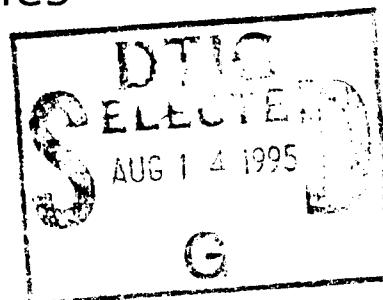




Fraunhofer Institut
Chemische Technologie

PYROTECHNICS

- Basic Principles
- Technology
- Application



19950811 043

26th International Annual Conference of ICT
July 4 - July 7, 1995
Karlsruhe, Federal Republic of Germany

DISTRIBUTION STATEMENT A

Approved for public release;
Distribution Unlimited

1995 0811 043

AD NUMBER	DATE	DTIC ACCESSION NOTICE
1. REPORT IDENTIFYING INFORMATION		<u>REQUESTER:</u> 1. Put your mailing address on reverse of form. 2. Complete items 1 and 2. 3. Attach form to reports mailed to DTIC. 4. Use unclassified information only. 5. Do not order document for 6 to 8 weeks.
A. ORIGINATING AGENCY FRAUNHOFER INSTITUTE, KARLSRUHE, GERMANY		
B. REPORT TITLE AND/OR NUMBER PYROTECHNICS - BASIC PRINCIPLES ETC.		
C. MONITOR REPORT NUMBER R&D 7731-AN-02		
D. PREPARED UNDER CONTRACT NUMBER N68171-95-M-6366		
2. DISTRIBUTION STATEMENT APPROVED FOR PUBLIC RELEASE - DISTRIBUTION UNLIMITED (FP)		<u>DTIC:</u> 1. Assign AD Number. 2. Return to requester.

DTIC Form 50
DEC 91

PREVIOUS EDITIONS ARE OBSOLETE

Herausgeber / Editor:

Fraunhofer-Institut für Chemische Technologie (ICT)
Joseph-von-Fraunhofer-Straße, Postfach 12 40
D-76318 Pfinztal (Berghausen)
Bundesrepublik Deutschland
Telefon (07 21) 46 40 - 0
Telefax (07 21) 46 40 - 111

Herstellung:

DWS Werbeagentur und Verlag GmbH, Karlsruhe
Printed in Germany

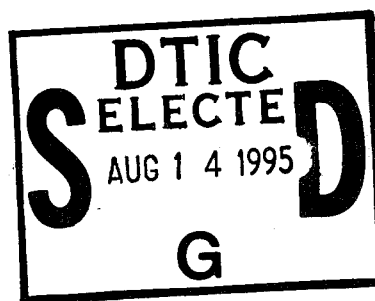
ISSN 0722-4087



Fraunhofer
Institut
Chemische Technologie

PYROTECHNICS

- Basic Principles
- Technology
- Application



N68171-95-M-6366

26th International Annual Conference of ICT
July 4 - July 7, 1995
Karlsruhe, Federal Republic of Germany

DISTRIBUTION STATEMENT A

Approved for public release;
Distribution Unlimited

DTIC QUALITY INSPECTED 5

DTIC QUALITY INSPECTED 5



26th International Annual Conference

PYROTECHNICS

- BASIC PRINCIPLES
- TECHNOLOGY
- APPLICATION

The International Annual Conferences, organized by the Fraunhofer-Institut für Chemische Technologie (ICT) over the last 25 years, have each dealt with a subject of particular interest in the field of energetic materials. As the subject of Pyrotechnics was last considered ten years ago (1985) it was high time to select it again. In this way we will have an opportunity to show the great deal of progress which has been made in this fascinating field.

The 26th International Conference of ICT is aimed at the discussion of the state of the art in research and development in the field of Pyrotechnics.

Main topics are

- Components and formulations
- Gas generators
- Initiation and ignition processes
- Test methods and criteria
- Performance, stability and compatibility
- Safety aspects
- Recycling and disposal

Chairman of the Conference

F. Volk,
ICT, Pfinztal, D

July 4 - July 7, 1995
Karlsruhe, Congress Center
Stadthalle, Weinbrenner-Saal
Federal Republic of Germany

Accession For	
NTIS CRA&I	<input checked="" type="checkbox"/>
DTIC TAB	<input type="checkbox"/>
Unannounced	<input type="checkbox"/>
Justification _____	
By _____	
Distribution /	
Availability Codes	
Dist	Avail and / or Special
A-1	

VORBEMERKUNG

Die Themen unserer Jahrestagung haben wieder ein breites internationales Echo gefunden. Die große Anzahl von eingegangenen Beiträgen machte, wie in den vorigen Jahren, eine Einteilung in Vorträge und Poster notwendig. Poster ermöglichen eine intensivere Diskussion und eine direkte Rückkopplung von interessierten Tagungsteilnehmern.

Der vorliegende Tagungsband erscheint zu Konferenzbeginn und enthält die schriftlichen Fassungen der Vorträge und Poster. Aus zeitlichen Gründen mußte die Drucklegung vor Eingang sämtlicher Beiträge erfolgen. Nachträglich eingegangene Manuskripte finden sich im Anhang oder wurden durch die Kurzfassung ersetzt.

PRELIMINARY REMARK

The subjects of the annual ICT-Conference have again found wide international response. The vast number of contributions necessitated - as in previous years - a division into oral presentations and posters. Posters enable an intensive discussion and direct feedback from interested conference participants.

The Conference Proceedings are published at the beginning of the conference and contain the written versions of the presentations and posters. Due to the shortage of time, printing had to commence prior to receipt of all contributions. Subsequently received manuscripts are either included in the Annex or the abstract is printed instead.

TABLE OF CONTENTS

LECTURES

V1

ENTWICKLUNG EINES EXTRUDIERTEN SCHNUR-FÖRMIGEN
COMPOSITGASGENERATOR-MATERIALS
*DEVELOPMENT OF AN EXTRUDABLE COMPOSITE CORDLIKE GAS-
GENERATING PROPELLANT*

J. Böhnlein-Mauß, G. Langer, K. Menke, R. Schäfer

V2

EINFLUSS DES BINDERGEHALTES AUF DAS REAKTIONSVERHALTEN
PYROTECHNISCHER MISCHUNGEN
*INFLUENCE OF THE BINDER CONTENT ON THE REACTION
BEHAVIOUR OF PYROTECHNIC MIXTURES*

B. Berger, B. Haas, G. Reinhard

V3

NEUE KONZEPTE BEI DER ENTWICKLUNG VON ZÜND- UND ANZÜND-
MITTELN
NEW CONCEPTS IN DEVELOPMENT OF EXPLOSIVES DEVICES

H. Zöllner

V4

AN EXPERIMENTAL INVESTIGATION OF THE ACCELERATION
INDUCED BURNING RATE INCREASE OF COMPOSITE SOLID
PROPELLANTS FOR GAS GENERATOR

J.-S. Hwang, C.-K. Kim, S.-H. Park

V5

PYROTECHNISCH ERZEUGTE TARNNEBEL - EIN ÜBERBLICK
PYROTECHNIC SMOKES FOR SCREENING - A SUMMARY

U. Krone

V6

A HYBRID GAS GENERATOR USING LOW CONCENTRATION HYDROGEN PEROXIDE FOR INFLATING AIRBAGS

N. Tsujikado, T. Saito, A. Iwama, T. Kazumi

V7

AN INFLUENCE OF THE CHEMICAL STRUCTURE OF SMOKE-PRODUCING MIXTURES ON THE LASER RADIATION EXTINCTION AT 1,06- μm AND 10,6- μm WAVELENGTHS

A. Paplinski, S. Cudzilo

V8

LOW TEMPERATURE SOLID SOURCES OF NITROGEN

V. Aleshin, S. Kurakin, G. Shirokova, Y.V. Frolov

V9

REDUCTION OF CO AND NO_x IN EFFLUENT GAS OF ADCA GAS GENERANT FOR AUTOMOTIVE AIRBAG INFLATORS

K. Hara, T. Hasegawa, S. Amari, Y. Otsuka, T. Yoshida

V10

DAS SELBSTSCHUTZSYSTEM MASKE, EIN MUNITIONSSYSTEM MIT KOMBINierter NEBELWIRKUNG IM SICHTBAREN UND INFRAROTEN BEREICH DES ELEKTROMAGNETISCHEN SPEKTRUMS
THE SELF-PROTECTION SMOKE SYSTEM MASKE WITH COMBINED EFFICACY IN THE VISIBLE AND INFRARED SECTIONS OF THE ELECTROMAGNETIC SPECTRUM

C. Hug, J. Grundler

V11

MESSUNGEN DES ENERGIEBEDARFS VON BRÜCKENANZÜNDPILLEN BEI NIEDRIGEM SPANNUNGSNIVEAU
TIME RESPONSE OF SQUIBS

M. Held

V12

THE HYDRODYNAMICAL METHOD TO ANALYSE THE COMBUSTION PRODUCTS COMPOSITION, THE CONCENTRATION AND TEMPERATURE FIELDS OF THE PYROTECHNICAL FUEL FLAME

V.P. Samsonov

V13

MECHANICAL IGNITION OF AN HETEROGENEOUS EXPLOSIVE
COMPOSITION SUBMITTED TO PROJECTILE PENETRATION

D. Lemoine, L. Gautier, H. Cherin

V14

STUDIES ON THE BURNING RATE OF
BUTACENE/AP/AL/CARBON FIBER COMPOSITE PROPELLANTS

H.-C. Yeh, D.-M. Chen, H.-C. Perng

V15

KINETICS AND MECHANISM OF ADN THERMAL DECOMPOSITION

G.B. Manelis

V16

ABBRANDEIGENSCHAFTEN VON VERZÖGERUNGSSÄTZEN AUF DER
BASIS VON BLEIOXID/SILICIUM
*COMBUSTION PROPERTIES OF DELAY COMPOSITIONS BASED ON
LEAD OXIDES/SILICON*

D. Cegiel

V17

VERBESSERUNG DER ANZÜNDEIGENSCHAFTEN VON TREIBLA-
DUNGSPULVERN DURCH APPLIKATION GEEIGNETER MODERATOREN
*IMPROVEMENT OF THE IGNITION PROPERTIES OF PROPELLANTS BY
THE APPLICATION OF SURFACE BALLISTIC MODIFIERS*

B. Vogelsanger, E. Brönnimann

V18

THE LASER INITIATION OF A SERIES OF ENERGETIC MATERIALS

A. L. Ramaswamy, R.W. Armstrong, J.E. Field

V19

BALLISTIC CHARACTERISTICS OF GUN PROPELLANTS AND CHARGES
CONTAINING METALLIC ADDITIVES

I.G. Assovskii, O.T. Chizhevskii, V.V. Sergeev

V20

EFFECT OF MOLECULAR STRUCTURE ON BURNING RATE

R.L. Simmons

V21

ZEITLICH PRÄZISE MEHRFACH-INITIIERUNG MIT ZÜNDSCHLÄUCHEN
(SHOCK TUBES) NONEL UND INDET
*MULTIPLE INITIATION WITH PRECISION TIMING USING SHOCK TUBES
NONEL AND INDET*

H.-U. Freund, W. Horning, G. Altmann

V22

SOLID PROPELLANT COMBUSTION

D.G. Voropaev, I.S. Zaslonko, V.N. Smirnov

V23

DEVELOPMENT OF THERMAL ANALYSIS TECHNIQUES FOR THE
STUDY OF PYROTECHNIC SYSTEMS

E.L. Charsley, S.B. Warrington, T.T. Griffiths

V24

BEHAVIOUR OF A PYROTECHNIC VALVE UNDER DIFFERENT
IGNITORS - THREE DIMENSIONAL FINITE ELEMENT MODELING

J.F. Guery, B. Cagnon, P. Brunet

V25

A DEVICE FOR QUANTITATIVE EVALUATION OF THRUST PRODUCED
BY SMALL FIREWORK ROCKETS

J. Akhavan, I. Grose, M. Williams, B. Cook

V26

APPLICATION OF THE COMPUTER-ASSISTED RETROSYNTHESIS TO
MODELING OF PROBABLE DECOMPOSITION REACTIONS FOR
ENERGETIC MATERIALS

T.S. Pivina, D.E. Lushnikov, E.V. Sokerina, A.A. Porollo, V.P. Ivshin

V27

CALCULATION OF THE EQUILIBRIUM THERMO-DYNAMIC PROPERTIES
OF THE ISOBARIC ADIABATIC COMBUSTION PRODUCTS OF AN/HTPB-
IPDI PROPELLANTS AT 7.0 MPA

P. Carvalheira

V28

THERMAL DECOMPOSITION STUDIES ON NTO AND NTO/TNT

J.C. Oxley, J.L. Smith, Z.L. Zhou, R. McKenney

V29

VISCOUS ENERGETIC LIQUID EXPLOSIVE FORMULATIONS
SENSITIZED WITH GLASS MICROBALLOONS - III. ANALYSIS OF THE
DETONATION DATA

J.L. Austing, A.J. Tulis

V30

FORTSCHRITTLICHE METHODEN ZUR BESTIMMUNG DER STABILITÄT
VON ZÜND- UND ANZÜNDSTOFFEN UND MUNITIONSKOMPONENTEN
*ADVANCED METHODS FOR THE DETERMINATION OF THE STABILITY
OF PRIMARY EXPLOSIVES AND COMPONENTS*

M. Kaiser, W. Scheunemann, U. Ticmanis

V31

AGEING OF MTV

C.A. van Driel, A.P.M. Leenders, J.J. Meulenbrugge

V32

ESTIMATION OF DETONATION PARAMETERS OF A NEW CLASS OF
EMULSION EXPLOSIVES

V.V. Odintsov, V.I. Pepekin

V33

KLASSIFIZIERUNG VON GROSSFEUERWERK
CLASSIFICATION OF DISPLAY FIREWORK

R. Basse, D. Eckardt, H.-J. Rodner

V34

PROBLEMATIK DER FORENSISCHEN UNTERSUCHUNGEN DER
DETONATIVEN EREIGNISSE IN GEBÄUDEN
*PROBLEMS OF THE FORENSIC INVESTIGATIONS CONCERNING
DETONATIVE EVENTS IN BUILDINGS*

O. Mueller

V35

MECHANICAL FAILURE OF HMX BASED PBXs AND ITS RELATIONSHIP
TO IMPACT SENSITIVITY

S.B. Langston

V36

GEFAHRKLASSIFIZIERUNG BEI DER HERSTELLUNG PYRO-
TECHNISCHER SÄTZE UND GEGENSTÄNDE
*HAZARD CLASSIFICATION FOR THE MANUFACTURING OF PYRO-
TECHNIC COMPOUNDS AND ARTICLES*

D. Eckhardt, N. Pfeil, H.-J. Rodner

V37

MODELING THERMAL / CHEMICAL / MECHANICAL RESPONSE OF
ENERGETIC MATERIALS

M.R. Baer, M.L. Hobbs, R.J. Gross, D.K. Gartling, R.E. Hogan

V38

THE STATIC ELECTRICITY HAZARDS: METHODS FOR ASSESSING
PYROTECHNICS SENSITIVITY AND APPROACH FOR HAZARD
REDUCTION

R. Rat, J. Isler

V39

ERMITTLUNG DER GRENZKONZENTRATIONEN DER EXPLOSIONS-
FÄHIGKEIT VON TNT IM GEMISCH MIT ERDREICH
*DETERMINATION OF THE EXPLOSIVE LIMITING CONCENTRATIONS OF
TNT IN SOIL*

E. Backof, B. Schieferdecker, F. Volk

V40

PHENOMENOLOGICAL ASPECTS OF BLAST OUTPUT FROM THE
HETEROGENEOUS DETONATION OF ENERGETIC COMPOSITIONS

A.J. Tulis, J.L. Austing, R. DiHu, D.L. Patel, D.C. Heberlein

V41

RECYCLING AND DISPOSAL OF PYROTECHNICS

N.H.A. van Ham, R. Eerligh

V42

PYROTECHNIC INCINERATION

D. Burch, M. Johnson

V43

BACTERIAL BIODEGRADATION OF NITRATE ESTER EXPLOSIVES

G.F. White, J.R. Snape, S. Nicklin

V44

RÜCKGEWINNUNG VON KOMPONENTEN KUNSTSTOFFGEBUNDENER TREIBMITTEL

RECOVERY OF INGREDIENTS FROM PLASTIC-BONDED PROPELLANTS

M.A. Bohn, R. Schweppe, W. Weisweiler

POSTER PRESENTATIONS

P45

EINFLUSS VON TEMPERATUR UND FEUCHTIGKEIT AUF PYROTECHNISCHE AUSGANGSKOMPONENTEN UND MISCHUNGEN

INFLUENCE OF TEMPERATURE AND HUMIDITY ON PYROTECHNIC MIXTURES AND THEIR COMPONENTS

F. Tschan, B. Berger, H.R. Bircher

P46

POLYVINYL ALCOHOLS AS BINDERS FOR PYROTECHNIC COMPOSITIONS

S.B. Langston

P47

ENERGETIC CHARACTERISTICS OF AMMONIUM PEROXOCOMPOUNDS OF NIOBIUM AND TANTALUM

G.D. Kozak, V.M. Raykova

P48

PYROTECHNIC COMPOSITIONS OF ZIRCONIUM AND CHROMATES OF ALKALINE EARTH METALS

R. Daniel, R.G. Sarawadekar, U.C. Durgapal

P49

ADHESION PROPERTIES OF LINER TO PROPELLANT AND METAL IN
HTPB BASED SYSTEMS

S.B. Haska, F. Pekel, S. Özkar, E. Bayramli

P50

STUDY ON HMX GRAIN SIZE CLASSIFICATION BY DMSO METHOD

Cheng Jingcai, Wu Xiaoqing, Guo Jianwen

P51

INVESTIGATION OF PENTAERYTHRITYL DIAZIDO DINITRATE

Wang Ping, Wang Xiaochuan, Huang Yue, Li Changqing

P52

THE ICT-THERMOCHEMICAL DATA BASE

F. Volk, H. Bathelt

P53

EINSATZ CHEMISCH EINBINDBARER FERROCENDERIVATE IN
COMPOSITTREIBSTOFFEN UND PYROTECHNISCHEN SYSTEMEN
*NEW CHEMICALLY BOUNDED FERROCENES FOR COMPOSITE
ROCKET AND GASGENERATING PROPELLANTS*

J. Böhnlein-Mauß, K.-P. Brehler, K. Menke, H. Jungbluth

P54

HERSTELLUNG VON EXPLOSIVSTOFFPARTIKELN DURCH SCHNELLE
EXPANSION FLUIDER ÜBERKRITISCHER LÖSUNGEN
*PARTICLE FORMATION OF EXPLOSIVES BY RAPID EXPANSION OF
SUPERCRITICAL SOLUTIONS*

U. Teipel, P. Gerber, H. Krause

P55

BINDERFREIE ANZÜNDMISCHUNGEN
BINDER FREE IGNITION MIXTURES

P. Jacob

P56

THE ROLE OF BISMUTH CHROMATE IN THE IGNITION REACTION OF
MOLYBDENUM AND POTASSIUM PERCHLORATE MIXTURES

R.G. Sarawadekar, R. Daniel, S. Jayaraman

P57

INFLUENCE OF ALUMINIUM ON COMBUSTION OF MAGNESIUM-
SODIUM NITRATE PYROTECHNIC MIXTURE

H. Singh, R. Bhaskara Rao

P58

ENERFOIL IGNITION FILM AS AN IGNITION CHARGE

S.K. Chan, S.J. Graham, G.A. Leiper

P59

UNTERSUCHUNG ÜBER DEN REAKTIONSMECHANISMUS DES
SCHWARZPULVERS UND SEINE ANWENDUNG
*INVESTIGATION OF THE REACTION MECHANISM OF BLACK POWDER
AND ITS APPLICATION*

T. Shimizu

P60

A STUDY ON THE PYROTECHNIC SYSTEM OF LC-RL-ATS-SI

O.S. Josyulu, E.G. Mahadevan

P61

AN INVESTIGATION OF THE CATALYTIC EFFECT OF IRON (III) OXIDE
ON THE BURNING RATE OF ALUMINIZED HTPB/AP COMPOSITE
PROPELLANT

E. Pinardag, A. Türkan, F. Pekel, S. Özkar

P62

IGNITION OF PYROTECHNICS SYSTEMS BY IRRADIATION

I.G. Assovskii

P63

THE INVERSION OF THE QUALITY OF RATIOS IN THE SYSTEM OF
INDEPENDENT CHEMICAL REACTIONS AT TRANSFER FROM
ISOTHERMAL HOLDING TO COMBUSTION

V.V. Klyucharev, A.P. Razumova

P64

THE COOPERATIVE PROCESSES OF MAGNESIUM OXIDATION IN
PERCHLORATE MIXTURES WITH OXIDE

V.V. Klyucharev, S.M. Sinelnikov, A.P. Razumova, V.D. Sasnovskaya

P65

THE CALCIUM COMPOUNDS AS THE COMPONENTS INCREASING THE ECOLOGICAL SAFETY OF PYROTECHNIC OXYGEN SOURCES

V.V. Klyucharev, S.M. Sinelnikov, A.P. Razumova, V.D. Sasnovskaya

P66

ESTIMATION OF THERMODYNAMIC STABILITY CONDITIONS AND PERSPECTIVES FOR SYNTHESIS OF COVALENT CARBON NITRIDE

V.V. Odintsov, V.I. Pepekin

P67

DEFLAGRATION AND DETONATION PREDICTIONS USING A NEW EQUATION OF STATE

L. Duraes, J. Campos, J.C. Gois

P68

MULTIDIMENSIONAL DDT MODELING OF ENERGETIC MATERIALS

M.R. Baer, E. Hertel, R. Bell

P69

BURNING RATE MODIFIERS FOR AN/HTPB-IPDI COMPOSITE SOLID PROPELLANTS FOR GAS GENERATORS

P. Carvalheira, J. Campos, G.M.H.J.L. Gadiot

P70

COMBUSTION PHENOMENA OF BORON CONTAINING PROPELLANTS

W. Eckl, N. Eisenreich, K. Menke, T. Rohe, V. Weiser

P71

HIGH-TEMPERATURE THERMOLYSIS; DEFLAGRATION AND IGNITION OF NITROCELLULOSE

G.T. Afanasiev, S.I. Postnov
(Manuscript not available)

P72

DEVELOPMENT PLAN OF A NEW DETONATION THEORY

F. Walker

P73

THE EXPERIMENTAL PHENOMENON OF DETONATION PROPAGATING
ALONG A CURVED SMALL CHARGE

Changgen Feng

P74

EIN FÜR SPRENGKAMMERN GEEIGNETER ÖKOLOGISCHER SPRENG-
STOFF FÜR EXPLOSIVSCHWEISSEN
*ENVIRONMENTAL FRIENDLY AGENT FOR EXPLOSIONWELDING IN
BLASTING CHAMBERS*

A. Vojtech

P75

TREIBSTOFF FÜR HÜLSENLOSE MUNITION AUF DER BASIS DES
PRESSBAREN NITROZELLULOSEGRANULATS
*PROPELLANT MASS FOR CASELESS AMMUNITION BASED ON
PRESSABLE NITROCELLULOSE GRANULAT*

T. Dosoudil

P76

SOLID PROPELLANT MOTOR IMPACT TEST

M. Chiba, R. Asano, H. Nakamura, Y. Hyodo, T. Matsunaga, K. Tanaka,
K. Arai, T. Nakayama, S. Suzuki, K. Kosaka

P77

GENERALIZATION OF THE RESULTS OF THE SOLID ENERGETIC
MATERIALS SENSITIVITY TO IMPACT AND FRICTION ESTIMATION

B.N. Kondrikov

P78

PYROTECHNIC GENERATOR OF FLYER DISK

J. Ribeiro, J. Campos, R. Mendes

P79

SPECTRAL EMISSION FROM POOL FIRES OF VARIOUS FUELS -
CONSIDERING TRANSIENT STRUCTURES

V. Weiser, M. Weindel, A. Hoffmann, W. Eckl, N. Eisenreich

P80

THERMAL ANALYSIS STUDIES ON THE ZIRCONIUM-POTASSIUM
PERCHLORATE-NITROCELLULOSE PYROTECHNIC SYSTEM

B. Berger, E.L. Charsley, J.J. Rooney, S.B. Warrington

P81

A PYROTECHNIC MULTI LAUNCH ROCKET SYSTEM SIMULATOR

M. Cartwright et al.

P82

OPTISCHE CHARAKTERISIERUNG VON ABBAUPROZESSEN
CHEMISCHER ENERGIETRÄGER IN ÜBERKRITISCHEM WASSER
*OPTICAL CHARACTERIZATION OF A HIGH PRESSURE REACTION
CHAMBER FOR DEGRADATION OF ENERGETIC MATERIALS IN
SUPERCRITICAL WATER*

B. Michelfelder, W. Eckl, N. Eisenreich, M. Herrmann, T. Hirth, H. Krause

P83

ANALYSIS OF THE LONG TERM STABILITY DATA

J. Petrzilek

P84

WÄRMEFLUSSKALORIMETRISCHE UNTERSUCHUNGEN AN
ANZÜNDMITTELN
HEAT FLOW CALORIMETRIC INVESTIGATIONS OF PRIMERS

S. Wilker, G. Pantel, M. Kaiser, U. Ticmanis

P85

THERMOANALYTISCHE CHARAKTERISIERUNG VON PYROPHOREN
METALLOORGANISCHEN VERBINDUNGEN
*THERMOANALYTICAL CHARACTERIZATION OF PYROPHORIC METAL-
ORGANIC COMPOUNDS*

T. Fischer, S. Rushworth, N. Eisenreich, A. Pfeil, A.C. Jones, A.B. Leese,
G. Williams

P86

THERMISCHES ZERSETZUNGSVERHALTEN VON AN/GAP-
MISCHUNGEN
THERMAL DEGRADATION OF AN/GAP-BLENDS

V. Weiser, S. Löbbcke, T. Keicher, T. Härdle, J. Böhnlein-Mauß, A. Pfeil

P87

EXPERIMENTAL STUDY OF DDT IN AN HETEROGENEOUS EXPLOSIVE COMPOSITION

D. Lemoine, L. Gautier, H. Cherin, R. Belmas

P88

withdrawn

P89

INVESTIGATION OF THERMAL DECOMPOSITION AND IMPACT SENSITIVITY OF PYROTECHNIC MIXTURES

W. Li, Q.C. Song

P90

THE DOUNREAY-SILVER-II-PROCESS AND ITS INDUSTRIAL APPLICATION FOR THE DISPOSAL OF PYROTECHNIC MATERIALS

J. Hedtmann

P91

GRÖSSENANALYSE VON FESTSTOFFPARTIKELN MIT HILFE DER LASERBEUGUNGSSPEKTRO-METRIE AM BEISPIEL VON GAS-GENERATOR-KOMPONENTEN
PARTICLE SIZE DETERMINATION OF GASGENERATOR COMPONENTS BY LASER LIGHT SCATTERING

U. Teipel, U. Förter-Barth

P92

STUDIES ON INFRARED SCREENING SMOKES

A. Singh, S.G. Avachat, L.K. Bankar, H. Singh

P93

A PROPOSED SCHEME FOR THE EVALUATION OF MATERIALS WITH PYROTECHNICS IN ROCKET MOTOR IGNITERS

B. Merchant, G.M. Keeton

P94

SPEKTROSKOPISCHE UNTERSUCHUNGEN ZUM ABBRANDVERHALTEN VON HTPB- UND GAP-PLATTEN MIT BORZUSATZ IN EINER EBENEN STUFENBRENNKAMMER

C. Hensel, H. Ciezki

P95

ENTWICKLUNG EINER KOMBINIERTEN GAS- UND PARTIKELPROBEN-
NAHMESONDE FÜR DEN EINSATZ IN EINER FESTSTOFFSTAUBRENN-
KAMMER

H. Ciezki, B. Schweln

P96

UV-VIS-SPEKTROSKOPISCHE ERFASSUNG VON IN UNTER- UND
ÜBERKRITISCHEM KOHLENDIOXID GELÖSTEN NITROAROMATEN

S. Löbbecke, G. Bunte, T. Härdle, H. Krause

DEVELOPMENT OF AN EXTRUDABLE COMPOSITE CORDLIKE GASGENERATING PROPELLANT

J. Böhnlein-Mauß, G. Langer, K. Menke

Fraunhofer-Institut für Chemische Technologie - ICT -
D-76327 Pfinztal (Berghausen)

R. Schäfer

Dornier GmbH, D-88039 Friedrichshafen

Zusammenfassung

Der Beitrag beschreibt die pyrotechnische Zusammensetzung und Konfiguration eines schnellbrennenden schnurförmigen Gasgeneratormaterials, das Abbrandzeiten im Bereich von 10 - 20 ms und eine hohe Weiterleitungsgeschwindigkeit der oberflächlichen Anzündung besitzt. Dabei wurde eine extrudierbare schnellbrennende Compositformulierung aus Ammoniumperchlorat und thermoplastisch verarbeitbarem Elastomer eingesetzt.

Der geforderte Druckanstieg im Millisekundenbereich konnte mit einem kleeblattförmigen Strangprofil, d.h. durch Einstellung von Hohlräumen zwischen pyrotechnischer Seele und umhüllenden Plastikschauch erreicht werden. Die geforderte hohe Fortpflanzungsgeschwindigkeit der Anzündung wurde durch Bepuderung des Treibstoffmaterials mit leicht durchzündbaren pyrotechnischen Sätzen ermöglicht. Die technischen Eigenschaften des neuen schnurförmigen Gasgeneratormaterials werden im Vergleich zu denen der ITLX 2000 Schnur dargestellt und diskutiert.

Abstract

The development of the pyrotechnical composition and configuration of a fast burning cord like gasgenerating propellant with burning times of 10 - 20 ms and a high propagation speed of surface ignition will be described. For this purpose an extrudable composite propellant formulation based on ammoniumperchlorate and thermoplastic elastomer was used.

The required pressure rise within milliseconds could be achieved by extruding a cloverleaf cord profile which enables the adjustment of free volume between the pyrotechnic core and the surrounding plastic hose. The required high propagation speed of ignition was made possible by powdering the propellant cord with easily ignitable pyrotechnic compositions. The technical properties of the new cordlike gas-generator material are discussed and compared with those of the ITLX 2000 ignition cord.

1. Einführung

Pyrotechnische Gasgeneratoren mit hohen Abbrandgeschwindigkeiten und Gaslieferung im Bereich von Millisekunden werden für Ausstoß- und Anzündladungen ebenso wie für Airbag-, Rettungs- und Feuerlöschsysteme benötigt. Schnurförmige Gasgeneratoren werden vornehmlich zur Anzündung von Raketen- und Gasgeneratortreibsätzen, Treibladungen oder Airbaggeneratoren eingesetzt. „Shock Tubes“ (Nonel Tubes) besitzen eine gepuderte Sprengstoffbeschichtung, z.B. aus PETN, RDX, HMX oder 2,2',4,4',6,6'-Hexanitrostilben (HNS) und Dipicramide (DIPAM) in einer Umhüllung aus Metall oder glasfaserverstärktem Kunststoff (1,2). Sie dienen u.a. zur Auslösung von Schleudersitzen (3). Anzündschnüre für Raketenmotoren bestehen nach Svejka und Kozera (4) aus Centralit, Nitrocellulose und Ammoniumperchlorat, nach Schulz aus Aluminium und Bleiazid (5), nach Montesi aus HNS, Bor und Kaliumnitrat (6).

Eine sehr schnellbrennende pyrotechnische Schnur mit Compositgasgeneratormaterial stellt die von der Firma Explosive Technologies entwickelte ITLX-Schnur dar (7). Sie wird sowohl für die Anzündung von Treib- und Airbag-Ladungen (8) als auch für schnelle Ausstoßvorgänge in speziell konzipierten Gasgeneratorkonfigurationen eingesetzt (9).

Das Ziel der Arbeiten war es, ein standardisierbares pyrotechnisches Material und eine entsprechende Gasgeneratorkonfiguration zu konzipieren, die einen schnellen Abbrand und Druckanstieg über 10 - 20 ms und eine Weiterleitungsgeschwindigkeit der Anzündung von 500 - 1000 m/s ermöglicht. Dies entspricht einer im Abbrand verlangsamen, aber dafür stärker gasliefernden Schnur als das ITLX-Modell. Weitere Anforderungen waren:

- * Funktionssicherheit von -50 °C bis +70 °C,
- * ausreichende chemische und mechanische Stabilität,
- * keine Selbstentzündung bei einstündigem Erhitzen auf 200 °C,
- * keine Detonationsempfindlichkeit,
- * Anzündbarkeit mit handelsüblichen elektrischen Anzündern,
- * leichte Konfektionierbarkeit,
- * Handhabungs- und Transportsicherheit,
- * niedriger Herstellungspreis.

2. Entwicklungskonzept

Um eine Standardisierung zu ermöglichen, ging das Entwicklungskonzept der Gasgeneratorschnur von einer extrudierten pyrotechnischen Seele aus schnellbrennendem Gasgeneratortreibstoff aus. Um eine gleichmäßige Anzündung über die gesamte Schnurlänge zu erreichen, sollte eine poröse oder gepuderte Anzündschicht aufgebracht werden. Damit waren im wesentlichen vier Problemstellungen zu bearbeiten:

- 1) Suche nach einer geeigneten extrudierbaren pyrotechnischen Formulierung mit hohen Abbrandgeschwindigkeiten im niederen Druckbereich.
- 2) Einstellung eines geeigneten geometrischen Strangprofils.
- 3) Formulierung und Aufbringung einer geeigneten Anzündschicht zur Einstellung der geforderten hohen Anzünd- und Weiterleitungsgeschwindigkeit.
- 4) Gestaltung und Applikation einer gleichmäßig verdämmenden, gut konfektionierbaren Stranghülle.

3. Durchführung

Entsprechend den äußeren Rahmenbedingungen wurde folgender Lösungsweg gewählt:

3.1. Pyrotechnische Formulierung

Zur Auswahl der pyrotechnischen Formulierung zeigt Tabelle 1 einen Eigenschaftsvergleich von extrudierbaren Gasgeneratormaterialien.

Traditionelle Doublebasetreibstoffe sind detonationsempfindlich und erreichen nicht die hohe geforderte Temperaturstabilität. Nitramintreibstoffe sind thermisch stabiler, aber in ihrer Abbrandgeschwindigkeit zu langsam.

Hohe Abbrandgeschwindigkeiten bei niedrigem Druck, hohe Temperaturstabilität und Detonationsunempfindlichkeit werden nur von perchlorathaltigen Compositformulierungen erreicht. Aus diesem Grunde wurde für das gasliefernde Material eine Composit-Formulierung gewählt. Zum Vergleich sind in Tab. 1 die Eigenschaften der sehr schnell abbrennenden ITLX-Schnur mit aufgeführt, die ebenfalls eine Compositformulierung in extrudierter Form enthält, aber durch den geringen Binderanteil und die hohe Porosität (s.u.) nur eine geringe mechanische Stabilität des pyrotechnischen Materials aufweist.

Um diesen Nachteil zu begegnen und eine Standardisierbarkeit zu erleichtern, wurde nach mehreren Entwicklungsschritten ein extrudierbarer pyrotechnischer Satz auf der Basis von Ammoniumperchlorat (AP) in kleiner, sehr fein vermahlener Korngröße, 4 % Abbrandbeschleuniger und einem Bindemittel, bestehend aus thermoplastisch verarbeitbarem Elastomer und Weichmacher, eingesetzt.

Zusammensetzung und Eigenschaftsprofil der pyrotechnischen Formulierung sind in Tabelle 2 wiedergegeben.

3.2 Geometrisches Strangprofil

Auch bei der Verwendung schnellbrennender pyrotechnischer Wirkmassen werden die geforderten kurzen Druckanstiegs- und Abbrandzeiten nur von einem offenen, hoch zerklüfteten Strangprofil mit großer Anbrennfläche erreicht; während eine hohe Weiterleitungsgeschwindigkeit der Anzündung vor allem durch Hohlraumkanäle in oder um der extrudierten pyrotechnischen Seele ermöglicht werden sollte. Abbildung 1 zeigt die mittels einer Topfpresse hergestellten und untersuchten Strangprofile der Gasgeneratormischung. Das Abbrandverhalten von jeweils 10 mm langen Stücken wurde exemplarisch von einem 2 mm Vollstrang und einem Strang mit 0,8 mm Innenloch in ummantelter und nicht ummantelter Form in einer 100 ml (10 g Ladungsgewicht) fassenden ballistischen Bombe bestimmt. Die Ladungen wurden jeweils mit einer Zündpille T7 und einer Beiladung von 0,5 g Bor/Kaliumnitrat gezündet. Druckmessung erfolgte mit Druckaufnehmern der Firma Kistler. Die erhaltenen Meßkurven

sind in Abb. 2 dargestellt. Wie erwartet, brennt der Vollstrang sehr langsam, der Strang mit Loch dafür in sehr kurzer Zeit ab.

Abbildung 3 zeigt die erhaltenen Druckkurven eines im Sternprofil extrudierten Stranges in offener (SGG 13/7) und mit Polyolefinschrumpfschlauch ummantelter Form (SGG 13/8). Die daraus gewonnenen Meßdaten sind in Tab. 3 zusammen- und denen der in den Abmessungen vergleichbaren ITLX-Schnur gegenübergestellt.

Die ummantelte Sternkonfiguration SGG 13/8 ist danach nur wenig langsamer als die nicht ummantelte Form SGG 13/7. Beide pyrotechnische Wirkmassen erreichen als Vollmaterial in dieser Form des Abbrandes fast die Schnelligkeit der porösen ITLX.(7)

3.3. Anzündschicht

Um eine hohe Weiterleitungsgeschwindigkeit und effektive Anzündung des Gasgeneratormaterials zu erhalten, wurde der Strang mit einer feinpulvrigen Anzündmischung bepudert. Tabelle 4 zeigt die thermodynamischen Daten von den Rezepturen der verwendeten pyrotechnischen Sätze. In den folgenden Versuchen stellte sich heraus, daß nur die Mischungen mit hoher spezifischer Energie und Abbrandtemperatur wie Aluminium/Oktogen und Kaliumperchlorat/Aluminium erfolgversprechend eingesetzt werden konnten.

3.4. Ummantelung und fertige Strangkonfiguration

Da für das Aufbringen der Ummantelung keine Extrusionsanlage zur Verfügung stand, mußten sich die Versuche auf eine im Labormaßstab durchführbare Methode beschränken. Für die Umhüllung bis zu 1 m langer Gasgeneratorstränge wurden in drei Lagen Polyolefinschrumpfschlauch, verstärkender Polyamidgewebeslauch und nochmals Polyolefinschrumpfschlauch verwendet. Die Bilder 4a und 4b zeigen Querschnitt und Außenansicht der auf diese Weise hergestellten Gasgeneratorschnur. In den Fotos sind die in Kleeblattform extrudierte pyrotechnische Seele, die durch Bepuderung aufgebraachte Anzündschicht und die dreilagige Ummantelung gut zu erkennen.

In den folgenden Abbrandversuchen zeigte sich, daß der vollständige Abbrand der pyrotechnischen Wirkmasse nur mit einer gleichmäßigen und druckbelastbaren Umhüllung zu erreichen war. Dementsprechend besteht der Mantel der zum Vergleich betrachteten ITLX-Schnur ebenfalls aus extrudierten, glasfaserversträtktem Polypropylenschlauch. Die vergrößerten Aufnahmen der Ansichten von Querschnitt und Schnur sind in den Bildern 5a und 5b dargestellt. In der Vergrößerung ist deutlich die Porosität und offene Struktur der pyrotechnischen Seele zu erkennen.

4. Abbranduntersuchungen

Der Abbrand der komplett montierten Gasgeneratorschnur wurde offen mit einer Hochgeschwindigkeitskamera, Typ Hycam, und in einer speziell gebauten, schlauchförmigen Druckbombe untersucht. Bild 6 zeigt die Versuchsanordnung des offenen Abbrandes. In dieser Anordnung wurde der Abbrand der in Bild 4 dargestellten Gasgeneratorschnur mit einer Filmgeschwindigkeit von 12.000 Bilder pro Sekunde aufgenommen.

Die erhaltenen Aufnahmen sind in Bild 7 wiedergegeben. Darin ist hell leuchtend der schnell fortschreitende Abbrand der pyrotechnischen Anzündschicht und der nachkommende, etwas ungleichmäßig verlaufende Abbrand des Gasgeneratormaterials mit punktuelltem Aufbrechen des Stranges erkennbar. Der mit 20.000 Bildern pro Sekunde aufgenommene Abbrand der ITLX 2000 (Bild 8) läuft durch die Porosität des Gasgeneratormaterials deutlich schneller ab. Der Strang reißt auf ganzer Länge einheitlich auf. Als Fortpflanzungs- oder Weiterleitungsgeschwindigkeit der Anzündung wird für den SGG 14 Gasgeneratorstrang 560 m/s und für die ITLX 2000 1100 m/s ermittelt.

Die Bilder 9 und 10 zeigen die beiden Gasgeneratorschnüre vor und nach dem Abbrand.

Um den Druckanstieg und die Fortpflanzungsgeschwindigkeit des Abbrandes quantitativ zu erfassen, wurde eine schlauchförmige Druckbombe gebaut, die es gestattete, den Abbrand von 470 mm langen Gasgeneratorschnüren über zwei Druckaufnehmer in 40 mm und 420 mm Entfernung vom Zündkopf und 6 Lichtleitern im Ab-

stand von jeweils 80 mm zu verfolgen. Bild 11 zeigt ein Foto der Versuchsanordnung.

Die beim Abbrand der SGG 14 Schnur erhaltenen Lichtleitersignale von vier besetzten Positionen sind in Bild 12 dargestellt. Sie zeigen ein ungleichmäßiges, mehrfaches Ansprechen der optischen Sensoren, bedingt durch das ungleichmäßige Aufreißen der Schnur. Es ergibt sich eine mittlere Fortpflanzungsgeschwindigkeit von 930 m/s. Die Signale der beiden Druckaufnehmer und der dazugehörige Druckanstieg zeigt Bild 13. Aus ihnen errechnet sich eine Fortpflanzungsgeschwindigkeit von 790 m/s. Die Zeitspanne bis zum Erreichen des Spitzendrucks von 180 bar liegt bei 15 ms.

Die unter gleichen Bedingungen vermessene ITLX-Schnur ergibt eine über Lichtleiter gemessene Abbrandgeschwindigkeit von 1150 m/s sowie einen über die Drucksensoren bestimmten Wert von 1380 m/s. Die Zeitspanne bis zum Erreichen des Spitzendrucks von etwa 100 bar liegt bei 0,5 ms. Die durch den schnellen Abbrand und das gleichmäßige Aufreißen der Schnur in schöner Periodizität erhaltenen Lichtleitersignale zeigt Bild 14.

5. Diskussion und Ergebnis

Tabelle 5 stellt die Eigenschaften der SGG 14 Schnur denen der ITLX 2000 gegenüber. Wie in den Druckbombenversuchen erkennbar, stellt die AP/TPE-Formulierung der SGG 14 auf Grund des höheren Binderanteils mehr Gas beim Abbrand zur Verfügung, als die ITLX-Schnur. Im Vergleich zur ITLX brennt der als Vollmaterial extrudierte SGG 14 Strang langsamer, d.h. in einer für Airbag Gasgeneratoren typischen Zeit ab.

Durch die Bepuderung wird im freien Abbrand wie in der Druckbombe eine Anzündgeschwindigkeit zwischen 500 und 1000 m/s erreicht. Ohne eine ausreichende Verdämmung erfolgt der Abbrand der pyrotechnischen Seele jedoch ungleichmäßig und über einen längeren Zeitraum gestreckt. Aus diesem Grunde wurde die Ausführung in einer doppelten Ummantelung mit Verstärkungsgewebe gewählt.

Im Vergleich zur SGG 14 besitzt die ITLX-Schnur eine sehr viel porösere und von Hohlräumen durchzogene Struktur des pyrotechnischen Materials. Der hohe Metall- und geringe Binderanteil führt zu einer hohen Abbrandtemperatur, aber insgesamt geringen Gaslieferung. Die poröse Struktur bewirkt ein schnelleres, blitzartiges Abbrennen. Dafür ist, ebenso wie für die schnelle Weiterleitung der Anzündung, eine gute Verdämmung wesentliche Voraussetzung. Die ITLX besitzt aus diesem Grunde einen aus zwei Lagen bestehenden extrudierten Doppelmantel aus glasfaserverstärktem Polypropylen (7).

Zusammenfassung

Ihre Abbrandeigenschaften machen die im Vergleich betrachtete ITLX zur idealen Anzündschnur, die eine hohe Energieübertragung, bedingt durch hohe Abbrandtemperaturen und eine hohe Konzentration heißer Metalloxidpartikel, mit einem schnellen Abbrand und hoher Weiterleitungsgeschwindigkeit der porösen pyrotechnischen Seele miteinander verbindet.

Demgegenüber stellt die SGG 14 Schnur ein schnellbrennendes, mehr Gas lieferndes, konfektionierbares Gasgeneratormaterial dar.

Die als extrudiertes Vollmaterial ausgeführte pyrotechnische Seele der SGG 14 brennt in einer kontrolliert verdämmenden Anordnung gleichmäßig und kontrollierbar im Bereich von Millisekunden ab. Ihre Abbrandeigenschaften werden von der Abbrandgeschwindigkeit der pyrotechnischen Formulierung, vom geometrischen Strangprofil, von Art und Aufbringung der Anzündschicht und von der verdämmenden Wirkung der Stranghülle bestimmt. Sie sind auf diese Weise variier- und einstellbar.

Das Hintereinanderschalten verschieden langer Schnurstücke bietet eine weitere Möglichkeit, Gas- und Drucklieferung den Anforderungen und der jeweiligen Anwendung entsprechend zu gestalten.

Der vorgestellte Schnurtyp bietet sich damit als Grundmaterial für Gasgeneratoren an, die für schnelle Aufblas-, Ausstoß- oder Schaltvorgänge eingesetzt werden sollen.

Literaturverzeichnis

- 1) C.O. Leiber, P. Steinbeiß, A. Wagner;
„On Apparent Irregularities of Pressure Profiles in Shock Tubes“
Contribution to DEA 7304, Bad Reichenhall (1992)
- 2) T. Rogers;
„Miniature Non Disrupting Detonating Delay Cord“
Contribution to 13th Intern. Pyrotechn. Seminar, London (1989)
- 3) L.J. Bement, E.G. Kayser, M.C. Schimmel;
„Service Life Evaluation of Rigid Explosive Transfer Lines“
NTIS Order N.N. 83 - 31596/0
- 4) O. Svejka, G. Kozera;
„Ignition Cord for Rocket Motor Charges“
CA 129074 (1968)
- 5) W.E. Schulz;
„High Velocity Ignition Propagating Cord“
US 332 0882 (1967)
- 6) L.J. Montesi;
„The Development of a Mild Detonating Cord (MDC) for a Gas Generator“
NTIS Order Nr. AD 878 854/9
- 7) „ITLX Ignition System
The Method for Linear Ignition“
Technical Specification from Explosive Technology Fairfield (1991)
- 8) Goepfert;
„ITLX-Schnur, Untersuchung zur Treibsatzanzündung“
DOK FIZ Bw Pok.Nr. EA 2186
- 9) A. Dietrich;
„Gasgenerator zum Erzeugen eines Gasdruckes in einer Expansionskammer“
DE 3403 352 (1984)

	DB-FTS	Nitramin PBX	Composit GG	ITLX
Zusammensetzung	NC/NGI	RDX/HMX TAGN/Binder	AP/KP Metall/Binder	AP/KP/Al + 6 % Binder
Gasausbeute	hoch ca. 1000 l/kg	hoch ca. 1000 l/kg	hoch 600 - 900 l/kg	285 l/kg
Abbrandgeschwindigkeit (100 bar)	20 - 30 mm/s	5 - 10 mm/s	50 - 60 mm/s	sehr hoch (Porosität)
Tieftemperatureigen- schaften < -30 °C	spröde	gut	gut	ungünstig
Chemische Stabilität	befriedigend	gut	gut	gut
Verpuffungstemperatur	180 - 190 °C	220 - 240 °C	240 - 280 °C	> 230 °C
Detonations- empfindlichkeit	++	++	θ	θ

Tabelle 1 : Eigenschaftsvergleich extrudierbarer pyrotechnischer Gasgeneratormaterialien

Tabelle 2: Zusammensetzung und Eigenschaftsprofil der pyrotechnischen Gasgeneratorformulierung SGG 14

◆ <u>Zusammensetzung</u>			
Ammoniumperchlorat	:	76 %	
Polybutadienstyrol TPE	:	19 %	
Polybutadien	:	1 %	
Kupferchromit	:	4 %	
◆ <u>Thermodynamische Daten (50 : 1)</u>			
Spez. Impuls (Ns/kg)	:	2029	
Abbrandtemperatur (K)	:	2022	
Charakteristische			
Geschwindigkeit (m/s)	:	1329	
Molzahl Gase	:	45,9	
mittl. Molgewicht der			
Abbrandprodukte	:	21,8	
◆ <u>Abbrandeigenschaften</u>			
Druck MPa	r (mm/s)		(IIr) _p
	+ 20 °C	+ 50 °C	
2	18,9	20,0	0,19
4	26,4	27,5	0,14
7	31,7	33,9	0,23
10	37,5	39,3	0,16
13	41,5	43,9	0,19
18	48,8	50,3	0,10
25	57,2	63,3	0,36
Druckexponent n:	0,43	0,44	
◆ <u>Chem. Stabilität</u>			
Verpuffungstemperatur:	281 °C		
(20°/min)			
Hollandtest:	- 0,34 %	Gewichtsverlust	
(8-72 h / 105°C)			
Vakuumstabilität:	0,184 ml/g	Gasentwicklung	
(40h / 100°C)			
◆ <u>Mechanische Eigenschaften</u>			
	- 40 °C	+ 20 °C	+ 50 °C
Zugfestigkeit (N/mm ²)	3,1	1,0	0,63
Reißdehnung (%)	3,4	2,6	1,9
E-Modul (N/mm ²)	655	64,2	37,0
◆ <u>Mechanische Empfindlichkeit</u>			
Reibempfindlichkeit:	72 N		
Schlagempfindlichkeit:	2,5 Nm		


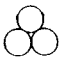
Tabelle 3: Aus den Abbranduntersuchungen in der ballistischen Bombe erhaltene Meßdaten (100 ml / Ladedichte 0,1 g / cm³):

Probe	max. Druck (bar)	Druckanstieg (m/s)	30 % Wert bar / ms	80 % Wert bar/ms	30 - 80 Zeit ms
D 22 Vollstrang	200	16	60/37	160/47	10
D 22 Vollstrang ummantelt	120 unvollständiger Abbrand	63 unvollständiger Abbrand	36/61 unvollständiger Abbrand	96/85 unvollständiger Abbrand	24 unvollständiger Abbrand
D 22 mit Loch	170	13	51/23	136/29	6
D 22 mit Loch ummantelt	130	25	39/36	104/46	10
SGG 13/7 Sternprofil	280	18	84/17	224/22	5
SGG 13/8 Sternprofil ummantelt	260	24	78/16	208/23	7
ITLX 2000	44	7	13/23	35/26	3

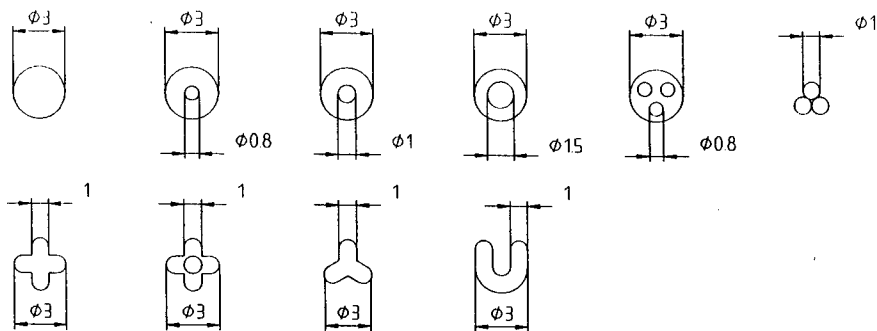
Tabelle 4: Thermodynamische Daten der zur Bepuderung verwendeten Anzündmittel

Anzündmittel	Temperatur (K)	Explosionswärme (cal/g)	spez. Energie (J/g)
B/KNO ₃ 25,9 : 74,1	2700	2043	314
Al/KClO ₄ 30 : 70	3801	2225	364
Al / Oktogen 20 : 80	3801	1912	1126

Tabelle 5: Vergleich der technischen Eigenschaften der SGG 14 und ITLX 2000 Schnur

	<u>SGG 14</u>	<u>ITLX 2000</u>
<u>Zusammensetzung:</u>	AP 80 % TPE 20 %	AP 33 % KP 40 % Al 21 % Binder 6 %
Molzahl Gas (Mol/kg):	43,74	14
Mittl. Molgewicht (g):	21	42,8
erzeugte Gasmenge (NI/kg):	980	314
Abbrandtemperatur (K):	2539	3800
Spez. Energie (J/g):	968	662
(Ladedichte 0,1 g/cm ³)		
Explosionswärme (cal/g):	838	2063
Form:		
Ummantelung:	3fach Kunstfaser verstärkt	3fach GFK extrudiert
Äußerer Durchmesser (mm):	6	3,5
<u>Ladungsgewicht:</u>		
g Pyro/m Schnur	5,8	2
g Gesamt/m Schnur	23	12,5
<u>Gasmenge:</u>		
g pro g Schnur	0,29	0,096
g pro m Schnur	5,54	1,2
NI/kg Schnur	247	50,2
NI/m Schnur	5,7	0,63
<u>Anzündgeschwindigkeit (m/s):</u>		
Offener Abbrand:	560	1100
Druckbombe:	790 - 930	1150 - 1380
Abbrandzeit,		
Druckanstiegszeit (ms):	15	0,5
Spitzendruck (bar)	180	100
(450 mm Schnur)		

Strangprofile



FRAUNHOFER-INSTITUT für Chemische Technologie Joseph-von-Fraunhofer-Str. 7507 Pfinztal 1		Zut. Abw.	Oberfläche	Maßstab:	Gewicht
		Datum	Name	Werkstoff:	
		Bearb.		Rohteil-Nr.	
		Geor.		Benennung:	Strangprofile
		Norm		Zeichnungsnummer:	1 Blatt
Zust.	Änderung	Datum	Name/Urspr.	Ers. f.	Ers. d.

Bild 1: Untersuchte Strangprofile der SGG 14 Formulierung

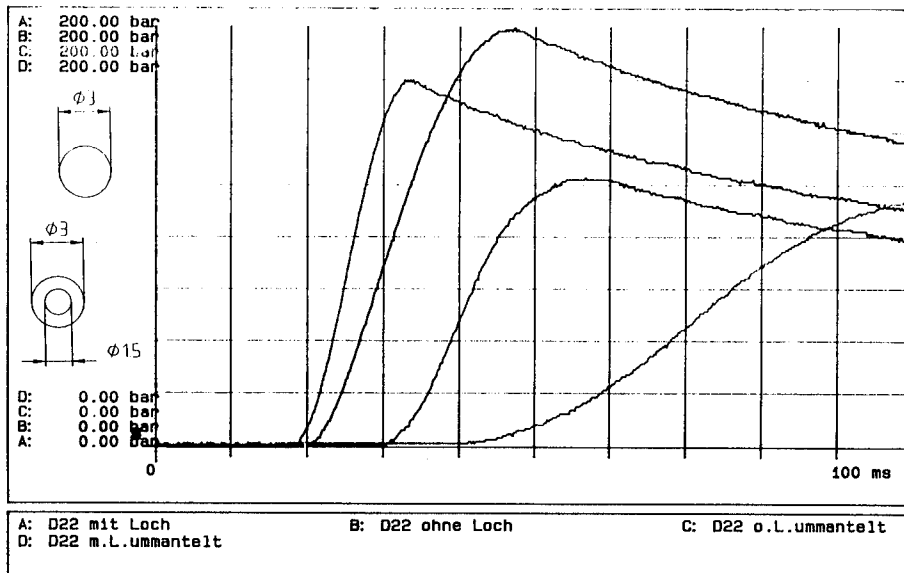


Bild 2: Abbrandverhalten von 10 mm langen Vollstrang- und Hohlzylindersträngen mit und ohne Ummantelung, gemessen in der ballistischen Bombe

1 - 15

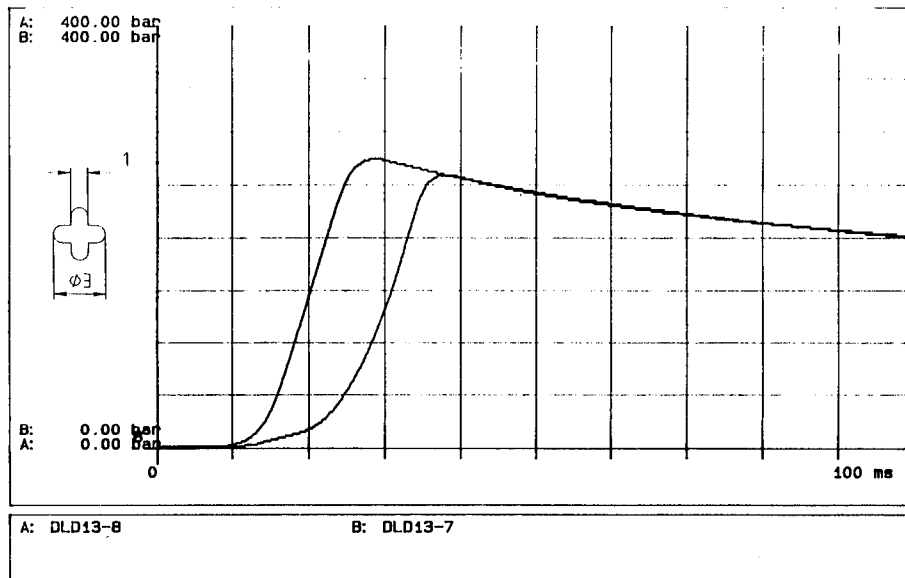


Bild 3: Abbrandverhalten von 10 mm langen Stücken eines im Sternprofil extrudierten Stranges mit und ohne Ummantelung, gemessen in der ballistischen Bombe

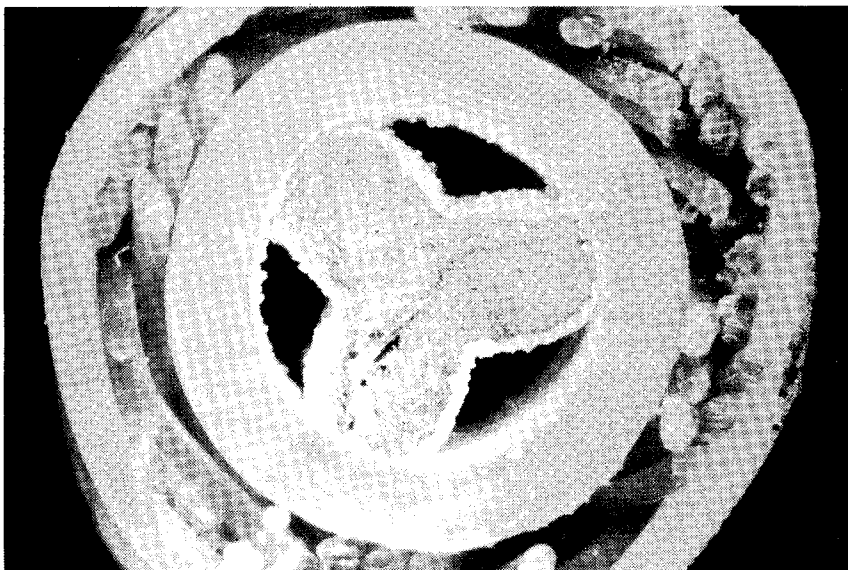


Bild 4a: Querschnittsaufnahme der ummantelten Gasgeneratorschnur SGG 14 (Vergrößerung 30 : 1)

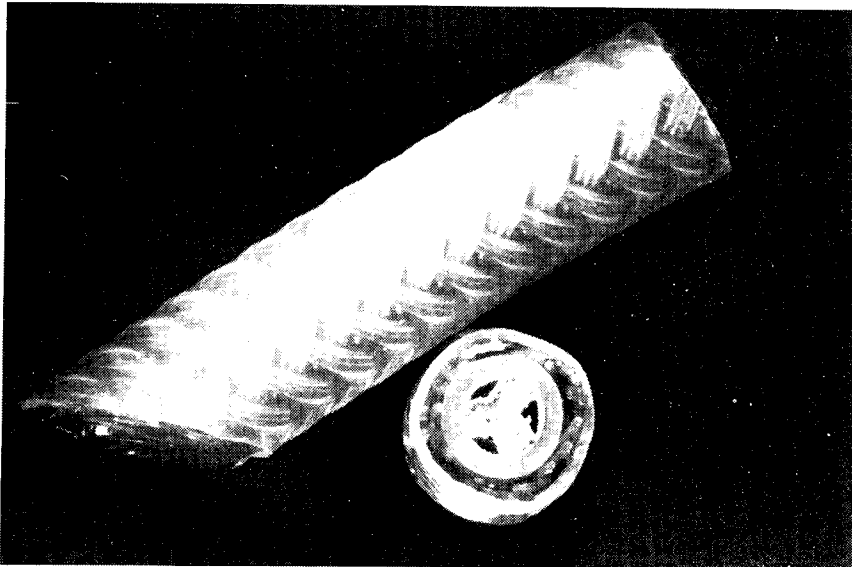


Bild 4b: Außenansicht der ummantelten Gasgeneratorschnur SSG 14
(Vergrößerung 7 : 1)

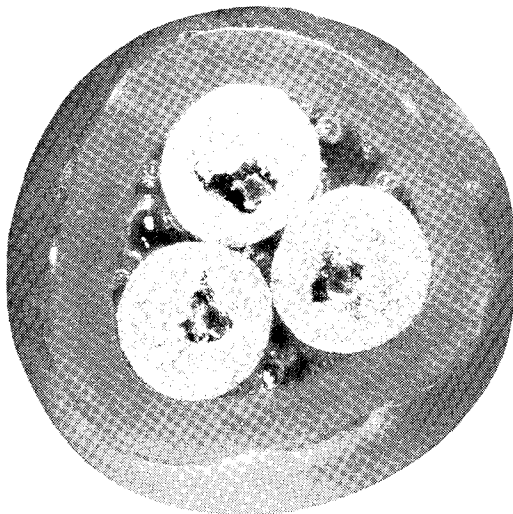


Bild 5a: Querschnittsaufnahme der Anzündschnur ITLX 2000

1 - 17

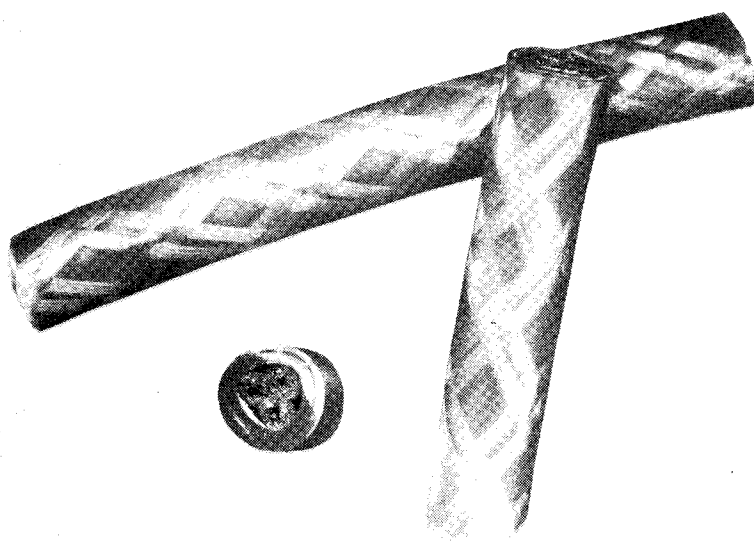


Bild 5b: Außenansicht der ITLX 2000

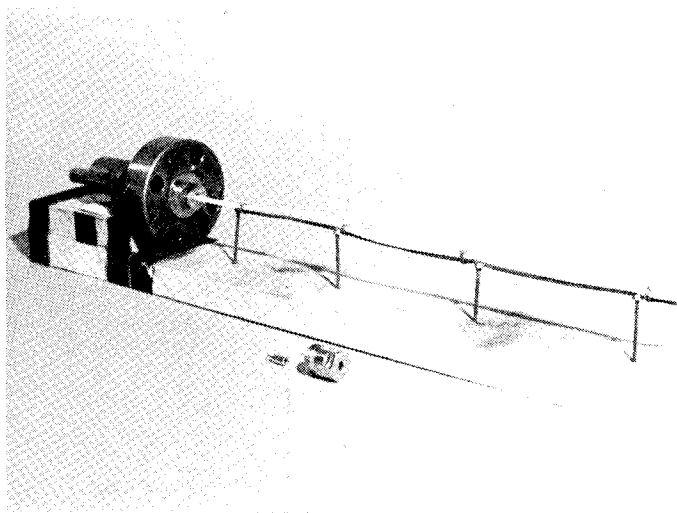


Bild 6: Versuchsanordnung für Untersuchungen des offenen Abbrandes

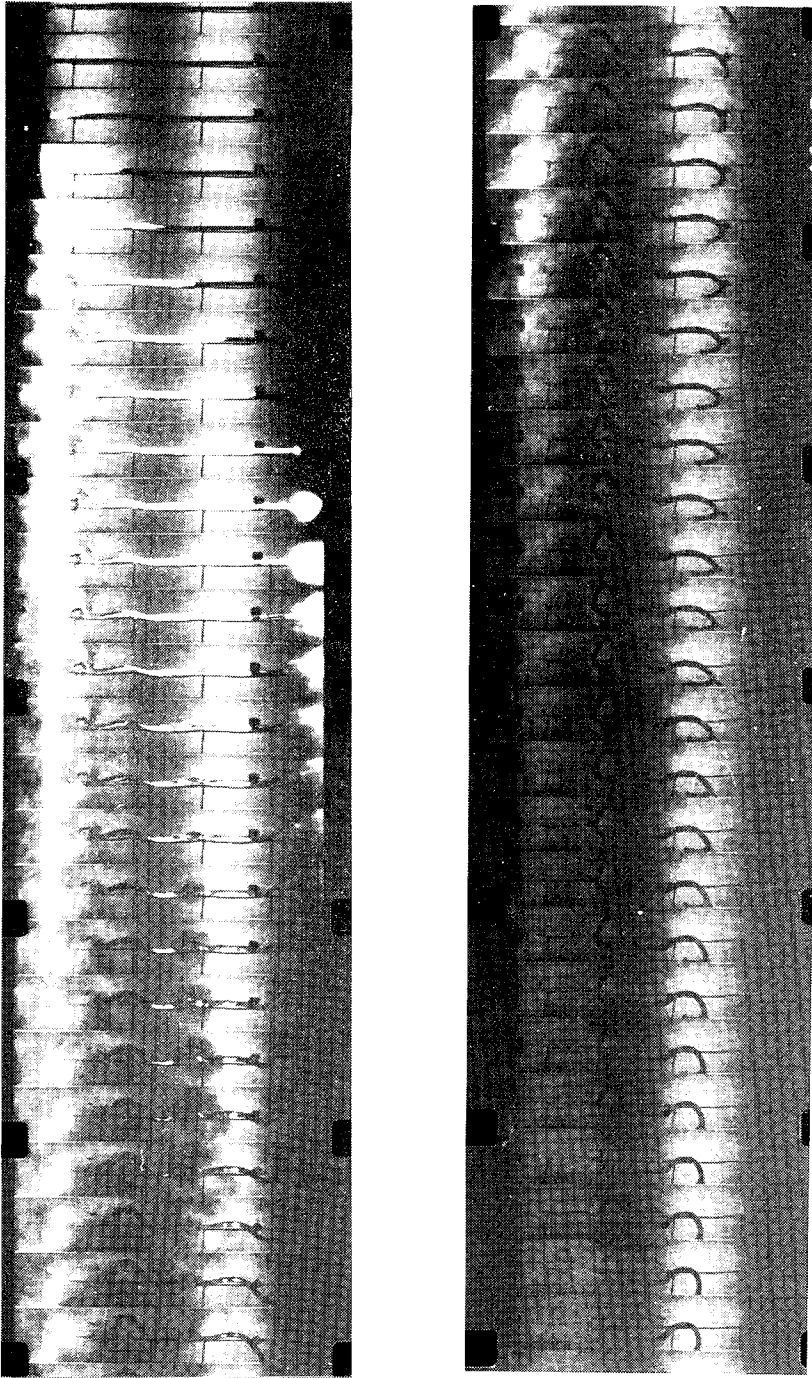


Bild 7: Aufnahme des offenen Abbrandes der SGG 14 Schnur mit der Hycam Hochgeschwindigkeitskamera, 12000 Bilder/s

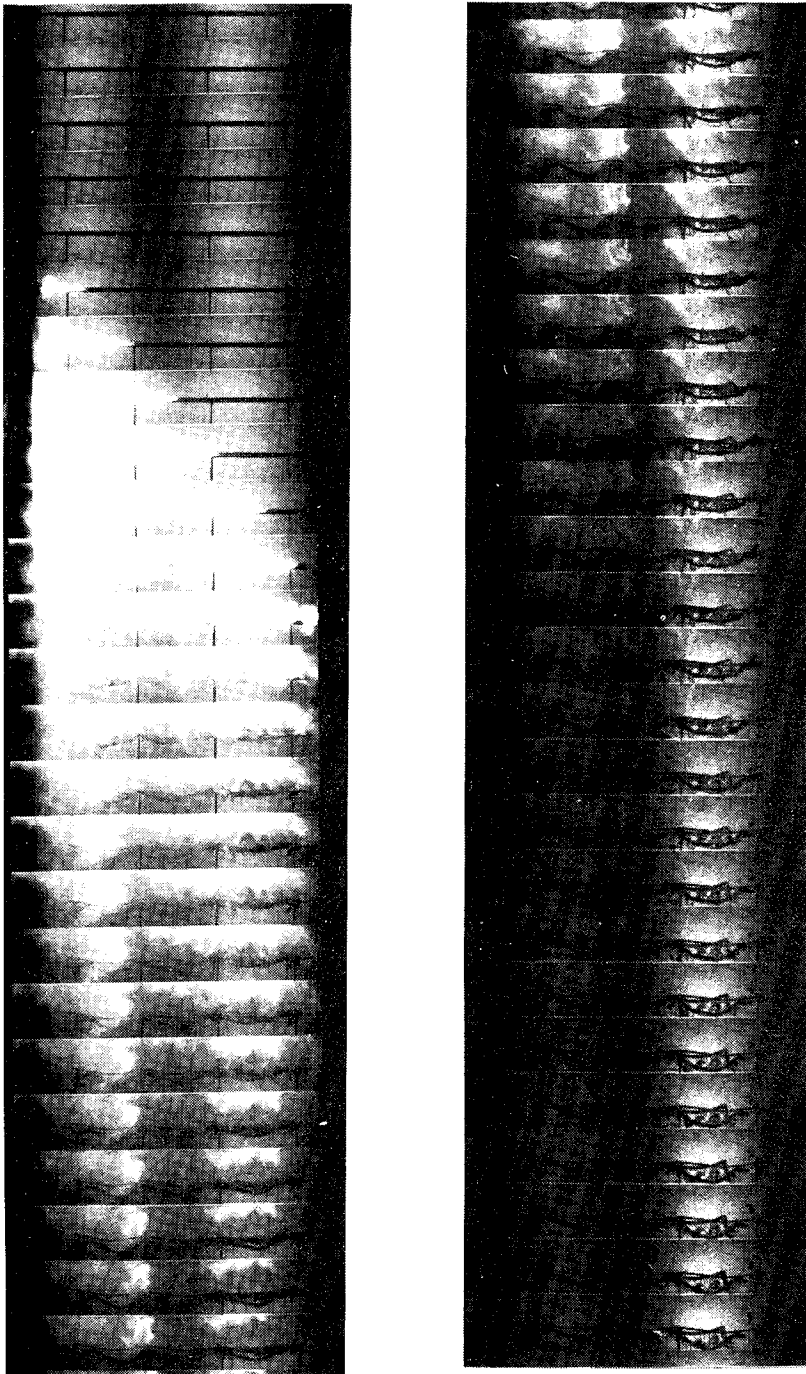


Bild 8: Gleiche Aufnahme der ITLX 2000 Schnur mit 20000 Bilder/s

1 - 20

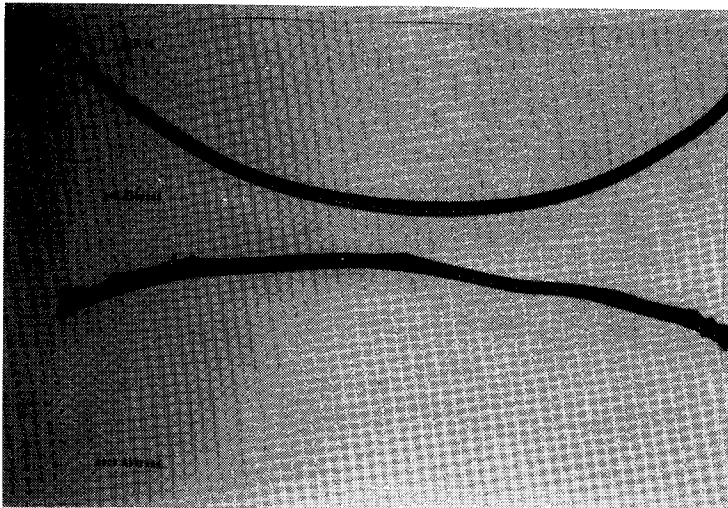


Bild 9: Bild der SGG 14 Schnur nach dem Abbrand

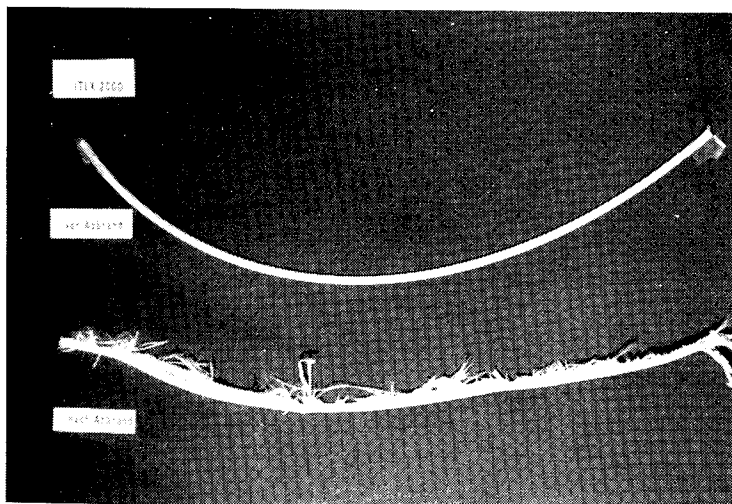


Bild 10: Bild der ITLX 2000 Schnur nach dem Abbrand

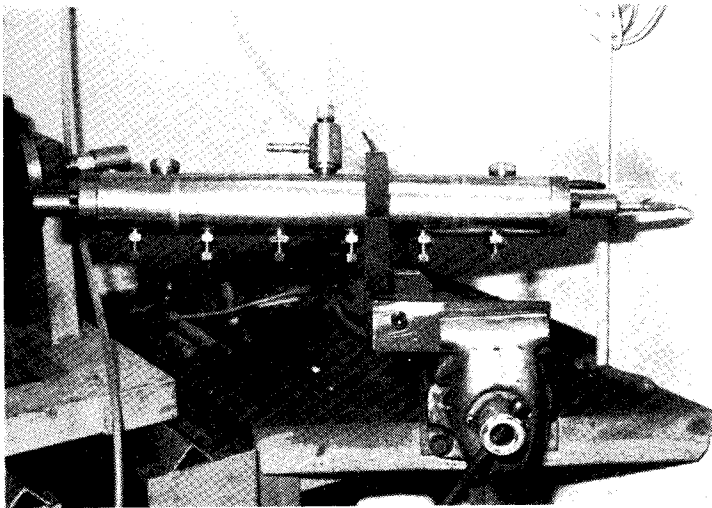


Bild 11: Versuchsanordnung der schlauchförmigen Druckbombe

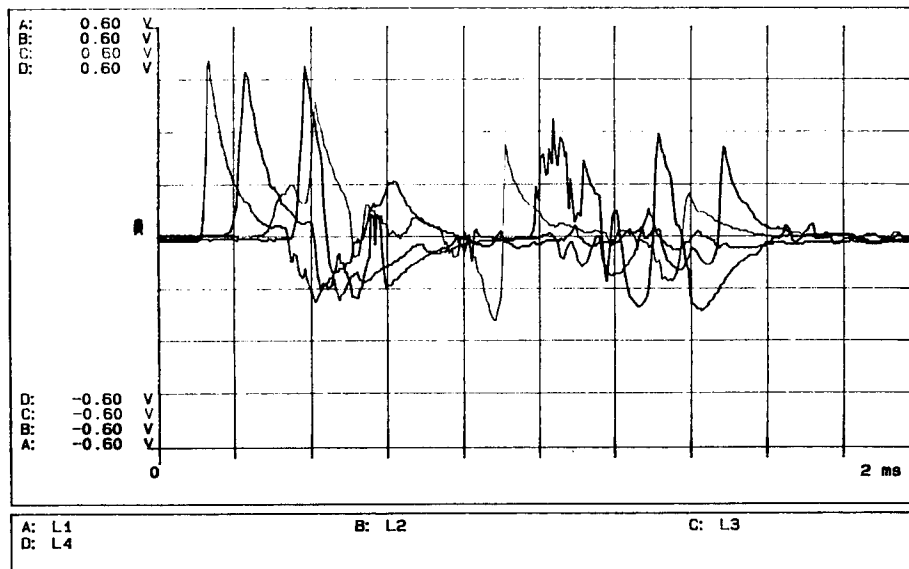


Bild 12: Lichtleitersignale beim Abbrand der SGG 14 Schnur

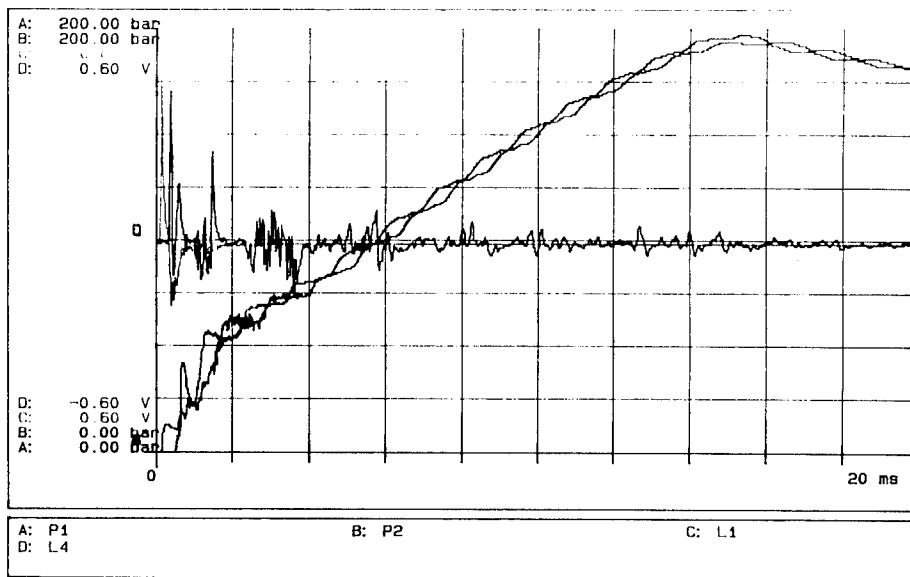


Bild 13: Signale der Druckaufnehmer beim Abbrand der SGG 14 Schnur

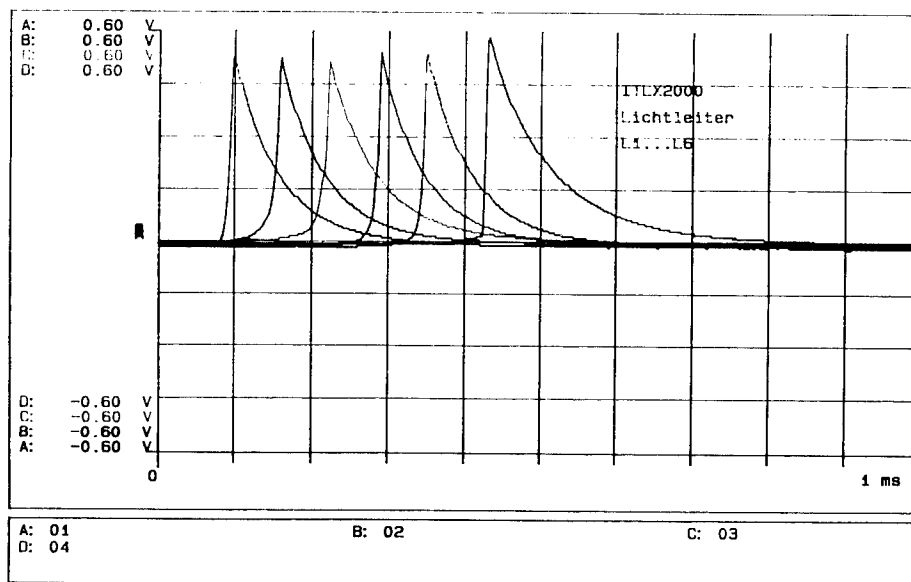


Bild 14: Lichtleitersignale der ITLX 2000 Schnur

EINFLUSS DES BINDERGEHALTES AUF DAS REAKTIONSVERHALTEN PYROTECHNISCHER MISCHUNGEN

B. Berger, B. Haas, G. Reinhard

Gruppe für Rüstungsdienste, Abt. Ballistik, Waffen und Munition
Feuerwerkerstrasse 39, CH-3600 Thun 2, CH

ABSTRACT

The influence of the binder ratio in pyrotechnic mixtures on their combustion and safety datas was studied taking the example of the high-energy polymer polynitro-polyphenylene (PNP). The pyrotechnic system used with this was zirconium-nickel-alloy 50:50 / potassium perchlorate. The binder ratios amounted from 1 to 4 weight percent.

The results show that despite a high-energy molecule, even small binder ratios reduce the rate of combustion.

On the other hand, it was not possible to ascertain any influence of the binder content on the heats of combustion of the different mixtures. The thermal behaviour of the mixtures is slightly influenced by the binder ratio.

The brisance and the maximum gas pressure of the mixtures become greater with an increasing binder ratio. However, the ignition delay is independent on the binder content.

With an increasing binder ratio, the mechanical stability of pressings becomes greater.

1. Einleitung

Zur Herstellung eines verarbeitbaren Granulates wird pyrotechnischen Mischungen häufig ein Binder zugegeben. Zusätzlich können dadurch die mechanischen Eigenschaften von aus dem Granulat hergestellten Presskörpern und Pellets verbessert werden. Die Auswahl verwendbarer Binder ist gross. Bei den meisten handelt es sich um inerte Polymere, die entsprechend der zugesetzten Menge kleinere bis grössere Leistungseinbussen bewirken. Der Einfluss des Binders sowie verschiedener Bindergehalte auf das thermische Verhalten von Mischungen der pyrotechnischen Redoxsysteme Magnesium/Strontiumperoxid bzw. Natriumnitrat und Titan/Strontiumperoxid bzw. Natriumnitrat wurde von E.L. Charlsley et al bereits untersucht [1]. Dabei wurde festgestellt, dass mit zunehmendem Binderanteil die Verbrennungswärme signifikant abnimmt. Dieser Effekt kann durch die Verwendung von energiereichen Bindern wie zum Beispiel Nitrocellulose (NC), Glycidyl-Acide-Polymer (GAP) oder Polynitropolyphenylen (PNP) vermindert werden. Bereits früher durchgeführte Untersuchungen haben jedoch gezeigt, dass ebenfalls unterschiedliche Typen von energiereichen Bindern das Abbrandverhalten pyrotechnischer Mischungen beeinflussen [2]. Hingegen ist über die Auswirkungen der eingesetzten Menge solcher Binder auf die pyrotechnisch relevanten Parameter wenig bekannt.

Im Rahmen einer Studie sind Mischungen des gut dokumentierten Redox-Systems Zirkon-Nickel-Legierung 50:50 / Kaliumperchlorat [3] mit unterschiedlichen Anteilen an energiereichem Binder Polynitropolyphenylen [4] granuliert und ihre Abbrandcharakteristika untersucht worden.

2. Ziel der Untersuchung

Das Ziel der Untersuchung ist es, vertiefte Kenntnisse bezüglich der Auswirkungen von unterschiedlichen Anteilen energiereicher Binder in pyrotechnischen Mischungen auf ihr Abbrandverhalten sowie auf ihre Leistungs- und Sicherheitskenndaten zu erhalten.

Zusätzlich ist zu ermitteln, wie sich ein variierender Binderanteil auf das Granulat sowie auf die mechanischen Eigenschaften von daraus hergestellten Presskörpern bzw. Pellets auswirkt.

3. Experimenteller Teil

3.1 Ausgangskomponenten

- Zirkon-Nickel-Legierung 50:50 A (Zr-Ni-Leg.) [5]

Spezifikation : NAVORD OS 10369

Korngrösse : 4 μm (Blaine)

Spez. Oberfläche: 0,58 m^2/g (BET)

Zündtemperatur : 565 K (292°C)

Reinheit : 96 %

- Kaliumperchlorat (KClO₄)

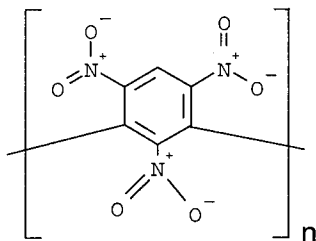
Spezifikation : MIL-P-217A

Korngrösse : < 60 μm

Reinheit : 99 %

- Polynitropolyphenylen (PNP) [4]

Strukturformel:



Mittleres Molekulargewicht : 2488

Beginn der Zersetzungsreaktion : 571 K (298° C)

3.2 Untersuchte Mischungen

Das Reduktions- und das Oxidationsmittel werden in einem Turbulamischer gemischt (Mischdauer 10 Min).

Anschliessend wird der in einem Lösungsmittelgemisch (Aceton/Ethanol 1:1) gelöste Binder zugefügt und die Mischung granuliert. Der Kordurchmesser des Granulates sollte danach $\leq 0,5$ mm betragen.

Tab. 1 Zusammensetzung der Mischungen mit 1 % Binder

Komp.	Zusammensetzung [Gew. %]																			
Zr-Ni-Leg.	25	30	35	40	45	50	52,5	55	57,5	59	60	62,5	65	70	72,5	75	80	85	90	95
KCl04	74	69	64	59	54	49	46,5	44	41,5	40	39	36,5	34	29	26,5	24	19	14	9	4
PNP	1	1	1	1	1	1	1	1	1	1	1	1	1	1	1	1	1	1	1	1

Tab. 2 Zusammensetzung der Mischungen mit 2 % Binder

Komponenten	Zusammensetzung [Gew. %]						
Zr-Ni-Leg.	40	50	60	65	75	85	95
KCl04	58	48	38	33	23	13	3
PNP	2	2	2	2	2	2	2

Tab. 3 Zusammensetzung der Mischungen mit 3 % Binder

Komponenten	Zusammensetzung [Gew. %]						
Zr-Ni-Leg.	40	50	60	65	75	85	95
KCl04	57	47	37	32	22	12	2
PNP	3	3	3	3	3	3	3

Tab. 4 Zusammensetzung der Mischungen mit 4 % Binder

Komponenten	Zusammensetzung [Gew. %]						
Zr-Ni-Leg.	40	50	60	65	75	85	95
KCl04	56	46	36	31	21	11	1
PNP	4	4	4	4	4	4	4

4. Ergebnisse

4.1 Abbrandgeschwindigkeit

In der nachfolgenden Abbildung sind die gemessenen Abbrandgeschwindigkeiten verschiedener Mischungen des untersuchten Redoxsystems dargestellt. Diese Werte sind Mittelwerte von jeweils 3-5 Messungen. Variablen sind das Verhältnis von Reduktions- zu Oxidationsmittel und der Anteil Binder.

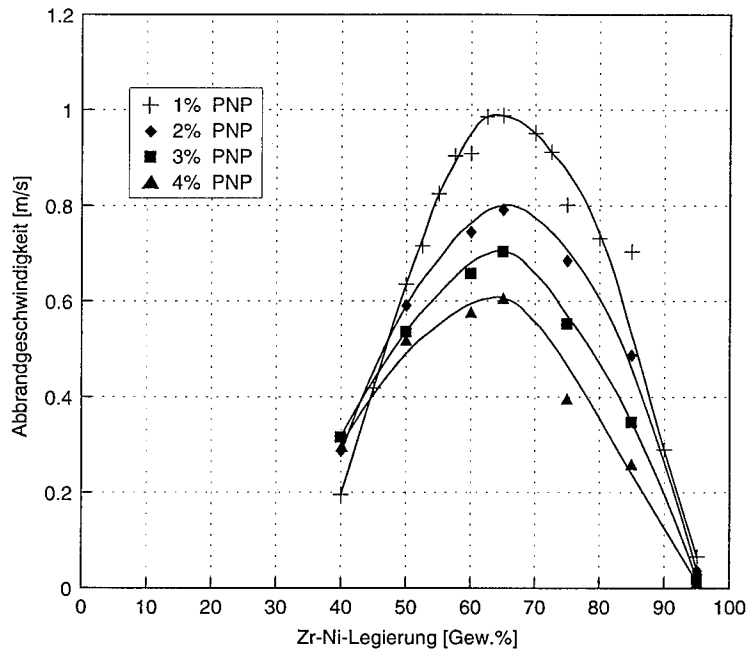


Abb. 1: Abbrandgeschwindigkeitskurven des Redoxsystems Zirkon-Nickel-Legierung 50:50 / Kaliumperchlorat mit unterschiedlichen Binderanteilen.

Die grössten Abbrandgeschwindigkeiten werden unabhängig vom Binderanteil stets bei der Mischung mit 65 Gew. % Reduktionsmittel gemessen. Die Abbrandgeschwindigkeit äquivalenter Mischungen wird durch den Anteil Binder jedoch beeinflusst. Am deutlichsten ist dies bei den Mischungen mit der grössten Abbrandgeschwindigkeit feststellbar. Sie nimmt von 1 m/s bei 1 Gew. % Binder auf 0,6 m/s bei 4 Gew. % Binder ab. Bemerkenswert ist die konstante Abnahme der maximalen Abbrandgeschwindigkeit bei Binderanteilen zwischen 2, 3 und 4 Gew. %. Die Abnahme zwischen 1 und 2 Gew. % Binder ist jedoch doppelt so gross.

4.2 Verbrennungswärme

Die gemessenen Verbrennungswärmen der verschiedenen Mischungen mit unterschiedlichem Binderanteil sind in der nachfolgenden Grafik eingetragen.

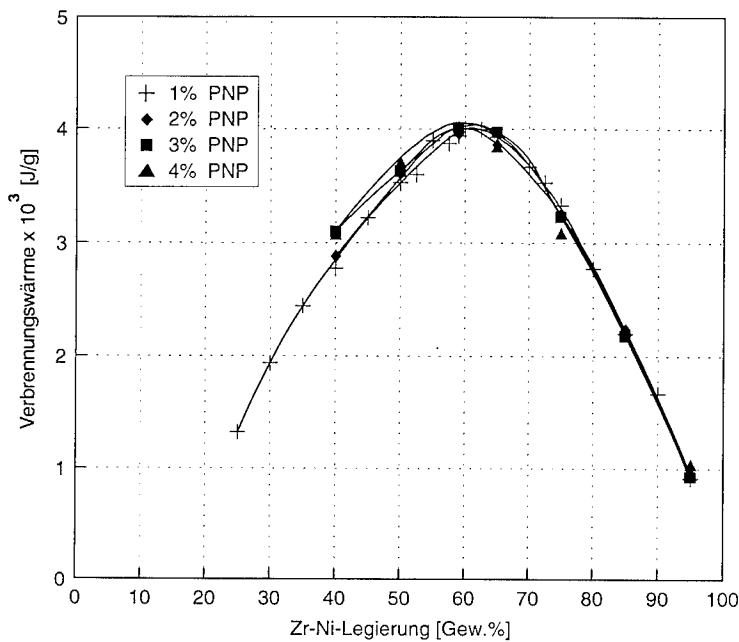


Abb. 2: Verbrennungswärmen verschiedener Mischungen des Redoxsystems Zirkon-Nickel-Legierung 50:50 / Kaliumperchlorat mit unterschiedlichen Binderanteilen.

Im Gegensatz zu den Untersuchungen von Charsley et al [1] zeigen die Messwerte des vorliegenden Redox-Bindersystems, dass eine Erhöhung des Binderanteils von 1 auf 4 Gew. % keinen signifikanten Einfluss auf die Verbrennungswärme hat.

4.3 Brisanz

Der Begriff Brisanz wird zur Beschreibung des Druckanstieges pro Zeiteinheit während des Abbrandes einer pyrotechnischen Mischung in einer Druckbombe verwendet. Die Ladedichte betrug bei unseren Untersuchungen $0,15 \text{ g/cm}^3$. Die in der folgenden Abbildung dargestellten Werte sind Mittelwerte aus 4-6 Messungen.

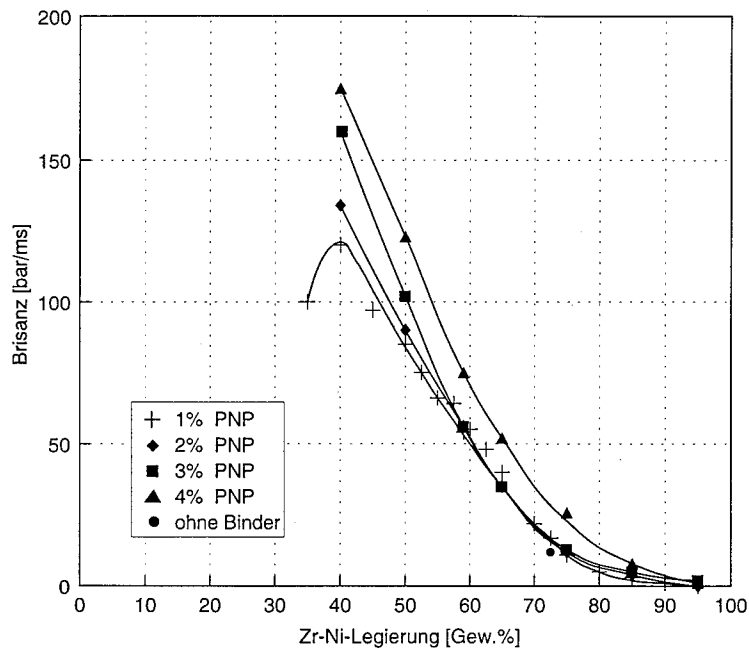


Abb. 3: Brisanzwerte verschiedener Mischungen des Redoxsystems Zirkon-Nickel-Legierung 50:50 / Kaliumperchlorat mit unterschiedlichen Binderanteilen.

Aus Abbildung 3 geht hervor, dass, mit einer Ausnahme, Mischungen mit einem Reduktionsmittelanteil kleiner 40 Gew. % in der verwendeten Messanordnung nicht angefeuert werden können.

Die grössten Brisanzwerte werden, unabhängig vom Anteil Bindemittel, bei 40 Gew. % Reduktionsmittel gemessen. Eine Erhöhung des Reduktionsmittelanteils in den Mischungen bewirkt eine nicht lineare Abnahme der Brisanz. Mit zunehmendem Binderanteil von 1 auf 4 Gew. % steigt der Höchstwert von 120 bar/ms auf 175 bar/ms an, d.h. der Binderanteil hat bei bestimmten Zusammensetzungen der Mischungen einen deutlichen Einfluss auf die Brisanz.

Als Vergleich ist in Abb. 3 ebenfalls der Brisanzwert einer Mischung des untersuchten Redoxsystems angegeben, die keinen Binder enthält. Er ist nur unwesentlich kleiner als die Werte der äquivalenten Mischungen mit 1, 2 und 3 % Binder.

4.4 Gasdruck

Der während des Abbrandes einer pyrotechnischen Mischung entstehende Gasdruck wurde mit der gleichen Versuchsanordnung gemessen wie die Brisanz (Ladedichte $0,15 \text{ g/cm}^3$). Die Mittelwerte dieser Messungen (4 Messungen/Mischung) sind in der nachfolgenden Grafik eingetragen.

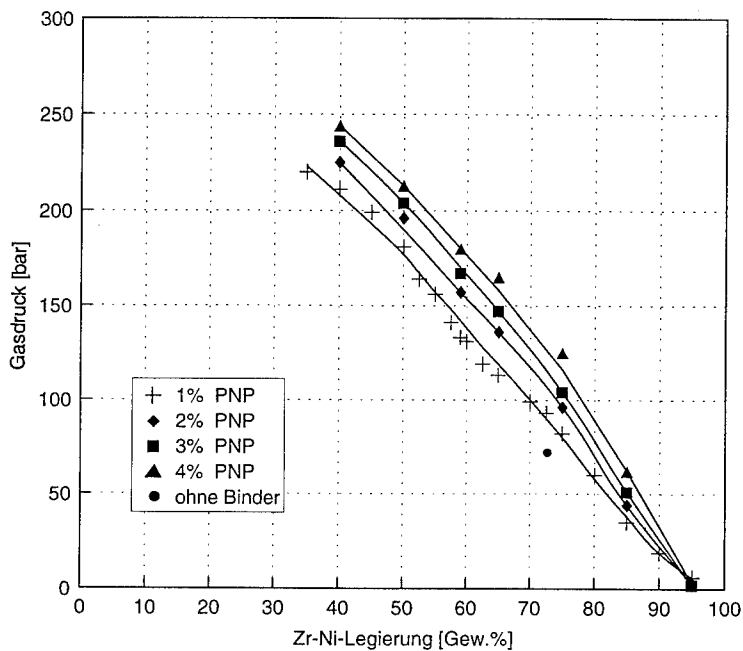


Abb. 4: Gasdruckwerte verschiedener Mischungen des Redoxsystems Zirkon-Nickel-Legierung 50:50 / Kaliumperchlorat mit unterschiedlichen Binderanteilen.

Wie in Abschnitt 4.3 erwähnt, konnten bis auf eine Ausnahme Mischungen mit Reduktionsmittelanteilen kleiner 40 Gew. % nicht zur Reaktion gebracht werden. Ausser bei der Mischung mit der Zusammensetzung 35 Gew. % Legierung/64 Gew. % KClO_4 /1 Gew. % PNP werden die höchsten Gasdrücke bei einem Reduktionsmittelanteil von 40 Gew. % gemessen. Dabei bewirkt die Erhöhung des Binderanteils von 1 auf 4 Gew. % eine Erhöhung des Gasdruckes von 210 auf 245 bar.

4.5 Anzündverzögerung

Die Anzündverzögerung ist definiert als die Zeit zwischen dem Anlegen des Anzündstromes und dem Erreichen von 10 % des Maximaldruckes. Die in der nachfolgenden Grafik eingetragenen Werte sind Mittelwerte aus vier Messungen.

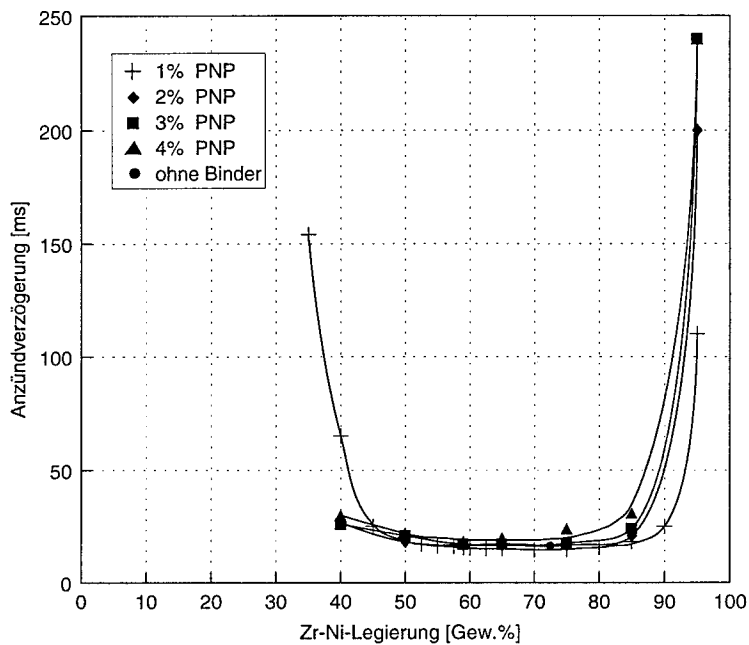


Abb. 5: Anzündverzögerungszeiten verschiedener Mischungen des Redoxsystems Zirkon-Nickel-Legierung 50:50 / Kaliumperchlorat mit unterschiedlichem Binderanteil.

Die Resultate zeigen, dass die Anzündverzögerungszeit bis auf zwei Ausnahmen durch den Binderanteil nicht beeinflusst wird. Die beiden Ausnahmen sind die Mischungen mit 35 bzw. 40 Gew. % Reduktionsmittelanteil und einem Bindergehalt von 1 %. Beide weisen eine wesentlich grössere Anzündverzögerungszeit auf.

4.6 Thermisches Verhalten

Der Einfluss des Binderanteils auf das thermische Verhalten von pyrotechnischen Mischungen wurde am Beispiel der Mischung mit ausgeglichener Sauerstoffbilanz (59 Gew. % Reduktionsmittel) untersucht. Die DSC-Aufzeichnungen der Mischungen mit einem Gehalt von 1, 2 und 3 Gew.-% PNP sind identisch, d.h. dass der Binder bis zu einem Anteil von 3 Gew. % keinen Einfluss auf den Beginn und den Verlauf der Redox-Reaktion hat. Ein Binderanteil von 4 Gew. % bewirkt eine Erhöhung der Temperatur der maximalen Energieabgabe um rund 10°C. Die Starttemperatur der Redox-Reaktion wird jedoch nicht verändert (Anhang).

4.7 Sicherheitskenndaten

Empfindlichkeit auf mechanische Einflüsse

Die Schlagempfindlichkeit wurde mit der Fallhammermethode nach BAM ermittelt. Die kritische Schlagenergie aller untersuchten Mischungen ist grösser als 20 J, d.h. im Prüfbereich der Methode ist kein Einfluss des Bindergehaltes der Mischungen auf ihre Schlagempfindlichkeit feststellbar.

Tab. 5: Kritische Reibempfindlichkeit der Mischungen

% Reduktions- mittel	Kritische Reibstiftbelastung [N]			
	1 % PNP	2 % PNP	3 % PNP	4 % PNP
40	> 360	> 360	> 360	> 360
50	> 360	> 360	> 360	> 360
59	320	> 360	> 360	324
65	192	252	240	252
75	216	180	180	160
85	120	144	120	160
95	> 360	> 360	> 360	> 360

Die Reibempfindlichkeit nimmt mit zunehmendem Binderanteil geringfügig ab.

Empfindlichkeit auf elektrostatische Entladungen

Mit Ausnahme der Mischungen mit einem Reduktionsmittelanteil von 40 Gew. % bewirkt ein höherer Binderanteil eine Abnahme der Empfindlichkeit gegenüber elektrostatischen Entladungen. Bei den Mischungen mit 40 Gew. % Reduktionsmittel wird die Empfindlichkeit mit höherem Binderanteil grösser.

Tab. 6: Empfindlichkeit auf elektrostatische Entladung

% Reduktions- mittel	Kritische Entladungsenergie [mJ]			
	1 % PNP	2 % PNP	3 % PNP	4 % PNP
40	3200	1000	560	32
50	32	32	56	56
59	5,6	18	5,6	18
65	3,2	5,6	10	10
75	3,2	1,8	10	5,6
85	1,0	5,6	18	18
95	1,8	10	32	56

4.8 Mechanische Eigenschaften von Presskörpern

Die nachfolgende Grafik zeigt die Druckfestigkeit von Presskörpern hergestellt aus Mischungen mit einem Reduktionsmittelanteil von 59 Gew. % und unterschiedlichen Anteilen an PNP-Binder. Als Vergleich ist ebenfalls die Druckfestigkeit eines Presskörpers eingezeichnet, der aus einer äquivalenten Mischungen hergestellt wurde, die als Binder jedoch 1 % NC enthielt. Die Resultate zeigen, dass die Druckfestigkeit mit zunehmendem Binderanteil linear zunimmt.

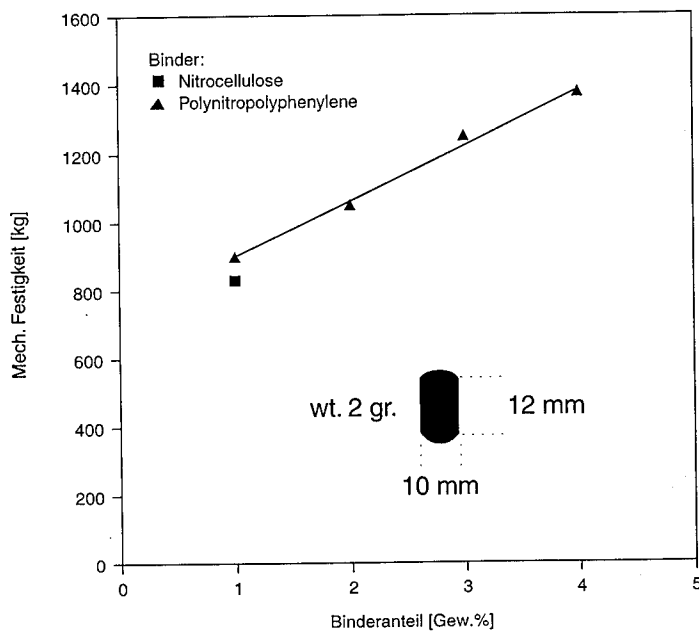


Abb. 6: Einfluss des Binderanteils in pyrot. Mischungen auf die Druckfestigkeit von Presskörpern.

5. Zusammenfassung / Folgerungen

Am gut dokumentierten pyrotechnischen Redoxsystem Zirkon-Nickel-Legierung 50:50 / Kaliumperchlorat wurde der Einfluss des Binderanteils auf die pyrotechnischen Parameter, auf die Sicherheitskennndaten sowie auf die mechanische Festigkeit von Presskörpern untersucht. Der verwendete Binder war das energiereiche Polymer Polynitropolyphenylen (PNP). Die Untersuchungen zeigen, dass ein signifikanter Zusammenhang zwischen dem Binderanteil und der Brenngeschwindigkeit bzw. der Brisanz besteht. Mit zunehmendem Binderanteil nimmt die Brenngeschwindigkeit ab bzw. die Brisanz zu.

Auffallend ist jedoch, dass die Brenngeschwindigkeitsmaxima der vier Versuchsreihen jeweils nahe bei der Zusammensetzung mit ausgeglichener Sauerstoffbilanz gemäss der für das System postulierten klassischen Reaktionsgleichung gemessen werden. Dieses Reaktionsverhalten steht im Gegensatz zu den Resultaten des gleichen wie auch anderer Redoxsysteme, bei denen als Binder Nitrocellulose verwendet wurde [2].

Dies weist darauf hin, dass der Bindertyp bzw. seine Zersetzungsprodukte die eigentliche Redoxreaktion beeinflussen können. Entsprechende Untersuchungen werden zur Zeit in Zusammenarbeit mit der Metropolitan University Leeds (UK) durchgeführt.

Die pyrotechnischen Parameter Verbrennungswärme, Gasdruck, Anzündverzögerung sowie die Starttemperatur der exothermen Redoxreaktion werden durch die unterschiedlichen Binderanteile in den Mischungen kaum beeinflusst.

Hingegen wird mit zunehmenden Binderanteil eine deutliche Verbesserung der Granulierung der Mischungen erreicht.

6. Literatur

- [1] Charsley E.L., Rumsey J.A., Barton T.J. Griffith T.
"An Investigation of the Influence of Organic Binders on the
Reaction of Pyrotechnic Systems using Thermal Analysis and Related
Techniques"
Thermal Analysis, 2, 1982

- [2] Berger B., Haas B., Reinhard G.
"High Energetic Polymer as Binder for Pyrotechnic Mixtures"
25. ICT-Jahrestagung, Karlsruhe, 1994

- [3] Berger B., Haas B.
"Determination of the Burning Characteristics of Zirconium and
Zirconium-Nickel-Alloys with Potassiumperchlorate"
4^e Congrès International de Pyrotechnie, La Grande Motte, 1989

- [4] Redecker K.H., Hagel R.
"Neuere Ergebnisse zur Herstellung und Eigenschaften von Poly-
nitropolyphenylen"
18. ICT Jahrestagung, Karlsruhe, 1987

- [5] Baudis U.
"Special Metals"
Chemetall GmbH, Frankfurt, 1992

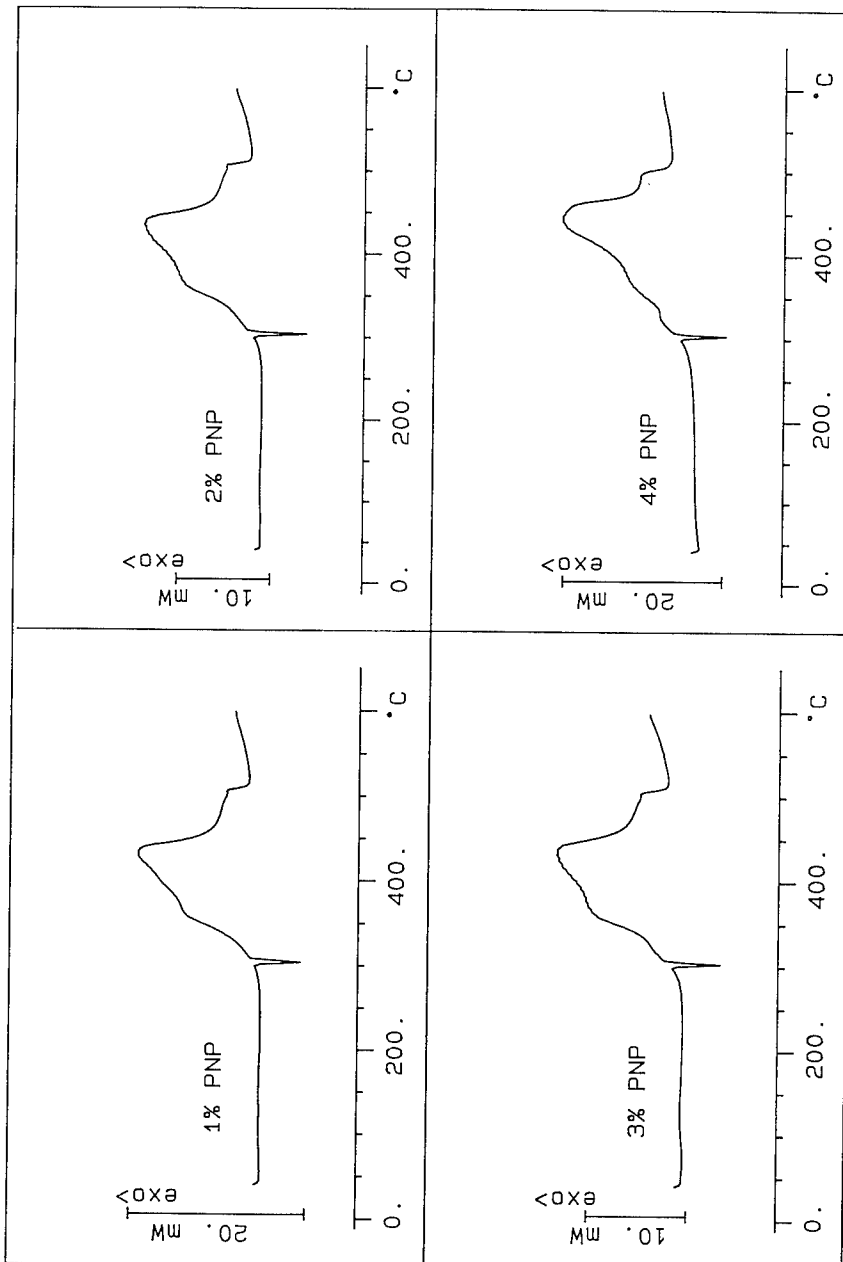
7. Anhang

Abb. 7: DSC-Kurven der Mischung mit ausgeglichener Sauerstoffbilanz, jedoch unterschiedlichen Binderanteilen

Dynamit Nobel Aktiengesellschaft

Kaiserstraße 1 • 53839 Troisdorf
Telefon (0 22 41) 89-0 • Telex 885666 dnd
Telefax 22414110=nobel
Telefax (0 22 41) 89 15 40**Beitrag zur 26. Internationalen Jahrestagung des ICT 1995****Titel:** Neue Konzepte bei der Entwicklung von Zünd- und Anzündmitteln**Autor:** H.Zöllner**Kurzfassung:**

Kostendruck und die Forderung nach kurzen Entwicklungszyklen setzen auch im Bereich der Zünd- und Anzündmittel neue Rahmenbedingungen. Diesen neuen Marktanforderungen kann im Entwicklungsbereich effizient nur mit modernen Methoden bei Versuchsplanung, Durchführung und Auswertung entsprochen werden. Die zum Teil sehr komplexen Zusammenhänge bei der Charakterisierung von Anzündmitteln entziehen sich oftmals einer analytischen Darstellungsform. Deshalb war in der Vergangenheit die gezielte Einstellung von kundenspezifischen Eigenschaften der Anzündmittel mit einem sehr hohen experimentellen Aufwand und einer großen Anzahl von Einzelschüssen verbunden. In der vorliegenden Arbeit wird nun ein neues Konzept vorgestellt, das drei wichtige Phasen der Entwicklung von Zünd- und Anzündmitteln hinsichtlich Effektivität, Zeitdauer und Kosten wesentlich beeinflusst:

1. Versuchsplanung
2. Versuchsdurchführung
3. Auswertung

In der ersten Phase läßt sich mit den Mitteln der statistischen Versuchsplanung die Anzahl der notwendigen Meßreihen drastisch reduzieren und in Hinblick auf die Auswertung eine optimale Auswahl der Meßreihen treffen. Bei der Versuchsdurchführung kann durch effiziente, attributive Prüfverfahren wie z.B. die Langlie-Methode oder durch eine echte Variablenprüfung eine deutliche Reduzierung der Einzelschüsse erreicht werden. Schließlich ist während der Auswertung mit Hilfe geeigneter Programme eine optimale Analyse und Darstellung der Meßergebnisse möglich.

Anhand eines Beispiels aus dem Bereich der elektrischen Anzündmittel wird die Leistungsfähigkeit dieses neuen Konzeptes vorgestellt. Dabei wird die Abhängigkeit der elektrischen Eigenschaften wie Streustromsicherheit, Zündimpuls und Reaktionszeit bei Anzündpillen von den Materialeigenschaften des Glühdrahtes, der Lamellen und des Satzes sowie den geometrischen Einbauverhältnissen im Bereich des Glühdrahtes untersucht.

26th International ICT-Conference
Karlsruhe, 4- 7 July, 1995

AN EXPERIMENTAL INVESTIGATION OF THE ACCELERATION INDUCED BURNING RATE INCREASE OF COMPOSITE SOLID PROPELLANTS FOR GAS GENERATOR

Jun-Sik Hwang, Chang-Kee Kim, Sang-Ilo Park*
ADD, Explosive Trains and Pyrotechnics Division,
P.O. Box 35 Yuseong, Taejon, Korea
* Hanwha Co., Ltd., Taejon, Korea

An experimental parametric study of the acceleration induced burning rate augmentation of composite propellant based on HTPB/AP in prototype gas generator for base bleed of a 155 mm artillery gun projectile is described. The effects of the spin rate, the aluminum content, the oxidizer content and particle size and the plasticizer content on the acceleration induced burning rate augmentation were investigated. The burning rate augmentation was found to be strongly affected by the spin rate, the aluminum content and the oxidizer particle size.

INTRODUCTION

Many studies have been conducted during the past 25 years to extend the range of a projectile in free flight by the injection of relatively small mass flows of various gaseous products into the base region, reducing base drag.¹⁻²⁾ The technique of base bleed is achieved by gas generator which is attached to the base of a projectile. The gas generator, which is usually called base bleed unit, produces gaseous products by burning solid propellant. The magnitude of base drag reduction depends on the combustion characteristics of solid propellant.

A spin-stabilized projectile rotates at high spin rate during flight and the acceleration field due to centrifugal force is formed in gas generator for base bleed. Numerous studies revealed that the acceleration loads increase the burning rate of solid propellant and the acceleration induced burning rate increase is affected by the acceleration level and the propellant composition.³⁾ The HTPB/AP composite propellant with fuel-rich composition is usually used as

This paper describes an experimental parametric study conducted to investigate the effect of the following parameters on the acceleration induced burning rate increase of solid propellant in prototype gas generator for base bleed of a 155 mm artillery gun projectile : the acceleration level, the aluminum content, the oxidizer content and particle size and the plasticizer content.

The gas generator for base bleed of 155 mm artillery gun projectile consists of cylindrical motor case and igniter assembly and propellant grain.⁴⁾ Propellant grain shown in Fig.1 has a cylindrical shape with two segments. External and end surfaces are inhibited so that combustion takes place on inner cylindrical surface and four planar surfaces separated by a slot. The centrifugal acceleration vector due to spin is perpendicular to the cylindrical surface and is parallel to the planar surface.



Ground Test Fixture

A schematic diagram of the spin fixture is shown in Fig.2. The rotor is supported by a set of duplex bearings at the two pedestal locations. The gas generator for base bleed is seen on the left side of the spin fixture. The rotor is connected to the electric motor by

the timing belt. Signal leads pass from the canister through the rotor shaft and are connected to the slip ring assembly which is on the far right of Fig.2. The signals, which are detected from pressure transducer and thermocouple mounted to the chamber of propellant grain, were transmitted to the computer system for data acquisition and analysis through the slip ring. The pressure transducers used in these experiments were purchased from the Kulite Corporation and are miniature, solid-state semiconductor strain gauge sensors with a four element bridge circuit. The transducers are rated for 25 psia full scale. A tungsten-rhenium thermocouple was used to measure temperature inside the propellant chamber. The slip ring assembly (Eaton Co.), rated at 8,000 rpm during continuous use, was used to acquire data signals from the rotating payloads. The slip ring assembly contained 12 epoxy-embedded coin silver slip rings. Two silver graphite brushes, which were easily replaceable, made contact with each of the rotating rings. The propellant was ignited by applying 20 volt to the electric match, igniting the black powder which in turn ignited the propellant grain. The analog signals which were transmitted through slip ring and conditioning amplifier (Measurement Group Co Model2310) were digitized at 1000 samples per second by a digitizer (Lecroy 6810) and were stored on a personal computer containing GPIB card.

The spin rate can be controlled within ± 50 rpm by a electronic controller and is obtainable up to 15000 rpm.

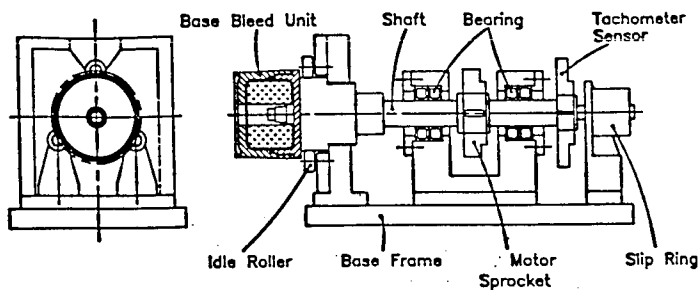


Fig.2 Schematic Diagram of the Spin Fixture

Ballistic Firing Tests

In order to investigate the acceleration induced burning rate increase in a gas generator of a projectile in flight, some projectiles with base bleed unit were fired. Firings were made at 820 m/s muzzle velocity and 900 mils quadratic elevation. The trajectory was measured by a combination of the doppler radar measuring the beginning of the trajectory and the pulse tracking radar covering the rest of the trajectory. The burning time of propellant grain can be calculated from the deceleration variation of a projectile in flight. The burn-out of propellant burning shows the sharp discontinuity in deceleration-time curve.

RESULTS AND DISCUSSION

The parameters that are thought to be important in the acceleration induced burning rate increase in this study are chosen as follows : the spin rate, the aluminium content, the oxidizer content and particle size and the plasticizer content. The three values chosen as the spin rate were 0, 10,000 and 15,000 rpm, which correspond to 0, 24,200 and 54,000 g of acceleration normal to cylindrical surface at $r = 22$ mm respectively. Four cases of the aluminium content are considered as follows : 0.0, 0.5, 1.5, 5.0 % The oxidizer contents are varied from 71 % to 80 %. In order to investigate the effect of oxidizer particle size, a bimodal 60/6 μm with a fraction ratio of 24/76, 50/50 and 76/24, respectively, was tested. In addition, two cases of the plasticizer content are tested as follows : 0.0 and 3.127 %

Base bleed unit with propellant grains were fired under the constant spin rate predetermined. The average burning rate at the various spin rate is calculated by dividing the web thickness by the burning time, determined from the measured pressure history. All tests were carried out after preconditioning propellant at a temperature of 21 °C .

Effect of the Spin Rate

The chamber pressure history as a function of time for various spin rate are plotted in Fig.3 . The burning rate is found to be strongly depend on the magnitude of the spin rate, that is to say, that of the acceleration level. The average burning rate increases from 1.12

mm/s at zero rpm to 3.16 mm/s at 10000 rpm and to 3.55 mm/s at 15000 rpm. It was reported in the literature⁴⁾ that no burning rate augmentation will occur until reaching a threshold acceleration sufficient to hold on the propellant surface AP (Ammonium Pechlorate) particles that would otherwise escape the surface and the burning rate will increase with acceleration as more of the AP particle mass is consumed in the propellant surface.

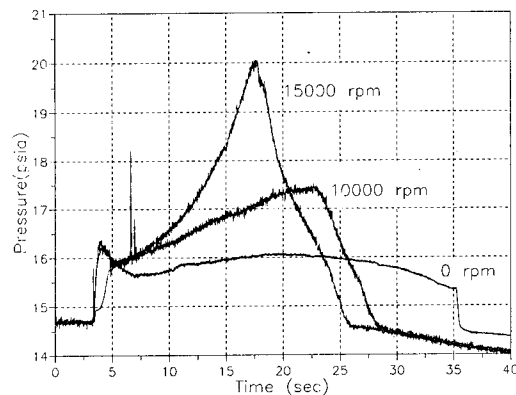


Fig.3 The chamber pressure trace with time for various spin rate

Effect of the Aluminum Content

The chamber pressure history as a function of time for various aluminum content at 3000 rpm is shown in Fig.4. Adding aluminum decrease the burning time considerably, or increased the chamber pressure as shown in the figure. This is due to the enhanced radiation heat transfer by aluminum combustion and enhanced retention of aluminium on the burning surface, increasing the burning surface area. The change of aluminum content from 0 % to 5 % gives 62 % increase of the burning rate from 1.74 mm/s at 0 % aluminium content to 2.82 mm/s at 5 % aluminium content.

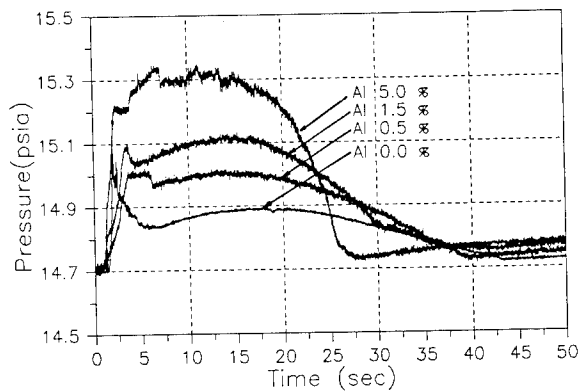


Fig.4 The chamber pressure trace with time for various aluminum content

Effect of the Oxidizer Content

A fuel-rich composite propellant gives more base drag reduction because higher temperature can be kept downstream of the base by a secondary combustion with a surrounding air.⁵⁾ However, too little oxidizer content decrease performance because of more unstable reignition after launch.

Fig.5 shows the chamber pressure history as a function of time for various oxidizer content. Considering that increase of AP content from 71 % to 80 % gives increasing of burning rate from 0.9 mm/s to 1.26 mm/s in the strand burner test at 14.7 psia, the effect of spin rate on burning rate decreases as AP content increase. As AP content increase from 71 % to 80 %, the pressure variation pattern as a function of time changed gradually from the progressive burning to the neutral burning.

Effect of the Oxidizer Particle Size

The effect of oxidizer particle size on the acceleration induced burning rate increase was studied by using firing test results.

The burning time was measured by reading the deceleration pattern showing the sharp burn-out discontinuity as shown in Fig.6. The change of the fine AP content from 76 to 24 % gives decrease of the burning time from 48 seconds to 37 seconds. The higher the fine AP content, the more sensitive the burning rate to the acceleration effect. This is because the retention of the fine AP oxidizer particles on the propellant surface was developed by the centrifugal force.

Effect of the Plasticizer Content

The chamber pressure history as a function of time for various plasticizer content at 3000 rpm is shown in Fig.7. The highly plasticized composition is more sensitive to acceleration effects. This is due to migration of the plasticizer to the wall side of the motor case by the centrifugal force, which increases the solid content ratio within the propellant grain, increasing the burning rate.

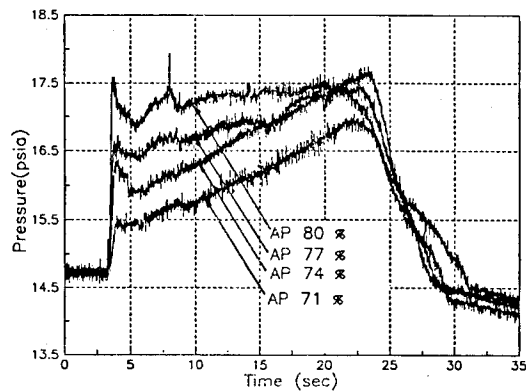
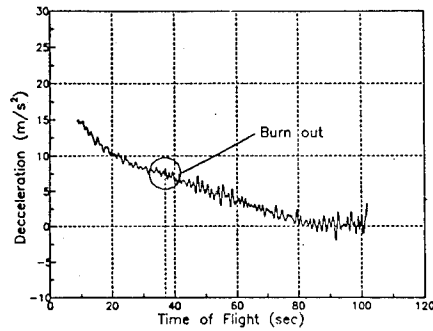
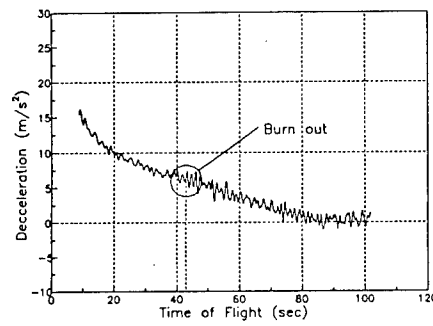


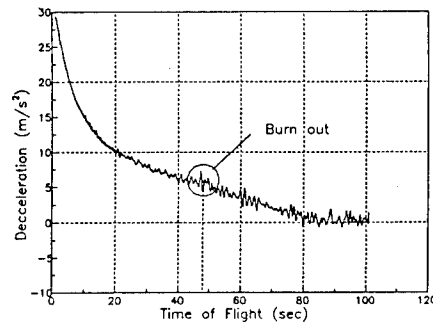
Fig.5 The chamber pressure trace with time for various oxidizer content



(a)



(b)



(c)

Fig.6 The acceleration variation of a projectile in flight with time for various oxidizer particle size

(a) Fraction ratio 24/76

(b) Fraction ratio 50/50

(c) Fraction ratio 76/24

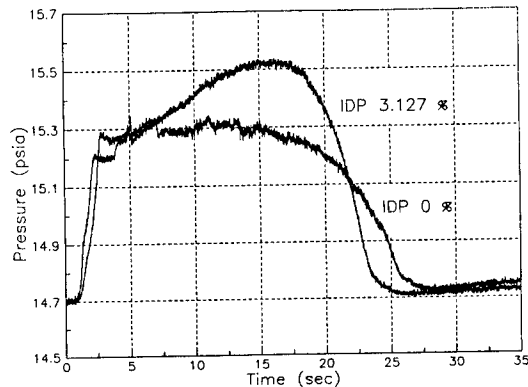


Fig.7 The chamber pressure trace with time
for various plasticizer content

CONCLUSIONS

A comprehensive experimental parametric study of the effect of acceleration on the burning rate of composite propellant based on HTPB/AP was carried out. The experiments were carried out in the spin rate range 0 - 15000 rpm. The results of this study may be used as guidelines for design of base bleed unit, and its propellant formulation.

REFERENCES

1. K. Anderson, N.E. Gunnars, R Hellgren," Propellant and Explosives, vol.1, Oct., p.69 (1976)
2. S. Jaramaz and M. Injac, Proceedings of First International Symposium on Special Topics in chemical Propulsion : Base Bleed, p.143, Greece(1988)
3. M.D. Fuchs and A. Peretz, J. Spacecraft, Vol.19, No.6, Nov.-Dec., (1982)
4. L.D. Kayser, J.D. Kuzan, and D.N. Vazquez, BRL-MR-3708, Ballistic Research Laboratory, Anderson Proving Ground, Maryland, (1988)

Pyrotechnisch erzeugte Tarnnebel

Ein Überblick

Dr. Uwe Krone
NICO-PYROTECHNIK
Hanns-Jürgen Diederichs GmbH & Co. KG
Postfach 1227, D-22 943 Trittau, FRG - Tel.: 49 4154 805 181

KURZFASSUNG:

Unter pyrotechnischen Tarnnebeln werden hier alle Fest/Flüssig-Aerosole verstanden, welche durch pyrochemische Reaktionen (chem. Bildung der aktiven Aerosolkomponenten) oder durch Explosivstoffdispersion gebildet werden (Ausbringung bereits fertiger aktiver Aerosolkomponenten durch pyrotechnische oder Explosivstoffladungen).

Beide Varianten werden mit typischen Beispielen erläutert. Schließlich werden diese Nebel mit ihren physikalischen Daten zur Verhinderung der Entdeckung oder zur Täuschung im visuellen, infraroten und RADAR-Bereich, respektive als mono-, bi- oder multispektrale Tarnnebel charakterisiert.

Ihre Anwendung in stationären Anlagen, Wurfkörpern, oder als Wirkladungen von Raketen und Artilleriegeschossen wird beispielhaft dargestellt. Aufgrund der Ergebnisse von Umweltverträglichkeitsuntersuchungen der FhG, Institut für Umweltchemie und Ökotoxikologie, wird auch auf Aspekte der toxikologischen und ökologischen Wirkung der Aerosole und der beim Abbrand entstehenden Rückstände eingegangen.

ABSTRACT:

Pyrotechnic smokes for screening, as referred to in this paper are solid/liquid aerosols being generated by pyrochemical reactions (chem. formation of the active aerosol component) as well as by explosive dissemination (dispersion of already preshaped aerosol components by HE or pyrotechnic bursting charges).

Both types will be presented with typical examples. The smoke types will be characterized by their physical properties and addressed as mono-, bi- or multispectral smokes being capable to attenuate or conceal in the visual, infrared or mm-wave region of the electromagnetic spectrum.

Their application in stationary installations, grenades or as effect charges of artillery ammunition (shells or rockets) is presented with examples. According to results of environmental compatibility tests also aspects of toxicity and ecological behaviour of the smokes (aerosol and ashes) are discussed.

PYROTECHNISCH ERZEUGTE TARNNEBEL - EIN ÜBERBLICK

Inhaltsübersicht

Begriffsbestimmungen und Lambert Beer'sches Gesetz

Pyrotechnische Nebelsätze

- 1. Bildung des Nebelstoffes durch pyrochemische Reaktion**
- 2. Dispergierung von Nebelstoff durch Anzünd- oder Zerlegerladungen**

Beispiele und Anwendungen pyrotechnischer Nebelsätze

- 1. Tarnnebel gegen optische Detektion**
- 2. Tarnnebel gegen optische, optronische und RADAR-Aufklärung**
- 3. Multispektrale Tarnnebel**

Sonderanwendungen und Ausblick

Literaturverzeichnis

Begriffsbestimmungen und Lambert Beer'sches Gesetz

Unter pyrotechnischen Tarnnebeln sollen hier vier Typen von künstlich erzeugten Aerosolen verstanden werden.

Durch pyrochemische Reaktionen gebildete hygroskopische oder andere Stoffe, welche durch die überschüssige Energie des pyrotechnischen Satzes verdampft oder sublimiert und mit den Reaktionsgasen ausgetrieben werden.

Nebelstoffe, die bereits als solche im pyrotechnischen Satz vorliegen und durch den Energieüberschuß der pyrochemischen Umsetzung des Nebelsatzes verdampft oder sublimiert oder mit den Reaktionsgasen ausgetrieben werden.

Durch Explosivstoffdispersion oder pyrotechnische Zerlegerladungen in der Atmosphäre dispergierte Feststoffe

Durch Explosivstoffdispersion oder pyrotechnische Zerlegerladungen in der Atmosphäre dispergierte, hygroskopische Flüssigkeiten.

Zur Abrundung und Begrenzung des Begriffs Tarnnebel wird außerdem das Lambert-Beer'sche Gesetz herangezogen, welches die Schwächung der Intensität einer Strahlung I_0 nach Durchgang einer Strecke l in Bezug zur Ausgangsstrahlung setzt. Die Schwächung findet durch Absorption, Reflektion und Streuung statt und ist außer von der Weglänge auch von der Partikel- oder Aerosolkonzentration c und einer Stoffkonstanten, dem Masseneextinktionskoeffizienten α abhängig^{1,2)}.

$$I(\lambda) = I_0(\lambda) \cdot e^{-\alpha(\lambda) \cdot c \cdot l}$$

$$\alpha(\lambda) \text{ [m}^2/\text{g]}$$

Daraus und mit den vorher beschriebenen Randbedingungen ergibt sich als allgemeine Definition für einen pyrotechnischen Tarnnebel:

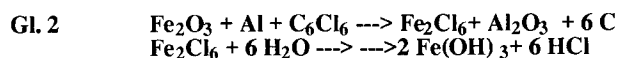
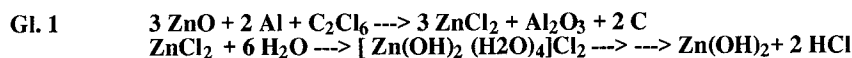
Tarnnebel ist ein künstliches Aerosol schwebfähiger Teilchen, das aus Tröpfchen, Feststoffen oder Gemischen von beiden besteht. Tarnnebel absorbiert, streut und reflektiert elektromagnetische Strahlung. Seine heutige Anwendung reicht von 0.1 µm bis 5 mm Wellenlänge. Tarnresultat ist immer eine Dämpfung der Ausgangs- oder Beobachtungsstrahlungsintensität.

Im Vortrag werden die beiden mit Explosivstoff dispergierten Typen nur der Vollständigkeit halber erwähnt. Durch Generatoren erzeugte künstliche Tarnnebel finden hier ebensowenig Berücksichtigung wie die Techniken zur Erzeugung künstlicher Scheinziele im Infraroten (decoys) und RADAR (chaff).

Pyrotechnische Nebelsätze

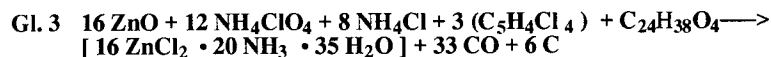
Bildung des Nebelstoffes durch pyrochemische Reaktion

Auf der pyrochemischen Bildung hygroskopischer, sublimierbarer Stoffe beruhen die klassischen HC-Nebelsätze. Das geschieht z.B. durch den Umsatz von organischen Chlordonatoren wie Hexachlorethan (C_2Cl_6) oder Hexachlorbenzen (C_6Cl_6) mit anorganischen Oxiden oder Metallpulvern. Die dabei gebildeten Chloride entstehen in sublimierbarer Form, entweichen mit den übrigen Verbrennungsgasen und bilden zusammen mit der Luftfeuchtigkeit dichte, im optischen Bereich wirksame Tarnnebel (Gleichungen 1 und 2).

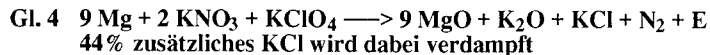


Die bei diesen Umsätzen immer zwangsläufig mitgebildete Salzsäure und die nicht immer vollständig verlaufende Dechlorierung der organischen Bestandteile mit der Folge der Bildung polychlorierter organischer Verbindungen mit hohem ökologischen Risikopotential hat die Verwendung dieser Nebelsätze in der Vergangenheit bereits stark eingeschränkt. Es hat daher nicht an Versuchen gefehlt, hier durch umweltfreundlichere Nebelbildner Abhilfe zu schaffen.

Ein Ansatz war der während der Jahrestagung 1981 vorgestellte NT-Nebel³⁾. Als Nebelkomponente wurde hier wie bei den HC-Nebelsätzen auch das ZnCl_2 gebildet, jedoch durch Amminkomplexe gebunden, sodaß seine starke Hydrolyse mit der Folge der Bildung von Salzsäure verhindert wurde.



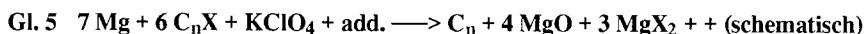
Die Verwendung des Schwermetalls Zink und die lediglich zeitlich verzögerte Hydrolyse waren jedoch nicht ausreichend, sodaß sich dieser Nebelsatz noch nicht voll durchsetzen konnte. Durch Arbeiten an Düngeaerosolen ^{4, 5)} gelang dann die Entwicklung eines KM-Nebel genannten Produktes ohne erkennbares toxisches Potential. ^{6, 7)}



Auch hier erzeugt der Umsatz der Chemikalien Kaliumperchlorat und Magnesium die Nebelbildner KCl und MgO. Die Ausbeute an Nebelpartikeln ist gemessen an den klassischen Nebelsätzen bereits erheblich eingeschränkt, da MgO überhaupt nicht mit der Luftfeuchte reagiert und KCl nur mit Luftfeuchten > 90% stärker wirksame Nebel bildet⁸⁾. KM-Nebel ist aufgrund seiner umweltfreundlichen Eigenschaften als Üb-Nebel bei der BW eingeführt worden.

In den USA, UK und AUS kam man zu anderen Lösungen, um die giftigen HC- und Phosphornebel für Übungszwecke zu ersetzen. Als Nebelbildner wurden sublimierbare organische Verbindungen wie Zimtsäure und Terephthalsäure⁹⁾ eingesetzt. Der Satzaufbau entspricht am ehesten Rauchsätzen und ist aus diesem Grunde nicht ganz unbedenklich. (Bildung choriierter organischer Stoffe durch KClO₃; Erzeugung teiloxydierter Verbindungen und CO aus Azidpolymeren).

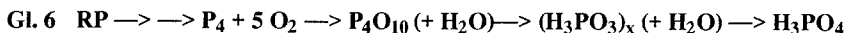
Es ist heute praktisch nicht mehr möglich, toxikologisch bedenkliche Nebelstoffe einzuführen. Umweltverträglichkeitsprüfungen vor der Einführung werden mehr und mehr obligatorisch. Auch ein neuer multispektraler Nebel von NICO¹⁰⁾, der ebenfalls auf dem pyrochemischen Prinzip der Bildung der aktiven Nebelspezies in einem pyrotechnischen Satz beruht, wurde einer solchen Prüfung durch das Fraunhofer Institut für Umweltchemie und Ökotoxikologie unterzogen. Es wurde kein ökotoxikologisches Potential festgestellt¹¹⁾.



Durch Umsetzung der energiereichen Komponenten KClO₄ und Mg wird die Graphit-Verbindung C_nX zersetzt und der dabei zurückgebildete Graphit mit den Verbrennungsgasen ausgetrieben. Aufgrund ihrer geometrischen Form sind diese Graphitpartikel im optronischen und HF-Bereich des RADAR-Spektrums tarnwirksam (siehe unten).

Dispergierung von Nebelstoff durch Anzünd- oder Zerlegerladungen

Die zweite große Gruppe der künstlich erzeugten Nebel hat die aktive Nebelspezies bereits vorgeformt im Nebelkörper (Stäube, hygroskopische Flüssigkeiten) oder der Nebel wird durch Umsetzung mit dem Sauerstoff der Luft gebildet (RP/WP-Nebel).



Eine Anzündladung, wie im Falle der Phosphornebel bzw. eine Zerlegerladung, die auch aus Sprengstoff bestehen kann, verteilt die Nebelpartikel am Wirkort.

Diese Art der Nebelerzeugung wird alleine oder in Verbindung mit der im vorigen Kapitel beschriebenen Methode immer dann eingesetzt, wenn die Tarnung bereits nach wenigen

Sekunden wirken soll. Man findet daher Anwendungsbeispiele besonders beim Selbstschutz von Kampfpanzern.

Beispiele und Anwendungen pyrotechnischer Nebelsätze

Die in den beiden vorhergehenden Abschnitten genannten Nebelstoffe, gebildet und dispergierbar durch pyrochemische Umsetzung oder Explosivstoff, werden in zahlreichen Nebelmunitionssorten eingesetzt. Ihre Verwendung kann in statischen Nebelkörpern (Nebelkerzen, Nebeltöpfe), in Nebelwurfkörpern (Nebelhandgranaten, Irritationskörper für polizeiliche Einsätze, Nebelkörper für Panzerselbstschutz; 40, 66, 76, 80, 81mm) oder in mit Rohr- oder Raketenartillerie verchossenen Wirkladungen (75, 81, 120, 155 mm, MLRS) erfolgen. Je nach Verwendungszweck werden örtlich begrenzte Szenarien für kurze Zeit vernebelt (Panzerselbstschutz) oder große Flächen der Beobachtung zum Teil über Stunden entzogen (Nebelgeneratoren, Objektschutz). Die Tarnung erfolgt hauptsächlich im Visuellen (0.4 - 0.7 μm), kann aber auch den IR-Bereich (0.7 - 1.6, 3 - 5, 8 - 14 μm) und den HF-Bereich des RADARS (1 - 5 mm) betreffen, oder für alle 3 Bereiche gleichzeitig dienen. Auf die Anwendung in den einzelnen spektralen Bereichen wird im folgenden näher eingegangen.

Tarnnebel gegen optische Detektion

Im VIS-Bereich von 0.4 - 0.7 μm Wellenlänge wurden bisher klassische Nebel, vor allem auf der Basis von HC-, HCB-, HCH- RP/WP-Nebelsätzen verwendet. Vorausgesetzt die Luftfeuchtigkeit ist > 50 %, dann wird dieser Bereich zuverlässig abgedeckt. Der Nebel besteht dabei zumeist aus einem Aerosol feinsten Wassertropfchen und kleiner Feststoffpartikel (Ruß, Oxide) und hat einen ausgesprochen niedrigen pH-Wert. In den Wassertropfchen sind die hygroskopischen Nebelstoffe gelöst, und darin spielen sich auch die Hydrolysevorgänge ab, die zur Bildung der Säure führen (HCl, H_3PO_4). Auch TiCl_4 und Chlorsulfonsäure ($\text{Cl-SO}_3\text{H}$) gehört zu diesem Nebeltyp (Explosivdispersion). Die Partikel und Wassertropfchen haben aerodynamische Durchmesser von ca. 0.1 - 1.0 μm in Form einer Gauß-Verteilung⁸), die auch bimodale Struktur haben kann¹²). Die Nebelausbeute ist neben der Abhängigkeit vom Wirkstoff selbst ausgesprochen luftfeuchteabhängig. Der Massenextinktionskoeffizient α liegt bei diesen Nebeln etwa zwischen 3 und 10 m^2/g .

Aufgrund ihrer ausgesprochen umweltunfreundlichen Eigenschaften hat es nicht an Versuchen gefehlt, sie durch weniger aggressive Stoffe zu ersetzen. Neben anderen sind hier NH_4Cl -Nebel, NT- und schließlich KM-Nebel zu nennen^{3, 6}), letzterer ohne erkennbares toxisches Potential⁷), jedoch bereits deutlich schwächer in der Nebelbildung⁸).

Tarnnebel gegen optische, optronische und RADAR-Aufklärung

Sind die im vorigen Kapitel erwähnten klassischen Nebel noch für den nächsten IR-Bereich bis etwa 1.2 μm wirksam, so fallen ihre α -Werte danach steil ab, es werden nur noch 0.05 - 0.2 m^2/g ¹) erreicht. Im sich anschließenden Fenster zwischen 3 und 5 μm und erst recht im fernen IR-Fenster zwischen 8 und 14 μm sind diese Nebel nicht mehr geeignet. Streuung, Absorption und Reflektion der Strahlung dieser Wellenlängen wird durch Lösungströpfchen und Partikel der genannten Größenordnung kaum mehr beeinflusst. Für wirksame Tarnnebel im IR-Bereich > 1.5 μm sollte sich der Massenextinktionskoeffizient α oberhalb von min. 1.5 m^2/g bewegen.

Effektive Tarnung bis etwa $14\text{ }\mu\text{m}$, den heute allgemein genutzten IR-Bereich für FLIR und Wärmebildtechnik wird besonders durch Metallstäube definierter Partikelgröße und Form erreicht. International hat sich hier das Messing durchgesetzt. Aber auch Graphitpartikel und Ruß, vorausgesetzt ihr Partikelspektrum ist geeignet, leisten in diesem Bereich beachtliche Tarnbeiträge.

Geht man von vorgeformtem, kompaktiertem Material aus, so wird dieses zur Ausbildung der Tarnwolke durch Zerlegerladungen, vorzugsweise aus Explosivstoff (z.B. RDX) dispergiert. Die so ausgebrachten "Nebel" haben zwar den Vorteil schneller Tarnwirkung, werden jedoch vom Wind sehr schnell verdünnt und verweht, sodaß "nachgefüttert" werden muß.

Ruß geeigneter Partikelgröße und Partikelform kann durch pyrotechnische Sätze erzeugt werden.
¹³⁾ Dadurch wird eine Tarnquelle erhalten, welche wie die klassischen Nebelsätze über eine gewisse Zeit die aufgebaute Nebelwand nachfüttert.

Neuere Entwicklungen im Hause NICO ¹⁰⁾ haben mit meßtechnischer Unterstützung durch das BICT ¹⁴⁾ pyrotechnische Nebelsätze hervorgebracht, die Graphitpartikel mit Multipoleigenschaften durch thermische Zersetzung von Graphitverbindungen bilden und diese als Aerosolwolke dispergieren. Mit diesen, bis zu einem gewissen Grade leitfähigen Aerosolwolken lassen sich nicht nur im IR-Bereich, sondern auch im HF-Bereich des RADARS, im sogenannten mmWellen-RADAR (MMW) gute Tarnwirkungen erzeugen. Die RADAR-Signale erfahren beim Durchgang durch diese Graphitwolken Dämpfungen $> 20\text{ dB}$ (siehe Abb. 1 und 2).

Multispektrale Tarnnebel

Mit den im mmWellenRADAR wirksamen Partikelaerosolen als Basis und pyrotechnischen Heisätzen (z.B. KClO_4/Mg), welche Abbrandprodukte haben, die im visuellen Bereich zwischen 0.4 und $0.7\text{ }\mu\text{m}$ Nebelwolken bilden können, lassen sich heute Nebelsätze herstellen, die beim Abbrand Tarnwolken erzeugen, welche den gesamten elektromagnetischen Spektralbereich mit Wellenlängen zwischen $0.4\text{ }\mu\text{m}$ und etwa 5 mm abdecken. Man hat diese **Multispektralnebel** inzwischen in NATO-Feldversuchen ¹⁵⁾ im Winter- und Sommerklima untersucht und ihre breitbandigen Tarn Eigenschaften bestätigt. Diese neuen Nebelsätze lassen sich in alle gängigen Nebelkörper laborieren. In Wurfkörpern für den Selbstschutz von Panzern ebenso wie in Rohr- und Raketenartilleriemunition helfen sie, sich der Bedrohung durch Multisensordetektion von Raketen suchköpfen, anderer fire and forget Munition sowie modernen Aufklärungsmitteln zu entziehen.

Sonderanwendungen und Ausblick

Wie mit Beispielen der pyrotechnisch erzeugten Tarnnebel gezeigt, gelingt es auf recht einfache Weise, die Abbrandprodukte pyrotechnischer Sätze oder besser: pyrochemischer Umsetzungen zu aerolysieren. Dieses Prinzip hat längst die lediglich leicht verdampfbaren oder sublimierbaren Aerosolbildner wie ZnCl_2 oder Anthrachinonfarbstoffe (Rauchsätze für farbigen Signalrauch) verlassen. Es gelingt heute, die richtige Energiequelle und Umsetzung vorausgesetzt, selbst unverdampfbare Stoffe wie Graphit als stetig fließendes Partikelaerosol aus pyrotechnischen Nebelkörpern zu dispergieren. Schon früher war gezeigt worden, daß auch Feststoffe wie CaO und MgO durchaus in aerosolfähiger Form herzustellen sind ^{4, 5)}. Damit ist das pyrotechnische Prinzip der **Bildung von Wirkstoffen** oder der Dispergierung von vorher in den **pyrotechnischen Satz integrierten Wirkstoffen** erheblich erweitert worden.

Abb. 1

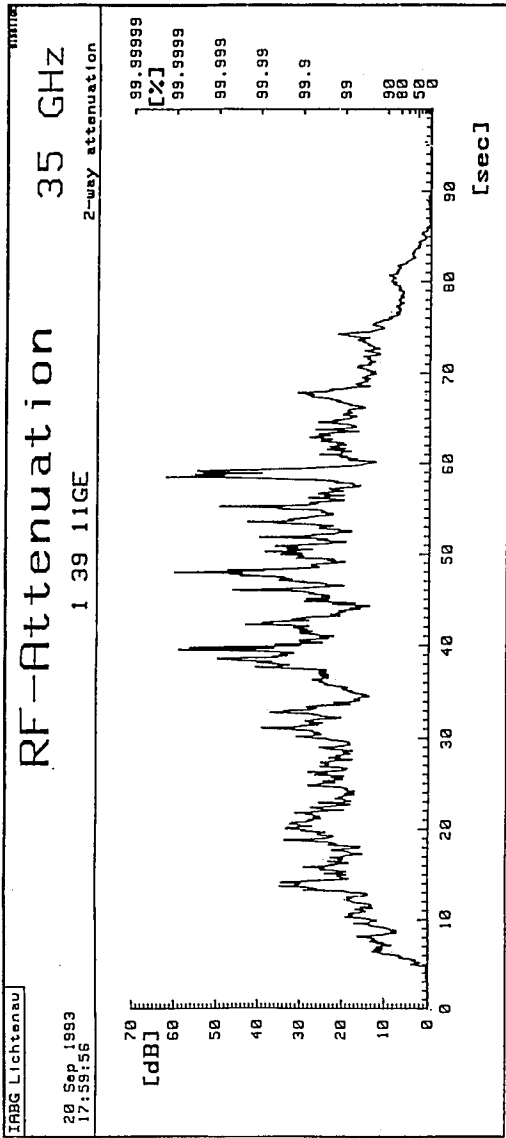
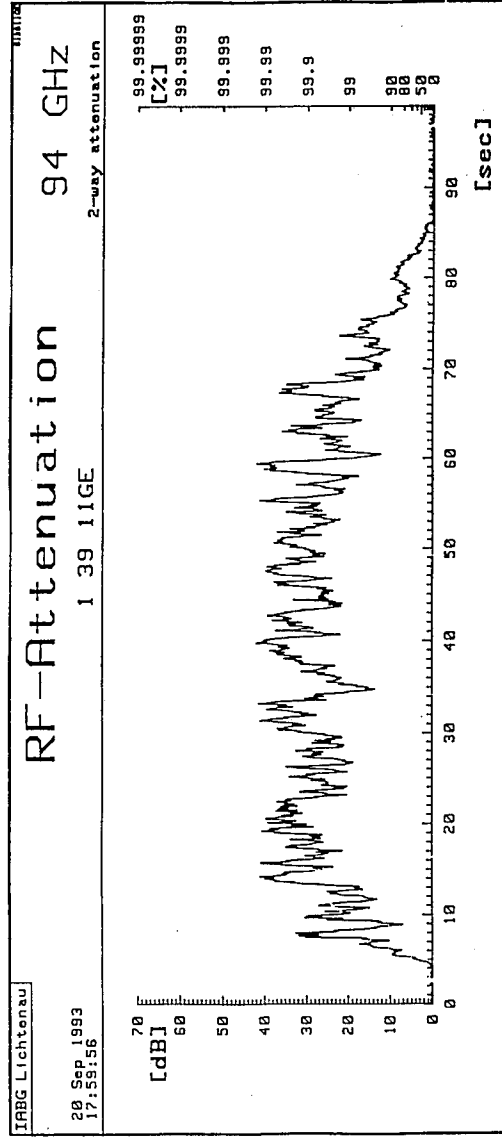


Abb. 2



Damit sollte es auch möglich sein, für zukünftige Anwendungen derartiger "Nebelsätze" toxikologische und Umweltrisiken besser zu beherrschen. Die Palette möglicher Aerosolkandidaten hat sich durch die Anwendung dieser Pyrotechnik, vor allem der Einführung hochenergetischer Heihsätze auf der Basis der Oxidation von Magnesium oder ähnlich energiereicher Metalle erheblich erweitert und sollte eine umweltverträgliche Auswahl geeigneter Wirkstoffe in Zukunft leichter machen.

LITERATURVERZEICHNIS

- 1) W. Scheunemann, Bericht über die optischen Eigenschaften von wässrigen Zinkchlorid-Lösungströpfchen im Infraroten. BICT-Bericht 3.2-3/4595/78
- 2) W. Scheunemann, Eine neue Methode zur Bestimmung des Massenextinktionskoeffizienten von RADAR-Tarnnebeln: Theorie und Experiment. BICT-Bericht 320/7513/88,
- 3) U. Krone, Herstellung und Bearbeitung eines neuen pyrotechnischen Nebelsatzes: NT-Nebel. Int. Jahrestagung ICT 1981, S. 211 ff
- 4) U. Krone, W. Kühn, B. Georgi, A. Hüttermann, Pyrotechnically Generated Ca- and Mg-Aerosols, Proceedings 9th Int. Pyrotechnics Seminar, P. 315 ff
- 5) U. Krone, W. Kühn, B. Georgi, Entwicklung und Anwendung pyrotechnisch erzeugter Calcium- und Magnesiumaerosole. Int. Jahrestagung ICT 1985, S. 36-1 ff
- 6) U. Krone, A Non-Toxic Pyrotechnic Screening Smoke for Training Purposes. Proceedings 15th Int. Pyrotechnics Seminar, P. 581 ff
- 7) F.J. Mönig, Untersuchungen zur toxikologischen und ökotoxikologischen Bewertung eines HC- und KMC- Nebels. FhG-Institut für Umweltchemie und Ökotoxikologie, 12.1990
- 8) W. Scheunemann, J. Franzen, Nebelwurfkörper-Üb M 88 KM, bes. Anlagen 13 und 14 zu BICT-Bericht 420/8536/90
- 9) US-Patent 5.098.488, Bickford, Smith, Cheng, Tracy, Composition
- 10) DE-Patent 43 37 071, U. Krone, K. Möller, E. Schulz, Pyrotechnischer Nebelsatz für Tarnzwecke und dessen Verwendung in einem Nebelkörper.
- 11) R. Debus, A. Flidner, Untersuchungen zur ökotoxikologischen Bewertung eines Nebelmittels. FhG-Institut für Umweltchemie und Ökotoxikologie, 12.1994
- 12) B. Georgi, U. Krone, Variation of the Particle Size Distribution During Dispersion Processes. Proceedings of the Smoke/Obscurants Symposium VII, 51, April 1983, Volume 1 OPM Smoke/Obscurants, Technical Report, DRCPM-SMK-T-001-83
- 13) DE Patent 40 30 430, H. Büsel, J. Schneider, IR-undurchlässigen Nebel erzeugende Zusammensetzung.

- ¹⁴⁾ W. Scheunemann, J. Franzen, Messungen an MMW-Tarnnebeln, BICT-Bericht 420/10815/92, VS-NfD
- ¹⁵⁾ NATO-SOCMET-TRIALS, 02./03.1993 Valcartier (Canada), 09.1993 Bourges (France)

A HYBRID GAS GENERATOR USING LOW CONCENTRATION HYDROGEN PEROXIDE FOR INFLATING AIRBAGS

Nobuo TSUJIKADO*, Takeo SAITO**, Akira IWAMA**,
Takashi KAZUMI***

* Faculty of Engineering, Tokai University

117, Kitakaname, Hiratsuka, Kanagawa 259-12, JAPAN

**The Institute of Space and Astronautical Science, Ministry of
Education, Culture and Science

3-1-1, Yoshinodai, Sagamihara, Kanagawa 229, JAPAN

***Nihon Koki Company, Shirakawa Plant

2-1, Aza Dobu, Nishigo-mura, Nagasaka, Nishi-shirakawa,
Fukushima 961, JAPAN

ABSTRACT

This paper presents a proposal to use 60 wt% or less concentration of hydrogen peroxide solution as the main gas generant of the hybrid gas generators for inflating the car airbags. The gas generants confined in the module are 50 ~ 100 ml of water solution with 60 wt% or less H_2O_2 , concentration, pressurized argon or nitrogen gas (0.1 ~ 10 MPa) and usual pyrotechnics applied to solid rocket vehicles including the decomposition catalyst $KMnO_4$ for H_2O_2 . Experimental modules have performed the severe requirements that The Federal Motor Vehicle Safety Standard (FMVSS) and Japanese car industries have imposed on airbag makers. An S-letter-type pressure build-up curve, arrival to the maximum pressure of 80 ~ 150 kPa within 30 ~ 80 ms in 60 liters tank test, and specified air bag inflation and contraction sequence aspect have been achieved. Employing experimental modules, results of a 60 liters tank and an airbag inflation test are described.

1. INTRODUCTION

Motive force to the progress in the passive system for protecting car drivers and passengers from vital injury in collision accident confronts the air bag producers with some stringent requirements¹⁾: downsizing,

decreased temperature on inflated airbag surface, no toxic gas emission, reduction in solid combustion products, lower cost, and easiness on disposal and recycling. Gas generators applied to current or near-future airbags of car vehicles are the consolidated mixtures of solid oxidizer and fuel chemicals such as sodium azide, triaminoguanizine, tetrazoles and so on²⁾. These materials encounter the some obstacles incapable of getting over. Azide type gas generants may contain not negligible Na_2O and Na_2O_2 in the burning gases. The mass production requests the high level of the safety control particularly regarding static electricity hazard, impact, and slight HN_3 generation due to the contact with the acidic atmospheres. Non-azide and hybrid gas generators using double-base propellants have a problem to control CO and NO emission, and further too highly elevated gas temperature conflicting with more quick response function in the event of collision is a common concern to azide-based gas generators.

Brede³⁾ proposed a liquid propellant composed of n-butane, nitrous oxide and carbon dioxide as the non-azide gas generants and demonstrated a downsized and light weight module with a higher performance. However, the oxidizer component, nitrous oxide is very expensive and not tender to human bodies on leaking in free air. The use of low concentration water solution of hydrogen peroxide less than 60 wt% proposed here, has expressed a high possibility to solve mostly the above problems by the combination with powerful starter and pressurized gas in a confined module.

2. CHARACTERISTICS OF LOW CONCENTRATION HYDROGEN PEROXIDE

Classical liquid rocket propulsion or attitude control device had employed widely 90 wt% H_2O_2 . The decomposition heat of hydrogen peroxide is as follows: $\text{H}_2\text{O}_2 \rightarrow \text{H}_2\text{O} + 1/2\text{O}_2 + 98.2 \text{ kJ}$. Consequently, once the decomposition start, the decomposition temperature of 90 wt% H_2O_2 would get immediately to around 1000 K at the maximum. This investigation avoids intentionally to apply such a high concentration H_2O_2 to airbag inflators. The reason consists in the property of H_2O_2 that, as shown in Fig. 1, the H_2O_2 solutions lower than 64.5 wt% in concentration, the heat of decomposition cannot make the remaining liquid temperature elevate further over the boiling point at once. Namely, the highest temperature at the outlet of the module is limited by the

boiling point determined under the ambient pressure. Figure. 1 also suggests that hazardous state would be no longer realized, provided the H_2O_2 solution remains in a region from 11.5 to 64.5 wt%.

Gases released through H_2O_2 decomposition are non-toxic and solid combustion products exclusive. In the hybrid system, oxygen gas liberated during a long time storage shall assist to convert carbon monoxide to carbon dioxide through the liquid and steam media in the event of collision as well as it becomes a working gas, and a high fraction of steam mist absorbs nitrogen oxides, hydrogen chloride and chlorine gas without any oxidizing catalyst and filter bed.

A further advantage of H_2O_2 water solution is an azeotrope property in term of the freezing point as indicated in Fig. 2. The minimum freezing point of 218 K appears at 60 wt% H_2O_2 fraction and even 40 wt% solution gives the freezing point of 233 K. Unfortunately, there is no azeotrope property on the boiling point, but as practically H_2O_2 solution is kept in confined module, the hazard because of an increase in the H_2O_2 concentration is not required to worry about.

On the other hand, it has been criticized that the vital disadvantage of H_2O_2 is related with the considerably high rate of the spontaneous decomposition even if it be kept in the specified material container. However, the recent products, 30, 35, 50 and 60 wt% H_2O_2 available in market guarantees high stability owing to the refining technology progress and stringent requirement from electronics industries. Table 1 shows an analysis example and Japan Industrial Standard(JIS)-K-8230 for the purity of 60 wt% H_2O_2 solution randomly sampled from market. This result means that the module guarantees ten to fifteen year product liability on the quality if it is assembled in the first class clean room and loaded in the confined cartridge made of a specified material. During long term storage, indeed, H_2O_2 solution shall incur extremely high temperature environment, for instance, more than 263 K and the decomposition rate might be accelerated. Nevertheless, H_2O_2 solution shall be able to perform the specification of FMVSS and Japanese car industries for ten years.

3. EXPERIMENTAL

Modules

Two different gas generator modules made of aluminum and stainless steels are machined for trial as shown in Fig. 3. The inner dimension of

an aluminum-made module is $\phi 45 \times h 60$ (95 ml) and stainless steel-made one $\phi 60 \times h 90$. A few pieces of copper screen sheets through which partially undecomposed H_2O_2 mist and vapor flow, plays both the roles of strainer and decomposition catalyst. Thus, in case of 60 wt% H_2O_2 solution the working gases composed of 18 wt% oxygen and the remainder of the mist and vapor of H_2O are exhausted into the airbags through the numerous tiny nozzles. The aluminum-made module has an upright sheath in which mixtures of pyrotechnics and decomposition catalyst is filled. The stainless steel-made module can be pre-pressurized with nitrogen or argon to realize an effective action in the air bag inflation against the aging deterioration of H_2O_2 and even under various environmental conditions. Hydrogen peroxide solutions are loaded with a cartridge. We tested also the starter containers made of three different materials: polyethylene bag, polymethyl methacrylate(PMMA) sheath and confined stainless steel.

Tank Test

According to the Japanese car industry specification, 4.1 and 60 liters capacity test tanks are prepared. Using 4.1 liters tank, at first, we tested a bag type starter in which 0.1 ~ 0.3 g pulverized black powder and 0.6 ~ 0.8 $KMnO_4$ catalysts for H_2O_2 decomposition are packed. The module sets the starter at the bottom, submerged in 50 ~ 100 ml of 60 wt% H_2O_2 solution. The pressure-time histories depicted the ideal S-pressure build-up curves. However, it took approximately 50 ms for the merging decomposition and 300 ms for the completeness of 60 liters airbag inflation respectively, which are a poor performance far from practical specification. Then, we assumed it difficult to meet the time budget of FMVSS only by such a catalytic decomposition and made a judgment that the simultaneous proceeding of catalytic reaction with thermal decomposition is indispensable for performing the outstandingly rapid gas generation.

Figure 4(a) is an example that the first module (I) has passed the time budget requested by FMVSS by employing a sheath type starter filled with black powder, a mixture of boron and potassium nitrate, propellant debris and fine $KMnO_4$ powder. With the 60 liters test(Fig.(b)), the stainless steel module also showed an achievement to pass the minimum requirements that the pressure build-up delay from the event of collision

is 10 ~ 25 ms, and the maximum pressures of 800 to 1500 kPa should attain in 30 ~ 80 ms as seen in Fig. 5.

Airbag Inflation Test

Adjusting the diameters of two vent holes from zero to 50 mm, the 60 liters airbag inflation tests were conducted with the modules installing the sheath starter. Figure 6 demonstrates a sequence of the inflation pictures taken at a rate of 250 frames per second. From the observations of the pictures obtained every four second, the airbag with the vent holes of ϕ 15 mm could inflate up to 90 % in volume within 50 ms. After it contracted slightly once, the airbag again has fully inflated till 150 ms. Because of the high heat of condensation the temperature and pressure of gases staying in airbags are maintained for a considerable time. Therefore, such a sequence of air bag inflation may make a relaxation against the rebound of human faces and bodies.

4. CONCLUSIONS

Water solutions of hydrogen peroxide in a region of 40 ~ 60 wt% can provide the rapid gas generation enough to inflate the car airbags within the specified time budget by promoting the H_2O_2 decomposition catalytically and thermally. The powerful pyrotechnics which are an igniter extensively used in solid rocket motors but include the decomposition catalyst powder of $KMnO_4$, were filled in a plastic sheath and a confined metal cartridge container. The starter has assisted for this system to achieve the time budget to meet the FMVSS requirements.

From the view point of production and operation safety, clean gas emission H_2O_2 solutions are a preferred property: the main reaction products are oxygen, and water mist and vapor harmless to human organs and solid combustion products are exclusive. Toxic gases, such as a small amount of carbon monoxide, hydrogen chloride, chlorine, sulfur dioxide brought about from the pyrotechnics, solid propellant and auxiliary solid non-azide gas generants, shall be oxidized or absorbed mostly through a contact and a mixing time with the liquid media. Therefore, no special catalyst bed or filter is needed except copper screens that plays a role of the catalyst for hydrogen peroxide.

The use of hydrogen peroxide would contribute to downsizing, reduced weight, cost lowering (two dollars per kilogram for 60 wt% H_2O_2 solution) and module design simplification.

It is believed with H_2O_2 that there are some concerns on the aging and stability at high ambient temperatures. However, advanced electronics industries requested recently a high grade purification on the H_2O_2 producers. Keeping 60 wt% H_2O_2 in a container made of a polyvinyl chloride at room temperature for five years, we noted the decomposed fraction remains less than 1 %. Furthermore, as the inner space of the modules must be pressurized much or less, the oxygen gas that has formed in the modules gradually during a long time storage, shall also become useful as the working gas for airbag inflation.

REFERENCES

- (1) James P. Karlow, J. John Jakovski and Brian Seymour: "Development of a Downsized Airbag System for Use in Passenger Vehicles", Presented at 1994 SAE International Congress and Exhibition. Society of Automotive Engineers, USA
- (2) L. Branbilla: "Chronik Einer Sicherheitsentwicklung Verbesselter Insassenschutz Durch Die Pyrotechnischen Systeme: Gurtstraffer und Airbag", Proceedings of 18th International Annual Conference of ICT Paper No. 29 (1987)
- (3) Uwe Brede: "Liquid Propellant Inflators", Paper No. 13 (1994)

Table 1 An analysis result of commercially available 60 wt% hydrogen peroxide solution

Metal	Concentration (ppb)	Specification (ppm)
Al	300 ~ 600	
Fe	2 ~ 5	
Cr	1 ~ 4	< 0.04
Ni	1	
Cu	0.3 ~ 0.5	< 0.01
Zn	ND*	< 0.05
Cd	ND	< 0.005
Pb	ND	< 0.02
As	ND	< 0.04
Total Hg	ND	< 0.005
Organic Phosphorus	ND	< 1

*ND: Not detectable

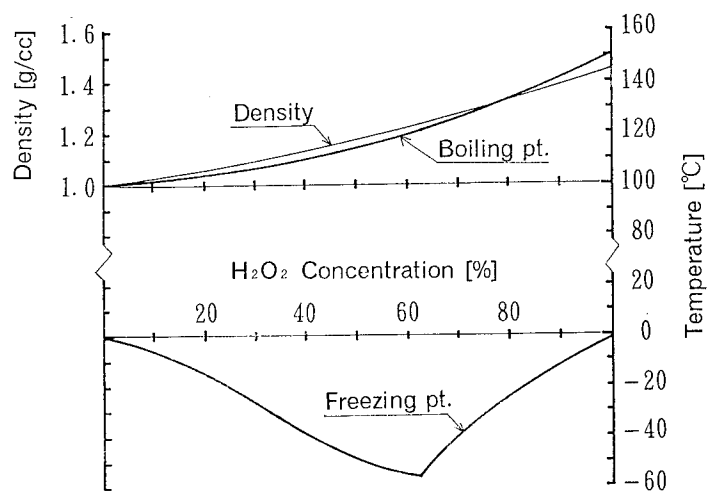


Fig. 1 Phase diagram of the mixtures of H₂O₂ and H₂O

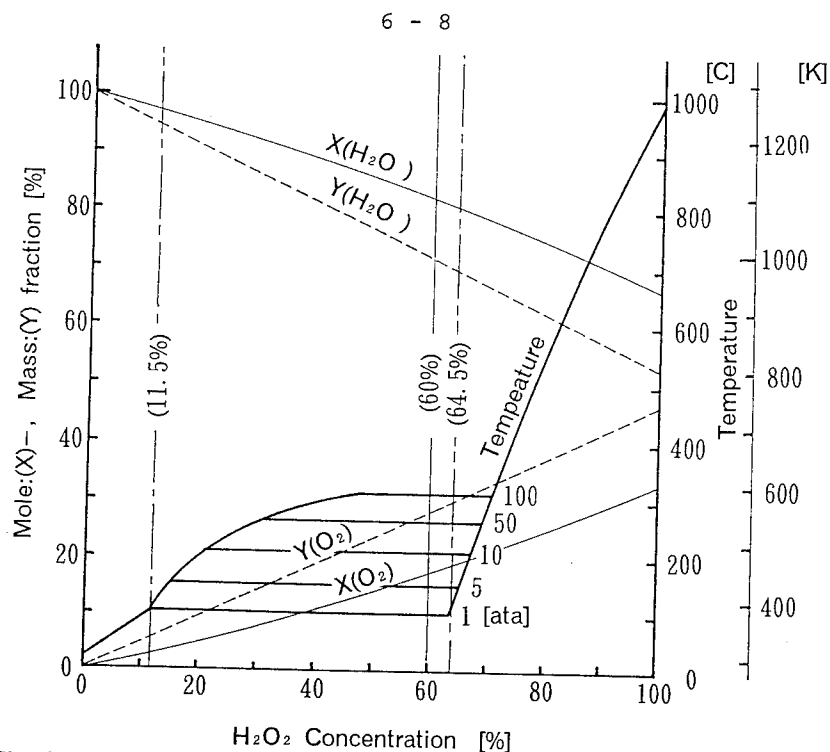


Fig. 2 Temperature and compositions of the decomposition products of mixtures of H_2O_2 and H_2O

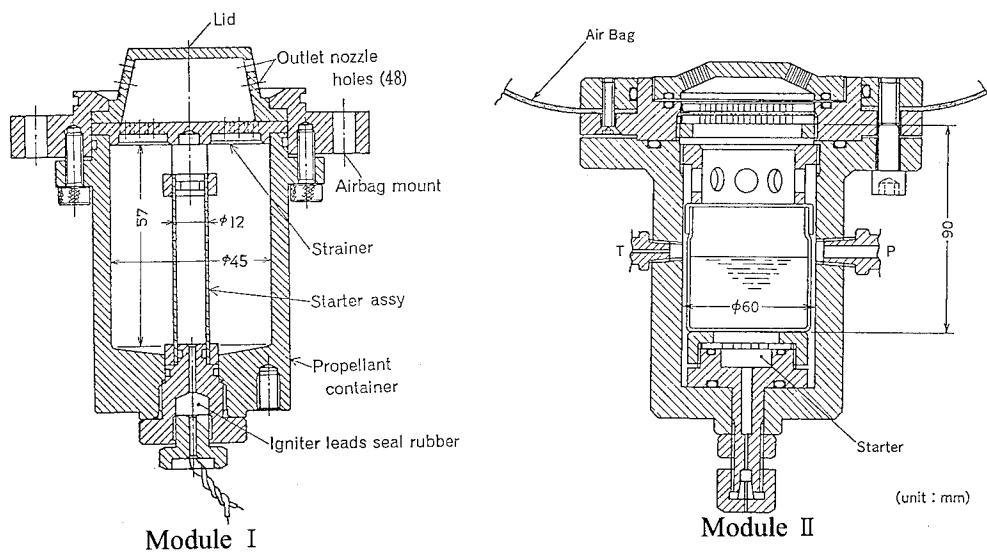
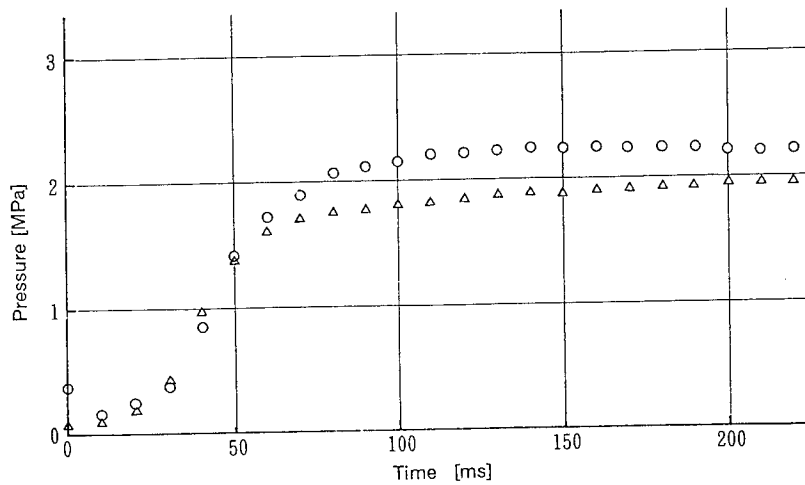
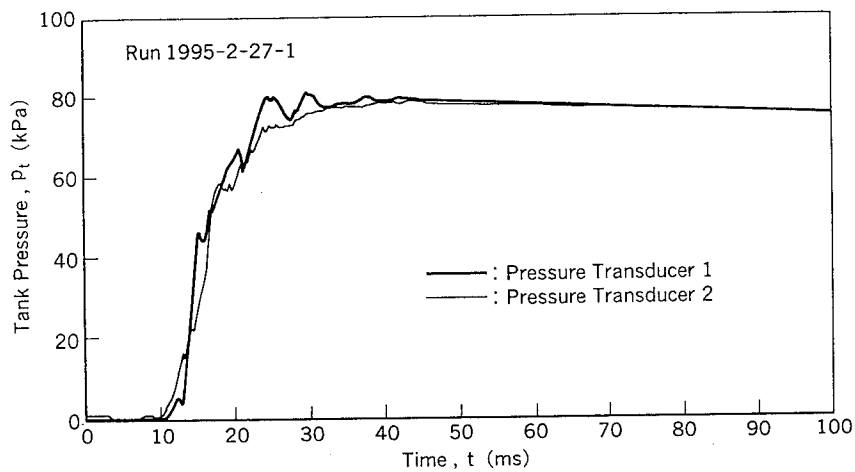


Fig. 3 Experimental modules (P: pressure transducer port and high pressure gas flow-in port, T: thermocouple port)



(a) 4.1 liters tank



(b) 60 liters tank

Fig. 4 An example of pressure-time histories in 4.1 and 60 liters tank (Module I, Sample: 60 wt% H_2O_2 70 ml. Starter: black powder 0.2 g, B/KNO_3 mixture 0.6 g, propellant debris 0.3 g, KMnO_4 0.7 g)

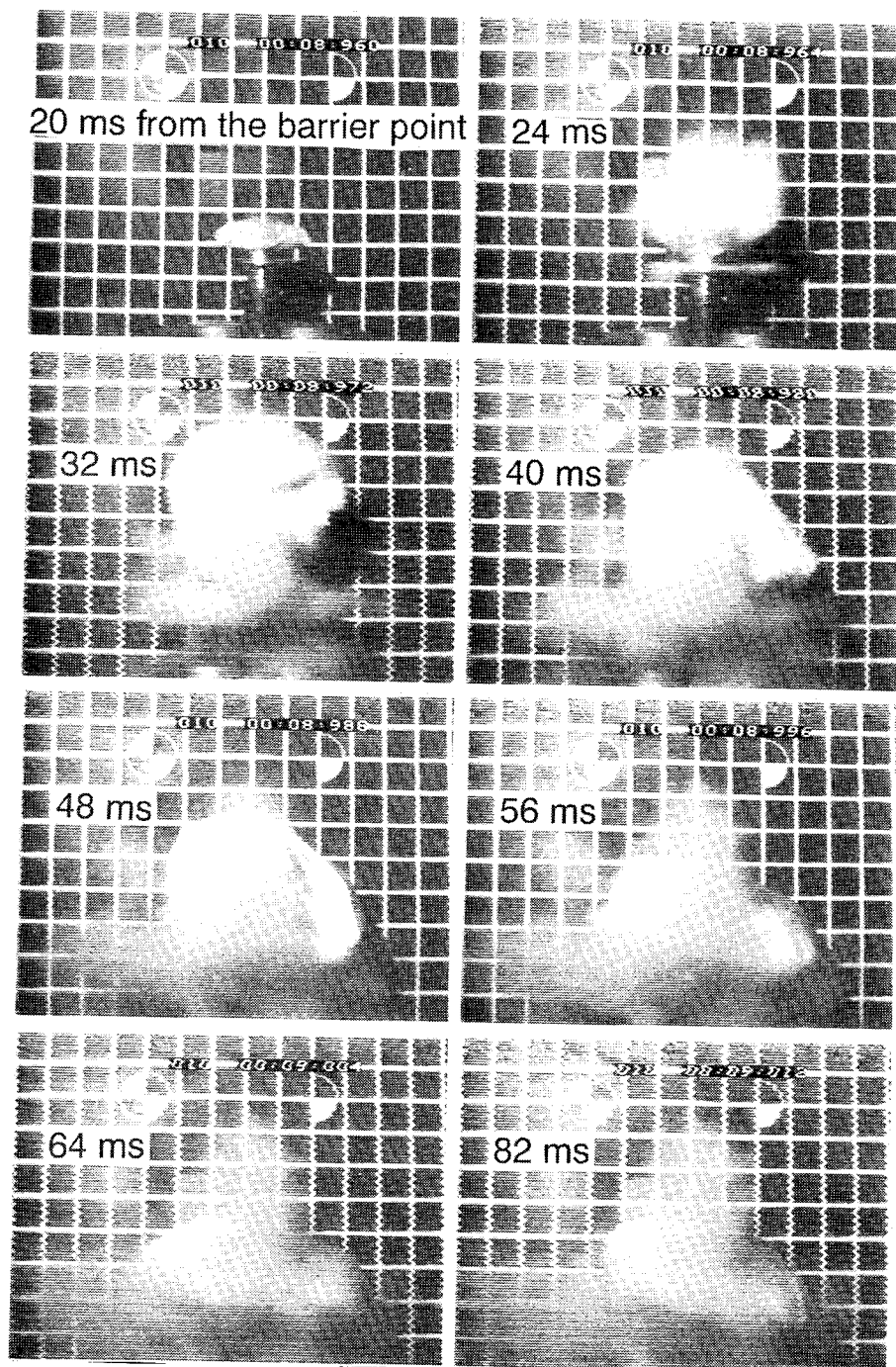


Fig. 5 An example of the inflation aspect of 60 liters airbag (Module I,
 Sample: 60 wt% H_2O_2 70 ml. Starter: black powder 0.2 g,
 B/ KNO_3 mixture 0.6 g, propellant debris 0.3 g, KMnO_4 0.7 g)

An Influence of the Chemical Structure
of Smoke-Producing Mixtures
on the Laser Radiation Extinction at 1,06- μm and 10,6- μm
Wavelengths

Andrzej Papliński and Stanisław Cudziło

Military University of Technology
01-489 Warszawa
Ul. Kaliskiego 2
Poland

In the paper an influence of the chemical composition of smoke-producing pyrotechnic mixtures upon their ability to the laser radiation attenuation is investigated. The transmission measurements were performed at laboratory conditions. The Nd:YAG and TEA CO₂ lasers with the energy density meters were used.

The chloroorganometallic mixtures containing oxidizing agents as well as mixtures which do not include oxidant ingredients were examined. In the investigated kinds of mixtures, the same elemental composition was preserved while chemical compounds being carriers of particular elements were changed. As chlorine carriers hexachloroethane (C₂Cl₆) and hexachlorobenzene (C₆Cl₆) were employed. The content of carbon was modified by introduction to the mixture of such compounds as polystyrene, naphthalene and biphenylene.

The obtained results of laser radiation transmission measurements in the aerosol clouds generated by burning of the mixtures with altered chemical composition enable us to infer about influence of the chemical structure of mixture constituents upon the screening efficiency of aerosols.

LOW TEMPERATURE SOLID SOURCES OF NITROGEN

V.ALESHIN, S.KURAKIN, G.SHIROKOVA, Yu.V.FROLOV.

INSTITUTE OF CHEMICAL PHYSICS RAS.

MOSCOW

RUSSIA

SOLID SOURCES OF GASES ARE GOING TO BE OF GREAT IMPORTANCE FOR TECHNICS AND OTHERS FIELDS.

AVAILABLE METHODS OF GAS GENERATION INCLUDE A SELF-PROPAGATION COMBUSTION PROCESSES OF SOLID COMPOUNDS SUCH AS POWDERS, SOLID PROPELLANTS AND PYROTECHNICS MIXTURES.

SOLID SOURCES OF GASES OFFER MANY POTENTIAL ADVANTAGES INCLUDING A POSSIBILITY TO HAVE DESTRED GAS ($N_2, O_2, CO_2, CL...$) JUST BEFORE USING IN ANY EXTERIOR CONDITIONS, LONG KEEPING TIME UNDER "ATMOSPHERE" PRESSURE, ETC.

VARIOUS ASPECTS OF THE NITROGEN GAS GENERATION BY THE COMBUSTION OF NaN_3 -BASED MIXTURES ARE DISCUSSED. THE INFLUENCE OF COMPOSITION AND INITIAL CONDITIONS ON THE GENERATION AND STRUCTURE FORMATION ARE SHOWN. .THUS, THE ALUMINA ADDITIVES TO THE COMPOUNDS RESULT IN THE DECREASE BURNING RATE AND REACTION TEMPERATURE. BUT IT WAS SHOWN THAT THIS "INERT" COMPONENT CAN CHEMTCALLY REACT WITH THE NaN_3 .

CONDITIONS OF THE SOLID POROUS FRAMEWORK FORMATION DURING COMBUSTION ARE DISCUSSED ALSO. IT IS PROVED THAT SUCH FRAMEWORK RESULT IN HIGHER GAS PURITIES BECAUSE OF AEROSOL FILTRATION DURING COMBUSTION.

THE PRINCIPLES OF COMBUSTION GAS GENERATION COMBINED WITH SOME ASPECTS OF APPLICATION.

REDUCTION OF CO AND NO_x IN EFFLUENT GAS OF ADCA GAS GENERANT FOR AUTOMOTIVE AIRBAG INFLATORS

by

Kazuo Hara, Takayuki Hasegawa, Satoru Amari, Yoshihiko Otsuka
and Tadao Yoshida

Department of Materials Chemistry, Hosei University,
3-7-2 Kajino-cho, Koganei-shi, Tokyo 184, Japan

ABSTRACT

Several experiments have been conducted for reducing the carbon monoxide (CO) and nitrogen oxides (NO_x) in the effluent gas from the combustion of azodicarbonamide (ADCA) based gas generants for automotive airbag inflators. Used apparatus is the 60L tank tester using a model inflator. Effects of CuO, oxygen balance, KNO₃ and other additives, catalysts and external oxidizers were examined for reducing the CO and NO_x from the burning of the ADCA gas generant. CO decreased and NO_x increased when the oxygen balance of the gas generant composition increased. Some catalysts showed effective activity for reducing CO and NO_x. Addition of external oxidizers such as potassium chlorate or nitrate was significantly effective for reducing the CO and NO_x.

INTRODUCTION

A new non-azide gas generant for automotive airbag inflators has been developed, and the concept¹⁾, performance^{1) 4)}, safety^{2) 5)}, health³⁾ and environment³⁾ aspects were already presented or published. The new gas generant contains azodicarbonamide (ADCA) as a most basic ingredient, and ADCA contains two carbon atoms in a molecule. Therefore our new gas generant releases the effluent gas including few amount of carbon monoxide (CO) and nitrogen oxides (NO_x). Here we describe results of our study on the reduction of CO and NO_x in the effluent gas released from the burning of the ADCA gas generant in a model inflator.

EXPERIMENTAL

Materials

Basic materials used are ADCA, KClO₄, CuO, soluble starch and SiO₂. Other

oxidizers such as KClO_3 , KNO_3 and CaO_2 were tried to be used. Examined catalysts are CuO , CoWO_4 , NiO , V_2O_5 , MoO_3 , WO_3 , Fe_2O_3 , Fe_3O_4 , $\text{Pb}(\text{NO}_3)_2$, NiMoO_4 , CoMoO_4 , MoS , Cr_2O_3 , Ni , MgO and Pb_3O_4 . NaHCO_3 and MgCO_3 were tried to be used as diluent.

A mixture of KClO_4 , soluble starch and some water is added to a mixture of ADCA, CuO , SiO_2 and other additives, and whole mixture is kneaded in a kneader. Formed pasty intermediate is feeded into a granulator and made to wet granules. The wet granules are dried in a oven at 80°C for one hour and then the dried granules are pressed to pellets by a pelletizing machine.

Test Apparatus

The test apparatus (Fig. 1) for evaluating CO and NO_x in the effluent gas from the burning of ADCA gas generant in the model inflator is composed of a 60L tank equipped with pressure and temperature sensors and gas sampling port, and a model inflator with a pressure sensor.

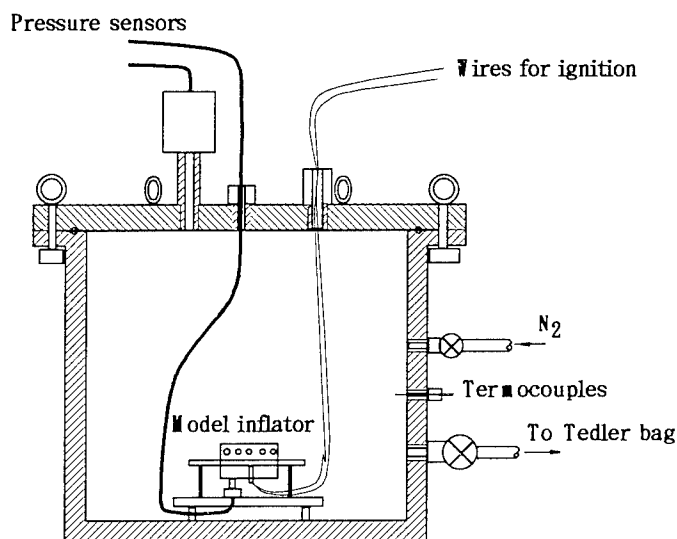


Fig. 1 60L tank tester

Gas Analysis

The effluent gas after the working of the inflator is introduced into a 1L Tedler bag from the 60L tank and the sampled gas is analysed for CO, NO_x and other component gases using gas detector tubes (Komyo Rika Co. Ltd. and Gastech Co. Ltd.).

Test Procedure

- (1) A filter assembly composed of stainless steel mesh and ceramic filter is inserted to the inside of the outer frame of the model inflator.
- (2) A separating ring and a coolant are placed on the filter assembly.
- (3) An inner frame is placed inside the filter and the coolant.
- (4) An Al cup is placed in the inner frame.
- (5) An enhansor assembly containing B/KNO₃ composition is pasted to the bottom of the Al cup.
- (6) The weighed gas genarant pellets (6mm ϕ and 5mm high) are poured into the cup with the enhansor.
- (7) A squib composed of Zr/KClO₄ ignitor composition and a bridge wire is screwed into the hole of the top cover of the model inflator.
- (8) The cover is screwed to the inflator.
- (9) The filled inflator is placed in the bottom of the 60L tank tester.
- (10) The circuit for ignition and pressure sensors are connected and the top cover of the 60L tank is closed.
- (11) The squib is ignited, and the pressures of the inflator and the tank, and the temperature inside the tank are recorded.
- (12) The gas in the tank is introduced into a Tedler bag and analysed for CO, NO_x and other gases.

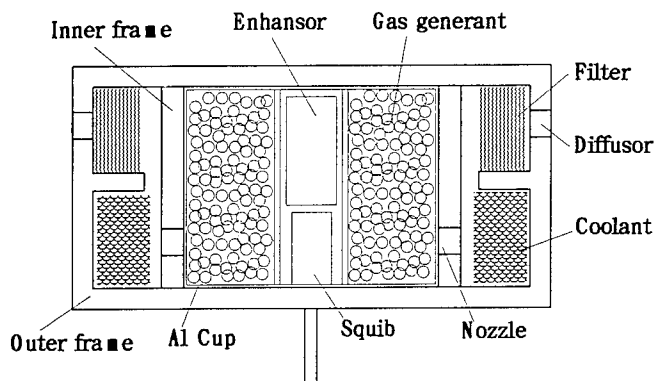


Fig. 2 Model inflator

RESULTS AND DISCUSSION

CO and NO_x from Base Composition

The CO and NO_x concentrations in the effluent gas from the burning of 30g of the basic AKCSSi composition (ADCA(A)45, KClO₄(K)55, CuO(C)10, starch(S)1.5 and SiO₂(Si)1.0 parts) were following:

	CuO(A)	CuO(B)
CO :	15000 ppm	1200 ppm
NO _x :	600 ppm	1000 ppm

Effect of CuO

CuO is one of the basic ingredients in our new gas generant composition. For the standard reaction conditions, CuO is necessary for stable burning of the gas generant. CuO is a catalyst for increasing burning rate of the gas generant and for reducing CO concentrations in the effluent gas. Two types of CuO(A) and CuO(B) were used. The latter is more reactive and gives more NOx and less CO than the former. CuO contents in the composition were changed and experimental results are listed in Table 1 and shown in Fig. 3. It is seen from Fig. 3 that CO decreases and NOx increases with increasing CuO content in the composition.

Table 1 Effects of CuO(B) and oxygen balance in AKCSSi on CO and NOx in the effluent gas

ADCA/KClO ₄ /CuO/Starch/SiO ₂	Mass in g	CO in ppm	NOx in ppm
45/55/10/1.5/1.0	30	13,500	800
45/60/15/1.5/1.0	30	7,500	1,500
45/65/20/1.5/1.0	30	3,200	1,800
45/60/10/1.5/1.0	30	15,000	1,200
45/65/5/1.5/1.0	30	17,000	1,300
45/65/10/1.5/1.0	30	10,000	1,300
45/60/0/1.5/1.0	30	48,000	600

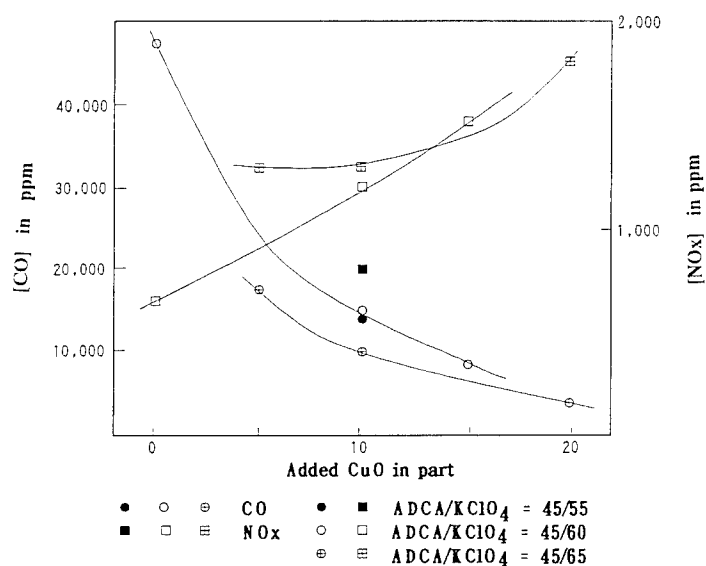


Fig. 3 Effect of added CuO on [CO] and [NOx]

Effect of Oxygen Balance

The oxygen balance of the gas generant composition AKCSSi was changed by increasing KClO_4 or by adding KNO_3 from 10 to 50 parts to the 113 parts of the base composition. Here CuO(B) was used. Result are listed in Table 2 and shown in Fig. 4.

CO decreased and NO_x increased with increasing KClO_4 or increasing KNO_3 added to the AKCSSi composition. Fig. 4 indicates that KNO_3 is more effective than KClO_4 as oxidizer. Fig. 4 also indicates that addition of KNO_3 gives minimum CO concentration at 30 parts addition. But, NO_x increases monotonically with increasing addition of KNO_3 .

Table 2 CO and NO_x concentrations in the effluent gas: effect of oxygen balance

ADCA/ KClO_4 / CuO(B) /St./ SiO_2 / KNO_3	mass in g	CO in ppm	NO_x in ppm
45/55/10/1.5/1.0/0	30	12,000	1,000
45/55/10/1.5/1.0/10	30	6,000	1,700
45/55/10/1.5/1.0/20	30	4,000	2,500
45/55/10/1.5/1.0/30	30	2,500	>4,000
45/55/10/1.5/1.0/40	30	3,500	>4,000
45/55/10/1.5/1.0/50	30	5,000	>4,000
45/60/10/1.5/1.0/0	30	15,000	1,200
45/65/10/1.5/1.0/0	30	10,000	1,300

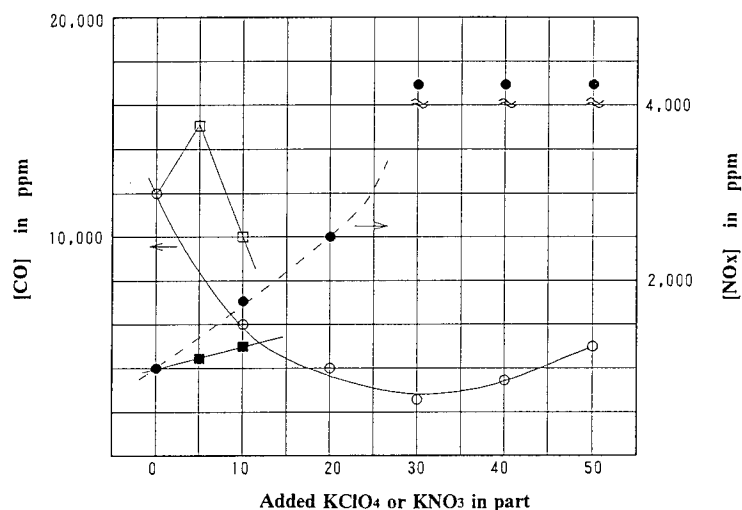


Fig. 4 Plot of [CO] and [NO_x] against KClO_4 or KNO_3 added to 113 part of the AKCSSi composition

Primary Evaluation

Fig. 5 shows the plot of $\log[\text{CO}]$ against $\log[\text{NO}_x]$ for the 30g AKCSSLN(N:KNO₃) gas generant in the 60L tank test. The solid line is for the best results of low CO and NO_x. Examples of the test results are listed in Table 3.

Table 3. Examples of best AKCSSLN compositions for low CO and NO_x

ADCA	KClO ₄	CuO	Starch	SiO ₂	KNO ₃	Mass in g	CO in ppm	NO _x in ppm
45	65	20(B)	1.5	1.0	0	30	3200	1800
45	55	10(A)	1.5	1.0	0	30	12000	450

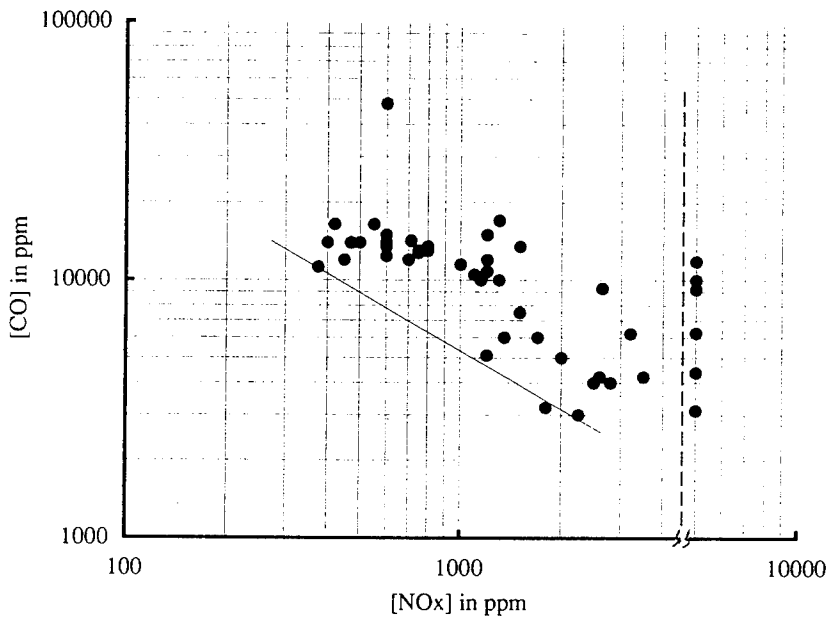


Fig. 5 Plot of $\log[\text{CO}]$ vs. $\log[\text{NO}_x]$ for 30g AKCSSLN gas generant in 60L tank test

Effect of Catalyst

Some experimental results of the burning test for examining the effect of catalysts on CO and NO_x are listed in Table 4. Fig. 6 shows the plot of $\log[\text{CO}]$ vs. $\log[\text{NO}_x]$ and a solid line in the Fig. 6 is for the best results. Examples of the best results obtained so far are listed in Table 5. By comparing Table 3 and 5, it can be realized that the best catalyst NiO is effective in higher oxygen balance region for reducing CO and NO_x and the catalyst CoMoO₄ is not effective in lower oxygen balance region.

**Table 4 Examples of effect of catalyst in AKCSSi on CO and NOx
in the effluent gas**

Composition:							Mass	CO	NOx
ADCA	KClO ₄	CuO(B)	Starch	SiO ₂	KNO ₃	Catalyst	in g	in ppm	in ppm
45	60	10	1.5	1.0	-	-	30	15,000	1,200
45	60	5	1.5	1.0	-	5(Cr ₂ O ₃)	30	10,000	1,750
45	60	5	1.5	1.0	-	5(Ni)	30	17,000	1,100
45	65	5	1.5	1.0	-	5(Fe ₃ O ₄)	30	12,000	1,300
45	55	10	1.5	1.0	10	-	30	4,200	2,600
45	65	10	1.5	1.0	-	-	30	10,000	1,300
45	55	10	2.0	1.0	10	5(CoWO ₄)	30	3,800	2,800
45	55	10	2.0	1.0	10	5(NiO)	30	3,000	1,900
45	55	10	2.0	1.0	10	5(V ₂ O ₅)	30	2,500	2,000
45	55	10	2.0	1.0	10	5(MoO ₃)	30	7,500	2,200
45	55	10	2.0	1.0	10	5(WO ₃)	20	3,300	1,800
45	55	10	2.0	1.0	10	5(Fe ₂ O ₃)	20	6,000	1,800
45	55	10	2.0	1.0	10	5(Fe ₃ O ₄)	20	1,600	2,300
45	55	10	2.0	1.0	10	5(Fe ₃ O ₄)	30	1,300	3,800
45	55	10	2.0	1.0	10	5(Pb(NO ₃) ₂)	20	2,800	2,400
45	55	10	2.0	1.0	10	5(NiMoO ₄)	20	3,500	2,000
45	55	10	2.0	1.0	10	5(CoMoO ₄)	20	4,200	2,000
45	55	10	1.5	1.0	5	10(NiO)	30	6,500	1,500
45	65	10	1.5	1.0	10	10(NiO)	30	3,000	2,600
45	55	10	2.0	1.0	10	5(V ₂ O ₅)	30	3,500	2,300
45	55	10	1.5	1.0	5	10(V ₂ O ₅)	30	6,500	1,600
45	55	10	1.5	1.0	5	5(V ₂ O ₅)	30	4,000	2,600
45	55	10	2.0	1.0	10	5(MoO ₃)	30	3,700	2,000
45	55	10	2.0	1.0	10	5(NiO)	40	2,800	2,300
45	55	10	1.5	1.0	5	10(NiO)	40	5,200	2,100
45	55	10	2.0	1.0	5	10(NiO)	40	7,800	2,200
45	55	10	1.75	1.0	7.5	7.5(NiO)	40	5,600	2,400
45	55	10(A)	1.5	1.0	0	5(NiO)	40	5,600	2,400

Table 5 Examples of best AKCSSiN-Catalyst compositions for low CO and NOx

ADCA	KClO ₄	CuO	Starch	SiO ₂	KNO ₃	Catalyst	Mass in g	CO in ppm	NOx in ppm
45	55	10(B)	2.0	1.0	10	5(NiO)	30	2100	1700
45	55	10(A)	1.5	1.0	0	5(CoMoO ₄)	30	1430	450

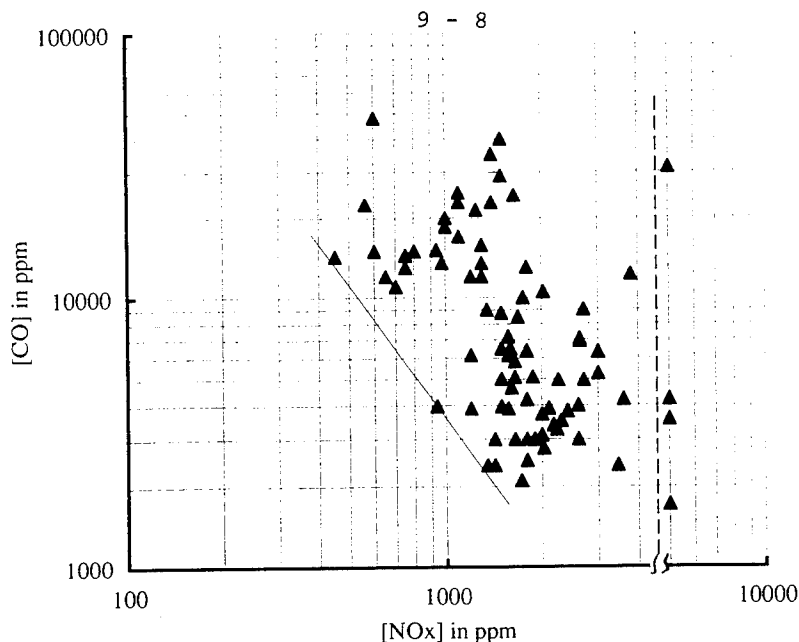


Fig. 6 Plot of $\log[\text{CO}]$ vs. $\log[\text{NO}_x]$ for 30g AKC(SiN+Catalyst gas generant in 60L tank test

Effect of External Oxidizers

It has been tried to reduce CO in the effluent gas by adding an external oxidizer in the combustion chamber or in the coolant chamber. The positions of the external oxidizers placed in the model inflator are shown in Fig. 7.

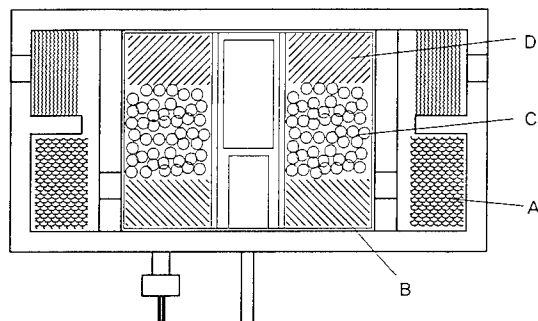


Fig. 7 Positions of outside oxidizer

Results are listed in Table 6 and shown in Fig. 8. The solid KClO_3 deposited on the coolant reduced CO significantly, but increased NO_x . KNO_3 powder in the position D had the similar effect as KClO_3 solid in the coolant chamber. KNO_3 and KClO_3 granules mixed with the gas generant were very effective for reducing CO, but increased NO_x significantly. So far the best result was obtained from the mixture of 30g AKC(B)SSi pellets and 20g KNO_3 pellets. In this method CO can be reduced without increasing NO_x .

Table 6 Effect of external oxidizers(E/O) on the CO and NOx in the effluent gas ADCA/KClO₄/CuO/Starch/SiO₂=45/55/10/1.5/1.0

CuO, X	AKCSSi Mass in g	E/O	Mass in g	Shape	Position	CO in ppm	NOx in ppm
A	30	-	-	-	-	13.500	600
A	30	KClO ₃	5	Solid	A	9.500	850
A	30	KClO ₃	10	Solid	A	8.000	850
A	30	KClO ₃	18	Solid	A	6.000	950
A	35	KClO ₃	20	Solid	A	8.000	850
A	30	KClO ₃	15	Solid	A	6.500	750
A	30	KClO ₃	10	Powder	B	9.500	950
A	30	KClO ₃	10	Powder	B	10.500	500
A	30	KNO ₃	10	Powder	D	10.000	750
A	30	KNO ₃	10	Powder	C	12.000	1.200
A	40	KNO ₃	10	Granule	C	8.000	1.500
A	40	KNO ₃	20	Granule	C	6.500	>2.000
A	40	KNO ₃	20	Granule	C	7.000	>2.000
	40	NaClO ₃	20	Solid	A		
A	40	KNO ₃	20	Powder	D	4.000	2.000
B	30	-	-	-	-	12.000	1.000
B	25	KNO ₃	20	Disk	D	9.000	750
B	30	KNO ₃	20	Pellet	C	3.000	700
B	40	KNO ₃	20	Powder	D	9.000	600
B	40	KNO ₃	20	Granule	C	4.000	2.000
B, +KNO ₃ (10)	30	-	-	-	-	6.000	1.700
B, +KNO ₃ (10)	30	KNO ₃	10	Granule	C	2.500	>4.000
B, +KNO ₃ (10)	30	KClO ₃	10	Granule	C	1.000	4.000

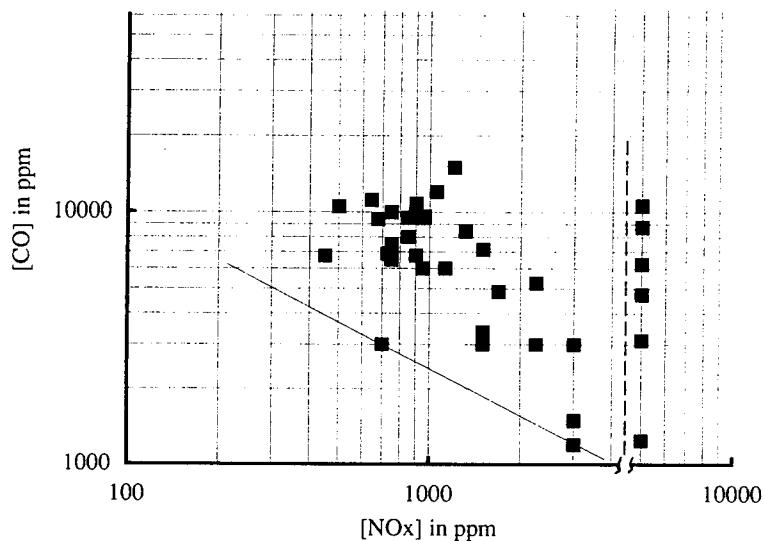


Fig. 8 Plot of log[CO] vs. log[NOx] for 30g AKCSSiN+External oxidizer in 60L tank test

Overall Evaluation

Three lines for the best results are shown Fig. 9. Some catalysts were effective in higher NO_x region, but not in low NO_x region. Some external oxidizers which were mixed with the gas generant pellets in pellet or granule form were very effective for reducing CO and NO_x in the effluent gas from the combustion of ADCA gas generant.

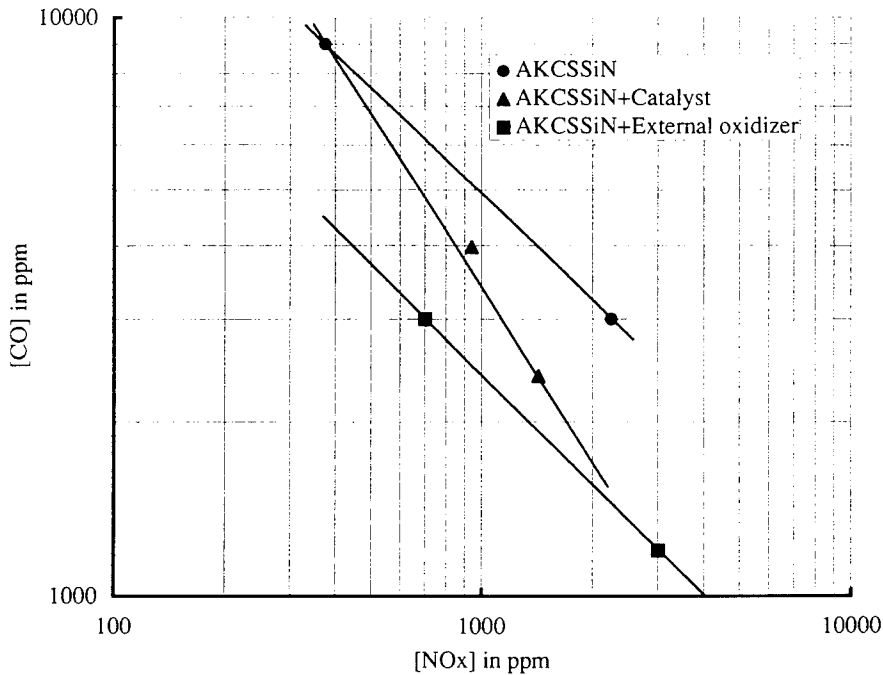


Fig. 9 Three lines for best results of AKCSSLiN, AKCSSLiN+Catalyst and AKCSSLiN+External oxidizer

Other Factors influencing to CO and NO_x Concentrations

CO and NO_x concentrations in the effluent gas was influenced by several other factors. Incomplete combustion of the pellets gave higher concentration of CO. Bursting of the inflator by the excessive pressure gave lower concentrations of both CO and NO_x.

REFERENCES

- 1) K. Hara, T. Misawa, T. Maekawa, S. Iyoshi, T. Yokoyama, T. Kazumi, M. Hayashi and T. Yoshida, "Concept and Performance of a Non - azide Propellant for Automotive Airbag Inflators", The 19th International Pyrotechnics Seminar, 20-25 February, 1994, Christchurch, New Zealand; Propellant, Explosive and Pyrotechnics, in Contribution.
- 2) T. Kazumi, K. Hara, Y. Yu, Y. Yamato, T. Takashi, Y. Shimizu and T. Yoshida, "Safety Aspect of a Non - azide Propellant for Automotive Airbag Inflators", *ibid.*, Energetic Materials, in Contribution.
- 3) Y. Yamato, T. Takahori, S. Iyoshi, Y. Shimizu, K. Hara, T. Kazumi, Y. Yu and T. Yoshida, "Evaluation of a Non - azide Propellant for Automotive Airbag Inflators on Environment and Health", *ibid.*
- 4) J. Kishimoto, M. Hayashi and T. Yoshida, "Simulation of Non - azide Gas Generant for Automotive Airbag Inflators", Proceedings of the 19th International Pyrotechnics Seminar, 20 - 25 February, 1994, Christchurch, New Zealand, p.517-530.
- 5) K. Hara, Y. Shimizu, K. Higashi, T. Nojima, T. Hasegawa and T. Yoshida, "Hazard Analysis of Manufacture of a Non - azide Propellant for Automotive Airbag Inflators", Proceedings of the 20th International Pyrotechnics Seminar, 25-29 July, 1994, Colorado Springs, USA, p.381-396.

**DAS SELBSTSCHUTZSYSTEM MASKE, EIN MUNITIONSSYSTEM MIT KOMBI-
NIERTER NEBEL-WIRKUNG IM SICHTBAREN UND INFRAROTEN BEREICH DES
ELEKTROMAGNETISCHEN SPEKTRUMS**

**THE SELF-PROTECTION SMOKE SYSTEM MASKE WITH COMBINED EFFICACY
IN THE VISIBLE AND INFRARED SECTIONS OF THE ELECTROMAGNETIC
SPECTRUM**

Carl Hug, SM Schweizerische Munitionsunternehmung, Allmendstrasse 74, CH-3600
Thun

Johannes Grundler, BUCK System GmbH, Hans-Buck Strasse 1, D-79395 Neuen-
burg / Baden

ABSTRACT

Presentation of the novel type smoke munition MASKE, developed in cooperation between SM Swiss Munition Enterprise and BUCK System GmbH. Its concept and characteristics will be discussed. The system provides instantaneous and sustained protection against sensors in the visible, near and thermal infrared sections of the electromagnetic spectrum. It is fired from 76 mm launcher systems already mounted on existing AFV's in series.

The concept of this ammunition is based on the sequential functions of an instantaneous flare module and a sustained smoke burner. Both modules are fired simultaneously from the same cartridge, but follow different trajectories with different ignition points. All system parameters are matched to obtain optimal screening.

The development of the smoke system MASKE has been initiated by the Swiss Army in 1993. The system now available will become the standard smoke ammunition on several AFV's of the Swiss Army in 1996/97.

Einleitung und Uebersicht

Die neuartige Nebelmunition MASKE soll in einem zweiteiligen Vortrag vorgestellt werden. Ein erster Vortragsteil wird dem Munitionskonzept, Einsatzmöglichkeiten und Schnittstellen zu den Werferanlagen gewidmet sein. Der nachfolgende, zweite Teil wird vornehmlich die Leistungen dieser Nebelmunition im sichtbaren und infraroten Teil des Spektrums diskutieren.

Das Konzept

Mit dem Munitionssystem MASKE soll ein Selbstschutzsystem für Kampffahrzeuge realisiert werden, wie es den Anforderungen auf dem heutigen Gefechtsfeld entspricht. Diese Anforderungen werden dominiert durch den wünschbaren Einsatz von Selbstschutzmitteln in Duellsituationen. Die vorliegende Bedrohung hat dabei ihren Ursprung in der Wahrnehmung der Signale des sichtbaren und infraroten Teils des elektromagnetischen Spektrums durch Visiereinrichtungen oder Sensoren. Mit der raschen und effizienten Unterbrechung dieser Wahrnehmung entfällt die Hauptbedrohung des Kampffahrzeuges durch direkt gerichtete Waffen.

Im Gegensatz zu den eingeführten Nebelsystemen mit ausschliesslicher Wirkung im sichtbaren Teil des elektromagnetischen Spektrums vermag MASKE sowohl im visuellen als auch im infraroten Bereich eine deckende Nebelwirkung zu entfalten.

Das System MASKE erfüllt die Forderung nach einer innerhalb weniger Sekunden vorhandenen und über eine definierte Zeit aufrechtzuerhaltende Nebeldeckung.

Das System wird in Salven aus den auf den Kampffahrzeugen vieler Nationen eingeführten Werferanlagen vom Kaliber 7.6 cm verschossen, kann jedoch auch auf andere Kaliber angepasst werden. Die hierzu notwendigen Modifikationen an den Werferbechern sind minimal.

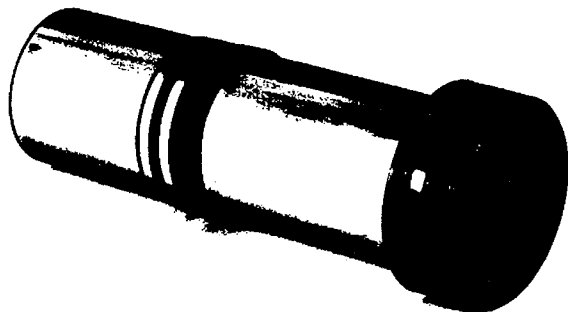
Die Entwicklungsgeschichte

Das im Auftrag der Schweizer Armee entwickelte System MASKE ist in einer Kooperation der beiden Firmen BUCK SYSTEM GMBH und SM SCHWEIZERISCHE MUNITIONSUNTERNEHMUNG, vormals MFT Munitionsfabrik Thun, in sehr kurzer Zeit realisiert worden.

Anschliessend an eine Machbarkeitsstudie im Jahre 1990, wurde im Mai 1993 mit der eigentlichen Entwicklung des Systems begonnen. Bereits im Sommer 1993 waren erste Versuchsmuster zur Erprobung vorhanden. Im Jahr 1994 wurde eine Funktionsmusterserie aufgelegt, eingehend erprobt und dem Auftraggeber zur Beurteilung vorgeführt. Aufgrund der ausgezeichneten Ergebnisse konnte bereits im Dezember 1994 die Phase Prototypserie freigegeben werden. Sie ist mittlerweile abgeschlossen.

Zurzeit befindet sich die Vorserie in der Technischen Erprobung und Truppenerprobung durch die Schweizer Armee. Wie in der Planung vorgesehen, wird im Herbst 1995 die entsprechende Beschaffungsreifeerklärung vorhanden sein und das System bereits 1996 eingeführt.

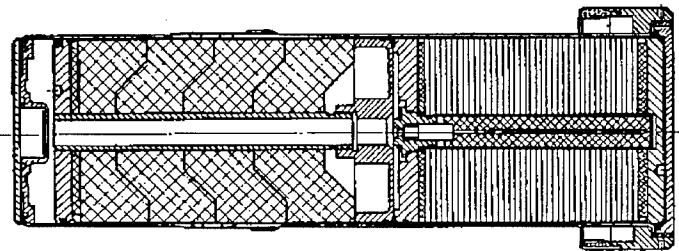
Während der kurzen zweieinhalb-jährigen Entwicklungszeit konnte das System mehrmals den Beschaffungsinstanzen der Bundeswehr und der Schweizer Armee präsentiert werden, letztmals im März und Mai dieses Jahres. Diese wertvollen Kontakte haben es uns in allen Entwicklungsphasen ermöglicht, die Bedürfnisse der Kunden optimal in das Produkt MASKE einfließen zu lassen.



Figur 1 : Die Selbstschutzmunition 7.6 cm MASKE

Das Produkt

Beim System MASKE handelt es sich um eine patronierte Munition. Sie birgt eine Treibladungskammer im Bodenteil der Patrone sowie zwei Wirkmodulen, die sogenannten Täusch- und Tarnmodule. Die Zündung erfolgt durch eine mit den aussen an der Patrone liegenden Kontaktringen verbundene Zündpille.



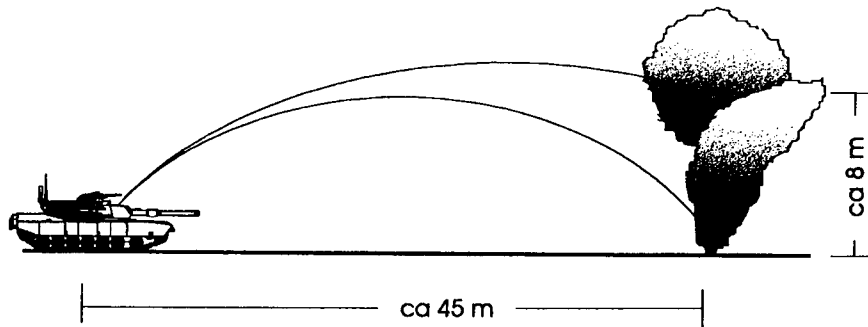
Figur 2 : Modularer Aufbau der Selbstschutzmunition 7.6 cm MASKE

Tarn- und Täuschmodul enthalten unterschiedliche Wirksubstanzen und entfalten ihre Wirkung in unterschiedlicher zeitlicher Abfolge

- das Täuschmodul nach < 3 Sekunden als Blendkomponente kurzer Wirkdauer
- das Tarnmodul als Langzeitnebler

Die zeitliche Abfolge beider Wirkungen ergibt eine durchgehende, visuell und infra-rot undurchsichtige Deckung während typisch 50 Sekunden.

Für das System Maske charakteristisch ist seine Ballistik ; Täusch- und Tarnmodul werden gleichzeitig aus dem Werferbecher verschossen und bewegen sich auf unterschiedlichen Flugbahnen zum Ort ihrer Wirkung. Die nachfolgend schematisch dargestellte Ballistik des Systems ist dabei so abgestimmt, dass die beiden Module ihre Wirkung vertikal untereinander entfalten.



Figur 3 : Ballistik von Tarn- und Täuschmodul im System MASKE

Das Täuschmodul wird in über 10 m Höhe zerlegt und überstrahlt die Kampffahrzeugsignatur grossflächig. Das Tarnmodul dagegen entfaltet seine Wirkung als Bodennebler unterhalb des Detonationspunktes der Täuschladung.

Die so definierte Ballistik wird über einen ausgeklügelten Mechanismus der Ladungstrennung während des Abschusses gesteuert. Er beruht auf dem Vorhandensein verschieden gestalteter Gasräume im Bodenteil der Patrone, als Bohrung durch das Tarnmodul und als Expansionsraum zwischen Tarn- und Täuschmodul. Letzterer erzeugt eine Ladungstrennung durch differentiell unterschiedliche Kräfte auf Tarn- und Täuschmodul.

Als Ergebnis dieses Abschusskonzeptes folgt eine im Temperaturbereich -35 C bis +63 C funktionierende Ballistik. Die Ausbringdistanz ist dabei je nach den vorliegenden Anforderungen im Bereich von 30 m - 50 m problemlos variierbar.

Das Verwenden einer patronierten Munition erlaubt eine maximale Erhöhung der abgeschossenen Wirkmassen, da nur diese selbst beschleunigt werden müssen. Sie erlaubt zudem eine Reduktion der Druckbelastung im Werferbecher. Trotz der im Vergleich zur bisher eingeführten Nebelmunition wesentlich höheren totalen Wirkmasse ergibt sich mit Hilfe der Patronierung eine wesentlich kleinere Belastung des Werfers.

Die Patronierung hat zudem den Vorteil, dass die Werferbecher durch keinerlei Rückstände verschmutzt werden. Die elektrische Zündung über die an der Aussen-seite der Patrone angebrachten Kontakttringe ist damit mit hoher Sicherheit gewährleistet.

Die Abschussanlagen

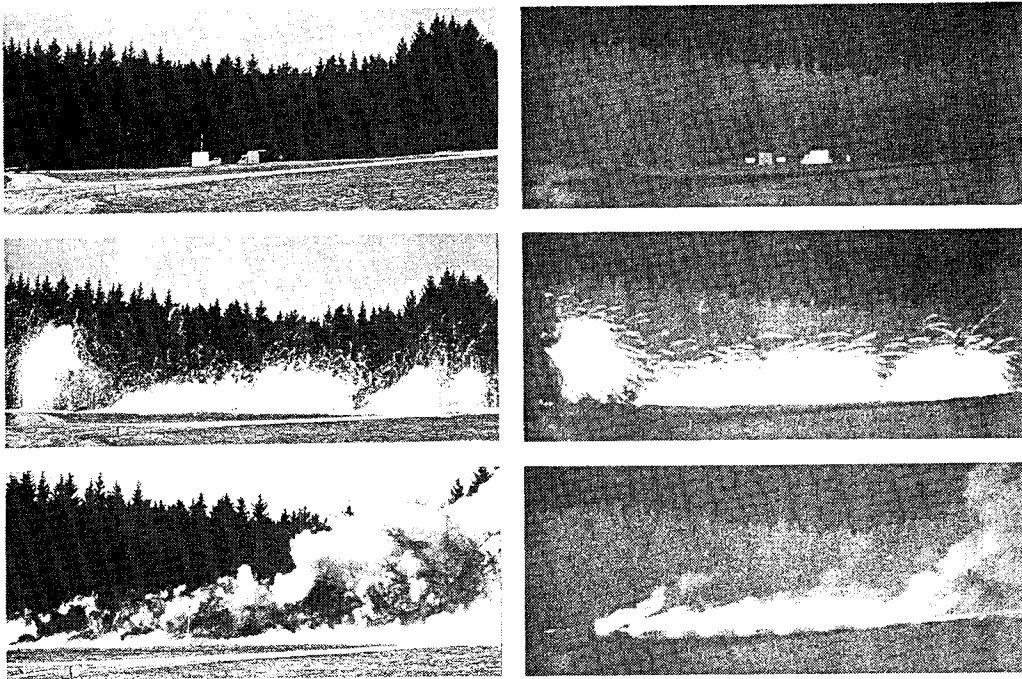
Das System MASKE ist so konzipiert, dass es aus den zahlreich eingeführten Wegmann-Nebelwerferanlagen verschossen werden kann. Das durch die Becher vorgegebene Werfervolumen wird dabei im Gegensatz zu den bereits eingeführten Nebelsystemen vollständig ausgenutzt. Dies bedingt eine geringfügige Modifikation des Bodenteils der Werferanlage. Das bisherige Bodenteil, das mit einem in den Werfer hineinragenden Zapfen den notwendigen Expansionsraum im Bodenteil des Bechers sicherstellte, kann durch ein wesentlich einfacheres Bodenteil ersetzt werden. Da dieses aufgrund der Patronierung der MASKE-Munition nur schwach belastet wird, können sogar Kunststofflösungen in Betracht gezogen werden.

Mit einer Anpassung der seitlichen Werferfächerung ergibt sich eine vollständig optimierte Leistung des Selbstschutzsystems MASKE. Auch bei einem Verzicht auf eine modifizierte Fächerung ist jedoch die Ballistik der MASKE-Munition so anzupassen, dass eine vollständige Nebeldeckung von ausreichender Breite erreicht wird, um eine taktische Absetzbewegung des Fahrzeuges zu gewährleisten.

Im Rahmen der Schweizer Armee ist eine Beschaffung des Systems MASKE in erster Priorität für die folgenden mit 2 x 4 bzw. 2 x 3 Werferanlagen ausgerüsteten Fahrzeuge vorgesehen :

- Panzer 87 Leopard
- Schützenpanzer M109
- Panzerjäger Mowag

Weitere Fahrzeuge werden längerfristig in die Beschaffung einbezogen. Ausgegangen wird dabei von einer angepassten Seitenfächerung der Werferanlagen. Im Falle des Panzer 87 Leopard soll zudem die Fähigkeit zu einer Zweitsalve ohne Nachladen durch die Auffächerung der zweiten turmparallelen 2 x 4 Werfer erzielt werden.



Figur 4 : Wirksequenz des Systems MASKE
links : visueller Bereich, rechts : infraroter Bereich

Die Wirksamkeit des Täuschmoduls

Beim Täuschmodul handelt es sich um ein Nebelmodul, das auf der Verwendung von rotem Phosphor basiert. Die Phosphorrezeptur wird in einem umweltverträglichen Herstellungsprozess in wässriger Phase auf ein Trägermaterial aufgebracht und anschliessend getrocknet. Die Schichtdicken, die hierbei Verwendung finden,

liegen im Bereich von einigen 100 µm. Nach entsprechender Konfektionierung - in diesem Falle Schneiden des beschichteten Trägermaterials und Vorfragmentierung der Wirkpartikel - werden die sogenannten Flare-Partikel in eine dünnwandige Metalldose laboriert. Die Initiierung der Flare-Partikel beim Einsatz erfolgt über eine zentral liegende Anzündzerlegerladung, die sich über die gesamte Länge des Täuschmoduls erstreckt. Diese Anzündzerlegerladung beinhaltet ein schadstoffarmes pyrotechnisches Verzögerungselement, das nach der vordefinierten Zeit die Anzündzerlegerladung aktiviert. Diese wiederum öffnet die Aussenhülle des Täuschmoduls und zündet gleichzeitig die Flare-Partikel an. Im vorliegenden Fall findet diese Zerlegung in 10 bis 15 m Höhe statt. Die kleinen und leichten Partikel werden brennend in der Luft verteilt, wobei sich im Moment der Zerlegung eine Wolke von über 10 m Durchmesser ergibt. Die anfänglich homogen in dieser Wolke verteilten Flare-Partikel sinken langsam zu Boden. Die Wirkung im sichtbaren Bereich erfolgt aufgrund der bekannten Eigenschaften von Phosphor über Streueffekte, die Wirkung im infraroten Bereich erfolgt mittels Ueberstrahlung. Dabei geben die vielen kleinen Flare-Partikel Infrarot-Strahlung ab, die im ganzen Spektralbereich von 0,8 bis 15 µm wirksam ist. Die beim Abbrand auftretende Infrarot-Strahlung überstrahlt die Strahlungen sowohl des Zieles - in diesem Fall des schiessenden Gefechtsfahrzeuges - als auch des Hintergrundes. Für den Beobachter, der mittels blossen Auge das Szenario betrachtet, ist eine grosse weisse Phosphornebelwand zu erkennen, während ein mit Wärmebild ausgerüsteter Beobachter eine helle unstrukturierte Fläche erkennt, hinter der sich das Ziel verbirgt.

Prinzipiell hält die Infrarot-Wirkung des Täuschmoduls für die Zeit an, in der sich genügend aktive Flare-Partikel in der Luft befinden. Feldversuche zur Wirksamkeit haben jedoch gezeigt, dass - auch nach dem Auftreffen der Flare-Partikel auf dem Boden - noch eine gewisse Täuschwirkung vorhanden ist. Dies erklärt sich dadurch, dass auch beim Abbrand am Boden noch warme Nebelschwaden produziert werden, die noch wirksam im Infraroten sind. Die Wirksamkeit des Phosphors im sichtbaren Bereich hält während der gesamten Brennzeit, d.h. für ca 50 s, an.

Zur optimalen Wirksamkeit des Gesamtsystems wird zur Ergänzung des Täuschmoduls das Tarnmodul als die zweite Komponente des Selbstschutznebelkonzeptes zur Wirkung gebracht.

Die Wirksamkeit des Tarnmoduls

Das Tarnmodul ist im Gegensatz zum Täuschmodul ein Punktnebler, der am Boden liegend abnebelt. Das MASKE-Konzept bietet den Vorteil, dass das Täuschmodul die Spontankomponente bietet, während das Tarnmodul als ortsgebundenes System auch unter schwierigen Bedingungen die Schutzfunktion am beabsichtigten Ort aufrechterhält.

Das Tarnmodul ist ein Nebelsystem, das aus Nebelpresslingen besteht, die lange Zeit wirksam sind. Die Reaktions- bzw. Anbrennzeiten dieser Presskörper sind so bemessen, dass die optimale Wirksamkeit des Tarnmoduls beim Nachlassen der Wirksamkeit des Täuschmoduls einsetzt.

Die Nebelpresslinge sind in eine dünnwandige Metalldose eingesetzt und werden mittels einer Anzündladung über den gesamten Querschnitt angezündet. Die Nebelkörper brennen als Stirnbrenner ab und geben dabei die wirksamen Kohlenstoffpartikel in die Luft ab. Bei diesen Kohlenstoffpartikeln handelt es sich um in den Nebelkörpern vorhandene nicht-toxische, aromatisch kondensierte Kohlenstoffverbindungen, die beim Abbrand umgewandelt und freigesetzt werden. Die Wirkung dieser Kohlenstoffverbindungen besteht in Ueberstrahlung, ähnlich zu der Wirkung des Täuschmoduls. Hinzu kommen beim Tarnmodul jedoch auch noch Dispersions- und Absorptionseffekte. Diese Effekte treten je nach Situation (Sonneneinstrahlung, Wind) in signifikant unterschiedlichen Anteilen auf. Eine Trennung und Quantifizierung auf allgemein gültiger Basis ist derzeit noch nicht möglich, entsprechende Arbeiten dauern noch an.

Die Wirksamkeit des Gesamtsystems

Die Wirksamkeit des Nebelwurfkörpers MASKE basiert im sichtbaren und infraroten Bereich auf den Wirksamkeitsprinzipien, wie sie oben geschildert wurden.

Die beiden Wirkmodule werden dabei so ausgebracht, dass sich eine Nebelwand ergibt, die im sichtbaren Bereich eine Breite von ca. 100 m und eine Höhe von ca. 10 m erreicht. Im infraroten Bereich ergeben sich, wie zahlreiche Feldversuche gezeigt haben, Nebelwandabmessungen von ca. 85 m Breite und 5 m Höhe, wenn die vor-

handene Nebelmittelwurfanlage unverändert verwendet wird. Mit der eingeführten 76 mm Nebelmittelwurfanlage sind Wirkzeiten von mindestens 50 s nachgewiesen.

Die Oekotoxikologie der pyrotechnischen Komponenten wurde bereits untersucht und bewertet. Das Täuschmodul wird dabei als gering toxisch (Wassergefährdungsklasse WGK 1) in der aquatischen Phase beurteilt, während das Tarnmodul als nicht-toxisch eingestuft wird. Aufgrund dieser Beurteilung steht dem Einsatz des Nebelwurfkörpers MASKE auch für Ausbildungs- und Übungszwecke nichts entgegen.

Mit dem Selbstschutznebel MASKE steht ein modernes Nebelsystem zur Verfügung, das zusätzlich zur Wirksamkeit im Sichtbaren auch im infraroten Bereich deckend ist und universell eingesetzt werden kann.

MESSUNGEN DES ENERGIEBEDARFS VON BRÜCKENANZÜNDPILLEN BEI NIEDRIGEM
SPANNUNGSNIVEAU

Manfred Held

TDW Gesellschaft für verteidigungstechnische Wirksysteme mbH
86523 Schrobenhausen, Germany

ABSTRACT

Es werden die verschiedenen Verfahren, mit denen Anzündpillen, elektrische Detonatoren oder allgemein Elektro-Explosive-Elemente auf ihren zum Ansprechen notwendigen Energie- bzw. Leistungsbedarf untersucht werden können, besprochen.

Die Meßmethode muß sich nach der Art der Energiequelle richten. Es ist ein Unterschied, ob die in einem Kondensator gespeicherte Ladungsmenge ein galvanisches Element mit konstanter Spannung oder ein magnetischer Stoßgenerator mit eingprägtem Strom das Elektro-Explosive-Element zum Ansprechen bringen soll.

Selbst die älteste Bauart einer Anzündpille, nämlich mit Brücken-draht, wie sie die P 65 Anzündpille repräsentierte, zeigt, wenn man sie nach den verschiedenen Methoden belastet, eine Reihe von interessanten Effekten, insbesondere in ihrem zeitlichen Ansprech-verhalten, welche nachfolgend eingehend diskutiert werden.

SUMMARY

We discussed the various methods to investigate the power necessary to ignite squibs or electro-explosive devices in general. The method of measurement has to be chosen according to the kind of energy source. It makes a difference if the energy stored in a capacitor, a galvanic element with constant voltage, or a magnetic generator with fixed current has to ignite an electro-explosive device.

1. Energiebestimmung durch Kondensatorentladung

1.1 Grenzenergie

Da in Zündschaltungen zumeist die in einem Kondensator gespeicherte Energie auf die Anzündpille oder den elektrischen Detonator geschaltet wird, wird der notwendige Energiebedarf von "Elektro-Explosiven-Elementen" - englisch "Electro-Explosive-Devices (EED)" - ebenfalls meistens mittels Kondensatorentladung bestimmt. Die im Kondensator gespeicherte Energie E_C (in Joule) wird durch die Beziehung

$$E_C = 1/2 C U^2 \quad (1)$$

berechnet, wobei die Kapazität C in Farad und die Spannung U des aufgeladenen Kondensators in Volt eingegeben werden. Diese in einem Kondensator gespeicherte Energie E_C wird möglichst mit einem prellfreien Schalter über die Anzündpille entladen.

Bei einer vorgewählten Kapazität C wurde hierbei durch schrittweises Erhöhen der Spannung U des Kondensators der Grenzenergiebedarf der Anzündpille bestimmt, wobei nach jeder Entladung der Widerstandswert der Anzündpille nachgeprüft wurde.

Durch diese Mehrfachbelastung der Anzündpillen oder der elektrischen Detonatoren können diese allerdings "formiert" werden, d.h., je nach Aufbau der Anzündpillen oder der elektrischen Detonatoren kann sich die Ansprechempfindlichkeit zu höheren oder niedrigeren Werten verschieben. Als Käufer von Anzündpillen kann man meist nicht mit allzu großen Stückzahlen arbeiten und alle Versuche mit unbelasteten Anzündpillen durchführen, um z.B. die statistische 50 %-ige Ansprechschwelle zu bestimmen. Bei dem kostensparenden Verfahren der Mehrfachbelastung muß man sich jedoch überzeugen, daß sich die Grenzwerte durch die Mehrfachbelastungen nicht allzu stark verschieben. Bei der Anzündpille P 65 konnte kein Einfluß der Ansprechempfindlichkeit durch diese mehrfache Belastung festgestellt werden.

Den Zündkreis mit dem Netzgerät, einem Vorschaltwiderstand R_V , dem Kondensator C und dem Quecksilberschalter Hg zeigt Fig. 1. Die Verwendung von Quecksilberschaltern ist notwendig, da mechanische Schalter nicht prellfrei arbeiten und die Ladung des Kondensators sozusagen tröpfchenweise abgegeben werden kann, ohne daß die Anzündpille ansprechen muß. Mit dem Zündimpuls wurde ein Oszillograph getriggert, mit dem der Spannungsabfall U an der

Anzündpille und gleichzeitig mittels einer Stromzange der Stromverlauf I registriert wurde. Mit dem Zündimpuls wurde auch ein Counter gestartet. Dieser Counter wurde durch den Lichtblitz der angesprochenen Anzündpille mittels einer Siliciumphotodiode (SGD 100) über einen Verstärker und eine Triggereinheit (Lichttrigger) wieder gestoppt, so daß gleichzeitig die Zeitdifferenz zwischen Anlegen der Spannung und Auftreten einer Lichtemission an der Anzündpille gemessen wurde.

Die Meßpunkte der mindestens notwendigen Energie E_C als Funktion der Kapazität C sind in das Diagramm Fig. 2 eingetragen. Die im Datenblatt der ehemaligen Firma Gevelot angegebene Grenzenenergie für die P 65 von ca. 3 mJ wird, wie Fig. 2 zeigt, bei Kondensatorentladungen im Kapazitätsbereich von 10 μF bis 100 μF leicht unterschritten. Bei 0,1 μF liegt der Energiebedarf allerdings bei etwa 3,5 mJ. Dies ist eine Folge der nicht genügenden elektrischen Anpassung an die niederohmige Anzündpille, wie die nachfolgenden Oszillogramme aufzeigen. Das Ansteigen des Energiebedarfes bei der Kondensatorkapazität von 1000 μF liegt an den nicht idealen Kondensatoren bei diesen großen Werten. Sie weisen bereits bei diesen kleinen Außenwiderständen einen nicht mehr zu vernachlässigenden Innenwiderstand auf, so daß die Klemmenspannung am Kondensator, die der Berechnung des Energiebedarfes zu Grunde gelegt wird, nicht dem wirklichen Spannungsabfall an der Anzündpille entspricht.

Außerdem benötigen Anzündpillen eine bestimmte Energie in einer bestimmten Zeit, also eine bestimmte Leistung, damit sie ansprechen. Man kann diese Anzündpille mit einem Strom von 0,05 A beliebig lange belasten, - hierbei geht die angebotene Energiemenge gegen unendlich - ohne daß die Anzündpille anspricht. Bei einem Widerstand von 2 Ω der Anzündpillen fallen bei 0,05 A Stromfluß 0,1 V Spannung daran ab, so daß nur 0,005 W (Leistung $N = U \cdot I$; $[W] = [V] \cdot [A]$) daran wirken. Diese geringe Leistung reicht wegen der immer gegebenen Wärmeableitung an den Zuleitungsdrähten und durch das Zündgemisch nicht aus, den Brückendraht auf die Zündtemperatur des Anzündgemisches aufzuheizen.

Aus dem Verlauf des Spannungsabfalles an den Anzündpillen und aus dem Stromverlauf, die mit einem Zweistrahls-Oszillographen registriert wurden, konnte das Entladungsverhalten der Kondensatoren

überprüft werden. Der Spannungsabfall nach einer e-Funktion für die Kapazitäten von 100 μF und 10 μF kann der Fig. 3 entnommen werden. Das Durchschwingen der Stromkurve kommt daher, daß eine Stromzange verwendet wurde. Das Überspringen des Spannungsverlaufes bei den Kapazitäten von 1 μF und besonders bei 0,1 μF (Fig. 4) stammt von der ungenügenden Anpassung des elektrischen Entladekreises mit den verwendeten Bauteilen und der Anordnung an diese niederohmigen Anzündpillen.

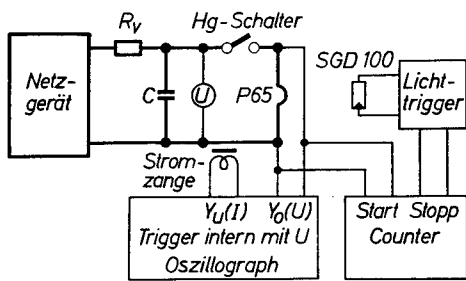


Fig. 1

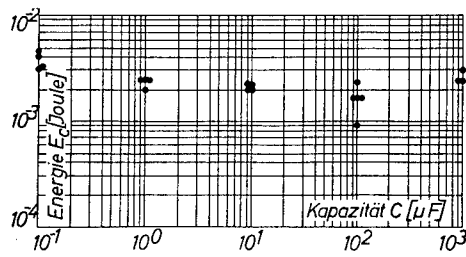


Fig. 2

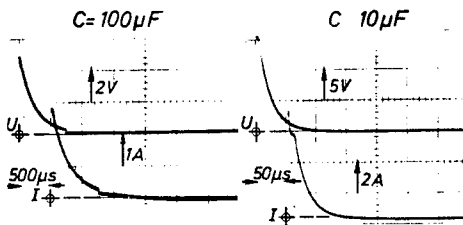


Fig. 3

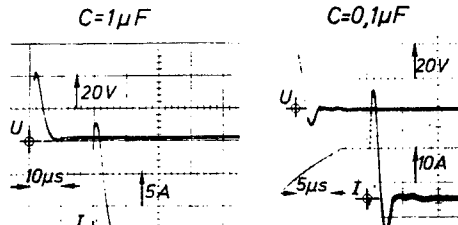


Fig. 4

1.2 10-fache Energie

Weiterhin wurde die Anzündzeit dieser Anzündpille mit dem 10-fachen Wert der Grenzenergie, also dem 3,1-fachen der Spannung gegenüber der Grenzspannung bei den verschiedenen Kapazitätswerten bestimmt. Hierbei ergaben sich einige bemerkenswerte Erscheinungen. Die als Beispiel wiedergegebenen Oszillogramme der 1000 μF -Entladung (Fig. 5 links - 2 Versuche) zeigen eine Unterbrechung des Brückendrahtes nach 0,42 ms bzw. 0,70 ms. Die Lichtmission

hierbei trat nach einer Zeitverzögerung t_{L-3U} von 5,9 ms bzw. 6,7 ms auf.

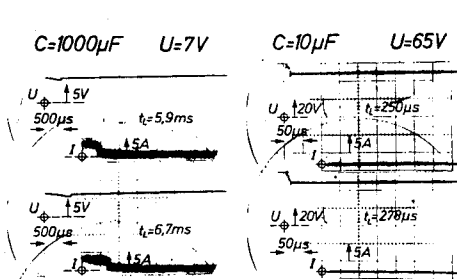


Fig. 5

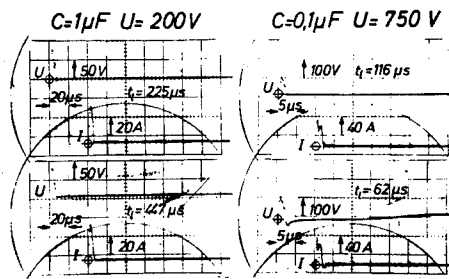


Fig. 6

Diese Oszillogramme zeigen außerdem deutlich, daß die Kondensatoren mit dieser großen Kapazität nicht den gewünschten niederohmigen Aufbau aufwiesen, wie er für derartige Untersuchungen benötigt wird, denn die Spannung bricht um etwa 15 % bei der Belastung an dem 2 Ω -Widerstand der Anzündpille zusammen. Nach Unterbrechung des Brückendrahtes steigt die Spannung im Oszillogramm wieder auf die Leerlaufspannung am Kondensator an.

Bei 10 μF hat sich die Kapazität ebenfalls nur zu einem geringen Bruchteil entladen. Hier wird der Brückendraht im Mittel bereits nach 15 μs unterbrochen, während die Lichtemission im Mittel nach 260 μs auftritt (Fig. 5 rechts).

Das Spannungsniveau beträgt bei der Kapazität von 1000 μF 7 V und bei 10 μF erst 65 V. Diese Spannungswerte steigen jedoch bei 1 μF auf 200 V oder bei 0,1 μF sogar auf 750 V an. Bei diesen hohen Spannungen entladen sich diese kleinen Kapazitäten vollständig, wie die Oszillogramme der Fig. 6 zeigen. Der Brückendraht wird bei 1 μF in 5 μs und bei 0,1 μF in 2 μs unterbrochen. Bei diesen hohen Spannungswerten tritt offensichtlich eine "Drahtexplosion" ein, so daß die gesamte gespeicherte elektrische Energie dann als Funkenentladung abgegeben wird.

Trotz dieser Drahtexplosion betragen die Verzögerungszeiten für die Lichtemission jedoch im Mittel 240 μs für 1 μF und 95 μs bei 0,1 μF . Die Zeitkonstanten der Entladekreise sind kürzer, bzw. in der gleichen Größenordnung, aber das abrupte Abbrechen der Strom- und Spannungskurven nach Fig. 6 deutet auf keine Entladung der

Kapazität nach einer e-Funktion, sondern auf einen steileren Abfall hin.

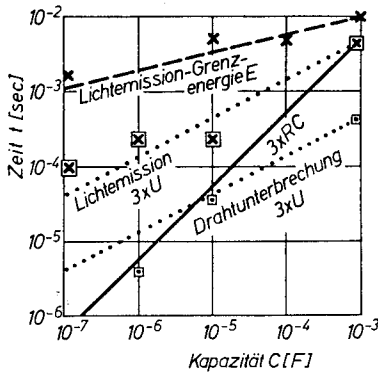


Fig. 7

Die stark streuenden Verzögerungszeiten bis zu einer Lichtemission bzw. Unterbrechung des Brückendrahtes sind in einem Diagramm mit doppel-logarithmischem Maßstab in Fig. 7 als Funktion der Kapazität eingezeichnet.

Bei Belastung der Anzündpille mit der Grenzenenergie nimmt die Zeitdifferenz bis zur Lichtemission t_L -Grenze von 10 ms bei 1000 uF auf 1 ms bei 0,1 uF ab. Die eingezeichnete linierte Gerade entspricht der Gleichung

$$t_L\text{-Grenze} = 56 \cdot 10^{-3} C^{1/4} \quad (2)$$

Da sich die Energie $E = 1/2 CU^2$ in diesem Bereich in erster Näherung als konstant erwies, kann die Kapazität C durch die Spannung U ersetzt werden.

$$C = \frac{2E}{U^2} = \frac{2 \cdot 3 \cdot 10^{-3}}{U^2} \quad (1b) \quad t_L\text{-Grenze} = \frac{16 \cdot 10^{-3}}{\sqrt{U}} \quad (3)$$

Aus den Oszillogrammen können keine Zeiten für die Unterbrechung des Brückendrahtes ausgewertet werden.

Bei der Kondensator-Entladung mit dem 10-fachen der Grenzenenergie treten kürzere Zeiten bis zur Lichtemission als bei Belastung mit der Grenzenenergie auf. Dies dürfte daher kommen, daß einmal der Brückendraht schneller und zu höheren Temperaturen aufgeheizt wird und zum anderen dadurch, daß das Anzündgemisch bei der größeren Wärmezufuhr schneller reagiert. In grober Näherung können die Mittelwerte wieder durch eine Gerade (punktierte Linie) in dem Diagramm mit doppel-logarithmischer Teilung verbunden werden, wobei die Verzögerungszeiten t_{L-3U} jetzt der Gleichung

$$t_{L-3U} = 0,15 \sqrt{C} \quad (4)$$

genügen. Die Kapazität C kann wieder durch die Spannung U substituiert werden

$$C = \frac{2E}{U^2} \quad \text{jetzt mit } E = 30 \cdot 10^{-3}, \text{ also } C = \frac{60 \cdot 10^{-3}}{U^2} \quad (5)$$

so daß sich die Zeitverzögerung t_{L-3U} zwischen Anlegen des Zündimpulses und der Lichtemission bei 10-facher Grenzenergie in dem untersuchten Kapazitätsbereich umgekehrt proportional der angelegten Spannung ergibt zu:

$$t_{L-3U} = \frac{37 \cdot 10^{-3}}{U} \quad (6)$$

Die Zeitdifferenz bis zur Drahtunterbrechung t_{D-3U} ist bei etwa 10-facher Grenzenergie um eine Zehnerpotenz kleiner als die Lichtemission und genügt somit der Gleichung

$$t_{D-3U} = \frac{3,7 \cdot 10^{-3}}{U} \quad (7)$$

2. Belastung mit konstanter Spannung

Um den Energiebedarf zum Ansprechen der Anzündpillen bei niedrigen Spannungen zu ermitteln, wurde diese Anzündpille mit Spannungen aus einer Spannungsquelle mit kleinem Innenwiderstand belastet (Fig. 8). Der Strom- und Spannungsverlauf und die Zeit, bis die Anzündpille Licht emittiert, wurden, wie vorher beschrieben, gemessen.

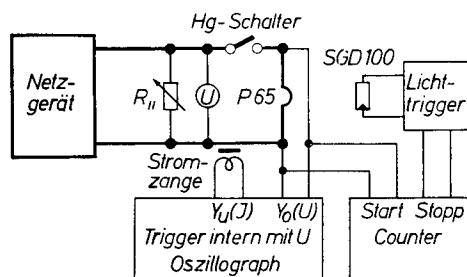


Fig. 8

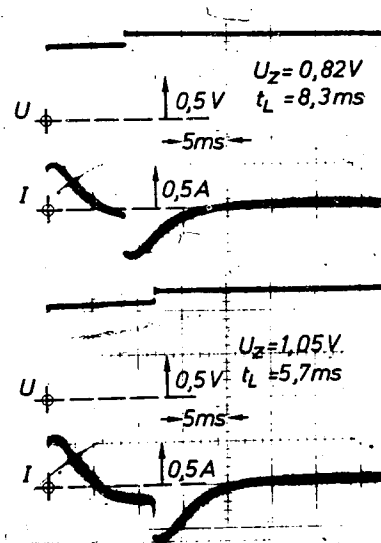


Fig. 9

Die Spannung steigt nach Unterbrechung des Zünddrahtes etwas an, wie die Oszillogramme der Fig. 9 zeigen, da die verwendete Konstantspannungsquelle nicht niederohmig genug war. Dadurch konnte jedoch die Unterbrechung des Zünddrahtes gut ausgewertet werden. Aus den oszillographischen Aufnahmen des Spannungsverlaufes kann außerdem der exakte Spannungsabfall an der Anzündpille für die Leistungsberechnung ausgewertet werden.

Die Zeitdifferenz zwischen Anlegen der Zündspannung und der Unterbrechung des Anzündpillendrahtes beträgt in dem als Beispiel wiedergegebenen Oszillogramm der Fig. 9 (obere Strahlen) 8,5 ms. Für die Zeitdifferenz zwischen Zündimpuls und Lichtemission wurden 8,3 ms mit dem Counter gestoppt. Hierbei betrug die Zündspannung 0,82 V. Im unteren Bildteil der Fig. 9 betrug trotz höherer Zündspannung von 1,05 V die Zeitdifferenz für die Zünddrahtunterbrechung 11,8 ms. Für die Zeitdifferenz der Lichtemission wurden nur 5,7 ms gemessen.

Hier kann nun, offensichtlich bei kleinen Spannungen, der umgekehrte Fall auftreten, wie bei der Kondensatorentladung, daß nämlich die Lichtemission **früher** als das Unterbrechen des nur langsam aufgeheizten Zünddrahtes auftritt. Dies bedeutet nun, daß nach einer bestimmten Erwärmung des Drahtes das Anzündgemisch bereits reagiert, ohne daß der Zünddraht vorher unterbrochen sein muß.

Dies bedeutet, daß auch die Zeitmessung bis zum Unterbrechen des Zünddrahtes t_D bei kleiner Potentialdifferenz am Zünddraht nicht repräsentativ für die notwendige Energie ($U \cdot I \cdot t_D$) ist, da die Zeit, die bereits ausreichend wäre, das Zündgemisch zum Reagieren zu bringen, hierbei nicht bestimmt wird. Wie vorher ausgeführt wurde, kann die Zeitverzögerung bis zur Lichtemission t_L ebenfalls nicht verwendet werden, da die Durchreaktionszeit des Zündsatzes, die außerdem eine Funktion des Wärmeschocks ist, nicht bekannt ist.

Außer Messungen bei kleinen Potentialdifferenzen (kleinen Spannungen) ab 0,75 V wurde die Messung der Zeitverzögerungen zwischen Anlegen von Spannung und Lichtemission bzw. Drahtunterbrechung bis zu konstanten Spannungen von 200 V Höhe fortgesetzt. Da hierfür unterschiedliche Lose von Anzündpillen verwendet wurden, streuten die Meßergebnisse stark. Trägt man die Zeitverzögerungen bis zur

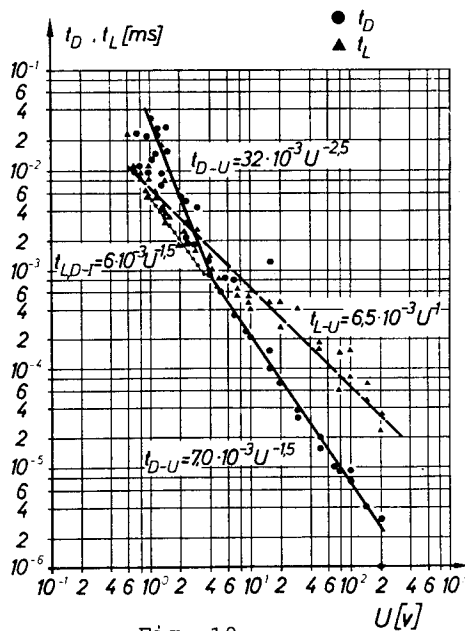


Fig. 10

Lichtemission bzw. Drahtunterbrechung als Funktion der Spannung in das doppellogarithmische Papier der Fig. 10 auf, so findet man folgendes:

Die Werte der "Lichtemission" liegen relativ gut um eine Gerade, welche folgender Gleichung genügen:

$$t_{L-U} = 6,5 \cdot 10^{-3} U^{-1} \quad (8)$$

Man kann das untersuchte Gebiet in Verbindung mit der Unterbrechung des Brückendrahtes in 3 Bereiche einteilen:

1. Einen Bereich bis ca. 3 V, in dem der Lichtblitz vor der Brückendrahtunterbrechung auftritt.
Der Brückendraht wird hier sehr langsam aufgeheizt, so daß das Anzündgemisch durchreagiert, bevor die Energie zur Unterbrechung des Brückendrahtes von außen zugeführt worden ist.
2. Einen Bereich von ca. 3 - 6 V, wo Brückendrahtunterbrechung und Lichtblitz praktisch gleichzeitig auftreten.
Dieser Bereich könnte durch einen Effekt bestimmt sein, daß der fast bis zur Unterbrechung aufgeheizte Brückendraht durch die zusätzlich hinzukommende Wärmeenergie bei Reaktion des Anzündgemisches unterbrochen wird.
3. Einen Bereich ab ca. 6 V, in dem der Brückendraht früher unterbrochen wird, als der Lichtblitz auftritt.
In diesem Bereich wird dem Brückendraht so viel Energie zugeführt, daß er unterbrochen wird, bevor das Anzündgemisch Zeit gefunden hat, durchzureagieren. Hierbei ist die Durchreaktionszeit des Anzündgemisches offensichtlich nicht

konstant, sondern hängt von der Aufheizgeschwindigkeit und damit der zugeführten Wärme ab. Ansonsten wäre es nicht verständlich, warum mit größer werdender Spannung und damit kürzeren Drahtunterbrechungszeiten auch die Zeiten bis zur Lichtemission immer noch kürzer werden.

3. Belastung mit eingprägtem Strom

Ein magnetischer Stoßgenerator als Energiequelle stellt keinen Spannungsgenerator, sondern einen Stromgenerator dar. Deshalb wurde der Energiebedarf der Anzündpille auch bei eingprägtem Strom untersucht. Um eventuelle Unterschiede in der Leistungsanpassung zu erkennen, wurden unterschiedliche Vorschaltwiderstände, nämlich 10, 30 und 100 Ohm eingesetzt.

Wie Voruntersuchungen zeigten, ist die Widerstandsänderung des Brückendrahtes beim Aufheizen kleiner als 0,1 Ohm. Dies heißt, bereits ab dem 10 Ohm Vorschaltwiderstand ist die Stromkonstanz trotz Änderung des Brückenwiderstandes dieser Anzündpille besser als 1 %. Der Spannungs- und Stromverlauf und die Zeitdifferenz zwischen Zündimpuls und Lichtemission wurde wie bei den vorhergegangenen Messungen bestimmt (Fig. 11).

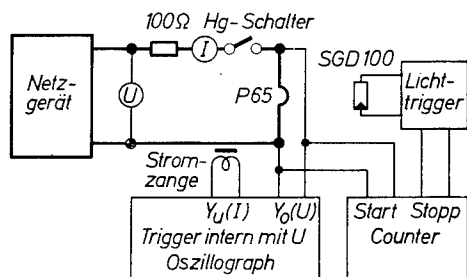


Fig. 11

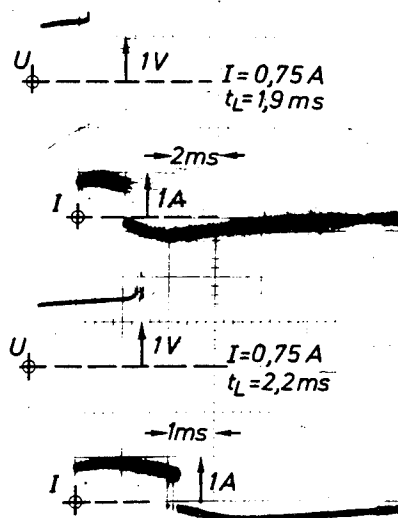


Fig. 12

In dieser Schaltanordnung unterbricht der Brückendraht den Stromkreis zum Teil mit Flutter- bzw. Prellerscheinungen wie bei einem mechanischen Schalter. Besonders deutlich zeigt dies, als Beispiel, das untere Oszillogramm von Fig. 12. Bei Unterbrechung des Drahtes steigt die Spannung auf die Leerlaufspannung des Netzgerätes an und deshalb läuft der Strahl des Oszillographen nach oben aus dem Bild heraus. Das Schwingen der Stromkurve ist wieder auf die Stromzange, die den Gleichstromanteil nicht überträgt, zurückzuführen.

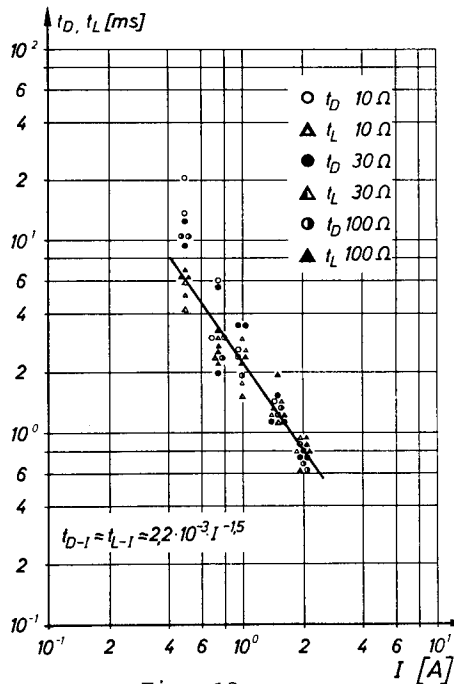


Fig. 13

Die Zeitdifferenzen vom Zündimpuls bis zur Unterbrechung des Anzündpillen-Brückendrahtes bzw. bis zur Lichtemission sind bei eingepprägtem Strom in erster Näherung gleich lang. Eine Abhängigkeit von den gewählten Vorschaltwiderständen konnte nicht gefunden werden. Alle Meßwerte, in Fig. 13 in doppellogarithmisches Papier als Funktion des eingepprägten Stromes mit den Vorschaltwiderständen als Parameter eingetragen, können durch eine Gerade gemittelt werden, welche durch folgende Gleichung beschrieben wird:

$$t_{L-I} = t_{D-I} = 2,2 \cdot 10^{-3} \cdot I^{-1,5} \quad (9)$$

Wird I durch U substituiert

$$(I = U/R = U/2; I^{-1,5} = (U/2)^{-1,5} = 2,8 \cdot U^{-1,5}),$$

so ergibt sich

$$t_{D-I} = t_{L-I} = 6,2 \cdot 10^{-3} U^{-1,5} \quad (10)$$

Diese Gerade wurde in Fig. 10 in dem untersuchten Bereich von 0,5 Ampere eingepprägten Stromes, entsprechend 1 Volt Spannungsabfall, und 2 Ampere entsprechend 4 Volt Spannungsabfall, als punktierte Linie eingetragen. Sie stellt interessanterweise bis auf eine ge-

ringe Abweichung der Konstanten (6,2 statt 7,0, was innerhalb der Meßgenauigkeit liegt) die Fortsetzung der Gleichung (8) in Fig. 10 mit gleicher Steigung dar.

Bei 1,5 und 2 Ampere, entsprechend 3 und 4 V, hat man innerhalb der Fehlergrenzen praktisch gleichzeitiges Auftreten der Lichtemission und der Drahtunterbrechung. Eine Erklärung dieser Erscheinung wäre, daß bei eingepprägtem Strom bei Unterbrechung des Brückendrahtes größere Leistungen in dieser Anzündpille als bei konstanter Spannung umgesetzt werden, die dann zu einem schnellen Reagieren des Anzündgemisches führen. Wie man Fig. 9 entnehmen kann, reagiert bei großer Spannung und damit großer Leistung das Zündgemisch unterhalb 100 μ s durch, was hier bei der gesamten Ansprechzeit von einigen Millisekunden dann innerhalb der Meßgenauigkeit liegt.

4. Belastung mit einem Stromimpuls

Da die Zeitdifferenz zwischen Zündimpuls und Zünddrahtunterbrechung oder Lichtemission weder bei geringen Spannungen an der Anzündpille, noch für die Verfahren der konstanten Spannung und auch des eingepprägten Stromes repräsentativ für die Zeit t in der Energieformel (1) ist, wurde eine Impulsschaltung mit einstellbarer Zeit für eingepprägten Strom aufgebaut. Hiermit kann die Anzündpille mit eingepprägtem Strom mit einstellbarer Zeitdauer belastet werden. Der Spannungsabfall an der Anzündpille wird wiederum oszillographisch gemessen und aus dem vorgegebenen Produkt $U \cdot I \cdot t$ kann der Energiebedarf ermittelt werden. Bei gewähltem eingepprägten Strom wurde die Zeit t des Impulses für jede Anzündpille so lange stufenweise verlängert, bis die Anzündpille ansprach.

Der Aufbau der Schaltung kann der Fig. 14 entnommen werden. Durch Vorschaltwiderstände von 10, 30 bzw. 100 Ω erhält man gegenüber dem Anzündpillenwiderstand von 2 Ω einen Stromgenerator mit fast konstanter Stromstärke.

Im Gegensatz zu den früheren Versuchen erfolgte die Messung des Stromverlaufes des Zündstromkreises über einen niederohmigen Widerstand von 0,1 Ohm. Der Spannungsabfall an diesem Shunt wurde

mit dem Doppelstrahloszillographen mitregistriert. Ein typisches aufgenommenes Oszillogramm zeigt Fig. 15.

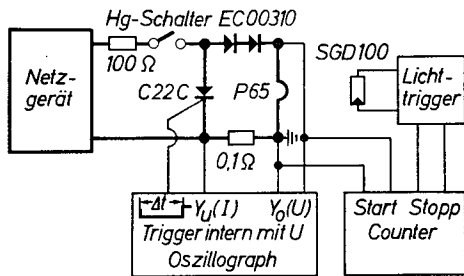


Fig. 14

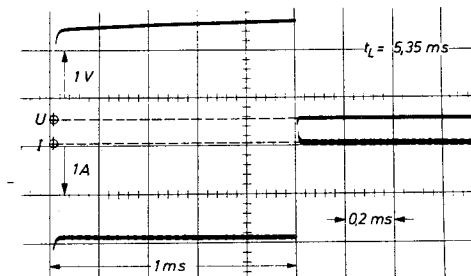


Fig. 15

Der Spannungsausschlag erfolgt nach oben, während der positive Stromausschlag nach unten geht. Mit dieser Meßanordnung kann die Zeit bis zur Drahtunterbrechung nicht miterfaßt werden und ein hierzu notwendiger Schaltungsaufwand wurde als nicht notwendig angesehen. Die Messung der Zeitdifferenz zwischen Zündimpuls und Lichtemission erfolgte, wie bei den vorhergehenden Versuchen, mit einem Counter.

Alle Meßwerte der Zeitdifferenz t zwischen Zündimpuls und

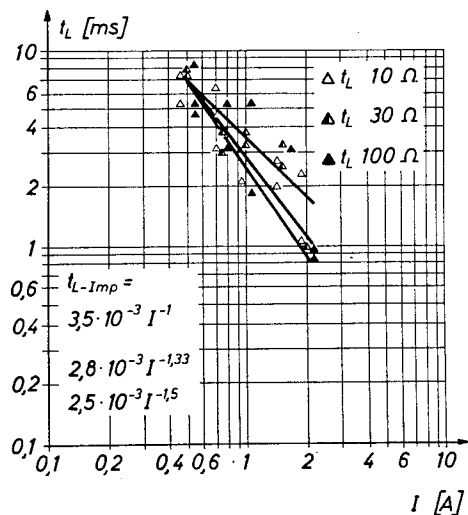


Fig. 16

Lichtemission für diese Anzündpille bei Stromimpulsbelastung mit Grenzenenergie sind als Funktion der Stromstärke I in ein doppel-logarithmisches Diagramm mit den Vorschaltwiderständen als Parameter in Fig. 16 eingetragen. Wie man sieht, streuen die einzelnen erhaltenen Meßwerte relativ stark und zeigen keine Signifikanz für die verschiedenen Vorschaltwiderstände von 10, 30 oder 100 Ω . Da der Meßbereich von 0,5 bis 2 A Stromstärke auch nur sehr klein war, kann nur schlecht eine mittellnde Gerade in die

stark streuenden einzelnen Meßwerte eingetragen werden.

Den Meßwerten würden die Geraden nach den folgenden Gleichungen gerecht werden:

$$t_{L-Imp} = 3,5 \cdot 10^{-3} I^{-1} \quad \text{oder} \quad (11)$$

$$t_{L-Imp} = 2,8 \cdot 10^{-3} I^{-1,33} \quad \text{oder} \quad (12)$$

$$t_{L-Imp} = 2,5 \cdot 10^{-3} I^{-1,5} \quad (13)$$

Durch Substitution von I durch U erhält man folgende Gleichungen:

$$t_{L-Imp} = 7 \cdot 10^{-3} U^{-1} \quad (14)$$

$$t_{L-Imp} = 7 \cdot 10^{-3} U^{-1,33} \quad (15)$$

$$t_{L-Imp} = 7 \cdot 10^{-3} U^{-1,5} \quad (16)$$

Die Gleichung (14) entspricht bis auf eine geringe Abweichung der Konstanten, was jedoch innerhalb der Meßgenauigkeit liegt, der Gleichung (8) für Zeidifferenz zwischen Zündimpuls und Lichtemission bei konstanter Spannungsbelastung. Die Gleichungen (13) bzw. (16) entsprechen weitgehend den Gleichungen mit konstanter Strombelastung (9) und (10).

Wie bereits vorher erwähnt, ist jedoch der untersuchte Meßbereich sehr klein, so daß die Aussagesicherheit der Gleichungen sehr gering ist. Bemerkenswert ist jedoch, daß man trotz ganz verschiedenartiger Belastung, wie konstante Spannungsbelastung oder Stromimpulsbelastung in dem Strombereich von 0,5 - 2 A gleiche Zeitdifferenzen zwischen Zündimpuls und Lichtemission erhält, d.h. die Zeit wird hier in erster Linie von der Reaktionszeit des Anzündgemisches bestimmt.

6. Zusammenfassung

Am Beispiel einer elektrischen Anzündpille mit Brückendraht wurde das zeitliche Ansprechverhalten bei den folgenden verschiedenen Belastungsfällen bestimmt und erläutert:

- Kondensatorentladung
- Konstante Spannung
- Eingeprägter Strom
- Stromimpuls

Die Reaktionsgeschwindigkeiten der in dieser Anzündpille gewählten Anzündmischung zeigt dabei eine sehr starke Abhängigkeit von der eingespeisten elektrischen Energie in den Brückendraht.

THE HYDRODYNAMICAL METHOD TO ANALYSE THE COMBUSTION PRODUCTS
COMPOSITION, THE CONCENTRATION AND TEMPERATURE FIELDS OF THE
PYROTECHNICAL FUEL FLAME

Victor Samsonov

Chuvash State Pedagogical Institute, K.Marx st. 38
428000, Cheboksary, RUSSIA

ABSTRACT

The method of the convective precipitation of the combustion products on the heat-transfer surface is developed to determinate the temperature fields and concentration fields in the flame of the gaseous and condensed fuels. The comparative calculations are made for the diffusion propane flame and the designed pyrotechnical fuels based on the mixtures of nitro-cellulose, polymethylmetacrilate and ammonia perchlorate. The method was tested at the various layout of the heat-transfer surface and the combustion products jet. The influence of errors of the gas velocity determination on the temperature values calculated is investigated. The conditions of the effective application of the method are formulated.

The necessary operating characteristics of the volatile pyrotechnical fuels are determined by evaporation and chemical transformation processes in gas phase. The planning of the concentration of initial components and the pyrotechnical fuel manufacture technology must be grounded on concentration data, composition of combustion products data, temperature gradients data in the flame. The data required can be obtained by testing of pyrotechnical fuel in chemical reactor, when heat-conducting walls of a reactor can be used to get a dimensional "portrait of a quickly frozen combustion reaction".

A "portrait" is a trace of intermediate reaction products those are carried off by chemically reacting flow to a reactor wall. The optical and mechanical properties of a trace are determined by his thickness, coagulating particles concentration and coagulation temperature. The "pencil

method" to determinate the temperature in the flame is known. This method uses the measurements of the mechanical hardness of the trace. It is a variety of contact methods of measurements.

The contactless method to analyse a trace has been developed in [1]. The velocity distributions, thickness distributions, the temperature dependence of the combustion products release rate and a classical model of volatile condensed system burning make it possible to build the closed algebraic equations system to calculate the temperature field and concentration field in gas phase.

This work deals with the basic principles of the method. The right algorithm must be developed in the specific case. It is stipulated by the features of the reactions kinetics, location and shape of the transformation zone, velocity field etc.

A flat massive stainless steel plate was used to obtain a trace. The gaseous and pyrotechnical fuels were being led through a round hole in a plate. It is possible to lead a liquid fuel through a capillary hole. The specimen of pyrotechnical fuels and gaseous fuel were being burnt in Hele-Shaw cell to obtain a two-dimensional flow. The Hele-Shaw cell is a chink, that is being formed by two plates. One of them is perspex, the other is steel. The surfaces were grinded and polished.

The traces were obtained in the following hydrodynamical situations those are possible:

- a combustion products jet and a surface flowed are parallel;
- a jet and a surface flowed are perpendicular. A combustion products velocity is directed to a surface or from off it;

The trace is not equally thick everywhere. The trace became as a thin transparent layer if the precipitation time reached some determined value. When the layer is being lighted, the interference picture has taken place. The figures 1,2 illustrate the sensitivity and the legibility ability of the method.

The algorithm of the temperature calculation is built in this way. The trace was covered by co-ordinate rectangular grid. The layer thickness δ is determined by interference or-

der k : $\delta = (k \cdot \lambda + \lambda/2)/2 \cdot n$, where λ is the light wave length, n is the light refraction in the layer. The mass of the combustion products, that comes on the unit of the surface in the time t is equal in XOY co-ordinate system:

$$m(x,y) = \rho_g(x,y) \cdot u(x,y) \cdot t \quad (1)$$

Here ρ_g is the combustion products concentration in gas phase



Figure 1.

The jet is being directed down. The plate is almost vertical. $Re=15$.



Figure 2.

The diameter of designed "PMMC-AP" fuel specimen is 2 mm. $Re = 7$. The surface is horizontal.

$u(x,y)$ is the perpendicular to a surface the gas velocity component. But the layer mass is proportional to his thickness:

$$m(x,y) = \rho_l (k \cdot \lambda + \lambda/2)/2 \cdot n \quad (2)$$

here ρ_1 is the combustion products density in layer. It follows from (1), (2):

$$\rho_g(x,y) = \rho_1(k\lambda + \lambda/2)/[2 \cdot n \cdot u(x,y) \cdot t] \quad (3)$$

The solid combustion products concentration in gas phase is proportional to their formation rate $\eta(x,y,T)$ and transformation time τ :

$$\eta(x,y,T) = \rho_g(x,y)/\tau(x,y). \quad (4)$$

Here $T=T(x,y)$ is the temperature distribution on the surface. The transformation time can be calculated, if the disperse particles motion trajectories are known. The combustion products formation rate as Arrhenius dependence is:

$$\eta(x,y) = k_0 \exp\{[T(x,y) - T_0]/\theta\},$$

where k_0 the combustion reaction rate constant, T_0 is the basic temperature of the Frank-Kamenetsky expansion [2], $\theta=RT^2/E$, R is the universal gas constant, E is the activity energy. It follows from last expression

$$T(x,y) = T_0 + \theta \ln[\eta(x,y)/k_0] \quad (5)$$

The equations (3)-(5) are the closed equations system for calculation of temperature distribution. Thus the equations system is based on the theory of volatile condensed fuels burning [3].

The boundary layer thickness l is $l \approx (\nu S/V)^{1/2} + 3 \cdot 10^{-3} \text{m}$, where V is an average flow velocity, ν is the kinematic viscosity. The extinction zone of many fuels flames is less as a rule. Because the temperature determined by expression (5) is not the surface temperature.

The equation system (3)-(5) is being presented as a recurrent expression, one realizes the calculation algorithm:

$$\rho_{gij} = C_1(k_{ij} + 1/2)/u_{ij}, \quad (6)$$

$$\eta_{ij} = \rho_{gij}/\tau_{ij}, \quad (7)$$

$$i_{\beta+1} \neq i_{\beta+1}, \quad j_{\beta+1} \neq j_{\beta+1}, \quad (8)$$

$$x_{\beta+1} = x_{\beta} + \Delta x \cdot \text{sign } u_{\beta}, \quad (9)$$

$$y_{\beta+1} = y_{\beta} + \Delta y \cdot \text{sign } v_{\beta}, \quad (10)$$

$$\tau_{\beta}(t_{N/2}, j_{N/2} | t, j) = \sum (\Delta x / u_{\beta}) = \sum (\Delta y / v_{\beta}), \quad (11)$$

$$T_{t,j} = T_0 + \theta \cdot \ln(\eta_{t,j} / k_0), \quad (12)$$

here t, j are the current numbers of the grid junctions along the axes X and Y , N, W are the numbers of the grid junctions, $C_1 = \lambda \cdot \rho_0 / 2nt$, ρ_0 is the layer density. The expressions (9), (11) calculate the the combustion time and the distance covered by particle. If the flow velocity is parallel to a plate and a free convective velocity is not great, then the combustion products velocity distribution is expressed as an automodel solution of the boundary layer equations [4] and one is controlled experimentally:

$$\begin{aligned} u &= 0,45 \cdot \left[\frac{K^2}{\nu x} \right]^{1/3} \cdot (1 - \text{th}^2 \xi), \\ v &= 0,55 \cdot \left[\frac{K\nu}{x^2} \right]^{1/3} [2\xi(1 - \text{th}^2 \xi) - \text{th} \xi], \\ \xi &= 0,27 \cdot \left[\frac{K}{\nu^2} \right]^{1/3} \cdot y/x^{2/3} \end{aligned}$$

The value of the kinematic impulse K is selected empirically.

The vortex flames are being observed if the combustion products velocity V and the gravitational acceleration g are opposite and $Re < 20$, $Fr \approx 1$. The photography of the vortex flame is presented in Fig.3.

The Reynolds number is $Re = ud/\nu$, Froude number is $Fr = V^2/gd$, where d is typical size. The velocity field of the vortex flame can be defined by measurements of the trajectories length on the trace. The calculations were made using following recurrent expressions:

$$\begin{aligned} \Delta u_{t,j} &= v_{kl} \cdot \cos \alpha_{kl} - v_{t,j} \cdot \cos \alpha_{t,j}, \\ \Delta v_{t,j} &= v_{kl} \cdot \cos \alpha_{kl} - v_{t,j} \cdot \cos \alpha_{t,j}, \\ k &= t+1, \text{ if } 0 < \alpha_{t,j} < \frac{\pi}{2}, \frac{3}{2}\pi < \alpha_{t,j} < 2\pi, \\ k &= t-1, \text{ if } \frac{\pi}{2} < \alpha_{t,j} < \frac{3}{2}\pi, \\ l &= j+1, \text{ if } 0 < \alpha_{t,j} < \pi, \end{aligned}$$

$$l = j - 1, \text{ if } \pi < \alpha_{t,j} < 2\pi$$

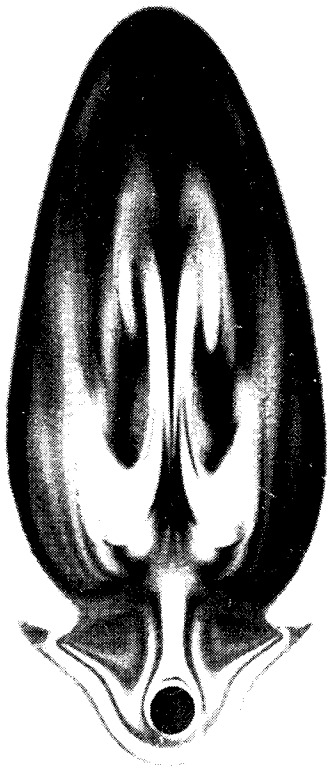


Figure 3.

The vortex flame corresponding to the burning of the "nitrocelullose - polymethylmetacrylat" composition. The plate is inclined, $Re=15$. The diameter of a specimen is 6 mm.

Here $\alpha_{t,j}$ is the angle between the trajectory and the axis X (or Y) in (l,j) -st. junction of the grid, k,l are the current junctions numbers.

It is necessary to know the precise values of the kinetic constants to define the absolute values of the temperature. It is not always possible to provide the information about combustion kinetics for the pyrotechnical composition. The temperature was being measured by thermocouple method in

the single typical point on the plate surface for this reason. Then the θ value was being varied in the expression (5) till the calculated temperature and the thermocouple temperature will become equal. The results of the temperature fields calculations are presented in Fig.4,5. They correspond to flames shown in Fig.1,3.

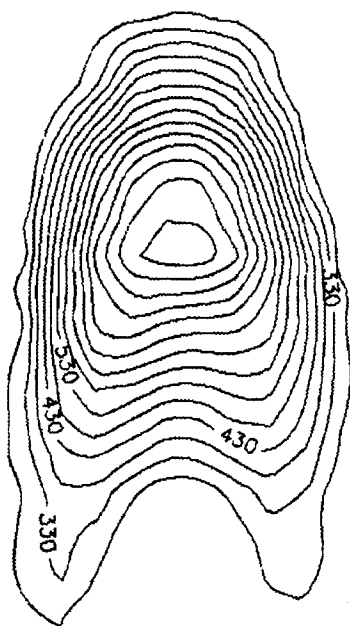


Figure 4

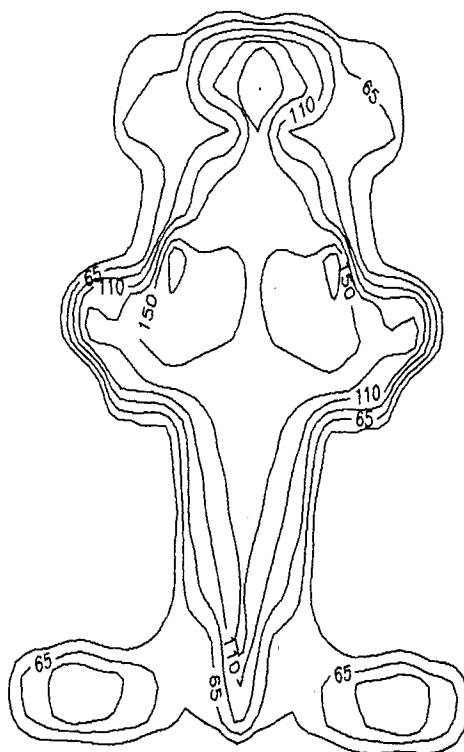


Figure 5

The temperature field of the hydrodynamical structure, which analogous the one shown in Fig.2, has been calculated. The "temperature crystal" is presented in Fig.6. The investigation of the solid fuel surface has shown the similarity of the surface relief and the "temperature crystal" one. This is the indirect corroboration of the calculation method.

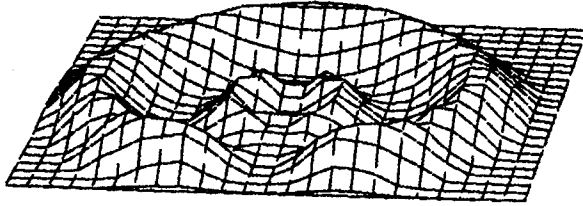


Figure 6.

The general defect of the method is the great error of the entered velocity values. The study of the influence of these errors has shown, that the velocity error $\Delta V/V = 1\%$ provides the temperature error $\Delta T/T < 0,1\%$. It is being explained by the faint dependence of a velocity on a temperature in the denominator of the logarithm expression (5). The other defect is the influence of the turbulence. The turbulence scale limits the legibility ability of the method.

The results of the calculations have made it possible to assert that the method can be applied to the volatile pyro-technical fuels flames diagnostics.

REFERENCES

- [1] Samsonov V.P. Khimicheskaja Fizika, 1992, 11, 1580 (in Russian).
- [2] Zel'dovich Ya.B., Barenblatt G.I., Librovich V.B. The Mathematical Theory of Combustion and Explosive, Moscow, Nauka, 1980 (in Russian).
- [3] Zel'dovich Ya.B., Leipunskij O.I., Librovich V.B. Theory of Non-Stationary Combustion of Gun Powder, Moscow, Nauka, 1975 (in Russian).
- [4] Schlichting G. Theory of boundary layer, Moscow, Nauka, 1974 (in Russian).

MECHANICAL IGNITION OF AN HETEROGENEOUS EXPLOSIVE COMPOSITION SUBMITTED TO PROJECTILE PENETRATION

D. LEMOINE, L. GAUTIER, H. CHERIN

COMMISSARIAT A L'ENERGIE ATOMIQUE

Centre d'Etudes du Ripault

B.P.N° 16

37260 MONTS (FRANCE)

1. Introduction

When an explosive device is impacted by a bullet, violent pyrotechnic reactions are observed for some configurations. These reactions are not the result of a SDT (Shock to Detonation-Transition), but of a DDT (combustion-to-Deflagration-to-Detonation Transition). It is therefore essential for the pyrotechnic safety to study the ignition process during the projectile penetration. Our purpose is to identify the mechanisms which can lead to a significant heating of the explosive and therefore to a possible ignition, and then, using well-adapted experiments, to select the predominant mechanism(s) governing the studied phenomenon.

Despite the large number of impact tests of this type performed worldwide, these mechanisms have still not been clearly identified up to now.

2. Phenomenology

As mentioned previously the assumed phenomenology is of the DDT type as presented in figure 1.

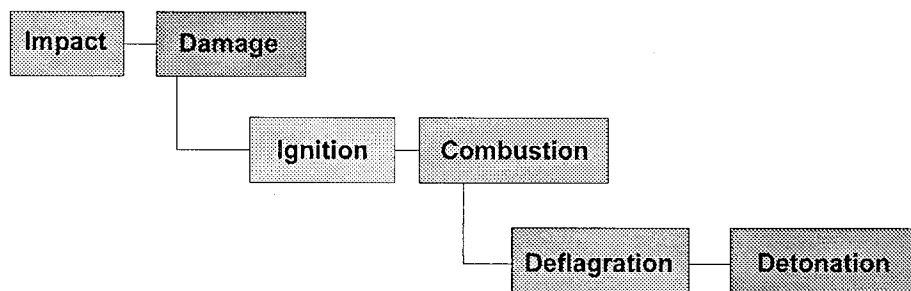


Figure 1

Upon impact and during penetration, the projectile induces an important damage in the target. This damage is located close to the axis of perforation, but also far from of it due to plastic deformations and propagation of cracks far from the perforation channel. If the input energy is sufficient, there is an ignition of the explosive followed by a combustion of the fragmented explosive. Depending on experimental conditions, this combustion may evolve into a deflagration or even a detonation.

3. Possible mechanisms

The different possible mechanisms leading to ignition can be classified into three categories :

- 1 - Influence of the structuration :
 - heating of the confinement during perforation,
 - case rupture with hot particles projection into the explosive.
- 2 - Influence of the projectile :
 - stripping of the front and back faces of the bullet (5.56 bullet),
 - heat exchange between the projectile and the explosive,
 - friction of the bullet into the explosive.
- 3 - Influence of the behavior of the explosive :
 - plastic deformations,
 - shear stress and fracturing,
 - outflow of explosive material.

Figure 2 below illustrates all these mechanisms.

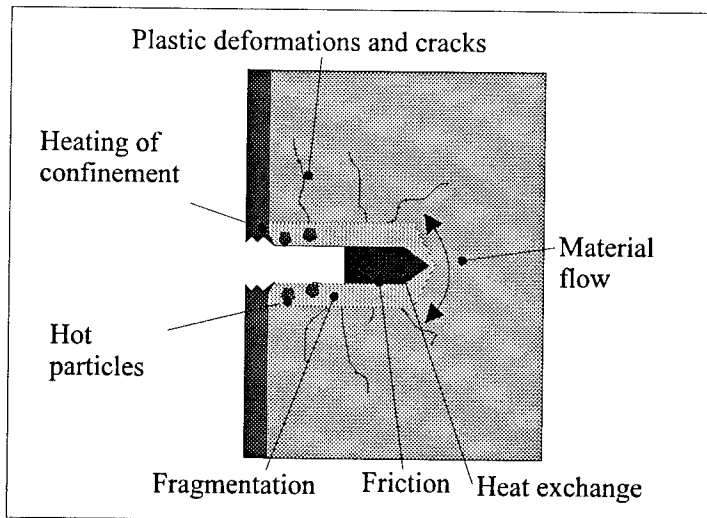


Figure 2

4. The experimental set-up

It is presented on Figure 3. The launcher is a 60 or 70 cm long grooved, 5.56 or 7.62 calibre gun. A system of optic barriers separated by a 50 cm distance is used to measure the velocity of the projectile. The experiments are filmed with an S-VHS camera, and recorded on a VCR.

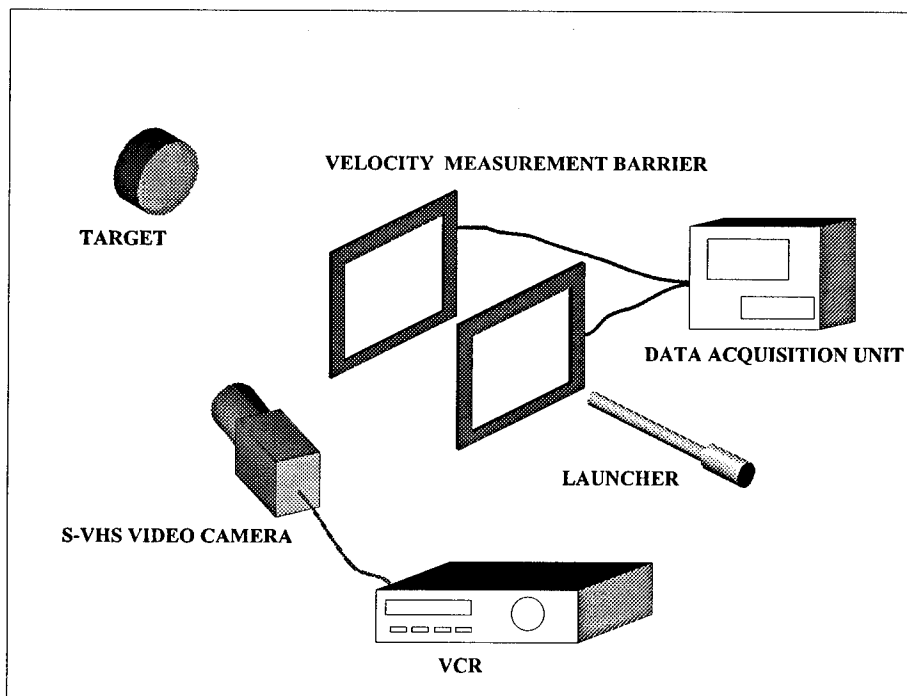


Figure 3

5. Experiments performed

A large number of tests were performed, the main characteristics of which are shown below :

- 5.56 armour piercing bullet velocity : 1,000 m/sec.
- 7.62 PPI bullet velocity : 900 m/sec.
- Lateral confinement : 20 mm thick steel cylinder.
- Front and back case : 3 mm thick steel plates.

The explosive tested is an HMX-based composition (X1) . The samples used are cylinders, Φ 100, h 40 mm, unless otherwise specified below.

Figure 4 presents a summary of the first tests performed with a 5.56 bullet.

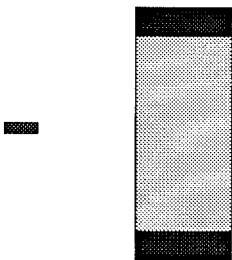
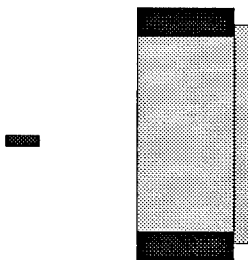
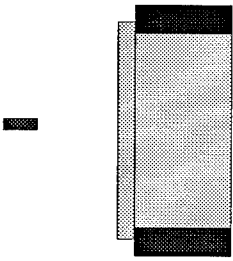
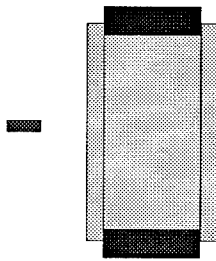
Configuration 1	Configuration 2
	
No reaction Dispersion of powdered explosive	Combustion
Configuration 3	Configuration 4
	
Deflagration	Detonation

Figure 4

In the tests performed in configuration 1, no pyrotechnic reaction was observed. The examination of the model after the test showed an important dispersion of powdered explosive. Furthermore, the perforation channel into the target had a diameter highly greater than the bullet one, but no trace of decomposition was identified. In configuration 2, a dispersion of the explosive from the front face occurred initially. It was followed by an ignition close to the perforation channel and by a complete combustion of the explosive after 2 minutes.

In the tests 3 and 4, a violent pyrotechnic reaction was obtained. Given the means of observation (24 images per second), the reaction type determination was only possible by examination of the models after the tests.

We subsequently performed an additional test, using a more complex structure integrating carbon insulator on both sides of the explosive, in order to eliminate the effects due to confinement heating and to the projection of hot particles (see Figure 5). After perforation of the model, smoke came out from the perforation holes. After 5 seconds, a violent pyrotechnic reaction was observed. The Combustion-to-Deflagration-to-Detonation transition was clearly evidenced in this case.

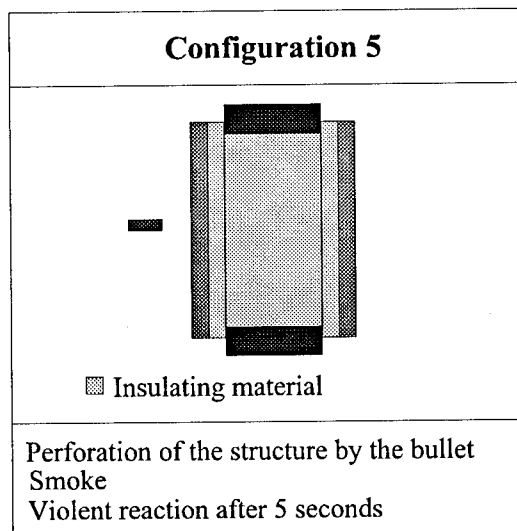


Figure 5

This first series of tests enabled us to eliminate from the list of potential ignition mechanisms those related to the confinement. This confinement has an effect only on the violence of the pyrotechnic reaction if ignition occurs. On the other hand, the nature of the armour piercing 5.56 bullet (insert + core) makes it impossible to determine any influence of the bullet. The two components behave in a random fashion upon impact : in certain cases, separation of the two parts of the bullet may occur, and the structure is then attacked by two projectiles. It therefore appeared essential to use a one-piece bullet, such as the 7.62 PPI, the slightly larger calibre of which can more over amplify the phenomena to be observed.

Figure 6 presents the tests which enabled us to get a better understanding of the phenomena involved, and to propose an interpretation of the effects of this kind of stimulus.

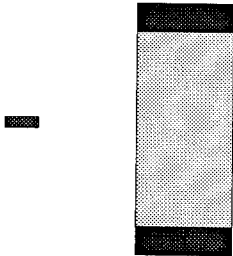
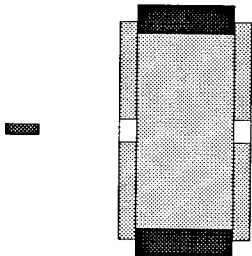
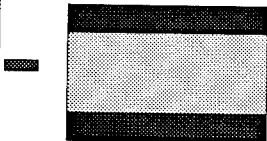
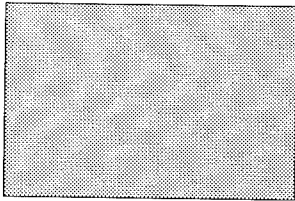
Configuration 6	Configuration 7
	
Explosive $\Phi 100$ h40	Explosive $\Phi 100$ h40
Ignition followed by extinction Dispersion of powdered explosive	Live combustion
Configuration 8	Configuration 9
	
Explosive $\Phi 40$ h200	Explosive 430 x 210 x 120
Deflagration	Detonation

Figure 6

In the case of the experiment on bare explosive (configuration 6), ignition appears quite clearly on the films. This flash of light is only visible on one image. The powdered explosive found after the test, and the fact that the scale model, analyzed after the test, showed no trace of combustion, indicates that ignition occurred in the most fragmented area of the explosive. The combustion stopped when the powdered burning explosive was expelled out of the target.

The following experiment (configuration 7) confirmed this hypothesis. The possibility of motion of the fragments was limited by the front and back plates and, in this case, a complete combustion of the scale model developed. The last two configurations tested also confirmed this hypothesis : the violent reactions observed were the results of an auto-confinement phenomenon. In this case the burning fragments could not be ejected. In configuration 9, the weight of explosive used (22 kgs in the case of the parallelepiped) enabled

the development of compressive and shock waves and the phenomenon evolved up to a detonation.

6. Proposed scenario

Submitted to the penetration of a bullet, the explosive is powdered all along the projectile trajectory. For the studied composition, there is a systematic ignition of this powdered explosive. If this powder can expand freely, the phenomenon stops. Otherwise, combustion in the bulk of the explosive develops. If the confinement is strong enough, the pressure generated by the combustion gases increases and a transition-to-deflagration, or even to-detonation, becomes possible. In the case of aggression on a large-sized explosive target, the pyrotechnic reaction obtained is a detonation, as a result from the auto-confinement of the material.

7. Conclusions

Among all the mechanisms identified, only the phenomenons associated to the mechanical behavior of the explosive and the friction of the bullet in the material appear to have an influence on ignition. Additional experiments, with high-performance diagnostic tools (ultra-fast integral imaging, infra-red imaging, optic fibers, etc.) will make it possible to situate precisely the ignition areas and to better understand the main phenomena governing ignition during projectile penetration.

STUDIES ON THE BURNING RATE OF
BUTACENE/AL/AP/CARBON FIBER COMPOSITE PROPELLANTS

Hsi-Cheng Yeh Dah-Ming Chen Huey-Cherng Perng

Chemical System Research Division
Chung-Shan Institute of Science and Technology
P.O. BOX 90008-17, Lungtan Taiwan, R.O.C.

ABSTRACT

The effect of carbon fiber in Butacene/Al/AP composite propellants has been studied in this work. Results indicated that the burning rate of the Butacene/Al/AP composite propellants increased significantly by the addition of 3% carbon fiber. These propellants exhibited burning rate higher than 51.4 mm/sec and 118.5 mm/sec at 16 kg/cm² and 100 kg/cm², respectively, while Butacene binder and ultrafine AP was employed. Besides, the effect of aluminum particle size on burning rate of the abovementioned propellants was also studied. Propellants with different size of aluminum, i.e. 60 μ m, 30 μ m and 16 μ m, their burning rate were 117 mm/sec, 107 mm/sec and 104 mm/sec (at 100 kg/cm²), respectively. The burning phenomena and mechanism of Butacene/Al/AP/Carbon Fiber composite propellants were investigated by strand burner, DSC, ARC, and window bomb. It is concluded that (1) Butacene is a good promoter for AP decomposition, (2) carbon fiber not only enhances the heat conduction of the propellants but also catalyzes the thermal decomposition of its ingredients or even participates the gas phase reaction, (3) because of the extremely short response time on the burning surface, a "pseudo-inert aluminum" hypothesis is proposed to elucidate the phenomenon of the larger the aluminum particle size, the higher the burning rate of this unique propellant. Carbon fiber containing propellant can be applied to any complex grain configuration, therefore, it is superior to metal wire embedded propellant which is restricted to the end-burning grain only. This is another merit of this propellant.

** Butacene is the trade mark of SNPE, France.

INTRODUCTION

Higher thrust of a rocket motor is always demanding, and the thrust F is related to specific impulse (I_{sp}), density (ρ), burning rate (R_b) and burning area (A_b) of the propellant grain, it can be shown by the equation: $F = I_{sp} \cdot \rho \cdot R_b \cdot A_b$. However, it is more and more difficult to promote density impulse ($I_{sp} \cdot \rho$) of the propellant extensively nowadays. In addition, the complex grain configuration are seldom in practical applications, mainly because of processing, structure and prohibited high cost. Consequently, grain configuration is generally restricted to several simple designs. Therefore, burning rate enhancement of solid propellant is a practical and crucial technology to improve the thrust characteristics of a rocket motor.

Generally speaking, there are several approaches to increase the burning rate of solid propellants. Such as using burning rate modifier, blending ultra fine AP, employing energetic binder, and embedding metal wire or fiber in the propellants etc.. There are some distinctive examples that achieved fascinating results in the past. For example, using porous ammonium perchlorate⁽¹⁾ to reach a burning rate of 154.94 mm/sec at 2000 psi; blending ultra-high-surface area ammonium perchlorate⁽²⁾ in the propellant, the burning rate achieved 83.1 mm/sec at 2000 psi; employing innovative carboranes as burning rate modifiers in CTPB/AP/NBC, HTPB/AP/IBC and HTPB(orCTPB)/AP/NF-MCA propellants⁽³⁾, the burning rate were 101.6 mm/sec at 1000 psi, 88.9 mm/sec at 1000 psi, 123.2 mm/sec at 2000psi, respectively. In 1970, the solid propellants embedded with metal wires⁽⁴⁾, displayed 21.8~68.7% increase in their burning rate. However, some drawbacks and limitation for the above-mentioned examples are existed. High surface area of AP or incompatibility problem causing processing of the solid propellant became extremely difficult, on the other hand, the metal wire can only be embedded in relative smaller diameter grains. Fortunately, for last decade, SNPE has developed a new prepolymer Butacene, which was to graft a silico-ferrocene derivative onto HTPB. This compound exhibits excellent burning rate capability, it is comparable to other ferrocene derivatives that generally used as combustion catalyst for solid propellants⁽⁵⁻⁷⁾. Besides, using Butacene in composite propellants, almost eliminate migration problem that encountered by the other ferrocene derivatives. Hence, the safety characteristics and ballistic performance of the Butacene propellants are superior to the propellants with conventional catalysts⁽⁷⁻⁸⁾. In this paper, the synergistic effect of carbon fiber on burning rate of Butacene/Al/AP composite propellants is emphasized. Specific goal of this

research is to formulate a composite propellant that the burning rate are higher than 40 mm/sec and 100 mm/sec at 16 kg/cm² and 100 kg/cm², respectively.

EXPERIMENTAL

Butacene and/or HTPB binder and other additives like carbon fiber 、Fe₂O₃ 、AP 、UFAP 、Al were blended together in a Baker Perkins mixer, certain processing aids and antioxidant were also incorporated. After curing in a 65°C oven for 5 days, the propellants are ready for testing. A propellant sample in 6x6x120mm coated with SBR is used for burning rate determination. DSC measurements were performed by a Perkin Elmer DSC 7 analyzer. Another important thermal analysis was carried out by an Accelerating Rate Calorimeter (ARC). The reaction vessels are 2.5cm in diameter and made by titanium, having a mass of approximately 10g. A pressure transducer with a 0~17200 KPa range is connected to the reaction vessel through stainless steel capillary tubing. In a typical experiment, a clean and weighed reaction vessel was charged with approximately 0.4g of sample, then sealed and reweighed. The reaction vessel was connected with Swagelok fitting to the pressure measurement device and enclosed in the calorimeter. At first, heated up the vessel to the setting temperature (100~120°C) and waited for 10 minutes to check if there is any detectable self-heating temperature rise (about 0.02°C), if no reaction, then the temperature is automatically raised by successive fixed increment (3°C). Once an exotherm has been detected, automatic recording of time, temperature and pressure data is carried out until the reaction is finished.

RESULTS AND DISCUSSION

Burning rate of HTPB/Al/AP composite propellants

Table 1. shows that Fe₂O₃, carbon fiber and Butacene are utilized separately and as co-catalysts in HTPB/Al/AP composite propellants. It is clear that the highest burning rate of these HTPB propellants is the one with 2% Fe₂O₃ and 3% carbon fiber, it reaches 71.12mm/s at 100kg/cm², but still fail to achieve the specific goal, although both Fe₂O₃ and carbon fiber are used as a combination. It is also interested to note that while Butacene is used as a catalyst in propellant C, the capability to enhance the burning rate is better than that of carbon fiber,

but inferior to Fe_2O_3 at high pressure and exceeds it at low pressure. It means that propellant with Butacene as a catalyst holds lower pressure exponent. Propellant D without any carbon fiber, and propellant E and F incorporate 1% and 3% of carbon fiber in replace of AP, the result reveals that higher content of carbon fiber gives higher burning rate.

Burning rate of HTPB and/or Butacene/Al/AP composite propellants

Propellants containing HTPB and/or Butacene binders are listed in Table 2. These propellants clearly display that the burning rate increases with the Butacene content. Moreover, the co-catalyst effect of Butacene and Fe_2O_3 is clearly demonstrated. For propellant I, the dual-function Butacene binder serves as the only catalyst, which has burning rate of 25.9mm/sec and 66.5mm/sec at 16kg/cm² and 100kg/cm², respectively. If fine AP in propellant I is replaced by Fe_2O_3 , then this co-catalyst propellant exhibits a burning rate increase of 30% and 41% for low and high pressure. The order of the burning rate at 100kg/cm² is H>G>I>D. However, none of these four composite propellants can achieve the special goal of this research.

Burning rate of Butacene/Al/AP/Carbon Fiber composite propellants

Table 3 shows the results of composite propellants that adopting the unique approach — employing Butacene as binder, Fe_2O_3 and carbon fiber as burning rate co-catalyst. There are four parameters are discussed in this case, including (1) Al content, (2) Al particle size, (3) AP particle size, (4) carbon fiber content, all of these 10 propellants satisfy the burning rate requirement of this research. Very short carbon fiber ($\leq 500 \mu$, see Fig. 1) is chosen in this case, in order to alleviate the burning rate variation problem which caused by the orientation of carbon fiber in propellant.

Fig. 2 shows that the burning rate of Butacene/Al/AP composite propellant is promoted as the content of carbon fiber is increased. The fastest burning rate of these 10% Al propellants are 110.4mm/sec and 45.4mm/sec at 100kg/cm² and 16kg/cm², respectively, as 3% carbon fiber is added. When the content of Al powder is increased from 10% to 17%, the burning rate still depends on the content of carbon fiber. However, the effect of carbon fiber diminished as the pressure higher than 70kg/cm². The results is showed in Fig. 3. In addition, the particle size effect of Al powder is also showed in Fig. 4. It is quite obvious that the larger the Al particle size, the faster the burning rate of these Butacene/Al/AP/Carbon fiber propellants.

The same phenomena are consistently recurred for propellants mixed with 20 μ m AP instead of 50 μ m AP, the results are exhibited in Fig. 5. The highest burning rates of this category propellant are 118.5mm/sec at 100kg/cm², and 51.4mm/sec at 16kg/cm², which accomplishes the specific goal of this study. Besides, the processing and mechanical properties are comparable to conventional propellant.

Burning rate mechanism of Butacene/Al/AP/Carbon Fiber composite propellants

Fig. 6 shows that the DSC thermograph of sample C59-4 containing Butacene binder, Al, AP had two stages decomposition. The most noticeable change is that the high temperature decomposition peak of AP is shifted tremendously from uncatalyzed AP's 420°C⁽¹⁰⁾ to 325°C. It is evident that the highly catalyzed power of Butacene on AP propellant. In addition, the sample C59-5 containing the same ingredients as sample C59-4 with 2% Fe₂O₃, a highly reactive deflagration took place at ~310°C. Moreover, the sample C59-6 is consisted of one more ingredient than sample C59-5, a 3% of carbon fiber is incorporated, and the onset temperature regarding deflagration is further reduced from 310°C to 250°C. This phenomenon strongly indicates that the carbon fiber is not only a thermal conductor (conductivity =50.14kcal/m · hr · °C) but also a good catalyst for Butacene propellant.

Table 4 and 5 listed the thermoanalytical data which obtained by ARC can also be used to elucidate the effect of carbon fiber on burning rate regarding the Butacene propellants. In comparison of three samples, it is clear that the burning rate of sample NO.1 is higher than that of sample NO.2 and NO.3. Simultaneously, the overall reaction rate of sample NO.1 is 2.3 times and 4.7 times faster than that of sample NO.2 and NO.3, respectively. This seems to imply that carbon fiber plays an effective role in augmenting the burning rate of the unique Butacene propellant. Therefore, it is another evidence to disclose that the carbon fiber behaves as both chemical and physical functions to promote burning rate in Butacene propellants. Besides, the synergetic effect of Butacene and carbon fiber is also revealed.

In addition to the DSC and ARC results, Fig. 7 exhibits the flame structures of propellant H and propellant R that were burned in a window bomb. Both propellant R and propellant H are prepared of Butacene, Fe₂O₃, AP and Al, and the only difference between them is the

propellant R has an extra 3% carbon fiber. As compared with propellant H, a very bright illuminous corona can be clearly observed above the burning surface of propellant R. It is believed that the carbon fiber catalyzed the thermal decomposition and/or even participated the gas phase reaction, thus increased the burning rate of this propellant.

Based on the burning rate data, one may easily conclude that the larger the Al particle size, the higher the burning rate for this unique type of propellant. Considering the characteristic high burning rate nature of this propellant, we proposed a "pseudo-inert aluminum" hypothesis to elucidate this phenomenon. Generally, the Al powder is enclosed by a layer of high-melting point (2323k) Al_2O_3 . Before realizing the high heating value of this fuel, the pure aluminum inside the shell must be heated up to its melting temperature (933k) first, then liquefied, and expanded to break through the Al_2O_3 shell, via vaporization and finally reacted with the adjacent oxidizing species as they diffuse into the gas phase. For conventional aluminized propellant, most of the heat generated by the metal fuel is not too far away from the burning surface, consequently, effective heat feedback to enhance the burning process is realized. Contrary to the above situation, the heat contribution of Al powder for this high burning rate propellant is almost impossible to receive by the burning surface. The main reasons are: (1) very thin (≈ 1 order thinner) thermal wave thickness and extremely short (≈ 2 order shorter) residence (response) time of Al powder on the burning surface, (2) Al powder ejected away from the burning surface with very high velocity, (3) the burning surface recessed away very fast. Therefore most of the Al powder only heated up and ejected to a distant gas phase followed by ignited and burned there, but with very limited heat feedback to the burning surface. Consequently, in the sense of burning rate, Al powder served temporarily as an inert "heat sink". Moreover, smaller Al powder has larger surface area caused more heat loss from burning surface and less effective heat absorbed by the other ingredients, therefore lead to lower burning rate. In addition, from the micro viewpoint when an larger Al particle ejects from the surface, a bigger hole will be generated, thus enhanced the burning rate, this inference also explains the phenomenon.

CONCLUSION

The Butacene propellant with Fe_2O_3 , carbon fiber as burning rate modifiers achieved very high burning rate at both low and high pressures. The burning phenomenon and mechanisms of these unique propellants were investigated by strand burner, DSC, ARC and window bomb.

The dual functions of carbon fiber are evidenced in this research.. In view of the ballistic, mechanical and processing properties, the practical application of this unique propellant is quite promising.

References

1. K. Klager, "Propellants Seminar" (1984)
2. David C. Sayles, U.S. Pat. 4,698,106 (1987)
3. William E. Hill and Lew R. Beason, U.S. Pat. 3,764,417 (1973)
4. Leonard H. Cavney, U.S. Pat. 3,508,494 (1970)
5. W.O. Munson, R.B. Walker and L.R. McGee, "Burning Rate Modifier Effects on a High Rate Tactical Propellant", AIAA-77-928 (1977)
6. S. Raynal and G. Doriath, "New Functional Prepolymers for High Burning Rates Solid Propellants", AIAA-86-1594 (1986)
7. B. Finck, C. Perut, J. Brunet, "Safety and Insensitivity Improvement by Using Butacene, a Ferrocene Grafted HTPB", ADPA Meeting New Orleans, Oct. 1992
8. Gilles Fonblance & Bruno Herran, "The Maturity of Butacene Based Composite Propellants", AIAA-94-3194 (1994)
9. K. Kishore and M.R. Sunitha, "Effect of Transition Metal Oxides on Decomposition & Deflagration of Composite Solid Propellant System: A Survey", AIAA, VOL.17, N.10, 1979
10. J. Richard Ward, "On the Copper(III)-Catalyzed Low Temperature Decomposition of Ammonium Perchlorate", BRL MR-2390, 1974

Table 1. Burning Rate of HTPB/Al/AP Composite Propellants

NO.		A	B	C	D	E	F
Item							
1	HTPB Binder, wt %	17	15	15	15	15	15
2	Fe ₂ O ₃ , wt%	—	—	—	2	2	2
3	Butacene, wt%	—	—	2	—	—	—
4	Carbon Fiber, wt%	—	2	—	—	1	3
5	Al fine, wt%	17	17	17	17	17	17
6	AP fine + UFAP, wt%	66	66	66	66	65	63
Burning Rate, mm/sec	@ 16 kg/cm ²	5.4	10.7	17.2	14.9	16.5	19.5
	@ 100 kg/cm ²	17.1	37.9	39.7	52.9	60.1	71.1
Pressure Exponent n		0.63	0.69	0.46	0.69	0.71	0.71

Table 2. Burning Rate of HTPB or Butacene/Al/AP Composite Propellants

NO.		D	G	H	I
Item					
1	HTPB Binder, wt %	15	8	—	—
2	Butacene Binder, wt %	—	7	15	15
3	Fe ₂ O ₃ , wt%	2	2	2	—
4	Al fine, wt%	17	17	17	17
5	AP fine + UFAP, wt%	66	66	66	68
Burning rate, mm/sec	@ 16 kg/cm ²	14.9	24.5	33.7	25.9
	@ 100 kg/cm ²	52.9	71.6	93.2	66.5
Pressure Exponent n		0.69	0.59	0.56	0.52

Table 3. Burning Rate of Butacene/Al/AP/Carbon Fiber Composite Propellants

Item	NO.	J	K	L	M	N	O	P	Q	R	S
Butacene Binder, wt%		15	15	15	15	15	15	15	15	15	15
Fe ₂ O ₃ , wt%		2	2	2	2	2	2	2	2	2	2
Carbon Fiber, wt%		1	2	3	1	3	3	3	3	3	3
Al 16 μ m, wt%		10	10	10	17	17	—	—	17	—	—
Al 30 μ m, wt%		—	—	—	—	—	17	—	—	17	—
Al 60 μ m, wt%		—	—	—	—	—	—	17	—	—	17
AP 20 μ m, wt%		—	—	—	—	—	—	—	17	17	17
AP 50 μ m, wt%		25	25	25	19	17	17	17	—	—	—
UFAP, wt%		47	46	45	46	46	46	46	46	46	46
Burning Rate, @16 kg/cm ²		40.7	43.7	45.4	39.5	42.6	41.8	49.8	41.4	46.5	51.4
mm/sec @100 kg/cm ²		105.4	108.4	110.4	104.2	104	107.1	117.3	107.9	109.7	118.5
Pressure Exponent n		0.54	0.48	0.49	0.53	0.49	0.51	0.47	0.52	0.47	0.46

Table 4. Ballistic Properties of Butacene/Al/AP/Carbon Fiber Composite Propellants

Item NO.	Composition, wt%	Ballistic Properties		
		Burning Rate, mm/sec		Pressure Exponent n
		16 kg/cm ²	100 kg/cm ²	
1	Butacene/Al/AP/Fe ₂ O ₃ /Carbon Fiber 15/ 17/ 63/ 2/ 3	51.4	118.5	0.46
2	Butacene/Al/AP/Fe ₂ O ₃ 15/ 17/ 66/ 2	33.7	93.2	0.56
3	HTPB/Al/AP/Fe ₂ O ₃ 15/ 17/ 66/ 2	14.9	52.9	0.69

Table 5. Thermoanalytical Data by ARC

Item NO.	T _m	T _i	t _m	t _i	r _i	$\frac{\Delta T^*}{\Delta t}$
1	302.7	183.8	514.2	440.2	0.06	1.61
2	325.8	169.2	631.8	406.2	0.02	0.69
3	268.9	179.7	622.1	356.4	0.02	0.34

Overall Reaction Rate:

$$* \frac{\Delta T}{\Delta t} = (T_m - T_i) / (t_m - t_i)$$

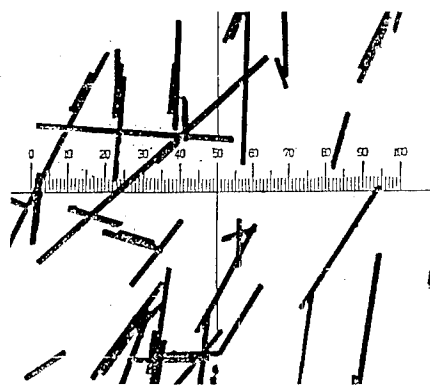
T_m : max. reaction temperatureT_i : initial reaction temperaturet_m : time to max. reactiont_i : time to initial reactionr_i : initial reaction rate

Fig. 1. Microscopic picture (200X)

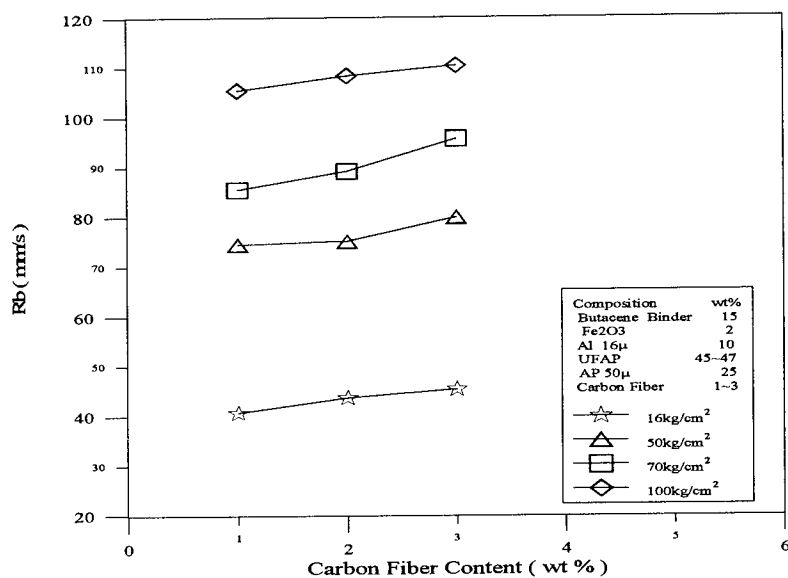


Fig. 2. Effect of concentration of carbon fiber on burning rate of Butacene/Al/AP/Carbon Fiber composite propellants.

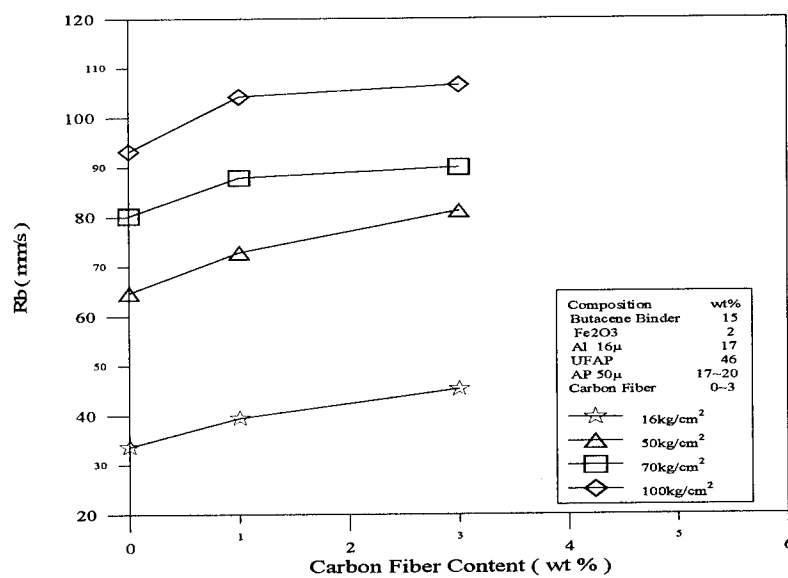


Fig. 3. Effect of concentration of carbon fiber on burning rate of Butacene/Al/AP/Carbon Fiber composite propellants.

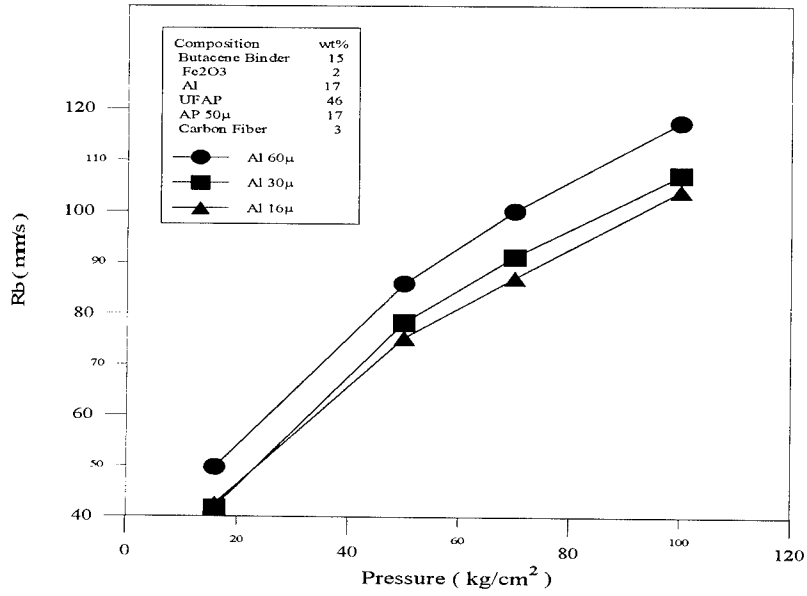


Fig. 4. Effect of different Al particle size on burning rate of Butacene/Al/AP/Carbon Fiber composite propellants.

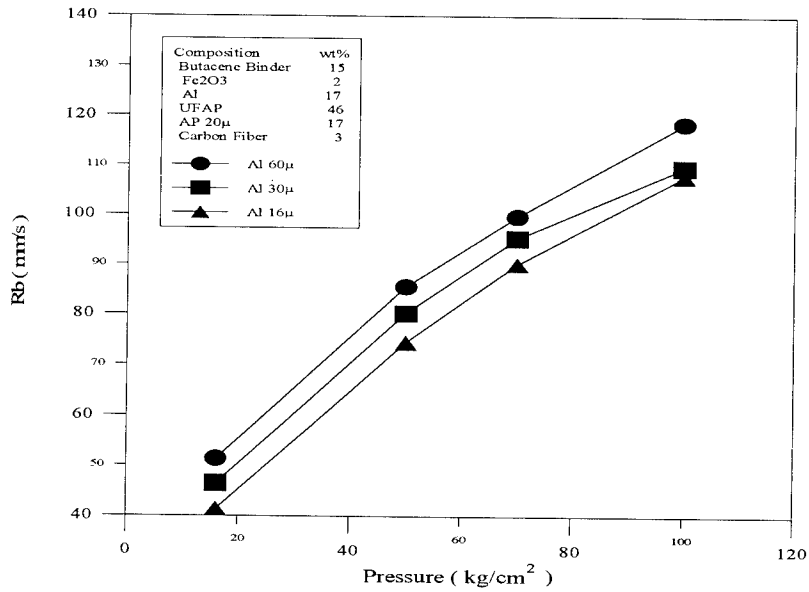


Fig. 5. Effect of different Al particle size on burning rate of Butacene/Al/AP/Carbon Fiber composite propellants.

Curve 1: DSC
File info: c596d Tue Aug 2 10:48:08 1994
Sample Weight: 1.074 mg
C59-6

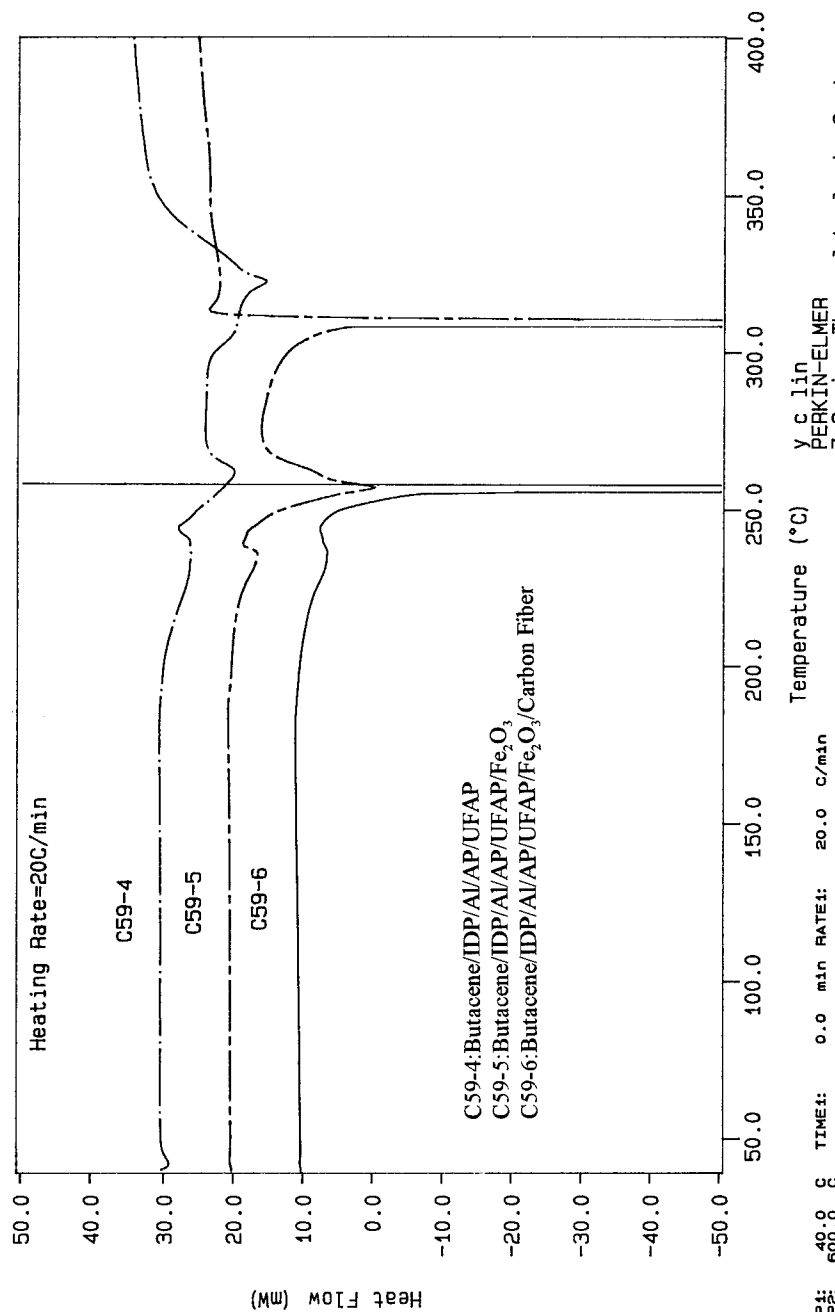
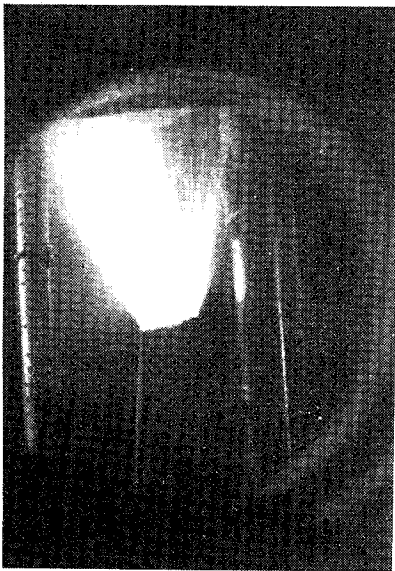


Fig. 6. DSC thermographs of Butacene/Al/AP/Fe₂O₃/Carbon Fiber



Propellant H without carbon fiber



Propellant R with carbon fiber

Fig. 7. Flame structures of propellant H & R

THERMAL DECOMPOSITION OF DINITRAMIDE AMMONIUM SALT

G.B. Manelis

Institute of Chemical Physics RAS in Chernogolovka

The kinetics of dinitramide ammonium salt $\text{NH}_4\text{N}(\text{NO}_2)_2$ (1) decomposition was studied by the manometric method. This method was adjusted by the spectrophotometric analysis of N_3O_4^- anion. The aqueous solution of 1 has the maximum of adsorption at 283.5 nm with the extinction coefficient $\Sigma = 5600 \pm 100$. Gaseous products were analyzed by LGC technique and mass-spectrometry, water - by the Fisher method, nitric acid in the products - by H^+ concentration. The special physical chemical methods has been elaborated for the determination of ammonium nitrate admixture in 1.

The degree of vessel filling with the substance (m/V , g/cm^3) was changed from 10^{-4} to 1. Large m/V allows to observe the reaction at the early stages beginning with the conversion degree of 0.01%.

Decomposition in the liquid phase

At the large free volume ($m/V < 6 \cdot 10^{-4}$) and the temperatures above 130°C the decomposition follows a first order equation (Figs 1 and 2). From 1 mole of 1 four moles of the gaseous products are formed. Composition of the products is the following: N_2O and N_2 (25% of each), H_2O (50%), NO and NO_2 traces. The condensed residue is NH_4NO_3 .

The rate constant of the first order takes the form:

$$k = 10^{14.4} \exp (-35500/RT) \text{ s}^{-1} \quad (1)$$

At the temperatures 100 - 120 °C and $m/V > 0.01$ the reaction has clearly defined autocatalytic character (Fig. 3). Up to the conversion degree of 15% (104 °C, $m/V = 0.3$) the curve is described with the first order equation of autocatalysis. Further the change in the rate follows the first order law with the rate constant 50 times more, than that of for the initial stage of the decay.

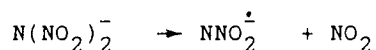
HNO_3 , water, ammonium nitrate and obviously N_2O_4 are accumulated in the melt 1 at large m/V up to the conversion degree of 15 - 20%. After that the formation of nitric acid and water is stopped. N_2O , N_2 and traces of NO and NO_2 are discovered in the gas phase. At the early stages N_2 and N_2O are formed in the equal amounts. Further the portion of N_2 is decreased and after 15 - 20% of decomposition N_2 is not formed at all. At the second stage of the catalytic process described with the first order equation (see Fig. 3) only N_2O and ammonium nitrate are formed. The total amount of the gaseous products at all stages comprises 1 mole per mole of 1.

The rate of the catalytic processes depends on m/V . The direct experiments proved, that HNO_3 and NO_2 play here the role of catalysts.

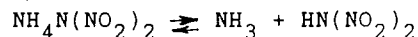
The rate of the initial stage decomposition does not depend on m/V and the rate constant is described with the equation (1)

obtained for the noncatalytic decay at high temperatures (Fig. 4).

The parameters of this equation correlate best of all to the N - N breaking in the anion:



There are some data indicating that an alternative way of decay through the salt dissociation is possible:



In the experiments with $\text{ND}_4\text{N}(\text{NO}_2)_2$ a kinetic isotope effect $K_H/K_D = 1.38$ at 98°C was discovered. On addition of NH_3 the initial rate decreases. The strong bases like urotropin which are capable to displace NH_3 from the salt operate in the same way. The decomposition in vacuum in the open vessel gives sublimation of 1.

All these facts are helpful in elucidation of the decomposition scheme of 1 in the melt (Fig. 5). The reactions (1) and (1') comprise respectively the main and side route of the anion primary decay. After the fast transformation reactions of the intermediate products the equilibrium (6) is set. As its consequence N_2 and N_2O are formed in the equal amounts by (7) and (8). The reaction (8) inhibits the catalysis by means of HNO_3 . The fast chain process (9 - 11) simulating a first order reaction exceeds (1) and (1') and brings the reaction to the end.

The time of 0.1% decomposition is 1 hour at 98 °C and 20 min at 105 °C.

Decomposition in the solid phase.

The decomposition in the solid phase possesses many features of the liquid-phase decomposition nearby the melting point, but stability of the solid 1 is significantly higher, than that of the molten.

Likewise the melt one mole of 1 gives about 1 mole of the gaseous products: N_2 , N_2O , traces of NO . The share of N_2 ranges from 10 to 30% and depends on sample purity.

The reaction takes place with self-acceleration, though the induction periods are very long. At 80 °C $\tau_{ind} = 120$ hours, at 60 °C it is 3 months. That is why the catalytic stage is not under study.

The initial stage of decomposition with the constant rate lasts to the conversion degree of 0.05%. The examples of the catalytic curves, gas evolution rates (W , sm^3/G hr) and times of 0.01 cm^3/g of gaseous products evolution at 40 - 80 °C ($\tau_{0.01}$) are shown in Figs 6 and 7. For the temperature dependence of $\tau_{0.01}$ the following expression has been obtained:

$$\lg \tau_{0.01} = -19.35 + 7353/T \text{ hr} \quad (2).$$

The activation energy of the solid 1 decomposition is equal to 33.6 kcal/mol, that is close to E_{liq} . From the correlation between equation (1) and (2) it follows, that solid-phase 1 is 50 times more stable, than the molten as regards the initial rates.

The solid-phase decay does not reveal evidence of salt dissociation to ammonium and acid. In particular, ammonium and strong bases like uropropin do not influence the initial decomposition rate of pure 1.

Water and ammonium nitrate admixtures strongly affect stability of solid 1. Both these substances form with 1 the eutectics having the approximate composition of 40% admixture / 60% 1. The melting point of the eutectics with NH_4NO_3 is 60 °C, with water it is about 15 °C. The rates of 1 decomposition in the saturated aqueous solution and in the liquid eutectics with ammonium nitrate are described with equation (1), that is, they are equal to the decay rate of molten 1. Water and ammonium nitrate are chemically inert to 1, but affect its decay by the mechanism of melting. Thus, at 80 °C one part of NH_4NO_3 melts with 6 parts of 1, and in one part of H_2O twenty parts of 1 are dissolved. On addition of 0.5% of nitrate the stability of 1 should decrease 2.5 times. The calculation agrees well with the experiment (Table). Water effect manifests itself only at the water content more, than 0.5%. At a less content water stays in the adsorbed state and does not form its own phase. At 80 °C the stability of 1 with 0.5 and 1.0% of water differs 6 times.

Equation (2) was obtained for the samples of 1 having H_2O - 0.4%, ammonium nitrate - 0.5%.

Abnormal decay.

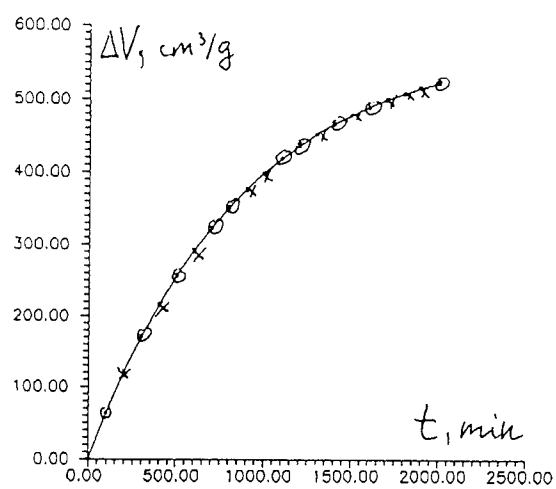
A unique phenomenon named the "abnormal decay" has been discovered at decomposition of 1. The essence of it is that severely dried samples of 1 have the initial decomposition rate at 60 °C significantly higher, than at 80 °C and thousands times exceeding that of the moistened sample (Fig. 8). At the temperatures below 60 °C the decomposition proceeds with higher rates and smaller activation energy, than the moistened samples have (Fig. 9). The transition boundary to the abnormal decay is approximately 0.2% H_2O . The abnormal decay takes place mainly on the surface and crystal defects. Its rate depends on the degree of drying. Water vapors, as a rule, strongly inhibit the abnormal decay.

To explain the phenomenon of "abnormal decay" the existence of two modifications of 1 differing in structure and anion stability was assumed. However this hypothesis is not rigorously proved.

To prevent the abnormal decay it is necessary to conduct the soft drying and to control the moisture content in storage.

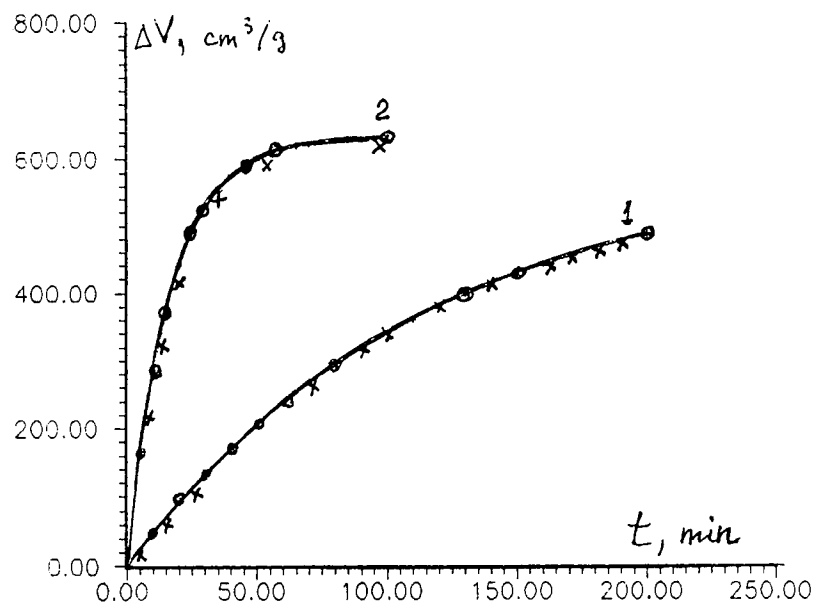
Conclusions

1. The initial decomposition of 1 proceeds via monomolecular breaking N - N bond in N_3O_4^- anion. In the melt the salt dissociation to ammonium and acid plays a definite part.
2. The stability of 1 in the molten state is not high. It is possible to handle 1 in isothermal conditions at the temperatures up to 100 °C for 1 hour.
3. The stability of 1 in the solid state is high enough to conduct technological processes at 60 - 70 °C. Long - term storage is possible at 20 - 25 °C.
4. Dried samples of 1 with the water content less, than 0.2% show the abnormal behavior in the decay, that is: the Arrhenius dependence of the rate is violated, at 60 °C the solid-phase decay proceeds faster, than in the melt at 100 °C. Abnormal samples are unstable. To avoid the abnormal decay it is necessary to control the moisture of 1.



Decomposition of ADN at 130 °C.
 m/V_f (g/cm^3): ○ - 0.0003, x - 0.0006

Fig.1

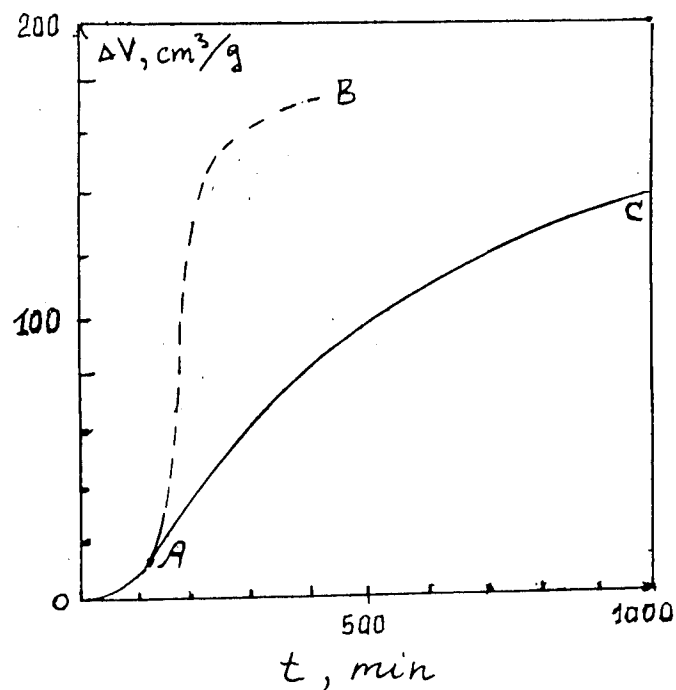


Decomposition of ADN.

$m/V_p = 0.0004 \text{ g/cm}^3$. 1 - 150 °C; 2 - 170 °C; \circ - before purification, \times - after purification.

$$k = 10^{14.4} \exp(-35500/RT), \text{ s}^{-1}$$

Fig. 2



. Decomposition of ADN in liquid state at 104 °C,
 $m/V_f = 0.3 \text{ g/cm}^3$. — experimental curve, ---- calculated curve for the first order autocatalytic reaction.

OA - autocatalytic reaction (catalysis by volatile products)

$$OB \quad \frac{d\eta}{dt} = k_1 (1-\eta) + k_2 \eta (1-\eta)$$

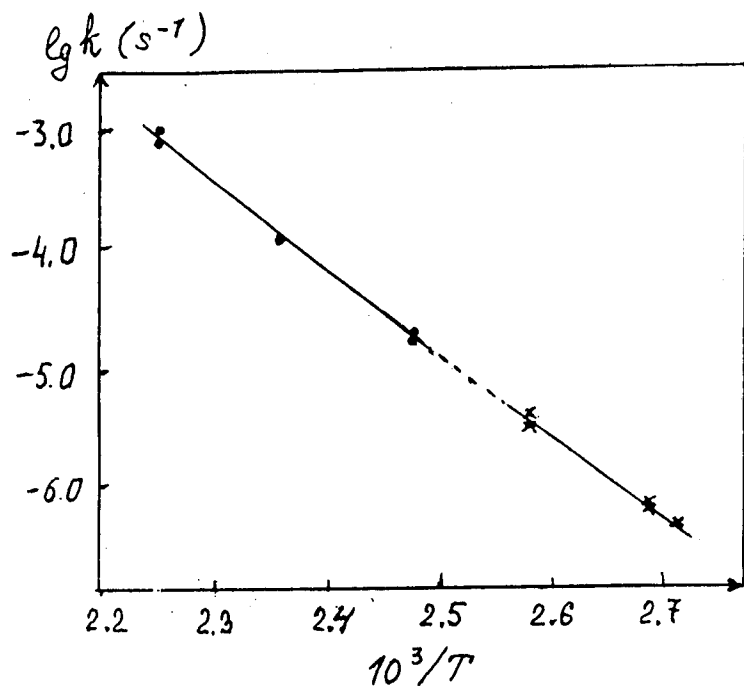
$$AC \quad \frac{d\eta}{dt} = k_3 (1-\eta)$$

reaction of ADN with
 $\text{N}_2 \text{O}_4$

$$k_1 = 9,92 \cdot 10^{-7} \text{ s}^{-1}, \quad k_2 = 5,6 \cdot 10^{-4} \text{ l/mol} \cdot \text{s}$$

$$k_3 = 5,0 \cdot 10^{-5} \text{ s}^{-1}$$

Fig. 3



Arrhenius plot for ADN decomposition in liquid state, noncatalytic step. • - points for 130, 150 and 170 °C, x - points for 97, 100 and 115 °C.

$$k = 10^{14.4} \exp(-35500/RT), s^{-1}$$

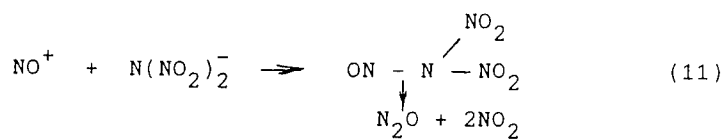
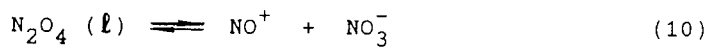
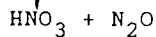
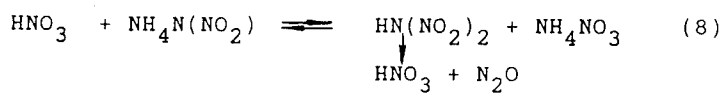
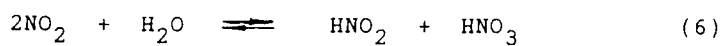
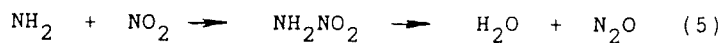
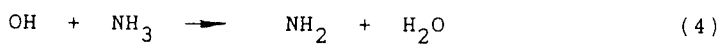
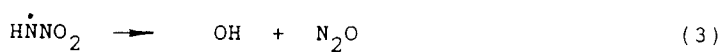
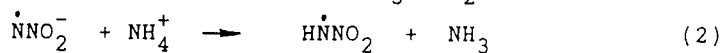
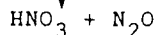
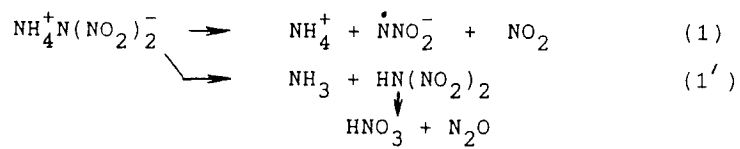
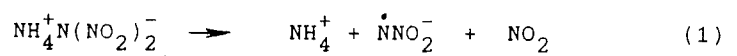
$$\lg \tau_{0.1\%} = -19.076 + \frac{7692}{T}, min$$

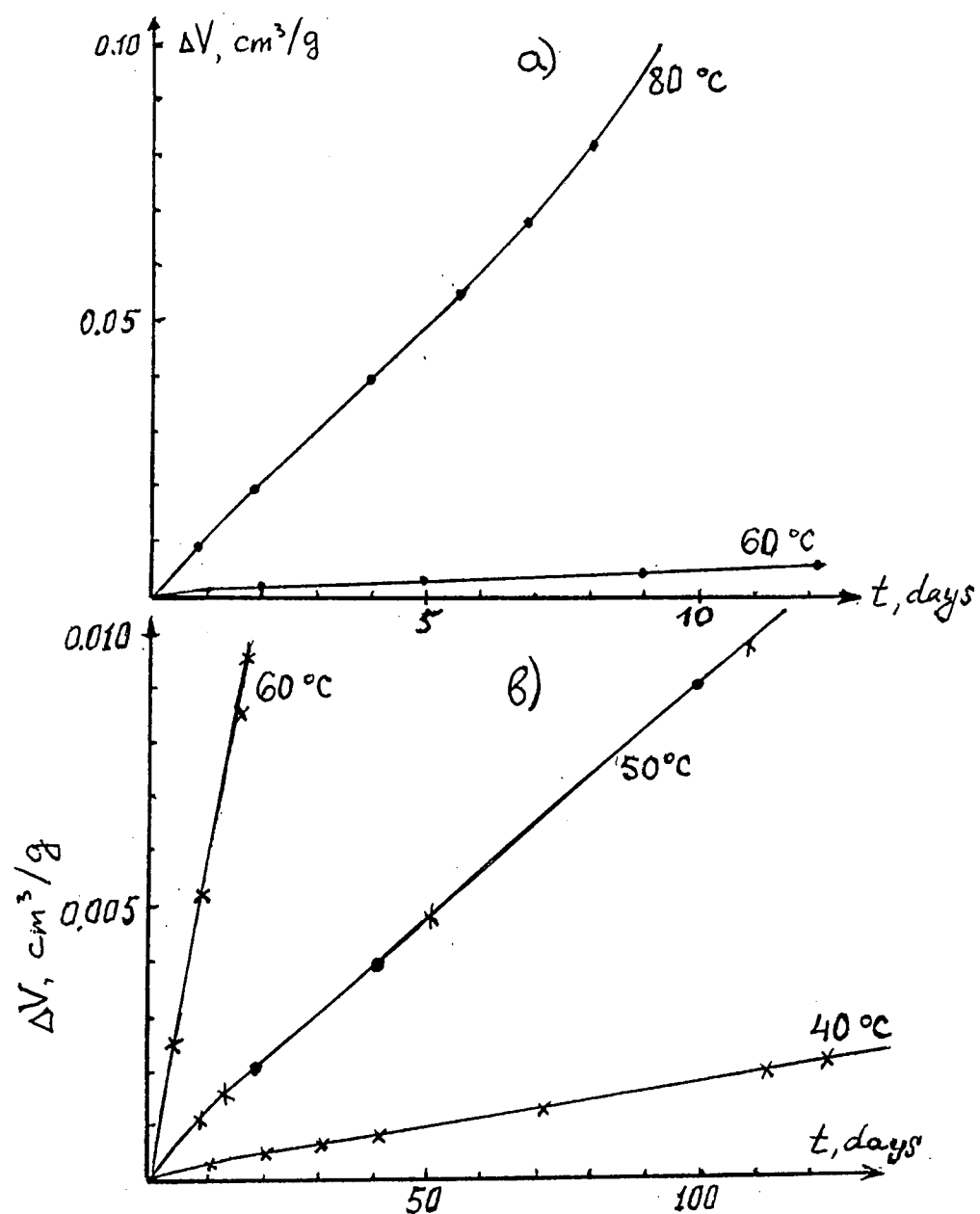
$$\tau_{0.1\%} = 67 min \quad at \quad 98^\circ C$$

Fig. 4

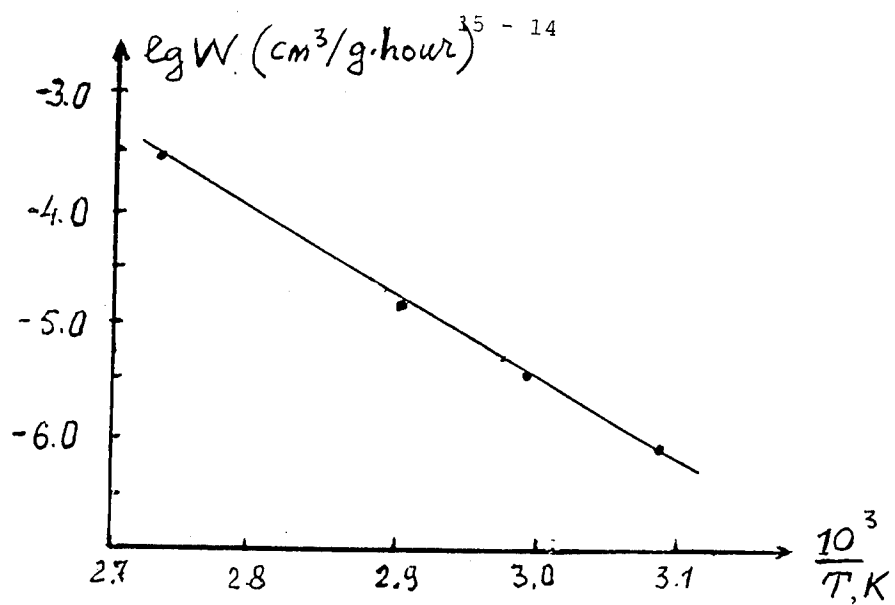
Fig. 5

MECHANISM OF DECOMPOSITION IN THE LIQUID PHASE





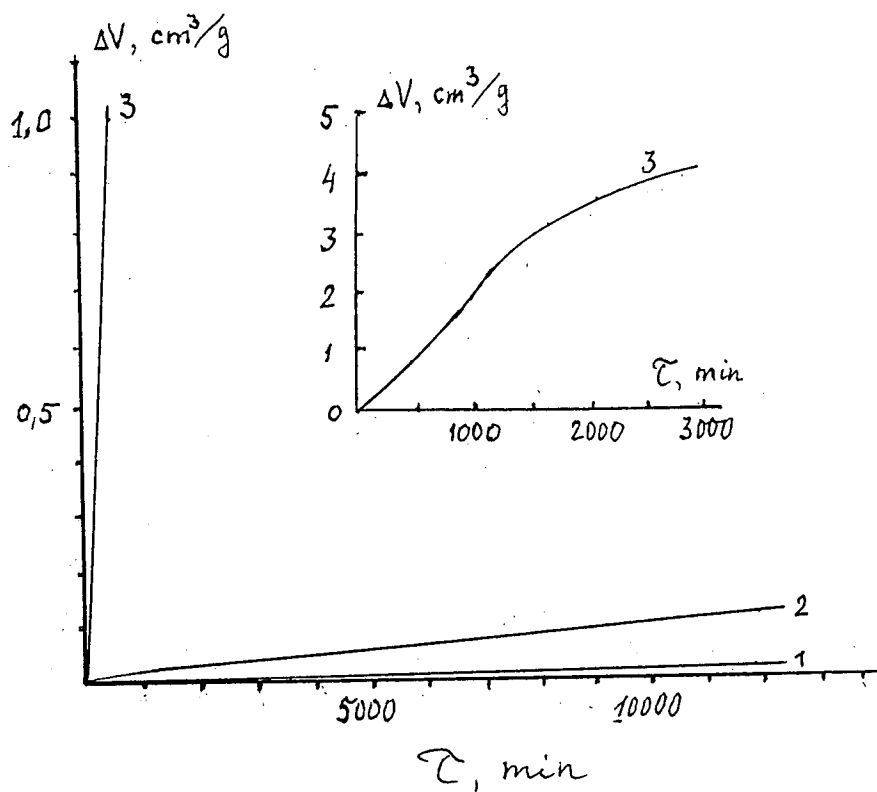
Decomposition of ADN a) 60 and 80 °C
 b) 60, 50 and 40 °C
 Points - $m/V_f = 0.4 \text{ g/cm}^3$; crosses - $m/V_f = 0.8 \text{ g/cm}^3$.



Arrhenius plot for the rate of gas evolution from solid ADN.

$$\lg \hat{r}_{0.01} \text{ cm}^3/\text{g} = -19.35 + \frac{7353}{T} \cdot \text{hour}$$

Fig. 7



The abnormal decay of an ADN sample with the moisture content of 0.5%

1 - 0.4% H_2O , 60 °C;

2 - 0.05% H_2O , 80 °C;

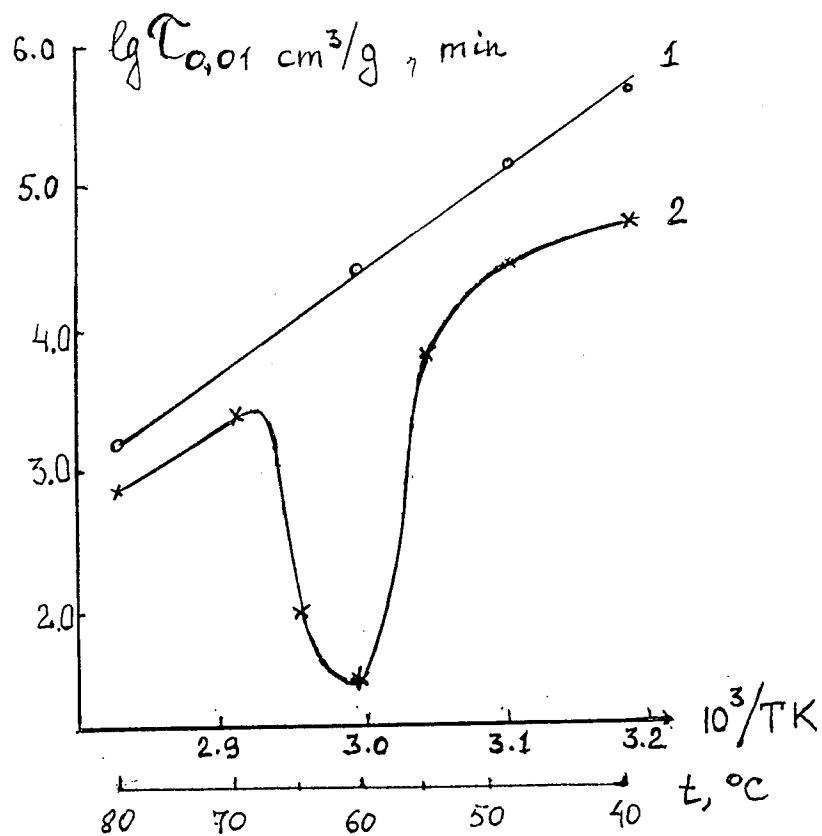
3 - 0.05% H_2O , 60 °C.

Fig.8

TABLE

AN influence on the ADN stability at 80 °C.

Amount of AN (mass %)	$\tau_{0.01 \text{ cm}^3/\text{g}, \text{ min}}$	
	calculated	experiment
0	2500	2500
0.5	1000	1100
1.0	635	700
2.0	365	-
2.5	300	300
3.0	250	-
4.0	190	-
5.0	160	150
8.0	100	-
10.0	80	-
15.0	55	-
17.0	50	50



The dependence of the evolution time of $0.01 \text{ cm}^3/\text{g}$ of products on temperature.

1 - the initial sample, $H_2O\% > 0.2$;

2 - the abnormal sample, $H_2O\% = 0.05$.

Fig.9

ABBRANDEIGENSCHAFTEN VON VERZÖGERUNGSSÄTZEN AUF DER BASIS VON BLEIOXID/SILICIUM

Dirk Cegiel

NICO-PYROTECHNIK, Hanns-Jürgen Diederichs GmbH & Co. KG, Trittau, FRG

Abstract

This paper presents the properties of combustion in silicon-red lead delay compositions. Factors influencing the burning rate, the burning behaviour and the mechanical sensitivity are described. These factors are the fuel/oxidant ratio, silicon particle size and the content of kieselguhr and binder. The relationship between burning rate, burning behaviour and mechanical sensitivity will be discussed.

1 Einleitung

Verzögerungssätze auf der Basis von Bleioxiden und Silicium werden seit mehr als 50 Jahren eingesetzt und haben große Bedeutung in vielen pyrotechnischen Verzögerungen erlangt. Gründe hierfür sind unter anderem die Bildung einer festen Schlacke, welche die Wirkung eines "Gasschlusses" hat [1] und die gute Alterungsbeständigkeit bei hoher relativer Luftfeuchtigkeit [2].

Ziel dieser Arbeit ist es, die Einflußgrößen, welche die Abbrandeigenschaften des Satzsystems Blei(II,IV)-oxid/Silicium beeinflussen, zu erfassen und Abhängigkeiten aufzuzeigen. Die betrachteten Eigenschaften sind neben der Verzögerungszeit die Abbrandcharakteristik und die mechanische Sensibilität.

2 Einflußgrößen auf die Verzögerungszeit

2.1 Experimentelles

Die Verzögerungszeit der einzelnen Sätze wird im offenen Abbrand ermittelt. Hierzu wird der Satz in Messingröhrchen ($d_i = 3,9$ mm, $d_a = 6,0$ mm, $l = 19$ mm) mit einem Druck von 238 MPa verpreßt. Die Länge der Satzsäule beträgt 18 mm. Die Ladedichte liegt in Abhängigkeit von der Satzzusammensetzung zwischen 2,14 und 4,58 g/cm³. Die so hergestellten Verzögerungsstücke werden mit einem elektrischen Brückenzünder angezündet. Gekoppelt mit dem Anzündimpuls wird ein elektronisches Zählwerk gestartet, welches nach dem Durchbrennen der 18 mm langen Verzögerungsstrecke über eine Photodiode gestoppt wird.

2.2 Einfluß des Mischungsverhältnisses Blei(II,IV)-oxid/Silicium

Die Verzögerungszeiten sind für Mischungsverhältnisse von 40:60 bis 90:10 Gew.% Pb₃O₄/Si nach der in Abschnitt 2.1 beschriebenen Methode ermittelt worden. Das verwendete Pb₃O₄ hat eine Reinheit von 96 % und eine mittlere Korngröße von 2,2 µm. Die Reinheit des Siliciums beträgt 98 %, die mittlere Korngröße liegt bei 2,7 µm. Die beiden Substanzen wurden unter Sicherheit trocken gemischt. In Abbildung 1 ist die Abhängigkeit der Verzögerungszeit vom Mischungsverhältnis Pb₃O₄/Si dargestellt. Aufgetragen ist die Verzögerungszeit gegen den Siliciumgehalt.

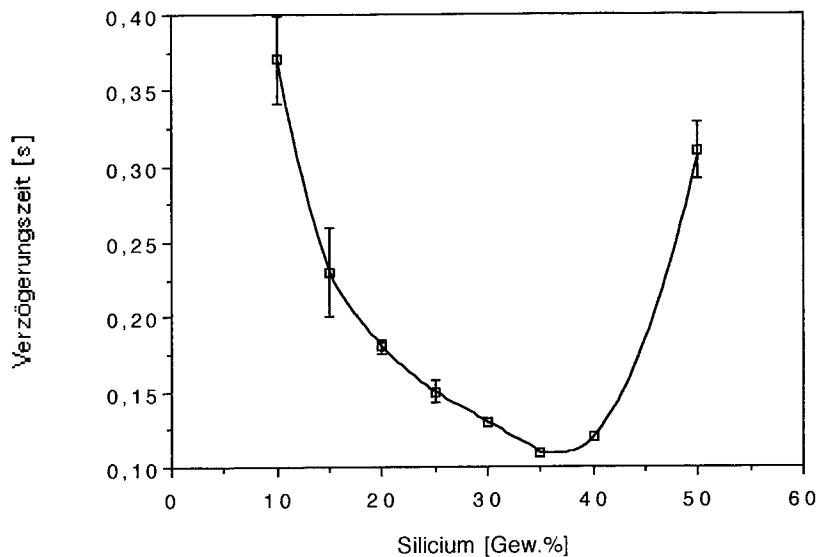


Abb. 1. Verzögerungszeit der 18 mm langen Satzssäule als Funktion des Si-Gehaltes in der Mischung. Die aufgetragene Verzögerungszeit ist der Mittelwert aus vier Messungen.

Man erkennt, daß die Verzögerungszeit bei einem Si-Gehalt von 35 Gew.% ein Minimum durchläuft. Die Schwankungen in der Brennzeit sind zwischen 30 und 40 Gew.% Si am geringsten. Die verpreßte Mischung mit einem Si-Gehalt von 60 Gew.% läßt sich mit Hilfe eines Brückenzünders nicht mehr anzünden.

Untersuchungen des Verzögerungssatzes $\text{Pb}_3\text{O}_4/\text{Si}$ im geschlossenen System (Messung der Verzögerungszeit in sprengkräftigen Millisekundenzündern) ergaben gleichartige Kurvenverläufe [3].

Interessant ist, daß die größte Abbrandrate (in cm/s und g/s) bei einem Si-Gehalt von 35 Gew.% liegt, obwohl die größte Reaktionsenthalpie bei einem Gehalt von 7,6 Gew.% Si gemessen wird [4, 5]. 7,6 Gew.% Si werden bei der stöchiometrischen Umsetzung von Pb_3O_4 und Si zu SiO_2 und Pb benötigt. Warum die maximale Abbrandrate und die maximale Reaktionsenthalpie bei derart unterschiedlichen Si-Gehalten liegen, ist möglicherweise auf die Passivierung der Si-Oberfläche durch das gebildete SiO_2 zurückzuführen. Die Bildung von SiO_2 auf einer Si-Oberfläche wird

stark herabgesetzt, sobald sich eine wenige Nanometer dicke Schicht von SiO_2 gebildet hat [6].

2.3 Einfluß der Korngröße des Siliciums

Es wurden drei unterschiedliche Silicium-Typen mit gleichem Si-Gehalt (98 Gew.% Si) aber unterschiedlichen Korngrößenverteilungen untersucht. Die Korngrößenverteilung wurde mittels Laserbeugung bestimmt. Die Summenkurven der Korngrößen für die drei untersuchten Si-Typen sind in Abbildung 2 dargestellt.

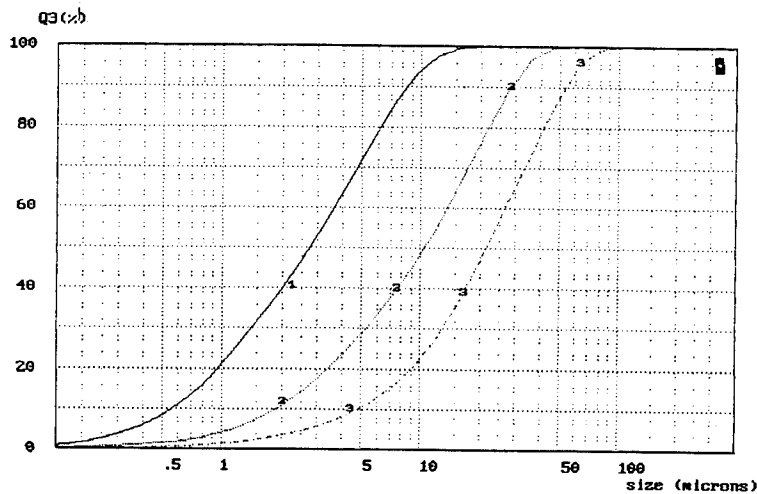


Abb.2. Summenkurven der Korngrößen der drei untersuchten Si-Typen.
Mittlere Korngrößen: 2,7 μm (1), 10,5 μm (2), 21,4 μm (3)

Von den drei Si-Typen wurden Verzögerungssätze mit der Zusammensetzung 75 Gew.% Pb_3O_4 /25 Gew.% Si hergestellt und die Verzögerungszeiten, wie in Abschnitt 2.1 beschrieben, bestimmt. In Abbildung 3 ist die Verzögerungszeit in Abhängigkeit von der mittleren Korngröße des Siliciums dargestellt. Auf den Einfluß des Binders wird in Abschnitt 2.5 noch näher eingegangen.

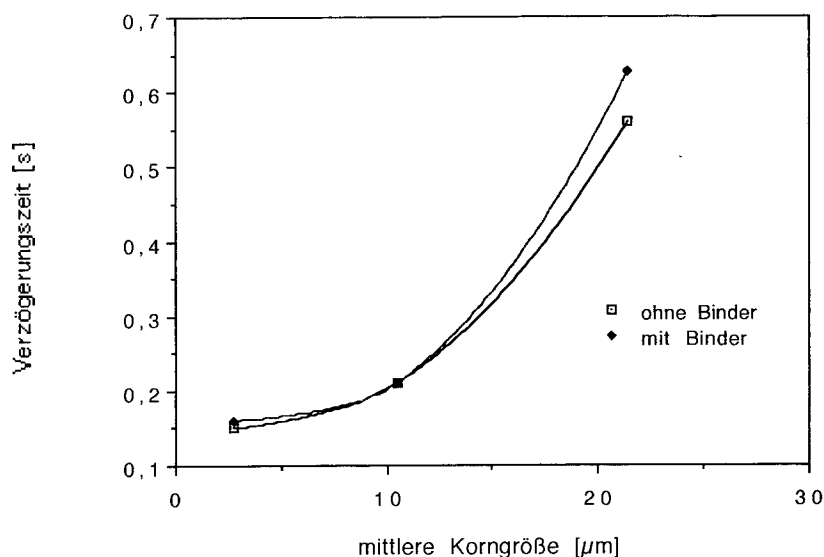


Abb. 3. a) Abhängigkeit der Verzögerungszeit von der Korngrößenverteilung des Siliciums. - b) Einfluß des Binders (Fluor-Elastomer) auf die Verzögerungszeit. Mischungsverhältnis $\text{Pb}_3\text{O}_4/\text{Si}$ 75:25 Gew.%.

Man erkennt, daß die Verzögerungszeit nicht direkt proportional zur mittleren Korngröße des Siliciums ist. Die Abhängigkeit der Verzögerungszeit von der Korngröße nimmt mit zunehmender Korngröße zu.

Geht man davon aus, daß mit abnehmender Korngröße die spezifische Oberfläche des Siliciums zunimmt, so ist der gleiche Zusammenhang auch von [3] beobachtet worden. So ist die Verzögerungszeit bei spezifischen Si-Oberflächen von $> 2 \text{ m}^2/\text{g}$ nicht mehr von der Größe der Oberfläche des Siliciums abhängig. Hingegen besteht ein linearer Zusammenhang zwischen Verzögerungszeit und Oberfläche bei einer spezifischen Oberfläche $< 0,25 \text{ m}^2/\text{g}$. Erklärt wird dieses Verhalten mit einer unterschiedlichen Reaktionskinetik bei großen bzw. kleinen spezifischen Oberflächen.

2.4 Einfluß von Kieselgur im Satzsystem Blei(II,IV)-oxid/Silicium

In Mischungen aus 75 Gew.% Pb_3O_4 /25 Gew.% Si (mittlere Korngröße des Si: $2,7 \mu\text{m}$) wurden zusätzlich 3 und 6 Gew.% Kieselgur homogen untergemischt. Die Ver-

zögerungszeiten wurden, wie im Abschnitt 2.1 beschrieben, bestimmt. In Abbildung 4 ist die Verzögerungszeit gegen den Zusatz an Kieselgur aufgetragen.

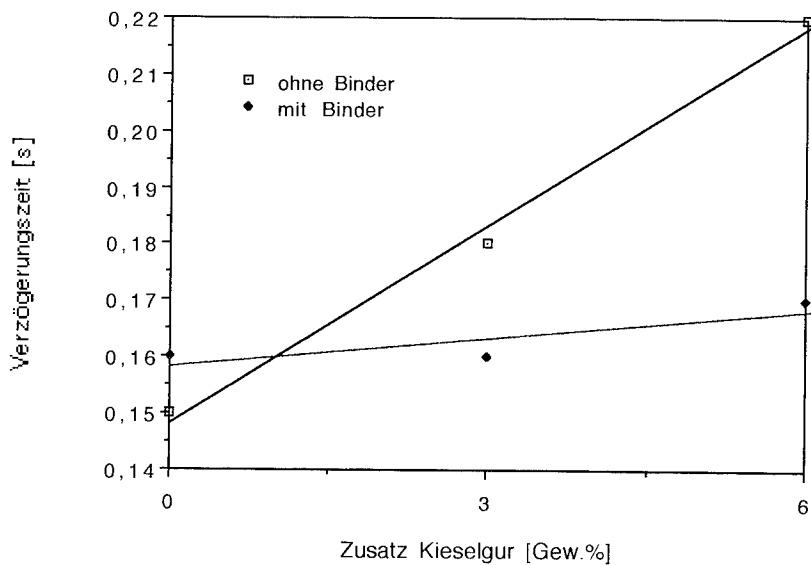


Abb.4. a) Verzögerungszeit als Funktion des Zusatzes an Kieselgur. - b) Einfluß des Binders (Fluor-Elastomer) auf die Verzögerungszeit.
Mischungsverhältnis $\text{Pb}_3\text{O}_4/\text{Si}$ 75:25 Gew.%.
Man erkennt, daß sich durch den Zusatz von 6 Gew.% Kieselgur die Verzögerungszeit um ca. 50 % verlängert. Dieses gilt jedoch nur für die Sätze, die keinen Binder enthalten.

2.5 Einfluß des Binders

In den Abbildungen 3 und 4 ist zusätzlich zu den schon besprochenen Einflußgrößen der Einfluß eines Binders dargestellt. Als Binder wurde ein Fluor-Elastomer in einer Konzentration von < 0,7 Gew.% eingesetzt.

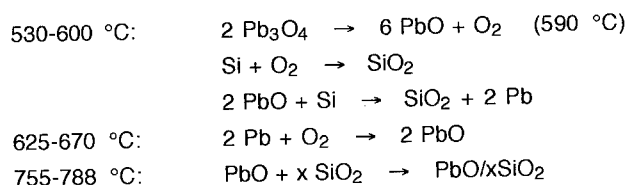
Der Einfluß des Fluor-Elastomer im Satzsystem $\text{Pb}_3\text{O}_4/\text{Si}$ ist in Abbildung 3 dargestellt. Bei einer mittleren Korngröße des Siliciums von $21,4 \mu\text{m}$ bewirkt der Binder

eine Verlängerung der Verzögerungszeit um ca. 12 %. In den Sätzen, welche aus den feineren Si-Typen hergestellt wurden, wirkt sich der Binder nur unwesentlich auf die Verzögerungszeit aus.

In Abbildung 4 ist der Einfluß des Fluor-Elastomers im Satzsystem $\text{Pb}_3\text{O}_4/\text{Si}/\text{Kieselgur}$ dargestellt. Man erkennt, daß die durch den Zusatz des Kieselgurs bedingte Herabsetzung der Umsetzungsgeschwindigkeit durch die Anwesenheit kleiner Mengen eines Fluor-Elastomers kompensiert wird.

Ein Vergleich der Abbildungen 3 und 4 in Bezug auf den Einfluß des Binders ergibt, daß die erzielte Wirkung im Satzsystem $\text{Pb}_3\text{O}_4/\text{Si}$ unterschiedlich von der im Satzsystem $\text{Pb}_3\text{O}_4/\text{Si}/\text{Kieselgur}$ ist. Einer Herabsetzung der Umsetzungsgeschwindigkeit im System $\text{Pb}_3\text{O}_4/\text{Si}$ steht eine Steigerung im System $\text{Pb}_3\text{O}_4/\text{Si}/\text{Kieselgur}$ gegenüber. Eine Erklärung hierfür liegt in den stattfindenden Reaktionen des Siliciums und des Kieselgurs (amorphes SiO_2) mit dem Fluor-Elastomer. Oberhalb von 350 °C zersetzen sich Fluorpolymere unter Bildung von Fluorwasserstoff [7]. Zum einen findet im Satzsystem $\text{Pb}_3\text{O}_4/\text{Si}$ eine Fluoroxidation des Siliciums statt, zum anderen reagiert im Satzsystem $\text{Pb}_3\text{O}_4/\text{Si}/\text{Kieselgur}$ das SiO_2 mit dem HF zu SiF_4 .

Die exotherme Reaktion, welche durch die Reaktion des Fluor-Elastomers hervorgerufen wird, ist mit Hilfe der Differentialthermoanalyse (DTA) gut identifizierbar. Die DTA ist mit einer Probenmenge von 50 mg und einer Aufheizrate von 10 °C/min in Luft durchgeführt worden. Neben den bekannten Reaktionen [4, 5] bei



findet eine exotherme Reaktion zwischen 300 und 370 °C statt.

3 Abbrandcharakteristik

Neben der gut meßbaren Brennzeit einer Verzögerung, sind andere Abbrandeigenschaften weniger gut erfaßbar, da sie sich nicht auf einfache meßbare physikalische Größen zurückführen lassen. Zu nennen sind hier:

- Anzündempfindlichkeit,
- Abbrandbild,
- Struktur der Schlacke.

Die genannten Größen beeinflussen neben der Brennzeit die gesamte Funktion einer Verzögerung und sind daher von großer Bedeutung. Das Problem liegt allerdings in der objektiven Erfassung und der anschließenden Bewertung dieser Größen. So ist die Anzündempfindlichkeit mit Hilfe eines Gap-Testes zu ermitteln. Das Problem liegt hier im Erzeugen eines definierten Anzündstrahls. Das Abbrandbild und die Struktur der Schlacke lassen sich visuell beurteilen. Die Bewertung ist jedoch immer subjektiver Natur und stark von der Erfahrung des Betrachters abhängig.

Faktoren, die die Abbrandcharakteristik beeinflussen sind:

- Satzzusammensetzung,
- Korngrößenverteilung der Ausgangsstoffe,
- Binder,
- Zusatzstoffe (z.B. Kieselgur).

Mit Hilfe dieser Parameter läßt sich die Abbrandcharakteristik beeinflussen und optimieren. Eine Optimierung der Abbrandcharakteristik bei vorgegebener Verzögerungszeit und fertigungstechnischer Machbarkeit ist eine sehr komplexe und schwierige Aufgabe. Dieses liegt daran, daß die Veränderung jedes Parameters im allgemeinen sowohl positive als auch negative Auswirkungen hat und sich alle Parameter gegenseitig beeinflussen. Ein Versuch diese Abhängigkeiten aufzuzeigen, würde jedoch den Rahmen dieses Vortrages sprengen.

Wie wichtig die Optimierung der Parameter ist, wird z.B. bei der Abhängigkeit der Verzögerungszeit und deren Streuung von der Schlackenstruktur deutlich. So beeinflußt die Porosität und der Schmelzpunkt der Schlacke den Verschluß der Verzögerung. Da in Verzögerungssystemen, die wie Pb_3O_4/Si nicht gaslos abbrennen,

eine Abhängigkeit der Verzögerungszeit vom Gasdruck besteht [1], ist der Verschluß der Verzögerung von großer Bedeutung [8]. In offenen Verzögerungssystemen, in denen der Verschluß nicht durch die Bauart vorgegeben ist (gasdichte Versiegelung), sondern lediglich durch den Grad der Verschlackung bestimmt wird, ist die Struktur der Schlacke ausschlaggebend für die Funktion der Verzögerung.

4 Mechanische Sensibilität

Die mechanische Sensibilität ist insbesondere aus fertigungstechnischer Sicht von großer Bedeutung. Sie ist auch ein Grund dafür, nach Zusatzstoffen, wie z.B. Kieselgur, zu suchen, die die mechanische Empfindlichkeit beeinflussen.

4.1 Experimentelles

Zur Beurteilung der mechanischen Sensibilität, wurde die Reibempfindlichkeit der schon im Kapitel 2 beschriebenen Sätze bestimmt. Die Bestimmung wurde nach dem in Anhang 1 zum SprengG beschriebenen Verfahren durchgeführt. Angegeben ist jeweils die kleinste Stiftbelastung in N, welche den untersuchten Satz zur Reaktion bringt.

3.2 Einflußgrößen auf die Reibempfindlichkeit

In den Abbildungen 5, 6 und 7 ist der Einfluß der Satzzusammensetzung, der Korngröße, des Binders und des Kieselgurs auf die Reibempfindlichkeit dargestellt.

16 - 10

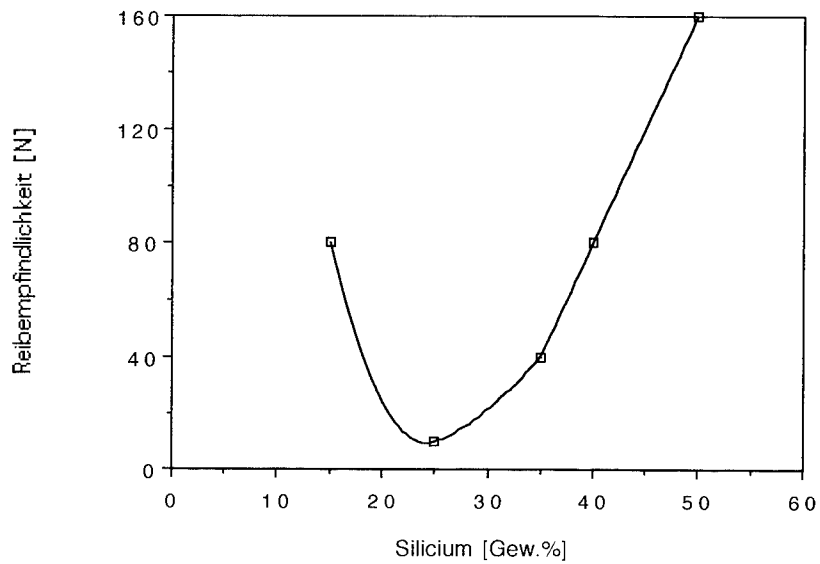


Abb. 5. Abhängigkeit der Reibempfindlichkeit von der Satzzusammensetzung.
Mittlere Korngröße des Siliciums: $2,7 \mu\text{m}$

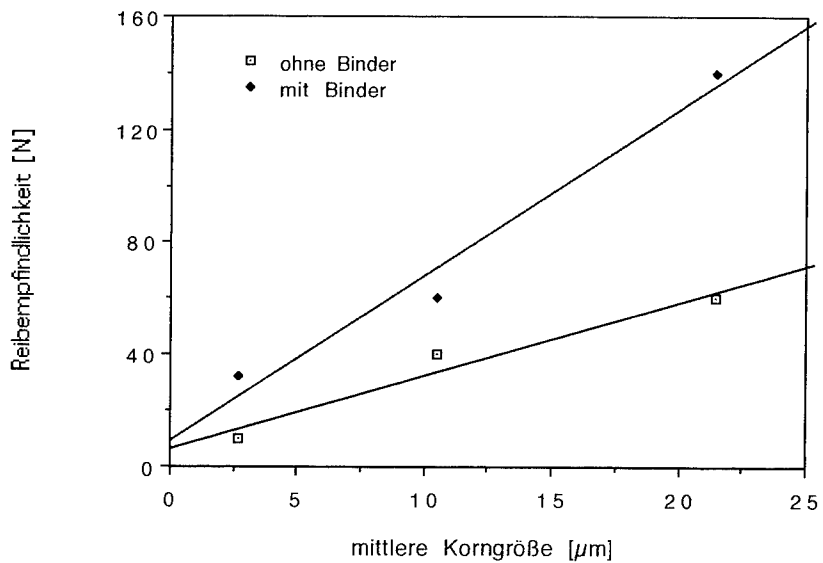


Abb. 6. Abhängigkeit der Reibempfindlichkeit von der Korngröße des Siliciums und dem Zusatz eines Binders ($< 0,7 \%$ Fluor-Elastomer).
Mischungsverhältnis $\text{Pb}_3\text{O}_4/\text{Si}$: 75:25 Gew.%

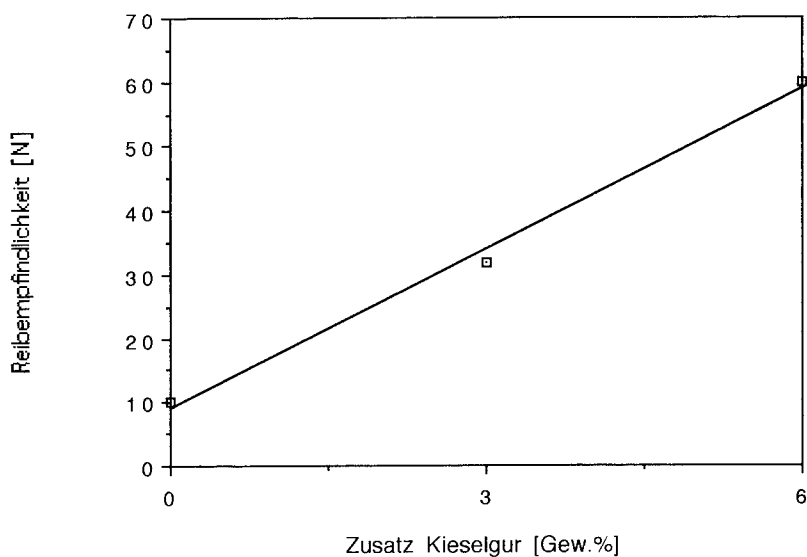


Abb. 7. Abhängigkeit der Reibempfindlichkeit von dem Zusatz an Kieselgur.
Mischungsverhältnis $\text{Pb}_3\text{O}_4/\text{Si}$: 75:25 Gew.%

Bei einer Zusammensetzung von 75 Gew.% $\text{Pb}_3\text{O}_4/\text{Si}$ und 25 Gew.% Si hat der Satz die größte Reibempfindlichkeit. Bei Verwendung der feinsten Si-Type, mit einer mittleren Korngröße von $2,7 \mu\text{m}$, beträgt die Gewichtskraft auf den Reibstift nur 10 N (s. Abb. 5, 6). Mit der Zunahme der Korngröße des Siliciums nimmt die Reibempfindlichkeit ab. Im Unterschied zur Abhängigkeit der Verzögerungszeit von der Korngröße des Siliciums (s. Abb. 3), besteht hier ein linearer Zusammenhang.

Das als Binder eingesetzte Fluor-Elastomer wirkt in Bezug auf die Reibempfindlichkeit als Phlegmatisator (s. Abb. 6). Ebenfalls läßt sich die Reibempfindlichkeit durch den Zusatz von Kieselgur stark herabsetzen (s. Abb. 7). Die Wirkung des Binders beruht auf seiner elastischen Eigenschaft. Im Fall einer homogenen Verteilung, läßt sich mit sehr geringen Binderkonzentrationen ($< 0,7$ Gew.%) eine Herabsetzung der Reibung zwischen den Partikeln untereinander und zwischen den Partikeln und der Materialoberfläche erzielen. Der Grund für die Herabsetzung der Reibempfindlichkeit durch den Zusatz von Kieselgur beruht wahrscheinlich auf Einlagerungs- und Verdünnungseffekten. Kieselgur hat ein geringes Schüttgewicht (150 g/l) und eine sehr große Porosität. 3 bzw. 6 Gew.% Kieselgur ergeben deshalb in der Volumenverteilung einen beachtlichen Effekt.

Auch durch Schmiermittel, wie z.B. Stearate oder Graphit, läßt sich die Reibempfindlichkeit stark herabsetzen. Diese Mittel wirken sich allerdings nachteilig auf die Abbrandcharakteristik aus.

5 Zusammenfassung

Die durchgeführte Untersuchung zeigt die Abhängigkeiten der Verzögerungszeit, der Abbrandcharakteristik und der mechanischen Sensibilität von den Parametern Satzzusammensetzung, Korngrößenverteilung der Ausgangsstoffe, Binder und Zusatzstoffe im Satzsystem Blei(II,IV)-oxid/Silicium auf.

Bei der Betrachtung der Verzögerungszeit in Abhängigkeit von der Satzzusammensetzung beobachtet man die kleinste Verzögerungszeit bei einem Si-Gehalt von 35 Gew.%. Der Einfluß der Korngröße des Siliciums nimmt im betrachteten Bereich (mittlere Korngröße 2,7-21,4 μm) mit zunehmender Korngröße zu. Der Zusatz von Kieselgur bewirkt eine Verlängerung der Verzögerungszeit. Das gleiche gilt beim Verwenden eines Binders (Fluor-Elastomer) im Satzsystem $\text{Pb}_3\text{O}_4/\text{Si}$. Ein entgegengesetztes Verhalten beobachtet man hingegen im Satzsystem $\text{Pb}_3\text{O}_4/\text{Si/Kieselgur}$.

Die mechanische Sensibilität wird von den gleichen Parametern beeinflusst. Die größte Reibempfindlichkeit ergibt sich bei einem Si-Gehalt von 25 Gew.% und gleichzeitiger Verwendung der feinsten Si-Type. Durch den Zusatz von Kieselgur und/oder Verwendung eines elastischen Binders läßt sich das Satzsystem $\text{Pb}_3\text{O}_4/\text{Si}$ phlegmatisieren.

Mit Hilfe der beschriebenen Faktoren läßt sich das Satzsystem $\text{Pb}_3\text{O}_4/\text{Si}$ beeinflussen und für die jeweilige Anwendung optimieren. Ziel muß es sein, die Parameter so festzulegen, daß sowohl die Funktion, als auch die fertigungstechnische Machbarkeit und die Handhabungssicherheit des Verzögerungssatzes und des Verzögerungselements gewährleistet ist.

6 Literatur

- [1] McLain, J. H.: Pyrotechnics; Chapter V; The Franklin Institute Press, 1980
- [2] Shortridge, R. G.; Hubble, B. R.: Microcalorimetric Study of the Aging Characteristics of Silicon Fuel in Pyrotechnic Ignition Compositions; Eighteenth International Pyrotechnics Seminar, 847-864, 1992
- [3] Hedger, J. T: Factors Influencing the Pyrotechnic Reaktion of Silicon and Red Lead; Propellants, Explosives, Pyrotechnics 8, 95-98, 1983
- [4] Al-Kazraji, S. S.; Rees, G. J.: The Fast Pyrotechnic Reaktion of Silicon and Red Lead Part 1. Differential Thermal Analysis Studies; Combustion und Flame 31, 105-113, 1978
- [5] Krien, G.: Thermoanalytische Ergebnisse der Untersuchung von pyrotechnischen Sätzen; BICT, 1981
- [6] Zeto, R.J.; Thornton, C. G.; Hrychowian, E.; Bosco, C. D.; J. Electrochem. Soc. 123, 1409, 1975
- [7] Saechtling, H: Kunststoff Taschenbuch, 23. Ausg., 1986
- [8] Jakubko, J.: Comparison of Burning Silicon-Red Lead Compositions in Closed and Vented Systems; Twentieth International Pyrotechnics Seminar, 497-504, 1994

VERBESSERUNG DER ANZÜNDEIGENSCHAFTEN VON TREIBLADUNGSPULVERN DURCH APPLIKATION GEEIGNETER MODERATOREN

B. Vogelsanger, E. Brönnimann

**SM Schweizerische Munitionsunternehmung,
CH-3602 Thun, Schweiz**

Zusammenfassung

Moderne Hochleistungs-Treibladungspulver (TLP) mit stark phlegmatisierter Oberfläche sowie TLP mit LOVA-Charakteristik (low vulnerability ammunition) zeigen oftmals Probleme bei der Anfeuerung. Durch Applikation geeigneter Moderatoren auf die Oberfläche des Pulverkornes kann eine deutliche Verbesserung der Anfeuerung erreicht werden.

Diverse Vertreter aus vier verschiedenen Stoffklassen (Oxidationsmittel, Anzündsätze, Katalysatoren und Sprengstoffe) wurden auf ein Hochleistungs-Mittelkaliber-TLP appliziert und in der Waffe geprüft. Einige der geprüften Moderatoren zeigten eine signifikante Anzündverbesserung. Im Falle der Oxidationsmittel wurde die erzielte Wirkung mit den Resultaten von thermoanalytischen Untersuchungen korreliert. Die Kompatibilität dieser Stoffe mit dem TLP wurde ebenfalls abgeklärt.

Abstract

Modern high-performance propellants (with deterred grain surface) as well as LOVA-propellants (low vulnerability ammunition) tend to be difficult to ignite. The ignition properties of such propellants may be significantly improved by the application of suitable surface ballistic modifiers.

Several substances and mixtures, all of them belonging to the four classes oxidizers, pyrotechnic mixtures, catalysts and high energy explosives, have been applied to the surface of a propellant and tested in a medium-calibre weapon system. Some of the modifiers were able to reduce the ignition delay time significantly. In case of the oxidizers, the improvement in performance was correlated to the results of thermoanalytical investigations. The compatibility of the modifiers with the base propellant was investigated as well.

1. Einleitung

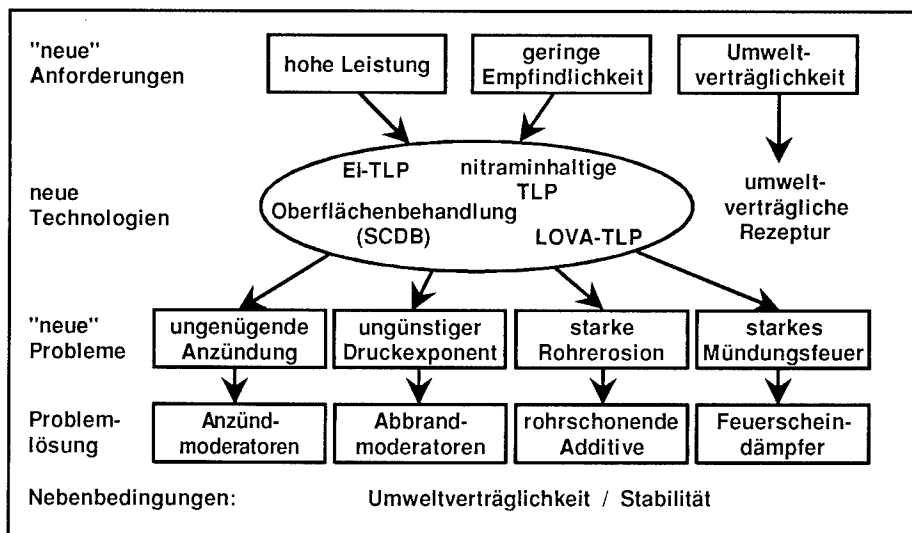
Die von modernen Treibladungspulvern (TLP) geforderten Eigenschaften wie hohe Leistung und geringe Empfindlichkeit können mittels verschiedener Methoden erreicht werden, z.B. durch (siehe auch Abbildung 1):

- Verwendung **neuer Rezepturen** (z.B. nitraminhaltige TLP),
- Verwendung **neuer Verfahren** (z.B. EI-extruded-impregnated-TLP),
- **Oberflächenbehandlung / Phlegmatisierung** konventioneller TLP.

Diese Verbesserung der Produkteigenschaften muss jedoch zumeist mit einigen Nachteilen erkauft werden, wie

- **schlechte Anzündung** des TLP beim Beschuss in der Waffe,
- **ungünstiger Druckexponent** (übermäßige Druckabhängigkeit der TLP-Brenn- geschwindigkeit, sodass die erhöhte Leistung in der Praxis nicht ausgenutzt werden kann),
- **starke Rohrerrosion**,
- **starkes Mündungsfeuer**.

Abbildung 1: Situationsanalyse "neue Anforderungen an TLP"



Diese unerwünschten Nebeneffekte können durch die Applikation geeigneter **Moderatoren** (Anzünd- und Abbrandmoderatoren, Rohrschoner und Feuerscheindämpfer) zumindest teilweise kompensiert werden. Ein Grossteil der zur Zeit international verwendeten Moderatoren zeichnen sich jedoch **durch schlechte Umweltverträglichkeit** (z.B. Bleiverbindungen!) oder durch **Inkompatibilität** mit den neuen TLP-Rezepturen aus. Letzteres hat eine **verminderte Stabilität** und damit eine Reduktion der TLP-Lebensdauer zur Folge. Weitere Moderatoren sind **stark korrosiv** oder zeigen **nur ungenügende Wirkung**. Somit sind viele der zur Zeit bekannten Moderatoren für den Einsatz unter den heutigen Rahmenbedingungen nicht oder nur beschränkt tauglich. Die Entwicklung neuer, besser geeigneter und umweltverträglicher Moderatoren sowie die entsprechende Konfektionierung in das TLP-System ist somit für die Zukunft der TLP-Produktion von essentieller Bedeutung.

Problematisierung ungenügender Anzündung:

Insbesondere moderne Hochleistungs-Treibladungspulver (TLP) mit stark phlegmatisierter Oberfläche sowie TLP mit LOVA-Charakteristik (low vulnerability ammunition) zeigen oftmals Probleme bei der Anfeuerung. Dies äussert sich durch das Auftreten von Zündverzügen sowie durch einen unvollständigen Abbrand des TLP. Letzteres führt zu einer Reduktion des thermischen Wirkungsgrades.

Aus der Kugelpulverherstellung ist bekannt, dass durch das Aufpolieren von Kaliumnitrat auf die Oberfläche des Pulverkornes eine deutliche Verbesserung der Anfeuerung erreicht werden kann. Durch diese Substanz wird jedoch die Stabilität (und damit die Lebensdauer) des TLP beträchtlich reduziert.

Im Mittelkaliberbereich hat sich Kaliumperchlorat als sehr wirkungsvoller Anzündmoderator erwiesen. Die beim Abbrand dieser Substanz freiwerdende Salzsäure führt jedoch zu starker Korrosion in der Waffe, was eine Verwendung von Kaliumperchlorat in der Praxis ausschliesst.

Die vorliegende Arbeit beschreibt die Suche nach neuen, geeigneten Anzündmoderatoren.

2. Anforderungsprofil und Lösungsansätze

An den gesuchten Anzündmoderator werden folgende Bedingungen gestellt:

Hauptbedingung: Verbesserung der Anzündung. Der Moderator soll über den gesamten Temperaturbereich von -50 °C bis +70 °C die Anzündung deutlich verbessern (Verkürzung der Zündverzögerungszeit t_2). Weiter sollen im gleichen Temperaturbereich auch bei Unterladung Anzündverzögerungen verhindert werden.

Nebenbedingung 1: Stabilität / Kompatibilität. Der Moderator darf die Stabilität des TLP nicht oder nur unwesentlich verschlechtern. Zudem muss der Moderator an sich auch stabil sein, d.h. er soll sich bei der Lagerung nicht chemisch verändern.

Nebenbedingung 2: Umweltverträglichkeit. Der Moderator darf keine oder nur eine geringe Human- und Umwelttoxizität aufweisen.

Nebenbedingung 3: keine Korrosion in der Waffe. Der Moderator darf beim Abbrand keine korrosiven Produkte bilden.

Nebenbedingung 4: vertretbarer Preis. Die Verwendung eines Moderators dürfte ab einem Kilopreis von ca. 500 US-Dollar unwirtschaftlich werden.

Eine potentielle Anzündverbesserung ist insbesondere von den folgenden vier Substanzklassen (bzw. Mischungen) zu erwarten:

Oxidationsmittel: Aufgrund der guten Anzündmoderation von Kaliumperchlorat und Kaliumnitrat ist die Verwendung von anderen Oxidationsmitteln naheliegend. Als Oxidationsmittel kommen eine grosse Anzahl von anorganischen Salzen und Oxiden in Frage, z.B. Chlorate, Perchlorate, Nitrate, Permanganate, Chromate und Perchromate.

Katalysatoren bzw. Abbrandmoderatoren: Es wurde gezeigt, dass in die Pulvermatrix eingearbeitete Abbrandmoderatoren nicht nur den Abbrand, sondern auch die Anzündung beschleunigen. Als gebräuchlichste Abbrandmoderatoren gelten Schwermetallverbindungen wie Oxide und Salze (Salicylate, Resorcyate) von Cu, Ni, Co, Cr, Pb usw.

Anzündsätze: Für die aus der Pyrotechnik bekannten Anzündsätze [1-5] vom Typ Oxidationsmittel + Brennstoff ist ebenfalls eine anzündbeschleunigende Wirkung zu

erwarten. Als Brennstoffe sollte sich Bor besonders eignen, sind doch Kaliumnitrat / Bor-Mischungen für ihre hervorragende Anzündwirkung (durch entstehende Gase, Dämpfe und feste Anteile) bekannt [6].

Sprengstoffe: Auch solch hochenergetische Stoffe könnten eine Abbrandbeschleunigung bewirken.

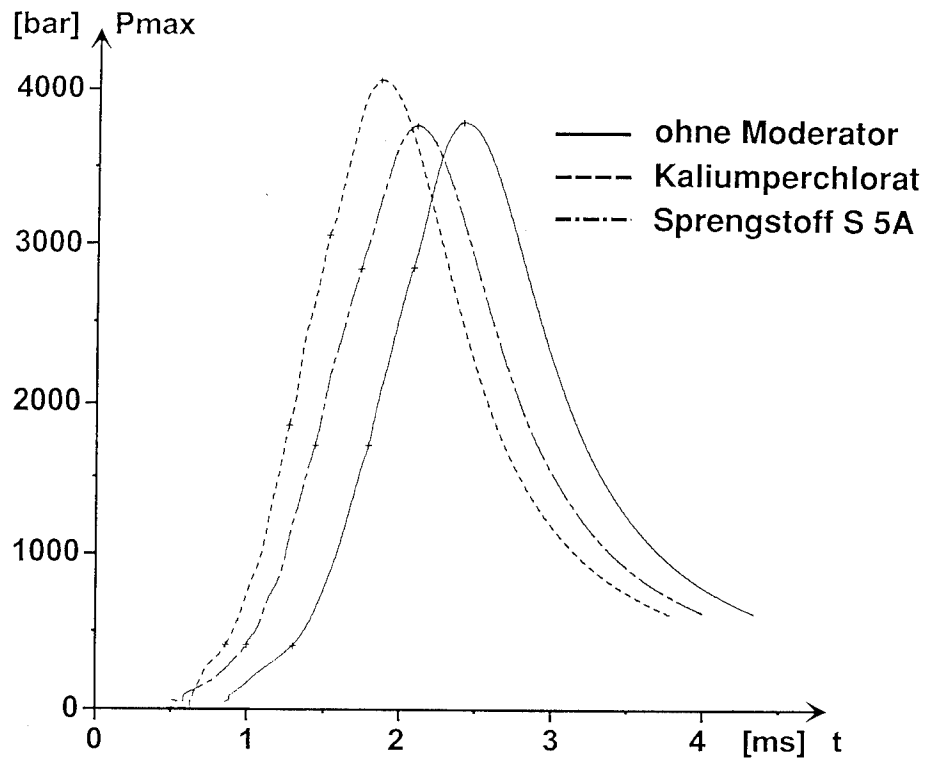
3. Auswahl der Moderatoren, Applikation und Prüfung

Basierend auf dem vorgängig beschriebenen Anforderungsprofil und weitergehenden Überlegungen wurde ein Beurteilungsschema für potentielle Anzündmoderatoren entwickelt. Mit Hilfe dieses Schemas konnten von einigen hundert möglichen Anwärtern (Stoffe und Mischungen) aus den vier Klassen "Oxidationsmittel", "Katalysatoren", "Anzündsätze" und "Sprengstoffe" der grösste Teil bereits aufgrund von Literaturdaten oder Vorversuchen ausgeschieden werden.

Die aussichtsreichsten 40 Moderatoren wurden beschafft oder selbst hergestellt und auf die Oberfläche eines Mittelkaliber-TLP aufpoliert. Die Prüfung erfolgte durch Beschuss in einer 20 mm Flugzeugabwehr-Kanone bei leichter Unterladung. Als Mass für die Anzündverbesserung wurde die Zündverzögerungszeit t_2 bei Raumtemperatur gewählt.

Ein Beispiel eines Druck-Zeit-Diagrammes (Druckverlauf in der Patronenhülse während dem Beschuss) ist in Abbildung 4 gegeben. Dabei ist die Wirkung der Anzündmoderatoren deutlich ersichtlich: Das TLP mit dem Moderator auf Sprengstoff-Basis zeigt praktisch den gleichen Verlauf der Kurve wie das Referenzmuster ohne Moderator, bis auf die deutlich kürzere Reaktionszeit (beide TLP bewirken denn auch praktisch identische Werte für maximalen Gasdruck und Geschossgeschwindigkeit). Das TLP mit Kaliumperchlorat zeigt zwar eine noch kürzere Reaktionszeit, dies ist jedoch verbunden mit einem deutlich stärkeren Druckanstieg sowie einem unerwünschten, höheren Maximalwert des Gasdruckes. Die Zündverzögerungszeit t_2 (zu dieser Zeit wird 10% des maximalen Gasdruckes erreicht) ist durch das erste Kreuz der jeweiligen Kurve gekennzeichnet.

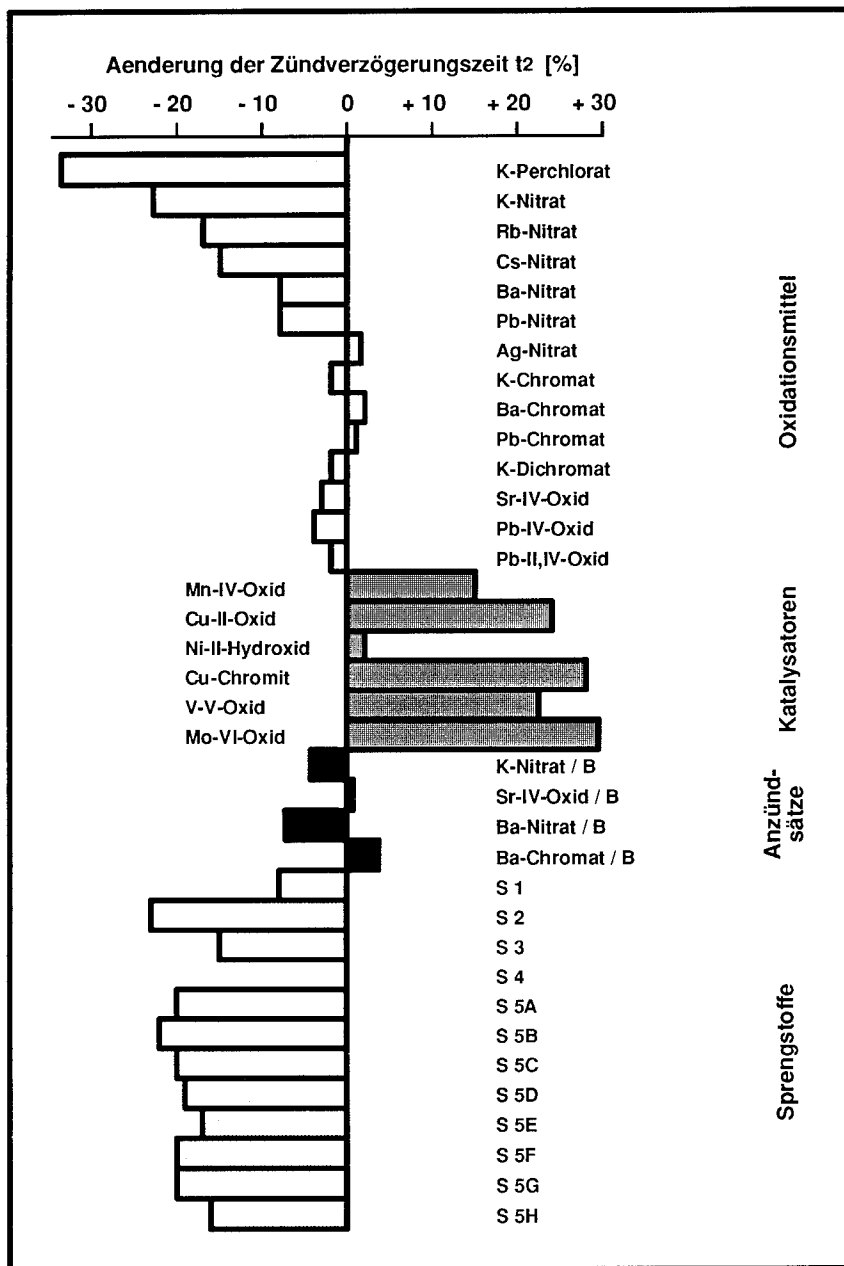
Abbildung 2: Druck-Zeit-Diagramm von TLP ohne und mit Anzündmoderatoren.



4. Innenballistische Resultate

Der Einfluss der verschiedenen Moderatoren auf die Zündverzögerungszeit t_2 ist in Abbildung 3 dargestellt (Hauptresultat dieser Untersuchung).

Abbildung 3: Wirkung der Anzündmoderatoren



Oxidationsmittel: Von dieser Gruppe zeigte *Kaliumperchlorat* klar die stärkste Anzündverbesserung - die Zündverzögerungszeit t_2 konnte gegenüber dem Referenz-TLP ohne Anzündmoderator um bis zu 35% verkürzt werden. Eine etwas geringere Anzündbeschleunigung zeigten die Nitrate der Alkalimetalle (*Kaliumnitrat*, *Rubidiumnitrat* und *Cäsiumnitrat*). Mit *Bariumnitrat* und *Bleinitrat* konnte nur noch eine geringfügige Verbesserung der Anzündung (ca. 25% der Wirkung von Kaliumperchlorat) erzielt werden. Alle anderen geprüften anorganischen Oxidationsmittel, wie *Silbernitrat*, *Kaliumdichromat*, *Kaliumchromat*, *Bariumchromat*, *Bleichromat*, *Strontiumperoxid*, *Bleiperoxid* und *Blei-II-IV-Oxid*, zeigten bezüglich Veränderung des Anzündverhaltens ein praktisch neutrales Verhalten (nur sehr schwache Anzündverbesserung oder gar geringfügige Verschlechterung der Anzündeigenschaften des TLP).

Katalysatoren bzw. Abbrandmoderatoren: Auf die Verwendung der bekannten bleihaltigen Moderatoren wurde aufgrund ihrer hohen Toxizität verzichtet. Stattdessen wurde die Wirkung von *Nickelhydroxid*, *Kupfer-II-oxid*, *Kupferchromit*, *Mangan-IV-oxid*, *Vanadium-V-oxid* und *Molybdän-VI-oxid* geprüft. Alle diese Stoffe bewirken gemäss Literaturangaben bei nitraminhaltigen TLP eine Abbrand- und zumindest teilweise auch eine Anzündbeschleunigung (bei Einarbeitung in die Pulvermatrix). Aufpoliert auf EI-TLP führten jedoch alle diese Substanzen zu einer deutlichen bis starken Verschlechterung der Anzündwirkung.

Anzündsätze: Es wurden TLP-Muster mit vier verschiedenen Anzündsätzen geprüft, nämlich mit *Kaliumnitrat / Bor*, *Bariumnitrat / Bor*, *Bariumchromat / Bor* und *Strontiumperoxid / Bor*. Die Wirkung dieser auf die TLP-Oberfläche aufpolierten Anzündsätze war eher enttäuschend. Die Anzündverbesserung der beiden Sätze mit Bor und den Oxidationsmitteln Kalium- bzw. Bariumnitrat entsprach nur 15 - 25% der Wirkung von Kaliumperchlorat. Die anderen beiden Sätze zeigten gar eine klare Anzündverschlechterung.

Sprenge Stoffe: Demgegenüber wurden mit einigen "Sprenge Stoffen" sehr gute Resultate erzielt. Die verschiedenen unbehandelten (S 1 - S 4) bzw. oberflächenbehandelten (S 5A - S 5H) Sprengstoffe zeigten bei 21°C praktisch durchwegs eine deutliche Verbesserung der Anzündwirkung - der Effekt erreichte bis zu 70 % der Wirkung von Kaliumperchlorat. Bei den Extremtemperaturen -54 und +71°C wurde immer noch eine Anzündverbesserung erzielt, diese war jedoch, verglichen mit dem Beschuss bei 21°C, deutlich geringer.

5. Abklärungen bezüglich der Wirkungsweise der Anzündmoderatoren

In Falle der **Oxidationsmittel** wurden weitergehende Abklärungen unternommen, mit dem Ziel, die Wirkungsweise dieses Moderatoren-Typs besser zu verstehen.

So wurde versucht, die Stärke der Anzündbeschleunigung auf die Einflussgrössen "Ergiebigkeit" und "Verfügbarkeit" der Sauerstoffabgabe zurückzuführen.

Als Mass für die **Ergiebigkeit** wurde die **Sauerstoff-Bilanz** der Moderatoren verwendet. Die Sauerstoffbilanz ist diejenige Sauerstoffmenge in Gewichtsprozent, die bei vollständiger Umsetzung des Oxidationsmittels frei wird.

Als Mass für die **Verfügbarkeit** zur Sauerstoffabgabe wurde die **Zersetzungstemperatur** der Moderatoren eingesetzt.

Die Werte für Sauerstoffbilanz und Zersetzungstemperatur wurden aus der Literatur gesammelt oder mit Hilfe der Stöchiometrie berechnet. Weiter wurden diese Werte durch eigene thermoanalytische Messungen überprüft: Durch Kombination der Resultate aus DSC- (differential scanning calorimetry) und TG- (thermogravimetry) Messungen konnte sowohl die Menge des abgespaltenen Sauerstoffes als auch der Temperaturbereich, in welchem diese Abspaltung stattfindet, bestimmt werden.

In Abbildung 4 wurde für die als Anzündmoderatoren wirkenden Oxidationsmittel die Anzündbeschleunigung (Verkürzung der Zündverzögerungszeit t_2) als Funktion der Sauerstoffbilanz aufgetragen.

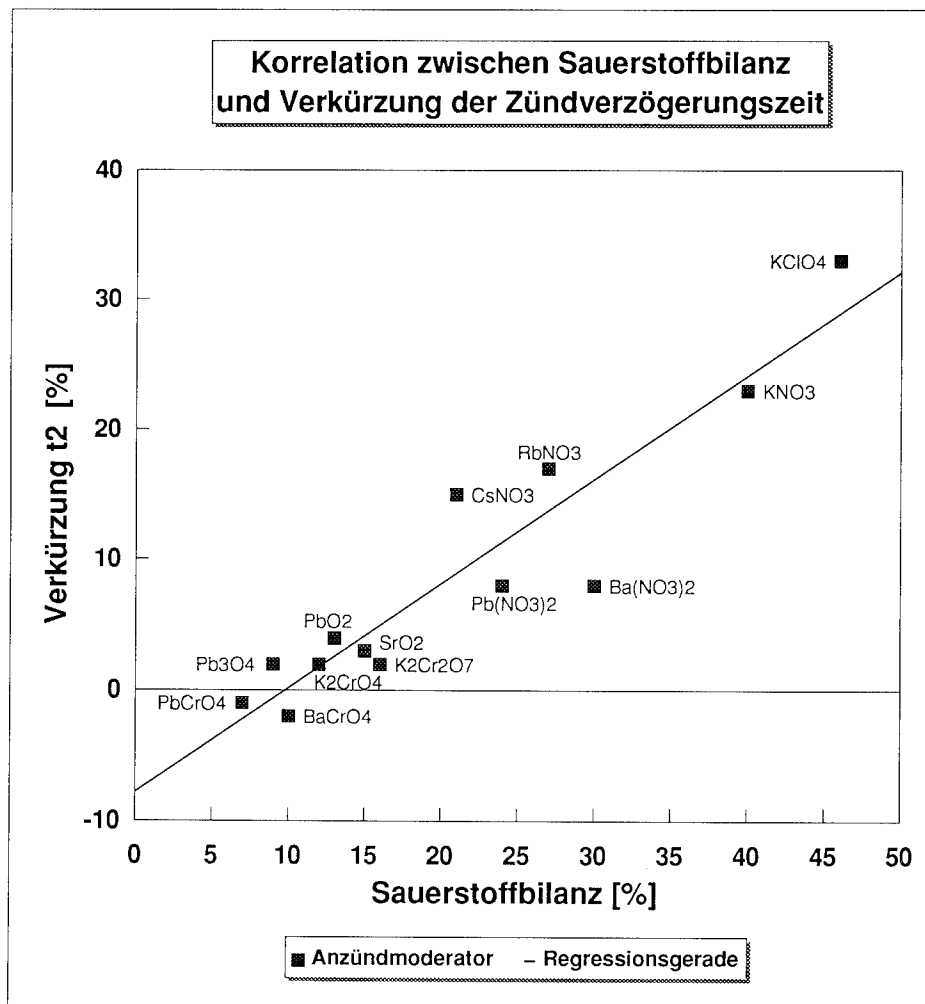
Daraus ist eine **klare Korrelation zwischen Sauerstoffbilanz und erzielter Anzündverbesserung** ersichtlich.

Weiter konnte auch ein klarer Einfluss der **Verfügbarkeit des Sauerstoffes** auf die Anzündwirkung gefunden werden. Substanzen mit tiefer Sauerstoffbilanz erreichen zwar trotz sehr hoher Verfügbarkeit des Sauerstoffes (tiefe Zersetzungstemperatur) kaum eine Anzündverbesserung. Demgegenüber vermag eine hohe Zersetzungstemperatur die Anzündwirkung der Oxidationsmittel (selbst bei hoher Sauerstoffbilanz) stark zu reduzieren oder, wie z.B. im Falle von Vanadium- und Molybdänoxid, sogar ganz aufzuheben.

Haupteinflussgrösse für die anzündverbessernde Wirkung von Oxidationsmitteln ist somit eindeutig die **Sauerstoffbilanz**. Diese Grösse bestimmt das **Poten-**

tial für die Anzündverbesserung. Eine **hohe Verfügbarkeit des Sauerstoffes** und damit eine **tiefe Zersetzungstemperatur** ist jedoch unabdingbar, um dieses Potential überhaupt ausschöpfen zu können.

Abbildung 4: Korrelation zwischen Sauerstoffbilanz und Verkürzung der Zündverzögerungszeit.



6. Resultate der Stabilitätsuntersuchungen

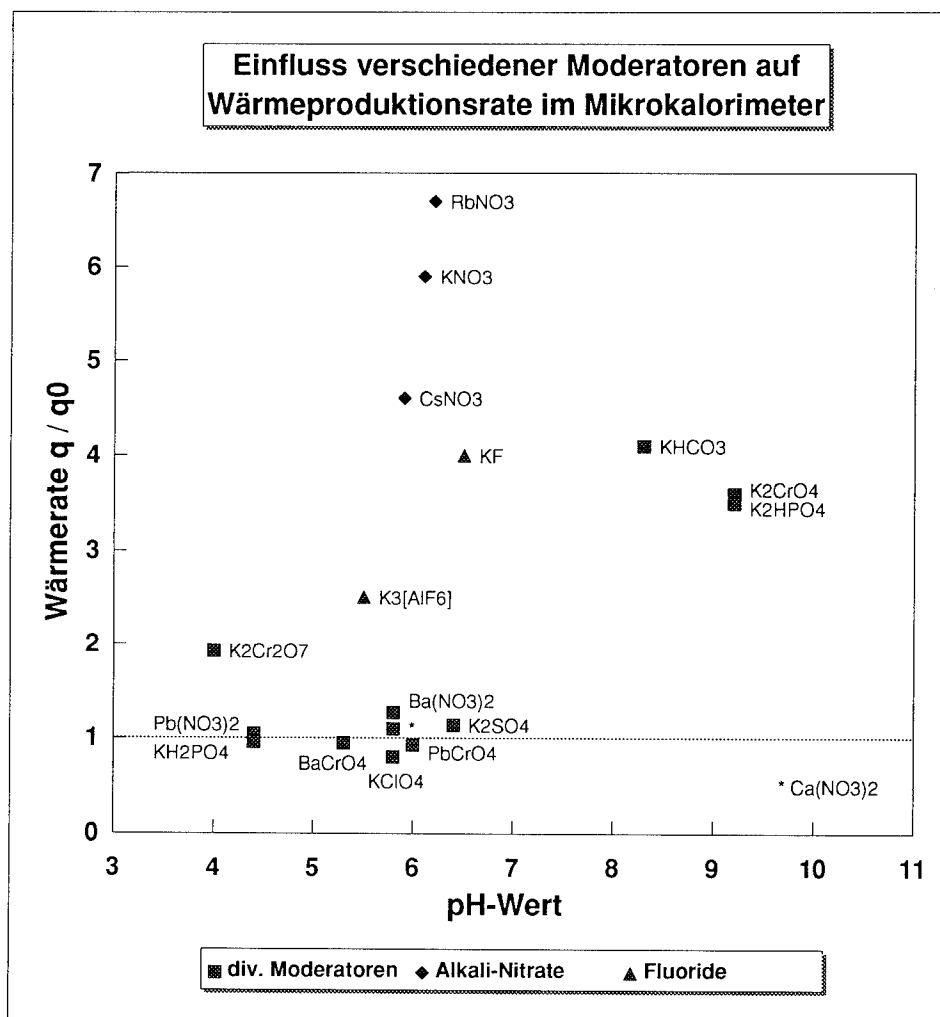
Gemäss Nebenbedingung 1 darf durch das Aufpolieren des Moderators die Stabilität des TLP nicht oder nur unwesentlich verschlechtert werden.

Der Einfluss der Moderatoren auf die TLP-Stabilität wurde durch Messung der Wärmeproduktion der jeweiligen TLP-Muster im Mikrokalorimeter (MK) bei 80°C überprüft. Neben den hier verwendeten Anzündmoderatoren wurden auch noch andere Substanzen, hauptsächlich Feuerscheindämpfer, getestet.

Bekanntlich vermögen stark saure oder basische Substanzen die Verseifung von Salpetersäureestern (Nitrocellulose oder Nitroglyzerin) zu katalysieren, wobei eine starke Beeinträchtigung der TLP-Stabilität zu erwarten ist. Im Folgenden wurde deshalb versucht, die Stabilitätsverminderungen der Moderatoren mit den jeweiligen pH-Werten zu korrelieren. So wurde in Abbildung 5 die relative Wärmeproduktion der TLP mit aufpoliertem Moderator im MK bei 80°C gegen den pH-Wert der 5%igen wässrigen Lösung des entsprechenden Moderators aufgetragen. Diese Auswertung erbrachte folgende Resultate:

- Erwartungsgemäss zeigten alle alkalischen Substanzen mit pH-Werten über 8 eine deutliche Reduktion der TLP-Stabilität.
- Demgegenüber zeigten die sauren Additive nur eine geringe bzw. überhaupt keine Reduktion der TLP-Stabilität.
- Die meisten der neutralen Substanzen (pH-Werte 5-7) ergaben erwartungsgemäss keinen signifikanten Einfluss auf die TLP-Stabilität. Lediglich die TLP mit aufpolierten **Alkalimetall-Nitraten** sowie mit **Kaliumfluorid** (und in etwas geringerem Masse auch mit **Kaliumaluminiumfluorid**) zeigten stark erhöhte Wärmewerte im MK. Die unerwünschte **Stabilitätsverminderung** durch diese Substanzen (Alkalimetall-Nitrate und -Fluoride) ist zwar schon seit langem bekannt - bis jetzt konnte unseres Wissens jedoch noch keine befriedigende Erklärung für diesen Effekt gefunden werden.

Abbildung 5: Relative Wärmeproduktion der TLP im Mikrokalorimeter (80°C) in Funktion des pH-Wertes des aufpolierten Moderators.



7. Resultatezusammenfassung und Diskussion

Von den anorganischen **Oxidationsmitteln** zeichneten sich nur Kaliumperchlorat sowie die Nitrate der Alkalimetalle durch eine brauchbare Anzündbeschleunigung aus. Diese Moderatoren zeigen jedoch eine stark korrosive Wirkung bzw. eine starke Reduktion der TLP-Stabilität und sind deshalb in der Praxis nicht anwendbar.

Die **Anzündsätze** zeigten nur eine beschränkte Anzündverbesserung, während die geprüften **Abbrandmoderatoren** (Katalysatoren) die Anzündung gar verschlechterten. Auch diese Stoffe scheiden für den praktischen Einsatz aus.

Demgegenüber konnte unter den Testbedingungen mit einigen **Sprengstoffen** auf Anhieb eine signifikante Anzündverbesserung bei unverminderter Stabilität erzielt werden. Leider liess sich diese Anzündverbesserung im tiefen und im hohen Temperaturbereich sowie in anderen Waffensystemen nur beschränkt reproduzieren.

Im Bereich dieser Explosivstoffe liegt sicherlich ein Potential zur Anzündverbesserung und eventuell auch zur Leistungssteigerung des TLP. Bis zur praktischen Anwendung solcher Stoffe als Anzündmoderatoren sind jedoch noch unzählige Abklärungen und Entwicklungsarbeiten vorzunehmen.

10. Literatur

- [1] A.A. Shidlovskiy: Principles of Pyrotechnics; Mashinostroyeniye Press (1964).
- [2] H.J. McLain: Pyrotechnics; Franklin Institute Press, Philadelphia (1980).
- [3] J.A. Conkling: Chemistry of Pyrotechnics; M. Decker, Inc., New York (1985).
- [4] Ullmanns Encyklopädie der Technischen Chemie, 4. Auflage, Band 19, S. 623 - 638; VCH, Weinheim (1980).
- [5] H. Ellern: Military and Civilian Pyrotechnics; Chemica Publishing Company, Inc., New York (1968).
- [6] A.M. Varney: Primers and Igniter; in L. Stiefel (Editor): Volume 109 Progress in Astronautics and Aeronautics; Gun Propulsion Technology; Published by the American Institute of Astronautics and Aeronautics, Washington (1988).
- [7] R. Meyer: Explosivstoffe; VCH, Weinheim (1985).

THE LASER INITIATION OF A SERIES OF ENERGETIC MATERIALS

Alba Lalitha Ramaswamy#, John E. Field*, Ronald W. Armstrong#

#Dept. of Mechanical Engineering

*Cavendish Laboratory

University of Maryland

University of Cambridge

College Park, Maryland 20742-3035

Cambridge CB3 0HE

USA

UK

ABSTRACT

A description is given of results obtained in four experimental studies on the laser initiation of a variety of energetic materials. The studies ranged from being application oriented to being more fundamental. The energetic materials and their conditions included powders and, where appropriate, crystals: the secondary explosives RDX (cyclotrimethylene trinitramine), TNT (trinitrotoluene), TNB (trinitrobenzene), tetryl and picric acid; the secondary/primary PETN (pentaerythritol tetranitrate) explosive; the pyrotechnic Mg Teflon Viton; and, the propellant oxidizer ammonium perchlorate. The experiments consisted of:-1)Laser initiated detonation of energetic material powders for safer detonation of explosives; 2)Laser ignition of energetic crystals relating to combustion of propellant compositions; 3)Laser initiation of energetic crystals for investigation of 'hot spot' origins; and, 4)Laser initiation for comparative energy densities and beam dimensions for ignition of different energetic materials.

1) LASER INITIATED DETONATOR

Introduction

The basic principle of a laser initiated detonator is shown in fig. 1. An explosive charge is set into ignition by irradiating it with a high energy density laser pulse emitted from a laser diode and is transferred to the explosive by means of an optical fibre.

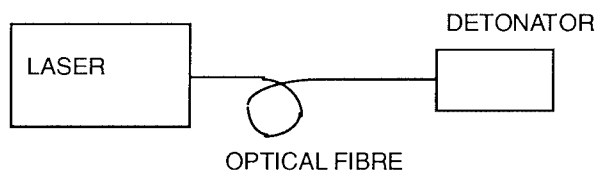


FIG. 1
Principle of a Laser Initiated Detonator

Such a system has an increased level of safety compared with traditional electrically initiated detonators. This is due to the fact that in electrically ignited systems, potential hazards arise from electrostatic discharges, currents induced in bridgewire circuits by sources of radiofrequency energy, and lightning. In addition there is some variability because of the bridgewire resistance-after-fire. Laser initiated detonator systems have not been fully developed yet, though research on their functioning has been ongoing from the late 1980's till now. Research results obtained at the Cavendish Laboratory relate to the application described here [1]. The explosive charge studied was PETN (pentaerythritol tetranitrate). Different physical parameters such as explosive grain size, percentage of added carbon and aluminium dopants and explosive compaction, were varied to find the optimum explosive charge conditions for laser initiation i.e. the conditions at which the laser energy density for initiation was a minimum.

Summary of Results

A non-Q switched Nd/glass laser (1064 nm) was used to irradiate ~ 15 mg of PETN explosive powders confined within an orifice 1 mm in depth and 5 mm in diameter, in a PMMA block. The PETN had been crystallized in the laboratory for increased crystalline perfection. A He/Ne laser was used to align the samples with the laser beam. The threshold energy is the value of laser energy at which the PETN is first observed to ignite. Figs. 2 and 3 show the plots of threshold energy density as a function of the percentage carbon and aluminium doping for different grain sizes of explosive.

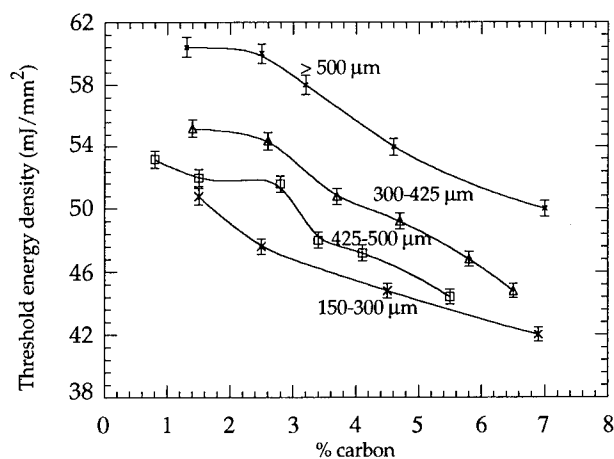


Fig. 2

Laser Threshold energy density as a function of percentage weight carbon doping

Activated carbon was used where the individual particle sizes were ~ 1 µm, with clumping occurring to produce larger particles ~ 10 µm in diameter. The aluminium consisted of flakes about 50 x 50 µm in size and a few µm in thickness. From curves

fitted to the measurements it has been found that the threshold energy $\sim Cr^n$, where C and n are constants and $n \sim 2/3$. This is believed to be indicative of a surface area to volume ratio burning dependency of the single explosive grains. The smaller the explosive grain size, the lower is the threshold energy density, though the strength of the induced combustion or reaction is reduced, thus, reducing the chance of a deflagration-to-detonation transition. Increasing the percentage of carbon and aluminium doping to an optimum value reduces the threshold energy for ignition. Carbon has been found to be a more efficient dopant than aluminium.

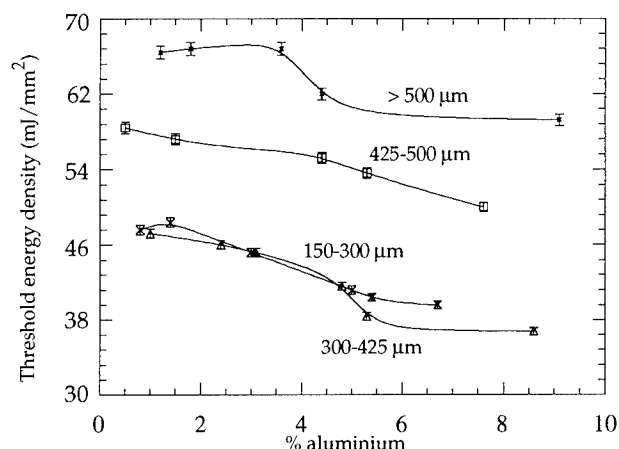


Fig. 3

Laser Threshold energy density as a function of percentage weight Al doping

The results summarized here, characterized the optimum explosive powder conditions for initiation in a laser detonator system. Threshold energy densities have also been measured as a function of the compaction pressure for 3.5 % carbon doping and two different grain sizes, as shown in fig. 4. The smaller grain size explosive is more susceptible to the applied pressure and this can be attributed to a better packing of

small grains compared with the larger grains. The increase in threshold energy density with compaction pressure is mainly due to the fact that the grains pack much closer together reducing the effective surface area to volume ratio for burning but it also affects the porosity and hence diffusion of the flame as well as the surface laser absorbance.

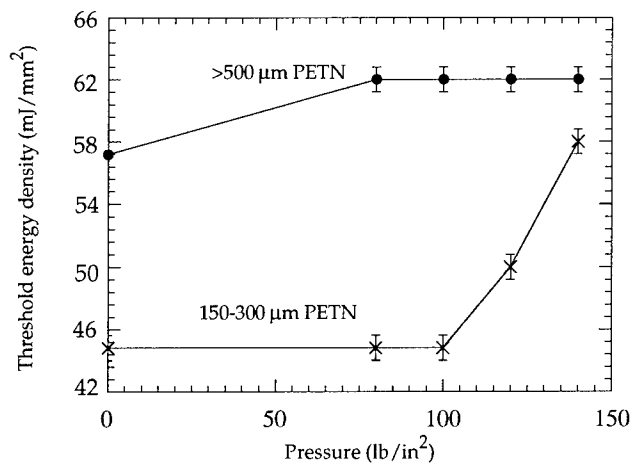


Fig. 4

Threshold energy as a function of the compaction pressure for 3.5 % carbon doping

2) LASER IGNITION OF AMMONIUM PERCHLORATE CRYSTALS; AN INGREDIENT OF PROPELLANT COMPOSITIONS

Introduction

Crystals of ammonium perchlorate constitute one of the most commonly used oxidizers in propellant mixtures. A solid propellant contains both oxidizer and fuel ingredients

and can burn at a very fast rate in the absence of air or other oxidizers. Nowadays, propellants are being used to produce propulsive thrusts in a broad range of applications which include rocket, gun and air-breathing propulsion systems, air-bags producing high pressure, and high temperature gases for joining heavy-duty electrical cables, etc. The significant commercial and military applications have made the development of insensitive propellants an important safety issue. An insensitive composition is one in which there is minimized possibility of initiation as a result of unintentional impact, electrostatic discharge, thermal and shock stimuli. Detailed research and understanding of the initiation, ignition and related mechanical deformations of ammonium perchlorate crystals are thus of vital importance. For this purpose, nanosecond and picosecond laser irradiation of ammonium perchlorate crystals has been used at the University of Maryland to study the initiation, ignition and associated mechanical deformation resulting in surface cracking on a time scale approaching the actual frequencies associated with energetic crystal decomposition during propellant combustion.

Summary of results

The nanosecond and picosecond laser pulses were obtained from two separate Nd/Yag lasers (1064 nm in wavelength). The decomposition has been detected by x-ray photoemission spectroscopy [2]. The surface mechanical deformations or cracking associated with the ignition have been studied by optical microscopy, see fig. 5, electron microscopy and atomic force microscopy. Extensive cracking was observed on the surface of the crystal. The directions of cracking have been identified and related to the crystallography and allotropy of ammonium perchlorate. It was found that with the nanosecond laser irradiation, the crystal exhibited cracking due to the orthorhombic structure overlying more shallow surface cracking produced by a rock-salt cubic

structure. This phenomenon had occurred as a result of the allotropic phase transformation of ammonium perchlorate from the orthorhombic to the cubic or rock salt structures at a temperature of 240 °C. The picosecond laser damage exhibited cracking solely due to the orthorhombic modification, see fig. 6. This is believed to be due to the fact that though the local temperature rise was undoubtedly also high enough to induce the rocksalt-type phase transition, the time for laser irradiation and hence heating of the crystal is too short for any significant amount of phase transformation to be detected.

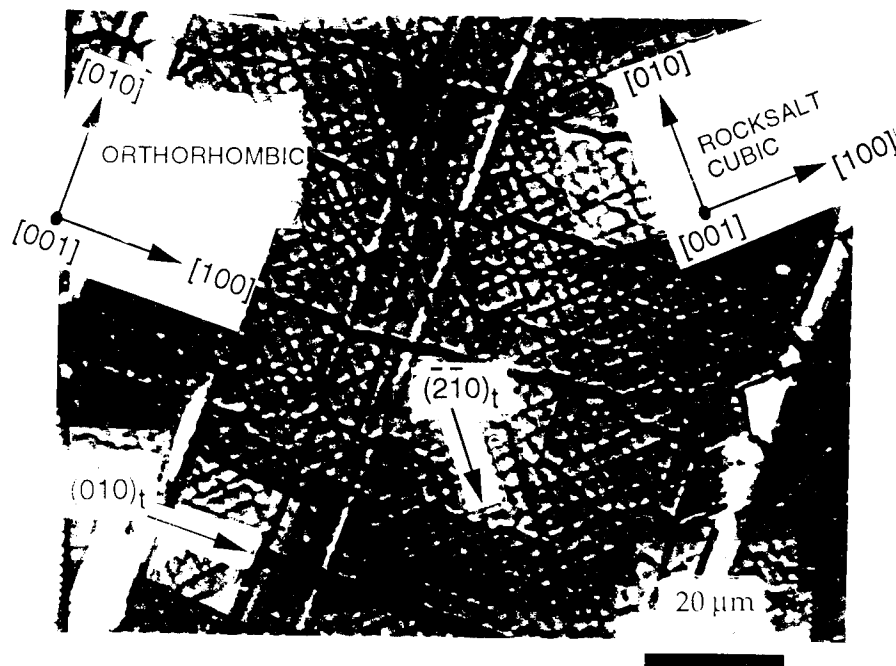


FIG. 5

TYPICAL CRYSTAL CRACKING PRODUCED BY FOCUSSED A ns LASER PULSE
 (14 MW/mm^2) ON THE (001) FACE OF AN AMMONIUM PERCHLORATE CRYSTAL

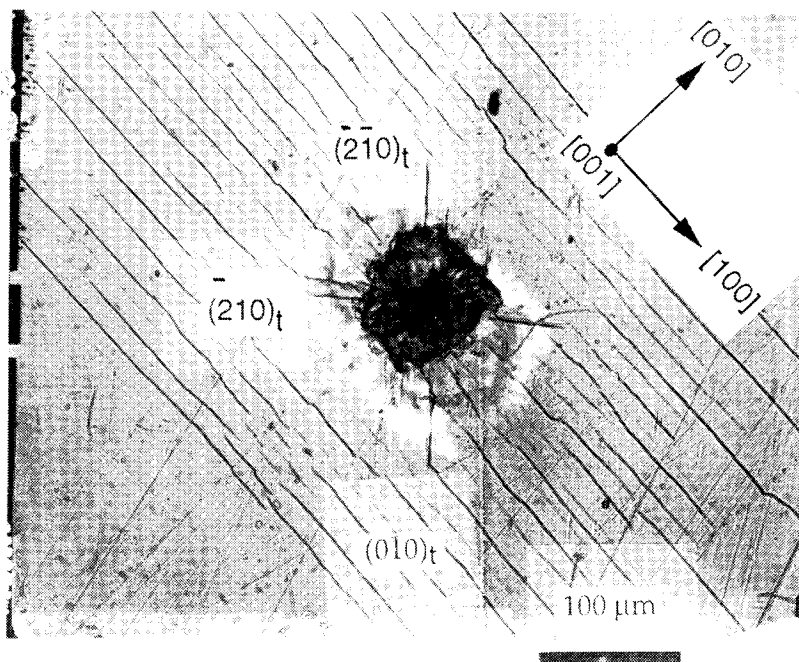


FIG. 6

TYPICAL CRYSTAL CRACKING PRODUCED BY FOCUSSED A ps LASER PULSE (9 GW/mm²) ON THE (001) FACE OF AN AMMONIUM PERCHLORATE CRYSTAL

The cracking produced in the rock salt structure even under nanosecond pulse conditions consisted of a very fine and extensive network and appeared to be subsurface by about a fraction of a micron dimension. This relates to propellant burning, since a finer network of cracking corresponds to a far greater surface area for decomposition, assuming that the decomposition sites are related to the surface cracks. This was confirmed with electron and atomic force microscopy, where individual initiation or 'hot spot' sites have been detected and their relation to the surface cracks determined. The initiation sites were found to be aligned along the major directions of cubic microcracking and not the (010) orthorhombic planes. A dislocation mechanism for the cracking observations is being proposed in a fuller account that is being prepared of this investigation [2].

3) LASER INITIATION OF SINGLE CRYSTALS OF ENERGETIC MATERIALS

Introduction

It is important to determine the microscopic mechanism/s which create the 'hot spots' or initiation sites in explosive crystals. A 'hot spot', after initiation, increases in size by propagating the chemical reactions to the remaining mass of explosive, eventually generating a detonation. The propagation of a deflagration-to-detonation can thus only be fully understood once the mechanism/s for 'hot spot' formation in single crystals have been fully identified. Also, if the factors that are involved in creating the 'hot spots' are identified e.g. dislocations or other crystal defects, then better control over the formation of initiation sites would be possible and, thus, safer conditions for handling explosives. The grains which make up the explosive powders consist of single crystals of the explosive. Here the results on the study of the initiation and ignition of single crystals of RDX (cyclotrimethylene trinitramine) undertaken at the Cavendish Laboratory are described [1,3].

Summary of Results

Single crystals of RDX have been irradiated on the (210) growth surface by a focused Nd/glass laser beam with an energy density of 1270 J/cm^2 and pulse duration at half maximum of $300 \text{ }\mu\text{s}$. Localized sites of initiation or 'hot spots' have been detected by high speed-photography. These sites have been found to be of the order of $20\text{-}30 \text{ }\mu\text{m}$ in size, they formed near the edges of the crystal remote from the incident laser beam and enlarged at the rate of $\sim 75 \text{ ms}^{-1}$, eventually propagating the deflagration to the entire surface of the crystal. Fig. 7 is a high-speed photograph of the laser irradiation of a single crystal of RDX of size $2\text{x}4\text{x}2 \text{ mm}$ being irradiated by a focused laser beam with 1

mm spot size and laser energy density of 1270 J/cm^2 . The interframe time was $20 \mu\text{s}$ and the first frame occurred $10 \mu\text{s}$ after the beginning of the laser pulse.

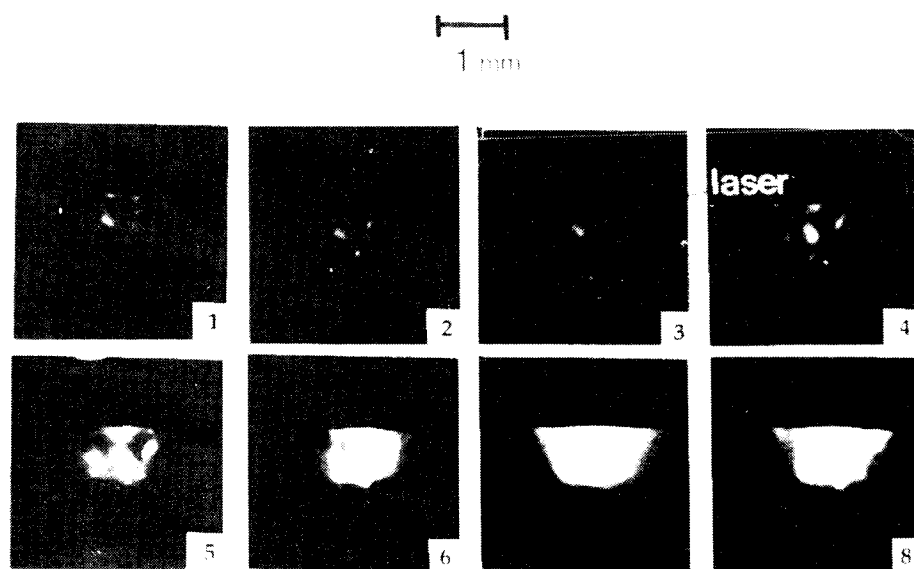


FIG. 7

HIGH-SPEED PHOTOGRAPHY OF AN RDX CRYSTAL (2X4X2 mm) IN DARKNESS, IRRADIATED BY A FOCUSED LASER PULSE

In frame 1 bright centres, believed to be initiation sites, have already formed. They are localized on the edges of the crystal as well as in the centre of the laser beam. By frame 4, $80 \mu\text{s}$ later, it can be observed that the centres are enlarging in size and propagating to the rest of the crystal until, by about frame 7, the whole crystal is illuminated by the reaction.

Various experiments have been performed to ascertain whether the initiation sites had been formed by a mechanism of internal reflection of the laser beam between the crystal faces and focusing at the crystal edges. These have been found to be negative. The

initiation sites were analyzed with an optical microscope, since they could be easily identified from the high-speed photographs and the whole almost intact crystal could be recovered after irradiation in those situations in which the laser energy density was just sub-threshold. It was noted that these sites are always associated with a very fine net-work of cracking.

4) LASER INITIATION OF POWDERS OF ENERGETIC MATERIALS

Introduction

The laser initiation of explosive powders can be used as an experimental tool to compare the threshold energy densities for initiation of different explosives. The technique can also be used to obtain more details on the initiation of one particular explosive, namely, the pyrotechnic Mg Teflon Viton (MTV). For this purpose the results of experiments performed at the Cavendish Laboratory are briefly described.

Summary of Results

The Nd/glass laser described in the above sections was used for the experiments. A summary of the threshold energy densities for powdered explosives is given in Table 1. The ignition temperatures and average grain sizes have also been given. The trend in laser ignition energies roughly follows the trend in ignition temperatures. No direct correlation can be made with the grain sizes showing that the laser ignition of explosive powders is also dependent on other factors such as grain perfection, explosive porosity etc. The critical radiation density versus beam diameter has been measured for the laser irradiation of pellets of MTV (Mg Teflon Viton) and is shown in fig. 8. This was done

by placing apertures of different diameters in the laser beam and measuring the laser energy necessary for ignition.

Explosive	Ignition temperature (°C)	Average grain size (µm)	Laser threshold energy for ignition (mJ/mm ²)
Tetryl	185	10-100	87.0
PETN	202	150-300	75.0
RDX	230	20-70	56.0
Picric acid	270	20-400	66.0
TNT	290	2-40	285.0
TNB	305	10-250	153.0

TABLE 1
Comparison of the threshold energy densities to laser ignition with ignition temperatures.

However, making the gross approximation that the energy density is constant across the beam and whose total energy in the beam is known, leads to a determination of the actual energy reaching the sample. A measurement was performed of the laser beam spatial profile and this approximation was found to be quite good in the limits of the aperture diameters used in the experiments. As can be seen from the graph in Figure 8, the critical radiation increases drastically for the lower beam diameters indicating that there is a minimum diameter for the initiating nucleus. This relates to the critical dimension necessary for the formation of an initiation site.

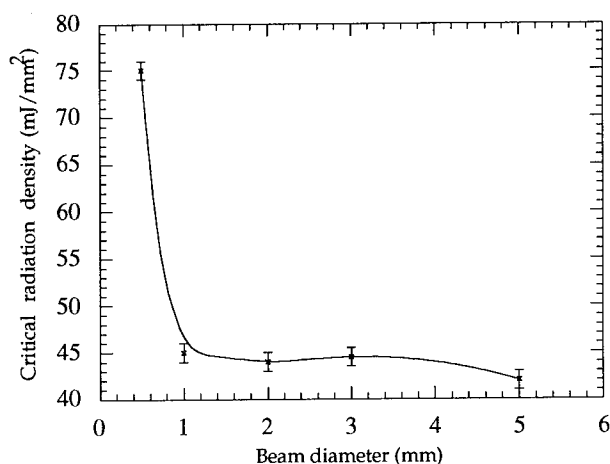


Fig. 8

Threshold energy density as a function of beam diameter for MTV explosive

CONCLUSIONS

The irradiation of explosives by a laser beam has been shown to be a useful experimental tool. It can be used to obtain information on fundamental physical processes taking place during explosive initiation, to compare the energetic and material properties of different explosives and has very high potential for research and development applications.

REFERENCES

- [1] Ramaswamy, A. L., PhD. thesis, Cambridge University (1993).
- [2] Ramaswamy, A.L., Shin, H., Armstrong, R.W., Sharma, J. and Lee, C.H., as in draft paper, "Nanosecond and Picosecond Laser Induced Cracking and Ignition of Single Crystals of Ammonium Perchlorate," to be submitted to *Journal of Material Sciences*.

[3] Armstrong, R.W., Ramaswamy, A.L. and Field, J.E., "Thermomechanical Influences on the Combustion of RDX Crystals," *ONR/SNPE/ONERA Workshop on Combustion Mechanisms*, ONREUR Report 91-02-W, p. 168, (1991).

Acknowledgments

Investigations 1, 3 and 4, performed at the Cavendish Laboratory, University of Cambridge, G.B. received support from Imperial Chemical Industries, Nobel Explosives Division. Investigation 2 performed at the University of Maryland, College Park, U.S.A., and 3 at the Cavendish Laboratory, were supported by the U.S. Office of Naval Research (ONR). The authors gratefully acknowledge help received from J. Sharma, H. Shin and C. H. Lee in achieving the results described in investigation 2.

BALLISTIC CHARACTERISTICS OF GUN PROPELLANTS AND CHARGES CONTAINING METALLIC ADDITIVES

I.G. ASSOVSKII , O.T. CHIZHEVSKII *, V.V. SERGEEV *

Semenov Institute of Chemical Physics RAS,
Kosygin St. 4, Moscow 117977 Russia

*GNPP "Pribor", Moscow 113519 Russia.

ABSTRACT

The purpose of the present paper is to show a possibility to improve the ballistic properties of conventional gun propellants by means of certain additives of fine grained metallic elements into the propellant composition or as a separate component of gun charge. The main attention is focused on the improvement of single- and double-base gun propellants using aluminium additives as powder or foil.

Such a possibility to obtain higher velocity of gun-launched projectile is proven theoretically, by means of the thermodynamic calculations and numerical simulation of the interior ballistics process, and experimentally by fire examinations using 30-mm/75-calibre gun. The addition of aluminium particles into the propellant composition as well as into the gunchamber is tested. The latter method allows one rather simply to increase thermal characteristics of powder gases and optimise the heatrelease process improving the flatness of the gun pressure-time curve.

This paper continues and summarises the author's investigations published in [1,2].

1. INTRODUCTION

Increasing of projectile velocity is a major objective of gun and rocket design. In order to achieve high speeds for projectile, a chemical propulsion system must use a hot light gas as driving agent, because the attainable maximum of projectile velocity is proportional to the speed of sound in the working substance used [3-6]. So, both of increasing in the propellant energy and decreasing in the average molecular weight of the combustion products are the basic methods for improving of the interior ballistic characteristics, as for conventional gun-tube as for rocket launchers [6-9].

Composite propellants containing metallic particles as energetic additives have long been in use for solid-propellant rocket motors. It is customary to assume that application of high-energy propellants in gun-tube systems is extremely limited, as it is accompanied by increasing of gun barrel wear, which is proportional to the propellant flame temperature [10,11]. The hot combustion gases in ordnance wear steel from the gun barrel, eventually rendering the barrel unserviceable.

Meanwhile, the experience of recent years indicates that the gun tube erosivity depends on the composition of combustion products and on the bore surface state as well as on the flame temperature (see, for example [11]). Therefore it is desirable to make up the increasing in the projectile muzzle velocity by means of optimisation of the combustion products composition, keeping the maximum gas temperature and pressure within the allowable limits. The theoretical and experimental results presented in this paper show that such approach can be realised using aluminium additives to conventional gun propellants.

2. THERMODYNAMIC AND BALLISTIC CALCULATIONS

Thermodynamic properties of propellants include the flame temperature T_f and composition B_j of the combustion products, their specific heats, average molecular weight M , and covolume under certain conditions [4,6]. The method that is used to calculate these properties for propellants containing metallic additives have been published in [1]. The pressure of condensed products, caused by the Brownian movement of particles, is neglected.

The calculations were carried out for given gas-pressures assuming the state equation corresponding to ideal gas. This assumption is permissible, as comparisons of results, computed with the ideal gas equation of state and equations for real gases, indicate that relatively small differences arise in flame temperature and in average molecular weight of gas [8,12]. Nevertheless, the calculation of gas-pressures for various loading densities D needs the state equation for real gas, for example, a virial equation [4,7,12], taking into account covolume and other characteristics of real gas-state.

The trustworthiness of the numerical method [1] was evaluated by comparison of the combustion products composition calculated for conventional gun powders and rocket solid propellants with appropriate literature data. A good conformity of the obtained results to literature data justifies the method [1] used in this work.

The gross coefficients B_j of compositions for single- and doublebase gun-propellants (pyroxylin and ballistite), with various contents of aluminium, and the enthalpies H of their formation under standard condition $T = 298$ K, are presented in Table 1.

Table 1.

Summary of Compositions and Thermochemical Properties of the Propellants.

Powder		Pyroxilin				Ballistite			
Addition* of Al, %		0	5	10	15	0	5	10	15
Al		0	1.765	3.369	4.834	0	1.765	3.369	4.834
Bj,	O	36.78	35.03	33.44	31.98	36.39	34.66	33.08	31.64
mol/kg	H	25.02	23.83	22.74	21.75	27.86	26.53	25.33	24.22
	N	9.709	9.247	8.827	8.443	10.46	9.965	9.512	9.098
	C	20.84	19.85	18.94	18.12	20.24	19.28	18.40	17.60
Enthalpy -H, MJ/kg		2.364	2.251	2.149	2.056	2.096	1.996	1.905	1.823

* It is the weight-ratio of the aluminum to the original propellant.

These thermochemical properties of propellants are the initial data for further thermodynamic and ballistic calculations. The results of thermodynamic and ballistic characteristics of original and metalliferous powders at pressure 3000 atm and temperature 298 K are shown in Table 2.

As we can see in Table 2, the introduction of aluminium leads to increasing maximum temperature T_f and powder force $F=RT_f/M$, where R is the universal gas constant. In result, the corresponding increase in muzzle velocity V of projectile is provided. It is of great interest for the interior ballistic problem to estimate the variation of thermodynamic characteristics by pressure change in range which is typical for gun-shot.

For this aim the calculations of maximum temperatures T_f and powder forces F were carried out for pressure values up to 5000 atm. The results of calculations

Table 2.

Thermodynamic and Ballistic Characteristics of Powders with Aluminum Additives

Powder	Pyroxilin				Ballistite			
Addition of Al, %	0	5	10	15	0	5	10	15
Tf, K	2878	3152	3403	3634	2947	3212	3454	3676
M, g/mol all products	26.27	27.60	28.92	30.25	25.48	26.77	28.06	29.35
gas-phase	26.27	25.11	23.95	22.80	25.48	24.36	23.24	22.12
Relative weight of Al ₂ O ₃	0	0.090	0.172	0.246	0	0.090	0.172	0.246
Relative weight of gas-products	1	0.956	0.912	0.868	1	0.956	0.912	0.868
W _{cond} /W _{prod} (Al ₂ O ₃)	0	0.008	0.015	0.021	0	0.008	0.015	0.021
(D ₀ -D)/D ₀ , %	0	3.29	5.39	6.89	0	2.85	4.75	5.70
W _{charg} /W _{chamb}	0.209	0.195	0.186	0.178	0.198	0.186	0.177	0.171
Density, g/cm ³	1.60	1.65	1.70	1.74	1.60	1.65	1.70	1.74
Heat of explosion cal/g	956	1086	1205	1313	1006	1134	1250	1357
Force F, J/g	911	1044	1181	1325	962	1096	1236	1382
F / F ₀	1	1.146	1.296	1.455	1	1.140	1.285	1.437
V / V ₀	1	1.047	1.087	1.124	1	1.044	1.082	1.117
Addition to covolume, l/kg	0	0.028	0.059	0.093	0	0.028	0.059	0.093

Table 3.

Combustion Products Temperature Tf and Force F vs Pressure.

Powder	Pyroxilin				Ballistite			
Pressure, atm	40	100	1000	5000	40	100	1000	5000
Tf, K	2833	2850	2872	2880	2890	2912	2940	2950
F, J/g	903.4	907.1	911.0	910.2	951.9	956.7	961.9	961.0

presented in Table 3 show that pressure influence is relatively small. So, the relative increase in temperature T_f by pressure variation from 40 to 5000 atm consists 1.72 %, and the maximum increase in powder force consists 1.0 %.

Such increase in temperature T_f takes place owing to the suppression of dissociation reactions, that simultaneously leads to some increase in average molecular weight M of gas mixture. The competing influence of these two factors leads to appearance of maximum on the curve $F(P)$ located in the pressure range 1000- 2000 atm. The effect of dissociation suppression influences the temperature T_f and powder force mainly at pressures up to 1000 atm. This effect can be neglected in the field of relatively high pressures 1000-5000 atm. So, the estimations obtained for $P=3000$ atm are true over a wide range of pressures. The weak dependence of powder force on pressure points indirectly to possibility to use the state equation for ideal gas instead of one for real gas.

3. DISCUSSION OF THE CALCULATIONS RESULTS

The thermodynamic calculations testify that addition of aluminum to conventional gun-powders may be one of the perspective method to increase their energy density. As we mentioned, the utilisation of high-energy propellants (HEP) is usually accompanied by increasing in temperature T_f and, as result, in erosivity of powder gases. For example, HEP containing the explosives, usually have the high temperature T_f together with high molecular weight M of combustion products, which is due to increase in CO_2 content in products. This circumstance is illustrated by thermochemical data for unmetalliferous powders, presented in Table 4.

Table 4.

Thermochemical Characteristics and Compositions of Combustion Products of Metallized and Conventional Gun Propellants*

Powder	T K	F J/g	M g/mol	Composition of Products, mol/kg					
				CO	CO ₂	H ₂ O	H ₂	N ₂	AL ₂ O ₃
M1	2480	928	22.2	22.8 0	2.40	6.10	9.10	4.50	-
Pyroxilin	2878	911	26.3	14.2 7	6.56	9.37	2.82	4.70	-
Ballistite	2947	962	25.5	14.3	5.92	10.20	3.34	5.05	-
M30	3021	1078	23.3	11.8 0	3.00	10.50	5.50	11.90	-
P+5% Al	3152	1044	25.1	15.3 3	4.50	7.99	3.50	4.43	0.090
B+5% Al	3212	1096	24.4	15.2 3	4.04	8.64	4.12	4.75	0.090
M5	3264	1079	25.1	16.5 0	4.90	9.30	4.00	4.90	-
P+10% Al	3403	1181	24.0	16.0 3	2.90	6.47	4.34	4.17	0.172
B+10% Al	3454	1236	23.2	15.8 0	2.60	6.94	5.06	4.47	0.172
P+15% Al	3640	1325	22.8	16.4	1.72	4.81	5.34	3.92	0.246
B+15% Al	3676	1382	22.1	16.0 0	1.56	5.14	6.12	4.20	0.246
M8	3716	1178	26.2	13.0 0	6.40	10.20	2.40	5.40	-

* Note : P is pyroxilin; B is ballistite; M1 - M30 are the conventional US gun-propellants [8,11].

It is desirable to make up the increase in powder force F , and consequently in muzzle velocity of projectile $V \sim F$, decreasing the molecular weight M , but keeping the temperature T_f within the allowable limits. This purpose is served for conventional propellants by means of aluminum addition, as the data presented in Tables 2 and 4 show.

The energy increasing of conventional propellants by introduction of aluminum leads simultaneously to lower molecular weight M of working gas, that is very desirable. This is due to the deoxidisation of CO_2 to CO by the oxidation of aluminum up to condensed phase Al_2O_3 . On the bases of carried out calculations with account of totality of defined factors exerted decisive influence in the end on the value of initial projectile velocity on the one hand and for the life of gun barrel on the other hand, it can be optimised the content of aluminium in powder [charge].

For ammunition of classic scheme round it is more acceptable content of aluminium in powder [charge] not more than 5- 8% of the charge mass. In such a case it is expected increasing of burning temperature up to 3100-3300 K, powder force up to 15-20%, and muzzle velocity up to 4-8%; that is highly substantial in comparison with other known methods, for example, the using of powder with fast-burning explosives.

4. FIRING TESTS OF GUN-CHARGES CONTAINING ALUMINUM ADDITIVES

In order to experimentally verify the proposed method for increasing in muzzle velocities of projectiles, some firings were done with charges containing aluminum additives taken in excess of 100% of powder mass. It was investigated the possibility of presence in conventional charges the aluminum powder ASD-1 or granulated aluminum AG-90 (on the base of 90% ASD-1 with 10% of pyroxylin).

It was investigated also the gun charges containing the aluminum foil particles of different thickness. The aim of these tests is to find the optimum form for aluminum foil elements and their distribution over the gun chamber volume. The

trials were carried out using conventional 30 mm ballistic gun-tube. The registration of projectile muzzle velocities were provided by solenoids. The maximum gas-pressures was measured by crasher device, and simultaneous registration of the pressure curve $P(t)$ by means of the piezometric pickup T-6000 was provided.

The results of ballistic trials show that the small addition of aluminum powder ASD-1 (or the composition of granulated aluminum AG-90) in amount of 2-6%, leads to increasing in the maximum pressure of powder gases. The more aluminum is contained in the charge the higher is the pressure increase. So, the addition of aluminum powder ASD-1 in amount of 4.4% leads to increasing the muzzle velocity up to 6.3% and the maximum pressure up to 20%. The addition of 4.6% of granulated aluminum AG-90 of different fractions into the same charge leads to increase in the muzzle velocity up to 2.5-6.0%, and maximum pressure increasing to 10-16%.

These experimental data confirming the theoretical forecast have been the base for further optimisation of the charge design to reduce temperature T_f keeping the increase in muzzle velocity V . The main goal for subsequent experiments was the looking for the optimum form of aluminum elements to improve thermodynamic characteristics of combustion products, and to optimise the dynamics of energy release during combustion of the metal-containing charges.

Results of these investigations for charges containing particles of aluminum foil indicate the peculiar dependence of the ballistic characteristics on foil thickness. So, the utilisation of foil having the certain thickness ensures the smaller rate for the maximum pressure increase in comparison with the rate of the muzzle velocity increase. This unordinary experimental fact can be explained by the influence of the time-delay of aluminum particles ignition, which depends on foil thickness.

The special investigation of interior ballistic process was carried out to check that hypothesis and to compare the burning processes for conventional and metalliferous charges. These experiments were provided by synchronous registration of pressure curves $P(t)$ at five different cross sections along the barrel. The maximum pressure for the charge containing the aluminum foil elements (3% of charge mass) is slightly lower (0.9%), than that one for conventional charge. At the same time the addition aluminium foil increases the muzzle velocity up to 2.3%.

This effect is accompanied by increase in the flatness of the pressure curves, i.e. the ratio of the mean pressure to the peak pressure. In the case of charge with aluminium foil the pressure measured at barrel point on distance of 7.5 clb. from the chamber is higher than corresponding one for conventional charge up to 8.3%. As the projectile moves along the bore, the pointed difference of pressures is lowering: at distance of 26 clb. it consists 3.3%, and near the muzzle end (75 clb) it consists only 2,0%.

A ballistic efficiency of the aluminum addition can be also estimated by comparison of the pressure impulses for conventional and metallized charges. These values were derived in according to experimental curves $P(t)$ for different cross-sections of bore. For the point on distance of 7,5 clb. from the chamber's bottom the pressure impulse for metallized charge exceeds the relevant one for the regular charge by 14,4%. For the next section corresponding to distance of 26 clb., this value is lowering up to 9,8%.

The high energy-release by aluminum burning is favourable for total combustion of powder charge in the bore during the pressure decrease period of shot cycle. The numerical estimation of burned out powder portion corroborates this effect.

along the bore. According to the theoretical estimations taking into account the foil ignition-delay, the temperature-time curve has the second maximum as result of aluminum burning. The optimization of aluminum content is directed to increase this second maximum of temperature but not exceed the level of first maximum gastemperature. In the case of metallized charge, the falling part of the curve $T(t)$, next to the second maximum, places above the same one for the original charge without aluminum.

5. CONCLUSION

The results of experimental and theoretical investigations presented in this paper show the possibility to improve the ballistic characteristics of conventional gun-propellants by addition of small amount of aluminum powder or foil particles of certain thickness.

The interior ballistic process for gun-tube systems using the multi-phase combustion products of metalliferous charges as working substance can be governed effectively by means of amount of additives and their sizes.

6. REFERENCES

1. Assovsii I.G., Boborykin V.M., and Leipunskii O.I.,
Ballistic Characteristics of the Gun Propellants with Metallic Additives.
The Thermodynamic Calculation, Report of Inst. Chem. Physics,
The USSR AS, Moscow, 1983 [in Russian].
2. Assovsii I.G., Sergeev V.V., and Toporkov D.L.,
Ballistic Characteristics of the Gun Powders with Metal Elements,
Proc. Int. Conf. on Combustion, Moscow St.Petersburg, IPC RAS, 1993.
3. Serebryakov M. E.,
Interior Ballistics,
Oborongiz, Moscow, 1949, [in Russian] .
4. Corner J.,
Theory of Interior Ballistics of Guns,
Wiley, New York, 1950.
5. Landau L. D., and Lifshitz E. M.,
Hydrodynamics,
Theoretical Physics, Vol. 6, Nauka, Moscow, 1986.
6. Sorkin R.E.,
Gas-thermodynamics of solid-propellant rocket motors,
Nauka, Moscow, 1967 [in Russian].
7. Krier H. and Summerfield M. (eds.),
Interior Ballistics of Guns,
Progress in Astronautics and Aeronautics, Vol. 66,
AIAA, Washington, D.C., 1979.
8. Stiefel L.
Gun Propellants, pp. 307-324, *ibid*.
9. Kuo K.K., and Summerfield M. (eds.),
Fundamentals of Solid Propellant Combustion,
Progress in Astronautics and Aeronautics, Vol. 90,
AIAA, Washington, D.C., 1984.
10. Orlov B.V., Larman E.K., and Malikov V.G.,
Arrangement and Design of Gun Barrels,
Mashinostroenie, Moscow, 1976 [in Russian].
11. Ward J.R., Stobie I.C., Kaste R.P., and Bensinger B.D.,
Effect of Surface Oxide on Gun Barrel Wear, Corrosion
NACE, Vol.39, No.10, pp. 384-385, (1983).
12. Baibuz V.F., Zitserman V.Yu., Golubushkin L.M., and Chernov Yu.G.,
Chemical Equilibrium in Nonideal Systems,
Inst.of High Temperatures, AS USSR, Moscow, 1985.

EFFECT OF MOLECULAR STRUCTURE ON BURNING RATE

R. L. Simmons
Naval Surface Warfare Center - Indian Head Division
Indian Head, MD 20640
301-743-4635
FAX 301-743-4683

ABSTRACT

This paper is a brief review of the molecular structure effects on the linear burning rate of energetic ingredients used in solid propellants. While it has long been known that the burning rate of propellants based on nitrocellulose (NC) and liquid nitrate ester plasticizers is a direct function of the flame temperature and heat of explosion, there are classes of ingredients for which this behavior does not always hold true -- specifically nitramines and azides.

There are new nitramine and azide ingredients emerging from research studies that offer drastically different burning characteristics -- which in turn will yield entirely new classes of advanced gun propellants. This paper will address how the molecular structure of various nitramine and azide ingredients affect the burning rate -- in ways that are significantly different than conventional NC-NG systems. For example, it is now possible to significantly increase the burning rate without the normal attendant increases in flame temperature -- and alternatively, reduce the flame temperature without sacrificing burning rate. These ingredients do not appear to obey the standard combustion theories and explanations.

INTRODUCTION

This paper is dedicated in memory of Otto K. Heiney, who was killed in an explosion on July 26, 1994 in the course of his work in advanced gun propellants. Otto was well known in the international solid propellant community as one who strongly believed in advancing the state-of-the-art of gun propellants, and was instrumental in funding many basic combustion and burning rate studies while at Eglin AFB. He was also keenly interested in improving a fundamental understanding of the interior ballistics of guns, especially at velocities > 2000 m/sec. He will be missed by his fellow workers.

Ever since the introduction of NC as a fully colloided solid propellant about 1880, virtually all gun propellants in use have been based on NC. Also, it was clearly recognized shortly after the introduction of double-base propellants that the burning rate is a direct function of the flame temperature and heat of explosion. If one wants faster burning, one simply uses a hotter and more energetic propellant. All of the known double-base combustion models are based on this fact.

It has been a challenge for many decades to find a way to tailor the burning rate relatively independent of flame temperature or heat of explosion. The results shown in this paper have been collected from a variety of sources, but primarily are based on work conducted at Eglin AFB and/or funded by Eglin during the past 20-25 years. In general, the results shown here have been not widely reported or readily available to burning rate researchers. One unique aspect about many of the burning rates reported here is that they were obtained in a high pressure strand burner (at Eglin AFB) at pressures up to 50,000 psi (345 MPa).

Nitrate Esters

For reference purposes, a literature review of 30 homogeneous double-base NC-NG propellants (including solvent and solventless extruded types as well as casting powder/casting solvent types) covering a wide range of heat of explosion (from 420 to 1650 cal/gram) showed the following relationship between heat of explosion (Qex) and burning rate:

$$R_1 = 0.08911 * 10^{0.0008928 * Q_{ex}} \quad (1)$$

where Qex is calories/gram and R_1 is inches/second at 2,500 psi (or 17.24 MPa). The pressure of 2,500 psi was chosen simply because many burning rate researchers used this as basis of comparison (in the 1940s-1950s), and much literature data were available. Unfortunately, much of the early data did not report flame temperature. For the simple NC-NG system, the relationship between Qex and isochoric flame temperature T_v (between 2200° and 4000°K) is as follows:

$$Q_{ex} = 247.8 * 10^{0.0001864 * T_v} \quad (2)$$

It should be recognized that Equation (2) may not be valid for other NC-based propellants, especially for ingredients that generate low MW combustion gases. However, based on these two relationships, the burning rate (at 2,500 psi) of homogeneous NC-NG propellants varies as follows:

<u>Tv (°K)</u>	<u>Qex (cal/g)</u>	<u>Rate (in/sec)</u>
2000	585	0.30
2500	725	0.40
3000	898	0.56
3500	1113	0.88
4000	1379	1.52

For gun applications, it is of more value to compare burning rates at significantly higher pressures -- and 40,000 psi (276 MPa) is typically used since it represents a value closer to the average pressure encountered during the gun ballistic cycle. Of course, burning rates at peak chamber pressures of 80,000 to 100,000 psi (550 to 700 MPa) would be even better, but no such high pressure strand burners are known to exist -- and closed bomb burning rates are always subject to much interpretation.

If the pressure exponent of all homogeneous NC-NG propellants is assumed to be essentially 0.90 above 5,000 psi (34.5 MPa), then the relationship between heat of explosion (Qex) and burning rate (at 40,000 psi or 276 MPa) is as follows:

$$R_2 = 0.8501 * 10^{0.0009454 * Q_{ex}} \quad (3)$$

where Qex is calories/gram and R_2 is inches/second at 40,000 psi.

From this, the following burning rates are to be expected at 40,000 psi:

<u>Tv (°K)</u>	<u>Qex (cal/g)</u>	<u>Rate (in/sec)</u>
2000	585	3.0
2500	725	4.1
3000	898	6.0
3500	1113	9.6
4000	1379	17.1

This relationship is believed to be reasonably good even though it is extrapolated from 2,500 psi. For instance, investigators working with solventless extruded JA-2 double-base propellant (where Qex = 1120 cal/g and Tv = 3440°K) have reported burning rates at 40,000 psi ranging from 9.5 to 11.1 inches/second -- in reasonably good agreement with the extrapolated rates. The pressure exponent of JA-2 is in the range of 0.86 to 0.90 at 40,000 psi. Actual observed rates at 40,000 psi are always better than predictions or extrapolations.

Strands of NC (12.6%N + 1% 2nDPA stabilizer) burned in the Eglin AFB high pressure strand bomb (as a baseline reference) from 4,000 to 50,000 psi (27.6 to 345 MPa) gave the following:

$$R_{NC} = 0.0004270 * P^{0.883} \quad (4)$$

where P is psi and R_{NC} is inches/second. At 40,000 psi, NC was found to burn at 4.96 inches/second -- slightly slower than the 6.4 inches/second expected from $Q_{ex} = 930$ cal/gram in equation (3) or 6.2 inches/second from $T_v = 3040^\circ K$ in equation (2). In summary, NC was observed to burn at the following rates:

<u>P (psi)</u>	<u>Rate (in/sec)</u>
4,000	0.65
10,000	1.45
20,000	2.68
30,000	3.83
40,000	4.96
50,000	6.02

In the period from 1945 to 1950, much work was done by B. L. Crawford (and others) at the University of Minnesota where they found polyvinyl nitrate (PVN) to be significantly faster burning than NC. A limited amount of testing was done at Eglin about 1983-1984 with PVN. Burning rate strands were prepared, and it was noted that PVN was completely miscible with NC (12.6%N) in all proportions. Results of the tests (and a comparison to neat PVN taken from the literature) are as follows:

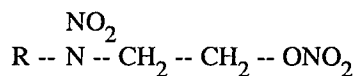
<u>% PVN</u>	<u>Q_{ex}</u>	<u>T_v</u>	<u>Rate</u>	<u>n</u>
0	930	3040	4.96	0.883
40	993	3154	6.00	0.984
100	1113	3372	7.96	1.035

where Q_{ex} is calories/gram, T_v is $^\circ K$, Rate is inches/second at 40,000 psi, and n is the pressure exponent.

The increase in burning rate (and the gradual increase in pressure exponent) as the concentration of PVN increased can either be attributed to the increase in Q_{ex} and T_v -- or to the simpler PVN molecule containing a greater proportion (or higher density) of nitrate groups per molecule than NC. On the other hand, NC-PVN appears to burn slightly slower than NC-NG at the same flame temperature (based on JA-2 propellant and extrapolated double-base behavior).

NENAs

Over a decade ago, alkyl NENA plasticizers (containing both a nitramine as well as a nitrate ester moiety) were researched extensively at Eglin AFB, and their burning rate properties determined in a NC binder. NENAs are mono nitrate nitramines as shown in the following structural formula:



where R = an alkyl group such as methyl, ethyl, propyl, etc. NENAs are completely miscible with NC in all proportions, and form homogeneous single-phase systems with no solid phases present.

Burning rates of strands were measured over the pressure interval from 4,000 to 50,000 psi (27.6 to 345 MPa). When examined at a fixed NENA concentration of 40% by weight (in NC), it was found that the burning rates changed in direct proportion to the individual Q_{ex} of the NENA studied. It was also noted that the NENAs burned faster than expected on the basis of Q_{ex} or T_v compared to NC. Pressure exponents were generally about unity, and varied little from one NENA to another. In summary, the following burning behavior was observed (where Rate is the burning rate in inches/second at 40,000 psi):

NENA	NENA Q_{ex}	40% in NC: Q_{ex}	T_v	Rate	n
Methyl	1113	993	3094	7.33	0.941
Ethyl	797	867	2741	5.95	1.005
Propyl	503	749	2453	4.72	1.022
Butyl	259	652	2245	3.95	1.006
Pentyl	47	567	2116	3.41	1.001
NC control	---	930	3040	4.96	0.883
NC-DBP	---	686	2370	3.02	0.862

In general, the NENAs burned about 45% faster than the NC and NC-DBP controls at the same flame temperature -- and the burning rate increased nearly linearly with increasing flame temperature. Presumably, the enhanced rate is due to the nitramine moiety in the NENA, or an interaction between the nitrate ester and nitramine. No predictions have been made for the neat NENAs, although it appears the rate of neat MeNENA ($T_v = 3225^\circ\text{K}$) could easily be greater than 15 inches/second (at 40,000 psi).

In another series of tests, EtNENA was diluted with an inert plasticizer DOS (dioctyl sebecate) to simulate the lower flame temperature of other members of the NENA family, ProNENA, BuNENA and PeNENA. Also, BuNENA was examined at a higher concentration to simulate the lower flame temperature of PeNENA, and PeNENA was examined at a lower concentration to simulate the higher flame temperature of ProNENA. NC (12.6%N) was the binder in all instances.

The burning rates observed were as follows (at 40,000 psi):

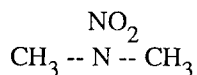
<u>NENA</u>	<u>Q_{ex}</u>	<u>T_v</u>	<u>Rate</u>	<u>n</u>
36% EtNENA+4% DOS	749	2450	4.99	1.001
40% ProNENA	749	2453	4.72	1.022
20% PeNENA	748	2452	4.37	0.844
34% EtNENA+6% DOS	652	2240	4.40	1.017
40% BuNENA	652	2245	3.95	1.006
50% BuNENA	582	2144	3.79	1.024
40% PeNENA	567	2116	3.41	1.001

In each instance, the smaller NENA molecule (with fewer attendant methylene groups) burned faster than the larger NENA molecule -- at the same or similar flame temperatures -- meaning it is more important to have methylene diluent groups in molecules other than the NENA itself.

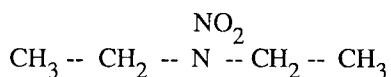
It is also believed to be significant that no slope breaks or pressure exponent changes were observed with any of these homogeneous NENA nitramine propellants over the entire pressure range tested, and in some instances this was from 2,000 to 50,000 psi.

NITRAMINES

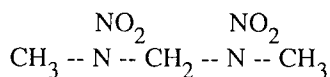
To help in understanding the enhanced burning rate of NENAs, three aliphatic nitramines were studied: dimethyl nitramine (DMN), diethyl nitramine (DEN), and dimethyl methylene dinitramine (DMMD) -- where no other energetic moieties are present. Structural formulas are as follows:



DMN



DEN



DMMD

Because of the lower flame temperature (and reduced energy) of DMN and DEN, they were studied at a lower concentration in NC than the NENAs.

Diethyl nitramine (DEN) burned as fast as ProNENA -- and at essentially the same flame temperature and heat of explosion -- when compared to NC, the flame temperature was lowered (by more than 600°K) without affecting the burning rate. Obviously, the nitramine moiety contributes greatly to the burning rate, as can be seen in the following (where Rate is inches/second at 40,000 psi):

<u>Nitramine</u>	<u>Q_{ex}</u>	<u>T_v</u>	<u>Rate</u>	<u>n</u>
NC - control	930	3040	4.96	0.883
15% DEN	733	2436	4.89	0.998
40% ProNENA	749	2453	4.72	1.022

Dimethyl nitramine (DMN), having a more favorable oxygen balance, was slightly hotter and faster burning than DEN -- not entirely unexpected. DMN is similar to ProNENA in both flame temperature and heat of explosion, yet its burned appreciably faster -- and almost as fast as EtNENA (which is hotter and more energetic). Results observed (at 40,000 psi) are as follows:

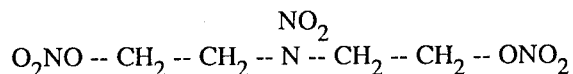
<u>Nitramine</u>	<u>Q_{ex}</u>	<u>T_v</u>	<u>Rate</u>	<u>n</u>
NC - control	930	3040	4.96	0.883
30% DMN	796	2542	5.77	0.940
40% EtNENA	867	2741	5.95	1.005

Dimethyl methylene dinitramine (DMMD) with two nitramine groups per molecule is more energetic than either DMN or DEN. It was studied at a concentration of 50% in NC, and found to burn much like MeNENA -- only cooler by more than 300°K. Results observed (at 40,000 psi) are as follows:

<u>Nitramine</u>	<u>Q_{ex}</u>	<u>T_v</u>	<u>Rate</u>	<u>n</u>
NC - control	930	3040	4.96	0.883
50% DMMD	893	2804	7.71	1.008
40% MeNENA	993	3094	7.33	0.941

The nitramines DMN, DEN, and DMMD appear to be excellent ingredients for adjusting the burning rate of NC propellants with little or no affect on flame temperature.

In addition to the three nitramines just mentioned, another key compound was studied -- the well known DINA (1,5-dinitrato-3-nitrazapentane). DINA contains two nitrate esters plus one nitramine group -- it can be considered to be a derivative of DEN with a nitrate ester on each end -- or as a derivative of EtNENA with a nitrate ester on the other end, as shown in the following formula:



DINA

Although DINA is a solid, melting at 51-52°C, it is soluble in NC in quite high concentrations. Strands were prepared of 40% DINA in NC (at the same level as for the NENAs), and burned at pressures from 4,000 to 50,000 psi.

As to be expected from such a very energetic ($Q_{\text{ex}} = 1337 \text{ cal/g}$) molecule, DINA increased the flame temperature considerably -- but did not burn appreciably faster than DMMD which is more than 500°K cooler. Results observed at 40,000 psi in comparison with others are as follows:

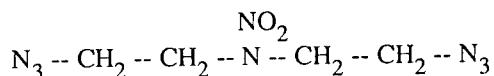
<u>Nitramine</u>	<u>Q_{ex}</u>	<u>T_v</u>	<u>Rate</u>	<u>n</u>
NC - control	930	3040	4.96	0.883
40% EtNENA	867	2741	5.95	1.005
40% MeNENA	993	3094	7.33	0.941
50% DMMD	893	2804	7.71	1.008
40% DINA	1083	3369	8.18	0.923

It appears that the two nitrate ester groups in DINA may be dominant over the nitramine group in determining the burning rate.

Azides

About the same time the NENAs and other nitramines were being studied, there were extensive studies on aliphatic azides at several different laboratories. Azides represent a substantial increase in energy over nitrate esters. Typically, the azide moiety contributes nearly +117 kcal/mole to the heat of formation when azide is substituted for the nitrate, and almost +80 kcal/mole when azide replaces a hydrogen. The combined effects of azide + nitramine in the same molecule made for extremely impressive molecules.

One diazido nitramine studied quite extensively in the early 1980s was DANPE (also known as DIANP) with the following structure:



DANPE

In a sense, where DINA can be considered to be a dinitrato version of EtNENA, DANPE is a diazido version. Both DINA and DANPE can be considered derivatives of DEN. DANPE is easily prepared from DINA by reacting with sodium azide, and the resulting DANPE is a liquid which readily plasticizes NC in all proportions. One of the most notable features of DANPE is fast burning, and a comparison with the precursors is shown below (at 40,000 psi):

<u>Compound</u>	<u>Q_{ex}</u>	<u>T_v</u>	<u>Rate</u>	<u>n</u>
15% DEN	733	2436	4.89	0.998
40% EtNENA	867	2741	5.95	1.005
40% DINA	1083	3369	8.18	0.923
40% DANPE	830	2857	11.74	0.822

From this comparison, it is seen that addition of a nitrate group (in EtNENA) increases the burning rate about 22%, while adding a second nitrate (in DINA) produces a 37% increase in burning rate. Even more impressive is the substitution of both azides for nitrate (in DANPE) which produced an additional 44% increase in rate -- with a simultaneous reduction in flame temperature of almost 500°K.

Since the flame temperature of DANPE is not appreciably higher than EtNENA (only 100°K) -- and an increase in temperature occurred with the second nitrate (in DINA), one might say that the increase in burning rate (observed with DINA) may have largely been due simply to the increased temperature.

Extrapolation of the 40% DANPE burning rate to lower pressures to compare it with literature values for 40% NG double-base propellants such as JPN (or JPT) reveals that 40% DANPE and NG burn at the same rate of 1.2 inches/second at 2500 psi -- though they have vastly different flame temperatures (2857 vs 3900°K).

Mixtures of DANPE with MeNENA, DINA, and RDX (with NC as the binder) showed that DANPE was the controlling factor in determining the burning rate. For instance, the following results (listed in order of decreasing burning rate at 40,000 psi) were obtained with equal parts of DANPE and other nitramines at a total concentration of 40%:

<u>Additive</u>	<u>Q_{ex}</u>	<u>T_v</u>	<u>Rate</u>	<u>n</u>
DANPE	830	2857	11.74	0.822
DANPE+RDX	962	3166	9.80	0.898
DANPE+DINA	957	3113	9.58	0.887
DANPE+MeNENA	912	2957	9.23	0.917
DINA	1083	3369	8.18	0.923
MeNENA	993	3094	7.33	0.941
RDX	1093	3436	7.12	1.062

The burning rate of 40% RDX in NC is not as high as expected considering the high Q_{ex} and T_v values. NC-NG of these same values will burn at about 9.0 inches/second -- approx 26% faster than the observed RDX rate. The fact that RDX does not burn as fast as NC-NG has been perplexing to propellant chemists for several decades. Much effort has been expended looking for ways to change the combustion behavior of RDX with no success until DANPE and other organic azides came on the scene.

There has been some research on the azide derivative of EtNENA -- it is known as EtAENA (ethyl azido ethyl nitramine), but no burning rate information is known. One might expect EtAENA to exhibit a rate of 8-10 inches/second at 40,000 psi.

GAP

Another interesting azide whose combustion has been examined at high pressure is glycidyl azide plasticizer/polymer, commonly known as GAP. It was studied at two different concentrations in NC, and found to burn as follows (at 40,000 psi):

<u>% GAP</u>	<u>Q_{ex}</u>	<u>T_v</u>	<u>Rate</u>	<u>n</u>
NC - control	930	3040	4.96	0.883
20% GAP	723	2476	5.19	0.823
30% GAP	609	2193	5.94	0.766

Higher concentrations were not studied because GAP is so oxygen deficient that the O/C ratio quickly falls under 1.00 above 40% GAP in NC. From these data, it is readily seen that the rate increases as the flame temperature decreases --- much like DANPE. And the pressure exponent also decreases -- much more than was seen for DANPE. GAP, in the above tests, was burned over the pressure interval of 2,000 to 50,000 psi (13.8 to 345 MPa) and found to have a constant pressure exponent over the entire interval.

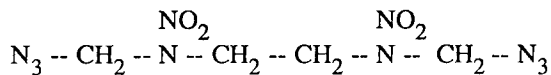
Comparing GAP with the NENAs, it is seen that 20% GAP has about the same flame temperature as 40% ProNENA (2476 vs 2454°K), yet burns about 10% faster. Even more impressive is 30% GAP with about the same flame temperature as 40% BuNENA (2193 vs 2245°K), yet 30% GAP burns 50% faster.

Neat GAP, with an empirical formula of $C_3H_5ON_3$ is quite oxygen deficient, yet burns rather fast at atmospheric pressure with no residue. Flanagan and Beckstead report that neat GAP burns at 0.80 inch/second at 1,000 psi (6.9 MPa) with a pressure exponent of 0.45 over the pressure interval 500 to 2,000 psi. Extrapolating the GAP concentration data above to neat GAP indicates a burning rate of at least 9-10 inches/second (at 40,000 psi) with a pressure exponent of about 0.6

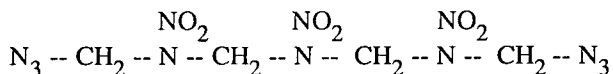
OTHER AZIDES

At least two other energetic aliphatic azides have been found of interest in propellant research studies where they offer high specific impulse to rocket propellants and high impetus for gun propulsion: DADNH (1,6-diazido-2,5-dinitrahexane) and DATH (1,7-diazido-2,4,6-trinitraheptane).

Though both DADNH and DATH have been in existence for over 25 years, and are known to be significantly faster burning than nitrate esters, their combustion behavior has not been well reported. Structural formulas are as follows:



DADNH



DATH

Burning rate studies of both of these diazides are available only at rocket operating pressures of 400 to 4,000 psi (2.76 to 27.6 MPa). Both DADNH and DATH are soluble in NC to about 30%, hence it is possible to make homogeneous propellants (with no solid phases). In studies at Hercules/Allegany Ballistics Laboratory in the early 1970s with DADNH and a dimethoxy analog known as DMDTH, the following burning rates were observed at 2,000 psi (13.8 MPa) -- the pressure interval from 400 to 4,000 psi was examined:

Nitramine	<u>Q_{ex}</u>	<u>T_v</u>	<u>Rate</u>	<u>n</u>
35% DMDTH	729	2387	0.25	0.64
NC - control	930	3040	0.32	0.64
1:1 DMDTH:DADNH	766	2587	0.57	0.58
35% DADNH	1005	3302	5.00	0.60

It is readily apparent that DADNH burns extremely fast. Extrapolation (with no increase in pressure exponent) indicates that 35% DADNH would burn at 30 inches/second at 40,000 psi.

From studies of DATH at Rocketdyne, the following were observed for 75% DATH in 25% NC ($Q_{\text{ex}} = 1166 \text{ cal/g}$ and $T_v = 3811^\circ\text{K}$) where the rates are in inches/second at 1,000 and 2,000 psi:

<u>R@1000 psi</u>	<u>R@2000 psi</u>	<u>n</u>
0.68	1.25	0.88

Extrapolation (with no change in pressure exponent) indicates 18 inches/second at 40,000 psi -- considerably less than for 35% DADNH. It is obvious that more study of DADNH and DATH is needed to determine their burning rate behavior. It also has been reported that relatively small amounts of DATH mixed with large amounts of RDX yield rather high burning rates -- actual numbers are unknown.

It has long been known that the fastest burning organic azide in the literature is TATNB (triazido trinitrobenzene) where researchers at Arthur D. Little reported (in 1956) that it burned at 5.0 inches/second at 1,000 psi. Pressure exponent was not reported -- but if it were typically 0.9, a rate greater than 100 inches/second at 40,000 psi would be predicted. In the same report, A.D. Little researchers observed nitramino triazole to burn at 1.7 inches/second, ortho-nitrophenyl azide to burn at 1.2 inches/second, and meta-nitrophenyl azide to burn at 0.6 inch/second at 1,000 psi.

CONCLUSIONS

From this collection of burning rate information, it is clear that nitramines burn faster than their nitrate ester counterparts -- and azides burn even faster -- when compared at the same flame temperature. The burning rate of azides also appear to be less sensitive to pressure. These classes of ingredients now offer the opportunity for the propellant formulator to tailor to a much wider range of burning rates without the usual associated flame temperature or heat of explosion changes.

ACKNOWLEDGMENTS

The author gratefully acknowledges the efforts of the following people who contributed data, information, and suggestions for this paper: Otto K. Heiney, Bertram K. Moy, Joseph E. Flanagan, John C. Gray, Gilbert B. Lancaster, J. Robert Martin, E. Hayes Zeigler, Thomas W. Christian, Norman S. Cohen, Bernie Strauss, and Sam Moy.

GLOSSARY

<u>Term</u>	<u>Definition</u>
BuNENA	Butyl nitrate ethyl nitramine
DADNH	1,6-diazido-2,5-dinitrahexane
DANPE	1,5-diazido-3-nitrazapentane; azido derivative of DINA
DATH	1,7-diazido-2,4,6-trinitraheptane
DB	Double base; usually NC + NG
DBP	Dibutyl phthalate
DEGDN	Diethylene glycol dinitrate
DEN	Diethyl nitramine
DIANP	1,5-diazido-3-nitrazapentane; also known as DANPE
DINA	1,5-dinitrate-3-nitrazapentane; dinitroxy ethylnitramine
DMDTH	1,6-dimethoxy-2,5-dinitrahexane
DMMD	Dimethyl methylene dinitramine
DMN	Dimethyl nitramine
EC	Ethyl centralite; sym-diethyl diphenyl urea
EtAENA	Ethyl azido ethyl nitrate; azido derivative of EtNENA
EtNENA	Ethyl nitrate ethyl nitramine
GAP	Glycidyl azide polymer/plasticizer
Impetus	Force constant in joules/gram
MeNENA	Methyl nitrate ethyl nitramine
2nDPA	2-nitrodiphenyl amine; stabilizer for nitrate esters
NENA	Nitrate ethyl nitramine moiety
NC	Nitrocellulose
NG	Nitroglycerin
OB	Oxygen balance to CO ₂ + H ₂ O in grams of [O] per 100 gm
O/C	Ratio of molecular oxygen to carbon
PeNENA	Pentyl nitrate ethyl nitramine
ProNENA	Propyl nitrate ethyl nitramine
PVN	Poly vinyl nitrate
Qex	Heat of explosion in cal/gram; also known as Hex and HOE
RDX	Cyclotrimethylene trinitramine; hexogen; cyclonite
RES	Resorcinol; stabilizer for nitrate esters
TATNB	Triazido trinitro benzene
TEGDN	Triethylene glycol dinitrate
Tv	Isochoric flame temperature in °K

Zeitlich präzise Mehrfach-Initiierung mit Zündschläuchen (Shock Tubes) NONEL und INDET ^{*)}

H.-U. Freund
W. Horning
G. Altmann

 **Battelle**
Ingenieurtechnik GmbH

Düsseldorfer Straße 9
65760 Eschborn

Einleitung und Zusammenfassung

Zündschläuche (engl. Shock Tubes) sind als nicht-elektrische Zündmittel seit vielen Jahren auf dem Markt; das Produkt NONEL ist auch in Deutschland zugelassen. Zündschläuche werden üblicherweise in Verbindung mit geeigneten pyrotechnischen Verzögerungsstufen im Tunnelbau und bei Gesteinssprengungen eingesetzt. Ein Vorteil ist die sehr geringe Sprengstoffmenge pro Längeneinheit, die bei der Detonationsweiterleitung die Hülle der Schnur unversehrt läßt. Die hier vorgestellten Untersuchungen, bei denen zur Diagnostik Röntgenblitzfotografie und Kurzschluß-Kontakte (Mikropins) eingesetzt wurden, zeigen, daß bei geeigneter Auslegung auch eine hohe zeitliche Präzision der Zündübertragung erreichbar ist. Damit erschließen sich neue Anwendungsbereiche.

Ergebnisse

NONEL und INDET stellen geeignete Übertragungsmittel zur Mehrfachinitiierung von Sprengladungen mit zeitlicher Präzision von $< 10 \mu s$ dar. Bei INDET-Tests erwies sich die zeitliche Präzision der Zündweiterleitung unbeeinflusst von starken Krümmungen des Schlauchs bis hin zum 180°-Knick. Alle Zündschläuche entstammten jeweils einem einzigen Fertigungslos. Damit die angegebene Zeitschwankung eingehalten bleibt, sind folgende Empfehlungen beim Aufbau einer Zündkette zu beachten:

1. Die Zündübertragung auf die Sprengladung muß über eine verzögerungslose Sprengkapsel und Übertragungsladung (PETN) vorgenommen werden.
2. Die NONEL-Schnüre sind präzise auf die geforderte Länge zu schneiden.
3. Die simultane Initiierung mehrerer Zündschläuche muß "end-on" mittels einer Sekundärladung (Verteilerladung) ausreichender Größe (bei 5 Schnüren beispielsweise 10 g) erfolgen.

Über die durchgeführten Tests wird im einzelnen berichtet.

^{*)} Hersteller-Produktbezeichnungen

SOLID PROPELLANT COMBUSTION. MODELING OF GAS-PHASE PRODUCTS AND
MICROPARTICLE FORMATION AND FIRE SUPPRESSION APPLICATIONS

Dmitrii Voropaev, Igor Zaslonko, Vladimir Smirnov
Semenov Institute of Chemical Physics, Russian Academy of
Sciences, Moscow, Russia

ABSTRACT

Computer model aimed at simulating the gas-phase and aerosol particles formation in solid propellant combustion was developed. Model calculations are in good agreement with experimental measurements of mean size and concentrations of combustion generated particles. Based on experimental data on quenching of small-scale fires in laboratory conditions, 2-D gasdynamic modeling of suppression of liquid fuel fires in large-scale semi-closed combustion chamber with the use of solid propellant aerosol generators was performed.

Introduction

Kinetic modeling of gas-phase products and aerosol particles formation during solid propellant combustion incorporates both the dispergation immediately from the propellant surface and particulate growth from the gas-phase species.

Evidently, it is unrealistic to try to work out detailed description of all aspects of this complicated phenomena. Instead of that, our approach is based on a detailed gas-phase kinetic block including the above mentioned factors. Especially difficult problem in computer modeling is simulation of kinetic processes with participation of solid microparticles.

Possibilities of our approach are illustrated by several actual examples: (a) formation of Al_2O_3 in burning of rocket propellant; (b) formation of K_2CO_3 in burning of solid compositions designed for fire-suppression.

Verification of our computer modeling results was performed based on comparison with experimental observations of the fire suppression action with the use of solid propellant combustion aerosols as applied to liquid fuel combustion in semi-closed volume.

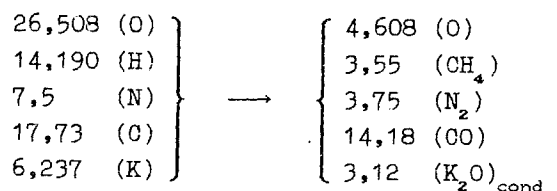
I. Formation and Evaporation of the Solid Microparticles

I.1 Simplified Model for Burning of Solid Propellant Compositions

The primary goal of this section is to model schematically the composition of combustion products flowing from the burning solid propellant surface. This surface serves as "flame holder" with an assigned combustion rate.

We used two solid propellant compositions PT-4 and PAS11-8, which are, in particular, very effective for fire suppression applications. The conversion of solid propellant to gas-phase products and aerosol particles was schematically presented by the following overall processes.

PT-4 (element composition, mole/kg)



PT-4

gasification
products

$$\Delta H_f = 4,125 \text{ kJ/kg}$$

$$\Delta H_f = -2946,07 \text{ kJ/kg}$$

PAS11-8 (element composition, mole/kg)

	1 variant	2 variant
26,33 (O)	5,07 (O ₂)	8,36 (O ₂)
16,51 (H)	8,25 (CH ₄)	8,25 (CH ₄)
38,1 (N)	1,61 (N ₂)	1,61 (N ₂)
14,82 (C)	6,57 (CO)	6,57 (C) _{sol}
6,42 (K)	3,21 (K ₂ O) _{cond}	3,21 (K ₂ O) _{cond}
27,09 (Cl)	2,71 (ClO ₂)	2,71 (ClO ₂)

PAS11-8

$$\Delta H_f = 853 \text{ kJ/kg} \quad \Delta H_f = -2205,6 \text{ kJ/kg} \quad \Delta H_f = -1479 \text{ kJ/kg}$$

It was assumed that the composition of gas-phase products is consistent with element composition of solid propellant and in the course of propellant gasification the methane and other poorly combustible components are predominantly emitted from burning propellant surface.

I.2 Boundary Conditions

General equations:

$$E_i = -D_i \frac{dC_i}{dx} + u \cdot C_i, \quad (1.1)$$

where D_i is the diffusion coefficient (cm²/s), C_i is the concentration of the i th component (mol/cm³), u is the gas flow velocity (cm/s), x is the distance from the fuel surface.

$$\frac{dE_i}{dx} = W_i, \quad (1.1)$$

where W_i is overall disappearance rate of i -th component

$$W_i = -C_i \cdot (\sum k_i + \sum k_{ij} C_j) + \sum k_{nm} C_n C_m, \quad (1.3)$$

where k_i is the rate constant of unimolecular reactions of C_i decomposition (1/s), k_{ij} is the rate constant of C_i interaction with C_j (cm³/mol/s), k_{nm} is the rate constant of C_i formation in reac-

tion between C_n and C_m .

$$h = -\lambda \frac{dT}{dx} + \sum [H(T) - H(0)]_i \cdot C_i, \quad (1.4)$$

$$\frac{dh}{dx} = \sum Q_i, \quad (1.5)$$

where λ is the heat-transfer coefficient, $[H(T) - H(0)]_i$ is the heat part of the i -th component enthalpy (kJ/mol).

$$\sum Q_i = -C_i \cdot (\sum k_{ij} q_{ij} + \sum k_{ij} q_{ij} C_j) + \sum k_{nm} q_{nm} C_n C_m, \quad (1.6)$$

where q_i , q_{ij} , q_{nm} are the heat effects of corresponding reactions.

$$u = \frac{A \cdot P^\nu \cdot \rho_{\text{propel}} \cdot \frac{\xi_{K_2O} \cdot \mu_{K_2O} + \xi_{K_2CO_3} \cdot \mu_{K_2CO_3} + \mu}{1000}}{\frac{P}{RT} \cdot \frac{\sum \xi_i \mu_i}{\sum \xi_i}}. \quad (1.7)$$

A (cm/s) and ν are parameters in the expression for burning rate.

Laser scattering measurements show that the mean size of solid particles formed in the course of solid propellant burning are equal to about 0,2 μ . Then, the concentration of solid particles equals:

$$N = \frac{P}{RT \cdot \frac{4}{3} \pi r^3 \rho_{K_2O}} \cdot \frac{\xi_{K_2O} \mu_{K_2O}}{\sum \xi_i}. \quad (1.8)$$

For example, the combustion of the composition FS-4 (first variant, $P = 1$ atm) gives $N \approx 1,8 \cdot 10^9 \text{ cm}^{-3}$

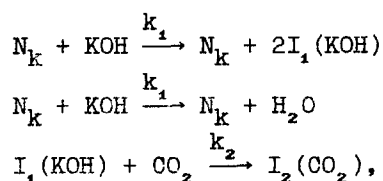
I.3 Modeling of Formation and Decomposition of K_2CO_3

Model assumptions:

- (1) KNO_3 decompose due to the contact burning on the KNO_3 (liquid) - organic component interfaces of propellant.
- (2) Main components formed in gas-phase state are: CH_2O , CH_4 , CO , and H_2 , O_2 , N_2 . Potassium oxide in the form of fine liquid K_2O microparticles of variable size.

(3) Burnout of products take place in the gas phase. Interaction of K_2O with CO_2 leads to K_2CO_3 formation. Other potassium-bearing particles (mainly KOH) are captured by K_2CO_3 particles in a diffusion-controlled regime.

To provide a possibility for describing heterogeneous processes in the framework of the formal kinetics, we propose a generalized symbolic form of kinetic equations

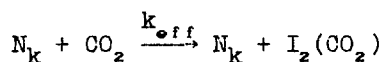


where N_K , the concentration of dispersed particles, is treated as an ordinary gas-phase species; I_1 and I_2 are the effective concentrations, which serve only for designating the amount of the gas-phase components deposited on the cluster surface and do not participate in any chemical transformations.

The mass of solid particles in a flame was calculated by equation:

$$m_{K_2O} \text{ (g/cm}^3\text{)} = \frac{P}{RT} \cdot \frac{\sum \xi_{K_2O} \cdot \mu_{K_2O}}{\sum \xi_i}$$

The CO_2 saturation of starting particles dispergated from propellant surface is presented by

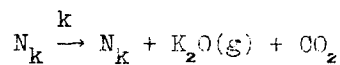


$$k_{eff} = 4\pi r_s D \cdot \left[\frac{|(N_K)_0 i_0 - I(CO_2)| + [(N_K)_0 i_0 - I(CO_2)]}{2 \cdot (N_K)_0 i_0} \right]^{1/3} \cdot N_A$$

where i_0 and $(N_K)_0$ are the initial size and concentration of particles.

Thermal decomposition of K_2CO_3 particles was modeled by the

simplified scheme



$$k = 4\pi r_s D \bar{N}_T(CO_2) N_A,$$

where k is effective decomposition rate constant in the diffusion regime expressed via reverse process and equilibrium constant, D is the diffusion coefficient for Brownian particles, N_A is Avogadro number.

$$\bar{N}_T(CO_2) = \frac{\exp(14,7 - 30450/T)}{82,05 \cdot T},$$

where $\bar{N}_T(CO_2)$ is the equilibrium CO_2 concentration over K_2CO_3 at the temperature T .

Coagulation was presented by simplified manner reflecting the fact that instead of two disappearing particles emerges only one particle.

I.4 Kinetic Scheme for Gas-Phase Reactions of K-bearing Species

In order to identify the main species, which play a dominant role in kinetic behavior of reacting system with K-bearing particles, we performed, as a first step, thermodynamic calculations of equilibrium compositions for some ballistite and composite solid propellants. As a further step, we composed the kinetic scheme for selected species which presented in Table 1.

II. Fire Suppression Efficiency of Propellant Generated Aerosols

The laboratory fire suppression experiments were performed in a closed chamber with small diffusion flames of n-heptane and acetone, which were quenched by aerosol combustion products of solid propellant PAS-47b composition. Detailed description of these experiments is presented elsewhere [4] and here we formulate only the main experimental findings:

(1) Under experimental conditions studied, the minimum charge of

solid propellant sample, needed for quenching, was around 23g/m^3 .

- (2) The characteristic quenching time strongly depends on a sample propellant weight. For large samples, this time is about the time of the propellant sample burn out.
- (3) The quenching time for acetone was about twice as short as that for heptane.
- (4) The repeated spark ignition of the residual unburned fuel was successful only for acetone, but not for heptane.
- (5) The percentage of K_2CO_3 - aerosol evolved during PAS-47 propellant combustion was $12 \pm 15\%$; the rest is gas-phase products and solid nonvolatile residue.
- (6) According to laser scattering measurements, the mean size of aerosol particles is equal to $0,2\ \mu$.
- (7) Critical particle concentration for fire suppression with aerosol generated by the PAS-47 burning was evaluated at $2,5 \cdot 10^7\ \text{cm}^{-3}$.

Some conclusions on mechanism of fire suppression:

- (a) Thermal factors in fire quenching are of minor importance.
- (b) Main factor determining the fire-suppression action is chemical prohibition caused by both radical termination on a microparticle surface of K_2CO_3 and K_2O or gas-phase inhibition by potassium-containing species. Estimates of a maximum rate of the radical termination, under conditions of our experiments lead to value of $k_{\text{max}} \approx 10^4\ \text{s}^{-1}$.

III Computer Modeling of Fire Suppression Action

The kinetic scheme for computer modeling includes the following basic blocks:

- (a) Gas-phase reactions for 49 species describing chemical kinetics in $\text{C}_1 + \text{C}_4$ -hydrocarbons/ O_2 systems.
- (b) Kinetic submodel describing the emission of microparticles and gas products from surface of burning solid propellant (see above).
- (c) Kinetic processes with participation of solid-phase particles.

The set of equations presented above was solved numerically for

some fire suppressing situations which are briefly illustrated below.

As the first step, the validity of our gas-phase methane combustion model was verified by comparison with experimental data on ignition delays in shock tubes. Then, we performed calculations of inhibition of methane combustion by K_2CO_3 aerosols and some results are presented in the Tables 2,3.

Table 2. Dependence of ignition delay on K_2CO_3 aerosol concentration ($T = 1300$ K, $\bar{d} = 2 \mu$)

Concentration of K_2CO_3 , g/m ³	τ_{ig} , s	τ_{ig}/τ_0
0	0,0079	1,0
0,28	0,011	1,39
2,8	0,023	2,95
13,2	0,06	7,5
27,9	0,07	8,7

Table 3. Dependence of ignition delay on mean size of aerosol particles ($T = 1300$ K, $[K_2CO_3] = 27,9$ g/m³)

\bar{d} , μ	τ , s	$\tau_d/\tau_{d=1}$
1	0,074	1,0
2	0,069	0,93
4	0,065	0,89
10	0,06	0,8

Comparing the experimental and calculated results we concluded that the proposed model satisfactorily describes the main features of the methane combustion inhibited by solid-propellant-generated K_2CO_3 aerosols.

IV. Computer Modeling of Gasdynamics and Thermal Processes in the Course of Fire Suppression in Large Semi-Closed Volumes

1. The dimensions of the experimental box are as follows: the

length is 6,5 m; the height is 4,5 m; the width is 2,85. The volume of the box is 83,4 m³. The embrasure is 2,0 m in width and 2,7 m in height (Fig.2).

2. Six aerosol generators are placed in this box. 4 units: mean discharge is 76 g/s, performance term (PT) is 66 s. 2 units: mean discharge is 137 g/s, PT is 73 s. Total discharge is 578 g/s. The arrangement of the generators and fire sources are shown in Fig.2. Surface of burning gasoline is 2 m². Overall gasoline consumption is 100 g/s

3. The gasoline combustion was modeled by well-stirred reactor approximation. Taking into account that characteristic combustion time under considered conditions was much shorter than characteristic gas-dynamic time, the composition of combustion products was calculated via chemical equilibrium assumption.

The flow field in the experimental box was determined by solution of gas-dynamic equations in two-dimension plane approximation.

The main results of computer modeling of gas-dynamic behavior are as follows:

(1) The air in the box has been dislodged by combustion products during 8 s. After that moment, the inflow of air into the box through the bottom part of the embrasure and the outflow of the products through the upper part was fairly stabilized.

(2) The steady-state regime of the gas-dynamic processes continued for ~30 s with the following parameters:

- the density of gasoline combustion products and air in the fire are 260 g/m³ and 65 g/m³, respectively;
- the temperature at the distance of 0,5 m from the fire source is 1100 K, that was consistent with experiments;
- flow rate over fire source is 3,7 m/s;
- inflow in the box and outflow in the atmosphere are 0,7 m/s and 0,25 m/s, respectively.

The fire suppressing generators were switched at $t \approx 80$ s.

Calculated results for q_{fs} as a function of time after switching the generators are listed below.

t, s	1	5	10	16	20	30	36	38	39	40
q_{FS} , g/m ³	0,5	11	16,9	20,4	22,8	32,5	43,9	47,7	49,7	51,6
T, K							644	615	603	593

To determine the moment of fire quenching we used the above results on critical quenching concentration measured experimentally for heptane combustion equal $q_{FS} \sim 23$ g/m³ (see above); q_{FS} is the actual density of solid propellant combustion products containing about 30% of fire suppressing K₂CO₃ aerosols. Note that, the widely accepted q_{FS} value in Russian fire suppressing practice is about 50 g/m³. This fact was the reason why the calculations presented in the above table were performed up to time attaining q_{FS} level about 50 g/m³.

The main results of computer modeling on the fire suppression action are as follows:

- (1) noticeable fire quenching starts at 25 s after generator is switched on;
- (2) duration of overall quenching ranges from 25 to 40 s;
- (3) termination stage in gasoline combustion occurs within 50 ÷ 60 s (from moment the generator switching on).

The calculation results are consistent with the experimental data on fire-suppression under full-scale experimental conditions. This work in particular, is a good illustration of solution of so called scaling problem. Thus, our approach based on laboratory investigation of fire suppression followed by computer modeling of full-scale fire suppression, using the laboratory data as input parameters is rather promising.

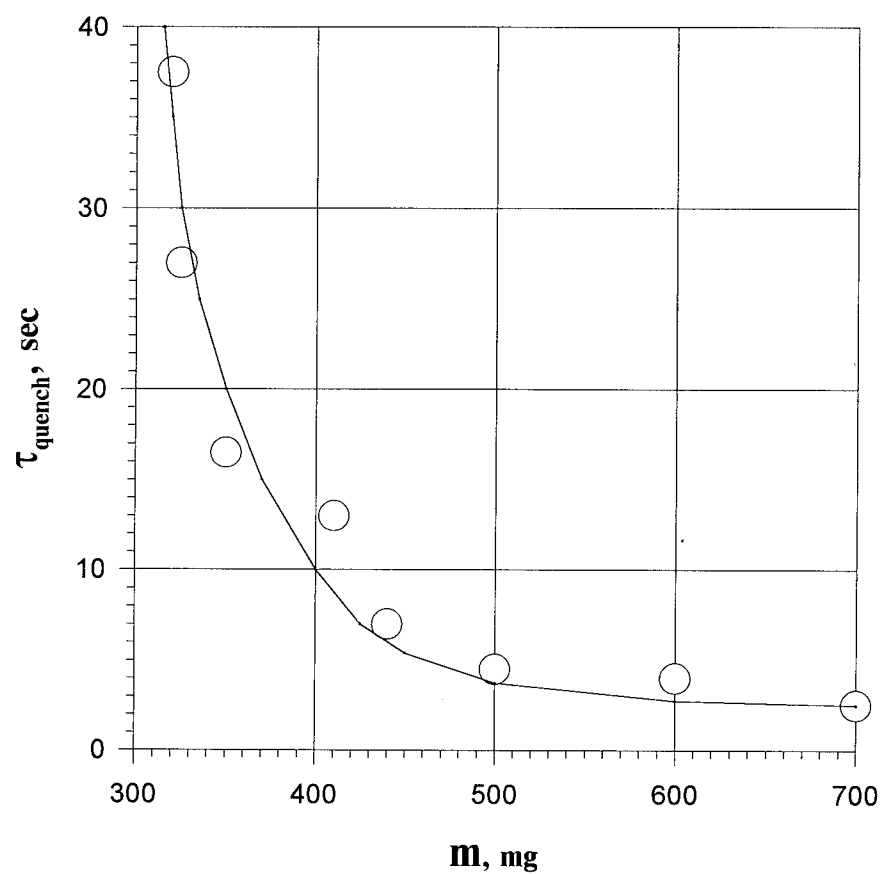


Fig.1. Characteristic time of fire quenching as a function of solid propellant sample mass. Volume of closed combustion chamber is $1,5 \cdot 10^4 \text{ cm}^3$, volume of liquid fuel is $0,4 \text{ cm}^3$, fire suppression composition is PAS-47.

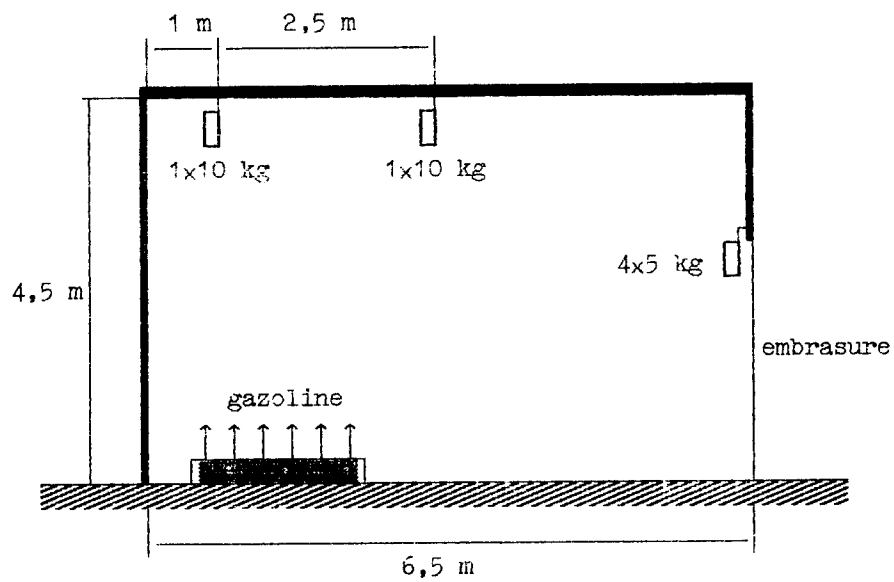


Fig.2. Plane schematic diagram of the semi-closed experimental chamber with gasoline fire source and the fire-suppressing aerosol generators disposal

Table 1

No	Reactions*	Lg A	n	E _a	Ref
1	$K + Cl + M \rightarrow KCl + M$	20,25	-1,0	0,0	[1]
2	$K + H_2O \rightarrow KOH + H$	13,6	0,5	37,7	[2]
3	$K + OH + M \rightarrow KOH + H + M$	22,84	-2,0	0,0	[2]
4	$K + O_2 \rightarrow KO + O$	12,8	0,5	53,6	[3]
5	$K + O_2 + M \rightarrow KO_2 + M$	21,73	-1,32	0,0	[2]
6	$K + HO_2 \rightarrow KO + OH$	12,8	0,0	1,99	[1]
7	$K + HO_2 \rightarrow KO_2 + H$	12,8	0,0	7,0	[3]
8	$K + HCl \rightarrow KCl + H$	14,38	0,0	8,5	[2]
9	$K + KOH \rightarrow K_2O + H$	14,5	0,0	34,0	est
10	$K + KO_2 \rightarrow KO + KO$	14,0	0,0	10,0	est
11	$KO + H \rightarrow K + OH$	12,8	0,0	3,2	[3]
12	$KO + OH \rightarrow KOH + O$	8,4	1,4	0,0	[3]
13	$KO + CO \rightarrow K + CO_2$	7,3	1,3	0,0	[3]
14	$KO + HO_2 \rightarrow KOH + O_2$	13,5	0,0	0,0	[3]
15	$KO + O + M \rightarrow KO_2 + M$	19,2	-1,0	0,0	[3]
16	$KO + H + M \rightarrow KOH + M$	22,6	-2,0	0,0	[3]
17	$KO + H_2 \rightarrow KOH + H$	14,28	0,0	1,5	[2]
18	$KO + CH_3 \rightarrow K + CH_3O$	13,5	0,0	1,5	est
19	$KO + CH_4 \rightarrow KOH + CH_3$	12,1	0,0	3,5	[3]
20	$KO + CH_2O \rightarrow KOH + CHO$	13,8	0,0	1,0	[3]
21	$KO + HCl \rightarrow KOH + Cl$	14,23	0,0	0,0	[2]
22	$KO + H_2O \rightarrow KOH + OH$	11,7	0,5	0,0	[2]
23	$KO_2 + O \rightarrow KO + O_2$	13,8	0,0	1,0	[3]
24	$KO_2 + Cl \rightarrow KCl + O_2$	13,8	0,0	0,0	[3]
25	$KO_2 + CO \rightarrow KO + CO_2$	13,8	0,0	23,0	[3]
26	$KO_2 + H \rightarrow KO + OH$	12,32	0,5	0,0	[2]
27	$KO_2 + OH \rightarrow KO + HO_2$	9,8	1,0	42,6	[3]
28	$KO_2 + HCl \rightarrow KCl + HO_2$	14,14	0,0	0,0	[2]
29	$KOH + Cl \rightarrow KCl + OH$	13,8	0,0	10,0	[3]
30	$KOH + HCl \rightarrow KCl + H_2O$	12,23	0,0	0,0	[2]
31	$K_2O + M \rightarrow K + KO + M$	20,6	-2,05	52,0	calc

* $k = A \cdot T^n \cdot \exp(-E_a/RT)$;

A [cm³/mol/s], T [K], E_a [kcal/mol]

REFERENCES

1. Jensen, D.E., J.Chem.Soc.Far.Trans., 1982, v.78, p.2835.
2. Zaslonko I.S. and Smirnov V.N., Kinetika i kataliz (Russian), 1995, in press.
3. Baratov, A.N., Dobrikov, V.V. and Shamonin, V.E., Khim.Fiz. (Russian), 1988, vol. 7, no. 6, p. 827.
4. Voropaev, D.G., Zaslonko, I.S. and Smirnov V.N., Fizika gorenia i vzriva (Russian), 1995, in press.

**DEVELOPMENT OF THERMAL ANALYSIS TECHNIQUES FOR
THE STUDY OF PYROTECHNIC SYSTEMS**

E.L.Charsley¹, S.B.Warrington¹, T.T.Griffiths², A.J.Brammer¹ & J.J.Rooney¹.

1. Thermal Analysis Consultancy Service, Leeds Metropolitan University, Calverley Street, Leeds, LS1 3HE, U.K.
2. Defence Research Agency, Fort Halstead, Sevenoaks, Kent TN14 7BP, U.K.

ABSTRACT

Recent developments in thermal analysis techniques for the characterisation of pyrotechnic systems are discussed. A high temperature differential scanning calorimeter is described which enables pyrotechnic systems to be studied, under both ignition and non-ignition conditions, over the temperature range ambient to 970°C, at heating rates up to 50°C min⁻¹. For studies at faster heating rates, a time to ignition apparatus, where the sample is introduced into a pre-heated furnace, is used. For both units, difficulties in defining the ignition temperature have been eliminated by the use of a photodetector system.

A thermomicroscopy system is also described which can be used to aid the characterisation of pyrotechnic systems and their components, under reflected light, at sample temperatures of up to 950°C. In addition to recording the observations using a colour video camera, in conjunction with a time-lapse video recorder, measurements can also be made of the intensity of the light reflected from the sample surface as a function of temperature.

INTRODUCTION

Thermal analysis techniques, in which a property of a material is measured as that material is heated or cooled at a controlled rate, are important methods for the characterisation of materials (1,2). Differential scanning calorimetry (DSC) and differential thermal analysis (DTA) where the energy changes in a system are measured as a function of temperature, are the most widely used of these methods and have been applied extensively to study pyrotechnic systems (3). Studies have been carried out under ignition conditions, where the sample undergoes a combustion reaction, and under non-ignition conditions, usually achieved by reducing the heating rate and sample weight, when the single peak seen on ignition may be resolved into several reaction stages.

In this paper we describe the development of a DSC system, designed to carry out measurements under both ignition and non-ignition conditions, in the sample temperature range up to 970°C. In addition to the DSC studies, recent developments in time to ignition and thermomicroscopy instrumentation will also be discussed.

DIFFERENTIAL SCANNING CALORIMETRY

We have previously reported on the development of a differential thermal analysis unit for the study of pyrotechnic systems under ignition conditions (4,5). The criteria for the design were to develop a head assembly which would:- (a) minimise heat losses from the sample and hence promote ignition, (b) provide reproducible temperature measurements over a large number of experiments and (c) resist attack from ignition products.

Although the original design performed very satisfactorily over a long period, it was decided that there would be significant advantages in upgrading the instrument to incorporate a heat flux DSC head. In addition to providing better reproducibility, the DSC technique, where the signal is given directly in mW, would also reflect the correct relative magnitude of the reaction peaks at different temperatures. This is in contrast to DTA where the instrument sensitivity decreases as a function of temperature (6).

A cross-section of the apparatus is shown in Fig.1. For ignition studies the sample and reference materials are contained in flat-bottomed quartz crucibles (C)

20mm in height and 6mm in diameter. The crucibles rest on a heat flux DSC plate (T) which forms part of the thermocouple measuring circuit. The plate, which is fitted with ears to locate the crucibles, is in direct contact with the inconel DSC block (H) which is supported on a four-bore alumina rod (R) carrying the thermocouple leads. The removable inconel lid (L) keeps the crucibles in place and prevents ejected ignition products from attacking the plate.

Light from an ignition reaction is transmitted to the silicon photodetector (S) (IPL Model 10530DAW) by the quartz rod (Q) which is positioned above the DSC head. The signal is used to activate a relay which switches from a zero voltage signal to a fixed voltage signal of 3.25V. The resultant step change in the voltage output signal enables a clearly defined ignition temperature to be determined. This avoids measurement problems in reactions where the majority of the sample is ejected on ignition and hence a sharp deviation is not observed on the temperature trace. Experiments are performed in an upwards flow of gas which leaves the furnace (F) via the porous plug (P). For experiments in inert gases, in cases where the atmosphere control is critical, a quartz sheath is placed over the DSC head and the experiment is carried out in a downward flow of gas. In addition, two inconel pans containing zirconium powder are placed on the lid of the DSC block to act as internal oxygen getters.

The temperature of the furnace is controlled by a digital programmer (Eurotherm Model 900 EPC) and experiments are normally carried out at heating rates within the range $3\text{--}50^{\circ}\text{C min}^{-1}$. For studies on non-ignition reactions, where the samples do not creep or bubble, improved quantitative performance may be obtained by using alumina or platinum crucibles 4mm in height and 6mm in diameter, in place of the quartz crucibles. These crucibles may also be used for measurements on pyrotechnic compositions where the sample is not displaced on ignition.

In the majority of high temperature DSC work carried out to date a chromel heat flux plate has been used, which forms part of a chromel-alumel thermocouple system. This provides a normal maximum operating temperature of 800°C , in an inert atmosphere. The temperature range of the equipment has recently been extended by replacing the chromel plate with a nisil plate, to form a nisil-nicrosil thermocouple system. This enables experiments to be carried out in an inert

atmosphere or in air to a sample temperature of 970°C, which is the maximum temperature obtainable with the nichrome wound furnace used in the present system.

The DSC and the photodetector system (PD) signals are logged using a 486-DX2 PC-compatible computer (Elonex model PC-450/VL) fitted with either a 12-bit data acquisition board (Strawberry Tree model AC-Jr) for the ignition studies, or where higher resolution is required for non-ignition studies a 16-bit board (Strawberry Tree model MINI-16) is used. The data is acquired using the icon-driven software provided with the boards (Quicklog PC, version 2.1.0). The resulting data in ASCII format is processed using a DOS-based graphics package (Biosoft Fig.P, version 6.0) which has been used to produce the graphs in this paper.

Both the chromel-plate and the nisl-plate heads were calibrated for temperature and enthalpy measurement using the fusion of high purity metals and the solid-solid phase transitions and fusions of inorganic compounds. The enthalpy measurements were used to convert the DSC signal to a mW output within the Fig.P software. The quantitative potential of the nisl-plate head is illustrated in Table 1, which shows the good reproducibility obtained in calibration experiments using the fusion of bismuth and the solid-solid transition of barium carbonate. The results are based on five experiments for each material.

Table 1

DSC Experiments Using the Nisl-Plate Head

(Sample weight, 20mg; heating rate, 10°C min⁻¹; atmosphere, argon)

Sample	Reaction	Crucible	*T _e /°C	Peak Area/J g ⁻¹
Bismuth	Fusion	Alumina	272.6 ± 0.1	53.2 ± 0.8
BaCO ₃	Phase change	Platinum	810.5 ± 0.3	97.7 ± 1.8

* T_e extrapolated onset temperature

Experiments on a 50% W-50% K₂Cr₂O₇ composition, in platinum crucibles, showed that the peak areas obtained under ignition conditions could be measured with a precision of ± 4%. Further work is to be carried out to evaluate the potential

of the unit for determining heats of ignition for "gasless" systems. Measurements using a random selection of the quartz crucibles used for ignition studies, which are produced by hand, showed a precision of $\pm 8\%$ for enthalpy measurements on the fusion of zinc. This is a factor of 2-3 times better than that obtained previously using the DTA apparatus.

A typical ignition experiment for a 46% Ti-46% $\text{Sr}(\text{NO}_3)_2$ -8% Alloprene composition is shown in Fig.2. This has been carried out under the standard ignition conditions where a 50mg sample is compressed under a 1kg deadload in the quartz crucible and heated at $50^\circ\text{C min}^{-1}$ in an argon atmosphere. Following the pre-ignition reaction between strontium nitrate and Alloprene in the region of 300°C (7), the sample ignited at 497°C . The ignition is thought to be initiated by the formation of a eutectic melt between strontium nitrate and the strontium chloride formed in the pre-ignition reaction.

An example of the use of the nisl-plate head to study reactions under non-ignition conditions is given in Fig.3 for a 7% B-93% $\text{K}_2\text{Cr}_2\text{O}_7$ composition which illustrates the baseline stability and wide temperature range which can be obtained with this system. The reaction can be seen to take place in two exothermic stages. The first stage, in the region of 400°C , involves the reaction of boron with potassium dichromate to produce potassium chromate and the second stage, at about 700°C , the reaction of the potassium chromate with unreacted boron (8).

TIME TO IGNITION STUDIES

A unit for time to ignition studies was described previously (9) and is shown in its present form in Fig.4. In this design the sample (M), contained in a quartz crucible (C) of the type used in the ignition DSC studies is seated on a plate type chromel-alumel thermocouple (T) and supported by the open inconel frame (I). This consists of two inconel discs with three inconel supporting strips and is mounted on a 4-bore alumina rod (R).

The water-cooled furnace (F), which is pre-heated to give the desired sample temperature, is rapidly lowered over the sample at the start of an experiment and forms a gas-tight seal against the base of the unit. Experiments are carried out in a flowing atmosphere and the gas is introduced at the top of the furnace and is diffused by a porous ceramic wool plug (P), which also serves as a trap for ignition products. The plug is held in place by an inconel liner (L), which prevents attack

of the furnace wall by ignition products.

Experiments using the chromel-alumel thermocouple have generally been limited to a maximum sample temperature of about 800°C, using an inert atmosphere. The temperature range and hence the effective heating rate has been extended recently by the use of a nisl-nicrosil plate thermocouple. Experiments may now be carried out in an inert atmosphere or in air to 970°C, which is the maximum sample temperature permitted by the furnace in current use.

As discussed earlier, difficulty was sometimes experienced in detecting ignition in DSC measurements on "gassy" pyrotechnic reactions, and this problem is accentuated in time to ignition experiments by the rapid rise in sample temperature. This has now been resolved by the incorporation of a similar system to that used in the DSC apparatus, where light from the ignition reaction is transmitted by the quartz rod (Q) to the silicon photodetector (S) and the resultant signal used to produce a step voltage change. This provides a precise indication of the time to ignition.

The temperature and photodetector system signals are logged at a rate of 10 points per second using a similar data collection system to that described above, incorporating the 16-bit board. Data is processed using the Fig.P software and in addition to the temperature and photodetector system curves, the heating rate curve is also plotted. This is obtained by dividing the individual temperature increments by the corresponding time increments. The data is lightly smoothed, before and after the ignition region, by the Savitsky-Golay routine provided in the Fig.P software.

An experiment therefore provides the time to ignition (TTI), the ignition temperature (T_{ig}) and the heating rate at ignition (HR_{ig}). Typical curves are shown in Fig.5 for an experiment on a 30mg sample of a 44% Mg-44% $NaNO_3$ -12% Alloprene composition, which gave a time to ignition of 20.9 seconds.

The advantage of obtaining the heating rate curve is that it offers the possibility of identifying pre-ignition reactions under fast heating rate conditions. This is illustrated in Fig.6, where the sample weight for the above ternary magnesium composition had been reduced to 15mg. It can be seen that the time to ignition had increased to 28.1 seconds and the temperature of ignition from 372°C to 477°C. The reaction, which resulted in ignition at the higher sample

weight can now be seen as a peak on the heating rate curve, in the region of 20 seconds. This is attributed to the exothermic reaction between sodium nitrate and Alloprene which, under fast heating rate conditions of the TTI experiment, has been found to be influenced significantly by the addition of magnesium (10).

THERMOMICROSCOPY STUDIES

Thermomicroscopy has been shown to be a valuable complementary technique for the characterisation of pyrotechnic systems (11). The hot stage unit used in these studies (Stanton Redcroft Model HSM-5) has been described previously (12). This unit enables samples to be examined using reflected light, under conditions of controlled heating rate and atmosphere, over the sample temperature range ambient to 950°C.

Although a similar hot stage unit to the original design was used, the remainder of the system, which is shown in Fig.7 has been completely updated. The sample, normally contained in a 6mm diameter alumina or platinum crucible, is viewed using a stereoscopic zoom-microscope (Olympus model SZ1145TR CTV) and illuminated with a twin fibre optic system (Olympus Highlight 3000) connected to a voltage stabiliser. Recordings are made using a CCD colour video camera (JVC model TK-1085E) in conjunction with a time-lapse S-VHS video recorder (JVC model BR-S920E). The camera output is viewed using a high-resolution colour monitor (JVC model TM-1500PS). Temperature programming is carried out using a Linkam programmer (modified model TMS91), which in conjunction with a video text overlay unit (Linkam model VTO 232) enables the sample temperature to be continuously displayed on the video recording.

The changes in the reflected light intensity (RLI) from the sample are monitored using a silicon photodetector (IPL model 16B) which is filtered to give an approximate eye response using a green filter (Schott type BG38). The RLI and the sample temperature signals are collected and processed using a similar system to that used in the DSC studies. The reflected light intensity measurements are approximately related to a common scale using precipitated barium sulphate as a reflectance standard.

The application of the system to studies on the zirconium-potassium perchlorate-nitrocellulose system has been described recently (13). The system is

currently being used to study the thermal behaviour of bismuth oxide as part of a work programme on the Si-Bi₂O₃ system (14). A light intensity curve for bismuth oxide (Johnson Matthey Puratronic grade) is shown in Fig.8. The reduction for the light intensity over the range ambient to 450°C was associated with the change in colour of the sample from pale yellow via golden-yellow to orange. Above this temperature the sample darkened to give a dull red solid in the region of 700°C. At 735°C the $\alpha \rightarrow \delta$ solid-solid phase transition (15) was clearly seen as a change from dull red to black and this was accompanied by a small step on the reflected light intensity curve. The sample was observed to melt in the region of 835°C, shrinking to form shiny black globules and this is shown in Fig.9. The exposure of the reflective base of the platinum crucible, which accompanied the fusion of the bismuth oxide, resulted in a sharp increase in the reflected light intensity signal.

REFERENCES

1. Thermal Analysis-Techniques & Applications, Eds. E.L.Charsley & S.B. Warrington, Royal Society of Chemistry, 1992.
2. Thermal Analysis, 3rd Edition, W.W.Wendlandt, Wiley, 1986.
3. P.G.Laye and E.L.Charsley, *Thermochim. Acta*, 120, 1987, 325.
4. E.L.Charsley, C.T.Cox, M.R.Ottaway, *Proc. Second European Symposium on Thermal Analysis*, Ed. D. Dollimore, Heyden, 1981, 593.
5. E.L.Charsley, C.T.Cox, M.R.Ottaway, T.J.Barton and J.M.Jenkins, *Thermochim. Acta*, 52, 1982, 321.
6. E.L.Charsley, *Chemistry in Australia*, 61, 1994, 188.
7. P.Emmott, T.T.Griffiths, J.Queay, E.L.Charsley, S.B.Warrington, *Proc.16th International Pyrotechnic Seminar*, Sweden, Sektion for Detonik och Forbranning, 1991, 937.
8. E.L.Charsley, T.Boddington, J.R.Gentle and P.G.Laye, *Thermochim. Acta*, 22, 1978, 175.
9. E.A.Robinson, G.I.Lindsley, E.L.Charsley and S.B.Warrington, *Proc. Joint 16th ICT Conference/10th International Pyrotechnic Seminar*, Fraunhofer-Institut fur Treib-und Explosivstoffe, 1985, 25.1.
10. T.T.Griffiths, J.Queay, E.L.Charsley and S.B.Warrington, *Proc.19th International Pyrotechnic Seminar*, South Pacific Information Services Ltd., Christchurch, 1994, 716.
11. E.L.Charsley and D.E.Tolhurst, *Microscope*, 23, 1975, 227.
12. E.L.Charsley and A.C.F.Kamp, *Thermal Analysis*, Vol.1, Ed. H.G. Wiedemann, Birkhauser Verlag, 1972, 499.
13. B.Berger, A.J.Brammer and E.L.Charsley, *Thermochim. Acta* in press.
14. E.L.Charsley & T.T.Griffiths, unpublished work.
15. H.A.Harwig & A.G.Gerards, *Thermochim. Acta*, 28, 1979, 121.

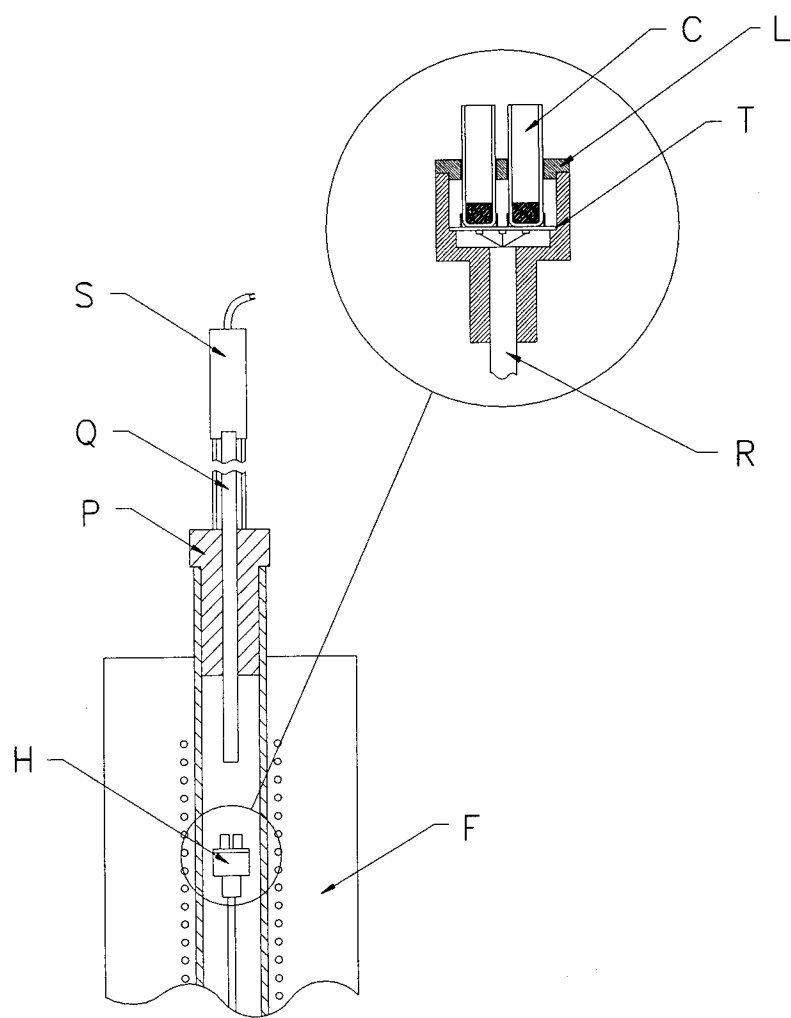


FIG.1 CROSS-SECTION OF HIGH TEMPERATURE DSC APPARATUS

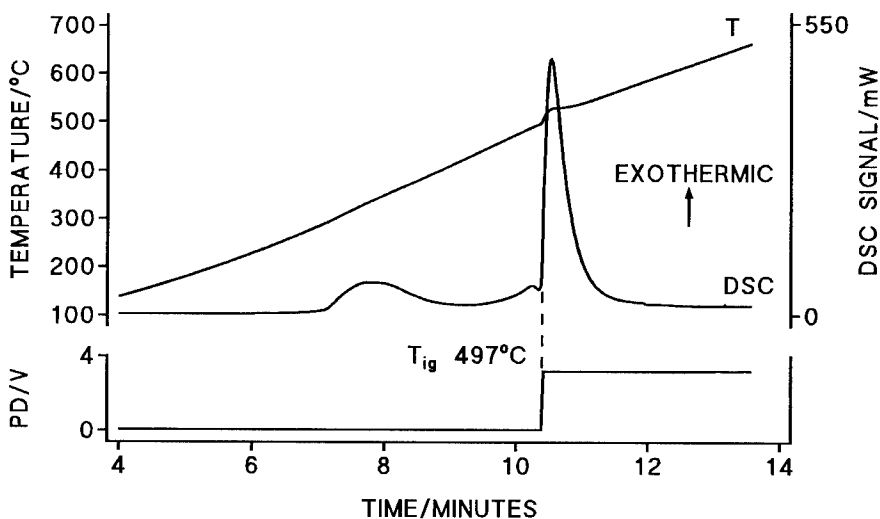


FIG.2 DSC CURVE FOR A 46% Ti-46% $\text{Sr}(\text{NO}_3)_2$ -8% ALLOPRENE COMPOSITION (Chromel-plate head, sample weight, 49.8mg; heating rate, $50^\circ\text{C min}^{-1}$; atmosphere, argon)

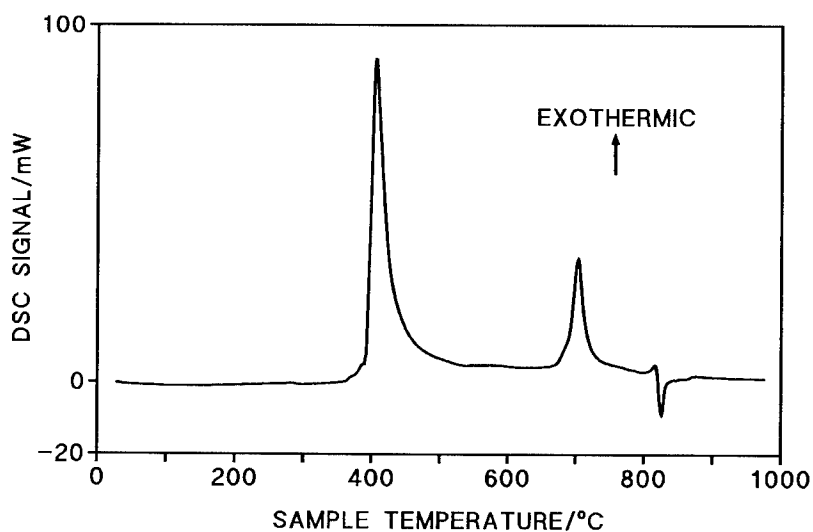


FIG.3 DSC CURVE FOR A 7% B-93% $\text{K}_2\text{Cr}_2\text{O}_7$ COMPOSITION (Nisil-plate head, sample weight, 9.9mg; heating rate, $10^\circ\text{C min}^{-1}$; atmosphere, argon)

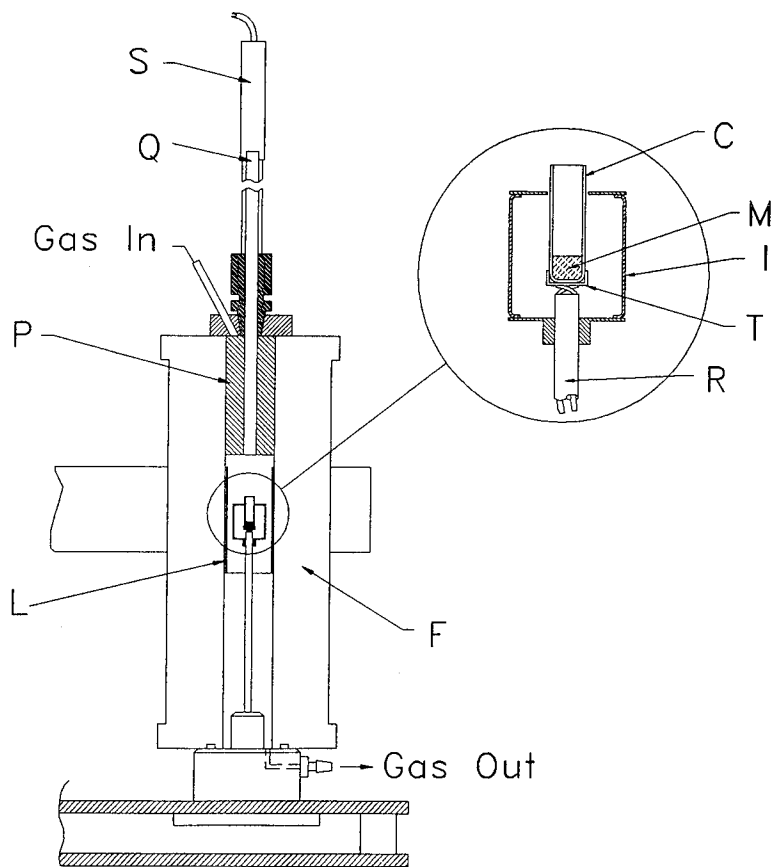


FIG.4 CROSS-SECTION OF TIME TO IGNITION APPARATUS

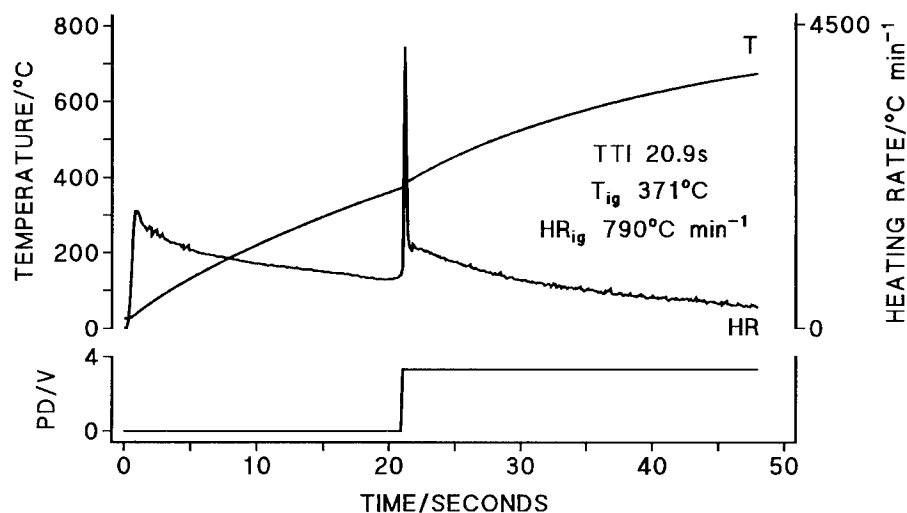


FIG.5 TIME TO IGNITION PLOT FOR A 44% Mg-44% NaNO₃-12% ALLOPRENE COMPOSITION (Sample weight, 30mg; temperature, 800°C; atmosphere, argon)

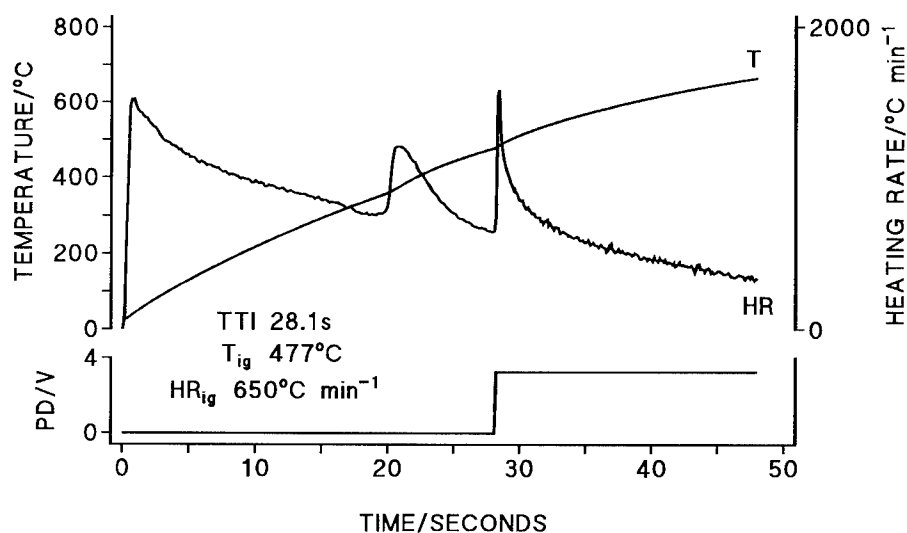


FIG.6 TIME TO IGNITION PLOT FOR A 44% Mg-44% NaNO₃-12% ALLOPRENE COMPOSITION (Sample weight, 15mg; temperature, 800°C; atmosphere, argon)

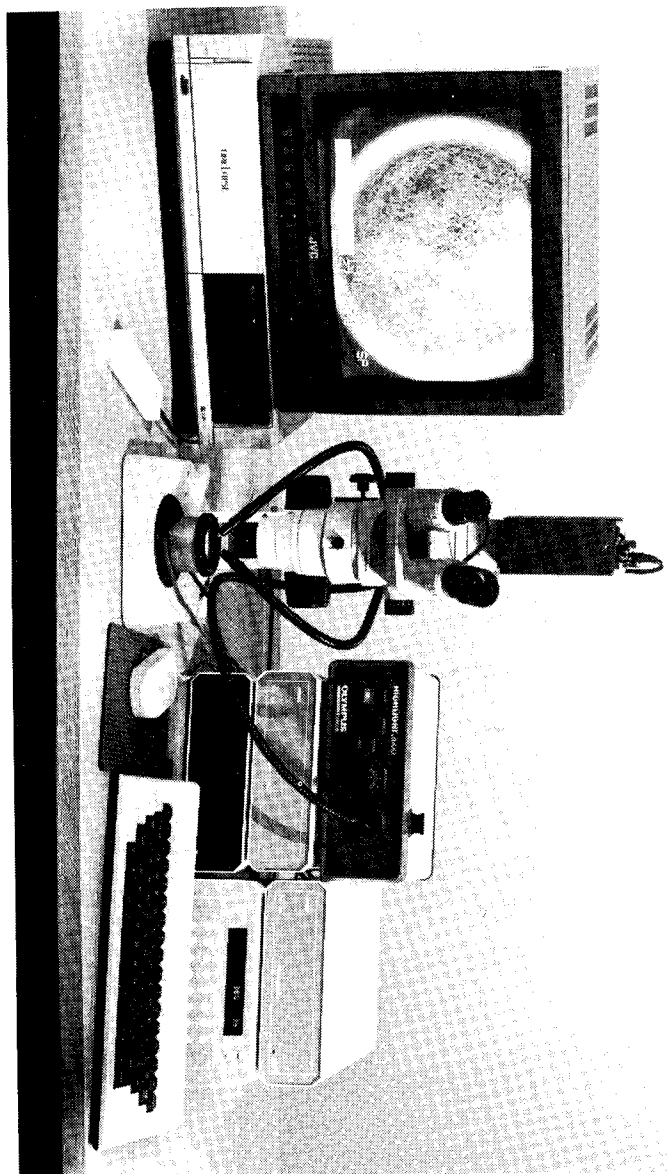


FIG. 7 PHOTOGRAPH OF THERMOMICROSCOPY SYSTEM

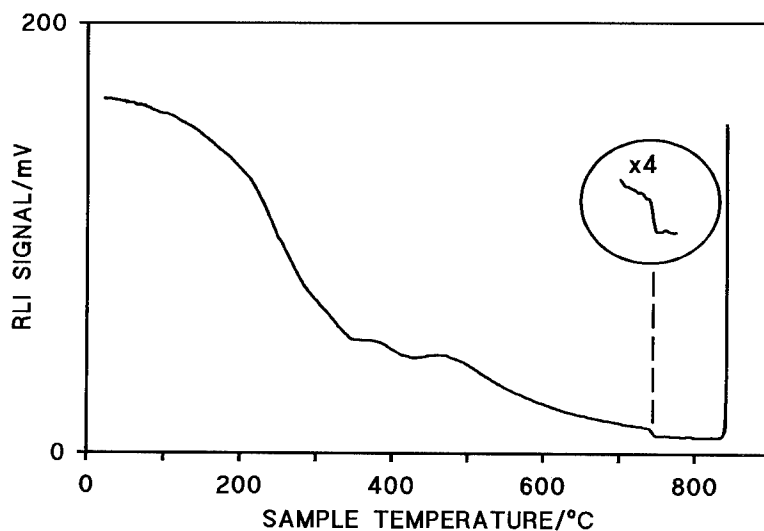


FIG.8 REFLECTED LIGHT INTENSITY CURVE FOR BISMUTH OXIDE (Sample weight, 15.1mg; heating rate, $10^{\circ}\text{C min}^{-1}$; atmosphere, argon)

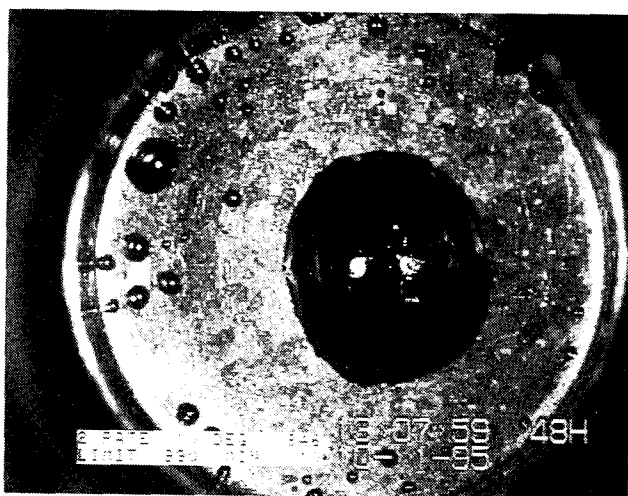


FIG.9 VIDEO PRINT SHOWING FUSED BISMUTH OXIDE AT 846°C (Sample weight, 15.1mg; heating rate, $10^{\circ}\text{C min}^{-1}$; atmosphere, argon)

BEHAVIOUR OF A PYROTECHNIC VALVE UNDER DIFFERENT IGNITORS. THREE DIMENSIONNAL FINITE ELEMENT MODELING

Jean-François GUERY, Brigitte CAGNON, Pierre BRUNET

SNPE Centre de Recherches du Bouchet
Rue Lavoisier - BP 2
91710 VERT LE PETIT - FRANCE

ABSTRACT

The dynamic behaviour of a pyrotechnic valve has been evaluated under two different ignitors through a three dimensionnal finite element analysis.

A detailed analysis has been performed for defining an appropriate constitutive law for the material used at high strain rates. Four different representative pressure histories have been applied in the booster chamber. Shearing and fracture of the nipples has been taken into account with an eroding model.

The computations show that there is no influence of the initiator on the process. The lack of symmetry of the housing and the ram can cause plastic strain localisation. Bending of the ram may also occur.

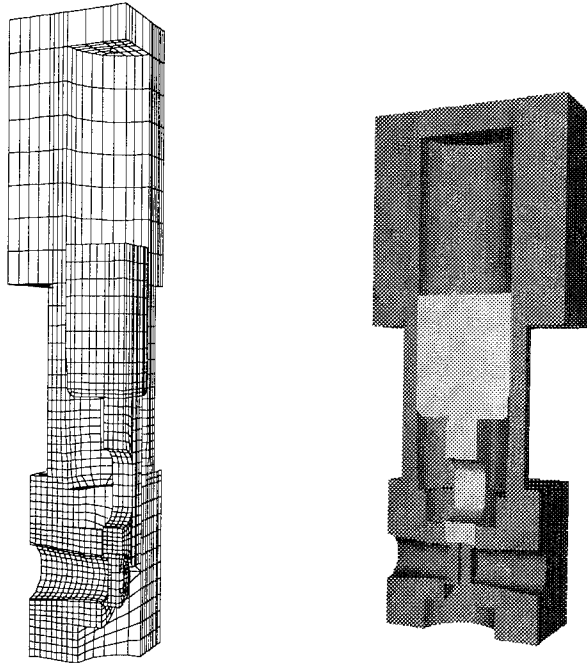
1 Introduction

The functioning of pyrotechnic systems may affect the safety of a space mission. In order to study the reliability of such systems, we have investigated the dynamic behavior of a pyrotechnic valve under different loadings through finite element analysis. The use of a three dimensional hydrocode was necessary to deeply understand the mechanisms involved in the process.

2 Three dimensional Finite Element Modeling

2.1 The FEM model

The three dimensionnal finite element analysis is performed with the non-linear dynamic analysis code LS-DYNA3D [1]. The three dimensionnal model is meshed with 8-node brick elements. There are about 7000 nodes.



2.1.1 Material properties

Housing, ram and pipe, are made of annealed TA6V. We have used Steinberg-Cochran-Guinan data for TA6V [2].

At high strain rates, the shear modulus and the yield stress are functions of pressure and temperature.

$$\sigma_y = \sigma_{y0} f(\epsilon^p) \frac{G(P, T)}{G_0}$$

$$f(\epsilon^p) = 1 + \beta(\epsilon^p + \epsilon^i)^n$$

$$G(P, T) = G_o(1 + A P/\eta^{\frac{1}{3}} - B(T - 300))$$

where σ_y is the yield stress, G the shear modulus, P the pressure, T the temperature and ϵ^p the plastic strain.

The hydrodynamic equation of state for the spherical part of the stress tensor is given in the Grüneisen form:

$$P = \frac{\rho_o c_o^2 \mu \left(1 + (1 - \frac{\gamma_o}{2})\mu - \frac{b}{2}\mu^2\right)}{(1 - (s_1 - 1)\mu)^2} + (\gamma_o + b\mu)E$$

for $\mu \geq 0$ and

$$P = \rho_o c_o^2 \mu + \gamma_o E$$

for $\mu \leq 0$ where:

$$\mu = \frac{\rho}{\rho_o} - 1$$

The parameters are the following:

μ_o	c_o	s_1	γ_o	b	σ_{yo}	A	B	β	n	ϵ_i
GPa	m/s				GPa	Mbar ⁻¹	K ⁻¹			
41.9	5130	1.028	1.93	0.17	1.33	1.15	$6.44 \cdot 10^{-4}$	12	0.10	0.

The material properties given by Steinberg are different from those published in reference books [3].

From Steinberg data, we can compute the bulk modulus from the bulk sound speed: $K = \rho_o c^2$, then the Poisson ratio from the classical relation:

$$\nu = \frac{\frac{K}{G} - \frac{2}{3}}{2\frac{K}{G} + \frac{2}{3}}$$

source	G	K	ν	σ_y
	GPa	GPa		GPa
Steinberg	41.9	116.29	0.339	1.33
MIL-HDBK	42.749	96.77	0.31	0.9

The difference in the bulk modulus can be attributed to the linear fit of the equation of state, which do not give a good approximation of the bulk sound speed in quasi-static conditions (MIL-HDBK). In the definition of the equation of state, the bulk modulus is not a constant but a function of the density. Rosenberg has studied the Hugoniot properties of the TA6V [4].

Rosenberg gives a Hugoniot elastic limit (HEL) of the alloy around 2.1 GPa and a velocity of the elastic precursor (u_e) of 6.45 mm/ μ s. With the classical formula:

$$u_e = \sqrt{\frac{K + \frac{4}{3}G}{\rho_0}}$$

$$HEL = \left(\frac{K}{2G} + \frac{2}{3} \right) \sigma_y$$

if we solve these equations assuming that the shear modulus is around 42 GPa, we find a value of 128 GPa for the bulk modulus, and 0.96 GPa for the yield strength. The HEL given by Follansbee [5] is a bit higher: 2.8 GPa. With this value, we find a yield strength of 1.28 GPa, close from Steinberg value. The strain rate giving that value of the HEL has been evaluated by Follansbee between 10^4 and 10^6 s $^{-1}$.

In the finite element model, friction is based on Coulomb formulation and is used in sliding interfaces. The coefficient of friction is defined as an exponential function for smoothing the transition between the static and dynamic coefficient:

$$\mu = \mu_d + (\mu_s - \mu_d)e^{-c\|\mathbf{v}\|}$$

where c is a decay constant and \mathbf{v} the relative velocity between two points on each surface. The value chosen is a standard value [7]. No further investigation has been made for fitting a value that would be more appropriate.

The erosive model implemented in LS-DYNA3D is used. This facility allows the full treatment of the nipples shearing. For activating the erosive model, a failure strain has been defined for and only for the nipples. The value that we have chosen, $\epsilon_r = 0.14$, enables the shearing of the nipples for an applied pressure of 27.6 MPa on the ram.

2.1.2 Boundary conditions

Due to symmetry planes, only a quarter of the structure is meshed. The FEM model is free in space.

2.1.3 Loads

Two ignitors are under evaluation. These ignitors are implemented with booster charges of increasing amplitudes: 80 %, 100 % and 130 % of nominal load.

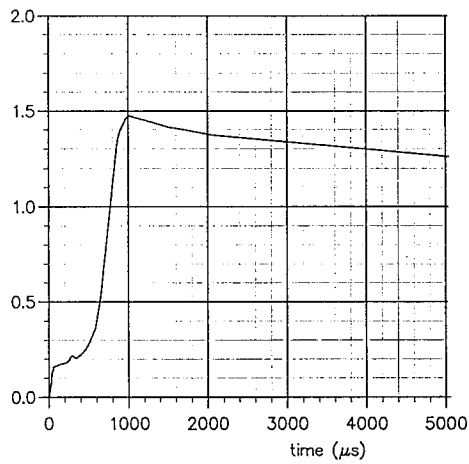
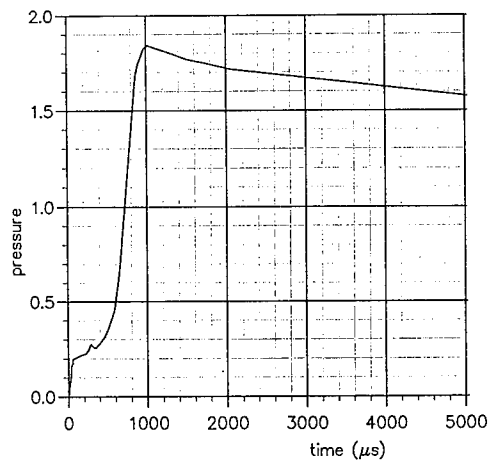
Four different pressure profiles have been applied to the top of the ram, and to the top of the housing as well. Each of these profiles is representative of a working scenario of the ignitors. For each load, the pressure has been measured in a closed-bomb test corresponding to the **maximum volume** of the chamber.

1. Curve 1, nominal load

2. Curve 2, 80 % load
3. Curve 3, 130 % load
4. Curve 4, 130 % with a different ignitor

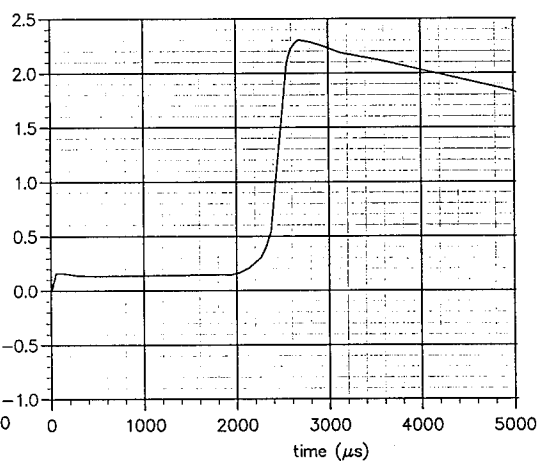
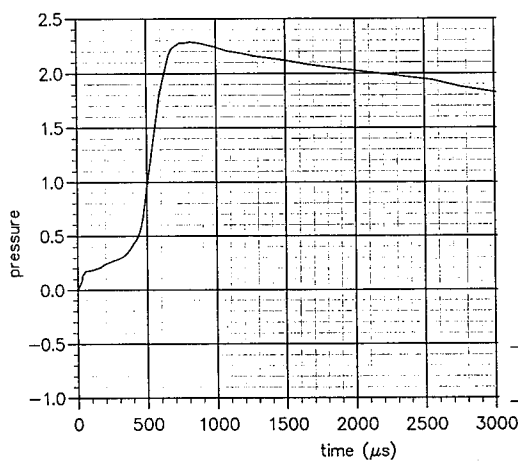
curve 1

curve 2



curve 3

curve 4



2.2 General results

The ignition of the booster charge will cause a rise of pressure at the top of the ram. Due to this pressure, the ram will start to travel inside the housing. The end of the ram is designed to punch the nipples on both ends of the pipe, and then will finally be stopped when the ram will reach the conical section of the housing. A plastic deformation and welding will result in the contact area.

In each computation, the pyrotechnics valve has worked in two stages: first the shearing of the nipples, and then, the running of the ram.

The loadings at 130 % of the booster charge with different ignitors lead to similar results and will not be distinguished in this paper.

2.2.1 Shearing of the nipples

The first stage is shared by the four working scenarios. Any pressure profile shows first a low magnitude level around 20. MPa, before increasing to a peak value: the ignition of the booster. During that level, whatever long it is, the ram does nothing else than positioning on the nipples. Shearing and then failure of the nipples will occur about a 27.6 MPa *static* pressure in the chamber, according to the failure strain that we have chosen for the erosive model. That value is actually reached only behind the plateau. Nipples are then thrown down the housing. Their velocity due to elastic energy release (nipples beyond the ram), is the same regardless of the four working scenarios: around 60. m/s.

2.2.2 Stopping of the ram

With the geometry we meshed, in any of the four pressure histories, the ram travels down as far as to hit the shoulder at the end of the tapered part of the housing. It needs the ram about 0.1 milliseconds to reach the shoulder after the time the nipples were punched.

An increase of the coefficient of friction, or a modification of the geometry (maximum tolerance limit on the ram with minimum tolerance limit on the housing) could stop the ram before it hits the inside shoulder of the housing.

– The housing

The tapered zone exhibits a plastic deformation pattern close to the one of a flexion: with neutral axis, outermost fibers in tension, and innermost fibers in compression.

Computation does not show a perfect axial symmetry: due to a greater rigidity of the ram, strains are higher next to the punching part of the ram.

— The ram

The lower part of the ram that hits the shoulder, exhibits plastic strain values above 3%. Besides, deformations of relatively high amplitude take place in the punching part of the ram. When punching the nipple, some bending occurs around the aperture designed through the punching part. That bending may lead to friction between housing and ram.

2.2.3 Analysis of failure

The nominal charge leads to a small plastic strain outside the housing, whereas 80% booster charge leads to no plastic deformation. An increase in the booster charge increases this plastic deformation.

If we take as a criterion that the failure probability is increased with an increase of plastic strain at the outside, we can say that the nominal charge is near the maximum permitted charge.

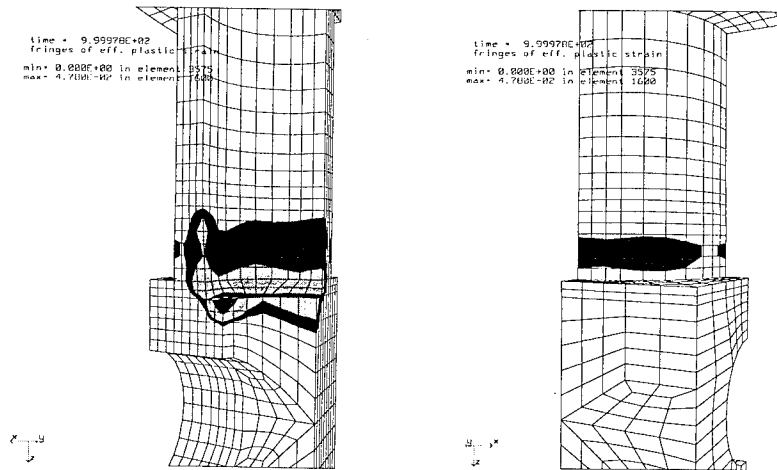
2.2.4 Sealing of the ram

The nominal charge enables a complete plastic deformation area in the tapered zone. This area is not increased at 130% booster charge. On the contrary, this area decreases at 80% booster charge.

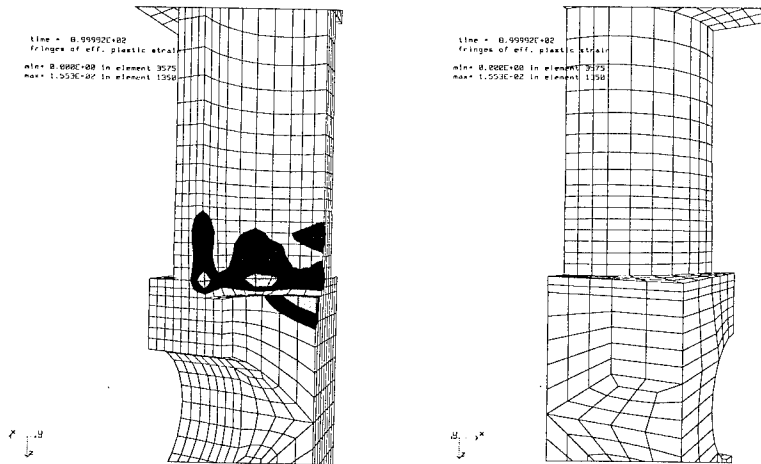
If we assume that the best sealing is done when that area is plastically deformed, then the nominal charge seems to be near the minimum permitted charge with respect to the sealing problem.

No heat transfer can be estimated for welding from these computations.

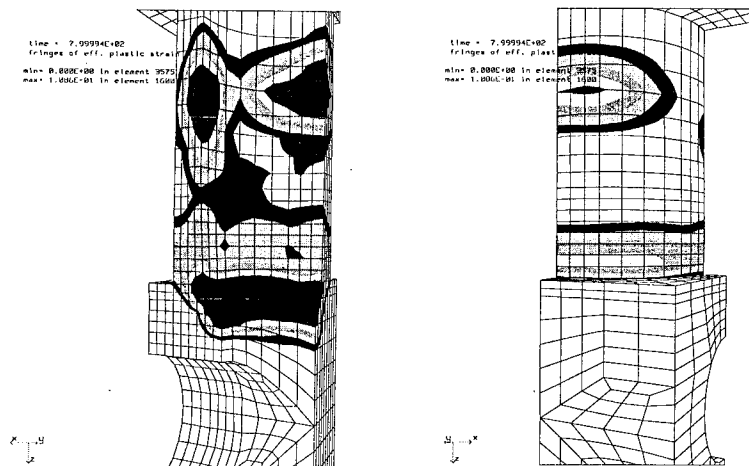
plastic strain for the nominal booster charge



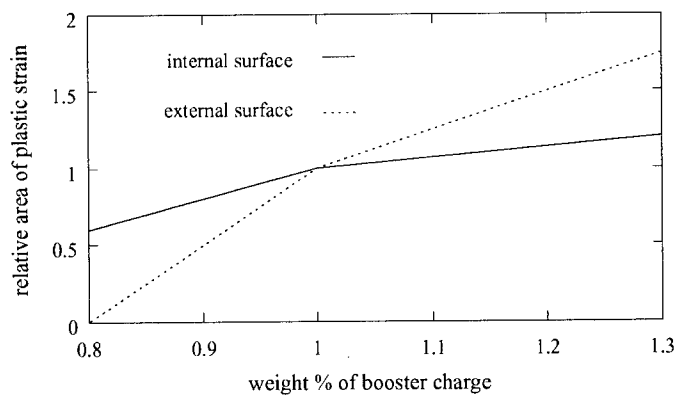
plastic strain for the 80 % booster charge



plastic strain for the 130 % booster charge



Failure and sealing are summarized in the following figure.



All the quantities are normalized to the nominal case. We consider the plastic strains greater than 0.5%. On the inner surface, we assume that sealing is realized by a plastic deformation in the surface. On the outer surface, we assume that a plastic strain can

lead to fracture. We see that increasing the booster charge does not improve the sealing but can lead to fracture, whereas a decrease in the booster charge leads to a bad sealing.

3 Concluding remarks

A simple FEM computation with literature material data and available tools lead to quite realistic results.

It is seen in the computation that the pressure level duration before the booster ignition does not affect the valve working: the nipples are punched when pressure rises above 27. MPa. The pressure loads used come from **closed-bomb tests** made at the **maximum volume** of the chamber. The pressure given by the combustion of only one ignitor has been computed with SNPE code BAGHEERA [8], [9]: it reaches 42 MPa. Then we can assume that the nipples can be sheared **before** the booster is ignited.

With the dimensions of ram and housing used in calculation, the constitutive law and friction coefficients for TA6V, whatever the amplitude of the booster charge will be, the ram will hit the shoulder inside the housing, even in the 80 % load case.

Up to the 100 % nominal loadcase, no significant plastic deformation occurs on the outer part of the housing. But 2.5 % values are reached outside with the 130 % load case.

The lack of symmetry of the housing and the ram can cause plastic strain localisation. Bending of the ram occurs.

Further investigations could be achieved with finer mesh that would make more explicit the extent of the plastic strain area. A more suitable constitutive law (a better fit of Steinberg-Guinan model on available data or on specific tests) would allow a better description of the physical state of the material in the contact area: residual stresses, temperature,... Failure of the material at high strain rate should be investigated.

The coefficients of friction could be discussed too, that would affect the motion of the ram.

More reliable load curves (pressure taken from experimental records) should be applied on the ram that could shear the nipples before the booster ignition.

This work was performed under the ESTEC/Contract N° 10543/93/NL/CC.

Références

- [1] John O. Hallquist, Douglas W. Stillman, Tsung-Liang Lin. LS-DYNA3D user's manual. Non-linear dynamic analysis of structures in three dimensions. Livermore Software Technology Corporation. January 1992.
- [2] Daniel J. Steinberg. Equation of state and strength properties of selected materials. LLNL, 1991.
- [3] MIL-HDBK-5F
- [4] Z. Rosenberg, Y. Meybar, D. Yaziv. Measurement of the Hugoniot Curve of the Ti-6Al-4V with Commercial Manganin Gauges. J. Phys. D: Appl. Phys., 14 pp 261-266, 1981
- [5] P. S. Follansbee. The HEL and Rate-dependant Yield Behavior. Proc. of the 1989 Topical Conference on Shock Compression of Condensed Matter, Albuquerque, 14-17 Aug. 1989.
- [6] P. S. Follansbee, G. T. Gray. An Analysis of the Low Temperature, Low and High Strain Rate Deformation of Ti-6Al-4V. Metall. Trans. A, vol 20 A, 5, pp 863-874, May 1989.
- [7] Handbook of chemistry and physics. 44th edition. The chemical rubber publishing co., 1962.
- [8] J. P. Bac
Bagheera, a Ballistic Thermodynamic Code
3rd Int. Gun Propellant Symp.,
Picatinny Arsenal, Dover, New Jersey, October 1984
- [9] Bureau Militaire de Standardisation OTAN
Accord de standardisation N° 4400
Dérivation des valeurs thermochimiques pour des calculs de balistique intérieure,
3 Juin 1993

A DEVICE FOR QUANTITATIVE EVALUATION OF THRUST PRODUCED BY SMALL FIREWORK ROCKETS

Jacqueline Akhavan, Ian Grose, Mike Williams
Chemical Systems Group, Royal Military College of Science
(Cranfield University), Shrivenham, Swindon, Wiltshire,
SN6 8LA, United Kingdom.

Barry Cook
Standard Brock Fireworks, Crosland Hill, Huddersfield,
West Yorkshire, HD4 7AD, United Kingdom.

ABSTRACT

The construction and operation of a small simple device for measuring the thrust developed by small firework rockets is described. The device has been used to obtain data on some rocket propellant formulations, and the results are shown to be in agreement with previous studies.

INTRODUCTION

The development of pyrotechnic items is an ongoing process, as improvements in colour, sound and lift are constantly being sought. The testing of new items produced during such development programmes is normally a qualitative procedure. Examples of new devices are compared alongside earlier ones, with quantitative measurements normally being restricted to timing the burning process. Whilst visual observation is important (after all, pyrotechnic devices are designed to be seen or heard), published systematic quantitative investigation is rare. This situation is especially true of rockets. It is considered desirable for a rocket to lift quickly, followed by a smooth steady flight. However, the exact definition of "quickly" and "smooth steady flight" differ markedly from observer to observer. Some form of quantitative measurement would minimise any "human error".

At Shrivenham, a research programme involving the development of new safer solid propellant for use in small commercial items is in progress. Although visual evaluation of

rockets under test is important, quantitative data is required to assess the relative performance of various compositions. A device was required to measure the thrust profile of small rocket motors, and such a device has been constructed, tested and is in routine use. This paper describes the principles and use of the device to obtain data on the performance of various propellant compositions and configurations.

THE THRUST MEASUREMENT DEVICE

The device consists of an adapted load cell. The load cell is a beam arranged so that an applied load will result in a proportional strain along that beam. The strain so produced is detected using an array of strain gauges, which convert the strain into an electrical signal, the magnitude of which is related to that of the applied strain [1].

A diagram of the instrument is given in figure 1. The load cell is mounted on a flat metal plate, which provides extra overload protection for the device.

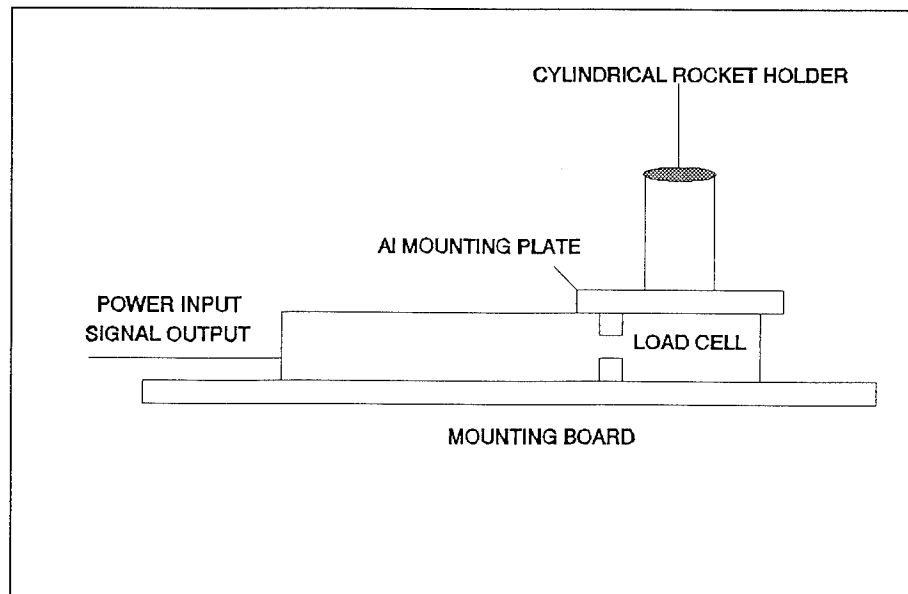


Figure 1 The thrust meter device

A cylindrical rocket holder is affixed to the top of the load cell via an aluminium mounting plate. Power input and signal output are regulated by a simple "black box", described by figure 2.

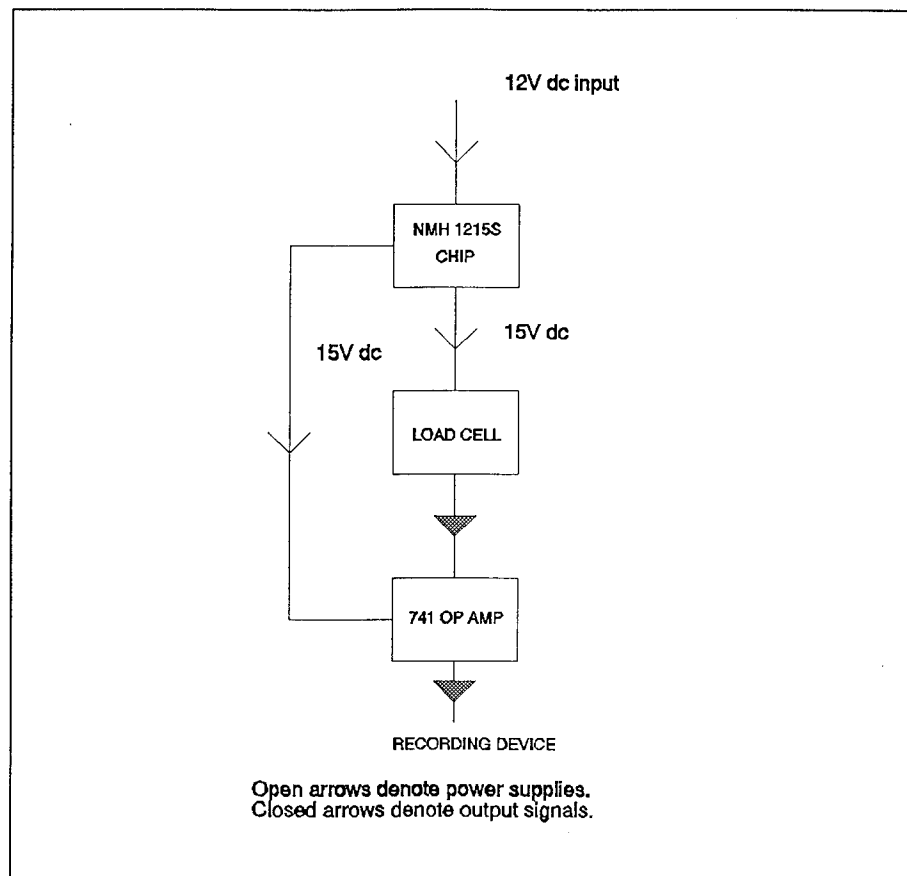


Figure 2 Schematic diagram of thrust meter circuitry

The load cell operates at 15V dc, as does the amplifier, so they are run off a common supply. The amplified load cell output is fed to a suitable recording device, such as a chart recorder or a data logger. Since the device is intended for outdoor use, where conditions are not normally as controlled as those in the laboratory, data collection using a computer (via a suitable ADC) has not been carried out, although the system can be so used if desired. A

25 - 4

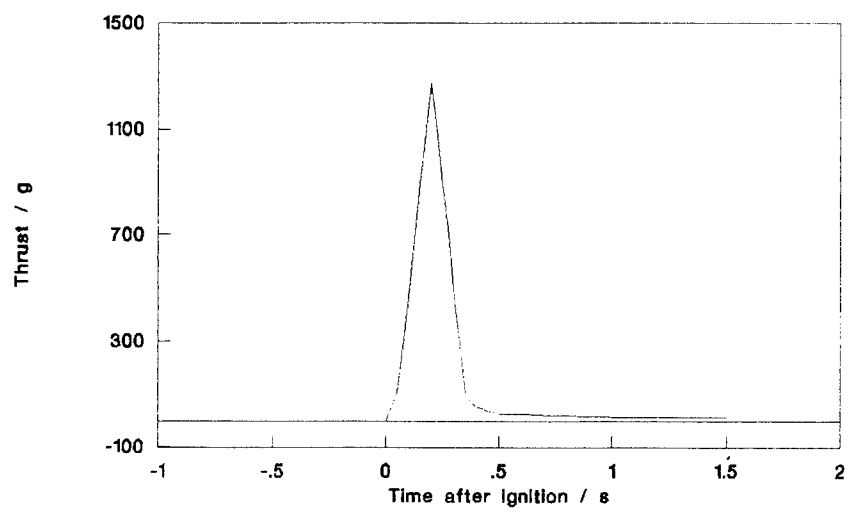


Figure 3 Typical thrust trace

typical trace obtained from a small firework rocket is given in figure 3.

USE OF THE THRUST MEASUREMENT DEVICE

1 - Effect of catalyst on propellant performance

The propellants under investigation incorporate a perchlorate oxidiser component, most commonly potassium perchlorate. It is well known that the rate of burn of propellants containing perchlorate oxidisers is speeded by the use of transition metal oxides in catalytic amounts [2-4]. Various catalysts were tested, with the results being presented in figure 4.

Figure 4 shows that copper (II) oxide is the best catalyst tested, as measured by peak thrust value. This confirms earlier findings [2-4]. Copper (II) chromite is also known to be effective, but its toxic properties precluded it from systematic investigation.

The values in figure 4 have been normalised to $\text{CuO} = 100$ in order to permit simple comparison. The thrust produced by the CuO composition in a small 12 mm diameter cardboard firework motor (with a 35 mm gallery and a 2 mm diameter circular nozzle) was around 1250 g, with a specific impulse of 35 s.

2 - Effect of catalyst level on propellant performance

Copper (II) oxide was selected as the catalyst for these investigations, since it was shown above that it was the best catalyst of those tested. The level of the catalyst was varied, and the thrust characteristics of the compositions were measured. The results are presented in figure 5.

Figure 5 clearly shows that peak thrust is at a maximum with 0.4 to 0.8 pts CuO , but falls off with increasing catalyst content. This also corresponds with earlier work [2-4]. Compositions including CuO burned smoothly, which was not the case for the composition which did not contain the CuO . The impulse produced by the rockets is also shown in figure 5 (the specific impulse follows a similar trend, since all rockets contained the same mass of composition).

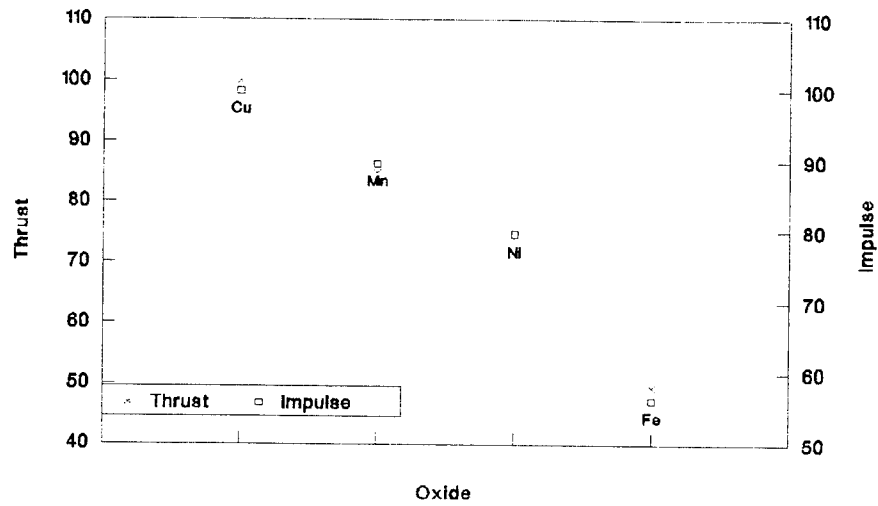


Figure 4 Effect of catalyst on propellant performance
(Data normalised to CuO = 100)

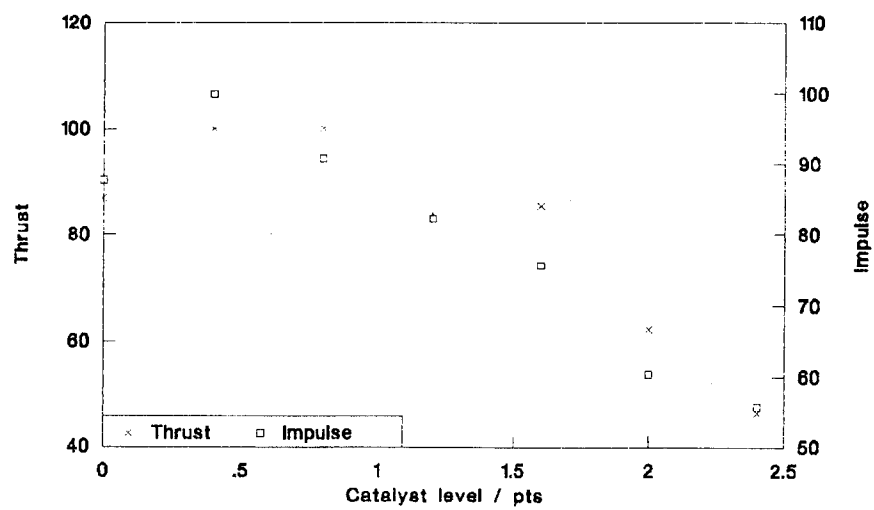


Figure 5 Effect of catalyst level on propellant performance
(Data normalised to 0.4 parts = 100)

3 - Effect of rocket geometry on performance

A typical rocket motor is shown in figure 6.

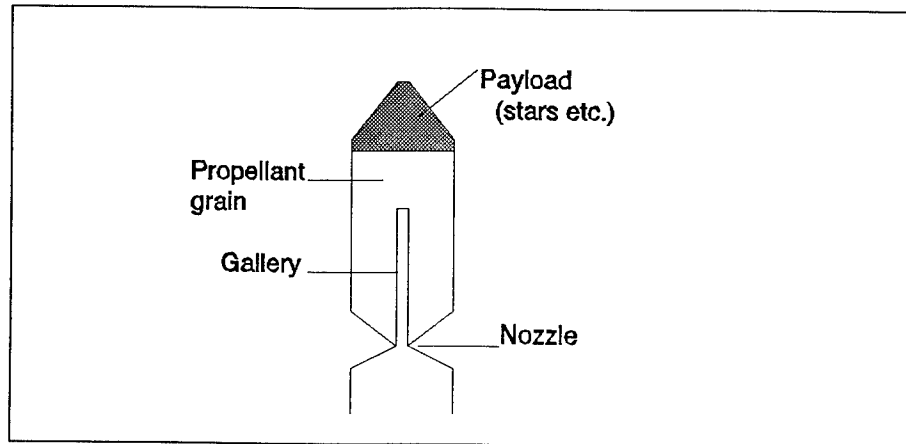


Figure 6 Rocket motor geometry

The role of the gallery is to enhance the liftoff characteristics of the rocket, since a greater surface area is available for combustion. Various shaped channels have been used, such as star-shaped and multiperforated [5], but the channel used in this work was a tapered cylindrical shape.

Figure 7 shows the effect of gallery length on the peak thrust values obtained from the rocket. As expected, smaller lengths produced lower thrust values, whilst longer gallery lengths resulted in much better thrust values, and therefore better lifting characteristics. This shows that the performance of propellants can be enhanced by adjusting gallery length, an effect which is well-known and utilised throughout the rocket propellant industry.

CONCLUSION

The use of large thrust measurement devices is common in development of propellant formulations for large civil and military devices, but use of smaller devices for testing firework rockets has not, to the best of our knowledge, been described in the open literature. This paper has described the construction and use of such a small device, and the results obtained from it have been found to be in good agreement with previous data obtained from other methods.

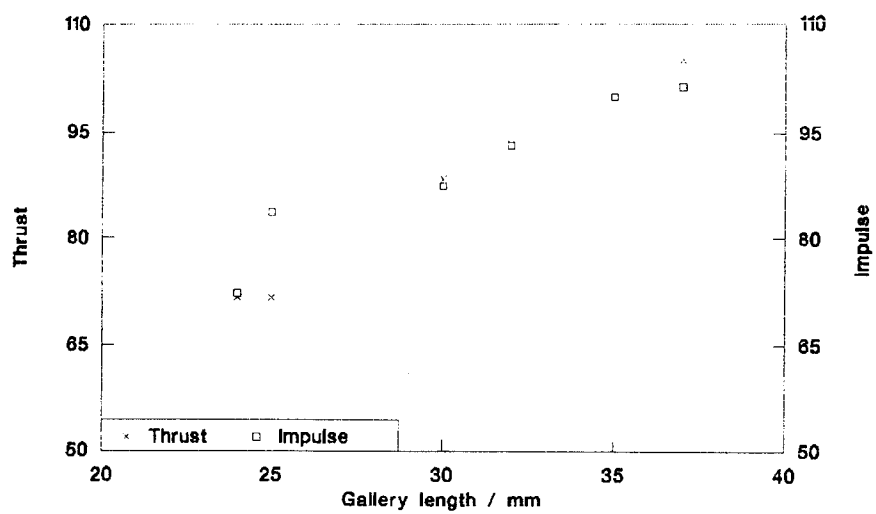


Figure 7 Effect of gallery length on propellant performance

(Data normalised to 35 mm = 100)

The device described is small, easily portable and relatively inexpensive to build and use. Data is produced in analogue form, which can be directly recorded onto a chart recorder or converted via an ADC unit to computer-readable form. The device has proved to be very useful in the development of propellants for small firework motors.

ACKNOWLEDGEMENTS

Funding for the project was provided by Standard Fireworks, Huddersfield, UK. Dr Colin Hodges assisted in the initial development of the device.

REFERENCES

1. RS Data Sheet 8155, RS Components Ltd., Corby, UK, 1987.
2. K. Kishore et al., AIAA Journal **18** (11) (1980), 1404-5.
3. K. Kishore et al., AIAA Journal **15** (11) (1977), 1649-51.
4. H.L. Girdhar and A.J. Arora, Comb. Sci. Technol. **17** (1978), 237-40.
5. A. Bailey and S.G. Murray, "Explosives, Propellants and Pyrotechnics", Brassey's (UK), London, 1989.

Application of the Computer-Assisted Retrosynthesis to Modeling of Probable Decomposition Reactions for Energetic Materials

Tatyana S. Pivina, Dmitry E. Lushnikov, Ekaterina V. Sokerina

N.D.Zelinsky Institute of Organic Chemistry,
Russian Academy of Sciences, Moscow 117913, RUSSIA

Aleksei A. Porollo and Victor P. Ivshin

Mari State University, Yoshkar-Ola, Mari El Republic, RUSSIA

ABSTRACT

We have formulated an approach to computer synthesis and retrosynthesis of organic compounds and have created the program code CASB (Computer-Assisted Structure Building) for this computer modeling. This approach was evaluated at the example of the computer generation of the probable channels for homolysis reactions of energetic materials decomposition.

All possible intermediates of homolysis reactions for molecules are generated by the program code at one step and are resubmitted for a further search of probable pathways for decomposition on the next steps, until the given maximum number of steps is achieved. Screening of advantageous pathways for these reactions has been arranged on the basis of a set of empirical rules and subsequent quantum chemistry calculations of some parameters of compounds decomposition.

The results of the suggested method and corresponding program code have been illustrated at the example of a classical compound within energetic materials - nitromethane.

INTRODUCTION

The theoretical prediction of possible pathways of decomposition for chemical substances is one of the urgent problems in the field of creation and application of energetic materials. However, the attempts to elaborate the methodology for describing thermostability and decomposition for energetic materials are not numerous and they were mainly aimed only at the interpretation and more deeper understanding of the results of experimental studies.

Meanwhile, the methods of computer chemistry and physics allow to develop certain approaches to elucidating problems at the theoretical-calculation level and to a greater extent than the experimental ones. Indeed, a computer possesses fantastic possibilities in generating and selecting possible pathways for decomposition reactions. Therefore, in many cases the computer prediction and subsequent screening of more advantageous ways, from the energy standpoint, for decomposition of energetic materials can be more effective and "economical" than the use of pure experimental results. Moreover, "the computer brain" has no their stereotypes and here we could expect interesting results.

Therefore we suggested the computer generation of possible pathways for homolysis reactions on the basis of a retrosynthesis idea and subsequent screening of thermodynamically advantageous channels for decomposition of energetic compounds.

Some theoretical rules for describing and predicting possible pathways of homolysis reactions can be formulated. In our approach elementary steps of homolysis reactions decomposition are modeled using a retrosynthetic approach. Each elementary reaction describes fragments of a must-be structure as well as some structural modifications that can be carried out to obtain reaction products.

Since among thermochemical properties one can define bond dissociation energies of molecular compounds and their subsequent intermediates as most principal, at the subsequent levels we can estimate thermodynamical advantages by assessing the enthalpy of decomposition and by comparing the results of these calculations for different channels of thermolysis reactions.

METHODOLOGY AND PROGRAM CODE

Presently, some methodologies and program codes have been created for organic synthesis computer modeling. In [1] a number of approaches for the computer-assisted prediction of reaction products under definite conditions were described. This methodology was modified for free radical chemistry in [2] and [3].

In general, a free radical module treats intermediates of chain reactions by iterative consideration of three fundamental radical processes: abstractions, additions, and fragmentations. All monoradical chain processes are divided into three discrete mechanistic phases: initiation, propagation, and termination.

CAMEO program [2,3] displays trapped products rather than free radical intermediates. A number of heuristics for the evaluation of philicity of radical intermediates, bond dissociation energies and steric effects has allowed us to obtain correct predictions of complicated reaction sequences [3].

But this methodology was not applicable to our case - for predicting possible channels for energetic compounds decomposition. Indeed, higher temperatures and pressures that take place during decomposition processes of these materials require a due regard to and selection of the complex set of possible radical intermediates.

Therefore, we suggested a somewhat different approach to the modeling of radical decomposition of explosives using a retrosynthesis idea.

For the modeling of this possible set of reactions we have created the program code CASB (The Computer-Assisted Structure Building) for the enumeration of all probable radical reactions between decomposition products. This program code is based, on the one hand, at the extensive combinatorial generation and selection of the pathways for decomposition of compounds and,

on the other hand, at the complex of simple rulesets that control more probable homolysis reactions. These rulesets are formulated by a user and allow him to define all possible transformations of particles in the system during computer modeling. Using this approach and experimental data we have investigated main processes of nitro compounds thermolysis reactions during the decomposition process.

We also have taken into account bond strengths, predictions of thermochemical stability based on the theoretical approaches, and specific features of formal kinetics. For example, in our ruleset in the case of nitroalkanes ($C_nH_{2n+1}NO_2$) we excluded a possibility of alkyl radicals (C_mH_{2m+1} , $m \geq 2$) formation, as well as the products of their interactions. This allowed us to avoid the "combinatorial explosion" limited by the build-up of a number of radicals. This is a vital assumption since the ratio concentration of these radicals is increasing with time and with the reaction progress and their encounters become less probable.

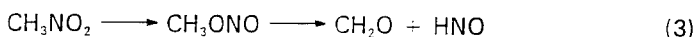
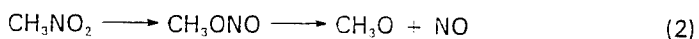
As a result of our analysis of thermochemical studies, a special ruleset for nitro compounds was formulated. We have defined the initiation step as the homolytic abstraction of the nitro group. Propagation steps form the main body of a chain reaction. They involve relocation of the unpaired electron by the rearrangement or by the reaction with a neutral molecule. The primary propagation phase is limited to intermolecular abstraction (S_H2 reactions). As usual, hydrogen atoms predominate in abstracting. The termination occurs as a result of the recombination of two radicals or by disproportionation between them.

All intermediates generated by the program code in one step are resubmitted for a further search on next steps until the given maximum number of steps is achieved. An important feature of the program is a possibility to check each radical intermediate as a potential particle for reactions with all molecules present in the system.

For estimating our approach and program code we have provided the computer generation of possible pathways for nitromethane and estimated the probability of these or other channels for decomposition of this compound on the basis of quantum chemistry methods.

EXPERIMENTAL DATA, RESULTS AND DISCUSSION.

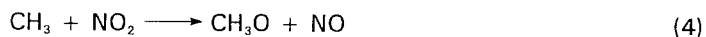
Gas-phase decomposition of nitromethane was studied by pyrolysis in static [4-8] and in flow [9-11] systems, by photolysis [12-18], by radiolysis [19] and shock-tube experiments [20-22]. Although experimental conditions used cover large pressure and temperature ranges, a close agreement with the mechanism of the reaction would be unlikely, thermolysis of nitromethane arises many doubts. In general, the initial step of thermal decomposition of nitromethane was commonly assumed to proceed via following routes [23]:



The other possibility, decomposition into nitrous acid and carben, even triplet carben, would be much more endothermic. It was shown [23] that at low temperatures (up to 700°C) the initial step of thermolysis nearly always took place via the rearrangement to methyl nitrite. Fission into radicals becomes more important with the temperatures growth.

The molecular rearrangement of nitromethane during thermal decomposition was often suggested in different studies. Substantial evidences that nitro compounds and isomeric nitrites can be thermally interconvertable appeared only recently [24,25]. Infrared multiple photon dissociation that does not differ greatly from pyrolysis was used in order to elucidate the collision-free "thermal" chemistry of nitromethane. This work became the first experimental confirmation of the importance of reaction (2).

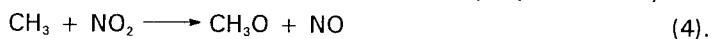
However, reaction (1) proves to play the predominating role during pyrolysis of nitromethane. Crawforth and Waddington [26] have observed high yield of methane, large amounts of nitromethane formed throughout the reaction, and nitrogen dioxide formed early in the reaction. The study on emission from the system of CH_3NO_2 -Ar [20] (temperature up to 2300°C) has shown that NO_2 appears after a shock, but it has very short lifetime, and it probably reacted according to



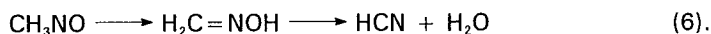
Gray [11] suggested that the nitrosomethane formation should proceed due to direct dissociation between methyl and nitrogen dioxide, although thermodynamically it is not the most feasible process. The confusion as to the primary process involved in the decomposition of nitroalkanes under different conditions still exists, but it is not our aim to discuss it here in detail.

The principal products, concentrations of which increase during decomposition of nitromethane, are methane, carbon monoxide, water, nitrogen and nitric oxide. Concentrations of formaldehyde and hydrogen cyanide reach a maximum when decomposition is about 70% complete, while concentrations of nitrogen dioxide and methanol - much earlier. Minor products are hydrogen, carbon dioxide, ethylene, ethane, methyl cyanide and methyl nitrite [5, 26].

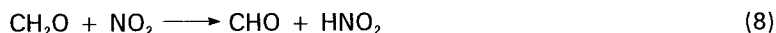
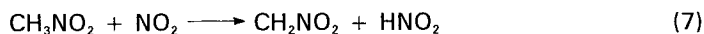
The detailed analysis of products has allowed to identify some of the most important reactions that take place during nitromethane thermolysis. So, at low temperatures nitrogen dioxide is a primary product, its concentration reaches a maximum early in the reaction [26]. It reacts rapidly with methyl radical:



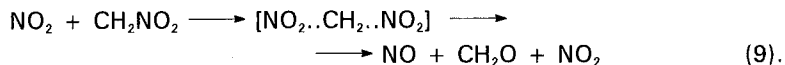
Nitrosomethane formed in reaction (5) can lead to hydrogen cyanide



The reaction of nitrogen dioxide with nitromethane is a follow-up of the chain process, and under these conditions it is slow [10, 26]

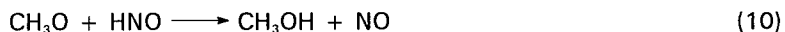


Formaldehyde is probably formed from CH_2NO_2 radicals:



Reaction (9) is not the only possible pathway suggested in literature for the formaldehyde formation.

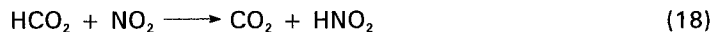
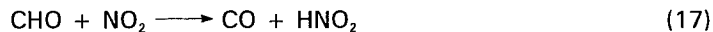
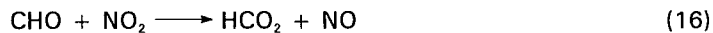
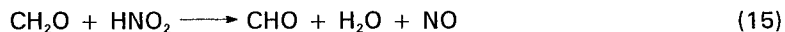
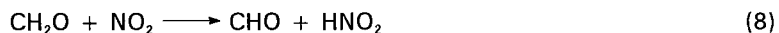
For the above reason we took into account pyrolysis of nitrosoalkanes. Gray and Williams [27] examined pyrolysis of CH_3ONO at 178-315°C in static and flow systems. Their results supported the mechanism developed by Levy for $\text{C}_2\text{H}_5\text{ONO}$ decomposition [28]:



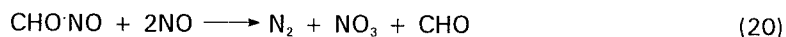
Pyrolysis of CH_3ONO was reexamined by Phillips [29] at temperatures between 150 and 240°C. He found that the reaction proceeded by



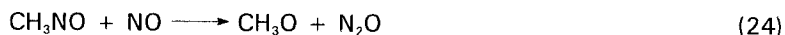
Phillips also proved a free-radical nature of the reaction by adding cyclohexane, a free-radical scavenger. It was shown that at low temperatures, CH_2O neither decomposed rapidly nor reacted with either nitrous oxide or nitric oxide [26], but it was rapidly oxidized by nitrogen dioxide [30, 31]



Concentrations of nitric oxide were probably increased by these reactions but the final mole fraction was reduced. One of the possible explanations to this fact is partial disproportionation of nitric oxide caused by formyl radicals [32]:



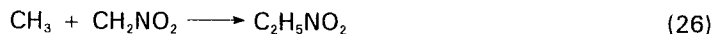
Nitrous oxide comes from HNO and nitroxyl [26]:



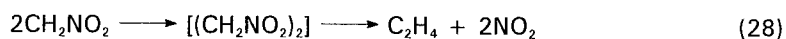
The following scheme was proposed for the formation of nitrogen [15, 33]:



Ethylene could be formed via nitroethane by cyclic elimination of nitrous acid [23, 26]



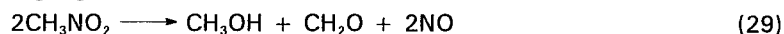
or from two CH_2NO_2 radicals [26]



As it follows from presented references, the reactions mentioned above do not completely describe the thermochemistry of nitromethane. Nevertheless, it is clear that even for such simple compound as nitromethane thermolysis pathways are not obvious and sometime really complicated. The attempts to formulate them were made, for example, by Melius [34]. He proposed to use theoretical chemistry techniques: the BAC-MP4 quantum chemistry method and detailed kinetics modeling. However, his approach is based only on empirical data and therefore cannot be taken as a complete one.

In order to find a general solution to the problem we have made an attempt to generate all possible pathways of thermolysis starting from the molecular structure of the compound in question. After the generation we screen the routes in order to eliminate wrong ones by applying a set of rules compiled using experimental data. On the next step of the screening procedure we analyze the results using quantum chemistry methods. As we noted, in our work we illustrated our approach on the classical example from the energetic material chemistry: nitromethane.

According to our approach and computer code CASB, we have studied the first stage ignition of nitromethane:



with the later conversion of formaldehyde to carbon monoxide



We were interested in the detailed mechanism of this process and as a result of our computer modeling the nitromethane decomposition tree was obtained. The results are in good agreement with the experimental data. The tree generated by CASB gives a clear pattern of the process occurring during nitromethane thermolysis. The fragment of this tree (four steps) is presented in Figure 1.

In order to estimate thermodynamical aspects of reactions proposed by the program CASB semi-empirical quantum chemistry method PM3 [35] was used. Currently this method gives such thermochemical characteristics for nitrogen-oxygen containing compounds that are apparently superior to those obtained by other semi-empirical calculations and close to the experiment [36]. The use of quantum methods gives way to basic screening of probable ways of the process course and to the elimination of less advantageous ones.

In our case the enthalpies of formations were close to the experimental data, though there were some exceptions (see Table 1).

Table 1. *Heats of formation on the basis PM3 method (in kcal/mol)*

Reaction	ΔH_f°	
$\text{CH}_3\text{NO}_2 + \text{CH}_3 \longrightarrow \text{CH}_2\text{NO}_2 + \text{CH}_4$	23.13	1
$\text{CH}_3\text{NO}_2 + \text{NO}_2 \longrightarrow \text{HONO} + \text{CH}_2\text{NO}_2$	21.27	2
$\text{CH}_3 + \text{NO}_2 \longrightarrow \text{CH}_3\text{ONO}$	-32.09	3
$\text{HONO} \longrightarrow \text{HO} + \text{NO}$	32.41	4
$\text{CH}_3\text{ONO} \longrightarrow \text{CH}_3\text{O} + \text{NO}$	10.71	5
$\text{CH}_3\text{NO}_2 + \text{NO} \longrightarrow \text{CH}_2\text{NO}_2 + \text{HNO}$	33.41	6
$\text{CH}_3\text{NO}_2 + \text{OH} \longrightarrow \text{CH}_2\text{NO}_2 + \text{H}_2\text{O}$	-21.98	7
$\text{CH}_3\text{NO}_2 + \text{CH}_3\text{O} \longrightarrow \text{CH}_2\text{NO}_2 + \text{CH}_3\text{OH}$	-7.29	8
$\text{CH}_3 + \text{CH}_3\text{O} \longrightarrow \text{CH}_4 + \text{H}_2\text{CO}$	-64.76	9
$\text{CH}_2\text{NO}_2 + \text{CH}_3\text{O} \longrightarrow \text{CH}_3\text{NO}_2 + \text{CH}_2\text{O}$	-58.07	10
$\text{NO}_2 + \text{CH}_3\text{O} \longrightarrow \text{HONO} + \text{CH}_2\text{O}$	-36.80	11
$\text{HONO} + \text{NO} \longrightarrow \text{NO}_2 + \text{HNO}$	12.14	12
$\text{HONO} + \text{CH}_3\text{O} \longrightarrow \text{NO}_2 + \text{CH}_3\text{OH}$	-28.56	13
$\text{HONO} + \text{OH} \longrightarrow \text{NO}_2 + \text{CH}_3\text{OH}$	-43.25	14
$\text{CH}_3\text{ONO} + \text{CH}_3\text{O} \longrightarrow \text{CH}_2\text{ONO} + \text{CH}_3\text{OH}$	-15.19	15
$\text{NO} + \text{CH}_3\text{O} \longrightarrow \text{CH}_2\text{ONO} + \text{CH}_3\text{OH}$	-24.67	16
$\text{OH} + \text{CH}_3\text{O} \longrightarrow \text{H}_2\text{O} + \text{CH}_2\text{O}$	-80.05	17
$\text{CH}_3\text{O} + \text{CH}_2\text{ONO} \longrightarrow \text{CH}_2\text{O} + \text{CH}_3\text{ONO}$	-50.16	18

Figure 1. Fragment of the reaction tree generated by the program CASB

As it follows from Table 1 (reaction **3**), the formation of nitromethane as a result of recombination of CH_3 and NO_2 radicals is thermodynamically beneficial. The following homolysis of CH_3ONO (reaction **5**) leads to the formation of radicals CH_3O and NO that are important in the subsequent chain development, this being a subject for the discussion of many experimentators. As our studies have shown, a step-by-step course of these reactions (**3** and **5**) is advantageous from the energy standpoint.

Reactions **9**, **10**, **11**, **13-16** are also energy-beneficial (enthalpies of these reactions are in the range of -64.76 kcal/mol (See reaction **9**, Table 1) to -15.19 kcal/mol (reaction **15**, Table 1), this being perfectly clear since they lead to the existence of stable particles that can be detected among final thermolysis compounds.

As for reaction **18**, which also results in the formation of formaldehyde and nitrosomethane, this reaction can serve as an example of the formation of another (except **5**) CH_3ONO channel and further involvement of this substance into the propagation step.

Generally, comparing the results of our calculations with the experimental data, we can mark a good agreement of our "pure" theoretical computer modeling of probable thermolysis pathways of CH_3NO_2 with the experimental thermochemical data.

The reaction tree generated by the program outlines several a priori unobvious pathways. Though some of them seem to be somehow strange or non-existent, all of them can occur in real process. Meanwhile the very nature of the explosive - extremely high temperature and pressure - could result in reactions products which are not possible under milder conditions.

CONCLUSION

As a result of our study we have formulated a general approach to computer extensive generation of possible pathways of decomposition for energetic materials. For screening of the most advantageous pathways from the energy standpoint a special ruleset for the class of nitro compounds has been created and at the subsequent levels of computer screening thermodynamical aspects of these reactions were estimated on the basis of quantum chemistry methods. In order to demonstrate the prospects of this methodology and the way program code CASB can be realized we have used nitromethane - a classical example in energetic material chemistry.

References

1. R.Barone and M.Chanon, *Computer-Aided Organic Synthesis*, In: Computer Aids to Chemistry; G.Vernin, M.Chanon, Eds.; E.Horwood, Chichester, p. 19-102
2. W.L.Jorgenson, E.R.Laird, A.J.Gushurst, J.M.Fleisher, S.A.Gothe, H.E.Helson, G.D.Paderes and S.Sinclair, *Pure Appl.Chem.*, 1990, **62**, 1921
3. E.R.Laird and W.L.Jorgenson, *J.Org.Chem.*, 1990, **55**, 9
4. H.A.Taylor and V.V.Vesselovsky, *J.Phys.Chem.*, 1935, **39**, 1095
5. T.L.Cottrell and T.J.Reid, *J.Chem.Phys.*, 1950, **18**, 1306
6. T.L.Cottrell, T.E.Graham and T.J.Reid, *Trans.Faraday Soc.*, 1951, **47**, 584
7. K.H.Mueller, *J.Amer.Chem.Soc.*, 1955, **77**, 3459
8. A.Makovky and T.B.Gruenwald, *Chem.Rev.*, 1958, **58**, 627
9. L.J.Hillenbrand and M.L.Kilpatrick, *J.Chem.Phys.*, 1951, **19**, 381
10. L.J.Hillenbrand and M.L.Kilpatrick, *J.Chem.Phys.*, 1953, **21**, 525
11. P.Gray, A.D.Yoffe and L.C.Rosenlaar, *Trans.Faraday Soc.*, 1955, **51**, 1489
12. Hirschlaff and R.G.W.Norrish, *J.Chem.Soc.*, 1936, 1580
13. H.W.Brown and G.C.Pimental, *J.Chem.Phys.*, 1958, **29**, 883
14. F.W.Dalby, *Canad.J.Phys.*, 1958, **36**, 1336
15. M.I.Christie, C.Gilbert and M.A.Voisey, *J.Chem.Soc.*, 1964, 3147
16. A.J.C.Nicholson, *Nature*, 1961, **190**, 143
17. J.I.McGarvey and W.D.McGrath, *Trans.Faraday Soc.*, 1964., **60**, 2196
18. I.M.Napier and R.G.W.Norrish, *Proc.Roy.Soc.A*, 1967, **299**, 317
19. S.Paszyc, *Photochem.Photobiol.*, 1965, **4**, 841
20. H.Hiraoka and R.Hardwick, *J.Chem.Phys.*, 1963, **39**, 2361
21. J.N.Bradley, *Trans.Faraday Soc.*, 1961, **57**, 1750
22. A.A.Borisov, S.M.Kogarko and G.I.Skachkov, *Kinetika I Kataliz*, 1966, **7**, 589
23. M.J.S.Dewar and J.P.Ritchie and J.Alster, *J.Org.Chem.*, 1985, **50**, 1031
24. A.M.Wodtke, E.J.Hintsa, and J.T.Lee, *J.Chem.Phys.*, 1986, **84**, 1044
25. A.M.Wodtke, E.J.Hintsa, and J.T.Lee, *J.Phys.Chem.*, 1986, **90**, 3549
26. C.G.Crawforth and D.J.Waddington, *Trans.Faraday Soc.*, 1969, **65**, 1334
27. P.Gray and A.Williams, *Nature*, 1960, **188**, 56
28. J.B.Levy, *J.Am.Chem.Soc.*, 1956, **78**, 1780
29. L.Phillips, *J.Chem.Soc.*, 1961, 3082
30. F.H.Pollard and R.M.H.Wyatt, *Trans.Faraday Soc.*, 1949, **45**, 760
31. D.Barton, *J.Phys.Chem.*, 1961, **65**, 1831
32. M.I.Christie and M.A.Voisey, *Trans.Faraday Soc.*, 1967, **63**, 2459
33. M.I.Christie, J.S.Frost and M.A.Voisey, *Trans.Faraday Soc.*, 1965, **61**, 674
34. C.F.Melius, *Phil. Trans.R.Soc.Lond.A*, 1992, **339**, 355
35. M.J.S.Dewar, E.E.Healy, A.J.Holder and J.C.Yaam, *J.Comp.Chem.*, 1990, **11**, 541
36. J.L.G.De Paz and J.Ciller, *Propellants, Explos., Pyrotech.*, 1993, **18**, 33

**CALCULATION OF THE EQUILIBRIUM THERMODYNAMIC
PROPERTIES OF THE ISOBARIC ADIABATIC COMBUSTION PRODUCTS
OF AN/HTPB-IPDI PROPELLANTS AT 7.0 MPa.**

P. Carvalheira

Departamento de Engenharia Mecânica, Faculdade de Ciências e Tecnologia da
Universidade de Coimbra, Largo de D. Dinis, P-3000 Coimbra, Portugal

ABSTRACT

Research on AN/HTPB-IPDI propellants has gained interest due to their advantages for certain gas generators applications. Combustion products that are chlorine free, low corrosive and have low flame temperature, are among the advantages. One disadvantage of AN is the phase transition IV to III in the AN crystal lattices that occurs at 305 K (32 °C) with a large volume change and that is detrimental to the mechanical properties of ammonium nitrate based propellants under cyclic thermal loading. Other disadvantages are the high hygroscopicity of AN and the low burning rate of AN based propellants. One solution for the phase transition problem is the incorporation of diammine complexes of transition metals, such as Ni, Cu and Zn, into the AN crystal lattice. The hygroscopicity problem of AN is not solved yet but has been contoured imposing the requirements of low humidity ambient conditions for AN/HTPB-IPDI propellants manufacture and storage. The problem of low burning rate has not been solved, but progress has been made. The investment in the development of new formulations and manufacturing processes for this kind of propellants might be interesting because they have a potential for low cost manufacture. The objective of this work is to contribute to the identification, in a systematic way, of the formulations including AN and HTPB-IPDI as main ingredients that might present high potential for practical applications in the near and far future. This is done by analysing the results of the NASA-Lewis CET89 equilibrium thermodynamic code in the aspects of combustion products composition and performance parameters. Four AN solid loading ranges were identified that present interesting characteristics. Their advantages and disadvantages were discussed in view of their suitability for industrial and practical applications.

1. Introduction

Research on AN/HTPB-IPDI propellants has gained interest due to their advantages for certain gas generators applications [1,2]. Combustion products that are chlorine free, low corrosive and have low flame temperature, are among the advantages [1,2]. One disadvantage of AN is the phase transition IV to III in the AN crystal lattices that occurs at 305 K (32 °C) with a large volume change and that is detrimental to the mechanical properties of ammonium nitrate based propellants under cyclic thermal loading [1,2]. Other disadvantages are the high hygroscopicity of AN and the low burning rate of AN based propellants [1,2]. One solution for the phase transition problem is the incorporation of diammine complexes of transition metals, such as Ni, Cu and Zn, into the AN crystal lattice [3]. It is also reported that it is possible to obtain phase stabilised ammonium nitrate, without additives, when particle size is in the range 63-88 μm and when it is dried to have humidity content lower than 0.2 wt.% [4]. The hygroscopicity problem of AN is not solved yet but has been contoured imposing the requirements of low humidity ambient conditions for AN/HTPB-IPDI propellants manufacture and storage [2]. The problem of low burning rate, usually 1-2 mm/s in the 2-10 MPa pressure range, has not been solved, but progress has been made [2,5]. The investment in the development of new formulations and manufacturing processes for this kind of propellants might be interesting because they have a potential for low cost manufacture [6] and specific impulse in the range 1888-2252 m/s. The objective of this work is to contribute to the identification, in a systematic way, of the formulations including AN and HTPB-IPDI as main ingredients that might present high potential for practical applications in the near and far future. This is done by analysing the results of CET89 [7] equilibrium thermodynamic code in the aspects of combustion products composition and performance parameters. Four AN solid loading ranges were identified and their advantages and disadvantages presented. Propellants with AN solid loading in the range 72-78 wt.% should present low variability of characteristics from batch to batch, have low flame temperature, low specific impulse and have high carbon (graphite) and high CO emissions. Propellants with 80 wt.% AN solid loading show similar characteristics to the previous range except that they should present medium variability of characteristics from batch to batch, and no carbon (graphite) emissions. Propellants with AN solid loading in the range 84-86 wt.% show medium specific impulse but should present high variability of characteristics from batch to batch and high CO emissions. Propellants with AN solid loading in the range 93-94 wt.% show relatively high specific impulse with moderate flame temperature and the lowest amount of pollutants but they can only be fully exploited in the far future when extrusion technology is fully developed for this kind of propellants.

2. Conditions of the Calculations

The calculations were performed using the computer code NASA-Lewis CET89 - Chemical Equilibrium with Transport Properties [7,8]. The calculations were performed assuming a combustion of the propellant in the combustion chamber at 7.0 MPa and than an expansion of the combustion products in chemical equilibrium flow,

through a convergent-divergent nozzle with a pressure ratio 70.0:1. Parameters of utmost importance are the specific impulse for the expansion in chemical equilibrium flow through the nozzle exit, temperature, molecular weight, isentropic compression exponent (Γ) and the composition of the combustion products in the combustion chamber and the temperature and the composition of the combustion products in the nozzle exit. Initial temperature of the reactants was 298.15 K. The effect of AN solid loading on each one of these parameters is presented in Tables 1 to 4 and in Figs. 1 to 6 and are discussed in this work.

3. Properties and Composition of Reactants

Table 1. Properties and composition of reactants

Reactant	Chemical Formula	$\Delta H_{f,298.15}^{\circ}$ /kcal.mol ⁻¹	$\rho_{298.15}$ /kg.m ⁻³	Reference
AN	H ₄ N ₂ O ₃	-87.27	1725	9
HTPB	C ₁₀ H _{15.6160} N _{0.2030} O _{0.1960}	-10.90	901	9, 10
IPDI	C ₁₂ H ₁₈ N ₂ O ₂	-111.40	1061	9

The AN is considered to include no phase stabilising agent and to be anhydrous. The HTPB-IPDI weight ratio in the binder is 92.32-7.68 wt.% and is typical of that used in practical composite solid propellant formulations. This binder system has excellent mechanical properties even in the low temperature end of the temperature range of most practical applications (- 60 °C to + 60 °C) [10]. The calculations were made using AN/HTPB-IPDI compositions where the AN solid loading varies in the range 70-100 wt.% with increments of 2.0 wt.% and in some sub ranges of interest with increments of 1.0 wt.%.

4. Analysis of Results and Discussion

4.1. Adiabatic Flame Temperature

The isobaric adiabatic flame temperature of the propellants in this AN solid loading range increases slightly from 1201 K to 1300 K in the range 70-78 wt.% AN. Then, after the transition range 78-82 wt.% AN, it increases strongly from 1511 K to 2261 K in the range 82-92 wt.% AN. Then, after the transition range 92-93 wt.% AN, there is the small range 93-94 wt.% AN, where it increases from 2335 K to 2344 K. After this, it decreases strongly from 2344 K to 1246 K in the range 94-100 wt.% AN. These results are shown in Fig. 1 and in Table 2.

4.2. Specific Impulse

The specific impulse of the propellants in this AN solid loading range increases slightly from 1876 m/s to 1936 m/s in the range 70-78 wt.% AN. Then, after the transition range 78-82 wt.% AN, it increases strongly from 1992 m/s to 2227 m/s in the range 82-92 wt.% AN. Then, after the transition range 92-93 wt.% AN, there is the small range 93-94 wt.% AN, where it increases from 2249 m/s to 2252 m/s. After this, it decreases strongly from 2252 m/s to 1578 m/s in the range 94-100 wt.% AN. These results are shown in Fig. 2 and in Table 2.

4.3. Combustion Products Composition

The combustion products of these compositions for AN solid loading in the range 70-100 wt.% is shown in Fig. 3 and Table 3 for combustion chamber at 7.0 MPa, and in Fig. 4 and Table 4 for the nozzle exit, after isentropic expansion in chemical equilibrium through a convergent-divergent nozzle to 0.1 MPa. The CET89 code only gives results for species concentrations larger than 5 ppm. For these AN/HTPB-IPDI reactant compositions the species in these conditions are the ones presented in Tables 3 and 4. The species considered as pollutants were CO, C(GR), NO_x (NO + NO₂), Non Methane HydroCarbons (NMHC) and HCN. NH₃, OH, H and O were not considered pollutants because we were not able to find in the literature accepted threshold concentration values above which they are considered pollutants and because OH, H, and O have short lives in normal ambient atmospheric conditions even if it is known that OH, H and O contribute to ozone layer depletion [11]. CO₂ was not considered a pollutant even if it can contribute to the global warming of the earth through the greenhouse effect [11].

4.3.1. Combustion Chamber and Nozzle Exit

CO

From an environmental point of view CO emissions should be kept lower than 80 ppm [13]. A CO level below 3.4 grams per mile (approx. 723-3613 ppm for 5-25 l/100 km fuel consumption) is already acceptable for the U. S. automobile industry standards [12]. Fig. 3 shows that for the combustion chamber the 1500 ppm goal can only be achieved for AN solid loading larger than or equal to 95 % and that the 80 ppm goal can only be achieved for AN solid loading larger than or equal to 96 %. Fig. 4 shows that for the nozzle exit the 80 ppm goal can only be achieved for AN solid loading larger than or equal to 94 %.

NO_x

Under the designation NO_x is included NO and NO₂. NO is thought to participate in the ozone layer depletion mechanism [11]. From an environmental point of view NO_x emissions should be kept lower than 300 ppm [13]. A NO_x level below 0.40 grams per mile (approx. 85-425 ppm for 5-25 l/100 km fuel consumption) is already acceptable for the U. S. automobile industry standards [12]. Fig. 3 shows that for the combustion chamber the 300 ppm goal can only be achieved for AN solid loading equal to or lower than 93 wt.% or for AN solid loading equal to 100 wt.%. Fig. 4 shows that for the nozzle exit the 300 ppm goal can always be achieved for AN solid loading in the range 70-100 wt.%.

NMHC (Non Methane HydroCarbons)

The HC observed as combustion products for this kind of propellants are methane (CH₄), ethene (C₂H₄) and ethane (C₂H₆) where CH₄ is the HC combustion product with larger amounts. A NMHC emission level below 0.25 grams per mile (approx. 53-266 ppm for 5-25 l/100 km fuel consumption) is already acceptable for the U. S. automobile industry standards [12]. Fig. 3 for the combustion chamber and Fig. 4 for the nozzle exit shows that the 100 ppm emission goal can always be achieved for AN solid loading larger than 70 %.

HCN

From an environmental point of view HCN emissions should be kept lower than 10 ppm (e.g.: South Korea Emissions Standards) [12]. Fig. 3 shows that for the combustion chamber this goal can always be achieved for AN solid loading larger than 80 wt.%. Fig. 4 shows that for the nozzle exit this goal can always be achieved for AN solid loading in the range 70-100 wt.%.

Solid Particles

The only solid particles observed as a result of the calculations for this kind of propellants are Carbon (Graphite), C(GR). An acceptable level of C(GR) content in combustion products is lower than 500 µg/m³ (about 400 ppm) [13]. Fig. 3 shows that for the combustion chamber the 400 ppm goal is possible for any AN solid loading in the range 70-100 wt.%. Fig. 4 shows that for the nozzle exit the 400 ppm goal is only possible AN solid loading larger than or equal to 80 wt.%.

4.4. Discussion of Results

To have repeatable performance in industrial applications the gradient of specific impulse and flame temperature relative to AN solid loading should be low. These results indicate that this is true for propellants with AN solid loading in the range 70-78 % or in the range 93-94 wt.%.

The first AN solid loading range of interest is 72.0-78.0 wt.%. The Oxidizer/Fuel weight ratio (O/F) in this range is 2.57-3.55. This first range is characterized by a specific impulse in the range 1888-1936 m/s, a flame temperature in the range 1215-1300 K, and by levels of emission in the combustion chamber that are acceptable for NO_x , C(GR) and NMHC emissions, and unacceptable for HCN and CO emissions. This first AN solid loading range is characterized by emission levels in the nozzle exit acceptable for NO_x , HCN and NMHC emissions, and unacceptable for C(GR) and CO emissions. It is expected low variability from batch to batch in this kind of propellants which is of special interest from an industrial point of view. The manufacture of castable propellants in this AN solid loading range presents no special difficulties to accomplish if a bimodal distribution is considered for AN solid loading larger than 75 wt.% [14].

The second AN solid loading of interest is 80 wt.%. The O/F weight ratio is equal to 4.00. This second AN solid loading is characterized by a specific impulse of 1960 m/s, a flame temperature of 1381 K, and by emission levels in the combustion chamber that are acceptable for NO_x , C(GR) and NMHC emissions, almost acceptable for HCN emissions and unacceptable for CO emissions. This second AN solid loading is characterized by emission levels in the nozzle exit acceptable for NO_x , C(GR), HCN and NMHC emissions, and unacceptable for CO emissions. It is expected low-medium variability from batch to batch in this kind of propellants which is of special interest from an industrial point of view. The manufacture of castable propellants in this AN solid loading range should presents no special difficulties to accomplish if a bimodal distribution is considered [14].

The third range of interest is the 84-86 wt.% AN solid loading which corresponds to the maximum AN solid loading that can be practically attained for castable propellants of this kind [14]. The O/F weight ratio in this range is 5.25-6.14. This third range is characterized by a specific impulse in the range 2032-2078 m/s, a flame temperature in the range 1656-1804 K, acceptable levels of NO_x , NMHC, HCN and C(GR) emissions and unacceptable levels of CO emissions both for the combustion chamber and for the nozzle exit. It is expected high variability from batch to batch in this kind of propellants which is not attractive from an industrial point of view. The manufacture of castable propellants in this range should presents no unsurpassable difficulties to accomplish if a bimodal or trimodal AN particle size distribution is considered to accomplish it [14].

The fourth AN solid loading range of interest is 93.0-94.0 wt.%. The O/F ratio in this range is 13.29-15.67. This range is characterized by a specific impulse in the range 2249-2252 m/s, and a flame temperature in the range 2335-2344 K. It is characterized by levels of emission in the combustion chamber and nozzle exit that are acceptable for NMHC, C(GR) and HCN emissions. At 93 wt.% AN solid loading it is characterized by acceptable levels of NO_x in the combustion chamber and in the nozzle exit and unacceptable levels of CO in the combustion chamber and in the nozzle exit. At 94 wt.% AN solid loading it is characterized by unacceptable levels of NO_x in the combustion chamber but acceptable levels in the nozzle exit and unacceptable levels of CO in the combustion chamber but acceptable in the nozzle exit. The manufacture of AN/HTPB-IPDI propellants in this range of AN solid loading is only possible to accomplish by extrusion or pressing processes [6].

5. Conclusions

Four AN solid loading ranges of interest have been identified in the AN solid loading range 70-100 wt.%. Propellants from each range present a group of special characteristics which make them more suitable for particular applications.

The first AN solid loading range of interest is 72.0-78.0 wt.%. This range is characterized by a low specific impulse, low flame temperature, unacceptable levels of CO and HCN emissions in the combustion chamber and unacceptable levels of CO and C(GR) emissions in the nozzle exit. Due to the high level of C(GR) emissions in the nozzle exit these propellants are expected to be smoky. It is expected low variability from batch to batch in this kind of propellants which is of special interest from an industrial point of view. The manufacture of castable propellants in this AN solid loading range presents no special difficulties to accomplish. In this range, the propellants with larger AN solid loading will have larger flame temperature, larger specific impulse and the advantages of presenting lower level of C(GR) and CO emissions.

The second AN solid loading of interest is 80 wt.%. This second AN solid loading is characterized by a specific impulse of 1960 m/s, a flame temperature of 1381 K, and by levels of emission in the combustion chamber and in the nozzle exit that are acceptable for NO_x , C(GR) and NMHC emissions and unacceptable for CO emissions. The level of emissions of HCN is almost acceptable for the combustion chamber and acceptable for the nozzle exit. It is expected low-medium variability from batch to batch in this kind of propellants which is of special interest from an industrial point of view. The manufacture of castable propellants with this AN solid loading should present no special difficulties to accomplish if a bimodal distribution is considered.

The third range of interest is the 84-86 wt.% AN solid loading which corresponds to the maximum AN solid loading that can be practically attained for this kind of

propellants to be castable. The propellants in this AN solid loading range are interesting from the point of view of performance but will be more difficult to manufacture and it is expected that they will present more variability than the previous AN solid loading in flame temperature and specific impulse from batch to batch. They are characterized by levels of emissions in the combustion chamber and in the nozzle exit that are acceptable for NO_x , C(GR), NMHC and HCN emissions and unacceptable for CO emissions.

The fourth AN solid loading range of interest is 93.0-94.0 wt.% AN. The propellants in this AN solid loading range are interesting because they present relatively high levels of specific impulse with relatively low flame temperature, they have the lowest overall pollutant emissions and are expected to have low variability in flame temperature and specific impulse from batch to batch, but will be extremely difficult to manufacture. Propellant grains of these compositions can only be manufactured by extrusion or pressing processes.

REFERENCES

1. Strecker, R. A. H., and Linde, D., "Gas Generator Propellants for Air-to-Air Missiles". AGARD CP-259, April 1979.
2. Korting, P. A. O. G., Zee, F. W. M., Meulenbrugge, J. J. (1987). "Performance of No Chlorine Containing Composite Propellants with Low Flame Temperatures". *AIAA/SAE/ASME/ASEE 23rd Joint Propulsion Conference*, June 29-July 2, San Diego, California.
3. Engel, W., Eisenreich, N., Deimling, A., Hermann, M., Lorenzo, M. J., Kolarik V., "Ammonium Nitrate, A Less Polluting Oxidizer". 24th International Annual Conference of ICT 1993, Karlsruhe, Federal Republic of Germany, (1993) pp. 3-1.
4. Kestilä, E. and Valkonen, J., DSC studies on the effect of particle size on NH_4NO_3 at temperatures between 25 °C and 100 °C. *Thermochimica Acta*, 223 (1994) 219-222.
5. Carvalheira, P., Gadiot, G.M.H.J.L. and de Klerk, W.P.C., Mechanism of Catalytic Effects on PSAN/HTPB Composite Solid Propellants Burning Rates. 25th International Annual Conference of ICT 1994, Karlsruhe, Federal Republic of Germany, (1994) pp. 65-1.
6. Cooke, E.M.G., The Manufacture of High Performance Composite Propellants and Novel Charges by Batch and Continuous Extrusion Processes. *Propellants, Explosives and Pyrotechnics* 15, 235-242 (1990).
7. McBride, B. J., CET89 - Chemical Equilibrium with Transport Properties, 1989. LEW-15113 Program, Cosmic Software, The University of Georgia, Athens, U.S.A..
8. Gordon, S. and McBride, B. J., "Computer Program for Calculation of Complex Chemical Equilibrium, Rocket Performance, Incident and Reflected Shocks, and Chapman-Jouguet Detonations, NASA SP-273, Interim Revision, March 1976.
9. ICT Thermochemical Data Base, Karlsruhe, Germany, June 15, 1994.

10. Hydroxyl Terminated Poly Bd Resins Functional Liquid Polymers in Urethane Elastomers, Atochem, Elf Aquitaine, October 1990.
11. McDonald, A. J., and Bennett R. R., Environmental Impacts From Launching Chemical Rockets, AGARD PEP 84th Meeting on Environmental Aspects of Rocket and Gun Propulsion, Alesund, Norway, 29 Aug.-2 Sept, 1994.
12. Patrick, David R. (Ed.), Toxic Air Pollution Handbook, Van Nostrand Reinhold, New York, 1994.
13. Boubel, R. W., Fox, D. L., Turner, D. B., and Stern, A. C., Fundamentals of Air Pollution, 3rd Ed., Academic Press, 1994.
14. Davenas, A., et collaborateurs, Technologie des Propergols Solides, Masson, Paris, 1989.

Table 2. Evolution in AN/HTPB-IPDI propellants with AN wt.% solid loading of isobaric adiabatic flame temperature, molecular weight, and Γ in combustion chamber at 7.0 MPa, and of specific impulse and vacuum specific impulse after isentropic expansion through a convergent divergent nozzle from 7.0 MPa to 0.1 MPa.

AN wt. %	Tf/K	Mw /(g/mol)	Γ	Isp /(m/s)	Ivac /(m/s)	Tne /K	Eq. Ratio	O/F
70	1201.1	18.737	1.1716	1876.0	2046.7	813.8	2.8038	2.333
72	1215.4	18.520	1.1767	1887.9	2059.1	816.1	2.6099	2.571
74	1233.5	18.331	1.1834	1901.5	2073.0	817.9	2.4257	2.846
75	1244.9	18.253	1.1879	1909.1	2080.5	818.7	2.3370	3.000
76	1258.8	18.190	1.1936	1917.3	2088.6	819.2	2.2506	3.167
78	1300.2	18.148	1.2125	1936.2	2106.9	819.9	2.0838	3.546
80	1381.4	18.347	1.2441	1960.3	2130.1	821.9	1.9248	4.000
82	1511.1	18.853	1.2531	1991.9	2160.2	825.3	1.7732	4.556
84	1655.9	19.478	1.2461	2031.6	2197.4	829.8	1.6282	5.250
85	1729.7	19.811	1.2416	2054.2	2218.4	833.3	1.5582	5.667
86	1804.2	20.156	1.2370	2078.1	2241.0	839.0	1.4897	6.143
88	1954.8	20.884	1.2274	2129.0	2290.9	868.5	1.3570	7.333
90	2107.4	21.667	1.2173	2179.8	2345.2	940.0	1.2299	9.000
92	2261.1	22.507	1.2056	2227.1	2397.4	1027	1.1080	11.50
93	2335.3	22.945	1.1961	2249.2	2422.1	1074	1.0489	13.29
94	2343.8	23.262	1.1792	2252.0	2426.0	1100	0.9910	15.67
95	2193.3	23.237	1.1958	2162.7	2327.0	994.1	0.9343	19.00
96	2022.3	23.173	1.2068	2066.1	2220.3	888.1	0.8787	24.00
98	1653.4	23.024	1.2296	1846.7	1978.8	675.4	0.7706	49.00
100	1246.0	22.870	1.2604	1578.2	1685.4	465.3	0.6667	infinite

AN wt. %	CO2	H2O	N2	O2	CO	H2	NO	CH4	C3GRI	NH3	ETHENE	ETHANE	HCN	HO2	NO2	OH	H	O
70	0.07214	0.13563	0.16904		0.22271	0.30523		0.09426		0.00093	0.00001	0.00002	0.00002					
72	0.0717	0.1506	0.17133		0.21595	0.31812		0.07133		0.00093		0.00001	0.00001					
74	0.07094	0.16653	0.17381		0.20937	0.32877		0.04965		0.00091		0.00001	0.00001					
75	0.07043	0.1751	0.17517		0.20608	0.3329		0.0394		0.00088		0.00001	0.00001					
76	0.06993	0.18433	0.17668		0.20272	0.33588		0.02969		0.00085		0.00001	0.00001					
78	0.06833	0.20644	0.1805		0.1953	0.3359		0.0128		0.00072		0.00001	0.00001					
80	0.0665	0.23938	0.1868		0.18493	0.31926		0.00251		0.0005		0.00001	0.00001					
82	0.06539	0.28598	0.1864		0.1693	0.28237		0.00025		0.00028								
84	0.06533	0.33776	0.20746		0.14992	0.23884		0.00002		0.00015								
85	0.06664	0.36459	0.21331		0.1391	0.21623		0.00001		0.00011								
86	0.06784	0.392	0.21935		0.12753	0.19316				0.00008								
88	0.07157	0.44863	0.2321		0.10194	0.14564				0.00004								
90	0.07747	0.50755	0.24579	0.00001	0.07254	0.09542				0.00002								
92	0.08649	0.56802	0.26048	0.00001	0.03818	0.04618	0.00004											
93	0.09253	0.59789	0.26812	0.00007	0.01868	0.02133	0.00018											
94	0.09418	0.61729	0.27382	0.00482	0.00245	0.00283	0.00153											
95	0.0801	0.61248	0.27567	0.02573	0.00034	0.0005	0.00258											
96	0.06412	0.60503	0.27768	0.04923	0.00005	0.00011	0.00234											
98	0.03188	0.58852	0.28186	0.09654			0.00098											
100		0.57143	0.28564	0.14278			0.00014											

Table 3. Evolution of combustion products composition of AN/HTPB-IPDI propellants with AN wt.% solid loading, in a combustion chamber at 7.0 MPa.

AN wt. %	CO2	H2O	N2	O2	CO	H2	NO	CH4	C(GR)	NH3
70	0.12578	0.1997	0.16603		0.04127	0.25276		0.08275	0.13156	0.00016
72	0.13473	0.20333	0.17434		0.04493	0.25767		0.08047	0.10437	0.00016
74	0.14428	0.20736	0.18319		0.04861	0.26226		0.07846	0.07569	0.00016
75	0.1493	0.20957	0.18783		0.05042	0.26439		0.07756	0.06077	0.00016
76	0.1545	0.21193	0.19263		0.0522	0.26639		0.07674	0.04546	0.00016
78	0.16551	0.21729	0.20275		0.05547	0.2698		0.07541	0.01362	0.00016
80	0.16812	0.2339	0.20925		0.05352	0.27239		0.06266		0.00016
82	0.1641	0.26031	0.21332		0.04778	0.27112		0.04321		0.00015
84	0.15944	0.291	0.21823		0.04157	0.26367		0.02595		0.00014
85	0.15663	0.30856	0.22108		0.03839	0.25698		0.01824		0.00013
86	0.15327	0.32829	0.2243		0.03523	0.24748		0.0113		0.00012
88	0.1433	0.38046	0.2329		0.02911	0.21244		0.00172		0.00007
90	0.12816	0.45708	0.24583		0.02185	0.14702		0.00003		0.00002
92	0.113	0.54216	0.26059		0.01171	0.07253				
93	0.10569	0.58658	0.26842		0.0056	0.03371				
94	0.09697	0.62379	0.27553	0.0037			0.00001			
95	0.08053	0.61491	0.27726	0.02729			0.00001			
96	0.06421	0.6061	0.27897	0.05072						
98	0.03188	0.58864	0.28237	0.0971						
100		0.57143	0.28571	0.14286						

Table 4. Evolution of combustion products composition of AN/HTPB-IPDI propellants with AN wt. % solid loading, in the nozzle exit, after expansion from a combustion chamber at 7.0 MPa to 0.1 MPa.

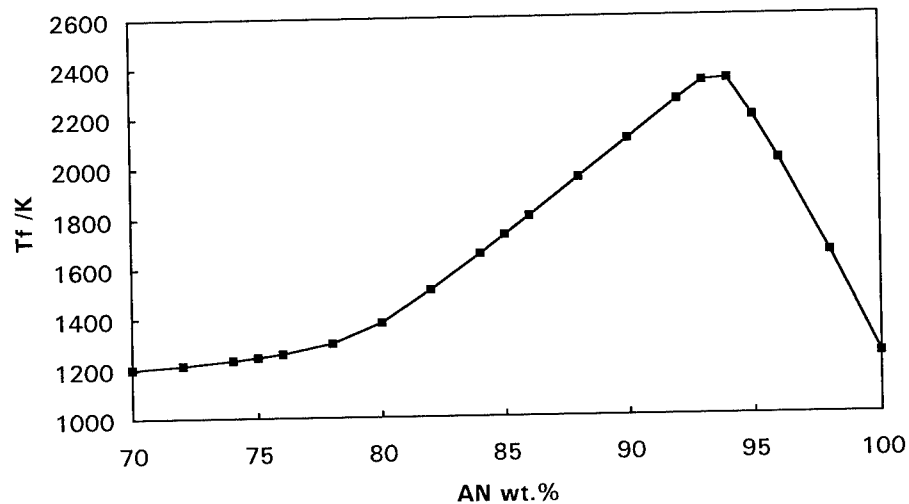


Fig. 1. Evolution of isobaric adiabatic flame temperature of AN/HTPB-IPDI propellants with AN wt.% solid loading, in a combustion chamber at 7.0 MPa.

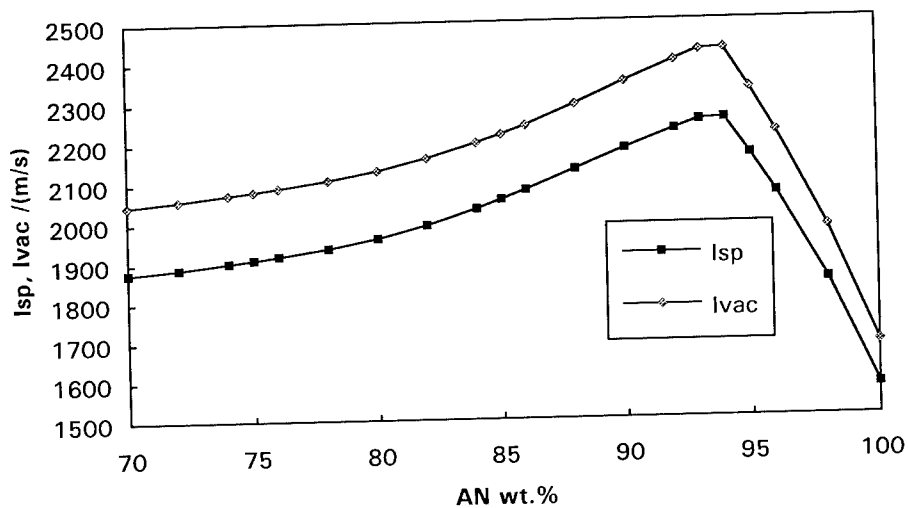


Fig. 2. Evolution of specific impulse and vacuum specific impulse of AN/HTPB-IPDI propellants with AN wt.% solid loading, after expansion from a combustion chamber at 7.0 MPa to 0.1 MPa.

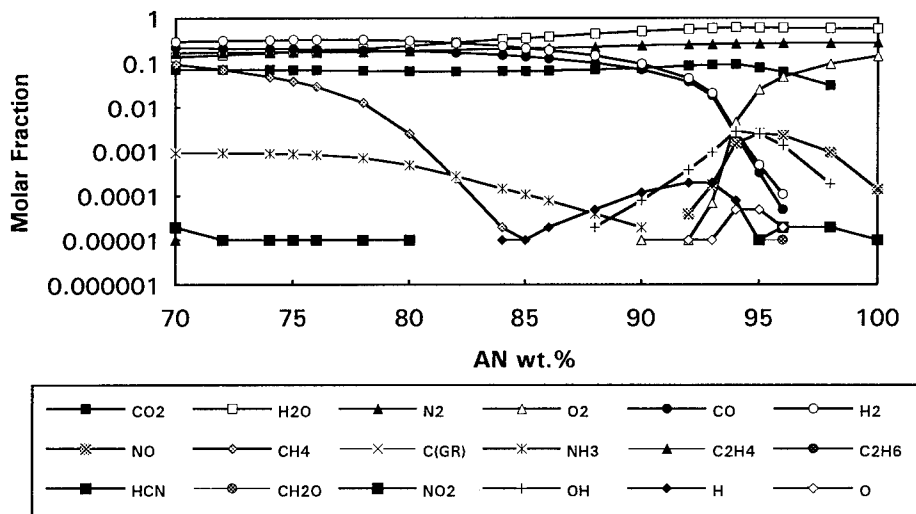


Fig. 3. Evolution of combustion products composition of AN/HTPB-IPDI propellants with AN wt.% solid loading, in a combustion chamber at 7.0 MPa.

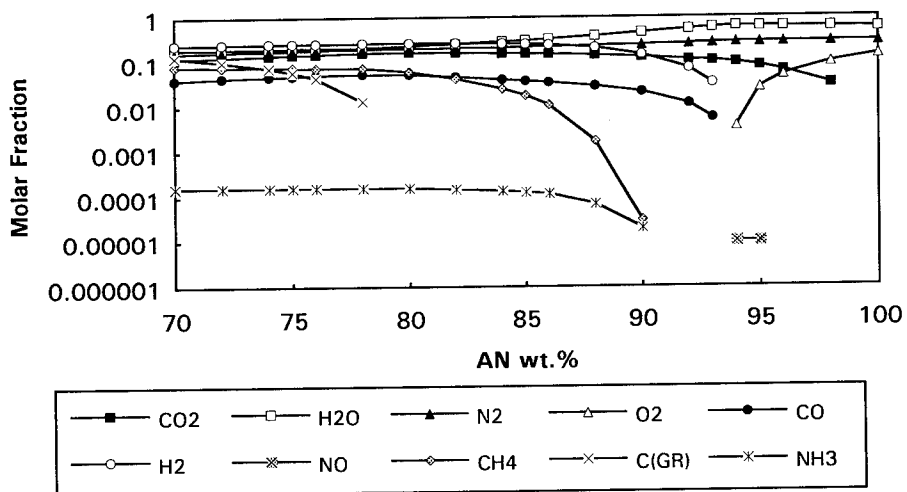


Fig. 4. Evolution of combustion products composition of AN/HTPB-IPDI propellants with AN wt.% solid loading in the nozzle exit, after expansion from a combustion chamber at 7.0 MPa to 0.1 MPa.

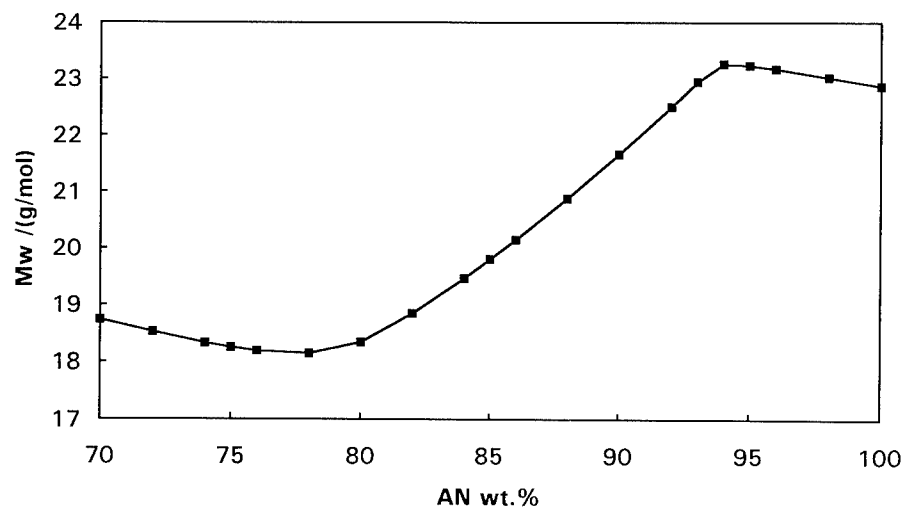


Fig. 5. Evolution of molecular weight of the combustion products of AN/HTPB-IPDI propellants with AN wt.% solid loading, in a combustion chamber at 7.0 MPa.

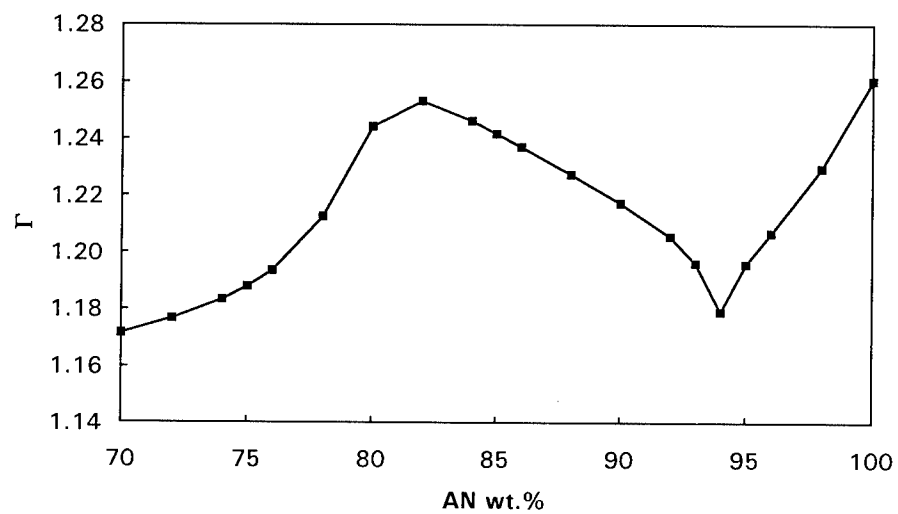


Fig. 6. Evolution of Γ of the combustion products of AN/HTPB-IPDI propellants with AN wt.% solid loading, in a combustion chamber at 7.0 MPa.

Thermal Decomposition Studies on NTO¹

Jimmie C. Oxley, James L. Smith, ZunLiang Zhou
Chemistry Department

New Mexico Institute of Mining and Technology
Socorro, New Mexico 87801

and

Robert L. McKenney
WL/MNME 2306 Perimeter Rd., Suite 9
Eglin Air Force Base, Florida 32542-5910

Abstract

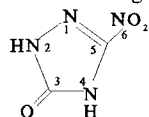
The thermal decomposition of 5-nitro-2,4-dihydro-3H-1,2,4-triazol-3-one (NTO) was examined over the temperature range 220° to 280°C using both neat NTO and NTO in aqueous and methanol solutions. The decomposition of NTO in the presence of 2,4,6-trinitrotoluene (TNT) was also examined. Activation parameters were calculated for all thermolyses. When mixtures of NTO and TNT were decomposed, the decomposition rate of both components was enhanced. Additives such as NO₂, ammonia, nitric acid, and ammonium nitrate also accelerated the decomposition of NTO and of TNT. Decomposition of deuterated NTO neat and in solution was noticeably slower than proteo-NTO, indicative of an intramolecular deuterium kinetic isotope effect (DKIE). An intermolecular DKIE was also observed when NTO was decomposed in deuterated solvent or in mixture with d₃-TNT. It was concluded that the rate determining step in at least one NTO thermolysis pathway involved hydrogen transfer to the nitro group followed by subsequent loss of HONO. This mechanism is believed to be dominate at low temperatures, while at high temperatures C-NO₂ homolysis is probably a competitive decomposition pathway.

Decomposition products from NTO thermolysis, neat, in solution, and in admixture with TNT, are reported for the first time. The condensed-phase thermolyses produced small quantities of 2,4-dihydro-3H-1,2,4-triazol-3-one (TO) and large amounts of an intractable tar for which the elemental ratio was roughly that of TO. Because TO was observed as a NTO decomposition product its thermal decomposition behavior was examined in the same fashion as that of NTO. Like NTO/TNT mixtures, TO/TNT mixtures exhibited mutual destabilization. However, unlike NTO, TO exhibited neither an inter- nor intra-molecular DKIE, and its decomposition rate was unaffected by the presence of NO₂. The elemental analysis of the TO residue differed from that of thermolyzed NTO. It was concluded that TO, while formed in the decomposition of NTO, was not an intermediate in the principal NTO decomposition pathway. Furthermore, while it appeared that NTO and TO promoted TNT decomposition by the same mechanism, hydrogen transfer to an arene nitro group, the mode by which TNT enhanced the decomposition of the two triazolone rings differed.

The kinetics and products of decomposition of eight other of triazole-like rings were examined. Thermal stability was related to ring substitution; rings with NO₂ and NH₂ substituents decomposed more rapidly at 270°C than those with O or H on carbon. The enhancement due to NO₂ gas was observed only on rings substituted with NH₂ or O groups, suggesting the carbonyl of NTO is the point subject to NO₂ attack. Hydrogen transfer to the nitro of NTO was supported by the observation that only rings substituted with either NO₂ or NH₂ exhibited an intermolecular DKIE.

Introduction

5-Nitro-2,4-dihydro-3H-1,2,4-triazol-3-one (NTO) is a candidate for an effective insensitive high explosive² and a potential bomb fill in admixture with TNT.³ NTO is a new explosive, and the literature available is sparse and contradictory. For example, Bruss et al.^{3,4} observed an intramolecular deuterium kinetic isotope effect (DKIE) of 1.67, but Burkey⁵ reported the complete absence of a DKIE. The activation energy of NTO decomposition has been reported as large as 88.0 kcal/mol³ (determined isothermally, 225°-245°C) and 77 kcal/mol⁶ or as small as 40.7 kcal/mol⁷ (using chemiluminescence to detect low levels of NO, 110°C-140°C) and 44.5 kcal/mol⁸ (monitoring the infrared stretching frequency of nitro, 195°-210°C).



NTO is unique among military high explosives in that it does not fall in the traditional classes--nitrate esters, nitramines, nor nitrobenzenes. Nitroarenes, nitramines, and nitrate esters have a common thermal decomposition mode: X-NO₂ homolysis. At temperatures over which thermal stabilities are normally examined, the trend in thermal stabilities is in line with the X-NO₂ bond dissociation energies: nitrate ester O-NO₂, 40 kcal/mol; nitramine N-NO₂, 47 kcal/mol; and nitroarene C-NO₂, 70 kcal/mol.⁹ For nitroarenes there is another common decomposition pathway--hydrogen transfer to the nitro group and subsequent loss of HONO. If NTO followed either of these traditional nitroarene decomposition pathways, the resultant radical could form 2,4-dihydro-3H-1,2,4-triazol-3-one (TO). This study attempts to clarify NTO thermal decomposition characteristics and examines the compatibility of NTO and TNT. To aid this effort other five-membered triazole-like ring systems were also examined at 270°C to determine their relative decomposition rates and products: 3-amino-5-nitro-1,2,4-triazole (ANTA); ammonium 3,5-dinitro-1,2,4-triazolate (ADNT); 3-nitro-1,2,4-triazole (NTR); 5-amino-1,2,4-triazole (ATR); 3,5-diamino-1,2,4-triazole (DAT); 5-amino-2,4-dihydro-3H-1,2,4-triazol-3-one (ATO); urazole; and 1,2,4-triazole (TRA).

Experimental Section

5-Nitro-2,4-dihydro-3H-1,2,4-triazol-3-one (NTO), 2,4,6-trinitrotoluene (TNT), and 2,4-dihydro-3H-1,2,4-triazol-3-one (TO) were received as white crystalline solids, from Eglin Air Force Base and Los Alamos National Laboratory, respectively. Synthesis of labeled compounds has been reported elsewhere.^{10,11} Samples, typically 1-2 mg, were heated isothermally in sealed capillaries tubes. After thermolysis, the soluble reaction residues were extracted with 100 uL of methanol, dimethylsulfoxide (DMSO), or water depending on their solubility. Residues from NTO, TRA, ATR, NTR, TO, DAT, ANTA, ADNT were extracted with methanol; the residue from urazole was extracted with water; and the residue of ATO was extracted with DMSO. Fraction remaining for TNT and ANTA and their mixture was determined by gas chromatography (GC) using a Varian 3600 GC equipped with an Alltech fused silica 5-BP capillary column (30 m x .32 mm i.d.) and a flame-ionization detector (FID). Quantifications of NTO, the NTO/TNT mixture, TO, urazole, ADNT, ANTA, ATR, DAT, and ATO were accomplished with a Beckman model LC-332 high performance liquid chromatograph (HPLC) equipped with an Alltech Econsphere C18 reversed-phase column, a Waters-486 tunable ultraviolet detector, and 20 uL sample loop. For NTO and the NTO/TNT mixtures, the mobile phase was 40% acetonitrile /

60% water containing 1% acetic acid. For the rest, a methanol/water (1/1) eluent was used. Typical retention times were three to four minutes with the exception of TNT which took 15 minutes; detection wavelengths varied from compound to compound: NTO 400 nm; TNT 350 nm; TO 225 nm; urazole 225 nm; ADNT 350 nm; ANTA 360 nm; ATR 210 nm; DAT 210 nm; ATO 265 nm. The NTO/TO mixture was monitored for loss of NTO only; this could be observed at 400 nm without interference of TO (at 225 nm the absorbance was due to both TO and NTO). The reaction progress of NTR, TRA and the TO/TNT mixture was analyzed directly using a Hewlett-Packard 5890A gas chromatograph equipped with a model 5971 quadrupole mass-selective detector and methyl silicone gum (HP-1, 12M x 0.2mm x 0.33um) GC column. For identification of decomposition gases a Varian 3600 GC equipped with a Supelco Porpack Q 80/100 SS (12' X 1/8") column in series across a thermal conductivity detector with a molecular sieve 13X 45/60 SS (9' X 1/8") column. Ammonia analysis was performed using a Hayesep D column (20' x 1/8"); the decomposition gases of all the triazoles were analyzed for ammonia; none was detected.

Results

Decomposition Kinetics of NTO, TNT, TO

Although the reaction was obviously autocatalytic after 50% conversion, first-order plots of the data were linear to at least 20% decomposition; therefore, first-order rate constants were calculated using only the first 20% of the curve. The activation energy and pre-exponential factor are given in Table I. Perdeutero-NTO was prepared and observed to decompose somewhat slower than the proteo-analog; a deuterium kinetic isotope effect (DKIE) of about 1.7 was calculated (Table II). To eliminate crystalline effects and to provide a medium in which radical intermediates might be trapped, thermal decompositions of NTO were performed in solution. In water or methanol (4wt%) solution, decompositions of NTO were first order (to 70% conversion), and the rates were generally faster than those of neat NTO (Table III). The decomposition of NTO was examined in the presence of other additives. Atmospheres of either NO_2 or NH_3 accelerated decomposition as did addition of nitric acid or 50 wt% ammonium nitrate or TO (Tables II and IV). Usually thermolysis was performed in sealed tubes, but at 250°C decompositions were also performed in open tubes. Though sublimation made determination of the exact rate constant difficult, first-order plots comparing the decomposition in open versus sealed tubes showed that in the open tubes first-order kinetics were followed out to 50% reacted, while in sealed tubes the reaction was notably autocatalytic after 25% reacted.

Since TO was considered a possible NTO thermolysis product, its decomposition kinetics were examined (Table I). TO decomposed considerably slower than NTO and exhibited first-order kinetics to over 70% conversion. In contrast to NTO, deuterated TO did not decompose any slower than the proteo-analog, and aqueous TO solutions (20wt%) decomposed more slowly than neat (Table V). While neither the presence of NO_2 nor NH_3 atmosphere accelerated TO decomposition, addition of TNT or nitric acid did (Table IV and V). The decomposition of TNT over the temperature range 220°C to 280°C approximated first order only to the first 20% conversion. The activation parameters (Table I) of TNT were sufficiently different from those of NTO that although at high temperatures TNT decomposed more slowly than NTO, below 240°C NTO decomposed more slowly than TNT. Decomposition of d3-TNT exhibited a primary kinetic isotope effect, as noted by a number of researchers (Table VI).^{9,11} Over the temperature range examined, TNT in methanol (4wt%) decomposed faster than neat TNT (Table III). Addition of NH_3 , NO_2 , HNO_3 or 50wt% TO accelerated TNT decomposition (Tables IV and VI).

Examination of one-to-one weight mixtures of NTO and TNT from 280°C down to 160°C indicated that each species enhanced the decomposition rate of the other (Table I). First-order plots were linear out to 70% conversion. The Arrhenius curves intersected so that, as was the case with neat NTO and TNT, the TNT in the TNT/NTO mixture decomposed more slowly above 220°C and the NTO in the mixture decomposed more slowly below that temperature (Fig. 1). This trend may continue down to storage temperatures, since typically NTO is considered a less sensitive explosive than TNT. The decomposition kinetics of each component in a methanol solution (4wt% NTO and 4wt% TNT) were only slightly faster than those of each component alone (4wt%) in methanol (Table III).

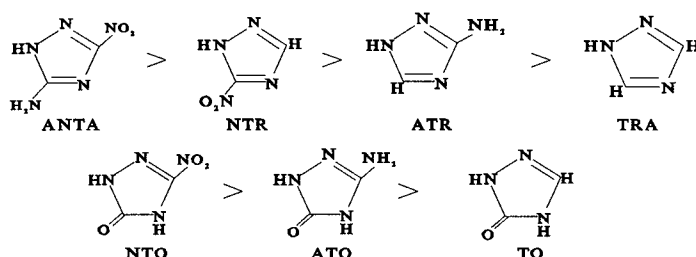
Decomposition Products of NTO, TNT, TO

Some reports cite CO₂ as the only identifiable decomposition product of NTO,⁴ whereas others⁶ have observed nitrogen-containing gases. Over the temperature range 240° to 280°C, GC analysis of thermolyzed NTO samples indicated a decomposition gas composition of NO 8%, N₂ 43%, N₂O 6%, CO 6%, and CO₂ 37%. The major condensed-phase product of NTO decomposition was an organic tar which was insoluble in even the most solvating solvents (water, methanol, ethanol, acetonitrile, and THF). The only form of analysis which was performed on this material was elemental analysis and infrared spectroscopy. Results of the former appear in Table VII. When NTO was heated to about 20% conversion (260°C, 2 min.), a small amount of the condensed-phase product was soluble. Using authentic samples and GC/MS analysis, we identified the soluble products as primarily TO with a small amount of 1,2,4-triazole. When NTO was heated one-to-one mass ratio with TNT, the products detected were similar to those found in neat NTO and neat TNT decompositions. TO and triazole produced in the decomposition of NTO were still among the decomposition products as were 2,4- and 2,6-dinitrotoluene, trinitrobenzene, and aminodinitrobenzoic acid, formed in the decomposition of neat TNT. Only thermolyses in methanol drastically affected the NTO decomposition products.

Decomposition of NTO in methanol (4wt%) produced a number of products, detectable by GC/MS, which appeared to originate from NTO (Tables VIII and IX). Based on the observed mass to charge ratio (m/e) for products of NTO, ¹⁵N(4)NTO, and ¹⁵N(6) in methanol (Table VIII) and of NTO in d4-methanol versus h4-methanol (Table IX), the following compositions were assigned: C₂N₃H₃(CH₃OH)₂ [A, 133 m/e]; B [253 m/e]; C₂N₃H₃O(CH₃OH) [C, 117 m/e]; D [188 m/e]; and C₂N₃(NO₂)(CH₃OH) [E and F, 144 m/e]. When TO was heated at 270°C for 10 minutes, 1,2,4-triazole (TRA) was found to be the only tractable condensed-phase product. The insoluble residue from TO decomposition was analyzed by elemental analysis; results are in Table VII. Typically TNT mixed with NTO produced the same principal decomposition products that it did neat.^{12,14} 1,3,5-tri-nitrobenzene, 2,6-dinitrotoluene, 2-amino-4,6-dinitrobenzoic acid, and 2,4-dinitrotoluene. Thermolysis of NTO/TNT mixtures formed minor amounts of products not observed in thermolyses of the neat materials; these have not been identified.

Decomposition Kinetics and Products of Other Triazoles

The decomposition kinetics and products of eight triazole-related ring compounds were examined. Results are shown in Table X where the compounds are arranged in rough order of their thermal stability. We observed that certain ring substituents appeared to enhance the decomposition; rings where a NO₂ was attached to carbon decomposed faster than those with NH₂. Those with NH₂ attached to carbon generally decomposed faster than those with O, but it should be noted that C=O changed the ring from XC=N₂H(X)C=N to XC=N₂H(O)CNH.



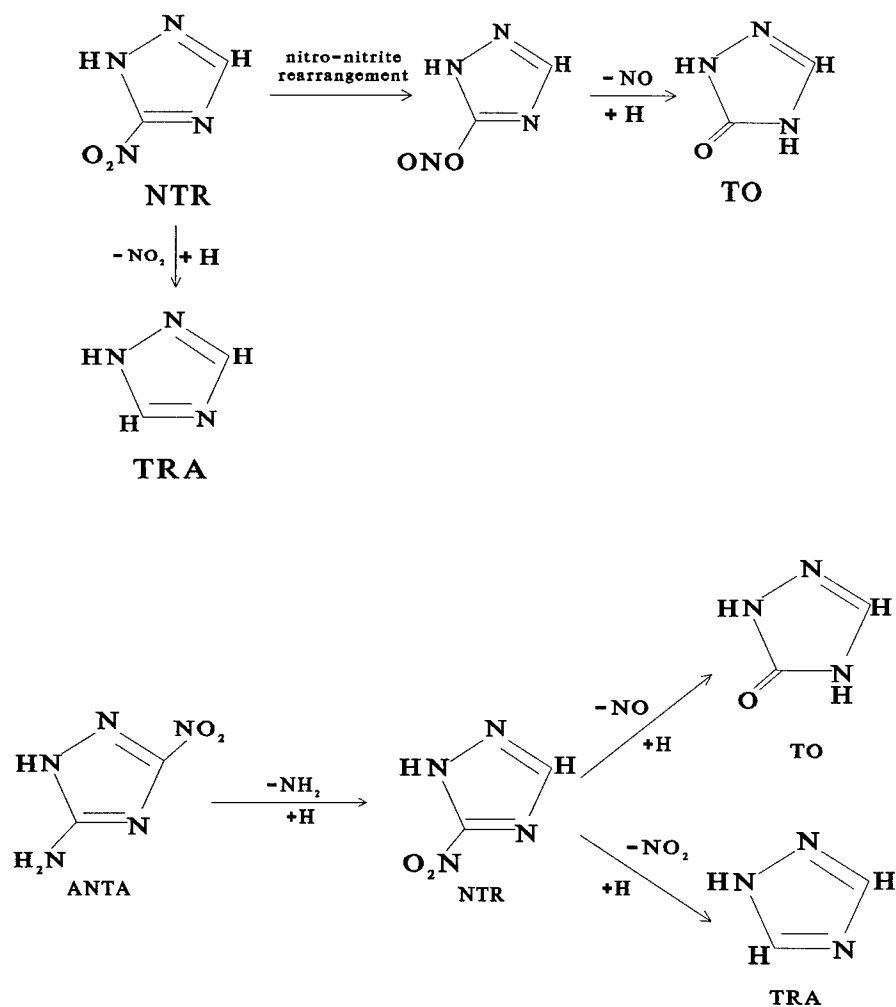
There were exceptions undoubtedly resulting from the fact that the degree of unsaturation is not the same in all the rings. The salt ammonium dinitrotriazolate, which has obvious aromatic character, decomposed more slowly than ANTA, even though it possessed two nitro groups compared to one nitro and one amino on ANTA. ATR decomposed much faster than would have been predicted. We expected it to decompose more slowly than DAT since it was observed in the decomposition of DAT, but its rate constant was consistently higher than that of DAT.

Since we had observed that the presence of NO_2 accelerated the decomposition rate of NTO but had no effect on that of TO, we examined the effect of NO_2 on the other ring compounds. For some triazoles, the decomposition rate was accelerated; for others there was no effect. Only rings with either NH_2 or O attached to carbon were affected by the presence of an NO_2 atmosphere. Similarly, some of the compounds, like NTO, exhibited a DKIE when decomposed in D_2O versus H_2O , whereas others, like TO, were unaffected (Table X). Only the rings with NO_2 or NH_2 groups exhibited an intermolecular DKIE.

The gaseous thermal decomposition products of the various triazole-like compound were readily identified by GC (Table X). Formation of large quantities of gas correlated with the presence of NO_2 groups, as the source of oxygen. ATR, DAT, and TRA, which contained no oxygen, produced only small quantities of N_2 gas. N_2 was the major nitrogen-containing gas for all the triazole compounds examined. In fact, N_2O was only observed in the decomposition of rings with NO_2 substituents (ANTA, ADNT, NTR, and NTO). Carbon dioxide was the major carbon-containing decomposition gas. The soluble condensed-phase decomposition products were identified by GC/MS. Urea was the only product identified from the decomposition of urazole.

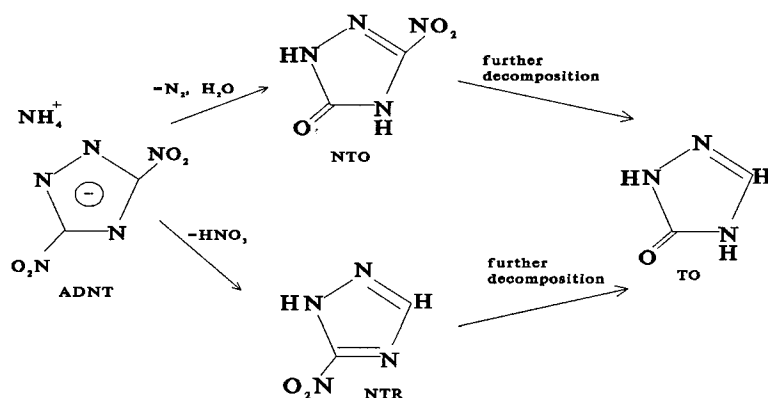
NTR was found to form TO, suggesting loss of NO through a nitro/nitrite rearrangement. TRA was also formed, presumably via C- NO_2 homolysis in NTR, although TO, itself, forms TRA during thermolysis.

The decomposition of ANTA produced NTR, TRA, and TO. TRA and TO may have been formed by the subsequent decomposition of NTR. Loss of NH_2 from ANTA could form NTR. The observation that rings with NH_2 exhibited an intermolecular DKIE suggest hydrogen addition might result in direct NH_3 loss. It is curious that in the decomposition of ANTA NTR (resulting from loss of NH_2 but with NO_2 remaining) is observed, while ATR (resulting from loss of NO_2 but with NH_2 remaining) is not. It is especially odd in light of the fact that comparison of their rate constants at 270°C showed NTR to decompose about four times faster than ATR.



Direct NH₂ loss appears to be operative in the thermolysis of DAT where both ATR and TRA were observed. The rate constant found for ATR (Table X) was about twice that of DAT; as discussed above, this is opposite to the expected result. This and the fact that ATR was formed in the decomposition of DAT questions the validity of this value.

ADNT formed NTO and NTR. The former could result from nitro/nitrite rearrangement followed by NO loss, possibly assisted by interaction with ammonium ion. The latter by hydrogen transfer to NO₂, from ammonium, and subsequent HONO loss. TO, a decomposition product of both NTO and NTR, was observed among the ADNT thermolysis products.



Decomposition Kinetics

The DKIE calculated for NTO by this work (1.7 at 260°C) and that of others (1.67)³ is large enough to be primary, but from these experiments alone the effect cannot be assigned as intra- or intermolecular or both. However, the presence of a DKIE when NTO was thermolyzed in CD₃OD or D₂O is definitive for intermolecular hydrogen transfer. Indeed, EPR observations³ of NTO in acetone suggested the formation of hydroxy 4-oxo-2,3,4-triazolyl-nitroxide. But, the observation that d2-NTO exhibited a DKIE in dilute (4wt%) solution indicates intramolecular

hydrogen transfer; therefore, both are operative in the thermolysis of neat NTO. Enhancement of intermolecular hydrogen transfer would explain the accelerative effect of aqueous acid on NTO decomposition. Enhanced decomposition rates were also noted when NTO was decomposed under ammonia. This is in line with reports that NTO salts are less thermally stable than NTO.¹³ Calculation of DKIEs comparing TNT/d3-TNT, TNT in methanol or d4-methanol, and d3-TNT or TNT in methanol confirm previous findings that TNT was susceptible to both intra- and intermolecular hydrogen transfer (Table VI).^{12,14}

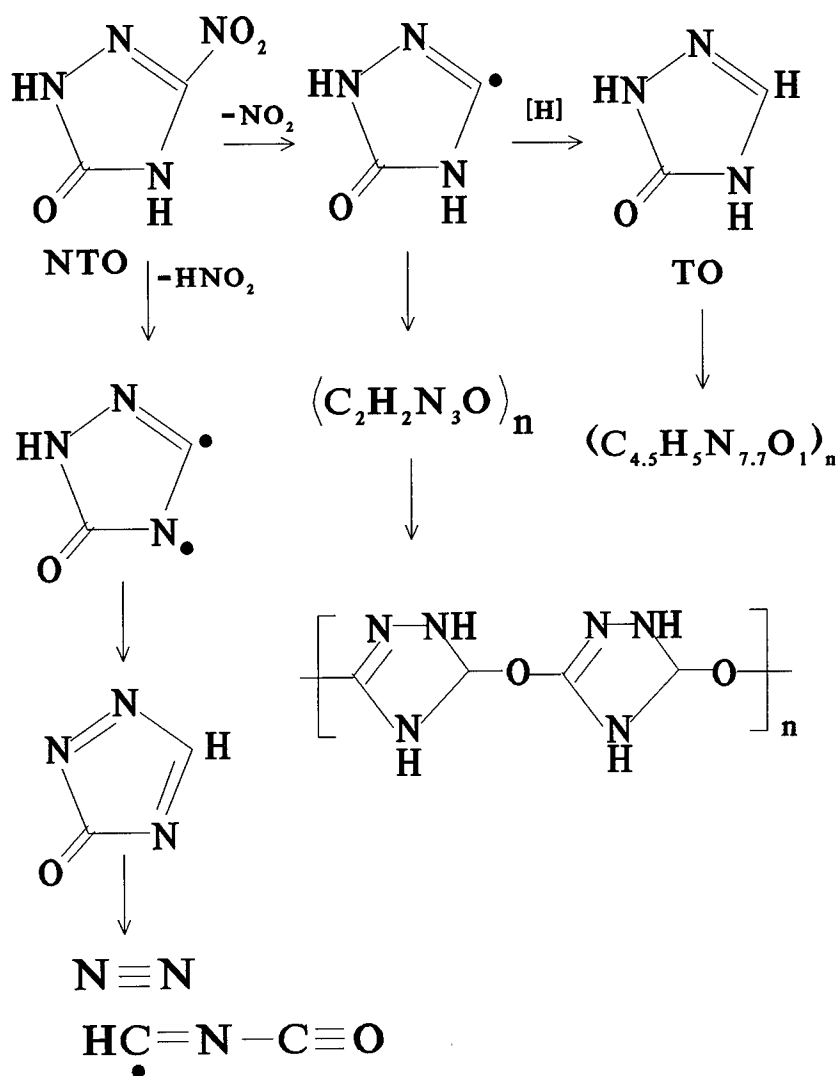
The combination of NTO and TNT was observed to be mutually destabilizing. Independent experiments showed that the decomposition of each species could be enhanced by addition of NO₂, ammonia, or protonic species; a detailed discussion of the effect of these additives on TNT is presented in reference 12. It seems likely that TNT could affect NTO decomposition by acting as a source of hydrogen or of NO₂ or HONO. The combination of TO and TNT was also mutually destabilizing. It was initially thought direct comparison of the decomposition of NTO and TO might be possible; however, neither kinetic results nor product analysis appear to support that hypothesis. Unlike NTO, the decomposition of TO exhibited neither an inter- nor intra-molecular DKIE (Table V). While TNT could accelerate the decomposition of NTO by acting as a source of hydrogen or of NO₂, neither of these mechanisms can explain the enhancement of TO decomposition. Since the only additive observed to accelerate TO decomposition was acid, generation of HONO by hydrogen transfer to a nitro group of TNT is postulated to explain the destabilizing effect of TNT on TO. The arguments used to explain the accelerative effect of TNT on NTO (source of H or NO₂) might also be used to explain the accelerative effect of NTO on TNT.

Decomposition Products

Since initial mass spectrometric analysis of NTO, showed strong peaks of m/e 85, 84, and 83, TO (molecular weight 85 g/mol) was considered a possible NTO decomposition product.¹¹

Furthermore, it seemed reasonable that if the decomposition of NTO proceeded through C-NO₂ homolysis, capping of the carbon radical with hydrogen from a neighboring species, would lead to TO. Indeed, extraction of the NTO residue after thermolysis revealed small amounts of TO, as well as TRA, had been formed. Since TO thermolysis also formed TRA, we cannot say whether TRA is a primary or a secondary NTO decomposition product. The decomposition of neat NTO, TNT, or their one-to-one mixture formed a residue which was insoluble in even the most polar solvents. The residue was analyzed by infrared spectroscopy (IR) and sent to a commercial laboratory for elemental analysis. The IR spectrum of the NTO residue showed the absence of the NTO stretching frequencies at 1719 cm⁻¹ (carbonyl) and at 1544 cm⁻¹ (nitro); otherwise, the spectrum was undifferentiated from that of the TO residue. Analyses indicated an elemental ratio of C₂H₂N₃O (Table VII), a formula consistent with "polymerized TO". However, we do not suggest that the ring structure is necessarily maintained in the polymer. We do know TO is not a direct intermediate in the formation of this residue. Independent decomposition of TO resulted in a residue of somewhat different elemental composition (Table VII): C_{4.5}H₅N_{7.7}O.

Thermolysis of TNT produced a number of decomposition products:^{12,14} 1,3,5-trinitrobenzene, 2,6-dinitrotoluene, 2-amino-4,6-dinitrobenzoic acid, and 2,4-dinitrotoluene. When TNT and NTO were thermolyzed in a one-to-one mixture, the principal products were those observed in the neat decomposition of each species. The same observation was made for the thermolysis of TNT/TO mixtures.



Conclusions

Thermal decomposition of NTO is speculated to proceed through C-N homolysis either by direct homolysis of C-NO₂, important at high temperature, or by initial transfer of hydrogen and subsequent C-NO₂H cleavage. That NTO is susceptible to hydrogen transfer is evidenced by the presence of both an intra- and an inter-molecular DKIE. The fact that the thermolysis of TO, which lacks a nitro group, does not evidence any type of DKIE suggests that NO₂ is the site accepting hydrogen on the NTO molecule. Examination of the decomposition of eight other

triazole-like compounds also supports this conclusion. The autocatalytic nature of the NTO decomposition is attributed to its generation of NO_2 during decomposition. Decomposition of NTO in solution or in open thermolysis tubes and decomposition of TO are strictly first order. NO_2 is thought to interact with the NTO carbonyl since a survey of ten triazole-like rings showed only those with carbonyl or a NH_2 substituent experienced enhanced decomposition in the presence of NO_2 . Decomposition of NTO results in formation of a certain amount of TO, presumably by hydrogen abstraction to fill the site vacated by NO_2 . The major condensed-phase NTO thermolysis product is a polymeric substance with a formula consistent with polymerization of the radical species remaining after NO_2 loss. TO thermolysis results in formation of 1,2,4-triazole and another polymeric residue, different from that NTO produces. TNT stimulates thermal decomposition of both NTO and TO. It is speculated that the ability of the methyl group of TNT to act as a source of H accelerates NTO decomposition, while it is the ability of TNT to generate HONO that adversely affects TO decomposition. Both NTO and TO are thought to destabilize TNT by hydrogen donation to an arene nitro group.

Acknowledgments

The authors thank the Armament Division of Eglin Air Force Base for funding through the Office of Naval Research. We also thank Ms. Hong Ye for her assistance.

References

1. Taken in part from the Master's Thesis of Z. Zhou, New Mexico Tech, May, 1994.
2. Lee, K.-Y.; Coburn, M.D. "3-Nitro-1,2,4-Triazol-5-One, A Less Sensitive Explosive," U.S. Patent 4,733,610, 1988.
Lee, K.Y.; Chapman, L.B., Coburn, M.D. *J. Energ. Materials*, **1987**, 5, 27.
Lee, K.-Y.; Stinecipher, M. *Propel., Explos., Pyrotech.*, **1989**, 14, 241-244.
Beard B.C.; Sharma, J. *J. Energ. Materials*, **1989**, 7(3), 181.
3. Menapace, J.A.; Marlin, J.; Bruss D.; Dascher, R. *J. Phys. Chem.*, **1991**, 95, 5509-5517.
4. Bruss, D.R.; Menapace, J.A. "Kinetic Studies on the Condensed Phase Thermal Decomposition of NTO" Am. Chem. Soc., 19 NE Reg Meet, Albany, June 1989.
5. Burkey, T.J.; Shackelford, S.A. "Thermal Decomposition of NTO and NTO/TNT Mixtures" Report on contract F49620-88-C-0053, 1992.
6. Rothgery, E.F.; Audette, D.E.; Wedlich, R.; Csejka, D. *Thermochim Acta*, **1991**, 185, 235.
7. Ostmark, H. "Thermal Decomposition of NTO" FOA Rep. D-201782.3, Nov. 1991.
8. Prabhakaran, K.V.; Naidu, S.R.; Kurian, E.M. "Spectroscopic and Thermal Analysis Studies on 3-Nitro-1,2,4-Triazole-5-one (NTO), preprint *Thermochim Acta*, 1993.
9. Melius, Carl F. Proceedings, *25th JANNAF Combust. Meetg.*, Huntsville, AL, **1988**.
10. Oxley, J.C.; Smith, J.L.; Zhou, Z. to be published *J. Phys. Chem.* May-June 1995.
11. Oxley, J.C.; Coburn, M.D.; Ott, D.G.; Smith, J.L.; Yeager, K.E. to be published *J. Energ. Materials*, Vol 13, No.1, 1995.
12. Oxley, J.C.; Smith, J.L.; Wang, W. "Compatibility of Ammonium Nitrate with Monomolecular Explosives Part II: Nitroarenes" *J. Phys. Chem.* **1994**, 89, 3901-3907.
13. Xie, Y.; Hu, R.; Yang, C.; Feng, G.; Zhou, J. *Propel, Explo, Pyrotech.*, **1992**, 17, 298-302.
Xie, Y.; Hu, R.; Wang, X.; Fu, X.; Zhu, C. *Thermochim Acta*, **1991**, 189, 283-296.
14. Oxley, J.C.; Smith, J.L.; Wang, J.; Ye, H.; Feng, H. "The 10th Intrnl Detonation Symposium," Boston, MA; July 1993.
Oxley, J.C.; Smith, J.L.; Ye, H. to be published *J. Phys. Chem.* May-June 1995.

Table I
Rate Constants of Neat NTO, TNT, TO and NTO/TNT One to One Mixtures

°C	NTO	NTO/TNT	TNT/NTO	TNT	TO
160		7.63E-07	1.37E-06		
180		4.28E-06	7.26E-06		
200		2.04E-05	3.20E-05		
220	2.85E-06	1.42E-04	1.10E-04	1.14E-05	9.93E-06
220	3.23E-06				
240	9.90E-05	1.73E-03	3.90E-04	4.76E-05	5.07E-05
240	8.72E-05				
250	3.19E-04	7.13E-03	5.70E-04	9.07E-05	
260	1.92E-03	1.32E-02	9.30E-04	2.32E-04	1.82E-04
260	1.84E-03			1.52E-04	
260	2.44E-03				
270	5.84E-03	3.99E-02	1.86E-03	6.12E-04	3.67E-04
270	5.75E-03	3.09E-02	1.82E-03	4.01E-04	
280	1.58E-02	7.06E-02	3.82E-03	1.22E-03	6.96E-04
280	1.62E-02				
Ea (kcal/mol)	78.6	47.7	30.4	41.6	46.5
A (sec ⁻¹)	2.53E+29	4.56E+17	3.34E+09	2.60E+13	4.10E+15
R ²	0.99	0.99	1.00	0.99	0.99

Table II
Rate Constants Reflecting Deuterium Isotope and Other Effects
NTO Thermolyses

°C	NTO	d ₂ -NTO	DKIE
250	3.19E-04	2.20E-04	1.45
260	2.07E-03	1.23E-03	1.68

NTO Thermolyses at 270°C

Compound	Rate Constant (sec ⁻¹)	DKIE or Factor*
NTO	5.84E-03	
NTO/CH ₃ OH	3.92E-03	0.67*
d ₂ -NTO/CH ₃ OH	2.79E-03	1.41
NTO/CD ₃ OD	2.98E-03	1.32
NTO/HOH	1.43E-02	2.4*
d ₂ -NTO/HOH	7.43E-03	1.92
NTO/DOD	6.71E-03	2.13
NTO/TNT	3.54E-02	6.1*
d ₂ -NTO/TNT	1.71E-02	2.07
NTO/d ₃ -TNT	2.77E-02	1.28
d ₂ -NTO/d ₃ -TNT	1.44E-02	2.46
NTO/TO	5.81E-02	10*
NTO/d ₂ -TO	5.50E-02	1.06
d ₂ -NTO/TO	2.58E-02	2.25

* indicates comparison to NTO without additive

Table III Rate Constants of NTO, TNT and One to One NTO/TNT Mixtures in Solution

°C	4% Methanol Solutions				4% Aqueous
	NTO	NTO/TNT	TNT/NTO	TNT	NTO
240	5.10E-04	7.97E-04	2.45E-04	1.38E-04	1.02E-03
240	4.30E-04				
250	8.40E-04	1.16E-03	3.72E-04	2.16E-04	2.46E-03
250	6.20E-04				
260	2.04E-03	1.74E-03	6.80E-04	3.50E-04	6.08E-03
260	2.78E-03				
260	3.27E-03				
270	3.41E-03	2.55E-03	1.17E-03	6.10E-04	1.43E-02
270	3.94E-03				
270	4.42E-03				
280	5.64E-03	3.97E-03	2.12E-03	1.11E-03	
280	6.27E-03			1.71E-03	
Ea (kcal/mol)	38.4	22.5	30.7	32.8	48.8
A (sec ⁻¹)	1.05E+13	3.06E+06	2.85E+09	1.19E+10	6.52E+17
R ²	0.93	1.00	0.99	0.96	1.00

Table IV
Effect of Additives on Rate Constants (sec⁻¹)

Additives	NO ₂	NH ₃	HNO ₃	NH ₄ NO ₃
NTO	2.07E-03	9.31E-05	3.79E-04	3.04E-06
NTO + additive	2.09E-02	6.98E-02	5.12E-03	2.03E-01
Factor	10.1	750	13.5	66776
Temperature (°C)	260	240	250	220
TNT	5.07E-04	1.92E-04	1.92E-04	1.92E-04
TNT + additive	2.93E-03	4.59E-03	5.98E-04	1.28E-03
Factor	5.78	23.9	3.11	6.67
Temperature (°C)	270	260	260	260
TO	3.67E-04	6.96E-04	6.96E-04	
TO + additive	4.31E-04	6.14E-04	4.13E-03	
Factor	1.17	0.88	5.93	
Temperature (°C)	270	280	280	

Table V
Rate Constants Reflecting Deuterium Isotope and Other Effects
TO Thermolyses at 270°C

Compound	Rate Constant (sec ⁻¹)	DKIE or Factor*
TO	3.67E-04	
d ₂ -TO	3.41E-04	1.1*
TO/HOH	2.98E-05	0.08*
TO/DOD	2.90E-05	1.03
TO/TNT	1.41E-03	3.8*
d ₂ -TO/TNT	1.37E-03	1.03
TO/d ₃ -TNT	1.31E-03	1.08

* indicates comparison to neat TO without additive

Table VI
Rate Constants Reflecting Deuterium Isotope and Other Effects

TNT Thermolyses at 270°C		
Compound	Rate Constant (sec ⁻¹)	DKIE or Factor*
TNT	5.07E-04	
TNT/NTO	1.84E-03	3.6*
d ₃ -TNT/NTO	1.15E-03	1.60
TNT/d ₂ -NTO	1.49E-03	1.23
d ₃ -TNT/d ₂ -NTO	1.06E-03	1.74
TNT/TO	3.99E-03	7.9*
TNT/d ₂ -TO	3.24E-03	1.23
d ₃ -TNT/d ₂ -TO	2.07E-03	1.93
TNT Thermolyses at 280°C		
TNT	1.22E-03	
d ₃ -TNT	7.06E-04	1.73
TNT/CH ₃ OH	1.41E-03	
d ₃ -TNT/CH ₃ OH	8.10E-04	1.74
TNT/CD ₃ OD	8.60E-04	1.64

* indicates comparison to neat TNT without additive

Table VII
Mole Fraction Ratios of NTO and TO Thermolysis Residues

NTO					TO				
C	H	N	O	N/C	C	H	N	O	N/C
2.76	3.25	4.21	1.00	1.53	4.55	5.04	7.77	1.00	1.71
2.73	3.28	4.22	1.00	1.55	5.52	4.91	7.80	1.00	1.73
1.84	1.62	3.01	1.00	1.64	4.47	5.31	7.63	1.00	1.71
1.84	1.73	3.00	1.00	1.63	4.59	5.42	7.87	1.00	1.72

Table VIII: GC/MS Analysis
 NTO & N15-Labeled Analogues after 3 Minutes at 260°C in Methanol (4%)

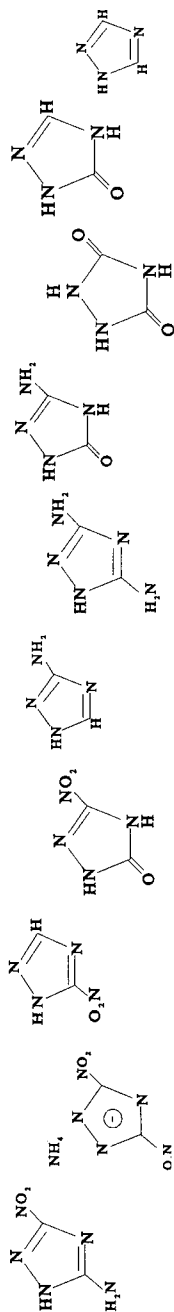
RT	A	N(4)	N(6)	C	N(4)	N(6)	D	N(4)	N(6)	E	N(4)	N(6)	F	N(4)	N(6)
	5.1				7.5			10.5			11.2			12.5	
	L	L	L	S	T	T	S	M	S	L	M	L	S	S	T
							188	189	189						
							158	159	159						
				148			157	158	144	145	145*	144	145	145*	
133	134	133					127	128	128	127	128	128	*		
					118	117*							128		
				117	116*	117									
				116*	116	116*									
							111	113	112	114		115	115	115	115
											114	114			
103				104									114		
102	104	103*													
	103	102	89				98			97	97			97	
			73			89	83	84		85	86	86	98	86	85
70	76	75											85		
	71	70					70	70	69	69	70	70		70	69
59	60		59										69		
58	59	59		59	59*						59	58		59	58
45		58					56	56	56	53	53	53		55	54
44	46	45	44	46	45	45*	45*	45*			46	47	54	45	44
32	45	44				44				44		44	44		
	32	30	32	28	30	32	30	30	30	30	30	31		30	28
													30		

RT = Retention Time (minutes) * indicates largest peak

Table IX: GC/MS Examination of NTO Decomposition Products
 NTO Heated in h4-Methanol or d4-Methanol at 270°C for 50 Seconds

RT	A	B	C	D	E	F
	h4	d4	h4	d4	h4	d4
	5.07	5.3	7.1	10.3	11.4	12.2
	L	T	T	S	M	M
			253*	259*		
			223	227		
					188	196
					156	158
					164	164
					158	144*
					148*	148
						174
						144
						180
133	140	119	120	117	120	128
104	108	104	106	116	119	112
103	106					
102	105				94	
75	80		86		83	86
70	70				73	74
59*	62*		62		62*	55
58	50			59*	50	50*
45	46		46	44	44	45
44	44	44	44	32	32	45*
32	30		30	28	28	30
		28	28		28	28

RT = Retention Time (minutes) * indicates largest peak



	ANTA	ADNT	NTR	NTO	ATR	DAT	ATO	Urazole	TO	TRA
Rate Constants (1/sec) at 270°C x 10 ³										
neat	73.9	16.3	9.6	8.87	1.65	0.71	0.026	0.47	0.38	0.33
+ NO ₂	252	16.1	10.4	21	6.4	4.7	0.79	1.9	0.43	0.33
DKIE	1.7	2.0	1.5	2.1	1.7	1.4	insoluble	none	none	none
(H ₂ O/D ₂ O)										
Thermolysis Residue Insoluble in Methanol										
Amount	lots	tiny	mod	lots	mod	lots	mod	none	tiny	tiny
Color	brown	cream	white	brown	yellow	white	tan		grey	
Gases after 99% Decomposition at 270°C in uL/mg										
NO			95	47						
N ₂	224	315	61	257	74	16	19	90	11	6
N ₂ O	2	14	7	36	0	0	0	0	0	0
CO	12	8	0	36	0	0	2	7	1	0
CO ₂	68	168	56	219	0	0	69	165	14	0
uL/mg	306	505	219	595	74	16	90	262	26	6

VISCOUS ENERGETIC LIQUID EXPLOSIVE FORMULATIONS SENSITIZED WITH GLASS MICROBALLOONS. III. ANALYSIS OF THE DETONATION DATA

James L. Austing and Allen J. Tulis

IIT Reserach Institute
Chicago, Illinois 60616 USA

Abstract

The complete detonation state data for viscous energetic liquid explosive mixtures have been analyzed to ascertain the degree of conformity to correlations that are generally applicable to ideally-detonating organic high explosives. The viscous energetic liquids were formulated from nitrocellulose, an organic nitrate ester liquid explosive, and fine RDX powder. Adequate sensitivity for initiation by a cloud of detonating dispersed explosive powder was achieved by incorporation of glass microballoons.

For conventional explosives, the detonation velocity is dependent on chemical composition and initial density, but for a given explosive is a direct linear function of density. The Chapman-Jouguet density and the adiabatic exponent, on the other hand, are *independent* of composition and are dependent *only* on the initial density. In the case of the viscous energetic liquids, the detonation velocity generally exhibited such a linear increase with density, but two of the charges with lesser amounts and smaller sizes of microballoons displayed velocities that were notably under the linear prediction. The Chapman-Jouguet density also increased in a linear relationship with density, but on the average was about 6 percent less than predicted for conventional explosives; this was attributed to measured pressures that were generally lower than expected. As a consequence, the scatter in the adiabatic exponent data was extreme, and on the average the adiabatic exponent was 40 percent higher than that for conventional explosives. It is not known whether these discrepancies were due to a systematic error in the measurements or to a phenomenon associated with the use of microballoons.

The results of the above analyses suggest that the detonation of the viscous energetic liquids did not propagate in accordance with those principles that govern classical, ideal detonation in conventional organic high explosives. This possibly can be attributed to the use of microballoons. The exact mechanism which was operating, however, is not clear at this time.

1. Introduction

The major thrust of the present effort was an investigation of liquid explosive mixtures that can be initiated by a detonating cloud of dispersed explosive powder. Such sensitivity has been achieved by incorporation of glass microballoons directly into the liquid formulation. We have termed these mixtures "*viscous* energetic liquids", because rather high viscosities were

required in order that the mixtures could be applied to essentially vertical surfaces without sagging.

The initial stages of the investigation were reported in two parts at the Twentieth International Pyrotechnics Seminar. The First Part (Austing et al., 1994b) surveyed the appropriate background relative to the use of microballoons, and described the formulation of the viscous energetic liquids and qualitative experiments to establish the initiation criteria. The Second Part (Austing et al., 1994a) was concerned with complete detonation state measurements on selected viscous energetic liquids, and with quantitative verification that these liquids could be initiated by the detonating cloud and subsequently propagate detonations as condensed explosives.

The present manuscript comprises the Third Part of the investigation, and is concerned with mathematical analyses of the complete detonation state data. In the balance of this manuscript, the previous portions of the investigation will be referred to as Part I and Part II, respectively.

2. Background

A considerable amount of activity concerning the incorporation of microballoons into emulsion and liquid explosive formulations has been reported in the open literature. In most of the applications, the objective has been to stabilize the detonation and to decrease the failure diameter (Chaudhri et al., 1993; Presles et al., 1989; and Yoshida et al., 1985). An alternative objective was to alter the shock sensitivity of the explosive; as a consequence, the shock initiation of liquid explosives containing microballoons has been modeled theoretically (Khasainov et al., 1993) and investigated experimentally (Gois et al., 1993).

The above investigators have stressed the importance of microballoon concentration and particle size in achieving their objectives; thus, Lee and Persson (1990) separated the fractured microballoons from the remainder of the lot. Chaudhri et al. showed that, for charges of a given density and of a diameter less than 25 mm, higher detonation velocity was achieved by use of *smaller* diameter microballoons; such charges had a smaller failure diameter. On the other hand, when the charge was greater than 50-mm diameter, use of *larger* size microballoons resulted in higher detonation velocities. These

observations are for a given weight fraction of microballoons, because Gois et al. showed that the detonation velocity decreases linearly with an increase in the microballoon concentration. These results are not necessarily in agreement with the data generated in Part II, which will be discussed in the next Section of this manuscript.

Alymova et al. (1994) and Lee et al. (1989) included experimental derivation of the unreacted shock Hugoniot for emulsion explosives as part of their investigations, in addition to detonation stability measurements. Alymova et al. utilized plastic microballoons in lieu of the glass variety in their formulations; however, the advantages and disadvantages of making this substitution were not discussed.

While an extensive amount of data concerning the detonation velocity of microballoon-sensitized explosives has been reported, very little data on the measurement of detonation pressure of these explosives has appeared. Granholm (1991) adapted a simplified manganin gauge technique and reported detonation pressures of nitromethane and several emulsion explosives. However, his paper did not include the detonation velocities, and thus analysis of his data in the manner discussed in this manuscript was not possible.

The viscous energetic liquids evaluated in the present program were formulated from an industrial grade nitrocellulose, an organic nitrate ester (BTTN, DEGDN, or TEGDN), and fine RDX powder, in proportions to achieve such viscosity that the mixtures did not sag when applied to a vertical surface. Adequate sensitivity for initiation by a detonating dispersed explosive cloud was achieved by incorporation of glass microballoons. The complete procedure for formulating the viscous energetic liquids is described in Part I. Table 1 specifies the composition of the viscous energetic liquids of concern in this manuscript, and the weight fraction and particle size of the microballoons. The final column tabulates the density of each mixture, which was calculated from the liquid or crystal density of each ingredient and the measured bulk density of the microballoons. The densities in Table 1 are slightly higher than those quoted previously, because here a correction has been applied to account for the approximately 26-percent interstitial voids in the bulk microballoons.

Table 1. Formulation Data for the Viscous Energetic Liquids^(a)

Liquid No.	Org. Nitrate Ester Type	Weight Fraction			Microballoon		Density (Mg/m ³)
		NC	O.N.E.	RDX	Weight Fraction	Particle Size (μm)	
34C	BTTN	0.03	0.503	0.462	0.005	88/63	1.524
35A	DEGDN	0.02	0.388	0.582	0.010	149/105	1.401
35B		0.02	0.389	0.583	0.0075	105/88	1.441
35C		0.02	0.390	0.585	0.005	88/63	1.493
35E		0.02	0.386	0.579	0.015	149/105	1.316
36E	TEGDN	0.02	0.386	0.579	0.015	149/105	1.297
36F		0.02	0.384	0.576	0.020	149/105	1.224

- (a) O.N.E. = Organic nitrate ester.
 BTTN = Butanetriol trinitrate.
 DEGDN = Diethylene glycol dinitrate.
 TEGDN = Triethylene glycol dinitrate.
 RDX = Class 5 RDX, 22-μm average particle size.
 NC = Aqualon nitrocellulose, Grade RS-18-25-cp.

3. Analysis of the Detonation State

There are two premises for the analyses that will be discussed in this Section. Both premises are based on observations of the performance of ideally-detonating high explosives:

1. The detonation velocity is determined by the chemical composition and density of the explosive. For a given explosive, the detonation velocity is a direct linear function of the density.
2. By way of contrast, the Chapman-Jouguet (CJ) density and the adiabatic exponent are independent of chemical composition and are *solely* a function of the initial density.

As a consequence, it was of interest to ascertain whether the viscous energetic liquids, which were formulated from conventional organic explosive compounds, would adhere to the above principles, and whether the presence of the microballoons would cause deviations from such classical behavior.

Accordingly, the measured detonation parameters as initially reported in Part II are tabulated in Table 2 in the order of decreasing liquid initial

Table 2. Computation of the Chapman-Jouguet (CJ) Density for Detonating Viscous Energetic Liquids

Liquid No.	ρ_0 , Initial Dens. (Mg/m ³)	D, Detonation Velocity (km/s)	Gauge Mounting	P_1 , Detonation Pressure (GPa)	ρ_1 , CJ Dens. (Mg/m ³)
34C	1.524	7.312	Wall	16.45	1.910
			End	18.86	1.983
35C	1.493	7.373	Wall	17.79	1.912
			End	21.36	2.026
35B	1.441	7.338	Wall	15.79	1.809
			End	15.27	1.794
35A	1.401	7.242	Wall	15.64	1.780
			End	15.28	1.769
35E	1.316	6.905	Wall	12.79	1.653
			End	15.46	1.746
36E	1.297	6.723	Wall	12.34	1.643
			End	17.79	1.862
36F	1.224	6.491	Wall	12.21	1.604

Applicable Equation:
$$\rho_1 = \rho_0 \left[1 - \frac{P_1}{\rho_0 D^2} \right]^{-1} \quad (1)$$

density; these parameters include the detonation velocity and the two independently-measured values of detonation pressure (from the responses of the carbon resistor gauges, mounted respectively in the wall of the instrumented channel apparatus and at the end of the charge*). In the final column, the CJ densities have been computed from Equation (1), which has been derived by appropriate combination of the expressions for conservation of mass and momentum for a stably-propagating detonation wave. Thus, Table 2 forms the basis for the three analyses which follow.

3.1 Correlation of the Detonation Velocity

The detonation velocities of the seven viscous energetic liquids have been graphed as a function of initial density in Figure 1, and a least squares linear correlation which excludes the two highest-density points has been derived and plotted. For purposes of comparison, the linear variation of deto-

* See Figure 1 of Part II.

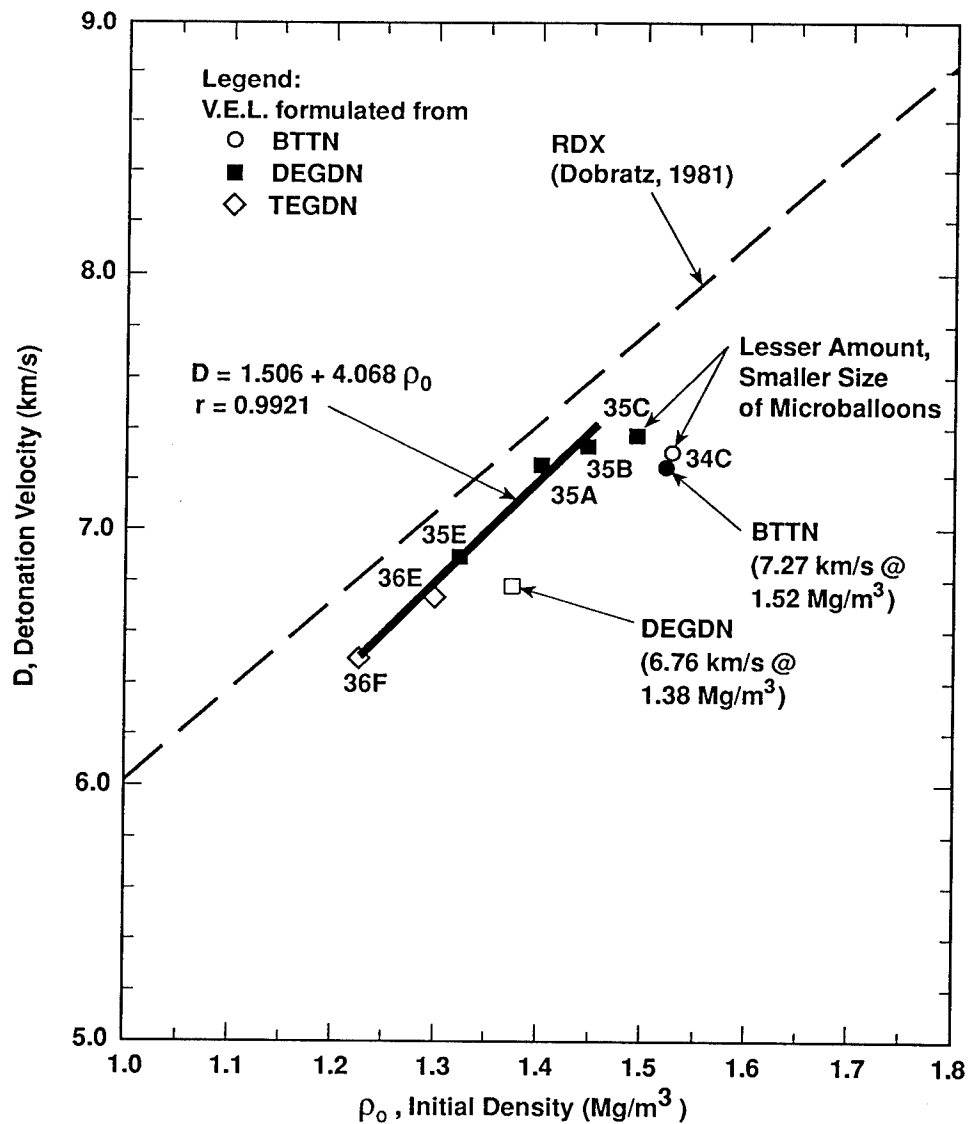


Figure 1. Detonation Velocity of Viscous Energetic Liquids as a Function of Initial Density.
(The data for RDX and two of the organic nitrate esters are also shown. r = the correlation coefficient for the viscous energetic liquids data. The correlation does not include the data for Liquids 34C and 35C.)

nation velocity of RDX (Dobratz, 1981) and the reported detonation velocities of BTTN and DEGDN (Federoff and Sheffield, 1962 and 1966) are also included*.

The correlation for the viscous energetic liquids in Figure 2 reveals two interesting aspects:

1. The detonation velocity of the five lower density charges increases in an essentially linear relationship with density, as is the case for all conventional organic explosives. In fact, the plotted correlation was based on these five points.
2. The detonation velocities of Liquids 34C and 35C notably deviate from the observed linear behavior, and exhibit velocities that are less than the values predicted from the correlation. Inspection of Table 1 reveals that these two viscous energetic liquids had the smallest weight fraction and particle size of microballoons.

It thus appears that the microballoons had a sensitizing influence on the detonation propagation in the viscous energetic liquids, but that this influence diminished as the amount and size of the microballoons decreased. One therefore wonders what the detonation velocity would have been if no microballoons had been utilized, or whether the detonation would even have been stable. These questions will be answered in the next phase of the investigation.

3.2 Correlation of the Chapman-Jouguet Density

The CJ densities of the viscous energetic liquids, as computed in Table 2, have been plotted as a function of the initial density in Figure 2, and a least-squares linear relationship has been derived and drawn through the points**. For purposes of comparison, the correlations of Cooper (1989) and of Roth (1994), based on experimental data, and the correlation of Hardesty and Kennedy (1977), based on computer-generated data, have been included in the graph. Except for two points which are in agreement with the referenced curves, in general the derived correlation predicts CJ densities that are in the range 4-7 percent less than those predicted by Cooper, Roth, and Hardesty and Kennedy. Nevertheless,

*The detonation velocity of TEGDN is not shown in Figure 1. As a pure material, its detonation is non-ideal, and the explosive requires very heavy confinement for propagation to occur. The detonation velocity under such conditions is reported to be less than 1.5 km/s.

**The CJ density of 1.862 Mg/m³ for Liquid 36E (Test No. 20) has not been plotted nor included in the correlation, because its value appears to be abnormally high.

the CJ density of the viscous energetic liquids collectively is a monotonically increasing function of the initial density.

At first glance, however, the premise that the CJ density is *independent* of chemical composition appears to have been violated, if one compares the derived correlation with respect to the standard correlations. All of these correlations depend on both the detonation velocity and the detonation pressure. The measurement of the former is accomplished with great accuracy, but unfortunately that of the latter is more an art than a science. Hence, uncertainties in the CJ density are directly attributed to uncertainties in the pressure. Equation (1) in Table 2 shows that a lower-than-expected detonation pressure will result in a similar error in the density, and this is verified by the derived correlation in Figure 2.

There are insufficient data to ascertain whether this inconsistency is due to a systematic error in the pressure measurements or to a phenomenon associated with the use of microballoons. With respect to the first possibility, Figure 1 in Part II shows that the surface of the viscous energetic liquids opposite the wall-mounted pressure gauges in the instrumented channel apparatus was unconfined. This in turn may have rendered the gauge calibration equations (Austing et al., 1995) not completely valid. In other words, some nonideality may have occurred in the detonations, even though the observations in Part I indicated that reliable propagation was obtained in viscous energetic liquids only 10 mm thick. One consequence of nonideal detonation would be lower-than-expected detonation pressure.

The possibility that the microballoons would have influenced the recorded detonation pressures can be resolved in future experiments in which complete detonation state measurements would be made on a given explosive formulation as a function of microballoon weight fraction and particle size, including tests on charges containing no microballoons. Perhaps it is not a coincidence that the data point associated with the end-mounted gauge for Liquid No. 35C (Test No. 14) yielded a CJ density of 2.026 Mg/m³, which in Figure 2 agreed very well with the Cooper and Roth data. Recall from Table 1 and Figure 1 that this charge had a lesser weight fraction and smaller particle size of microballoons, and that the detonation velocity deviated from the observed linear behavior of the other charges. This observation prompts us to speculate that indeed the presence of the microballoons affected the magnitude of the

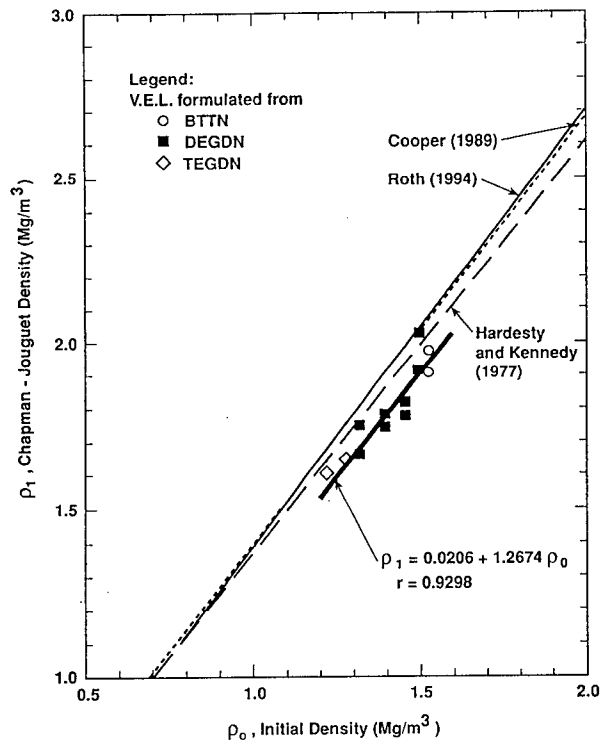


Figure 2. The Chapman-Jouguet Density of Detonating Viscous Energetic Liquids and Conventional Explosives as a Function of Initial Density.

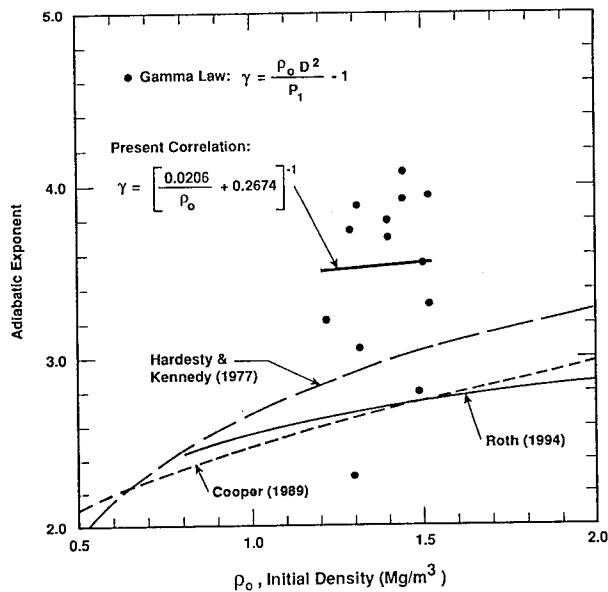


Figure 3. The Adiabatic Exponent for Detonating Viscous Energetic Liquids (Individual Points) and Conventional Explosives (Smooth Curves) as a Function of Initial Density.

(The equation for the correlation is based on the density correlation in Figure 2.)

Table 3. Computation of the Adiabatic Exponent by Four Methods

Liquid No.	ρ_0 , Initial Density (Mg/m ³)	Adiabatic Exponent			
		Gamma Law, Equ. 2	Present Effort, Equ. a	Roth, Equ. b	Hardesty and Kennedy, Equ. c
34C	1.524	3.95 3.32	3.56	2.76	3.06
35C	1.493	3.56 2.80	3.56	2.75	3.04
35B	1.441	3.91 4.08	3.55	2.73	3.01
35A	1.401	3.70 3.81	3.54	2.72	2.98
35E	1.316	3.87 3.06	3.53	2.70	2.93
36E	1.297	3.75 2.30	3.53	2.69	2.92
36F	1.224	3.22	3.52	2.66	2.86

Applicable Equations:

$$\text{Gamma Law:} \quad \gamma = \rho_0 D^2 / P_1 - 1 \quad (2)$$

$$\text{Density Correlation:} \quad \gamma = [\rho_1 / \rho_0 - 1]^{-1} \quad (3)$$

$$\text{Present Effort:} \quad \gamma = [0.0206 / \rho_0 + 0.2674]^{-1} \quad (a)$$

$$\text{Roth (1994):} \quad \gamma = [0.08003 / \rho_0 + 0.3101]^{-1} \quad (b)$$

$$\text{Hardesty and Kennedy (1977):} \quad \gamma = [0.136 / \rho_0 + 0.238]^{-1} \quad (c)$$

recorded pressures for all of the viscous energetic liquids.

3.3 Attempted Correlation of the Adiabatic Exponent

The adiabatic exponent has been calculated from the gamma law relationship and from the various density correlations in Figure 2, and the results are tabulated in Table 3 and plotted as a function of initial density in Figure 3. The adiabatic exponent according to the gamma law is very sensitive to the uncertainty in the measured pressure, which accounts for the tremendous scatter

of the individual points; hence, Roth stresses that computations based on normalized density correlations provide a more satisfactory estimate.

The present correlation in Figure 3 predicts adiabatic exponents that are about 20 percent higher than the data of Hardesty and Kennedy, and about 40 percent higher than the data of Roth and Cooper. The objective was to demonstrate that the adiabatic exponent of the detonating viscous energetic liquids was independent of chemical composition and dependent only on the initial density. If such were true, the present correlation should have lain much closer to those of Cooper, Roth, and Hardesty and Kennedy. Its failure to do so means that this objective cannot be satisfied, and must await the resolution of the dilemma concerning the pressure measurements. To repeat what was stated earlier, either there was a systematic error in these measurements or the presence of the microballoons influenced the results in some manner.

In the previous section, we discussed the possibility that nonideal detonation may have exerted an influence on the recorded pressures. Roth discusses the role of nonideal detonation, and presents a derivation to show that incomplete reaction (one of the attributes of nonideality) will result in higher values of the adiabatic exponent. Thus, while it is difficult to comprehend that the viscous energetic liquids reacted incompletely and detonated nonideally, nevertheless it is a possibility that must be accepted and appropriately considered in future experimentation.

4. Conclusions

This manuscript represents one portion of a continuing investigation of viscous energetic liquid explosives which can be initiated by a cloud of detonating dispersed explosive particles. These viscous explosives were formulated from nitrocellulose, a liquid organic nitrate ester, and fine RDX powder; the desired sensitivity was achieved by incorporation of glass microballoons. The initiation and detonation measurements were reported in two papers at the Twentieth International Pyrotechnics Seminar, and these respectively comprised Part I and Part II of the investigation. The objective of the effort herein, which comprises Part III, was to ascertain whether the detonation performance of these explosives was in agreement with that for conventional high explosives.

For ideally detonating explosives, it has been established that the deto-

nation velocity is dependent on the chemical composition, but for a given explosive is described by a direct linear relationship with initial density. On the other hand, the Chapman-Jouguet (CJ) density and the adiabatic exponent are *independent* of chemical composition and are functions *only* of the initial density.

The detonation data for the viscous energetic liquids did not meet *all* of the above criteria, although *some* were partially satisfied. For example, the detonation velocity in general did exhibit a monotonic increase with initial density, but two of the charges containing lesser amounts and smaller sizes of microballoons achieved velocities that were notably less than what was predicted by the linear correlation. Likewise, the CJ density correlated with initial density, but on the average was about 6 percent less than predicted by investigators such as Cooper and Roth. This was attributed to lower-than-expected detonation pressures; it is not known whether this discrepancy was due to a systematic error in the measurements or to the use of microballoons. Whatever the reason, a definitive conclusion that the CJ density of the viscous energetic liquids was independent of chemical composition could not be drawn.

The uncertainty in the pressure measurements resulted in a large scatter in the individual values of the adiabatic exponent, and so no correlation with initial density was apparent. An equation was derived from the CJ density relationship, but this equation predicted the adiabatic exponent to be a weak function of the initial density and about 40 percent greater than the data of Cooper and Roth. The possibility that nonideal detonation with incomplete reaction was the cause of this discrepancy was considered, but not proven.

Based on the above observations, it is concluded that the detonation in the viscous energetic liquids as formulated for this investigation did not propagate in accordance with the principles that govern classical, ideal detonation in conventional explosives. The contribution of the microballoons to this behavior, if indeed they played a role, is not understood at this time.

Future effort will include complete detonation state measurements on viscous energetic liquids containing no microballoons, and further analysis of the detonation data. The methodology of Walker (1990) will be invoked to calculate the detonation velocities of the viscous energetic liquids, in a manner similar to the calculation for TNT/Dinitrogen Tetroxide by Austing et

al. (1995a). Finally, analysis of the mechanism by which microballoons affect the sensitivity, in the context of the observations of Leiber (1985, 1986), will be undertaken.

5. References

- Alymova, Ya. V., V. E. Annikov, and B. N. Kondrikov, "Detonation of the Emulsion Explosive", *Proc., Twentieth International Pyrotechnics Seminar*, IIT Research Institute, Chicago, Illinois, USA, p. 11, 1994.
- Austing, J. L., A. J. Tulis, D. E. Brzycki, C. E. Foxx, G. R. Gribbon, D. E. Baker, D. L. Patel, and D. C. Heberlein, "Viscous Energetic Liquid Explosive Formulations Sensitized with Glass Microballoons. II. Quantitative Initiation and Detonation Measurements", *ibid.*, p. 47, 1994a.
- Austing, J. L., A. J. Tulis, D. E. Brzycki, D. L. Patel, and D. C. Heberlein, "Viscous Energetic Liquid Explosive Formulations Sensitized with Glass Microballoons. I. Formulation Data and Initiation Criteria", *ibid.*, p.31, 1994b.
- Austing, J. L., A. J. Tulis, R. P. Joyce, C. E. Foxx, D. J. Hrdina, and T. J. Bajzek, "Carbon Resistor Gauges for Measuring Shock and Detonation Pressures. III. Revised Calibration Data and Relationships", *Propellants, Explos., Pyrotech.*, in press, 1995.
- Austing, J. L., A. J. Tulis, D. L. Patel, and D. C. Heberlein, "Analysis of the Complete Detonation State of Solutions of TNT in Advanced Oxidizers", *Proc., 6e Congrès International de Pyrotechnie (EuroPyro 95)*, Association Française de Pyrotechnie, La Ferté Saint Aubin, France, 1995a.
- Chaudhri, M. M., L-A. Almgren, and A. Persson, "Detonation Behavior of a 'Water-in-Oil' Type Emulsion Explosive Containing Glass Microballoons of Selected Sizes", *Paper Summaries, The Tenth International Symposium on Detonation*, Naval Surface Warfare Center, Dahlgren Division, Report No. NSWCDD/MP-92/456, p. 4, 1993.
- Cooper, P. W., "Estimation of the C-J Pressure of Explosives", *Proc., Fourteenth International Pyrotechnics Seminar*, RARDE, Fort Halstead, U.K., p. 569, 1989.
- Dobratz, B. M., "LLNL Explosives Handbook", Report No. UCRL-52997, Lawrence Livermore Laboratory, Livermore, California, USA, Table 8-2, 1981.
- Federoff, B. T., and Sheffield, O. E., "Encyclopedia of Explosives and Related Items", Volume 2, Report No. PATR 2700, Picatinny Arsenal, Dover, New Jersey, USA, 1962.
- Federoff, B. T., and Sheffield, O. E., *ibid.*, Volume 3, 1966.
- Gois, J. C., J. Campos, and R. Mendes, "Shock Initiation of Nitromethane-PMMA Mixtures with Glass Microballoons", *Paper Summaries, The Tenth International Symposium on Detonation*, Naval Surface Warfare Center, Dahlgren Division, Report No. NSWCDD/MP-92/456, p. 24, 1993.
- Granholm, R. H., "Detonation Pressure Measurement using the Manganin Gauge", *Proc., Seventh Annual Symposium on Explosives and Blasting Research*, Society of Explosives Engineers, Solon, Ohio, USA, p. 35, 1991.

- Hardesty, D. R., and Kennedy, J. E., "Thermochemical Estimation of Explosive Energy Output", *Comb. and Flame*, 28, 45, 1977.
- Khasainov, B. A., B. S. Ermolaev, and H-N. Presles, "Shock Wave Initiation of Chemical Reaction in Liquid High Explosives Sensitized by Glass Microballoons", *Paper Summaries, The Tenth International Symposium on Detonation*, Naval Surface Warfare Center, Dahlgren Division, Report No. NSWCDD/MP-92/456, p. 40, 1993.
- Lee, J., and Persson, P-A., "Detonation Behavior of Emulsion Explosives", *Propellants, Explos., Pyrotech.*, 15, 208, 1990.
- Lee, J., F. W. Sandstrom, B. G. Craig, and P-A. Persson, "Detonation and Shock Initiation Properties of Emulsion Explosives", *Proc., Ninth Symposium (International) on Detonation*, Office of Chief of Naval Research, Arlington, Virginia, USA, Report No. OCNR-113291-7, p. 573, 1989.
- Leiber, C-O., "Approximate Quantitative Aspects of a Hot Spot", *J. Hazardous Materials*, 12, 43, 1985.
- Leiber, C-O., "Approximate Quantitative Aspects of a Hot Spot, Part II. Initiation, Factors of Safe Handling, Reliability and Effects of Hydrostatic Pressure on Initiation", *J. Hazardous Materials*, 13, 311, 1986.
- Presles, H-N., J. Campos, O. Heuse, and P. Bauer, "Effects of Microballoons Concentration on the Detonation Characteristics of Nitromethane-PMMA Mixtures", *Proc., Ninth Symposium (International) on Detonation*, Office of Chief of Naval Research, Arlington, Virginia, USA, Report No. OCNR-113291-7, p. 925, 1989.
- Roth, J., "The Adiabatic Exponent in Steady Detonation", *Proc., Twentieth International Pyrotechnics Seminar*, IIT Research Institute, Chicago, Illinois, USA, p. 845, 1994.
- Walker, F. E., "Calculation of Detonation Velocities from Hugoniot Data", *Propellants, Explos., Pyrotech.*, 15, 157, 1990.
- Yoshida, M., M. Iida, K. Tanaka, S. Fujiwara, M. Kasakabe, and K. Shiino, "Detonation Behavior of Emulsion Explosives containing Glass Microballoons", *Proc., Eighth Symposium (International) on Detonation*, Naval Surface Weapons Center, Silver Spring, Maryland, USA, Report No. NSWC MP 86-194, p. 993, 1985.

Fortschrittliche Methoden zur Bestimmung der Stabilität von Zünd- und Anzündstoffen und Munitionskomponenten

Manfred Kaiser, Winfried Scheunemann, Uldis Ticmanis
Bundesinstitut für chemisch-technische Untersuchungen beim BWB (BICT)
Großes Cent, D-53913 Swisttal

Abstract

Advanced methods for the determination of primary explosives and components

It is a major problem to predict the long term shelf life of ammunition from short term experiments in connection with the unavoidable temporal extrapolation of the results.

Also, extreme environmental conditions e.g. in "out of area" regions must be covered by the tests. Especially, high temperatures may have greater influence on the stability of the explosives. Therefore, a reliable estimation of the shelf life can only be based on reaction kinetics using thermoanalytical tools such as DSC, TGA or heat flow calorimetry combined with functional testing of the relevant explosive components. In this context it is of fundamental importance to use optimized temperature test profiles, which is demonstrated by experiments and as well by model calculations because a deviation of the optimal programs can lead to even catastrophically wrong estimations about the stability of explosives.

To calculate the shelf life of ammunition and its components as a function of time and temperature, it is necessary - besides the description of the kinetics of decomposition - to test the function of thermally stressed material and to estimate a critical reaction degree.

Zusammenfassung

Die langjährige Einsatzdauer militärisch verwendeter Explosivstoffe muß im allgemeinen durch relativ kurzfristige Untersuchungen gewährleistet werden. Deshalb ist eine Zeitextrapolation der Meßergebnisse stets erforderlich. Andererseits müssen auch zwischenzeitliche Sonderbelastungen - etwa bei Einsätzen in anderen Klimagebieten - berücksichtigt werden. Hinreichende Sicherheit der verschiedenartigen Voraussagen kann nur unter Einbeziehung kinetischer Reaktionsmodelle erreicht werden. Das jeweils zutreffende Modell kann nur bei geeigneter Versuchsführung unter gleichzeitiger Berücksichtigung der verfügbaren Meßgenauigkeit ermittelt werden. Aus diesen Überlegungen resultieren für die thermoanalytischen Verfahren (DSC, TG, statische Kalorimeter) einzusetzende Meßprogramme, deren Anwendung zu tragfähigen Resultaten führt. Demgegenüber wird anhand von Modellrechnungen und Meßbeispielen gezeigt, daß Abweichungen von diesen optimalen Programmen zu katastrophalen Fehleinschätzungen der Stabilität von Explosivstoffen führen können.

Um die Lebensdauer von Munitionskomponenten als Zeit- und Temperaturfunktion berechnen zu können, muß neben der kinetischen Beziehung durch Funktionsprüfungen gezielt belasteter Prüflinge zusätzlich ein kritischer Reaktionsgrad ermittelt werden.

1. Anforderungen an Prüfmethoden für die thermische Stabilität

In Deutschland militärisch eingesetzte Munition soll i. a. zehn Jahre lang sicher und funktionsfähig bleiben. Im Zeichen schwindender Mittel kann künftig mit noch längeren Gebrauchszeiten gerechnet werden.

Darüberhinaus sind neben den normalen Belastungen beim Umgang und bei der Lagerung in wachsendem Maße besondere Einwirkungen - etwa beim Einsatz in anderen Klimagebieten - zu berücksichtigen.

Leistungsfähige Prüfmethoden sollten es ermöglichen, solche Fragestellungen - möglichst quantitativ - zu beantworten. Um die Qualifikationsprozeduren nicht übermäßig zu verzögern, ist dazu eine Prüfdauer von höchstens einigen Wochen zu fordern; die extreme Zeitextrapolation bis zur Gebrauchslebensdauer erfordert eine zuverlässige Theorie.

2. Normierbarkeit der Prüfmethode

In eingeführten Prüfvorschriften wird versucht, das Problem mit festgelegten Belastungstemperaturen und -zeiten zu lösen, z.B.:

- Stabilitätstest im Vakuum

Messung der Gasabspaltung von Explosivstoffen nach 40 h Lagerung bei 100 °C.

- Prüfung der Lagerbeständigkeit bei extremen Temperaturen

4-wöchige Lagerung von Zündern oder Zündmitteln bei 71 °C (oder -54 °C) mit anschließender Funktionsprüfung (nach MIL-STD 331B, PV C 6).

Die thermische Zersetzungsreaktion von Explosivstoffen wird durch die Temperatur und die Expositionszeit bestimmt und - wie später zu formulieren sein wird - durch eine kinetische Gleichung beschrieben. Der für die Temperaturextrapolation entscheidende Parameter ist dabei die Aktivierungsenergie E . Für Explosivstoffe sind in der Literatur zahlreiche, häufig widersprüchliche Angaben dieser Größe zu finden. Es kann jedoch als sicher gelten, daß der glaubwürdige Bereich sehr groß ist. Einige Beispiele sind in Tabelle 1 aufgelistet.

Tabelle 1: Aktivierungsenergie der thermischen Zersetzung von Explosivstoffen

Aktivierungsenergie [kJ/mol]	Explosivstoff	Literatur
33,3	TLP A 5020	Frey ¹⁾
58,7	TLP A 5020	Bohn und Volk ²⁾
67	Diazodinitrophenol (DDNP)	Yamamoto ³⁾
87,4	Nitroguanidin	Rogers ⁴⁾
127	Hexanitrostilben	Rogers ⁴⁾
132	Silberazid	Bartlett, Tompkins, Young ⁵⁾
146	Tetryl	Connick, May, Thorpe ⁶⁾
162	Nitropenta	Connick, May, Thorpe ⁶⁾
198	Tetrazen	Patel, Chaudhri ⁷⁾
220	Oktogen	Robertson ⁸⁾
259	Tetrazen in Sinoxid	Ticmanis, Scheunemann ⁹⁾

Der große Streubereich der Werte bedeutet praktisch, daß die der Prüfzeit bei höherer Temperatur äquivalente Lagerzeit bei Raumtemperatur sich von Stoff zu Stoff um viele Größenordnungen unterscheiden kann. Fehlbeurteilungen in beide Richtungen - Aussondern eines hinreichend stabilen und Akzeptanz eines instabilen Zündmittels - sind ohne weiteres möglich (9).

In der Bilanz ist festzustellen, daß aufgrund der sehr unterschiedlichen Stoffreaktionen Prüfmethoden zur Bestimmung der thermischen Langzeitstabilität nicht generell normierbar sind.

3. Richtlinien für Prüfmethode

Planung, Führung und Auswertung von Versuchen sind durch die Art der zu prüfenden Theorien, dem Untersuchungsziel und der verfügbaren Meßgenauigkeit bestimmt. Unter Beachtung dieser Wechselwirkung lassen sich Richtlinien für eine quantitative Behandlung ableiten:

Richtlinien für Prüfmethode

- P 1 Erkennen der dominierenden Reaktionen
- P 2 Formulierung der Reaktion
- P 3 Ermittlung (Abschätzung) des kritischen Reaktionsgrades
- P 4 Wahl der Untersuchungsmethode
- P 5 Hinreichende Varieierung der Einflußgrößen Temperatur und Reaktionsgrad
- P 6 Unabhängige Varieierung der Einflußgrößen

- P 7 Prüfung der Formulierungen durch Regressionsrechnung, Wahl der Besten
 P 8 Extrapolationstest
 P 9 Wenn vertretbar, Akzeptanz.

Soweit erforderlich, werden im folgenden die einzelnen Punkte der Richtlinien in Kürze erläutert.

P 1 Erkennen der (dominierenden) D-Reaktion

Die Wahrscheinlichkeit, daß in Explosivstoffgemischen und sogar in Munitionsteilen mit mehreren Gemischen eine einzige Komponente die Schädigung dominiert, ist aufgrund sehr unterschiedlicher Reaktionsraten der Stoffe recht hoch. Eine zuverlässige Auswahl ist meist aus den vorhandenen thermoanalytischen Datensammlungen oder aus Analysen nach Belastung möglich.

P 2 Formulierungen der Reaktion

Nach unserer Erfahrung genügt in den meisten Fällen die allgemeine Gleichung

$$d\alpha/dt = f(\alpha) \cdot A e^{-E/RT} \quad (1)$$

- α Reaktionsgrad (0→1)
 t Reaktionszeit
 T Reaktionstemperatur
 $d\alpha/dt$ Reaktionsgeschwindigkeit (Reaktionsrate)
 $f(\alpha)$ Reaktionsmodell (RM)
 A Frequenzfaktor (vorexponentieller Faktor)
 E Aktivierungsenergie

Zwar sind thermische Zersetzungen von Explosivstoffen überwiegend mehrstufige Prozesse, doch können konkurrierende und konsequente Reaktionen in aller Regel vernachlässigt werden.

Die wichtigsten Reaktionsmodelle in Gl. 1

- | | | |
|------|---|--------------------------------------|
| RM 1 | $f(\alpha) = (1-\alpha)^n$ | Reaktion n. Ordnung |
| RM 2 | $f(\alpha) = (1-\alpha) \cdot [1+(a-1) \cdot \alpha]$ | Reaktion 1. Ordnung mit Autokatalyse |
| RM 3 | $f(\alpha) = (1-\alpha) \cdot (-\ln(1-\alpha))^p$ | Reaktion nach Avrami-Erofeev |
| RM 4 | $f(\alpha) = (1-\alpha)^r \cdot \alpha^m$ | Prout-Tompkins |

Explosivstoffe reagieren in aller Regel autokatalytisch, bevorzugt nach Typ RM 2.

P 3 Ermittlung des kritischen Reaktionsgrades

Als kritischer Reaktionsgrad wird hier der maximale Umsatz der D-Reaktion verstanden, bei dem die Funktion der Munitionskomponente („Gegenstand“) noch hinreichend ist.

Dieser Wert wird i.a. durch Beschußversuche belasteter Gegenstände zu ermitteln sein. Ist eine Bestimmung nicht möglich, sollte im Zweifelsfall auf ein sehr niedriges Niveau - z.B. 1 % - geschätzt werden.

P 8 Extrapolationstest

Insbesondere bei Methoden, deren Arbeitstemperaturen beträchtlich über den zu erwartenden Belastungstemperaturen liegen, empfiehlt sich ein Isotherm-Test der erhaltenen Beziehung. Bei diesem wird geprüft, inwieweit der vorausgesagte Umsatzgrad nach z.B. 20 h Lagerung zutrifft. Wurden keine kompletten kinetischen Beziehungen, sondern nur die Aktivierungsenergie ermittelt, können für die modellfreie Schätzung der Isotherm-Zeiten zwei Gleichungen eingesetzt werden, die sich auf jeweils gleiche Umsatzgrade für Messungen und Extrapolation beziehen.

E aus Isothermmessungen:

$$t = C_{\text{iso}} \cdot e^{E/RT} \quad (2)$$

E aus dynamischen Messungen:

$$t = C_{\text{dyn}} \cdot e^{E/RT} \quad (3)$$

t isotherme Lagerzeit

T dazugehörige konstante Lagertemperatur

C_{iso} $t_p \cdot e^{E/RT_p}$

C_{dyn} $1/H \cdot \int_0^{T_{\text{dyn}}} e^{-E/RT} dT$

t_p isotherme Lagerzeit in der Prüfung

T_p konstante Lagertemperatur in der Prüfung

T_{dyn} dynamische Temperatur, bei der der Referenzreaktionsgrad erreicht wurde

H Heizrate des dynamischen Versuchs

Die Konstanten der Formeln 2 und 3 sind leicht zu bestimmen, sie sind für viele Problemlösungen bereits hinreichend.

4. Temperaturführung

In diesem Abschnitt wird im wesentlichen der Punkt 6 unserer Richtlinien - unabhängige Variation der Einflußgrößen - abgehandelt. Diese Sonderbehandlung ist jedoch gerechtfertigt, da die Nichtbeachtung dieses Punktes immer noch die Hauptquelle von Fehleinschätzungen ist, insbesondere bei Methoden mit ansteigender Temperaturführung. Dabei werden Temperatur und Reaktionsgrad zwar maximal, jedoch gleichsinnig variiert. Dieses indiziert a priori eine schlechte

Trennung der Wirkung der Einflußgrößen und hohe gegenseitige Kompensationsfähigkeit. Wir haben das vielfach vorhandene Unbehagen durch Modellrechnungen quantifiziert.

Dau wurden „Versuchsdaten“ aus der integrierten Form der Gl. 1 mit den drei autokatalytischen Modellen RM 2, RM 3 und RM 4 gerechnet und die Qualität der Wiedergabe durch die best-angepaßte Reaktion n-ter Ordnung (RM 1) - ebenfalls in der integrierten Form - geprüft. Die Heizrate wurde zu 1 K/min gewählt.

Tabelle 2: Anpassung autokatalytischer Reaktionen durch n-Ordnungsreaktionen

Erzeugungsreaktion			angepaßte Reaktion n.Ordnung					
RM	A [s ⁻¹]	E [kJ/mol]	Konstanten		A [s ⁻¹]	E [kJ/mol]	n	S (%)
RM2 1.Ordn. mit AK	10 ⁶	100	a		9,449·10 ¹³	177,2	1,264	1,9
	10 ⁶	100	5		9,455·10 ²³	269,8	1,333	2,1
	10 ⁶	100	20		7,540·10 ³⁹	408,1	1,449	1,8
RM3 Avrami- Erofeev	1,80·10 ¹	50	p		5,553·10 ⁴	88,9	0,996	0,032
	6,75·10 ¹	50	0,4		1,617·10 ¹⁰	136,9	0,995	0,040
	3,40·10 ²	50	0,6		2,516·10 ²⁶	280,7	0,998	0,030
RM4 Prout- Tompkins	3,328·10 ⁶	100	r	m	8,444·10 ⁸	125,4	0,846	0,079
	1,113·10 ⁷	100	0,8	0,2	4,556·10 ¹³	167,0	0,663	0,20
	4,189·10 ⁷	100	0,6	0,4	9,140·10 ²²	249,6	0,441	0,30

s Standardabweichung der α -Werte beider Reaktionen

Die ausgezeichnete Anpassung wird auch in den folgenden Darstellungen erkennbar (Abb. 1, 2 und 3).

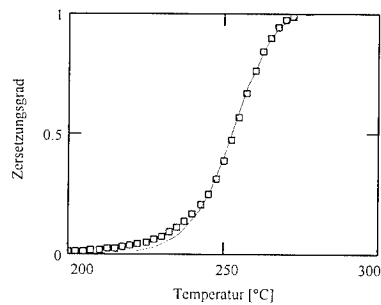


Abb. 1. Anpassung einer Reaktion 1. Ordnung mit Autokatalyse ($a = 20$)

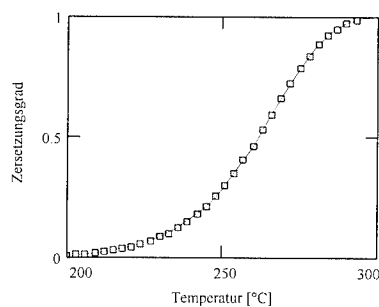


Abb. 2. Anpassung einer Reaktion nach Avrami-Erofeev ($n = 0,6$)

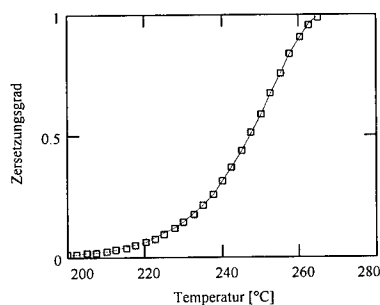
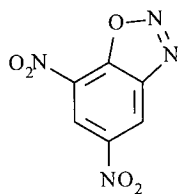


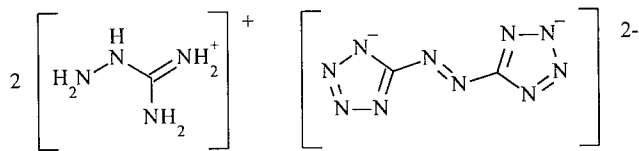
Abb. 3. Anpassung einer Reaktion nach Prout-Tompkins ($r = 0,6$, $m = 0,4$)

Aus der Standardabweichung und den graphischen Darstellungen erkennt man die überraschende Genauigkeit, mit der die autokatalytischen Reaktionen durch eine falsche Reaktion n.Ordnung wiedergegeben werden. Dabei ist insbesondere auf die viel zu hohen Werte der gefundenen Aktivierungsenergie hinzuweisen, die zu einer katastrophalen Überschätzung der Stabilität führen kann.

Thermogravimetrische Messungen an Diazodinitrophenol (DDNP, Diazol) und Di(aminoguanidinium)-azotetrazolat (DAGAT)



Diazol (2,4-dinitro-6-diazophenol)



Di-(aminoguanidinium)-azotetrazolat

beweisen, daß solche guten, aber falschen Anpassungen auch praktisch alltäglich sind, wenn Messungen mit **einer** Heizrate ausgewertet werden.

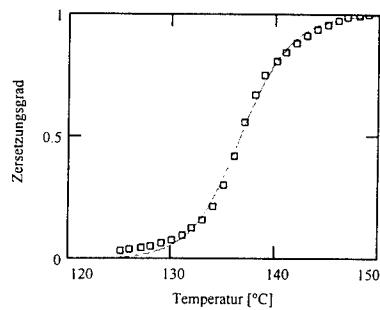


Abb. 4. Anpassung einer TG-Messung von DDNP ($H = 0,1 \text{ K/min}$)
Parameter der n-Ordnungsreaktion:
 $A = 2,980 \cdot 10^{72} \text{ s}^{-1}$, $E = 593,2 \text{ kJ/mol}$,
 $n = 2,063$

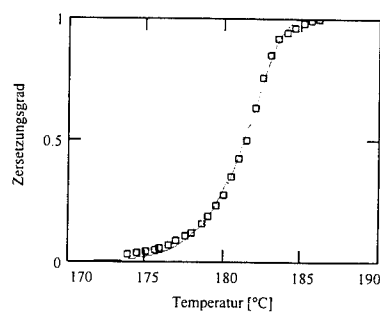
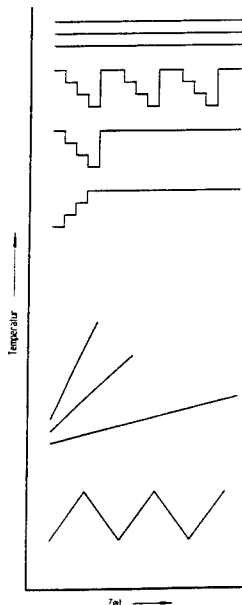


Abb. 5. Anpassung einer TG-Messung von DAGAT ($H = 0,1 \text{ K/min}$)
Parameter der n-Ordnungsreaktion: $A = 1,682 \cdot 10^{104} \text{ s}^{-1}$,
 $E = 934,5 \text{ kJ/mol}$ $n = 1,07$

Später wird gezeigt, daß beide Stoffe autokatalytisch und sehr viel niedriger aktiviert reagieren.



Führt man zusätzlich einen zweiten dynamischen Versuch bei deutlich verschiedener Heizrate durch, so verschiebt sich der Temperaturbereich der Reaktion. Gleiche Reaktionsgrade können bei verschiedenen Temperaturen ermittelt werden. Die Zwangskombination der Einflußgrößen ist damit aufgehoben, die Trennung der Wirkung der Einflußgrößen wird scharf, wenn die Daten beider oder besser mehrerer Messungen vereint und gemeinsam ausgewertet werden; es paßt nur noch ein wenigstens angenähert richtiges Reaktionsmodell.

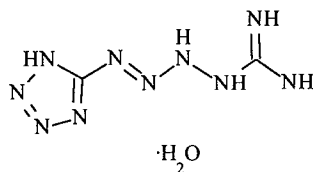
Aus Überlegungen dieser Art wurden geeignete Meßprogramme (Temperaturführungen) abgeleitet, mit denen ein Datenfeld erzeugt werden kann, das „scharf“ genug ist, um die kinetischen Parameter mit einiger Sicherheit zu ermitteln.

Abb. 6. Meßprogramme zur Ermittlung kinetischer Parameter

5. Anwendungsbeispiele

Im folgenden werden einige Untersuchungen schematisch vorgestellt, bei denen wir recht zuverlässige und extrapolationsfähige kinetische Daten ermittelt haben.

Tetrazen



Tetrazen

Methoden:	TG, DDK (DSC)
Probengröße:	ca. 1 mg in Al-Tiegeln mit Deckel und Loch
Versuchsführung:	dyn. bei Heizraten von 0,1 bis 1 K/min (Nr. 5 in Abb. 6)
Temperaturbereich:	110 bis 130°C
Auswertung:	Bestimmung der Aktivierungsenergie nach Kissinger
Ergebnisse:	E = 181,1 kJ/mol aus DTG E = 200,0 kJ/mol aus DDK Reaktion ist autokatalytisch
Extrapolation:	20 h Isothermtest gibt geringe Abweichung (ca. 5 %) gegenüber Voraussage nach Gl. 3 (DTG) geringe Abweichungen gegen Wärmeflußmessungen bei 60-80 °C ¹⁰⁾

DAGAT

Methode:	TG
Probengröße:	ca. 1 mg
Versuchsführung:	dyn. bei Heizraten von 0,1 bis 1 K/min (Nr. 5 in Abb. 6)
Temperaturbereich:	180-200 °C
Auswertung:	Bestimmung der Aktivierungsenergie nach Kissinger
Ergebnis:	E = 207,8 kJ/mol (nicht 934,5!)
Extrapolation:	20 h-Isothermlagerung gibt eine Abweichung von ca. 3 % gegenüber der Voraussage nach Gl. 3 Reaktion ist extrem autokatalytisch

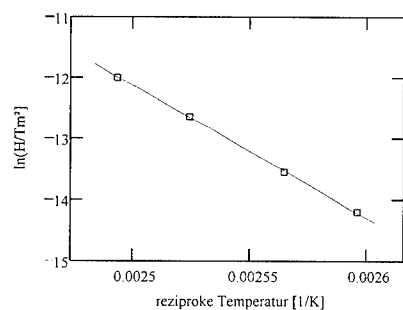


Abb. 7. Kissinger-Auswertung¹¹⁾ der TG-Messungen an Tetrazen

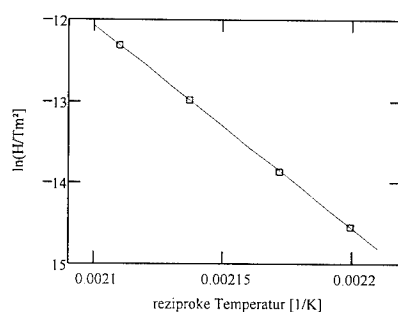


Abb. 8. Kissinger-Auswertung der TG-Messungen an DAGAT

Nitropenta-Tetryl-Eutektikum

Methode: TG
 Probengröße: 20-50 mg in Tiegel mit Deckel
 Versuchsführung: isotherm bei 4 Temperaturen (Nr. 1 in Abb. 6)
 Temperaturbereich: 130-150°C
 Auswertung: Iso- α -Plot über den gesamten Reaktionsbereich, selektive Bestimmung der Aktivierungsenergie und des Reaktionsmodells mit finaler Totalregression
 Ergebnis: Der Stoffumsatz entspricht einer Reaktion 1. Ordnung mit Autokatalyse
 ($a = 7,235$, $A = 3,887 \cdot 10^{14} \text{ s}^{-1}$ und $E = 154,3 \text{ kJ/mol}$)

TLP T 5700 (Oktogen/Binder)

Methode: TG
 Probengröße: 50 mg in Tiegel mit Deckel
 Versuchsführung: Ansteigende Isothermperioden mit langer Endperiode (Nr. 3 in Abb. 6)
 Temperaturbereich: 150 bis 190°C
 Auswertung: Bestimmung von Näherungswerten von A und E aus den Kurzperioden und des Reaktionsmodells aus der Langperiode.
 Die Konstanten werden durch Regression der integrierten Form der kompletten Beziehung endoptimiert.
 Ergebnis: Der Stoffumsatz entspricht mit hoher Genauigkeit und bis zu einem Gewichtsverlust von 77 % einer Reaktion n.-Ordnung ($n = 0,2048$, $A = 1,225 \text{ s}^{-1}$, $E = 162,9 \text{ kJ/mol}$).

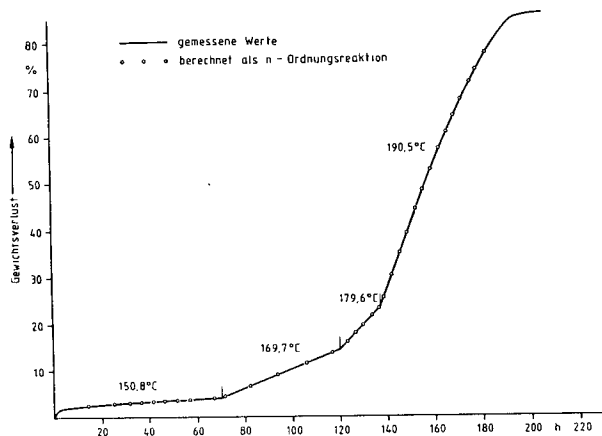


Abb. 9. Anpassung einer n-Ordnungsreaktion an TG-Messungen von TLP T 5700

Diazodinitrophenol (DDNP) ¹²⁾

Methoden:	DDK, TG, NMR
Probengröße:	1 bis 100 mg in Al-Tiegeln mit Deckel
Versuchsführung:	DDK, dyn. bei 4 Heizraten (Nr. 5) DDK, isoth. bei 3 Temperaturen (Nr. 1) TG, isoth. Zyklen (Nr. 2) NMR, isoth. (Nr. 1)
Temperaturbereich:	90 - 150°C
Auswertung:	Bestimmung der Aktivierungsenergie aus allen Methoden. Ermittlung des Reaktionsmodells aus NMR-Daten.
Ergebnis:	Reaktion entspricht bis 20% Massenverlust 1. Ordnung mit Autokatalyse ($a = 67,0$, $A = 5,218 \cdot 10^{22} \text{ d}^{-1}$, $E = 178 \text{ kJ/mol}$)

Tetrazen im Sintox-Anzündhütchen DM 1448 ¹³⁾

Aufgrund der Anwesenheit von drei weiteren zersetzlichen Komponenten (DDNP, TLP und Zinkperoxid) bereitete in diesem Fall die Erkennung der Tetrazenzersetzung als dominierender Reaktion einige Mühe.

Methode:	TG
Probengröße:	1 Anzündhütchen mit ca. 30 mg Sintox-Satz
Versuchsführung:	dyn. bei Heizraten von 0.1 bis 1 K/min (Nr. 5 in Abb. 6)
Temperaturbereich:	120-135°C

Auswertung: Soweit möglich, Bestimmung der Aktivierungsenergie aller zersetzlichen Komponenten und daraus Abschätzung der Dominanz im relevanten Temperaturbereich von 20-100°C.

Ergebnis: Tetrazen bestimmt das Langzeitverhalten
 $E = 175,9 \text{ kJ/mol}$

Extrapolation: Lagerungen bis zu 84 h ergaben nur geringe Fehler in der Voraussage nach Gl. 3 (vgl. Tab. 3)

Tabelle 3
 Isothermer Extrapolationstest der dynamischen Kinetik
 am Anzündhütchen DM 1448

Lagertemperatur [°C]	Zeit, ber. nach Gl.3 [h]	Zeit, exp. [h]	rel. Fehler [%]
109,5	3,94	4,08	3,6
100,1	15,9	16,4	3,1
89,8	79,8	84,0	5,3

Vergleichspunkt: Massenverlust des dynamischen Maximums des Tetrazens
 2,6 % auf Satzgewicht)

Tetrazen im Sinoxid-Anzündhütchen

Methoden: TG, Funktionsprüfungen mit Messung der Anzündverzugszeit

Probengröße: 33 Anzündhütchen mit je 33 mg pro Satz

Versuchsführung: Isotherm TG in 4 Zyklen (Nr. 2 in Abb. 6)

Temperaturbereich: 85-95°C

Auswertung: Funktionsprüfungen mit TG-vorbelasteten Anzündhütchen liefern den kritischen Schädigungsgrad
 Regression der integrierten Formen von 3 Reaktionsmodellen

Ergebnis: Der Umsatz entspricht einer Reaktion nach Avrami-Erofeev mit $A = 2,656 \cdot 10^{33} \text{ min}^{-1}$, $E = 259,4 \text{ kJ/mol}$ und $p = 0,094$
 Der kritische Umsatzgrad wurde zu $d = 0,6$ gefunden.

Wärmeflußmessungen im Bereich von 65-80°C an den gleichen Anzündhütchen liefern praktisch identische Aussagen für Lagerzeitextrapolationen und eine nahezu gleiche Aktivierungsenergie von $252 \text{ kJ/mol}^{10)}$.

Die „Meilensteine“ der Prozedur sind in den Abb.10 und 11 dargestellt.

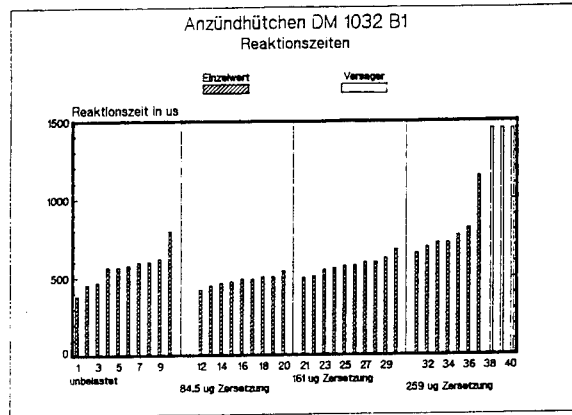
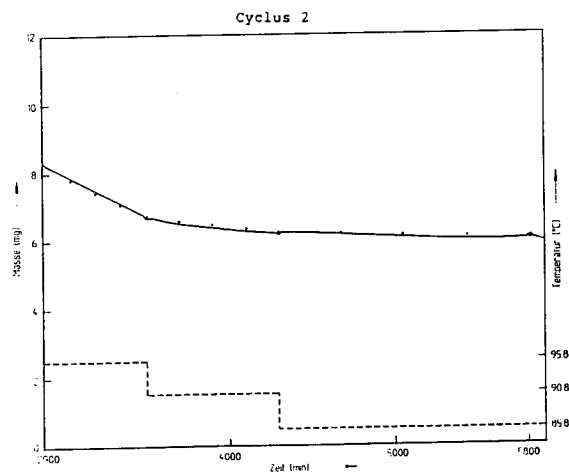
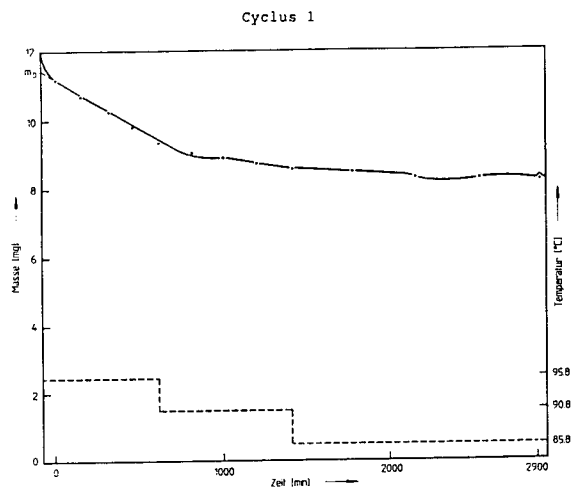


Abb.10. Bestimmung des kritischen Zersetzungsgrades

Der Wert von 161 µg vor den Versagern wurde als Grenze angenommen; aus dem Massenverlust kann später aus der Kinetik ein Reaktionsgrad zugeordnet werden.



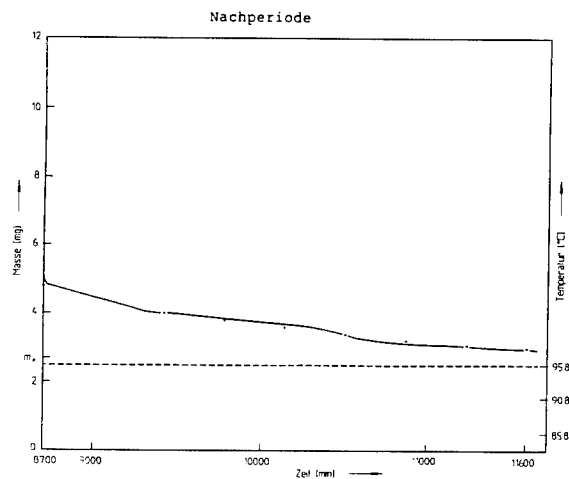
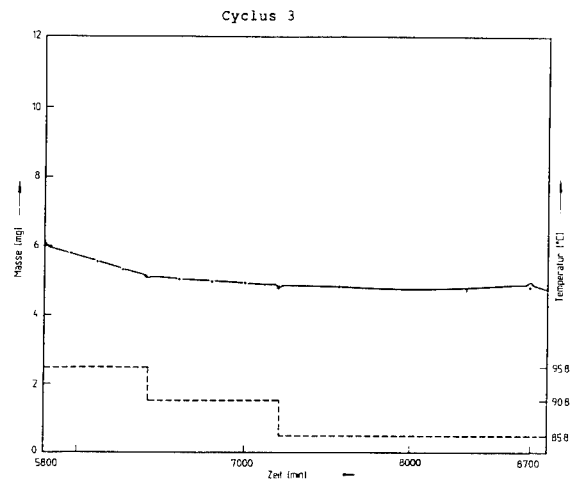


Abb.11. Anpassung des Arami-Erofeev-Reaktionsmodells
(durchgezogene Kurve: experimentelle Werte)

Im Rahmen der damals zur Verfügung stehenden Meßgenauigkeit der Thermowaage sind die Abweichungen des Modells vom Experiment gering.

Literatur

- 1) Frey, M., *BICT-Bericht* 1.1/7040/86.
- 2) Bohn, M.A., Volk, F., *Propellants, Explosives, Pyrotechnics* **17** (1992) 171-178.
- 3) Yamamoto, K., *Explosives* **18** (1965).
- 4) Rogers, R.N., *Thermochim. Acta* **11** (1975).
- 5) Bartlett, B.E., Tompkins, F.C., Young, D.A., *Proc. R. Soc. (London)* **A 246** (1958).
- 6) Connick, W., May, F.G.J., Thorpe, B.W., *Aust. J. Chem.* **22** (1969).
- 7) Patel, R.G., Chandhri, M.M., *Proc. Symp. Chem. Probl. Conn. Stab. Explos.* **4**, (1967).
- 8) Robertson, A.J.B., *Trans. Faraday Soc.* **45** (1949).
- 9) Ticmanis, U., Scheunemann, W., *Vortrag 16. Sprengstoffgespräch* 4.-6.11.1992 in Meppen, *BICT-Bericht* 330/11993/92.
- 10) Wilker, S., Pantel, G., Kaiser, M., Ticmanis, U., *Proc. Annu. Conf. ICT* **26** (1995).
- 11) Kissinger, H.E., *Anal. Chem.* **29** (1957) 1702-1706.
- 12) Kaiser, M., Ticmanis, U., *Thermochim. Acta* **250** (1995) 137-149.
- 13) Scheunemann, W., Ticmanis, U., *BICT-Bericht* 330/13683/94.

TNO Prins Maurits Laboratory

AGEING OF MTV

Chris van Driel, Jeannette Leenders, Jan MeulenbruggeLange Kleiweg 137
P.O. Box 45
2280 AA Rijswijk
Netherlands

ABSTRACT

Ageing of MTV (Magnesium, Teflon, Viton) is caused by the reaction of magnesium with water into magnesium hydroxide and hydrogen gas. This reaction continues until all magnesium is converted into magnesium hydroxide. The coating of magnesium with Teflon and Viton has a minor effect on the progression of the ageing process.

The conversion rate during ageing of an MTV composition is modelled on the basis of calorimetric measurements during ageing of MTV under various conditions. In the model the conversion is insignificant until time t_1 which can be considered as an induction time. t_1 is temperature dependent but not affected by the humidity of the surrounding air. After t_1 the reaction rate increases linearly in time. This linear increase depends on temperature and relative humidity. After 15 to 20 % of the magnesium is converted at time t_2 the reaction rate decreases linearly in time until the conversion is complete.

The increase of the reaction rate after t_1 is caused by the so-called 'peeling-effect': during conversion magnesium hydroxide shells are peeled off from the magnesium particles, in this way enlarging the reacting magnesium surface area. The decrease of the reaction rate after t_2 is caused by a decrease of the available free magnesium surface area.

The proposed model is confirmed by measurements of the conversion of MTV that was aged in a climatic cabinet. The model can be used to predict the conversion in time as a function of temperature and relative humidity.

1. INTRODUCTION

Magnesium is used in pyrotechnics as a fuel. The pyrotechnic composition MTV is, for instance, applied in infra red flares and igniter compositions for rocket propellants or low vulnerability gun propellants [1]. The aim of this study is to investigate the influence of temperature and humidity on the ageing of MTV in order to gain a better understanding of the deterioration of magnesium containing compositions under various conditions. At TNO-PML a preliminary model of the ageing behaviour is set up which will be used and subsequently refined in a future study.

The ageing of MTV was followed by various techniques, like microcalorimetry, IR-spectroscopy, and X-ray diffraction. In order to study the effects of ageing on the performance of the MTV the dimensions, mechanical properties, and burning characteristics of pressed igniter MTV pellets have been determined.

2. EXPERIMENTAL

Materials

For all experiments a single batch of MTV was prepared consisting of 65 wt% Mg, 30 wt% Teflon, and 5 wt% Viton. The magnesium particles were coated with Teflon and Viton. Pellets were pressed from this batch with a height and diameter of 15.85 mm and a porosity of 29.6 vol%. This MTV composition is used as igniter composition [1].

Calorimetry

Calorimetric measurements were performed using MTV powder, MTV pellets, or magnesium powder. The heat released correlates with the amount of reacted magnesium [2]. The relative humidity (RH) of the air in the calorimeter was set using saturated aqueous salt solutions. Conditions under which the measurements were performed are given in Table 1. For each measurement approximately 5 g MTV was used.

Table 1 Conditions under which the calorimetric measurements were performed.

code	T [°C]	RH [%]	code	T [°C]	RH [%]
PW80-80	80	80	PW50-80	50	80
PW80-60	80	60	PW50-60	50	60
PW80-50	80	50	PW50-50	50	50
PW80-20	80	20	PW50-0	50	0
PW80-0	80	0	PL80-80 ^{*)}	80	80
PW60-80	60	80	MG80-80 ^{**)}	80	80
PW60-60	60	60	MG80-0 ^{**)}	80	0
PW60-50	60	50			

^{*)} Experiment performed with a pellet instead of powder.

^{**)} Experiment performed with magnesium powder instead of MTV powder.

Accelerated Ageing of MTV

MTV-pellets were artificially aged in a climatic cabinet at a constant temperature of 80°C and a constant RH of 80 %. At specific time intervals length, diameter and mass of these pellets were measured after reducing the RH for 1 hour to less than 1 % at 80°C in order to remove the water from of the porous pellets.

Mechanical characteristics

Compressibility, stress and compression modulus of MTV pellets were determined by compression of the pellets. These measurements were performed in threefold under ambient conditions.

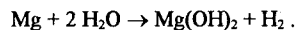
Burning behaviour

A closed vessel with a volume of 700 ml was used to determine the burning characteristics of the MTV pellets [3]. For each measurement a single pellet was ignited by a squib. Measurements were performed in threefold.

3. RESULTS AND DISCUSSION

3.1 Ageing mechanism of MTV

IR-spectroscopy and X-ray diffraction show that ageing of MTV is caused by the reaction of magnesium with water into magnesium hydroxide:



This agrees with the fact that, after being aged in a climatic cabinet for a long time, the mass of MTV pellets is increased by a factor of 1.91 which corresponds to a conversion of 100 %. Chemical analysis also confirms the formation of magnesium hydroxide.

The coating of the magnesium particles, consisting of Teflon and Viton, deteriorates not measurably during ageing.

The MTV pellets increase in mass and size during ageing. Table 2 shows the averages of the mass and size increase as a function of time for pellets which were stored at 80°C and 80 % RH.

Table 2 Increase of mass and volume of MTV-pellets during ageing at 80°C and 80 % RH.

Ageing time [h]	Mass increase [%]	Volume increase by factor
32	4.2 ± 0.1	1.038 ± 0.002
81	38.9 ± 0.5	1.552 ± 0.020
143	72.7 ± 0.5	2.272 ± 0.022
336	91.1 ± 0.2	3.68 ± 0.13

The observed mass increase is a result of the ageing reaction, given above. The volume increase is only partly caused by the formation of magnesium hydroxide, which has a different density than magnesium. The main cause of the volume increase is the fact that during the ageing process magnesium hydroxide shells are peeled off from the magnesium particles, the so-called 'peeling effect' [4]. These shells also push the Teflon/Viton matrix aside, hence enlarging the porosity of the pellets considerably.

3.2 Calorimetry

The microcalorimetric measurements show no heat production if the RH is zero. In all other cases initially a small decrease in heat production is found during a relatively short time interval, t_1 . After this time interval the heat production starts to increase almost linearly in time. t_1 was found to vary with temperature as is shown in Table 3 and is independent of the RH (for RH > 0). No correlation could be found between the level of the heat production until t_1 and the RH. From the results obtained at 80°C and 20 % RH (exp. PW80-20) it could be determined that only a fraction of $8 \cdot 10^{-6}$ of the magnesium has reacted during this time interval which means that only a negligible amount of magnesium was converted into magnesium hydroxide, probably due to the reaction of adsorbed moisture with unprotected magnesium.

After t_1 the heat production was observed to increase linearly in time. The slopes of the curves after t_1 measured at 80 % RH (exps. PW80-80, PW80-60, and PW80-50) are also given in Table 3. Because of the short time during which the measurements at other humidities were performed the correlation between the linear heat increase and the RH could not be performed reliably.

Table 3 Time interval t_1 and slope of the curve after t_1 at 80 % RH at various temperatures.

T [°C]	t_1 [h]	slope [$\text{mW} \cdot \text{kg}^{-1} \cdot \text{h}^{-1}$]
80	11	101.6
60	100	1.2
50	$3 \cdot 10^2$	0.12

In this preliminary set of experiments during only one measurement (exp. PW80-20) the heat production was recorded sufficiently long to show that the linear increase of the heat production after t_1 is followed by a decrease of the heat production which is also nearly linear in time. Because this experiment was stopped after 600 hours for technical reasons it is not known how the heat production proceeded at the end of the conversion. The result of this measurement is shown in Figure 1.

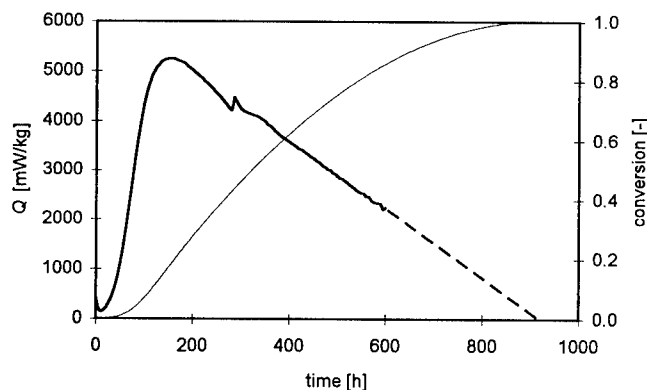


Figure 1 Heat production, Q , of 5 g MTV at 80°C and 20 % RH. The measured data are extrapolated for time exceeding 600 hours.
— : Q ; — : conversion

The increase in heat production after t_1 is caused by an increase of the reaction rate. This increase is a result of the peeling effect mentioned in section 3.1: during conversion shells of magnesium hydroxide with magnesium are peeled off from the magnesium particles, thus enlarging the free reacting magnesium surface area. When the total available magnesium surface area reduces (after t_2) the reaction rate decreases.

One measurement (PL80-80) was performed using an MTV pellet instead of MTV powder in order to determine whether pressing has any influence on the ageing of MTV. No significant differences with respect to the results of exp. PW80-80, however, were found as shown in Figure 2: both the time interval after which the heat production starts to increase, t_1 , and the slope of the curve after that time interval, a_1 , are

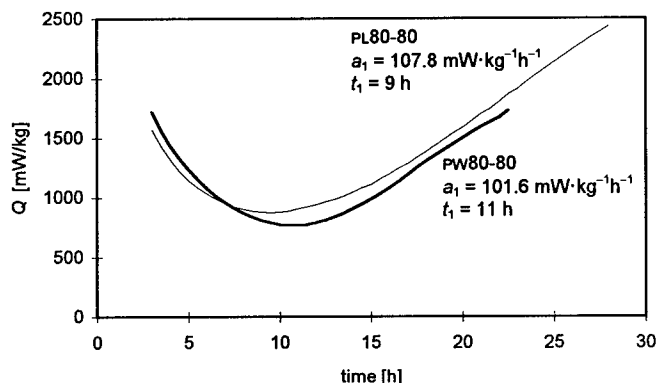


Figure 2 Heat production, Q , at 80°C and 80 % RH during ageing of MTV powder and an MTV pellet (exps. PW80-80 and PL80-80).
 — : powder; - - : pellet

almost similar. This means that moisture can penetrate freely into the pellet. Pressing may cause some protection if the pellet is pressed to a much higher density.

Another measurement was performed with magnesium powder instead of MTV (exp. MG80-80). In this case a similar shape of the heat production curve was found as for MTV. For the measurement with magnesium t_1 equals 6 hours and the slope of the curve after t_1 equals 289 mW·kg⁻¹·h⁻¹. In order to compare the latter value with the one obtained for MTV powder it has to be multiplied by the mass fraction of magnesium in MTV which is 0.65. This results in 188 mW·kg⁻¹·h⁻¹ which is nearly twice the value found for MTV powder. Thus the binder system consisting of Teflon and Viton provides some protection during the ageing process though not a very effective one.

On the basis of the results of the various microcalorimetric measurements the dependence of the ageing of MTV on temperature and RH can be modelled. This will be described in the next section. The model will be refined in a future study.

3.3 Modelling of the ageing of MTV

The conversion curve of the ageing of MTV can be derived from the heat production curve if it is assumed that finally all magnesium converts into magnesium hydroxide. The fact that the mass of MTV pellets after complete conversion was increased by a factor of 1.91, which corresponds to 100 % conversion, confirms this assumption. The heat production is proportional to the reaction rate. The conversion curve at 80°C and 20 % RH is plotted in Figure 1 together with the heat production curve. Figure 3 shows a schematic representation of a model which describes the reaction rate.

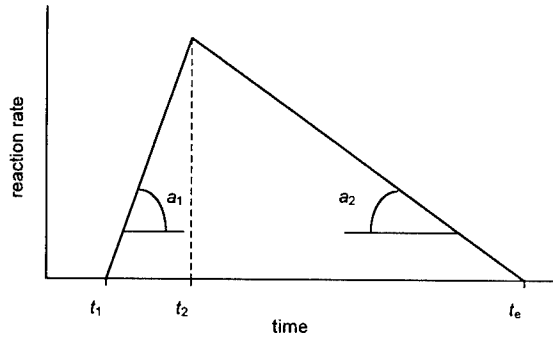


Figure 3 Schematic representation of the modelled reaction rate.

For the derivation of the model the following symbols are used:

- t_1 [h] = moment at which the heat production starts to increase
- t_2 [h] = moment at which the increase of the heat production stops and a decrease starts
- t_e [h] = moment at which all magnesium in the MTV is converted
- a_1 [h⁻²] = slope of the curve of the reaction rate (in [fraction·h⁻¹]) between t_1 and t_2
- a_2 [h⁻²] = slope of the curve of the reaction rate between t_2 and t_e

Dependence of t_1 on temperature and relative humidity

From the values of t_1 given in Table 3 it follows that t_1 decreases by a factor of approximately $\sqrt{10}$ at an increase of the temperature by 10°C. t_1 is independent on the RH as described in section 3.2. Using these data the next equation can be calculated for t_1 :

$$t_1 = 8.0 \cdot 10^4 e^{(-0.1151 \cdot T)} \quad [\text{h}]. \quad (1)$$

Dependence of a_1 on temperature and relative humidity

From the values of the slopes of the heat production curves given in Table 3 it follows that the slope increases by a factor of approximately 9 at an increase of the temperature by 10°C. From these data the influence of the temperature on the slope can be calculated:

$$a_1 = A \cdot e^{(0.2197 \cdot T)} \quad [\text{h}^{-2}], \quad (2)$$

in which A is a factor which depends on the RH. The duration of these preliminary measurements was not sufficient to determine the influence of the RH on this slope accurately. Theoretically a quadratic dependence is expected because for the reaction 2 moles of H₂O are needed per mole Mg. If this correlation is taken the constant A follows from:

$$A = A' \times \text{RH}^2 \quad [\text{h}^{-2}]. \quad (3)$$

The value of A' can be calculated if the slope between t_1 and t_2 of the heat production curve which was measured at 80°C and 20 % RH ($a_1 = 1.375 \cdot 10^{-5} \text{ h}^{-2}$) is fitted to these equations: $A' = 8.0 \cdot 10^{-16} \%^{-2} \text{ h}^{-2}$. The complete equation for the positive slope, a_1 , of the curve between t_1 and t_2 becomes:

$$a_1 = 8.0 \cdot 10^{-16} e^{(0.2197 \cdot T)} \times \text{RH}^2 \quad [\text{h}^{-2}]. \quad (4)$$

Derivation of t_2 and a_2

It is assumed that the heat production will decrease linearly to zero until all the magnesium is converted into magnesium hydroxide. Exp. PW80-20 was stopped too early to confirm this assumption. The reaction rate can now be described by two straight lines as depicted in Figure 3. The conversion at t_2 , ξ_{t_2} , appears to be approximately 0.15. a_2 , t_2 , and t_e can now be determined mathematically since the total area under the reaction rate curve represents 100 % conversion of magnesium:

$$a_2 = -a_1 \times \frac{\xi_{t_2}}{1 - \xi_{t_2}} \quad [\text{h}^{-2}], \quad (5)$$

$$t_2 = t_1 + \sqrt{\frac{\xi_{t_2}}{0.5 \cdot a_1}} \quad [\text{h}], \quad (6)$$

$$t_e = t_2 + (t_2 - t_1) \frac{1 - \xi_{t_2}}{\xi_{t_2}} \quad [\text{h}]. \quad (7)$$

The main uncertainty in this model is the value of ξ_{t_2} which probably mainly depends on material characteristics like the size and shape of the magnesium particles.

Measurements of the conversion from the mass increase of pellets which were aged in the climatic cabinet at 80°C and 80 % RH confirm the proposed model. Figure 4 shows the conversion of the pellets determined from their weight changes together with the calculated conversion as a function of time. The measured points plot at best on the calculated conversion curve if a value of 0.17 is chosen for ξ_{t_2} .

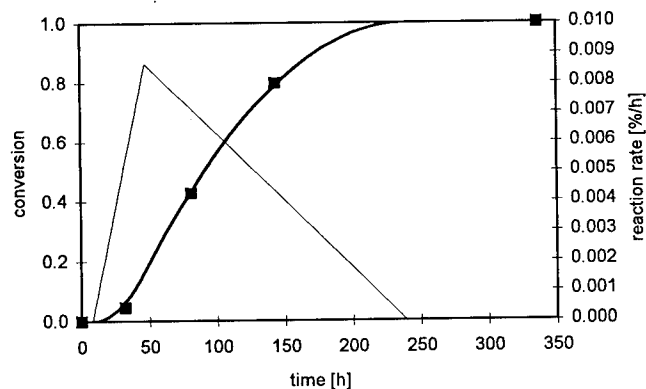


Figure 4 Ageing of MTV pellets at 80°C and 80 % RH.
 ■ : measured data; — : calculated conversion;
 — : calculated conversion rate

3.4 Mechanical characteristics and burning behaviour

The mechanical characteristics of MTV pellets which were aged in the climatic cabinet at 80°C and 80 % RH have been determined by compression tests. The maximum stress (σ_{\max}), compression ($\epsilon_{\max} = (L_0 - L_{\min})/L_0 \cdot 100 \%$), and compression modulus ($E = \Delta\sigma/\Delta\epsilon$) were determined. Figure 5 shows the results of the pressing experiments.

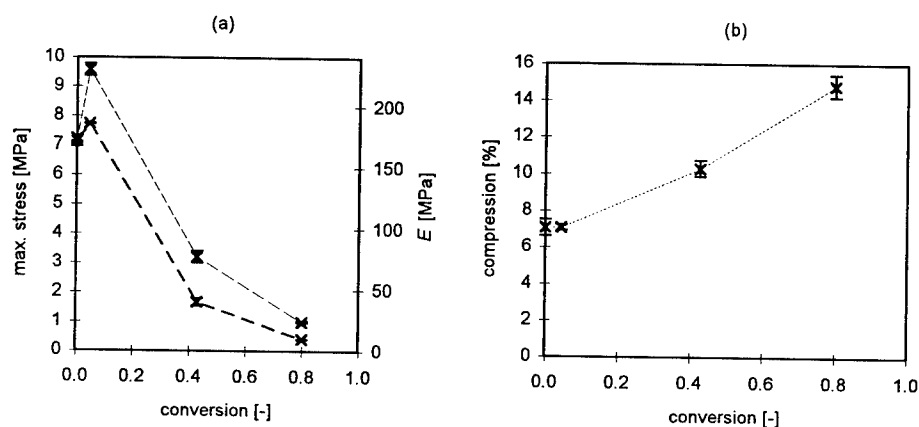


Figure 5 Change of mechanical properties of MTV pellets due to ageing at 80°C and 80 % RH.
(a) — — — : maximum stress; — — — : E ; (b) : compression

These figures show that the maximum stress and modulus initially increase. At a conversion above approximately 10 % the mechanical properties deteriorate. The initial improvement of the mechanical properties can be attributed to the formation of magnesium hydroxide which contributes to a higher maximum stress and modulus than MTV. Further conversion of magnesium into magnesium hydroxide, however, causes deterioration of the internal structure of the MTV pellet which results in a decrease of the mechanical properties. Another possibility is that magnesium itself breaks up as a result of the so called peeling effect of oxidising magnesium, mentioned above (sections 3.1 and 3.2). The pellets which were aged until 100 % conversion could not be tested due to disintegration of the pellets.

The burning behaviour of MTV pellets which were aged at 80°C and 80 % RH for various periods was determined by performing closed vessel experiments. Maximum pressure and the time till maximum pressure were determined. Figure 6 shows the results of these experiments. The pellets which were aged until 80 % conversion and until complete conversion could not be tested because of their poor mechanical properties.

This figure shows that time till maximum pressure increases with increasing conversion which means that aged MTV appears to be more difficult to ignite and to burn slower than unaged MTV. The maximum pressure slightly increases as a result of ageing. This seems to be illogical because an increase in burning time will also increase the heat losses in the closed vessel, which will cause a decrease in maximum pressure. The amount of MgF_2 , which is the main cause for the pressure build up, does not change

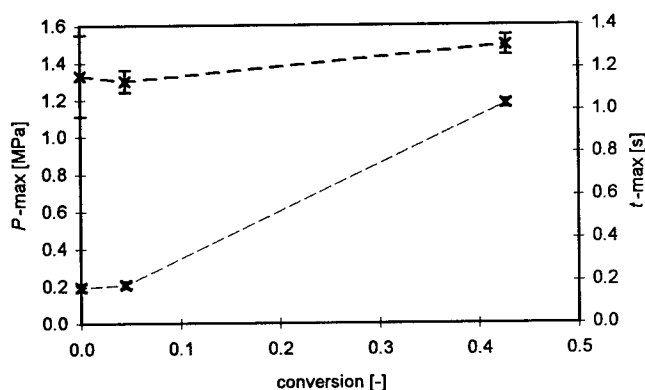
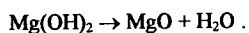


Figure 6 Change of burning characteristics maximum pressure, P_{max} , and time till maximum pressure, t_{max} , of MTV pellets due to ageing at 80°C and 80 % RH.
 — — — : P_{max} ; — — — : t_{max} .

considerably because of the excess of magnesium: the MTV contains 65 wt% magnesium while the stoichiometric proportions are 32 wt% Mg and 68 wt% Teflon/Viton. An explanation for the observed slight pressure increase is that heating of the magnesium hydroxide which is formed during ageing results in the formation of water vapour according to the reaction



At 42 % conversion during ageing 42 wt% of magnesium is converted into magnesium hydroxide which results in 0.046 moles of water vapour per pellet, which causes a significant pressure increase.

4. CONCLUSIONS

- Ageing of MTV is caused by the conversion of magnesium into magnesium hydroxide in the presence of moisture. The binder system, consisting of Teflon and Viton, provides some protection against ageing, though not a very effective one. The binder system itself deteriorates not measurably.
- On the basis of preliminary microcalorimetric measurements a model has been set up which describes the influence of temperature and humidity of surrounding air on the ageing rate and conversion of an MTV composition. The model is confirmed by measurements of the conversion of MTV pellets, determined from their mass increase due to ageing.
- As a result of ageing the MTV pellets increase considerably in mass and volume while their mechanical properties deteriorate during ageing. The burning characteristics of aged MTV pellets, the maximum pressure and in particular the burning time, are changed with respect to unaged pellets. These changes greatly affect the performance of magnesium containing compositions.

REFERENCES

- 1 J. Leenders, J.J. Meulenbrugge. "Igniter development for lova gun propellants." Europyro 93, 5^e Congrès International de Pyrotechnie du Groupe de Travail. Strasbourg, 6 – 11 June 1993, p. 611.
- 2 R.G. Shortridge, A. Chin, B.R. Hubble. "Microcalorimetric study of the aging reactions of atomized magnesium powder." NSWCCR/RDTR-92/0003, Naval Surface Warfare Center Crane Division Ordnance Engineering Directorate Crane, In 47522-5050, 20 February 1992.
- 3 J. Spasojevic, Batinic-Haberle, D. Barisin. "Functional and chemical characterization of the aging process of an igniter." 20th International Conference of ICT, Karlsruhe, 1989, p. 61-1 – 61-13.
- 4 L.G. Svensson, private communication.

ESTIMATION OF DETONATION PARAMETERS OF A NEW CLASS OF EMULSION EXPLOSIVES

Victor Odintsov, Vitaly Pepekin
Institute of Chemical Physics, Russian Academy of Sciences,
4 Kosygin Street, Moscow, 117977, Russia.

ABSTRACT

The work is devoted to a quantitative estimation of detonation parameters of mixtures of emulsion explosive with powder on the base of thermodynamic computations of the ideal and non-ideal detonations. The two models of the BKW equation of state are used in computations for gaseous detonation products — BKW-RDX and BKW-RR. The three thermodynamic models of detonation are considered: 1) the ideal detonation — total chemical equilibrium of the detonation products at the Chapman-Jouguet point; 2) the slightly non-ideal detonation — the detonation products consist of the two chemical subsystems (the products of decomposition of emulsion matrix and those of powder) which are equilibrium inside themselves but do not chemically reacting one with another; 3) the strongly non-ideal detonation — the products consist of the three chemical subsystems (the products of decomposition of the aqueous solution of ammonium nitrate, those of the mixture of hydrocarbons, and those of powder) which are equilibrium inside themselves but do not chemically reacting one with another. It is shown that the estimations of detonation parameters on the base of thermodynamic computations and common reasonings on the sensitivity mechanism of emulsion explosives allow to consider it possible to increase the power characteristics of such explosives by 10–20% and higher by means of replacing sensitizing hollow glass microballoons or gas-producing additions with dispersed high explosives and, in particular, powders the problem of utilization of which in connection with military conversion is still rather far from the resolution.

In [1] it is proposed that the power characteristics of the known and applied in practice emulsion explosives could be significantly improved by introducing gun-powders in them. The present work is devoted to estimation of detonation parameters of mixtures of emulsion explosive with powder.

Emulsion explosives have good water-resistance and explosion safety, i.e.

Table 1.

Compound	Chemical formula	Mass part, %	Enthalpy, kJ/kg
Ammonium nitrate	$H_4N_2O_3$	77	-4563
Water	H_2O	16	-15860
Saturated liquid hydrocarbon	$(CH_2)_n$	6	-2088
Oleic acid	$C_{18}H_{34}O_2$	1	-2841
Powder	$C_{24}H_{33.13}N_{13.19}O_{46.68}$	over 100%	-2272

low sensitivity to detonation initiation. However, the advantage at the time of production and transportation — low sensitivity — transforms in the disadvantage at the time of direct application since the common sensitization by means of introduction into emulsion matrix of hollow microballoons or chemicals producing gaseous bubbles leads to the decrease in charge density and, accordingly, to the fall in efficiency of action of detonation products of emulsion explosives.

To overcome the mentioned shortcoming when applying emulsion explosives it seems to be perspective to add dispersed gun-powder to emulsion matrix instead of microballoons or gas-producing chemicals. In this case one can expect the smaller decrease and possibly even the increase in detonation parameters along with the increase of addition quantity in contrast to the sharp fall in detonation parameters when adding hollow glass microballoons to the emulsion matrix [2].

The composition of the emulsion matrix is given in Table 1 and is identical to that considered in [2]. The gross composition of powder, the detonation parameters of which were studied in [3] (powder #3) and which was considered as an addition to industrial explosives in [1], is given in Table 1 as well as enthalpies of compounds.

The density of the emulsion matrix was defined to be 1353 kg/m^3 [4]. For the sake of generality the two values of powder density are considered — 1600 and 1353 kg/m^3 . The latter value is chosen to reveal the effect of powder addition in contrast to that of the charge density. Thus, the two different cases of determination of the charge density are consi-

Table 2.

Explosive	Density, kg/m ³	Model of EOS	Detonation velocity, m/s	Pressure, GPa	Temperature, K
Powder	1353	BKW-RR	6706	15.68	3375
—"	1353	BKW-RDX	6568	15.44	2834
Emulsion	1353	BKW-RR	6613	13.95	1781
matrix	1353	BKW-RDX	7134	16.04	976

dered: 1 — the charge density is rising from 1353 kg/m³ while adding powder with density of 1600 kg/m³; 2 — the charge density is constant and equals to 1535 kg/m³ irrespective of powder quantity in a mixture.

The thermodynamic computations of detonation of emulsion explosives were conducted with the use of the Automated System of Thermodynamic Reckonings and Algorithms ASTRAL based on the methods described in [5]. The Becker-Kistiakowsky-Wilson (BKW) equation of state were used to describe behavior of the gaseous phase of detonation products; both dispersed diamond and dispersed graphite crystals of condensed carbon were allowed to be formed in detonation products [6], the behavior of graphite being described by the Cowan's equation of state and the diamond phase being considered as incompressible. The two sets of coefficients of the BKW equation were used: BKW-RDX and BKW-RR. The problem of selection of these models for detonation computations of emulsion explosives was discussed in [2].

The computed equilibrium dependences of detonation velocity on powder quantity in mixture with the emulsion matrix are depicted in Fig. 1. The results of computations with the BKW-RDX and BKW-RR models differ not only by absolute values, but by the characters of dependences. Indeed, at the constant initial density of charge (1353 kg/m³) the detonation velocity computed with the BKW-RDX equation decreases along with the increase in powder amount in mixture, whereas the BKW-RR equation gives the small increase in detonation velocity. This is a consequence of the fact that the computed values of detonation velocity of powder differ insignificantly for the BKW-RDX and BKW-RR models whereas the detonation velocity of the emulsion matrix computed with the BKW-RDX equation significantly surpasses the one computed with the BKW-RR equation

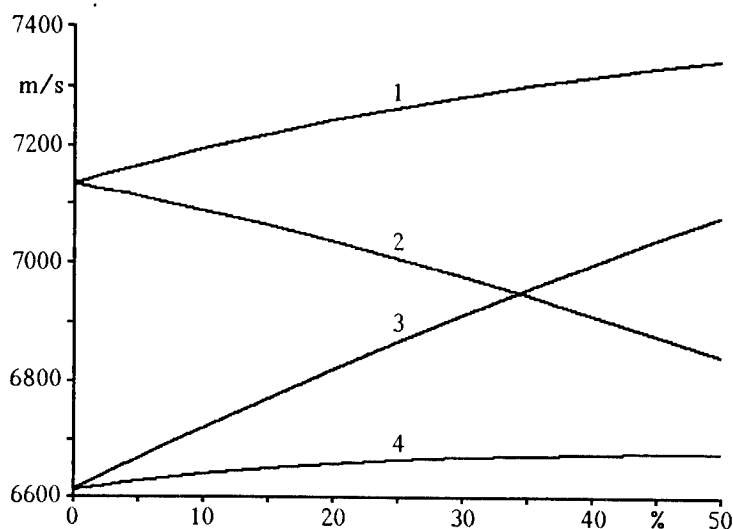


Fig. 1. Dependences of ideal detonation velocity on mass percentage of powder in mixture with emulsion matrix. Lines: 1 — the BKW-RDX model, powder density is 1600 kg/m³; 2 — BKW-RDX, 1353; 3 — BKW-RR, 1600; 4 — BKW-RR, 1353.

(see Table 2). What is more, the detonation velocity of the emulsion matrix computed with the BKW-RDX model noticeably exceeds the one of powder at the equal initial density of charge.

A somewhat different picture is observed in behavior of detonation pressure dependences on powder quantity in mixture presented in Fig. 2. At the constant initial density of mixture (1353 kg/m³) the detonation pressure remains almost constant for the BKW-RDX model (being changed from 16.04 GPa for the emulsion down to 15.44 GPa for powder) and increases for the BKW-RR model from 13.95 GPa (emulsion) up to 15.68 GPa (powder).

While increasing initial density of mixture due to higher density of powder (the first case of mixture density definition) the velocity and pressure of detonation rise together with increasing powder amount.

The temperature of detonation products of the considered explosives behaves itself in a similar way both for the different models and for the different cases of initial density definition. This is connected to the fact

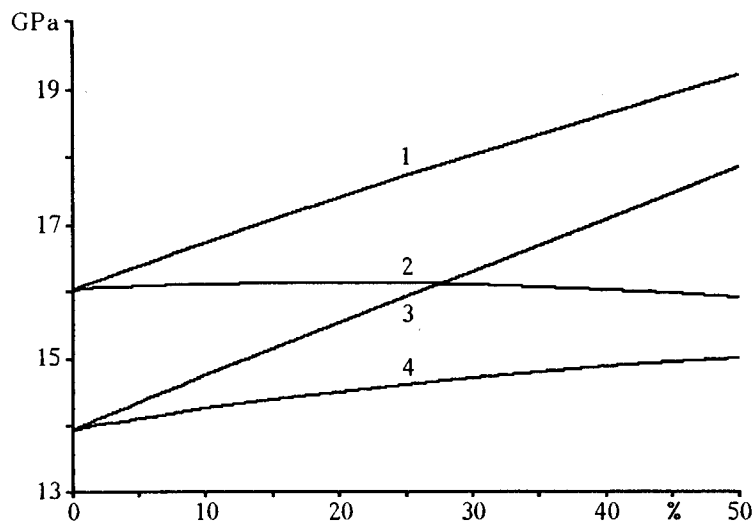


Fig. 2. Dependences of pressure of ideal detonation on mass percentage of powder in mixture with emulsion matrix. Lines: 1 — the BKW-RDX model, powder density is 1600 kg/m^3 ; 2 — BKW-RDX, 1353; 3 — BKW-RR, 1600; 4 — BKW-RR, 1353.

that the temperature of detonation products of powder significantly surpasses the one of the emulsion matrix. As it should be expected for the BKW equation of state the detonation temperature of the more dense mixture is lower than that of the less dense mixture. One should pay attention to the very low temperature of detonation of the emulsion computed with the BKW-RDX model (see Table 2).

The advantage of the use of powder instead of hollow microballoons in mixture with the emulsion matrix can be clearly illustrated by the ratio of detonation velocities of these mixtures at the equal mass content of additions. In Fig. 3 there are presented dependences of ratio of detonation velocities of emulsion mixtures with powder to those with microballoons for the considered equation of state models and the two ways of charge density definition of mixtures with powder. The values computed with the use of the BKW-RDX and BKW-RR models from [2] were used as the values of detonation velocity of the emulsion matrix with microballoons mixtures. They were obtained in assumption of partial reaction of detonation products by means of correlating slopes of the computed and experimental dependences of detonation velocity versus initial density. It follows from Fig. 3

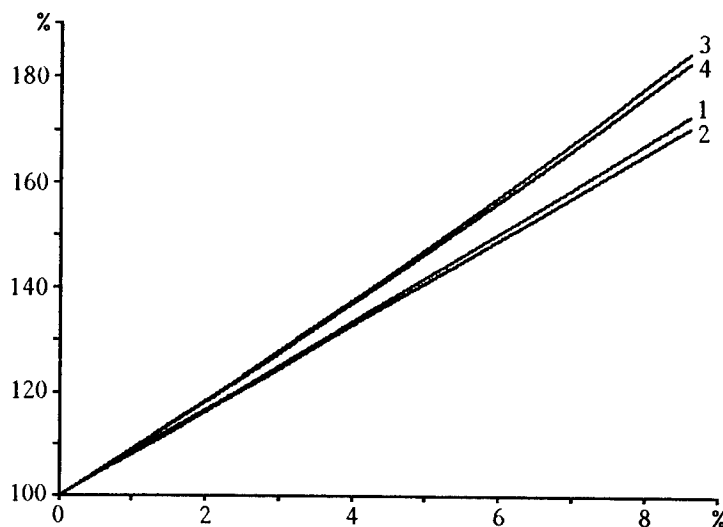


Fig. 3. Dependence of ratio of ideal detonation velocity of mixture with powder to detonation velocity of mixture with microballoons [2] on mass percentage of addition. Lines: 1 — the BKW-RDX model, powder density is 1600 kg/m³; 2 — BKW-RDX, 1353; 3 — BKW-RR, 1600; 4 — BKW-RR, 1353.

that an increase in amount of addition to the emulsion leads to a sharp rise in detonation velocity ratio value. Thus, the computed detonation velocity of emulsion explosive with powder is almost twice as much as the one of mixture with microballoons at mass content of addition about 10%.

However these results are obtained in the case when the detonation of mixtures with powder was considered as the totally ideal one, but the detonation of mixtures with microballoons — as the thermodynamically non-ideal one with incomplete reacting of detonation products by the Chapman-Jouguet point. Therefore, to reveal the effect of the possible thermodynamic non-ideality of detonation of mixtures of the explosive emulsion with powder let us consider two more cases one of which is most unfavorable and can serve as the bottom border of estimation of detonation parameters of these mixtures.

The first case of the thermodynamic non-ideality of detonation can be modelled by the supposition that the detonation products of the emulsion matrix and powder do not chemically interact one with another. Then the

detonation products consist of the two subsystems which are totally equilibrium inside themselves but do not enter in chemical interaction one with another and at the same time all other parameters of state in both subsystems have the equal values. Later on we will call this case for short as the thermodynamically slightly non-ideal detonation.

The second, most unfavorable for detonation, case of thermodynamic non-ideality consists in the supposition that each of the basic compounds of mixture reacts by itself. In this case the whole system is considered to consist of the three chemical subsystems (1 — aqueous solution of ammonium nitrate, 2 — mixture of hydrocarbons, and 3 — powder) the products of each of which are chemically equilibrium. Chemical interactions between subsystems are absent. In other respects the system is equilibrium, i.e. the parameters of state throughout the whole system at the Chapman-Jouguet point are uniform.

The results of computations show that the absence of chemical interaction between products of decomposition of the emulsion matrix and powder does not practically affect the detonation parameters of mixture. It is expressed in indistinctness of the lines depicting the dependences of detonation parameters of mixtures of the emulsion matrix with powder for the totally ideal and thermodynamically slightly non-ideal (2 subsystems) detonations. The dependences of the ratio of detonation velocities of the emulsion—powder mixtures to detonation velocities of the emulsion—microballoons mixtures on the mass part of addition amount in the considered case of slight non-ideality of detonation practically coincide with the corresponding dependences for the totally ideal detonation.

The different picture is observed in the case of thermodynamic non-ideality with formation of the three subsystems in detonation products. This case corresponds to the considered in [2] thermodynamic non-ideality of detonation with the zero extent of reacting of products. For short we will call in this work the case under consideration (3 subsystems) as the thermodynamically non-ideal detonation with the zero extent of reacting. Since the decomposition products of the oxidizing subsystem (aqueous solution of ammonium nitrate) do not react with the decomposition products of the combustible subsystem (hydrocarbon mixture) then far from the whole of the chemical part transforms into the thermal and elastic parts of the internal energy by the Chapman-Jouguet point. As a result the detonation parameters occur to be significantly lower than in the cases considered above.

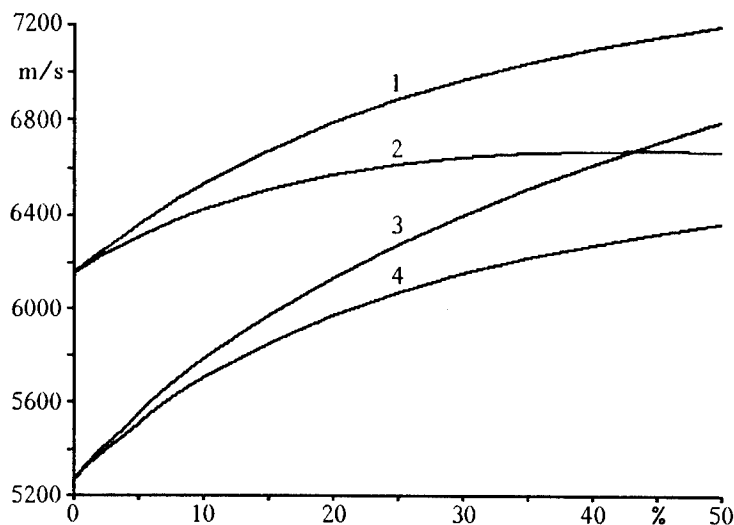


Fig. 4. Dependence of substantially non-ideal detonation velocity versus mass percentage of powder in mixture with emulsion matrix. Lines: 1 — the BKW-RDX model, powder density is 1600 kg/m^3 ; 2 — BKW-RDX, 1353; 3 — BKW-RR, 1600; 4 — BKW-RR, 1353.

In Fig. 4 there are presented the computed dependences of the thermodynamically non-ideal detonation velocity of the emulsion—powder mixture on the addition amount for the two models of equation of state and for the two ways of initial density definition in the case of zero extent of reacting. The character of the dependences differs from that for the cases of the ideal and slightly non-ideal detonations. The detonation velocity values for the neat emulsion at the zero extent of reacting are significantly less than those at the ideal and slightly non-ideal detonations for the both models. The increase in the powder amount in mixture leads to the increase in detonation velocity approaching that of the ideal and slightly non-ideal detonations.

The possibility to obtain the higher values of detonation parameters by adding to the emulsion matrix the powder instead of hollow microballoons even in the case of detonation with zero extent of reacting is illustrated by the dependences of ratio of detonation velocities of emulsion mixtures with powder at zero extent of reacting of products to detonation velocities of emulsion mixtures with microballoons versus addition amount in mixture with the emulsion matrix which are given in Fig. 5.

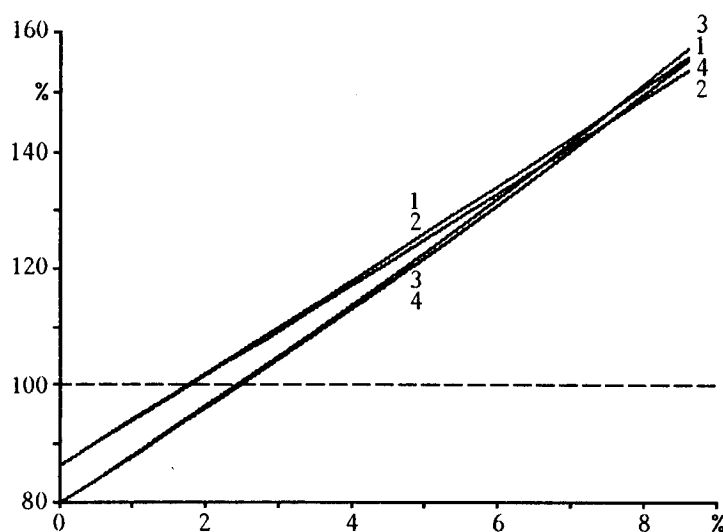


Fig. 5. Dependence of ratio of substantially non-ideal detonation velocity of emulsion mixture with powder to detonation velocity of emulsion mixture with microballoons [2] versus mass percentage of addition. Lines: 1 — the BKW-RDX model, powder density is 1600 kg/m^3 ; 2 — BKW-RDX, 1353; 3 — BKW-RR, 1600; 4 — BKW-RR, 1353.

The detonation velocity of neat emulsion in the case of zero extent of reacting makes up about 80% of the velocity of ideal detonation which is supposed to be the detonation of emulsion matrix from comparison in [2] with the experimental data. However, while increasing addition amount in mixture at least to 1.5–2.5% by mass the velocity of substantially non-ideal detonation in mixture with powder becomes equal to the velocity of partially non-ideal detonation in mixture with microballoons. Further increase in addition amount leads to the quick rise in velocity ratio. Thus, already at 9% of addition by mass the detonation velocity of mixture with powder at zero extent of reacting of products exceeds the velocity of partially non-ideal detonation of mixture with microballoons by 50–60%.

It follows from the experimental data [4] that the critical diameter of detonation of mixture with microballoons characterizing sensitivity of a charge reaches 25 mm and practically ceases to decrease at densities less than 1200 kg/m^3 that corresponds to about 1.6% of microballoons in mixture by mass. At about the same value the experimental dependences of detonation velocity on initial density reach the maximum [4]. It seems

possible to consider the values of partially non-ideal detonation of emulsion mixture with microballoons computed by the BKW-RDX and BKW-RR models at the mentioned charge density as the optimal ones for practical application by correlation of detonation velocity and critical diameter. Therefore the indicated detonation velocity values computed with the use of the two models of equation of state can be assumed to be bench-marks for estimating an effectiveness of adding powder instead of microballoons by referring to these values the detonation velocity values of emulsion mixtures with powder computed with the use of the corresponding models for the two ways of charge density definition.

In Figs. 6 and 7 there are presented the quantities of ratios of detonation velocities of emulsion mixtures with powder with respect to the bench-mark values of detonation velocities of emulsion mixture with microballoons in dependence on powder amount in mixture for the two different ways of mixture density definition.

It is seen from Fig. 6 that in the case of constant mixture density while adding powder one can expect increase in detonation velocity by 10–15% in comparison with the bench-mark values. The expected value of detonation velocity of emulsion mixture with powder should be placed in a region limited at top by the ideal detonation velocity dependence and at bottom by dependence of detonation velocity with zero extent of reacting. One can notice the different character of dependences of the ideal detonation velocity computed with the different models of equation of state. With the increase in powder amount in mixture the relative velocity of ideal detonation insignificantly increases in the case of the BKW-RR model and decreases in the case of the BKW-RDX model. Relative velocity of detonation with zero extent of reacting increases for the both models but in different degrees. In any case the velocity of detonation with zero extent of reacting exceeds the bench-mark detonation velocity of emulsion mixture with microballoons at mass content of powder in mixture with the emulsion matrix higher than 12%.

In the case of increasing density of mixture along with increasing in mass content of powder of density 1600 kg/m^3 in it (see Fig. 7) the raise of ideal detonation velocity while adding powder in comparison with the bench-mark values for mixture with microballoons reaches 15–20%. The characters of dependences of relative velocities of the ideal and substantially non-ideal detonations for the both models of equation of state are

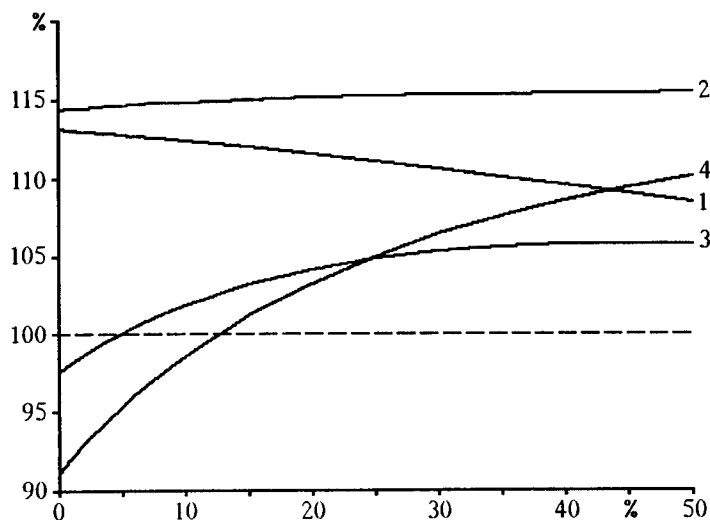


Fig. 6. Dependence of the relative detonation velocity on mass percentage of powder (1353 kg/m^3) in mixture. Lines: 1 — the ideal detonation, the BKW-RDX model; 2 — ideal, BKW-RR; 3 — substantially non-ideal, BKW-RDX; 4 — substantially non-ideal, BKW-RR.

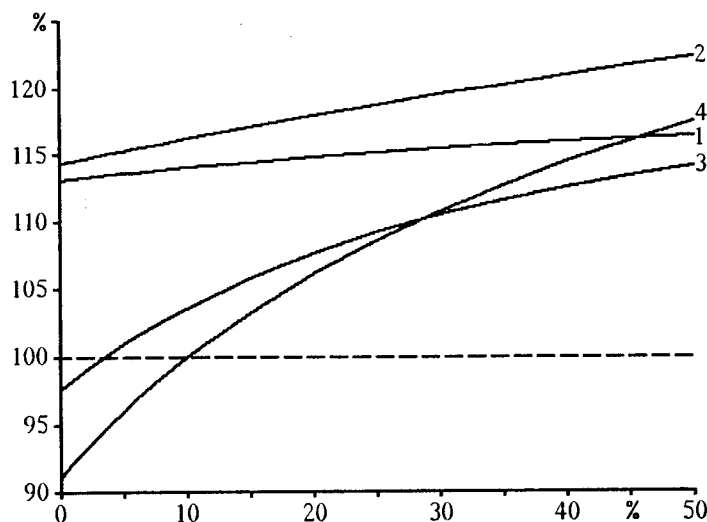


Fig. 7. Dependence of the relative detonation velocity on mass percentage of powder (1600 kg/m^3) in mixture. Lines: 1 — the ideal detonation, the BKW-RDX model; 2 — ideal, BKW-RR; 3 — substantially non-ideal, BKW-RDX; 4 — substantially non-ideal, BKW-RR.

similar — the detonation velocity increases while increasing in mass part of powder in mixture for the all considered cases. The difference consists only in values of the dependence slopes. Detonation velocities even in the case with zero extent of reacting of products exceed the bench-mark values at mass content of powder in mixture higher than 10%.

In [2,4] it is supposed that detonation of the emulsion matrix proceeds ideally from the thermodynamic point of view, i.e. the detonation products completely gets mixed up and reacts by the Chapman-Jouguet point. The increase in quantity of hollow microballoons raises sensitivity of mixture but leads to the increase in thermodynamic non-ideality of detonation which is modelled in [2] by the decreasing in extent of chemical reacting of decomposition products of aqueous solution of ammonium nitrate and hydrocarbon mixture.

Under the influence of leading shock wave the hollow glass microballoons are closed down creating the "hot spots" in the nearest vicinity of which the chemical reactions in the emulsion matrix are initiated and accelerated at the beginning stages. However, the creation of significant local raises in temperature — hot spots — is accompanied by the decrease in total energy quantity per unit of mass or volume of mixture because of supplanting an energetic substance from a part of volume and partial replacing it with inert glass. This leads to a reduction in completeness of chemical reactions at the later stages of process of reacting after hot spots dissipating. As a result the rise of temperature of products in the chemical reaction zone while approaching the Chapman-Jouguet point is significantly reduced because of the less average concentration of energy in the system. This in turn leads to the reduction in rates of chemical interactions and energy release. One obtains the exclusive circle or, in other words, a system with positive feedback.

Thus, the sensitizing an emulsion explosive by the means of adding the hollow microballoons results in a reduction of extent of reacting of detonation products.

As it is noticed in [3] reaching the detonation conditions in powders requires a powerful initiation and quite big diameter of a charge. However, the systematic data on sensitivity of powders to shock wave initiation and their critical diameters have not been found in literature. Therefore we can only discuss here some common reasonings for verifying which it is

necessary to conduct systematic experimental researches.

Concerning the possibility of occurrence of the detonation mode of chemical decomposition propagation in powder under influence of a shock wave coming from emulsion matrix one can say only that the velocity and pressure of the neat emulsion detonation are comparable with those of the powder detonation (see Table 2). Hence one can expect that the power of shock wave is quite enough for initiation of detonation in a powder particle.

The critical diameter of detonation, even if it exceeds size of a powder particle, cannot be directly applied to the considered case since the particle is surrounded by quite dense and heated substance being the detonation products of emulsion.

The proposed mechanism of sensitizing an emulsion explosive by means of adding the powder particles is based on the same principle as in the cases of hollow microballoons and gaseous bubbles. The temperature of powder detonation products is substantially higher (by 1500–2000 K for the different models of equation of state) than that of neat emulsion so that the powder particles play a part of "hot spots". For all this the detonation products of powder particles play a part of the hot spots not only for the nearest vicinity as in the case with microballoons but for significantly farther neighbourhoods since the molecules of powder store energy not less than the molecules of explosion emulsion itself.

Therefore, by a very careful estimation one can expect that the extent of reacting of detonation products of the mixture of emulsion matrix with powder particles would be not less than by detonation of the emulsion mixture with microballoons. As the more reasonable estimations one can consider assumptions on the thermodynamic ideality of detonation of mixture with powder or the non-ideality of detonation caused by total or partial non-mixing of detonation products of emulsion and powder in consequence of the sizes of macro-particles of the latter. The latter case is modelled by the considered above variant of slightly non-ideal detonation with formation of the two chemical subsystems in detonation products the results of computations for which are practically identical with those for the ideal detonation.

Thus, the estimations of detonation parameters on the base of thermodyna-

mic computations and common reasonings on the sensitivity mechanism of emulsion explosives allow to consider it possible to increase the power characteristics of such explosives by 10–20% and higher (in dependence on the bench-mark values) by means of replacing sensitizing hollow glass microballoons or gas-producing additions with the dispersed powders the problem of utilization of which in connection with military conversion is still rather far from the resolution.

References

1. Odintsov V.V., Pepekin V.I., Gubin S.A., Korsunsky B.L. Explosive Properties of Systems Based on Water-filled Powders. — *Khimicheskaya Fizika* (Chemical Physics), 1994, V.13, No.8-9, p.179. (Russ.).
2. Odintsov V.V., Pepekin V.I., Kutuzov B.N. Estimation of Thermodynamic Non-ideality of Emulsion Explosive. — *Khim. Fiz.*, 1994, V.13, No.11, p.79. (Russ.).
3. Odintsov V.V., Pepekin V.I., Gubin S.A. Theoretical Study of Detonation Characteristics and Efficiency of Powders. — *Khim. Fiz.*, 1993, V.12, No.10, p.1404. (Russ.).
4. Lee J., Sandstrom F.W., Craig B.G., Persson P.-A. Detonation and Shock Initiation Properties of Emulsion Explosives. — *Proc. 9-th Symp. (Int.) on Detonation*. 1989, p.263.
5. Gubin S.A., Odintsov V.V., Pepekin V.I. Thermodynamic Computations of Complex Chemical Systems. — Moscow: Mosc. Phys.-Eng. Inst., 1987. (Russ.).
6. Odintsov V.V., Gubin S.A., Pepekin V.I., Akimova L.N. Determination of Shape and Size of Diamond Crystals Behind Detonation Wave in Condensed Explosives. — *Khim. Fiz.*, 1991, V.10, No.5, p.687. (Russ.).

26th International ICT-Conference, July 4 - July 7, 1995, Karlsruhe, FRG
Pyrotechnics - Basic Principles - Technology - Application

KLASSIFIZIERUNG VON GROSSFEUERWERK
(Classification of display firework)

Dr. Klaus Basse
Verband der pyrotechnischen Industrie
Kaiserwerther Str. 135
40474 Düsseldorf

Dr. Dietrich Eckhardt,
Dr. Hans-Jochen Rodner
Bundesanstalt für Materialforschung und -prüfung
Unter den Eichen 87
12205 Berlin

Kurzfassung

Ziel der Untersuchungen war es eine Gefahrgutklassifizierung und eine Lagergruppenzuordnung für Großfeuerwerksgegenstände durchzuführen. Auf der Basis einer Systematisierung und einer kodierten Beschreibung der in Deutschland vorhandenen Großfeuerwerksgegenstände wurden experimentelle Prüfungen nach den UN-Richtlinien für den Transport gefährlicher Güter vorgenommen und allgemeine Kriterien für die Einordnung der Gegenstände in Gefahrklassen abgeleitet. Es zeigt sich, daß in Abhängigkeit von der Verpackung eine differenzierte Zuordnung von Großfeuerwerksgegenständen zu den Gefahrklassen 1.1 bis 1.4 möglich ist. Eine entsprechende Verfahrensanleitung wird angegeben.

Abstract

The object of the tests was the Hazard Classification and the Storage Group Classification for articles of display firework. It was introduced a system for the display firework. A code helps to conduct the tests in accordance to the UN - Recommendations on the Transport of Dangerous Goods. Universally applicable criteria were derived for the Classification of display firework. It was shown, that a different classification of class 1.1 to class 1.4 is possible in the dependence on the packaging. A Classification method was explained.

Inhalt/ Content

1. Einleitung/ Introduction
2. Systematisierung des Großfeuerwerk/ Classification in categories
 - 2.1 Gegenstandskategorien/ Categories of the articles
 - 2.2 Großfeuerwerk in Deutschland/ Display firework in Germany
3. Klassifikationsverfahren und Versuchsplanung/ Classification and tests
4. Prüfergebnisse und Diskussion/ Test results and discusion
5. Schlußfolgerungen/ Conclusions

1. Einleitung

Pyrotechnische Gegenstände werden nach ihrer Gefährlichkeit und ihrem Verwendungszweck eingeteilt. In Deutschland unterscheidet man:

Klasse	Bezeichnung	Zulassungszeichen
Klasse I	Kleinstfeuerwerk	BAM-PI-...
Klasse II	Kleinf Feuerwerk	BAM-PII-...
Klasse III	Mittelfeuerwerk	BAM-PIII-...
Klasse IV	Großfeuerwerk	nicht zulassungspflichtig
T ₁	pyrotechnische Gegenstände für technische Zwecke	BAM-PT ₁ -...
T ₂	pyrotechnische Gegenstände für technische Zwecke	BAM-PT ₂ -...

Die Anforderungen an diese Gegenstände sind in der Anlage 1 zur 1. SprengV in der Fassung der Bekanntmachung vom 31.01.1991 (BGBl. I, S. 169), letzte Änderung der ersten Verordnung zum Sprengstoffgesetz vom 26. Oktober 1993 (BGBl. I, S. 1782) /4/ festgelegt. Das Sprengstoffgesetz regelt den Umgang, den Verkehr, die Beförderung und die Einfuhr der o.g. Gegenstände.

Zur Pyrotechnik gehört in Deutschland noch die pyrotechnischer Munition. Der Umgang mit der pyrotechnischer Munition allerdings wird im Waffengesetz vom 19. September 1972 (BGBl. I, S. 1797) geregelt. Die Anforderungen an die pyrotechnische Munition, gegliedert in die Klassen PMI und PMII, sind in der Anlage I, Nr. 5 der 3. Verordnung zum Waffengesetz in der Fassung vom 2. Oktober 1991 (BGBl. I, S. 1872) /2/ beschrieben. Baugruppen oder ganze Gegenstände werden auch für Großfeuerwerk verwendet.

Großfeuerwerk ist nach § 3 1. SprengV /3/ im Gegensatz zu den anderen Klassen nicht zulassungspflichtig. Allerdings besteht trotzdem die Notwendigkeit diese Gegenstände der Klasse IV nach dem Transportrecht /4/ und §4 der 2. SprengV /5/ entsprechenden Gefährklassen bzw. Lagergruppen zuzuordnen.

Die Zuordnung nach dem Transportrecht wird innerhalb eines international harmonisierten Prüfverfahrens vorgenommen. Ähnlich aufgebaut ist auch das Prüfverfahren zur Zuordnung einer Lagergruppe. In der Vergangenheit wurde eine Zuordnung des Großfeuerwerkes generell zur Gefährklasse/ Lagergruppe 1.1 G vorgenommen. Da es das größte Gefahrenpotential darstellt, das von einem verpackten Gegenstand mit Explosivstoff ausgehen kann, wurde bisher auf Prüfungen verzichtet.

In den Niederlanden und in Kanada durchgeführte Tests ergaben jedoch, daß nicht alle Gegenstände des Großfeuerwerkes das typische Verhalten einer Gefährklasse - 1.1 - Gegenstandes aufweisen. Die Prüfungen in Kanada ergaben eine Zuordnung auf der Basis von

vergleichenden Betrachtungen, die sich an den Kalibern der einzelnen Gegenstände orientierten. Gegenstände mit Blitzsatz werden generell der Gefahrklasse 1.1 G zuordnet. Nach Meinung der BAM sind detailliertere Aussagen möglich. Diese Überlegungen sind durch erste Versuche bestätigt worden. Es wurde entschieden in Zusammenarbeit mit dem Verband der pyrotechnischen Industrie auf der Grundlage einer Systematisierung des Großfeuerwerkes in Deutschland eine komplexe Versuchsserie zur Bewertung des Verhaltens von Großfeuerwerk unter verschiedenen Belastungen zu untersuchen.

2. Systematisierung des Großfeuerwerkes

2.1 Gegenstandskategorien

Auf der Grundlage einer Analyse des verwendeten Großfeuerwerkes in Deutschland wurde eine Systematisierung des in Deutschland verwendeten Großfeuerwerks in 8 Gegenstandskategorien (Raketen, Bomben, Römische Lichter/ Bombenrohre, Feuertöpfe, Fontänen/..., Lichterbilder/ Frontstücke, Baugruppen, Feuerwerksbatterien) vorgenommen.

Über eine codierte Darstellung wird die Einteilung der Gegenständen übersichtlicher und erleichtert. Diese Systematisierung ermöglichte auch als wichtige Einflußgröße für die Transportsicherheit die Verpackung in die Codierung einzubeziehen.

Die Codierung ist wie folgt aufgebaut:

Typ	-	Unterteilung des Großfeuerwerkes in acht Gegenstandsgruppen
Aufbau	-	Baugruppen, die Explosivstoff enthalten
Masse	-	Nettoexplosivstoffmasse (NEM) des Gegenstandes
Verpackung	-	Art und Material der Außenverpackung (entsprechend Transportvorschriften z.B. 4G - Kiste aus Pappe), Angabe der Nettoexplosivstoffmasse innerhalb eines Versandstückes;
Unterverpackung	-	Füllmaterial, Trennwände, auch Innenverpackung

Anmerkung zur Verpackung:

Als Verpackung (Außen- bzw. Transportverpackung) ist grundsätzlich eine nach UN-Richtlinien geprüfte Gefahrgutverpackung einzusetzen. Der Typ ist anzugeben (z.B. Kiste aus Pappe - 4G oder Kiste aus Holz - 4C1 usw.).

Als Unterverpackung gelten Pappkartons oder gleichartige Verpackungen, die

- gleiche mechanische Stabilität sowie
- gleiche Dämpfungseigenschaften hinsichtlich Flammenwirkung und Detonationsunterdrückung haben (z.B. Schaumeinsätze oder dicke Plastfolien u.ä.).

Die 8 Gegenstandskategorien sind wie folgt aufgebaut:

1. Raketen - (R)**Aufbau:**

	Treibladung
1	Effekte (außer Knalleffekte, andere als Schwarzpulver)
2	Effekte mit Knallerzeugnissen oder Chloratsätzen
3	Gegenstände mit reinen Blitz- oder Knallsätzen
Z	Zerlegerladungen (außer Schwarzpulver)

Massen: Nettoexplosivstoffmasse (NEM)

1	< 50 g
2	50g.....250g
3	250g.....500g

Verpackung: (Nettoexplosivstoffmasse pro Verpackung)UN geprüfter Karton (z.B.: ... - **4G**)

1	≤ 5 kg
2	≤ 20 kg

Unterverpackung:Unterverpackung (UVP) **A** = PappkartonUnterverpackung (UVP) **B** = Pappkarton mit Füllstoff (z.B. Recycling-Papier, Chips)

Beispiel:

Typ	/	Aufbau	/	Masse	/	Verpackung	/	UVP
R	/	1 Z	/	3	/	2 - 4 G	/	A

2. Bomben - (B)**Kaliber:**

- Ø 100 mm
- Ø 150 mm
- > Ø 150 mm

Aufbau:

T	Treibladung
1	Effekte (außer Knalleffekte, andere als Schwarzpulver)
2	Effekte mit Knallerzeugnissen oder Chloratsätzen
3	Gegenstände mit reinen Blitz- oder Knallsätzen (nur Blitzbomben)
Z	Zerlegerladungen (außer Schwarzpulver)

Masse: Nettoexplosivstoffmasse (NEM)

	≤ 100 mm	150 mm	> 150 mm
1	≤ 350 g	≤ 500 g	≤ 750 g
2	≥ 350 g	≥ 500 g	≥ 750 g

Verpackung: (Nettoexplosivstoffmasse pro Verpackung)

UN geprüfter Karton (z.B.: 4G /...)

1 ≤ 5 kg**2** ≤ 20 kg mit Füllstoff**Unterverpackung:**Unterverpackung (UVP) **A** = Pappkarton 3-5 mmUnterverpackung (UVP) **B** = Pappkarton mit Füllstoff (z.B. Recycling Papier, Chips)

Beispiel:

Typ	/	Kaliber	/	Aufbau	/	Masse	/	Verpackung	/	UVP
B	/	150	/	T 2	/	2	/	2 - 4 G	/	B

3. Römische Lichter / Bombenrohre - (RL)**Aufbau:**

- | | |
|----------|--|
| T | Treibladung |
| 1 | Effekte (Sterne, Bombetten, außer Knalleffekte andere als Schwarzpulver) |
| 2 | Effekte mit Knallerzeugnissen oder Chloratsätzen |
| 3 | Gegenstände mit reinen Blitz- oder Knallsätzen |

Massen: Nettoexplosivstoffmasse (NEM)**1** < 150 g**2** 150 g ... 500 g**3** > 500 g**Verpackung:** (Nettoexplosivstoffmasse pro Verpackung)

UN geprüfter Karton (z.B.: ... - 4 G)

1 ≤ 5 kg**2** ≤ 20 kg**Unterverpackung:**Unterverpackung (UVP) **A** = PappkartonUnterverpackung (UVP) **B** = Pappkarton mit Füllstoff (z.B. Recycling Papier, Chips)

Beispiel:

Typ	/	Aufbau	/	Masse	/	Verpackung	/	UVP
RL	/	1	/	2	/	1 - 4 G	/	B

4. Feuertöpfe - (FT)**Kaliber:** 60 mm...80 mm...100 mm...**Aufbau:**

- | | |
|----------|--|
| T | Treibladung |
| 1 | Effekte (außer Knalleffekte, andere als Schwarzpulver) |
| 2 | Effekte mit Knallerzeugnissen oder Chloratsätzen |
| 3 | Gegenstände mit reinen Blitz- oder Knallsätzen |

Massen: Nettoexplosivstoffmasse (NEM)

- | | | |
|----------|-----------------------|-----------------------|
| | $\leq 100 \text{ mm}$ | $\geq 150 \text{ mm}$ |
| 1 | $< 150 \text{ g}$ | $< 500 \text{ g}$ |
| 2 | $> 150 \text{ g}$ | $> 500 \text{ g}$ |

Verpackung: (Nettoexplosivstoffmasse pro Verpackung)

UN geprüfter Karton (z.B.: ... - 4G.)

- | | |
|----------|----------------------|
| 1 | $\leq 5 \text{ kg}$ |
| 2 | $\leq 20 \text{ kg}$ |

Unterverpackung:Unterverpackung (UVP) **A** = PappkartonUnterverpackung (UVP) **B** = Pappkarton mit Füllstoff (z.B. Recycling-Papier, Chips)

Beispiel:

Typ	/	Kaliber	/	Aufbau	/	Masse	/	Verpackung	/	UVP
FT	/	80	/	T 1 .	/	2	/	2 - 4 G	/	B

5. Fontänen, Bränder, Wasserfälle, Lichter, Lanzen - (F)**Aufbau:**

- | | | |
|----------|--------------------|--|
| 1 | Satzgruppe 3, 4, 5 | {Satzgruppenzuordnung gemäß UVV 55k /7/} |
| 2 | Satzgruppe 2 | |

Masse: Nettoexplosivstoffmasse (NEM)

- | | |
|----------|------------------------------------|
| 1 | $\leq 50 \text{ g}$ |
| 2 | $50 \text{ g} \dots 200 \text{ g}$ |
| 3 | $> 200 \text{ g}$ |

Verpackung: (Nettoexplosivstoffmasse pro Verpackung)

UN geprüfter Karton (z.B.: ... - 4G.)

- | | |
|---|---------|
| 1 | ≤ 5 kg |
| 2 | ≤ 20 kg |

Unterverpackung:

Unterverpackung (UVP) **A** = Pappkarton

Unterverpackung (UVP) **B** = Pappkarton mit Füllstoff (z.B. Recycling Papier, Chips)

Beispiel:

Typ	/	Aufbau	/	Masse	/	Verpackung	/	UVP
F	/	2	/	3	/	1 - 4 G	/	B

6.Lichterbilder, Frontstücke - (LB)

Aufbau:

- | | |
|---|--|
| 1 | Zusammenstellung von Einzelementen als Teilbild oder Teilfrontstück |
| 2 | Zusammenstellung von Einzelementen als komplettes Bild oder Frontstück |

Masse: Nettoexplosivstoffmasse (NEM)

- | | |
|---|---------|
| 1 | ≤ 20 kg |
|---|---------|

Verpackung: (Nettoexplosivstoffmasse pro Verpackung)

- | | |
|---|--|
| 1 | UN- Verpackung (z.B.: ... - 4 G) |
| 2 | unverpackt, Anzündstellen abgedeckt, auf dem Fahrzeug befestigt. |

Beispiel:

	Typ	/	Aufbau	/	Masse	/	Verpackung
	LB	/	1	/	1	/	1 - 4 G
oder	LB	/	2	/	1	/	2 -

7. Baugruppen - (BG)

(Kreisel, Sterne, pyrotechnische Munition u.s.w.)

Aufbau:

- | | |
|---|--|
| 1 | Effekte (Sterne, Kreisel, Pfeifen, u.s.w.) |
| 2 | Effekte mit Knallerzeugnissen oder Chloratsätzen |
| 3 | Blitzladung (Bombetten) |
| 4 | Treibladung (schubfähig mit Düse) |

Masse : Nettoexplosivstoffmasse (NEM)

- | | | |
|---|---------|-------|
| 1 | < 50 g | |
| 2 | 50 g | 100 g |
| 3 | > 100 g | |

Verpackung: (Nettoexplosivstoffmasse pro Verpackung)

UN geprüfter Karton (z.B.: ... - 4G)

- | | |
|---|---------|
| 1 | ≤ 5 kg |
| 2 | ≤ 20 kg |

Unterverpackung:

Unterverpackung (UVP) **A** = Pappkarton

Unterverpackung (UVP) **B** = Pappkarton mit Füllstoff (z.B. Recycling Papier, Chips)

Beispiel:

Typ	/	Aufbau	/	Masse	/	Verpackung	/	UVP
BG	/	2	/	1	/	1 - 4 G	/	B

8. Feuerwerksbatterien - (FB)

Aufbau:

(T - Treibladung) - stets vorhanden, daher nicht mit anzugeben !

- | | |
|---|--|
| 1 | Effekte außer Knall (incl. Schwarzpulver als Zerlegerladung) |
| 2 | Effekte mit Knallkörpern oder Chlorat - Sternen |
| 3 | Gegenstände mit reinen Blitz- oder Knallsätzen |

Massen: (Nettoexplosivstoffmasse /Batterie)

- | | |
|---|-------------|
| 1 | <1 kg |
| 2 | 1 ... 5 kg |
| 3 | 5 ... 10 kg |

Verpackung: (Nettoexplosivstoffmasse pro Verpackung)

UN geprüfter Karton (z.B.: ... - 4G)

- | | |
|---|---------|
| 1 | ≤ 5 kg |
| 2 | ≤ 20 kg |

Unterverpackung:

Unterverpackung (UVP) **A** = Pappkarton

Unterverpackung (UVP) **B** = Pappkarton mit Füllstoff (z.B. Recycling Papier, Chips)

Beispiel:

Typ	/	Aufbau	/	Massen/	Verpackung	/	UVP
FB	/	1	/	1	1 - 4G	/	B

2.2 Großfeuerwerk in Deutschland

In Deutschland stellen nur einige der pyrotechnischen Fabriken Großfeuerwerk her. Ein Großteil des verwendeten Großfeuerwerkes wird jedoch importiert. Unter Heranziehung der vorstehend beschriebenen Systematisierung geben die folgenden Tabellen eine Übersicht über das in Deutschland verwendete Großfeuerwerk, sowie die in den einzelnen Gegenständen enthaltene Nettoexplosivstoffmasse.

Tabelle 1 Systematisierung vorhandener Großfeuerwerkssysteme

Typ	Aufbau Treiber (T)	Metall-Chlorat (1)	Cl. (2)	Bk (3)	Zerl. (Z)	Verpackungen		20 kg		Bemerkungen	
						5 kg	A	B	A	B	
Raketen (R)	x	x	x	x	x	-	x	x	x	-	
Bomben (B)	x	x	x	x	x	x	x	x	x	x	
Römische Licht. Bombenrohre (RL)	x	x	x	x	-	x	x	-	x	-	
Feuertöpfe (FT)	x	x	x	x	-	x	x	-	x	-	
Fontänen Bränder (F)	-	x	x	-	-	x	x	-	x	-	
Lichterbilder (LB)											vielfältige Zusammenstellung z.B. Fontänen, Wasserfälle usw.
Baugruppen (BG)	x	x	x	x	-	x	x	x	x	x	z.B. dragierte Sterne (1.1 -1.3), Sternbomben reine Chloratsterne (1.1) Metallchlorat (1.3) Vogelschreckpatronen (1.1 -1.3)

Bk - Blitzknall, Zerl. - Zerlegerladung, Metall-Chlorat - Metallsätze, Cl. - Chloratsätze, A - Unterverpackung aus Pappe, B - Unterverpackung aus Pappe mit Füllstoff
x - existiert in D

Tabelle 2 Großfeuerwerk in Deutschland

Typ	Nettoexplosivstoffmasse pro Gegenstand							
	≤ 50g	≤ 100g	≤ 150g	≤ 200g	≤ 250g	≤ 350g	≤ 500g	≤ 750g
Raketen (R)	x	x	x	x	x	x	x	
Bomben (B)	x	x	x	x	x	x	x	x
Römische Lichter Bombenrohre (RL)	x	x	x	x	x	x	x	
Feuertöpfe (FT)	x	x	x	x	x	x	x	
Fontänen Bränder (F)	x	x	x	x	x	x	x	
Lichterbilder (LB)	x	x	x	x	x	x	?	?
Baugruppen (BG)	x	x						

x in Deutschland verwendet

Entsprechend den Angaben aus den beiden Tabellen wurde die Versuchsplanung hinsichtlich der Gefahrgutklassifizierung erstellt und die Versuchsmuster ausgewählt.

3. Klassifizierungsverfahren und Versuchsplanung

Die Versuchsmuster wurden aus den 8 Gruppen zusammengestellt. Die Gegenstände mit der größten Nettoexplosivstoffmasse aus jeder Gruppe wurden als erste geprüft.

Für die Gefahrgutklassifizierung wurden vom Oktober/ November 93 bis zum Dezember 94 folgende Prüfungen durchgeführt und die entsprechenden Kriterien nach UN - Empfehlungen zur Beförderung von gefährlichen Gütern angewandt:

4 (b)	-	Fallprüfung " 12 m Falltest "	-	/5/
6 (a)	-	Innenzündung eines Einzelpackstückes	-	/5/
6 (c)	-	Außenbrandtest eines Holzstapels mit Prüfmuster	-	/6/

Die bisherigen Ergebnisse der Prüfungen werden im folgenden dargestellt und bewertet.

4. Prüfergebnisse

Die Prüfungen von Großfeuerwerksgegenständen im 12 m - Falltest (UN - Test 4(b)) ergaben zwar eine Beschädigung der Verpackung und vereinzelt auch der Gegenstände. Es traten aber keine Beschädigungen auf, die auf eine explosive Reaktion oder Auslösung der Gegenstände hinweisen. Es wurden keine Brand- und Explosionsgefahren festgestellt. Das "Aufreißen" der Verpackung wird auch nach UN - Bewertungskriterien nicht als positives Ergebnis gewertet.

Im Einzelpackstücktest 6(a) wird ermittelt, ob die für eine 1.1 - Klassifizierung typische Reaktion - eine gleichzeitige Explosion des gesamten Inhaltes der Verpackung (Massenexplosion) - bei Zündung eines Gegenstandes auftritt.

Fontänen und Bränder werden meistens in Verpackungen dicht gepackt. Es besteht dadurch die Gefahr der Überzündung zwischen den Gegenständen. Es wurde keine massenexplosive Wirkung festgestellt. Gefahren für die Umgebung traten nicht auf. Eine Klassifizierung in die Unterklasse 1.1 nach den Kriterien des Testes 6(a) war nicht gerechtfertigt. Die Gefahr der Überzündung besteht bei anderen Gegenständen ebenfalls, wie z.B. bei Bomben, durch deren Zündmechanismus. Aufgrund der Optimierung der gesamten Prüfablaufes und dem Bestreben die Anzahl der Versuchsmuster gering zu halten, wurde darauf verzichtet mit allen Gegenstandgruppen die Innenzündung im Einzelpackstücktest durchzuführen.

Der Außenbrandtest - Prüfmethode 6(c) - spielt bei der Zuordnung zu den einzelnen Unterklassen im Klassifizierungsverfahren eine zentrale Rolle. Durch die Zuordnung zu einer Unterklasse ergeben sich Zusammenpackverbote und Zusammenladeregelungen für die einzelnen Gegenstände, außerdem müssen bestimmte Lademengen auf Beförderungseinheiten eingehalten werden.

Die Ergebnisse sind in der Tabelle 3 zusammengefaßt dargestellt.

Tabelle 3 Geprüfte Großfeuerwerkssysteme und Klassifizierung

33 - 17

Typ	Nettoexplosivstoffmasse pro Gegenstand								
	≤ 50g	≤100g	≤150g	≤200g	≤250g	≤350g	≤500g	≤750g	Z
Raketen (R)	☞	☞	☞	☞	☞	☞	1Z/4G2/A(*)	-	1.3
Bomben (B)	☞	☞	☞	☞	☞	45/1Z/4G1/A 60/1Z/4G1/A 60/T2Z/4G2/ 80/1Z/4G1/A 100/T2Z/4G1/A	100/T2Z/4G2 100/T2Z/4D2 125/T1Z/4G1/A 150/T2Z/4G2	210/T1Z/4G1/A ^(*) 1.3 /α1.1	
Römische Lichter Bombenrohre (RL)	☞	☞	☞	2/2/4G2	☞	2/2/4G2	(☞ ^(*))	-	1.3/ 1.2 (ab .50mm)
Feuertöpfe (FT)	☞	☞	60/T2/1/4G2	☞	☞	80/T2/4G2	-	-	1.3
Fontänen Bränder (F)	☞	☞	☞	☞	☞	☞	1/3/4G2/	-	1.3
Lichterbilder (LB)	☞	☞	☞	☞	☞	1/4G/	☞	☞	1.4
Baugruppen (BG)	☞	☞	☞	☞	☞	☞	☞	☞	1.1-1.4 ^(xx)
Feuerwerksbatterien (FB)	☞	☞	☞	☞	☞	☞	☞	☞	1.2/1.3

(*) - Kaliber/Aufbau/Masse /Verpackung/Unterverpackung (z.B. 100/T2Z/1/4G1/A)

♣ - ausstehende Versuche; (♣^(*)) - eventuell zusätzliche Versuche; ♣ - keine Versuche geplant, Zuordnungen fest; - - nicht vorhanden, Z - Zuordnung entspr. Prüfungen
alle Gegenstände mit Aufbau = Ziffer 3 (Blitzknall) sind Gefährklasse 1.1G; (xx) - Zuordnung anhand von vorhandenen Prüfergebnissen analoger oder ähnlicher Gegenstände

Zu den einzelnen Gegenstandgruppen können folgende Bemerkungen gemacht werden:

Alle Gegenstände mit Blitzknallsätzen werden aufgrund der Gefahr einer Massenexplosion der Gefahrklasse 1.1 zugeordnet.

Es zeigte sich erwartungsgemäß, daß viele Gegenstände (siehe Tabelle 3) ein Verhalten der Gefahrklasse 1.3 zeigen. Die Kriterien für die Gefahrklasse 1.3 G, wie die auftretenden hohen Wärmemengen (siehe Diagramme - Anlage 1) und die registrierten Wurfweiten von aus Holz, Pappe oder Kunststoff bestehenden Wurf-/ Splitterstücken, werden erfüllt. Bei höheren Nettoexplosivstoffmassen (siehe Tabelle 3 - Kaliber 210 mm/Bombe) ist eine Tendenz zur Gefahrklasse 1.1 G festzustellen.

Die Gegenstände für die Zusammenstellung von Lichterbildern, wie z.B. Fontänen, Bränder sind teilweise zugelassene Gegenstände entsprechend Sprengstoffgesetz. Aufgrund der Vielfalt der verwendeten Gegenstände kann sich eine differenzierte Zuordnung zu den Gefahrklassen ergeben. Es ist hilfreich die vorhandenen Prüfergebnisse und die Bewertung von ähnlichen bereits klassifizierten Gegenständen zur Zuordnung der Lichterbilder/ Frontstücke einzubeziehen.

Die verwendeten Gegenstände für Großfeuerwerksbaugruppen - "Baugruppen" - weisen sowohl das Verhalten der Gefahrklasse 1.1, 1.2, 1.3 als auch der Gefahrklasse 1.4 auf. Viele Baugruppen wie z.B. pyrotechnische Munition, pyrotechnische Sätze, verschiedene zugelassene Feuerwerkskörper besitzen schon eine Zuordnung.

Da das Klassifizierungsergebnis u.a. auch von der Art der Verpackung abhängig ist, muß auf der Suche nach einer geeigneten Verpackung überlegt werden, ob der Aufwand für eine neue Verpackungstechnologie oder -materialien auch dem Nutzen bezüglich der Möglichkeit höhere Ladungsmengen zu befördern, die Gefahrklasse herabzusetzen oder eventuell Beförderungseinheiten ohne spezielle Anforderungen zu verwenden, entspricht. Hier besteht bei der Beurteilung eine gegenseitige Abhängigkeit.

Folgende Hinweise zur Verwendung von Verpackungen können gegeben werden:

Überzündungen zwischen den Gegenständen werden durch einzeln verpackte Gegenstände, Trennwände, Füllmaterialien verhindert. Gegenstände können schon durch die Festlegung in Abschlußrohren separiert werden. Dadurch ergibt sich eine Abbrandverzögerung. Die Dauer der Reaktion der Versuchsmustern während des Außenbrandtestes wird durch die zeitversetzte Auslösung verlängert. Der Explosivstoff setzt sich nicht kurzfristig um. Die freiwerdenden

Wärmemenge erreicht keine Spitzenwerte, wie es bei kurzen heftigen Bränden vorkommen kann.

Als Materialien werden vorzugsweise Pappe, Holz oder Kunststoff verwendet. In die Außenverpackung integrierte Metallgitter verhindern das Auswerfen von Splittern, Spreng- und Wurfstücken. Um eine sichere Handhabung auf dem Abbrandplatz und während der Beförderung zu gewährleisten, wird versucht Mehrwegverpackungen z.B. auch mit Schubeinsätzen, die gleichzeitig Abschußkonfigurationen darstellen, aus Holz oder Kunststoff anzuwenden.

Allerdings ist es entsprechend den gesetzlichen Regelungen bisher nicht gestattet komplette Abschußbatterien bestehend aus den pyrotechnischen Gegenständen und aus Zündmitteln in den entsprechenden Abschußrohren zu befördern. Abschußrohre stellen keine geschlossene Innenverpackung dar. Erst auf dem Abbrandplatz soll das Großfeuerwerk aus seiner Ursprungsverpackung entnommen und komplettiert werden. Bei den vorgenommenen Testserien wurden auch komplettierte Abschußbatterien mit unterschiedlichen Kalibern in Holzkisten mit verschließbaren Seitenöffnungen im Außenbrandtest geprüft.

Es kam zu keiner Überzündung zwischen den Gegenständen, die in den Rohren festgelegt waren. Die Gegenstände wurden bestimmungsgemäß ausgelöst. Beim Test mit einer Kiste wurden die Gegenstände in vorbestimmter Richtung ausgeschleudert. Die Effekte reagieren bestimmungsgemäß in Ausstoßrichtung bei verringerter Flughöhe. Sind die Kisten übereinander gestapelt, zünden die Effektkörper schon in den unteren Kisten. Die Effektkörper in den obenliegenden Kisten werden bestimmungsgemäß herausgeschleudert. Durch das Auftreten von Überzündungen und gefährlichen Wurfstücken kann es zu einer Zuordnung in die Gefahrklasse 1.1 G und 1.2 G kommen. Eine Prüfung wird notwendig für eine differenzierte Gefahrgutklassifizierung. Ohne Prüfung werden die Großfeuerwerksgegenstände der Gefahrklasse 1.1 G zugeordnet.

Bei den "Römischen Lichtern" können die Gegenstände sowohl der Gefahrklasse 1.3 G als auch der Gefahrklasse 1.2 G zugeordnet werden. Es war ab Kaliber 50 mm festzustellen, daß die Effektkörper beim bestimmungsgemäßen Ausstoß die Nachweisschirme, die 4 m vom Holzstapel aufgestellt werden und dem Nachweis der Wirkung von Splittern und Wurfstücken dienen, durchschlagen können. Damit wurden die Kriterien für die Gefahrklasse 1.2 G erfüllt. Das Durchschlagsverhalten ist abhängig von der Konfiguration des aufschlagenden Körpers. Haben diese Gegenstände eine zylindrische Gestalt und bestehen sie aus einem Material mit einer größeren Härte als Pappe z.B. Kunststoff oder Aluminium, so kann es ab Kaliber 50 mm zu Durchschlägen kommen, wenn die entsprechende Aufschlaggeschwindigkeit die entsprechende kinetische Energie des "Geschosses" bestimmt. Bei Gegenständen mit abgerundeter Auftrefffläche und Pappumhüllung ist ein derartiges Verhalten nicht festzustellen.

Integriert man in die Außenverpackung ein Metallgitter verhindert man den Auswurf solcher "Geschosse" wirkungsvoll. Eine Zuordnung in die Gefahrklasse 1.3 G ist möglich.

Die Ergebnisse in Form der vollzogenen vorläufigen Zuordnung werden in der Tabelle 4 in zusammengefaßter Weise dargestellt.

Tabelle 4 Klassifizierung von Großfeuerwerk (Stand 03.95)

Gegenstands- gruppen	Gefahrklassen			
	1.1	1.2	1.3	1.4
Raketen (R)	R/3/...	-	R/...	-
Bomben (B)	B/.../3/... B/(>150)/...	B/(>125)/...(x)	B/...	-
Römische Lichter (RL)	RL/3/...	RL/...	RL/...	-
Feuertöpfe (FT)	FT/.../3/... FT/(>150)/...	-	FT/...	-
Fontänen (F)	-	-	F/...	-
Lichterbilder (LB)	-	-	-	LB/..
Baugruppen (BG)	BG/...	BG/...	BG/...	BG/..
Feuerwerksbatt. (FB)	FB/3/...	FB/...	FB/...	- (xx)

(x) - zylindrische Gegenstände

(xx) - es sind noch Versuche notwendig

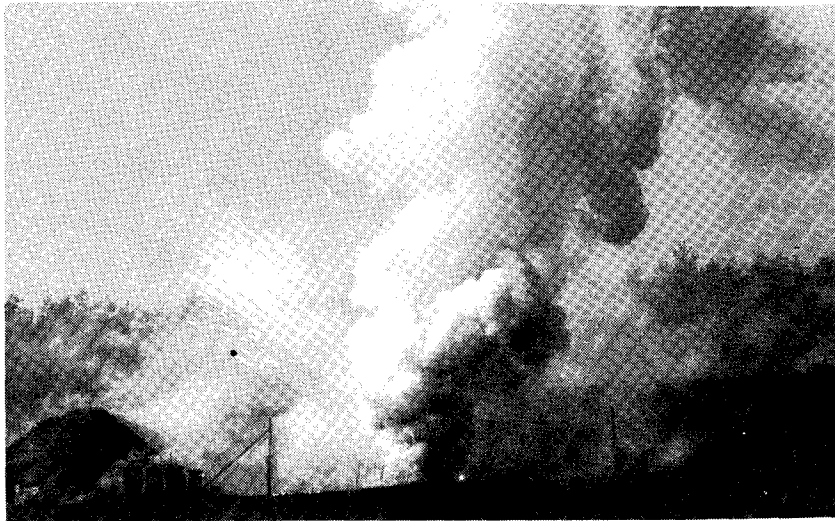


Abbildung 1 Außenbrandtest mit Feuertöpfen (FT)

5. Ausblick und Schlußfolgerungen/ Conclusions

Erwartungsgemäß kann eine große Anzahl von Gegenstände in die Gefahrklasse 1.3 G zugeordnet werden. In einigen Gegenstandskategorien sind alle Gefahrklassen von 1.1 bis 1.4 vertreten.

Ausstehende Prüfungen, wie z.B. für die Gruppe der Feuerwerksbatterien, werden ergänzenden Charakter haben und im Verlauf der nächsten Zeit in die Bewertungstabelle einbezogen. Neue Gegenstände oder Gruppen können nach Prüfung in die Tabelle eingebaut werden.

Wie soll man nun mit den vorhandenen Ergebnisse umgehen?

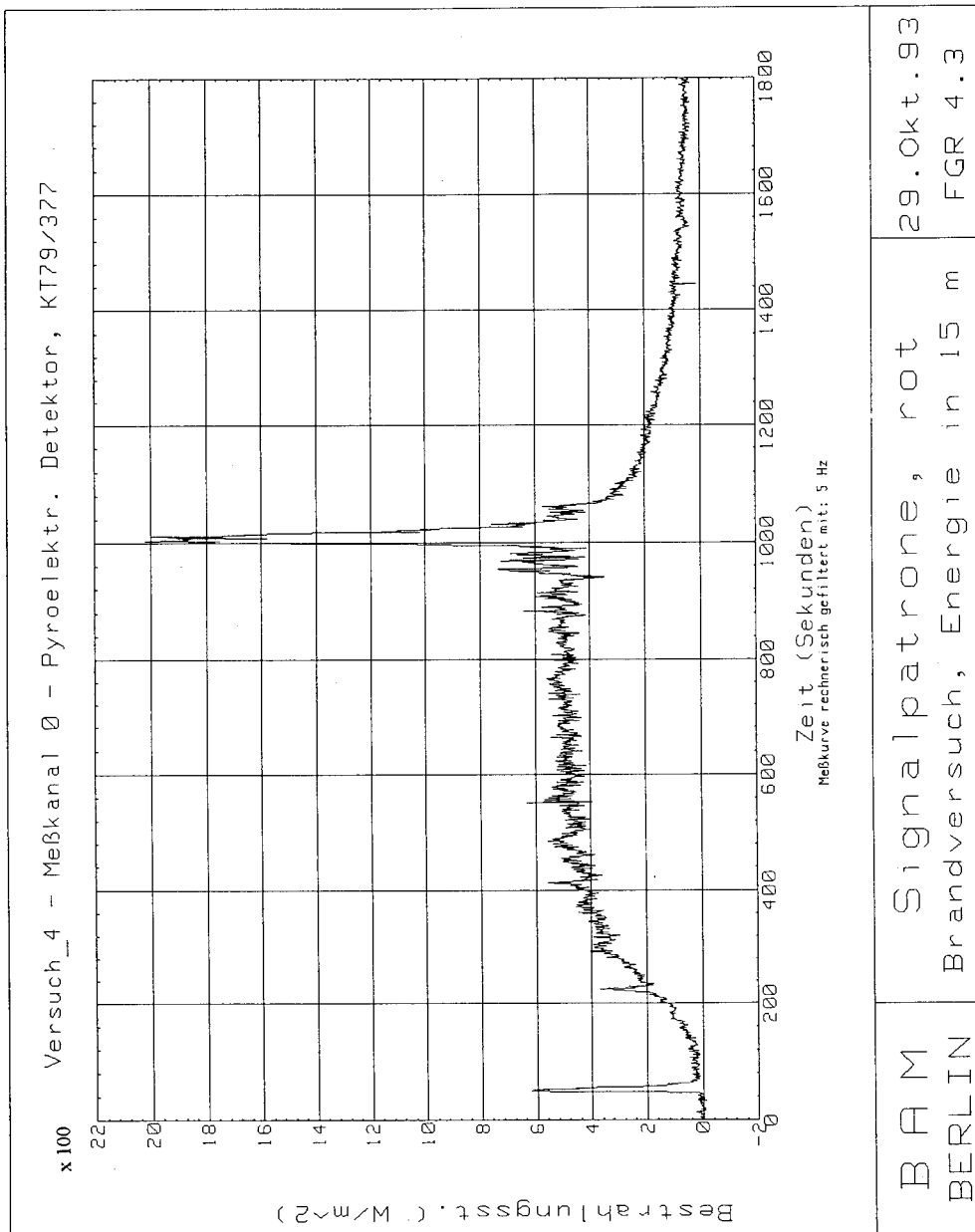
Die Verantwortung für die ordnungsgemäße Vorbereitung der Gefahrgutklassifizierung durch die BAM liegt bei den Herstellern. Die vorliegende Codierungsmöglichkeit hilft den Herstellern ihre Gegenstände einzuordnen bzw. eine Vorbewertung durchzuführen und damit für die Klassifizierung durch die BAM vorzubereiten.

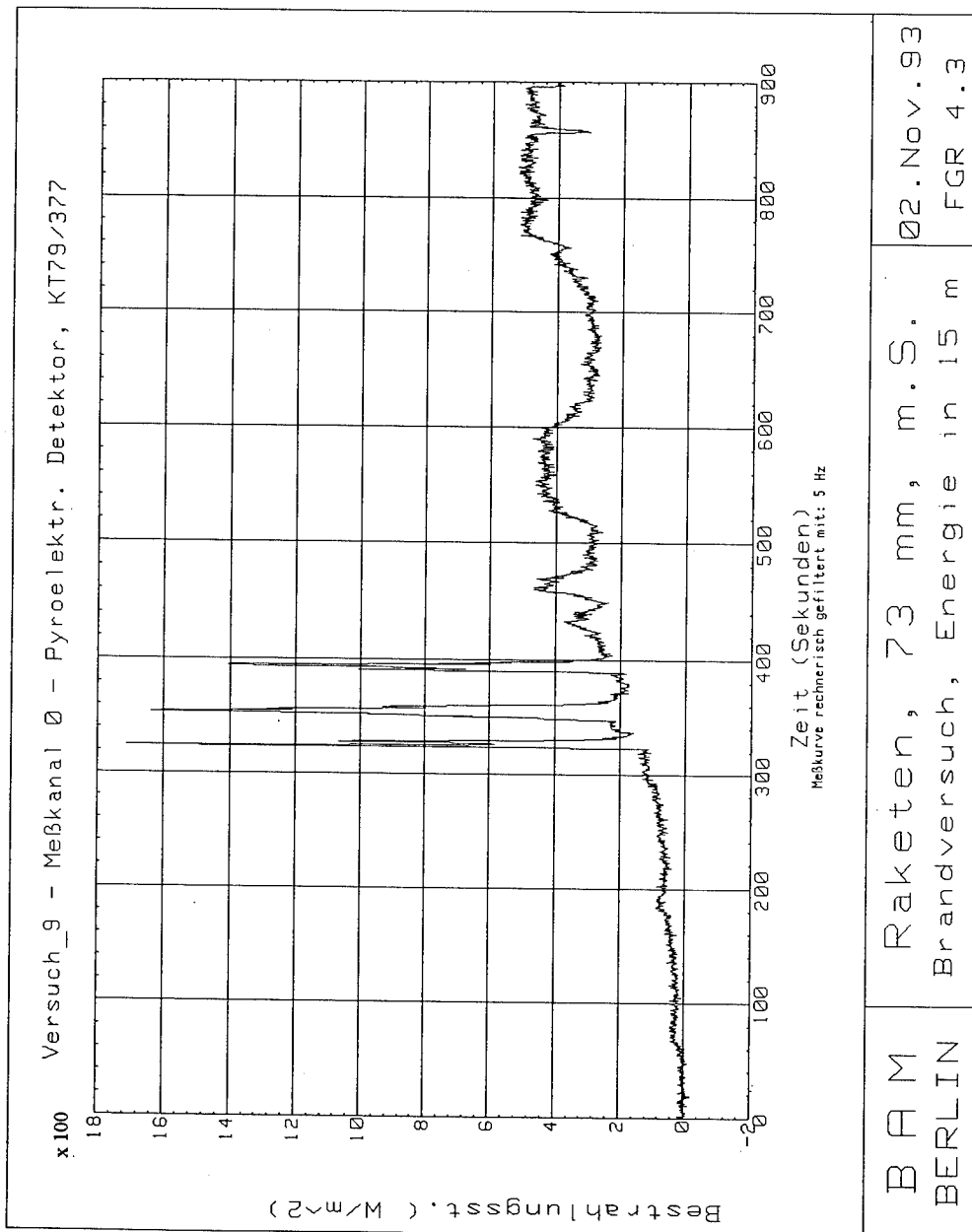
Anhand der eingereichten Anträge kann die BAM auf der Grundlage von Analogiebetrachtungen entsprechende Zuordnungsbescheide für die Beförderung als auch für die Lagerung erteilen oder ergänzende Prüfungen vornehmen. Es ist nicht ausgeschlossen, daß der eine oder andere Gegenstand auf der Grundlage von Prüfungen Neubewertet werden muß.

Die Notwendigkeit der Lagergruppenzuordnung, die analog und zusammen mit der Gefahrgutklassifizierung durchgeführt werden kann, wird durch den § 4 der 2. SprengV begründet.

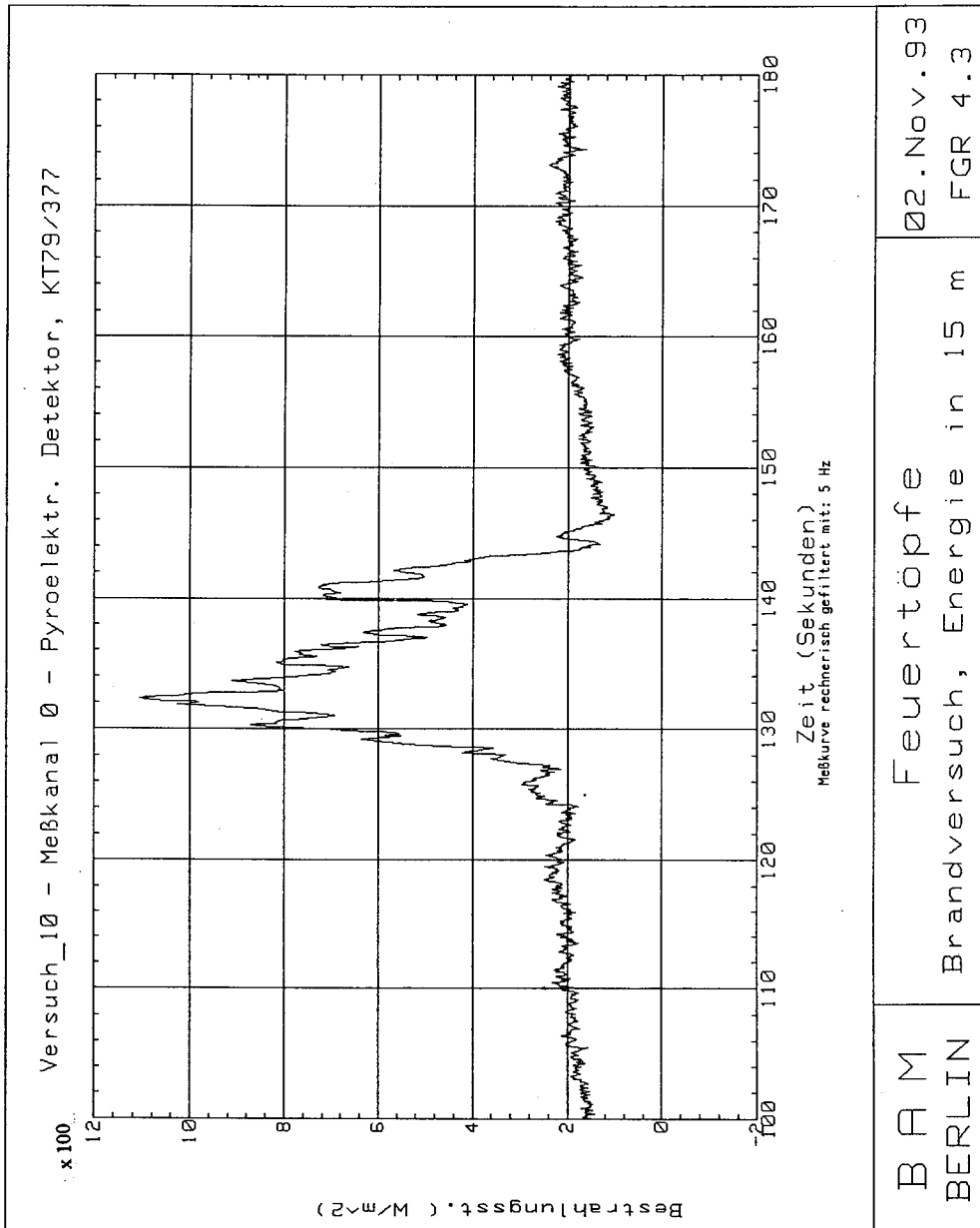
Literaturverzeichnis

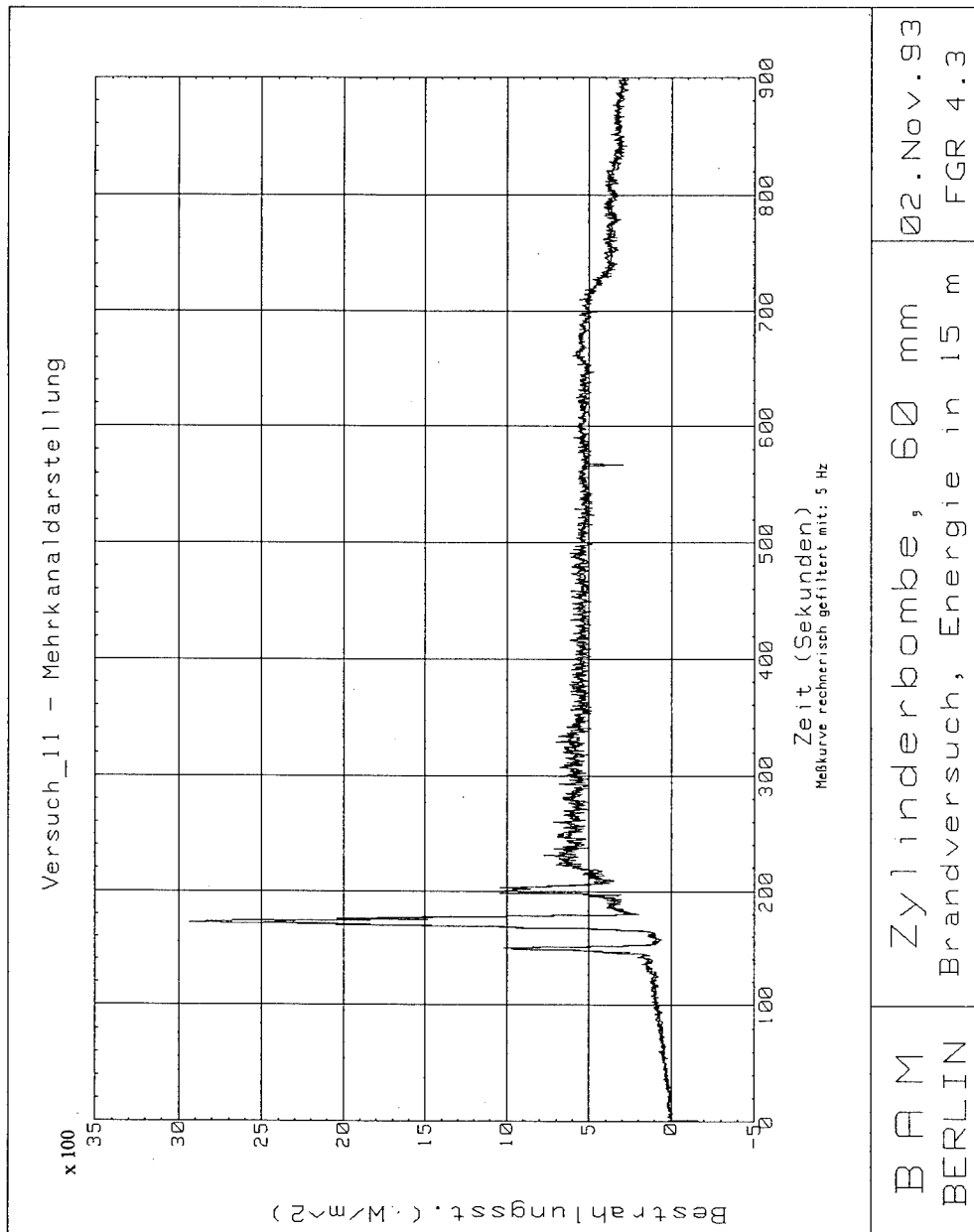
- /1/ Sicherheitsmaßnahmen für das Abbrennen von pyrotechnischen Gegenständen der Klassen III und IV (Anlage 1)
- persönliche Information von Zink Feuerwerk - 31.08.94
- /2/ Projektieren von Feuerwerken
Kegler, 1993
Grundlehrgang für Abbrenner von Feuerwerk
(Lehrmaterial herausgegeben von der Berufsgenossenschaft Chemie, Ausbildungsstätte für Arbeitssicherheit Laubach/ 1991)
- /3/ Gesetz über explosionsgefährliche Stoffe (Sprengstoffgesetz - SprengG)
in der Fassung der Bekanntmachung vom 17. April 1986 (BGBl. I, S. 577)
letzte Änderung vom 19. Oktober 1994 (BGBl. I, S. 2978)
- /4/ 1. SprengV in der Fassung der Bekanntmachung vom 31.01.1991 (BGBl. I, S. 169),
letzte Änderung der ersten Verordnung zum Sprengstoffgesetz vom 26. Oktober 1993
(BGBl. I, S. 1782)
- /5/ Empfehlungen für die Beförderung gefährlicher Güter - Prüfungen und Kriterien -
(Amtliche Übersetzung der "Recommendations on the Transport of Dangerous Goods -
Test and Criteria - First Edition. United Nations, New York, 1986,
ST/SG/AL.10/11"), 1990, ISBN 3-88314-990-K
- /6/ Beförderungen von Gegenständen mit Explosivstoff
- Außenbrandprüfungen als Teil der Gefahrgutklassifizierung -
H.-J. Rodner, M.-M. Zindler
in: Sprengstoffe, Pyrotechnik 2/93 Schönebeck
- /7/ Unfallverhütungsvorschrift 55k (UVV)
- Herstellen pyrotechnischer Gegenstände -
Berufsgenossenschaft der chemischen Industrie (BG Chemie) - 1. April 1991

Anlage 1 Wärmesignaturen vom Außenbrandtest ausgewählter Prüfmuster (1)


Anlage 1 Wärmesignaturen vom Außenbrandtest ausgewählter Prüfmuster (2)


Anlage 1 Wärmesignaturen vom Außenbrandtest ausgewählter Prüfmuster (3)



Anlage 1 Wärmesignaturen vom Außenbrandtest ausgewählter Prüfmuster (4)


PROBLEMATIK DER FORENSISCHEN UNTERSUCHUNGEN DER DETONATIVEN ER-
EIGNISSE IN GEBÄUDEN

Dr. Ing. Othmar Mueller, Direktor

Technisches Gerichtssachverständigeninstitut Ungarns /IMSZI/ ,
H - 1406 Budapest, VII. Postfach 15., Damjanich utca 12. Ungarn

ABSTRACT

Also in Hungary had been occurred some detonative events in connection with buildings: damages caused by explosions of gasses, powders and by criminal actions using commercial or military explosives, homemade explosives, pyrotechnic compositions. The investigation of a detonative event begins with a forming of a special team with criminalists, criminal technicians, forensic experts. The first step - simultaneously with the rescue action - consists of the search for the cause/s/ of the detonative event. Later the team will work to clear the full facts to support the law-court procedures. The lecture tries to give an overview of the steps on the forensic investigations.

Einleitung.

Es erfolgt ein Ereignis, das man vorerst als einen "detonativen Vorgang" signalisiert, weil es noch nicht klar ist, was wirklich geschehen ist. Die Feuerwehr, die Polizei, bei "Katastrophengrösse" der Zivilschutz erscheint am Ort des Ereignisses. Hier finden sie oft ein Feuer von verschiedenen Grössen und Intensitäten vor, ggf. mit Explosionen oder nicht. Es gibt detonative Ereignisse ohne Feuer mit kleineren oder grösseren Materialschäden, mit Verwundeten, Toten, ggf. mit annehmbar verschütteten Personen. Vorerst sollte natürlich das Rettungs- verfahren eingeleitet werden parallel mit der Gefahrverminde- rung bezüglich eventuellen labilen Konstruktionen. Bei detona- tiven Vorgängen fängt die Polizei sofort mit ihren Investigatio- nen an um möglichst alle Einzelheiten des "Ereignisortes" bild- lich fixieren zu können. Sogleich muss auch ein Sachverständigen- team bestehend aus verschiedenen Kompetenzgebieten gebildet werden.

Aufgabenstellung des Untersuchungsteams

Oft ist es sogleich klar, das das Ereignis "nur" ein einfaches Feuer ist, das gelöscht werden muss und nachher soll die Feuerursache festgestellt werden. / Ggf. ob ein Verdacht auf eine Brandstiftung bekräftigt werden kann. /

Bei "komplexen Feuerstellen", besonders in /Chemie-/ Industrieanlagen ist die Untersuchung viel problematischer, besonders im Zusammenhang mit Gasen und Pulvern. Hier treten auch Umweltaspekte, z.B. im Zusammenhang mit giftigen, gefährlichen Belastungen auf. Hierbei sind gekoppelte terroristische Sabotageaktionen auch nicht auszuschliessen. / Gekoppelt sind solche Aktionen bei welchen ein Sprengsatz grundsätzlich einere weit grössere detonative Umsetzung auslösen sollte. /

Auch bei "einfachen", relativ kleinen Sprengaktionen / die Ladung wird vor dem Objekt gezündet, bzw. sie besteht nur aus 500-1000 g Explosivstoff / ist der Detonationsort leicht festzustellen, bzw. es ist eindeutig, dass dort eine Explosivstoffdetonation stattfand.

Obzwar bei Explosivstoffanschlägen katastrophalen Ausmasses, wie z.B. beim World Trade Center in New York, oder bei Autobomben mit 400-1000 Kilogramm im Kofferraum / auf Strassen neben Gebäuden stehenden Pkw-s / ist es eigentlich auch sofort annehmbar, dass eine Explosivstoff-Detonation stattgefunden hat, aber es ist nicht überblickbar, wie, mit welchem Sprengstoff, durch welche Zündung, usw. die Detonation durchgeführt wurde.

Das zu bildende Team ist nicht einfach - wie es so oft in den Nachrichten steht - eine Gruppe von Sprengstoffexperten, sondern ist vielmehr ein Komplexteam von oft vielen Kompetenzgebieten der forensischen und technischen Wissenschaften, der Gerichtssachverständigen.

Je nach der Komplexizität des Ereignisses ist die Aufgabenstellung des Teams ein solches, oft aus mehreren Gutachten bestehendes Untersuchungsergebnis zu erarbeiten, aufgrund dessen die Polizei, die Staatsanwaltschaft die Ursache des Ereignisses eindeutig klar sieht, die Täter eruieren kann und beim späteren Gerichtsverfahren die Anklage stabil untermauern kann.

Aufgabenteilung und Mitglieder des Sachverständigenteams

Der Vorgang und Arbeitsweise der "Feuerbeschauung" ist allgemein bekannt, deshalb wird im Vortrag auf die kriminellen /terroristischen/ Explosivstoffaktionen der Schwerpunkt gesetzt. Der Leiter des Teams ist allgemein ein solcher Kriminalist, der auf dem Gebiete der Sprengstoffattentate eine längere Erfahrung besitzt. Der Teamleiter muss anlässlich der Einführungs-Lagebesprechung die Aufgabengebiete abstimmen und auch die Zusammenarbeit der verschiedenen Sachverständigen festlegen, damit z.B. der eine Sachverständige die Untersuchungstätigkeit des anderen nicht stört, bzw. die spezifische Beweissicherung zunichte macht. Obwohl an Ort und Stelle viel untersucht werden kann, ist die Arbeit des Teams ohne sog. Laborhintergrund nicht ausschlaggebend. Es ist auch deshalb notwendig, dass das Untersuchungsorgan, allgemein die Polizei über eine Personenkartei der in Betracht kommenden Sachverständigen verfügt, um die kompetenten Personen je nach Notwendigkeiten des Tatortes heranziehen kann.

Welche Kompetenzgebiete kommen in Betracht?

- Der Gerichtsmediziner kann durch die Verletzungserscheinungen, durch das Sichern eventueller Splitter und Wundgegenständen in und aus Verletzten, bzw. Toten wertvolle Hinweise geben, besonders hinsichtlich Überdruck- und ballistischen Einwirkungen.
- Die Spurenfahnder bilden selber eine Gruppe. Wichtige Spuren können sein: Detonationsschmauch, Metallteile, Verpackungsmaterialreste, Zündmittelstücke, Glassplitter und besonders interessant in letzterer Zeit sind "Gestankfixierungen".
- Die Spurenanalysatoren sind allgemein in Laboratorien tätig, die Fachgebiete sind sehr breit gestaffelt: Analyse von Spurenmaterialien, Chemikalien, Papieren, Metallen, Kunststoffen, und Dokumentenuntersuchungen können auch von Wichtigkeit sein.
- Die Bausachverständigen, besonders aber die Konstruktionsfachleute und Statiker sind im letzten Jahrzehnt wichtig geworden. Aufgrund der schwedischen Untersuchungen ist es möglich, durch zusammengesetzte komputerisierte Analyse der Verrückung der Bauteile durch die Einwirkung von Detonationen festzustellen wie die Ladungsgrösse gewichtsmässig und wo sie gelagert war.

- Der Fahrzeug-Sachverständige kann besonders durch die Untersuchung des detonierten Fahrzeuges wertvolle Hinweise auf die Detonationsvorgänge, bzw. auf den Eigentümer des Fahrzeuges, usw. geben.
- Der Toxikologe kann in der Explosivstoffanalyse /auch/ behilflich sein, bzw. in der Untersuchung der Schmauchspuren. Auch soll er über die eventuellen toxischen Ausmasse des detonativen Vorganges eine Expertise geben.
- Der Entschärfungsspezialist soll eigentlich im Falle einer noch nicht detonierten weiteren "Höllenmaschine" zum Entschärfen eingesetzt werden. Andererseits aber ist er ein Sachverständiger für die "gruppenspezifischer", bzw. personenspezifischen Merkmale der Attentatsmittel zuständig im Vergleich mit früheren Aktionen.
- Der daktyloskopische Spezialist ist zuständig bei nicht detonierten, bzw. nicht berührten Sprengeinrichtungen auf der Suche nach Fingerabdrücken.
- Die gerichtlichen Sachverständigen für Elektronik errangen eine Wichtigkeit in letzterer Zeit. Es werden verdeckte Höllenmaschinen in elektronischen Mitteln /Kofferradio, Lap-tops, Telefon, Videogeräte, usw./ eingebaut; zur Zündung von USBV-s /Unkonventionelle Spreng- und Zündvorrichtungen/ werden elektronische Elemente, Funkgeräte usw. verwendet; Sprengrezepte und -handbücher werden durch Computernetze vermittelt und abgerufen; die Stimmenanalyse von Drohtelephonaten und "Verantwortungsübernahmen" kann auch zum Beweismittel gehören.

Kurzüberblick der Ausrüstungen des Sachverständigenteams.

In die Geräte und Ausrüstungen der Vielzweckausrüstungen der kriminalistischen, toxikologischen, chemischen Laboratorien soll hierbei nicht eingegangen werden, besonders in die immer komplexer arbeitenden Analysegeräte, Chromatographen, usw. Die an Ort und Stelle zu verwendenden Ausrüstungen sind auch immer vielseitiger. Die biologischen Detektoren sind die Hunde. Sie konnten durch die effektiver arbeitenden Schnüffelschweine nicht verdrängt werden. /Das hat praktische Gründe./ Laut amerikanischen Untersuchungen wären die Ratten noch effektiver, aber praktisch sind sie auch nicht einsetzbar.

Das Team muss über verschiedene Teleskop-Spiegel verfügen, sowie über Bendoskope und Boreskope. Die Explosivstoffe /insofern sie nicht detonierten, bzw. teilweise detoniert sind und verstreut wurden/ können durch die ETK-s /Explosives Testing Kits/ primär festgestellt werden. /Die ETK-s sind aber auch Einwirkungen von anderen "energetischen Materialien" anfällig, deshalb ersetzen sie die Laboruntersuchungen nicht, sie sind auch kein grundsätzliches Beweismittel./

Die verschiedensten Explosivstoffdetektoren sind eigentlich nur für das Auffinden von nicht detonierten Explosivstoffen geeignet. Hierbei soll erwähnt werden, dass tragbare Röntgen-Durchleuchtungsgeräte beim Untersuchen von aufgefundenen, intakten Höllenmaschinen besonders zwecksmässig sein können.

Natürlich darf die "übliche" Tatortausrüstung nicht fehlen./Z.B. Fotogeräte, Messgeräte, Tonbandgeräte, usw./

Konklusionen.

Auch in Ungarn erschienen terroristische Sprengaktionen, die besonders von Ausländern verübt worden sind. Eine potentielle Gefahr bedeuten die "Hinterlassenschaften" der Sowjetarmee, sowie die Schmuggelwaren aus den Krisengebieten. Einige einheimische Racheaktionen wurden - hauptsächlich durch Handgranaten - verübt. Eine gewisse Interesse erwachte für Selbstlaborate, die aber bisher noch rechtzeitig entdeckt wurden. /Zu einem naturwissenschaftlichen Wettbewerb einer Zeitschrift schickte ein Schüler sein "Sprengpulver" ein. Er erhielt keinen Preis./ Die im Vortrag beschriebenen Teams und Vorgangsweisen wurden bei den bisher eher spärlichen Fällen erfolgreich verwendet. Es wurden weitere Untersuchungen zur Vervollständigung der Untersuchungsmethoden und der in Betracht kommenden Teammitglieder eingeleitet.

MECHANICAL FAILURE OF HMX BASED PBXs AND ITS RELATIONSHIP TO IMPACT SENSITIVITY

S B Langston

School of Mechanical, Materials and Civil Engineering,
Cranfield University,
Royal Military College of Science,
Shrivenham, Swindon, SN6 8LA, UK.

ABSTRACT

HMX (1,3,5,7-tetranitro-1,3,5,7-tetrazacyclooctane) recovered from polymer bonded explosive compositions (PBXs) was investigated using Scanning Electron Microscopy (SEM). Each composition consisted of 95% HMX Type B and 5% polymeric binder. Dissolution of the polymer permitted HMX particulates to be recovered from pressed and unpressed PBXs. On examination, a number of fractured particulates were located. The impact sensitivity of recovered HMX had increased compared to the original ex-works material. Cylindrical pressed pellets of each PBX were subjected to mechanical testing in the compression mode. The mechanical properties of pressed pellets and the impact sensitivity of the unpressed moulding powders were shown to depend, in most cases, upon the degree of polymeric binder plasticisation. Tough and brittle binders were found to produce sensitive compositions.

INTRODUCTION

A series of polymer bonded explosive compositions (PBXs) based on HMX with either water soluble binders or Cariflex was prepared. After pressing, pellets of each PBX were subjected to mechanical testing in the compression mode and a series of load/displacement curves were produced. Further pellets of all the water soluble binder based PBXs and some Cariflex based compositions (10 & 14) were broken down on addition to either water or cyclohexane. Scanning Electron Microscopy (SEM) was carried out on the recovered HMX. HMX recovered from compositions 1-5 was subsequently impact tested using the Rotter Impact Machine. It was then possible to assess the effect processing and compaction had on the degree of particle cracking and other characteristics of HMX. All PBX moulding powders were subjected to the Rotter Impact Test and Figures of Insensitivity (F of I) obtained.

A number of water soluble polyvinyl alcohols^{1,2} were assessed for their suitability as binders for recoverable PBXs. The polyvinyl alcohols used in this investigation were Alcotex 72.5, supplied by Harlow Chemical Company Ltd and Mowiol GE4-86, manufactured by Hoechst (available through Harlow Chemical Company). Alcotex 72.5 is a cold water soluble, 72.5% hydrolysed (27.5% residual acetate groups) polyvinyl alcohol. Mowiol GE4-86 is an internally plasticised, hot water soluble analogue of Alcotex 72.5. The polyethylene glycols, PEG 200, PEG 300, PEG 400 and glycerol used as the low molecular weight plasticisers for the polyvinyl alcohols were supplied by Aldrich Chemical Company Ltd.

A series of PBXs based on HMX with either Cariflex TR-1101 or TR-1102 styrene-butadiene-styrene (SBS) block co-polymer thermoplastic elastomers were manufactured. Cariflex was supplied by Shell Chemicals UK limited. Cariflex TR-1102 is similar to Cariflex TR-1101 but with a lower modulus of elasticity. The Mechanical Pump Oil No.8A, used as a plasticiser for the thermoplastic elastomer based binders was supplied by Edwards High Vacuum International.

PREPARATION OF COMPOSITIONS

Compositions 1-5 were hand mixed at the 50g level with a horn spatula inside a stainless steel beaker using a water based paste-mix process. The water was removed by placing the beaker on a hot water heated hotplate in a forced air draught. All remaining traces of water were removed by placing the beaker in a vacuum desiccator. It was found that Alcotex 72.5

showed a marked reduction in water solubility above its cloud point (30-35°C); undergoing a phase change from a solution to a dispersion. On reaching the cloud point the mixture of HMX, binder and water tended to gel with a subsequent drop in viscosity. On cooling below the cloud point the binder rapidly re-dissolved with an immediate increase in viscosity. This effect made preparation of the water based PBXs time consuming. On further investigation it was found that Alcotex 72.5 is able to remain in solution, even at the boiling point and high solids loading by simply substituting water for a 1 part water to 1 part methanol mixture. Compositions 3B, 7 and 9 were successfully prepared in a 1 part water to 1 part methanol mixture, whereas compositions 6 and 8 were manufactured using binders dissolved in a mixture of 2 parts water to 1 part methanol. The best results were achieved by dissolving the polymer in water prior to adding the methanol and plasticiser. On heating and stirring the composition the alcohol/water mixture readily evaporated in a forced air draught. The Cariflex based compositions were similarly produced. The polymeric binder and plasticiser as required were dissolved in cyclohexane prior to the addition of HMX. The formulations are presented in tables 1 and 2.

PRESSING OF PBXs INTO PELLETS

The compositions were pressed at 82°C as small cylindrical (2.5g / 13mm diameter / 10-11mm length) pellets to a pressure of 15 tons in⁻² (2.4 tonnes cm⁻² / 225MPa), with a dwell time of 30 seconds. Compositions based on the water soluble binders were also pressed as small (1.8g/4.5mm thick) pellets at 10 tons in⁻² (150 MPa / 1.6 tonnes cm⁻²). Each pellet was placed in approximately 20cm³ of water for the dissolution process to take place. Material extracted in this manner was examined using SEM (see figures 6-9). Compositions 10 and 14, based on HMX and Cariflex were similarly treated, by dissolution in cyclohexane. HMX recovered from compositions 1-5, on washing with further water and drying, were subjected to impact testing. The results are presented in table 5.

IMPACT TESTING

Impact testing of PBX moulding powders (unpressed) was carried out at DRA Fort Halstead using the Rotter Impact Tester, according to the S.C.C. Manual of Tests³. This test is also described in the UN 'Orange Book' Recommendations on the Transportation of Dangerous Goods - Tests and Criteria⁴. The greater the value of the F of I for each composition the more insensitive it is to impact. A brief description of impact sensitiveness is given in the

paper by Leach et al⁵, and a summary of the results are shown in tables 3 and 4. The F of I for each PBX plotted against percentage plasticiser is given in figure 3.

COMPRESSIVE TESTING OF PBX PELLETS

Cylindrical pellets pressed from compositions 1-18 were tested in compression mode using an Instron 4206 Universal Test Machine incorporating the Series IX Automated Materials Testing System. All work was carried out in a humidity and temperature controlled environment (23°C / 50%RH). The results are presented in tables 3 and 4. Load/Displacement curves for composition 1 (brittle binder) and Composition 11 (thermoplastic elastomer) are given in figures 1 and 2.

MICRO-MECHANICAL FAILURE OF HMX

HMX recovered from PBXs was examined using a Joel JSM-840A Scanning Electron Microscope⁶. Each composition examined consisted of 95% HMX Type B and 5% water soluble polymeric binder. Dissolution of the polymer in water permitted HMX particulates to be recovered from pressed and unpressed PBXs. On examination, a number of fractured particulates were located. HMX was also recovered from unpressed PBXs consisting of 95% HMX and 5% unplasticised SBS thermoplastic elastomer block copolymer by dissolution with cyclohexane. Contact time with the solvent was kept to a minimum and comparisons were made to similarly treated uncoated HMX. Fractured particulates were found. No micro-cracking was detected in the uncoated HMX.

DISCUSSION AND CONCLUSIONS

The mechanical properties of each binder for example, modulus of elasticity, were found to depend on the plasticiser contents. Unplasticised polyvinyl alcohols were found to be hard and brittle, whereas a high level of plasticiser resulted in soft and flexible binders⁶. The compressive strength (stress at maximum load) of the pressed PBXs and the impact sensitivity of each (unpressed) composition appeared in most cases to correspond to the degree of binder plasticisation (see figures 4 and 5). Particle size and micro-mechanical failure (fracture) of HMX particulates was found to depend on the mechanical properties of the binder, although the efficiency of a particular binder at wetting and coating HMX may be equally important. These microscopic fractures may be the potential sites of ignition under dynamic load, or at least, indicate the susceptibility of a particular composition to ignite under impact. It was

found that particulates of HMX fractured under conditions of both high mechanical load⁶ (during pressing), and minimum load conditions (during the manufacture of PBXs). Considerable surface damage was noted on some particulates recovered from Cariflex based compositions (see figure 8).

Compositions containing unplasticised binders, in particular, those based on thermoplastic elastomers were found to be very sensitive to impact, usually more so than uncoated HMX. PBXs containing plasticised binders were found to be relatively insensitive to impact. Work by Leach et al⁵ has shown that impact sensitivity for a series of plasticised thermoplastic elastomer PBXs is proportional to the viscosity of the plasticiser if the ratio of HMX to polymer binder to plasticiser remains constant. Figure 4 shows that the compressive strength for PBXs containing Cariflex based binders, is proportional to the degree of plasticisation.

The high elasticity, elongation to break of approximately 900% combined with resistance to viscous flow and tensile strength in excess of 30 MPa for unplasticised Cariflex TR-1101 could result in sudden releases of energy under conditions of high dynamic load or shearing forces. According to current thinking, stress concentrations could arise, leading to the generation of hot spots within the polymer matrix. Hot spots may also occur due to adiabatic compression of air or frictional forces within the cracks of individual particulates. The rate of crack generation may be proportional to velocity and magnitude of impact combined with the mechanical, physical and chemical properties of the binder.

The pressed pellet densities of each composition also varied according to the level of plasticisation. With the Cariflex based binders, pellet densities varied from 1.71 g.cm⁻³ for composition 10 to 1.800 g.cm⁻³. The water soluble binders produced pellets with greater densities and varied from 1.80 g.cm⁻³ for composition 1 to 1.86 g.cm⁻³ for composition 5. Composition 5 was interesting in that it contained nearly 98% HMX after pressing (2-3% PEG 200 was squeezed out on compaction), yet was relatively insensitive to impact in powder form. The compressive strength of composition 5 as pressed pellets was also found to be relatively high.

Compo- sition	HMX	Alcotex 72.5	Mowiol GE4-86	PEG 200	PEG 300	PEG 400	Glycerol
No.	Percentage by weight						
1	95.00	5.00	-	-	-	-	-
2	95.00	3.75	-	1.25	-	-	-
3	95.00	2.50	-	2.50	-	-	-
4	95.00	1.25	-	3.75	-	-	-
5	95.00	-	-	5.00	-	-	-
6	95.00	2.50	-	-	2.50	-	-
7	95.00	2.50	-	-	-	2.50	-
8	95.00	2.50	-	-	-	-	2.50
9	95.00	-	2.50	2.50	-	-	-

Table 1: PBX Formulations Based on HMX and Water Soluble Binders

Composition No.	HMX	Cariflex TR-1101	Cariflex TR-1102	Edwards No.8 oil
Percentage by weight				
10	95.00	5.00	-	-
11	95.00	3.75	-	1.25
12	95.00	2.50	-	2.50
13	95.00	1.25	-	3.75
14	95.00	-	5.00	-
15	95.00	-	3.75	1.25
16	95.00	-	2.50	2.50
17	95.00	-	1.25	3.75
18	95.00	-	-	5.00

Table 2: PBX Formulations Based on HMX, Cariflex and No.8 Oil

Composition No.	Impact Sensitivity F of I	Load at Max. Load kN	Stress at Max. Load MPa	Strain at Max. Load mm/mm
1	50	8.206	62.98	0.1419
		8.645	66.35	0.1592
		8.734	67.04	0.2191
2	54	3.334	25.59	0.1643
		3.217	24.69	0.2065
		3.149	24.17	0.1811
3	67	2.017	15.48	0.0957
		1.897	14.56	0.0768
3A	77	1.949	14.96	0.0820
		2.299	17.65	0.0994
		1.840	14.12	0.2889
3B	55	2.114	16.23	0.1064
		1.993	15.30	0.1170
		1.941	14.90	0.1124
4	97	1.281	9.832	0.0941
		1.293	9.924	0.1811
		1.401	10.75	0.1376
5	89	1.909	14.65	0.0790
		1.764	13.54	0.0671
		1.458	11.19	0.1312
6	58	1.828	14.03	0.0555
		1.848	14.18	0.0586
		1.897	14.56	0.0779
7	56	1.941	14.90	0.2507
		1.832	14.06	0.0722
		1.953	14.99	0.0779
8	57	2.247	17.25	0.0968
		2.344	17.99	0.1654
		2.227	17.09	0.1282
9	66	1.136	8.719	0.0743
		1.172	8.995	0.1039
		1.156	8.873	0.0566

Table 3: Impact Sensitivity and Mechanical Properties of PBXs Based on HMX and Water Soluble Binders

Composition No.	Impact Sensitivity F of I	Load at Max. Load kN	Stress at Max. Load MPa	Strain at Max. Load mm/mm
10	31	2.029 2.110 2.009	15.57 16.19 15.42	0.1430 0.1566 0.1695
11	39	1.434 1.478 1.723	11.01 11.34 13.23	0.1292 0.1512 0.1042
12	72	1.236 1.264 1.204	9.487 9.701 9.241	0.0942 0.1020 0.0979
13	78	0.8738 0.8658 0.8658	6.707 6.645 6.645	0.0539 0.0606 0.0535
14	68	2.311 2.291 2.235	17.74 17.58 17.15	0.1256 0.1251 0.1394
15	64	1.619 1.723 1.639	12.43 13.22 12.58	0.1456 0.1395 0.1202
16	66	1.240 1.220 1.236	9.517 9.364 9.487	0.0653 0.1459 0.0729
17	66,73	0.8617 0.8496 0.8295	6.614 6.521 6.367	0.0282 0.0411 0.0500
18	77	0.2698 0.2577	2.071 1.978	0.1215 0.1265

**Table 4: Impact Sensitivity and Mechanical Properties of PBXs Based on HMX,
Cariflex and Edwards No.8 Oil**

Composition No. from which HMX was recovered from	Percentage plasticiser in original binder	Impact test F of I
1	0.0	48
2	25.0	46
3A	50.0	48
4	75.0	48
5	100	54
HMX unpressed	-	60

Table 5: Rotter Impact Results for HMX Recovered from PBXs Based on HMX Water Soluble Binders

REFERENCES

1. C A Finch, Polyvinyl Alcohol - Developments, John Wiley & Sons, Chichester, 1992.
2. Mowiol Polyvinyl Alcohol (brochure), Hoechst Aktiengesellschaft, Marketing Kunstharze/Polymerisate, D-6230 Frankfurt am Main 80, December 1991.
3. Sensitiveness Collaboration Committee, Manual of Tests, RARDE, Fort Halstead, Kent, October 1988.
4. UN 'Orange Book' Recommendations on the Transportation of Dangerous Goods - Tests and Criteria.
5. C J Leach, S B Langston, J Akhavan, A Plasticisation Study of Thermoplastic Elastomer Bound Pressable Explosives, 25th International ICT-Conference, Karlsruhe, Germany, 28 June - 1 July 1994.
6. S B Langston, J Akhavan & A S Cumming, Water Soluble Polymers as a Diagnostic Tool for the Examination of Pressed Plastic Bonded Explosives Based on HMX, 25th International ICT-Conference, Karlsruhe, Federal Republic of Germany, 28 June - 1 July 1994.

ACKNOWLEDGEMENT

This work was undertaken at RMCS under the sponsorship of DRA Fort Halstead.

35 - 10

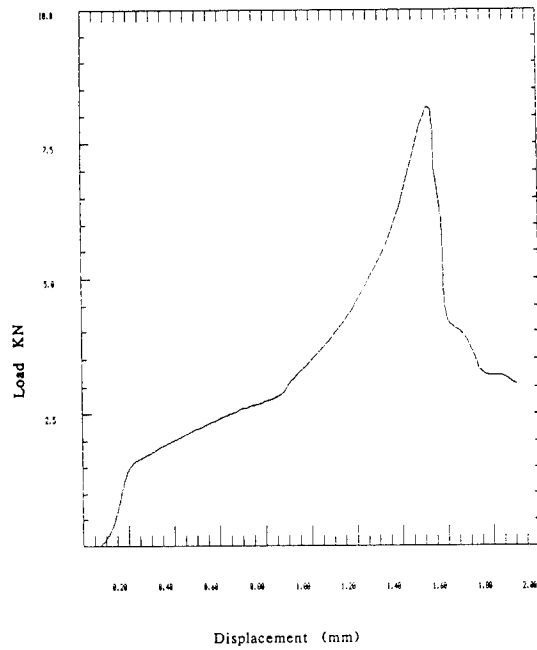


Figure 1: Load/Displacement Curve for Composition 1 - Pellet No.1

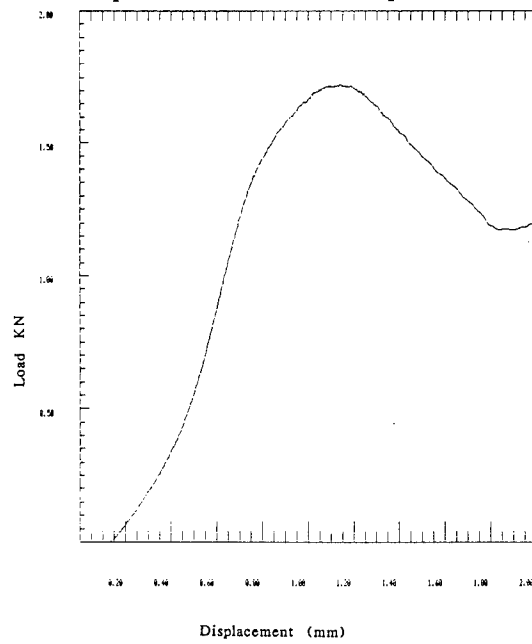


Figure 2: Load/Displacement Curve for Composition 11 - Pellet No. 3

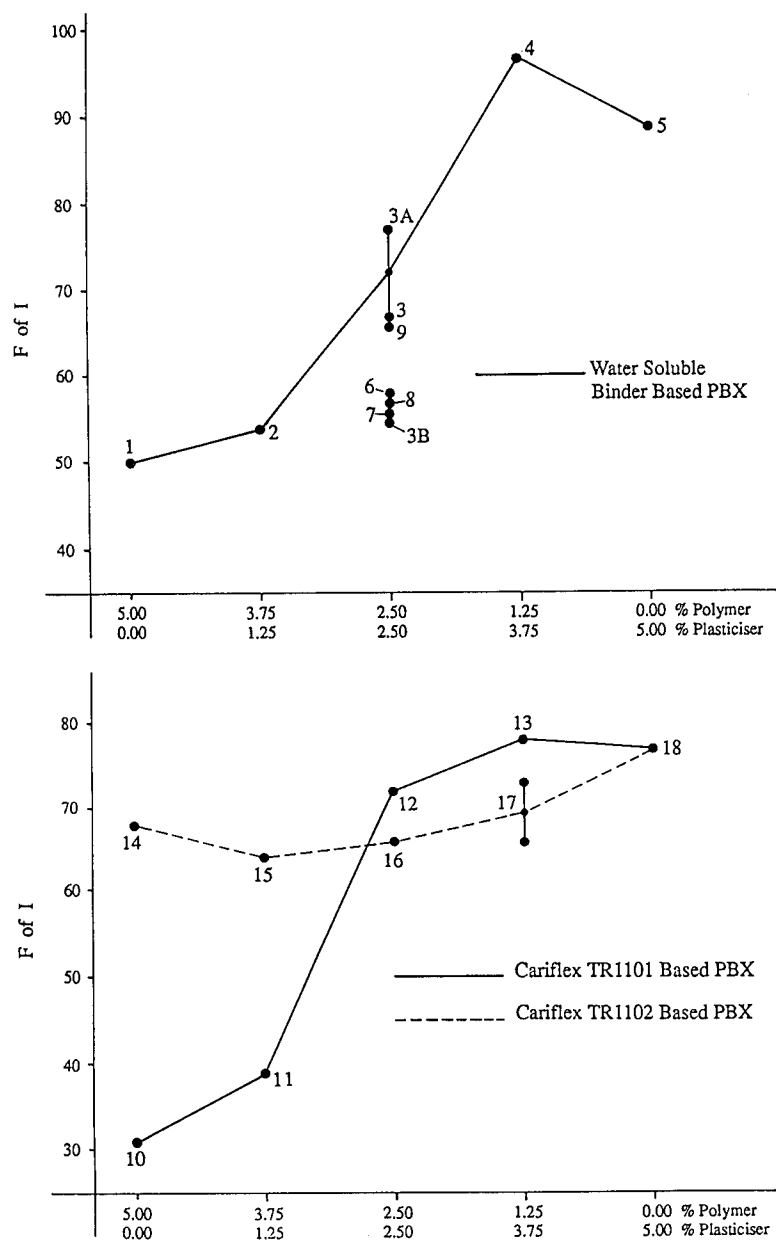


Figure 3: Impact Sensitivity of PBXs Versus Binder Composition

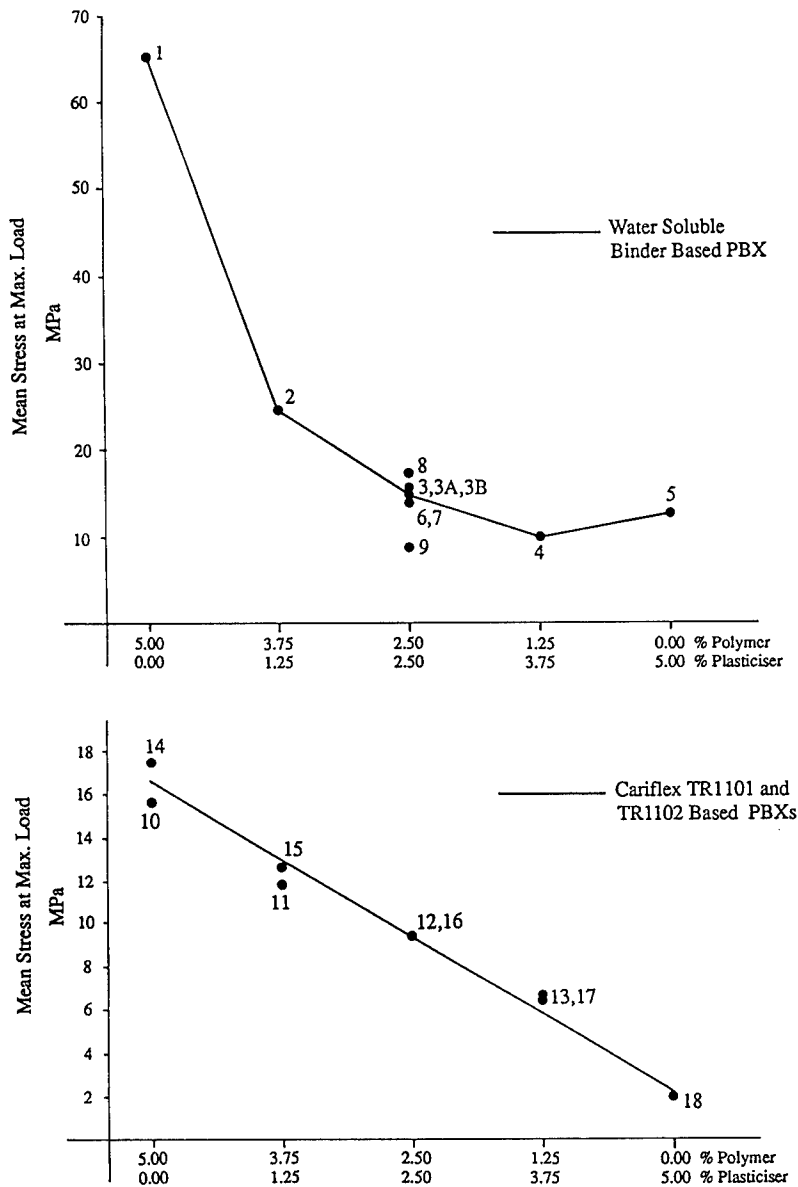


Figure 4: Mean Stress at Maximum Load For Pressed PBXs Versus Binder Composition

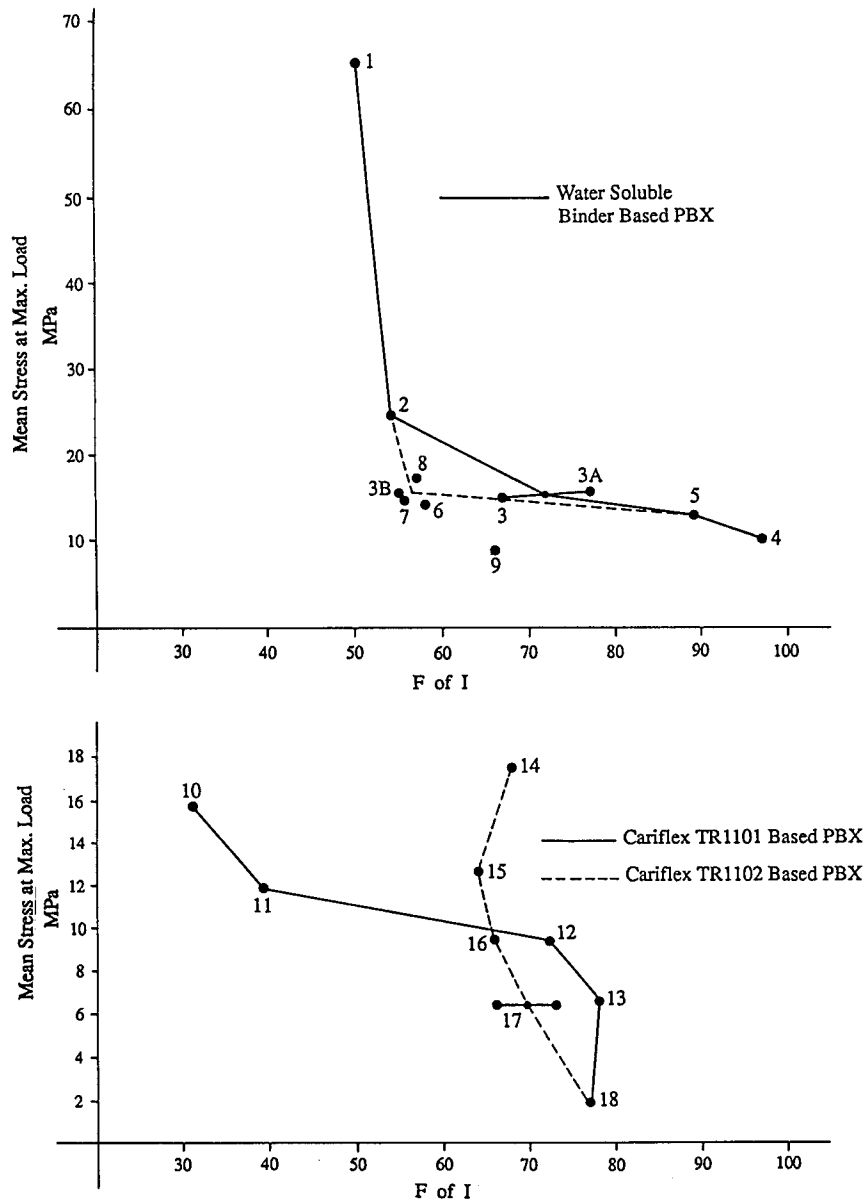


Figure 5: Mean Stress at Maximum Load for Pressed PBXs versus Impact Sensitivity

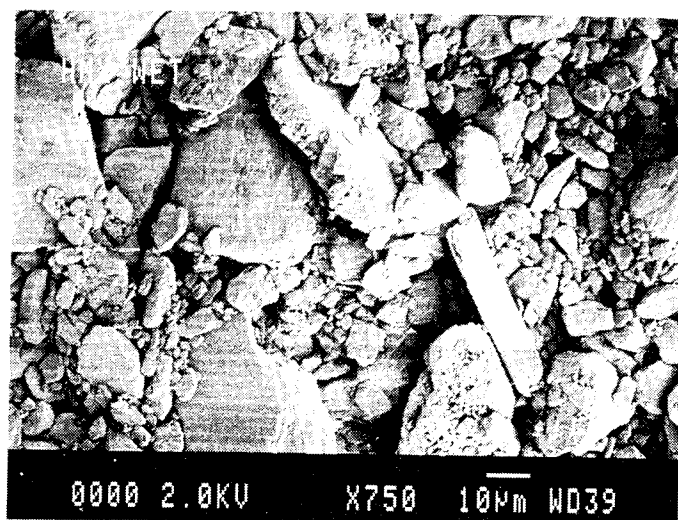


Figure 6: Unpressed HMX Type B (SEM X750) - No visible cracking

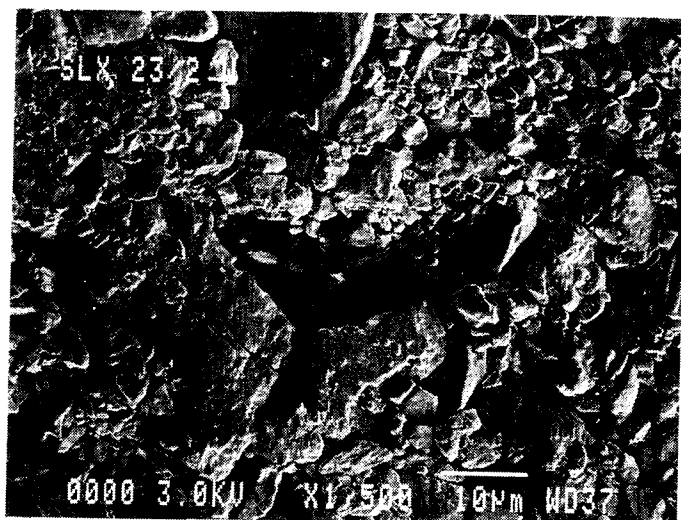


Figure 7: HMX Recovered From Composition 1 (unpressed) (SEM X1500)
The presence of a hard, brittle binder has resulted in cleavage of several particles

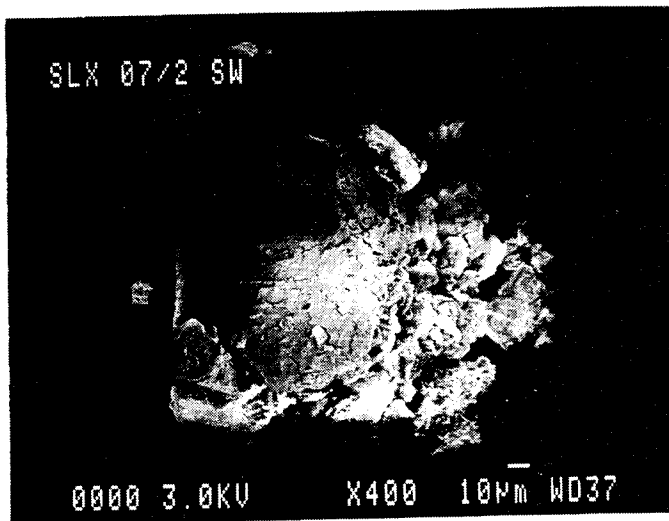


Figure 8: HMX Recovered From Composition 10 (unpressed) (SEM X400) - The presence of a tough rubbery binder has resulted in severe surface damage

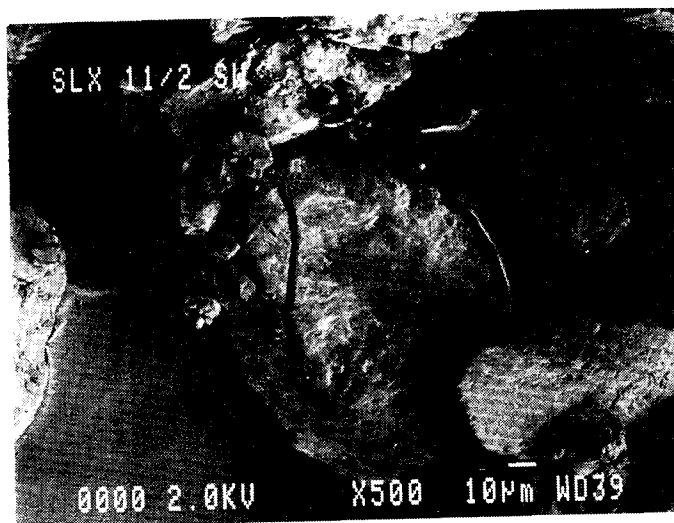


Figure 9: HMX Recovered From Composition 14 (SEM X500) - The presence of a tough rubbery binder has resulted in a severely cracked particle



Figure 6: Unpressed HMX Type B (SEM X750) - No visible cracking



Figure 7: HMX Recovered From Composition 1 (unpressed) (SEM X1500)
The presence of a hard, brittle binder has resulted in cleavage of several particles



Figure 8: HMX Recovered From Composition 10 (unpressed) (SEM X400) -
The presence of a tough rubbery binder has resulted in severe surface damage



Figure 9: HMX Recovered From Composition 14 (SEM X500) - The presence of a
tough rubbery binder has resulted in a severely cracked particle

GEFAHRKLASSIFIZIERUNG BEI DER HERSTELLUNG PYROTECHNISCHER SÄTZE UND GEGENSTÄNDE

Dietrich Eckhardt, Norbert Pfeil, Hans-Jochen Rodner

Bundesanstalt für Materialforschung und -prüfung (BAM)
Unter den Eichen 87
D-12205 Berlin

ABSTRACT

In the Federal Republic of Germany the manufacture of pyrotechnics is subject to the safety rules of the Industrial Injuries Insurance (Berufsgenossenschaft) of the chemical industry. The safety provisions of the safety rules "Manufacture of pyrotechnic articles" (VBG 55k) are based on the classification of pyrotechnic compositions and pyrotechnic articles. Which are divided in five hazard groups.

For certain application it is necessary to classify pyrotechnics in accordance with the safety rules "Explosives - general provisions" (VBG 55a) which based on the same principle as like as the hazard classification for transport or storage of explosives.

The relations between both hazard classification systems are discussed.

1. Einleitung

Die Herstellung pyrotechnischer Mittel, worunter sowohl solche die dem Sprengstoffrecht unterliegenden pyrotechnische Sätze und Gegenstände als auch die dem Waffenrecht unterstellte pyrotechnische Munition verstanden wird, ist in der Bundesrepublik Deutschland den Unfallverhütungsvorschriften der Berufsgenossenschaft der chemischen Industrie unterworfen, speziell der VBG 55k "Herstellen pyrotechnischer Gegenstände" [1].

In einer Reihe von Anwendungsfällen sind aus bestimmten Gründen bei der Herstellung pyrotechnischer Gegenstände nicht die Vorschriften der VBG 55k, sondern die der Unfallverhütungsvorschrift VBG 55a "Explosivstoffe und Gegenstände mit Explosivstoff - Allgemeine Vorschrift" [2] anzuwenden. Die VBG 55a sieht hingegen eine Gefährlichkeitsgruppeneinteilung vor, die sich von der VBG 55k unterscheidet, dafür aber den Prinzipien der Lagergruppenzuordnung nach dem Sprengstoffgesetz bzw. der gefahrgutrechtlichen Zuordnung von explosiven Stoffen und Gegenständen zu Unterklassen der Klasse 1 folgt.

Im weiteren sollen die unterschiedlichen Grundlagen beider Gefährlichkeitsklassifizierungen diskutiert und dargestellt werden, in welcher Beziehung die Gruppen gemäß VBG 55k zu denen der VBG 55a stehen.

2. Gruppeneinteilung gemäß VBG 55k

Die VBG 55k "Herstellen pyrotechnischer Gegenstände" teilt sowohl pyrotechnische Sätze, das sind die explosionsgefährliche Inhaltstoffe der pyrotechnischen Mittel, als auch pyrotechnische Halberzeugnisse und Gegenstände in jeweils 5 Gruppen unterschiedlicher Gefährlichkeit ein. Der Begriff "Gefährlichkeit" ist im Sinne des üblichen Risikobegriffs zu verstehen, also die Verknüpfung der Eintrittswahrscheinlichkeit eines unerwünschten Ereignisses (Empfindlichkeit, Auslösbarkeit) mit dem zu erwartenden Schadensausmaß (Abbrandverhalten, Wirkung).

Aus der Zuordnung zu diesen Gruppen ergeben sich die in Herstellungsräumen bzw. -gebäuden zulässigen Satzmassen und Personenzahlen für die verschiedenen Fertigungsschritte vom Mischen der Sätze bis zum Verpacken der fertigen Gegenstände.

Charakterisiert sind die Sätze der verschiedenen Gruppen durch ihr Abbrandverhalten sowie ihre mechanische oder thermische Empfindlichkeit. Die Tabelle 1 beinhaltet eine tabellarische Zusammenstellung der verbalen Charakterisierungen für das Abbrandverhalten und die Empfindlichkeit der Sätze, die in den Gruppenbeschreibungen Verwendung finden.

3. Gefahrgruppen gemäß VBG 55a

Nach der Unfallverhütungsvorschrift VBG 55a werden Explosivstoffe und Gegenstände mit Explosivstoff in 4 Gefahrgruppen eingeteilt. Die Definitionen dieser Gefahrgruppen stimmen mit denen, die für die Bestimmung der Lagergruppen gemäß Zweiter Verordnung zum Sprengstoffgesetz (2. SprengV) bzw. für Unterklassen der Klasse 1 der gefahrgutrechtlichen Zuordnung Verwendung finden, überein.

Die Gefahrgruppen werden in der Neufassung der VBG 55a [3] wie folgt charakterisiert:

Gefahrgruppe 1.1

Die Explosivstoffe dieser Gefahrgruppe können in der Masse explodieren. Die Umgebung ist durch Druckwirkung (Stoßwellen), durch Flammen und durch Spreng- oder Wurfstücke gefährdet.

Gefahrgruppe 1.2

Die Explosivstoffe dieser Gefahrgruppen explodieren nicht in der Masse. Gegenstände explodieren bei einem Brand zunächst einzeln. Im Verlauf des Brandes nimmt die Zahl der gleichzeitig explodierenden Gegenstände zu. Die mittelbare Umgebung ist durch Druckwirkung (Stoßwelle), die weitere Umgebung ist durch Sprengstücke und durch Flugfeuer gefährdet.

Gefahrgruppe 1.3

Die Explosivstoffe dieser Gefahrgruppen explodieren nicht in der Masse. Sie brennen sehr heftig und unter starker Wärmeentwicklung ab, der Brand breitet sich rasch aus. Die Umgebung ist hauptsächlich durch Flammen, Wärmestrahlung

Tabelle 1 Verbale Charakterisierung für das Abbrandverhalten und die Empfindlichkeit pyrotechnischer Sätze entsprechend der Gruppeneinteilung der Unfallverhütungsvorschrift VBG 55k

Gruppe	Die Sätze brennen	Die Abbrandgeschwindigkeit	Die Sätze können	Die Sätze sind mechanisch oder thermisch	Die Gefährlichkeit
1	sehr heftig ab	-	bereits ohne Verdämmung in kleinen Mengen explodieren	sehr empfindlich	in der Druck- und Flammenwirkung
2	heftig ab	steigt bei Eigenverdämmung stark an	bei Verdämmung (auch kleiner Mengen) explodieren	empfindlich	in der Druck- und Flammenwirkung
3	schnell ab	ändert sich nur geringfügig bei Erhöhung der Menge	bei Verdämmung auch explodieren oder deflagrieren	empfindlich	hauptsächlich in der Flammenwirkung
4	mit langsamer bis mittlerer Geschwindigkeit ab	erhöht sich bei zunehmender Menge im allgemeinen nicht	in verdämmten Zustand auch deflagrieren	verschieden empfindlich	im wesentlichen in der Flammen- und Hitzewirkung
5	langsam ab	-	-	wenig empfindlich	(Die Umgebung ist gefährdet)

und Flugfeuer gefährdet. Im allgemeinen ist mit Druckwirkung (Stoßwellen) nicht zu rechnen.

Gefahrgruppe 1.4

Die Explosivstoffe dieser Gefahrgruppen stellen keine bedeutsame Gefahr dar. Sie brennen ab, einzelne Gegenstände können auch explodieren. Die Auswirkungen sind weitgehend auf das Packstück oder den Arbeitsplatz beschränkt. Sprengstücke gefährlicher Größe und Flugweite entstehen nicht. Ein Brand ruft keine Explosion des gesamten Inhaltes einer Packung oder der Menge von Explosivstoff am Arbeitsplatz hervor.

Während die Gruppeneinteilung nach der VBG 55k sowohl die Empfindlichkeit als auch die Wirkung berücksichtigt, werden die Gefahrgruppen der VBG 55a ausschließlich aus der Wirkung heraus definiert. Die Empfindlichkeit geht lediglich über die Fähigkeit zur Weiterleitung der eingeleiteten Reaktion, z. B. bei der Massenexplosion, impliziert ein.

Zum Zeitpunkt der Erarbeitung dieses Manuskriptes war noch die unter [2] zitierte VBG 55a gültig. Es ist aber vorgesehen, zum 01.04.1995 die überarbeitete Fassung der VBG 55a "Explosivstoffe - Allgemeine Vorschrift" [3] in Kraft zu setzen. Diese enthält u. a. hinsichtlich der Ermittlung der Gefahrgruppen wesentlich veränderte Bestimmungen. In der "alten" VBG 55a [2] waren die Eigenschaften der Stoffe und Gegenstände, insbesondere ihr Verhalten in der Versandpackung bei einem Brand, einer Deflagration oder Detonation und den sich daraus ergebenden Gefahren, für die Einteilung in Gefahrgruppen maßgebend. Gemäß der "neuen" VBG 55a [3] sind für die Festlegung der Gefahrgruppen "..... die Wirkungen der Explosivstoffe bei der Auslösung durch die möglichen Beanspruchungen in den jeweiligen Arbeitsgängen" zu bestimmen. Es wird weiterhin gesagt, daß die nach der 2. SprengV bestimmten Lagergruppen nur dann als Gefahrgruppen übernommen werden können, wenn denkbare ungewollte Reaktionen aufgrund möglicher Beanspruchungen während der Arbeitsgänge nicht anders sind, als die für die Ermittlung der Lagergruppen angenommenen.

Durch dieses geänderte Verfahren der Zuordnung der Explosivstoffe zu Gefahrgruppen soll erreicht werden, daß ausgehend von den Stoffeigenschaften, den

Darstellungen sind die Subdiagramme für die Satzgruppen 1 bis 5 von links nach rechts abnehmender Gefährlichkeit entsprechend angeordnet. Innerhalb der Subdiagramme gilt dies in gleicher Weise für die in Klassen eingeteilten Prüfergebnisse. Daraus resultiert für alle diese Darstellungen eine mehr oder minder ähnliche Struktur, die sehr deutlich im Bild 1 für den Koenen-Test zu erkennen ist: etwa 80 % der Gruppe-1-Sätze befinden sich in der Ergebnisklasse, die der höchsten Gefährlichkeit entspricht (linke Säule), und etwa 90 % der Gruppe-5-Sätze sind eingekehrt in einer Ergebnisklasse, in der die untersuchte Eigenschaft als ungefährlich anzusehen ist (recht Säule).

Häufigkeit in %

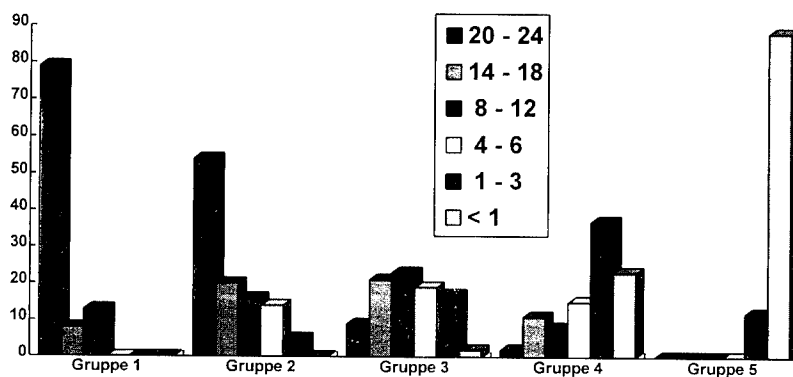


Bild 1: Verteilung der Grenzdurchmesser beim Koenen-Test innerhalb der Satzgruppe der VBG 55k

Die Gruppe-3-Sätze zeigen eher eine Gleichverteilung mit einem schwachen Häufigkeitsmaximum bei mittleren Grenzdurchmessern.

Die Fähigkeit mit oder ohne Einschluß zu explodieren kann am besten durch den Grenzdurchmesser beschrieben werden (vgl. Tabelle 1). Typische Grenzdurchmesser für Gruppe-1-Sätze und Gruppe-5-Sätze sind ≥ 20 mm und < 1 mm. Verglichen mit den verbalen Charakterisierung bedeutet dies, daß pyrotechnische Sätze mit Grenzdurchmesser ≥ 20 mm bereits ohne Verdämmung in kleiner Menge explodieren können.

Die verbalen Charakterisierung der Satzgruppen nennen einerseits die Gefährdung der Umgebung durch Druck- und Flammenwirkungen (Gruppe 1 und 2) und andererseits durch im wesentlichen thermische Wirkungen (Gruppe 3 und 4), wobei keine Aussage über die zu berücksichtigenden Mengen getroffen werden. Aufgrund der Verteilung des Verhaltens pyrotechnischer Sätze in Stahlrohren innerhalb der verschiedenen Satzgruppen (Bild 2)

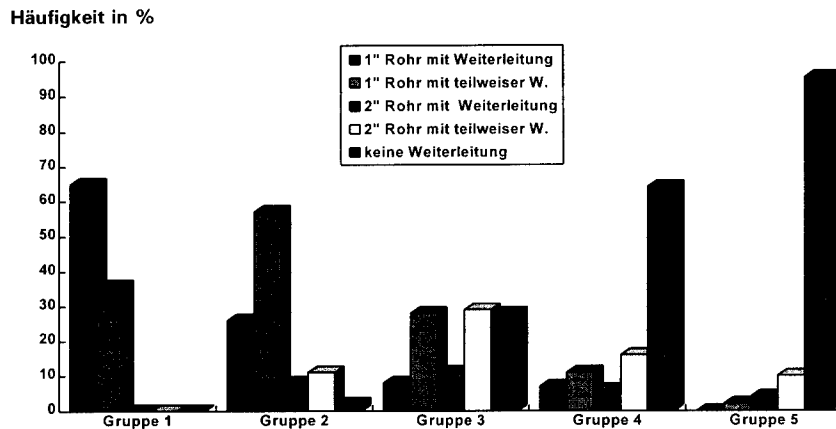


Bild 2: Verteilung der Verhaltensweise gegenüber Detonationsstoß im Stahlrohr innerhalb der Satzgruppen der VBG 55k

kann davon ausgegangen werden, daß auch relativ kleine Satzmengen, d. h. Mengen, die üblicherweise in Arbeitsräumen vorhanden sind und nicht unbedingt unter Sicherheit gehandhabt werden, dann zu gefährlichen Druckwirkungen führen können, wenn sie im 1"-Stahlrohr eine positive Reaktion, d. h. Weiterleitung oder teilweise Weiterleitung zeigen.

Für die Beziehung der Gruppen gemäß VBG 55k zu den Gefährgruppen der VBG 55a im Ergebnis obiger Darlegungen, d. h. sowohl nach den verbalen Beschreibungen der Satzgruppe als auch nach den gezeigten experimentellen Daten, muß zunächst davon ausgegangen werden, daß die Gruppen 1, 2 und 3 der Gefährklasse 1.1, die Gruppen 4 bzw. 5 den Gefährgruppen 1.3 bzw. 1.4 zuzuordnen sind.

Die in Bild 1 und 2 dargestellten Untersuchungsergebnisse für die Gruppe 2 zeigen aber auch Merkmale, die auf eine mögliche Zugehörigkeit zur Gefahrgruppe 1.3 hinweisen.

Eine Entscheidung darüber, ob eine Zuordnung zur Gefahrgruppe 1.3 vorgenommen werden kann, ist im Rahmen (praxisnaher) Untersuchungen, wie sie üblicherweise zur Ermittlung der Gefahrgruppen nach der VBG 55a durchgeführt werden, zu erbringen.

Für derartige Untersuchungen müssen die tatsächlichen Bedingungen an den jeweiligen Arbeitsplätzen hinsichtlich der Mengen, des Einschlusses, der Auslösemöglichkeiten usw. zugrunde gelegt werden. Neben der Ermittlung der Gefahrgruppe bieten diese Untersuchungen gleichzeitig die Möglichkeit die Wirksamkeit eventuell vorgesehener Schutzeinrichtungen zu überprüfen.

5. Literaturverzeichnis

- [1] Unfallverhütungsvorschrift "Herstellen pyrotechnischer Gegenstände"
(VBG 55k) vom 1. April 1981
i. d. F. vom 1. April 1991
Berufsgenossenschaft der chemischen Industrie
Jedermann-Verlag Dr. Otto Pfeiffer oHG, Heidelberg

- [2] Unfallverhütungsvorschrift "Explosivstoffe
und Gegenstände mit Explosivstoff - Allgemeine Vorschrift"
(VBG 55a) vom 1. August 1978
i. d. F. vom 1. April 1991
Berufsgenossenschaft der chemischen Industrie
Jedermann-Verlag Dr. Otto Pfeiffer oHG, Heidelberg

- [3] Unfallverhütungsvorschrift "Explosivstoffe - Allgemeine Vorschrift"
Gelbdruck, Berufsgenossenschaft der chemischen Industrie
Beschlusseifer Entwurf Juli 1994

- [4] Treumann, H.
Quantification of the degree of hazard of pyrotechnic compositions
Proceeding of the 7th International Pyrotechnic
Seminar, Vail/Colorado 1980, S. 878 - 897

- [5] Pfeil, N.; Krüger, G.; Treumann, H.
Empfindlichkeits- und Wirkungsparameter pyrotechnischer Sätze
für die Einteilung in Satzgruppen abgestufter Gefährlichkeit
Sprengstoffe Pyrotechnik, Schönebeck, 30. Jahrgang (1993) 4

MODELING THERMAL/CHEMICAL/MECHANICAL RESPONSE OF ENERGETIC MATERIALS

M. R. Baer, M. L. Hobbs, R. J. Gross, D. K. Gartling and R. E. Hogan

Sandia National Laboratories, Albuquerque, New Mexico 87185 USA*

ABSTRACT

An overview of modeling at Sandia National Laboratories is presented which describes coupled thermal, chemical and mechanical response of energetic materials. This modeling addresses cookoff scenarios for safety assessment studies in systems containing energetic materials. Foundation work is discussed which establishes a method for incorporating chemistry and mechanics into multidimensional analysis. Finite element analysis offers the capabilities to simultaneously resolve reactive heat transfer and structural mechanics in complex geometries. Nonlinear conduction heat transfer, with multiple step finite-rate chemistry, is resolved using a thermal finite element code. Rate equations are solved element-by-element using a modified matrix-free stiff solver. This finite element software was developed for the simulation of systems requiring large number of finite elements. An iterative implicit scheme, based on the conjugate gradient method, is used and a hemi-cube algorithm is employed for the determination of view factors in surface-to-surface radiation transfer.

The critical link between the reactive heat transfer and mechanics is the introduction of an appropriate constitutive material model providing a stress-strain relationship for quasi-static mechanics analysis. This model is formally derived from bubble nucleation theory and parameter variations of critical model parameters indicates that a small degree of decomposition leads to significant mechanical response. Coupled thermal/chemical/mechanical analysis is presented which simulates experiments designed to probe cookoff thermal-mechanical response of energetic materials.

INTRODUCTION

It is well accepted that the response of energetic materials subjected to abnormal thermal environments involves a variety of thermal, chemical and mechanical processes. Prior work has centered on the onset of runaway reaction based only on thermal-chemical effects with little regard to mechanical behavior of the energetic material or the pressurization induced during decomposition. Recent studies have suggested that a small degree of decomposition leads to significant pressure buildup in confined systems¹. Traditional cookoff modeling, such as that of Zinn and Rogers², estimate pressurization effects using a gaseous equation of state without any considerations of material distortion or strain of the energetic material. This modeling approach only provides leading order effects for fast cookoff and is incorrect for slow cookoff conditions. Such analyses are strictly limited to thermal runaway and do not correctly address the complex issues related to mechanical response.

*This work performed at Sandia National Laboratories supported by the U.S. Department of Energy under contract DE-AC04-94AL85000

In this study, a new approach in cookoff modeling is explored which couples thermal, chemical and mechanical behavior. Modern finite element analysis can be used to solve problems having a large number of elements while also including complex physical models necessary to assess the onset and violence of reaction of energetic materials. Complex geometry, multiple boundary conditions, sliding surfaces/gaps, material strength, and material deformation are aspects of simulations that must be considered in finite element analysis needed to resolve energetic material response in real systems.

Much prior finite element analysis has been decoupled, *i.e.* the stress field is resolved as a separate calculation for a specified thermal state. However, fully-coupled multidimensional thermal/chemical/mechanical analysis capability is currently available which builds upon state-of-the-art software for mesh generation, input/output, visualization, and shared databases. A driver analysis package, TREX3D, under development at Sandia National Laboratories, updates coupled thermal/chemical and mechanical analysis in a time step to time step consistent manner whereby material and meshing is revised with properties and boundary conditions resulting from coupled response.

In the sections to follow, brief descriptions of the finite element solvers are discussed and the reactive mechanics material model is reviewed. Demonstrative calculations of coupled response are then presented which illustrates the importance of coupling mechanical response to reactive heat transfer. Multidimensional simulations of small-scale cookoff experiments are also shown representing capabilities for better linking modeling with experimentation.

THEORETICAL/NUMERICAL DESCRIPTIONS OF MODELING

TREX3D is the analysis software which links reactive heat transfer with mechanics. This next generation finite element software is an extension of a coupled thermal/chemical/mechanical solver for one-dimensional geometries --TREX1D which consisted of a thermal/chemistry solver, XCHEM,³ and a quasi-static mechanics finite element code, SANTOS⁴. In multidimensions, the thermal/chemical finite element solver is COYOTE II⁵ and the quasi-static finite element code JAS⁶. TREX3D uses an operator splitting technique whereby thermal/chemical fields are advanced using a fixed mechanics field; then mechanics is advanced over the same time interval using the updated thermal/chemical fields. This technique provides for a rapid solution since the mechanical solver is inactive during the small time steps required by the thermal/chemistry solver.

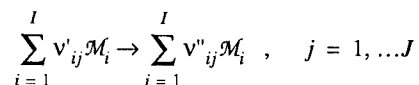
In the one-dimensional method-of-lines solver, thermal chemistry is resolved using a high resolution stiff solver enhanced with adaptive gridding. Mesh interpolation is required to communicate the temperature and reacted fraction from the thermal chemistry code to the quasi-static mechanics code. However, in the multidimensional finite element solver, common mesh and element basis functions and database structures are used which simplifies communication between the solvers.

The reactive material model, discussed later, uses temperature and species information as input from the thermal solver and a stress-strain history is resolved. The effects of material strain are manifested in the heat transfer finite element analysis through a distorted mesh. Gaps can form

between material interfaces and thermal contact resistance changes heat transfer paths. Stress is communicated back from the mechanics solver to the chemical kinetics routines as mixture pressure allowing pressure-dependent combustion mechanisms. Predicted spatial history variables include temperature, chemical species, principle stress, engineering strain, solid/gas pressure, solid/gas density, local yield stress, and gas volume fraction. The specific surface area of the thermally-damaged energetic material is then estimated from calculated volume fractions given initial state information of nucleation density and defect size.

Reactive heat transfer in one-dimension - The eXplosive CHEMical kinetics code, XCHEM³ was developed to solve the reactive diffusion equations associated with thermal ignition of energetic materials. This method-of-lines code uses a stiff numerical method and adaptive meshing to resolve relevant combustion physics. Solution accuracy is maintained between multi-layered materials consisting of blends of reactive components and/or inert materials. Phase change and variable properties are included in multi-layer one-dimensional slab, cylindrical, and spherical geometries. Temperature-dependent thermal properties are incorporated and the modification of thermal conductivities to include decomposition effects are estimated using solid/gas volume fractions determined by species fractions. Gas transport properties, including high-pressure corrections, are also considered. Time-varying temperature, heat flux, convective and thermal radiation boundary conditions, and layer-to-layer contact resistances are implemented.

Nonlinear heat conduction with differential reaction sources is the basis for the thermal-chemistry solvers. Multiple step chemistry is modeled upon consideration of a mechanism expressed as:



\mathcal{M}_i denotes the chemical symbol for the i^{th} species, and v_{ij} represents a stoichiometric coefficient for the i^{th} species in the j^{th} reaction step. Reactive heat transfer is described by the conduction equation given as

$$\rho C_p \frac{\partial T}{\partial t} = \lambda \nabla^2 T + \sum_{i=1}^I \sum_{j=1}^J \mathcal{H}_{ij} \rho_i r_j \quad (1)$$

where

$$r_j = T^{\beta_j} A_j \exp(-E_j/RT) \prod_{i=1}^I N_i^{\mu_{ij}}, \quad j = 1, \dots, J$$

and

$$dN_i/dt = \sum_{j=1}^J v_{ij} r_j, \quad i = 1, \dots, I \quad (2)$$

For the sake of brevity, details of the XCHEM code are not discussed here and the interested reader is encouraged to review reference 3 for complete documentation of the numerical method and its implementation.

Multidimensional reactive heat transfer - For higher dimensional problems, a finite element solution of reactive heat transfer is preferred using COYOTE II⁵. COYOTE II employs an extensive element library including triangles, quadrilaterals, hexahedrons, prisms, tetrahedrons, bars, and shells. Several general purpose mesh generation programs for finite element analysis have been developed at Sandia National Laboratories to provide mesh connectivity, material pointers and boundary condition specifications compatible with COYOTE II. For example, FASTQ⁷ is an interactive two-dimensional automatic mesh generation program which includes a paving algorithm. Paving provides an optimized element mesh by layering elements along boundaries toward the interior of a region and then seams and smoothly joins them. Three-dimensional finite element meshes are created by mapping (*i.e.* translating or rotating surfaces) using the program GEN3D⁸. Other meshing programs include GJOIN⁹ which merges separate meshed regions into a single domain, and GREPOS¹⁰ which repositions a finite element mesh by translating, rotating, or exploding two-dimensional or three-dimensional meshes.

Having established a discrete element mesh, a set of finite element basis functions is defined for each element which are a functional representation of the independent variables. COYOTE II allows linear or quadratic basis functions. Equation (1) is approximated as a residual, *i.e.* all terms are collected on one side, multiplied by an appropriate weighting basis function, and integrated over the entire domain. The resulting Galerkin approximation yields a set of nonlinear equations given in matrix form as:

$$\mathbf{M}(\mathbf{T}) \dot{\mathbf{T}} + \mathbf{K}(\mathbf{T}) \mathbf{T} = \mathbf{F}_Q(\mathbf{T}, N) \quad (3)$$

where $\mathbf{M}(\mathbf{T})$ is the mass matrix, $\mathbf{K}(\mathbf{T})$ is the stiffness matrix and \mathbf{F}_Q is the forcing function vector. Information concerning chemistry variables are contained in the forcing vector at the Gauss quadrature integration points. Rate equations for the chemistry variables are defined at these locations (in contrast to nodes) to avoid ambiguities associated with elements adjoining material interfaces.

The time derivatives in Equations (3) are discretized in COYOTE II using one of several user-specified numerical options including: first order backward Euler, a second order trapezoidal method, or a first order explicit method. The resulting discretized equations are then linearized using a Picard method or a Newton method, producing a set of linear first order equations of the form, $\mathbf{A}x = \mathbf{b}$, where \mathbf{A} is the Jacobian matrix, x is the unknown vector representing nodal temperature, and \mathbf{b} is the residual vector.

Chemical reaction is introduced through the forcing vector. An operator-splitting method is used which first advances the temperature in time with all chemistry variables remaining unchanged. Then, the second operator fixes the temperature field and the species rate equations are advanced in time using a modification of CHEMEQ¹¹, which is a matrix-free hybrid stiff solver. Following the second operator, the endothermic and/or exothermic heat sources are re-evaluated as input for the next time step. Adaptive time stepping is based on time scales relevant for both the heat transfer and the chemistry¹². Because the solver for the chemistry does not use Jacobian evaluation requiring a large start-up overhead, the system of reaction equations are efficiently solved element-by-element at Gauss integration points.

A unique capability of COYOTE II is the means to determine view factors for large problems involving surface-to-surface radiation heat transfer. Thermal radiation from a fire source is an example of an abnormal thermal environment for surety and weapon safety analyses. The code, CHAPARRAL¹³, uses either a hemi-cube algorithm¹⁴ or FACET¹⁵, which has been made into a subroutine library, to compute view factors. For large three-dimensional problems, the hemi-cube algorithm has been shown to be a computationally superior method for radiation heat transfer analysis.

Although the assembly of the set of linear equations is computationally expensive, a large fraction of computation time is spent in obtaining the solution of $Ax = b$. The inverse of the Jacobian matrix directly determines the solution vector, and thus, direct matrix methods have been traditionally used in finite element analysis. Unfortunately, direct methods become prohibitively expensive in terms of both CPU time and computer memory, especially in multidimensional simulations requiring many elements. In COYOTE II, the direct matrix solvers have been replaced by iterative methods using the conjugate gradient approach¹⁶. This substantially improves the performance of the code with no compromise in accuracy. Conjugate gradient algorithms are among the most robust and fastest methods currently available. Further, these methods require far less memory than direct methods. Because finite element simulations in three-dimensional routinely require 50,000 or more elements, this is a critical feature of analysis.

Multidimensional mechanics - Quasi-static, large deformation, nonlinear mechanical response of inert and reactive materials is resolved using finite element solvers, SANTOS⁴ and JAS⁶. Elastic-plastic and creep behavior are included as finite strain constitutive material models. Thermal expansion can be simulated for reactive materials. Quasi-steady solution of the mechanics is obtained using a self-adaptive dynamic relaxation scheme based on explicit central difference pseudo-time integration and artificial damping. Gap formation is implemented in the finite element solution using a master-slave algorithm for sliding interfaces. In applying the mechanics operator, mechanical energy is preserved consistent with mass conservation constraints. The energy equation states that the variation of total internal energy equals the sum of the surface work and the work by body forces:

$$\delta \int_V \rho e dv = \oint_S t_{(n)k} \delta x_k da + \int_V \rho f_k \delta x_k dv \quad (4)$$

where $t_{(n)k}$ is the surface traction, ρ is the material density, e is the material internal energy, and δx_k is material deformation along direction k . Variations are denoted by δ and the integration spaces correspond to finite element surfaces, S and volumes, V . All variations are subject to conservation of mass: $\delta \int_V \rho dv = 0$.

Commonly used stress-strain relationships are elastic-plastic, viscoelastic, and elastic-plastic power law hardening materials as described in Reference 18. Total energy conservation over a time interval is enforced with the sequential solution of the equations (1) and (4). The thermal/chemical energy equation is first resolved assuming that the mechanics field is unchanged, and thereafter mechanical energy contributions are incorporated assuming frozen thermal and chemical fields. Thus, on a time step to time step basis, all thermal, chemical and mechanical effects are included as a fully coupled model. In the present work, the elastic-plastic constitutive model is used for inert structural materials. This model uses standard von Mises yield

with kinematic and isotropic hardening. To describe the mechanical behavior of decomposing energetic materials a new algebraic stress-strain constitutive law has been developed for determined temperature and species fields.

REACTIVE, ELASTIC-PLASTIC CONSTITUTIVE MODEL

Recovery tests of thermally-degraded TATB (2,4,6-trinitro-1,3,5-benzenetriamine) show clear evidence of macroscale pore formation.¹ In these tests, pressed samples are confined with O-rings, heated 5 K/minute to 523 K, and held at 523 K for 1 hour until confinement is breached at ~100 atm. In typical tests, the total mass loss is estimated to be ~5% which confirms that a small degree of decomposition leads to significant mechanical response. Thermal decomposition of energetic materials produces gaseous products which accumulate at defects or nucleation sites and contribute to local pressurization. This physical observation has motivated the development of a new constitutive model based on bubble nucleation theory.

A complete derivation of this model is not presented here and only the salient features are discussed. The interested reader can find the details in reference 19. The conceptual model considers a region of space or element filled with a collection of defects which act as nucleation sites. For simplicity, spherical inclusions are assumed and the ensemble of defects is considered in a unit cell with a uniformly-distributed, statistically-average size. Volume fraction is directly related to the geometric variables and the nucleation density. Similarly, the specific surface area of the thermally degraded material is derived from these internal state variables.

The micromechanical model is described by the six algebraic equations 1) the conservation of gas mass; 2) the conservation of total mass; 3) the gas-phase equation of state (EOS); 4) the condensed-phase EOS; 5) the force balance between gas pressure, solid pressure, and yield stress of the skeleton solid; and 6) the mixture pressure. For the unit cell, a uniform thermal state is considered and the decomposition products are equally distributed to all of the defects. Hence, the micromechanical model requires input of temperature (T) and the reacted gas fraction (F) as determined by reactive heat transfer analysis. Given T and F, the six equations have seven unknowns describing the stress-strain relationship. Closure of the model is obtained by determining the stress field (average mixture principle stress) that is consistent with material strain determined by the finite element analysis. All of the model assumptions and material parameters for the energetic material are given in reference 19. This stress-strain relationship is implicit in porosity and for a given set of material parameters and input T and F, stress fields are determined iteratively or with a general root solving algorithm. Figure 1 shows representative stress-strain states as estimated using material parameters relevant for decomposing TATB at 523 K.

Variations are shown corresponding to varied degree of material decomposition (i.e., F, fraction of material mass decomposed to a gas phase). For a given strain, the mixture pressure changes four orders of magnitude when the reacted gas percent increases from 0 to 5%, consistent with experimental observations. Clearly, a small degree of material decomposition has a significant influence on the mechanical response of the energetic material which, in turn, leads to a strong interaction between thermochemistry and mechanics.

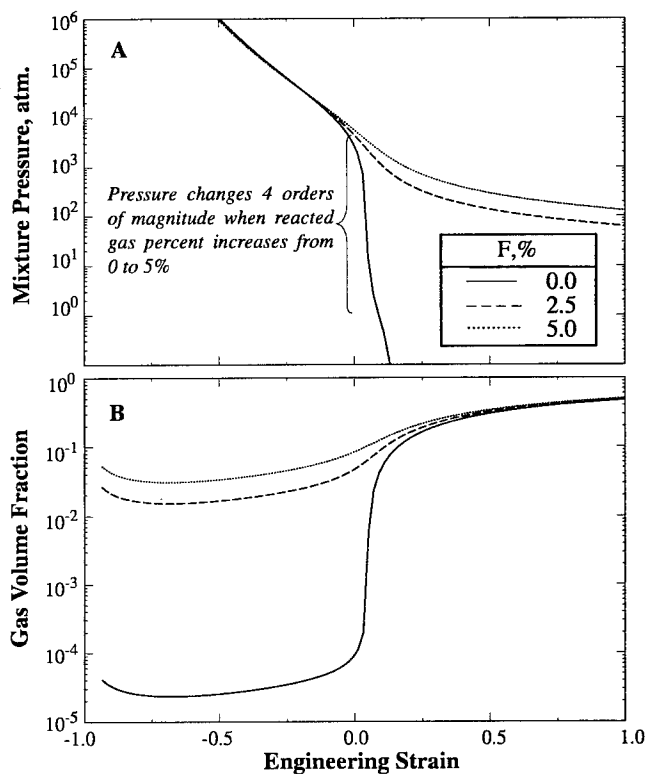


Figure 1. Stress-strain relationship for thermally-degraded TATB
A) principle stress B) volume fraction vs. material strain.

SIMULATION OF CONFINED EXPLOSIVES

In spherical ODTX experiments conducted at the Lawrence Livermore National Laboratory²⁰, preheated aluminum anvils confine 1.27 cm diameter spherical samples of explosive. Heaters control the temperature of the anvils to ± 0.2 K, and the primary measurement is the time to "explosion" at confinement failure. The anvil confinement is sealed hydraulically to 1500 atm.

Several spherical ODTX experiments have been modeled using TREXID; calculated results are displayed in Figure 2 for TATB and PBX 9404. Typically, the logarithm of time to confinement failure versus the reciprocal of the surface temperature T_f is linear over a large region, but sharply bends upward near the critical temperature, T_c , as shown in Figure 2.A for

TATB. The dashed line represents calculated thermal runaway, the solid line represents the time when pressure venting is estimated to occur. The symbols correspond to experimental data. For conditions of fast heating, thermal runaway and mechanical failure coincide. However, for slow cookoff, failure of confinement is largely due to thermal-chemical-mechanical response of the energetic material.

For PBX 9404, a plateau at fast cookoff conditions is observed as shown in Figure 2B. This plateau results from low temperature reactions of nitrocellulose resulting in substantial pressurization. To our knowledge, the features in Figure 2 have never before been calculated with a true estimate of confinement rupture. Tarver²¹ assumed a heat release for NC that was twice as large as calorically possible (excluding any cross-catalytic chemistry effects) assuming that the plateau is entirely a thermal response of the NC binder. The two-step kinetic mechanism may be inadequate to capture the abrupt change in failure times shown for both the aged and new PBX 9404 data shown in Figure 2B. The experimental data of Chen and Brill²² suggest that the kinetics for fast heating rates are different from those measured at slow heating rates. Although a change in mechanism with temperature may explain the abrupt change in failure times, small amounts of additives can also affect results. For example, the stabilizer used in PBX 9404, 0.1% diphenylamine, has a noticeable effect on the ODTX results as seen in Figure 2B; the aged PBX 9404 reacts sooner than the new PBX 9404. The kinetic rate mechanisms used in this work were obtained from the original fits to the ODTX data which did not include mechanical behavior or pressure effects of the chemical rates. Clearly, improved kinetic rates are warranted to explain the time to failure observed for PBX9404.

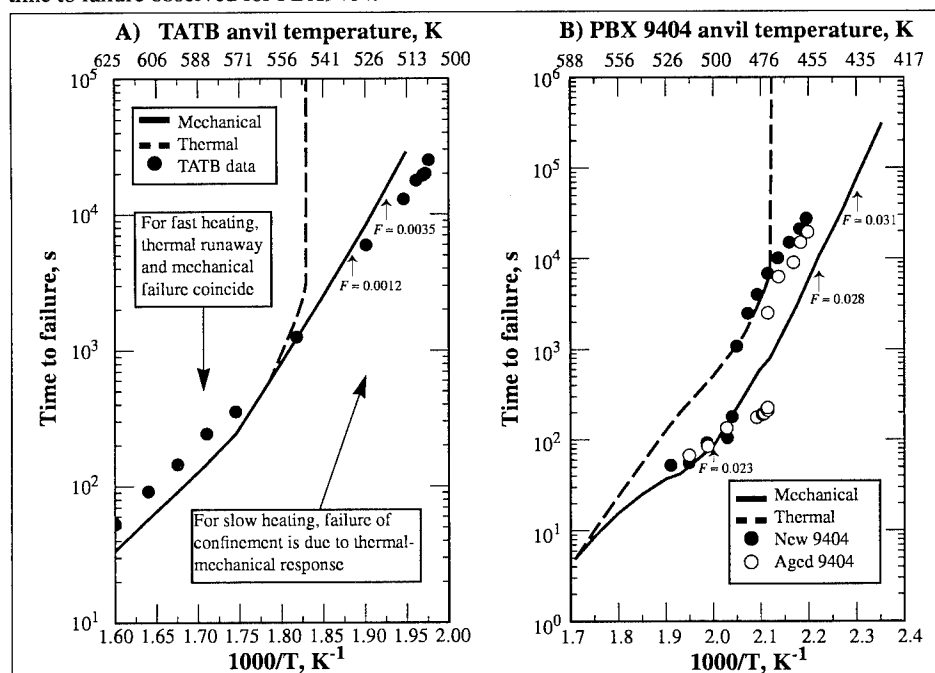


Figure 2 Calculated and experimental time to failure for 1.27 cm diameter spheres of A) TATB and B) PBX 9404

MULTIDIMENSIONAL SIMULATION OF COOKOFF EXPERIMENTS

As a demonstrative three-dimensional simulation of a typical cookoff experiment, the small-scale cookoff bomb developed by Pakulak²³ at NAWC, China Lake, CA is modeled. This experiment consists of steel-cased cylinder cast with a propellant containing a center bore. Two heating band sleeves are used to heat the energetic material at a fixed rate. The combustion bomb is mounted to a steel support structure using four bolts. Representative propellant properties and a single step global reaction kinetics (obtained from DSC estimates)²⁴ are used in this simulation treating a 75 F/hr heating rate.

Figure 3 shows the finite element mesh and an overlay of thermal contours after 14400 seconds of heating (a time prior to ignition). The heat transfer effects of the mounting plate and mounting bolts are calculated to be insignificant. The thermal field is nonuniform and is, at least, two-dimensional and axisymmetric. Figure 4 displays a 45° slice through the combustion prior to the onset of thermal runaway. At 14600 seconds significant propellant decomposition supplements the heat transfer and thermal runaway initiates at an interior location within the propellant. The experimentally-observed onset to thermal runaway occurs at 19000 sec. Given that a simplistic chemistry model is used (no endothermic steps), this cookoff simulation predicts only leading order effects - *numerical simulation is only as accurate as the model inputs*. A true benchmark experiment requires well-defined initial and boundary conditions and accurate material characterization. In these calculations, 58,000 finite elements are used and computation time, simulating 15000 sec of heating to ignition, requires 3 hr CPU on a IBM SP/2 multiple processor computer.

A different type cookoff experiment is being developed by Renlund²⁵ at Sandia National Laboratories to provide simultaneous measurements of thermal and mechanical behavior of confined energetic materials. Figure 5 is a pictorial representation of this experiment. In this hot-cell device, a steel block confines a cylindrical plug of energetic material supported by axial rods fixed to a support structure and a water-cooled load cell. The hot-cell is heated by a band heater which is controlled by thermocouples in the steel block. Simultaneous temperature and load cell measurements provide time-resolved information on thermal-mechanical behavior.

In recent experiments, a support rod is replaced with transparent material which allows optical access to the energetic material interface whereupon laser-based diagnostics (Raman spectroscopy) are used to probe time-resolved species information as the sample undergoes thermal decomposition. Most importantly, species are measured at realistic confinement conditions. Figure 6 displays the time history of temperature and the measured load cell force for thermally-degrading TATB. At later time, decomposition of the material causes pressurization in the cell. Typically, tests are quenched prior to thermal runaway to minimize damage to the hot-cell apparatus.

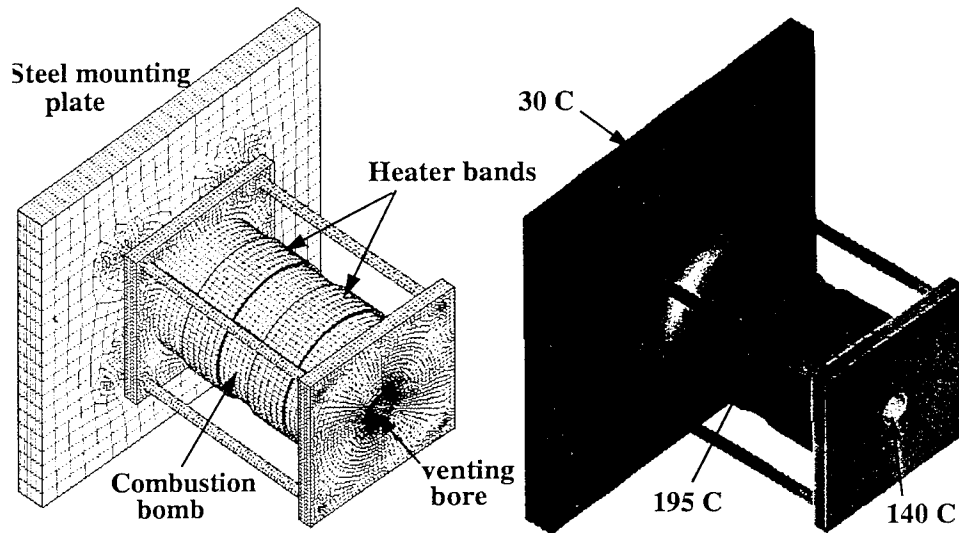


Figure 3. Three dimensional finite element mesh used in COYOTEII simulation of the small-scale cookoff combustion bomb experiment. The right figure displays contours of the thermal field.

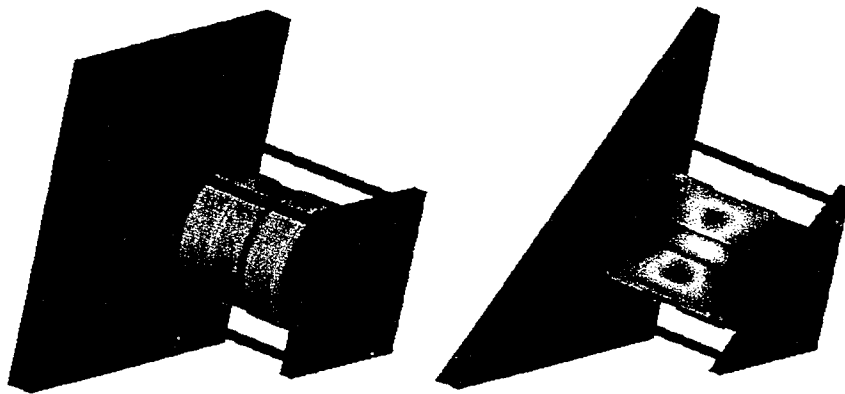


Figure 4. Thermal fields exterior and interior of the combustion bomb prior to thermal runaway. A localized ring of thermally-degraded material forms as chemical energy supplements the heat transfer.

Figure 7 displays axisymmetric finite element calculations of the thermal and stress fields prior to the onset of decomposition. Variations of these fields are shown as shaded contours. On the left, thermal fields are displayed which show that the temperature of the hot-cell is uniform. Cooling of the support structure and the load cell induces thermal and stress gradients. Despite the uniformity of the thermal field, stress fields shown on the right are clearly nonuniform as axial variations in the hot-cell are predicted. In this preliminary study, the displacement of the load cell was not included, thus higher stresses are predicted. Subsequent calibration calculations using inert material (Teflon) have been modeled and the load cell is treated as an elastic material with properties that mimic the measured response of the load cell. With this calibration, modeling studies can now address fully-coupled behavior.

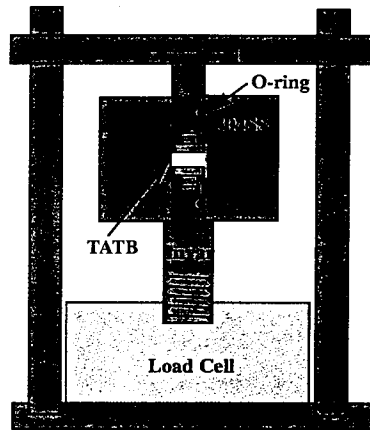


Figure 5. Pictorial of the hot-cell experiment used in simultaneous measurement of temperature and stress of confined energetic materials.

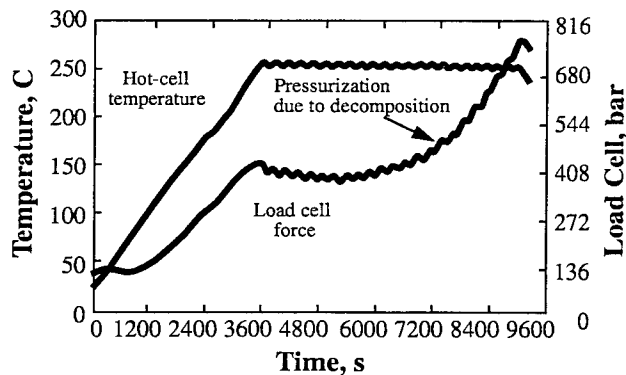


Figure 6. Hot-cell cookoff data for confined TATB.

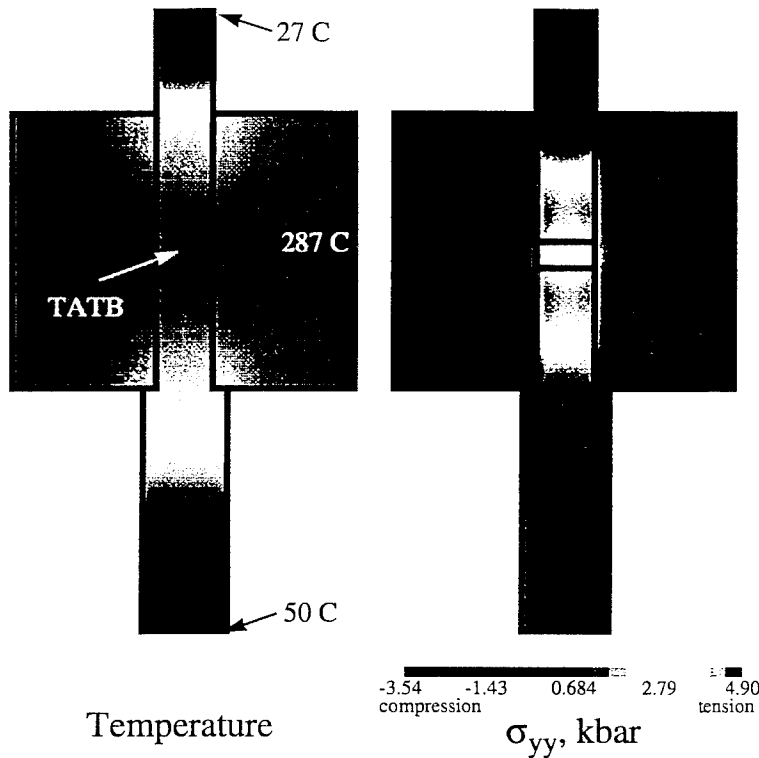


Figure 7. Left: Temperatures in the hot-cell. Right: Stress fields in hot-cell apparatus.
No displacement of the load cell is considered in these calculations.

SUMMARY AND CONCLUSIONS

This work reviews modeling of fully coupled thermal, chemical, and mechanical cookoff analysis under study at Sandia National Laboratories. This effort is being developed for safety assessments of systems containing energetic materials. Finite element analysis has been extended to couple thermal and mechanics behavior. A critical aspect of this coupling involves development of a stress-strain model for thermally-degrading materials. This constitutive relationship is based on bubble nucleation theory which indicates that a small degree of decomposition has a significant influence on pressure buildup and/or material expansion.

Confined ODTX experiments are simulated to conditions of pressure failure at 1500 atm. The spherically confined ODTX simulations compared favorably to experimental data. Slow cookoff is dominated by significant pressure buildup. Even in fast cookoff conditions, small

amounts of decomposition products results in large pressures loading, demonstrating that *mechanics must be considered in any cookoff analysis.*

Multidimensional simulations of realistic cookoff geometries have also been demonstrated. Thermal conduction heat transfer is resolved in finite element analysis including thermal radiation and multiple step condensed phase chemistry. A unique feature of this finite element analysis is the development of solution schemes that can handle a large system of elements with many degrees of freedom. The common use of element structures and databases is critical in coupled analysis. A fully-couple thermal/chemical/mechanical capability has been demonstrated and modeling studies of hot-cell cookoff experiments with inert and energetic materials are ongoing. Future work will extend calculations of experiments for model verification and assess improved kinetic mechanisms and rate data.

REFERENCES

1. Renlund, A. M., personal communication, Sandia National Laboratories, Albuquerque, New Mexico, 1994.
2. Zinn, J. and Rogers, R. N., "Thermal Initiation of Explosives," *J. Phys. Chem.*, **66**, 2646, 1962
3. Gross, R. J., Baer, M. R., and Hobbs, M. L., "XCHEM-1D, A Heat Transfer/Chemical Kinetics Computer Program for Multilayered Reactive Materials," SAND93-1603, Sandia National Laboratories, Albuquerque, NM, 1993.
4. Stone, C. M., "SANTOS - A Two-Dimensional Finite Element Program for the Quasi-static, Large Deformation, Inelastic Response of Solids," SAND90-0543, Sandia National Laboratories, Albuquerque, New Mexico, unpublished personal communication (1994), for more information see Stone, C. M., Krieg, R. D., and Beisinger, Z. E., "SANCHO, A Finite Element Computer Program for the Quasistatic, Large Deformation, Inelastic Response of Two-Dimensional Solids," SAND84-2618, UC-32, 1984.
5. Gartling, D.K., and Hogan, R.E., "COYOTE II - A Finite Element Computer Program for Nonlinear Heat Conduction Problems," SAND94-1173, Sandia National Laboratories, Albuquerque, New Mexico, September, 1994.
6. Biffle, J. H., Blanford, M. L., "JAC2D - A Two-Dimensional Finite Element Computer Program for the Nonlinear Quasi-Static Response of Solids with Conjugate Gradient Method", SAND93-1891, Sandia National Laboratories, Albuquerque, New Mexico; JAS is the 3D extension of this work and documentation is currently in progress.
7. Blacker, T.D., "Paving: A New Approach to Automated Quadrilateral Mesh Generation," *International Journal for Numerical Methods in Engineering*, **32**, 811-847, 1991.
8. Gilkey, A. P., and Sjaardema, G. D., "GEN3D: A GENESIS Database 2D to 3D Transformation Program," SAND89-0485, Sandia National Laboratories, Albuquerque, New Mexico, March, 1989.
9. Sjaardema, G.D., "GJOIN: A Program for Merging Two or More GENESIS Databases," SAND92-2290, Sandia National Laboratories, Albuquerque, New Mexico, December, 1992.
10. Sjaardema, G.D., "GREPOS: A Genesis Database Repositioning Program," SAND90-0566, Sandia National Laboratories, Albuquerque, New Mexico, June, 1993.
11. Young, T.R., "CHEMEQ - Subroutine for Solving Stiff Ordinary Differential Equations," NRL Memorandum Report 4091, Naval Research Laboratory, Washington, D.C., 1979.
12. Gresho, P.M., Lee, R.L., and Sani, R.L., "On the Time Dependent Solution of the Incompress-

- ible Navier-Stokes Equations in Two and Three Dimensions," *Recent Advances in Numerical Methods in Fluids*, Vol. 1, 27-81, Pineridge Press, Swansea, U.K., 1980.
13. Glass, M. W., "CHAPARRAL: A Package for Solving Large Enclosure Radiation Heat Transfer Problems," SAND94-0840, Sandia National Laboratories, Albuquerque, NM, June, 1994.
 14. Cohen, M.F., and Greenberg, D.P., "The Hemi-Cube: A Radiosity Solution for Complex Environments," *Computer Graphics*, **19** (3), 31-40, 1985.
 15. Shapiro, A.B., "FACET - A Radiation View Factor Computer Code for Axisymmetric, 2D Planar, and 3D Geometries with Shadowing," UCID-19887, Lawrence Livermore National Laboratory, Livermore, California, August, 1983.
 16. Schunk, P.R., and Shadid, J.N., "Iterative Solvers in Implicit Finite Element Codes," SAND92-1158, Sandia National Laboratories, Albuquerque, New Mexico, 1992.
 17. Eringen, A. C., *Mechanics of Continua*, second edition, Robert E. Krieger Publishing Company, Malabar, Florida, 142, 1980.
 18. Taylor, L. M., and Flanagan, D. P., "PRONTO 3D: A Three-Dimensional Transient Solid Dynamics Program," SAND87-1912, UC-32, Sandia National Laboratories, Albuquerque, New Mexico, 1992.
 19. Hobbs, M. L., Baer, M. R., and Gross, R. J., "A Constitutive Mechanical Model for Energetic Materials" *Twentieth International Pyrotechnics Seminar*, Colorado Springs, Colorado, IIT Research Institute, Chicago, Illinois, 1994.
 20. McGuire, R. R., and Tarver, C. M., "Chemical Decomposition Models for the Thermal Explosion of Confined HMX, TATB, RDX, and TNT Explosives," *Seventh Symposium (International) on Detonation*, NSWC MP 82-334, 56, 1981.
 21. Tarver, C. M., personal communication, Lawrence Livermore National Laboratory, California 1993.
 22. Chen, J. K., and Brill, R. B., "Thermal Decomposition of Energetic Materials 50. Kinetics and Mechanism of Nitrate Ester Polymers at High Heating Rates by SMATCH/FTIR Spectroscopy," *Comb. Flame*, **85**, 479, 1991.
 23. Pakulak, J. M., "USA Small-Scale Cookoff Bomb (SCB) Test," *21st Explosive Safety Seminar*, Vol. 1, China Lake, CA, August 1984.
 24. Dimararanan, L., personal communication, Naval Air Warfare Center, China Lake, CA, 1995.
 25. Renlund, A., personal communication, Sandia National Laboratories, Albuquerque, NM, 1995.

THE STATIC ELECTRICITY HAZARDS : METHODS FOR ASSESSING PYROTECHNICS SENSITIVITY AND APPROACH FOR HAZARD REDUCTION

Roger RAT, Jean ISLER,

**SNPE - Centre de Recherches du Bouchet - BP N° 2
91710 VERT LE PETIT - FRANCE**

ABSTRACT

Within energetic materials, pyrotechnics are often among the most sensitive to static electricity.

According to the processing conditions, and to the system configuration, they can be submitted to different kinds of electrical stimuli :

- sparks like those delivered by the human body,
- capacitive discharge due to charge accumulation within a system

The paper will describe the experimental devices which allow to measure the sensitivity to each of these two kinds of stimuli. Typical results will be presented, as well as an analysis of the different behaviors observed with pyrotechnics.

On another hand, a procedure is recommended for the choice of a test method depending on the real situation, and on the threats to take into account.

1 - INTRODUCTION

The static electricity is frequently involved in accidental ignition of flammable mixtures, and of course of energetic materials. This is often the result of a complicated process, with at least three main steps : [1].

① A charge generation must first occur, generally by triboelectrical effect during the separation of dissimilar parts of the concerned system.

So static electricity can be generated in different ways, well summarized by C.J. DAHN in [2] :

- charging of powders, of large solid particles or of mixtures, by pneumatic transport, sieving, grinding, mixing, blending operations, ...
- charging of poorly conductive substances, which can come in contact with an explosive material, like plastic coatings on rocket motor mandrels.
- charging of personnel, which can occur from walking on nonconducting flooring, wearing shoes with nonconducting soles, rising from a chair, brushing against an object, or even acquiring the charge from another object in the vicinity by induction.
- charging of metal objects isolated from ground, which can occur by separation with insulating items, or more often by induction.

② The consequent electrical field, due to charge accumulation has to be enhanced up to reach the breakdown field. This can be done macroscopically, by the presence of a sharp metal corner within the electrical field, or microscopically, like in the case of energetic materials made of metallic particles inside an insulating matrix : solid propellants [3], MTV, ...

③ The energy delivered during this discharge can then lead to ignite the flammable mixture, or the energetic material, depending on its level and time duration, and also on thermodynamical conditions related to the confinement or pressure.

2 - ELIMINATING THE ELECTROSTATIC IGNITION DANGERS

The example of the chemical industry, which often handles flammable mixtures much more sensitive than explosives and pyrotechnics, shows that eliminating the third point above can be a good way for the reduction of static electricity hazards.

When not completely feasible, then measures concerning the two others points can be taken in order to :

- minimize the charge generation and accumulation,
- avoid the situations likely to allow a breakdown discharge.

This approach can be summarized on a flowchart like on table 1.

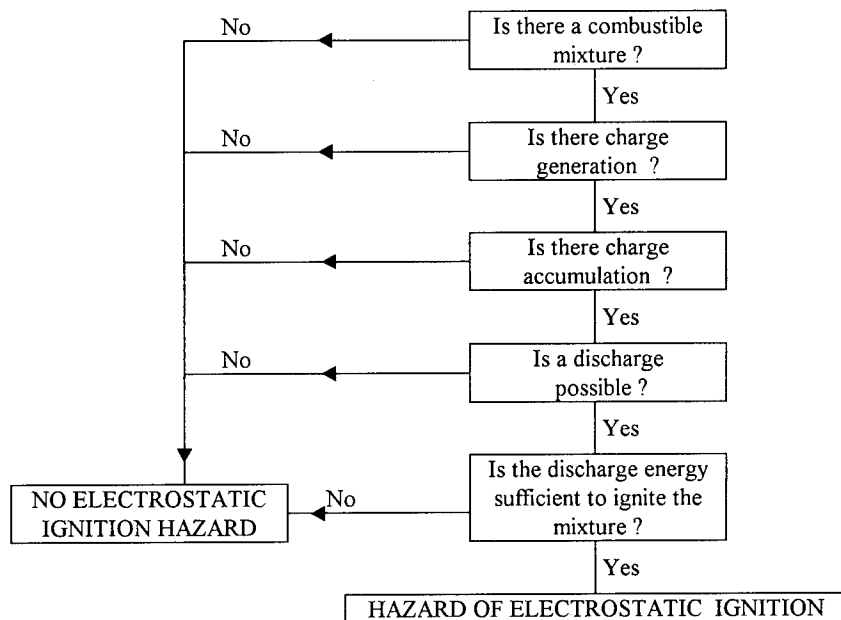


Table 1 : Example of hazard analysis for electrostatic ignition

3 - ELECTROSTATIC IGNITION HAZARDS WITH PYROTECHNICS

Using the previous approach to identify the electrostatic ignition hazards with pyrotechnics means then to be able to list, during all steps of the manufacturing process, all the possible combustible mixtures and all the environment features.

And this can become a difficult work in the case of some pyrotechnics, due to the wide diversity of situations that can be met. Indeed, we may have to consider in a hazard analysis :

- different kinds of flammable ingredients : solvents with minimum ignition energy (MIE) much lower than 1 mJ, metal powders with MIE near some mJ, and of course redox mixtures with unknown MIE.
- different physical states of the composition, depending on the process : granular mixture with more or less solvent, pressed material, chips, ...
- different confinement conditions, which can lead to various situations on an electrical point of view (capacity of the system, time constant ...) and on a thermodynamical point of view (heat conduction ...)

The aspects of solvents and fine metallic particles ignition will not be treated here, since quite wellknown from the chemical industry experience. But according to our experience in the fields of secondary high explosives and rocket motor propellants, we have rather tried to see how can the sensitivity of pyrotechnics range beside these more classical kind of energetic materials.

This analysis is mainly based on results obtained with the two kinds of apparatus commonly used at SNPE :

- a spark sensitivity test,
- a capacitive discharge apparatus.

4 - SPARK SENSITIVITY OF PYROTECHNICS

4.1. Test description

The study of the spark sensitivity of granular energetic materials, mainly primer explosives and secondary high explosives, can be performed with an apparatus like described on figure 1. [3]

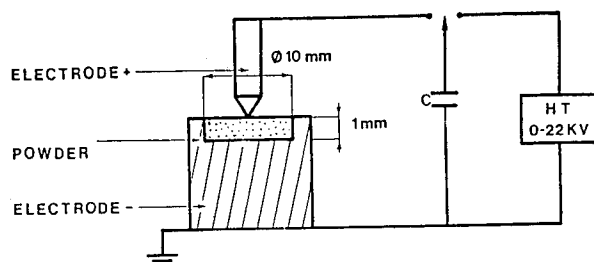


Figure 1 : Schematic arrangement of ignition test by electrostatic spark

In this test, the discharge of a maximum 3000 pF capacity charged up to 22 KV produces a spark between the two electrodes. The maximum energy delivered by the spark is 726 mJ.

The principle of testing is to determine the minimum ignition energy, i.e. the lowest level at which one ignition occurs, with twenty no reaction at the level just below.

4.2. Typical results

The next table summarizes results obtained with this test, and provides a good basis for the comparison between some kinds of pyrotechnics and classical secondary high explosives.

	Ingredients	"No reaction" energy measured by the test of figure 1 (mJ)
SECONDARY HIGH EXPLOSIVES (Granular)	PETN RDX HMX	73 (1) 120 to > 726 (2) 225 to > 726 (2)
PYROTECHNICS (Granular)	Zr/CuO Zr H ₂ /CuO Zr/Ba Cr O ₄ /AP Mg/CuO BaO ₂ /PbO ₂ /Si ₂ Ca/Fe ₂ O ₃ /Al Mg/MnO ₂ /KMnO ₄ /Fe ₂ O ₃ /Si ₂ Ca AP/Al Mg/Teflon KNO ₃ /Si ₂ Ca/Sb ₂ S ₃ KNO ₃ /Fe ₂ O ₃ /Al/Si/C	< 1 < 1 2 25 30 20 541 661 > 726 > 726
COMPACT MATERIALS	All kinds of composite materials for PBXs and Rocket motor propellants	Not sensitive at this test (> 726). Samples only sometimes perforated in their middle
	New compositions recently tested : - AP / Al / Binder - AP / Mg / B / Binder - AP / Al / C / Binder	37 13 121

Table 2 : Spark sensitivity results

- (1) Fine : the medium particle size is 10 μ m
 (2) Depending on the particle size

5 - SENSITIVITY OF PYROTECHNICS TO CAPACITIVE DISCHARGE

5.1. Test description

The analysis of accidental events with some propellants declared not sensitive to the spark test led us to design a new test with increased values for the following parameters [3] :

- size of samples (mass effect or confinement)
- duration of discharge in the RC circuit, where R is the sample resistance, and C the capacity applied to the sample extremities (time required for ignition)
- energy delivered, up to 15.6 J

In view of the above parameters, an equipment was developed, shown in figure 2.

The sample to be tested is a cylindrical 90 mm diameter grain, 100 mm long. The grain is located between two electrodes. The electrode system is a "point-plane type", which is very penalizing because the electric field close to a sharp area is more intense. In order to get an adequate contact area and distribution of the electric current, the grounded surface of the sample facing the negative electrode is coated with a silver lacquer.

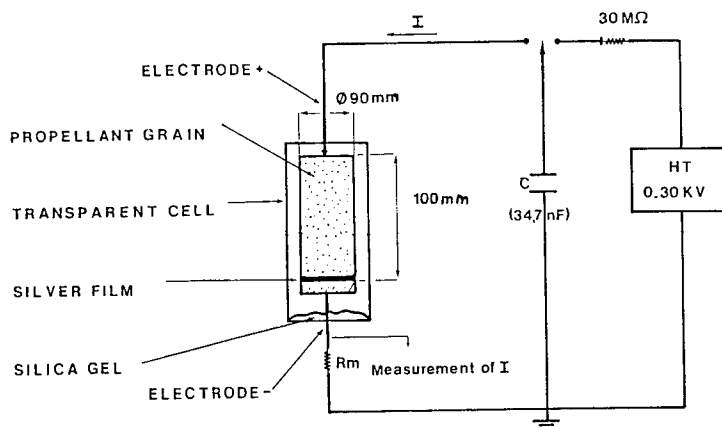


Figure 2 : Schematic arrangement for capacitive discharge test on the propellant grains.

Each tested composition is studied by performing, on three different samples, thirty consecutive discharges with the 34.7 nF capacitance charged to 30 KV.

Different kinds of results may be observed : cracking, ignition, violent explosion ...

A tested composition is declared not sensitive if no one of these events is observed after the thirty discharges on three samples.

5.2. Typical results

The next table summarizes results obtained with the capacitive discharge test.

	Ingredients	Sensitivity to the capacitive discharge (34.7 nF / 30 KV)
ROCKET MOTOR PROPELLANTS AND PBXs	HTPB Binder AP, RDX, ... Aluminum	The compositions with a high content of fine aluminum particles are sensitive. Ignition are observed after some discharges
PYROTECHNICS	AP / Mg / B / Binder AP / Al / C / Binder Mg / Teflon	Not sensitive Sensitive (ignition after 6 discharges) Not sensitive

Table 3 : Capacitive discharge results

6 - DISCUSSION

Due to the wide range of ingredients used in pyrotechnics, and to the variety of operations performed during their manufacturing, it appears that particular care must be taken with such energetic materials.

The analysis of results obtained with our two classical ESD tests shows three particular behaviors with pyrotechnics :

- ① The combination of oxydants with some metals can lead to a sensitivity to sparks with very low energy (less than one mJ), as observed with some granular mixtures with Zirconium for instance. A "spark test" like described in 4.1. is well adapted to detect such sensitive mixtures.
- ② Such sensitive to spark compositions are not found systematically sensitive to the capacitive discharge test, when in a compact presentation.
- ③ But some compositions have been found sensitive to spark with energy in the range of 10 mJ, when in a compact presentation, or in a polymerized binder. This behavior was quite new for us, since never observed before with more classical formulations like propellants and PBXs.

On another hand, this sensitivity appeared to be variable with the sample preparation and also probably with the sample presentation in the measurement cell.

7 - CONCLUSION

For many years, the electrostatic hazard assessment of energetic materials has been based on the simple statements that only granular mixtures are sensitive to sparks and that compact materials may only be ignited by a capacitive discharge mechanism.

Our recent experience shows that with some pyrotechnics, we have also to consider the ignition by low energy sparks with compact materials.

And in this area, there is still the need of much more information, to improve the knowledge of all kinds of mechanism, and to establish better correlation between real situations and test configurations.

REFERENCES

- [1] R.W. LARSON et al, A Microphysical Model for the Electrostatic Discharge Susceptibility of Solid Rocket Propellants, 24th DOD Explosives Safety Seminar, St Louis, 28-30 August 1990.
- [2] C.J. DAHN et al, New Concepts in Studying Electrostatic Discharge Hazards of Propellants, Pyrotechnics and Explosives, 24th DOD Explosives Safety Seminar, St Louis, 28-30 August 1990.
- [3] R. KENT and R. RAT, Static Electricity Phenomena in the Manufacture and Handling of Solid Propellants, Journal of Electrostatics, 17 (1985), 299-312.

Ermittlung der Grenzkonzentration der Explosionsfähigkeit
von TNT im Gemisch mit Erdreich
Determination of the Explosive Limiting Concentration
of TNT in soil

E. Backof, H.G. Farr, B. Schieferdecker, F. Volk

Fraunhofer-Institut für Chemische Technologie (ICT)
Joseph-von-Fraunhofer-Straße, D-76327 Pfinztal 1 (Berghausen)
Bundesrepublik Deutschland

Kurzfassung

Im Rahmen der thermischen Entsorgung von kampfstoff- und explosivstoffhaltigem Erdreich in einem Verbrennungsofen wird ein Prüftest zur Bestimmung der Explosionsfähigkeit von Sand/TNT-Mischungen in Abhängigkeit von den Korngrößen und vom Wassergehalt der Ausgangsprodukte eingesetzt.

Als Prüftest wurde der Stahlrohrtest TNO 50/70 der "Recommendations on the Transport of Dangerous Goods - Tests and Criteria, Second Edition, United Nations, New York, 1990", modifiziert.

Der Test wird beschrieben, und über Versuchsergebnisse wird berichtet.

ZIELSETZUNG

Das Bundesministerium der Finanzen (BMF) der BRD hat die Planung und den Bau einer zentralen Verbrennungsanlage zur Entsorgung explosivstoff- und kampfstoffkontaminierter Böden in Auftrag gegeben. Im Rahmen des Planungsauftrags führte das Fraunhofer-Institut für Chemische Technologie Realisierbarkeitsuntersuchungen über das Aufbereitungsverfahren und die thermische Entsorgung explosivstoff/kampfstoffkontaminierter Böden durch. Die Verbrennungsanlage wird bei der Wehrwissenschaftlichen Dienststelle der Bundeswehr (WWD Bw) in Munster errichtet.

1 SICHERHEITSTECHNISCHE BETRACHTUNGEN

1.1 Sicherheitstechnik und Umweltverträglichkeit

Für das thermische Verfahren zur Entsorgung von sprengstoffhaltigen Kampfstoffen sind sicherheits- und umweltrelevante Betrachtungen von entscheidender Bedeutung. Die Konzeption des Entsorgungsverfahrens muß die Gewähr bieten, daß einerseits die Anlage selbst vor unkontrollierten explosionsartigen Umsetzungen des Explosivstoffanteils, andererseits die Umwelt vor Austritt von Kampfstoffen geschützt wird. Der Schutz der Anlage vor unkontrollierten Verpuffungen kann durch Begrenzung des Sprengstoffes im Ofen auf eine Menge erreicht werden, die bei plötzlicher Umsetzung die kurzzeitige, dynamische Belastbarkeit des Ofenraums nicht übersteigt.

1.2 Explosionsfähigkeit

Zur Ermittlung der Grenzkonzentration von TNT im Aufgabegut haben wir die Explosionsfähigkeit von TNT/Sandgemischen bestimmt. Es ist zu unterscheiden zwischen Explosionsgefährlichkeit und Explosionsfähigkeit eines Stoffes oder Stoffgemisches.

Explosionsfähige Stoffe sind feste, flüssige oder gasförmige Stoffe oder Stoffgemische, die sich in Form einer Explosion umsetzen können. Die Auslösung der Umsetzung (Zündung) kann durch thermische Einwirkung (z.B. Funken, Flamme, glühende Stoffe), durch mechanische Beanspruchung (z.B. Schlag, Reibung) oder durch Detonationsstoß (z.B. Sprengzünder, Detonator, Verstärkerladung) erfolgen; Einschränkungen hinsichtlich der Zündarten bestehen nicht.

Explosionsgefährliche Stoffe sind durch das Sprengstoffgesetz definiert /1/. Die Prüfmethode zur Klassifizierung von explosionsgefährlichen Stoffen wurden von der Bundesanstalt für Materialprüfung (BAM) ausgearbeitet.

Explosionsgefährliche Stoffe können für sich allein oder im Gemisch mit Inertstoffen auftreten. Die Explosionsgefährlichkeit einer Komponente sagt allerdings noch nichts über die Explosionsfähigkeit eines Stoffgemisches aus, da selbst explosionsgefährliche Stoffe (Stoffgemische) bestimmter Mischungsverhältnisse außerhalb ihrer Explosionsgrenzen auch ungefährlich, d.h. nicht explosionsfähig sein können.

Für feste Sprengstoffe im Gemisch mit Inertstoffen kommen neben dem Mischungsverhältnis weitere Faktoren hinzu, die Randbedingungen für die Explosionsfähigkeit darstellen, z.B.:

- Schichtdicke bzw. kritischer Durchmesser, abhängig von den Stoßwelleneigenschaften der Umgebung der Proben (Einschluß, Entrapment, Verdämmung etc.). Die Umgebung der Probe beeinflusst die einleitende Zündstoßwelle durch unterschiedliches Transmissions- bzw. Reflektionsverhalten nach Maßgabe der jeweiligen Impedanz (Dichte x Schallgeschwindigkeit) der Umgebung. Dabei tritt Verstärkung oder Dämpfung der Zündstoßwelle im Medium auf.

- Unstetigkeiten im Explosivstoff(gemisch), verursacht durch Lufteinschlüsse (Poren, Risse, Lunker) oder Fremdstoffe, die an der chemischen Umsetzung unbeteiligt sind (Inertstoffe höherer oder niederer Dichte, versch. Korngrößen etc.), bewirken eine Dämpfung der Zündstoßenergie. Die eingeleitete Detonation läuft dann nach mehr oder weniger großen Laufstrecken aus.

Im Grunde ist die dem Explosivstoff jeweils unter bestimmten Randbedingungen zugeführte Zündenergie (Triggerschwelle) die eigentliche Klassifizierungsgröße, die von hochempfindlich bis unempfindlich reicht. Eine mittlere Empfindlichkeit hat z.B. eine Probe mit der Schlagenergie von 2 mkg = 19,6 Joule (Fallhammer 2 kg, Fallhöhe 1 m). Als unempfindlich werden Substanzen mit einer Schlagenergie über 60 Joule eingestuft.

Der UN-Sachverständigenausschuß "Beförderung gefährlicher Güter" hat in seinen Empfehlungen über die Beförderung gefährlicher Güter /2/ Prüfmethoden und Kriterien für die Klassifizierung von explosiven Stoffen vorgeschlagen.

Zu den einfachsten Prüfmethoden gehört die Schlag- und Reibempfindlichkeit. Die beinahe winzige Probengröße (10-40 mg) macht sie jedoch ungeeignet für Tests an kompakten Körpern oder Schüttungen grober Körnung.

Zu den härtesten Randbedingungen gehört der starkwandige Einschluß im TNO-Rohr (Innen- ϕ 50 mm, Wandstärke 10 mm) mit 200 g-Booster-Anfeuerung (Booster: Hexogen/Wachs, hochempfindlich, Zündung mit Sprengkapsel) /2/. Ein Stoffgemisch, das unter diesen "extrem harten" Randbedingungen nicht mehr "durchdetoniert" (über eine Strecke von 1100 mm), ist unter anderen "weicheren" Randbedingungen als ungefährlich, d.h. als nicht explosionsfähig zu bezeichnen.

Aus diesem Grunde wurde der Stahlrohrtest TNO 50/70 als Kriterium für "go" oder "not go" gewählt. Alle sonstigen in praxi vorkommenden Einschlußarten (Erde, Schmelze im Reaktor) sind weniger hart bzw. liefern geringere Triggerschwellenenergien. Stoffmischungen, die bei diesem "Sensitivity-Test" von der eingeleiteten Detonation in langsame Deflagration übergehen oder auf Nullumsatz innerhalb der Teststrecke auslaufen (erlöschen), sind zwar immer noch explosionsgefährlich, aber nicht mehr als explosionsfähig einzustufen.

Eine gleichzeitige Messung der Explosionsgeschwindigkeit im Testrohr erlaubt - neben dem Splitterbild - weitere Aussagen.

Explosivstoff/Erde-Gemische wurden schon früher untersucht /3/, da sie als Sediment in Abwasserteichen von Sprengstoff-Fabriken vorkommen.

So wurde z.B. festgestellt, daß TNT/Sediment-Gemische durchaus schlagempfindlicher sein können als reines TNT:

TNT, 100%:	6 mkp = 59 Joule,
TNT/Humus-Sediment 40/60:	0,42 mkp = 4 Joule.

Erst Gemische hoher Verdünnung ($\text{TNT/Humus} \leq 5/95$, trocken) erreichen wieder die "Unempfindlichkeit" von TNT, 100% /3/ (Tab. 1). Explosivstoffe höherer Empfindlichkeit wie TNT/RDX 60/40 oder TNT/RDX 40/60 erreichen die Unempfindlichkeit des reinen TNT erst wieder bei einer Verdünnung auf 2,5% Sprengstoff im Humus-Sediment.

Die höchste Schlagempfindlichkeit von $0,25 \text{ mkp} = 2,5 \text{ J}$ erreichen die Mischungen des TNT/RDX 40/60-Sprengstoffs mit 50% Humus-Sedimentanteil im Gemisch sowie des TNT/RDX 60/40-Sprengstoffs mit 60% Humus-Sedimentanteil im Gemisch /3/ (Tab. 2).

Die mit steigendem Sedimentgehalt zunächst ebenfalls steigende Schlagempfindlichkeit und die erst bei weiter steigendem Sedimentgehalt wieder abnehmende Schlagempfindlichkeit von TNT/Sedi-

mentgemischen, die schließlich erst bei einer Verdünnung von 2,5% TNT den Wert des reinen TNT wieder erreicht, hat das BICT wohl veranlaßt, eine Grenzkonzentration von 2,5 TNT vorzuschlagen /4/.

Für **feuchte Gemische** brisanter Explosivstoffe (HE) mit Humus-Sediment (40% Sprengstoff im Gemisch) - das Gemisch der höchsten Schlagempfindlichkeit - wurde eine Unempfindlichkeit gegen Schlag bei Wassergehalten von 10-25% ermittelt /3/.

Eine Fortpflanzung der Detonation unter Einschlußbedingungen wurde jedoch für Sprengstoffgehalte $\leq 30\%$ - für trockene Gemische mit Sediment und nasse Gemische mit Sediment (Wassergehalt 20%) - nicht mehr beobachtet /3/ (Tab. 3).

Mit 40% Sprengstoffgehalt im Sediment wird sowohl für trockene als auch nasse Mischungen (selbst bei höheren Wassergehalten $>30\%$) eine detonative Reaktion unter Einschluß propagiert (shock sensitivity test) /3/ (Tab. 3).

Es galt nun, in dieser Arbeit den erwähnten harten Test im TNO-Rohr (detonation propagation of shock waves under confinement) zu verfeinern in Bezug auf Korngrößeneinfluß von Explosivstoff und "Sediment" (versch. Erden: Feinsand, Grobsand etc.). Als Modell-sand bot sich Quarzsand an, der in allen Korngrößen erhältlich ist. TNT handelsüblich (1-1,5 mm Korngröße) kann durch Naßmahlen bis zu ca. 10 μm zerkleinert werden.

2 VERSUCHE IM TNO-ROHR

2.1 Stahlrohrtest TNO 50/70

2.1.1 Beurteilungskriterien

Für die Beurteilung der Explosionsfähigkeit von TNT/Erdreich wurde die Zerlegung des TNO-Rohres in Splitter und die Weiterleitung des detonativen Umsatzes durch das Reaktionsgemisch untersucht (Bild 1).

Das Stoffgemisch ist dann detoniert, wenn das TNO-Rohr über die ganze Länge vollständig in Splitter zerlegt ist. Wird keine vollständige Zerlegung des Rohres in Splitter festgestellt, ist dennoch auf eine Detonation zu schließen, wenn

- die Reaktion über die ganze Länge der Meßsonde verlaufen ist,
- die Weiterleitungsgeschwindigkeit im hinteren Teil des Rohres konstant ist und
- die konstante Reaktionsgeschwindigkeit größer als die Schallgeschwindigkeit des Stoffgemisches ist.

Es wurden daher das Splitterbild fotografiert, die Detonations- bzw. Reaktionsgeschwindigkeit und die Reaktionsstrecke im TNO-Rohr bestimmt.

2.1.2 Ausgangsmaterial

Für die Versuche im TNO-Rohr wurde der Explosivstoff TNT NST 26, Güteklasse 80.6 gemäß TL 1376 801 von der BOFORS EXPLOSIVES AG, Schweden, eingesetzt:

Für Grobmischungen wurde das Ausgangsmaterial mit einer mittleren Korngröße von 1,5 mm ohne Nachbehandlung verwendet.

Für Mischungen mit feinem TNT wurde das Ausgangsmaterial in einer Naßmühle auf eine mittlere Korngröße von 0,015 mm gemahlen und im Gefriertrockner getrocknet.

Für Mischungen mit kompakten TNT-Körpern wurden zylindrische TNT-Preßlinge aus Original-TNT NST 26 hergestellt ($\phi = 30$ mm; $h = 32$ mm; $\rho = 1,5$ g/cm³; $G = 34$ g). Die P 30-Preßlinge wurden anschließend mit einer axialen Bohrung $\phi = 3$ mm versehen.

Zur Untersuchung des Korngrößeneinflusses von Bodenmaterial auf die Detonationsfähigkeit der Mischungen wurden mehrfach gewaschener, getrockneter und gesiebter Kies und Sand der FRIEDRICH QUARZSANDWERKE, Karlsruhe, verwendet:

Sandqualität	Korngröße in mm
S 60 T	4,00 bis 6,00
K 30	2,00 bis 4,00
K 15	0,80 bis 1,50
K 6	0,30 bis 0,60
W 6	0,00 bis 0,20

Die Siebanalyse des Quarzmehls W 6 ergab eine mittlere Korngröße von 0,030 mm.

Wasserfeuchte TNT/Erdreichsimulate hoher Feuchtigkeit wurden mit Ton, Quarzmehl und gemahlenem TNT angesetzt. Als Ton wurde Bentonit (Calcigel) der SÜD-CHEMIE AG verwendet. Bentonit hat in grubeuchte Zustand einen auffallend hohen Wassergehalt von durchschnittlich 35 bis 40%. Wasser wird an das wegen seiner Lamellenstruktur besonders quellfähige Mineral Montmorillonit, das im Bentonit enthalten ist, angelagert.

Der Siebrückstand von Calcigel trocken beträgt bei einer Maschenweite von 0,063 mm maximal 25%.

2.1.3 Probenvorbereitung

Die trockenen Mischungen wurden unter Sicherheitsvorkehrungen in einem Zwangsmischer (Pflugscharmischer) hergestellt. Für die Herstellung feuchter Mischungen wurden den trocken vorgemischten Proben im Pflugscharmischer die entsprechenden Wassermengen zugegeben und eingearbeitet.

Die Rohre wurden portionsweise unter ständigen leichten Hammerschlägen gegen die Rohrwand gefüllt. Diese Arbeit mußte zur Schonung der Geschwindigkeitssonde mit großer Vorsicht ausgeführt werden. Die Sonde ist nämlich axial durch den Boden des Rohres eingeführt und am freien Ende mit einer Öse arretiert.

Von jeder Mischung wurde die Stampfdichte nach DIN 51 916 bestimmt, um die berechnete Dichte des Materials im TNO-Rohr mit der Stampfdichte vergleichen und die Qualität der Befüllung kontrollieren zu können. Es zeigte sich, daß die Materialdichten im Rohr überwiegend gleich oder höher als die Stampfdichten nach DIN waren.

Erdreichsimulat-Mischungen aus Bentonit und Quarzmehl wurden im Pflugscharmischer zunächst trocken vorgemischt und anschließend mit dem gemahlenden TNT versetzt. Bei Wassergehalten oberhalb 20% ergaben sich leicht bewegliche Schlämme, die sich luftfrei in das TNO-Rohr einfüllen und verdichten ließen. Bei Wassergehalten unterhalb von 20% wurden je nach Wasser/Bentonit-Verhältnis pulverige bis bröckelige Massen erhalten, die sich nicht luftfrei verdichten ließen. Um handhabbare Mischungen mit Wassergehalten von 5 bis 35% herstellen zu können, wurden den Erdreichsimulat-Basismischungen unterschiedliche Mengen an Quarzmehl zugegeben.

Bei Mischungen mit größeren TNT-Stücken wurden die Preßkörper auf die axial im TNO-Rohr angeordnete Geschwindigkeits-Meßsonde aufgefädelt. Zwischen den TNT-Preßlingen wurden zwecks Einhaltung der vorgegebenen Distanzen abgewogene Sandmengen eingefüllt. Nach je-

der Sandzugabe wurde durch leichte Hammerschläge gegen das Rohr für gleichmäßige Verdichtung der Mischung gesorgt. Für die Mischungen mit TNT-Preßlingen wurde Feinsand K 6 (Korngröße: 0,30 bis 0,60 mm) verwendet.

2.1.4 Versuchsdurchführung

Unmittelbar vor der Zündung wurde die Verstärkerladung (200 g Hexogen) angebracht; die Zündung wurde durch eine Sprengkapsel in Normalausführung (Nr. 8) initiiert.

Das TNO-Rohr wurde in einem liegenden Schutzrohr ($\phi = 1000$ mm, $l = 2000$ mm, $d = 40$ mm) konzentrisch aufgehängt. Das Meßsignal wurde mit einem Speicheroszillographen aufgezeichnet.

Nach jedem Versuch wurden die Splitter, in die das TNO-Rohr zerlegt worden war, eingesammelt und zur Dokumentation fotografiert. Die Bilder 2 und 3 zeigen Splitterbilder und Meßsignale von je einer detonierten und nicht detonierten TNT/Sand-Mischung.

2.2 Versuchsauswertung

Die Versuchsergebnisse sind in den Diagrammen Bild 4 - Bild 9 zusammengestellt. Die darin angegebenen TNT-Konzentrationen beziehen sich auf die Trockenmassen der TNT/Sand/(Wasser)-Gemische.

Die grünen (hellen) Felder kennzeichnen die Versuche, bei denen die Detonation nicht weitergeleitet wurde, und die roten (dunklen) die mit Weiterleitung der Detonation. Die zweifarbigten Felder markieren die Versuchsergebnisse, bei denen die Detonation des Stoffgemischs zwar angesprungen, aber nach einer kurzen Reaktionsstrecke wieder erloschen war. Versuche im Übergangsbereich fielen durch starke Rußentwicklung, d.h. durch unvollständigen Umsatz auf.

In die Diagramme sind folgende Größen eingetragen:

- Detonationsgeschwindigkeiten D in m/s
- Reaktionsgeschwindigkeit v in m/s
- Reaktionsstrecke RS in cm.

Angaben von Reaktionsstrecken RS in den grünen (hellen) Feldern der Diagramme bedeuten, daß zwar Stoffumsatz stattgefunden hat, die Reaktion sich aber nicht zur Detonation entwickeln konnte. Die Meßstrecke zur Bestimmung der Detonations- bzw. der Reaktionsgeschwindigkeit und der Ausbreitungslänge betrug 111 cm. Die in den Diagrammen angegebenen Reaktionsstrecken können, z.B. durch Quotientenbildung, mit der Gesamtmeßstrecke verglichen werden.

2.3 Bewertung der Ergebnisse

Der Stahlrohrtest TNO 50/70 liefert Daten, mit denen die Explosionsfähigkeit von Stoffen und Stoffgemischen bestimmt werden kann. Die Detonationsgeschwindigkeit und das Splitterbild aus dem zerlegten Rohr geben Hinweise auf die Brisanz und die Arbeitsfähigkeit des Gemisches. Länge der Reaktionsstrecke und die Reaktionsgeschwindigkeit lassen auf die Reaktivität des Stoffes bzw. Stoffgemisches schließen.

Mit dem Stahlrohrtest TNO 50/70 wurden die Grenzkonzentrationen Detonation/Nichtdetonation von TNT/Sand-Gemischen in Abhängigkeit von der Sandkörnung und dem Wassergehalt mit TNT grob (mittlere Korngröße 1,5 mm) und TNT fein (mittlere Korngröße 0,015 mm) bestimmt.

Die Untersuchung wasserfeuchter Mischungen mit gemahlenem TNT wurde nur mit Feinsand von 0,3-0,6 mm und Quarzmehl <0,2 mm (mittlere Korngröße 0,030 mm) durchgeführt, weil größere Körnungen im Flotationsverfahren nicht zu erwarten sind. Wasserfeuchte Mischungen mit einem Wassergehalt über 20% konnten nicht herge-

stellt werden, weil Wasserausscheidungen festgestellt wurden. Da in den Flotaten und in den anfallenden Schlämmen der Aufbereitungsanlage Wasssergehalte bis 40% zu erwarten sind, wurde die Testreihe ergänzt durch Versuche, bei denen Mischungen aus feinkörnigem Bentonit, Quarzmehl und gemahlenem TNT sukzessive mit Wasser (bis max. 35%) versetzt und dem TNO-Rohr-Test unterworfen wurden.

Aus den ermittelten Daten wurden die Grenzkonzentrationen für die Explosionsfähigkeit der untersuchten Stoffgemische abgeschätzt und der maximal zulässige TNT-Gehalt für die Aufgabe in den Reaktor vorläufig festgesetzt. Weitere Untersuchungen sind im Rahmen des Versuchsbetriebs der Anlage vorgesehen.

Die ermittelten TNT-Grenzkonzentrationen gelten nur für die im Stahlrohr TNO 50/70 getesteten Mischungen, sofern sie - fein verteilt - kontinuierlich in den Reaktor aufgegeben werden. Während der thermischen Behandlung im Reaktor dürfen sich durch Ausschmelzen von TNT keine neuen Explosivstoffansammlungen bzw. explosionsfähige Mischungen bilden.

Die Versuchsergebnisse der Stahlrohrtests sind in den Diagrammen Bild 4 bis Bild 9 zusammengefaßt.

Bei den **trockenen Mischungen mit TNT** verläuft die Grenze der Explosionsfähigkeit quer über das Diagramm (Bild 4 und 5).

Trockene Mischungen mit TNT fein (0,015 mm) sind bei einigen Kornfraktionen etwas reaktiver als die mit TNT grob. Die Grenze der Explosionsfähigkeit ist nach links zu niedrigeren TNT-Konzentrationen verschoben (Bild 5).

Die Versuchsergebnisse der TNO-Tests mit **wasserfeuchten Mischungen aus TNT + Erdreichsimulaten** hoher Feuchtigkeit sind in Bild 9 dargestellt.

Bei Wassergehalten von mehr als 20% waren die Mischungen von breiartiger Konsistenz, ohne jedoch Wasser auszuscheiden. Wassergehalte von weniger als 20% ergaben pulverförmige bis bröckelige Massen, die sich nur mit Mühe im TNO-Rohr verdichten ließen (siehe Abschnitt 2.1.3 Probenvorbereitung). Die Dichten der lockeren Mischungen betrugen 1,2 bis 1,3 kg/dm³, die der breiförmigen 1,5 bis 1,6 kg/dm³. Die Dichteunterschiede waren auf den unvermeidlichen Luftgehalt der lockeren Mischungen zurückzuführen.

Lockere Mischungen wurden erwartungsgemäß mit zunehmendem Wassergehalt unwirksamer in Bezug auf Detonationsübertragung. Stieg der Wassergehalt bis zum Bereich breiartiger Konsistenz, nahm die Detonationsfähigkeit sprunghaft zu. Bei weiterer Erhöhung des Wassergehaltes wurden die Mischungen wieder unempfindlicher.

Die Zunahme der Detonationsfähigkeit oberhalb der Konsistenzänderung, hervorgehoben durch die dick ausgezogene Trennungslinie im Bild 9, war auf die sprunghafte Änderung der Dichte zurückzuführen.

TNT/Erdreichsimulate 20/80 sind in allen Mischungsverhältnissen mit Wasser auch oberhalb des Dichtesprungs, nicht detonationsfähig.

Bei **TNT/Erdreichsimulaten 30/70** macht sich der Dichtesprung auf die Explosionsfähigkeit der Mischungen bemerkbar: Die Mischung mit 25% Wasser ist detonationsfähig. Bei stärkerer Verdünnung mit Wasser und bei Wassergehalten unter 25% sind die Mischungen nicht mehr explosionsfähig.

TNT/Erdreichsimulate 40/60 sind nur noch in dem schmalen Band zwischen 10 und 20% Wasser nicht mehr detonationsfähig. Trockene Mischungen mit 5% und nasse Mischungen oberhalb 25% Wasser sind dagegen sehr reaktiv (Bild 9).

Aus Sandmischungen mit TNT-Preßlingen wurden drei Ladungen mit TNT-Gehalten von 10%, 15% und 19% hergestellt und im TNO-Rohr angesprengt. Die Ladungen enthielten pro Rohr 10, 15 und 19 zylindrische TNT-Preßlinge mit einem Stückgewicht von 34 g. Die Preßlinge waren in Abständen von 71, 42 und 28 mm angeordnet. Sämtliche Ladungen detonierten nicht vollständig durch.

Dies bedeutet, daß bei Transport und Handhabung (auch bei mechanischer Beanspruchung?) von Erdreich, das 15% TNT in Stücken mit einem Durchmesser von 30 mm enthält, eine initiierte Detonation nicht weitergeleitet wird. Die Ergebnisse der Modellversuche bedürfen allerdings der Bestätigung durch Versuche im TNO-Rohr mit Gemischen aus Erde + TNT.

Die Annahme, daß beim Eintauchen von TNT-Stücken in eine Schmelze mit einer Temperatur von 1600°C trotz des Temperaturschocks keine explosionsartige Zersetzung des Sprengstoffs erfolgt, muß noch untersucht werden.

3 FOLGERUNGEN AUS DEN TESTS IM TNO-ROHR

Für trockene Gemische aus TNT und Boden (Erde, Sand, Lehm) lassen sich unter extremen Einschlußbedingungen Abhängigkeiten der Explosionsfähigkeit erkennen, die je nach Partikelgrößen, sowohl des TNT als auch des Inertstoffs Sand, einer größeren Schwankungsbreite unterliegen: 15-40% TNT im Gemisch mit Sand, trocken (Bild 4 und 5).

Bei nassen TNT-Sandgemischen bis zu 20% Wassergehalt ist die Explosionsfähigkeit weniger von der Korngröße des Sandes abhängig. Die Schwankungsbreite beträgt 30-40% TNT; sie ist wesentlich schmaler als bei trockenen Mischungen (Bild 6-8).

Da Feuchtegehalte über 20%, besonders in grobem Sand, wegen der Wasserausscheidung nicht ohne weiteres verifiziert werden konnten, mußte die Versuchsreihe mit feuchtem Sand modifiziert fortgesetzt werden: Es wurden feinkörnige Bentonit/Quarzmehl-Mischungen (TNT/Erdreichsimulate) hergestellt, die sich durch ein hohes Wasserrückhaltevermögen auszeichnen.

Die Erweiterung der Naßversuche brachte ein überraschendes Ergebnis: Nicht explosionsfähige trockene TNT/Erdreich-Grundmischungen können bei schrittweiser "Verdünnung" mit Wasser unversehens explosionsfähig werden und oberhalb eines bestimmten Wasseranteils die Explosionsfähigkeit wieder verlieren (Bild 9: TNT/Erdreich 30/70 nach Zusatz von 5, 25 und 35% Wasser). Andererseits können explosionsfähige Grundmischungen ab einem bestimmten Wasseranteil ihre Explosionsfähigkeit verlieren und bei noch höherem Wassergehalt wieder explosionsfähig werden (Bild 6: TNT/Erdreich 40/60).

Die Ursache dieses Phänomens ist im Dichtesprung der TNT/Erdreich-Mischungen ab einer bestimmten Wasserkonzentration zu suchen: Unterhalb des Dichtesprungs sind die Mischungen locker mit unvermeidlichen Lufteinschlüssen, oberhalb des Dichtesprungs werden die Mischungen plastisch und enthalten keine Lufteinschlüsse mehr.

Nach Bild 9 sind TNT/Erdreich-Mischungen jedoch bis zu 20% TNT in der Grundmischung (trocken) nicht explosionsfähig, unabhängig vom Wassergehalt.

Eine weitere Überraschung lieferten die Versuche mit TNT-Körpern, die in Sand eingebettet waren. Die Abstände der TNT-Körper wurden schrittweise bis auf 28 mm verkürzt. Trotz des geringen Ladungsabstandes und der starken Verstärkungsladungen von 200 g Hexogen wurde die Detonation nicht weitergeleitet.

Generell ist zu den TNO-Rohr-Tests folgendes anzumerken:

Die erzielten Ergebnisse - der Abhängigkeit vom TNT-Gehalt, von der Korngröße und der Feuchtigkeit - zeigen zwar eindeutig Tendenzen auf, wie in den Bildern 4-9 dargestellt. Es ist aber zu bedenken, daß bei allen Arten der Sensitivity-Tests (auch für das TNO-Rohr) gewisse Imponderabilien mitspielen, die eine Unsicherheit beinhalten. Mit anderen Worten: es muß zur Erhärtung der Sensitivity-Grenzen ein Minimum an Statistik betrieben werden (wie z.B. zur Bestimmung der Schlag- und Reibempfindlichkeit bekannt ist).

Bei der Schlagempfindlichkeitsbestimmung nach BAM darf von 6 Wiederholungen eines Meßwertes keiner eine Reaktion zeigen. In den USA werden 30 Wiederholungen vorgezogen, von denen max. 50% Reaktion zeigen dürfen. Ein solcher Aufwand ist jedoch enorm arbeits- und kostenintensiv und hier nicht realisierbar.

Die von uns meßtechnisch verfeinerte, gleichzeitige Messung der Reaktionsgeschwindigkeit im TNO-Rohr mittels Widerstandssonde läßt Geschwindigkeitsmessungen bis unter 1000 m/s zu. Beispielsweise ist die Schallgeschwindigkeit $V_S = \text{ca } 200 \text{ m/s}$ eines Gemisches noch meßbar.

Daneben steht das Splitterbild des Versuchsrohres nach einer Reaktion als Kriterium für die "Arbeitsfähigkeit" eines Explosivstoffs bzw. Explosivstoff/Erde-Gemischs zur Verfügung. Wie sich in den bisherigen Versuchen gezeigt hat, kann Splitterbildung auch bei erheblich "verdünntem TNT" auftreten, das rein kalorisch betrachtet (Kalorimeterbombe) keine hohe Arbeitsfähigkeit liefern kann. Die guten Übertragungseigenschaften (Impedanz) des inertten "Füllstoffs Sand" erhöhen aber die Wirkung des Explosivstoffs auf die, die Reaktionsstrecke umhüllende Umgebung. Die Wirkung des reinen Explosivstoffs (Wirkungsgrad der Arbeitsfähigkeit) wird "in fester Umgebung" gegenüber gasförmiger Umgebung (Schüttung

mit Luftporen in Atmosphäre) stark erhöht. (Vgl. die schiebende Wirkung im Bohrloch mit Sprengstoff niedriger Detonationsgeschwindigkeit).

4 LITERATUR

- /1/ Apel/Keusgen: Sprengstoffgesetz, Band 1, Sprengstoffrechtliche Vorschriften, 37. Lieferung, August 1994.
Carl Heymanns Verlag KG, Köln

- /2/ Recommandations on the Transport of Dangerous Goods. Tests and Criteria. Second Edition, United Nations, New York, 1990. ISBN 92-1-139033-8, ISSN 1014-7160

- /3/ Kirshenbaum, M. S. : Reactivity of Explosive/Sediment Mixtures. AD-A 118012, Techn. Report ARLCD-TR-82007/1982

- /4/ Zierath, J: Gutachten zu explosivstoffbezogenen Sicherheitsfragen im Zusammenhang mit dem Neubau einer Sonderabfallverbrennungsanlage in Munster. Bundesinstitut für Chemisch-Technische Untersuchungen beim Bundesamt für Wehrtechnik und Beschaffung (BICT). Ber.-Nr.: 100/8112/89

5 ANHANG (Tabellen/Bilder)

Table 1: Impact sensitivity as a function of TNT-humus sediment concentration (after /3/, table 3)
(ERL-Type 12 Tool, 2¹/₂-kg drop weight)

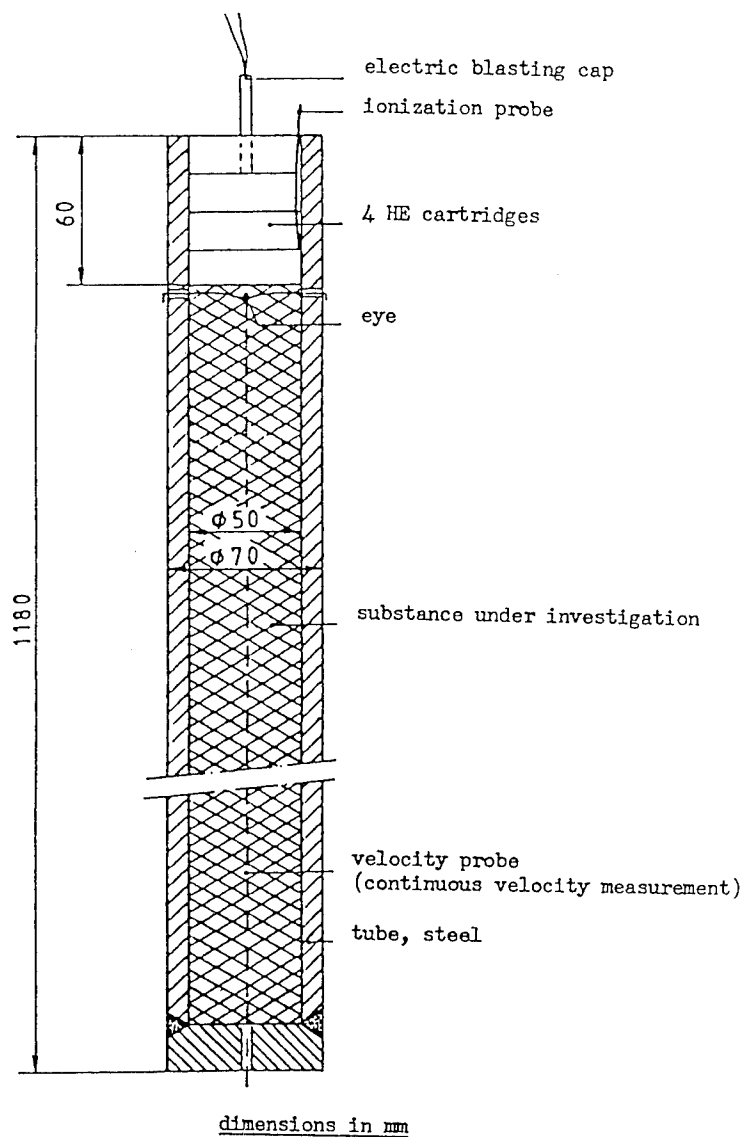
TNT concentration (% by wt)	Height (cm)	Fired (%)	Type reaction
100	240	55	Explosion
100	240	70	Burn
80	92	50	Explosion
80	23	50	Burn
40	78	50	Explosion
40	17	50	Burn
20	34	50	Burn
10	131	50	Burn
5	240	52	Burn

Table 2: Impact sensitivity as a function of 60/40 TNT/RDX-humus sediment concentration (after /3/, table 4)
(ERL-Type 12 Tool, 2¹/₂-kg drop weight)

Explosive concentration (% by wt)	Height (cm)	Fired (%)
100	84	50
40	<10	50
10	77	50
5	111	50
2.5	240	0

Table 3: Shock test results as a function of explosive-humus sediment concentration (after /3/, table 7)

Explosive	Concentration (% by wt)	Results
=====		
TNT	60	Propagation - hole in steel witness plate
	50	Propagation - hole in steel witness plate
	40	Propagation - steel witness plate split in two
	30	No propagation
RDX	40	Propagation - hole in steel witness plate
	30	No propagation
	20	No propagation
60/40 TNT/RDX	40	Propagation - hole in steel witness plate
	30	No propagation
	25	No propagation
40/60 TNT/RDX	40	Propagation - hole in steel witness plate
	30	No propagation
	25	No propagation
60/40 TNT/RDX (20% by wt H ₂ O)	50	Propagation - steel witness plate split into three pieces
	40	Propagation - steel witness plate split into two pieces
	30	No propagation



FOR SOLIDS

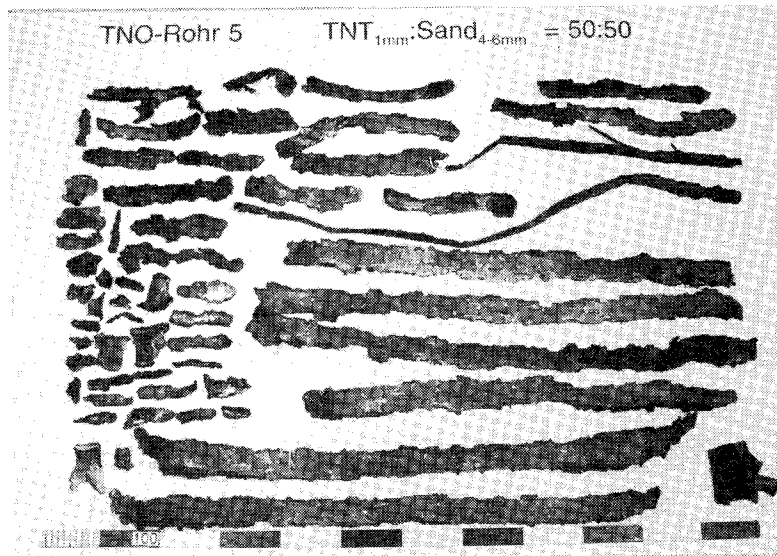
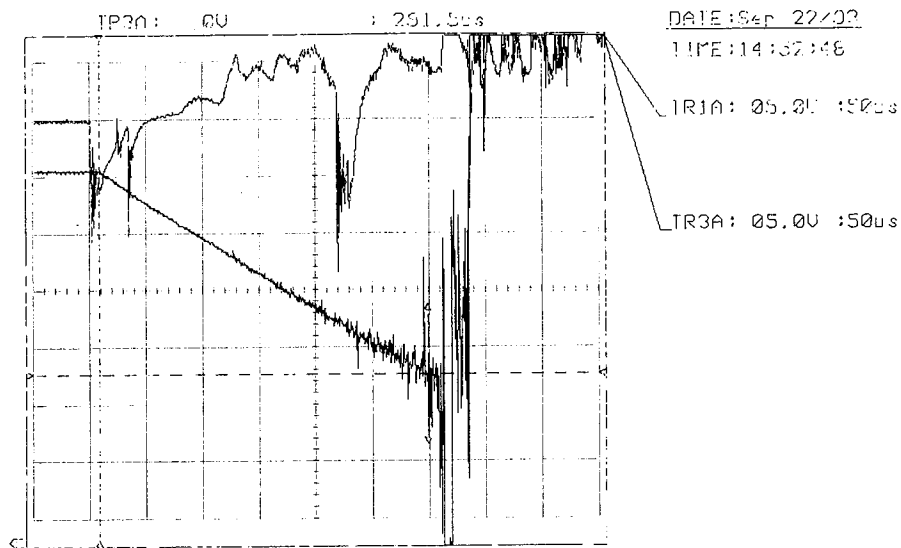


Bild 2: TNO-Rohr 5
 TNT_{grob}:Sand_{grob} = 50:50
 D = 3800 m/s

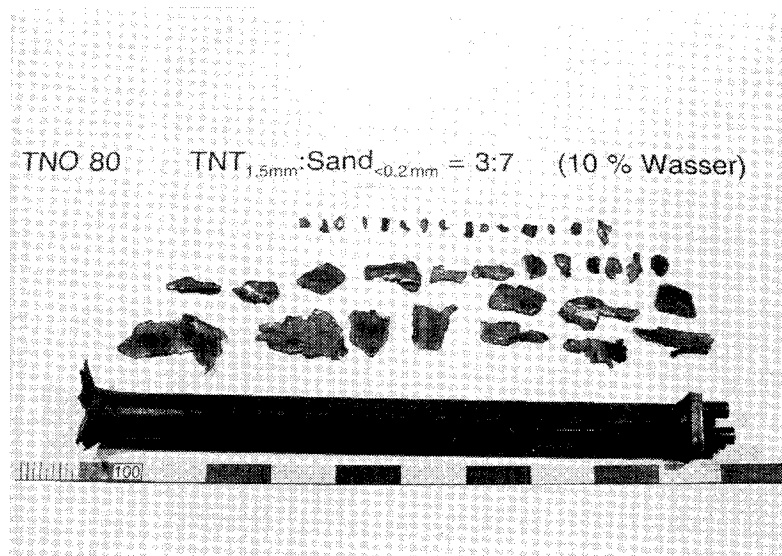
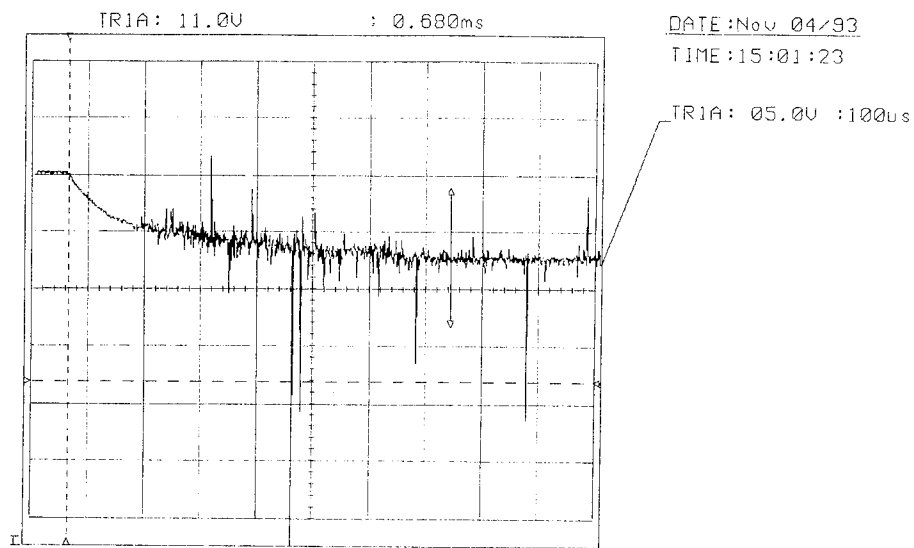


Bild 3: TNO-Rohr 80
 TNT_{grob}: Sand_{fein} = 3:7 (10% Wasser)
 TNT/Sand/Wasser = 27/63/10
 v = 275 m/s RS = 44 cm

TNT% Sand	0	5	10	15	20	25	30	35	40	45	50
S 60 T 4,0 - 6,0 mm				23 D=690	14 D=1130		12 D=3250		6 D=3360		4 D=3600
					38 D						5 D=3830
K 30 2,0 - 4,0 mm				34 D=650	19 D=1200						
					33 D=2100						
K 15 0,8 - 1,5 mm						54 D=1600	31 D=1600				
						26 D	55 D				
K 6 0,3 - 0,6 mm						57 RS=63	52 RS=50	53 RS=71			
						30 RS=26	94 RS=44				
W 6 <0,2 mm							18 D=3200	56 D=3900	10 D=3760		7 D
									11 D		

o = Fußstück abgerissen
c = Schweißnaht des Fußstücks
angegrissen

D = Detonationsgeschwindigkeit in m/s
v = Reaktionsgeschwindigkeit in m/s
RS = Reaktionsstrecke in cm

Erläuterungen

Bild 4: TNT grob/trocken

TNT% Sand	0	5	10	15	20	25	30	35	40	45	50
S 60 T 4,0 - 6,0 mm											
K 30 2,0 - 4,0 mm		RS-29 117	116 D=690	112 D=1840	109 D=4260	87	109 D=4260				
K 15 0,8 - 1,5 mm		RS-29 118	RS-36 119	73	42 D=3200	37 D=4370					
K 6 0,3 - 0,6 mm			RS-29 72	61 D=4000	27	32 D=3400	46 D=4800				
W 6 <0,2 mm			RS-27 75		50	62	84 D=4020	91 D=3240			

o = Fußstück abgerissen
c = Schweißnaht des Fußstücks
angerissen

Erläuterungen D = Detonationsgeschwindigkeit in m/s
v = Reaktionsgeschwindigkeit in m/s
RS = Reaktionsstrecke in cm

Bild 5: TNT_{fein}/trocken

TNT% Sand	0	5	10	15	20	25	30	35	40	45	50
S 60 T 4,0 - 6,0 mm											
K 30 2,0 - 4,0 mm											
K 15 0,8 - 1,5 mm											
K 6 0,3 - 0,6 mm											
W 6 <0,2 mm											

Bild 6: TNT_{grob}/10% Wasser

Erläuterungen D = Detonationsgeschwindigkeit in m/s o = Fußstück abgerissen
 v = Reaktionsgeschwindigkeit in m/s c = Schweißnaht des Fußstücks
 RS = Reaktionsstrecke in cm angerissen

TNT fein 0,015 mm / 10% H₂O

TNT% Sand	0	5	10	15	20	25	30	35	40	45	50
S 60 T 4,0 - 6,0 mm											
K 30 2,0 - 4,0 mm											
K 15 0,8 - 1,5 mm											
K 6 0,3 - 0,6 mm						RS=61 v=340	76 RS=60	65 D=3750	100		
W 6 <0,2 mm						RS=50	69 RS=46	99			
							0 RS=60	57 RS=55	77 D=4370		
						RS=60 (5% H ₂ O)	29	83 RS=40 v=370	64 RS=70		

Bild 7: TNT fein/10% Wasser

Erläuterungen: D = Detonationsgeschwindigkeit in m/s
v = Reaktionsgeschwindigkeit in m/s
RS = Reaktionsstrecke in cm

o = Fußstück abgerissen
c = Schweißnaht des Fußstücks
angerissen

TNT% Sand	0	5	10	15	20	25	30	35	40	45	50
S 60 T 4,0 - 6,0 mm											
K 30 2,0 - 4,0 mm											
K 15 0,8 - 1,5 mm											
K 6 0,3 - 0,6 mm											
W 6 <0,2 mm							RS 45 v = 10 m/s	RS 45 v = 10 m/s	82 D = 5000 o = Fußstück abgerissen c = Schweißnaht des Fußstücks angerissen		

Erläuterungen: D = Detonationsgeschwindigkeit in m/s
 v = Reaktionsgeschwindigkeit in m/s
 RS = Reaktionsstrecke in cm

Bild 8: TNT_{fein}/20% Wasser

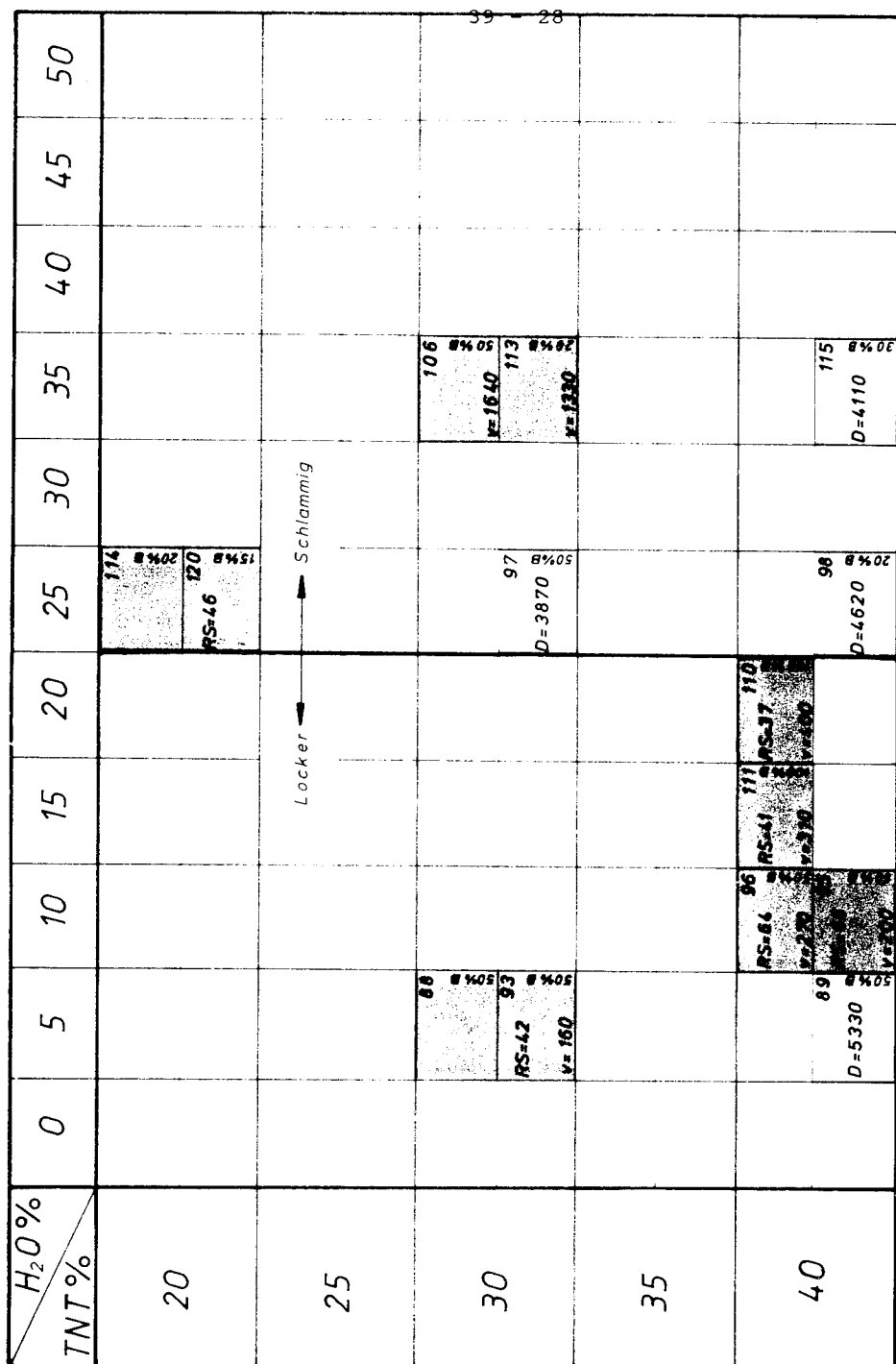


Bild 9: TNT_{fein}/Erdreichsimulat, 5 - 35% Wasser

**PHENOMENOLOGICAL ASPECTS OF BLAST OUTPUT FROM THE
HETEROGENEOUS DETONATION OF ENERGETIC COMPOSITIONS**

Allen J. Tulis, James L. Austing, and Remon Dihu
IIT Research Institute
Chicago, Illinois 60616, U.S.A.

Divyakant L. Patel and David C. Heberlein
U.S. Army CECOM
Fort Belvoir, Virginia 22060, U.S.A.

ABSTRACT

The detonability of heterogeneous fuel/oxidizer compositions, in particular various carbohydrates such as starch and lactose, to which small amounts of flaked aluminum powder are added, has been previously demonstrated; these were tested as condensed compositions in one-dimensional confined steel tubes and as dispersions in air in a detonation tube. In this paper the characterization and associated phenomenological aspects of these compositions, when dispersed in air in an unconfined manner, is presented. These compositions were explosively dispersed in air upon an instrumented blast-pad arena so that both detonation pressures and impulses within the dispersed dust clouds could be monitored using piezoelectric pressure transducers located flush with the ground in the blast pad. In support of the earlier one-dimensional detonation tube experiments, results demonstrated various phenomena such as multiple fronts and extended reaction zones in the detonations that were achieved. In most cases variable amounts of high explosive powder (RDX) were added to the compositions in order to assure the propagation of detonation in the grossly inhomogeneous concentrations that are obtained in explosively dispersed powders; also ammonium perchlorate oxidizer was added to balance the stoichiometry. Based on analytical computations using the TIGER Code for Chapman-Jouguet characteristics, the composition selected for this initial evaluation was 60(70/30)/40 by weight [lactose/aluminum]/ammonium perchlorate, at average calculated concentrations ranging from 0.77 to 5.5 kg/m³, and sensitized with RDX powder amounts from zero to 50 weight percent. Observed average detonation velocities were in the range of 1400 to 1700 m/s, compared to Chapman-Jouguet velocities of about 1950 m/s. Observed detonation pressures often displayed multiple peaks with extended plateaus, indicating multiple detonation fronts with extended reaction zones. In numerous instances multiple blast-pressure responses were also observed at various distances outside of the detonating linear-type clouds at locations orthogonal to the clouds.

INTRODUCTION

Carbohydrates such as starch and lactose, whose molecules are composed of carbon, hydrogen, and oxygen (CHO molecules), become extremely energetic when mixed with a highly calorific metallic powder such as aluminum (Al) and subsequently combusted in air (Tulis et al., 1994a). Both starch powders (Kauffman et al., 1984) and Al powders (Tulis and Selman, 1982) have demonstrated their potential of detonating when suitably dispersed in air. The criteria, however, are very severe, especially in regard to particle size; but also in regard to stoichiometry with oxygen of the air and homogeneity of the dispersed concentrations. In the absence of oxygen from air, although CHO/Al mixtures have sufficient exothermic energy release to detonate (Tulis et al., 1989), they are very deficient in oxidizer. Hence, by providing additional oxidizer such as ammonium perchlorate (AP) to these mixtures, detonation of these compositions can become independent of air. This has been demonstrated by achieving detonation of various compositions of CHO/Al/AP *without RDX* dispersed in nitrogen gas in a detonation tube investigation (Tulis et al., 1995a).

Analytical TIGER Code Chapman-Jouguet (CJ) computations have been conducted on the CHO/Al/AP compositions in regard to the composition and concentration parameters (Dihu et al., 1995). These computations provided a basis for selecting the specific compositions that have been investigated in the detonation tube experiments by Tulis et al., as well as in the explosively dispersed unconfined CHO/Al/AP powders in air experiments, which are the subject of this paper. However, in both the detonation tube studies and in these unconfined experiments, various amounts of RDX powder sensitizer were added to most of these CHO/Al/AP compositions in order to sustain stable, self-propagating detonations. This was an experimental expedient, since analytical computations have demonstrated that the addition of RDX does not appreciably influence the detonation characteristics (Tulis et al., 1994b). The work presented in this paper involves an experimental investigation of the CHO/Al/AP composition 6C(70/30)/40 by weight [lactose/aluminum]/ammonium perchlorate, at average calculated concentrations ranging from 0.77 to 5.5 kg/m³, sensitized with RDX powder amounts from zero to 50 weight percent. The RDX component, especially at the upper limit of 50 percent, would probably detonate even if the other 50 percent were an inert powder.

Detonation of the CHO/Al/AP components, especially without any RDX present, is a truly heterogeneous mechanism involving several separate, but

inter-dependent, sequential and/or concurrent mechanisms of decomposition, oxidation, reduction, and perhaps other complex parameters dependent upon system chemical and physical factors such as particle size and distribution of the various components.

EXPERIMENTAL PROCEDURES

The experimental procedure for achieving a sufficiently long linear-type dispersion (cloud) was to use five individual canisters placed in a line along the north section of the blast pad. Figure 1 illustrates this experimental set-up as observed from above the blast pad. Four of the five individual canisters contained nominally 4.5 kg of the test composition. The first canister contained an identical amount of an 89:11 weight ratio of RDX:Al powder; this initiation scheme has been found to be useful for achieving detonation initiation of experimental cloud compositions by providing an initiation wave of comparable detonation velocity to that anticipated in the experimental clouds.

The spacing of the canisters was an experimental parameter determined by the requirements of a specific experiment. For example, as depicted in Figure 2, the times for initiation of the dispersal explosive charge were varied in canisters 2 through 5; thus, when the detonation initiation charge, frequently termed the second event, was detonated at the far end of the first canister, the four test canisters had dispersed their powders each for a different duration, hence forming a different size cloud with an attendant concentration variation. The spacing of the canisters was selected to provide a moderate overlap between adjacent clouds to allow detonation coupling of these cylindrical clouds.

It should be noted that, based on past investigations of similar experimental methodology, the detonation does not progress through the five cloud dispersions in a truly linear fashion. Rather, it follows a somewhat circuitous path around each canister due to the fact that the concentration is variant in a gradient about each canister, with the greatest concentration somewhere between the canister and the furthest extremity of the dispersed cloud. For this reason the measured (piezoelectric pressure transducers) and observed (high speed cine records) data yield detonation velocities that are probably somewhat lower than the actual "circuitous" routing would yield. This circuitous detonation routing has been previously observed in high speed cine records taken from an overhead perspective.

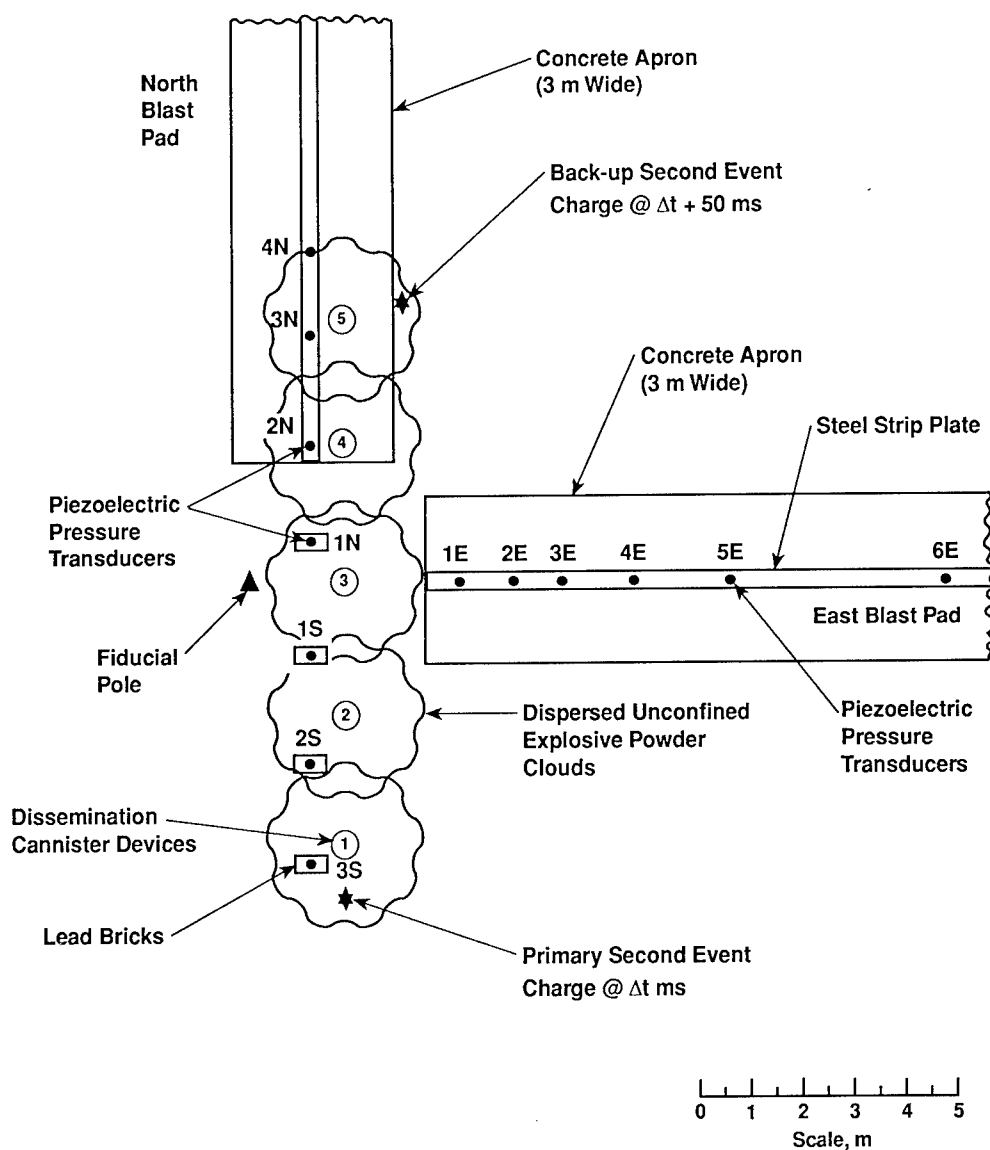
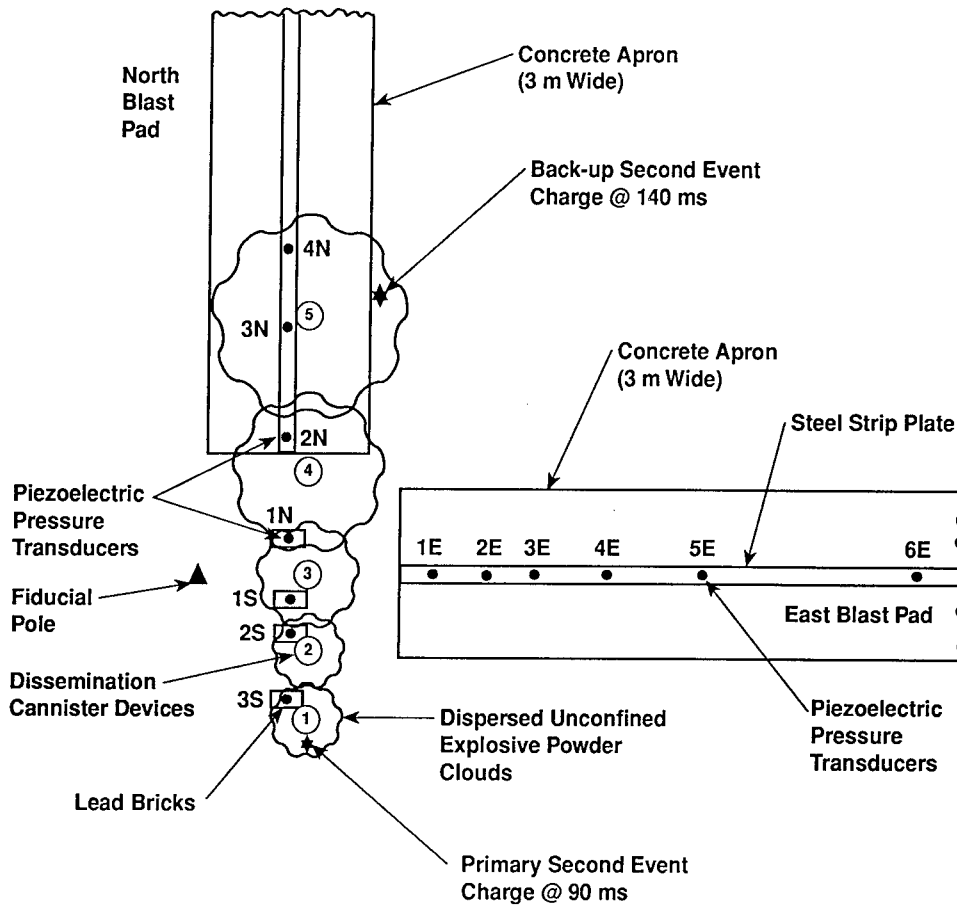


Figure 1. Experimental Arrangement for the Majority of the Linear Cloud Detonation Tests, as viewed from Above.

Test No. IDE - 11



Cannister No.	Powder Type	Nominal Disp. Density, kg/m ³
1	RDX/Al	5.5
2	Lac/Al/AP/RDX	5.5
3	Lac/Al/AP/RDX	2.7
4	Lac/Al/AP/RDX	1.3
5	Lac/Al/AP/RDX	0.78

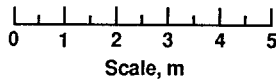


Figure 2. Experimental Arrangement for the Linear Cloud Detonation Tests in which an Incrementally-Decreasing Dispersed Density was Utilized, as viewed from Above.

EXPERIMENTAL EFFORT

Each experiment provided four individual test canisters which allowed the imposition of up to four variables per experiment. In this effort, these variables were: (1) the amounts of RDX powder sensitizer and (2) the concentrations. Obviously, other variables could also be imposed, such as variation of CHO/Al/AP composition, particle size of individual components, etc. The investigation of these additional variables, and others such as another type of oxidizer in lieu of the AP (for instance ammonium nitrate or ammonium dinitramide), are presently planned and are expected to be conducted in the future.

It needs to be emphasized that, contrary to the detonation tube experiments wherein concentration is fairly well controlled, in these explosively dispersed clouds there exists much greater variability of concentrations. Explosive dissemination modeling of explosive dispersions in air as were conducted here (Gidaspow et al., 1988) showed very non-uniform powder distributions, with the powder emanating as a concentrated slug of material initially, with the bulk of the dispersed powder near the periphery of the dispersed cloud. This accounts for the previous reference to the concentration gradients within the cloud.

Several initial experiments were conducted in which the dispersed concentrations were similar; i.e., all were dispersed at the same time and initiated at the same time. Therefore, the concentration profiles (and associated cloud sizes) were quite similar, as is illustrated in Figure 1. The parameter in these experiments was the amount of RDX powder sensitizer that was added. This variation was 50, 40, 30, and 20 weight percent in an initial experiment, and then 20, 15, 10, and 5 percent, and 15, 10, 5, and 0 percent, respectively, in subsequent experiments. Of course, the dissemination time was also critical, so that this test parameter needed to be tested so that variable concentrations would be achieved with the same composition. In this case an alternative methodology was used, in which the dissemination times were variable. In this case the four canisters contained identical compositions and RDX sensitizer but yielded different concentrations (and associated cloud sizes) as is illustrated in Figure 2. Finally, for conclusively ascertaining true stability of detonation propagation, experiments were conducted in which all four canisters were identical, both in composition and in dispersed concentration. In this manner the stabilities and more precise detonation

velocities could be established, as linear-type clouds of the experimental compositions more than 10 m long were achieved, so that incremental detonation velocities were obtained at multiple stations along the full lengths of the linear-type clouds.

Some typical results, as well as phenomenological aspects, of the experiments conducted will now be presented. Figure 3 illustrates the *observed linear* progression of detonation along the north leg of the blast pad, as determined from the arrival times of the detonation pressure at the flush-mounted piezoelectric pressure transducers in the blast pad. In this experiment the basic composition was used with 30 weight percent RDX powder sensitizer additive: 70(60(70/30)/40)/30, or 29:13:28:30 of CHO:Al:AP:RDX, respectively, by weight ratio. All four dispersed clouds were of identical composition and the same concentration, which was estimated to be approximately 1.12 kg/m^3 on average, based on the total mass of the powder distributed homogeneously within the cloud volume as grossly calculated from the high speed cine records. It is seen that the detonation velocity, which started low at the dispersed RDX/Al detonation initiation, increased to a fairly uniform velocity within the major portion of the linear-type cloud, with some fall-off near the end of the cloud (as concentration was dissipated). This "slow start" could be a manifestation of induction time for initiation of the test composition at the interface of the RDX/Al detonation, a "coupling" phenomenon we have previously observed in many initiations of detonation in dispersed powders, including RDX. Even with this slow start and the end fall-off of velocity, the average experimental velocity was only about 300 m/s slower than the analytically predicted CJ velocity of 1960 m/s; and this, we might add, is based on ideal detonation of the composition.

Regarding detonation pressures, the results are much more complex in that classical pressure responses were generally not obtained; i.e., the phenomena of multiple pressure fronts and extended pressure plateaus were observed. In some instances, the initial peak pressure was substantially lower than a subsequent pressure, lagging the incident pressure by as much as 150 μs , and even more in some very complex waveforms. Figure 4 displays a comparison between two typical detonation pressure waveforms in one experiment observed: (1) within the RDX/Al canister initiating detonation cloud and (2) at a section of the dispersed linear-type cloud where the CHO/Al/AP/RDX dispersion detonated. It is apparent that in (1) a nearly classical-type pressure waveform was achieved whereas in (2) a complex, multiple front and extended reaction zone waveform was manifest.

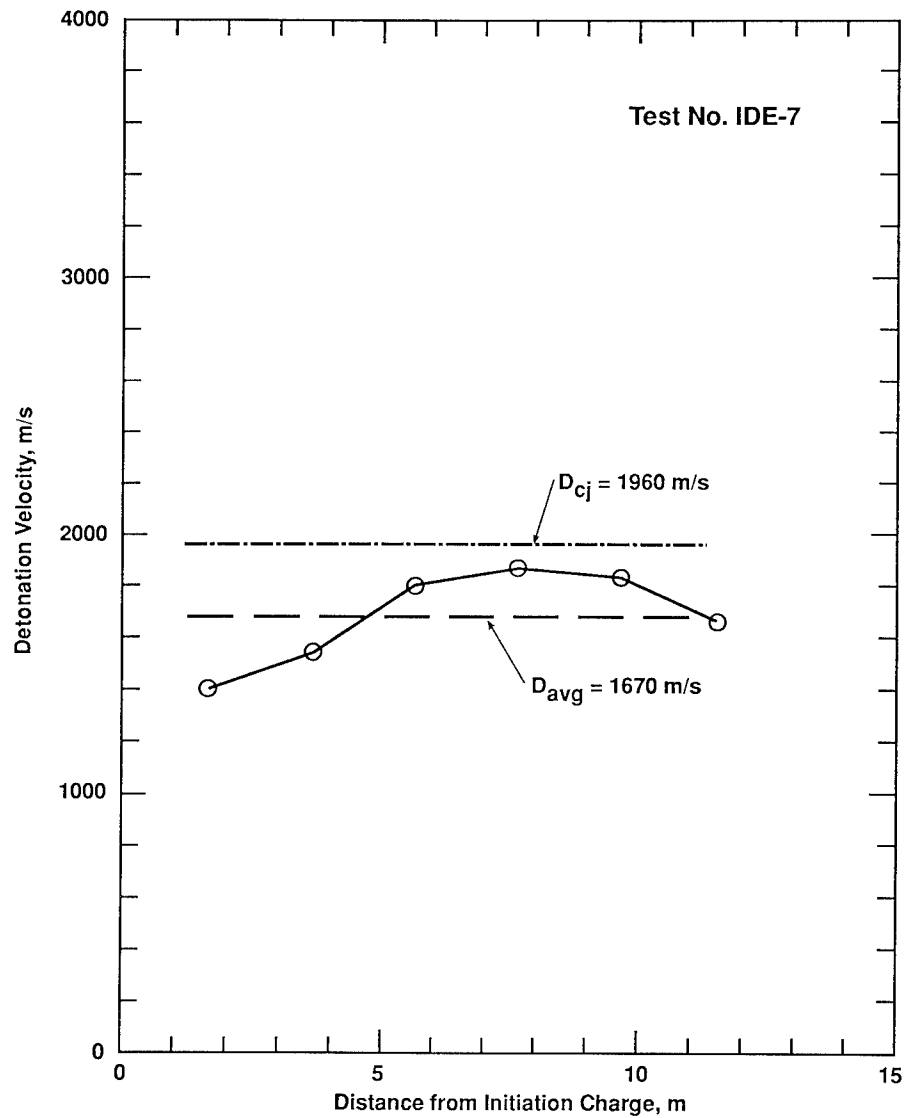


Figure 3. Incremental, Average, and CJ Detonation Velocities for Dispersed Lactose/Aluminum/Ammonium Perchlorate at an Average Concentration of 1.12 kg/m^3 .

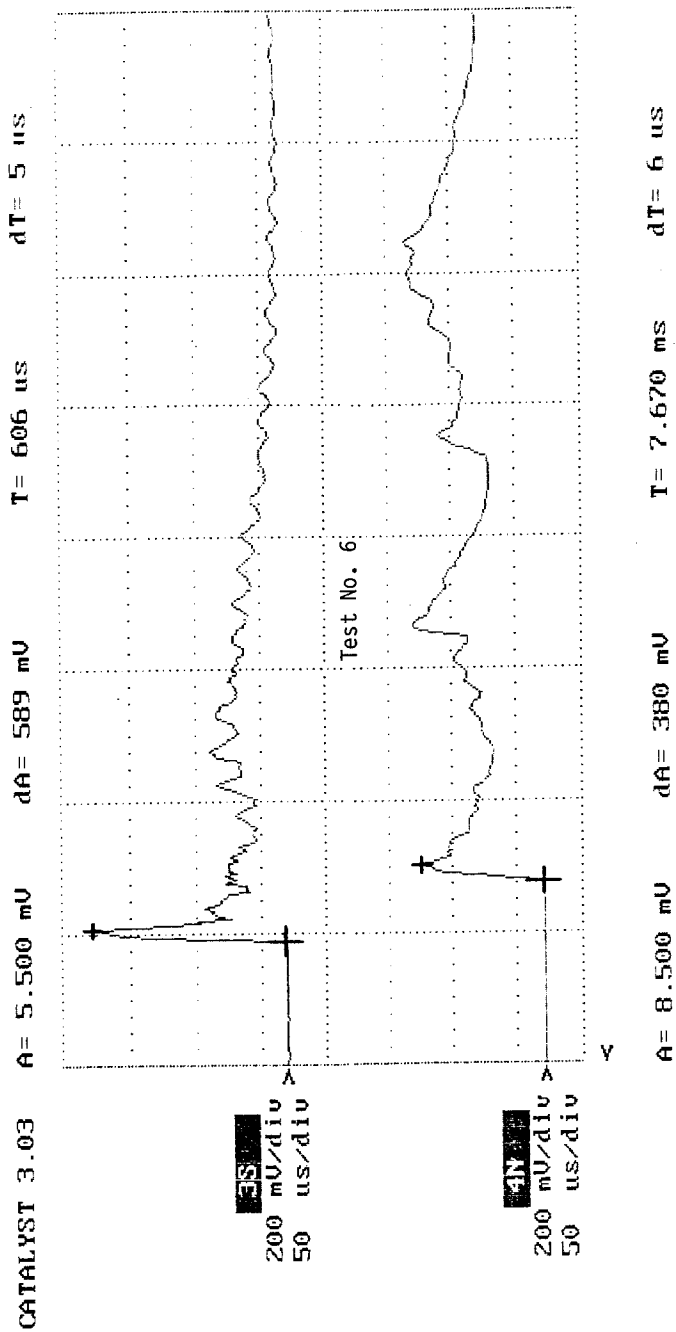


Figure 4. Pressure-Time Signatures for two High-Pressure Transducers.

Upper Trace: "Classical" Detonation Pressure Signature.

Lower Trace: CHO/Al/AP/RDX "Complex Heterogeneous Detonation" Signature.

Figure 5 illustrates four more such typical detonation pressure waveforms observed in a number of other experiments, in the CHO/Al/AP/RDX linear-type cloud detonation regions.

Many of the much more complex waveforms that were observed are not illustrated here since they are not at present confirmed not to be anomalous instrumental behavior. It is, nevertheless, believed that they represent true manifestations of the complex nature of these heterogeneous detonations and perhaps indicate waveform coalescence and other physical manifestations of the detonation process. Since the detonation probably travels in a circuitous route about the individual clouds, it can readily coalesce at some points, resulting in overdriven observed pressures, and possibly inducing spikes in the measured detonation velocities as well. It must be emphasized, however, that these phenomenological aspects have been unequivocally observed in detonation tube experiments of CHO/Al/AP compositions detonated in nitrogen and that these results of unconfined CHO/Al/AP/RDX cloud detonations were anticipated and support the detonation tube experiments.

This investigation is continuing, both in detonation tube experiments and in these unconfined experiments, with the intent to better resolve the nature of these heterogeneous detonations of highly promising insensitive explosive compositions for use in dispersed, as well as condensed, applications.

CONCLUSIONS

The detonation of insensitive energetic compositions based on CHO/Al/AP mixtures, sensitized with RDX in most cases, is readily achieved when these powders are dispersed in air in an unconfined manner. In accordance with analytical TIGER Code CJ computations, the detonation characteristics appear to be directly related to composition concentrations independent of the presence of oxygen from ambient air. In related detonation tube studies (Tulis et al., 1995b) involving the detonation of various CHO/Al/AP compositions in nitrogen *in the absence of RDX sensitizer*, heterogeneous mechanisms involving the individual CHO, Al, and AP components of the compositions were determined to be involved. Results yielded multiple detonation fronts as well as extended reaction zones. When RDX sensitization was included, the detonation mechanisms were especially complex; primary detonation fronts involved the RDX, but the presence of flaked Al had a tendency to reduce the induction time between the shock and the flame (reaction) fronts. The major critical requirement for achieving detonation was

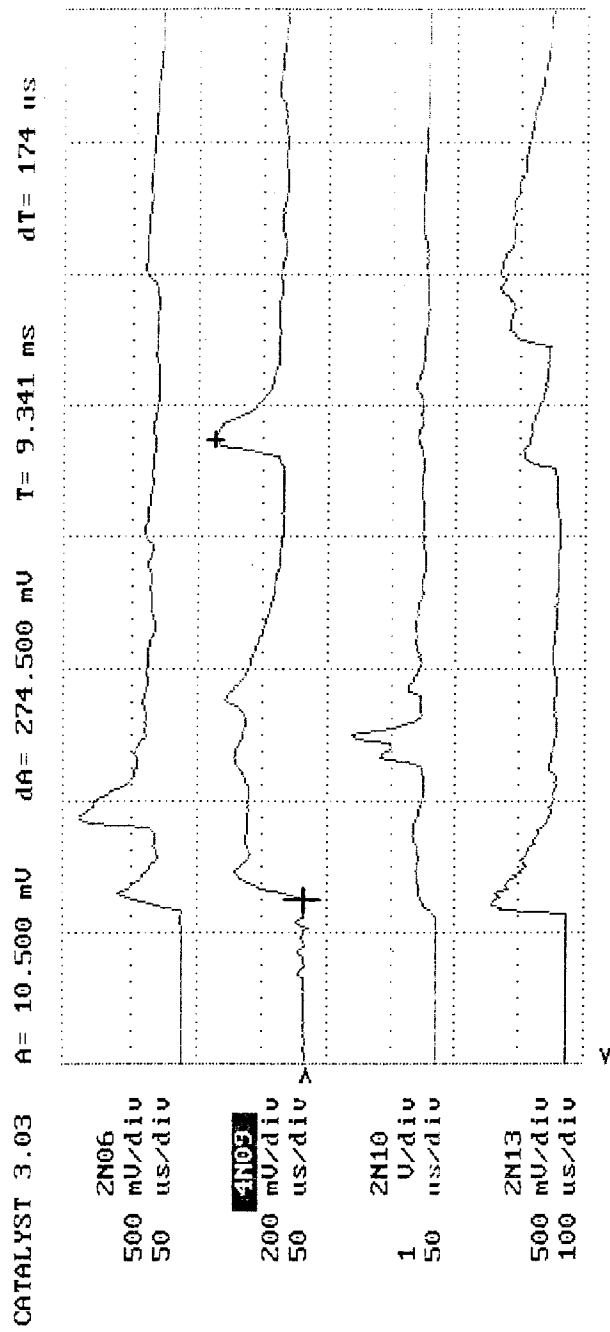


Figure 5. Selected Detonation Pressure-Time Signatures from a number of other CHO/AL/AP/RDX Experiments.

determined to be sufficiently small particle sizes of the components, especially of the Al, which plays a major role in the energetics of the compositions.

As the detonation tube experiments confirmed, and these unconfined experiments support, the proviso that if the stoichiometry of the compositions is adequate; e.g., by the inclusion of an oxidizer such as AP, the detonation of CHO/Al/AP compositions becomes independent of oxygen from air. The unconfined experiments described in this paper were conducted at average concentrations as high as 5.5 kg/m^3 , which is more than an order of magnitude higher than the stoichiometric concentration in air if combustion in air were the criterion, yet near-CJ detonations were achieved.

Another aspect of these unconfined CHO/Al/AP detonations is the probability that chemical reactions *continue* after the primary heterogeneous detonation itself; in particular as the hot, reactive and often insufficiently oxidized products expand into the surrounding air, allowing further exothermic energy releases which may enhance the overall detonation blast outputs, probably manifested as extended blast pressures and/or secondary blast waves. As was noted in the results of these unconfined detonations, blast pressures measured orthogonal to the linear-type clouds often resulted in such multiple blast pressure waves.

Finally, although not an issue in this paper, these insensitive CHO/Al/AP explosives provide explosive energies comparable to those of typical secondary high explosives such as TNT and RDX, whether condensed or dispersed in air.

REFERENCES

- Dihu, R., Tulis, A.J., Sumida, W.K., Patel, D.L., and Heberlein, D.C., "Analytical TIGER Code Assessment of Detonation Characteristics", *6th Congress International de Pyrotechnie du Groupe de Travail de Pyrotechnie (EUROPYRO 95)*, June 5-9, 1995; in press.
- Gidaspow, D., Syamlal, M., Austing, J.L., Tulis, A.J., Burhmaster, E., and Heberlein, D.C., "The Explosive Dissemination of Particulate Pyrotechnic and Explosive Powders", *Thirteenth International Pyrotechnics Seminar*, pg. 347, 1988.
- Kauffman, C.W., Wolanski, P., Arisoy, A., Adams, P.R., Maker, B.N., and Nicholls, J.A., "Dust, Hybrid, and Dusty Detonations", *AIAA*, 94: pg. 221, 1984.
- Tulis, A.J. and Selman, J.R., "Detonation Tube Studies of Aluminum Particles Dispersed in Air", *Nineteenth Symposium (International) on Combustion*, The Combustion Institute, Pittsburgh, pg.655, 1982.

- Tulis A.J., Austing, J.L., Sumida W.K., Baker, D.E., and Hrdina, D.J.,
"Explosive potential of Carbohydrate-Metal Composites", *Ninth Symposium
(International) on Detonation*, OCNR-113291-7, pg. 972, 1989.
- Tulis, A.J., Sumida, W.K., Norikane, K., Heberlein, D.C., Patel, D.L., and
Egghart, H., "Influence and Characterization of Aluminum Powder Additive on
the Detonability of CHO Compounds Dispersed in Air", *Twenty-fifth
International Annual Conference of ICT*, pg. 3-1, 1994a.
- Tulis, A.J., Dihu, R., Sumida, W.K., Patel, D.L., and Heberlein, D.C.,
"Parametric analytical TIGER Code Assessment of Chapman-Jouguet
Characteristics of Starch/Aluminum/Ammonium Perchlorate Dispersions in Air",
Twentieth International Pyrotechnics Seminar, pg. 1081, 1994b.
- Tulis, A.J., Sumida, W.K., Norikane, K., Dihu, R., Patel, D.L., and Heberlein,
D.C., "Characterization of Heterogeneous Detonations of Powders Dispersed in
Nitrogen", *Twentieth International Symposium on Shock Waves*, July 23-28,
1995a.
- Tulis, A.J., Sumida, W.K., Austing, J.L., and Dihu, R., "Insensitive Dispersed
Explosives", IITRI Technical Progress Report Nos. 25-27, Contract No.
DAAK70-93-C-0011, U.S. Army CECOM, January 1 through March 31, 1995.

RECYCLING AND DISPOSAL OF PYROTECHNICS

26 International ICT-Conference, July , 1995, Karlsruhe, FRG

Nico van Ham, Reinier Eerligh

TNO Prins Maurits Laboratory, PO Box 45,
2280 AA RIJSWIJK, Netherlands

Abstract

TNO-PML has investigated some alternative methods for the disposal of munitions, as was published before (ref. 8).

From our investigations it turned out that controlled combustion is the most mature, promising and universally applicable technique. Controlled combustion makes use of a closed furnace system; most promising for the situation in the Netherlands seems the fluidized bed oven (FBO). Additional scrubbing systems (dry chemical / wet) are needed to remove the remaining hazardous products like HCl, SO₂, NO_x.

In this article we describe the succesfully combustion of slurries of explosives and propellants in the FBO, altogether more then 1000 kg.

Special attention was paid for the disposal of pyrotechnics and initiators.

Calculations for a complete disposal unit were made.

41 - 2

1. Problem description.

The disposal of munitions and explosives is in fact the last phase in the life time cycle of these ordnance items. To put them in the right perspective it is necessary to overview the whole cycle:

<i>Procurement- phase</i>	tactical study demands trials comparative bids contract
<i>In service- phase</i>	transportation storage trials exercises usage maintenance modifications like: *other fuze * other warhead *exercise from HE
<i>End of life time- phase</i>	sell reversed assembly recycle disposal

This scheme was discussed in detail in one of our previous publications (ref.8)

2. Pre-treatment

A good separation between the explosive and the metal parts of the munitions is mandatory for a more economic disposal procedure. In this way materials can partly be reused and the controlled combustion will be more efficient.

Reverse assembly or disassembly is the conventional pre-treatment of munitions: it includes the separation of the projectiles from the cartridges, the defuzing of the projectiles and the removal of the explosives from the projectiles. The reverse assembly is applicable to most regular munitions.

Waterjet washout was developed by the Royal Dutch Navy with the assistance of TNO-PML. By means of a high pressure waterjet the explosives can be removed from the munitions. This was demonstrated with 155 mm HE projectiles. Advantages above the classical melt-out technique are: Less time needed to remove the explosive from one projectile, applicable to all explosives including plastic bonded explosives, less energy compared to melt-out, less pollution because the water is reused, less TNT vapour in the buildings so better for the health of the personell, better removal of explosives; in the melt-out process a TNT film remains on the inside of the projectiles, with the waterjet all TNT including the inner coating of the projectile is removed.

Water jet cutting is a powerful variance on the conventional metal cutting tools. By means of a high pressure water jet and some abrasive, munitions can be cut with high speed. Nevertheless it is a relatively safe method as the water cools the metal and possible ignition of the explosive is suppressed.

This technique can be utilised on those munitions that cannot be opened by reversed assembly (non regular munitions) , e.g. munitions in bad condition or munitions that originate from World War II and have been buried in the ground for a long time.

The system consists of a water jet cutting system. The water with possible explosives is collected. After filtering, the water can be used again. This technique has been tested in practise by the Royal Netherlands Navy. TNO has also tested the water jet cutting technique with all kinds of munitions such as 40 mm HE, 105 mm HE, 155 mm HE, 81 mm mortar with pyrotechnic flare composition (Mg!). The deliberate cutting action on very sensitive parts like the fuze and the igniter did not result in a reaction, so the safety of the system is proven in practise.

Shredding looks favourable for pyrotechnic items. Trials are performed by the Royal Netherlands Navy with a variety of pyrotechnic munitions. The shredding was performed under water. The metal parts are separated from the explosives. Most explosives can be transformed into slurry as a fuel for the fluidised bed incinerator. Some explosives has to be neutralised beforehand.

41 - 4

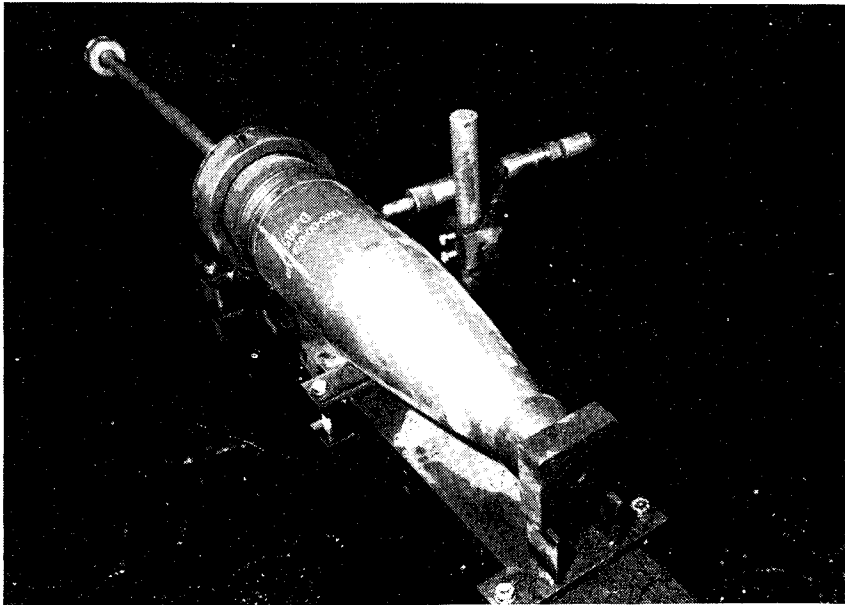


Fig. 1. Test set-up for water jet cutting of 155 mm projectile

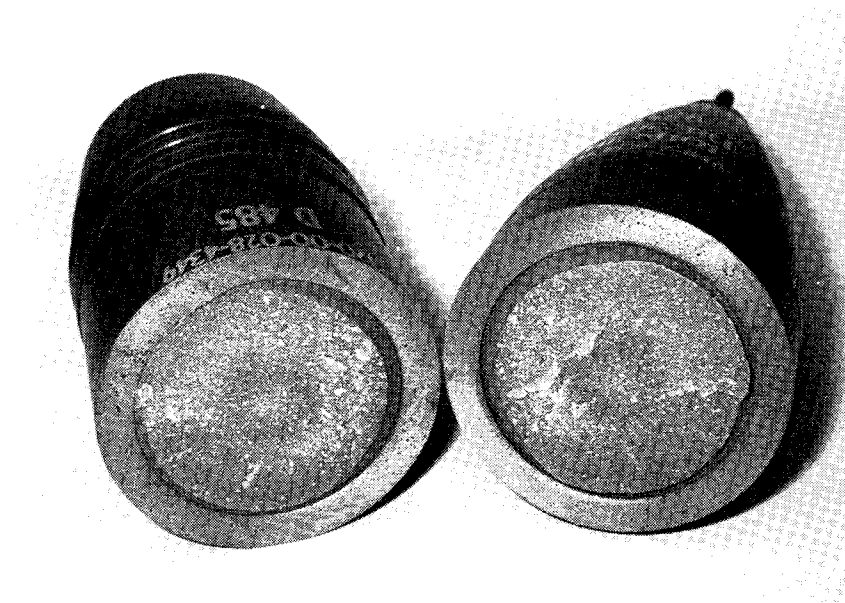


Fig. 2. View of 155 mm projectile after water jet cutting

3. Slurry preparation

The explosive fillings (including pyrotechnics) which were washed out of the munitions by means of a water jet technique are milled under water and transformed into a stable slurry. The propellants are collected, mixed with water and made into a separate slurry.

The initial explosives from the igniter and the fuze are also separated from the metal parts with the water jet and collected for chemical pretreatment.

Both the explosive slurry and the propellant slurry are transformed into the desired concentration of approx. 50 % explosive . This is realised by filtering techniques. In order to prevent the settling of explosives from the slurry, additives are used to create a stable slurry. Also a pumping system is used to prevent the explosive particles to settle.

The explosion safety of the installation is realised by the design of the pipes necessary to transport the slurry from the storage to the fluidized bed furnace. The diameter of these pipes must be under the critical diameter for a stable detonation of the slurry in the pipes.

Special attention is paid to the injection of the slurry into the fluidized bed furnace. The special safety features of the injector prevent a pressure build up and a possible backwards reaction in the slurry feed.

The storage of the explosive slurry is very safe as this slurry can only detonate if initiated by the powerful shock of a donor explosive.

4. Fluidized bed combustion

The principle of controlled combustion is the well defined feed of fuel (slurry from explosives and water) to a closed combustion chamber or furnace. In this way the explosives can react portion by portion with excess air to give the cleanest combustion products. This in connection with the further treatment of the reaction products to satisfy the threshold values defined in the National Environmental Protection Laws.

On the other hand the amount of explosives present in the furnace at the same time can be regulated, to avoid pressures that can damage the furnace.

A fluidized bed furnace (see fig. 3) makes use of a flow of hot air through a packed bed of silicon oxide particles (sand).

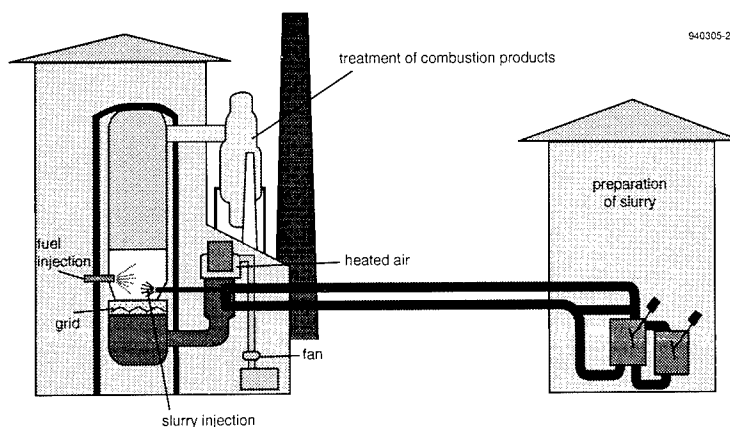


Fig. 3. Principle of fluidized bed furnace.

Due to the action of the air flow the particles of the bed are floating and act like a liquid. The fuel is injected in this floating bed in the form of fine droplets ensuring optimum mixing with air. It is of importance that the particles have reacted completely before they reach the top of the bed. A CO-monitor is installed to control the proper functioning.

Catalyst like NiO can be added to the bed to facilitate the decomposition of explosives and to suppress the NO_x formation. The bed material can be varied in composition between pure silicon oxide and aluminium oxide. That is the reason that fluid bed incineration has often been used for the clean combustion of waste. Due to the efficient and complete combustion, the use of a separate afterburner can in most cases be omitted. During the experiments described in this article, the FBO was filled with river sand.

An advantage of the fluidized bed furnace over a rotary retort is the energy balance: due to the efficient combustion (especially when catalyst are used) and the possibility to use the excess heat from the bed for preheating the air and energy recovery. Another interesting possibility is the large heat capacity of the bed; when this has reached its working temperature (800 °C) there will be no need for extra heating other than generated by the combustion of the explosive in water slurry. Once the process is stopped the bed remain at

high temperature for a long time, even over the weekend. After 16 hours the temperature is still 600 °C so the furnace can be started up easily at low energy cost (thermal fly-wheel). Starting up time of the fluidised bed from ambient temperature to 850 °C will take 2-3 hours.

5. Exhaust cleaning

The solid reaction products (mainly from pyrotechnics) can be collected in a cyclone or a bag house, while the gaseous products are emitted through the exhaust stack.

Explosives can react with oxygen to harmless substances like CO₂ and H₂O for the mayor part. However there will be harmful compounds formed like NO_x, CO, HCl, HF, SO₂, depending on the composition of the explosive. Research on laboratory scale by ICT Germany (Dr Volk, see ref. 6) has revealed some figures for the combustion of the most common explosive materials.

Table 1. Harmful exhaust gases due to the combustion of explosives (w %).

Explosive	NO _x	HCl	SO ₂	H ₂ S
Single Base	10			
Double Base	19			
TNT	0,01			
Rocket Prop.		25		
Black Powder	-	-	0,1	6-8

At TNO-PML we have found in small scale laboratory experiments for TNT 3-7 weight % NO_x and for a Single Base Propellant 2-3 weight %; it is obvious that the reaction is strongly dependent on the conditions in the furnace.

In the Netherlands the gaseous exhaust products should fulfil the limits given in table 2:

Table 2. EC Exhaust Threshold Limits

Component	Threshold value (mg/m ³)
Total solid dust	5
HCl	10
CO	50
SO _x	40
NO _x	70
Heavy metals	1
Cd/Hg	0,05
PCD's (dioxins)	0,1 nanogr. TEQ/m ³

TEQ= Toxicity Equivalence

During pilot scale testing in the Flued Bed Oven (FBO) with slurry feeds between 50 and 300 kg / hour, the NO_x emission varried between 2000 and 3000 ppm. It seems that by carefull tuning of the gas equilibrium the NO_x emission can be reduced considerdably compared to the combustion in the open air. However the application of additional exhaust cleaning will remain necessary.

41 - 8

removal of CO/C_xH_y

This can be realised by correct functioning of the furnace and its afterburner section: The temperature in the afterburner section should be well above 850 °C, the % oxygen should be above 6 vol. %, the residence time of the reaction products in the afterburner should be above 2 seconds.

removal of NO_x

By careful design of the furnace burners and the use of clean fuels such as natural gas, the excess formation of NO_x due to the reaction between N₂ and O₂ can be suppressed. Furthermore, NO_x can be decomposed by the use of catalysts. This is most conveniently realised in the fluidized bed furnace. Other possibilities are the chemical binding of NO_x with NH₃ and the wet scrubbing technique.

removal of HCl, SO_x

HCl can be removed by use of a wet scrubber in combination with a chemical scrubber (Na₂CO₃).

SO_x can be suppressed by the addition of limestone in the bed. This is of importance in the combustion of black powder (fire works).

removal of dioxins

During the combustion processes of explosives, all the necessary conditions are present for the formation of dioxins. Suitable techniques for the removal of dioxins are: injection of active carbon together with CaO, and the use of active carbon filters.

6. Cost estimate for complete design

In table 3 the following calculation was made for the situation in the Netherlands : all prices in Kfl. (ref. 7)

Table 3. Cost estimate for the construction of an explosives incineration plant for 100 kg/hour

element	fluidized bed	rotary retort furnace
furnace	1000	4500
water jet cutting	220	220
shredder for pyrotechnics	100	
control apparatus	300	150
scrubber(wet)	175	175
denox(chem.)	50	50
dioxin filter	50	50
<u>site preparation</u>	<u>1155</u>	<u>1355</u>
total cost	3050	6500

The investment cost of the furnace dominates the total cost; the fixed capacity of the rotary retort exceeds the annual Dutch need many times, whereas the fluidized bed furnace can be tailored to the actual needs.

For the fluidized bed the annual exploitation costs are calculated at 1000 Kfl.

References

- 1 P.C. Kearney et al., Chemosphere 12 (1983) 1583
- 2 J.C. Hoffsommer et al., Report NSWC/WOL-TR-77-146
- 3 W.R. Maby et al., Chemosphere 12 (1983) 3
- 4 D.L. Kaplan et al., Natick TR-81/019
- 5 D.B. Hill, Explosive Safety Seminar 19 (1980) vol II, p. 995
- 6 F.Volk, Chemistry and Physics of Energetic Materials
Kluwer 1990, p. 511
- 7 H.Bartelds, H.M.G. Temmink, TNO-IMET Report 91-453
Haalbaarheidsstudie verbrandingsinstallatie voor het explosieven
opruimingscommando (in Dutch)
- 8 N.H.A. van Ham, H.Bartelds
Environmentally acceptable disposal of munitions and explosives
25 th Explosives Safety Seminar, Anaheim,CA,USA,18-20 August 1992.

PYROTECHNICS INCINERATION

Dan Burch, Michael Johnson
Crane Division
Naval Surface Warfare Center
300 Highway 361
Crane, IN 47522-5000 USA

ABSTRACT:

The United States Department of Defense (DoD) faces many environmental issues and concerns in the demilitarization and disposal of obsolete, excess and unserviceable munition items. Pyrotechnic materials present an especially difficult problem for disposal. Formulated to yield brilliant colors, the items contain organic dyes and heavy metals which are carcinogenic. There is no current available technology for the treatment of the colored smokes and dyes.

Crane Division, Naval Surface Warfare Center (NAVSURFWARCENDIV Crane) has been working with Los Alamos National Laboratory (LANL) in developing incineration technology to dispose of colored smokes and dyes. LANL, as a result of conducting test burns on mixtures of chemicals representative of Navy smokes with an existing incinerator, designed and built a transportable prototype Controlled Air Incinerator (CAI) for the Navy. The CAI, which consists of a slurry feed system, combustion chamber and emission control system was tested at the Naval Air Warfare Center (NAWC) China Lake. Two series of environmental tests were performed which consisted of monitoring the stack emissions of the CAI while processing simulated Navy smoke formulations doped with metal salts and hexachlorobenzene. Results of the testing showed that the incinerator met RCRA Hazardous Waste Incinerator standards, i.e. particulate and HCl emission limits and Destruction Removal Efficiency for hexachlorobenzene.

NAWC China Lake, as an alternative to conventional captive sampling techniques, has developed instrumentation and sample methodology for continuous monitoring of the heavy metals in the incinerator exhaust stream using an inductively coupled plasma (ICP) spectrometer. NAWC China Lake utilized an isokinetic sampling system to withdraw a representative air sample from the incinerator stack during the combustion of the slurry spiked with copper sulfate, barium nitrate and strontium nitrate. The ICP detected the metals of interest but the results for all the metals were lower than the result obtained by the captive sampling technique.

BACKGROUND:

In August 1980, the Surgeon General placed a moratorium on the open burning of pyrotechnic colored smoke, flare, and dye material as a disposal method. Currently the DOD does not possess the capability to dispose of this material. The Navy, therefore, tasked the Los Alamos National Laboratory to design, fabricate, and test a

transportable pyrotechnic incinerator. Naval Weapons Support Center Crane (NWSCC) was tasked by Naval Sea Systems Command, Washington, DC (NAVSEA) to develop thermal treatment technology for the destruction of Navy colored smoke and flare material. The only method of disposal for colored smoke, flare, and dye material is open burning. Ordnance items containing these materials have been placed in long term storage, due to the fact that the Department of Defense does not possess the capability to dispose of this material.

HISTORY OF PYROTECHNIC DYE INCINERATOR:

In March of 1985, Navy colored smokes were tested at Los Alamos National Laboratory's (LANL) controlled air incinerator. The LANL incinerator is a stationary dual chamber transuranic waste incinerator. The destruction removal efficiency (DRE) was on the scale of 99.96%, which is below the 99.99% DRE required by RCRA 40 CFR Part 264 Subpart O for the removal of principal organic hazardous constituents (POHC's). With the test data information amassed on Navy colored smokes, a design for the prototype pyrotechnic incinerator was completed by T.K. Thompson and Associates, this was completed in September 1986. One of the main requirements of the incinerator was that it be transportable, and fit on a conventional 40 foot trailer.

In January 1992, with the fabrication of the incinerator completed, it was decided to transport the incinerator to Naval Air Warfare Center, China Lake (NAWC) Ridgecrest, CA. in order to obtain proper permitting to perform the necessary testing of the incinerator. The task of relocation was completed in April of 1992, and with this complete, initial testing commenced.

Environmental testing began in April 1993, and was completed in December 1994. The incinerator is now located at the Los Alamos National Laboratory (LANL) where it is undergoing routine maintenance in anticipation of transfer to an Army facility.

DESIGN OF INCINERATOR:

The prototype incinerator consists of three portable modules: a utility module, a feed module, and an incinerator module. All three modules are designed to be transported on one 40 foot trailer. Controls and analytical equipment are mounted on a 30 foot trailer.

The utility module includes an electric steam generator, an electric air compressor, an air dryer, and electric switch gear. The feed module includes a feed tank, slurry mixing equipment, a feed pump system, and a caustic addition system. The incinerator module includes the incinerator and off-gas equipment.

The incinerator is a single-chamber design with controlled air, the air added as both primary and secondary air. The fired duty is 0.5 million Btu per hour. Gas leaving the incinerator is quenched with water sprays in a quench vessel. The off-gas leaving the quench vessel goes through a high-energy venturi scrubber and through a cyclone

separator and mist pad to the vent stack. The normal differential pressure of the venturi is 60 inches of water. Scrubber solution collected in the cyclone is recycled to the quench vessel. The quench vessel blowdown rate is based on the solution density and the pH is adjusted by caustic addition.

The incinerator is equipped with a firing management system for safe operation. The control system purges the incinerator before the pilot is lit and after the burner is shut down. All fuel sources are shut off on flame failure, loss of combustion air flow and/or low propane pressure. The slurry feed is shut down by a high quench exit temperature, loss of atomizing air or steam, high or low incinerator exit temperature, and high incinerator pressure. All fuels are automatically shut off by an electrical failure.

INCINERATOR EQUIPMENT OPERATION:

Feed Module: The waste feed system is designed to accept Navy colored smoke and flare compounds and mix with other constituents to produce a waste feed form that is suitable for injection into an incinerator. Smoke and flare compounds are mixed with varying concentrations of water, fuel oil, and surfactant. The solution is mixed with a blade mixer and by circulating through the recycle pump and nozzle. A feed pump takes slurry from the recycle pump suction and either recycles slurry to the tank or feeds it to the slurry feed nozzle in the burner.

The slurry feed tank is a cone-bottom, stainless steel tank with a capacity of 100 gallons. The tank mixer, recycle pump, and the slurry tank eductor mix the slurry. Both the pump and the eductor impart mixing shear on the slurry and maintain good mixing even when the tank level is drawn below the impeller of the tank mixer. The recycle loop resuspends solids that settle out of the slurry in the tank. The recycle pump requires compressed air pressure of 20 to 40 psig to cycle properly.

A small cone-bottom tank is used for mixing sodium hydroxide crystals into water. This caustic solution is recycled by means of a diaphragm pump into the quench tank, and is used as a neutralizing agent on the mineral acids absorbed in the scrub solution. The caustic solution is available upon demand from the pH control loop.

Utility Module: 480 Volt 200 Amp power is distributed from the utility module to the other modules and control trailer through power cables. All cables are sized for the proper amp load and voltage and have spark-proof, weather tight connectors.

Saturated 100 psig steam is generated with an electric boiler on the utility module and supplied to the incinerator module. Compressed dry air at 80 psig is provided by an electric air compressor and the air dryer mounted on the utility module. Propane for the burner fuel is provided from a 500 gallon LPG tank. Propane is delivered to the incinerator during start up phase at 2 psig. A water tank, on site, provides water to the quench tank, electric steam boiler, demister pad spray, and process pump seal flush.

Incinerator Module:

Blower: The combustion air blower provides 4 psig air as both primary combustion air to the burner and secondary air to the incinerator. The total combustion air flow at high burn rate is approximately 120 SCFM.

Burner: The burner is a dual fuel vortex-type burner with the waste atomizing nozzle at the center of the burner. The slurry enters the burner as a fine spray, this promotes vaporization and mixing with air prior to combustion. Propane exits the burner tip through an outer ring of holes where it mixes with primary combustion air. Primary combustion air enters the burner tangentially which creates a swirling turbulence causing more efficient burning and a higher hold up time.

Incinerator: The incinerator is a chamber where complex hazardous constituents are converted by combustion to simpler, more benign compounds. The geometry, orientation, materials of construction, and ancillary equipment have been designed to optimize the combustion of the Navy waste liquid fuels. The incinerator, lined with high-alumina refractory lining, was designed to minimize particle impact on the ceramic lining, while providing for desirable plug-flow conditions after volatilization and mixing of reactants.

The incinerator is brought up to operating temperature by heat supplied by the propane burner. Once the waste is being injected into the incinerator, the combustion of the mix will supply most of the heat required to keep the incinerator at the desired temperature. It has been demonstrated that 60 pph of slurry feed will maintain temperature above 2100 degrees F.

The incinerator volume, 40 cu. ft., was sized to allow enough residence time for combustion reactions with Navy colored smoke and dye compounds mixed with oxygen and water vapor to reach equilibrium. Orientation of the incinerator is vertical (firing down) in order to enhance the movement of salt slag out of the chamber.

Quench Vessel: Combustion products leaving the incinerator pass downward into the quench tank. These products include offgasses, entrained particulates, and salt slag. The offgasses and entrained particulates are cooled by cross-flow contact with recycled quench solution. The quench solution is atomized by six spray nozzles and is partially evaporated by the hot offgasses and particulates. The latent heat exchange associated with evaporation provides the primary cooling of the off-gas. Evaporation continues until the offgasses are saturated with water contained in the quench solution. Saturation of the offgasses also serves to improve the performance of the venturi scrubber.

The unevaporated quench liquid collects in the bottom of the quench tank where it quenches and dissolves any salt slag that drains from the incinerator.

Venturi Scrubber: Offgasses leaving the quench tank pass through the venturi scrubber, a device that removes particulates entrained in the offgas. The offgas is forced through large, slow moving water droplets, and caused to accelerate by moving through a duct section with diminishing diameter. Particulates larger than 1/2 micron are removed from the offgas stream by direct impact with target quench solution droplets injected into the converging section of the venturi scrubber. Smaller particles have insufficient momentum for direct impact but are collected by being moved to the target droplets by the flow of water vapor being condensed on the cooler target droplets. The water droplets and cleaned offgas are then separated by gravity.

The venturi scrubber is designed with an adjustable throat that can be opened or closed to maintain the desired offgas pressure drop across the venturi. This pressure is maintained at 60 inches of water. It was noted during testing that if the pressure dropped below this, the quench tank suction pressure was insufficient for proper quench pump operation, and the quench flows dropped off.

Demister Pad: The velocity of offgasses leaving the venturi scrubber tends to entrain a small amount of process liquid. Most of this liquid is removed by passing the offgasses through a mesh pad where the liquid coalesces on the mesh fibers and drains to the bottom of the demister pad.

Vent Stack: The vent stack exhausts the cleaned offgasses from the system. The geometry of the stack is designed to provide a correct internal offgas flow pattern for reliable sampling of the offgasses by established procedures.

CONTROL TRAILER:

The control trailer consists of two control panels consisting of controllers, recorders, totalizers, air regulators, interlock logic controllers, switches, and alarms. Also in the control trailer are the polycyclic aromatic hydrocarbon monitor, and the air inductively-coupled heavy metals monitor.

Control Panels:

Controllers: The controllers consist of the slurry feed flow, quench pH control, primary air flow, oxygen analyzer, quench spray flow, and venturi quench spray flow. All of these variables can be controlled from within the control trailer.

Recorders: The recorders are as follows: slurry feed tank level, slurry feed temperature, slurry pressure, incinerator top temperature, steam or air flow (atomizing), secondary air pressure, secondary air flow, venturi scrubber differential pressure, quench tank temperature, quench tank pressure, and quench tank differential pressure. All are continuously recorded and analyzed during post data analysis.

Totalizers: The totalizers used for cumulative data are as follows: propane flow, combustion air flow, and stack gas flow.

Pressure Switches: The following switches provide interlock contacts that are inputs to the Allen Bradley programmable controller on the back of the control panels: propane pressure (low), propane pressure (high), steam/air pressure, combustion air pressure, quench pump discharge pressure, and low water pressure.

Interlocks: Safety interlocks shut down the incinerator or prevent startup under unsafe conditions. Two devices provide interlock protection: The Honeywell burner controller controls the incinerator startup sequence and monitors the burn conditions. When in operation this controller checks to see if all pre-ignition interlocks are off. The second controller utilized is an Allen Bradley programmable controller, which provides interlock protection for the total incinerator system.

Regulators: The control panel has an air manifold which provides regulated air to the slurry tank recirculation pump, pinch valve, and dip tube.

Alarms: The alarm panel alarm lights and buzzer turn on whenever an alarm condition exists. This provides the operator with a warning that conditions are not normal or that an interlock has occurred.

Polycyclic Aromatic Hydrocarbon Monitor:

A spectrofluorimeter with a heated flow-through cell was configured for continuous emissions monitoring of polycyclic aromatic hydrocarbons (PAH's). The instrument was programmed to scan over spectral regions associated with a group of ten target PAH's. Stack air and clean reference air were alternately introduced into the instrument to permit baseline subtraction measurements. The PAH monitor is capable of detecting airborne PAH's at concentrations less than one part per million. The PAH monitor was operated continuously during incinerator operation on propane and when waste slurry was burned. No PAH's were detected during the monitoring period by the monitor.

Air Inductively-Coupled Plasma Heavy Metals Monitor:

As an alternative to conventional captive sampling techniques for monitoring the metals emissions in incinerator effluent, instrumentation and methodology for real-time detection of airborne metals has been developed. Conventional measurement techniques involve the capture of airborne particulates on filter media, chemical digestion of the samples, and spectrochemical analysis of the sample digests. These techniques do not provide analytical data in the timely fashion required for active process control aimed at minimizing or eliminating the fugitive emission of metals into the atmosphere. By the time the sample is analyzed in a laboratory, the information obtained may have only historical value. Real-time, continuous emissions monitoring

offers nearly instantaneous measurements that are more useful in tracking the transient behavior of an emissions source.

To accomplish the goal of real-time, in-the-field measurement of airborne metals, an inductively coupled plasma (ICP) spectrometer was modified to allow introduction of sample air. The ICP is normally used as a laboratory instrument capable of sensitive measurement of the metal content in a variety of real samples. The high temperature (6000-8000 K) of the plasma ensures efficient sample decomposition and excitation. The metal atoms and ions in a given sample, upon entering the plasma emit light of characteristic wavelengths as a result of excitation within the plasma. The intensity of this light is proportional to the concentration of a given metal in the sample. Adapting this technique for the detection of airborne metals is straight forward. The plasma used in the present application is sustained on air and therefore is readily amenable to the introduction of sample air. An isokinetic sampling system was used to withdraw a representative air sample from the incinerator stack during the combustion of waste slurry spiked with copper sulfate, barium nitrate, and strontium nitrate. The three optical detectors employed by the ICP were tuned to the appropriate wavelengths to detect these metals and the instrument was calibrated with standard solutions. The relationship between metals introduced as airborne aerosols and as aqueous solutions had been previously established in the laboratory. The results of continuously monitoring the stack effluent for a period of fifty minutes yielded concentrations of 1290, 700, and 1030 micrograms per cubic meter for airborne copper, barium, and strontium. These compared reasonably with measurements obtained by conventional captive sampling techniques: 3260 (Cu), 1810 (Ba), and 2270 (Sr). The real-time measurements were more than a factor of two lower due to sample loss in the fifty foot heated sample line located between the stack and the control trailer.

MOBILE CHEMICAL LABORATORY TRAILER:

The mobile chemical laboratory at the incinerator site at NAWC China Lake was installed and monitored by NAVSURFWARCENDIV Crane Code 4054 personnel. The trailer is equipped with all necessary equipment in order to obtain all data necessary to meet the requirements set forth by the Hazardous Waste Incinerator Standards promulgated under the United States Environmental Protection Agency (EPA) Resource Conservation and Recovery Act (RCRA).

With the advent of RCRA regulations and the classification of demilitarization furnaces as hazardous waste incinerators, it has become necessary to expand the previous sampling parameters to include organic/explosive, hydrochloric acids and metals emissions. The Federal Incinerator Environmental Standards that were followed during testing were as follows:

(1) Organic Emissions. A destruction and removal efficiency (DRE) of 99.99% for each designated principal organic hazardous constituent (POHC) must be demonstrated.

(2) Particulate Emissions. Particulate emissions may not exceed 0.08 grains per dry standard cubic foot, corrected to 7% oxygen content of the exhaust gas.

(3) Hydrogen Chloride Emissions. Hydrogen chloride (HCL) emissions are limited to 4 pounds per hour or 1% of the HCL that was present in the exhaust gas prior to the air pollution control system, whichever is higher.

(4) Metals Emissions. Included in Part B of operating permit.

(5) Non-Methane Hydrocarbons. This was measured due to the fact that it is a very good indicator of the amount of organics being emitted.

(6) Continuous Gas Monitoring. Operational requirements listed in 40 CFR Part 264.345 and trial burn requirements of 40 CFR Part 270.62 call for the continuous monitoring of carbon monoxide and oxygen. The information collected from the monitoring of these gasses was used to evaluate the incinerator performance and will also provide a background on which operational parameters of the RCRA permit will be specified.

TEST METHODS:

Nine separate one hour tests were conducted on the incinerator during the week of 14-18 June 1993. Three separate slurry mixtures were utilized for the testing; Slurry mixture #1, which was used during the hydrochloric acid emission testing, consisted of fuel oil, water, surfactant, and Mk 13 smoke composition (this consists of potassium chlorate, sugar, diatomaceous earth, graphite, xylene-azo-b-naphthol, and red dye #9). Slurry mixture #2 used for the metals emissions testing consisted of all components in slurry mixture #1 with copper, barium, and strontium added. Slurry mixture #3 used for the POHC/DRE testing consisted of all components in slurry mixtures #'s 1 and 2 with hexachlorobenzene added as the POHC.

The sampling method used for the hydrochloric acid emissions testing, and the metals emissions testing was a modified Method 5 train as found in 40 CFR Part 60, Appendix A. The metal concentrations in the stack gas were calculated by using formulas in EPA Method 12, and the determination of metals in the stack gas was accomplished by Atomic Absorption Spectroscopy. The sampling train used during POHC testing was an EPA approved United States Army Environmental Hygiene Agency (USAEHA) Modified Method 5 procedure, with the quantification of the POHC and it's surrogate, tetrachlorobenzene, determined by using Gas Chromatography Analysis.

TEST RESULTS:

Slurry Mixture #1
 Incinerator Temperature: 2150 degrees F
 Combustion Air Flow: 108 SCFM
 Slurry Feed Flow: 73 lb/hr

<u>HCL Testing</u>	<u>HOURL #1</u>	<u>HOURL #2</u>	<u>HOURL #3</u>
HCL Emissions (pounds per hour)	0.00076	0.01915	0.01252

All HCL emissions were well below RCRA Incinerator limits of four pounds per hour or less.

Slurry Mixture #2
 Incinerator Temperature: 2120 degrees F
 Combustion Air Flow: 92 SCFM
 Slurry Feed Flow: 75 lb/hr

<u>Metals Testing</u>	<u>HOURL #1</u>	<u>HOURL #2</u>	<u>HOURL #3</u>
Copper (captive) (AIR-ICP) (Micrograms/DSCM)	2831	3864	3261 1290
Barium (captive) (AIR-ICP) (Micrograms/DSCM)	1882	2840	1812 700
Strontium (captive) (AIR-ICP) (Micrograms/DSCM)	2080	3155	2269 1030
Particulate Emission (gr/DSCF)	0.0194	0.0238	0.0264

The particulate emissions were well below the RCRA limits, which specifies particulate emissions of not more than 0.08 gr/DSCF.

42 - 10

Slurry Mixture #3
Incinerator Temperature: 2020 degrees F
Combustion Air Flow: 70 SCFM
Slurry Feed Flow: 57 lb/hr

<u>DRE Testing</u>	<u>HOURL #1</u>	<u>HOURL #2</u>	<u>HOURL #3</u>
POHC DRE	99.9998%	99.9968%	99.9705%
hexachlorobenzene			

Tests #1 and #2 pass the requirements of a DRE of 99.99% or greater. The lower DRE in Test #3 was believed due to problems in feeding the added ingredients is slurry mixture #3 as surges were noted during the test run.

EXPERIMENTAL NAVY SMOKE COMPOSITION TESTING:

In December 1993, the incinerator was used to test an experimental Navy smoke composition for development of a demilitarization plan. The composition consisted of the following materials: amorphous boron, potassium perchlorate, algoflon (PTFE), and viton A copolymer. These materials were slurried with fuel oil and water for the POHC testing, utilizing the PTFE for the DRE testing. During the second day of testing, copper, barium and strontium were added for the metals emissions testing. The third of testing included all of the above materials while monitoring for dioxin/furan emissions.

The formulation for the destruction removal efficiency testing was as follows:

<u>ITEM</u>	<u>PERCENTAGE</u>
Fuel Oil	26.8%
Water	56.1%
Surfactant	0.6%
Experimental Comp.	16.5%

The sampling method used for the DRE testing was EPA Method 5 Modified sampling train. Note that PTFE was chosen as the Principal Organic Hazardous Constituent as contained in 40 CFR Part 261, Appendix VIII. DRE results were as follows:

First Hour Destruction Removal Efficiency: 99.9996%
Second Hour Destruction Removal Efficiency: 99.9996%

The formulation for the metals emissions testing was as follows:

<u>ITEM</u>	<u>PERCENTAGE</u>
Fuel Oil	26.8%
Water	56.1%
Surfactant	0.6%
Experimental Comp.	16.3%
Barium Nitrate	0.06%
Strontium Nitrate	0.06%
Copper Sulfate	0.06%

The sampling method used for the metals emission testing was EPA Method 5 Modified sampling train. The Metals emissions results for the two one-hour tests were as follows:

<u>METAL</u>	<u>MICROGRAMS/DSCM</u>		<u>REMOVAL PERCENTAGE</u>	
	<u>HR #1</u>	<u>HR #2</u>	<u>HR #1</u>	<u>HR #2</u>
Copper	1576	1230	99.61	99.65
Strontium	1715	814	99.59	99.78
Barium	1379	976	99.74	99.79
Boron	27914	11491	99.28	99.66

The slurry formulation for the dioxin/furan emissions testing was the same as that used during the metals emissions test. The sampling method used was USAEHA Modified Method 5 sampling train. The emission rates of dioxins/furans were reported in two different units, pounds per hour and nanograms per dry standard cubic meter. As of the writing of this paper, Destruction Removal Efficiency requirements are included in the hazardous waste incinerator performance standards as per 40 CFR Part 264, and also Boiler and Industrial Furnace (BIF) performance standards found in 40 CFR Part 266, Appendix IX. The DRE requirement is 99.9999% removal for the designated POHC when the slurry contains dioxin/furan compounds. The DRE results presented here represent what the DRE would be if the designated POHC, PTFE were a dioxin/furan containing compound. As noted in the "Environmental Reporter", the EPA is in the process of changing the current standard for dioxin/furan emissions from a 99.9999% DRE to that of 30 nanograms per DSCM. Therefore, the results are given in both standards. The results of the testing are as follows:

<u>ITEM</u>	<u>DESTRUCTION REMOVAL EFFICIENCY</u>	
	<u>HR #1</u>	<u>HR #2</u>
Total dioxin/furans based on PTFE feed rate of 1.73 lb/hr	99.9999993%	99.9999992%
Total dioxin/furans based on PTFE feed rate of 1.73 lb/hr using Toxicity Equivalency Method as per 40 CFR Part 266, Appendix IX	99.999999991%	99.999999986%

42 - 12

NANOGRAMS/DSCM

<u>HR #1</u>	<u>HR #2</u>
35.1	43.44

TOXICITY EQUIVALENCY METHOD

NANOGRAMS/DSCM

<u>HR #1</u>	<u>HR #2</u>
0.45	0.741

EMISSIONS RESULTS ANALYSIS:

DRE Results: The Destruction Removal Efficiency obtained for the PTFE as listed above were well above the 99.99% DRE required in 40 CFR, Part 264, Subpart O, Paragraph 264.343, for Hazardous Waste Incinerators.

Dioxins/Furans Results: The EPA has included in the BIF emission regulations (40 CFR Part 266, Appendix IX, Section 4.0) a method of estimating risks posed by different dioxin/furan congeners. The resulting 2,3,7,8 TCDD (Tetrachlorodibenzodioxins) equivalency values are used in the subsequent risk calculation and modeling efforts as discussed in the BIF final rule. The toxicity equivalency emission concentrations were less than 1 ng/dscm, well below the limits to be imposed by the EPA (30 ng/dscm), and also below the limits imposed of European incinerators of 1 ng/dscm.

TCLP Results: The Toxicity Characteristic Leaching Procedure results indicate that for the hazardous waste determination of the sludge produced during the environmental testing, it is not a hazardous waste. This was determined as per 40 CFR Part 261. Barium concentrations were below the 100 mg/L upper limit and only trace elements of PTFE were found. No limits exist for the other metals.

Oxides of Nitrogen Emissions Results: The NOx emissions for the test burns ranged from 0.048 to 0.133 pounds per hour. This is considered to be too high, and for any future testing, a more starved air atmosphere ratio will be used to control NOx production. This method may in fact cause higher carbon monoxide emissions, and if this is the case, different burners will be analyzed for incorporation to the CAI.

CONCLUSIONS:

The incinerator proved efficient for the destruction of the organics as the DRE for the designated POHC was greater than the 99.99% requirement on two of the three tests. The lower DRE in Test #3 was believed due to problems in feeding the added ingredients in the slurry mixture as surges were noted during the test run. Also the selected POHC, hexachlorobenzene, is considered by the EPA to be more difficult to incinerate than the majority of organic hazardous constituents. The emission control system also proved effective for the control of acid gasses and particulate as the pounds per hour HCL and grains per standard cubic foot of particulates were below the RCRA hazardous waste incinerator standards.

The real time measurements using the Air-ICP developed by NAWC China Lake were more than a factor of two lower than the EPA prescribed multiple metals train method.

This is believed due to sample loss in the fifty foot heated sample line located between the stack and the control trailer housing the Air-ICP.

CURRENT STATUS/FUTURE PLANS:

The incinerator is currently at Los Alamos National Laboratory. It has undergone routine maintenance repairs in anticipation of siting it at an Army facility.

NAVSURFWARCENDIV Crane is currently conducting a market survey of existing incineration systems to see if any are qualified for Navy smokes and dyes. With this market survey will also be a final design for the prototype incinerator in order to incorporate any necessary changes due to the data analysis.

The AIR-ICP unit is currently being reconfigured so that lead detection is possible. This effort is being funded by the Army.

BACTERIAL BIODEGRADATION OF NITRATE ESTER EXPLOSIVES

Graham F. White,^a Jason R. Snape^a and S. Nicklin^b

^aSchool of Molecular and Medical Bioscience, University of Wales Cardiff,
PO Box 911, Cardiff CF1 3US

^bDefence Research Agency, Fort Halstead, Sevenoaks, Kent, TN14 7BP

ABSTRACT

Glycerol trinitrate (GTN) is used as a high explosive. Its sensitivity to detonation by mechanical shock, and its pharmacological potency, while critical to its utility, also constitute problems for handling and treating wastes arising from the production and use of the compound. This paper describes bacterial biodegradation of GTN, which may offer a means of removal of GTN from waste streams and bioremediation of contaminated land sites.

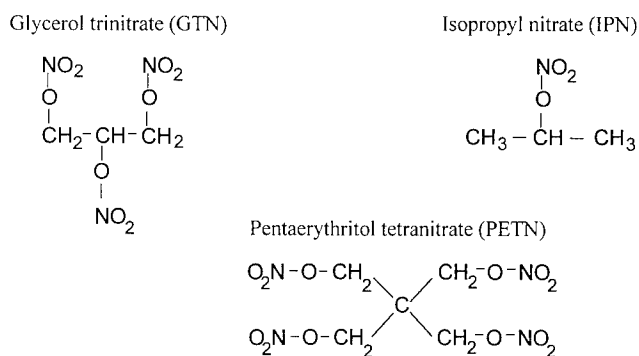
Pseudomonas sp. strain RING2 was isolated from river sediment by enrichment culture on minimal salts/glycerol/GTN medium. Batch culture experiments established that this isolate utilised GTN as its sole source of nitrogen. Analysis of the growth medium using HPLC showed the presence of glycerol dinitrates and glycerol mononitrates. Isomeric glycerol 1,2-dinitrate and glycerol 1,3-dinitrate were produced simultaneously and concomitantly with the disappearance of GTN, with significant regioselectivity for the production of the 1,3-isomer. After GTN disappearance was complete, the dinitrates were further degraded to glycerol 1- and 2-mononitrates. Preliminary experiments indicate that the nitro group is liberated as nitrite, not nitrate. The bacterial biodegradation of GTN thus shows parallels with GTN metabolism in eukaryotic (mammalian and fungal) systems.

INTRODUCTION

Nitrate esters of aliphatic alcohols are industrially important as a result of two major, though incongruous, applications. First they are widely used as powerful explosives, and secondly they are effective vasodilators in the treatment of heart disease such as *angina pectoris*. Glycerol trinitrate (GTN; propane-1,2,3,-triyl trinitrate) and pentaerythritol tetranitrate (PETN; 2,2-bis[nitrooxymethyl]propane-1,3-diyl dinitrate) are among the most widely known and are used in both applications. They are produced by direct nitration of the parent alcohol with nitric acid, usually with

sulphuric acid present as catalyst (Urbanski, 1965), and may be regarded as the nitric acid tri- and tetra-esters, respectively, of glycerol and pentaerythritol (Fig. 1). Thus structurally these nitrate ester groups are analogous to phosphate and sulphate esters. However it has recently been emphasised that whereas the latter groups occur ubiquitously in the biosphere, nitrate esters have never been detected as naturally-occurring compounds in living organisms and thus constitute a true xenobiotic challenge to biological systems (White & Snape, 1993). The microbial biodegradability of nitrate esters is therefore not only academically intriguing but is also relevant to development of methods for the elimination of nitrate esters from production waste-waters and for the bioremediation of land-sites contaminated during production, storage and use of such compounds (Kaplan, 1992; Walker & Kaplan, 1992; Gorontzy *et al.*, 1994).

Figure 1. Structures of some nitrate esters



Before embarking on a search for bacteria competent in the biodegradation of nitrate esters, it is helpful first to appreciate *why* they might do so. Low-nutrient (oligotrophic) environments are often considered among the "extremes" to which microorganisms have become adapted. Yet, oligotrophic conditions are so ubiquitous in the microbial biosphere, as to be the norm (Morgan and Dow, 1986). Moreover, nutrient status is determined not only by carbon availability but also by other bio-elements (predominantly P, S, N), and in oligotrophic environments it is likely that microbial growth is constrained by all these, either simultaneously, or sequentially. Faced with such privation, microorganisms have evolved numerous strategies for surviving nutrient limitation, including chemotaxis, surface-attachment, and in more recent times diversification of metabolic capabilities to include catabolism of the industrial products of human-kind.

Examination of the structures of nitrate ester explosives shows that they contain abundant carbon derived from polyhydric alcohols (e.g. glycerol, pentaerythritol) which are readily assimilable by bacteria. Moreover nitrate esters also contain abundant nitrogen and thus they may also serve to supply this element for microbial growth. A very few bacterial species can fix dinitrogen from the air to synthesise amino acids and other organonitrogen compounds, but many more can reduce nitrate and/or nitrite to ammonia prior to its assimilation into amino acids. A further group (the denitrifiers) use nitrate or nitrite as an oxidizing agent in place of dioxygen to oxidise organic fuels under anaerobic conditions to yield energy (Payne, 1981). If there are routes for utilization of nitrate ester nitrogen, these involving nitrate and/or nitrite seem the most likely.

The well-documented metabolism of GTN in mammalian systems (Taylor *et al.*, 1987) involves conversion to nitric oxide (Feelisch & Noack, 1987; Schror *et al.*, 1991) which currently enjoys new-found importance in mammalian physiology as a chemical messenger with roles in vascular function (Moncada *et al.*, 1988), neurotransmission (Knowles *et al.*, 1989) and immune response (Knowles *et al.*, 1990). Fungi such as *Phanerochaete chrysosporium* and *Geotrichum candidum* also metabolise GTN and are serving as model systems for the study of eukaryotic metabolism of nitrate esters (Ducrocq *et al.*, 1989, 1990; Servent *et al.*, 1991). Fungal fission of the nitrate ester linkage is also reductive with the formation of nitrite and NO-protein complexes. Published work on bacterial metabolism of GTN is confined to an earlier study (Wendt *et al.*, 1978) which established sequential denitration via glycerol dinitrates (GDN) and glycerol mononitrates (GMN) to glycerol.

The present work was undertaken as part of a wider programme to isolate bacteria competent in the biodegradation of nitrate esters and to determine the kinetics of metabolite production during the biodegradation process. The enrichment substrates used were GTN, PETN and propane-2-yl nitrate (isopropyl nitrate, IPN). The last was chosen because it is a readily available mononitrate which is structurally related to GTN, and it is analogous to propane-2-yl sulphate which is known to undergo bacterial biodegradation (Crescenzi *et al.*, 1984, 1985).

MATERIALS AND METHODS

Chemicals

Three esters, viz. GTN, PETN and isopropyl nitrate (IPN), were used for the initial isolation of bacteria. Research quantities of GTN (adsorbed on Kieselguhr, 20% w/w), glycerol 1-mononitrate (1-GMN), glycerol 1,2-dinitrate (1,2-GDN), glycerol 1,3-

dinitrate (1,3-GDN) and PETN were supplied by Fort Halstead, Sevenoaks, Kent. IPN was purchased from Aldrich Chemicals, Poole, Dorset.

Working solutions of GTN were prepared by extracting 20mg of GTN-on-Kieselguhr into 0.5ml ethanol. The mixture was shaken vigorously for 15min, then centrifuged at 2500 rpm for 5min. The supernatant (0.4ml) was used for the preparation of microbial growth media.

HPLC eluents were prepared using HiperSolv quality methanol (Merck-BDH) and ultra-pure water from a Millipore Milli-Q 50 system which produced 0.22 μ m-filtered, 18Mohm deionised water.

Other chemicals were the purest available from Merck (BDH) or Sigma Chemical Co.

Isolation and culturing of competent bacteria

Standard enrichment culturing techniques were used to isolate bacteria from a variety of sources (see Table 1) for ability to use one of the three nitrate esters GTN, PETN, and IPN as source of nitrogen for growth. Samples of inoculum material were added to culture flasks containing a minimal salts medium lacking nitrogen (see below) and 1% v/v glycerol as carbon source, plus the appropriate nitrate ester as sole source of nitrogen. Flasks were incubated in a gyratory incubator at 25°C for 1-2 weeks and samples were sub-cultured at weekly intervals thereafter into fresh medium. After 4-8 sub-cultures, samples from flasks showing visible growth were plated out onto nutrient agar plates and single colony-types separated and re-plated to purity. Axenic strains were re-inoculated into the basal salts/ glycerol/ nitrate ester medium to check that they had retained the capacity for growth.

For isolation and subsequent culturing, the basal salts medium contained (per litre) K₂HPO₄, 3.5g; KH₂PO₄, 1.5g; NaCl, 0.5g; MgSO₄, 0.12; 1ml of trace elements solution. Trace elements solution contained (per litre) sodium borate, 0.57; FeCl₃.6H₂O, 0.24g; CoCl₂.6H₂O, 0.04g; CuSO₄.5H₂O, 0.06g; MnCl₂.4H₂O, 0.03g; ZnSO₄.7H₂O, 0.31g; Na₂MoO₄.2H₂O, 0.03g; this solution was stored in the dark at 4°C. Culture flasks were prepared by adding 2ml glycerol to 100ml basal salts medium immediately before autoclaving. After autoclaving and cooling, 0.4ml of ethanolic GTN working solution was added to give the desired final concentration of GTN as sole added source of nitrogen for growth. Cultures were agitated at 100 rpm and 25°C and growth of bacteria was monitored by measuring optical density at 450nm in Pharmacia/LKB Novaspek II spectrophotometer.

Storage and maintenance of microorganisms

Bacterial isolates were maintained on working and short-term back-up nutrient agar slopes stored at 4°C. Cultures were plated out every 2 months to ensure purity, and fresh slopes made. Long-term storage was at -70°C in glass embroidery beads with 15% glycerol in nutrient broth as cryo-protectant (Jones *et al.*, 1991).

Geotrichum candidum was obtained from Birkbeck College Culture Collection and maintained on nutrient agar plates with 2-monthly transfers.

Analysis of nitrate esters and their metabolites

Residual GTN and the di- and mono-nitrated analogues arising from bacterial biodegradation were analysed by HPLC using a Dionex DX300 Series Ion Chromatograph (Dionex UK, Camberley) equipped with a variable wavelength UV detector and a Spectra Physics 4400 Integrator. The column was a Lichrosorb ODS 10 µm-bead size, 260 x 4.6mm (Phase Separations, Clwydd, Deeside) eluted with a water/methanol linear gradient from 5% to 50% methanol over 30 minutes. Eluents were prepared from HPLC grade solvents and degassed by sparging with helium and maintaining under a helium atmosphere. Analytes were detected by their absorbance at 217nm.

HPLC retention times for GTN and glycerol 1-mononitrate (1-GMN) were determined by elution of authentic materials, and calibration curves were obtained using standard solutions, the concentrations in which were determined using published extinction coefficients (Dunstan *et al.*, 1965). Calibration of the HPLC system for glycerol dinitrates presented some problems because the chemical preparation of pure samples is difficult. Thus the available sample of "1,2-GDN" contained 2 peaks and it was impossible to assign one or other to 1,2-GDN. To circumvent this difficulty, a mixture of the dinitrates was prepared from standard solutions of GTN by incubation with *Geotrichum candidum*. This microorganism is known (Ducrocq *et al.*, 1989) to yield a mixture of dinitrates but with the 1,3-isomer dominating over the 1,2-isomer, thus enabling the HPLC peaks to be identified by relative size. Calibration was achieved from the known initial and measured (HPLC) residual concentrations of GTN. The available sample of 1,3-GDN contained 4 peaks, 3 of which were identified with 1-GMN, 1,2-GDN and 1,3-GDN. The fourth peak, eluting between 1-GMN and the dinitrates, was tentatively attributed to 2-GMN.

Nitrite was detected using the Greiss-Romijn reagent (sulphanilic acid/ N-1-naphthylethylenediamine in acid) as described by Tan-Walker (Tan-Walker, 1987).

RESULTS

Isolation of bacteria

Table 1 summarises the distribution of isolates obtained from each of the source samples, using each nitrate ester separately as source of nitrogen. Of the three esters used, GTN and PETN appeared to be the most readily biodegradable, judging by the number of isolates obtained. No isolates were obtained which could utilise IPN. Of the various source samples, the sewage, soil and river samples were the most productive.

Some of the isolates in Table 1 were selected for further study. The remainder of this paper is devoted to the results obtained for strain RI-NG1, isolated from river sediment for its ability to biodegrade GTN, and tentatively identified as a *Pseudomonas* sp. using the BIOLOG bacterial identification (BIOLOG, Hayward, Ca, USA) system.

Table 1. Number of isolates obtained from various sources by enrichment on different nitrate esters.

Source of organisms	Nitrate ester		
	GTN	IPN	PETN
Sewage (SW)	2	0	4
Soil (SL)	3	0	4
River (RI)	1	0	4
Rat faeces (RF)	0	0	2

Dependence of growth on ester availability

In order to establish that disappearance of nitrate esters was the result of microbial metabolism, experiments were initiated to show that growth was dependent on the presence of nitrate esters. Cells pre-adapted by growth on basal salts, glycerol/GTN (250µM) medium for 72h, were used to inoculate (0.1% v/v) a second flask, designated A and containing 200 ml of the same medium. Growth in flask A was monitored for 240h. *Pseudomonas* sp. RI-NG1 grew with a doubling time of about 24h, reaching a final OD₄₅₀ of about 0.4 (Fig. 2). In view of the high concentration of glycerol and low concentration of GTN, it was likely that growth was nitrogen-limited.

Figure 2. Growth of *Pseudomonas* sp. RI-NG1 with GTN as sole source of nitrogen. Flask A (○, 200ml basal salts/ 1% glycerol and 250μM GTN) was inoculated with *Pseudomonas* sp. RI-NG1 in similar medium. After 120h, 100ml was transferred from flask A to a clean flask B (●) and supplemented with more GTN. Simultaneously, flask C (▽, fresh whole medium) and flask D (▼, fresh medium lacking GTN) were inoculated from flask A (0.1% v/v). Growth was measured as OD₄₅₀.

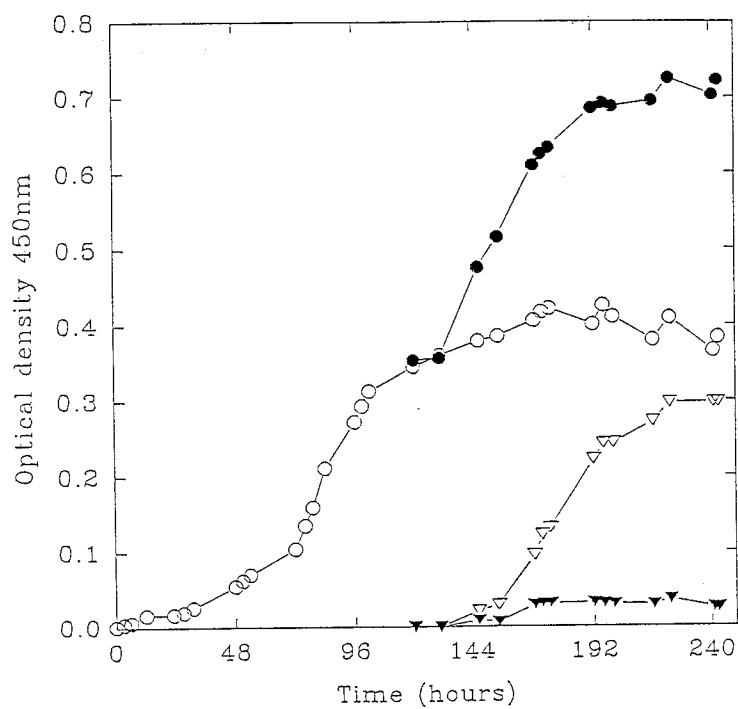
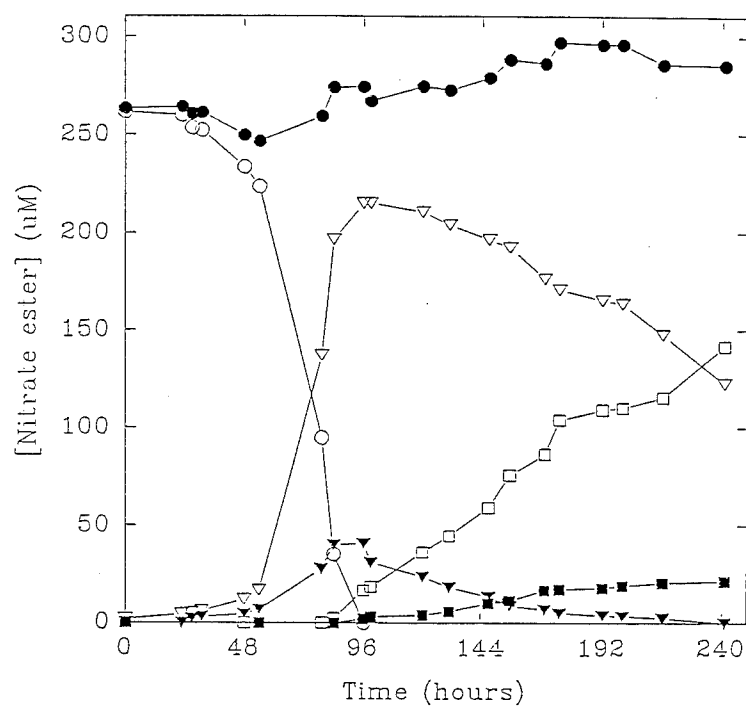


Figure 3. Production of metabolites from GTN by *Pseudomonas* sp. RI-NG1.
 ○ , GTN; ▽ , 1,3-GDN; ▼ , 1,2-GDN; □ , 1-GMN; ■ , 2-GMN; ● , total
 residual GTN and its metabolites.



To confirm this, at 120h the culture in flask A was sub-divided as follows:- 100 ml of the residual culture was transferred aseptically to a clean sterile flask (B) and supplemented with a further aliquot of GTN; 1ml aliquots from flask A were used to inoculate flask C which contained fresh sterile whole media (i.e. including GTN), and flask D which contained fresh sterile media lacking GTN; the residual culture medium in flask A was left untreated. All four flasks A-D were returned to the incubator and monitored for growth over a further 5-day period. Fig. 2 shows that after the initial 120h period, the culture in flask A was entering stationary phase. Addition of fresh GTN to the culture at this point (flask B) led to a second burst of growth which approximately doubled the cell density. Dilution (100-fold) of the first culture into fresh whole medium (flask C) gave a very similar burst of growth, suggesting that growth in the flask A at 120h was limited only by GTN availability. Transfer from flask A to flask D lacking GTN produced no growth at all.

Metabolite production

The samples removed from flask A for measurements of growth, were also analysed by HPLC for GTN and its metabolites (Fig. 3). Growth was accompanied by disappearance of GTN which was complete at 96h, and by appearance of both isomers of GDN. 1,3-GDN was the major metabolite, its rate of appearance exceeding that of the 1,2 isomer by about 5-fold. 1-GMN and 2-GMN first appeared after about 80h, and increased in concentration at the expense of decreasing concentrations of the dinitrates throughout the remainder of the experiment. The rate of production of 1-GMN exceeded that of the 2-isomer by about 6-fold. Fig. 3 also shows that the total concentration of all the glycerol nitrates detected was constant throughout the 240h period of incubation.

Preliminary experiments using broth-grown resting cells incubated with GTN showed that disappearance of GTN was accompanied by formation of nitrite ions in solution.

DISCUSSION

The growth experiments demonstrated unequivocally that GTN was serving as the sole source of nitrogen for growth of *Pseudomonas* sp. RI-NG1 under these conditions. During growth, GTN was converted stoichiometrically (Fig. 3) to its dinitrate analogues which were produced simultaneously but with 1,3-GDN appearing about 5 times faster than the 1,2-isomer. This is significantly higher than the ratio of 1.2-1.8 for 1,3-GDN/1,2-GDN produced by *G. candidum* (Ducrocq *et al.*, 1989). Moreover, bearing in mind that GTN offers only one way of making 1,3-GDN

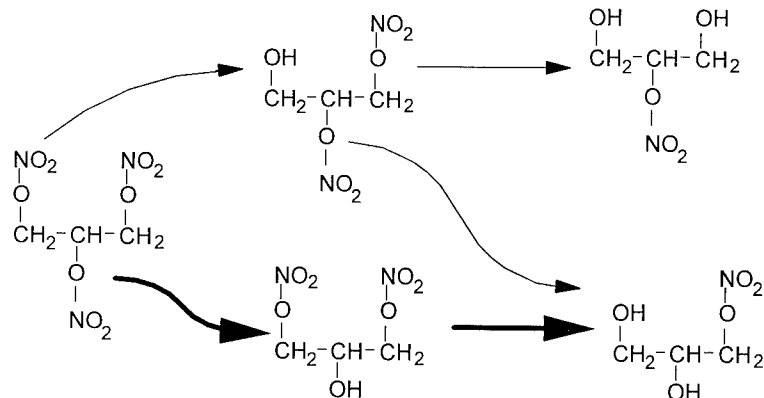
(denitration at the central nitrate) but two ways for making 1,2-GDN (attack at either end) the selectivity for attack at the central nitrate group (C2) is about ten-times that at the terminal esters.

When all the GTN had disappeared, and the GDNs were approaching their maximum concentrations, the mono-nitrates 1-GMN and 2-GMN began to appear, again simultaneously but in the ratio of about 6:1. Whichever of its nitrate esters is removed, 1,3-GDN can only give rise to 1-GMN. Thus because 1,3-GDN is the dominant intermediate, the bulk of the 1-GMN production (Fig. 3) is attributable to the biodegradation of 1,3-GDN. In contrast, denitration of 1,2-GDN can produce either 1-GMN or 2-GMN depending on whether the attack occurs at C2 or C1 respectively. After 96h, GTN degradation was complete and no more dinitrates could be made. Examining the data after this point in Fig. 3, it is clear that most but not all of the 1,2-GDN is converted to 2-GMN, indicating a preference for attack at C1 in 1,2-GDN. Thus the regioselectivity for C1/C2 denitration in GTN is different from that in 1,2-GDN. Whether this difference reflects either the operation of different enzyme systems or different modes of substrate binding to a common enzyme, is unknown.

The total recovery of residual GTN plus all isomers of GDN and GMN was close to 100% throughout the period of the experiment. This indicated that no other GTN derivative or metabolite was produced in significant quantities and also suggested that the organism was incapable of biodegrading either of the mononitrates.

Based on the data presented herein, Fig. 4 summarises the sequence of metabolite production, and heavy arrows are used to indicate that the major route for biodegradation is via initial attack at C2, then C1 to yield mainly 1-GMN. The detection of nitrite in incubations of resting cells with GTN is consistent with a reductive mechanism enabling the ester nitrogen to enter the assimilation pathway at the level of nitrite. Although not yet tested, denitrifiers may also be able to denitrify nitrate esters via nitrite to dinitrogen gas.

Figure 4. Pathway for the biodegradation of GTN in *Pseudomonas* sp. RI-NG1.



REFERENCES

- Crescenzi, A.M.V., Dodgson, K.S. & White, G.F. (1984). *Biochem. J.*, **223**, 487-494.
- Crescenzi, A.M.V., Dodgson, K.S., White, G.F. & Payne, W.J. (1985). *J. Gen. Microbiol.*, **131**, 469-477.
- Ducrocq, C., Servy, C. & Lenfant, M. (1989). *FEMS Microbiol. Lett.*, **65**, 219-222.
- Ducrocq, C., Servy, C. & Lenfant, M. (1990). *Biotechnol. Appl. Biochem.*, **12**, 325-330.
- Dunstan, I., Griffiths, J.V. & Harvey, S.A. (1965). *J. Chem. Soc.*, **120**, 1325-1327.
- Feelisch, M. & Noack, E.A. (1987). *Biochem. Pharmacol.*, **139**, 19-30.
- Gorontzy, T., Drzygza, O., Kahl, M.W., Bruns-Nagel, D., Breitung, J., von Loew, E. & Blotevogel, K.-H. (1994). *Crit. Rev. Microbiol.*, **20**, 265-284.
- Jones, D., Pell, P.A. & Sneath, P.H.A. (1991). In *Maintenance of microorganisms and cultured cells*, ed. B. E. Kirsop & A. Doyle, Academic, London, pp. 45-50.
- Kaplan, D.L. (1992). *Curr. Opin. Biotechnol.*, **3**, 253-260.
- Knowles, R.G., Pallacios, M., Palmer, R.M.J. & Moncada, S. (1989). *Proc. Natl. Acad. Sci. U.S.A.*, **86**, 5159-5162.
- Knowles, R.G., Salter, M., Brooks, S.L. & Moncada, S. (1990). *Biochem. Biophys. Res. Comm.*, **172**, 1042-1048.
- Moncada, S., Radoski, M.W. & Palmer, R.M.J. (1988). *Biochem. Pharmacol.*, **37**, 2495-2501.
- Morgan, P. & Dow, C.S. Bacterial adaptations for growth in low nutrient environments. In: *Microbes In Extreme Environments*, (Herbert, R.A. & Codd, G.A., Eds), 1986, pp.187-214, Academic Press, London.
- Payne, W.J. (1981) *Denitrification*. New York. Wiley.
- Schorr, K., Woditsch, I. & Forster, S. (1991). *Blood Vess.*, **28**, 62-66.
- Servent, D., Ducrocq, C., Henry, Y., Guissani, A. & Lenfant, M. (1991). *Biochim. Biophys. Acta*, **1074**, 320-325.
- Servent, D., Ducrocq, C., Henry, Y., Servy, C. & Lenfant, M. (1992). *Biotechnol. Appl. Biochem.*, **15**, 257-266.
- Tan-Walker, R.L.B. (1987). *Techniques for analysis of explosive vapours*, PhD thesis, University of London
- Taylor, T., Taylor, I.W., Chasseaud, L.F. & Bonn, R. (1987). In *Progress in Drug Metabolism*, ed. J. W. Bridges, L. F. Chasseaud and G. G. Gibson, Taylor and Francis, London, **10**, 207-386.
- Urbanski, T. (1965). *Chemistry and Technology of Explosives*. PWN-Polish Scientific Publishers and Pergamon Press, Warsaw and Oxford,
- Walker, J.E. & Kaplan, D.L. (1992) *Biodegradation* **3**, 369-385.
- Wendt, T.M., Cornell, J.H. & Kaplan, A.M. (1978). *Appl. Envir. Microbiol.*, **36**, 693-9.
- White, G.F. & Snape, J.R. (1993). *J. Gen. Microbiol.*, **139**, 1947-1957.

Rückgewinnung von Komponenten kunststoffgebundener Treibmittel

M.A. Bohn¹, R. Schweppe¹, W. Weisweiler²

¹ Fraunhofer-Institut für Chemische Technologie (ICT), D-76327 Pfinztal

² Institut für Chemische Technik, Universität Karlsruhe, D-76128 Karlsruhe

Kurzfassung

Wirtschaftlichkeit und der Schutz der Lebensumgebung fördern Entsorgungsmethoden, die eine Rückgewinnung und Wiederverwendung von Einsatzstoffen gestatten sowie die Entstehung unerwünschter Produkte vermeiden. Dies trifft auch für Treibmittel zu. Neuere Treibmittelentwicklungen enthalten teure kristalline Energiesubstanzen wie die Nitramine Hexogen und Oktogen, gebunden in einer dreidimensional vernetzten Polyurethanmatrix; sie werden 'kunststoffgebundene Treibmittel' genannt. Zur Rückgewinnung von Komponenten wurde die Polyurethanmatrix mit reinem Wasser und alkalischem Wasser (0,05n bis 0,5n NaOH) bei Temperaturen zwischen 130 °C und 170 °C in einer Druckeinschlußzelle solvolytisch aufgespalten. Aus einem Modelltreibstoff, bestehend aus einem Polyetherdiol-Gemisch (Lupranol 1000/2021) vernetzt mit Desmodur T80 und 60 % Ammoniumperchlorat (AP) wurde die Polyetherpolyolkomponente zu 84 % bis 90 % rückgewonnen und der AP-Anteil zu 98 % im wäßrigen Solvolysat bestimmt. Die Polyetherdiole wurden auch bei einer hohen solvolytischen Belastung von 170 °C und 2 h kaum verändert, wie die Molmassenverteilungen, bestimmt mit Gelpermeationschromatographie, zeigen. Das Treibladungspulver KHP, bestehend aus 86 % Hexogen und 14 % GAP-Desmodur N100-Binder wurde bei 130 °C, 150 °C und 170 °C mit reinem Wasser und mit 0,05 n NaOH jeweils 10 min, 30 min und 60 min solvolysiert. Hexogen ist in hohen Ausbeuten und hoher Reinheit rückgewinnbar. GAP ist ebenfalls ein Polyetherdiol, formal auf der Basis von Propan-1,2-diol mit Azidgruppen an den Methylseitengruppen. Es verhält sich nicht wie die Lupranol-Polyetherdiole. Durch solvolytische Belastung wird die Molmassenverteilung verbreitert und der Azidgehalt vermindert, welcher über die Infrarotabsorption der asymmetrischen N₃-Streckschwingung und

44.2

über den Energiegehalt mit DSC relativ zum Azidgehalt des originalen GAP bestimmt wurde. Der GAP-N100-Binder wird nicht aufgespalten, GAP ist nicht rückgewinnbar. Beim Abspalten von Stickstoff aus der N_3 -Gruppe werden über das entstehende Nitren durch intermolekulare Insertionsreaktionen solvolytisch nicht spaltbare C-N-Bindungen gebildet. Die gasförmigen Hauptreaktionsprodukte bei der Solvolyse des KHP sind N_2 und N_2O , daneben etwas CO_2 , O_2 und CO . NH_3 und CH_2O wurden nicht quantifiziert. An ionischen Zersetzungsprodukten wurden gefunden: NO_2^- , NO_3^- , HCO_3^- , $HCOO^-$, NH_4^+ . Mit den in der Literatur angegebenen Mechanismen und Reaktionsprodukten für die Zersetzung des Hexogens sowie durch Reaktionen der Zersetzungsprodukte mit dem Solvolysenmittel und Reaktionen zwischen den Zersetzungsprodukten kann das Produktspektrum gedeutet werden.

1. Einleitung

Für die Entsorgung von Treib- und Explosivstoffen kommen folgende Möglichkeiten in Betracht: Verbrennen, hydrolytisches Zersetzen, Umsetzung in überkritischem Wasser (auch bei Sauerstoffzufuhr), Wiederverwendung und selektive Rückgewinnung von Komponenten. Bei der Verbrennung von Treib- und Explosivstoffen entstehen immer Schadgase wie HCN , NO_x , HCl und auch Ruß in größeren Mengen /1,2/, so daß eine aufwendige Abgasreinigung nötig ist. Aufgrund der neuen Gesetze zur Abfallverminderung und zur stofflichen Verwertung sind Entsorgungsverfahren gefragt, die eine Wiederverwendung oder eine Rückgewinnung von Einsatzstoffen gestatten. Von der Automobilindustrie wird eine Wiederverwendung oder Rückgewinnung schon ab einem Materialerzeugerpreis von 3 DM/kg als wirtschaftlich angesehen /3/. Die kristallinen Energiestoffe Hexogen und Oktogen in neuartigen Treibmittelformulierungen sind teure Komponenten, ihr kg-Preis liegt bei 35 DM und 100 DM. Auch die verwendeten Präpolymere für die dreidimensional vernetzten Polyurethanelastomerbinder sind teuer, HTPB (hydroxyterminiertes Polybutadien) kostet etwa 20-25 DM/kg, GAP (Glycidylazidpolymer) noch über 700 DM/kg.

Wegen der dreidimensionalen Vernetzung der Polyurethanmatrix ist ein einfaches Auflösen der Treibstoffe in Lösungsmitteln nicht möglich. Für eine Rückgewinnung der Energiestoffe stehen zur Wahl die Extraktion mit Lösungsmitteln und ein Aufschluß des Kunststoffbinders und Freisetzen des Energiestoffs. Beim Aufschluß

wird auch die Polyolkomponente des Polyurethanbinders zugänglich. Hier werden Ergebnisse eines Aufschlußverfahrens vorgestellt.

Die in den Treibmitteln verwendeten energetischen Substanzen wie GAP und Hexogen (RDX) weisen Entzündungstemperaturen zwischen 200 °C und 220 °C auf. Die Aufschlußtemperaturen müssen daher niedriger liegen, der Bereich zwischen 130 °C und 170 °C wurde gewählt. Das ideale Aufschluß- oder Solvolysmittel soll die Urethangruppierung schnell spalten, die Kettenlänge der Polyole nicht verändern, die energetischen Komponenten nicht angreifen und von den gewünschten Stoffen leicht abtrennbar sein. Mit Blick auf die technische Realisierung soll das Verfahren sicher handhabbar und preiswert sein. Diesem Anforderungsprofil kommen reines und alkalisches Wasser am nächsten. Um im vorgesehenen Temperaturbereich solvolysieren zu können, ist ein Druckeinschluß der Solvolysmischung erforderlich.

2. Ziel

Aus einem Treibmittel soll Hexogen (RDX) gebunden mit GAP-Desmodur N100 durch wäßrige Solvolyse zurückgewonnen werden. Die Ausbeute wird als Funktion des Solvolysmittels, nämlich reines Wasser und 0,05 n NaOH, der Solvolysezeit und der Solvolys temperaturen zwischen 130 °C und 170 °C bestimmt. Der Einfluß der Solvolysebedingungen auf die Polyolkomponente GAP wird untersucht und mit den Ergebnissen für eine nichtenergetische Polyetherpolyolkomponente verglichen. Gasförmige und ionische Zersetzungsprodukte werden ermittelt.

3. Substanzen

Für die Solvolysen wurde das Rohrwaffentreibmittel KHP verwendet, welches etwa 86 Ma.-% feinkörniges RDX gebunden in 14 Ma.-% GAP-Desmodur N100 enthält. GAP und KHP wurden im ICT hergestellt /4/, RDX von Dyno Industrier AS, Norwegen, und Desmodur N100 von Bayer AG, Leverkusen, bezogen. GAP ist ein Polyetherdiol, formal ein kondensiertes Propan-1,2-diol mit Azidgruppen an den Methylseitengruppen. Zum Vergleich wurde ein Kunststoffbinder aus den handelsüblichen Polyetherpolyolen Lupranol 1000 und 2021 (BASF AG, Ludwigshafen) herge-

stellt, Vernetzer war Desmodur T80 (80 Ma.-% 2,4- und 20 Ma.-% 2,6-Toluoldiisocyanat, Bayer AG). Der Binder bestand aus 78,8 Ma.-% Lupranol 1000, 11,7 Ma.-% Lupranol 2021, 8,3 Ma.-% Desmodur T80, der Rest sind Hilfsstoffe. Mit diesem Bindertyp wurde auch ein Modell-Raketenfesttreibstoff mit 60 Ma.-% Ammoniumperchlorat hergestellt /4/.

4. Apparatur

Die Solvolysen wurden in einer zylindrischen Druckeinschlußzelle durchgeführt, Abb. 1, welche aus einem warmfesten, korrosionsbeständigen Edelstahl vom Typ Thermanit 4575 (1880 SST, Werkstoffnr. 1.4575) im ICT hergestellt wurde /5/. Der Zellkörper hat eine Höhe von 140 mm und einen Außendurchmesser von 68 mm. Das Innenvolumen beträgt 44 ml, der Innendurchmesser 23 mm. Der Reaktionsraum wird mit einem in einer Nut des Stempels S gehaltenen O-Ring aus Viton gedichtet. Durch eine Bohrung im Stempel S wird ein Fe/CuNi-Mantelthermoelement, eingelötet in einer Druckverschraubung, in den Reaktionsraum eingeführt, so daß zur Temperaturmessung und zur Regelung der elektrischen Außenheizung (Widerstandsheizband gewickelt auf einen Aluminiumträger) die Temperatur der Solvolysenmischung verwendet werden kann, welche mit einem teflonummantelten Rührstabmagneten gewirbelt wird. Der Druck wird mit einem Dehnungsmeßstreifen (DMS)-Druckaufnehmer gemessen und über ein kalibriertes Anzeige- und Versorgungsgerät (Burster GmbH, Gernsbach) in bar angezeigt. Die beim Aufschluß gebildete Gasmenge wird mit einer Gasbürette oder mit einem Kolbenprober bestimmt.

5. Durchführung der Solvolysen, Aufarbeitung der Solvolysate und Analyse der Solvolyseprodukte

Für die Solvolysen wurde das Reaktionsvolumen der Druckeinschlußzelle zu etwa 60 % mit der Solvolysenmischung, 1 g zerkleinerte Probensubstanz und 20 g bis 25 g Solvolysenmittel gefüllt. Der freie Reaktionsraum wurde evakuiert und mit 1 bar Helium wieder aufgefüllt. Nach der Solvolyse wurde schnellstmöglich auf Raumtemperatur abgekühlt und die entstandene Gasmenge bestimmt.

Als Solvolysat erhält man eine wäßrige Phase mit ionischen Reaktionsprodukten und beim KHP einen festen Rückstand, der aus Hexogen und Binder besteht. Die wäßrige Phase wurde vom festen Rückstand abgetrennt und das Hexogen mit Aceton ausgewaschen. Das Aceton wurde abgezogen und die trockenen Rückstände ausgewogen. Neben der gravimetrischen Bestimmung wurde das Hexogen auch mit Hochleistungsflüssigkeitschromatographie (HPLC) quantifiziert. Bei der Solvolyse des Lupranolbinders entstand neben der wäßrigen Phase eine ölige Phase, bestehend im wesentlichen aus den freigesetzten Polyolen, welche mit Dichlormethan extrahiert wurden.

Die Molmassenverteilungen der Lupranole und des GAP wurden mit einem Gelpermeationschromatograph bestimmt, bestehend aus dem Hewlett-Packard Flüssigkeitschromatograph 1084B, dem ERMA-Brechungsindexdetektor ERC 7510 und aus vier in Serie geschalteten Polymer Laboratories GPC-Säulen mit den Porenweiten 10^3 nm, 10^2 nm, 10 nm und 5 nm sowie $10\text{ }\mu\text{m}$ Teilchengröße. Laufmittel war Tetrahydrofuran, kalibriert wurde mit engverteilten Polystyrolstandards.

Die Ionen Nitrat, Nitrit, Hydrogencarbonat, Formiat und Ammonium wurden mit einem GAT-Ionenchromatograph mit Alltech Wescan 315 Leitfähigkeitsdetektor analysiert. Die Säulen waren für HCO_3^- , NO_2^- , NO_3^- eine Wescan Anion/R-Säule, für Formiat eine Wescan Anionenausschlußsäule und für NH_4^+ eine Wescan Cation/S-Säule.

Die Gase Stickstoff, Sauerstoff, Methan und Kohlenmonoxid wurden mit einer Molsieb 5\AA -Säule getrennt, Kohlendioxid und Distickstoffmonoxid mit einer Poropak Q-Säule, nachgewiesen wurde mit einem Wärmeleitfähigkeitsdetektor, Trägergas war Helium. Der Gaschromatograph war von der Fa. FISONs, Typ GC 6000 VEGA, Serie 2. Die Gase NO/NO_2 wurden mit dem NO_x -Analysator 951A der Fa. Beckman Instruments quantifiziert.

Für die HPLC-Analyse wurde eine Anlage der Fa. Waters mit der Millennium 2010-Datenerfassung und -auswertung verwendet, zusammen mit dem Waters Photodiodenarraydetektor 996. Die Trennsäule war eine Umkehrphasensäule Typ C-18, mobile Phase Wasser/Methanol.

6. Ergebnisse und Diskussion

6.1 Solvolyse eines Festtreibstoffbinders mit inerten Polyetherpolyolen

Zwei Modell-Festtreibstoffproben und die dafür verwendeten Polyetherdiole Lupranol 1000 und Lupranol 2021 wurden bei 170 °C mit reinem Wasser, 0,1 n NaOH und 0,5 n NaOH zwei Stunden solvolysiert. Die Einwaagen lagen zwischen 0,4 g und 1 g. Es wurden bewußt drastische Bedingungen gewählt, um eine abbauende Wirkung zu erkennen. Beide Diole werden praktisch nicht verändert, wie die Molmassenverteilungen (MMV) der unbelasteten und belasteten Proben zeigen, Abb. 2 und Abb. 3. Die charakteristischen Molmassenwerte M_n (Zahlenmittel), M_w (Massenmittel), M_z (Z-Mittel) und M_{max} (Maximumlage der MMV) sind nur sehr wenig zu niedrigeren Werten verschoben, Tabelle 1.

Der Binder mit 60 % Ammoniumperchlorat (FTS-1) und der reine Binder (FTS-2) sind bei 170 °C mit 0,5 n NaOH vollständig aufschließbar. Die Polyolkomponenten sind in hohen Ausbeuten erhältlich. Aus FTS-1 sind im Mittel 84 %, aus FTS-2 über 90 % an Lupranol wiedergefunden worden. Der Anteil an freigesetztem Ammoniumperchlorat wurde über das Perchloratanion bestimmt, er lag bei 98 %. Bei FTS-1 kam es zu leichter Gasbildung, etwa 8,1 ml pro g FTS-1. Bei den anderen Solvolysen wurde keine Gasbildung festgestellt. Die MMV-Daten der Lupranole aus FTS-1 und FTS-2 sind in Tabelle 1 enthalten; auch hier fielen die Änderungen der MMV gegenüber den originalen Diolen gering aus.

Im Gegensatz dazu ließ sich der FTS-Binder HTPB-IPDI (Hydroxyterminiertes Polybutadien-Isophorondiisocyanat) durch einfache Hydrolyse nicht aufspalten /6/.

6.2 Solvolyse des energetischen Polyetherpolyols GAP und Azidgruppenbestimmung

Als Polyetherdiol sollte sich GAP solvolytisch wie die Lupranole verhalten. Es wurde ebenfalls zunächst bei den hoch belastenden Solvolysebedingungen, 170 °C, 2 h, untersucht. Solvolysenmittel waren reines Wasser, 0,05 n NaOH sowie zusätzlich n-Heptan und Toluol. Alle behandelten GAP-Proben waren wie unbehandeltes GAP in

Dichlormethan löslich und ähnlich viskos, letzteres bis auf die mit 0,05 n NaOH solvolysierte Probe, sie war deutlich weniger viskos. Die Molmassenverteilungen der behandelten Proben unterscheiden sich im Vergleich zu dem Ergebnis bei den Lu-
pranolen viel mehr von der originalen Probe. Die Verteilungen werden niedriger und breiter, besonders nehmen die Anteile auf der höhermolekularen Seite zu, Abb. 4.

Um die belasteten Proben weiter zu charakterisieren, wurde der Azidgruppengehalt mit der Infrarotabsorption der asymmetrischen N_3 -Streckschwingung bei 2100 cm^{-1} und über den mit der DSC bestimmten Energiegehalt ermittelt. Die IR-Azidgruppenbestimmung erfolgte mit dem schon beschriebenen Verfahren /7/. Mit Kalibrierlösungen von unbehandeltem GAP in Dichlormethan wurde die spezifische Absorption der asymmetrischen N_3 -Streckschwingung erhalten. Zur Steigerung der Genauigkeit wurden integrierte Bandenintensitäten verwendet /8/. Da die niederfrequente Halbbande nur im Auslauf Störungen aufweist, wurde vom Bandenmaximum bei 2104 cm^{-1} bis zu 2064 cm^{-1} integriert.

Nach Lambert-Beer gilt

$$(1) \quad A(\sigma) = \lg \frac{I_R(\sigma)}{I_p(\sigma)} = \epsilon(\sigma) \cdot c \cdot l$$

mit:

σ :	Wellenzahl [cm^{-1}]
$A(\sigma)$:	Absorbanz (Extinktion)
$I_R(\sigma)$:	Intensitätsspektrum der Referenzprobe
$I_p(\sigma)$:	Intensitätsspektrum der Probe
$\epsilon(\sigma)$:	Massenabsorptivität [Fläche/Masse]
c :	Konzentration [Masse/Volumen]
l :	geometrische Schichtlänge [Länge].

Referenzprobe war Dichlormethan. Die Spektren wurden mit einem Fourier-Transform-IR-Spektrometer der Fa. Nicolet, Typ 60SX, in einer Flüssigkeitszelle mit NaCl-Fenstern bei 4 cm^{-1} Auflösung aufgenommen. Die Schichtlänge betrug $5,02 \cdot 10^{-3}\text{ cm}$. Mit der integrierten Intensität, Gl. (2), wurde die N_3 -Gehalt-Abnahme relativ zum N_3 -Gehalt des unbelasteten GAP, Gl. (3), bestimmt.

$$(2) \quad B(\sigma) = \int_{\sigma_1}^{\sigma_2} \varepsilon(\sigma) d\sigma = \int_{\sigma_1}^{\sigma_2} \frac{A(\sigma)}{l \cdot c} d\sigma$$

$$(3) \quad \text{relativer N}_3\text{-Gehalt} = \frac{B(\sigma) [\text{behandeltes GAP}]}{B(\sigma) [\text{unbehandeltes GAP}]}$$

Der Energiegehalt des GAP ist proportional dem N₃-Gehalt. DSC-Thermogramme, Aufheizrate 2 °C/min, der GAP-Proben wurden zwischen 170 °C und 260 °C ausgewertet. Unbehandeltes GAP setzt eine Energie von 2447 J/g frei. Das Verhältnis der Zersetzungsenergien der behandelten GAP-Proben zu originalem GAP ist ein Maß für den relativen N₃-Gehalt. Mit der Infrarotabsorption ist auch der absolute N₃-Gehalt bestimmbar /7/. Die Ergebnisse sind zusammen mit den Molmassenwerten in Tabelle 2 aufgelistet. Beide Bestimmungsmethoden für den relativen N₃-Gehalt stimmen im Rahmen der Reproduzierbarkeit (DSC ± 3 %, IR-Absorption ± 2 %) gut überein.

Das Polyetherdiol GAP sollte als Binder aus GAP und Desmodur N100 wie die Lupranolbinder völlig aufgespalten werden. Es wurde bei 170 °C eine Stunde mit 0,05 n NaOH solvolysiert. Der GAP-Binder verhält sich allerdings nicht wie der Lupranolbinder. Es entstand ein in Dichlormethan löslicher Anteil von nur 1 % der Einwaage. Der feste Rückstand konnte auch in Lösungsmitteln nicht gelöst werden. Die Ursache ist vermutlich eine Vernetzung über die Stabilisierungsreaktion des bei der Stickstoffabspaltung aus der N₃-Gruppe gebildeten, sehr reaktiven Nitrens, welches sofort intra- und intermolekulare Insertionsreaktionen eingeht und somit zu solvolytisch nicht spaltbaren C-N-Bindungen führt. Bei den Solvolysen des GAP und des GAP-N100-Binders war auch eine Gasentwicklung zu beobachten. Gefunden wurden N₂, N₂O, wenig CO, CO₂, O₂ und NO_x in ppm-Mengen. An ionischen Produkten wurde Ammonium nachgewiesen, NH₃ in der Gasphase wurde nicht bestimmt. Die Tabelle 3 zeigt die gefundenen Gasmengen für 20 °C, 1 atm bezogen auf 1 g Probe.

6.3 Solvolyse des KHP

Das KHP wurde bei 130 °C, 150 °C und 170 °C mit reinem Wasser und mit 0,05 n NaOH über jeweils 10 min, 30 min und 60 min solvolysiert. Abb. 5 zeigt die Hexogenausbeuten sowohl graphisch als auch tabellarisch. Mit steigender Alkalität, Solvolysezeit und Solvolysetemperatur nimmt die Ausbeute ab. Bereits eine zehnminütige Hydrolyse bei 130 °C erlaubt eine Rückgewinnung des Hexogens zu über 95 %. Mit DSC und Schmelzpunktbestimmung wurde die Reinheit des Hexogens nachgewiesen, die Übereinstimmung mit dem eingesetzten Hexogen erwies sich als sehr gut. Es gab immer ein Binderrückstand aus den Gründen wie in Abschnitt 6.2 diskutiert.

Bei allen Solvolysen des TLP KHP trat eine Gasentwicklung auf. Abb. 6 zeigt die bestimmten Gesamtgasvolumina. Hauptkomponente war N₂, gefolgt von N₂O, CO₂, O₂ und CO. In Abb. 7 sind für eine Solvolyse bei 170 °C, 1 h für beide Solvolysemittel die Gasmengen der Einzelkomponenten pro g KHP angegeben. Der Binderanteil beträgt beim KHP nur 14 %. Entsprechend den Daten aus Tabelle 3 für die GAP-Solvolysen erkennt man, daß die Hauptmengen der gasförmigen Produkte aus der Zersetzung des Hexogens stammen.

Von einigen Solvolyselösungen sind in der Tabelle 4 die ionischen Reaktionsprodukte Nitrit NO₂⁻, Nitrat NO₃⁻, Hydrogencarbonat HCO₃⁻ und Ammonium NH₄⁺, zusammengestellt. Beim Abbau des Hexogens wird auch Formiat gebildet. In der Literatur, siehe Abschnitt 6.4.2, wird für die wäßrige alkalische Hydrolyse die Bildung von Formaldehyd CH₂O, und Ammoniak NH₃, angegeben. Formaldehyd wurde organoleptisch erkannt, konnte aber nicht quantifiziert werden. Die zitierte Arbeit sagt nichts über die Bildung von Nitrat aus, welches hier in deutlichen Mengen gefunden wurde. Die dortigen Untersuchungsbedingungen waren jedoch auch andere: 25 °C, 35 °C und 45 °C und nur geringe Konzentrationen an RDX gelöst in Wasser.

6.4 Zersetzungsmechanismen für Hexogen

Da bei relativ hohen Temperaturen solvolysiert wurde, sollte auch mit thermischer Zersetzung gerechnet werden. Aus der adiabatischen Selbstaufheizung, gemessen mit dem 'Accelerating Rate Calorimeter' (ARC, Columbia Scientific Industries, USA) /9/, kann auf eine thermisch ausgelöste Zersetzung in der kristallinen Phase schon unterhalb von 180 °C geschlossen werden. In verdünnten Lösungen von Cyclohexanon oder Wasser liegt der mit dem ARC erkennbare Zersetzungsbeginn bereits um 120 °C.

6.4.1 Thermische Zersetzung des Hexogens

Die thermische Zersetzung des Hexogens und ihre kinetisch-mechanistische Deutung ist kompliziert, schon vielfach untersucht worden und noch Gegenstand der Forschung. Die Reaktionsprodukte der Zersetzungsreaktion wurden im Temperaturbereich von 180 °C bis 300 °C von mehreren Arbeitsgruppen bestimmt. Sie variieren etwas quantitativ aber auch qualitativ, je nach Versuchsführung und wohl auch mit der analytischen Leistungsfähigkeit.

Eine der früheren umfangreichen Arbeiten ist von Robertson /10/. Er untersuchte die RDX-Zersetzung im Temperaturbereich 213 °C bis 299 °C mit Mengen zwischen 4 mg und 45 mg und fand folgende Reaktionsprodukte (mol/mol RDX): N₂ (1,16), N₂O (0,98), NO (0,54), CO₂ (0,48), CO (0,40), H₂ (0,09) und nicht quantifiziert CH₂O und H₂O. Er wies kein NO₂, NH₃ und HCN nach.

Rauch und Fanelli /11/ fanden zusätzlich HCN, konnten NO₂ bei der Gasphasenzersetzung nachweisen, geben aber kein N₂ an.

Batten /12/ erkannte, daß CH₂O die Zersetzung des RDX in der festen und flüssigen Phase beschleunigt. NO₂ hat eine retardierende Wirkung, was auf die Reaktion des NO₂ mit CH₂O und damit dessen Entfernung zurückgeführt wird.

Cosgrove und Owen /13/ versuchten das Produktspektrum vollständig zu erfassen.

Sie fanden bei 195 °C folgende Reaktionsprodukte (mol/mol RDX): N₂ (1,26), N₂O (1,08), NO (0,51), CO₂ (0,70), CO (0,36), CH₂O (1,04), HCOOH (0,37), NH₃ (0,34), NO₃⁻ (0,1), NO₂⁻ (0,02). Als Zersetzungsrückstand wurde N-Hydroxy-N-Methylformamid identifiziert. Auch sie fanden, daß CH₂O die Zersetzung von RDX fördert. Bei ihrer Versuchsführung war die Zersetzung in der Gasphase dominierend.

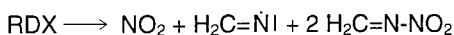
Hoffsommer und Glover /14/ untersuchten die Zersetzung von RDX in Benzol und D6-Benzol zwischen 180 °C und 200 °C und in der Schmelze bei 210 °C. In den benzolischen Lösungen nahm RDX nach einer Reaktion 1. Ordnung, in der Schmelze nach 0. Ordnung ab. Sie identifizierten als Reaktionsprodukt im geschwindigkeitsbestimmenden Schritt N-Nitroso-'RDX', eine NO₂-Gruppe ist durch eine NO-Gruppe ersetzt. Die N-NO-Gruppe entstand durch die Abspaltung einer OH-Gruppe aus N-NO₂ nach der Protonenabstraktion vom Lösungsmittel Benzol.

Pfeil, Krause und Eisenreich /15/ untersuchten die thermische RDX-Zersetzung bei sehr unterschiedlichen Aufheizraten: IR-spektroskopische Analyse der Gasentwicklung bei etwa 5 °C/min, Abbrand in der optischen Bombe bei 10⁵ bis 10⁶ °C/min mit UV-VIS-Analyse der Flammenreaktionsprodukte NH, CH, OH und CHO/CH₂O sowie Laserimpulsaufheizung mit etwa 10¹¹ °C/min und flugzeitmassenspektrometrischer Analyse der Pyrolyseprodukte NO, H₂CN, CN, HCN und je nach Pulsenergie Ringfragmente wie H-C-N, N-CH₂-N, N-CH₂-N-CH₂, N-CH₂-N-CH₂-N. Die Ringbruchstücke spalten schnell NO₂ ab. Bei langsamer thermischer Zersetzung (5 °C/min) wurden folgende Reaktionsprodukte gefunden: N₂O, CH₂O, HCN, NO, CO₂, CO, H₂O, CH₃OH und NH₃. Nicht detektiert werden konnte eventuell gebildetes N₂. Aus der zeitlichen Entwicklung der Reaktionsprodukte wurde geschlossen, daß N₂O, CH₂O und HCN primäre Reaktionsprodukte sind, NO und CO₂ sowie die anderen Produkte entstehen durch Reaktion aus oder zwischen den Reaktionsprodukten, vermutlich unter NO₂-Beteiligung. Diese Ergebnisse lassen auf ein C-N-Bindungsbruch als Hauptreaktion bei langsamer Zersetzung schließen. Bei schneller Aufheizung zerfällt das RDX-Molekül isoliert in der Gasphase, so daß hier N-N-Bindungsbruch und NO₂-Abspaltung zu den primären Reaktionsschritten zählen. C-N-Bindungsbruch dominiert in der kondensierten Phase.

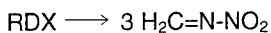
Behrens und Bulusu /16/ teilen die bisherigen Ergebnisse in ein Schema der Hauptzersetzungswegen ein:

44-12

- N-N-Bindungsspaltung mit NO₂-Bildung



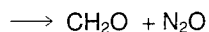
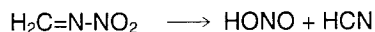
- konzertierte Dreifach-Spaltung



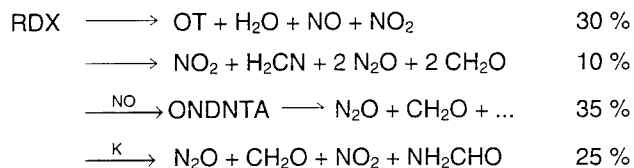
- HONO-Eliminierung



Das Methylennitramin kann in zwei Weisen zerfallen:



In der kristallinen Phase zersetzt sich RDX langsam, sehr viel schneller in der flüssigen Phase bzw. in der Schmelze. Die Autoren fanden folgende Reaktionsprodukte (keine Umsatzangaben): N₂O, CH₂O, NO, CO, HCN, H₂O, NO₂, HONO, NH₂CHO, CH₃-NH-CHO, Oxytriazin (OT), 1-Nitroso-3,5-Dinitrohexahydrotriazin (ONDNTA). Bei ihrer Reaktionsführung in einer speziellen TGA-MS-Apparatur wurde kein N₂ gefunden, auch nicht NH₃, HCOOH, CO₂. Für ihre Ergebnisse geben sie folgende vier Zersetzungswege mit einer Vorkommenswahrscheinlichkeit an:



K ist ein Katalysator aus dem Produktspektrum, der nicht näher bezeichnet wurde.

Die Bildung des Produkts Oxytriazin ist in der Abb. 8 dargestellt. Die Reaktionswege zu seiner Bildung wurden aus Isotopenmarkierungsergebnissen geschlossen. ONDNTA bildet sich durch Abspalten eines NO₂-Radikals und anschließende Addition eines NO-Radikals.

6.4.2 Zersetzung des Hexogens in wäßrigen Lösungen

Das Produktspektrum der Zersetzung des Hexogens bei der wäßrigen und alkalischen Hydrolyse ist ähnlich zu dem bei der thermischen Zersetzung. Die Bildung ionischer Produkte ist jedoch stark ausgeprägt.

Somlo /17/ fand 1940 bei der alkalischen Hydrolyse des RDX bei 60 °C in 1 n NaOH folgende Reaktionsprodukte pro mol umgesetztem Hexogen:

0,8 m als Summe von NO_3^- und NO_2^- ,

3,5 m Säuren, davon 2,7 m organische Säuren, er vermutete HCOOH ,

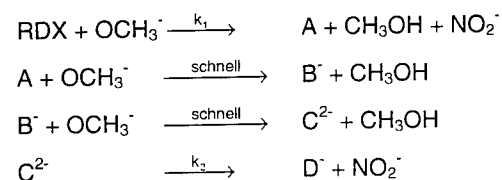
0,88 m NH_3 ,

1,89 m N_2

und nicht quantifizierter Formaldehyd.

Epstein und Winkler /18/ führten eine alkalische Hydrolyse in acetonischer Lösung bei 0 °C und 15,5 °C durch. Ihr RDX wurde schnell zersetzt, sie gaben keine Reaktionsprodukte an.

Jones /19/ untersuchte die Reaktion von RDX in methanolischer Lösung mit $\text{CH}_3\text{OH}/\text{KOH}$, CH_3ONa und CH_3OLi zwischen 19 °C und rund 45 °C. Er stellte aus seinen Ergebnissen folgendes Reaktionsschema auf:



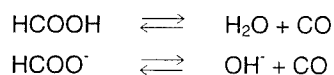
Die Reaktionsgeschwindigkeitskonstanten k_1 und k_2 haben folgende Eyring-Parameter:

	ΔH^\ddagger [kJ/mol]	ΔS^\ddagger [J/K/mol]	E_a [kJ/mol]	Δn^\ddagger
k_1	116,7	98,7	121,7	-1
k_2	92	-33	92	1

Eine detaillierte Arbeit wurde von Hoffsommer, Kubose und Glover /20/ bei 25 °C, 35 °C und 45 °C und mit 0,02 n bis 0,25 n NaOH durchgeführt. Sie verwendeten zur mechanistischen Deutung auch deuteriertes RDX. Die Autoren fanden folgende Hydrolyseprodukte (mol/mol RDX): NO_2^- (1,1), N_2O (1,2), CH_2O (1,1), N_2 (0,12), NH_3 (0,9), HCOO^- (0,7). Nicht gefunden wurden: NO_3^- , CO , CO_2 , NO , NO_2 und O_2 . Aus dem H/D-kinetischen Isotopeneffekt schlossen sie auf die Abspaltung von H^+ durch OH^- von einer Methylengruppe des RDX als ersten Reaktionsschritt, verbunden mit einer konzertierten Abspaltung eines Nitritions. Es entsteht 1,3,5-Triaza-3,5-Dinitrocyclohexen-1, siehe Abb. 9, (I). Dieser Reaktionsschritt wurde auch schon von Jones /19/ vermutet. Das Produkt (I) wurde aber von Hoffsommer u.a. nicht definitiv nachgewiesen, es wird nur darauf geschlossen. Es ist zu vermuten, daß ein weiteres Molekül HONO in einer schnellen Reaktion eliminiert wird und erst dieses Produkt (II), Abb. 9, weiter hydrolysiert wird. Dies ist ein ähnlicher Weg wie bei der Bildung des Oxytriazins, Abb. 8. Die Autoren isolierten ein Hydrolyseprodukt und nahmen (I) an, doch im Massenspektrum konnten sie nur (II) nachweisen.

Die $-\text{N}=\text{CH}$ -Gruppen in den Hydrolyseprodukten (I) oder (II) werden zu HCN und dieses bei den hier vorliegenden Solvolysebedingungen weiter zu HCOOH und NH_3 hydrolysiert, womit ein Weg zu diesen Reaktionsprodukten gegeben ist. Nach der Abspaltung der zwei HCN-Gruppen in (II) kann das Methylennitramin zerfallen in CH_2O und N_2O , Abb. 10, es ist auch der Weg zu HCN und HONO möglich. Aus dem Produktspektrum der KHP-Solvolyse kann man schließen, daß in der wäßrigen Phase die Bildung von CH_2O und N_2O überwiegt, da eine relativ starke N_2O -Bildung gefunden wurde.

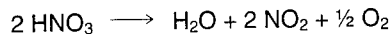
Die bisher angegebenen Zerfallsreaktionen erklären nicht alle Reaktionsprodukte, es fehlen noch CO_2 , CO , N_2 , O_2 und NO_3^- . Bildungsmöglichkeiten sind Reaktionen von und zwischen den Produkten. Ameisensäure kann zu H_2O und CO zerfallen:



Nitrit wird in größerer Menge gebildet. Da der pH-Wert während der Solvolyse durch Verbrauch des OH^- abnimmt, kann die salpetrige Säure disproportionieren:

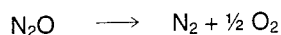


Dies erklärt das Auftreten von NO_3^- und die geringen Konzentrationen an NO_2^- in den vorliegenden Hydrolysen. NO selbst kann unter diesen Bedingungen, da die Versuche unter Heliumatmosphäre durchgeführt wurden, wieder zu HNO_2 reagieren. Da jedoch O_2 als Reaktionsprodukt gefunden wurde, wäre eine mögliche Quelle der Zerfall der HNO_3 :

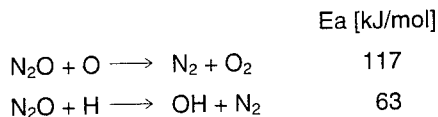


NO_2 kann CO zu CO_2 und CH_2O zu HCOOH oxidieren.

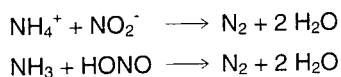
N_2O ist bei den Temperaturen der Solvolysen thermodynamisch instabil, die Zerfallsreaktion ist aber durch die mittelhohe Aktivierungsenergie von etwa 250 kJ/mol gehemmt.



Es gibt jedoch Reaktionen mit niedrigeren Aktivierungsenergien, z.B. /21/



Für Stickstoff als Reaktionsprodukt fehlt noch ein bei diesen Reaktionsbedingungen möglicher Entstehungsweg. Es ist bekannt, daß NH_4^+ und NO_2^- zu N_2 und H_2O reagieren:



Dieser Entstehungsweg vermindert sowohl NO_2^- als auch NH_3 bzw. NH_4^+ im Reaktionsproduktspektrum, wie auch in weiteren Arbeiten gefunden wurde.

7. Zusammenfassung

Es wurde die Rückgewinnung von Polyetherpolyolen und Ammoniumperchlorat (AP) aus einem Modell-Festtreibstoff (FTS) mit 60 % AP und von Hexogen und GAP aus dem Treibladungspulver KHP durch Solvolyse mit reinem Wasser und alkalischem Wasser (0,05 n bis 0,5 n NaOH) zwischen 130 °C und 170 °C untersucht.

Der FTS-Binder, hergestellt aus den Polyetherdiolen Lupranol 1000 und 2021 und dem Vernetzer Desmodur T80, ist solvolytisch gut aufschließbar, die Polyole können in Ausbeuten bis über 90 % rückgewonnen werden. Der freigesetzte AP-Anteil wurde über das Perchloratanion ionenchromatographisch bestimmt, er lag bei 98 %. Die Lupranole werden auch bei hohen solvolytischen Belastungen, 170 °C, zwei Stunden Solvolysezeit, kaum verändert, wie der Vergleich der Molmassenverteilungen (MMV) zwischen den originalen und den rückgewonnenen Diolen zeigt.

GAP ist ebenfalls ein Polyetherdiol auf der Basis Propan-1,2-diol mit Azidgruppen. Ein GAP-Binder sollte sich solvolytisch wie ein Lupranol-Binder verhalten. Das ist nicht der Fall. Durch die Abspaltung von Stickstoff aus der N_3 -Gruppe bildet das dadurch entstehende sehr reaktive Nitren intermolekulare C-N-Bindungen, welche solvolytisch nicht spaltbar sind. Die N_3 -Gehaltabnahme durch die solvolytische Belastungen wurde über die Infrarotabsorption der asymmetrischen N_3 -Streckschwingung und über die Abnahme des mit der DSC bestimmten Energiegehalts untersucht. In reinem Wasser bei 170 °C und einer Stunde Solvolysezeit nimmt der N_3 -Gehalt um etwa 9 % bis 10 % ab, bei zwei Stunden sind es 18 %. Die MMV der solvolysierten GAP-Proben werden niedriger und breiter, der höhermolekulare Anteil nimmt zu.

Das KHP wurde bei 130 °C, 150 °C und 170 °C mit reinem Wasser und 0,05 n NaOH solvolysiert, mit Solvolysezeiten von jeweils 10 min, 30 min und 60 min. Mit steigender Alkalität, Solvolysezeit und Solvolysetemperatur nimmt die Ausbeute an Hexogen ab. Bereits eine zehnminütige Hydrolyse bei 130 °C erlaubt eine Rückgewinnung des Hexogens von über 95 %. Dessen Reinheit war hoch, wie die Übereinstimmung des Schmelzpunktes mit dem für das KHP verwendeten Hexogen zeigte. Die Rückgewinnung des GAP war nicht möglich.

Bei allen Solvolysen des KHP entstanden als Zersetzungsprodukte Gase und Ionen. Bei den Gasen war N_2 die Hauptkomponente, gefolgt von N_2O , daneben wurden noch CO_2 , O_2 und CO nachgewiesen. NH_3 und CH_2O wurden nicht quantifiziert. Ionische Produkte sind NO_2^- , NO_3^- , HCO_3^- , $HCOO^-$ und NH_4^+ . Aus den Untersuchungen zum Zersetzungsverhalten von Hexogen sowohl thermisch, in Lösung von organischen Lösungsmitteln als auch in wäßrigen, alkalischen Lösungen kann man schließen, daß N_2 , O_2 , CO , CO_2 , $HCOOH$ und NH_3 erst durch Reaktionen zwischen den Zersetzungsprodukten und der Zersetzungsprodukte mit dem Solvolysenmittel gebildet werden.

8. Literatur

- /1/ F. Volk, H. Bathelt, R. Jakob
„Reaktionsprodukte von Treib- und Sprengstoffen.“
19th Internat. Annual Conference of ICT, Karlsruhe, 1988,
Fraunhofer-Institut für Chemische Technologie.

M. A. Bohn, F. Volk
„Reaction Products of Propellants and Explosives and their Influence on the Environment.“
Proceed. 17th ADPA-Environmental Symposium, Atlanta, Georgia, USA, 1990.
- /2/ P. Ase, W. Eisenberg, S. Gordon, K. Taylor, A. Snelson
„Propellant Combustion Product Analysis on a M16 Rifle and a 105 mm
Caliber Gun.“
J. Environ. Sci. Health A20, 337 (1985).
- /3/ Proceed. 2nd Internat. Symposium on Sophisticated Car Occupant Safety
Systems, 'airbag 2000', Karlsruhe 1994, Fraunhofer-Institut für Chemische
Technologie.
- /4/ GAP: Dr. Wasmann, ICT,
KHP: Dr. Schedlbauer, ICT,
Modell-FTS: Dr. Menke, Herr Eisele, ICT.
- /5/ Mithilfe von Dr. Hirth, ICT.
- /6/ M.A. Bohn, H. Neumann
„Rückgewinnung von Treibmittelkomponenten durch Hochdruck-
Hochtemperatur-Solvolyse.“
Proceed. 22nd Internat. Annual Conference of ICT, Karlsruhe, 1991,
Fraunhofer-Institut für Chemische Technologie.

- /7/ R. Schweppe, M.A. Bohn
„Bestimmung des Azidgruppengehalts in Azidbindern und Azidowechmachern.“
Proceed. 25th Internat. Annual Conference of ICT, Karlsruhe, 1994, Fraunhofer-Institut für Chemische Technologie.
- /8/ M.A. Bohn
„Untersuchung der intermolekularen Wechselwirkung und der Dynamik von CHClF_2 bis zu hohen Temperaturen und Drücken mit Infrarotabsorption zwischen 9200 cm^{-1} und 10 cm^{-1} .“
Dissertation, Universität Karlsruhe, 1984.
- /9/ M.A. Bohn, F. Volk
„Adiabatische Selbstaufheizung bei Treib- und Explosivstoffen.“
Proceed. 24th. Internat. Annual Conference of ICT, Karlsruhe, 1993, Fraunhofer-Institut für Chemische Technologie.
- /10/ A.J.B. Robertson
„The Thermal Decomposition of Explosives II. RDX and HMX.“
Trans. Farad. Society 45, 85 (1949).
- /11/ F.C. Rauch, A.J. Fanelli
„The Thermal Decomposition of RDX above the Melting Point: Evidence for Both a Gas and Liquid Phase Decomposition.“
J. Phys. Chem. 73, 1604 (1969).
- /12/ J.J. Batten
„The Thermal Decomposition of RDX at Temperatures below the Melting Point.“
Aust. J. Chem. 24, 945 (1971).
- /13/ J.D. Cosgrove, A.J. Owen
„The Thermal Decomposition of RDX-Part I: The Products and Physical Parameters.“
Combust. Flame 22, 13 (1974).
- /14/ J.C. Hoffsommer, D.J. Glover
„Thermal Decomposition of RDX: Kinetics of Nitroso Intermediates Formation.“
Combust. Flame 59, 303 (1985).
- /15/ A. Pfeil, H. Krause, N. Eisenreich
„Zersetzungsmechanismen von RDX in unterschiedlich thermischer und chemischer Umgebung.“
Proceed. 19th Internat. Annual Conference of ICT, Karlsruhe, 1988, Fraunhofer-Institut für Chemische Technologie.
- /16/ R. Behrens, S. Bulusu
„Thermal Decomposition of Energetic Materials.“
J. Phys. Chem. 96, 8877 (1992) und
J. Phys. Chem. 96, 8891 (1992).

- /17/ F. Somlo
„Einige Bemerkungen über die Beständigkeit von Hexogen und Penthrit gegen Alkali.“
Zeitschrift für das gesamte Schieß- und Sprengstoffwesen 35, 175 (1940).
- /18/ S. Epstein, C.A. Winkler
„Studies on RDX and Related Compounds.“
Can. J. Chem. 29, 731 (1951)
- /19/ W.H. Jones
„Mechanism of the Homogeneous Alkaline Decomposition of RDX: Kinetics of Consecutive Second- and First-Order Reactions. A Polarographic Analysis for RDX.“
J. Am. Chem. Soc. 76, 829 (1954).
- /20/ J.C. Hoffsommer, D.A. Kubose, D.J. Glover
„Kinetic Isotope Effects and Intermediate Formation for the Aqueous Alkaline Homogeneous Hydrolysis of RDX.“
J. Phys. Chem. 81, 380 (1977).
- /21/ W.C. Gardiner
„Combustion Chemistry“
Springer-Verlag, New York, Berlin, Heidelberg, Tokyo, 1984.

9. Tabellen und Abbildungen

Tabelle 1: Solvolysen der Lupranole 1000 und 2021 bei 170 °C und 2 h.

Probe	Solvolysemittel	rückgew. Lupranolanteil [Ma.-%]	Mn	Mw	Mz	Mmax
Lupranol 1000	-	-	3280	3430	3560	3490
	H ₂ O	98	-	-	-	-
	0,1 n NaOH	79,5	3120	3280	3420	3380
	0,5 n NaOH	88	3100	3250	3390	3340
Lupranol 2021	-	-	6220	6540	6840	6790
	H ₂ O	97	5650	5990	6300	6250
	0,1 n NaOH	78	5880	6230	6550	6500
	0,5 n NaOH	85	5940	6250	6550	6470
Lu-FTS-Mischung Lu1000 Lu2021	-	-	3190	3370	3530	3470
			6790	6940	7110	6490
FTS-1 (mit AP) Lu1000 Lu2021	0,5 n NaOH	84	3330	3530	3720	3660
			6910	7030	7150	7010
FTS-2 (ohne AP) Lu1000 Lu2021	0,5 n NaOH	91	3330	3490	3650	3610
			7080	7320	7610	6920

Die Mischung Lu1000/Lu2021 wurde jeweils im Minimum der MMV aufgeteilt.

Tabelle 2: Charakterisierung des GAP und der solvolytierten GAP-Proben mit GPC, IR-Absorption und DSC.

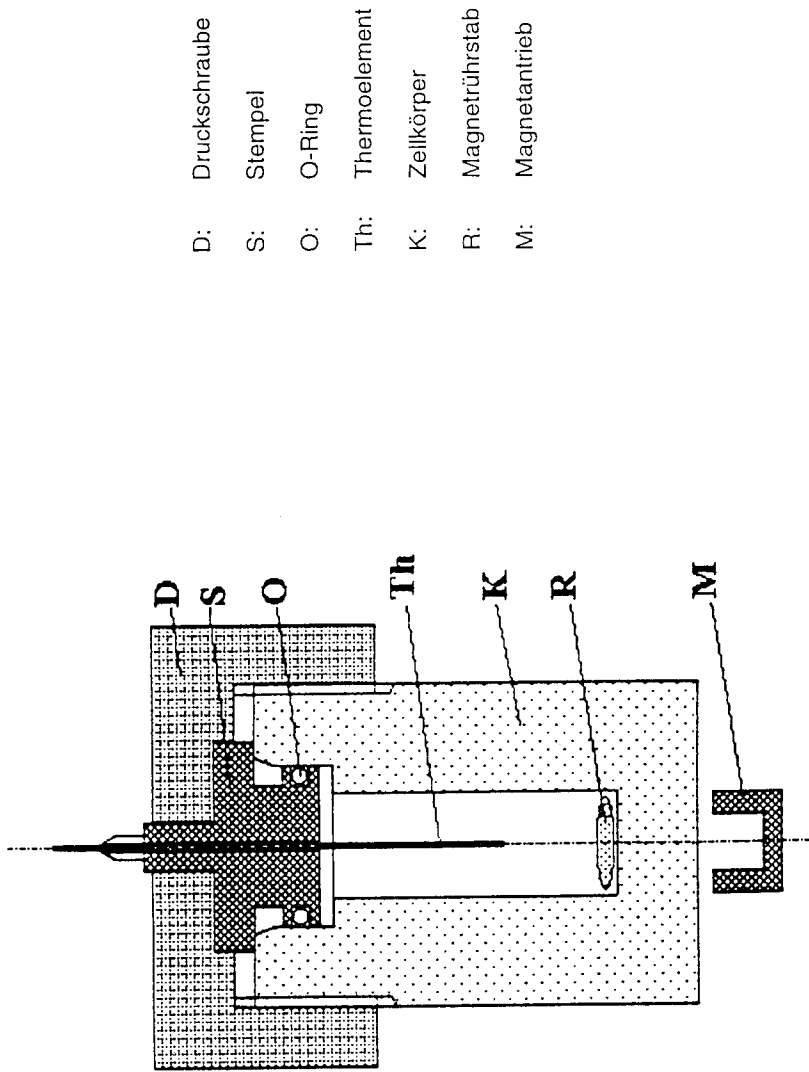
Solvolysemittel	Solvolysezeit [h]	IR-N ₃ -Gehalt [%]	DSC-N ₃ -Gehalt [%]	Mn	Molmassen in g/mol			Mmax
					Mw	Mz		
-	-	100	100	2940	3500	4320		3140
n-Heptan	2	88	89	2840	4200	6930		2930
Toluol	1	98	98	2910	3830	5470		3040
Toluol	2	80	81	2990	4180	6410		2960
Wasser	1	90	92	2850	4000	6260		2980
Wasser	2	80	82	2710	4210	7340		2790
Wasser	2	84	84	2570	4140	7270		2790
0,05 n NaOH	2	30	33	2630	3610	5310		2850

Tabelle 3: Entwickelte Gase bei den Solvolysen des GAP und des GAP-N100-Binders.

Probe	Solvolyse- mittel	Solvolyse- zeit [h]	Solvolyse- temp. [°C]	Gase in ml [20 °C, 1 atm] pro g Probe					
				N ₂	N ₂ O	O ₂	CO	CO ₂	NO _x
GAP	H ₂ O	2	170	10,2	0,61	0,68	0,02	0,24	0,21
GAP	0,05 n NaOH	2	170	4,43	0,15	0,18	-	-	0,0004
GAP-N100	0,05 n NaOH	1	170	3,96	0,02	0,79	-	-	0,0003

Tabelle 4: Ionische Reaktionsprodukte aus einigen Solvolysen bei 170 °C.

Probe	Solvolysen- mittel	Solvolysenzeit [h]	Solvolysentemp. [°C]	Ionen in mg/g Probe				
				NO ₂ ⁻	NO ₃ ⁻	HCO ₃ ⁻	NH ₄ ⁺	
GAP	H ₂ O	2	170	-	-	-	4,0	
KHP	H ₂ O	1	170	-	89,1	-	-	
KHP	0,05 n NaOH	0,5	170	0,7	38,9	32,6	2,8	
KHP	0,05 n NaOH	1	170	1,0	149,3	202,0	5,0	
Hexogen	0,05 n NaOH	1	170	1,2	344,2	236,5	12,7	



- | | |
|-----|----------------|
| D: | Druckschraube |
| S: | Stempel |
| O: | O-Ring |
| Th: | Thermoelement |
| K: | Zellkörper |
| R: | Magnetrührstab |
| M: | Magnetantrieb |

Abb. 1: Schematische Darstellung der Druckeinschlußzelle.

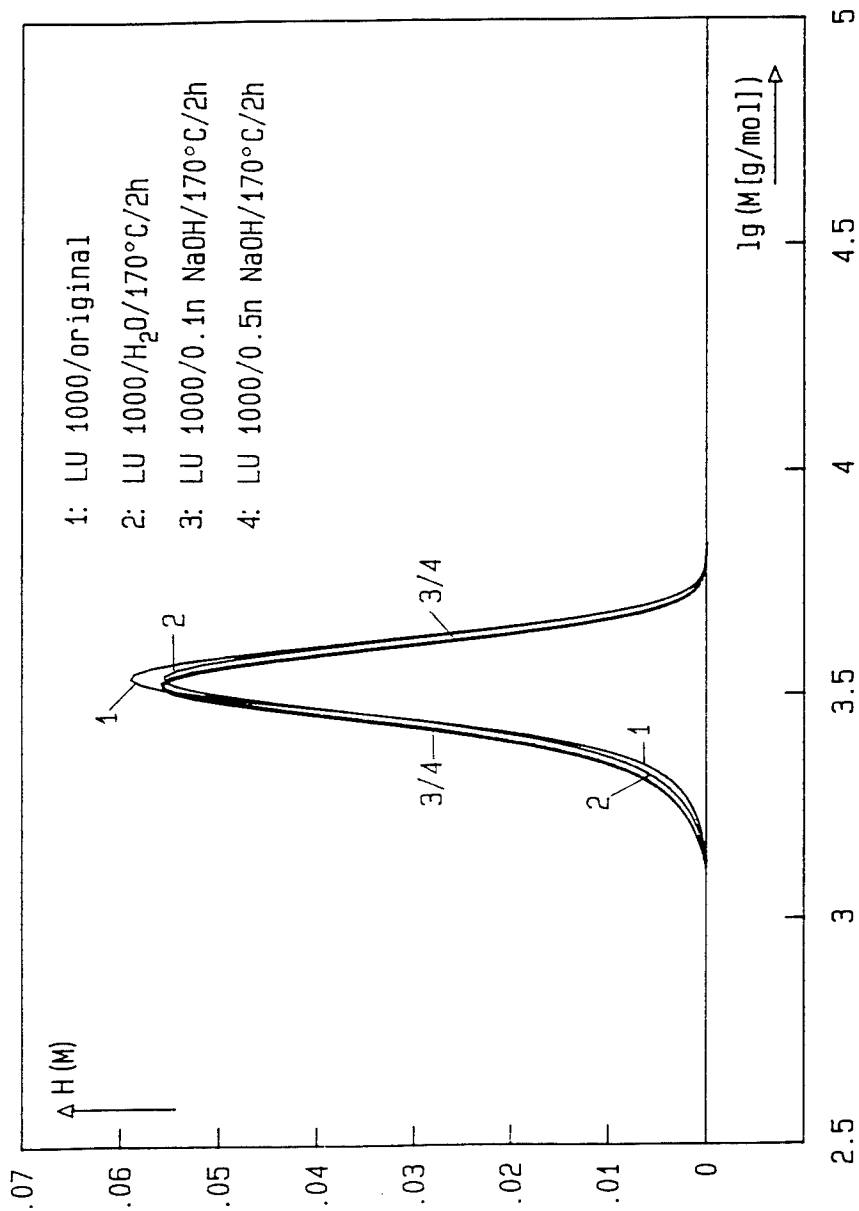


Abb. 2: Molmassenverteilungen des unbehandelten und solvolysebelasteten Polyetherdiols Lupranol 1000.

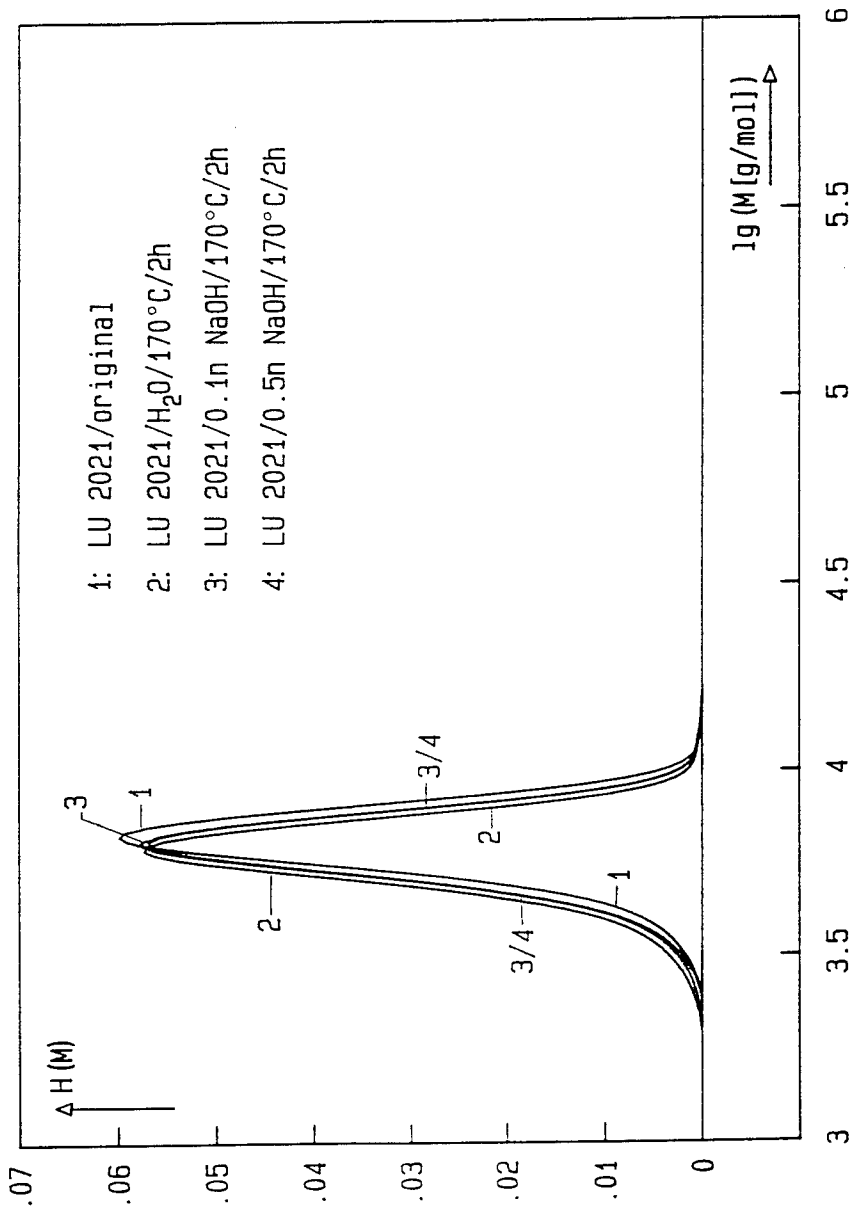


Abb. 3: Molmassenverteilungen des unbehandelten und solvolysebelasteten Polyetherdiols Lupranol 2021.

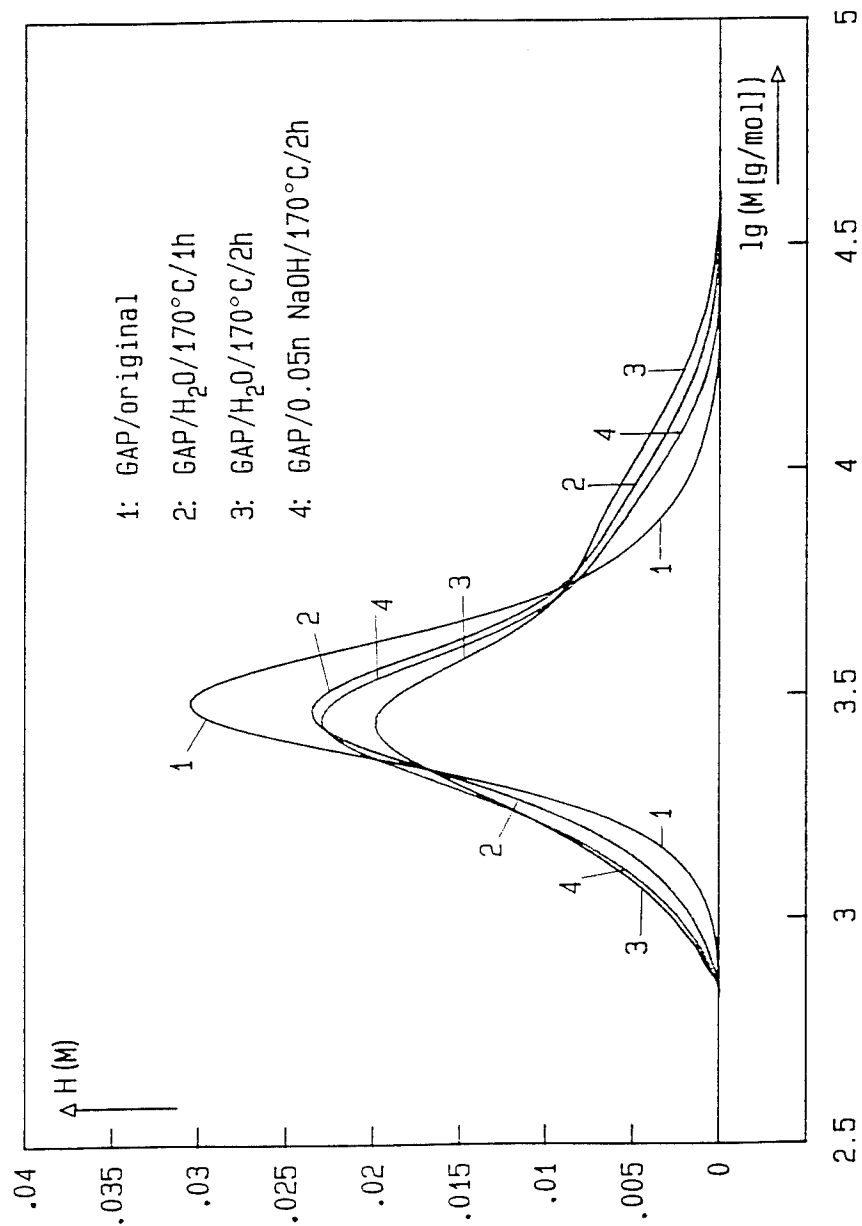


Abb. 4: Molmassenverteilungen des unbehandelten und solvolysebelasteten Azido-Polyetherdiols GAP.

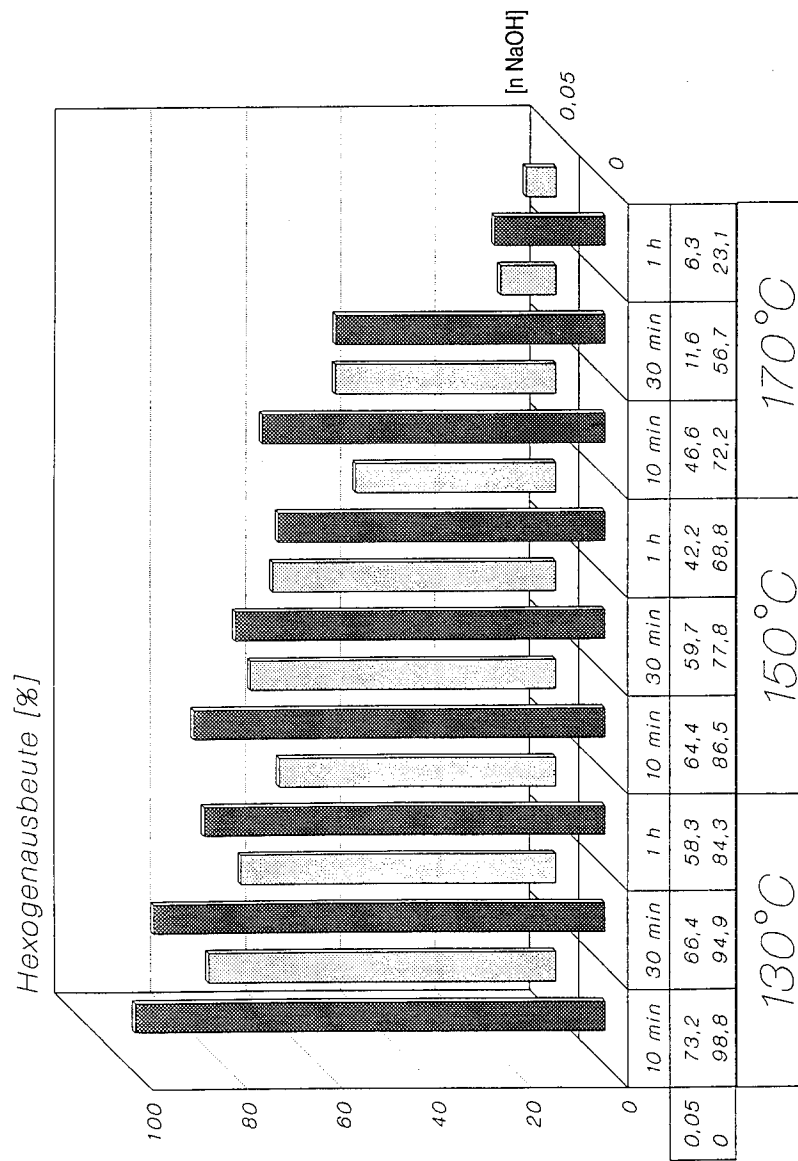


Abb. 5: Hexogenausbeuten der Solvolysen des Treibladungspulvers KHP.

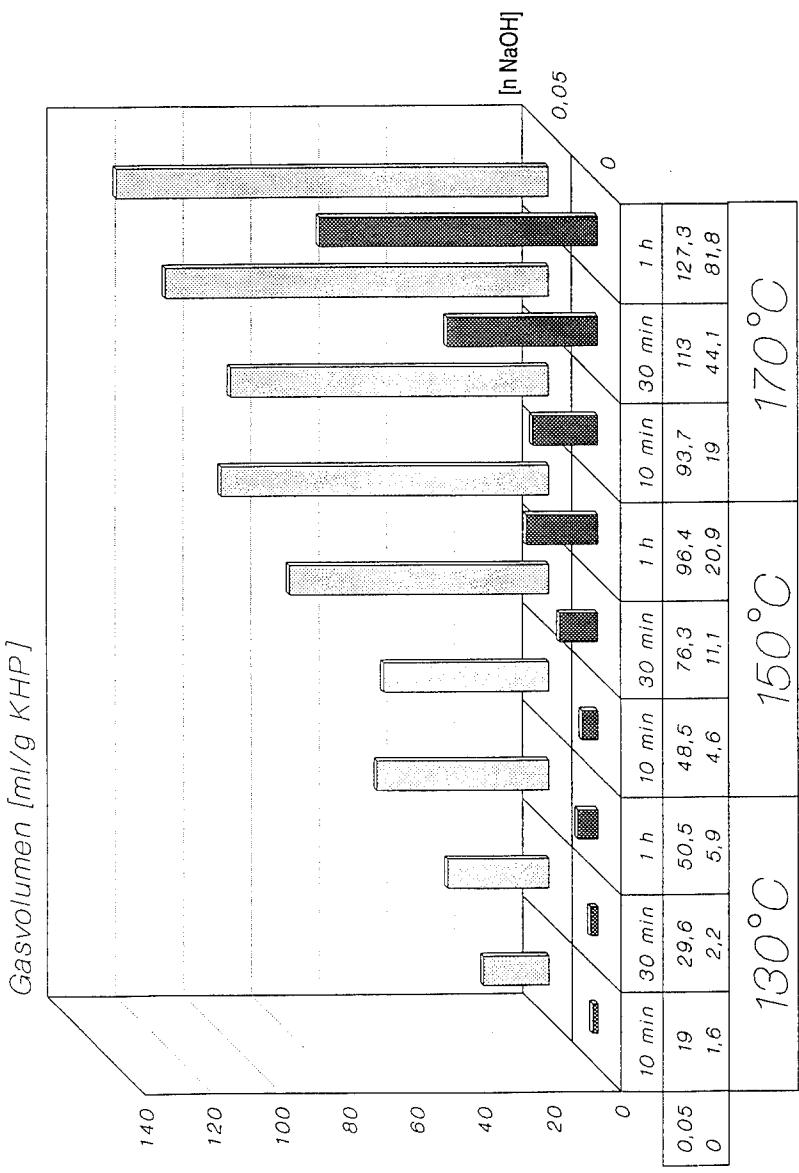


Abb. 6: Entwickelte Gesamtgas Mengen bei den Solvolysen des KHP in ml pro g KHP.

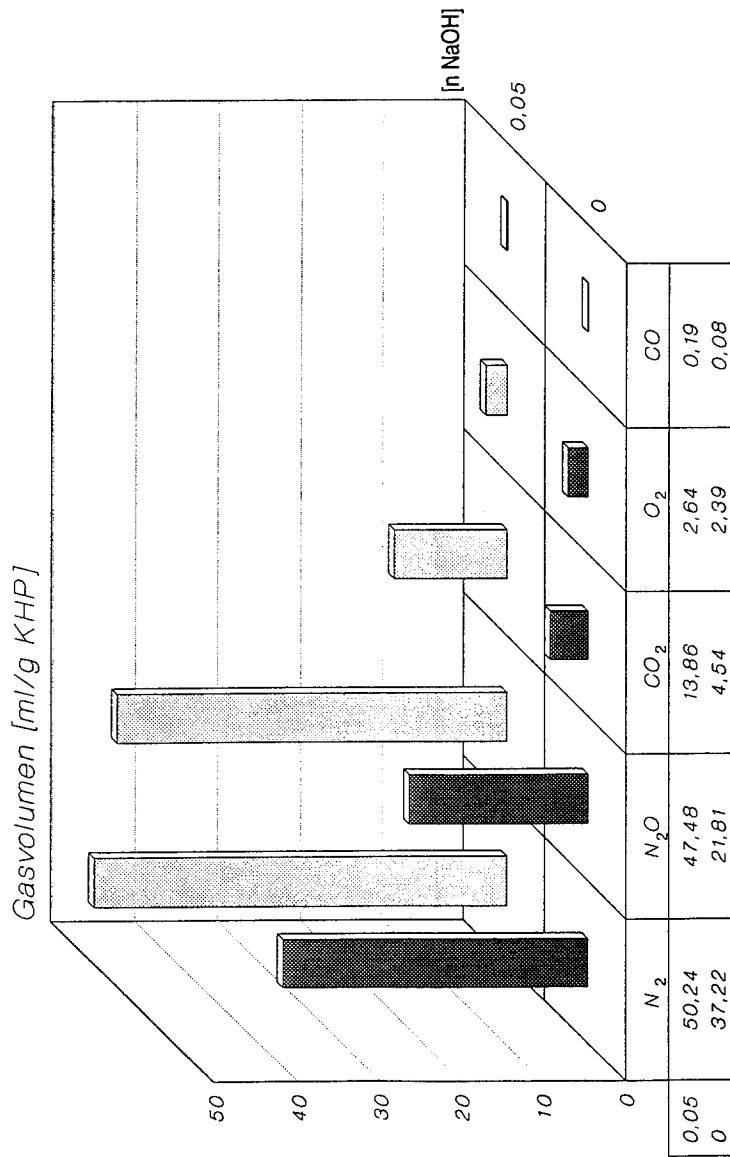


Abb. Z: Hauptgaskomponenten in ml pro g KHP der Solvolysen bei 170 °C und einer Stunde.

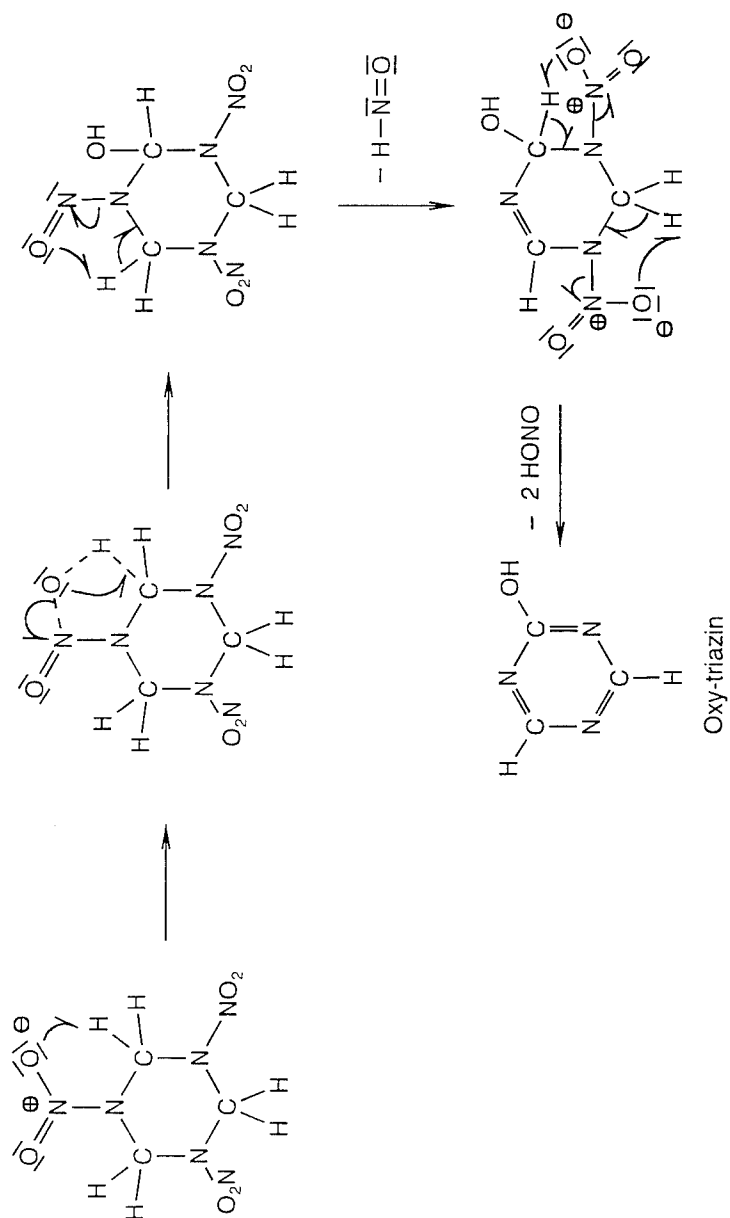


Abb. 8: Zersetzung des Hexogens zum Oxytriazin /nach 16/.

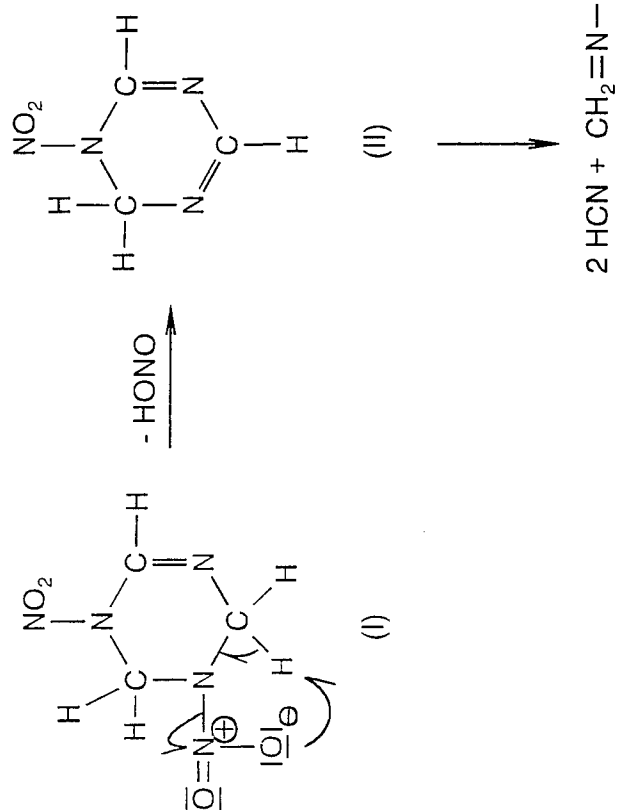
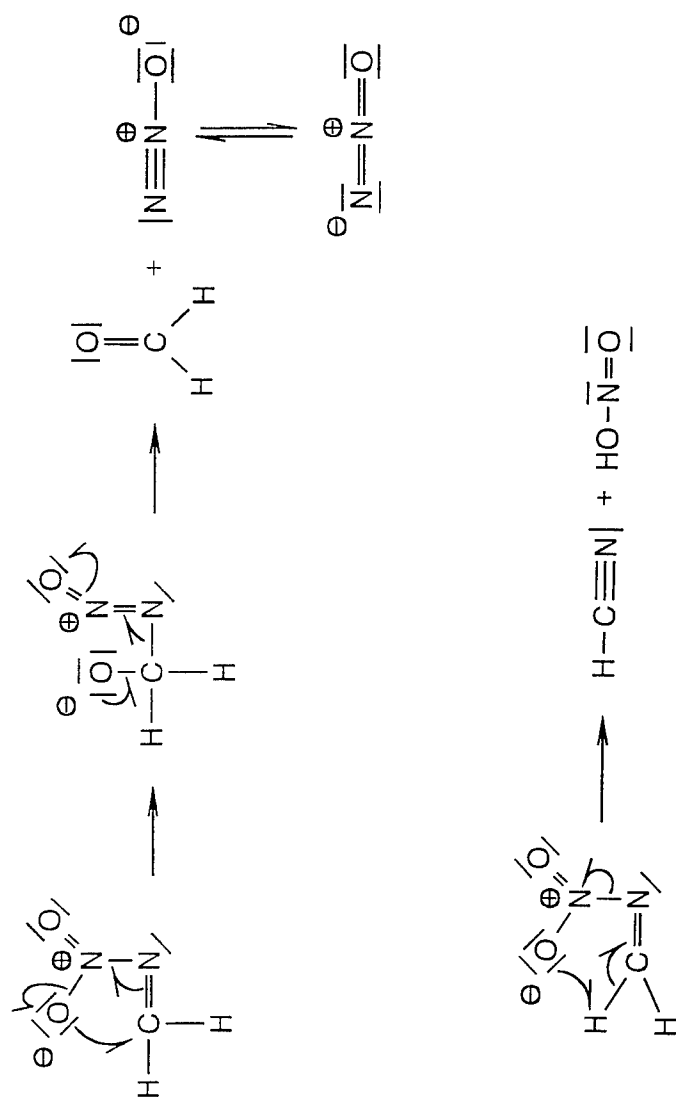


Abb. 9: Zerfall des Hexogens nach der konzentrierten NO_2^- - H^+ -Eliminierung durch OH^- -Angriff /20/.

Abb. 10: Zerfallswege des Methylennitramin $\text{CH}_2=\text{N}-\text{NO}_2$.

Einfluss von Temperatur und Feuchtigkeit auf pyrotechnische Ausgangskomponenten und Mischungen

F. Tschan, B. Berger, H.R. Bircher

Gruppe für Rüstungsdienste
Abt. Ballistik, Waffen und Munition
Feuerwerkerstrasse 39
CH-3600 Thun 2

Abstract

Der Einfluss von Temperatur und Feuchtigkeit auf vier, in der Pyrotechnik häufig verwendete Reduktionsmittel sowie auf entsprechende pyrotechnische Mischungen wurde mittels Mikrokalorimetrie und "Gas Flow Ampoule System" (GFAS) ermittelt. Die untersuchten Reduktionsmittel waren Zirkon, Zirkonhydrid, Zirkon-Nickel-Legierung 70:30 und Titan. Als pyrotechnische Modellmischungen dienten Zirkon / Kaliumperchlorat, Zirkonhydrid / Kaliumperchlorat, Zirkon-Nickel-Legierung 70:30 / Kaliumperchlorat sowie Titan / Kaliumperchlorat.

Die Messergebnisse zeigen, dass sowohl an der Zirkonoberfläche als auch an der Zirkonhydridoberfläche bei erhöhter Temperatur und Feuchtigkeit Reaktionen stattfinden, wobei die Reaktion bei Zirkonhydrid schwach ist. Kaum einen Einfluss hatten die Testbedingungen auf Titan und Zirkon-Nickel-Legierung sowie auf die vier pyrotechnischen Mischungen.

The influence of temperature and humidity on four reducing agents and on four pyrotechnic mixtures, very often used in pyrotechnics, was determined by means of microcalorimetry and "Gas Flow Ampoule System" (GFAS). The following reducing agents have been tested: Zirconium, zirconium hydride, titanium and zirconium-nickel-alloy. The mixtures of zirconium and potassium perchlorate, zirconium hydride and potassium perchlorate, titanium and potassium perchlorate and zirconium-nickel-alloy and potassium perchlorate have been tested as applied compounds.

The results indicate, that there are reactions at increased temperature and humidity on the surface of zirconium as well as of zirconium hydride, whereby zirconium hydride shows a slight reaction. The stability of titanium and zirconium-nickel-alloy and the four investigated pyrotechnic mixtures seems not to be influenced by humidity at 70 °C.

1. Einleitung

1975 beschrieb Prof. Dr. Schubert, Leiter des Fraunhofer Institutes für Chemische Technologie in Pfinzthal, die Situation in der militärischen Pyrotechnik mit den folgenden treffenden Worten [1]:

"Die Pyrotechnik macht meist nur dann von sich reden, wenn durch das Versagen pyrotechnischer Anordnungen das Waffensystem in Frage gestellt wird oder infolge geringer Lebensdauer umlaboriert werden muss. Meist ist dann das Lamento gross - aber nur selten ändert sich damit die Situation".

Eine der Ursachen für das Fehlverhalten von pyrotechnischen Komponenten liegt häufig schon bei den Ausgangskomponenten bzw. deren Lagerung. Die Ausgangskomponenten von pyrotechnischen Mischungen sind Reduktions- und Oxidationsmittel mit Korngrössen von einigen wenigen Mikron und demzufolge mit grossen Oberflächen. Bei den Reduktionsmittel handelt es sich oft um reine Metallpulver, auf deren Oberfläche in Zusammenhang mit Luftfeuchtigkeit und Wärme leicht Oxide gebildet werden, was zu einer wesentlichen Herabsetzung der Reaktivität des Reduktionsmittels führt. Da die meisten pyrotechnischen Reaktionen topochemische Redoxreaktionen [2] sind, kann eine solche Desaktivierung der Oberfläche des Reduktionsmittels zu einer Beeinträchtigung bzw. zu einem vollständigen Ausfall von pyrotechnischen Komponenten führen. Eine Desaktivierung des Reduktionsmittels kann ebenfalls bei pyrotechnischen Mischungen erfolgen, wenn das verwendete Oxidationsmittel hygroskopisch ist und so Feuchtigkeit in die Mischung eingebracht wird.

In einer Grundlagenstudie wurde mittels Mikrokolorimetrie und einem "Gas Flow Ampoule System" [3, 4] das Verhalten von einigen, in der militärischen Pyrotechnik häufig verwendeten Reduktionsmittel sowie entsprechender pyrotechnischer Mischungen in feuchter Atmosphäre und bei erhöhter Temperatur untersucht.

2. Ziel

Ziel der Untersuchung ist es, den Einfluss von Feuchtigkeit und Temperatur auf die Reaktivität von, in der Pyrotechnik oft verwendeten, Metallpulvern sowie entsprechender pyrotechnischer Mischungen abzuklären. Das Oxidationsmittel der geprüften Mischungen war Kaliumperchlorat.

3. Experimenteller Teil

3.1. Untersuchungsmethode

Zur Abklärung des Einflusses von Feuchtigkeit und Temperatur auf die Reaktivität von Metallpulvern sowie entsprechender pyrotechnischer Mischungen wurden mikrokalorimetrische Wärmeflussmessungen durchgeführt. Die Messungen erfolgten mit einem "Thermal Activity Monitor 2277" (TAM) der Firma LKB AB in Bromma/Schweden. Die Untersuchungen unter erhöhter Feuchtigkeit erfolgten mit Hilfe des "Gas Flow Ampoule Systems" der Firma Bofors/Schweden. Die Standardausführung, wie sie bei uns verwendet wird, erlaubt Messungen bei verschiedenen relativen Luftfeuchtigkeiten (RH).

3.2 Untersuchungsbedingungen

Bei unserer Versuchsanordnung wurden jeweils 500 mg Metallpulver bzw. 500 mg einer pyrotechnischen Mischung eingewogen und deren Wärmefluss bei 60% RH gemessen. Die Versuchstemperatur betrug 70° C. Die Versuchsdauer erstreckte sich über 30 Tage. Die gemessenen Wärmeflüsse wurden auf eine Masse von 1000 mg referenziert. Als Vergleich wurden die Wärmeflusskurven von je 1000 mg Metallpulver bzw. pyrotechnischer Mischung unter Normalbedingungen gemessen. Die Differenz der Wärmeflüsse bei 60% RH und unter Normalbedingungen ist ein Mass für die Abhängigkeit der Stabilität bei erhöhter Luftfeuchtigkeit. Vor dem eigentlichen Messbeginn wurden die Proben während 16 Stunden unter den gleichen Bedingungen, unter denen der Wärmefluss bestimmt wurde, vorkonditioniert.

3.3 Untersuchte Metallpulver

Bei den untersuchten Metallpulvern handelt es sich um frisch hergestellte Muster der Chemetall AG, Frankfurt, die unter Inertgas angeliefert wurden. Das Verhalten der folgenden Reduktionsmittel wurde abgeklärt:

- Zirkon, Typ FA
- Zirkonhydrid, Typ F
- Titan, Typ S
- Zirkon-Nickel-Legierung 70:30, Typ A

Die Spezifikationen sind im Anhang aufgeführt.

3.4 Untersuchte Mischungen

Mischung 1	Mischung 2	Mischung 3	Mischung 4
56.8 Gew.% Zr	47.3 Gew.% ZrH ₂	40.9 Gew.% Ti	58.5 Gew.% Zr-Ni-Leg.
43.2 Gew.% KClO ₄	52.7 Gew.% KClO ₄	59.1 Gew.% KClO ₄	41.5 Gew.% KClO ₄

Die aufgeführten Mischungen entsprechen den jeweiligen Redoxsystemen mit ausgeglichener Sauerstoffbilanz.

4. Resultate

4.1 Allgemeines

Die qualitative Bestimmung der Reaktionsprodukte erfolgte mittels Röntgendiffraktion. Um eine Abschätzung des Umsetzungsgrades von den Metallpulver zu den entsprechenden Oxiden vornehmen zu können, wurden die freigesetzten Energien durch numerische Integration der Wärmeflusskurven ermittelt. Aufgrund der Standardbildungsenergien der Oxide konnte eine Abschätzung des Umsetzungsgrades für die Messzeit von 30 Tagen bestimmt werden. Dabei ist zu beachten, dass sich die Umsetzungsgrade bei den pyrotechnischen Mischungen stets auf ein Gramm Reduktionsmittel beziehen. Zudem wurde bei der Zirkon-Nickel-Legierung die Berechnung nur auf Zirkon bezogen.

4.2 Zirkon

Unter Normalbedingungen weist Zirkon zu Beginn der Messung einen hohen exothermen Wärmefluss auf, der aber schnell abnimmt und sich asymptotisch der Nulllinie nähert. Erfolgt die gleiche Messung bei 60% RH, so misst man einen hohen Wärmefluss, der nur langsam abnimmt und nach 30 Tagen immer noch über 60 μ W/g aufweist. Die Röntgendiffraktionsanalyse zeigt, dass sich sowohl unter Normalbedingungen wie auch bei 60% RH Zirkonoxid bildet. Der berechnete Umsetzungsgrad unter Normalbedingungen beträgt 0.021 %, derjenige bei 60 % RH 0.107 %. Somit erfolgt die Umwandlung von Zirkon zu Zirkonoxid bei 60 % RH rund fünf Mal schneller.

4.3 Zirkonhydrid

Zirkonhydrid zeigt unter Normalbedingungen das gleiche Verhalten wie Zirkon, jedoch ist der Wärmefluss zu Beginn um rund einen Faktor drei kleiner. Die glei-

che Messung bei 60% RH ergibt einen ähnlichen Kurvenverlauf, jedoch liegt dieser zu Beginn um etwa $10 \mu\text{W/g}$ und nach 30 Tagen um knapp $20 \mu\text{W/g}$ höher. Mittels Röntgendiffraktion konnte nachgewiesen werden, dass sich wiederum in beiden Fällen Zirkonoxid bildet. Die Umsetzungsgrade betragen bei Normalbedingungen 0.011 % und unter 60 % RH 0.032 %. Die Erhöhung der Luftfeuchtigkeit begünstigt die Bildung von Oxid um den Faktor drei.

4.4 Titan

Die Verläufe der Wärmeflusskurven unter Normalbedingungen und unter 60% RH weisen einen ähnlichen Verlauf auf, jedoch liegt auch hier diejenige bei erhöhter Feuchtigkeit etwas höher. Der Einfluss ist aber sehr gering. Mit Hilfe der Röntgendiffraktion konnten keine Reaktionsprodukte nachgewiesen werden. Unter der Annahme, dass sich Titanoxid bildet, errechnen sich die Umsetzungsgrade unter Normalbedingungen zu 0.005 % und bei erhöhter Feuchtigkeit zu 0.011 %. Der Einfluss der Feuchtigkeit auf die Oxidationsrate ist auch hier feststellbar.

4.5 Zirkon-Nickel-Legierung

Der Einfluss der Feuchtigkeit scheint bei dieser Legierung kaum einen Einfluss auf die chemische Stabilität zu haben. Die berechnete Differenz der beiden Wärmeflusskurven bewegt sich zwischen -8 und $+8 \mu\text{W/g}$. Mittels qualitativer Röntgendiffraktionsanalyse konnte nachgewiesen werden, dass sich Zirkonoxid bildet, jedoch wurde kein Nickeloxid gefunden. Der Umsetzungsgrad unter Normalbedingungen beträgt 0.018 % und derjenige unter erhöhter Feuchtigkeit 0.020 %.

4.6 Zirkon / Kaliumperchlorat

Unter Normalbedingungen tritt zu Beginn der Messung eine starke exotherme Wärmetönung auf, die aber rasch abklingt und gegen den Wert Null geht. Bei einer RH von 60 % registriert man einen exothermen Wärmefluss, der während der Versuchszeit von $30 \mu\text{W/g}$ gegen $20 \mu\text{W/g}$ absinkt. Mittels Röntgendiffraktion konnten keine Reaktionsprodukte bestimmt werden. Unter der Annahme, dass sich Zirkonoxid bildet, ist der berechnete Umsetzungsgrad unter Normalbedingungen 0.022 %, derjenige bei einer RH von 60 % beträgt 0.051 %. Ein Einfluss der Feuchtigkeit auf die Reaktionsfreudigkeit scheint gegeben zu sein.

4.7 Zirkonhydrid / Kaliumperchlorat

Bei dieser Mischung scheint sich eine erhöhte Feuchtigkeit entgegen aller Erwartungen positiv auf die chemische Stabilität auszuwirken. Mit Ausnahme der Startwerte liegt die Wärmeflusskurve unter Normalbedingungen stets höher als diejenige bei 60 % RH. Die Röntgendiffraktionsanalyse ergab als Reaktionsprodukt Zirkonoxid. Für die Messung unter Normalbedingungen wird ein Umsetzungsgrad von 0.018 % berechnet, während derjenige bei 60 % RH nur 0.006% beträgt. Die Bildung von Zirkonoxid verläuft im Vergleich unter Normalbedingungen bei einer RH von 60 % um den Faktor drei langsamer. Dieser Effekt ist Gegenstand weiterer Untersuchungen.

4.8 Titan / Kaliumperchlorat

Unter Normalbedingungen ist diese pyrotechnische Mischung chemisch sehr stabil. Daher ist es nicht verwunderlich, dass mittels Röntgendiffraktion keine Reaktionsprodukte nachgewiesen werden konnten. Unter der Annahme, dass sich Titanoxid bildet, beträgt der Umsetzungsgrad 0.003 %. Die Wärmeflusskurve unter einer RH von 60 % verläuft im endothermen Bereich zwischen 0 μ W/g und -5 μ W/g. Auch hier lassen sich keine Reaktionsprodukte nachweisen. Eine Erklärung für dieses Verhalten konnte (noch) nicht gefunden werden. Jedoch scheint die erhöhte Feuchtigkeit auf die Reaktionsrate nur einen geringen Einfluss zu haben.

4.9 Zirkon-Nickel-Legierung / Kaliumperchlorat

Unter Normalbedingungen scheint diese Mischung chemisch ziemlich stabil zu sein. Der gemessene Wärmefluss liegt zu Beginn der Messung bei 7.5 μ W/g und sinkt nach 30 Tagen auf 2.5 μ W/g ab. Unter der Annahme, dass nur Zirkon an der Reaktion teilnimmt, ist der berechnete Umsetzungsgrad 0.013 %. Wird die gleiche Messung bei 60 % RH durchgeführt, so wird ein leicht erhöhter Wärmefluss registriert. Wird wiederum angenommen, dass nur Zirkon an der Reaktion teilnimmt, beträgt der Umsetzungsgrad 0.020 %. Der Einfluss der Feuchtigkeit scheint hier eine grössere Rolle zu spielen.

5. Zusammenfassung / Folgerungen

Die Untersuchungen haben gezeigt, dass die chemische Stabilität der Reduktionsmittel Zirkon und Zirkonhydrid stark von der Luftfeuchtigkeit abhängen. Bei Titan ist diese Abhängigkeit schwächer und bei der Zirkon-Nickel-Legierung konnte keine Abhängigkeit der chemischen Stabilität von der Feuchtigkeit im gemessenen Bereich festgestellt werden. Die pyrotechnische Mischung Zirkon / Kaliumperchlorat weist eine Abhängigkeit ihrer chemischen Stabilität von der Luftfeuchtigkeit auf, die aber im Vergleich zum Zirkon viel schwächer ist. Im Falle der Mischung von Zirkonhydrid und Kaliumperchlorat scheint sich die Beimengung von Oxidationsmittel positiv auf die chemische Stabilität auszuwirken. Auch die Mischung von Titan mit Kaliumperchlorat weist eine bessere chemische Stabilität auf als diejenige des reinen Reduktionsmittels. Eher negativ wirkt sich die Zunahme der Feuchtigkeit auf die chemische Stabilität bei der Mischung von Zirkon-Nickel-Legierung mit Kaliumperchlorat aus.

Grundsätzlich darf festgestellt werden, dass sich die Beimengung von Kaliumperchlorat auf die chemische Stabilität der untersuchten Reduktionsmittel eher positiv auswirkt.

6. Literatur

- [1] H. Schubert
"Forschungsziele in der Pyrotechnik"
Jahrestagung ICT, Karlsruhe, 1975
- [2] N.H.A. van Ham
"Deflagration of Gasless Pyrotechnic Mixtures"
PLM, TNO, NL
- [3] F.R. Taylor, L.R. Lopez, P.L. Farnell
"Study of the Storage Stability of a Zirconium-Nickel Delay System using
Ampoule Microcalorimetry"
Picatinny Arsenal, Dover, New Jersey, USA
- [4] L.G. Svensson, H. Nyhlén, C.K. Forsgren, N.G. Gellerstedt,
"A Study of Long-term Pyrotechnic Degradation using Microcalorimetry and
Burnig Rate Tests"
Bofors AB, S, 1988

7. Anhang

7.1 Spezifikation von Zirkon-Metallpulver, Typ FA

Delivered form	Greyish-black powder				
Bulk density	1.2 g/cm ³				
Ignition point	190 ± 15°C				
Combustion rate	60 ± 10 sec/50 cm				
Particle size	100 % < 40 µm; acc. to Blaine 2.3 ± 0.5 µm				
Specific surface (BET)	1.1 m ² /g				
Oxidation value	28.5 ± 1.0 % (weight increase by combustion)				
Analysis	Zr + Hf	total	92	± 1	%
	Zr + Hf	metallic	78	± 3	%
	Si	max.	3		%
	Hf	approx.	2		%
	(natural content)				
	H		0.3	± 0.05	%
	Mg	max.	0.3		%
	Ti	max.	0.15		%
	Al	max.	0.1		%
	Fe	max.	0.08		%
	Ca	max.	0.05		%

7.2 Spezifikation von Titan-Metallpulver, Typ S

Delivered form	Grey powder				
Bulk density	1.3 g/cm ³				
Melting point	1727 °C				
Ignition point	440 ± 20 °C				
Combustion rate	50 ± 10 sec/50 cm				
Particle size	100 % < 40 µm; acc. to Blaine 9 ± 1.5 µm				
Specific surface (BET)	0.3 m ² /g				
Oxidation value	64.5 ± 0.5 % (weight increase by combustion)				
Analysis	Ti	total	98.5	± 0.5	%
	Ti	metallic	96.5	± 1.0	%
	N	max.	0.1		%
	H	max.	0.1		%
	Fe	max.	0.09		%
	Cl	max.	0.06		%
	Ni	max.	0.05		%
	Si	max.	0.05		%
	Mg	max.	0.04		%
	C	max.	0.03		%

7.3 Spezifikation von Zirkonhydrid-Pulver, Typ F

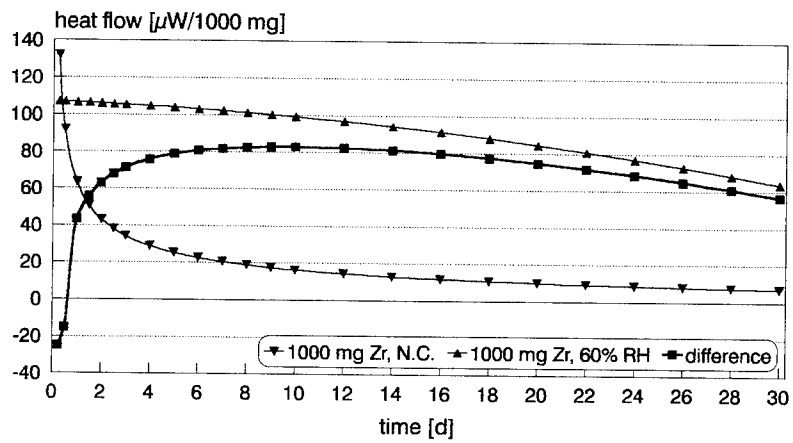
Delivered form	Greyish-black powder				
Bulk density	0.9 g/cm ³				
Ignition point	280 ± 20 °C				
Combustion rate	320 ± 40 sec/50 cm				
Particle size	100 % < 40 µm; acc. to Blaine 2.5 ± 0.5 µm				
Specific surface (BET)	1.2 m ² /g				
Oxidation value	29.5 ± 1 % (weight increase by combustion)				
Analysis	Zr + Hf	total	95.5	± 1	%
	Hf	approx.	2		%
	(natural content)				
	H		1.6	± 0.2	%
	Si	max.	0.5		%
	Mg	max.	0.2		%
	Ti	max.	0.15		%
	Al	max.	0.1		%
	Fe	max.	0.1		%
	Ca	max.	0.01		%

7.4 Spezifikation von Zirkon-Nickel-Legierung 70:30, Typ A

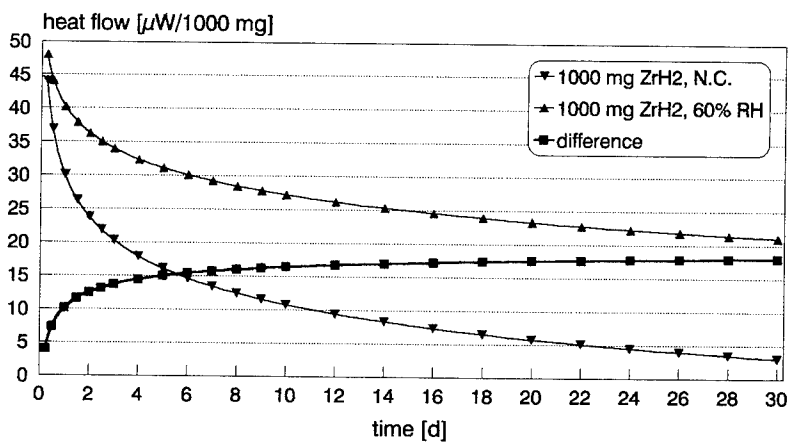
Delivered form	Fine, greyish-black powder				
Bulk density	1.8 g/cm ³				
Tab density	2.7 g/cm ³				
Melting point	1140 °C				
Ignition point	260 ± 15 °C				
Combustion rate	200 ± 20 sec/50 cm				
Particle size	100 % < 40 µm; acc. to Blaine 4 ± 2 µm				
Specific surface (BET)	0.6 m ² /g				
Oxidation value	31 ± 1 % (weight increase by combustion)				
Analysis	Zr (+Hf)	total	70	± 3	%
	Ni	total	30	± 3	%
	Zr + Ni (+Hf)	min.	97		%
	H	total	0.2	± 0.05	%
	Fe	max.	0.2		%
	Ca	max.	0.15		%
	Al	max.	0.15		%
	S	max.	0.01		%

7.5 Wärmeflusskurven

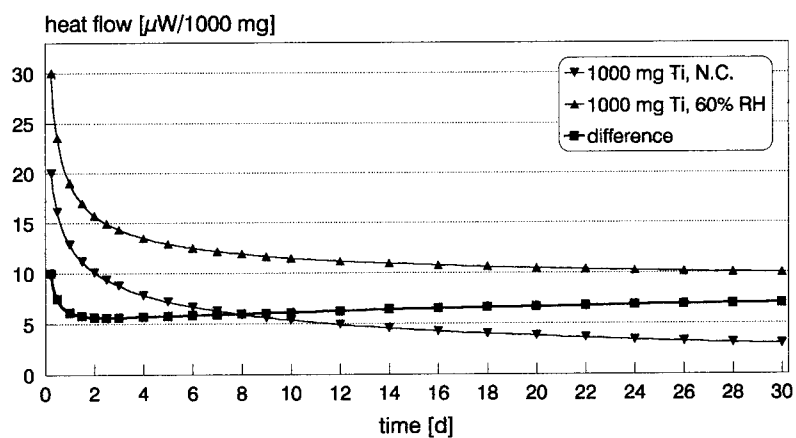
Stability of Zirconium Heat Flow Measurement at 70 °C



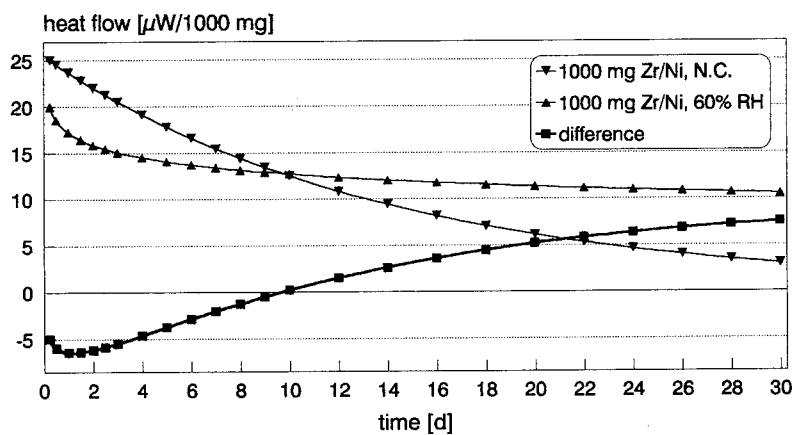
Stability of Zirconium Hydride Heat Flow Measurement at 70 °C



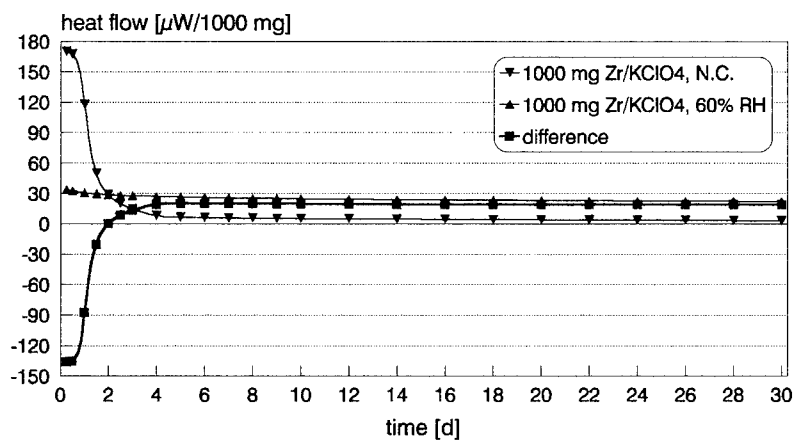
Stability of Titanium Heat Flow Measurement at 70 °C



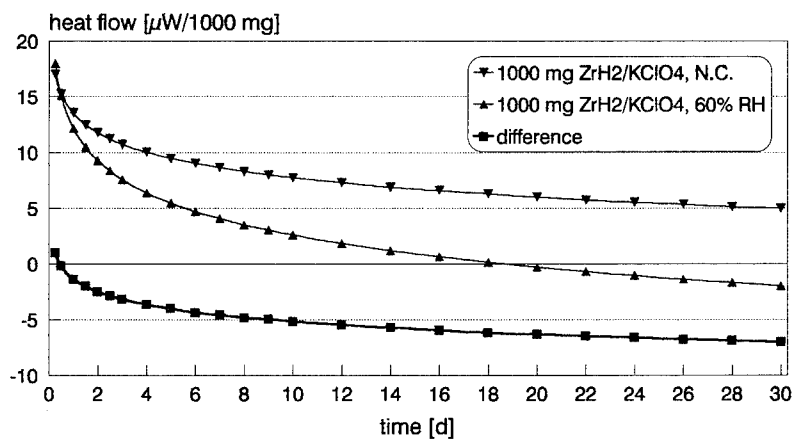
Stability of Zirconium-Nickel-Alloy Heat Flow Measurement at 70 °C



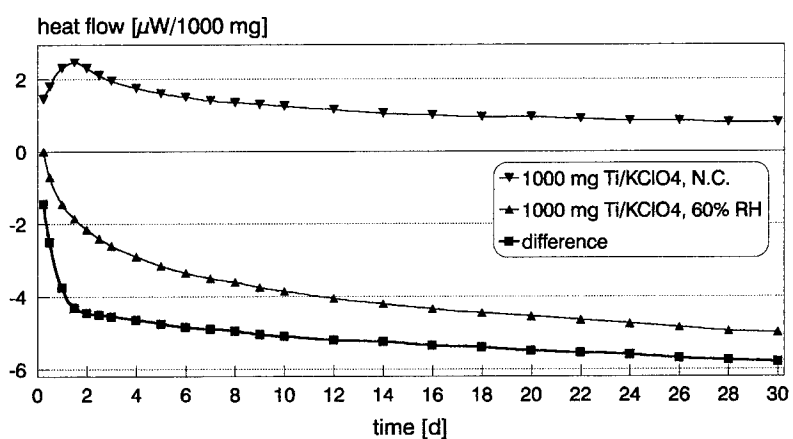
Stability of a Mixture of Zirconium and Potassium Perchlorate
Heat Flow Measurement at 70 °C



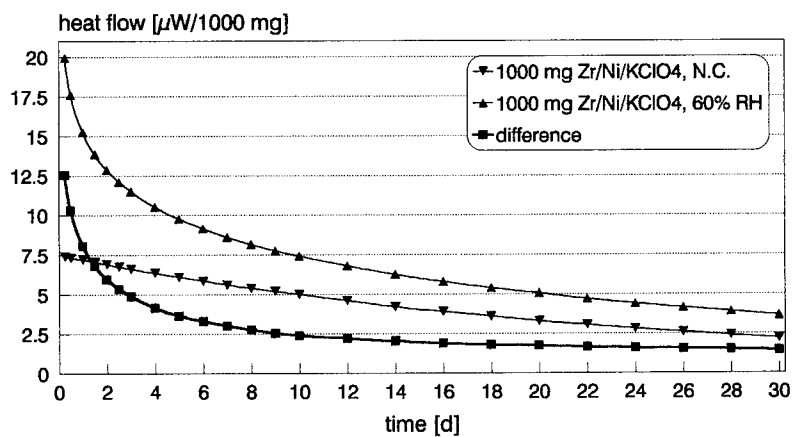
Stability of a Mixture of Zirconium Hydride and Potassium Perchlorate
Heat Flow Measurement at 70 °C



Stability of a Mixture of Titanium and Potassium Perchlorate
Heat Flow Measurement at 70 °C



Stability of a Mixture of Zirconium-Nickel-Alloy and Potassium Perchlorate
Heat Flow Measurement at 70 °C



POLYVINYL ALCOHOLS AS BINDERS FOR PYROTECHNIC COMPOSITIONS

S B Langston

School of Mechanical, Materials and Civil Engineering,
Cranfield University,
Royal Military College of Science,
Shrivenham, Swindon, SN6 8LA, UK.

ABSTRACT

Poly(vinyl acetate, vinyl alcohols) or Vinyl Alcohol Acetate Resins (VAAR) have been used successfully as binders for pyrotechnic compositions over a number of years. These polymers also known as polyvinyl alcohols or hydrolysed polyvinyl acetates, depending on the degree of hydrolysis, are efficient binders and are effective at desensitising pyrotechnic compositions. New compositions based on Alcotex poly(vinyl acetate, vinyl alcohol) resins were prepared. The challenge of recycling materials was examined and the problems of disposing of waste pyrotechnics, addressed.

INTRODUCTION

Traditional binders for pyrotechnic compositions are often based on natural or semi-natural resins. Although serving the pyrotechnic industry well for many years, natural resins are of complex and variable composition and can be difficult to source. On coating magnesium or other similarly reactive fuel metals with natural hardening oils spontaneous ignition may occur during curing. The viscous nature of natural resins and the tendency of manufacturers to coat magnesium manually by hand, results in a process where product quality can be operator dependent. Any coating deficiency can lead to premature aging and subsequent poor performance or failure. Synthetic polymers generally do not suffer from these disadvantages and can offer other benefits over natural resins, for example; improved physical and mechanical properties, tighter specifications and reduced material and manufacturing costs.

Polyvinyl alcohols are soluble in either lower alcohols or water depending on their degree of hydrolysis and average molecular weight. These are solvents of choice within the pyrotechnic industry. Polyvinyl alcohol solutions are efficient coating agents and effective binders once dry. The polymer film strength is high and many polyvinyl alcohols are remarkably impervious to moisture.

POLYVINYL ALCOHOL BINDERS

A number of water soluble polyvinyl alcohols^{1,2} were assessed for their suitability as binders for pyrotechnics. The polyvinyl alcohols (or partially hydrolysed polyvinyl acetate) used in this investigation were Alcotex 20-009 and Alcotex 47P, supplied by Harlow Chemical Company Ltd. Although often referred to as polyvinyl alcohols, these polymers are strictly vinyl acetate, vinyl alcohol co-polymers. The distribution of the hydroxyl groups can be either random or blocky. They are manufactured by the alkaline hydrolysis (saponification) or alcoholysis (ester interchange) of polyvinyl acetate. Alcotex 47P is a 47% hydrolysed poly(vinyl acetate, vinyl alcohol) supplied as a solution consisting of 40% solids, 49% methanol, 9% methyl acetate and 2% water. Alcotex 20-009 is a 20% hydrolysed poly(vinyl acetate, vinyl alcohol) with a molecular weight of approximately 50,000, supplied as a solution consisting of 28% solids, 49% methanol, 9% methyl acetate and 2% water. Many polyvinyl alcohols can be readily plasticised with for example: polyethylene glycols, polypropylene glycols or glycerol. On plasticisation, polyvinyl alcohols become more rubbery by nature and can hold between twice and three times their own weight in plasticiser. Water

is also a very efficient plasticiser of polyvinyl alcohols with a high hydroxyl content. The ability of these polyvinyl alcohols to absorb moisture and remain dry, could be useful in removing any traces of water present in a sealed system. The recovery of explosive fillers for example, HMX, from pressable polymer bonded explosives (PBXs) has already been demonstrated^{3,4} and the recycling of such explosives described⁵. Polyvinyl alcohols exhibit a number of properties that may be advantageous to their use as binders in pyrotechnics and PBX's. These advantages include the following:

1. Good mechanical properties and easily plasticised.
2. Can be produced in either cold water soluble or hot water soluble forms.
3. Efficient binder - effective bonding, weldable.
4. Resistant to most solvents.
5. Non toxic and physiological inertness.
6. Readily forms films, can form thermoplastic mouldings.
7. Impermeable to most gases, can be moisture resistant.
8. Wash waters are biodegradable.
9. Very stable and resistant to degradation in the dry state.

The wash waters containing polyvinyl alcohols can be processed² in a number of ways. The polyvinyl alcohol solution could be concentrated by precipitation, evaporation or ultrafiltration. Polyvinyl alcohols will precipitate very efficiently from solution with iron or aluminium salts or as a calcium/boric acid complex (Hoechst process). The recovered material can then be incinerated or recycled. With ultrafiltration the polyvinyl alcohol is removed from the wash water by filtration under pressure through modular polymer membranes. The polyvinyl alcohol can then be recovered. As aqueous solutions of polyvinyl alcohols are readily biodegraded by adapted micro-organisms any polyvinyl alcohol remaining in the wash water can finally be treated by biological purification.

POLYVINYL ALCOHOL BASED COMPOSITIONS

Polyvinyl alcohols as binders for pyrotechnic compositions have been used extensively in the United States since the 1960's. The poly(vinyl acetate, vinyl alcohol), or VAAR⁶ described is a co-polymer consisting of 18% vinyl alcohol and 82% vinyl acetate, dissolved in technical grade methyl acetate. A UK specification⁷ exists, although this describes a fully hydrolysed polyvinyl alcohol used to coat electric fuseheads and as an inhibitor for propellant strands used in the Crawford Bomb Test. VAAR has been successfully incorporated as a binder in

a wide range of pyrotechnic compositions⁸⁻¹⁶. According to Taylor and Jackson⁸, VAAR was no longer commercially available in the US (from 1986) and attempts were made by the users to manufacture something similar. They considered VAAR to be one of the most important binders used by the US Army. Fortunately Alcotex 20-009 is a good replacement for VAAR and was one of the binders described here in the manufacture of illuminating flare compositions (see experimental).

Crane et al⁹ and Manno¹⁰ describe the use of VAAR as a binder for pyrotechnic smoke compositions based on potassium chlorate, sugar and organic dyes. Martin and Danner¹¹ describe in their patent a combination of polyvinyl alcohol and gelling agent as a binder in match formulations. This is a replacement for traditional animal glue based binders. VAAR has been shown¹² to be a suitable binder for First Fire compositions. VAAR was found to be an effective binder and produced a composition that was significantly less sensitive to accidental ignition by impact, friction and electrostatic discharge. A reduction in production costs was realised. The use of VAAR as a binder for tracer compositions has been demonstrated¹³. These compositions were found to be particularly successful when used in tracer cartridges for small calibre, high velocity small arms rounds. Carrazza and Kaye¹⁴ discussed the long term and high temperature storage stability of VAAR based coloured flare compositions. They concluded that VAAR was a suitable binder for pyrotechnics with a long storage life. The MIGRAD mixer has been demonstrated^{15,16} as a suitable means of manufacturing sensitive pyrotechnic compositions. VAAR was used in these trials for first fires, ignition mixtures, delay and tracer compositions.

DISPOSAL OF WASTE PYROTECHNIC MATERIALS AND ARTICLES

There are two main sources of waste pyrotechnics; factory waste and time expired munitions/devices. Traditionally, methods of disposal include the following:

1. Landfill
2. Open pit burning
3. Closed pit burning (open top bunkers)
4. Sea dumping
5. Reworking

Factory waste was traditionally landfilled on site, although this practice has effectively ceased, mainly as a consequence of no more land being available, toxic emissions into

ground water and the occasional disastrous ignition of the waste. At present most factory waste is destroyed by open or closed pit burning (vented bunker), for articles that could project fragments or are otherwise too dangerous to dispose of by open pit burning. Many time expired marine pyrotechnics are disposed of by their owners by removing protective seals or caps and dropping overboard at sea. Sea dumping of munitions has been subject to a European ban since 1993. The en masse disposal of pyrotechnics could also be affected by this ban, but in any case the disposal of individual pyrotechnics at sea is undesirable. The pyrotechnic materials may be toxic and if articles have been disposed of incorrectly, they could be washed ashore posing a threat in particular to young children. Many time expired pyrotechnic devices failing a satisfactory method of disposal are often badly stored or unsafely discarded creating a hazard to the general public. Schemes for returning time expired civilian pyrotechnics to the manufacturer may have an environmental impact if there is no proper and safe method of disposal available. Large scale disposal of unwanted or time expired military pyrotechnics not consumed during training is presently impossible for most manufacturers, who lack the required facilities. Much of this waste is disposed of by the military or specialist companies, usually by open pit burning.

Open pit burning of pyrotechnics and composite rocket propellants can place a considerable burden on the local environment, the toxic emissions are often much greater than from the similar disposal of high explosives or gun propellants. Stores containing phosphorus emit clouds of phosphorus pentoxide / phosphoric acid and composite propellants containing perchlorates will yield hydrochloric acid. Pollution from metal oxide particulates and toxic metals such as barium are not insignificant.

RECYCLING PYROTECHNICS

Certain pyrotechnics, for example, flare compositions containing polyvinyl alcohol binders, may be recyclable. The oxidising agent component, if water soluble, can be washed out. As some polyvinyl alcohols, especially if fully hydrolysed, tend to retard burning rate, oxalate moderators may be omitted from the formulation, leaving behind various grades of coated magnesium. Polyvinyl alcohols thermally degrade to carbon dioxide and water leaving little or no ash and therefore pure magnesium can then be recovered from the melt. The oxidising agent for example, sodium or potassium nitrate could also be recovered and reused, perhaps as chemical fertilizer. Care is required in selecting a first fire that will not cause processing

difficulties, although the quantities of such material are generally very small compared to that of the main pyrotechnic component. The whole life cost of ownership may be subsequently reduced, coupled with an environmentally acceptable and profitable method of disposal. Polyvinyl alcohol wash waters are also biodegradable. Water based polyvinyl alcohols are probably unsuitable as binders for pyrotechnics where reactive metals are incorporated into the composition. The methanol or methyl acetate soluble, partially hydrolysed, polyvinyl alcohols are probably more suitable, whereas water soluble binders are particularly suitable for use with pyrotechnics containing water insoluble fuels and oxidising agents.

EXPERIMENTAL

The following illuminating flare compositions containing magnesium, sodium nitrate and polyvinyl alcohols were manufactured (see table 1). The magnesium - 50 mesh was supplied by Aldrich Chemical Company Ltd., and the magnesium - 325 mesh was supplied Ventron-Alfa Produkte. Alcotex 20-009 contained 28% solids whereas Alcotex 47P contained 40% solids.

	COMPOSITION 1 % by wt.	COMPOSITION 2 % by wt.
Magnesium - 50 mesh	50	50
Magnesium - 325 mesh	5	5
Sodium Nitrate	40	40
Alcotex 47P*	5	-
Alcotex 20-009*	-	5

*Dry weight - Polymers are supplied dissolved in methanol/methyl acetate

Table 1: Illuminating Flare Compositions Containing Polyvinyl Alcohol Binders

The following procedure was used in the manufacture of the compositions. The sodium nitrate was ground, dried and sieved prior to use. In a fume cabinet (hood) Alcotex binder solution was added to the magnesium in a plastic beaker. The contents were well stirred with a wooden spatula. The mixture was placed on a paper sheet and was well rubbed by hand to ensure effective coating of the magnesium. Care was taken that agglomerates did not form

during the coating procedure. After a period of about 15 minutes most of the solvent had evaporated and dry, coated magnesium powder was produced. The coated magnesium was hand blended with the sodium nitrate and passed three times through a coarse sieve. The composition was pressed as 25 g pellets at 3.4 tons in⁻² (0.54 tonnes cm⁻² / 50 MPa).

The pellets were successfully ignited using a small quantity of silicon/red lead igniting composition and plastic igniter cord to produce an intense yellowish white flame. Burning rate was between 3 and 4 mm/s.

The dissolution trial was carried out by placing a pellet of each composition in separate beakers containing 250 cm³ cold water. Both pellets completely broke down in less than 10 minutes - unstirred and approximately 3-4 minutes with occasional agitation.

DISCUSSION

Composition 2 was found to burn more quickly than Composition 1. Composition 2 contained Alcotex 20-009 which is less hydrolysed than Alcotex 47P used in Composition 1. This result indicates that the more hydrolysed the polyvinyl alcohol, the greater the retarding effect on the burn rate. This aspect could be useful when formulating compositions to burn at a specific rate, many pyrotechnics are liable to burn faster than desired. Polymer binders, especially polyvinyl alcohols, tend to desensitise pyrotechnic compositions towards impact and friction, which is a major safety consideration. Granulation with a binder can make a powdery pyrotechnic composition easier to handle and process.

Compositions containing polyvinyl alcohol binders can be readily manufactured using specially adapted mixers under remote control. The MIGRAD mixer^{15,16} and the MATRIX mixers supplied by T K Fielder in the UK are particularly suitable. The MATRIX mixers have been used for many years within the UK pyrotechnics industry for the manufacture of coloured and screening smokes, often with the incorporation of water soluble binders to assist in granulation and binding of the composition.

As little as 2% by weight polyvinyl alcohol binder is sufficient to produce compositions of very high tensile and compressive strengths. A composition has been reported⁴, consisting of HMX / polyvinyl alcohol 95/5 with a high compressive strength. This composition pressed

as a cylindrical pellet was capable of withstanding in compression a stress greater than 60MPa.

CONCLUSIONS

1. Polyvinyl alcohols are excellent binders for pyrotechnic compositions.
2. The lower hydrolysis polyvinyl alcohols as supplied in liquid form are very easy to use.
3. Polyvinyl alcohols can help desensitise pyrotechnic compositions from accidental ignition.
4. Polyvinyl alcohols can provide both oxygen and fuel to the pyrotechnic reaction.
5. Polyvinyl alcohols can form the basis of recoverable and recyclable compositions.

REFERENCES

1. C A Finch, Polyvinyl Alcohol - Developments, John Wiley & Sons, Chichester, 1992.
2. Mowiol Polyvinyl Alcohol (brochure), Hoechst Aktiengesellschaft, Marketing Kunstharze/Polymerisate, D-6230 Frankfurt am Main 80, December 1991.
3. S B Langston, J Akhavan & A S Cumming, Water Soluble Polymers as a Diagnostic Tool for the Examination of Pressed Plastic Bonded Explosives Based on HMX, 25th International ICT-Conference, Karlsruhe, Federal Republic of Germany, 28 June - 1 July 1994.
4. S B Langston, Mechanical Failure of HMX Based PBXs and its Relationship to Impact Sensitivity, 26th International ICT-Conference, Karlsruhe, Federal Republic of Germany, 4-7 July 1995.
5. S B Langston, Recoverable Explosive Compositions Based on the High Explosive HMX and Water Soluble Binders, R'95 "Recovery, Recycling, Re-Integration", Palexpo-Geneva, Switzerland, 1-4 February 1995.
6. Mil-V-50433 (MU), Military Specification, Vinyl Alcohol-Acetate Resin Solution (VAAR) (For use in Ammunition), 3 July 1969.
7. TS10235A, Polyvinyl Alcohol for Lacquers Type QX, MQAD Headquarters Building, Royal Arsenal East, London.
8. F R Taylor and D E Jackson, Development of a Polymer Binder for Pyrotechnic Compositions, 11th International Pyrotechnic Seminar, Vail, Colorado, USA, July 1986.

9. E D Crane, B Werbel and G Weingarten, Development of Burning-Type Colored Smokes, Technical Report 3273, Pyrotechnics Laboratory, Feltman Research Laboratories, Picatinny Arsenal, Dover, N.J., USA, August 1966.
10. R Manno, Use of Organic Dyes in White Smoke Formulations, Technical Memorandum 1839, Picatinny Arsenal, Dover, New Jersey, USA, September 1968.
11. R R Martin, J R Danner Jr., U.S. Patent 3650712, Combination of Polyvinyl Alcohol and Gelling Agent as a Binder in Match Formulations, 21 March 1969.
12. J A Carrazza, S M Kaye, F R Taylor, Development of a Safer Intermediate and First Fire Formulation for the M49A1 Surface Trip Flare, Feltman Research Laboratory, Picatinny Arsenal, Dover, New Jersey, USA, July 1974.
13. W W Cavell, W E Perkins & J J Caven, Smaller, Faster, Brighter, Frankford Arsenal Report FA-A67-15, August 1967. (Ordnance July-August 1967).
14. J A Carrazza Jr., S M Kaye, Storage Stability of Pyrotechnic Compositions Containing Vinyl Alcohol Acetate Resin, Technical Report 3357, Picatinny Arsenal, Dover, New Jersey, USA, November 1966.
15. L M Aikman, T E Snook, R M Lehr & E Robinson, Improved Mixing, Granulation and Drying of Highly Energetic Pyromixers, Pine Bluff Arsenal, Pine Bluff, Arkansas, US. (supplied through APV Chemical Machinery Ltd., Cooper Street, Hanley, Stoke-on-Trent, England)
16. W Miller, MIGRAD System for Pyrotechnic Mixes, Live Testing, Technical Paper for ADPA Joint Symposium, Virginia Beach, Virginia, 23-25 October 1989.

ACKNOWLEDGEMENT

The author wishes to thank Dr Peter Shaw of Harlow Chemical Company Ltd., for his valuable assistance in supplying polymer samples and background information relating to polyvinyl alcohols.

**ENERGETIC CHARACTERISTICS OF AMMONIUM PEROXOCOMPOUNDS
OF NIOBIUM AND TANTALUM.**

Georgy Kozak, Vlada Raykova
Mendeleev University of Chemical Technology,
Miuskaya sq. 9, Moscow A-190, 125-190 Russia

ABSTRACT

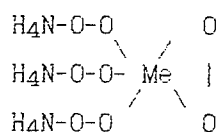
The results of investigation are proposed of the explosive behavior of ammonium tetraperoxoniobate and tetraperoxotantalate, (APONb and APOTa) of the general formula of $(\text{NH}_4)_3 \text{MeO}_8$. The slow thermal decomposition reaction of both compounds: $2 (\text{NH}_4)_3 \text{MeO}_8 \rightarrow 6 \text{NH}_3 + \text{Me}_2\text{O}_5 + 3 \text{H}_2\text{O} + 4 \text{O}_2$, was performed in the glass test tube supplied by the thermocouple. The temperature of the beginning of the quick reaction accompanied by the essential temperature rise of the dry sample (1-1.5 g) was $43 \pm 2^\circ \text{C}$ for APONb, and $74 \pm 3^\circ \text{C}$ for APOTa. The high temperature decomposition had a rather violent character but did not lead to selfignition of the sample. Moistened samples of APONb and APOTa decomposed slower than dry ones. Both of the peroxocompounds burned at atmospheric pressure by electric ark like flame. The failure diameter of detonation in the conical paper tube of APONb ($\rho_0 = 0.7 \text{ g/cm}^3$) was 3 mm, of APOTa ($\rho_0 = 0.3 \text{ g/cm}^3$) - 1.5 mm. The detonation velocity of APOTa at the charge density of $0.9\text{-}2.1 \text{ g/cm}^3$ in the thick-walled steel tubes of $d = 10 \text{ mm}$ $D = 0.43 + 2.07 \rho$, km/s.

Introduction

Ammonium tetraperoxoniobate and tetraperoxotantalate (APONb and APOTa) are used as catalysts of some reactions in organic chemistry, as sources of especially pure oxides of tantalum and niobium but unfortunately up to date they are not investigated as energetic materials and correspondingly as the potentially dangerous substances. Some of physicochemical and crystallographic properties of them are described in [1].

47 - 2

APONb and APOTa of the general formula of $(\text{NH}_4)_3\text{MeO}_8$, or structural one:



are rather unusual but perspective pyrotechnic components possessing a rather big but till now still indefinite quantity of potential energy.

It is well known [2], that enriching of substances by peroxogroups leads to increase of explosion hazard, so in conformity with their structural formula APONb and APOTa could be expected to be an explosives.

Experimental data

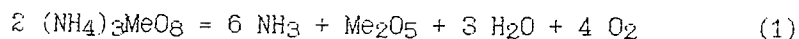
Preparation.

APONb and APOTa were produced by action of mixture of ammonia water solution with hydrogen peroxide on a solution of metal oxide in hydroflouric acid. The neat products precipitated from solution as a fine powdered yellow crystalline substances.

The chemical composition of investigated compounds corresponded to foregoing formula. The experiment elements percentage differed from theoretical one not more than 0.2-0.4%.

Slow thermal decomposition

APONb and APOTa decompose in accordance with equation [1]:



The slow thermal decomposition of both compounds was performed in the glass air thermostate constructed from two test tubes (diameter of inner tube was 13 mm, air clearance

was 2,5 mm). The wall of outside test tube was heated by electrical coil. The thermocouple inserted into quartz capillary was placed into layer of sample ($m=1-1.5$ g). The temperature rise velocity by external heating was in limits of $V_h = 0.2-0.5$ K/s. The time-temperature dependences $T(t)$ were registered in every run by automatic recorder.

The $T(t)$ curves of dry samples of APONb and APOTa are showed at Fig.1-2. The first period (from $t=0$, to $t=t_r$) was linear heating of the samples by electrical coil. After reaching $T=T_r$ a linear character of curves broke and sharp growth of temperature appeared. T_r - the temperature of beginning of quick reaction. Quick reaction was accompanied by selfheating and essential rise of temperature of the sample from T_r to maximal temperature - T_m (period of time from t_r to t_m).

Curves $T(t)$ for APONb and APONTa are similar each other, they are compared on the Fig.2. The high temperature decomposition had a rather violent character but did not lead to selfignition of the sample obviously due to the high ignition temperature of $NH_3-O_2-H_2O_{(vap)}$ mixture obtained as a main gaseous products of the decomposition. The smell of ammonia was felt during decomposition.

If gas above test tube was ignited by a source of flame laminar front burning propagated in gas to bottom of test tube and then burning damped. This procedure could be repeated two-three times during decomposition.

The results of runs are collected in Table 1. The temperature of beginning of the quick exothermic reaction of APONb (T_r) was $43 \pm 2^\circ C$. The maximum temperature of sample $T_m=150^\circ C$. The temperature of beginning of the quick reaction of APOTa was much more $T_r=71-78^\circ C$. The maximal temperature of APOTa was much more too.

Moistenining (15-28% of water) of APONb and APOTa changed the character of decomposition curves $T(t)$ in comparision with dry samples (Fig.3). The region of very slow temperature rise was appeared on the curves (t_o-t_r). The acceleration of temperature rise began after this

period. Ammonia was produced during the period of slow temperature rise and apparently the hydrolysis of APONb and APOTa proceeded.

The results of investigation of moistened samples are collected in Table 2. The temperature of beginning of hydrolysis of APONb was $T_0 = 75^\circ\text{C}$ and of APOTa $T_0 = 84-92^\circ\text{C}$. The temperature of beginning of the quick exothermic decomposition was the same for both moistened substances - $T_r = 92-96^\circ\text{C}$. Maximal temperature of APOTa ($T_m = 198-228^\circ\text{C}$) was higher than of APONb ($T_m = 165-182^\circ\text{C}$).

The enthalpies of formation of APONb and APOTa have not been found in literature. Using the nearly adiabatic calorimeter we determined the approximate heat of decomposition of APONb ($Q_r = 48 \text{ kJ/mol}$). It permitted to estimate the enthalpy of formation of APONb in accordance with equation (1): $\Delta H_f = -1.4 \pm 0.2 \text{ MJ/mol}$.

Burning and detonation of peroxocompounds

The burning rate is one of the main characteristics which defines an explosion hazard of energetic material.

Both of dry powdered peroxocompounds were ignited easily from source of flame and burned at atmospheric pressure by electric arc like flame. The rest after burning was the almost pure powdered metal oxide. Burning rate of APOTa of density $\rho = 0.12 \text{ g/cm}^3$ at atmospheric pressure was measured in the quartz tube ($d = 8 \text{ mm}$): $U_1 = 0.09 \text{ cm/s}$. In charge of $\rho = 0.75 \text{ g/cm}^3$ the burning damped quickly after ignition.

Ability to detonation of APOTa and APONb was characterized by the size of failure diameter (d_f). Detonation velocity (D) was an additional characteristic.

d_f was defined in cone shape (angle at the top $\alpha = 1.6^\circ$) paper tube. The charge was fixed at aluminium plate-witness. Detonation was initiated by standard detonating cap from the side of large size diameter. The place of interruption of the detonation dent on plate-witness defined the value of failure diameter.

Detonation velocity was measured in steel tubes ($d = 10$

mm, thickness of wall - 13 mm). The radial holes ($d=2$ mm) were drilled in wall of tube with step of 25 mm to have an opportunity to receive the streak-camera records by the Russian analog of streak-camera - VFU-2.

The failure diameter of APONb ($\rho=0.7$ g/cm³) was $d_f=3$ mm, of APOTa ($\rho=0.3$ g/cm³) - $d_f=1.5$ mm.

Detonation velocity of APONb ($\rho=0.93$ g/cm³) was $D=2.06$ km/s. The dependence $D(\rho)$ of APOTa in region $0.9<\rho<2.1$ g/cm³ was measured:

$$D = 0.43 + 2.07 \rho, \text{ km/s}$$

(six runs, coefficient of correlation $R=0.995$)

The pressed pellets ($d=h=12$ mm) of retarded by paraffin (5%) APOTa ($\rho=2.1\pm0.02$ g/cm³) were received at pressure of pressing of 0.165 GPa. The charge gathered from nine pressed pellets (common length ~ 100 mm) was tested without any confinement and had detonation velocity $D=4.68$ km/s. The attempt of pressing APOTa without retarder led to explosion of pellet at ejection from press filter.

Some runs were carried out with mixtures of peroxocompounds with inert diluents. One of them bromoform had density (2.82 g/cm³) almost equal to density of crystalline APOTa (2.87-2.91 g/cm³). Detonation velocity of mixture 50/50 APOTa and bromoform was measured. This mixture of density (2.72, 2.83, and 2.87 g/cm³) detonated in three runs in glass tubes ($d=14$ mm) with velocity 4.36, 4.57, and 4.65 km/s accordingly. The second diluent - water was interesting as technological addition at production of peroxocompounds. Detonation of moistened samples of APOTa (15% of water) of density 1.87 g/cm³ in steel tube ($d=10$ mm, thickness of wall 13 mm) was stable. The mixture of APONb with higher percentage of water (30%) did not detonate in these conditions.

It is necessarily to note that mixtures of APOTa with bromoform (50%) and water (15%) did not burn at atmospheric pressure.

The impact sensitivity of APOTa and APONb was investigated on impact machine (Russian model K44-II) in stemp tool N1 (mass of sample 0.05 g, rollers of 10 mm

diameter with facets). The sensitivity was characterized by frequency of explosion at the falling weight $m=10$ kg at the high of weight fall down $H=50$ cm in twenty five runs. The frequency of explosion of APONb was 20% and of APOTa was 70%. The explosion of APONb and APOTa was accompanied with the same sound of shot and flame as in the case of usual high explosives. Impacts on dry peroxocompounds at steel plate by hammer initiated no failure explosions.

Effect reminding explosion (a snap) took place sometimes at investigation of impact sensitivity of moistened peroxocompounds, nevertheless a flame have never been observed in this case.

Conclusion.

APONb and APOTa are able to selfheating and selfpropagating decomposition but selfignition was not observed though the maximal temperature of selfheating reached in some runs to 250°C . It must be noted that ammonia and oxygen are formed at decomposition and their volume ratio is closed (3:2) to explosive limits of $\text{O}_2\text{-NH}_3$ mixture (15-57% of ammonia).

Investigated peroxocompounds are able to detonation and their failure diameter is smaller at low density than of some nitrocompounds and ammonites.

Burning rate of APOs is closed to one of such high explosives as RDX and dinitrate ethylen glycol.

Moistening (15-30% of water) of APONb and APOTa increases greatly the delay time of exothermic decomposition, makes difficult ignition, decreases impact sensitivity. However small quantity (15%) of water and significant quantity (50%) of bromophorm does not prevent detonation of peroxocompounds. The possibility of drying and corresponding rise of explosion hazard must take into account at treatment of these products.

It can be concluded that both of the ammonium peroxocompounds investigated are rather dangerous explosives and treatment of them in practice has to be

performed with necessary carefulness.

ACKNOWLEDGEMENTS

We are most grateful to Prof. B.N.Kondrikov for useful discussion and to Dr.L.M.Avdonina who synthesized investigated substances.

References

1. Volnov I.I. Peroxokomplexy vanadiya, niobiya i tantala. Moskva. Nauka. 1987.
2. Andreev K.K., Belyev A.F. Teoriya vzryvchatykh veschestv. Moskva.Oborongiz. 1964

Table 1

The parameters of the slow thermal decomposition
of APONb and APOTa

Subst.	m, g	V _h , K/s	Temperature, °C		Time, s	
			T _r	T _m	t _r	t _m
APONb	1	0.3	46	155	76	86
	1	0.2	41	140	100	120
APOTa	1.5	0.3	71	253	188	205
	1.5	0.26	78	226	228	247

Table 2

Influence of water on the parameters of slow thermal
decomposition of APONb and APOTa

Subst.	H ₂ O %	m, g	V _h , K/s	Temperature, °C			Time, s		
				T ₀	T _r	T _m	t ₀	t _r	t _m
APONb	28	1	0.47	75	92	182	136	280	430
	28	1	0.38	75	92	170	136	280	400
	28	1	0.35	75	94	165	136	280	390
APOTa	15	1.5	0.37	92	96	198	218	352	414
	15	1.5	0.36	84	92	228	210	376	490

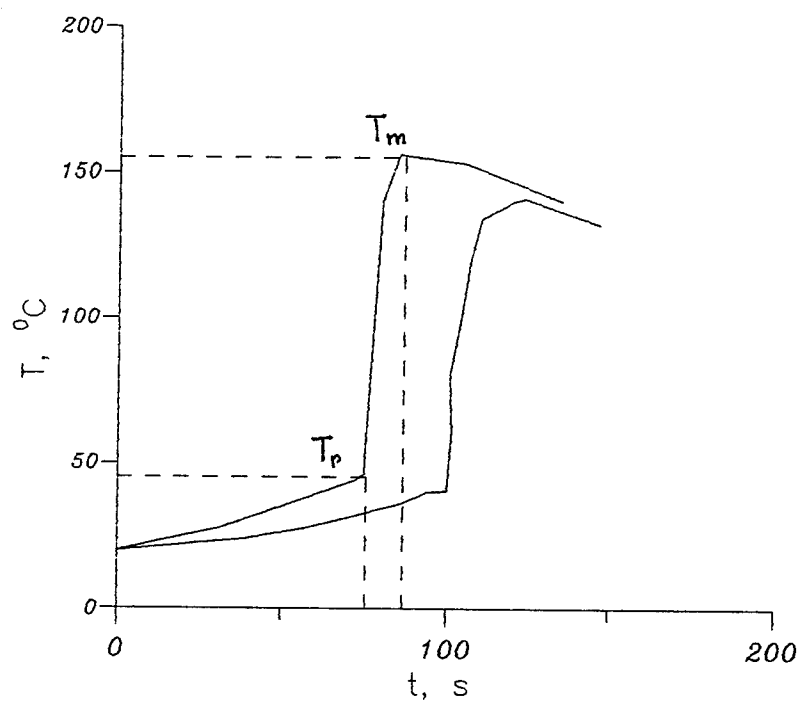


Fig.1. Time-temperature dependence for APONb.

T_p - temperature of the beginning of quick reaction.

T_m - maximal temperature.

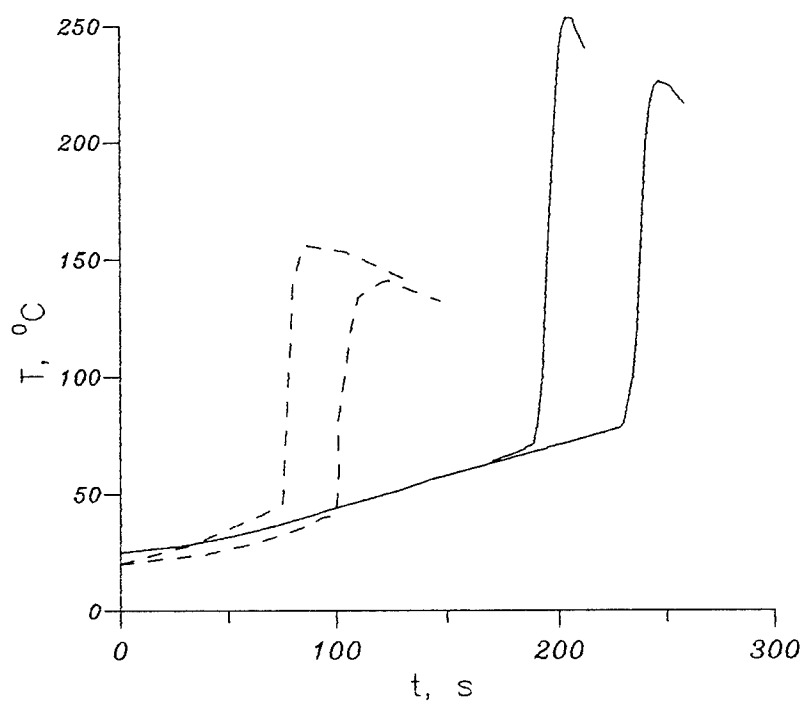


Fig.2. Comparison of time-temperature dependences for APONb (dotted line) and APOTa (solid line).

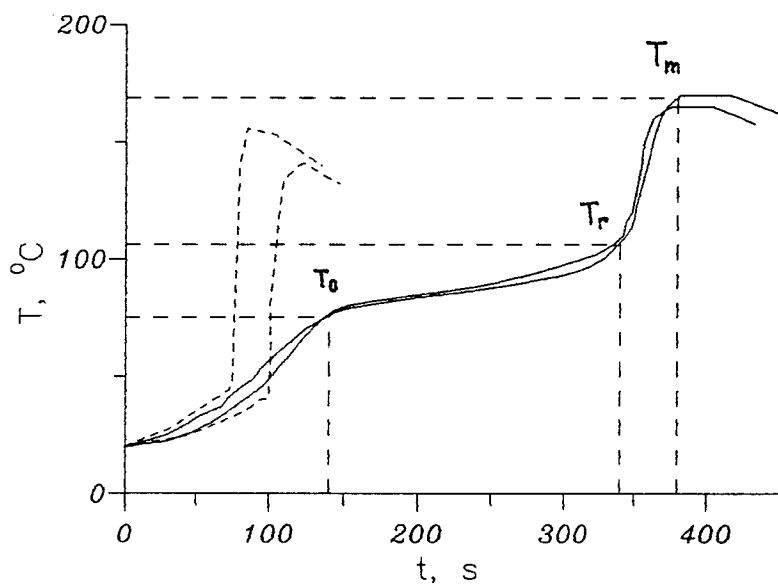


Fig.3. Influence of water (28%) on time-temperature dependence for APONb.

Dotted line - dry sample, solid line - moistened sample. T_0 - temperature of beginning of hydrolysis, T_r - temperature of beginning of the quick reaction, T_m - maximal temperature.

**PYROTECHNIC COMPOSITIONS OF ZIRCONIUM AND CHROMATES OF
ALKALINE EARTH METALS**

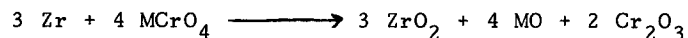
Reuben Daniel, R.G.Sarawadekar
Explosives Research & Development Laboratory
Pashan, Pune, India
and
U.C.Durgapal*
Institute of Armament Technology
Girinagar, Pune, India

ABSTRACT

A study was carried out of pyrotechnic compositions based on zirconium metal as fuel and chromates of Group IIA elements viz. Mg, Ca, Sr and Ba as oxidizers. Burning rates of mixtures containing 10 to 90% zirconium as fuel were determined, in steps of 10% by the lead tube method. Generally, the compositions containing 30-70% zirconium were ignitable and burnt uniformly. The compositions containing 50% Zr showed a decrease in burning rate from 4.88 cm/s to 2.16 cm/s when passing from magnesium chromate to barium chromate. This could be related to ionic character and ionisation potential of the elements.

DTA thermograms in air showed main exothermic peaks at 426 °C for Zr-MgCrO₄ while zirconium with other chromates showed peak at about 326 °C. Another prominent peak at 600 + 20 °C was observed for air oxidation of excess zirconium in all cases. All the peaks were very broad which indicated that the combustion reaction between zirconium and metal chromates was quite slow. A general equation for

the reactions can be written as:



Where M = Mg, Ca, Sr, Ba.

*Correspondence author.

The slag obtained from combustion was analysed by X-ray diffraction and IR spectra. It was observed that ZrO_2 was formed alongwith metal oxide and Cr_2O_3 . Presence of metal zirconates was also detected. Similarly, analysis by IR spectra indicated the formation of ZrO_2 , Cr_2O_3 , ZrO_3 etc.

The composition containing MgCrO_4 exhibited impact sensitivity in a fall hammer apparatus, but the height of 50% explosion was above 100 cm. Other composition were insensitive upto 175 cm height for 2 Kg drop weight. The compositions studied were also found insensitive to friction upto 36 Kg load. It is concluded that these compositions are safe to handle and may find practical applications in medium to fast pyrotechnic delays.

1. INTRODUCTION

Zirconium powder has been used as a fuel alongwith various oxidizers and studies have been reported for the systems Zr/PbO_2 (1,2), Zr/KClO_4 (3) and Zr/BaCrO_4 (4). In the present work oxidation of zirconium by chromates of alkaline earth metals namely Mg, Ca, Sr and Ba has been studied employing differential thermal analysis, thermogravimetry, infrared spectroscopy and x ray diffraction spectroscopy. Their burning rates and their sensitivity to impact and friction have also been studied.

2. EXPERIMENTAL

2.1 Materials

Zr metal powder used in the present study had an average particle size of 4.4 micron and its purity was

99.5%. Alkaline earth chromates were of 99% purity.

2.2 Methods

The compositions were granulated by using 2% nitrocellulose binder. DTA/TG was carried out on a Netzsch STA 409 thermal analyser in air. Infrared spectra of slags were done on a Perkin-Elmer IR spectrophotometer model 683 in KBr matrix, and x-ray diffraction patterns of the same were recorded on an x-ray diffractometer of the type 1730/90 PHILLIPS (Holland) using Cu-K radiations at room temperature. Friction sensitivity tests were carried out on Julius Peters apparatus.

3. RESULTS AND DISCUSSIONS

3.1 Burning Rate

The burning rates of various Zr/Chromate mixtures determined by the lead tube method are presented in Table I. All the mixtures having 10% Zr were not ignitable in the lead tube. In addition Zr/CaCrO₄ containing 20% and 80% Zr and Zr/BaCrO₄ containing 20% Zr did not ignite. While Zr/MgCrO₄ burnt with a bright flame, the mixtures of Zr and chromates of Ca, Sr, Ba gave smooth gasless combustion.

In all cases the burning rate increases with increasing percentage of zirconium, reaches a maximum value and decreases again. High burning rate of 5.714 cm/s in case of 40:60 Zr/SrCrO₄, leading to a nearly flat burning rate region could not be explained. It was also interesting to note that the burning rate for 50:50 mixtures increased in the order Ba Sr Ca Mg whereas the ionic radii of these elements decreased in that order. The trend is observable for all mixtures in the range 30:70 to 70:30 except for strontium which behaves differently.

In general the compositions burn fast and may be applicable to fast or medium-fast pyrotechnic delays.

3.2 Thermal Analysis

In a pyrotechnic delay system the onset of ignition is governed by the ignition temperature which in turn is governed by the composition itself (i.e. fuel-oxidiser ratio). The oxidiser content also governs the kinetics of the reaction, the total heat produced in the reaction and the mechanism of the reaction.

Another common observation is that though the majority of oxides and other oxidants have high decomposition temperatures, the reaction with a reactive, metal starts at a much lower temperature. Zirconium on oxidation always yields the oxide ZrO_2 , the oxidation reaction being highly exothermic. The chromates of the alkaline earth metals decompose at very high temperatures. It is expected that on heating zirconium with the chromates the onset of the reaction will take place at much lower temperature and the same has been observed in the present study.

3.2.1 Zirconium : Magnesium Chromate System

DTA/TG data of this system is presented in Table II. There are three endotherms and two exotherms. The three endotherms appear in the temperature range of 67-135°C, 167-243°C and 238-337°C. All these endotherms are due to stepwise removal of four molecules of water of crystallisation of $MgCrO_4$ which is confirmed by TG data which shows weight loss in three steps. The first exotherm which is due to the main reaction of zirconium and magnesium chromate starts at around 411°C and ends at 467°C with peak at 426°C. Only in the case of 70:30 the peak has shifted to 442°C. The exotherm due to air oxidation of excess zirconium begins at around 490°C and ends at 694°C with the peak at 563°C with 2.5% weight gain for 30% Zr, 8.0% weight gain for 50% Zr and 18.5% weight gain for 70% Zr.

3.2.2 Zirconium : Calcium Chromate System

The DTA data (Table III) of the system shows three exotherms. The first exotherm starts at 148°C and ends at 260°C with a peak at 203°C which is attributed to the decomposition of the binder i.e. nitrocellulose whose decomposition is reported at 162-170°C. The small weight loss accompanying this exotherm is likely to be due to loss of half a molecule of water of crystallisation. The second exotherm appears between 260°C to 391°C with peak at 315°C; this exotherm is the result of the main reaction between zirconium and calcium chromate. It appears that the reaction is by diffusion process without the liberation of any gases. The third exotherm between 319-680°C with the peak at 588°C is attributed to the air oxidation of zirconium which is supported by TG data which shows a weight gain of 9.5% for 30% zirconium showing that oxygen is taken up from the atmosphere for the oxidation process. TG also shows an increase in weight during oxidation as the % of Zr is increased.

3.2.3 Zirconium : Strontium Chromate System

The DTA curves of all the mixtures of this system show three exotherms and gain in weight is shown by TG alongwith the third exotherm. The first exotherm appears in the range of 175-230°C with peak at 200°C which is due to nitrocellulose binder. The second exotherm is due to the main reaction between zirconium and strontium chromate and is in the range of 250-416°C with peak at 315°C and the third exotherm due to oxidation of excess zirconium is in the range of 412-650°C with peak at 568°C, also confirmed by gain in weight by TG, thus showing that excess unreacted zirconium is available for air oxidation. Data is presented in Table IV.

3.2.4 Zirconium : Barium Chromate System

This system also showed three exotherms the first

one in the range 160-260°C and peak at 215°C, second one from 270-400°C with peak at 321°C and the third from 400-780°C with peak at 600°C (Table V).

It is thus seen that peak temperatures were increasing from top to bottom in the II-A group chromates. Hence, the reactivity of the chromates with zirconium decreases in this order.

3.3 X-ray Diffraction of Combustion Residues

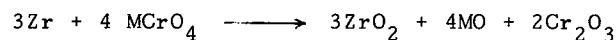
The combustion residues were analysed by x-ray diffraction. X-ray diffraction patterns of Zr-MgCrO₄ and Zr-CaCrO₄ are shown in Fig 1 & 2 respectively. It is observed that zirconium dioxide is formed along with zirconate (5). It also shows the formation of MgO (3.06, 2.97, 2.09 Å°), Cr₂O₃ (2.66, 2.46, 2.09, 1.57 Å°), ZrO₂ (2.97, 2.65, 1.86 Å°), and CaO (2.40, 2.34, 1.71, 1.63 Å°), Cr₂O₃ (3.62, 2.67, 2.48, 1.80 Å°), ZrO₂ (3.17, 3.00, 2.86, 1.99, 1.85 Å°) and CaZrO₃ (4.01, 3.96, 2.89, 2.82, 1.63 Å°). These values are comparable with ASTM cards (6).

3.4 IR Spectra of Combustion Residues

IR spectra of the slags shows the formation of ZrO₂ (490, 430, 428, 375 cm⁻¹), Cr₂O₃ (628, 550 cm⁻¹), MgZrO₃ (310, 320 cm⁻¹). In the system Zr-CaCrO₄ it showed the formation of ZrO₂ (486, 430, 375 cm⁻¹), Cr₂O₃ (628, 552 cm⁻¹) & CaZrO₃ (715, 510, 325 cm⁻¹). Similarly in the systems Zr-SrCrO₄ and Zr-BaCrO₄ the slags show the formation of oxides and zirconates (7). Absorption peak values are compared with IR spectra given in the literature (8).

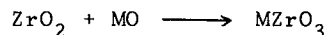
3.5 Reaction Mechanism

The basic mechanism of the reaction of all these systems can be written as follows:



Where M = Alkaline earth metal.

The combustion products of the above reaction have been confirmed by IR spectra. The presence of zirconate was also detected with all the four cases, thus showing that the following additional reaction may be taking place.



Where M = Alkaline earth metal.

3.6 Sensitivity of the Compositions to Impact and Friction

Out of all the compositions studied it was found that only Zr/MgCrO₄ mixtures were sensitive to impact. All the compositions were found to be insensitive to friction upto 36 kg pistil load on a Julius Peters apparatus thus showing that they are safe to handle from the point of view of friction sensitivity.

4. CONCLUSION

DTA data of zirconium/alkaline earth chromates shows that exothermic reactions between Zr and the chromates in most of the cases are within the temperature range 250-450°C. Study of combustion residues has indicated formation of ZrO₂, alkaline earth oxides and zirconates.

Burning rate studies indicate very fast burning rates in all cases. The fastest burning rate is 8.26 cm/s in the case of Zr:SrCrO₄ system at 70:30 ratio and the slowest burning rate is 0.374 cm/s in the case of Zr:MgCrO₄

system at 20:80 ratio. All these burning rate values are quite high and indicate the possibility of applications of the systems to fast or medium fast pyrotechnic delays. Burning rate data also broadly indicate that there could possibly be some correlation between ionic radii of the elements Mg, Ca, Sr, Ba and burning rates of their chromates with Zirconium.

REFERENCES

1. Earl E. Kilmer, Patent US 3, 150, 020 (1964).
2. AMC Pamphlet, "Engineering Design Handbook Military Pyrotechnic Series", Part I - Theory and Application, HQ US Army 28th April 1967, P-5.34-5.35.
3. Durgapal UC, Dixit AS, Sarawadekar RG, Proc. 13th Int. Pyrotechnic Seminar, IIT Research Institute, Chicago, 1988, p-209.
4. Fumio Kondo : Patent Japan 2624 (1956).
5. Tadashi, Nishino, Kasakichi, Moteki and Shusaku Nishiyama, "Reactions in the System $\text{CaO-Cr}_2\text{O}_3\text{-ZrO}_2$ and $\text{CaCrO}_4\text{-ZrO}_2$ ", Kogyo Kagaku Zasshi 69(4), p 622-5, (1966), Japan.
6. Alphabetical and Grouped Numerical Index of X-ray Diffraction Data, ASTM Cards (1950).
7. Galkin Y.M. and Chukhlantsev V.G., "The system BaO-ZrO_2 in the BaO rich region" 1 (11) p-1952-4, (1965), (Russian).
8. Nyquist R.A. and Kagel R.O., "Infrared Spectra of Inorganic Compounds", Academic Press, New York.
9. Cackett J.C., "Monograph on Pyrotechnic Composition", Royal Armament Res & Dev Estt, 1965, p 82.

TABLE I
COMPARISON OF BURNING RATES OF ZIRCONIUM/ALKALINE EARTH
CHROMATES

Zr/ Chromate ratio	BURN RATE, cm/s			
	Magnesium Chromate	Calcium Chromate	Strontium Chromate	Barium Chromate
20:80	0.374	*	0.586	*
30:70	2.105	0.775	1.739	1.039
40:60	3.636	2.146	5.714	1.482
50:50	4.878	4.550	4.219	2.164
60:40	5.495	5.182	5.555	3.077
70:30	6.173	4.762	8.264	4.348
80:20	5.525	4.000	7.299	4.762
90:10	4.717	*	1.695	2.353

* Did not burn.

TABLE II
 THERMOANALYTICAL DATA OF ZIRCONIUM/MAGNESIUM CHROMATE IN
 AIR

Composi- tion ratio (W/W) Zr: MgCrO ₄ ·4H ₂ O	Differential Thermal Analysis				Thermogravimetric Analysis			
	Endotherm		Exotherm		TG Steps	Temp Range °C	% Loss in wt	% Gain in wt
	Temp Range °C	Peak Temp °C	Temp Range °C	Peak Temp °C				
30:70	67-122	102	-	-	1st	67-116	16	-
	173-238	203	-	-	2nd	161-321	9	-
	238-326	300	-	-	3rd	348-385	1	-
	-	-	411-462	426	-	-	-	-
	-	-	523-612	573	4th	478-588	-	2.5
50:50	67-135	102	-	-	1st	67-109	11.5	-
	167-243	201	-	-	2nd	142-209	3.5	-
	243-337	294	-	-	3rd	243-411	6	-
	-	-	411-467	426	-	-	-	-
	-	-	493-694	563	4th	467-755	-	8
70:30	71-109	89	-	-	1st	74-96	6.5	-
	167-220	197	-	-	2nd	167-209	2.5	-
	249-305	288	-	-	3rd	271-294	1.0	-
	-	-	400-498	442	-	-	-	-
	-	-	498-694	563	4th	342-741	-	18.5

TABLE III
THERMOANALYTICAL DATA OF ZIRCONIUM/CALCIUM CHROMATE IN AIR

Composition ratio (W/W) Zr:CaCrO ₄ · 0.5 H ₂ O	Differential Thermal Analysis		Thermogravimetric Analysis			
	Exotherm		TG Steps	Temp Range °C	% Loss in Wt	% Gain in Wt
	Temp Range °C	Peak Temp °C				
30:70	148-260	203	1st	148-277	4.5	-
	260-391	315	2nd	353-713	-	9.5
	391-680	588	-	-	-	-
50:50	167-260	200	1st	191-283	2.93	-
	260-411	326	2nd	348-732	-	16.09
	411-680	588	-	-	-	-
70:30	179-271	209	1st	185-266	1.5	-
	271-462	342	2nd	332-713	-	23.25
	462-713	593	-	-	-	-

TABLE IV
THERMOANALYTICAL DATA OF ZIRCONIUM/STRONTIUM CHROMATE IN AIR

Composition ratio (W/W) Zr:SrCrO ₄	Differential Thermal Analysis		Thermogravimetric Analysis		
	Exotherm		TG Steps	Temp Range °C	% Gain in Wt
	Temp Range °C	Peak Temp °C			
30:70	185-232	200	-	-	-
	249-416	315	-	-	-
	416-651	568	1st	416-700	9.0
50:50	173-220	197	-	-	-
	220-315	277	-	-	-
	422-637	533	1st	406-685	-
70:30	179-226	200	-	-	-
	249-416	326	-	-	-
	421-666	578	1st	348-670	21.0

TABLE V
THERMOANALYTICAL DATA OF ZIRCONIUM/BARIUM CHROMATE IN AIR

Composition Differential ratio (W/W) Thermal Analysis		Thermogravimetric Analysis			
Zr: BaCrO ₄					
Exotherm					
Temp Range °C	Peak Temp °C	TG Steps	Temp Range °C	% Gain in Wt	
30:70	160-268	215	-	-	-
	268-406	321	-	-	-
	406-751	598	1st	406-751	13.26
50:50	179-249	209	-	-	-
	288-395	321	-	-	-
	395-779	600	1st	395-779	16.83
70:30	188-260	215	-	-	-
	271-411	326	-	-	-
	411-797	598	1st	411-797	26.66

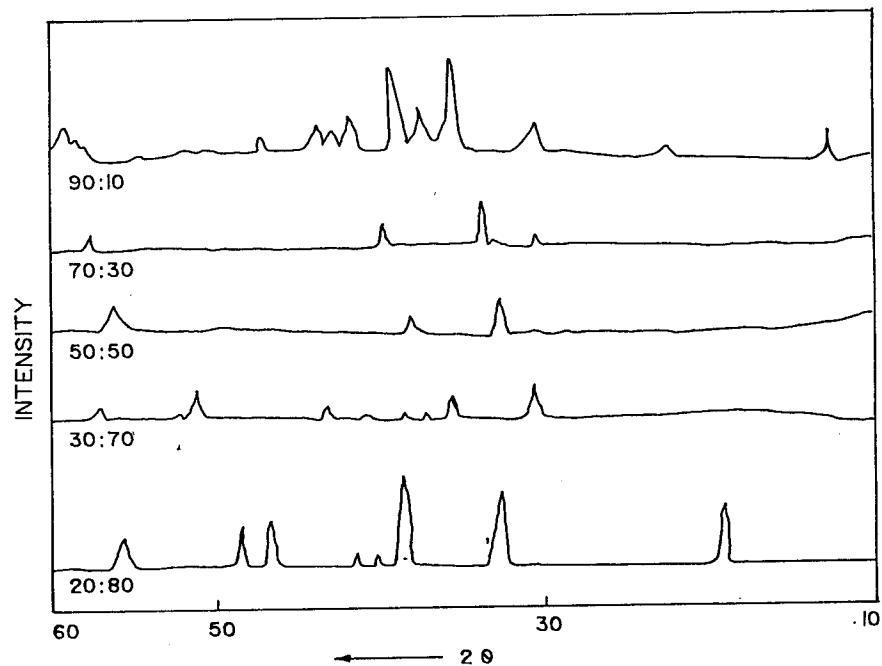


FIG. 1 - X-RAY DIFFRACTION PATTERNS OF SLAGS OF ZIRCONIUM-MAGNESIUM CHROMATE SYSTEM.

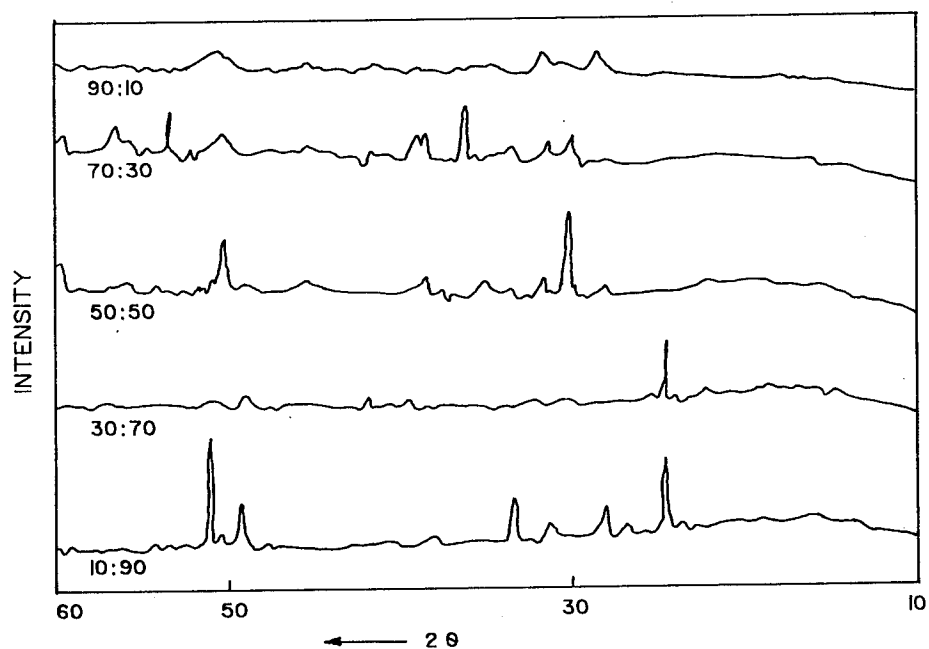


FIG. 2 - X-RAY DIFFRACTION PATTERNS OF SLAGS OF ZIRCONIUM-CALCIUM CHROMATE SYSTEM.

ADHESION PROPERTIES OF LINER TO PROPELLANT AND METAL IN HTPB BASED SYSTEMS

Serkan Burak Haska, Fikret Pekel,

Defense Industries Research and Development Institute, TÜBİTAK, P.K. 16 Mamak,
06261 Ankara, TURKEY

Erdal Bayramlı, Saim Özkar,

Department of Chemistry, Middle East Technical University,
06531 Ankara, TURKEY

Summary

A liner composition was developed for an aluminized HTPB/AP composite propellant using HTPB (R45-M) as binder, isophoron diisocyanate (IPDI) as curing agent, dioctyladipate (DOA) as plasticizer, carbon black (Printex-U) as filler, and an aziridine-based bond promoter. The propellant-liner bonding was tested by several bond failure analysis including the mechanical, shear and peel tests. The effects of various components were optimized to obtain a reliable liner formulation which possesses good bonding, and a soft tacky state during contacting the matrix. The shear and peel tests were used to study the adhesion between the metal-liner and the propellant-liner matrix systems. The adhesion strength of the system was measured on tensile test specimens. In the compositions achieved by this way, the adhesion of liner to propellant was found to be stronger than the cohesive strength of the matrix so that the failure occurred from the matrix. The effect of bond promoter was investigated in adhesion tests and it was found that bond promoter in the liner composition up to 2% increases the adhesion strength significantly. The shear and tensile tests applied to the liner-metal system showed that the adhesive strength of the system is better than cohesive strength of the liner. Adhesion of liner to aluminum was found to be better than that of liner to steel.

Introduction

The complexity of case bonded HTPB liner systems has forced studies towards refining the lining process variables with the goal of increasing the reliability of bonds at all interfaces between layers. The similarity of the matrix and the liner in their chemical structure and composition is vital to assure optimum compatibility and effective adhesive bonding. The main objective of this study is to develop an efficient and reliable matrix for a liner chemical bonding system that fails cohesively in the propellant, any other failure mode being unacceptable.⁽¹⁾ The desired liner compositions should also provide heat-insulation together with a reliable adhesive bond having an adhesive strength at least equal to the cohesive strength of the propellant.⁽²⁾ Partially cured liners are used in bonding studies. Compositions studied consist of HTPB (R45-M), isophoron diisocyanate (IPDI) as curing agent, dioctyladipate (DOA) as plasticizer, carbon black (Printex-U) as filler, and an aziridine-based bond promoter. In order to have good bonding, the liner should be in a soft and tacky state during contacting the matrix. The propellant-liner bonding was tested by a combination of several bond failure analyses including the mechanical, shear and peel tests. The effects of various components were optimized to obtain a reliable liner formulation.

Background to Liner Formulations

The construction of case bonded liner system for solid rocket motors involves a series of processes designed to satisfy a variety of launch parameters. There are many processing variables in the complex liner chemistry which affect the interfacial bonding properties in the liner-propellant system. Since the liner and the propellant are specifically designed to maximize the adhesive and protective properties, an understanding chemistry of the liner system is of importance.

In this work, partially cured (precured) liner compositions were investigated. The control of barrier layer cure is therefore essential, not only to reduce the migration of reactants and plasticizer from propellant to liner, but also to provide active surface for adhesion of the propellant to the liner. It has been shown that the isocyanate groups remained on the surface of the liner after precuring process react with hydroxyl groups of the HTPB on the propellant surface to form strong bonds between the liner and propellant.⁽³⁾ In order to produce reliable bonds between the liner and the propellant, one has to perform a controlled precuring which is a complex process. The curing rates of the binder in the liner and propellant together with diffusion rates of ingredients in both matrixes must be considered in the design of a liner-propellant system. The

difference between the curing rates of two integral parts in the interfacial zone is minimized by using the same curing agent in the liner and propellant formulations. The compositions were tested for the achievement of a liner which is compatible with an aluminized HTPB/AP composite propellant. All liners used contained 10% carbon black and 90% total binder.

The presence of plasticizer in the propellant binder results in a less tight polymer structure that causes poor propellant-liner bond formation. The migration of unreacted curing agent with the plasticizer is the most serious cause of poor propellant-liner linkage. In order to control the diffusion of plasticizer between the two integral parts of the system its relative concentration with respect to the binder must be equal in both matrixes.⁽⁴⁾

Another bonding material that assists in the interfacial bonding between the liner and propellant is the bond promoter which improves the interaction at the binder-oxidizer interface and thus the mechanical properties. Its presence in the liner renders the surface of the liner to be more active for adhesion to the propellant. Bond promoter in the liner increases the adhesion by making hydrogen bonding with the ammonium perchlorate at the interface. It is also used to control the migration of small molecules from propellant to liner or interface. The bond promoter is also known to react with the hydroxyl groups of HTPB to form amides which is accelerated by the catalytic effect of ammonium perchlorate particles.⁽⁵⁾

The proper adhesion of liner to the metal surface is provided by primer application. For this purpose, a triisocyanate, usually in solution, is applied to the surface of an adherent prior to its contact with liner adherend. Metal surface is freshly coated with a triisocyanate solution. After drying, the liner is applied to the coated metal surface.

Experimental

HTPB (R45-M, ARCO Chemical Company, Philadelphia, USA), IPDI (Fluka AG, Leverkusen, Germany), carbon black (Printex-U, Degussa A.G. Frankfurt, Germany), and dioctyladipate (DOA, Kimtaş Kimya San. Tic. A.Ş. Istanbul, Turkey) were used as purchased.

The liner was applied with an aluminized HTPB/AP composite propellant. The aluminum and steel surfaces were sand-blasted and degreased by trichloroethane prior to the liner application.

A preliminary examination of a series of liner compositions showed that only three of them were promising and therefore chosen for detailed tests. These liner compositions denoted as S-1, S-3 and S-4 are given in Table 1.

All the ingredients except the curing agent and the curing catalyst were put in the mixing bowl of a horizontal mixer and blended thoroughly for about 10 min at 65°C. The mixing was then continued under vacuum for another 45 min. After addition of curing agent to the slurry, the mixture was blended for 15 min under dry nitrogen gas blanket.

The liner viscosity was measured by Brookfield viscosimeter at 65°C to be 168, 136 and 196 poise for S-1, S-3 and S-4 compositions, respectively. The relative concentration of plasticizer with respect to the binder in the liner and the propellant was kept equal to prevent diffusion of the plasticizer and the other ingredients.

Liner Tensile Test

Dog-bone shaped liner specimens of about 50 mm gage length and 3x6 mm cross-section were prepared by casting into Teflon molds, and cured for 7 days at 65°C. The tensile strength, elongation at break and initial modulus of the cast polyurethane liner were measured on an Instron tensile testing machine by the standard procedure (ASTM D 638-77a) at a crosshead speed of 50 mm/min at 25°C.

Lap Shear Tensile Test

Lap-shear tensile tests of the liner supported on steel or aluminum sheet treated with triisocyanate were carried out on the tensile testing machine at a crosshead speed of 1 mm/min. The specimens (Figure 1) were cured 7 days at 65°C before testing (ASTM D-1002).

T-Peel Test

The liner samples of 1 mm thickness were prepared between 0.4 mm aluminum shims and cured at 65°C for 7 days. The T-peel tests were performed according to ASTM D-1876 (Figure 2).

Metal-Liner-Propellant Tensile Test

The rectangular shaped bond specimen (Figure 3) consisted of a block of propellant and liner system (25 mm thick, 25 mm high, 50 mm wide) that is fully bonded to the metal case. Freshly prepared liner was applied onto a special pool on the metal case. The lined system was precured at 65°C for 3-4 hours. The freshly

prepared propellant was casted onto the lined pool and the system was cured for 7 days at 65°C. The load was applied normal to the plane of the bonding at a cross-head speed of 1 mm/min on tensile testing machine. At the end of the test, mode of failure was reported.

This is a reliable method in deciding the type of failure between the liner and the propellant (cohesive or adhesive). A successful case bond liner system is one that fails cohesively in the propellant, any other mode of failure in the system is not acceptable, therefore the liner should have enough internal cohesive strength and adhesive bond capability both to the propellant and to the metal case. ⁽¹⁾

Multiaxial Shear Test

In this method the whole system, propellant-liner-metal, was tested by using specifically designed shear test apparatus (Figure 4). The liner was applied to four surfaces of the metals which adhere to the propellant and precured about 3-4 hours at 65°C. Then, the propellant was casted between metallic supports. The setup was cured for 7 days at 65°C. Test was performed by using tensile tester at a crosshead speed of 50 mm/min. At the end of the test, mode of failure was noted.

Results and Discussion

The stress-strain behavior of the liners tested are given in Fig 5. The S-3 and S-4 formulations are similar in terms of their mechanical behavior. The S-1 liner formulation is quite elastomeric (about 900 % elongation before rupture) in nature compared to the other two. The maximum stress, strain, and Young's Modulus (E values) calculated from the initial linear portion of the curves are given in Table 2.

The results of the lap-shear tensile tests are given in Table 3. In general the shear stress values between the liner and the steel substrate are greater for S-1, S-3 compared to aluminum substrate. However, for the S-4 system the aluminum value is superior. The values for the lap-shear tensile test are the averages of a minimum of 20 tests. The S-4 composition has extremely good failure behavior which is always cohesive in the liner, and more reproducible as understood from the standard deviation results.

In Table 3, the maximum shear stress values for the metal-liner-propellant specimen were obtained from the multi-axial shear tests. The failure in these tests always occurred cohesively in the propellant. It is interesting to note that, S-4

composition which gives the highest shear stress values with respect to steel and aluminum is the least effective composition in protecting the propellant from cohesive failure. It can be said that S-4 is inferior in shock absorption capacity and transfers the stress applied more or less directly into the propellant. With S-4 liner composition, the propellant fails at an average of 3,22 kg/cm² compared to 5,56 kg/cm² for S-1 and 4,29 kg/cm² for S-3 compositions.

The typical test results for the metal-liner-propellant specimens are presented in Figure 6. The average values of stress at failure are 6.30 ± 0.98 , 5.92 ± 1.43 , and 5.51 ± 0.76 kg/cm² for S-1, S-3, and S-4, respectively. The failure is either cohesive in the propellant phase or near the interface with a small amount of ammonium perchlorate remaining on the liner side. Again, the more elastomeric liner composition S-1 functions better than the S-3 and S-4 compositions.

The 90° peel test carried out between 0.4 mm aluminum sheets (Figure 2) give as load 6800 ± 350 , 6000 ± 500 , 4700 ± 350 g/cm for S-1, S-3 and S-4, respectively. These values are average of a minimum of 10 tests for each liner formulation. Typical experimental results for S-1, S-3 and S-4 are given in Figure 7. The load fluctuates around an average value signifying the tearing action where the stresses are relieved and followed by the accumulation of stresses, repeatedly. Again in the more rigid formulations, S-3 and S-4, the propagation of cracks occur at lower values of load compared to S-1.

Conclusion

The liner composition tested in this study, in general, fulfills the requirements for a metal-liner-propellant system. The viscosity's were adjusted with the addition of a plasticizer for the processing ease. As expected, the elastomeric nature of the S-1 composition functions better in absorbing stresses and protecting the propellant phase against mechanical stresses as observed in multiaxial shear stress test and metal-liner-propellant tests. Also, in the T-Peel test and Lap-shear tests where the liner used alone with the primer the S-1 composition has larger average resistivity against load before failure and larger lap shear stress values. It should be noticed that these results can be deducted from the stress-strain behavior of the liner materials.

References

1. T.W. Giants "Case Bond Liner System for Solid Rocket Motors", April 1991, Report No AD-A242 297, The Aerospace Co. El Segundo, California.
2. J.M. Wrightson "Polyurethane Compositions for Rocket Casing Liners", May 1980, UK Patent Application GB 2 033 410 A, Aerojet General Corporation, El Monte, California.
3. H.T. Sampson "Process for Case Bonding Cast Composite Propellant Grains" US Patent 3,734, 982, May 1973, China Lake, California.
4. L.A. Dee, L.J Emmanuel, M.E. Fiske, L. Ninomiya, "Solid Propellant Ingredient Migration Studies", June 1982, Air Force Rocket Propulsion Lab., Edwards, California.
5. B.M.Broline, "Acylaziridine Reactivity in the Liner and Propellant Environments", Oct 1985, Boeing Aerospace Company, Seattle, Washington.

Table 1 The liner compositions tested. Quantities given show the weight percentages.

Material	Composition S-1	Composition S-3	Composition S-4
HTPB (R-45M)	75	74	73
IPDI	6.9	6.8	8.8
Bond promoter	0.5	2.0	0.5
Carbon Black	10	10	10
DOA	6	6	6

Table 2 Average stress, strain, and E values for S-1, S-3, and S-4 liner compositions. The values are the average of 3 for S-1, 15 for S-3, and 13 for S-4 measurements.

Liner	Composition	Stress (kg/cm ²)	Strain (%)	E (kg/cm ²)
S-1		8.30± 0.20	864±16.6	0.91±0.19
S-3		11.70± 1.63	331±88.9	5.978±0.58
S-4		15.94± 3.34	221±34.8	11.21±1.75

Table 3 Maximum shear stress values (kg/cm²) between steel, aluminum, propellant and liner with the composition S-1, S-3, and S-4.

Composition	Steel-Liner	Alum-Liner	Metal-Liner- Propellant
S-1	11.82 ±2.43	8.13 ±1.42	5.56 ±0.16
S-3	7.97 ±1.06	7.05 ±1.25	4.29 ±0.42
S-4	13.97 ±3.05	15.93 ±3.03	3.22 ±0.33

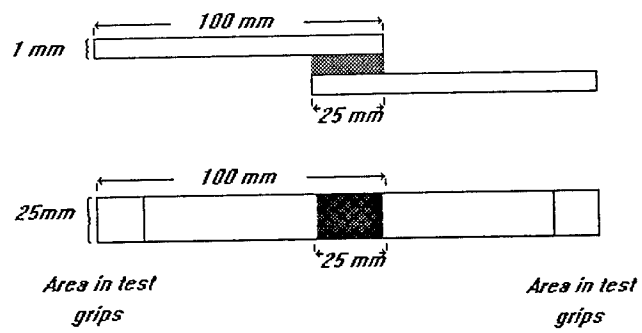


Figure 1 Lap shear test specimen.

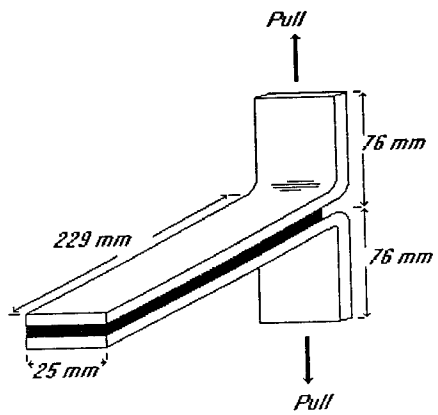


Figure 2 T-Peel test specimen.

49 - 10

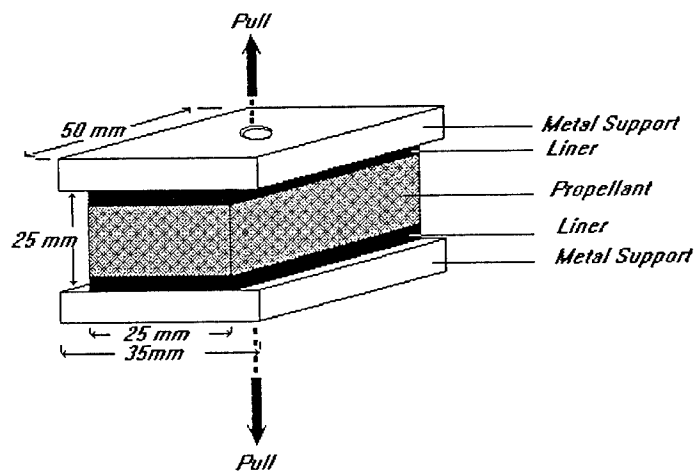


Figure 3 Metal-liner-propellant tensile test specimen.

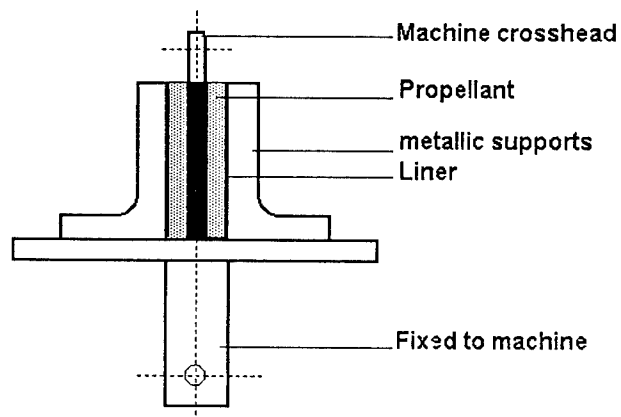


Figure 4 Multi-axial shear test specimen.

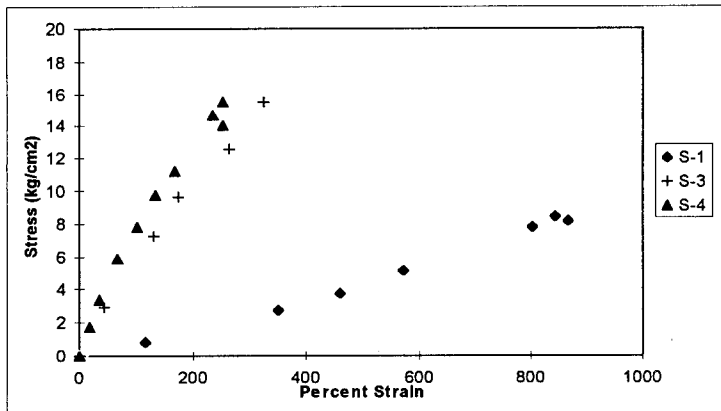


Fig 5. Stress/Strain behavior of typical S-1, S-3 and S-4 specimens. The values for S-1 are the average of 3, average of 15 for S-3, and average of 13 for S-4 measurements.

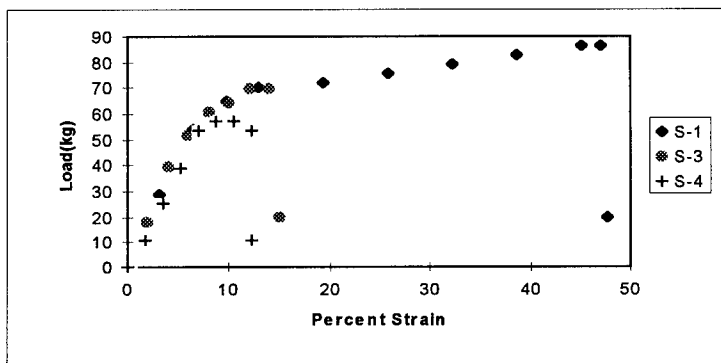


Fig 6. Typical tensile test for the metal-liner-propellant system

49 - 12

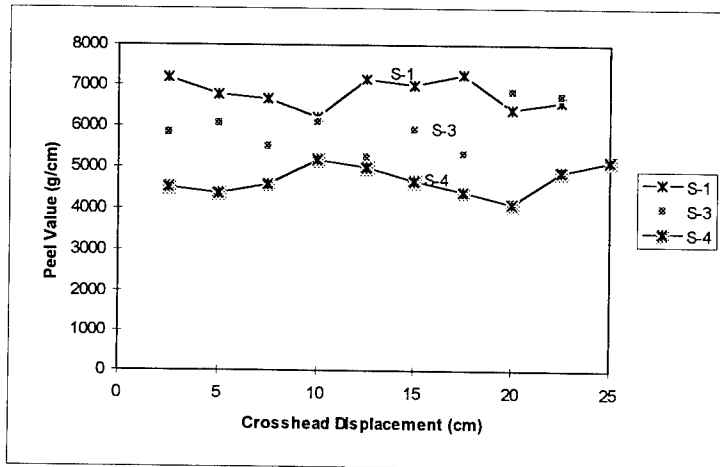


Fig 7. A typical Peel test for the Aluminum-Liner system.

STUDY ON HMX GRAIN SIZE
CLASIFICATION BY DMSO METHOD

Cheng Jingcai, Wu Xiaoqing, Guo Jianwen
Taiyuan Institute of Machinery,
(Taiyuan, 030051, P. R. China)

ABSTRACT

Based on the discussion of the principle for the selection of solvents this paper points out the advantages of using DMSO as solvent and the application of solvent-nonesolvent precipitation in the control of conditions for different crystallization process, so to make HMX products perfectly satisfy American Field data Class 6 grain size.

KEY WORDS

DMSO, HMX, Clasification of Grain Size, Technics of Solvent-Nonesolvent Precipitation

DMSO=dimethyl sulfoxide.

HMX=Cyclotetramethylenetetranitramine or Octogen.

HMPA=hexamethylphosphoramide.

PREFACE

HMX is the world's best explosive for its great power, good property and heat stability. It is used to be mixed in propellants so as to increase their power. This is the major trend of today's development of explosives.

In the modern production of HMX, the main problem besides its low production and high cost is the singleness of its grain size. Different propellant mixtures need HMX of different grain sizes. For instance, Octols need C, D class HMX of

greater of grain size and RX-08 cast compound explosive needs B class HMX of less grain size. Therefore the grain size of the HMX is a matter that needs a quick solution and the object of the study on HMX home and abroad.

Both mechanical mixing and chemical crystallization can be used to realize grain size classification. As for HMX, it is better to use the method of chemical crystallization. There are quite a number of report about refined HMX and crystal transformation, but few about HMX grain size classification.

According to a report from U. S. P. 2900381, American Thatcher studied first to refine HMX by DMSO and got HMX of high quality. And according to a report from UCRL- 50612, American California University's Lawrence Radiation Lab has worked together with Pantex AEC on the evaluation of re-crystallized RDX and HMX used for DMSO by Holston ground force ammunition, and found that DMSO is better than acetone and other solvents and is a most appropriate solvent.

According to a report from ADA 0232, America has made in its factories 14 tests on re-crystallization of HMX by DMSO-H₂O, and has only worked out products of four classes: A, B, E and F. They could not work out HMX of C and D classes.

From the above observation, we choose DMSO as solvent and work on controlled crystallization under different conditions by using DMSO as solvent and H₂O as non-solvent in the solvent-non-solvent precipitation, so as to realize HMX grain size classification.

METHOD OF EXPERIMENT

Generally speaking, the course of crystallization includes the stage of formation of saturated solution, formation of the

core of crystals, growth of the crystals and re-crystallization. In the course of crystallization, super-saturation and super-cool are the main factors.

There are many different methods for crystallization, such as cooling down, evaporation, vacuum cooling, salting-out and reversed crystallization. Ours adopt both the cooling and saltout methods, in other words, to cool down and add solvent. The method is to add certain matters into the process so as to reduce the dissolvability of the solute in the solvent, and is a widely used method in industry. The added matter can be either solid or liquid or gas, and is often called solvent or precipitant. Requirement to added matter is that it should be soluble in the solution but non-soluble to the crystals, and easy to be separated from the solution when necessary. Our selection of DMSO as solvent and H₂O as non-solvent satisfy the requirement.

Advantages for the adoption of cooling and saltout methods are: 1. Increase the HMX recovery in the DMSO-H₂O solution. 2. Easy to control the crystal temperature at any degree so as to benefit the growth of the crystals. 3. DMSO-H₂O makes impurities stay in the mother liquor and thus purifies the HMX.

In summary, the different grain sized HMX can be obtained by controlling the temperature and the adding ratio and speed of the solvent.

Crystal products are classified by their average grain size and consisting grain sizes. Methods to determine their grain size include sieve method, microscope method and photo method.

Our tests is made by classifying HMX grain size according to American Army Standard of 6 classifications, and to grade the products by water sieve method from samples. For we don't have

the standard American sieves, we use Chinese standard sieves that are similar to them according to the principals of substitution. Mesh sizes of MIL-H-4544B standards is shown on the Table 1. and Chinese standards in comparing to it is shown on Table 2.

Table 1. American MIL Standard in Grading HMX

STANDARD MESH	CLASS A %passed	CLASS B %passed	CLASS C %passed	CLASS D %passed	CLASS E %passed	CLASS F %passed
8				100		
12			No less than 99	No less than 85		No less than 99
35				25±15		
50	96±6	100	40±15			No less than 90
100	50±10		20±10	No less than 15		65±15
120	No less than 98					
200	20±6		10±10			30±15
325	8±5	No less than 75			No less than 98	15±10

Table 2. Comparison of American and Chinese Standards

AMERICAN	MESH	8	12	35	50	10	120	200	325
STANDARD	SIZE mm	2.38	1.68	0.50	0.297	0.149	0.125	0.074	0.044
CHINESE	MESH	8	12	35	50	10	120	200	325
STANDARD	SIZE mm	2.50	1.68	0.50	0.30	0.154	0.125	0.075	0.045

Table 3. List of Different HMX Grain Size Classes

Item %passed No.	M8	M12	M35	M50	M100	M120	M200	M325	Up to the Class of
TAI				96	56		18	11	A
TBI				100		99		96	B
TCI		100		55	16		2		C
TDI	100	100			3				D
TEI								98	E
TFI		100					15	11	F

RESULTS OF EXPERIMENT

Test made by re-crystallizing interrupted method, DMSO as solvent, nonesolvent H₂O as diluent in the process of solvent-

non-solvent precipitation and by controlling the temperature and changing the ratio and amount of $\text{DMSO-H}_2\text{O}$, as well as its dosing speed has produced HMX with standard grain sizes fully satisfy American MIL Standards. All products are qualified β type crystals. This method has the advantages such as simple, wide range of process conditions, easy to control and stable.

DISCUSSION

1. Factors such as properties, price, safety and toxicity are to be considered in the selection of solvent. HMX has the characters of great dissolvability and with moderate relationship with solution temperature as shown in Fig. 1.

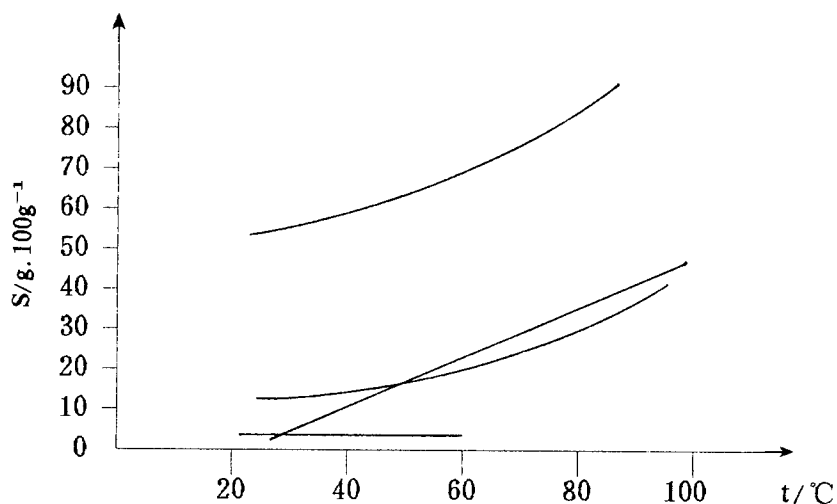


Fig. 1. Dissolvability of HMX in different Solvents and at different Temperatures

From Fig. 1. we can see that HMPA has the greatest dissolvability coefficient and is followed by DMSO and butyrolactone. although HMPA has a greater dissolvable temperature coefficient, it's dissolvability is much less than DMSO,

Moreover, a big dissolvent temperature co-efficient needs strict control of temperature and thus make operation difficult. Therefore DMSO is the best selection. From the figure we can see that at 25°C DMSO still has considerable dissolvability, which means that to sure only DMSO is not good for HMX recovery. But when we adopt the cooling method at the same time and use H₂O as diluent, the shortcoming becomes advantage. Our tests show that HMX production is high and more than 86% can be obtained for each class.

According to document and experiments, the using of DMSO as solvent helps the growth of crystals and all product will be β type crystals.

2. The control of degrees of solution supersaturation affects directly the result of the tests. We adopt both cooling and deluent method to control the degree of supersaturation. A speedy cooling down and adding of the deluent will cause greater degree of saturation and helps to produce more crystals with small grain sizes. On the contrary, a slow cooling down and adding of deluent helps to produce greater grain sizes. Therefore when products of B, E grades are needed, the colling down should be fast and the adding of the deluent should be speedy. When products of C, D grdes are needed, the cooling down should be slow and the adding of deluent should be prolonged.

3. The solvent-nonesolvent ratio has a significant influence on the grain sizes of HMX. The DMSO-H₂O proportion is used to control the size of the crystals: If 100% of nonesolvent is used, a fastest diluted condition will be accomplished and smallest crystals will be created; If a ratio of 1:1 of solvent-nonesolvent is used, a moderately rapid diluted condition will be accomplished and crystals of greater sizes will be created. Therefore when crystals of C, D classes are needed,

the ratio of DMSO-H₂O should be 1:1, and when crystals of E class is needed, pure H₂O should be used for dilution.

4. HMX-DMSO solutions have advantages such as high temperature, high HMX dissolvability, less differential concentration compared with other solutions with same concentration, and are thus good for the growth of the crystals. According to the study of crystallization, when crystallizing and dissolving are big crystals are likely to grow. Therefore when crystals of D, C classes are needed, the crystallizing temperature is to be controlled around 80°C, and when that of other classes are needed, the temperature should be lower. The temperature should not be too high, for DMSO is volatile and high temperature will cause more loss and air pollution. Crystallizing temperature has to be controlled properly according to the grain size requirement of the product.

5. Speed of agitation also influences the forming of crystals. When agitation speed is too low, crystals are settled in the bottom and remain small, which prevents mass transfer. When the agitating speed is good for mass transfer. Therefore the speed of agitation should be determined by a comprehensive consideration of the apparatus, type of the impeller and the grain size requirement.

REFERENCE BOOKS:

1. ADA 023275
2. MIL-H-45444 B.
3. OCRL-50612.
4. U.S.P 2900381
5. ADA 023274
6. "Growth of Crystals" by Zhang Lehui, Beijing Publish House, 1981.
7. "Industrial Crystallization" by Ding Zhuhui and Tan Qiu, Beijing Chemical Industry Publish House, 1985.

INVESTIGATION OF PENTAERYTHRITYL DIAZIDO DINITRATE

Wang Ping, Wang Xiaochuan, Huang Yue, Li Changqing

Institute of Chemical Materials, CAEP

P. O. Box 513, Chengdu 610003. China

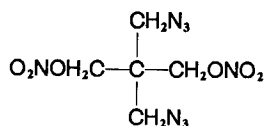
Abstract

Pentaerythrityl diazido dinitrate (PDADN) is hopeful to be used as a component in pyrotechnics and propellant, especially, in the liquid gun propellant formulations because of the two kinds of energetic groups in its molecule which would play the roles of both improving the oxygen balance of the composition and increasing the nitrogen gas in the combustion products needed to enhance the impulse and decrease the temperature in the gun bore.

PDADN was synthesized and characterized in our laboratory. The results show that PDADN is a crystalline compound at ambient temperature with melting point of $39.6 \sim 39.7^{\circ}\text{C}$, which disagrees with the report in US Patent 4 683 086 (1987) concluding that PDADN was a colorless oil with refractivity of $n_D^{25} 1.5165$.

The infrared spectrum of our PDADN gives the same characteristic wave number for $\text{C}-\text{N}_3$ and $\text{C}-\text{ONO}_2$, respectively, as described in the above-said patent.

All data of element analysis, mass spectrum (MS) and nuclear magnetic resonance (NMR) agree with the molecular structure of



The differential scanning calorimetry (DSC) analysis show an acceptable thermal stability of PDADN for practical application.

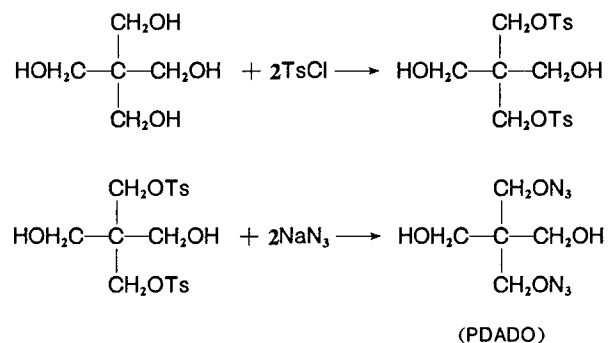
Key Words

Pentaerythrityl diazido dinitrate, Pyrotechnics, Liquid propellant.

1. Introduction

According to analysing the properties of pentaerythrityl tetranitrate (PETN) and pentaerythrityl tetrazide (PETA)^[1] combined with a series of aliphatic azide related data, we consider, if two nitrate groups ($-\text{ONO}_2$) in PETN was replaced by azido groups ($-\text{N}_3$), the expected product, pentaerythrityl diazido dinitrae (PDADN), would be an oil or a compound with low melting point and much accepted stability compared with that of PETN. The compound with such properties would be a promising energetic plasticizer for polymer bonded explosive (PBX), pyrotechnics and propellant, especially, a component in high energy and low fume liquid gun propellant because of the two kinds of energetic groups in its molecule which would play the roles of both improving the oxygen balance for the composition and increasing the nitrogen gas in the combustion products needed to enhance the impulse and decrease the temperature in the gun bore.

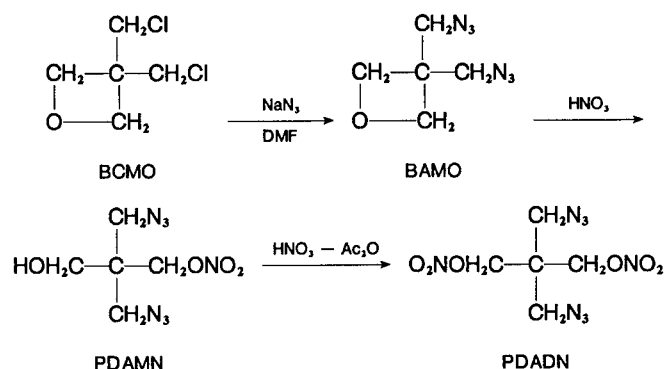
We tried different methods to synthesize PDADN. One of the routes was aimed at synthesizing pentaerythrityl diazido diol (PDADO):



Where Ts=tosyl or phenylsulfonyl.

No matter how to stoichiometrically reduce the quantity of TsCl or NaN₃, we could not reserve the hydroxy group (—OH) on the matrix of pentaerythrityl. Except reduction of the yield, PETA was the only azidation product, no mono-, di- or triazido derivative were found.

Dr. Milton Frankel^[2] who used bis (chloromethylene) oxetane (BCMO) as starting material to synthesize PDADN:



The intermediate, bis (azidomethylene) oxetane (BAMO), was nitrated by two steps to convert into pentaerythritol diazido mononitrate (PDAMN) and dinitrate (PDADN) respectively.

Frankel reported that PDADN was nearly a colorless oil at 25°C, n_D^{25} 1.5161, the infrared spectrum of strong absorption peaks 2083cm^{-1} (—N₃), and 1626cm^{-1} (—ONO₂) agreed with the expected molecular structure.

Simulating Frankel's way, we obtained PDAMN which is a pale-yellow oil and agrees with the report, but the PDADN we obtained is an off-white crystalline with melting point 39.6~39.7°C. Although we made some modification in the nitration condition, the results were the same.

2. Synthesis

2.1 PDAMN

43ml nitric acid (NA) of 70% (wt) was slowly dropped into a solution of 51g BAMO in 61ml methylene chloride (MC) under stirring at ambient temperature. A remarkable exotherm occurred. The reaction temperature was controlled at 22~30°C. After the addition of BAMO was completed, the reactants were kept stirred for about 70 hrs. Then the solution was washed with water and neutralized with dilute aqueous NaHCO_3 , until $\text{pH}=7$. The organic solution layer in the vessel was separated out and distilled at reduced pressure to dispel MC. The product of PDAMN obtained was a viscous oil with pale-yellow color. The infrared spectrum (Fig. 1) agrees with that reported in reference[2], and the strong absorption peaks at 2083cm^{-1} , 1626cm^{-1} and 3400cm^{-1} imply the groups of $-\text{N}_3$, $-\text{ONO}_2$ and $-\text{OH}$, respectively, in the molecule.

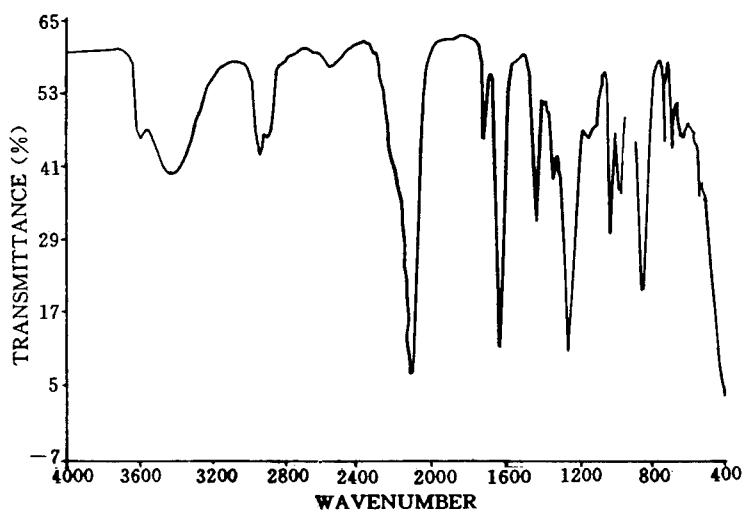


Fig. 1 Infrared spectrum of PDAMN

2.2 PDADN

32g acetic anhydride was mixed with 168ml MC and cooled down to $0\sim 5^{\circ}\text{C}$. 13g fuming NA (98%) was slowly added into the flask under agitation and cooling. Then 42g PDAMN in 48ml MC was added dropwise into the nitration mixture. The temperature was kept below 5°C for all the time when PDAMN solution was added. 5 min latter the temperature was enhanced to $20\sim 30^{\circ}\text{C}$ and agitation was continued for 10 minutes. The reaction mixture was diluted with cold water. The water-insoluble phase was separated and treated with dilute aqueous NaHCO_3 and water until $\text{pH} = 7$. The organic phase was dried with anhydrous MgSO_4 , purified in a column filled with neutral alumina. The eluate was condensed in vacuum then a wax-like solid formed. After crystallization of the product from MC, a near white crystalline with m. p. $39.6\sim 39.7^{\circ}\text{C}$ was obtained.

To observe the influence of nitration temperature on the result, we canceled out the step of temperature enhancement after the addition of PDAMN was finished and kept the reaction at $0\sim 5^{\circ}\text{C}$ for 20 minutes. The final product was the same crystal with the same m. p. as stated above.

3. Identification of PDADN

3.1 Physical Properties

PDADN is an off-white crystalline at ambient temperature and melts at $39.6\sim 39.7^{\circ}\text{C}$. The refractivity at its molten state is $n_D^{20} 1.5082$, and supercooling occurs until the melt freezes completely when the temperature is down to 20°C .

Fig. 2 Shows the microphotograph of PDADN magnified 90 times of the crystals.

3.2 Element analysis

The results of 5 PDADN samples' element analysis were shown in table 1. The

reaction conditions of synthesis were somewhat different for the samples, but the analyzing data of theirs are similar to each other in the error range allowed and basically agree with those of the theoretical values of PDADN.

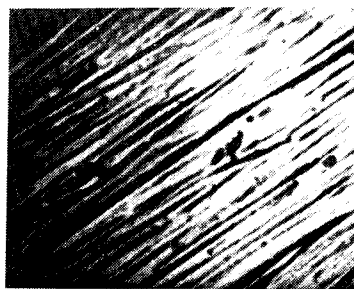


Fig. 2 Microphotograph (90 times) of PDADN

Table 1. Element analysis data of PDADN

No	C (%)	H (%)	N (%)
1	22.52	2.98	40.74
2	22.57	2.98	40.80
3	22.63	2.93	39.95
4	22.87	2.98	40.33
5	22.54	2.99	40.14
Average	22.63	2.97	40.39
Theoretic	21.74	2.90	40.58
Deviation (%)	+4.1	+2.4	-0.47

3.3 Infrared spectrum

Fig. 3 are two infrared spectra of PDADN obtained from different nitration conditions. (a) is the nitration product of PDAMN under 0~5°C for 20 min; (b) is that under 0~5°C for 5 min and then 30°C for 10 min. It is clear that there is no essential difference between two spectra. The strong absorption peaks conform to

that reported in reference[2]. But, compared with Fig. 1, the characteristic peak at 3400cm^{-1} disappeared, which means the hydroxy group has converted to $-\text{ONO}_2$.

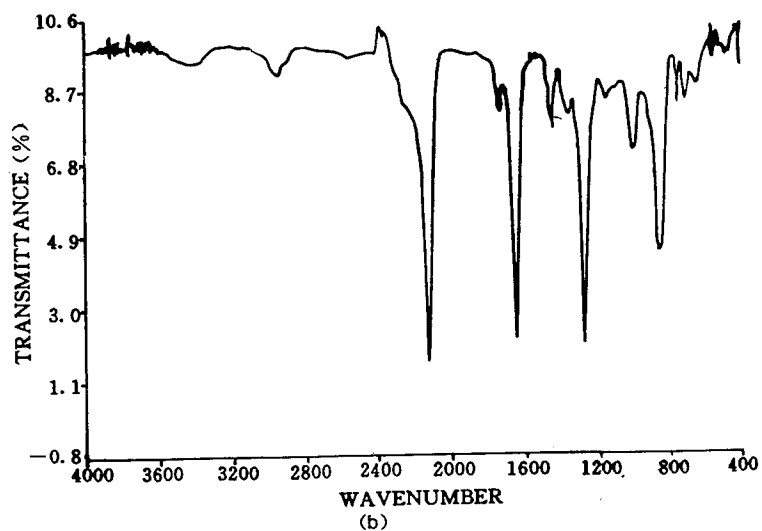
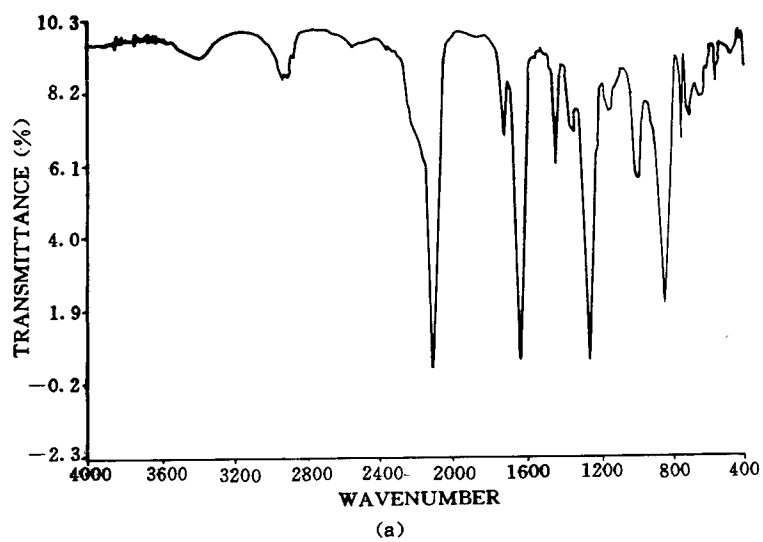
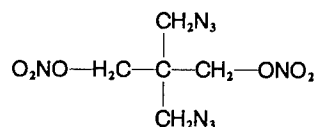


Fig. 3 Infrared spectra of PDADN

3.4 Mass spectrum (MS)

Fig. 4 is the mass spectrum of PDADN obtained from bombarding the specimen with an electronic energy of 70eV. It can be seen that the maximum mass to charge ratio, M/z , of the molecular or "parent" ion is 277. According to the "nitrogen rule", the mass of molecular ion is 276 which conforms to the mass number of PDADN. The low intensity of peak implies that PDADN is rather unstable under the condition of electron's bombardment, and quite a lot of ionic fragments are formed because of the fracture of chemical bonds in the molecule. The relatively intensive peaks of M/z 46, M/z 56 and M/z 69 correspond to the fragment of $^+\text{NO}_2$, $^+\text{CH}_2\text{N}_3$ and $\text{CH}_2 = \text{C}^+ - \text{N}_3$ rearranged from the former. These fragments indicate the existence of $-\text{NO}_2$, $-\text{CH}_2\text{N}_3$ and $-\text{C}-\text{CH}_2\text{N}_3$ in the PDADN molecule. The fragmental ions with M/z 84 and M/z 99 imply the $-\text{CH}_2 - \text{O} -$ structure.

Combining the FTIR data, the results of MS above can identify that the molecular structure of PDADN is



3.5 Nuclear magnetic resonance (NMR)

Fig. 5 and Fig. 6 are the H- and C-spectrum of PDADN obtained from 300MHz nuclear magnetic resonator. The peaks in Fig. 5 indicate there exist only two types of hydrogen in PDADN molecule. The peaks in chemical shift of $\delta=3.52$ ppm and 4.43 ppm correspond the H-spectrum in $-\text{C}-\text{CH}_2-\text{ONO}_2$ and $-\text{C}-\text{CH}_2-\text{N}_3$ respectively. Fig. 6 shows the existence of three types of carbon in PDADN molecule. The single peak at $\delta=42.35$ ppm, the triple peaks at $\delta=50.29$ ppm and

the tetradic peaks at $\delta=68.83$ ppm are correlated to the carbon of $\begin{array}{c} | \\ -\text{C}- \\ | \end{array}$,
 $-\text{CH}_2-\text{ONO}_2$ and $-\text{CH}_2\text{N}_3$ in their order. These data give a further evidence for the
 structure of PDADN as identified with FTIR and MS.

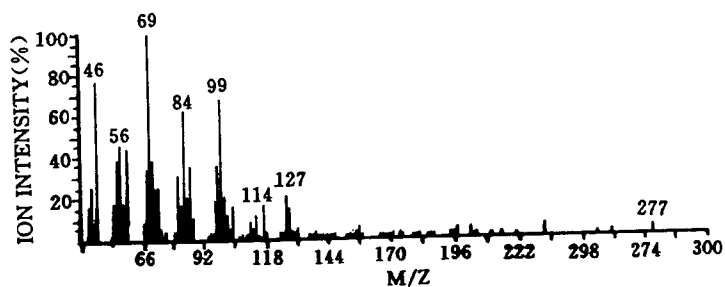


Fig. 4 Mass spectrum of PDADN

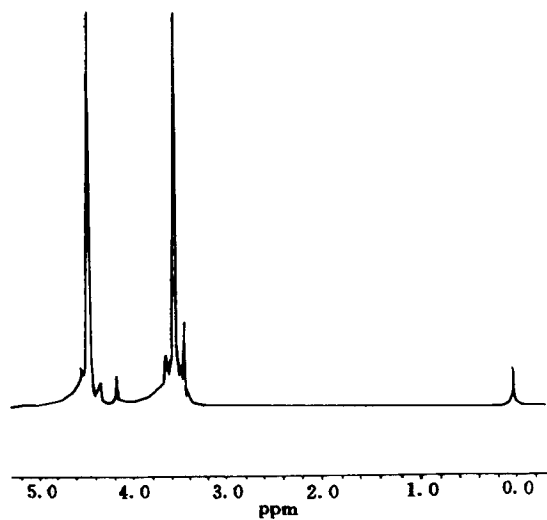


Fig. 5 H-NMR spectrum of PDADN

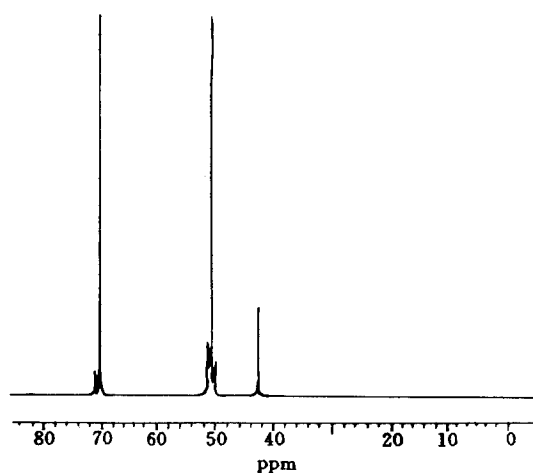


Fig. 6 ^{13}C -NMR spectrum of PDADN

4. Thermal properties

Table. 2 and Fig. 7 show the data of BAMO, PDAMN and PDADN in DSC analysis. It can be seen, all the chemical bonds except $-\text{N}_3$ are very stable in BAMO, therefore, only the exothermal peak, 271°C , characteristic to $-\text{N}_3$ appears in its DSC data. The exothermal peaks of PDAMN and PDADN locate at the temperature near 200°C which agrees with the decomposition temperature specified to $-\text{ONO}_2$.

5. Conclusion

All the analysis data prove that PDADN is a crystalline substance at ambient temperature with low melting point of $39.6 \sim 39.7^\circ\text{C}$. Our preliminary work shows PDADN is promising to be used as a ingredient in liquid propellant for impulse enhancement and reduction of the combustion temperature in the gun bore. Because

of its crystallinity, PDADN is rather sensitive to impact and friction according to our test, which seems not favorable for PDADN to be used as an energetic plasticizer in PBX as we thought before.

Table 2 DSC data of BAMO, PDAMN and PDADN

No	Sample	Onset (°C)	Exo. peak (°C)	ΔH_{decomp} (J/g)
1	BAMO	214.6	271.2	—
2	PDAMN -1	182.3	199.5	-2572
3	-2	181.1	199.7	-2667
4	PDADN -2	190.9	204.3	-2587
5	-5	192.3	204.6	-2570

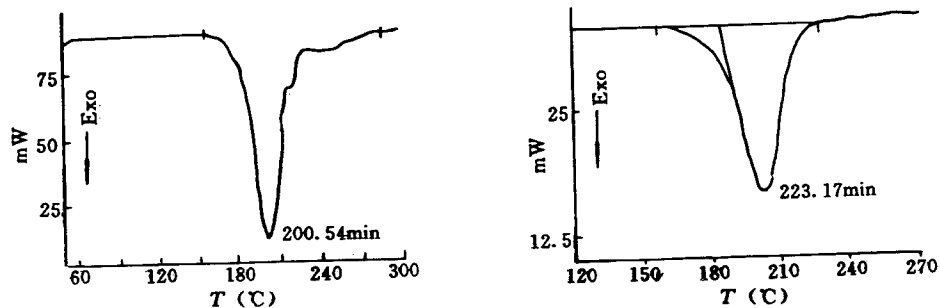


Fig. 7 DSC curve of (a) PDAMN and (b) PDADN

Acknowledgement

The authors sincerely thank the following colleagues for their warm help in different analysis: Ms. Pu Junli, Zhang Zhenglan, Wang Huilian and Cheng Jie; Mr. Wang Zhaoming, Zhang Xiaoyi, Hu Qingxian and Lu Zijian.

References

1. Anderson W S. Some New Aliphatic Polyazides Derived from Pentaerythritol.
AD-A103 844, 1981.
2. Frankel M B. Azido Derivatives of Pentaerythriol. USP 4 683 086, 1987.

ICT - THERMOCHEMICAL DATA BASE

F. Volk
H. Bathelt

Fraunhofer - Institut für
Chemische Technologie
Joseph-von-Fraunhofer-Straße 7
D - 76327 Pfinztal, FRG

Thermodynamic calculations are nowadays an indispensable part of scientific and technical investigations. The fast improvement of computer capabilities did enhance the calculation of chemical equilibria, which is of interest for the evaluation of the performance of energetic materials, rocket and gun propellants, but also for optimization purposes of combustion processes with regard to temperature, pressure and product formation. Such calculations can be performed for example with the ICT - Thermodynamic Code, which is running on PC.

The reliability of the results of thermochemical calculations depends primarily on the accuracy of the data used. Therefore the Fraunhofer - Institute für Chemische Technologie (ICT) began very early to collect data on energetic materials. In 1971, tables with properties of substances related with the preparation of rocket and gun propellants were published:





F. Volk, H. Bathelt, R. Kuthe

*Thermodynamische Daten von Raketentreibstoffen,
Treibladungspulvern und Sprengstoffen sowie deren Komponenten*

A supplement was published in 1981.

Meanwhile, properties of a lot of new energetic substances have been published. Therefore, instead of compiling an additional supplement, we decided to store the main properties of all substances in a THERMOCHEMICAL DATA BASE on PC. Compared with printed tables, this has the advantage that data can be retrieved very fast; updates can be made easily and regularly.

The Thermochemical Data Base

-  contains data of 2228 substances
-  contains especially data of energetic materials
-  is available in English and German
-  is updated regularly

The following data is stored:

- Sum formula
- State of aggregation
- Name(s)
- Molecular weight
- Oxygen balance
- Density
- Melting point
- Boiling point
- Enthalpy of formation (up to four values)
- Energy of formation
- Energy of combustion
- References

Structure formulas of the stored organic substances are given in the manual.

The Thermochemical Data Base

allows to search for

- **Names**
- **Parts of names**
- **Names beginning with a certain letter**
- **Sum formulas**
- **Parts of sum formulas**
- **Substances consisting of certain elements**
- **Substances containing certain elements**
- **Substances with certain properties**
(for example with a positive oxygen balance)
- **Substances belonging to certain classes**

for example: Primary explosives

Stabilizers

Liquid fuels

Pyrotechnics

. . .

C 3 H 6 N 2 O 6					Liquid
PROPYLENEGLYCOL DINITRATE METHYLNITROGLYCOL 1,2-DINITROXYPROPANE 1,2-PROPANEDIOL DINITRATE					
Molecular Weight:		166.090 [g]	Oxygen Balance:		-28.90 [%]
Density [g/cm ³]:		1.377 at 20°C	Source:		B013
Melting Point [°C]:		-42.5	Source:		57
Boiling Point [°C]:		92 (10mm)	Source:		B013
Enthalpy of Formation			Energy of Formation		Source
[KJ/Mol]	[Kcal/Mol]	[Kcal/kg]	[KJ/Mol]	[Kcal/Mol]	
-294.97	-70.50	-424.47	-277.63	-66.36	36
-277.65	-66.36	-399.54	-260.31	-62.22	175
-347.69	-83.10	-500.33	-330.35	-78.96	57
Samples of the stored values					1- 109

C 4 H 7 N 3 O 9					Liquid
1,2,4-BUTANETRIOL TRINITRATE BTTN					
Molecular Weight:		241.114 [g]	Oxygen Balance:		-16.59 [%]
Density [g/cm ³]:		1.520 at 20°C	Source:		99
Melting Point [°C]:		-5.8-(-3.2)	Source:		202
Enthalpy of Formation			Energy of Formation		Source
[KJ/Mol]	[Kcal/Mol]	[Kcal/kg]	[KJ/Mol]	[Kcal/Mol]	
-285.52	-68.24	-283.02	-261.98	-62.62	99
-398.02	-95.13	-394.54	-374.49	-89.51	9
Energy of Combustion:					Source: 27
522.7 [Kcal/Mol] = 2167.9 [cal/g]					1- 156

C 5 H 9 N 3 O 9					Liquid
METHYLTRIMETHYLOLMETHANE TRINITRATE METRIOL TRINITRATE TMETN					
Molecular Weight:		255.141 [g]	Oxygen Balance:		-34.49 [%]
Density [g/cm ³]:		1.488	Source:		68
Melting Point [°C]:		15.7-17.1	Source:		202
Boiling Point [°C]:		182 D	Source:		57
Enthalpy of Formation			Energy of Formation		Source
[KJ/Mol]	[Kcal/Mol]	[Kcal/kg]	[KJ/Mol]	[Kcal/Mol]	
-442.67	-105.80	-414.67	-416.66	-99.58	68
-443.50	-106.00	-415.46	-417.49	-99.78	STB
-476.14	-113.80	-446.03	-450.13	-107.58	57
-388.69	-92.90	-364.11	-362.68	-86.68	99
Energy of Combustion:					Source: 57
674.0 [Kcal/Mol] = 2641.7 [cal/g]					1- 208

C 12 H 5 N 7 O 12					Solid
2,4,6,2',4',6'-HEXANITRODIPHENYLAMINE HEXYL HEXAMINE					DIPICRYLAMINE
Molecular Weight:		439.211 [g]	Oxygen Balance:		-52.82 [%]
Density [g/cm3]:		1.64	Source:		EX
Melting Point [°C]:		244 D	Source:		H
Enthalpy of Formation			Energy of Formation		Source
[KJ/Mol]	[Kcal/Mol]	[Kcal/kg]	[KJ/Mol]	[Kcal/Mol]	
41.42	9.90	22.54	71.15	17.00	STB
-45.61	-10.90	-24.82	-15.88	-3.80	129
Energy of Combustion:			Source:		ME
1315.2 [Kcal/Mol] =			2994.5 [cal/g]		1- 493

C 14 H 6 N 6 O 12					Solid
trans-2,2',4,4',6,6'-HEXANITROSTILBENE					HNS
Molecular Weight:		450.235 [g]	Oxygen Balance:		-67.52 [%]
Density [g/cm3]:		1.74	Source:		63
Melting Point [°C]:		318	Source:		194
Enthalpy of Formation			Energy of Formation		Source
[KJ/Mol]	[Kcal/Mol]	[Kcal/kg]	[KJ/Mol]	[Kcal/Mol]	
78.24	18.70	41.53	107.97	25.80	29
78.24	18.70	41.53	107.97	25.80	63
67.78	16.20	35.98	97.51	23.30	33
57.74	13.80	30.65	87.47	20.90	C
Energy of Combustion:			Source:		63
1540.3 [Kcal/Mol] =			3421.1 [cal/g]		1- 554

C 6 H 6 N 12 O 12					Solid
HEXANITROHEXAHAZ ISOWURTZITANE HNIW					
2,4,6,8,10,12-(HEXANITRO-HEXAHAZ)-TETRACYCLODODECANE					CL 20
Molecular Weight:		438.187 [g]	Oxygen Balance:		-10.95 [%]
Density [g/cm3]:		2.1	Source:		73
Melting Point [°C]:		> 195 D	Source:		156
Enthalpy of Formation			Energy of Formation		Source
[KJ/Mol]	[Kcal/Mol]	[Kcal/kg]	[KJ/Mol]	[Kcal/Mol]	
415.47	99.30	226.62	452.63	108.18	71
					1- 876

C 4 H 6 N 4 O 12					Solid
TETRANITROERYTHROL NITROERYTHROL ERYTHROL TETRANITRATE					
Molecular Weight:		302.111 [g]	Oxygen Balance:		5.30 [%]
Density [g/cm3]:		1.6	Source:		EX
Melting Point [°C]:		61.5	Source:		EX
Enthalpy of Formation			Energy of Formation		Source
[KJ/Mol]	[Kcal/Mol]	[Kcal/kg]	[KJ/Mol]	[Kcal/Mol]	
-502.50	-120.10	-397.54	-475.25	-113.59	CTI
Energy of Combustion:			Source:		S
467.1 [Kcal/Mol] =		1546.1 [cal/g]			1- 154

C 4 H 8 N 8 O 8					Solid
CYCLOTETRAMETHYLENE TETRANITRAMINE OCTOGEN HMX 1,3,5,7-TETRANITRO-1,3,5,7-TETRAAZACYCLOOCTANE					
Molecular Weight:		296.156 [g]	Oxygen Balance:		-21.61 [%]
Density [g/cm3]:		1.902	Source:		63
Melting Point [°C]:		280 D	Source:		211
Enthalpy of Formation			Energy of Formation		Source
[KJ/Mol]	[Kcal/Mol]	[Kcal/kg]	[KJ/Mol]	[Kcal/Mol]	
75.02	17.93	60.54	104.75	25.03	STA
47.28	11.30	38.16	77.01	18.40	63
87.86	21.00	70.91	117.59	28.10	17
90.29	21.58	72.87	120.02	28.68	10
Energy of Combustion:			Source:		63
660.7 [Kcal/Mol] =		2230.9 [cal/g]			1- 159

C 4 H 2 N 8 O 10					Solid
1,3,4,6-TETRANITROGLYCOURIL SORGUYL					
Molecular Weight:		322.107 [g]	Oxygen Balance:		4.97 [%]
Density [g/cm3]:		2.01	Source:		32
Melting Point [°C]:		250 D	Source:		189
Enthalpy of Formation			Energy of Formation		Source
[KJ/Mol]	[Kcal/Mol]	[Kcal/kg]	[KJ/Mol]	[Kcal/Mol]	
-15.06	-3.60	-11.18	9.71	2.32	137
-48.95	-11.70	-36.32	-24.18	-5.78	31
50.21	12.00	37.25	74.98	17.92	199
56.99	13.62	42.28	81.76	19.54	32
Energy of Combustion:			Source:		32
463.0 [Kcal/Mol] =		1437.4 [cal/g]			1- 198

N 3 NA 1					Solid
SODIUM AZIDE NaN ₃					
Molecular Weight:		65.010 [g]	Oxygen Balance:		-12.31 [%]
Density [g/cm ³]:		1.846 at 20°C	Source:		264
Melting Point [°C]:		275 D	Source:		30
Enthalpy of Formation			Energy of Formation		Source
[KJ/Mol]	[Kcal/Mol]	[Kcal/kg]	[KJ/Mol]	[Kcal/Mol]	
21.25	5.08	78.14	24.97	5.97	21
21.71	5.19	79.83	25.43	6.08	SE

C 5 H 6 N 6 O 14					Solid
BIS(2,2,2-TRINITROETHYL)FORMAL TEFO 1,1,1,7,7,7-HEXANITRO-3,5-DIOXAHEPTANE BIS(2,2,2-TRINITROETHOXY)METHANE					
Molecular Weight:		374.134 [g]	Oxygen Balance:		4.28 [%]
Density [g/cm ³]:		1.72 at 25°C	Source:		22
Melting Point [°C]:		65	Source:		22
Enthalpy of Formation			Energy of Formation		Source
[KJ/Mol]	[Kcal/Mol]	[Kcal/kg]	[KJ/Mol]	[Kcal/Mol]	
-403.30	-96.39	-257.63	-371.09	-88.69	72
-402.08	-96.10	-256.86	-369.88	-88.40	72
-403.34	-96.40	-257.66	-371.13	-88.70	86
Energy of Combustion:			Source:		93
579.1 [Kcal/Mol] =			1547.8 [cal/g]		1- 224

C 6 H 8 N 6 O 18					Solid
NITROMANNITOL MANNITOL HEXANITRATE HEXANITROMANNITOL					
Molecular Weight:		452.159 [g]	Oxygen Balance:		7.08 [%]
Density [g/cm ³]:		1.8 at 20°C	Source:		H
Melting Point [°C]:		112.3	Source:		H
Boiling Point [°C]:		120 E	Source:		H
Enthalpy of Formation			Energy of Formation		Source
[KJ/Mol]	[Kcal/Mol]	[Kcal/kg]	[KJ/Mol]	[Kcal/Mol]	
-644.34	-154.00	-340.59	-604.70	-144.53	STC
Energy of Combustion:			Source:		L
683.8 [Kcal/Mol] =			1512.3 [cal/g]		1- 260

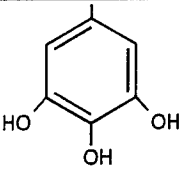
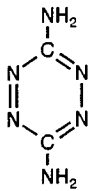
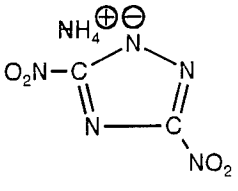
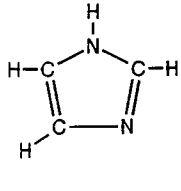
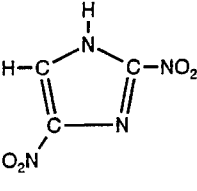
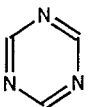
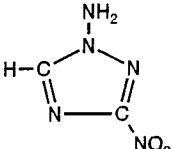
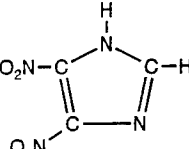
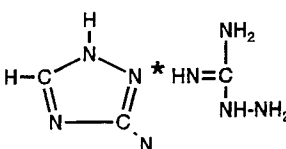
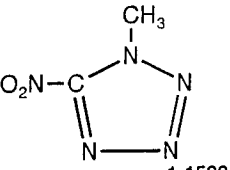
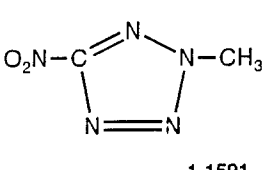
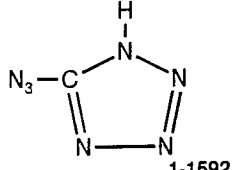
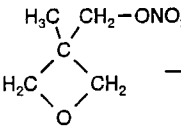
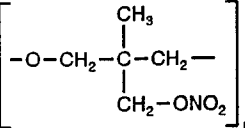
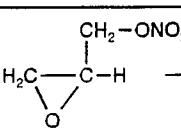
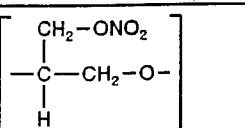
1- 613 TETRAFLUORO METHANE
 1- 188 TETRAFORMALTRIAZINE
 1-1462 1',2',3',4'-TETRAHYDRO-1,2'-DINAPHTHYLMETHANE
 1- 745 TETRAHYDRO-3,3,5,5-TETRAKIS(HYDROXYMETHYL)-4-HYDROXYPYRAN
 1- 814 TETRAHYDROCARBAZOLE CARBOXAMIDE
 1- 814 TETRAHYDROCARBAZOLE UREA
 1- 484 *exo*-TETRAHYDRODICYCLOPENTADIENE
 1- 795 *exo*-TETRAHYDRO-DI(METHYLCYCLOPENTADIENE)
 1-1172 TETRAHYDROFURAN
 1-1221 TETRAHYDROFURFURYL ALCOHOL
 1-1386 1,2,3,4-TETRAHYDRONAPHTHALENE
 1-1183 TETRAHYDROPYRROLE
 1- 747 TETRA(HYDROXYMETHYL)METHANE
 1- 437 TETRAKIS-2,2,2-TRINITROETHYL ORTHO ESTER
 1-1749 1,2,4,5-TETRAKIS(DIAZIDOMETHYL) BENZENE
 1- 748 2,2,4,4-TETRAKIS(HYDROXYMETHYL NITRATE)PYRANOL NITRATE
 1- 748 2,2,4,4-TETRAKIS(NITRATOMETHYL)-1-PYRANOL NITRATE
 1- 622 TETRAMETHYLAMMONIUM-DECAHYDRODECABORATE
 1- 170 TETRAMETHYLAMMONIUM NITRATE
 1-1389 1,2,4,5-TETRAMETHYLBENZENE
 1-1033 2,2,3,3-TETRAMETHYLBUTANE
 1- 761 TETRAMETHYLBUTYNE DIOL
 1-1640 1,1,2,2-TETRAMETHYLCYCLOPROPANE
 1- 650 TETRAMETHYL-DIBORANE
 1-1060 TETRAMETHYLENE
 1-1172 TETRAMETHYLENEOXIDE
 1-1688 TETRAMETHYLLEAD
 1- 468 TETRAMETHYLOLCYCLOHEXANOL PENTANITRATE
 1- 467 TETRAMETHYLOLCYCLOHEXANONE TETRANITRATE
 1- 441 TETRAMETHYLOLCYCLOPENTANOL PENTANITRATE
 1- 440 TETRAMETHYLOLCYCLOPENTANON TETRANITRATE
 1- 747 TETRAMETHYLOLMETHANE
 1- 187 TETRAMETHYLOZONIDE
 1- 159 1,3,5,7-TETRANITRO-1,3,5,7-TETRAAZACYCLOOCTANE
 1- 868 1,3,5,5-TETRANITRO-1,3-DIAZACYCLOHEXANE
 1- 868 1,3,5,5-TETRANITRO-1,3-DIAZINE
 1- 323 *trans*-1,4,5,8-TETRANITRO-1,4,5,8-TETRAAZADECALIN
 1-1153 2,4,6,8-TETRANITRO-2,4,6,8-TETRAAZACYCLOOCTANON-1
 1-1199 2,4,6,8-TETRANITRO-2,4,6,8-TETRAAZADICYCLO(3,3,0)-OCTANDIONE-(3,7)
 1-1152 2,4,6,8-TETRANITRO-2,4,6,8-TETRAAZADICYCLO(3,3,0)OCTANE
 1-1143 2,4,6,8-TETRANITRO-2,4,6,8-TETRAAZADICYCLO(3,3,0)OCTANON-3
 1-1167 1,3,5,7-TETRANITRO-2,6-DIOXO-1,3,5,7-TETRAAZACYCLOOCTANE
 1-1263 1,3,6,8-TETRANITRO-3,6-DIAZA-*n*-OCTANE
 1- 872 2,2,6,6-TETRANITRO-4-AZAHEPTANE
 1- 238 2,3,4,6-TETRANITROANILINE
 1- 312 1,2,4,5-TETRANITROBENZENE
 1-1239 1,2,3,5-TETRANITROBENZENE
 1-1240 1,2,3,4-TETRANITROBENZENE
 1-1736 4,5,6,7-TETRANITROBENZOFUROXANE
 1- 789 1,3,8,10-TETRANITROBENZOTRIAZOLO[1,2-*a*]BENZOTRIAZOLE
 1- 507 1,3,7,9-TETRANITROBENZOTRIAZOLO[2,1-*a*]BENZOTRIAZOLE
 1- 967 1,1,3,3-TETRANITROBUTANE
 1- 171 2,2,3,3-TETRANITROBUTANE
 1- 204 1,1,1,4-TETRANITROBUTANE
 1- 491 1,3,6,8-TETRANITROCARBAZOLE
 1-1537 TETRANITRODIGLYCEROL
 1-1413 2,2',4,4'-TETRANITRODIPHENYLAMINE
 1- 154 TETRANITROERYTHROL

Sample page
 of the list of substances
 (Manual)

<p>Sample page of the list of sources (Manual)</p>
--

- 142 M.B. Frankel, E.F. Witucki, D.N. Vincent
US Patent No. 3907907, 23. Sept. 1975
- 143 Sicherheitsdatenblatt der Firma FLUKA AG
Produkt-Nr. 50040, Ausgabedatum 4.10.89
- 144 C.V. Hart
Carbonic Acid Azides
Journal American Chemical Society, 50 (1928), 1922-1930
- 145 M. Tremblay
Spectres Infrarouges de Composes Riches en Azote
Canadian Journal of Chemistry, Volume 43 (1965), 1154-1157
- 146 R.A. Henry
2-Amino-4,6-diazido-1,3,5-triazine
J.Org. Chemistry 31, 1973-1974 (1966)
- 147 M. Tremblay
Synthesis of some Tetrazole Salts
Canadian Journal of Chemistry, Volume 43 (1965), 1230-1232
- 148 Dictionary of Organic Compounds
Fifth Edition
Chapman and Hall, 1982
- 149 K.-Y. Lee, L.B. Chapman, M.D. Coburn
3-Nitro-1,2,4-Triazol-5-One, a Less Sensitive Explosive
Journal of Energetic Materials, Vol.5, 27-33 (1987)
- 150 M.F. Zimmer, R.A. Robb, E.E. Baroody, G.A. Carpenter
Heat of Formation and Other Properties of Trinitrofluoromethane
Journal of chemical and engineering data,
Vol. 11, No.4, October 1966, 577-579
- 151 A.E. Fogelzang et al.
FLAME - Database on Combustion of Explosives and Propellants
Russian Mendeleev University of Chemical Technology,
9, Miusskaya sq., Moscow 125190, Russia
- 152 B.B. Ebbinghaus
Thermodynamics of Gas Phase Chromium Species:
The Chromium Oxides, the Chromium Oxyhydroxides,
and Volatility Calculations in Waste Incineration Processes
Combustion and Flame 93: 119-137 (1993)
- 153 J. Lee, A. Block-Bolten
Correlation of Physical and Chemical Properties of
C-H-N-O Explosives (Part II)
Propellants, Explosives, Pyrotechnics 18, 161-167 (1993)
- 154 O. Kubaschewski, E.L.L. Evans
Metallurgical Thermochemistry
Pergamon Press
- 155 D. Miksovsky, J. Korinek, A. Vojtech
An Optimized Process for Making MEDINA
Propellants, Explosives, Pyrotechnics 18, 51 (1993)

B-99

$\text{N}_3-\text{CH}_2-\text{CH}_2-\text{N}-\text{CH}_2-$ NO_2		<div style="border: 1px solid black; padding: 5px; text-align: center;"> Samples of structure formulas (Manual) </div>		$\text{N}-\text{CH}_2-\text{CH}_2-\text{N}_3$ NO_2
				1-1578
$\text{CH}_3-\text{N}-\text{CH}_2-\text{N}-\text{CH}_2-\text{O}-\text{CH}_3$ $\text{NO}_2 \quad \text{ONO}_2$			$\text{O}_2\text{N}-\text{N}-\text{CH}_2$ $\text{H}_2\text{C}-\text{C}-\text{NO}_2$ NO_2	
1-1579		1-1580	1-1581	
				
1-1582	1-1583	1-1584	1-1585	
				
1-1586	1-1587	1-1588	1-1589	
				
1-1590		1-1591		
CH_2-N_3 $\text{N}-\text{NO}_2$ CH_2 CH_2 $\text{N}-\text{NO}_2$ CH_2-N_3		$\text{H}_3\text{C}-\text{CH}_2-\text{ONO}_2$ $\text{H}_2\text{C}-\text{C}-\text{CH}_2$ O		
1-1593				
				
		Nimmo → PolyNimmo 1-1594		
				
				
		Glyn → PolyGlyn 1-1595		

The price of the ICT - Thermochemical Data Base
- English or German version -
is DM 990.-

**For an order during the ICT - Conference the
Reduced Price of DM 800.-
will be charged.**

Order Forms are available at the Conference Office

Please send your order to:

Fraunhofer - Institut für
Chemische Technologie
Attn: Mr. H. Bathelt
Postfach 1240
D-76318 Pfinztal - Berghausen

New Chemically Bound Ferrocenes for Burn Rate Modification of Composit Rocket and Gas Generating Propellants

Jutta Böhnlein-Mauß, Klaus-Peter Brehler, Klaus Menke

Fraunhofer-Institut für Chemische Technologie

D-76327 Pfinztal

Hubert Jungbluth

Chemische Betriebe Pluto GmbH

D-44649 Herne

Zusammenfassung

Es wird der Einsatz von drei neuen über OH-Gruppen chemisch einbindbaren Ferrocenderivaten in hochgefüllten AP, Al, HTPB-Compositformulierungen vorgestellt. Dabei werden der Einfluß auf die Verarbeitbarkeit, die Ausbildung guter mechanischer Eigenschaften mit vernetzenden Triol- und Isocyanatkomponenten und die Wirksamkeit auf die Erhöhung der Abbrandgeschwindigkeit im Vergleich zum 2,2'-Bis(ethylferrocenyl)propan (Catocen®) untersucht.

Es zeigt sich, daß ein Derivat bis zur Konzentration von 1,5 Gew% alle wesentlichen Eigenschaftsforderungen für den Treibstoffeinsatz erfüllt, chemisch eingebunden wird und in der Erhöhung der Abbrandgeschwindigkeit ebenso wirksam ist wie Catocen.

Abstract

Three new ferrocene derivatives are introduced which are chemically bound by OH groups to the binder system of AP, Al, HTPB-composite propellants with high solids loading. Their influence on processing parameters like casting viscosities, formation of good mechanical properties with suitable triol and isocyanate compounds and their efficiency on burn rate enhancement is examined in comparison to 2,2'-Bis(ethylferrocenyl)propane (Catocen®).

It is demonstrated that one ferrocene compound fulfills all essential property requirements for the application in composite propellants up to a concentration of 1,5 %. It is chemically bound to the binder without disturbing network formation and is as effective (or even more) as Catocene in the enhancement of burning velocities.

1. Einführung und Zielsetzung

Mit Ferrocenverbindungen können Raketentreibstoffe für hochbeschleunigende Flugkörperantriebe formuliert werden, die hohe Füllstoffanteile feinkörniger AP-Fraktion enthalten und auf diese Weise hohe Leistung und hohe Abbrandgeschwindigkeiten in sich vereinigen.

Flüssige Ferrocenderivate wie 2,2'-Bis(ethylferrocenyl)propan (Catocen®) sind in der Lage, die Abbrandgeschwindigkeiten von Composittreibstoffen signifikant zu erhöhen, ohne daß die Leistung, die Verarbeitbarkeit oder die mechanischen Eigenschaften wesentlich beeinflußt werden.

Der Nachteil dieser hoch wirksamen Abbrandkatalysatoren liegt in ihrer Tendenz zur Migration und leichten Oxidierbarkeit durch Luftsauerstoff.

Dies führt zu einem schlechteren Alterungsverhalten und einer geringen Zuverlässigkeit des Treibstoffs sowie zu einer geringeren Lebensdauer und erhöhten Empfindlichkeit. Wie Böhnlein-Mauß et al (1,2) zeigen konnten, verringert sich die Migrationstendenz der Ferrocenderivate beim Einbau sperriger Liganden am Ferrocen. Zugleich sind aber auch die sterisch gehinderten Ferrocene bei der Erhöhung der Abbrandgeschwindigkeit nicht so wirksam wie die weniger substituierten Derivate. In diesem Sinne erhöht z.B. bei gleichem Eisengehalt im Treibstoff n-Butylferrocen die Abbrandgeschwindigkeit eines Composittreibstoffs auf der Basis AP, Al und HTPB weniger stark als Ethylferrocen (2).

Ethylferrocen migriert aber auch stärker als das ohnehin schon schnell wandernde n-Butylferrocen. Ferrocenderivate mit hoher Wirksamkeit, die nicht mehr migrieren sollen, müssen deshalb mit dem polymeren Bindersystem chemisch gebunden sein. Verschiedene mono- und difunktionell substituierte Derivate sind in der Patendliteratur beschrieben (3-5). Die meisten davon sind nicht flüssig oder lassen sich nicht unter Erhalt von Gießfähigkeit und guten mechanischen Eigenschaften in hochgefüllte Composittreibstoffe einarbeiten.

Ein neues Präparat, das hoch wirksam ist und alle Anwendungseigenschaften erfüllt, ist Butacen®, ein am Polybutadien gekoppeltes Ferrocen (6). Es erfordert jedoch hohe Einsatzkonzentrationen und ist aufwendig zu synthetisieren.

Aus diesem Grunde war es das Ziel der Arbeit, leichter zu synthetisierende chemisch einbindbare Ferrocenderivate auf ihre Wirksamkeit der Abbrandbeschleunigung und Anwendbarkeit in hochgefüllten Composittreibstoffen zu untersuchen.

2. Ferrocenderivate

Die in dieser Arbeit untersuchten Ferrocenderivate wurden ausgewählt auf Grund ihrer strukturellen Integrierbarkeit und Mischbarkeit mit den Binderkomponenten eines Composittreibstoffs auf der Basis von Ammoniumperchlorat, Aluminium und hydroxyterminiertem Polybutadien (HTPB) sowie auf Grund ihrer leichten und preisgünstigen Herstellbarkeit aus kommerziell in größeren Mengen verfügbaren Ferrocenverbindungen. Alle untersuchten Ferrocenderivate wurden von der Chemische Betriebe Pluto GmbH im Labormaßstab synthetisiert und mittels GC bzw. HPLC auf Reinheit und Isomerenverteilung untersucht. Das verwendete Catocen® („PLUTORAC EFP“) enthielt etwa 3,5 % Ethylferrocen. Abbildung 1 zeigt die auf Grund ihres Abbrandverhaltens, Verarbeitbarkeit und mechanischen Eigenschaften der Treibstoffe näher untersuchten einbindbaren Ferrocenverbindungen. Das verwendete Ferrocenderivat B ist strukturell ähnlich aufgebaut wie das literaturbekannte Bisferrocenylpentanol (7). Es verleiht dem Treibstoff hinsichtlich Verarbeitbarkeit und mechanischer Struktur deutlich bessere Eigenschaften als das literaturbekannte Derivat.

3. Composit Raketentreibstoffe

Der Einfluß der Ferrocenderivate wurde in zwei Treibstoffformulierungen mit jeweils 85 Gew% Feststoffgehalt untersucht, bestehend aus 70 % AP, 15 % Aluminium und 15 % HTPB-Binderanteil inkl. Abbrandkatalysator, Stabilisator, Haftvermittler und Diisooctyladipat (DOA) als Weichmacher.

Um die monofunktionell OH-substituierten Ferrocenderivate einzubinden und trotzdem die Ausbildung eines vollständigen Bindernetzwerkes zu ermöglichen, wurden

Triole wie Trimethylolpropan (TMP) als vernetzende OH-Komponente oder trifunktionelle Isocyanate eingesetzt. Als HTPB-Komponenten wurden R 45 HT und R 45 M der Firma Atochem verwendet. Mit Isophorondiisocyanat (IPDI) als Härter wurde jeweils mit einem NCO/OH-Äquivalentverhältnis von 0,8 - 0,9 gearbeitet.

Bei einer Konzentration von jeweils 1,5 Gew% Ferrocenderivat kamen folgende Grundrezepturen zur Anwendung:

	Treibstoff I	Treibstoff II
<u>Feststoff:</u>	<u>85 Gew%</u>	<u>85 Gew%</u>
AP 30 µm:	49 %	28 %
AP 5-7 µm:	21 %	42 %
Al 5 µm:	15 %	15 %
 <u>Binder:</u>	 <u>15 Gew%</u>	 <u>15 Gew%</u>
Ferrocenderivat:	1,5 %	1,5 %
Irganox:	0,15 %	0,19 %
DOA:	3,0 %	3,75 %
R 45 M/HT)		
+ HX 878 (Tepanol))	10,35 %	9,56 %
+ IPDI)		
+ TMP)		

Bezugsquellen und Funktion der Bestandteile sind in Tabelle 1 wiedergegeben.

4. Ergebnisse

4.1 **Verarbeitbarkeit, mechanische Eigenschaften und Empfindlichkeit**

Der Einfluß von OH-funktionalisierten einbindbaren Ferrocenverbindungen auf Verarbeitbarkeit und mechanische Eigenschaften wurde im wesentlichen mit Treibstoffsystem I untersucht. Tabelle 2 zeigt die mit Catocen, Derivat B und BFDEGE jeweils mit R 45 HT und R 45 M erhaltenen Werte.

Die Viskositäten wurden mit einem Brookfield Spindel Viskosimeter gemessen. Sie sind als auf die Meßmethodik bezogene Vergleichswerte zu betrachten.

Schlagempfindlichkeiten wurden mit dem BAM-Hammer, Reibempfindlichkeiten mit dem BAM'schen Reibempfindlichkeitsmeßgerät gemessen. Zur Bestimmung der mechanischen Eigenschaften wurde eine Instron-Maschine mit uniaxialem Zug verwendet. Die Werte für Zugfestigkeit, Bruchdehnung und Elastizitätsmodul wurden bei 20 °C und einer Zuggeschwindigkeit von 50 mm/min gemessen.

Mit Ausnahme von Treibstoff Nr. 1067 weisen alle Formulierungen gute Gießviskositäten und Verlaufseigenschaften auf. Bei der Verwendung von R 45 HT sind allgemein die Gießviskositäten besser, die mechanischen Eigenschaften aber ungünstiger als bei der Verwendung von R 45 M. Auffällig ist, daß die Treibstoffe mit dem einbindbaren Derivat B trotz des Zusatzes von Trimethylolpropan kleinere Gießviskositäten und bessere mechanische Eigenschaften als die gleichartigen Catocenhaltigen Formulierungen zeigen.

Treibstoff Nr. 1067 mit 1,5 % BFDEGE war nach Härterzugabe nicht gießfähig. Das als Härter verwendete trifunktionelle Isocyanat N 3400 ist als HDI-Abkömmling für die Umsetzung mit HTPB zu reaktiv, um den Treibstoffslurry in ausreichendem Maße fließfähig zu halten. Nach den mechanischen Eigenschaften sind die Treibstoffe mit Derivat B und BFDEGE günstig eingestellt. Das Netzwerk des polymeren Binders erscheint ausgebildet.

Die Reib- und Schlagempfindlichkeiten der Treibstoffe mit 1,5 % Ferrocengehalt sind in etwa gleich und entsprechen der Treibstoffformulierung ohne Abbrandkatalysator. Nur die Formulierung mit 3 % Catocen scheint empfindlicher zu sein.

4.2 Abbrandverhalten

Die Abbrandeigenschaften aller Formulierungen wurden in der Crawford-Bombe im Druckbereich von 2 - 25 MPa bei 20 °C gemessen. Die Abbrandgeschwindigkeiten wurden an Strands mit quadratischer Querschnittsfläche und einer Länge von 50 mm und 100 mm gemessen. Tabelle 3 zeigt die Werte der Abbrandgeschwindigkeiten bei 2 MPa und 10 MPa und die sich im gesamten Druckbereich nach dem Vieille'schen Gesetz ergebenden Druckexponenten.

Abbildung 2 zeigt die logarithmische Auftragung der Abbrandgeschwindigkeit über den Druck von Treibstoffsystem I ohne sowie mit 1,5 % und 3 % Catocen. Die Wirkung des Ferrocenkatalysators kommt dabei gut heraus. Bei niederem Druck werden die Abbrandgeschwindigkeiten signifikant erhöht, der Druckexponent jedoch gesenkt. Insgesamt bewirkt die Ferrocenverbindung eine deutliche Verbesserung des Abbrandverhaltens in Bezug auf anwendungstechnische Anforderungen.

In Abbildung 3 ist das Abbrandverhalten des Treibstofftyps I mit den einbindbaren Ferrocenverbindungen Derivat B und BFDEGE im Vergleich zu den Formulierungen mit Catocen und ohne Abbrandkatalysator dargestellt. Die beiden neuen einbindbaren Verbindungen zeigen im Vergleich zu Catocen gleichwertige und im Falle des Derivat B sogar verbesserte Wirksamkeit. Bezieht man die Erhöhung der Abbrandgeschwindigkeit auf den Eisengehalt im Treibstoff, sind beide einbindbaren Ferrocene deutlich wirksamer als Catocen.

Abbildung 4 stellt das Abbrandverhalten von Treibstofftyp 2 mit jeweils 1,5 % Catocen, BFDEGE, FMHPE und Derivat B dem Abbrandverhalten des Treibstoffs ohne Katalysator gegenüber. Durch den höheren Anteil des feinkörnigen AP sind die Effekte in Bezug auf Erhöhung der Abbrandgeschwindigkeit und Senkung des Druckexponenten noch ausgeprägter. Gegenüber den FMHPE- und Derivat B-haltigen Treibstoffen fällt die Erhöhung der Abbrandgeschwindigkeiten durch BFDEGE in diesem Fall geringer aus. Der Druckexponent ist jedoch deutlich reduziert, das Abbrandverhalten erscheint gut eingestellt.

Derivat B und FMHPE zeigen zusammen mit Catocen die höchsten Wirksamkeiten. Ab 4 MPa fallen die nach dem Vieilleschen Gesetz gefitteten Funktionen der Treibstoffe mit FMHPE und Catocen praktisch übereinander. Bezieht man die Erhöhung der Abbrandgeschwindigkeiten auf den Eisengehalt, besitzen beide Verbindungen auch gegenüber dem traditionell verwendeten Ferrocenkatalysator höhere Effektivität.

5. Diskussion

Aus den Ergebnissen ergeben sich verschiedene Ansatzpunkte für die Diskussion:

1. Die unterschiedliche Wirksamkeit der Abbrandkatalysatoren ist wahrscheinlich auf molekulardynamische, strukturelle sowie elektronische Unterschiede der Ferrocenverbindungen zurückzuführen. Ebenso dürfte die Integration der Komponente in das Netzwerk des polymeren Binders von Bedeutung sein.

Wie Böhnlein-Mauß et.al. (1,2) zeigen konnten, sind sterisch gehinderte Ferrocene zwar weniger migrationsfähig, aber in Bezug auf Erhöhung der Abbrandgeschwindigkeit weniger wirksam. Dies trifft u.U. auch für die geringere Wirksamkeit des n-butylsubstituierten BFDEGE zu. Gleichwohl dürften elektronische Faktoren eine Rolle spielen, da BFDEGE als estercarbonylsubstituiertes Ferrocen ein höheres Oxidationspotential besitzt als Derivat B und FMHPE.

2. Deutliche Unterschiede gibt es bei den einbindbaren Ferrocenderivaten in Bezug auf Beeinträchtigung der Verarbeitbarkeit des Treibstoffslurries und Netzwerkintegration. BFDEGE- und FMHPE-haltige Treibstoffe sind vermutlich durch die Häufung polarer Gruppen am Ferrocen und deren Komplexbildungstendenz mit vernetzenden Triolen und Urethangruppierungen schwer zu verarbeiten.

Derivat B zeigt diese Nachteile nicht. Treibstoffe mit 1,5 Gew% Derivat B sind mit TMP sowohl mit R 45 HT als auch R 45 M gießfähig und besitzen nach Aushärtung gute mechanische Eigenschaften.

3. Über die Anwendbarkeit einer Ferrocenverbindung werden das gesamte Eigenschaftsprofil der Treibstoffformulierung ebenso wie Preis und Verfügbarkeit der Komponente entscheiden.

Die Auswahl der getesteten Verbindungen wurde deshalb von der Chemische Betriebe Pluto GmbH vor dem Hintergrund einer preisgünstigen und gut aufskalierbaren Synthese vorgenommen.

Alle vorgestellten Ferrocenderivate lassen sich ohne Schwierigkeiten auch in größeren Mengen herstellen.

Für den HTPB-Treibstoff erfüllt derzeit das Derivat B alle wesentlichen Forderungen wie:

- * gute Einarbeitbarkeit ohne Beeinträchtigung der Gießviskosität des Treibstoff-slurries,
- * gute Netzbildung unter Beifügung eines vernetzenden Triols,
- * keine Beeinträchtigung der mechanischen Treibstoffempfindlichkeit und Stabilität,
- * hohe Wirksamkeit in Bezug auf Steigerung der Abbrandgeschwindigkeit und Senkung des Druckexponenten.

BFDEGE und FMHPE sind in HTPB-Treibstoffen weniger gut, d.h. nur mit anderen noch zu definierenden Härtern und Netzbildnern problemlos zu verarbeiten. Sehr gute Verwendungsmöglichkeiten bestehen jedoch für Raketen- oder Gasgenerator-treibstoffe mit Polyether- oder Polyesterurethanbindern (8).

6. Zusammenfassung

In zwei AP, AI, HTPB-Compositformulierungen mit jeweils 85 Gew% Feststoffgehalt zeigt das einbindbare Derivat B bis zu einer Konzentration von 1,5 Gew% in Bezug auf Erhöhung der Abbrandgeschwindigkeit, Verarbeitbarkeit, mechanische Eigenschaften und Empfindlichkeit des Treibstoffs gute Ergebnisse. Mit dem Zusatz von TMP gelingt eine gute Netzbildung unter Einbindung des Ferrocens, die dessen Migration verhindert. Die Erhöhung der Abbrandgeschwindigkeit entspricht und übersteigt teilweise die Wirkung des Catocens.

Die beiden über Ether- und Estergruppen funktionalisierten Ferrocene FMHPE und BFDEGE sind im HTPB-Treibstoff deutlich schwerer zu verarbeiten. FMHPE ist in der Erhöhung der Abbrandgeschwindigkeit ebenso wirksam wie Catocen, BFDEGE liefert ein insgesamt sehr gut eingestelltes Abbrandverhalten. Beide Verbindungen empfehlen sich für den Einsatz in Raketen- oder Gasgenerator-treibstoffen mit Polyether- oder Polyesterurethanbindern.

Literaturverzeichnis

- 1) J. Böhnlein-Mauß et.al.;
„Structural Influences of Ferrocenes on Burn Rate Modification of Composite Rocket Propellants“
24. Intern. ICT-Conf. 71-1 ff (1993)
- 2) J. Böhnlein-Mauß et.al.;
„Abbrand- und Migrationseigenschaften von zweikernigen Ferrocenverbindungen als Abbrandmodifikatoren in Composittreibstoffen“
25. Intern. ICT-Conf. 105-1 ff (1994)
- 3) C. Gotzmer et.al.;
„Non Migrating Ferrocene Modifiers for Composite Propellants“
JANNAF Prop. Meeting Vol. 2. 475 ff (1979)
- 4) W.P. Norris et.al.;
US-Patent 3 968 126 (1976)
- 5) F.M. Dewey;
„Ferrocene Polyglycols“
US-Patent 3 598 850 (1971)
- 6) S. Raynal, G. Doriath;
„New Functional Prepolymers for High Burning Rates Solid Propellants“
AIAA 22nd Joint Prop. Conf. Huntsville (1986)
- 7) J.D. Braun et.al.;
„Burning Rate Modifying Binder for Propellant and Method“
US-Patent 3 932 240 (1976)
- 8) J. Böhnlein-Mauß, K.P. Brehler, K. Menke;
unveröffentlichte Ergebnisse

Tabelle 1: Treibstoffkomponenten

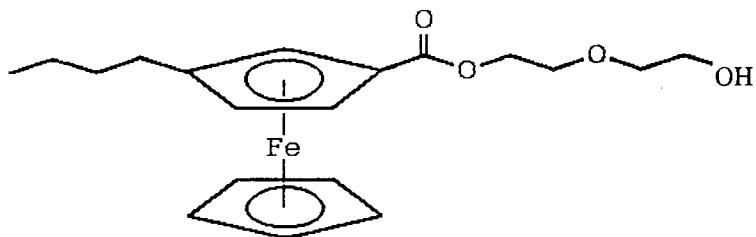
Bezeichnung	Funktion	Hersteller
R 45 HT/M	HTPB-Precursorpolymer	Atochem
HX 878 (Tepanol)	Haftvermittler	3 M
Irganox 565	Antioxidanz	Ciba Geigy
TMP	OH-Vernetzer	Aldrich
IPDI	Isophorondiisocyanat-Härter	Hüls AG
N 3400	Triisocyanat-Härter	Bayer AG
DOA	Plastifizierer	BASF AG
AP 30 μm	Oxidator	Mitsubishi
AP 5-7 μm	Oxidator	Kerr McGee
Al Alcan 400	Brennstoff	Alcan Toyo

Tabelle 2: Empfindlichkeit, Verarbeitungs- und mechanische Eigenschaften

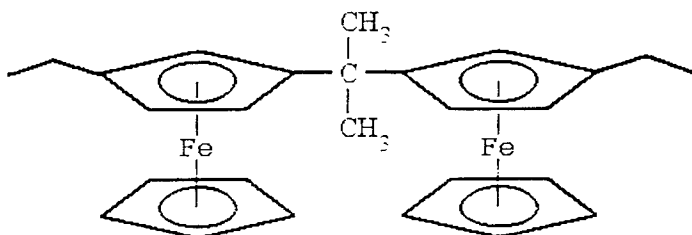
FTS Nr.	Ferrocen	Gew. %	Gießvis- kosität (Pas)	Schlag- empfind- lichkeit (Nm)	Reib- empfind- lichkeit (N)	mechanische Eigenschaften (20°C / 50 mm/min)			HTPB OH-Vern.	Isocyanat	NCO/OH (Eq)
						Zugfestig- keit (N/mm ²)	Dehnung (%)	E-Modul (N/mm ²)			
<u>Treibstoff I</u>											
1060	-	-	152	3	36	1,57	11	14,38	R 45 HT	IPDI	0,8
1058	Catocen	1,5	128	3	40	1,75	10	23,02	R 45 HT	IPDI	0,8
1059	Catocen	3	160	2	32	1,76	14	8,70	R 45 HT	IPDI	0,8
1061	Derivat B	1,5	112	3	40	2,41	15	14,9	HT/TMP	IPDI	0,9
1066	Catocen	1,5	224	3	40	0,51	44	1,95	R 45 HT	IPDI	0,8
1065...	Derivat B	1,5	184	3	36	1,34	22	8,62	M/TMP	IPDI	0,9
1067	BFDEGE	1,5	800	4	40	1,34	27	6,81	R 45 M	N 3400	0,87

Tabelle 3: Abbrandgeschwindigkeiten und Druckexponenten bei 20 °C

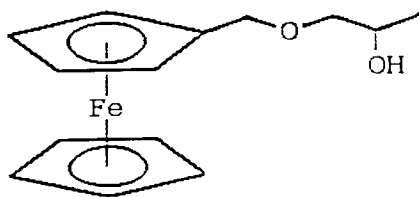
FTS Nr.	Ferrocen- derivat (HTPB-Type)	Gew. %	Abbrandgeschwindigkeit (mm/s) r (2 MPa)	Abbrandgeschwindigkeit (mm/s) r (10 MPa)	Druck- exponent	Druckbereich (MPa)	Fe-Gehalt im Treibstoff (%)
Treibstoff I							
1060	-	-	13,5	27,3	0,47	2 - 25	-
1058	Catocen HT	1,5	20,6	31,9	0,21 0,43	2 - 7 7 - 25	0,36
1066	Catocen M	1,5	17,4	31,4	0,39	2 - 25	0,36
1061	Derivat B HT	1,5	21,1	33,4	0,33	2 - 25	0,33
1066	Derivat B M	1,5	20,3	36,6	0,34	2 - 25	0,33
1067	BFDEGE M	1,5	17,7	31,4	0,43 0,12	2 - 7 7 - 18	0,22
1059	Catocen HT	3,0	21,6	38,6	0,38	2 - 25	0,72
Treibstoff II (HT)							
991	-	-	12,6	34,2	0,51	2 - 25	-
993	Catocen	1,5	20,7	47,7	0,32	4 - 18	0,36
1053	BFDEGE	1,5	19,1	35,0	0,33	2 - 22	0,22
1052	FMHPE	1,5	27,5	44,2	0,32	2 - 25	0,31
1055	Derivat B	1,5	22,8	41,8	0,36	2 - 25	0,33



n-Butylferrocenecarbonsäurediethylenglycolester = BFDEGE



2,2'-Bis(ethylferrocenyl)propan = Catocen



Ferrocenylmethyl-(2-hydroxypropyl)ether = FMHPE

Abbildung 1:

Molekülstrukturen der untersuchten Ferrocenverbindungen

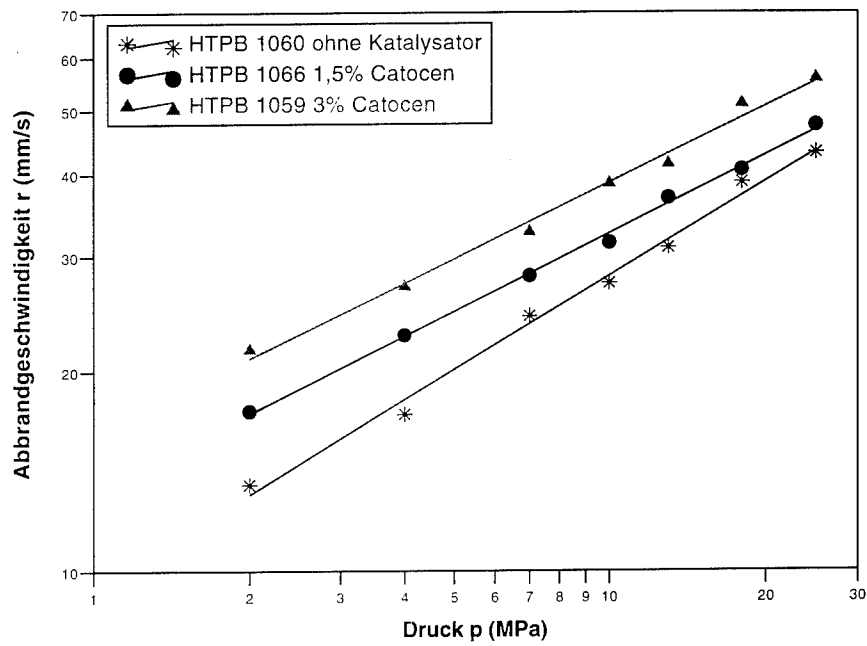


Abbildung 2:

Abbranddiagramm $\lg r = f(\lg p)$ von Treibstofftyp I ohne und mit Catocen Abbrandmodifikator

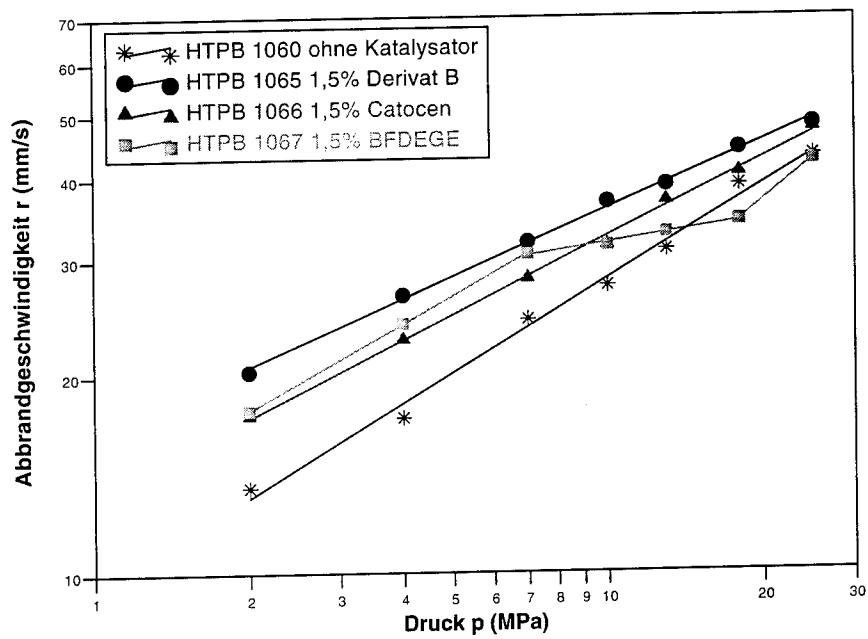


Abbildung 3:

Abbranddiagramm $\lg r = f(\lg p)$ von Treibstofftyp I mit jeweils 1,5 % Derivat B, BFDEGE und Catocen

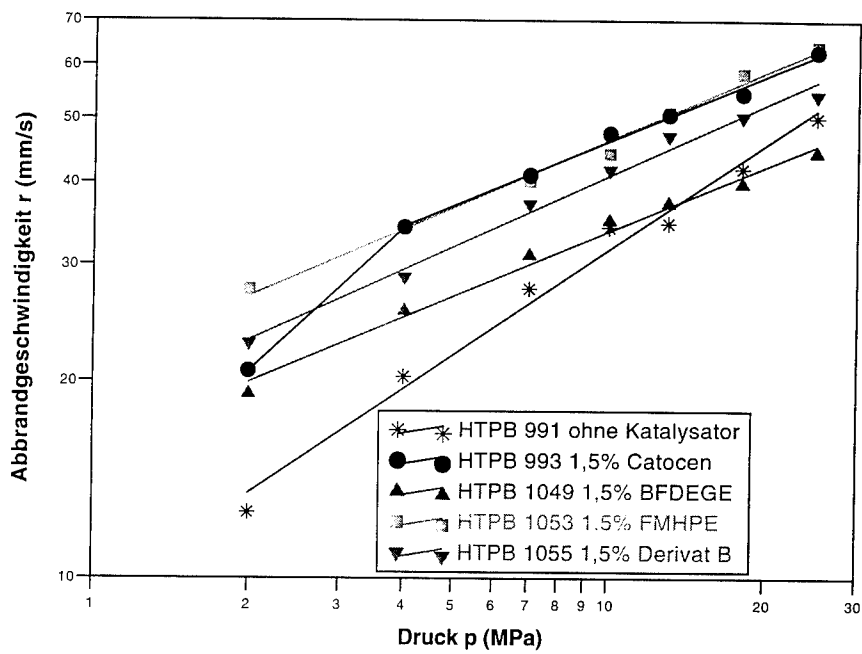


Abbildung 4:

Abbranddiagramm $\lg r = f(\lg p)$ von Treibstofftyp II mit jeweils 1,5 % Catocen und einbindbaren Ferrocenderivaten

Herstellung von Explosivstoffpartikeln durch schnelle Expansion fluider überkritischer Lösungen

Particle Formation of Explosives by Rapid Expansion of Supercritical Solutions

U.Teipel, P. Gerber, H. Krause

Fraunhofer - Institut für Chemische Technologie (ICT)
Postfach 1240, D - 76318 Pfinztal, Germany

Abstract

Bei der Formulierung von Explosivstoffen kommt den Partikeleigenschaften, wie z.B. der Partikelgröße, der Partikelgrößenverteilung und der Partikelform eine besondere Bedeutung zu. In dem vorliegenden Beitrag wird ein neues Verfahren zur Herstellung von Partikeln aus überkritischen Lösungen vorgestellt. Bei diesem Verfahren wird in einem ersten Schritt Explosivstoff durch überkritisches CO₂ extrahiert. Anschließend wird das beladene Fluid über eine Düse entspannt. Durch den Entspannungs Vorgang sinkt die Löslichkeit des Explosivstoffes im Fluid, wodurch der Explosivstoff nach der Entspannung als Partikel vorliegt.

In diesem Beitrag wird das Verfahren zur Herstellung von Explosivstoffpartikeln durch schnelle Expansion fluider überkritischer Lösungen näher beschrieben und erste Ergebnisse vorgestellt.

1. Einleitung

Für die Beurteilung von Explosivstoffen sind Aussagen über deren Stabilität und Empfindlichkeit von Interesse. Die Empfindlichkeit eines Explosivstoffes gibt die Sensibilität gegen Wärme und mechanische Einwirkungen wie Schlag, Stoß und Reibung an. Um möglichst unempfindliche kristalline Explosivstoffe zu erhalten, wird ein neues Verfahren konzipiert, bei welchem die Kristalle möglichst wenig Kristallfehler in Form von Einschlüssen und Fehlstellen aufweisen.

Ziel des konzipierten Prozesses ist es, Partikel mit kleinem mittleren Durchmesser ($x < 10 \mu\text{m}$) und einer engen Partikelgrößenverteilung herzustellen. Die durch den Prozeß gewonnenen Partikel weisen hierbei eine enge Partikelgrößenverteilung auf. Erste Vorversuche zu diesem Prozeß im Labormaßstab /1/ bestätigen diese Erwartungen. Durch Variation verschiedener Prozeßparameter wird die Partikelgröße sowie die Partikelgrößenverteilung beeinflusst.

Das für diesen Prozeß eingesetzte Lösungsmittel muß bestimmte Bedingungen erfüllen, welche näher erörtert werden. Auf den Einsatz von klassischen Lösungsmitteln kann je nach Verfahrensvariante verzichtet werden. Um den Einsatz von Lösungsmittel zu minimieren, wird bei diesem Verfahren das überkritische Lösungsmittel im Kreislauf gefahren.

Die Lösungsmiteleigenschaften überkritischer Fluide wurde schon 1879 durch Hanay und Hogarth /2/ festgestellt. Sie beobachteten, daß sich ein Feststoff ohne meßbaren Dampfdruck in einem Gas löst, wenn der Druck des Gases über den kritischen Druck erhöht wird. Reduziert man den Druck, fällt der zuvor gelöste Feststoff kristallin aus. /3, 4, 5/

2. Grundlagen

2.1 Eigenschaften überkritischer Fluide

Wird ein Gas oder eine Flüssigkeit über den kritischen Druck p_c komprimiert, bzw. über die kritische Temperatur T_c erhitzt, so befindet sich das Fluid im überkritischen Zustand. Für Kohlendioxid ist in Abbildung 1 die Existenzbereiche der verschiedenen, von Druck und Temperatur abhängigen, Aggregatzustände dargestellt.

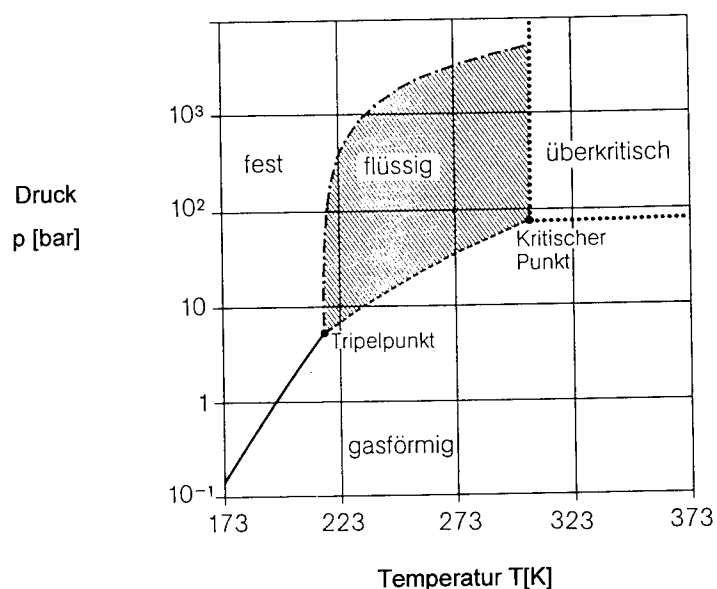


Abb. 1: p,T - Phasendiagramm für CO_2 /6/

Ein Vergleich der physikalischen Eigenschaften von Gasen, verdichteten Gasen und Flüssigkeiten zeigt Tabelle 1. Trotz der im Vergleich zu Flüssigkeiten nur geringfügig niedrigeren Dichte (ρ) verdichteter Gase entspricht die dynamische Viskosität (η) dem Wert von Gasen bei 1 bar und $\vartheta = 25^\circ\text{C}$. Der Diffusionskoeffizient (D^*) eines verdichteten Gases ist in der Nähe des kritischen Punktes um mehr als das Zehnfache höher als der einer Flüssigkeit.

Eine besondere Eigenschaft verdichtete Gase, ist ihr schnelles Massentransportverhalten. Sie eignen sich daher prinzipiell besser, im Vergleich zu klassischen Lösungsmitteln dazu, in das zu extrahierende Trägermaterial einzudringen, die löslichen Bestandteile aufzunehmen und weiterzutransportieren. Das verdichtete Gas als Lösungsmittel muß jedoch eine genügend hohe Lösungskapazität für den zu lösenden Stoff aufweisen. Die Löslichkeit eines Feststoffes in einem Lösungsmittel hängt von Druck und Temperatur und somit von der Dichte des Lösungsmittels ab. Im Bereich des kritischen Punktes ist die Dichteänderung schon bei geringer Variation von Temperatur und Druck besonders groß.

		ρ [kg/m ³]	η [Pas · 10 ³]	D^* [m ² /s]
Gase bei 1 bar, $\vartheta = 25\text{ }^{\circ}\text{C}$		0,6 – 2,0	0,01 – 0,03	$1 - 4 \cdot 10^{-5}$
überkritische Fluide	T_C, p_C	200 – 500	0,01 – 0,03	$7 \cdot 10^{-8}$
	$T_C, 4 \cdot p_C$	400 – 900	0,03 – 0,06	$2 \cdot 10^{-8}$
Flüssigkeiten bei $\vartheta = 25\text{ }^{\circ}\text{C}$		600 – 1600	0,2 – 3,0	$0,2 - 2 \cdot 10^{-9}$

* Selbstdiffusion für Gase und verdichtete Gase, binäre Mischungen für Flüssigkeiten

Tab. 1: Größenordnungsvergleich physikalischer Daten von Gasen, verdichteten Gasen und Flüssigkeiten /7/

Durch Zusatz einer Komponente mittlerer Flüchtigkeit, zwischen Gas als Lösungsmittel einerseits und kondensierter bzw. fester Phase andererseits, eines sogenannten Schleppmittels, kann die Lösungskapazität des verdichteten Gas wesentlich erhöht werden. Durch Temperaturänderung besteht z.B. durch Ausnutzung von Mischungslücken die Möglichkeit einer günstigen Regeneration des Lösungsmittels.

2.2 Auswahl des Lösungsmittels

Für die Auswahl eines geeigneten Lösungsmittels ist es von Vorteil, wenn sich das Lösungsmittel durch niedrige kritische Parameter (Druck, Temperatur) auszeichnet. Somit können niedrige Prozeßrandbedingungen gewählt werden, welche sich günstig auf die Prozeß- und Investitionskosten auswirken. Desweiteren sollte ein Lösungsmittel gewählt werden, welches nicht toxisch ist und mit Luft keine explosionsfähigen Gemische bildet. Als interessantestes Gas ist in diesem Zusammenhang Kohlendioxid zu nennen. Dieses Gas steht in großen Mengen zu günstigen Konditionen zur Verfügung, die Bevorratung großer Mengen in verflüssigter Form ist Stand der Technik.

Tabelle 2 zeigt ein Vergleich der kritischen Temperaturen und Drücke für verschiedene Fluide.

Fluid	T_c [°C]	p_c [bar]
n - Pentan	196,5	33,7
n - Butan	152,0	38,0
Propan	96,6	42,5
Methan	-82,8	46,0
Ethylen	9,2	50,4
Kohlendioxid	30,9	73,7
Distickstoffoxid	36,4	72,4
Methanol	239,4	80,9
Ammoniak	132,3	113,5
Wasser	374,1	221,2

Tab. 2: Physikalische Daten verschiedener zur Extraktion geeigneter Gase /1,8/

Chemische Formel	CO ₂	
Molare Masse	M _{CO₂} = 22,263	kg / kmol
Molares Normvolumen	V _{mN} = 22,263	m ³ / kmol
Kritische Temperatur	T _c = 304,1	K
Kritischer Druck	p _c = 73,7	bar
Kritische Dichte	ρ _c = 467,6	kg / m ³
Tripelpunkt	T _{Tr.} = -56,6	°C
	p _{Tr.} = 5,18	bar
Sublimationspunkt (Trockeneis)	T _s = -78,9 ,	°C
	bei p _s = 0,981	bar
Zersetzungstemperatur	ab ca 1200 °C, bei einem Zersetzungsgrad von ca. 0,032 Vol %	

Tab. 3: Eigenschaften von Kohlendioxid, /6, 8/

Tabelle 4 zeigt den Einfluß von Druck und Temperatur auf die Dichte von Kohlendioxid /6/. Tabelle 4 zeigt für den Prozeß zur Herstellung von Partikeln typische Temperatur- und Druckwerte. Innerhalb des Prozesses variiert die Dichte von CO₂ um fast zwei Dekaden.

T [°C]	10	20	40	50	150
p [bar]					
1	1,88	1,82	1,70	1,64	1,27
40	108,32	97,51	83,77	78,87	54,60
50	870,49	140,53	113,02	104,80	69,60
300	1020,70	985,35	910,50	870,90	526,04

Tab. 4: Dichte von Kohlendioxid [kg/m³] in Abhängigkeit von Druck und Temperatur

Es ist von Vorteil, wenn das Lösungsmittel ausreichende Lösungsmiteigenschaften gegenüber dem Feststoff aufweist, sodaß auf den Einsatz von Schleppmitteln verzichtet werden kann. Für die in diesem Beitrag vorgestellten Versuche wurde das Dummy-Material Naphthalin ausgewählt. Im Vergleich zu einem Explosivstoff besitzt Naphthalin ähnliche physikalische Eigenschaften bezüglich der Dichte und der Lage des Schmelzpunktes. Außerdem weist Naphthalin eine ausreichende Löslichkeit in Kohlendioxid auf. Wie Abbildung 2 zeigt, läßt sich durch Variation von Druck und Temperatur die Konzentration von gelöstem Naphthalin um zwei Dekaden variieren.

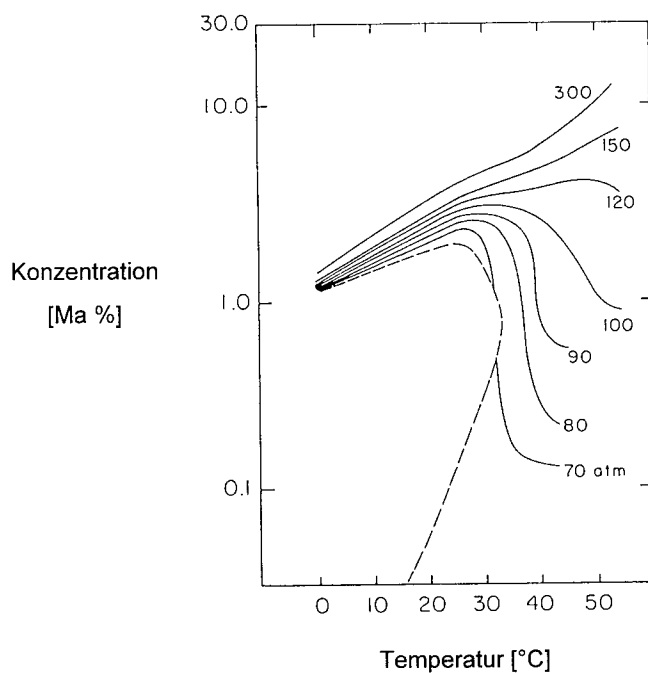


Abb. 2: Löslichkeit von Naphthalin in CO₂ /9/

Naphthalin bildet farblose, monokline Kristalle. Es ist bei Normaldruck und -temperatur leicht löslich in Benzol, Äther und Chloroform, löslich in Ethanol und praktisch unlöslich in Wasser. Tabelle 5 zeigt weitere Eigenschaften von Naphthalin.

Chemische Formel	$C_{10}H_8$	
Molare Masse	128,18	kg / kmol
Schmelzpunkt	80,29	°C
Dichte (25 °C, 1 bar)	1,17	kg / m ³
kritische Temperatur	475	°C
spezifische Wärme bei 25 °C	1294	J / kg
Dampfdruck bei 70 °C	5,25	mbar

Tab. 5: Eigenschaften von Naphthalin /10/

3. Düsenströmung

Die Strömung lässt sich in zwei unterschiedliche Bereiche aufteilen, in eine **adiabate Düsenströmung** und eine **isentropen Freistrahlexpansion** im Überschallbereich. Als Düse wurde die in Abbildung 3 dargestellte Expansionsdüse eingesetzt. Die Düse ist 1,5 mm lang, der Durchmesser des engsten Querschnittes beträgt 100 µm.

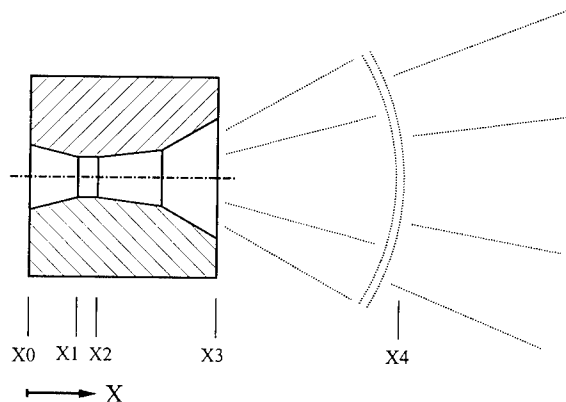


Abb. 3: Expansionsdüse

Vor dem Eintritt in die Düse, befindet sich die Lösung im überkritischen Zustand. Nach der Düse liegt das CO_2 gasförmig vor; der zuvor gelöste Feststoff liegt in kristalliner Form vor. Für die im folgende betrachtete Strömung werden vom Düsenanfang stromabwärts folgende Annahmen getroffen:

- Druck und Temperatur ändern sich nur in x-Richtung, die Strömung wird näherungsweise als eindimensionale Strömung betrachtet.
- Die Expansion in der Düse erfolgt aufgrund der kurzen Aufenthaltszeit adiabatisch.
- Der Druckunterschied in der Düse ist ausreichend groß, um das Fluid im engsten Querschnitt auf Schallgeschwindigkeit zu beschleunigen.
- Die Strömung ist stationär.

Für die Strömung im Bereich $x_0 < x_4$ gelten folgende differentielle Erhaltungssätze:

- Massenerhaltung:
$$\frac{d\rho}{\rho} + \frac{dw}{w} + \frac{dA}{A} = 0 \quad (1)$$

- Energieerhaltung:
$$d\left(u + pv + \frac{w^2}{2}\right) = 0 \quad (2)$$

mit $u + pv = h$ gilt:
$$(3)$$

$$dh + wdw = 0 \quad (4)$$

Die Energiebilanz lautet somit:
$$h + \frac{w^2}{2} = H_0 = \text{konst.} \quad (5)$$

Für die Düse $x_0 < x < x_3$ lautet die Enthalpiedifferenz:

$$H_0 - H_3 = \frac{w_3^2}{2} - \frac{w_0^2}{2} \quad (6)$$

Da sich Kohlendioxid im vorliegenden Druck- und Temperaturbereich wie ein reales Gas verhält, gilt für die Enthalpie: $H = H(T, p)$

Im Bereich $x_0 < x < x_2$ gilt:

- Impulserhaltung allgemein:
$$w dw = -\frac{1}{\rho} dp \quad (7)$$

$$\rho w A w_1 - \rho w A w_0 = p_1 A_1 - p_2 A_2 + \int_0^1 p dA \quad (8)$$

- Impulserhaltung innerhalb der Düse:

$$-A dp + \overline{\tau_w} dA_w = m dw \quad (9)$$

$$\text{mit } \overline{\tau_w} = \frac{\rho}{8} \overline{c_m}^2 \lambda_{\text{turb.}} \quad (10)$$

Der turbulente Verlustbeiwert $\lambda_{\text{turb.}}$ kann in Abhängigkeit der Reynoldszahl und der Wandrauhigkeit bestimmt werden.

Im Bereich $x_2 < x < x_4$ kann die Strömung als isentrop angesehen werden. Nach dem engsten Querschnitt in der Düse bei $x=x_2$ ($M=1$), findet eine Freistrahlexpansion im Überschallbereich statt, bis daß bei $x > x_4$ sich die Zustandsgrößen aufgrund eines Verdichtungsstoßes unstetig ändern.

4. Herstellungsprozeß

Bei der Herstellung von Partikeln mit Hilfe überkritischer Fluide sind zwei verschiedene Verfahrensvarianten zu unterscheiden:

- **RESS** - Prozeß (**R**apid **E**xpansion of **S**upercritical **S**olutions)

Die überkritische Lösung wird mittels einer Düse entspannt. Durch die Verminderung der Parameter Druck und Temperatur durch den Entspannungsvorgang sinkt das Lösevermögen des Fluides stark herab, der zuvor gelöste Feststoff liegt nach der Entspannung in kristalliner Form vor.

- **GAS** - Prozeß (**G**as **A**nti - **S**olvent process)

Bei diesem Prozeß wird der Feststoff durch ein klassisches Lösungsmittel gelöst. Die Zugabe eines überkritischen Fluides, welches sich im Lösungsmittel löst, bewirkt eine volumetrische Expansion des Lösemittels. Durch das vergrößerte spezifische Volumen des Lösungsmittels, sinkt die Löslichkeit des Feststoffes im Lösemittel, wodurch der gelöste Feststoff auskristallisiert.

Der wesentliche Vorteil des **RESS** - Prozeß gegenüber dem **GAS** - Prozeß ist, daß keine klassischen Lösungsmittel für diesen Prozeß eingesetzt werden. Hierdurch werden Kristallfehler durch Lösungsmiteleinschlüsse vermieden. Andererseits kann der **GAS** - Prozeß vorteilhaft eingesetzt werden, wenn keine Löslichkeit des festen Explosivstoffes im überkritischen Fluid vorliegt.

In den weiteren Ausführungen wird ausschließlich der **RESS** - Prozeß vorgestellt, da er neben den genannten Vorteilen, durch die gezielte Strömungsführung in der Düse, eine engere Partikelgrößenverteilung als beim **GAS**-Prozeß erwarten läßt.

Abbildung 4 zeigt die Hochdruck-Extraktion-Kristallisationsanlage. Diese Pilotanlage ist für einen maximalen Betriebsdruck von 300 bar und eine maximale Betriebstemperatur von 200 °C ausgelegt.

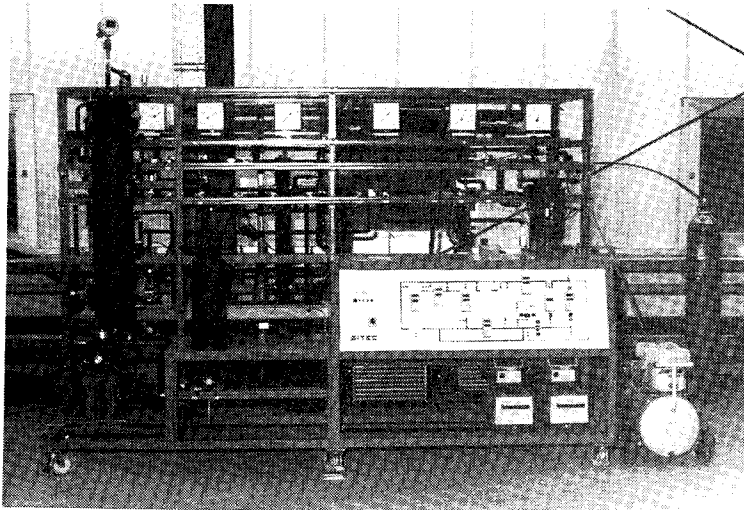


Abb. 4: Hochdruckpilotanlage

Beim **RESS** - Prozeß wird flüssiges, bzw. gasförmiges CO_2 aus einer Vorratsflasche in die Anlage eingespeist, im Wärmetauscher (W3) kondensiert und im Flüssigkeitsspeicher (LS) zwischengespeichert. Nach der Bestimmung des Massenstromes wird das Lösemittel zur Vermeidung von Kavitation im Wärmetauscher (W4) unterkühlt und anschließend mit der Flüssigkeitspumpe (P1) auf den Extraktionsdruck verdichtet. Im Wärmetauscher (W1) wird das Fluid auf die gewünschte Extraktionstemperatur erhitzt, so daß ein überkritischer Zustand erreicht wird. Im Extraktor (B1) wird der zu lösende Stoff extrahiert. Die beladene fluide Lösung wird mittels einer elektrischen Heizung (EI) auf eine höhere Temperatur erwärmt und anschließend über eine Düse in die Kolonne (B3) entspannt. Der zuvor gelöste Feststoff kristallisiert aus, und liegt in der Form von Feststoffpartikeln vor. Diese Partikel verbleiben in der Kolonne, während das CO_2 gasförmig abgezogen wird. Im Separator (B2) wird das Lösungsmittel nochmals entspannt, sodaß noch eventuell gelöster Feststoff ausfällt. Damit das Lösungsmittel im Kreislauf gefördert werden kann, wird das noch gasförmige CO_2 im Wärmetauscher (W3) kondensiert.

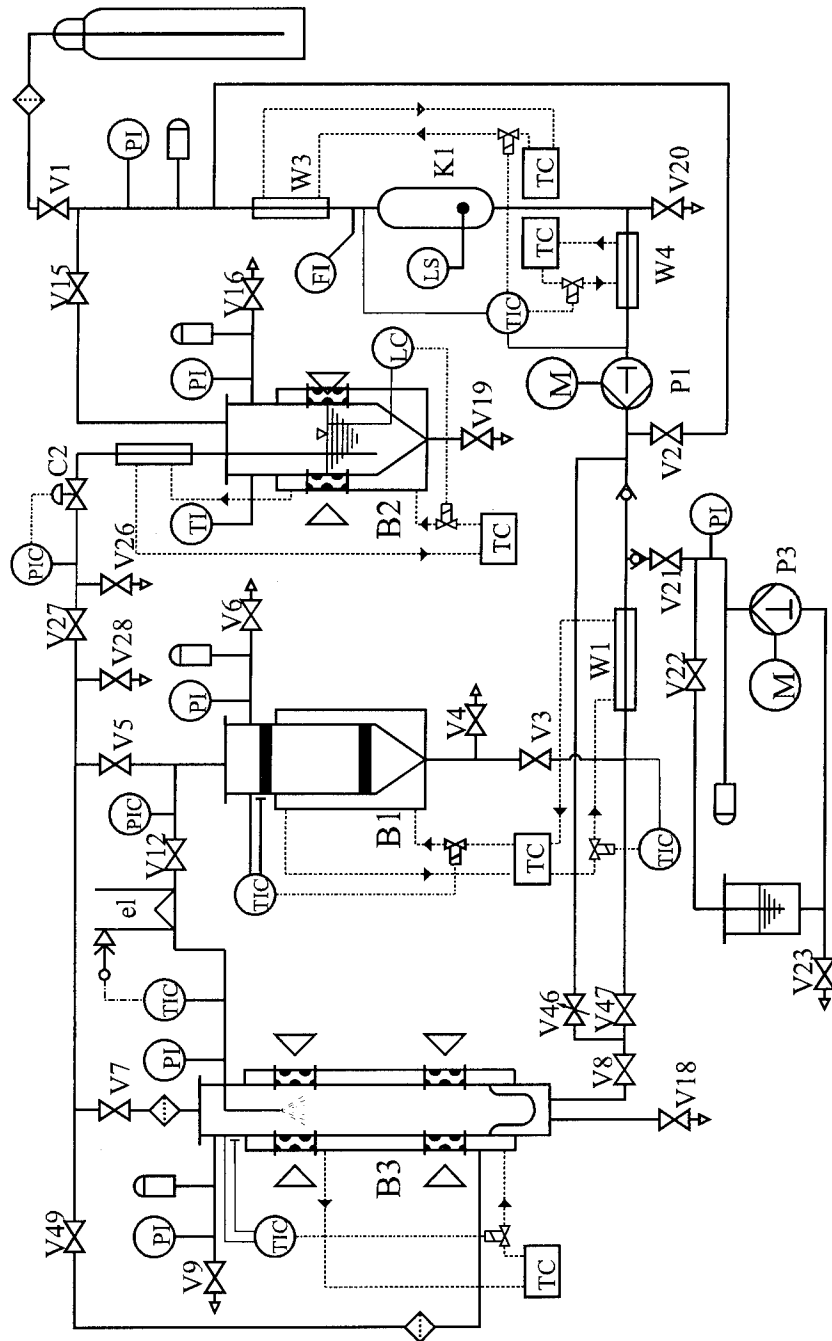


Abb. 5: Fließbild der Hochdruck-Extraktions-Kristallisationsanlage

Abbildung 6 zeigt den Verlauf des idealen **RESS** - Prozesses für unbeladenes Kohlendioxid in ein $p - h$ Diagramm. Bei dem realen Prozeß sind jedoch Reibungs- und Druckverluste, sowie Verluste durch Wärmestrahlung zu berücksichtigen. Da die Entspannung in der Düse nicht über Gleichgewichtszustände erfolgt, wird diese Zustandsänderung durch eine gestrichelte Linie gekennzeichnet.

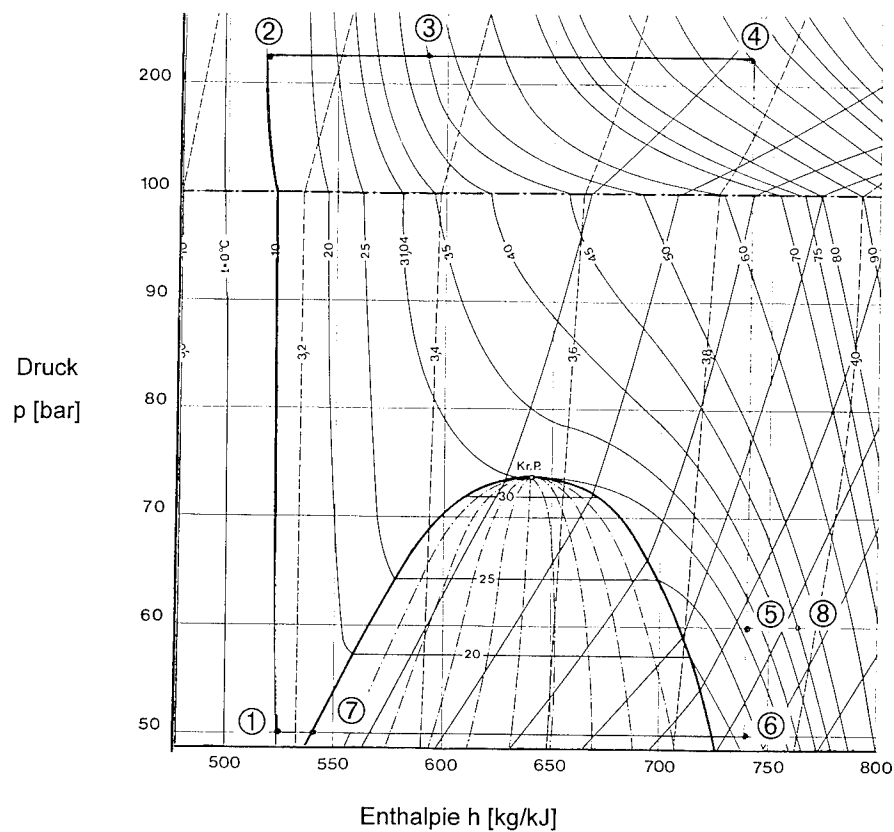


Abb. 6: Schematische Darstellung des RESS - Prozesses im $p - h$ Diagramm

Der ideale **RESS** - Prozeß läßt sich durch folgende Zustandsänderungen beschreiben:

- | | | | |
|-------|--------------------------------------|-------|-------------------------|
| 1 - 2 | isentropische Kompression | 6 - 7 | isobare Kondensation |
| 2 - 3 | isobare Wärmezuführung | 7 - 1 | isobare Unterkühlung |
| 3 - 4 | isobare Wärmezuführung | | |
| 4 - 5 | irreversible Entspannung in der Düse | 3 - | Zustand im Extraktor B1 |
| 5 - 6 | isenthalpe Expansion im Separator | 8 - | Zustand der Kolonne B3 |

5. Versuchsergebnisse

Zur Charakterisierung des RESS-Prozesses wurden vor der Herstellung von Explosivstoffpartikeln, Versuche mit Dummy-Material durchgeführt. Als Versuchsmaterial wurde Naphthalin gewählt. Mit diesem Dummy-Material, von welchem die Löslichkeit in CO_2 bekannt ist, wurde zur Charakterisierung des RESS-Prozesses Parameterstudien durchgeführt.

Folgende Einflußparameter sind beim RESS-Prozeß von besonderer Bedeutung: p , T , \dot{m}_{CO_2} , Düsendurchmesser d sowie die Düsengeometrie. Die Zielgröße dieses Prozesses ist die Partikelgröße bzw. die Partikelgrößenverteilung. Die Bestimmung der Partikelgrößenverteilung erfolgt nach dem Prinzip der Laserbeugungsspektrometrie. Beispielhaft ist in Abbildung 7 die Partikelgrößenverteilung von Naphthalinpartikel, mit folgenden Herstellungsparametern dargestellt:

- Düsendurchmesser, $d = 100 \mu\text{m}$
- Temperatur der Kolonne $T_{\text{Kol.}} = 45^\circ\text{C}$
- Massenstrom CO_2 , $\dot{m} = 6,5 \text{ kg/h}$
- Extraktionsdruck $p_{\text{Extr.}} = 220 \text{ bar}$
- Extraktionstemperatur $T_{\text{Extr.}} = 45^\circ\text{C}$
- Druck in der Kolonne $p_{\text{Kol.}} = 20 \text{ bar}$
- Temperatur vor der Düse $T_{\text{Dü.}} = 110^\circ\text{C}$

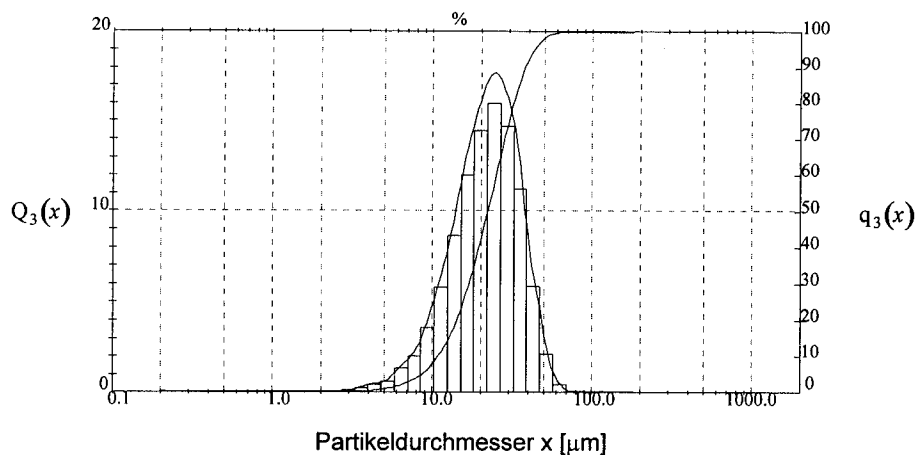


Abb. 7: Volumensumme $Q_3(x)$ und Volumendichteverteilung $q_3(x)$ von Naphthalin, RESS-Prozeß

Die mittlere Partikelgröße $x_{50,3}$ für den in Abbildung 7 dargestellten Versuch beträgt 22 μm . Die Breite der Verteilung stellt sich wie folgt dar: $x_{10,3} = 11 \mu\text{m}$; $x_{90,3} = 38 \mu\text{m}$.

6. Zusammenfassung

Der vorgestellte RESS - Prozeß zur Herstellung von Partikeln aus überkritischen Lösungen wurde am Beispiel von Naphthalin dargestellt. Beim vorgestellten RESS - Prozeß erfolgt die Partikelherstellung durch schnelle Expansion der überkritischen Lösung mittels einer Düse. Als Lösungsmittel wird Kohlendioxid verwendet. Feststoffe welche keine Löslichkeit in Kohlendioxid aufweisen, lassen sich durch Zugabe von Schleppmittel ebenfalls lösen.

Grundsätzlich können mit dem RESS - Prozeß kleine Partikel mit enger Partikelgrößenverteilung hergestellt werden [12,13]. Die erzielbare Partikelgröße und die Partikelgrößenverteilung ist insbesondere von der Geometrie der Düse sowie vom Druck und der Temperatur vor und nach der Düse abhängig. Desweiteren hängt die Übersättigung der Lösung in der Düse von der Konzentration der überkritischen Lösung ab. Die Einflüsse dieser Parameter, auf die Partikelgrößenverteilung, soll in weiteren Versuchen mit Explosivstoffen näher untersucht werden.

7. Literatur

- /1/ Berends E.M., *Supercritical Crystallisation*, Dissertation Technische Universität Delft, 1994
- /2/ Hannay J.B., Hogarth J., *On the solubility of solids in gases*, Proc. Roy. Soc. London 29 (1879), 324.
- /3/ Debenedetti P. G., Tom J. W., Kwauk X., *Rapid Expansion of Supercritical Solutions (RESS): Fundamentals and Applications*, Fluid Phase Equilibria, 82 (1993) 311 - 321, Amsterdam
- /4/ Krukoniš V.J., *Processing of Polymers with Supercritical Fluids*, Polymer News, 1985, Vol. 11, pp 7 - 16
- /5/ Matson D.W., Petersen R. C., Smith R. D., *Production of powder and films by the rapid expansion of supercritical solutions*, Journal of Material Science, (1987) 1919 - 1928
- /6/ *Eigenschaften der Kohlensäure*, Fachverband Kohlensäure - Industrie e. V., 1992
- /7/ Stahl, E., *Verdichtete Gase zur Extraktion und Raffination*, Springer - Verlag, Berlin, 1987
- /8/ Span R., *Eine neue Fundamentalgleichung für das fluide Zustandsgebiet von Kohlendioxid bei Temperaturen bis zu 1100 K und Drücken bis zu 800 MPa*, Fortschr. Ber. VDI Reihe 6 Nr. 285, Düsseldorf 1993
- /9/ McHugh M.A., Krukoniš V.J., *Supercritical Fluid Extraction, Principles and Practice*, Butterworth Publisher, 1986
- /10/ Falbe I., Regnitz M., *Röempp Chemie Lexikon*, 9. Auflage, Band 4, Stuttgart 1991
- /11/ Luckenbach R., *Beilsteins Handbuch der Organischen Chemie*, 4. Ergänzungswerk, 5. Band, 3. Teil, Springer Verlag, 1979
- /12/ Mohamed R.S. et. al., *Solids Formation After the Expansion of Supercritical Mixtures*, ACS Symp. Serie 406, Am. Chem. Soc. (1989 b)
- /13/ Tom J. W., Debenedetti P. G., *Particle Formation with Supercritical Fluids - A Review*, J. Aerosol Sc., Vol 22, No. 5 , pp 555 - 584, 1991

BINDERFREIE ANZÜNDMISCHUNGEN

Peter Jacob

Bayern Chemie
Gesellschaft für flugchemische Antriebe mbH
Liebigstr. 15 - 17
84544 Aschau/Inn

ABSTRACT

The succesfull introduction and widespread application of the airbag as a protection system for motorists required the development of ignition mixtures which on combustion produce minimal toxic gases (CO, NO_x). Bayern-Chemie were already engaged in producing binder free ignition mixtures in the early seventies. Because there are no organic compounds in the composition, there are only a small amount of toxic gases in the reaction products.

Two mixtures are used for the airbag which differ from each other mainly in formulation, heat of explosion and ballistic properties. The method of production is quite similar for both ignition mixtures. After the production of a homogeneous premix, there follows a wet granulation step as the first stage of the granulation process. To achieve the desired distribution of particle size the material is passed through a sieve and afterwards dried. The mechanical stability of the granules is due to recrystallisation of the partly dissolved potassium nitrate during the drying process. The product shows a very good rub-off-strength.

The results of the following tests and calculations are reported: theoretical properties based upon thermodynamic calculations, physical, chemical and ballistic properties, impact and friction sensitivity, aging characteristics and hazard classification.

Einleitung

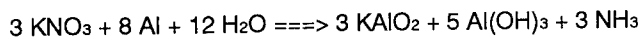
Der Airbag als passives Rückhaltesystem in Kombination mit dem Sicherheitsgurt hat seine Effizienz in zahlreichen Tests und Ernstfallsituationen bewiesen. So gilt heute die Ausstattung eines Fahrzeuges mit Fahrer- und Beifahrerairbag, Gurtstraffer und neuerdings auch Seitenairbags als Standardausrüstung nicht nur für Luxuslimousinen.

Eine pyrotechnische Ladung löst hierbei innerhalb weniger ms in genau abgestimmter Weise die Entzündung des eigentlichen Treibstoffes aus. Wesentlich dafür ist der Energieinhalt, die Kornverteilung und die daraus folgenden ballistischen Kenndaten. Die Anhäufung der pyrotechnischen Sätze in einem Fahrzeug machen natürlich eine genaue Betrachtung der emittierten Schadstoffe (CO, NO_x, Feinstaub etc.) notwendig, deren Grenzwerte immer wieder Diskussionsgrundlagen bieten. So ist es auch für kleinere Baugruppen sinnvoll, den von ihnen verursachten Schadstoffausstoß zu minimieren. Binderhaltige Anzündmischungen (AZM) benötigen zur Ausbildung eines stabilen Granulats einen Harzanteil von ca. 5 %. Aufgrund der starken Sauerstoff-Unterbilanzierung findet sich diese Komponente in Form von Kohlenmonoxid im ausströmenden Gas wieder. Durch die Entwicklung und Fertigung binderfreier Anzündmischungen wurde dieses Problem umgangen. Die dennoch hohe Festigkeit der binderlosen AZM's wird durch die Ausbildung einer stabilen Matrix erzielt, welche nach der wäßrigen Granulation während der Trockenphase durch die Rekristallisation des gelösten Kaliumnitrats entsteht.

Herstellung

Das Herstellungsverfahren für AZM 6 BG 02, AZM 6 BG 03 und AZM 7 ist in den wesentlichen Schritten identisch. Zunächst werden die Rohstoffe, soweit sie nicht schon in der gewünschten Korngröße vorliegen, gemahlen. Nach der Erzeugung einer homogenen trockenen Vormischung erfolgt der eigentliche Granulationsschritt. Hierzu wird in die Granulationseinrichtung eine bestimmte Menge Wasser dosiert, welche einen Teil des in der Vormischung enthaltenen Kaliumnitrats löst. Die Festigkeit des Korns wird durch die Bildung einer stabilen Matrix erhalten, die durch die Rekristallisation des Salzes bei der anschließenden Trocknung entsteht. Auftretendes Überkorn (lockere Agglomerate des Produktes oberhalb der gewünschten Korngröße) wird im Durchreibeverfahren gebrochen und dem Gutkorn zugeführt. Ein Beispiel für die Kornverteilung von AZM 6 BG 02 und AZM 7 findet sich in der Abbildung 1. Die einzelnen Batches werden in einer Homogenisiertrommel zu einem Los vereinigt, automatisch abgefüllt und stehen nach einer umfangreichen Qualitätskontrolle zum Versand bereit.

Die chemische Stabilität während der Feuchtphase ist bei den Bor/Kaliumnitrat-Mischungen kein Problem. Allerdings erfordert die Herstellung der Anzündmischung 7 während der Feuchtphase erhöhte Vorsicht und schnelles Arbeiten. Durch die dabei gleichzeitige Anwesenheit von Aluminium, Kaliumnitrat und Wasser läuft eine Reaktion gemäß nachfolgendem Schema ab:



Durch das amphotere Verhalten von Aluminium löst sich bekanntlich der an der Oberfläche anhaftende Oxidfilm und bietet für Wasser Angriffsmöglichkeiten. Die fortschreitende Alkalisierung der Mischung begünstigt eine autokatalytisch beschleunigte Reaktion, welche unter ungünstigen Umständen zur Selbstentzündung führen kann. Dieses Verhalten kann bis zu einem gewissen Grade durch den Zusatz von Fettadditiven verhindert werden. Selbstverständlich ist auf diesen Umstand auch bei der Verwendung von AZM 7 zu achten. Hierbei ist ein zuverlässiger Schutz vor Feuchtigkeit unabdingbar.

Ballistische Untersuchungen

Zur Beurteilung der ballistischen Eigenschaften der bei der Bayern-Chemie hergestellten Anzündmischungen wird eine standardisierte Prüfbombe verwendet, welche bei einer Einwaage von 0,5 g einen Maximaldruck von 100 - 150 bar erzeugt. Im Rahmen unseres Qualitätssicherungssystems aber auch bei Neuentwicklungen oder Verfahrensüberprüfungen werden routinemäßig Prüfbombenabbrände durchgeführt.

Bei Vergleich der Daten (sh. ballistische Kurven in der Abbildung 2) wird deutlich, daß die AZM 7 nicht nur einen um rund 1000 J/g höheren Energieinhalt besitzt, sondern auch eine deutlich höhere Druckanstiegsrate (dieser Wert ergibt sich aus der Beziehung: $0,8 \times p_{\max} / (0,9 \times p_{\max} - 0,1 \times p_{\max})$), verbunden mit einem um 30 bar höheren Maximaldruck. Dieses Verhalten ergibt sich aus der erhöhten Reaktivität des aluminiumhaltigen Satzes verbunden mit einer erhöhten Gasausbeute in der Brennkammer.

Tabelle 1: Ballistische Kenndaten

		AZM 6 BG 02	AZM 7
Zündverzugszeit	[ms]	1,9	1,8
t _{20 bar}	[ms]	1,94	1,84
t _{50 bar}	[ms]	2,52	2,15
t _{p max}	[ms]	6,36	3,72
p _{max}	[bar]	103	132
Druckanstiegsrate	[bar/ms]	29	91

Eigenschaften von AZM 6 BG 02 / AZM 6 BG 03**ZUSAMMENSETZUNG**

Bor / Kaliumnitrat

THEORETISCHE EIGENSCHAFTEN ($p = 100 \text{ bar}$)

Flammentemperatur	T_c	=	3250 K
Spezifischer Impuls	I_{sp}	=	171 s
Charakteristische Geschwindigkeit	c^*	=	950 m/s

SPEZIFIKATION

Explosionswärme		>	6900 J/g
Schüttgewicht		>	0,83 g/cm ³
Abriebfestigkeit		<	10 %
Korngrößenbereich (0,4 - 1,0 mm)	AZM 6 BG 2	>	95 %
Korngrößenbereich (0,9 - 2,0 mm)	AZM 6 BG 3	>	95 %

GASZUSAMMENSETZUNG (100:1, Massenprozent)

Kaliummetaborat	KBO_2	g	50,8 %
Bormonoxid (dimer)	$(BO)_2$	g	18,9 %
Bormonoxid (monomer)	BO	g	3,1 %
Bortrioxid	B_2O_3	g	3,0 %
Bornitrid	BN	s	16,2 %
Bor	B	l	2,4 %
Kalium	K	g	4,4 %
Stickstoff	N_2	g	1,2 %

Gasausbeute in der Brennkammer:	67,5 %
Gasausbeute in der Düse:	81,4 %

Eigenschaften von AZM 7**ZUSAMMENSETZUNG**

Bor / Kaliumnitrat / Aluminium / Kaliumperchlorat / Mineral. Öl

THEORETISCHE EIGENSCHAFTEN (p = 100 bar)

Flammentemperatur	T_c	=	3150 K
Spezifischer Impuls	I_{sp}	=	180 s
Charakteristische Geschwindigkeit	c^*	=	1010 m/s

SPEZIFIKATION

Explosionswärme	>	7825 J/g
Schüttgewicht	>	0,9 g/cm ³
Abriebfestigkeit	<	15 %
Korngrößenbereich (0,3 - 0,8 mm)	>	95 %

GASZUSAMMENSETZUNG (100:1, Massenprozent)

Kaliummetaborat	KBO_2	g	40,2 %
Bormonoxid (dimer)	$(BO)_2$	g	10,4 %
Bormonoxid (monomer)	BO	g	1,6 %
Bortrioxid	B_2O_3	g	1,5 %
Bornitrid	BN	s	12,5 %
Aluminiummetaboration	$Al(BO_2)^{++}$	g	14,9 %
Kalium	K	g	4,1 %
Kaliumchlorid	KCl	g	4,5 %
Stickstoff	N_2	g	0,5 %
Kohlenmonoxid	CO	g	1,0 %
Rest			9,8 %

Gasausbeute in der Brennkammer: 90,2 %
 Gasausbeute in der Düse: 87,5 %

Thermochemische Untersuchungen

Aus den Ergebnissen der thermochemischen Messungen wird deutlich, daß innerhalb eines normalen Arbeitsbereiches ($< 110\text{ °C}$) mit keinerlei Phasensprüngen, verbunden mit Volumenänderungen zu rechnen ist, welche die mechanische Stabilität des Granulats beeinträchtigen könnte (sh. DSC/TG-Kurven in den Abbildungen 3 und 4). Ferner können die Anzündmischungen aufgrund der hohen Entzündungstemperatur sicher gehandhabt werden.

Tabelle 2: DSC-Messungen

	AZM 6 BG	AZM 7
Probenmenge	0,482 mg	0,544 mg
Aufheizgeschwindigkeit	10 °C / min	10 °C / min
Atmosphäre	N ₂	N ₂
Kristallumwandlung KNO ₃	135 °C	135 °C
Schmelzvorgang KNO ₃	333 °C	333 °C
Zersetzungsbeginn AZM	420 °C	440 °C
Verpuffung AZM	530 °C	580 °C

Alterungsuntersuchungen

Im Rahmen der Qualitätssicherung werden in gewissen Abständen aus der laufenden Produktion Proben zur Überprüfung der Langzeitstabilität gezogen. Als Kriterium wird die Abnahme der Explosionswärme herangezogen. Dazu wird eine definierte Menge von AZM in ein lose verschlossenes (d. h. ohne Sicherung) Reagenzglas mit Schliffstopfen über einen Zeitraum von 168 h mit 110 °C belastet. Dieses Modell simuliert eine Einsatzdauer von ca. 10 Jahren. Während dieses Vorganges nimmt die Anzündmischung geringfügig an Masse zu. Dies erklärt sich durch die Bildung von Stickstoffdioxid (NO₂), welches sich mit einem Teil des Bors zu Bortrioxid und Stickstoffoxid (NO) umsetzt. Das freigesetzte Stickstoffoxid wird durch den im Reagenzglas befindlichen Sauerstoff wieder zu NO₂ und nimmt solange an der Reaktion teil, bis der Sauerstoff vollständig verbraucht ist.

AZM 7 besitzt unmittelbar nach der Produktion eine Explosionswärme von durchschnittlich 8000 J/g, welche sich nach durchlaufen der oben genannten Prozedur um 3,4 % auf 7725 J/g verringert. Dieser Wert liegt lediglich 1 % unterhalb der Spezifikationsgrenze (bezogen auf die unbelastete Substanz). In der Praxis ist kein Fall bekannt, der aufgrund dieser Tatsache eine Fehlfunktion aufgewiesen hätte.

Analoge Untersuchungen für die AZM 6 BG ergaben einen Abbau der Explosionswärme um 2,5 % von 7280 J/g auf 7100 J/g. Dieser Wert liegt deutlich oberhalb der Spezifikationsgrenze. Bekanntermaßen erleidet eine B/KNO₃-Mischung mit 91proz.

Bor durch den produktionsbedingten hohen Magnesiumanteil im Laufe der Zeit eine starke Degradation. Das hohe Reduktionsvermögen von Magnesium führt zu einem Abbau von Kaliumnitrat mit simultaner Oxidation von Bor zu Bortrioxid. Bayern-Chemie verwendet deshalb für ihre Anzündmischungen ausschließlich 97proz. Bor, wo diese Problematik nicht auftaucht. Der Magnesiumanteil wird hier von Seiten des Herstellers durch einen zusätzlichen Waschschriff mit Flußsäure (HF) auf einen geringen Anteil gedrückt.

Amorphes Bor besitzt durch seine hohe Oberfläche eine gewisse Affinität zu Sauerstoff. Die sachgerechte Lagerung und Verwendung der Anzündmischungen bedingt demzufolge eine von ständiger Luftzufuhr und Feuchtigkeit geschützte Umgebung (geschlossener Behälter, Anzündeinheit, geschlossener Gasgenerator).

Klassifizierung

Die Durchführung der Sicherheits-Tests erfolgte mit dem Fallhammer nach BAM (gem. TL 1376 -950 Blatt 16) bzw. dem Reibapparat nach BAM (gem. TL 1376-950 Blatt 15)

Die Entzündungstemperatur wurde mittels thermochemischer Methoden (TG, DSC) (Heizrate: 10 °C/min in N₂-Atmosphäre gemessen) untersucht.

Tabelle 3: Sicherheitsdaten

	AZM 6 BG	AZM 7
Schlagempfindlichkeit	0,75 kpm	0,5 kpm
Reibempfindlichkeit	> 36 kg	> 24 kg
Entzündungstemperatur	> 500 °C	> 500 °C
Sicherheitseinstufung: 1.1 G		

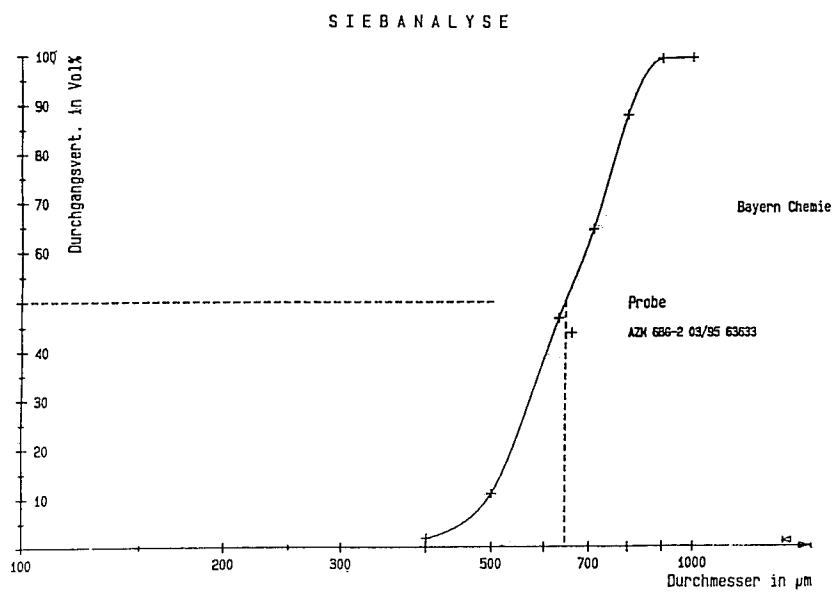
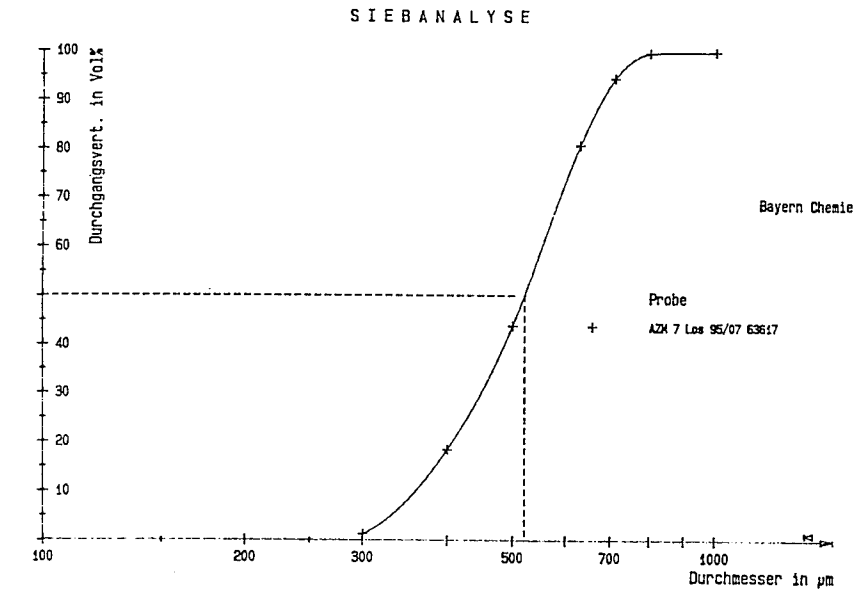
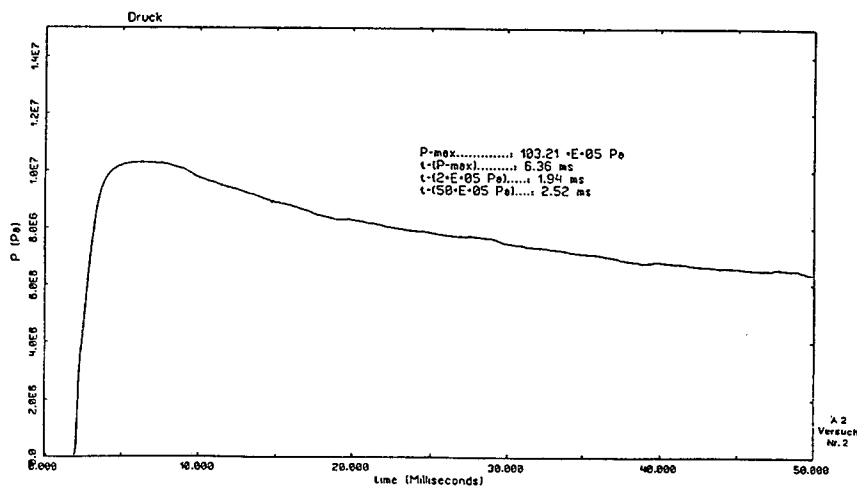


Abbildung 1: Kornverteilung von AZM 6 BG 02 und AZM 7

AZM 6BG 20510 20 GrdC *BAYERN-CHEMIE*
 Pruefbombe 31-Jan-94 Gesellschaft fuer Flugchemische Antriebe mbH

Bomben-Nr. 521-781W848 AZM-Masse 0.5 Los 14/93



AZM 7 20494 20 GrdC *BAYERN-CHEMIE*
 Pruefbombe 31-Jan-94 Gesellschaft fuer Flugchemische Antriebe mbH

Bomben-Nr. 521-781W848 AZM-Masse 0.5 Los 92/33

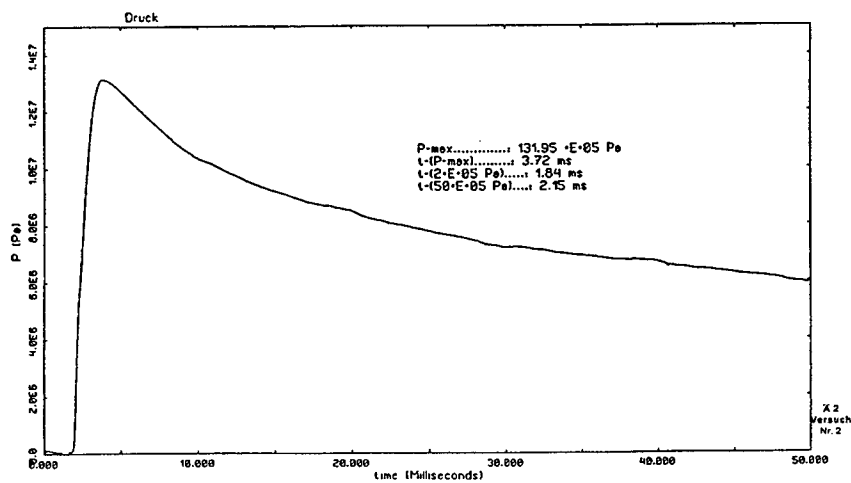


Abbildung 2: Ballistische Kurven

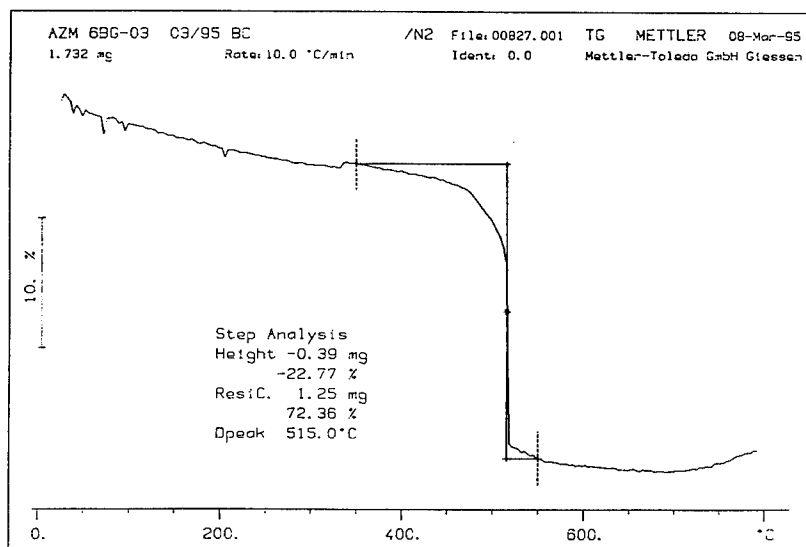
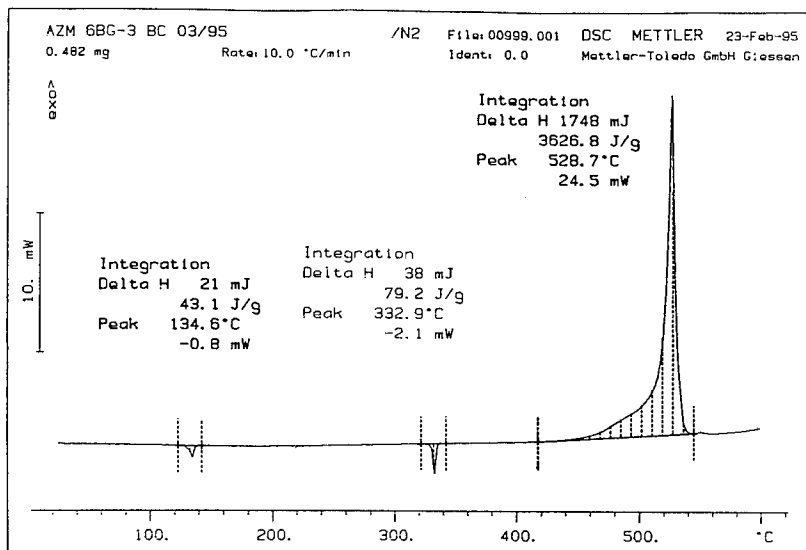


Abbildung 3: DSC- und TGA-Messungen von AZM 6 BG

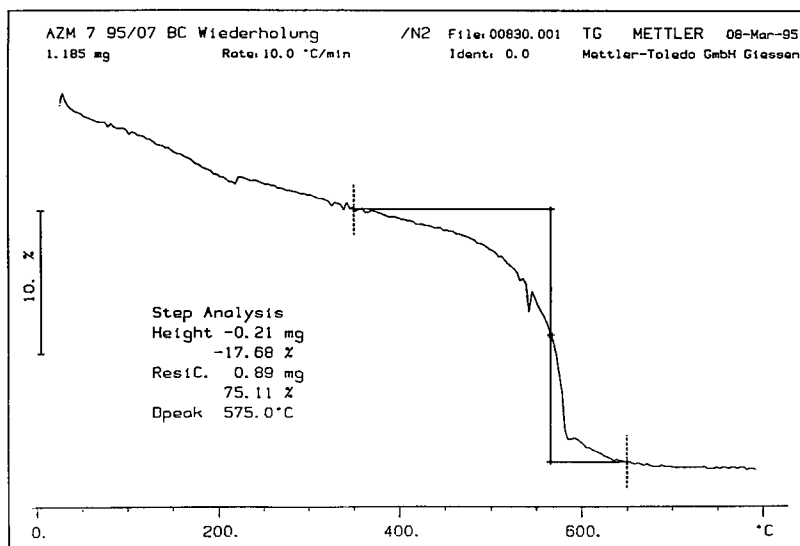
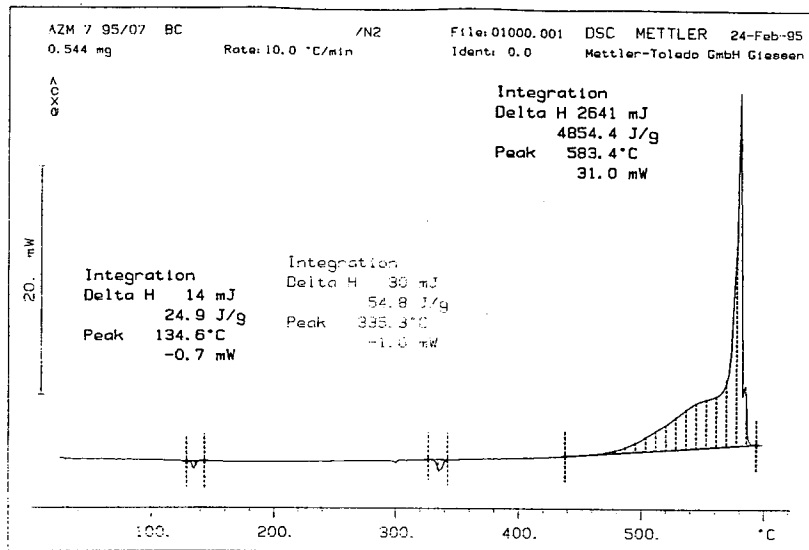


Abbildung 4: DSC- und TGA-Messungen von AZM 7

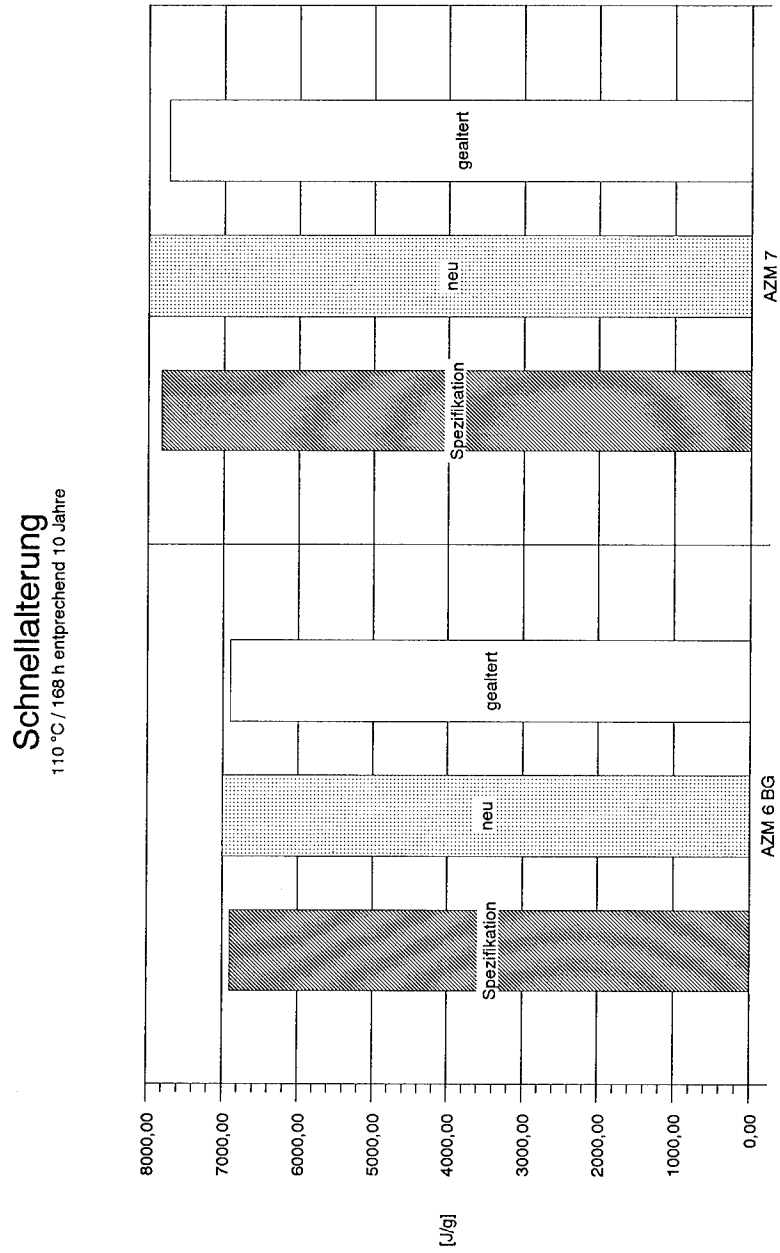


Abbildung 5: Schnellalterung von Anzündmischungen

THE ROLE OF BISMUTH CHROMATE IN THE IGNITION REACTION
OF MOLYBDENUM AND POTASSIUM PERCHLORATE MIXTURES

*

R.G.Sarawadekar, R.Daniel & S.Jayaraman

High Energy Materials Research Laboratory (HEMRL)

Sutarwadi, Pune. 411 021. INDIA

ABSTRACT

Mixtures of Mo - KClO_4 show exothermic ignition reactions, while mixtures of molybdenum and bismuth chromate do not show ignition reactions. Mixtures in which the KClO_4 content is less at about 10% show very good propagation properties when bismuth chromate is included even upto an extent of 70%.

Inclusion of bismuth chromate to a mixture of molybdenum and potassium perchlorate reduces the violent nature of the mix and decreases the burning rate. Bismuth chromate reduces the decomposition temperature of KClO_4 as shown by DSC experiments. Though the heat output of mixes of Mo - KClO_4 - bismuth chromate is just about half that of Mo - KClO_4 (40 /60) these show good propagation characteristics in lead tubes, whereas Mo - KClO_4 does not in open systems because of the formation of MoO_3 (sublimes). KCl , MoO_3 , Bi_2O_3 and Cr_2O_3 have been identified in the products of combustion.

-oo0oo-

* To whom all correspondence should be addressed.

1. INTRODUCTION :-

Delay compositions with molybdenum powder as fuel and a few oxidants have been reported. Mo - BaO₂ mixtures gave burning rates in the range of 3.3 cm/ s (1). C.H. Miller plotted the burning rate against fuel content for mixtures of Mo - PbCrO₄ and reported a parabolic curve (2). A model for solid -solid propagation reaction rates of Mo - KClO₄ system is described by Bernard M.L. et.al. (3). A more detailed account of Mo - KClO₄ system is given by Riffault (4). HSU Ywonkeng has studied the burning rates of mixes containing Mo -KClO₄ and the effect of additives on their burning rates (5). Barium chromate decreases the burning rate of the composition. Thermal studies on Mo - KClO₄ -BaCrO₄ delay has been reported (6). It has been reported that higher percentage of KClO₄ leads to production of KCl which retards the reaction.

In the present work, the effect of bismuth chromate on Mo -KClO₄ system has been studied. Thermal analysis has been carried out and reaction products have been analysed by X-ray diffraction and infrared spectroscopy.

2. EXPERIMENTAL :

2.1 Materials :

Electrolytic grade molybdenum metal powder with an average particle size 2.6 micron was used. Bismuth chromate of purity 99% and 3.4 micron particle size was used. Potassium perchlorate having particle size between 106 and 125 micron was

used. The mixtures with varying percentages of molybdenum and bismuth chromate and 10% KClO_4 were granulated using 2% NC.

2.2 Methods :

The mixes were filled in lead tubes and the tubes were drawn through successive dies. Burning rates were determined. Ignition DTA were carried out on locally fabricated apparatus, using 25 mg sample mass in platinum cups and a heating rate of $10^\circ\text{C}/\text{min}$ in static air.

TG:DSC studies were performed using STA-409 EP thermal analyser of NETZCSH in static air with 25 mg sample mass in alumina cups and heating rate $10^\circ\text{C}/\text{min}$. The reaction exothermicities were measured in argon atmosphere in a Parr adiabatic calorimeter. X-ray diffraction patterns of combustion residue of various compositions were recorded on Phillips X-ray diffractometer model No.1730/90 using CuK radiations at room temperature. Infra red spectra of slags were recorded on Perkin-Elmer IR spectrophotometer model No.457 in nujol mull at room temperature.

The sensitivity to impact was measured on a fall hammer apparatus using 2 kg drop weight and a sample size of 20mg. The sensitivity towards friction was determined using Julius Peter friction sensitivity apparatus.

3. RESULTS AND DISCUSSIONS :

3.1 Calorimetric data

The calorimetric value of the mix $\text{Mo} - \text{KClO}_4$ (40 / 60) was determined in argon at 5 atm. and found to be 604 cal / g .

The calorimetric values of the mixes Mo - KClO_4 - $\text{Bi}_2\text{Cr}_2\text{O}_9 \cdot \text{H}_2\text{O}$ containing 10% KClO_4 , Mo between 20-40% and bismuth chromate 50-70% were determined in argon. These values are shown in Table 1. A comparison of the heat output reveals that the heat output of the compositions containing bismuth chromate are much less compared to that of the mixture containing only Mo and KClO_4 . The heat of reaction increases with increase in Mo content upto about 45% Mo.

3.2 Burning Rate :

Bernard et.al. have mentioned that mixes containing less than 40% Mo do not ignite whereas HSU Ywenkeng has reported the ignition of mixes containing 33% Mo also. We also tested Mo- KClO_4 mixes in lead tubes with 2mm diameter of the pressed column and found that the column does not propagate at 40% Mo level. When bismuth chromate is added to the mixes containing Mo and KClO_4 , it is found that the compositions containing as little as 20% Mo propagate burning satisfactorily. The proportion of KClO_4 was maintained constant at 10%. These compositions show good burning characteristics. The burning rates are given in Table-1. The mixture containing 15% Mo does not burn, whereas in the rest of mixtures it is seen that burning rate increases with increase in molybdenum content.

It was very surprising to note that the composition Mo - KClO_4 on ignition gives a heat output twice that of Mo - KClO - bismuth chromate but does not show propagation of burning in the

lead tube. On the other hand , the mix Mo - KClO_4 (40/60) was tested in a closed system and it was found to propagate smoothly with a burning rate of 3.7 s/cm when loaded with a pressure of 3750 Kg/cm². To investigate the matter further, the temperature of the burning layer was measured with the R type thermocouple. It was found that the temperature of the reaction front was 540° C for the mix Mo - KClO_4 (40/60) and 370° C for the mix Mo - KClO_4 - Bismuth Chromate (40/10/50). This confirms that in an open system the products of the combustion of Mo - KClO_4 being volatile escape from the reaction front carrying the heat away thus causing failure in propagation. In the case of Mo - KClO_4 - $\text{Bi}_2\text{Cr}_2\text{O}_9 \cdot \text{H}_2\text{O}$ the temperature is low and so the heat does not escape from the system.

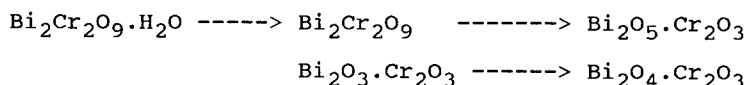
3.3 THERMAL ANALYSIS

The DTA curve of Mo metal powder shows a broad exotherm beginning at 420 ° C and ending at 600 °C, which is due to air oxidation of Mo. X - ray diffraction shows the formation of only MoO_3 which crystallizes in the rhombic form. It belongs to Pb_{nm} (6_2) group where $Z=4$ and $d=4.710$ (7). TG data shows 39.4% increase in weight as against the theoretical value 50% for MoO_3 . This lower increase in weight may probably due to the loss of MoO_3 by sublimation, which occurs simultaneously.

TG-DSC of KClO_4 was carried out in air. DSC curve shows two endotherms and one exotherm. The first endotherm at 309.4°C is due to crystalline transition. The second endotherm is observed at 584.8°C for fusion. The exothermic peak is observed at 600.9°C

corresponds to the decomposition of KClO_4 with evaluation of heat (8).

DSC data of bismuth chromate shows four endotherms. between (i) 229.7 to 303.3°C (ii) 488 to 533.2°C (iii) 818.8 to 847.5°C and (iv) 915.8 to 941.9°C. The possible reaction mechanism is given below, which was described in an earlier paper (9).



DSC of Mo-KClO_4 (40/60) shows one endotherm at 308°C corresponding to the crystalline transition of KClO_4 and one exotherm at 450°C corresponding to oxidation of molybdenum. It gives a sharp peak in the range 448.9 to 462.8°C with evolution of heat. It is observed that KClO_4 decomposes at 448.9°C and air oxidation of Mo also takes place in the same range. Fig.1 shows that the reaction between Mo-KClO_4 is violent.

DSC curve for the composition containing molybdenum and bismuth chromate (20/80) in air is given in Fig 1. It shows main exotherm in the range 542.6 to 659.9°C with peak temperature at 620.2°C.

To understand the role of bismuth chromate, compositions were prepared containing bismuth chromate and potassium perchlorate with varying proportions such as 1:1 to 1:7. DSC curves show that there is a reduction in the decomposition temperature of KClO_4 as shown in Fig.2. The mixture containing 1:1 ratio begins to melt at 420°C with simultaneous decomposition as shown by weight loss, with peak temperature at 501.6°C. When the proportion of bismuth chromate is increased,

the main exotherm of decomposition of KClO_4 vanishes and only one endotherm appears at 453.5°C . As bismuth chromate content increases, exotherm peak height also decreases, clearly showing that bismuth chromate absorbs all the heat evolved during the decomposition of KClO_4 . At this temperature range bismuth chromate also decomposes. Thus it can be seen that addition of bismuth chromate brings down the decomposition temperature of KClO_4 , but reduces the exotherm. This explains the satisfactory propagation of burning of the composition containing low percentages of Mo, but high percentage of bismuth chromate. DSC curves under non-ignition condition of the mixtures containing $\text{Mo-KClO}_4\text{-Bi}_2\text{Cr}_2\text{O}_9$ indicate an exothermic peak near about 446°C . This can be attributed to the reaction between Mo-KClO_4 . This peak is sharp for compositions containing less than 30% Mo. The rate of reaction is slow for compositions containing more than 30% Mo which show two more exotherms. Second exothermic peak is broad at about 520°C and third exotherm is sharp at $630\pm 3^\circ\text{C}$.

3.4 IGNITION DTA

DTA of $\text{Mo-KClO}_4\text{-Bi}_2\text{Cr}_2\text{O}_9\cdot\text{H}_2\text{O}$ containing 15-40 % Mo were carried out under ignition conditions in air. In all cases a single sharp exotherm is observed in the range of 452 to 468°C . The temperature of ignition of these mixes does not show any significant variation due to change in Mo content. The ignition occurs at around the same temperatures as the air oxidation of Mo. The values of ignition temperatures are given in Table -2.

3.5 REACTION PRODUCTS

The reaction products were analysed by X-ray diffraction technique. It is observed that generally MoO_3 is formed. In addition, the formation of Bi_2O_3 , Cr_2O_3 and higher oxides of Mo is also indicated (7). X-ray diffraction patterns are shown in Fig - 3, which were analysed by comparing with standard patterns of each compound from X-ray diffraction Philip computerised data library. It is noticed that the oxides of molybdenum react with Bi_2O_3 and form molybdenum bismuthates.

The infra red spectra of the slags shows absorption peaks at 625 and 560 cm^{-1} for Cr_2O_3 , 842, and 540 cm^{-1} for MoO_3 and Bi_2O_3 shows peaks at 640 and 515 cm^{-1} . These are comparable with literature values. (10)

3.6 IMPACT AND FRICTION SENSITIVITY :

It is observed that in all the compositions initiation by impact was only 20-50 % at an impact energy of 62 J/cm^2 . All compositions studied here are insensitive to friction upto 36 kg. load in the Julius Peters apparatus.

4 CONCLUSIONS :

Mixtures of Mo - KClO_4 show exothermic ignition reactions, while mixtures of molybdenum and bismuth chromate do not show ignition reactions. Mixtures in which the KClO_4 content is less at about 10% show very good propagation properties when bismuth chromate is included even upto an extent of 70%.

Molybdenum-potassium perchlorate-bismuth chromate mixes in proper proportions present a good delay system. These

compositions (20 - 40 % Mo) show ignition in DTA experiments even though their heat output is less. Bismuth chromate decreases the decomposition temperature of potassium perchlorate and absorbs the heat liberated in the process due to endothermic decomposition reactions.

DTA experiments under ignition conditions indicate that the ignition temperatures are of the same order for compositions containing either molybdenum-potassium perchlorate or molybdenum-potassium perchlorate-bismuth chromate. The heat output of Mo-KClO₄ (40/60) is almost double that of mixes containing bismuth chromate. But the former does not burn satisfactorily in open system whereas the latter shows good propagation characteristics. This is because in the case of Mo-KClO₄, the reaction temperature is high and the product MoO₃ which is volatile at the flame temperature and must be carrying the heat away from the reaction zone, whereas in the case of compositions containing bismuth chromate the flame temperature is low, and therefore MoO₃ does not volatilise and the products of combustion form hot slag, which transfers the heat effectively to the unburnt composition resulting in satisfactory propagation. This was confirmed by testing the Mo - KClO₄ in a closed system where it showed fast burning characteristics.

ACKNOWLEDGEMENT

We thank the Director, HEMRL Pune for permission to publish this work.

REFERENCES

1. Ganlay, Robert and July, Gerard, Patent, French, 1, 587,420 (1968)
2. C.H.Miller, Third Symp. on chemical problems connected with the stability of explosives at Ystad., 1973 PP 285.
3. Bernard, M.L.,Espagnacq, A.L. and Branka, R., Proc.Int. Pyrotech. Semin., 1980, 7th (2) PP. 826-45.
4. Riffault, M.L.;Third Symp. of Chemical Problems connected with the stability of explosives at Ystad, 1973 PP 302.
5. HSU Ywonkeng, Proc.7th Int. Pyrotech. Semi. 1980, PP 771-784.
6. A.G. Rajendran, C. Ramchandran and V.V. Babu, Propellants, Explosives, Pyrotechnics, 14, 113 - 117 (1989).
7. JCPOS " X - ray powder diffraction file, " (1967).
8. R.G. Sarawadekar and N.S. Bankar, in Proc. of the 8th Int. Pyrotech, Semin., Colorado, USA (1982) pp 574 - 87.
9. R.G.Sarawadekar and S.Jayaraman, Defence Science Journal, Vol.42, No.3, July 1992 PP 177-181.
10. N.T. McDevit and W.L. Daun, Spectrochim. Acta., 20, 799 (1964).

TABLE 1 : BURNING RATE AND CALORIMETRIC DATA

COMPOSITION Mo + KClO ₄ + B.C.	BURNING RATE cm/s	CAL VAL Cal/g (Argon)
20 - 10 - 70	0.21	253
25 - 10 - 65	0.33	271
30 - 10 - 60	0.40	289
35 - 10 - 55	0.44	304
40 - 10 - 50	0.56	315
45 - 10 - 45	0.41	330
50 - 10 - 40	0.44	313
60 - 10 - 30	0.44	290

TABLE: 2 : THERMOANALYTICAL DATA

Composition %	IGNITION Temp °C	NON IGNITION EXO °C	DTA/ TG % Wt.loss
Mo+KP+BC			
15/10/75	452	448	27.8
20/10/70	465	446	22.2
25/10/65	468	446	--
30/10/60	457	444	15.2
35/10/55	462	445	13.7
40/10/50	459	446	16.7

KP = KClO₄
 BC = Bi₂Cr₂O₉·H₂O

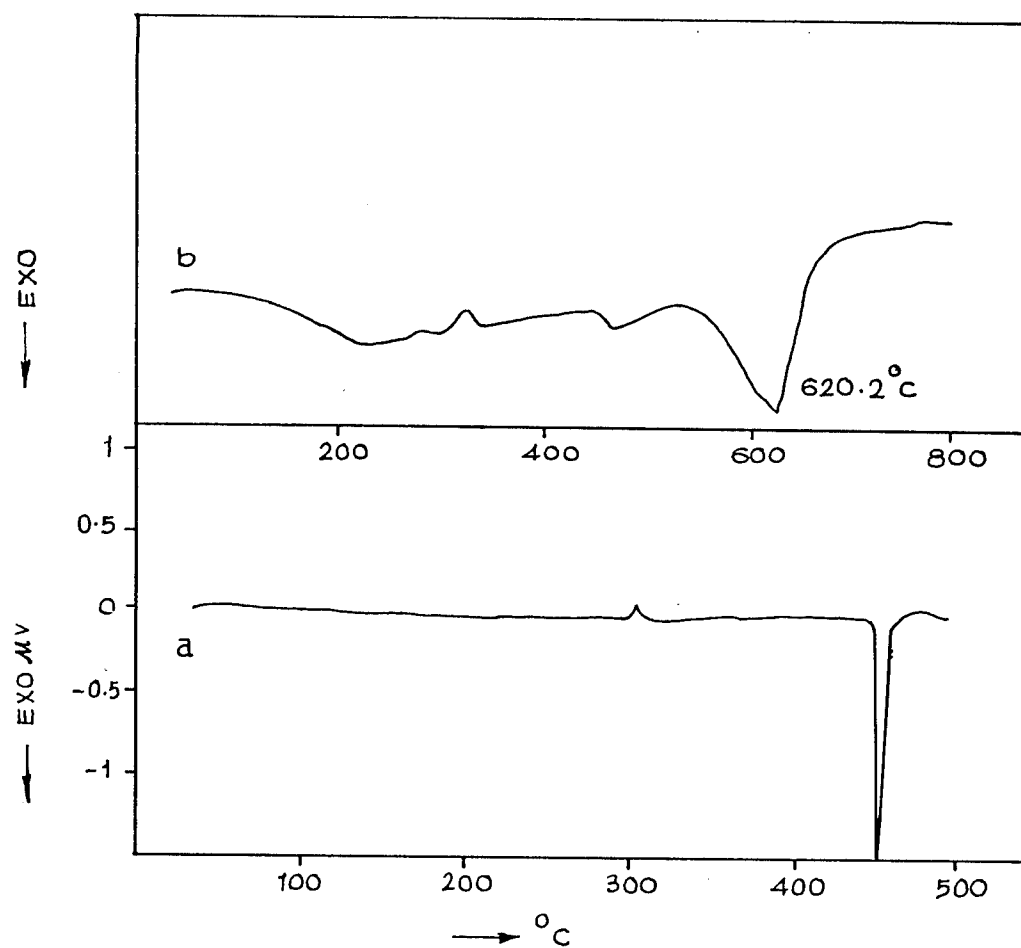


FIG.1 - a) DSC CURVE FOR Mo·KClO₄ (40/60)

b) DSC CURVE FOR Mo·Bi₂Cr₂O₉ (20/80)

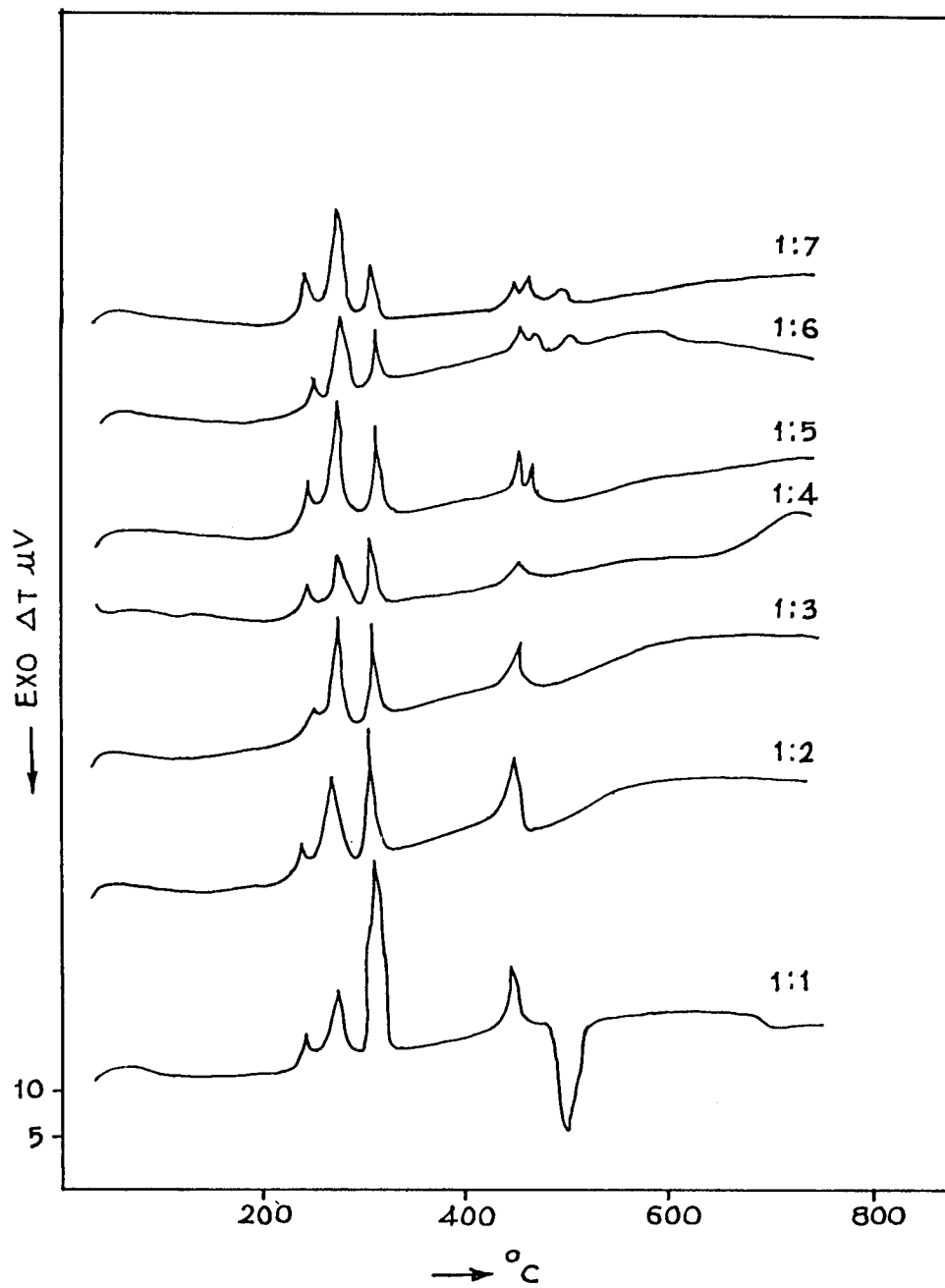


FIG.2 - DSC CURVES OF $\text{KClO}_4\text{-Bi}_2\text{Cr}_2\text{O}_9$
AT DIFFERENT RATIOS (W/W)

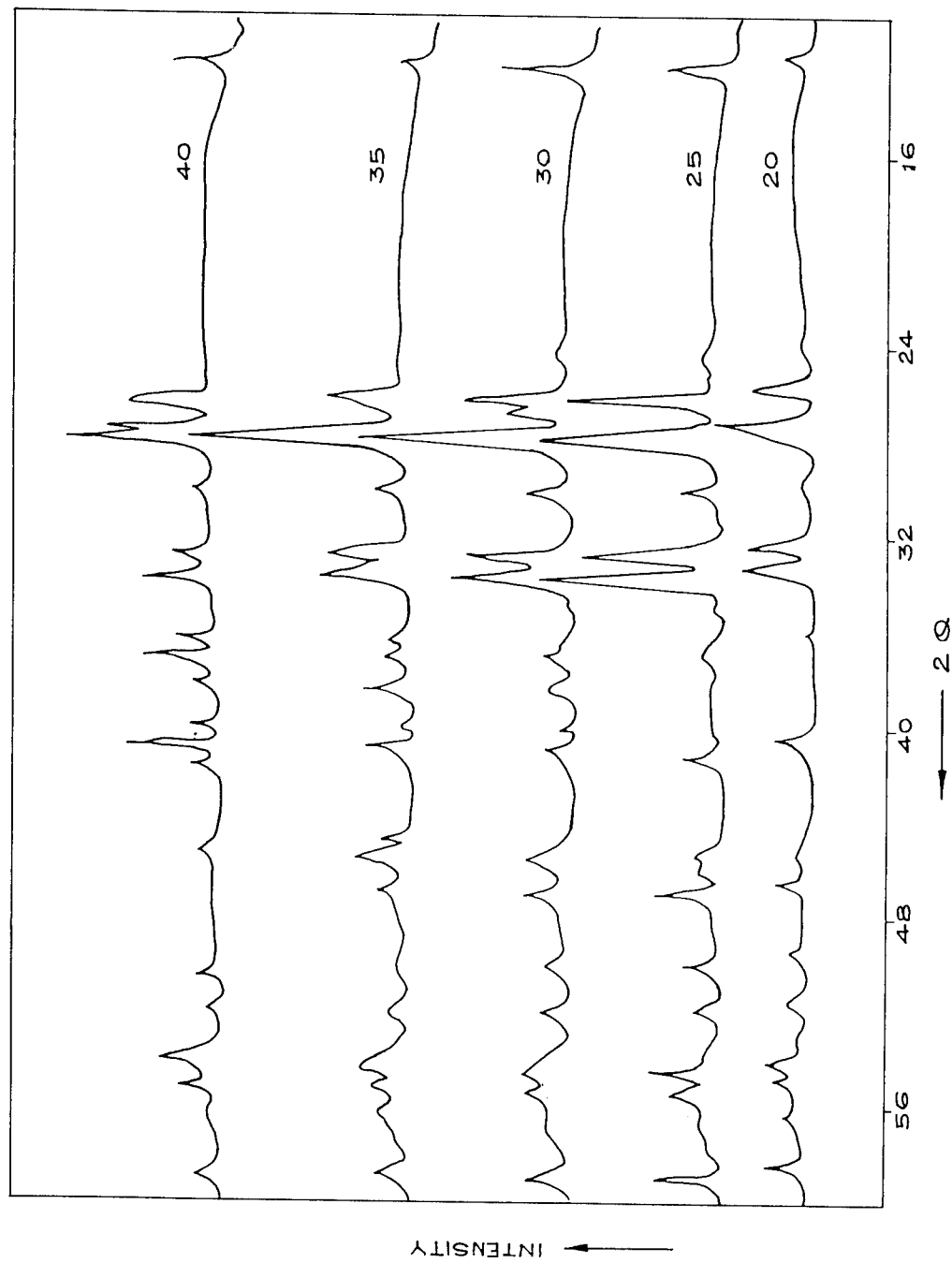


FIG:3.XRD PATTERNS OF SLAGS CONTAINING MO

INFLUENCE OF ALUMINIUM ON COMBUSTION OF MAGNESIUM-SODIUM NITRATE PYROTECHNIC MIXTURE

Harihar Singh and R.Bhaskara Rao
Explosives Research & Development Laboratory (Cell),
Kanchanbagh, Hyderabad-500258 (INDIA)

ABSTRACT

Burning rate and energetics of Mg-NaNO_3 and Al-NaNO_3 pyrotechnic mixtures have been studied to elucidate their combustion mechanism and to understand the influence of addition of Al particles on the combustion of Mg-NaNO_3 gas generating systems at different oxidiser levels. Results indicate that the burning rate of Mg-NaNO_3 system is higher at fuel-rich ratio due to high condensed phase heat release and decreases with increasing oxidiser content and shows a minimum value at stoichiometric ratio due to the formation of metal agglomerates at the burning surface. On the other hand the burning rate of Al-NaNO_3 composition is lower at fuel-rich ratio due to the presence of high degree of metal agglomeration and increases with the increase of oxidiser content and has a maximum value at stoichiometric ratio due to release of high heat energy in the vapour phase combustion.

The burning rate of Mg-NaNO_3 at fuel-rich ratio on addition of Al particles upto 10%, further increases due to enhanced exothermic reactions at the burning surface resulting in the increase of surface heat energy, while at higher contents of Al particles the burning rate decreases due to the accumulation of Al particles and formation of agglomerates at the burning surface with its increased concentration and shifts the reactions to the vapour phase away from the surface. At stoichiometric ratio of Mg-NaNO_3 addition of Al particles further reduces the burning rate alongwith energy content due to enhanced metal agglomeration.

It was also found out that the addition of Al-Mg alloy particles to Mg-NaNO_3 composition decreases the burning rate alongwith the energy content at all mixture ratios due to the higher stability of the alloy particles for the reactions in comparison to its component elements and also due to the lower melting temperature of the alloy particles below the decomposition range of NaNO_3 leading to high degree of metal agglomeration. The burning surface temperature data also support the suggested mechanism.

INTRODUCTION

Study of metal based pyrotechnics has shown a great interest in the recent past as gas generators for advanced air-breathing propulsion systems due to their high density and high heat potential⁽¹⁻³⁾. Among the various pyrotechnic formulations, Mg-NaNO₃ mixture is known to be efficient as a gas generator because of its high combustion efficiency and wide spectrum of burning rate. Since the performance realisation of a composition depends on its kinetic and energetic parameters, the performance augmentation studies for use as gas generator have been carried out using aluminium powder as an additive which is a known energetic material commonly being used in pyrotechnics and propellants.

In the present study, the burning rate and energetics of Mg-NaNO₃ and Al-NaNO₃ compositions have been studied in order to understand the influence of Al particles in free form as well as in the form of alloy particles with Mg, on the combustion of Mg-NaNO₃ formulations. Attempts have also been made to develop a suitable combustion mechanism.

EXPERIMENTAL

Compositions containing Mg/NaNO₃, Al/NaNO₃, Mg/Al/NaNO₃ and Mg/Al-Mg(1:1)alloy/NaNO₃ at different fuel/oxidiser ratios were formulated. Pellets of 100 mm diameter and 50 mm length were pressure moulded to a density of 1.6 g/cc and inhibited with epoxy resin for the measurement of burning rate and surface temperature. Burning rate of the compositions was determined by static firing. The pellet was loaded in a test motor of 110 mm diameter and ignited electrically with an igniter composition Mg-KNO₃-EC. The burning rate was determined from the pressure-time profile.

Heat of combustion values of the samples were determined with a Julius Peters adiabatic bomb calorimeter of 300 cc volume. Samples corresponding to 0.01 g/cc loading density was ignited in an argon atmosphere. Burning surface temperature of the samples were measured during the static firing with micro-thermocouples embedded within the pellet. Micro-thermocouples made of platinum and platinum-rhodium 10% of 50 μ diameter was used.

Thermal decomposition of the samples was carried out with STA 409 Netzsch Gerätebau Gm bH differential thermal analyser (DTA). Experiments were conducted using 5 mg sample with a heating rate of 10°C/min in an argon atmosphere.

RESULTS AND DISCUSSION

Burning rate of the compositions at different weight percent of NaNO_3 is shown in Figure 1 and energy content shown in Figure 2. It can be observed that the burning rate of Mg-NaNO_3 increases with increasing oxidiser content, shows a maximum at 30% NaNO_3 and reaches a low value at stoichiometric point (ie 58% NaNO_3) in contrast to the energy content. On the otherhand the burning rate of Al-NaNO_3 increases continuously with increasing NaNO_3 alongwith the energy content and shows a maximum at stoichiometric point (ie 65% NaNO_3). Further the burning rate as well as energy content of Mg-NaNO_3 are higher at fuel rich ratio than Al-NaNO_3 and are lower at stoichiometric ratio.

Addition of Al particles upto 10% in Mg-NaNO_3 further increases the burning rate significantly by about 20% at fuel-rich ratio with an increase in the energy content. On further addition of Al particles beyond 10%, the burning rate decreases though the energy content increases upto 50% of Al content. On the other hand at stoichiometric ratio of the composition, the addition of Al particles decreases the burning rate alongwith energy content at all Al concentrations.

To obtain the information on the heat flux at the burning surface, the burning surface temperature was determined. The results indicate (Figure 3) that with all the compositions the surface temperature is higher at stoichiometric ratio than at fuel rich ratio. Also the surface temperature is lower for Mg-NaNO_3 and it increases on addition of Al particles and shows higher value with Al-NaNO_3 (785°C at fuel-rich ratio and 1100°C at stoichiometric ratio).

Thermal decomposition studies of Mg-NaNO_3 (Figure 4) indicate two exotherms. The first exotherm appears at 460°C and the second exotherm at 465°C with fuel rich composition with a higher heat release and at 523°C with stoichiometric composition with a lower heat release. At different concentrations of Al in Mg-NaNO_3 at fuel rich ratio, though the decomposition starts at 460°C, the heat release in the exotherms varies with a delay in the ignition temperature. Thermal decomposition of Al-NaNO_3 occurs at 695°C

with a lower heat release at fuel rich ratio and at 723°C with a higher heat release at stoichiometric ratio after a melting transition at 660°C due to Al particles. These results indicate that the decomposition of Mg-NaNO₃ occurs before the Mg particles reaches melting temperature (660°C) whereas the decomposition of Al-NaNO₃ occurs after the Al particles attain the melting temperature at the burning surface. Also the presence of Al particles in Mg-NaNO₃ shifts the decomposition range to a higher temperature.

Based on the above observations attempt was made to explain the mechanism of combustion of the compositions. It is suggested⁴ that the decomposition of NaNO₃ starts at 460°C from nitrate to nitrite with the release of atomic oxygen. This oxygen atom reacts with Mg for the exothermic heat release in the condensed phase and facilitates total ignition of the sample. The exotherm at 460°C with Mg-NaNO₃ before the Mg particles reach the ignition temperature (528°C) indicates the release of high condensed phase heat⁵ leading to high burning rate at fuel rich ratio of the composition.

An increase in concentration of NaNO₃ increases inert heating of the metal particles due to the presence of molten layer of NaNO₃ resulting to thicker oxide coating of the metal particles. This reduces the heat release in the condensed phase and leads to delay in the ignition. This results in the formation of metal agglomerates which eject into the flame zone burn inefficiently and cause low burning rate. Diffusion of agglomerates take place to the flame zone only after the particles attain a sufficient temperature on the burning surface. This may cause rise in burning surface temperature (Figure 3) when the composition approaches stoichiometric value.

Decomposition of Al-NaNO₃ composition (Figure 4) occurs at 695°C with a lower heat release at fuel rich ratio and at 723°C with a higher heat release at stoichiometric ratio after the transition due to melting of Al particles at 660°C. The higher temperature decomposition compared to Mg-NaNO₃ composition is due to the formation of protective oxide layer exists around Al particles preventing the surface oxidation at lower temperature. Hence the molten Al droplets at the burning surface coalesce into large slow burning agglomerates and diffuse out to the vapour phase after attaining sufficient temperature. The combustion in the vapour phase conducts heat to the burning surface for further regression of the composition. This explains the high burning surface temperature and also the increase of burning rate when the composition approaches from fuel rich to stoichiometric value due to the vapour phase combustion.

The addition of Al particles in Mg- NaNO_3 composition at fuel rich ratio, thermal decomposition also starts at 460°C for the condensed phase heat release. Further, the additional heat release in the exotherm at low concentration of Al is expected due to the oxidation of Al particles and the reduction of Al_2O_3 in presence of excess of Mg. Hence the additional heat release in presence of Al particles upto 10% increases the surface heat potential and causes an increase in the burning rate.

At higher concentration of Al particles in Mg- NaNO_3 , the particles are expected to accumulate at the burning surface and form metal agglomerates as the reaction of Al in presence of NaNO_3 occurs after the melting of Al particles at the burning surface. Hence the agglomerates which increases with increasing concentration of Al and when ejected into the flame zone burn inefficiently and cause low burning rate. The reduced exothermicity in the DTA with delay in ignition indicates the vapour phase combustion of the particles away from the burning surface. The increase in burning surface temperature with increasing Al content in Mg- NaNO_3 also supports the particle agglomeration at the burning surface.

The addition of Al particles at stoichiometric ratio of Mg- NaNO_3 further reduces the heat release in the DTA (Figure 4) with longer ignition delay and without any condensed phase heat release. As the combustion of Mg- NaNO_3 composition at this ratio provide low burning rate due to metal particle agglomeration followed by inefficient burning in the vapour phase, the presence of Al particles are expected to enhance the metal agglomeration and further reduce the burning rate of the composition.

Further it is also found out that the addition of Al-Mg (1:1) alloy particles in Mg- NaNO_3 composition lowers the burning rate and energy content at all mixture ratios of the composition and at all concentrations of the alloy particles (Figure 1 and 2). DTA data of Mg- NaNO_3 in presence of alloy particles indicate (Figure 4) an endothermic transition at 442°C due to the melting of alloy particles and an exothermic decomposition at 535°C with a lower heat release with fuel rich composition and at 565°C with a higher heat release with stoichiometric composition.

The melting of alloy particles of the composition earlier to the decomposition range of NaNO_3 ($460\text{--}720^\circ\text{C}$) indicate that the Mg particles at the burning surface of the composition are enveloped by the stable molten alloy layer and hence are difficult to undergo oxidation at the surface thus form high degree of metal agglomerates. These

agglomerates when ejected into the flame zone burn inefficiently and provide low heat release and conduct lower heat to the burning surface and causes reduced burning rate. The higher burning surface temperature recorded on addition of alloy particles due to the formation of high degree of metal agglomerates at the surface supports the phenomena. The lower heat of combustion of the Mg-NaNO₃ composition on addition of alloy particles is probably due to their higher stability of alloy particles in comparison to its component elements.

CONCLUSIONS

Burning rate of Mg-NaNO₃ pyrotechnic composition is higher at fuel-rich ratio as the metal particles react exothermically in the condensed phase before the particles acquire sufficient energy for ignition and release high condensed phase heat. Increase of oxidiser content reduces the heat release in the condensed phase due to oxide coating of metal particles in presence of higher concentration of molten oxidiser leading to low burning rate.

Burning rate of Al-NaNO₃ composition is low at fuel-rich ratio and increases with increasing oxidiser content as the metal particles react in the vapour phase after melting at the burning surface without any condensed phase reactions. This leads to particle agglomeration and the ejection of the agglomerates to the vapour phase causing increase of burning rate with increasing oxidiser content.

Addition of Al particles upto 10% in Mg-NaNO₃ composition augment the burning rate at fuel-rich ratio due to the additional exothermic reactions occurring just above the burning surface while at higher contents of Al particles the burning rate decreases due to the particle accumulation of Al with its increased concentration and formation of agglomerates at the burning surface and shifts the reactions to the vapour phase away from the surface. At stoichiometric ratio of Mg-NaNO₃ the addition of Al particles further decreases the burning rate due to enhanced metal agglomeration.

Addition of Al-Mg alloy particles decreases the burning rate and energy content of Mg-NaNO₃ composition at all mixture ratios due to the higher stability of the alloy particles for the reactions than its component elements and also due to the lower melting point of alloy particles below the decomposition range of NaNO₃ leading to high degree of metal

agglomeration.

Study carried out has indicated that the combustion efficiency of Mg-NaNO_3 gas generator fuel-rich composition could be augmented significantly by about 20% on addition of Al particles upto 10% for use in advanced air-breathing propulsion system.

ACKNOWLEDGEMENT

The authors are grateful to Dr. Haridwar Singh, Director, ERDL, Pune (India) for his valuable guidance and encouragement in the preparation of this paper.

REFERENCES

1. A.Gany and D.W.Netzer, "Combustion Studies of Metallized Fuels for Solid-Fuel Ramjets", J.Propulsion 5, 423-427 (1986).
2. M.K.King, A Report on "Combustion Studies of Fuel Rich Propellants", Kinetics and Combustion group, Atlantic Research Corporation, Alexandria, Virginia, pp.19-141, August (1976).
3. J.Richard Ward, Leon J.Decker and Austin W.Borrows, "Burning Rates of Pressed Strands of a Stoichiometric Magnesium-Sodium Nitrate", Combust. and Flame, 51, 121-123 (1983).
4. B.D.Bond and P.W.M.Jacob, "Chemical Reactions of Magnesium and Sodium Nitrate", Combust. and Flame, 10, 349-354 (1966).
5. Harihar Singh, M.R.Somayajulu and R.Bhaskara Rao, "A Study on Combustion Behaviour of Magnesium-Sodium Nitrate Binary Mixtures", Combust. and Flame, 76, 57-61 (1989).

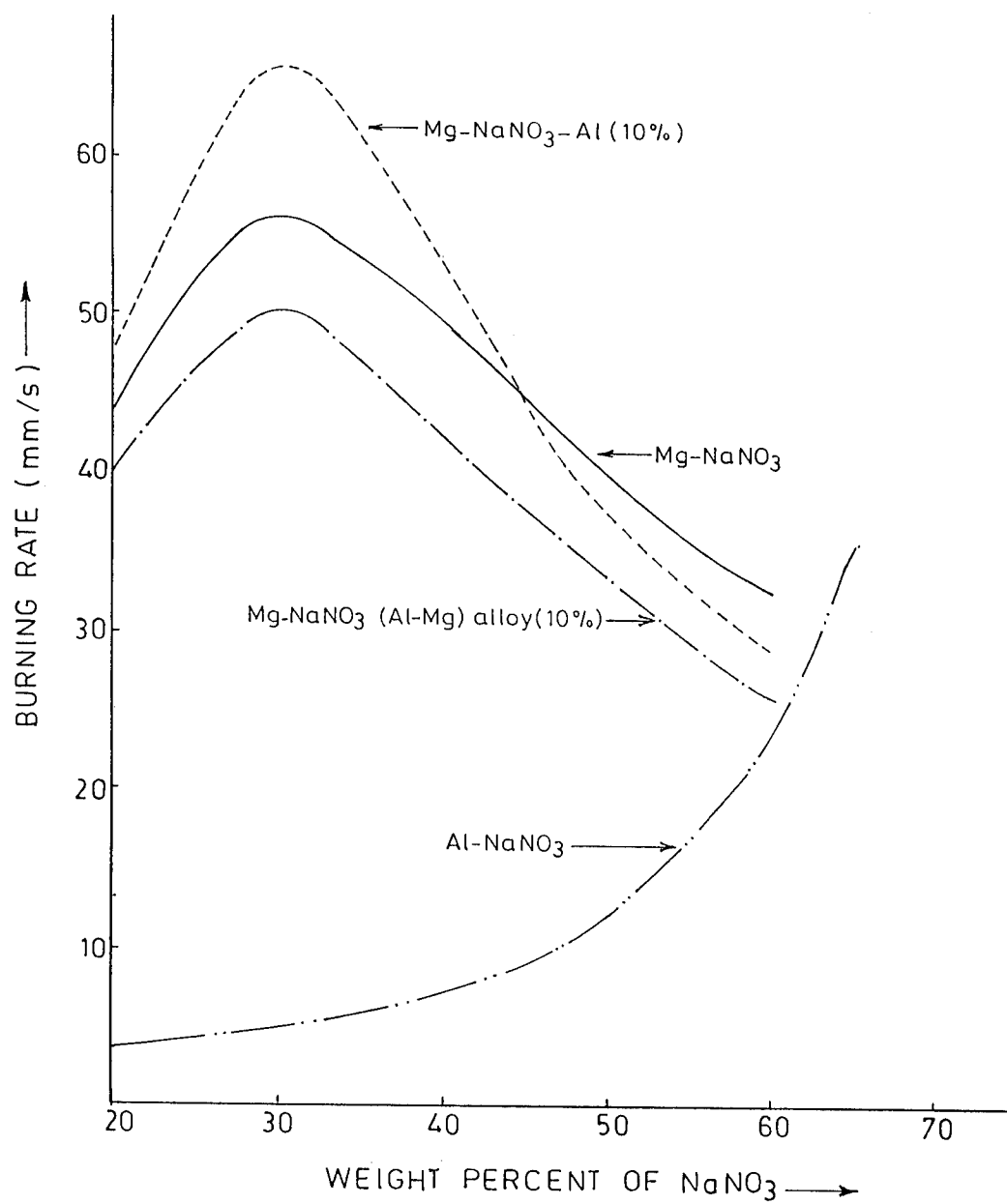


FIGURE 1 Burning rate data of compositions as a function of NaNO_3 concentration

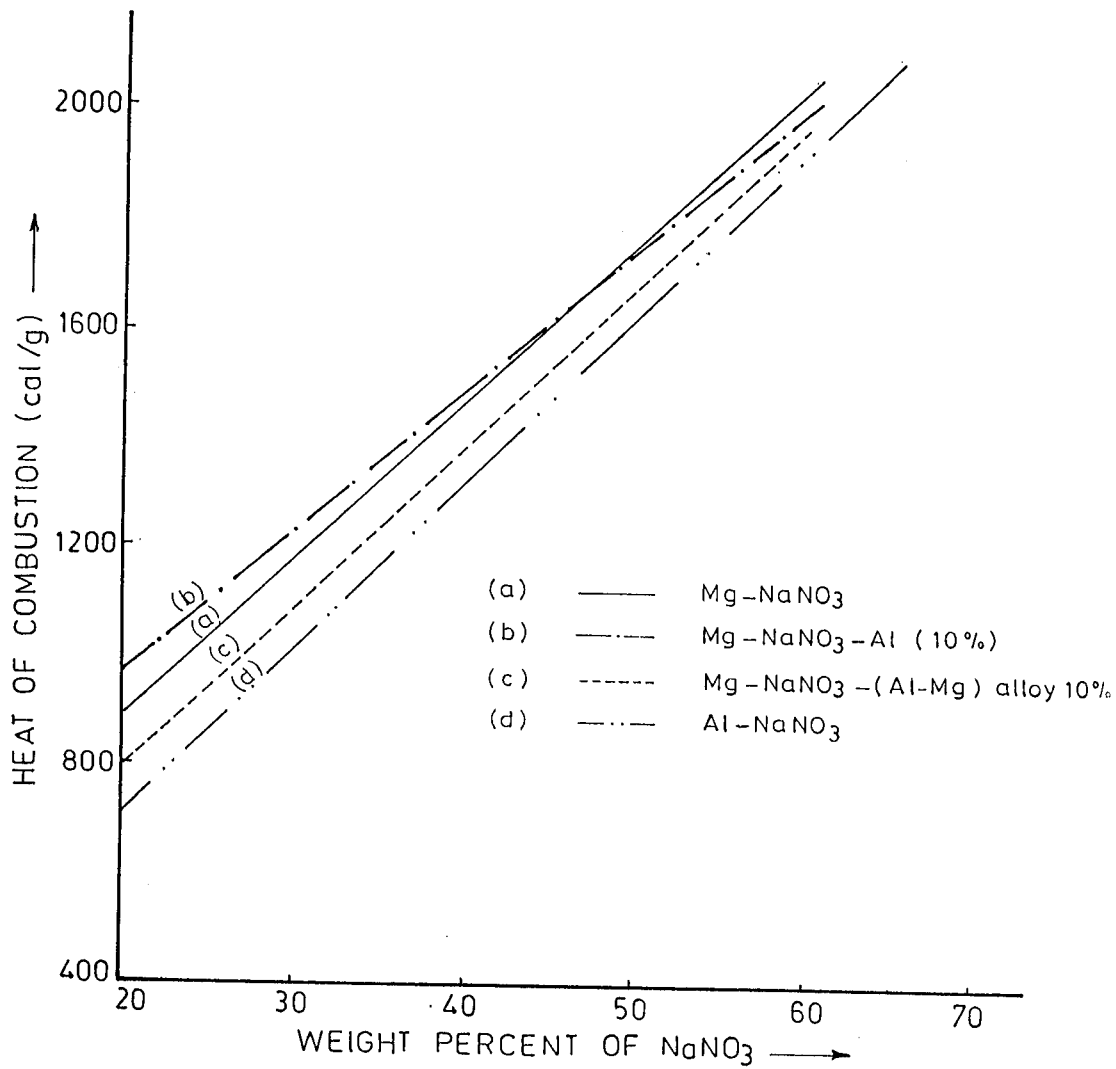


FIGURE 2. Heat of combustion data of compositions as a function of NaNO₃ concentration.

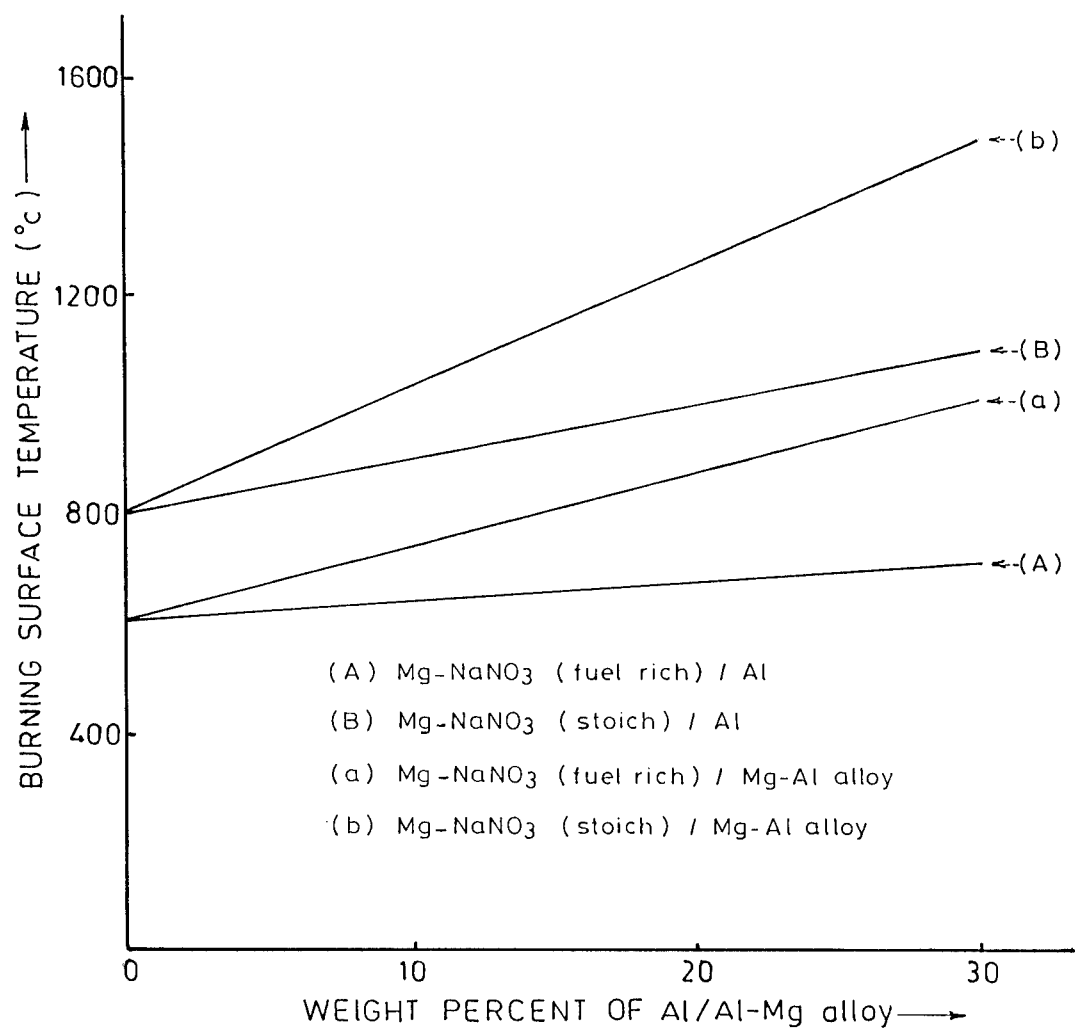


FIGURE 3. Burning surface temperature data of Mg-NaNO₃ composition replacing Mg with Al/Al-Mg alloy particles.

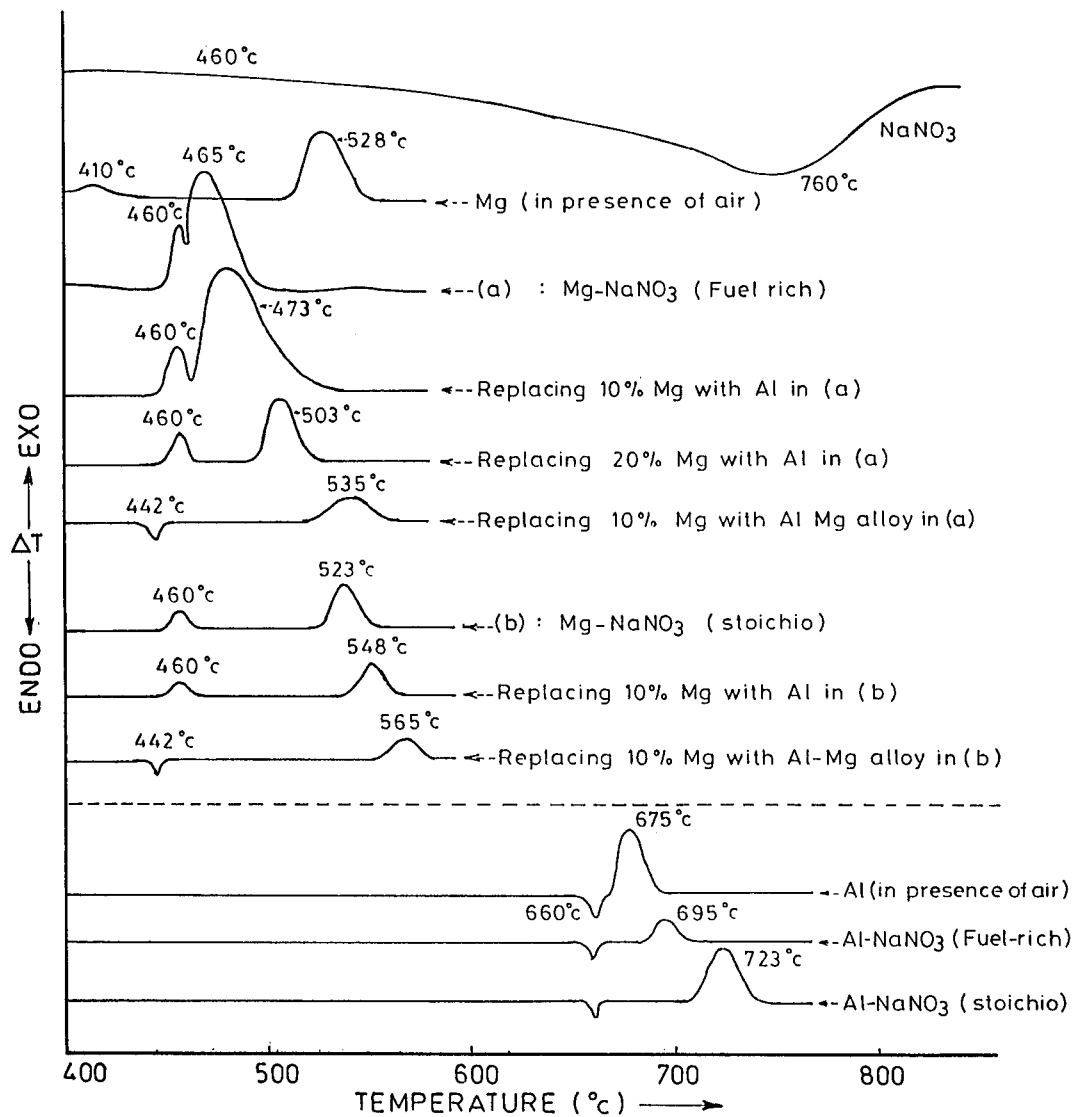


FIGURE 4. Thermal decomposition data of compositions.

ENERFOIL™ IGNITION FILM AS AN IGNITION CHARGE

Se Kwan Chan, ICI Explosives, Richlieu Blvd., McMasterville, Quebec, Canada

Steven J. Graham, ICI Explosives, Stevenston, KA20 3LN, U.K.

Graeme A. Leiper, ICI Explosives, Stevenston, KA20 3LN, U.K.

ABSTRACT

In propellant based gas generation systems, there are a number of pyrotechnic elements comprising an ignition train. These elements convert a mechanical or electrical impulse into a combustion wave of sufficient magnitude to ignite the propellant charge, thereby beginning the gas generation process. In this paper, typical ignition trains as used in passive vehicle restraint systems, and the pyrotechnic elements therein are described. In particular, the role of the ignition enhancer in providing a prompt and controlled ignition stimulus to the propellant is examined.

Special reference is made to a new pyrotechnic product, ENERFOIL™ Ignition film. The material has been characterised in terms of both its ballistic performance and its sensitivity to common hazardous stimuli. This material is shown to have increased performance over conventional pyrotechnic powders in terms of ballistic, environmental and cost considerations. The manufacturing method, based on vacuum vapour deposition is reviewed, and is shown to be intrinsically more controllable than conventional powder mixing, giving a uniform and reliable product.

Conversion of the film into enhancers for use in passenger side airbag inflators is described, and examples given of the ballistic performance of such systems. Use of ENERFOIL™ film based enhancers along with MICROSAF™ advanced propellant grains as an integrated pyrotechnic unit is detailed. Data on passenger side generator performance is provided and conclusions drawn as to the likely

performance available from such systems in terms of ballistic response over the complete operational temperature range.

INTRODUCTION

The use of propellant gas generators to inflate automobile passive occupant restraint systems, "airbags", has become commonplace. The technology associated with the design of these generators relies heavily on that used in defence applications, in particular the use of sodium azide propellants as a means of generating hot clean nitrogen gas. Because of the high burn rate of such systems, large web dimensions can be used, notwithstanding the very short burn times required in airbag systems.

Typical propellant grains are pressed as single or multi-holes disks. These are assembled into a stack, which is inserted into a filter and then into the body of the generator. The filter system acts to remove unwanted particulates from the generator efflux, and reduce the temperature of the gas to a level compatible with the polymeric material used to manufacture the air bag itself. The generator body has a number of nozzles on the outer surface of the body orientated to give thrust neutral characteristics. A schematic of a typical passenger side generator is shown in Figure 1.

For a passenger side generator, the ballistic specification of the generator requires that the seals on the nozzle system open within about 8 ms., and complete combustion is achieved within about 65 ms, at ambient temperature. Nozzle opening is controlled primarily by the promptness of propellant ignition and the free volume within the generator. Burn out is controlled by the propellant web thickness, and the uniformity of ignition of the propellant grain.

The gas generation rate is closely prescribed throughout the operation of the generator, requiring reproducible ignition of all of the surfaces of propellant grains, without significant grain damage due to the ignition event.

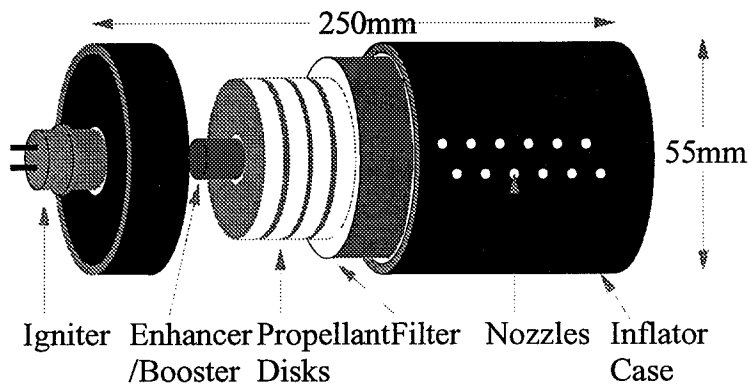


FIGURE 1
SCHEMATIC OF PASSENGER SIDE GENERATOR

The ignition system used to ensure adequate performance has until recently comprised an igniter containing various quantities of metal - oxidant powders, for instance boron and potassium nitrate or titanium and potassium perchlorate, and an "enhancer", comprising a perforated tube containing a large quantity of boron - potassium nitrate powder and deflagrating cord. An electric igniter is mounted in the head end of the generator, and an enhancer inserted down the central conduit formed by the propellant grains.

The enhancer unit suffers from numerous drawbacks including complexity, cost and safety in manufacture and handling. The performance can be variable, and can lead to significant grain damage during ignition of the generator, which can be less than optimal. It is the most unsatisfactory part of the generator design.

Recently a novel pyrotechnic material has been invented at the Defence Research Agency, Fort Halstead, Sevenoaks, U.K. that promises to revolutionise the design of ignition enhancing systems. Details of this novel material have been published by Allford and others elsewhere ^{1,2,11}. In this paper an overview of the material is given, and a specific application described.

NATURE OF ENERFOIL® IGNITION FILM

ENERFOIL™ Ignition film is a variant of magnesium - polytetrafluoroethene, PTFE. It is manufactured by the novel process of physical vacuum vapour deposition. In this process, a sheet of PTFE is coated on each side with magnesium to give a sandwich structure of well controlled dimensions. Typically the thickness of the PTFE film is of the order of 25 microns, and that of the magnesium, 8 microns per side, that being the stoichiometric composition.

Surprisingly it has been found that the pyrotechnic properties of the material are significantly better than that of an identical chemical composition manufactured by a powder route. Allford has suggested that this is due to the lack of a magnesium oxide layer between the magnesium and PTFE. An oxide coating on the magnesium powder retards the reaction by limiting diffusion of oxidising moieties toward the metal in the early stages of combustion.

Standard hazard testing on the film has been carried out in our laboratories, and the results are summarised in table 1. The direct and frictional impact data are impressive, and the static ignition threshold ³ for sustained burning is exceptionally high. Thermal stability data has been obtained ⁴ that shows the material to be extremely insensitive to heat. Together these properties greatly increase the inherent safety of the material during handling operations, over that associated with typical powder systems.

Ballistic properties have been computed by thermochemical calculations, and by calculation from closed vessel combustion tests. These are summarised in table 2. The pyrotechnic has a very high flame temperature and heat of reaction, but a very low force constant. Such a combination of properties is ideal for ignition systems, as there is little generation of high transient forces which can damage the propellant grain or grain bed. Ignition is primarily due to the condensation of the reaction products onto the propellant, with the resulting release of large amounts of energy.

TABLE 1: HAZARD AND SENSITIVITY DATA

BAM Impact sensitivity	16J
BAM Friction sensitivity	>360N
Static Ignition threshold	20J
Thermal stability by DSC	>450C
Time to ignition at 550C	30s

TABLE 2: COMPUTED AND MEASURED BALLISTIC PROPERTIES

Isochoric flame temperature	5010K
Isobaric flame temperature	3800K
Heat of reaction	9.1MJ/kg
Force constant	0.165 MJ/kg
Mass of gas generated	78% at flame temperature
	0% at STP
Flame spread rate	~1m/s at 10^5 Pa.
	~300m/s at 10^6 Pa.

Flame spread rates across the film have been measured and been found to be sensitive to the local pressure and geometry. Flame spread across an unconfined sheet occurs rapidly. Upon confinement, the flame spread reaction becomes close to sonic, allowing the material to be used in flash tubing, and in applications where uniform ignition over large distances is required.

METHOD OF MANUFACTURE

The production process used to manufacture the pyrotechnic film has been the subject of intensive research over the last three years. The initial method proposed by Allford ¹¹ was not well suited to mass production, and ICI has developed a reliable and robust production process based on novel physical vapour deposition technology ^{9,10,12}. This technology combines the process monitoring, quality techniques and reproducibility standards common to the films industry with the high safety and environmental standards required by the pyrotechnics and automotive industries respectively.

A full scale production manufacturing facility for ENERFOIL™ ignition film has been constructed and commissioned by ICI Explosives Airbag Products Group at our facility at Tamaqua, PA., USA. Process development is complete, and product will be available for supply from Quarter 3, 1995.

USES OF ENERFOIL™ FILM

In principle, the film can be used to replace any pyrotechnic composition used in ignition, flash transfer or flare systems. It is particularly suited to applications that require the generation of hot particles. In this respect it can be used with great efficacy in effecting the ignition of insensitive propellant.

The nature of the product lends itself to the formation of self-supporting structures created through the use of winding and processing techniques, common in the

packaging and films industries. Thus it can be configured into long spirals that might be introduced into propellant assemblies as novel components. For instance, it is possible to load the central conduit of propellant grains or propellant-containing modules with the film to give abrupt and uniform ignition along the length of the inner surface of the grain or grain module. It is ideally suited to the ignition of generators commonly used in car airbag systems. In the remainder of this paper, the use of the film in such a fashion is described.

In the introduction, details were given of the internal structure of a passenger side generator for automobile passive occupant restraint systems. Inside the generator there was an enhancer system used as part of the ignition train. Given the geometry of the generator, this enhancer was a good candidate for replacement by a wound roll of ENERFOIL™ ignition film.

Significant cost and reliability advantages accrue from the replacement. The film itself is a very cost competitive material, given the simplicity, safety, and robustness of the manufacturing route. The high quality standards inherent in the manufacturing process contribute to more uniform and reliable performance. Conversion of the film into an ignition enhancer, by cutting and winding, is again simple and highly reproducible, in marked contrast to the problems of filling tubes with dusty and ill-flowing powders.

Initial enhancer trials were carried out in a generator simulator. The simulator, figure 2, comprised a cylindrical pressure vessel, tapped to take an igniter in one face, and two pressure transducers in the cylinder wall: one close to the igniter and one far from the igniter. A third transducer could also be mounted directly opposite the igniter.

Within the vessel there was a charge volume compensation block, that was used to correct the free volume of the simulator to that of the generator being simulated. The enhancer itself was loaded into a central conduit within the block.

Various types of blocks were used to alter the degree of confinement of the enhancer, and hence model the degree of resistance caused by the grain stack to the flow of the enhancer combustion products from the central conduit into the ullage next to the internal surface of the bomb. The material of construction of the block could also be altered to increase or decrease the heat loss from the enhancer products as they flowed into the ullage.

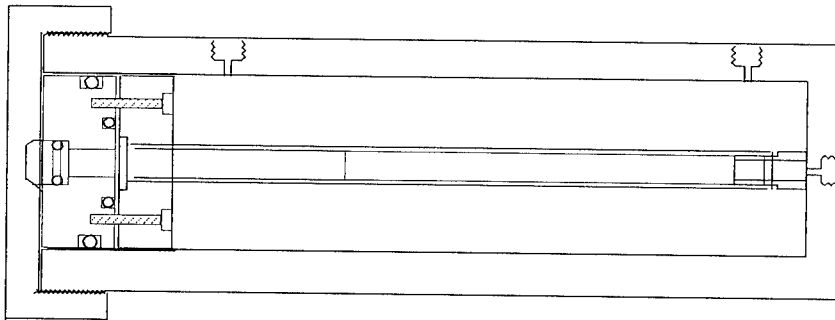


FIGURE 2
SCHEMATIC OF BALLISTIC BOMB

The enhancer used in the tests comprised about 0.004 kg of ENERFOIL™ film, wound into a cylinder roughly 0.22 m. long and 0.012 m. in diameter. The film was pre-treated by embossing¹³, to aid ignition and flame spread. The end closest to the igniter was spiral cut to aid ignition of each layer in the roll^{5,8}. An ICI Explosives IGN 184 igniter was used in all experiments unless otherwise indicated.

The first series of experiments concentrated on examining the effect of confinement upon the combustion rate of the enhancer. The charge volume compensation block was altered to give either a large or small open area for gas flow into the ullage, figures 3 and 4 respectively. The ballistic results clearly demonstrated that the combustion rate was greatly improved by confining the combustion products within the central conduit, and hence increasing the local pressure. It was also noted that

for good confinement, the total combustion time for the enhancer was of the order of 2 ms., well within the time required for airbag applications.

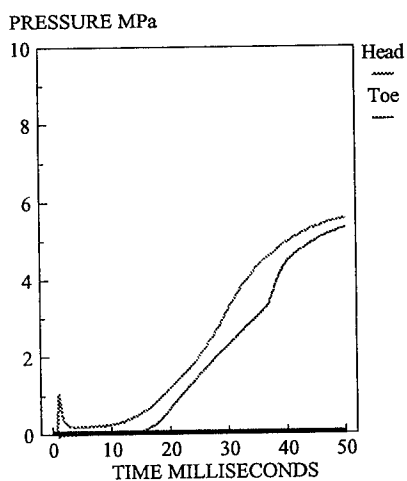


FIGURE 3

Ballistic performance in
open bomb

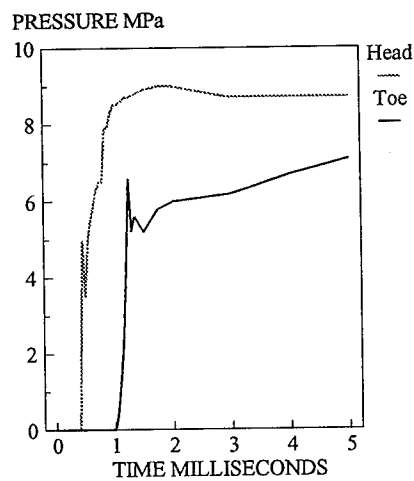


FIGURE 4

Ballistic performance in
confined bomb

Other data collected in the simulator tests included the effect of various external variables such as temperature and igniter strength. (It should be noted that as the geometry of the enhancer was being continually optimised, not all data was available for one enhancer geometric design. The effect is thus illustrated in comparative form for the particular design trialled in each test.)

The effect of initial temperature was examined by cooling the pre-loaded ballistic bomb assembly in a freezer at temperature of 238K. The bomb was removed and the pyrotechnic charge ignited. The rate of reaction at 238K was found to be slightly lower than that at room temperature. The maximum pressure developed was reduced by about 20%, but the time to maximum pressure was still short, of the

order of 3 ms as measured by the axial gauge, figures 5,6. A small amount of after-burning was seen as a slow pressurisation of the chamber at late time. This was thought to be due to a small fraction of the film being almost extinguished by impact against the cold wall of the bomb.

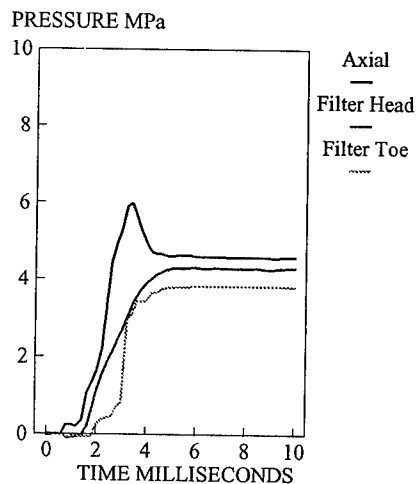


FIGURE 5

Ballistic performance

298K

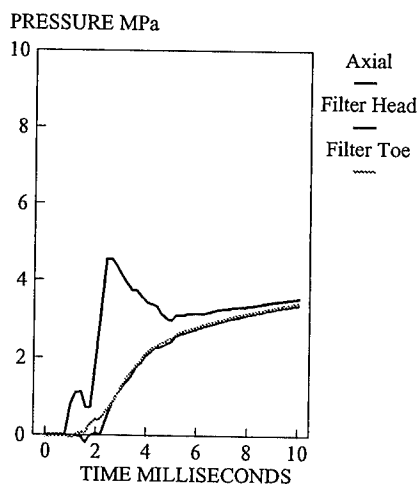


FIGURE 6

Ballistic performance

238K

Finally the effect of igniter pyrotechnic charge mass was investigated. The standard igniter used in the trials had a charge of 154 mg of powder. This was systematically reduced in steps to 50 mg.

Initially, as the powder mass was reduced, no effect was observed in the ballistic traces. However, for igniter charges of less than 100 mg., a progressive decrease in pressurisation rate was noticed, figures 7,8. However, it was found that the charge mass effect could be mitigated by optimisation of the geometry of the igniter to enhancer interface.

In practice igniter charge mass was not a limiting factor on the use of the film, and successful tests were obtained with igniters with as low a charge as 70 mg. of boron - potassium nitrate composition.

Once the performance of the enhancer unit had been optimised, a live generator test was performed. The generator consisted of a stack of MICROSAF™ propellant grains, pressed into thin annular disks, The disks were loaded into a steel generator body with integral filter system, as shown in figure 1. An ENERFOIL™ film enhancer was loaded into the central conduit formed by the annular disks, and the generator sealed. A standard igniter as previously described was used.

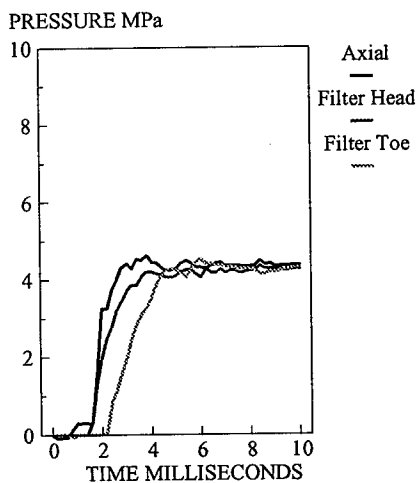


FIGURE 7
Ballistic performance
normal igniter

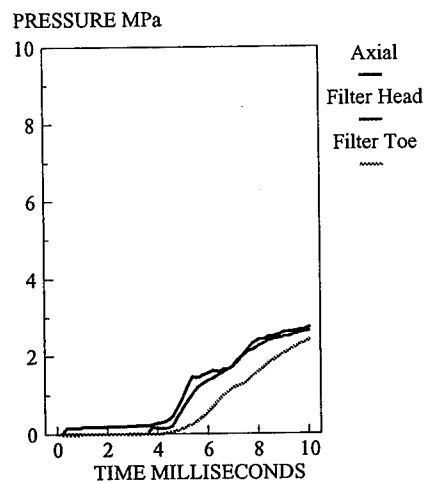


FIGURE 8
Ballistic performance
low strength igniter

The generator assembly was chilled to 243 K, a common low temperature operational specification for airbag gas generators. It was then placed in a 60 l. tank and a firing pulse applied to the igniter. Pressure transducers were attached to

record the pressure inside the central conduit of the generator, and the pressure in the 60 l tank.

Upon activation, prompt ignition of the generator occurred, figure 9. The nozzles opened in about 8 ms, causing a transitory depressurisation of the generator, until the combusting propellant balanced the gas efflux at about 15 ms. Combustion finished promptly at about 70 ms. The lack of sliver burn indicated uniform ignition of the propellant grains by the enhancer charge. The performance was within the specification required for the system.

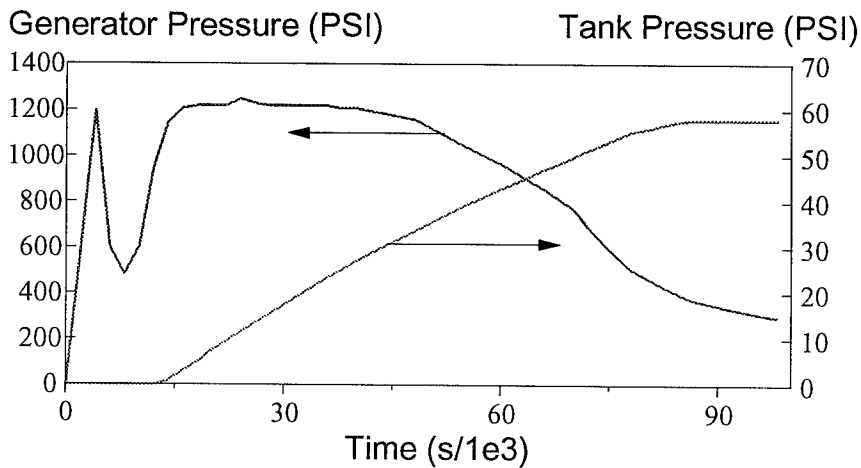


FIGURE 9

TYPICAL GENERATOR RECORD AT 243K

CONCLUSION

The use of a novel film pyrotechnic material in igniting propellant charges has been described. The material has been shown to have unusually good safety characteristics compared to conventional powder pyrotechnic materials. The ballistic performance, in particular the exothermicity and speed of reaction has been shown

to be especially suited to the ignition of insensitive propellant systems. A brief outline of the associated manufacturing technology for film production, and conversion into a useful ignition element has been given.

Typical applications have been described. The use of the film has been exemplified in the successful development of an ignition enhancer for a gas generator used for inflating passenger side passive occupant restraint systems in cars.

ACKNOWLEDGEMENTS

The permission of Imperial Chemical Industries PLC, allowing publication of this work is acknowledged. Much of the experimental data presented in this paper were the result of painstaking ballistic measurements by R Lebrun, M Logan, and B Underwood, their contribution is noted with grateful thanks.

ENERFOIL™ and MICROSAF™ are registered trademarks of Imperial Chemical Industries PLC.

REFERENCES

1. Allford F., Patent filing PCT WO 90/10724
2. Allford F., Place M., Proceedings of the 15th International Symposium on Pyrotechnics, Boulder, Co., U.S.A, 1990, p 1-16.
3. Gorton, W., Private communication
4. Charlesly E., Warrington S., Private communication
5. Chan S.K., Graham S.J., Leiper G.A., Patent EP050502A1
6. Chan S.K., Graham S.J., Leiper G.A., UK patent application 9216517.4

7. Chan S.K., Graham S.J., Leiper G.A., Chan S.K., Graham S.J, Leiper G.A., UK patent application 9423445.7
8. Chan S.K., Graham S.J., Leiper G.A., UK patent application 9500719.1
9. Baxter I, Bishop C., McGee D.C., Wadkins K., UK patent application 93230033.2
10. Baxter I., Bishop C., McGee D.C., Wadkins K., UK patent application 9323034
11. Allford F., Place M., Proceedings of the 15th International Symposium on Pyrotechnics, Boulder, Co., U.S.A, 1990, p 17-32
12. Gorton W., et al , Proceedings or the 1995 Conference of the Society of Vacuum Coaters, Chicago, Il., USA.
13. Chan S.K., Graham S.J., Leiper G.A., UK patent application pending

UNTERSUCHUNG ÜBER DEN REAKTIONSMCHANISMUS DES SCHWARZPULVERS UND SEINE ANWENDUNG

Takeo Shimizu

KOA-Feuerwerk AG, 350-12 Hidaka-shi, Japan

KURZFASSUNG

Burning Mechanism of Black Powder and its Applications.

It is said that black powder is the oldest explosive. However, even at present black powder is one of the most important explosives. The burning reaction mechanism of materials in the mixture is yet obscure. The purpose of this study is to make the mechanism clear and to find some applications of it.

The burning reaction of black powder has been for long time denoted by various formulas which included potassium carbonate or sulfate which we can find in the ash. The author made an effort to make clear the formation of such materials at the burning. Such a method would be the most effective to make clear the burning reaction mechanism.

By experiments the author has found that the potassium carbonate or sulfate are formed not only in the case of black powder, but also in the case of mixtures of potassium nitrate and charcoal or potassium nitrate and sulfur. It is clear that the formation of the potassium carbonate or sulfate is not peculiar to black powder, but to the nitrate.

The ash holds both of the substances. Therefore, the reaction of the formation will be not in the vapor, but in the solid or liquid state. The excellent ignition characteristics of black powder would be caused by such a reaction.

Applications of the mechanism of the burning reaction of black powder could be found to make ignition of some other compositions more effective.

1. Einleitung

Schwarzpulver ist wegen seiner ältesten Historie in dem Feld des Explosivstoffs berühmt. Dennoch waren seinen Untersuchungen seit der Erfindung des rauchlosen Pulvers in Verfall gekommen. Aber, sogar heutzutage hat das Schwarzpulver eigentümlichen Eigenschaften, die man mit anderen Explosivstoffen nicht zu substituieren. Zum Beispiel, sehr gute Zündfähigkeit, sehr hohe Lebhaftigkeit oder sehr schwieriges Feuerlöschen usw.

Der Zweck dieser Untersuchung liegt darin, den obscuren Abbrennungsmechanismus des Schwarzpulvers zu erklären und seine Anwendung weiter zu finden.

In der Vergangenheit wurde dieses Problem im 19. Jahrhundert von vielen Fachmännern studiert: Bunsen-Schischkoff, Links, Karolyi, Noble-Abel, Sarrau, Berthelot und Debus usw. Im Jahre 1940 in Japan arbeitete Dr. N. Yamaga an der Berechnung der charakteristischen Werte für Ballistik.

2. Analysen der Abbrandprodukte des Schwarzpulvers von Bunsen, Karolyi und Noble-Abel, und eine Begründung von N. Yamaga dafür

Die chemischen Zusammensetzungen, die von Bunsen, Karolyi und Noble-Abel geprüft wurden, sind wie in Abb.1 angegeben.

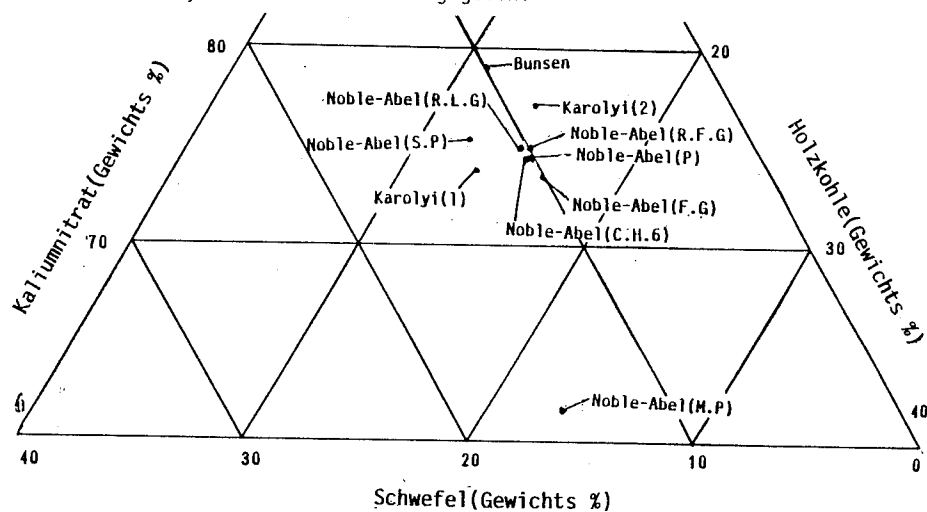


Abb.1. Die Probepulver von Bunsen, Karolyi und Noble-Abel. ^{(1),(2),(3)}

Zeichen: P.: Waltham-Abbey Pebble powder, R.L.G.: Waltham-Abbey Gifle Large Grain, R.F.G.: Waltham Abbey Rifle Fine Grain, F.G.: Waltham-Abbey Fine Grain, S.P.: Spanish spherical pebble powder, C.H.6: Curtis Harvey No.6 sporting powder, M.P.: Mining powder.

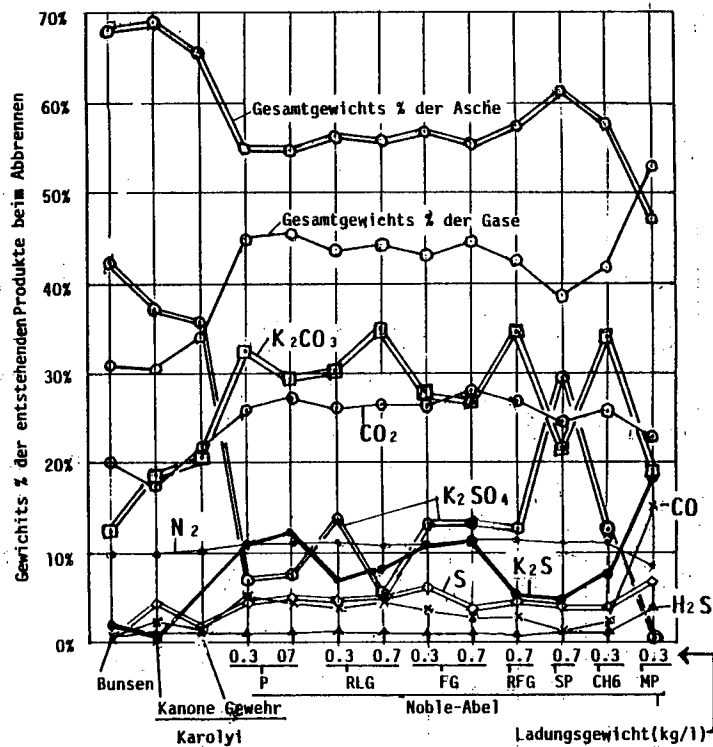
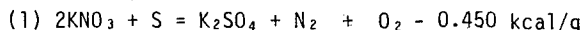


Abb.2. Hauptprodukte bei den Abbrennungen der Probepulver von Bunsen, Karolyi und Noble-Abel.

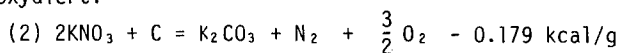
Abb.2. zeigt die Ergebnisse der Prüfung. Die Zeichen an den Kurven zeigt die Hauptprodukte. Es gab andere z.B. $K_2S_2O_3$, $(NH_4)_4H_2(CO_3)_3$ oder $KSCN$, aber sehr wenig. In Vergleichung der Kurve vom Gesamtgewichts % der Asche mit der der Gase kann man verstehen, daß die Menge der Asche größer war als die der Gase, das Bergwerkpulver ausnehmend. Das Bergwerkpulver hatte den kleinsten Gehalt an Kaliumnitrat von allen pulvern. Daher wäre der Abbrandmechanismus von dem der andere etwas verschieden. In Abb.2. befinden sich CO_2 , CO , N_2 und H_2S als Gase, die man in gewöhnlichen Abbrandreaktion finden kann. Dagegen gibt es K_2CO_3 , K_2SO_4 , und K_2S als Asche, die man in gewöhnlichen nicht leicht finden kann. Daher wäre die untersuchung der Entstehungsreaktionen von K_2CO_3 , K_2SO_4 und K_2S der effektivste Schlüssel, den Abbrandmechanismus des Schwarzpulver zu erklären.

(4)
Die Begründung des Abbrandmechanismus von Dr. Yamaga war wie folgt:

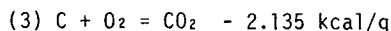
Erstens wird der Schwefel durch das Kaliumnitrat oxydiert:



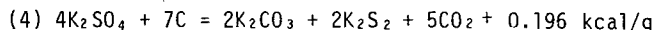
Wenn der Schwefel ausgenützt wird, dann wird die Holzkohle durch das Kaliumnitrat oxydiert:



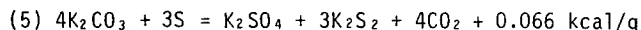
Der Sauerstoff von den zwei Reaktionen (1) und (2) oxydiert die Holzkohle:



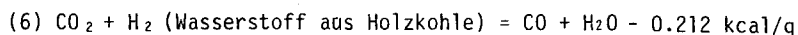
Wenn die Holzkohle nicht ausgenützt wird, geht es wie folgt:



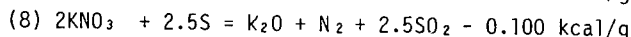
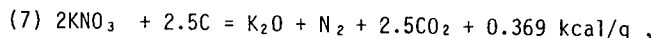
Wenn der Schwefel nicht ausgenützt wird, dann folgt es:



Wenn die Holzkohle noch bleibt, geht es:



Außer den obigen Gleichungen, (1)-(6), benutzt man gewöhnlich folgende Gleichungen, (7), (8), um den Sauerstoffsättigungspunkt einer Reaktion zu rechnen.



Es ist sehr aufmerksam, daß sich Kaliumoxyd, K_2O , trotz sehr sorgfältiger Analysen von Fachleuten befindet nicht (Abb.2).

3. Experimentelle Prüfung

Die Experimente vom Verfasser wurden in freier Luft ausgeführt, um die Abbrandphänomene gut zu beobachten. Die Arten von den Produkten in der Luft von Bunsen sind mit der im Hochdruck von den Karolyi und Noble-Abel dieselben (Abb.2). Daher wäre der Abbrandmechanismus im niedrigeren Luftdruck mit dem im höheren nicht so viel verschieden.

Die erste Frage: Die Entstehung der Verbindungen, Kaliumkarbonat oder Kaliumsulfat usw., die man bei der Abbrennung der anderen Pulvern nicht leicht bekommen kann, ist beim Schwarzpulver sehr leicht wie in Abb.2 angesehen wird. Ist die Entstehung der Verbindungen dem Schwarzpulver, einem Gemisch von Kaliumnitrat, Holzkohle und Schwefel, eigentümlich?

Zur Prüfung diese Sache hat der Verfasser über die Gemische von Oxydierstoffen (Kalium-, Natrium-, Barium-, Strontium-, oder Ammoniumnitrat) und Brennstoffe (Accroidesharz, Holzkohle, Schwefel, oder Schwefel+zufügende Holzkohle) probiert (Tabellen 1. und 2. und Abb.3).

Tabelle 1. Die Abbrennungen der Gemische von Nitraten und kohlenstoffhaltigen Stoffen (Accroidesharz oder Holzkohle)

Brennstoff \ Nitrat	KNO_3	NaNO_3	$\text{Ba}(\text{NO}_3)_2$	$\text{Sr}(\text{NO}_3)_2$	NH_4NO_3
Accroidesharz					
(a) Menge des Gemisches	9.65g	10.14g	10.06g	10.27g	9.70g
(b) Menge der Asche	5.61g	5.00g	6.23g	-	-
Verhältnis (b)/(a)	58.1%	49.3%	61.9%	-	-
Brenndauer	19.4s	18.5s	19.2s	-	-
Aussehen der Abbrennung	langsam mit einer gelben Flamme	langsam mit einer orangen Flamme	langsam mit einer gelben Flamme	nicht brannte ab	nicht brannte ab
Befund der Existenz des Karbonats in der Asche	K_2CO_3	Na_2CO_3	BaCO_3	-	-
Holzkohle(Paulownia)					
(a) Menge des Gemisches	10.14g	10.61g	9.85g	10.76g	10.13g
(b) Menge der Asche	3.65	1.10	2.28	-	0.53
Verhältnis (b)/(a)	36.0%	10.4%	23.1%	-	5.2%
Brenndauer	34.2s	16.2s	42.3s	-	21.5s
Aussehen der Abbrennung	langsam mit einer orangen Flamme	langsam mit einer gelben Flamme	sehr langsam mit einem dünnen Licht der Flamme	nicht brannte ab	langsam mit einer durchsichtigen Flamme
Befund der Existenz des Karbonats in der Asche	K_2CO_3	Na_2CO_3	BaCO_3		

Anmerkungen für Tabellen 1 und 2.

- (1) Gewichtsverhältnis Nitrat/Brennstoff = 80:20 (Tabellen 1 und 2).
- (2) Gewichtsverhältnis Nitrat/Schwefel/Holzkohle = 80:20:5 (Tabelle 2).
- (3) Analyse der Holzkohle(Paulownia): Wassergehalt: 7.09%, Asche: 4.92%, in der 14.18%Ca, 13.63%K für 100% Asche enthalten wurden.

Wie es in der Tabelle 1. angegeben ist, ist es die allgemeine chemische Tendenz, daß ein Karbonat entsteht, wenn ein Gemisch von Nitrat und nicht nur mit Holzkohle, sondern auch mit einem kohlenstoffhaltigen Stoff abgebrannt wird. Die kürzere Brenndauer jedes Gemisches zeigt, daß die Entstehung des Karbonats sehr leicht geht. In der Tabelle 2 sehen wir an, daß ein Sulfat schwierig entsteht, wenn ein Gemisch von Nitrat und Schwefel abgebrannt wird, wie die sehr lange Brenndauer zeigen. Wenn sogar aber eine kleine Menge Holzkohle zum Gemisch zugefügt wird, das Sulfat sehr leicht entsteht.

Tabelle 2. Die Abbrennungen der Gemische von Nitraten und Schwefel oder von denselben Gemischen, wozu eine kleine Menge Holzkohle zugefügt wurde.

Brennstoff	Nitrat	KNO_3	$NaNO_3$	$Ba(NO_3)_2$	$Sr(NO_3)_2$	NH_4NO_3
Schwefel						
(a) Menge des Gemisches		9.53g	9.95g	10.58g	10.30g	9.76g
(b) Menge der Asche		4.73	9.44	6.82	10.21?	9.00?
Verhältnis (b)/(a)		49.6%	94.9%	64.5%	-	-
Brenndauer		69.5s	länger als 120s	36.0s	-	-
Aussehen der Abbrennung		sehr langsam mit einer stark weißen Flamme	sehr langsam mit einer durchsichtigen Flamme	langsam mit einer weißen Flamme	schwer abzubrennen	nicht brannte ab
Befund der Existenz des Sulfats in der Asche		K_2SO_4	Na_2SO_4	$BaSO_4$	-	-
Schwefel + zufügende Holzkohle (Paulownia)						
(a) Menge des Gemisches		10.39g	11.13g	110:20	9.94	
(b) Menge der Asche		4.26g	6.16g	5.17g	-	
Verhältnis (b)/(a)		40.6%	55.4%	33.5%	-	
Brenndauer		4.0s	12.0s	15:5s	-	
Aussehen der Abbrennung		sehr schnell, heftig mit einer großen weißen Flamme	heftig mit einer gelben Flamme	stark weiße Flamme	nicht brannte ab	
Befund der Existenz des Sulfats in der Asche		K_2SO_4	Na_2SO_4	$BaSO_4$		

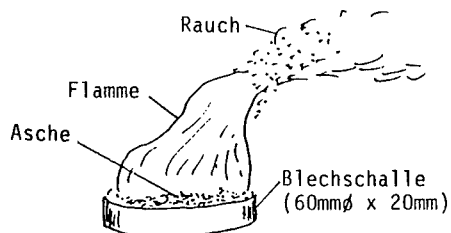


Abb. 3. Abbrennungsphänomen des Probegemisches in der Luft.

Die zweite Frage: In welchem Zustand brennt das Schwarzpulver ab? Wie es in der Abb.3 gezeigt wird, bleibt sehr viel Menge von Asche auf der Abbrennungsfläche. Die Asche muß von dem festen oder flüssigen Zustand kommen, weil ob die Asche vom gasartigen kommt, muß die Asche durch die Flamme als Rauch in die Luft entweichen (s. auch Abb.2 und Tabelle 2.). Daher brennt das Schwarzpulver ungefähr halb in festem Zustand und ungefähr halb in flüssigem ab. Es bedeutet, daß Schwarzpulver mit kleinerem Wärmeentweichen abbrennt. Das verursacht dem Schwarzpulver sehr gute Zündungsfähigkeit.

Die dritte Frage: Warum ist der Druck- und Reibungsprozeß ans Gemisch

Tabelle 3. Die Abbrennungen der Gemische, die aus Holzkohle(Paulownia) und Kaliumnitrat von verschiedenen Korngrößen entstanden.

von verschiedenen Korngrößen entstanden.								
Korngröße des Nitrats	G4		G5		G6		G7	
Menge des Gemisches(a)	22.46g	21.81g	23.78g	21.22g	20.20g	21.70g	19.88g	19.23g
Länge des Gemisches	95mm	93mm	100mm	87mm	88mm	98mm	94mm	88mm
Brenngeschwin- digkeit(mm/s)	0.84	1.07	3.14	2.93	4.86	5.10	8.39	8.30
Menge der Asche (b)	12.41g	11.01g	9.38g	9.26g	4.66	4.64	4.31g	2.94g
(b)/{a}	55.3%	50.5%	39.4%	43.7%	23.1%	21.4%	21.7%	15.3%
Kalium- karbonat in Asche(c)	8.66g	8.81g	6.96g	8.01g	5.19g	4.79g	4.27g	2.86g
(c)/(b)	71.0%	65.9%	63.0%	73.1%	99.8%	96.6%	96.8%	99.3%
Kalium- nitrit in Asche(d)	3.53g	4.56g	4.08g	2.95g	0.01g	0.17g	0.14g	0.02g
(d)/(b)	29.0%	34.1%	37.0%	26.9%	1.5%	3.4%	3.2%	0.7%

Anmerkungen:

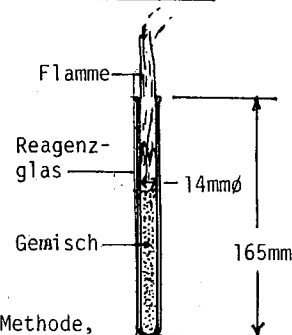
(1) Die Korngrößen sind wie folgt angegeben:

Zeichen	Sieboffnung
G4	0.295 ~ 0.208mm
G5	0.208 ~ 0.104mm
G6	0.104 ~ 0.053mm
G7	< 0.053mm

(2) Das Gewichtsverhältnis von Kaliumnitrat zu Kohlenstoff in den Gemischen ist 8:2.

(3) Die Korngröße der Holzkohle gehört zu G7.

Abb. 4. Die Methode, Asche zu empfangen



beim Herstellen des Schwarzpulvers nötig? Kaliumnitrat von vier Klassen der Korngröße wurde bereit gemacht (s. Anmerkungen (1) und (2) in der Tabelle 3). Die Gemische vom Kaliumnitrat und Holzkohle(Paulownia) wurden abgebrannt und die Aschen wurden analysiert (Tabelle 3., Abb.5 und 6).

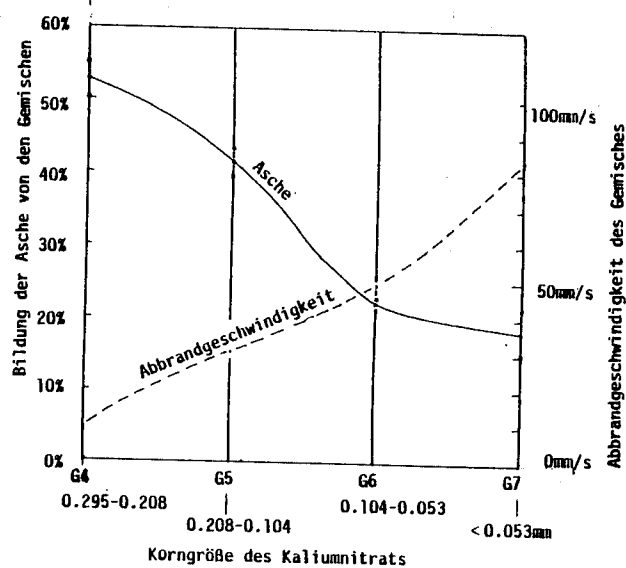


Abb. 5. Die Abbrandeffekte mit den Korngrößen des Kaliumnitrats I : Die Abbrandgeschwindigkeit und die Menge der entstehenden Asche.

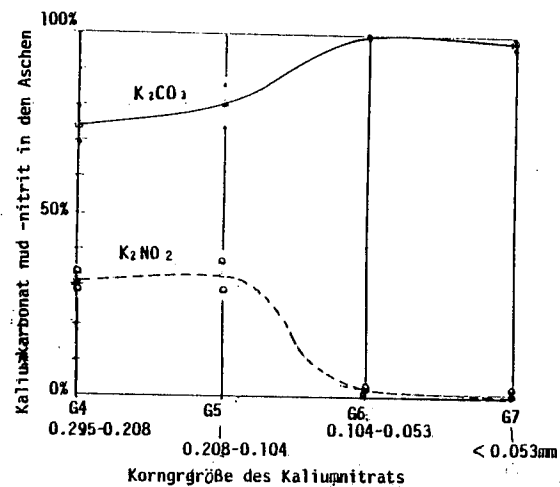


Abb. 6. Die Abbrandeffekte mit den Korngrößen des Kaliumnitrats II : Die Gehalte von Kaliumkarbonat und Kaliumnitrit in der Asche.

Wie es in den Abbildungen 5. und 6. angesehen wird, je kleiner die Korngröße des Kaliumnitrats wird, desto schneller wird die Abbrandgeschwindigkeit, weniger wird die Entstehung der Asche, mehr wird die Menge des Kaliumkarbonats und weniger wird die Menge des Kaliumnitrits in der Asche. Diese Sache zeigt, daß die Abbrandreaktion mit aneinander dichtem Kontakt der Bestandteile vollkommen wird. Dieser Mechanismus ist besonders der Abbrandreaktion in festem Zustand eigentümlich. Davon versteht man die Notwendigkeit des Druck- und Reibungsprozesses beim Herstellen des Schwarzpulvers.

Die vierte Frage: Wovon kommt die ausgezeichnete Zündungs- oder Entzündungsfähigkeit des Schwarzpulvers kommt? Zur Prüfung wurden 7mm kubische Sterne bereit gemacht, die aus verschiedenartigen chemischen Zusammensetzungen bestanden. Drei Probesterne wurden jedesmal in einem kleinen Mörser geladen und abgefeuert (Abb.7). Die Zahl der Sterne, die dabei entzündet wurden, verzeichnet wurde (Tabellen 4.-9). (S. auch die zweite Frage!)

Anmerkungen zu Tabellen 4-9 :

- (1) Die erste Kolonne zeigt die Zeichen der Gemische.
- (2) Die zweite Kolonne zeigt die chemischen Zusammensetzungen der Gemische im Gewichtsverhältnis.
- (3) Die dritte Kolonne zeigt die Zahl der Sterne, die bei der Abfeuerung entzündet wurden: Die Zeichen oder Ziffern x, 1, 2, 3 zeigen jeder für sich keine, ein, zwei und drei entzündete Sterne von den drei. Das Zeichen * bedeutet eine verspätete Entzündung.
- (4) Die Wörter "gestrichen auf" in der dritten und in der fünften Kolonne in der Tabelle 9. bedeutet eine Konstruktion der Probesterne wie z.B. in Abb.8 gezeigt wird.

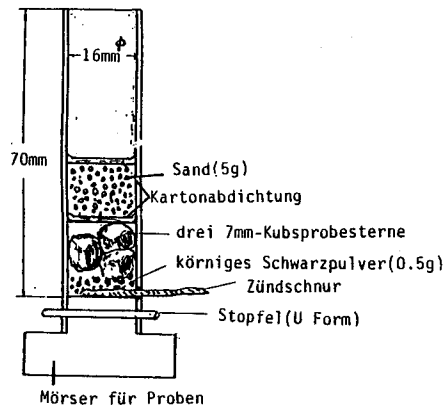


Abb.7. Vorrichtung für die Zündproben der Probesterne

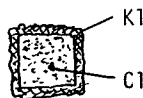


Abb.8. Mit einem Gemisch K1 gestrichener Stern C1.

Tabelle 4. Zündprüfung der Sterne im Gebrauch:
die Effekte des Zusatzes der Nitate

	A1	A2	B1	B2	C1	C2	C3	C4
KClO ₄	66	66	60.8	60.8	68	68	68	68
KNO ₃	-	5	-	-	-	11	-	10
NaNO ₃	-	-	-	-	-	-	-	-
Ba(NO ₃) ₂	-	-	-	5	-	-	-	-
Sr(NO ₃) ₂ · 4H ₂ O	-	-	-	-	-	-	-	-
NH ₄ NO ₃	-	-	-	-	-	-	-	-
Holzkohle	-	-	-	-	-	-	-	-
Accroidesharz	13	13	9.0	9.0	13	13	13	13
Schwefel	-	-	-	-	-	-	5	5
K ₂ CO ₃	-	-	-	-	-	-	-	-
Na ₂ CO ₃ · H ₂ O	-	-	-	-	-	-	-	-
BaCO ₃	-	-	-	-	-	-	-	-
SrCO ₃	12	12	-	-	12	12	12	12
CaCO ₃	-	-	-	-	-	-	-	-
CuCO ₃ · Cu(OH) ₂	-	-	12.3	12.3	-	-	-	-
CuO	-	-	-	-	-	-	-	-
K ₂ SO ₄	-	-	-	-	-	-	-	-
Na ₂ SO ₄	-	-	-	-	-	-	-	-
BaSO ₄	-	-	-	-	-	-	-	-
SrSO ₄	-	-	-	-	-	-	-	-
CaSO ₄ · 1/2H ₂ O	-	-	-	-	-	-	-	-
Vinylchlorid	2	2	-	-	-	-	-	-
Parlon	-	-	13.1	13.1	2	2	2	2
Klebreisstarke	5	5	4.8	4.8	5	5	5	5
Mal 1.	x	3	x	x	x	3	x	1
2.	1	2	x	x	x	3	x	x
Zahl des	x	3	x	x	x	2	x	1
Entzündens	x	2	x	x	x	3	x	x
4.	1	3	x	x	x	3	x	1
5.								

Die Antwort wird von den Ergebnissen in den Tabellen 4-9 indirekt oder direkt gegeben.

Tabelle 4: Durch einen Zusatz von einiger Menge Kaliumnitrat ergibt sich sehr gute Zündfähigkeit der Sterne im Gebrauch (A2 und C2). Der Zusatz von Schwefel vermindert den Entzündungseffekt (C3 und C4). Der Zusatz von Bariumnitrat ist ungünstig (B2).

Tabelle 5: Man findet keinen guten Effekt.

Tabelle 6: Der Zusatz von Kaliumkarbonat gibt einen besseren Effekt, noch gibt der von Natriumkarbonat den besten (E6 und E11).

Tabelle 7: Schwarzpulver gibt den besten Entzündungseffekt (FS1 und FS2). Noch ist es bemerkenswert, daß ein Gemisch von Kaliumperchlorat, Kaliumnitrat und Accroidesharz (H1) einen besseren Entzündungseffekt gibt.

Tabelle 5. Zündprüfung der Sterne im Gebrauch:
die Effekte des Zusatzes der Nitrate
oder Karbonate

	D1	D2	D3	D4	E1	E2	E3	E5
KClO ₄	63	63	66	66	68	68	68	68
KNO ₃	-	-	-	-	-	-	-	-
NaNO ₃	-	-	-	-	-	-	-	-
Ba(NO ₃) ₂	-	11	-	10	-	-	-	-
Sr(NO ₃) ₂ ·4H ₂ O	-	-	-	-	-	-	-	-
NH ₄ NO ₃	-	-	-	-	-	-	-	-
Holzkohle	-	-	-	-	-	-	-	-
Accroidesharz	9	9	10	10	13	13	13	13
Schwefel	-	-	5	5	-	-	-	-
K ₂ CO ₃	-	-	-	-	-	-	-	-
Na ₂ CO ₃ ·H ₂ O	-	-	-	-	-	-	-	-
BaCO ₃	-	-	-	-	-	-	-	12
SrCO ₃	-	-	-	-	-	-	-	-
CaCO ₃	-	-	-	-	-	-	-	-
CuCO ₃ ·Cu(OH) ₂	13	13	-	-	-	-	-	-
CuO	-	-	13	13	-	-	-	-
K ₂ SO ₄	-	-	-	-	-	-	-	-
Na ₂ SO ₄	-	-	-	-	-	-	-	-
BaSO ₄	-	-	-	-	-	-	12	-
SrSO ₄	-	-	-	-	-	-	-	-
CaSO ₄ ·1/2H ₂ O	-	-	-	-	-	-	-	-
Vinylchlorid	-	-	-	-	-	-	-	-
Parlon	15	15	6	6	2	2	2	2
Klebreisstärke	5	5	5	5	5	5	5	5
Mal 1.	1	1*	x	x	x	x	x	1
2.	1	x	x	x	x	x	1	x
Zahl des	3.	1	1*	x	1	2	x	x
Entzündens	4.	1	x	x	x	x	x	x
5.	1	x	x	x	x	1	x	2

Tabelle 8: Einige Gemische von Nitrat und Holzkohle geben besseren Entzündungseffekt (I1 und I3, die Kaliumnitrat oder Bariumnitrat enthalten). Die Gemische von einem Nitrat und Schwefel geben keinen guten Effekt.

Tabelle 9: Schwarzpulver K1 auf C3 oder ein Gemisch von Bariumnitrat und Holzkohle K4 auf C1 oder C3 geben einen besseren Effekt. Aber K4 wirkt mit Zündverspätung.

Durch die obigen Ergebnisse versteht man, daß ein Gemisch von Kaliumnitrat, Holzkohle und Schwefel den besten Entzündungs- oder Zündungseffekt ergibt. Aber man kann bemerken, daß ein anderes Gemisch von Kaliumnitrat und Holzkohle den besseren Effekt gibt, aber noch ein anderes Gemisch von Kaliumnitrat und Schwefel nicht.

Tabelle 6. Zündprüfung der Sterne der Probegemische:
die Effekte der Karbonate oder Sulfate
mit keinem Nitrat

	E6	E7	E8	E9	E10	E11	E12
KClO ₄	68	68	68	68	68	68	68
KNO ₃	-	-	-	-	-	-	-
NaNO ₃	-	-	-	-	-	-	-
Ba(NO ₃) ₂	-	-	-	-	-	-	-
Sr(NO ₃) ₂ · 4H ₂ O	-	-	-	-	-	-	-
NH ₄ NO ₃	-	-	-	-	-	-	-
Holzkohle	-	-	-	-	-	-	-
Accroidesharz	13	13	13	13	13	13	13
Schwefel	-	-	-	-	-	-	-
K ₂ CO ₃	12	-	-	-	-	-	-
Na ₂ CO ₃ · H ₂ O	-	-	-	-	-	12	-
BaCO ₃	-	-	-	-	-	-	-
SrCO ₃	-	-	-	-	-	-	-
CaCO ₃	-	12	-	-	-	-	-
CuCO ₃ · Cu(OH) ₂	-	-	-	-	-	-	-
CuO	-	-	-	-	-	-	-
K ₂ SO ₄	-	-	-	-	12	-	-
Na ₂ SO ₄	-	-	-	-	-	-	12
BaSO ₄	-	-	12	-	-	-	-
SrSO ₄	-	-	-	-	-	-	-
CaSO ₄ · 1/2H ₂ O	-	-	-	12	-	-	-
Vinylchlorid	-	-	-	-	-	-	-
Parlon	2	2	2	2	2	2	2
Klebreisstarke	5	5	5	5	5	5	5
Mal 1.	1	x	x	x	x	3	1
Zahl des	2.	1	x	x	x	3	x
Entzündens	3.	2	x	x	?	3	1
	4.	2	x	x	x	3	x
	5.	3	x	x	x	3	x

4. Diskussion

Durch die obigen Ergebnisse der Experimente (Tabellen 4 -9) versteht man, daß ein Gemisch von Kaliumnitrat, Holzkohle und Schwefel den besten Entzündungs- oder Zündungseffekt ergibt. Trotzdem kann man bemerken, daß ein anderes Gemisch von Kaliumnitrat und Holzkohle den besseren Effekt gibt. Schwefel ist zum Zweck der Entzündung oder Zündung nicht wirksam.

Daher kann man vermuten, daß Nitrat und Kohlenstoff oder Karbonat, das bei der Abbrandreaktion im festen Zustand entsteht, für die Entzündung oder Zündung wirksam sind. Schwefel oder Sulfat, das bei der Abbrandreaktion entsteht, sind nur eine Hitzequelle, weil das Schwefel bei der Reaktion

Tabelle 7. Zündprüfung der Sterne der Probegemische:
die Effekte des Schwarzpulvers oder der
Nitratre

	FS1	FS2	H1	H2	H3	H4
KClO ₄	-	-	77	77	77	77
KNO ₃	75?	75	10	-	-	-
NaNO ₃	-	-	-	10	-	-
Ba(NO ₃) ₂	-	-	-	-	10	-
Sr(NO ₃) ₂ · 4H ₂ O	-	-	-	-	-	10
NH ₄ NO ₃	-	-	-	-	-	-
Holzkohle	15?	15	-	-	-	-
Accroidesharz	-	-	15	15	15	15
Schwefel	10?	10	-	-	-	-
Vinylchlorid	-	-	-	-	-	-
Parlon	-	-	2	2	2	2
Klebreisstarke	6	6	6	6	6	6
Mal 1.	3	2	2	x	1	x
Zahl des	2.	3	2	2	3	1
Entzündens	3.	3	2	2	1	1
	4.	2	3	x	1	1
	5.	3	3	1	1	1

Tabelle 8. Zündprüfung der Sterne der Probegemische,
die aus Nitraten und Holzkohle oder
Accroidesharz entstanden.

	I1	I2	I3	I4	J1	J2	J3	J4
KClO ₄	-	-	-	-	-	-	-	-
KNO ₃	80	-	-	-	75	-	-	-
NaNO ₃	-	80	-	-	-	75	-	-
Ba(NO ₃) ₂	-	-	80	-	-	-	75	-
Sr(NO ₃) ₂ · 4H ₂ O	-	-	-	80	-	-	-	75
NH ₄ NO ₃	-	-	-	-	-	-	-	-
Holzkohle	20	20	20	20	-	-	-	-
Accroidesharz	-	-	-	-	-	-	-	-
Schwefel	-	-	-	-	25	25	25	25
Klebreisstarke	6	6	6	6	6	6	6	6
Mal 1.	x	2	3	1	x	x	x	x
Zahl des	2.	3	1	2	1	x	x	x
Entzündens	3.	3	1	2	1	x	x	x
	4.	3	2	3	1	x	x	x
	5.	3	1	3	1	x	1	x

mit Kaliumnitrat mehr Hitze erzeugt als die Kohlenstoff mit Kaliumnitrat.
Die Hitze werde die Reaktion des Kohlenstoffs mit Kaliumnitrat sehr schnell
machen (Formeln (1) und (2) und Tabelle 2).

Zur Anwendung des Abbrandmechanismus des Schwarzpulvers rät der Ver-

Tabelle 9. Entzündungseffekte der Probegemische, die auf den Probesternen gestrichen waren.

	K1	K2	K3	K4	K5
KClO ₄	-	-	-	-	-
KNO ₃	75	80	86	-	-
NaNO ₃	-	-	-	-	-
Ba(NO ₃) ₂	-	-	-	84	88
Ba(NO ₃) ₂ · 4H ₂ O	-	-	-	-	-
NH ₄ NO ₃	-	-	-	-	-
Holzkohle	15	20	-	16	-
Accroidesharz	-	-	-	-	-
Schwefel	10	-	14	-	12
Klebreisstarke	5	5	5	5	5
gestrichen auf	C1	C1	C1	C1	C1
Mal 1.	3	1	x	1*	2*
2.	1	1	x	3*	3*
Zahl des	3.	2	x	3*	2*
Entzündens	4.	1	x	2*	x
5.	1	1	x	3*	3
gestrichen auf	C3	C3	C3	C3	C3
Mal 1.	1	3	x	3*	1
2.	3	2?	1	2*	2
Zahl des	3.	3	2	3*	2
Entzündens	4.	3	x	2*	2
5.	3	2	2	1*	2

fasser, daß man eine Menge Nitrat oder Karbonat in die chemischen Zusammensetzung zufügt, die Tabellen 4.-9 betreffend, um zu Zündfähigkeit eines Gemisches zu verbessern.

Die Reaktion des Schwefels mit Kaliumnitrat (Formel (1)) geht sehr schwer, dagegen geht die der Holzkohle mit Kaliumnitrat (Formel (2)) sehr leicht. Daher muß die Holzkohle mit Kaliumnitrat erstens reagieren, und dann das Schwefel.

Sehr schwieriges Feuerlöschen beim Abbrennen des Schwarzpulvers kommt von der aktiven Asche wie z.B. der Asche Kaliumsulfid enthält ⁽⁵⁾.

5. Schluß Noch eine Frage, warum man einen guten Zündungs- oder Entzündungseffekt meistens durch Zusatz oder durch Entstehung des Karbonats bei einer chemischen Zusammensetzung bekommen kann, bleibt chemisch ungelöst.

Literaturen: (1) Pogg. Annalen, cii, 1857, 325., (2) Ann. d. Chemie cix, 1858, 325, (2) Ann. d. Chemie cix, 1858, 53, (3) Sir Andrew Noble, Artillery and Explosives. London, p. 101-384(1906); Trans. Roy. Soc. 1875, 1879.(4) N.Yamaga and T.Denawa, Kaheigaku-kaishi, 1940, 435, T.Shimizu, FEUERWERK, 1976, 67.

A STUDY ON THE PYROTECHNIC SYSTEM OF LC-RL-ATS-Si

O. S. JOSYULU

IDL CHEMICALS LIMITED, HYDERABAD, INDIA

ABSTRACT :

The introduction of non electric shock tube initiating system like Raydet DTH for down the line applications and Raydet TLD for surface hook up has opened a technology in mining wherein a detonator is embedded at the bottom of the bore hole in the primary cartridge. It is a common practice to use the delay elements based on chemical technology coupled with lead tube technology. However in large scale production, the problems like lead coverage over the elements or improper filling of composition can lead to non initiation of detonator, which is highly unwarranted. The direct dosing of compositions on the initiatory filled shells will be helpful in many ways to overcome such problems. In this connection, a pyrotechnic system consisting of LC-RL-ATS-Si was studied for its suitability. The compositions were studied to show the effect of ATS and Si on the burning time which varied from 50 m.sec to 1100 m.sec with a dosing of 10 cgs. to 60 cgs. The study includes the effect of free chamber on the burning characteristics of the compositions which showed interesting results on the delay timings coupled with binder effects on the performance. The data and delay times have shown interesting results and these are discussed in the paper along with the method of granulation.

INTRODUCTION :

The development of non electric initiating systems like Raydets^{*} and DIDETS^{*} (nonel and anodet) have given flexibility in designing the bigger blasts with minimum inventory. The concept of Delay detonators will initiate successive holes at a pre-determined delay intervals. Pyrotechnics play an important role in giving various delay intervals like Milli second and Half second intervals in the delay detonators. In addition the initiatory systems between the holes and between the rows have increased the flexibility of the usage of non electric detonators. The usual delay intervals will be either 225/250m.sec or 475/500/525 in the bore hole. The use of delay intervals, will help in controlling the ground vibrations, muck profile, fragmentation, charge distribution and for conducting large scale blasts. In this senerio, the delay time in the detonator plays an important role.

The delay in the detonator can be obtained by different methods. The first and fore-most is use of pyrotechnic material which will give a delay by chemical burning of composition. This can be achieved by two methods.

By filling the pyrotechnic composition into the lead tube, drawing lead tube to the pre-determined dimensions, and subsequently cutting, calibration and consolidation of the composition. This process is simple and is helpful in large scale manufacture. However, certain difficulties like void formation, density variation from tube to tube and variations in the cutlength of the elements can cause the scatter in delay timing. The formation of blind elements where the lead will flow and cover the pyrotech composition during the consolidation is a major concern for mal-functioning of the detonator.

The second method is to fill the composition in pre-determined length of aluminium tubes/sleeves by multiple filling and pressing operations and subsequently inserting the element into the detonator. This requires more sophisticated technology for simultaneous dosing of non flowy composition and pressing. It can give raise to problems like fall out of composition, improper pressing and insertion defects etc.

With this background the concept of direct dosing of delay compositions on to the initiatory composition in the detonator to obtain the necessary delay is a new concept. This in turn, will eliminate all the problems associated with the lead tube technology and the processed element pressing technology.

In this paper, a pyrotechnic system was taken up which can give a delay of 500 m.sec with direct dosing.

Investigation objective :

The aim of this work is to find out a suitable composition to give the required delay timing (475 m.sec/500 m.sec) by direct dosing on to the primary explosive in the detonator. In this connection it is necessary to know effect of the method of preparation, composition effect fuel-oxidiser ratio, free space chamber, nature of binder and method of granulation.

Tested compositions :

Pyrotechnic compositions were made from the fuel oxidiser system, Lead Chromate, Red Lead, Antimony tri sulphide, Silicon. All the materials are in powder form passing through 200 BSS. The various compositions are given in Table No.1

TABLE NO.1
Weight proportions of composition

LC	RL	ATS	Si	Binder
60	15	25	15	BA
40	35	20	15	BA
50	25	20	15	BA
50	25	10	20	BA
20	50	0	30	BA
75	25	0	15	BA
50	25	10	20	BA
50	25	10	15	BA
50	25	10	10	BA
50	25	10	15	B
0	70	15	15	BA
0	70	15	15	IPA
75	0	25	10	-
20	50	0	30	-

Binders are Butyl acetate (BA), Bentonite (B), Isopropyl alcohol (IPA).

Experiment :

The above materials are taken in different weight proportions and premixing was carried out employing the angular mixer. Different binders like butyl acetate, IPA, Bentonite were added and granulation was carried out on the BSS 18 sieve maintaining the moisture ratio of 18-20% and dried.

Detonator shells of different lengths (47 mm to 77 mm) of normal diameter i.e. OD of 7.2 mm and ID 6.4 mm with PETN/ASA as base charge and initiatory charge were taken and the granulated

material was dozed on to the initiatory charge and prezzed at 80 kg. load. The pyrotechnic composition was initiated with electric squib. The delay times so obtained are given in table Table No.2.

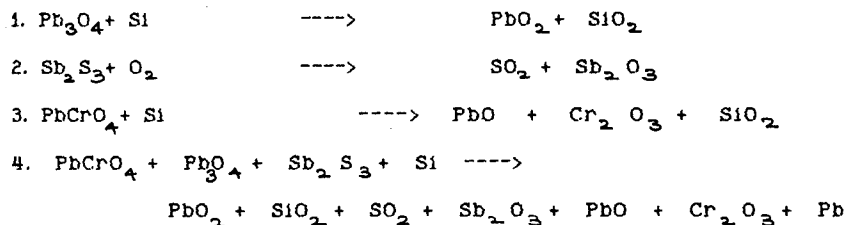
Table No.2
Delay time vs. dosages of compositions

Composition	quantity	average			
75/0/25/10	20 cgs + IC	514			
75/0/25/10	51 cgs + IC	885			
75/0/25/10	31 cgs + IC	719			
75/0/25/10	20 cgs + IC	513			
75/0/25/10	20 cgs + IC	515			
75/0/25/15	20 cgs + IC	473			
75/0/25/15	26 cgs + IC	494			
75/0/25/15	26 cgs + IC	543			
60/15/25/15	20 cgs + IC	605			
60/15/25/15	20 cgs + IC	596			
60/15/25/15	30 cgs	729			
40/35/20/15	20 cgs + IC	232			
	40 cgs + IC	300			
50/25/20/15	40 cgs + IC	300	47	mm	
	40 cgs + IC	521	57	mm	
	40 cgs + IC	509	59	mm	
	40 cgs	388	47	mm	
	40 cgs	570	59	mm	
	40 cgs	673	77	mm	
50/25/10/25	32 cgs + IC	280	57	mm	
	38 cgs + IC	345	57	mm	
	40 cgs + IC	374	57	mm	
50/25/10/20	40 cgs	189	59	mm	
50/25/10 (W)/20	40 cgs	84	59	mm	

The delay time was measured using an electronic timer employing the electronic circuitry which will be actuated by a firing pulse and stopped by a sound signal from the detonator.

Theory :

Earlier, the system RL, Fe₂O₃ Si was studied¹ The gasless compositions RL, Fe₂O₃ Si were identified to burn unaffected with gas pressure as pyrotech delay in the detonator shell. However, the addition of ATS in place of Fe₂O₃ enhances the gas generation and the addition of LC will complicate the burning phenomena. The addition of LC will help to achieve higher delays. The probable mechanism is (unbalanced equations).



The amount of gas generation in the present context is significant and it shows an effect on the burning time. In this connection, the effect of the free space in the detonator and the quantity for required delaytime become significant along with the shell material properties to withstand the sudden spurt in the gas generation and flame sensitivity of the composition.

Delay time vs dosing quantity :

The delay time depends on the burning of the composition and the quantity of the material forming the layer. In delay composition burning propagates by reignition from layer to layer along the burning path and therefore depends on the thermal conductivity of

mixture. Addition of active materials can increase the heat transfer through the mix and hasten the reaction. Increased contact between the reactions accelerate the solid reaction due to diffusion in lattice components. Stoichiometry, heat of reaction and burning rate are inter related.

The delay times so obtained will depend on the quantity of the material. The higher quantity can give rise to longer delays. But linearity can not be seen with increased dosing quantity due to many factors. (i.e.) the gas generated by the reactants, the free chamber area, the binder effect, the conducting media.

From the Table 2, it is observed that delaytime, increased with the quantity of composition. The composition 50/25/10/15 gave 280 m.sec at 32 cgs.dosing to 518 m.sec at 48 cgs dosing. Similarly 75/0/25/10 gave 514 m.sec at 20 cgs. level to 719 m.sec at 31 cgs. level. Another important factor to be considered is it is always better to obtain the negative delay time with higher dosages as it accomodates the variations in the volumetric filling of composition.

Flame sensitivity :

Another factor which effects is ability of the composition to pick up from the spit of the squibs. If the flame sensitivity and continuous burning of compositions are not satisfactory then all the effort is lost. These compositions are of slow burning nature hence the response to the spit is marginal. The burning can be hastened by adding a flame sensitive, gasless composition on the top of the pyrotech composition. The data in the table No.2 indicate that the IC hastenes the reaction as is seen in case of

composition 60/15/25/15 and 50/25/20/15. The IC ensures for continuous flame propagation in the composition by giving proper initial stimulus - for initiation.

Heat transfer of the material :

The ATS in the composition acts like an inhibitor and also as fuel. The addition of Tungston (W) in place of ATS will definitely enhances the thermal conductivity by making it a faster burning composition. The delay time ATS was 189 m.sec. while it is 84 m.sec in case of Tungston (W). (Table 2).

Effect of free space in the detonator :

In the detonator between the squib and the pyrotechnic material a free space is available. This free space varies with the varying length of shell (i.e) from 47 mm shell to 77 mm shell. The delay compositions are basically gas generating and the free space available plays an important role on the burning of the composition. The more free space can accomodate the gas and the gas pressure on the burning of the composition is less significant. The smaller gap will definitely hasten the burning and faster delay time can be obtained. However, a criticality exists where the gas can not be accomodated and the shell can burst leading to total failure. The results in Table 3 shows that the free chamber volume effects the delaytime.

The effect of pressure on the burning of BaCrO_4 , KClO_4 , Fe_2O_3 system was studied by Lucas R. Lopez et al⁷. They concluded that the composition exhibit an approximately 20-25% decrease in the burning time with 1 atm. increase in external pressure. As the pressure increases, the reactive gases are held closer to the reaction surface, thereby increasing energy transfer back in to the composition with subsequent decrease in burning time.

Secondly, the presence of more ATS can generate higher volume of gas leading to slowing down the composition. The ATS will act as an inhibitor in this context.

Table No. 3

Shell length in delaytime in the composition

LC/RL/ATS/Si 50/25/20/15 (40 cgs + 5 cgs IC)		LC/RL/ATS/Si 50/25/10/15	
Shell length 47 mm	388	57 mm	275
57 mm	521	59 mm	325
59 mm	570	65 mm	401
77 mm	673		

Effect of silicon on the burning :

In the system LC, RL act like oxidiser while ATS will play an active role like inhibitor. The Silicon is the fuel. The higher concentration of Silicon lead to fasten the reaction also contributing to higher heat coefficient. A variation of 10 to 20% of silicon contributes the delay time to vary from 442 to 189 m.sec. Similarly, LC and RL both act as oxidants but RL generates less gas and burns faster compared to LC. A reduction of RL in the composition enhances the delay time. This is evident from the results in Table 4.

Table No. 4

Effect of Silicon and LC on delay times

LC/RL/ATS/Si	Delay time in 47 mm shell
50/25/10/20	189 m.sec
50/25/10/15	345 m.sec
50/25/10/10	442 m.sec
75/0/25/15	438.3 m.sec
75/0/25/10	513 m.sec

Effect of binder/granulation :

The binder has a unique role in the surface contact of the ingredients. The binder if inactive can inhibit the burning between the fuel oxidiser causing it to slow down. In the direct dosing the binder's role is significant. The composition being powdery nature is non flowy. The density differences in Si & RL can cause segregation and inhomogeneity in the composition leading uncontrollable delay timing. Proper binder is necessary so that the composition can be made into loosely bound flowable granules, which can be crumbled under pressure. The data confirms the significant role.

Table No. 5

Effect of binder on the delay time

Binder	LC/RL/ATS/Si	Delay time noticed
Dry mix	75/0/25/10	250 m.sec
BA	75/0/25/10	514 m.sec
dry mix	0/70/15/15	very fast
BA	0/70/15/15	45 m.sec
IPA	0/70/15/15	80 m.sec
Bentonite	0/70/15/15	60 m.sec
as dry mix 20 cgs.	20/50/0/30	10 m.sec
as compacted element 25 mm length	20/50/0/30	150 m.sec
as granules	20/50/0/30	63 m.sec
Bentonite 1%	50/25/10/15	441
BA	50/25/10/15	275 m.sec

CONCLUSIONS :

From this study the following conclusions can be drawn :

1. The LC/RL/ATS/Si is suitable to achieve higher delays by direct dosing technique.
2. It is always proper to select a suitable ratio when higher delay time can be obtained with larger dosing of composition to nullify the variations in volumetric filling of composition.
3. Granulation of the composition is a must for free flowy nature of the composition.
4. The composition should be developed as per the need and length of the shell.

ACKNOWLEDGEMENT :

The authors are thankful to M/s. IDL Chemicals Limited, Hyderabad, India for allowing the publication of the data..

REFERENCES :

1. OS. JOSYULU & SR YOGANARASIMHAN, Def Scientific Journal vol. 37, No.1, 1987, pp 73-83.
2. Conkling J.A, Chemistry of Pyrotechnics - Basic Principles & theory (Marcel Dekker Inc.) 1985.
3. Abdolsamad, Moghaddam and Rees G J. Fuel, 60 (1981) 629-632.
4. Anton B. Weber, 18th International pyrotechnic seminar, Colorado (1992) 925-938.
5. L.V.De Yong, 18th international pyrotechnic seminar, Colorado (1992), 195-212.
6. O.S. JOSYULU, Thesis on statistical analysis of delay composition, 1984.
7. Lucas R. Lopez, Francis R. Taylor and Russel N Broad. 16th International pyrotechnic seminar, Sweden (1991), 599-610.

AN INVESTIGATION OF THE CATALYTIC EFFECT
OF IRON(III) OXIDE ON THE BURNING RATE
OF ALUMINIZED HTPB/AP COMPOSITE PROPELLANT

Fikret Pekel, Eralp Pınar dağ, Ali Türkan,
Defense Industries Research and Development Institute, TÜBİTAK, P.K. 16 Mamak,
06261 Ankara, TURKEY.

Saim Özkar
Department of Chemistry, Middle East Technical University,
06531 Ankara, TURKEY.

Abstract

The catalytic effect of iron(III) oxide on the burning rate of an aluminized HTPB/AP composite propellant with a constant solid content of 87 % by weight was studied. Two types of well characterized iron(III) oxides with different specific surface area were added to HTPB/AP propellant in various amount. The burning rate, viscosity and mechanical properties of the samples were measured and evaluated for studying the catalytic effect. The binder percentage of the propellant and the amount of metallic fuel were kept constant. The distribution of AP was bimodal with a constant ratio between the coarse (200 μm) and fine (5-7 μm) particles. The iron(III) oxide content was the only parameter varied in the range of 0-2 % by weight which replaced for the equal amount of AP. The cured samples were tested for their mechanical properties at room temperature and with a cross-head speed of 50 mm/min. by a conventional uniaxial testing system (INSTRON). The burning rates of the propellant were measured by firing of 2-inch motors or by an home made Crawford Bomb testing system at 25°C under variable pressure (20 - 140 kg/cm²). The burning rate and the pressure exponent of the propellant were found to increase with the increasing iron(III) oxide content of the propellant. The catalytic activity of the iron(III) oxide was found to be dependent on its particle size and surface area. The mechanical properties and viscosity of the propellant were affected slightly by the increasing weight percentage of iron(III) oxide.

Introduction

Transition metal oxides (TMO) are known to promote the thermal decomposition and deflagration of ammonium perchlorate (AP) and the combustion of AP-composite solid propellants.^(1,2) The mechanism of the catalyzed combustion of solid propellants is not fully understood. However, it has been shown that the catalytic activity of transition metal oxides is mainly in the gas phase and transition metal oxide promotes the electron transfer process which lowers the activation energy of the exothermic decomposition of the gaseous perchloric acid and ammonia formed by a proton transfer reaction from the ammonium cation to the perchlorate anion at the surface of the solid propellant.⁽³⁾ Much work has been done to study the catalytic activity of various transition metal oxides on the combustion of different AP-based solid propellants as well as of oxidant and binder. A differential thermal analysis (DTA) study on the decomposition of AP has shown that the presence of 1% transition metal oxides reduces the decomposition temperature in the order $\text{Co}_2\text{O}_3 > \text{MnO}_2 > \text{Ni}_2\text{O}_3 > \text{Fe}_2\text{O}_3$.^(2,4) However, the combustion rate of AP has been found to be affected only by Fe_2O_3 and MnO_2 . In the same study the combustion rate of a CTPB-based propellant has been found to be affected by the presence of 1% transition metal oxide in a similar order $\text{Ni}_2\text{O}_3 \approx \text{Fe}_2\text{O}_3 > \text{MnO}_2 \approx \text{Co}_2\text{O}_3$ while for a AP/PS-propellant the order has been found to be $\text{Fe}_2\text{O}_3 > \text{Co}_2\text{O}_3 > \text{Ni}_2\text{O}_3 > \text{MnO}_2$. A nice correlation between the thermal decomposition and the burning rate in AP/HTPB propellants has recently been reported.⁽⁵⁾ The burning rate of the AP/HTPB propellants follows the same order of the catalytic effect of the transition metal oxides as observed in its catalyzed thermal decomposition. From these results it is evident that the catalytic effectiveness in the propellant decomposition is different than that observed for AP. Therefore one anticipates the decomposition of the binder to be affected by the presence of transition metal oxide. Indeed a mass spectrometric study of the catalytic effect of iron(III) oxide on the HTPB/AP system has shown that the transition metal oxide catalyzes not only the decomposition of AP but also the degradation of HTPB.⁽⁶⁾

Iron(III) oxide is one of the commonly used burning rate catalyst for the HTPB/AP propellants.⁽⁷⁻⁹⁾ The particle size of iron(III) oxide has been found to affect

its catalytic activity on the burning rate of the propellant.^(10,11) Although the surface area of the catalyst is expected to affect the burning rate of both the binder and the oxidizer, experiments showed that the calcination of iron(III) oxide does not influence the combustion of AP.⁽¹²⁾ Here we would like to report our study on the catalytic effect iron(III) oxide on the burning rate of an aluminized HTPB/AP composite propellant. Two types of well characterized iron(III) oxides with different specific surface area were added to the aluminized HTPB/AP composite propellant in various amount. The burning rate, viscosity and mechanical properties of the samples were measured and evaluated for studying the catalytic effect.

Experimental

The propellant tested is an aluminized HTPB/AP composite propellant with a constant solid content of 87 % by weight. The binder percentage of the propellant was kept constant throughout the study. The amount of metallic fuel, aluminum, which is the most important parameter affecting the specific impulse was kept constant at 18 % as well. The distribution of AP was bimodal with a constant ratio between the coarse and fine particles. The coarse particles were 200 μm , and the fine particles were in the range 5-7 μm in size. The fine particles were prepared by grinding the coarse particles and measured in size. The only parameter varied was the iron(III) oxide content which replaced for the equal amount of AP. The iron(III) oxide content of the propellant was varied in the range of 0-2 % by weight..

The propellant was prepared by mixing AP, binder, aluminum and the other additives in batches followed by casting into the samples and curing at 65°C for 7 days. The viscosity measurements of the propellant samples were carried out at 65°C after the addition of curing agent by a Brookfield viscosimeter with spindle Nr. 7 at 10 rpm.

The burning rates of the propellant were measured by firing of 2-inch motors or by using a Crawford Bomb testing system at 25°C under variable pressure (20 - 140 kg/cm^2). The results of two methods were found to be in good agreement.

The cured samples were tested for their mechanical properties at room temperature and with a cross-head speed of 50 mm/min by using a conventional uniaxial testing system (INSTRON). Particle sizes of the used powders were determined on a Quanta-Sorb Surface Area Analyzer of Quantachrome, Eurasburg, Germany.

The X-ray powder pattern of the iron (III) oxide samples were recorded on a HUBER 642 Guinier powder diffractometer combined with a generator Enraf Nonius Delft Diffractis 582.

Two different Iron(III) oxides, denoted as $\text{Fe}_2\text{O}_3\text{-M}$ and $\text{Fe}_2\text{O}_3\text{-B}$, were purchased from Merck Darmstadt, Germany and from BASF Ludwigshafen, Germany, respectively.

Results and Discussion

Both of the two iron(III) oxide samples gave the same powder pattern on the x-ray diffractometer. Their analysis showed that both of them have the hematite structure ($\alpha\text{-Fe}_2\text{O}_3$, Rhombohedral, $R\bar{3}c$). However, they differ in color, $\text{Fe}_2\text{O}_3\text{-M}$ is red and $\text{Fe}_2\text{O}_3\text{-B}$ is brown. The difference in the color is attributed to the differences in their particle sizes. Indeed the average particle sizes were found to be about 7 micron for $\text{Fe}_2\text{O}_3\text{-M}$ and smaller than 1 micron for $\text{Fe}_2\text{O}_3\text{-B}$. In consistent with the particle size, the BET surface area were determined to be $1.65 \text{ m}^2/\text{g}$ for $\text{Fe}_2\text{O}_3\text{-M}$ and $18.0 \text{ m}^2/\text{g}$ for $\text{Fe}_2\text{O}_3\text{-B}$. The densities of both iron(III) oxide samples were found to be 5.24 g/cm^3 .

The mechanical properties of the propellant samples were found to be affected by increasing weight percentage of iron(III) oxide. Both the strain and the stress values decreased with the increasing amount of iron(III) oxide in the propellant. However, the variations in both of the mechanical properties remained within the acceptable range (40-50% for the strain and $0.10\text{-}0.12 \text{ kg/mm}^2$).

The change in the slurry viscosity of the propellant mixture at 65°C was monitored by using a Brookfield viscosimeter. The addition of iron(III) oxide increases the slurry viscosity of the propellant as expected for a solid additive. However, since

the iron(III) oxide replaces another solid ingredient (AP) the change in the viscosity with the increasing weight percentage of iron(III) oxide is not large and remains within the acceptable range (The increase in the slurry viscosity after 3 h is less than 50 % of its initial value).

Figure 1 and 2 show the variations in the burning rate with the pressure for the HTBP/AP propellant samples containing various amount of iron(III) oxide. All the values of the burning rates were fitted by the method of least squares to an exponential function defined by the Vieille's equation, $r = aP^n$, where r is the burning rate in cm/s, P the pressure in kg/cm² and n the pressure exponent; the nonlinear correlation coefficients⁽¹³⁾ were found to be greater than 0.985. The comparison of these two figure indicates that two types of iron(III) oxide have noticeably different catalyzing effect on the burning rate. In order to appreciate this difference, the burning rates at a pressure of 65 kg/cm² were plotted against the iron(III) oxide content for the both types in Figure 3. From this graphic one can immediately see that the Fe₂O₃-B gives remarkably higher burning rates than Fe₂O₃-M does at the same concentration. The main causes for this significantly great difference in the catalytic activities of two types of iron(III) oxides are obviously the particle size and the specific surface areas. Recall that the specific surface area is 18 m²/g for Fe₂O₃-B and 1.64 m²/g for Fe₂O₃-M. By comparison of the graphs in Figure 1 and 2, it is interesting to note that the propellant containing 1.0 % Fe₂O₃-M has almost the same trend as the sample with 0.08 % Fe₂O₃-B with respect to the burning rate.

In composite solid propellants, the three key ballistics parameters are the specific impulse, the density, and the burning rate. The latter parameter depends upon pressure. This pressure dependence is most conveniently expressed by the pressure exponent referred to as n value or combustion index in Vieille's law which enables the expression of burning rates at varying pressure range. The pressure exponent has usually the values between 0.3 and 0.7 for the composite solid propellants excluding the ones with very high burning rates. The n values for the propellant samples were elucidated from the best curve fitting of the burning rates versus pressure data in Figure 1 and 2. The n -values obtained in this way were plotted against the iron(III)

oxide content of the propellant (Figure 4). As one can see from Figure 4, the n -value increases almost linearly with the increasing percentage of iron(III) oxide for both types in the range of 0 - 1 % Fe_2O_3 . However, the slope of line is found to be larger for Fe_2O_3 -B than that for Fe_2O_3 -M. This can also be attributed to the larger surface area of Fe_2O_3 -B. Of course, it must be kept in mind that there are many other factors affecting the n value of a composite propellant, e.g., the particle size distribution of the oxidant and the metallic fuel. Since all of the other parameters were kept constant in the preparation of the propellant samples the observed increase in the n -value with the increasing weight percentage of iron(III) oxide provides an additional access to tune the pressure dependence of the burning rate.

Conclusion

Two types of well characterized iron(III) oxides with different specific surface area were added to HTPB/AP propellant in various amount. The burning rate, viscosity and mechanical properties of the samples were measured and evaluated for studying the catalytic effect. The burning rate and the pressure exponent of the composite solid propellant increase with the increasing weight percentage of iron(III) oxide as anticipated. Furthermore the catalytic effect of iron(III) oxide on the burning rate of a HTPB/AP propellant was found to be dependent on the surface area of the catalyst. The catalysis has shown to proceed through an electron transfer process whereby the decomposition of the oxidant is activated. The contact of the oxidant with the iron(III) oxide particles is essential for the catalytic activity either in the solid or in the gaseous phase. Therefore increasing surface area of the catalyst enhances its activity.

References

- 1) K.Kishore and M.R.Sunitha, "Effect of Transition Metal Oxides on decomposition and Deflagration of Composite Solid Propellant Systems", AIAA Journal, 17, 1118-1119, (1979).
- 2) K.Kishore, V.R.Pai Verneker, and M.R.Sunitha, "Action of Transition Metal Oxides on Composite Solid Propellants", AIAA Journal, 18, 1404-1405, (1980).
- 3) K.K.Kuo, Fundamentals of Solid Propellant Combustion. progress in Astronautics and Aeronautics, Volume 90, AIAA, New York, 1984.
- 4) K.Kishore, V.R.Pai Verneker, and M.R.Sunitha, "Effect of Manganese dioxide on the thermal Decomposition of Ammonium Perchlorate", J.Applied Chemistry and Biotechnology, 27, 415-422 (1977).
- 5) W.Zhang, H.Zhu, R.Zhang, "Correlation Between Thermal Decomposition and Burning Rate in AP/HTPB Propellant", Int. Jahrestagung Fraunhofer Institut für Treib- und Explosivstoffe, 62, 1-6, (1991).
- 6) A.Langlet, R.Sanden, and H.Ostmark, "Study of the effect of Iron oxide on the degradation of HTPB by Mass Spectrometry", Int. Jahrestagung Fraunhofer Institut für Treib- und Explosivstoffe, 52, 1-8, (1991).
- 7) S. Krishnan, and R. Jeenu, "Combustion Characteristics of AP/HTPB Propellants with Burning Rate modifiers", J.Propulsion and Power, Vol. 8, (1992) 748-755.
- 8) S. Krishnan, and C.Periasamy, "Low-Pressure Burning of Catalyzed Composite Propellants", AIAA Journal, 24, 1670-1675 (1986).
- 9) A.L.Leu, and R.J.Wu, "Formulation Effects on The Burning Rate of Aluminized Solid Propellant", J.Propulsion, 4, 22-26 (1988).
- 10) T.K.Engen, and T.C.Johannessen, "The Effects of Two Types of Iron Oxide on The Burning Rate of A composite Propellant", in:H.Schubert, K.Menke (eds),

- "Technology of Polymer Compounds and Energetic Materials", Proceedings of 21st International Annual Conference of ICT, Karlsruhe, 82, 1-8, (1990).
- 11) C.H.Burnside, "Correlation of Ferric oxide Surface Area and propellant Burning Rate", AIAA paper, 75-234 (19759).
 - 12) Y.Rongjie, and M. Qingyun, "Catalytic Combustion of Ammonium Perchlorate", in: H.Schubert, K.Menke (eds), "Technology of Polymer Compounds and energetic Materials", Proceedings of 21st International Annual Conference of ICT, Karlsruhe, 82, 1-8, (1990). R.P.Rastogi, G.Singh, and B.L.Dubey, J. Catalysis, 65 (1980) 25.
 - 13) L.Sachs, Applied Statistics: A Handbook of Techniques, Second ed., Springer Verlag, New York, 1984.

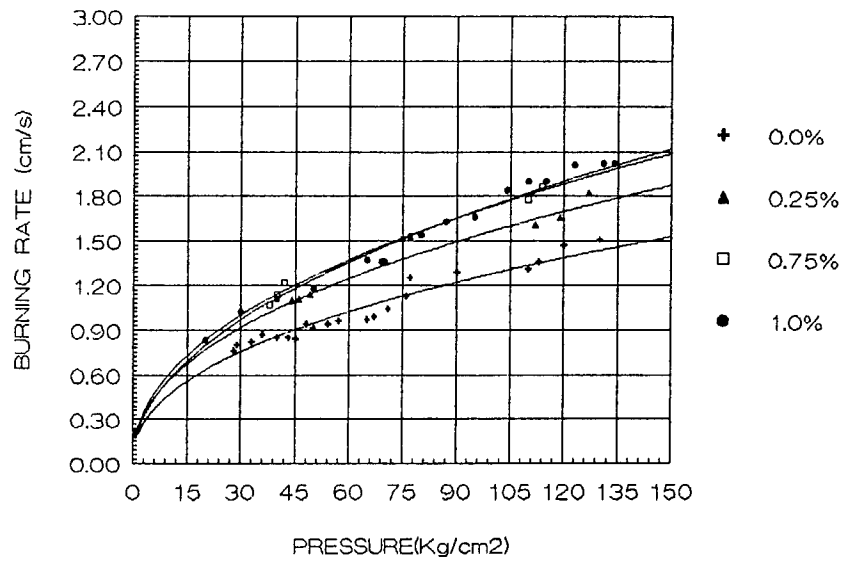


Figure 1 Burning Rate/Pressure curves for the propellant samples containing Fe₂O₃-M in various weight percentage.

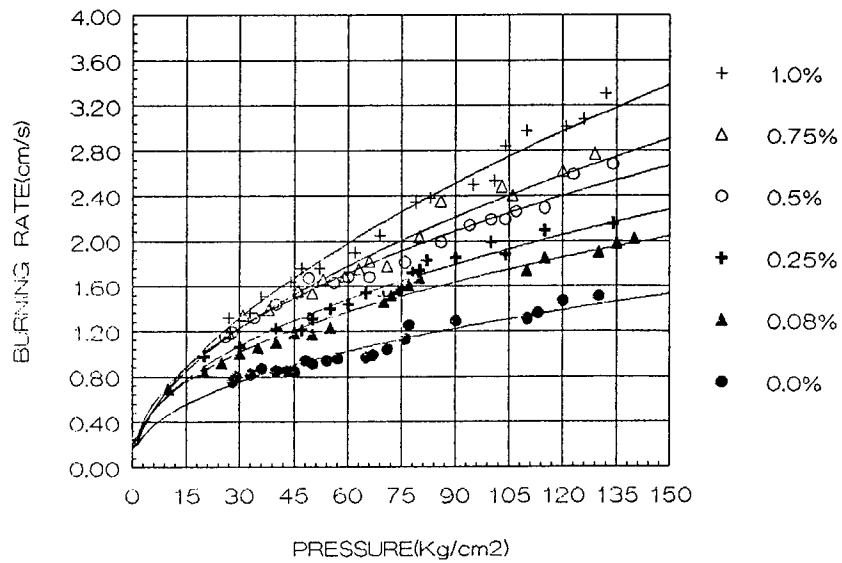


Figure 2 Burning Rate/Pressure curves for the propellant samples containing Fe₂O₃-B in various weight percentage.

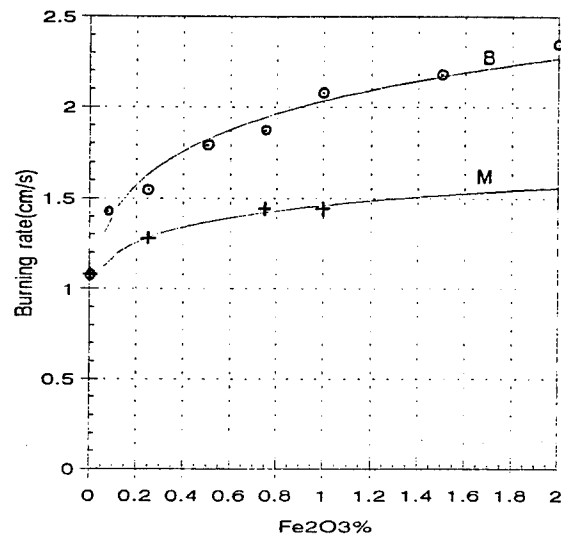


Figure 3 The Burning Rate as a function of the weight percentage of iron(III) oxide in the solid propellant at a constant pressure of 65 kg/cm².

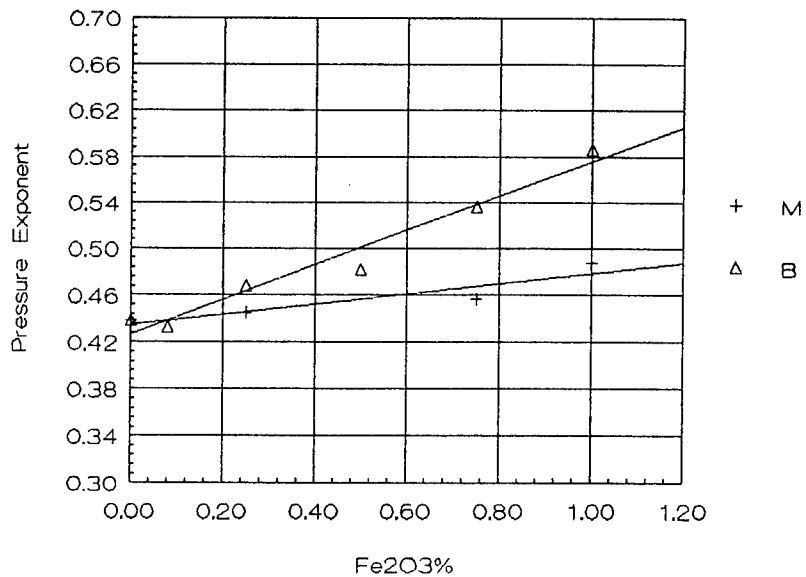


Figure 4 The pressure exponent as a function of the weight percentage of iron(III) oxide in the solid propellant.

IGNITION OF PYROTECHNICS SYSTEMS BY IRRADIATION

Igor G. ASSOVSII

Semenov Institute of Chemical Physics RAS

Kosygin St. 4, Moscow 117334, RUSSIA

E-mail: Assov@sms.ccas.msk.su

Fax: (7 095) 938 2156

The purpose of this review paper is an analysis of critical phenomena by interaction of pyrotechnics systems with polychromatic or monochromatic pulse-irradiation. The role of absorbing microinclusions or optical discontinuities is considered. Emphasis is placed on determining the critical conditions of the ignition by laser-pulse irradiation of propellants and explosives. The work is based on the theoretical ideas of [1,2] as well as on publicized experimental results.

A critical relationship between the reaction rate constants of the flammable substance and the characteristics of irradiation is proposed for determination of the interaction thermal regime and the ignition possibility. Specific features of ignition and subsequent combustion induced by laser-pulse irradiation is considered for optically uniform and non-uniform pyrotechnic systems. The stable ignition region on the 'pulse time'- 'flux intensity' plane has the shape of a peninsula. Its boundaries are defined by kinetics of thermal decomposition of system and by the system combustion low.

It is shown that absorbing particles can significantly influence the boundaries of the stable ignition peninsula if the particle diameter exceeds the critical one. This critical diameter depends on initial temperature and reaction rate constants as on radiation intensity. It is directly proportional to the characteristic space-scale of reaction zone in the system. The product of the particle critical diameter and the radiation intensity is approximately constant.

It is also shown that continuous irradiation of pyrotechnic system can induce the system ignition if the laser-beam diameter exceeds the critical one. This critical diameter depends on radiation intensity and on thermochemical characteristics of system.

The main results of consideration are illustrated by instances with NC-propellants, HMX, RDX, and lead azide.

1. I.G. Assovskii, Doklady Phys. Chem., Proc. RAS, Vol. 337, No. 6, (1994).
2. I.G. Assovskii and Z.G. Zakirov, Proc. 25th Intern. Symp. on Combustion, The Comb. Institute, 1994.

**THE INVERSION OF THE QUALITY OF RATIOS IN THE SYSTEM OF
INDEPENDENT CHEMICAL REACTIONS AT TRANSFER FROM ISOTHERMAL
HOLDING TO COMBUSTION.**

Valentin Klyucharev, Alla Razumova.

Institute of New Chemical Problems, Russian Academy of Science.
142432, Chernogolovka, Russia.

ABSTRACT

The transfer from isothermal to nonisothermal conditions can lead to the inversion of the quality of ratios in the system of independent chemical reactions. At the same components and contents, over the same temperature range, at the same one-sided position of the range with respect to isokinetic point, at the total conservation of the chemical reactions mechanisms, the same substance can act solely as a catalyst under isothermal conditions and as a inhibitor under nonisothermal conditions. The experiments show the availability of such switch in medium of perchlorates and chlorates with oxides and peroxides even if the heating rate is $2.5-10^{\circ}\text{C/min}$.

The customary set of active components exerting an effect on the O_2 evolving from perchlorates and chlorates incorporates MnO_2 , Fe_2O_3 , Co_2O_3 , NiO , CuO , Cu_2O , CaO [1-10], CaO [11], BaO [12,13], Li_2O [14-16], Na_2O [17,18], K_2O [19]. The modern-day theory treats these substances as catalysts for the degradation of the salts. However, in pyrotechnic gasgenerating sources containing a perchlorate or chlorate with a metal fuel, oxide and peroxide can promote and can retard the burning rate [20-24]. These results make very difficult the application of existing systematized knowledge in order to forecast the real effects of chemical agents on combustion.

Discussing the problem, Glazkova [23-24] pointed out that the known experimental data on the reactivity of the substances were obtained either at low heating rate ($10-50^{\circ}\text{C/min}$) or under

isothermal conditions at low temperatures. On the contrary, a thermoshock or very high temperatures often take place at combustion. As a consequence, the ignored transfer over isokinetic point or a discrepancy between reaction mechanisms give rise to mistaken forecasts.

The explanation for the known evidence offered by Glazkova is of chemical interest, however calls into question the use of thermal analysis in studies of combustion [24,25].

The paper presents just one more possibility to retard the reaction rate by catalysts, which is not connected with added changes of mechanisms or transfer over isokinetic point, in going from isothermal holding to heating.

The problem can be specified by giving a ideal object, for example a system of chemical processes with Arrhenius kinetics proceeding independently of one another.

Let us assume that the starting components, final products and mechanisms of the chemical conversions are constant. The fundamental equation of nonisothermal kinetics [11-13] will be considered to take place for all reactions. In the case:

$$K_i = A_i \exp (-E_i/RT) \quad (1)$$

at constant temperature and

$$K_i = A_i \exp [-E_i/R(T_0 + vt)] \quad (1a)$$

at linear heating with constant rate v , where i , K , A , E , t , T , T_0 , R are the number, the rate constant, the activation energy, the pre-exponential factor of the chemical reactions, time, temperature, the initial temperature of heating, the universal gas constant, respectively.

The growth of K in the sequence

$$K_{i+1} > K_i \quad (2)$$

will be denoted the catalysis.

As a simplification, assume that the relationship A_i vs. E_i is defined in the following manner:

$$\ln (A_i) = bE_i, \text{ where } b = \text{const} > 0 \quad (3)$$

In the case

$$K_i = \exp \left[\frac{(bRT - 1)E_i}{RT} \right] \quad (4)$$

and

$$\frac{dK_i}{dE_i} = \exp \left[\frac{(bRT - 1)E_i}{RT} \right] * \frac{bRT - 1}{RT} \quad (5)$$

For $bRT - 1 = 0$, the condition

$$b = 1/RT \text{ or } T = 1/bR \quad (6)$$

defines the isokinetic point, in which the value of K_i is constant with any frequency of E_i . When $bRT - 1 > 0$, then taking into account $b > 0$ (3), $R > 0$, $T > 0$, it turns out that

$$b > 1/RT \text{ or } T > 1/bR \quad (7)$$

and any elevation of E_i increases the K_i . If $bRT - 1 < 0$ then

$$b < 1/RT \text{ or } T < 1/bR \quad (8)$$

and any fall of E_i brings about a rise of the K_i .

Together with (2) the conditions (7) and (8) define the advent of a catalysis if the activation energy, in the considered system of the chemical reactions, elevates or falls. By force of habit to connect a catalytic action to a decrease of activation energy [29], the following analysis has been made with reference to inequalities (8).

Let us consider the same chemical reactions (1 and 1a), (3), (4), (8) at linear heating, that is under conditions which are usually for differential thermal analysis (DTA). With (3) it turns out that

$$K_1 = \frac{\exp \{ [bR(T_0 + vt) - 1] E_1 \}}{R(T_0 + vt)} \quad (9)$$

Insight into the chemical aspect of a process in which the source materials pass into products gives the time of the conversion for every step of the interaction between reagents [11]. For its specific estimation, and consequently the estimation of chemical significance of different properties inherent in function $K = f(E)$, the start and finish points of the process are to be determined, reasoning from particular constraints.

Every so often, in nonisothermal experiments the onset of chemical conversion, in fact, has been referred to the start of heating in a furnace. Only in the case a temperature shift of a chemical process under nonisothermal conditions can be treated as the sign of a positive or negative catalysis [1-10, 12, 14, 20-24]. However, the approach is able to give misinterpretations of experimental data, because the time of heating and the time of chemical reaction can be attributed to processes very different by its nature [11, 28, 30, 31]. Besides, the statement that a reaction takes place all along, if the temperature of reacting species is above 0oK, makes no particular sense [32].

In this work, the estimation of chemical significance of different changes in the pre-exponential factor and the activation energy was carried out by the data given: the reference and ultimate degree of conversion were 0.01 and 0.99 respectively. The approach allows to determine the time of reagents interactions with regard to the significance of the chemical event [32].

Let us explain, the selection of the part from unity does not signify to overlook all history of a sample; it merely takes down the rigorous correspondence between the structure of a process and the structure of the time, which is generated by the process [33,34].

The calculated values of conversion time can be obtained at the estimation of the integral (10) by Simpson method

$$\int_0^t \frac{C * \exp \{ [bR(T_0 + v_t) - 1] E_i \}}{R(T_0 + vt)} dt \quad (10)$$

for the system of first order reactions, requirement that the condition (9) is met. C is calibrating coefficient. The result is presented in Table 1.

In the numerical experiments, at heating rate $10^\circ\text{C}/\text{min}$, the initial temperature was 173.15°K (-100°C). From the time of conversion at $b = 3.933 \cdot 10^{-4}$, $C = 0.01$ (Table 1, column 6) it will be obvious that the temperature (Table 1, column 5) lies below that of isokinetic point $T_z = 1273^\circ\text{K}$ (equation 6). It follows that the conditions (8) should be met. For example, if the observable temperature $T = 773.15^\circ\text{K}$, then $b = 6.477 \cdot 10^{-4}$. Hence the accepted value $b = 3.933 \cdot 10^{-4} < 6.477 \cdot 10^{-4} = 1/RT$ at $T = 773.15^\circ\text{K}$ and the inequality (8) is true. The fulfilment of the condition (8) implies that on isothermal holding the elevation of E leads to the rise of conversion time.

The calculated values of conversion time on heating, however show, beginning in certain values of activation energy E_i , the inversion of the quality of ratios arises in considered k system of independent chemical reactions.

If $E_i < E_k$ then with elevation E , $E_{i+1} > E_k$, the times of conversion match up to one another as follows: $t(E_{i+1}) > t(E_k)$. (Table 1, column 6.), that is to say in the same fashion as for isothermal holding.

If $E_i > E_k$ then the relations between E remain as before ($E_i > E_k$), however, the quality of ratios can be changed: $t(E_{i+1}) < t(E_k)$. (Table 1, column 6.)

The obtained result indicate: at the same components and contents, over the same temperature range, at the same one-sided position of the range with respect to isokinetic point, at the total conservation of the chemical reactions mechanisms, the same substance can act solely as a catalyst under isothermal and as a inhibitor under nonisothermal conditions [30,31].

The experiments show the availability of like switch in medium of perchlorates and chlorates with oxides and peroxides, even if the heating rate is $2.5-10^\circ\text{C}/\text{min}$. The Fig. 1 presents the mixture KClO_4 with NiO . The $0.01 - 0.015 \text{ M NiO}$ as a dope to the perchlorate 4 increases the temperature range of rapid oxygen evolution about 2 times: from $600-650^\circ\text{C}$ for KClO_4 , to $500-610^\circ\text{C}$ for KClO_4 with NiO . The $0.07 - 0.08 \text{ M CaO}$ in KClO_4 2 retards the process about 2 times too (Fig. 2). By this means, 4 the oxide additives can act as inhibitors for breakdown of perchlorate salt under nonisothermal conditions, despite the fact that on standing at constant temperature in range $450-550^\circ\text{C}$ these substances promote the oxygen evolution. A similar result had been obtained for KClO_4 with Fe_2O_3 [35], BaO , and for binary mixtures of the other alkali metal perchlorates.

The possibility of a correlation between changes of the last step of salt oxidizer decomposition going with highest rate in DTA experiments for NaClO_4 with CaO at $10^\circ\text{C}/\text{min}$, and changes of the burning rate in compacted mixtures with $2 - 2.3 \text{ g/cm}^3$ of these substances and metal Mg was studied for the materials with $65 - 100 \text{ mk}$ for all components. The tests shown that the rates of the decomposition and the burning have a minimum at molar ratio $\text{CaO}/\text{NaClO}_4$ about $0.13 - 0.15$. At this takes place, a maximum temperature of combustion was seen over the region. (The temperature for the heterogeneous system was determined by thermocouples as a arithmetic mean value from $10 - 17$ runs.

The revealed chemical switch or changer, based on the inversion of the quality of ratios in the system of independent chemical reactions at transfer from isothermal holding to combustion, in all probability, will have a strong impact on the choices of approaches to the solution of problems in chemical engineering. It should be remarked, that at this takes place, the case of point is not only the self-propagating processes or pyrotechnic materials. The change in the classification of substances as catalysts and inhibitors can influence on views about the biochemical activity or ecological safety of chemical agents in nature.

This work was carried out by financial backing of International Science Foundation (Grant N9K 000) and Department of Science and Scientific Politics of RF. We are indebted to Dr. I.B.Kudinov (Kurnakov's Inst. of Inorg. Chem., Moscow) and Dr. G.I.Nikishin (Zelinskii's Inst. of Org. Chem., Moscow) for helpful discussion and support.

REFERENCES

1. S.Yamamoto, T.Asaba, Kogyo Kayaku, **1952**, 13, 235.
2. W.K.Rudloff, E.S.Freeman, J. Phys. Chem., **1970**, 74, 3317.
3. M.Shimokawabe, R.Furuichi, T.Ishii, Thermochim. Acta, **1977**, 20, 347.
4. L.W.Collins, Inorg. Chim. Acta, **1980**, 39, 53.

5. T.Nagaishi, J.Yoshimura, M.Matsumoto, S.Yoshinaga, Kyushu Sangyo Daigaku Kogakubu Kenkyu Hokoku, **1981**, 18, 19.
6. S.Morishima, H.Iwakura, N.Kakuta, Nippon Kagaku Kaishi, **1991**, 1172.
7. H.Iwakura, N.Kakuta, A.Ueno, K.Kishi, J.Kato Ind. ang Eng. Chem. Res., **1991**, 30, 778.
8. Y.C.Zhang, G.Kshirsagar, J.E.Ellison, J.C.Cannon, Ind. and Eng. Chem. Res., **1993**, 30, 2863.
9. Y.C.Zhang, G.Khirsagar, J.E.Ellison, J.C.Cannon, Thermochim. Acta, **1993**, 228, 147.
10. J.C.Cannon, Y.C.Zhang, J. Thermal. Anal., **1994**, 41, 981.
11. V.V.Klyucharev, A.P.Razumova, S.V.Karachinskii, I.V.Solopov Inorg. Mater., **1995**, 31, 111.
12. Y.C.Zhang, G.Kshirsagar, J.C.Cannon, Ind. and Eng. Chem. Res., **1993**, 32, 966.
13. Z.K.Nikitina, V.Ya.Rosolovskii, Zh. Inorg. Chem., **1993**, 38, 1465.
14. M.M.Markowitz, D.A.Boryta, J. Phys. Chem., **1965**, 69, 1114.
15. D.G.Lemesheva, V.Ya.Rosolovskii, Zh. Inorg. Chem. **1977**, 23, 2055.
16. Y.C.Zhang, J.C.Cannon, PCT Int. WO 93.17.962 from 16.09.**1993**.
17. T.L.Thompson, Pat. Ger. DE 2.142.185, from 02.03.**1972**.
18. Z.K.Nikitina, V.Ya.Rosolovskii, Zh. Inorg. Chem., **1989**, 34, 322.
19. Z.K.Nikitina, A.I.Karelin, V.Ya.Rosolovskii, Zh. Inorg. Chem. **1991**, 36, 3063.
20. G.B.Northam, G.L.Pellet, W.R.Cofer, AIAA J., **1972**, 10, 1068.
22. N.N.Bakhman, V.S.Nikiforov, V.I.Avdyunin, A.E.Fogelzang, Yu.S.Kichin, Comb. and Flames, **1974**, 22, 77.
23. A.P.Glazkova, AIAA J., **1975**, 13, 438.
24. A.P.Glazkova, The Catalysis of the Explosive Substances Combustion. M.: Nauka. 1976. Pp. 179-181, 201, 230, 248 (in Rus.).
25. L.H.Caveni, C.U.Pittman, AIAA J., **1968**, 6, 1461.
26. W.W.Wendland, Thermal Methods of Analysis. M.: Mir. 1977. (In Rus.)

27. Ya. Sestak, Theory of Thermal Analysis. M.: Mir. 1987.
(In Rus.)
28. V.V.Klyucharev, A.P.Razumova, V.V.Aleshin, Inorg. Mater.,
1994, 30, 421.
29. V.A.Kireev, Handbook of Physical Chemistry. M.: Khimiya.
1975. P.668. (in Rus.)
30. V.V.Klyucharev, A.P.Razumova, in Actual Problems of the
Fundamental Sci., V.5. Chemistry. M.: MGTU. P.11. (in Rus.)
31. V.V.Klyucharev, A.P.Razumova, in Workshop of the 10th
Congress on Thermal Analysis. Hatfield. ICTA. 1992. P.107.
32. M.G.Slinko, Izv. Vyssh. Ucheb. Zav. (Khim. and Khim.
Tech.), **1993**, 36, (N.10), 3.
33. L.N.Gumilev, Doklady Otdelenii i Komissii Geograficheskogo
Obshchestva SSSR, **1970**, (N.15), 143.
34. I.A.Grudzinskaya, Dokl. Ac. Sci. Rus., **1993**, 329, 802.
35. V.V.Klyucharev, A.P.Razumova, V.D.Sasnovskaya, in Thes. of
the 11th Conf. on Thermal Analysis. Samara.: SGTU. 1993.
P.71. (in Rus.)

Table 1.

$v = 10^{\circ}\text{C}/\text{min.}$ $b = 3.933 \cdot 10^{-4},$ $C = 0.01.$ $T_z = 1273.15^{\circ}\text{K.}$					
E kkal	t(ons)	T(ons) $^{\circ}\text{C}$	t(end)	T(end) $^{\circ}\text{C}$	Tau min
30000	69.08	590.8	108.22	982.2	39.14
20000	56.72	467.3	103.28	932.8	46.56
12500	41.91	319.1	94.51	845.1	52.60
8000	28.68	186.8	83.36	733.6	54.68
5000	16.68	66.8	69.65	596.5	52.97
2000	1.83	-81.7	42.76	327.6	40.93
$v = 10^{\circ}\text{C}/\text{min.}$ $b = 8.737 \cdot 10^{-4},$ $C = 0.01.$ $T_z = 573.15^{\circ}\text{K.}$					
E kkal	t(ons)	T(ons) $^{\circ}\text{C}$	t(end)	T(end) $^{\circ}\text{C}$	Tau min
30000	31.36	216.1	42.82	328.2	11.46
25000	30.02	200.2	42.91	329.2	12.89
20000	27.81	178.1	42.95	329.5	15.14
15000	24.55	145.5	42.78	327.8	18.23
7000	14.27	42.7	40.41	304.1	26.14
6000	12.08	20.8	39.48	294.8	27.40
5000	9.51	- 4.9	38.16	281.6	28.65
3000	3.22	- 67.8	33.26	232.6	30.04
2000	0.82	- 91.8	28.43	184.3	27.61
$v = 10^{\circ}\text{C}/\text{min.}$ $b = 1.833 \cdot 10^{-3},$ $C = 0.01.$ $T_z = 273.15^{\circ}\text{K.}$					
E kkal	t(ons)	T(ons) $^{\circ}\text{C}$	t(end)	T(end) $^{\circ}\text{C}$	Tau min
30000	8.48	- 15.2	11.40	14.0	2.92
25000	8.12	- 18.8	11.57	15.7	3.45
20000	7.58	- 24.2	11.79	17.9	4.21
15000	6.71	- 32.9	12.11	21.1	5.40
10000	5.10	- 49.0	12.35	25.5	7.25
5000	1.64	- 83.6	13.09	30.9	11.45
3000	0.36	- 96.4	12.98	29.8	12.62
2000	0.13	- 98.7	12.45	24.5	12.32

E is activation energy; **t(ons)**, **T(ons)** are the time in min. and the temperature in $^{\circ}\text{C}$, at which the degree of the chemical conversion runs to 0.01, respectively; **t(end)**, **T(end)** are the time in min. and the temperature in $^{\circ}\text{C}$, at which the degree of the chemical conversion runs to 0.99; **Tau** is the time in min. of the chemical conversion from 0.01 degree to 0.99 degree.

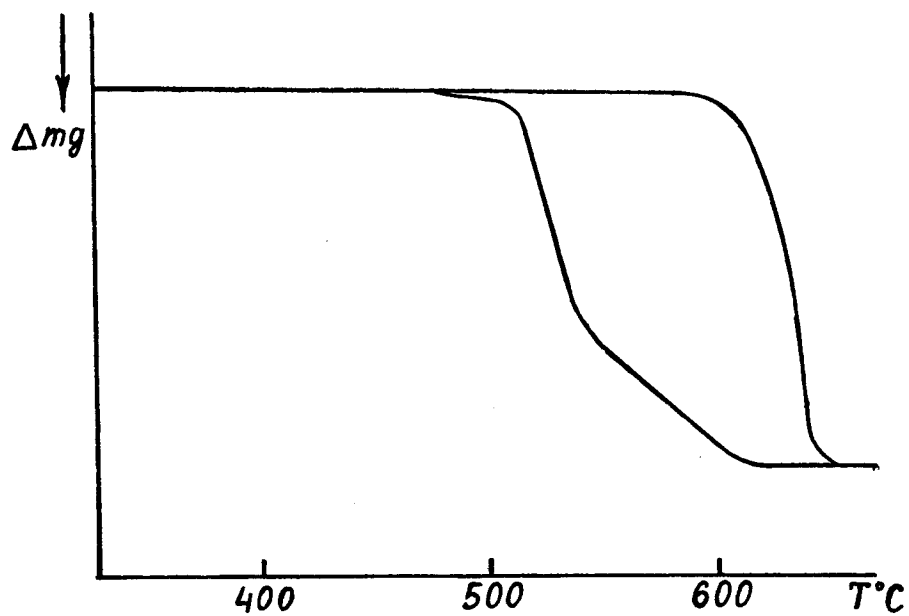


Figure 1.

- A). TGA profile of pure sodium perchlorate
- B). TGA profile of sodium perchlorate with nickel oxide at mol. ratio 1 NaClO_4 - 0.01 NiO .

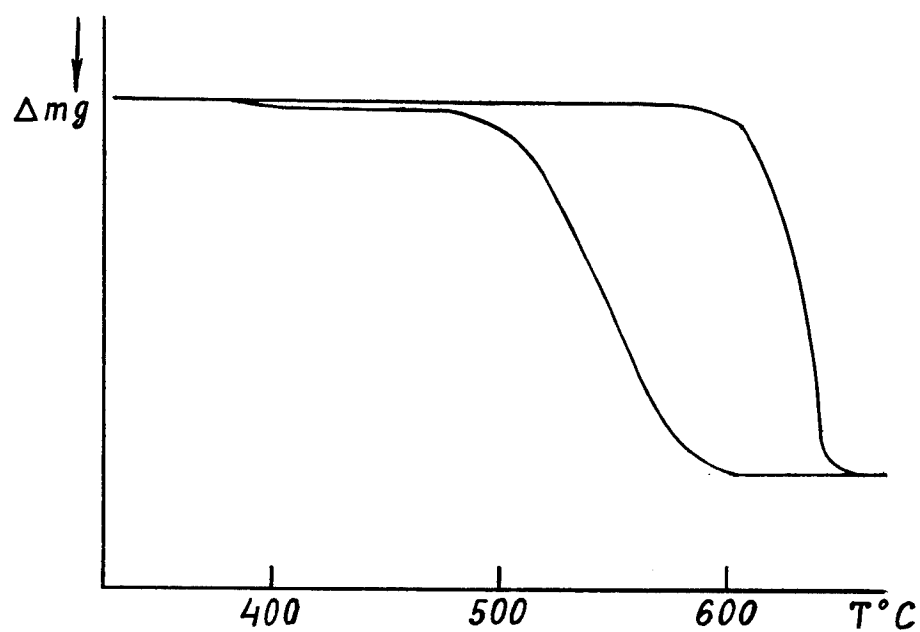


Figure 2.

- A). TGA profile of pure sodium perchlorate.
- B). TGA profile of sodium perchlorate with calcium peroxide at mol. ratio $1 \text{ NaClO}_4 - 0.08 \text{ CaO}_2$.

THE COOPERATIVE PROCESSES OF MAGNESIUM OXIDATION IN PERCHLORATE MIXTURES WITH OXIDE.

Valentin Klyucharev, Stanislav Sinelnikov, Alla Razumova, Valentina Sasnovskaya.

Institute of New Chemical Problems, Russian Academy of Science.
142432, Moscow Region, Chernogolovka, RUSSIA.

ABSTRACT

The particular cooperative reaction of oxygen evolution from perchlorate source with simultaneous oxidation of metal fuel, in the system of three bodies, was made out in ternary mixtures of magnesium, perchlorates and calcium oxide. The reaction allows to increase the degree of low-temperature burning of the fuel and to decrease the specific heat value of pyrochemical oxygen candles.

For production of high-quality oxygen by SHS must be afforded a sufficient yield, cleanness, time of synthesis and economical consumption of energy. On many occasions, the solution of the problems is determined by conditions of metal fuel oxidation in combustion front of perchlorate or chlorate candle. The paper presents the magnesium's investigations which were undertaken in order to increase the degree of metal conversion into oxide at once in the front.

The reactivity of substances was made by "Derivatograph Q1500D" thermal analyzer in alundum or quartz cylindrical tubes at heating rates from 2.5 to 10°C/min. The experimental procedure was described in [1,2].

The combustion was studied in air for cylindrical blocks with diameter 28-30 mm and height 40-60 mm.

The powders were analyzed with DRON-3M-INKHP X-ray diffractometer and UR-20 IR-spectrometer [1,2].

The metal magnesium particles had diameters about 2 mk.

The sodium and potassium perchlorates was prepared by double recrystallization from distilled water and dried as noted in [1,2]. The calcium oxide was introduced from the peroxide as a precursor [1,2].

The Table 1, (N.3,4) and Table 2, (N.1,2) present the catalytic effect of CaO_2 on sodium perchlorate and potassium perchlorate decomposition.

The experiments with CaO_2 and Mg at $10^\circ\text{C}/\text{min}$ showed that the endothermic oxygen evolution and CaO formation occurred at $360\text{--}430^\circ\text{C}$, the Mg burnt after $580\text{--}590^\circ\text{C}$ (Table 1, N.1). A like picture is in system NaCl-Mg-CaO_2 (Table 1, N.2). In the case, the magnesium oxidation came into prominence about 520°C , next was gradually speeded up, however after the complete oxygen evolution from peroxide.

The binary mixtures of Mg with NaClO_4 and KClO_4 liberate the O_2 at lesser temperature than the pure perchlorate⁴. However, the complete burning of metal can occur after final salt breakdown (for example at $540\text{--}570^\circ\text{C}$) and indicate just one more exoeffect at $600\text{--}650^\circ\text{C}$ (Fig. 1, Table 1, N.5; Table 2, N.3). The result was obtained in alundum crucible.

The binary mixtures of sodium perchlorate and metal magnesium, in some DTA and TGA tests, were analyzed in quartz tubes. The experiments are caused by Freeman e.a. [3], which had conducted a research in the Vicor glass.

Our experiments showed that the SiO_2 had effect on reactivity of substances in binary mixtures of the NaClO_4 and the metal magnesium (Table 1, N.5,12-13). Moreover, at mol. ratio 4 M Mg / 1 M NaClO_4 the complete evolution of four oxygen gram-atoms are observed at $440\text{--}480^\circ\text{C}$. It is clear, in the case the process occurs without the appreciable oxidation of the Mg by melts of perchlorate or perchlorate with chlorate and chloride.

The effect of quartz glass on reactivity of Mg in perchlorate mixtures is attributable to formation of chemical compounds at the metal surface. An attack of reaction products in SiO₂ tubes by hydrochloric acid solution we observe a garlicky explosive gas, evoking headache. It is usual behaviour of silanes. Thus, following experiments have been carried out in alundum dish.

When CaO₂ is added to mixture containing NaClO₄ and Mg, a new low-temperature process take place at 420-460°C (Fig. 2-4 and Table 1, N.6-11) which can afford complete oxidation of fuel with simultaneous O₂ evolution containing in the salt source. The process exists only in ternary mixtures, consequently it is a cooperative reaction. Its ΔT (temperature range) is below the ΔT of the decomposition for binary samples of NaClO₄ with equimolar content of CaO₂ (after 430-450°C, Table 1, N.4) and much below the ΔT of complete Mg oxidation in binary mixtures with CaO₂ or NaClO₄ (after 590°C, Table 1, N.1,5). A similar reaction is in system KClO₄-Mg-CaO₂ (Table 2).

Degree of Mg conversion at the cooperative process depends on the relationship of the all three components.

The DTA profiles show that the perchlorate addition at constant Mg/CaO₂ ratio increases the first exothermic peak corresponding to the metal oxidation with simultaneous oxygen evolution. In the mixture contained 0.125 M NaClO₄ (Fig. 2) the heat evolving at 410-425°C is very small. In going from the composition to ternary mixtures contained 0.5 - 1.0 M NaClO₄ (Fig. 3) the area ratio between the first and second peaks can turn approximately equal to one. For systems: 0.5 M NaClO₄ - 0.5 M Mg - 1 M CaO₂ and 1 M NaClO₄ - 0.5 M Mg - 1 M CaO₂ the heat of perchlorate conversion to chloride and oxygen is about 2.5 - 6 kkal/mol (8.4-25.1 kJ/mol) [4]. The Mg conversion to MgO evolves 0.5*141 = 70.5 kkal/mol (295.4 kJ/mol) [4]. This result reports that the magnesium oxidation gives alms to the first exoeffect. The loaded sodium perchlorate increases the contribution of fuel oxidation to heat evolving at cooperative stage. The first and second exothermic peak are connected with magnesium oxidation.

The data in Fig. 4 and Table 1, N.10,11 give evidence that the low temperature exothermic process in the ternary mixtures can be complex. The first peak is composed of two overlapped effects with maximums about 435°C and $466-474^{\circ}\text{C}$. It is quite possible that the different, cooperative and catalytic decomposition of the salt oxygen source take place in the ternary mixtures.

The degree of magnesium conversion is a function of peroxide content. The increase of CaO_2 in initial samples can favour or hinder the low temperature cooperative stage of Mg oxidation (Table 2). Doping the binary mixtures by the peroxide from the molar ratio $\text{CaO}_2/\text{KClO}_4 = 0.05$ to 0.12 decreases the part of metal which burns out in oxygen after 600°C . At 0.12 , the Mg is complete oxidized in the low-temperature cooperative stage. However, the dose of the CaO_2 from 0.13 to 0.5 throws away the metal at high temperatures. The transfers between 0.1 and 0.13 M CaO_2 vs. 1 M KClO_4 agrees with singular point which had been observed in binary systems of the perchlorate and oxides [5].

The consideration of the magnesium characteristic properties allows to develop the cartridges which generate oxygen with lesser heat-evolving, temperature or rate of combustion. The decrease of the minimal content of metal as a fuel, by increasing the part of a peroxide, had been presented in paper [6]. The authors [7] detected an cooperative action in system barium nitrate, metal magnesium in presence of BaO . In the case it has been found that the oxidation of Mg about 80°C in humid air proceeds with largest rate if all components exist jointly. The results obtained for the ternary mixtures of perchlorates, suggest the unified nature of the effects [6,7] which can be attributed to specific low temperature cooperative reaction between the salt oxidizers, a metal and oxides or peroxides.

This work was carried out by financial backing of International Science Foundation (Grant N9K 000) and Department of Science and Scientific Politics of RF. We are indebted to Dr. I.B.Kudinov (Kurnakov's Inst. of Inorg. Chem., Moscow) and Dr. G.I.Nikishin (Zelinskii's Inst. of Org. Chem., Moscow) for helpful discussion and support.

REFERENCES

1. V.Klyucharev, S.Sinelnikov, A.Razumova, V.Sasnovskaya, in 26th Int. Annual Conf. of Fraunhofer-Inst. f'r Chem. Technologie. July 4 - July 7, 1995.
2. V.V.Klyucharev, A.P.Razumova, S.V.Karachinskii, I.V.Solopov Inorg. Mater., **1995**, 31, 111.
3. E.S.Freeman, V.D.Hogan, D.A.Anderson, Comb. and Flames, **1965**, 9, 19.
4. Thermal Constants of Substances, Ed. V.P.Glushko, V.9-10, M.: VINITI, 1981. (In Rus.)
5. V.V.Klyucharev, S.M.Sinelnikov, A.P.Razumova, E.S.Rumyantsev, in Thes. of the 10th Allunion Conf. on Kinetics and Mechanism of Chemical Reactions in Solids. V.2. Chernogolovka.: OIKHF. 1989. P.106. (In Rus.)
6. W.H.Schechter, R.R.Miller, R.M.Bovard, C.B.Jackson, J.R.Pappenheimer, Industr. and Engin. Chem., **1950**, 42 2348.
7. D.Barisin, I.Spasojevich, I.Batinic-Haberle, R.Ferko, Proc. of the Pyrotech. Seminar. **1991**, 16, 107.

Table 1.

Number of sample	Mixtures (mol. ratio)	Temperature °C					
		I	II	III	IV	V	VI
1	Mg-CaO ₂ (0.5/1)	---	---	---	---	584	602
2	NaCl-Mg-CaO ₂ (5/0.5/1)	---	---	---	---	570	578
3	NaClO ₄	---	---	529	582	---	---
4	NaClO ₄ -CaO ₂ (1/0.5)	---	---	447	502	---	---
5	NaClO ₄ -Mg (1/0.5) [in alundum]	---	---	457	540	572	600
6	NaClO ₄ -Mg-CaO ₂ (0.125/0.5/1)	410	422	410	422	556	very high
7	NaClO ₄ -Mg-CaO ₂ (0.2/0.5/1)	415	441	415	441	546	very high
8	NaClO ₄ -Mg-CaO ₂ (0.5/0.5/1)	415	439	415	439	[500]	[570]
9	NaClO ₄ -Mg-CaO ₂ (1/0.5/1)	415	441	415	441	[500]	[560]
10	NaClO ₄ -Mg-CaO ₂ (1.7/0.5/0.9)	420	434	420	466	[520]	[584]
11	NaClO ₄ -Mg-CaO ₂ (5/0.5/1)	374	433	374	474	610	626
12	NaClO ₄ -Mg (1/0.5) [in quartz]	---	---	457	482	507	558
13	NaClO ₄ -Mg (1/4) [in quartz]	---	---	440	462	---	---

- I.) Start of the cooperative reaction of simultaneous Mg combustion and salt oxidizing agent decomposition.
 II.) Exothermic peak of the cooperative reaction.
 III.) Start of the oxygen exothermic evolution from perchlorate oxidizer.
 IV.) Exothermic peak of the evolution.
 V.) Start of the magnesium oxidation (combustion) in evolved oxygen. [In brackets: oxidation with no ignition.]
 VI.) Exothermic peak of the oxidation.

Table 2.

Number of sample	Mixtures (mol. ratio)	Temperature °C					
		I	II	III	IV	V	VI
1	KClO ₄	---	---	609	646	---	---
2	KClO ₄ -CaO ₂ (1/0.1)	---	---	560	610	---	---
3	KClO ₄ -Mg (1/0.5)	---	---	537	570	640	646
4	KClO ₄ -Mg-CaO ₂ (1/0.4/0.05)	505	525	505	525	630	640
5	KClO ₄ -Mg-CaO ₂ (1/0.4/0.1)	485	510	485	510	---	---
6	KClO ₄ -Mg-CaO ₂ (1/0.4/0.13)	496	527	496	527	640	650

The designations are in accord with table 1.

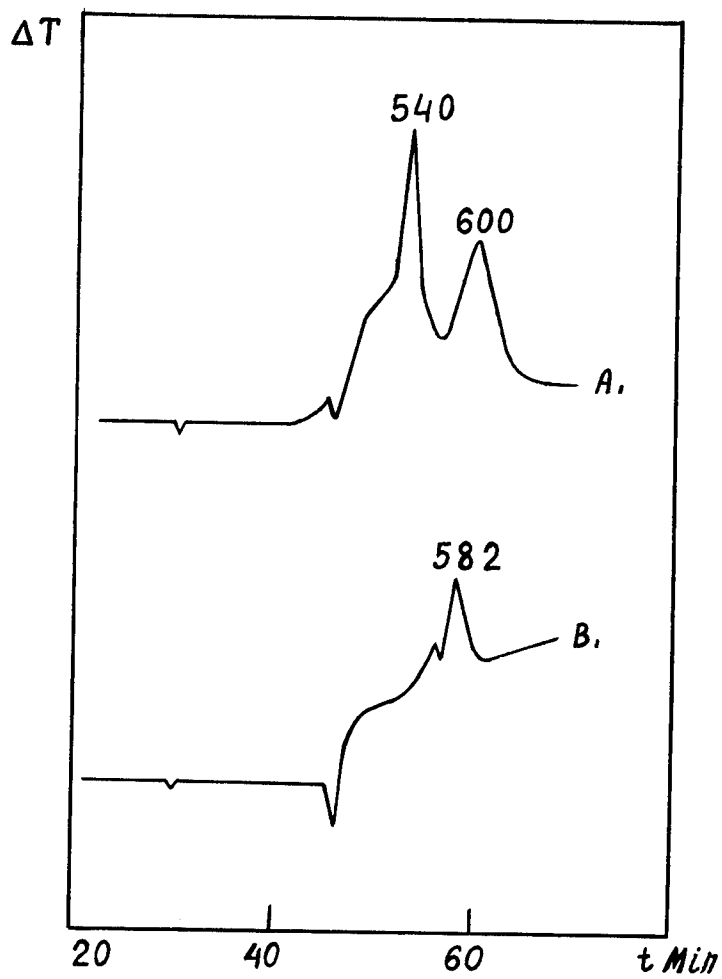


Figure 1.

A). The DTA profile of sodium perchlorate and metal magnesium binary mixture at mol. ratio 0.5 Mg - 1 NaClO₄.

B). The DTA profile of sodium perchlorate.

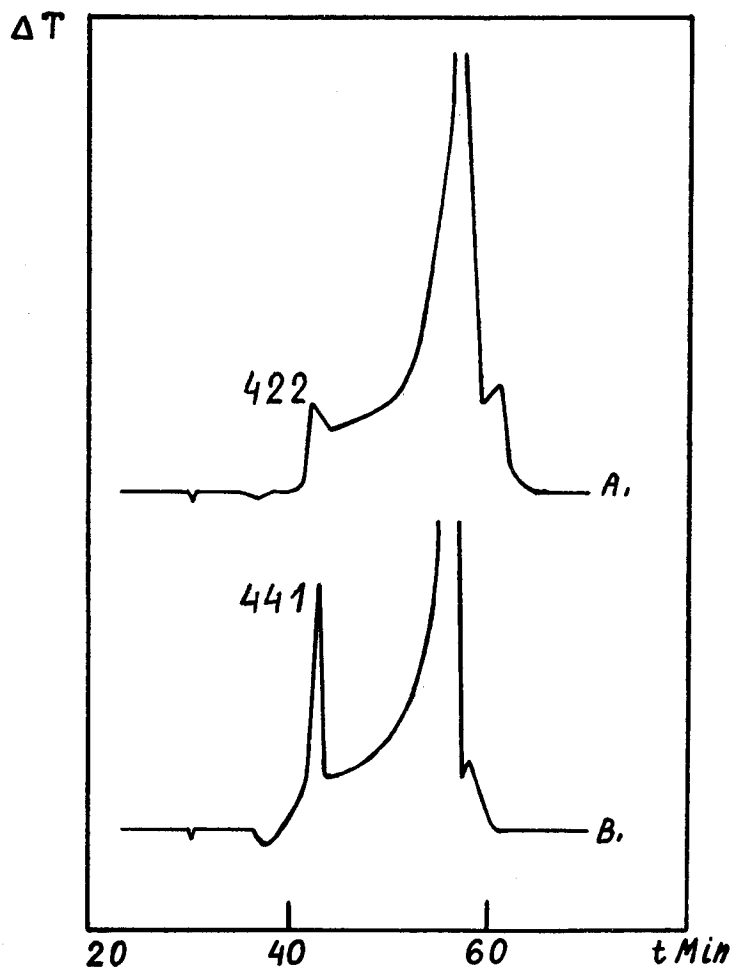


Figure 2.

- A). DTA profile of sodium perchlorate metal magnesium and calcium peroxide ternary mixture at mol. ratio $0.125 \text{ NaClO}_4 - 0.5 \text{ Mg} - 1 \text{ CaO}_2$.
- B). DTA profile of sodium perchlorate metal magnesium and calcium peroxide ternary mixture at mol. ratio $0.2 \text{ NaClO}_4 - 0.5 \text{ Mg} - 1 \text{ CaO}_2$.

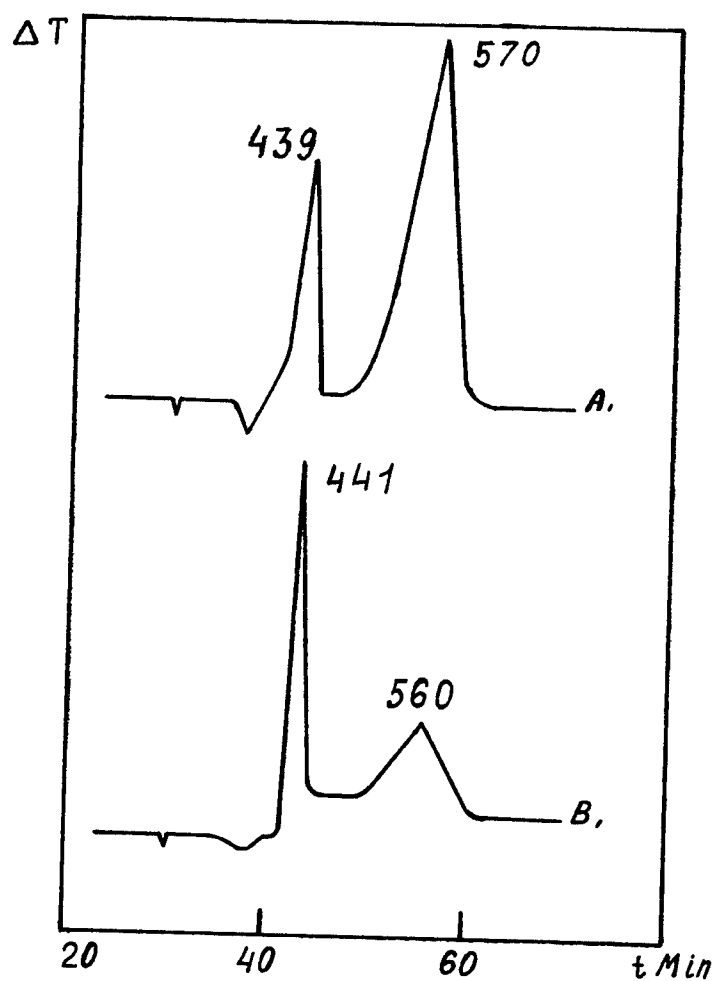


Figure 3.

- A). DTA profile of sodium perchlorate metal magnesium and calcium peroxide ternary mixture at mol. ratio $0.5 \text{ NaClO}_4 - 0.5 \text{ Mg} - 1 \text{ CaO}_2$.
- B). DTA profile of sodium perchlorate metal magnesium and calcium peroxide ternary mixture at mol. ratio $1 \text{ NaClO}_4 - 0.5 \text{ Mg} - 1 \text{ CaO}_2$.

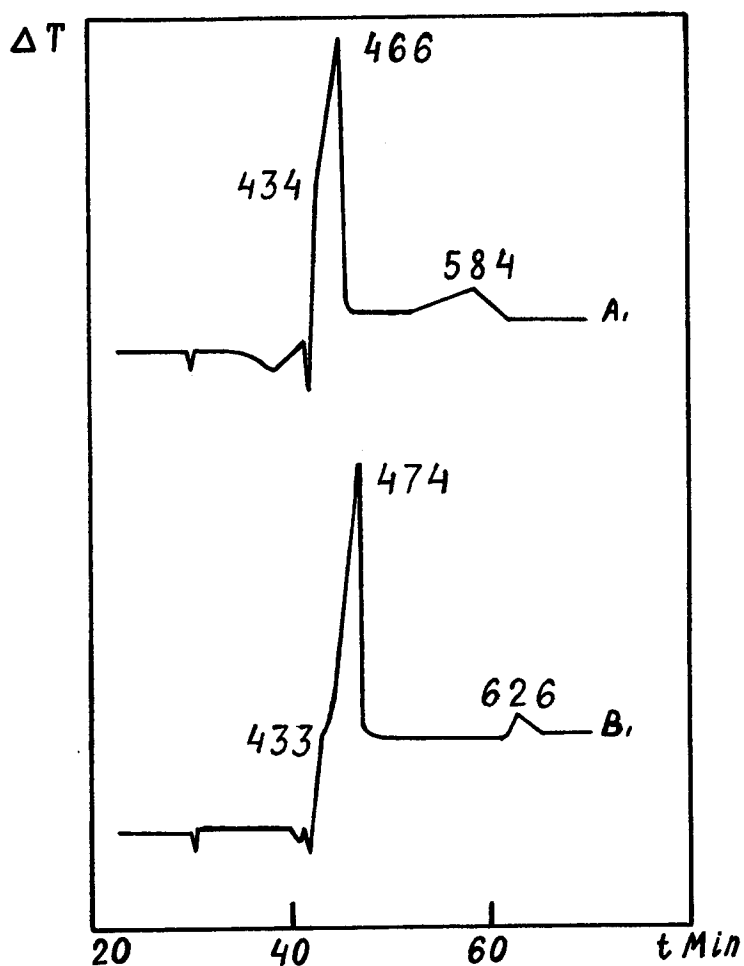


Figure 4.

- A). DTA profile of sodium perchlorate metal magnesium and calcium peroxide ternary mixture at mol. ratio $1.7 \text{ NaClO}_4 - 0.5 \text{ Mg} - 0.9 \text{ CaO}_2$.
- B). DTA profile of sodium perchlorate metal magnesium and calcium peroxide ternary mixture at mol. ratio $5 \text{ NaClO}_4 - 0.5 \text{ Mg} - 1 \text{ CaO}_2$.

THE CALCIUM COMPOUNDS AS THE COMPONENTS INCREASING THE ECOLOGICAL SAFETY OF PYROTECHNIC OXYGEN SOURCES.

Valentin Klyucharev, Stanislav Sinelnikov, Alla Razumova,
Valentina Sasnovskaya.

Institute of New Chemical Problems, Russian Academy of Science.
142432, Moscow Region, Chernogolovka, RUSSIA.

ABSTRACT

The catalytic activity of calcium oxide, peroxide and hydroxide are considered for oxygen evolution from sodium and potassium perchlorate. It has been found that a dope of CaO can lead to the total disintegration of the perchlorates in much the same temperature range that the oxides of Mn, Co, Ni, Cu. The result allows to depress the toxic impurities in evolving oxygen not only by their absorption, but decreasing the temperature of the salt decomposition as well. The calcium peroxide is advisable to use as a precursor of CaO in pyrotechnic systems.

The stable chlorates and perchlorates with 45 - 60 wt. % O₂ are of great interest to makers of life support systems. However, the decomposition of the salts at high heating rate often leads to evolving Cl₂ and ClO₂ [1-3]. There is only a little of substances which can avoid the toxic impurities: the oxygenous compounds of alkaline metals [4-7] and barium [1,8-12], KMnO₄ [13], MgFeO₃ [14] CaO, Ca(OH)₂, CaO₂ [15-19].

BaO₂ more often has use in pyrotechnic oxygen generators. The substance effectively inhibits the Cl₂-evolution, at the same time acting as a catalyst for chlorate₂ [20,21] and perchlorate [21] decomposition. In the last case, the catalytic effect of BaO₂, estimated from the temperature shift of chemical process can be similar to effect induced by oxides [2, 22-35] and salts [36-38] of d-elements.

At the same time, the barium peroxide has great molecular mass and own high toxicity. As a consequence, the offers arise to substitute the BaO in pyrotechnic materials. The most simple decision is in use² of CaO , $Ca(OH)_2$, $CaCO_3$, $Mg(OH)_2$, $MgCO_3$ for absorption of chlorine and heat. In addition, the² dope by oxides of d-elements can compensate the known low catalytic activity of the light alkaline-earth metal compounds for reactions of oxygen evolving from chlorates and perchlorates [3,15-19,22-24,28,31-35].

The application of materials containing Co, Mn, Ni, Cu, states problems in terms of ecological safety [39]. For this reason, the outlook of calcium and magnesium compounds as components of gasgenerating formulas arouses great interest in using their own catalytic influence, in order to promote the processes of oxygen evolution from salts of the perchloric and chloric acids. The present paper shows the results obtained for CaO , CaO , $Ca(OH)_2$ in binary mixtures with sodium and potassium perchlorates.²

The scope for using the calcium oxide as a catalyst of oxygen evolution from the salts of the perchloric acid had been studied before [3,22-24]. Experimental findings presented in the papers give evidence that the CaO offers a some catalytic activity for processes leading to perchlorate decomposition, however, does not stand a competition with many oxides of d-elements [2,22-27]. When the mixture of $KClO_4$ with manganese dioxide [2,22,23-26], cobalt oxides [22,23,25],⁴ nickel oxide [23,25], or copper oxide [27] began to evolve a gas about 460-480°C and reaction was completed about 500-520°C, then in presence of the CaO the process was observed at temperatures too high by 30-40°C.

The idea, a second time to study the mixtures of perchlorates and compounds of alkali-earth elements, sprang up as a result of detailed analysis of the experiments [23] carried out by Shimokawabe e.a. As follows from the description, a part of d-metal oxides, prior to mixing with the salt, was calcined for

removal of water and hydroxide groups. In the cases of CaO , the starting material was not exposed to like thermal treatment.

The surface calcium hydroxide can critically change the estimation of catalytic activity of the CaO [40]. The rapid transport of products which arise at chemical destruction of hydroxides [41-45], a modification of surface involving the hydrogen evolution in such process [46-50] call for high degree of drainage, so that the oxide surface showed itself in chemical action [44].

The reactivity of source substances and their mixtures was made with "Derivatograph Q1500D" thermal analyzer in quartz or alundum cylindrical tube (6 mm and 10 mm respectively) protected by covers with V-tap. The initial atmosphere was air, further self-forming. The heating rate was $10^\circ\text{C}/\text{min}$ in the interval 25 - 750°C , the standard Al_2O_3 . Weight of samples, about 100 mg, was selected so that the rate of oxygen evolution was increased in proportion to the temperature, in consequence of the stationary heat transfer between a sample and surrounding medium [51, 52].

The powders were analyzed with DRON-3M-INKHP X-ray diffractometer for samples in paste form with fluorined oil. A quartz dish was waterproof thanks to fluoroplast film [53]. IR-experiments were carried out with UR-20 apparatus using the nujol technique.

The sodium and potassium perchlorates was prepared by double recrystallization from distilled water. The sodium salt was dried in a vacuum at heating rate $6^\circ\text{C}/\text{min}$ to 320°C [54], the potassium salt isothermally at 120°C in air. The specimens contained no less 99.8 % of perchlorate. The chemical analysis was carried out for Cl^- , ClO_3^- and ClO_4^- , after Mohr, by SO_2 and nitron acetate, respectively [53].

In the work was used NiO "OSCh 10-2" calcined at 600°C in the course of 5 hours, and $\text{Ca}(\text{OH})_2$ "ChDA" (reagent grade).

The present study was conducted with two specimens of CaO .

In the first case, a calcium oxide was introduced from peroxide as a precursor. The thermal decomposition: $2 \text{CaO}_2 = 2 \text{CaO} + \text{O}_2$ [55] proceeds at heating rate $10^\circ\text{C}/\text{min}$ in interval $330\text{--}460^\circ\text{C}$ with formation water-free CaO . Lemesheva obtained this starting CaO by reaction of exchange between CaCl_2 and water-ammonia solution of H_2O_2 [56]. The specimen was dried at 150°C in air. The samples contained no less 95,7 % of peroxide. The ballast is carbonate. The product leaves traces of chloride.

In the second case, a calcium oxide had been prepared from the CaO by shock calcination in air at 900°C with subsequent cooling to 700°C in the course of 10 minutes. Idea, to obtain a calcium oxide by explosive decomposition, had been carried over from [57]. The granules [57] produced by thermoshock of $\text{Ca}(\text{OH})_2$ and CaCO_3 evoked particular interest to the approach.

In both cases X-ray diffraction patterns of the oxides were in agreement with ASTM-standard [58]. The fact is consistent with results of $\text{Ca}(\text{OH})_2$ and CaCO_3 explosive disintegration [57] and X-ray analysis of solid products of CaO_2 decomposition [55].

Experimental data obtained for source salts and its binary mixtures with CaO , CaO_2 , $\text{Ca}(\text{OH})_2$, NiO , in mol. ratios 1:1, are shown in table 1.

The calcium peroxide evolved oxygen in the $330\text{--}460^\circ\text{C}$ region with DTA endothermic peak about 401°C . The CaCO_3 impurity was decomposed in the case between $625\text{--}760^\circ\text{C}$. The $\text{Ca}(\text{OH})_2$ had endothermic effect with start about 380°C and sharp minimum at 529°C . The error of temperature measurements at a point of extremum are $\pm 3^\circ\text{C}$.

DTA-curve of the potassium perchlorate in quartz dish turned out to be very near to result by Anderson and Freeman [59]. Endothermic effect at 300°C conforms to phase transformation of

KClO₄ that is consistent with recommendation of ICTA-committee on standardization [60].

In alund tube the KClO₄ decomposition was finished at 620-625°C.

Phase conversion of the NaClO₄ was observed at 302°C. The result practically agrees within experimental data by Shimokawabe e.a. [23] if there to standardize on temperature of KClO₄ phase transition at 300°C, as well as the lower limit of the transfer obtained under cooling in [61]. The complex nature of NaClO₄ phase conversion [61-63], probably, cause a discordance into 5-6°C with known literary data [62,64,65], but not experimental errors.

The picture of sodium perchlorate decomposition after 525°C fits the result by Markowitz and Boryta [2].

The systems: KClO₄ - CaO and NaClO₄ - CaO were studied in interval of molar ratios² CaO /MClO₄ from 0.01 to 10 (M = Na,K). At reference endothermic stage² of perchlorate decomposition the chlorate had been accumulated; it was noted by chemical, X-ray and IR analysis. At exothermic stage, the sample was crushed with formation of the chloride.

In quartz tubes, at increasing the peroxide part, 0.1 M CaO₂ in mixture with 1 M KClO₄ had reduced the temperature of complete salt decomposition approximately into 90°C. At such proportion between the components, the catalytic action of forming CaO leads to retarding the reactions of the oxygen evolution, if the process is carried out under nonisothermal conditions with heating rate 10°C/min [51]. The switch based on the inversion of the quality of ratios in the system of independent chemical reactions in going from isothermal holding to continuous temperature elevation brings about the effect [51,66-67]. The further increase of the CaO₂ part leads to rise of an catalytic action (table 1). At determined molar ratios the

forming oxide can accelerate the oxygen evolution from perchlorate source on heating too [51].

Experimental data obtained for mixtures: KClO_4 - CaO are by far distinguished from results presented by Shimokawabe e.a. [23] for system KClO_4 - CaO . In the last case, the start of heat evolving at decomposition of sample (about 525°C) and the largest rate of its exothermic disintegration (about 545°C) practically check with picture of KClO_4 chemical conversion in presence of Ca(OH)_2 in our experiments⁴ (table 1). Taking account of results² obtained in [40-47], we assumed that the hydroxide and even peroxide groups can prevent or hinder a catalytic action of CaO for thermolysis of alkali metal perchlorates.

The experimental data obtained for samples, which contained beforehand prepared calcium oxide, give evidence (table 1) that the free surface of CaO at specific ratios oxide/salt can quickly and completely decompose: NaClO_4 at $430 - 460^\circ\text{C}$, KClO_4 at $480 - 500^\circ\text{C}$. The decrease ($120-140^\circ\text{C}$)⁴ of the temperature for the final oxygen evolution is close to effect of Fe, Co, Cu, Ni oxides [2,22-27].

The experimental study of combustion processes in molded blocks contained a metal magnesium fuel, sodium or potassium perchlorate oxidants, and calcium peroxide showed that a CaO dope can work similarly to BaO in Schechter's candle [1]. The dosed rise of the peroxide content, in both cases, allows to decrease the content of a fuel. In both cases one can diminish the amount of toxic impurities in gas, the temperature and rate of combustion front. In our experiments with CaO , a burning composition were obtained which had the temperature in the front about 650°C .

The results of present paper, as against [15-19,22-24,28,31-35] make possible a new estimation of outlook of applying the oxides, peroxides, and hydroxides of calcium with the purpose

forming oxide can accelerate the oxygen evolution from perchlorate source on heating too [51].

Experimental data obtained for mixtures: KClO_4 - CaO are by far distinguished from results presented by Shimokawabe e.a. [23] for system KClO_4 - CaO . In the last case, the start of heat evolving at decomposition of sample (about 525°C) and the largest rate of its exothermic disintegration (about 545°C) practically check with picture of KClO_4 chemical conversion in presence of Ca(OH)_2 in our experiments⁴ (table 1). Taking account of results² obtained in [40-47], we assumed that the hydroxide and even peroxide groups can prevent or hinder a catalytic action of CaO for thermolysis of alkali metal perchlorates.

The experimental data obtained for samples, which contained beforehand prepared calcium oxide, give evidence (table 1) that the free surface of CaO at specific ratios oxide/salt can quickly and completely decompose: NaClO_4 at $430 - 460^\circ\text{C}$, KClO_4 at $480 - 500^\circ\text{C}$. The decrease ($120-140^\circ\text{C}$)⁴ of the temperature for the final oxygen evolution is close to effect of Fe, Co, Cu, Ni oxides [2, 22-27].

The experimental study of combustion processes in molded blocks contained a metal magnesium fuel, sodium or potassium perchlorate oxidants, and calcium peroxide showed that a CaO_2 dope can work similarly to BaO_2 in Schechter's candle [1]. The dosed rise of the peroxide content, in both cases, allows to decrease the content of a fuel. In both cases one can diminish the amount of toxic impurities in gas, the temperature and rate of combustion front. In our experiments with CaO_2 , a burning composition were obtained which had the temperature in the front about 650°C .

The results of present paper, as against [15-19, 22-24, 28, 31-35] make possible a new estimation of outlook of applying the oxides, peroxides, and hydroxides of calcium with the purpose

of promoting the decomposition of oxidants traditional for pyrotechnic oxygen generators.

Ca(OH)_2 can find application as a component taking up the heat and stabilizing the rate of combustion, as a substance having an influence on decomposition of alkali metal perchlorates (table 1) and, to all appearances, chlorates.

CaO as a effective catalyst of the oxidants thermolysis (Table 1) probably can have limited use through hygroscopicity.

The calcium peroxide is of the greatest interest. The use of CaO additions in order to lower the temperature of decomposition of perchlorate and chlorate oxygen carrier in absence of perceptible metallate formation leads to the decrease of Cl_2 -impurities in evolving gas. The CaO has the low toxicity of thermolysis products, the low molecular weight, the sufficiently low degradation rate in humid air [68]. These properties allows to see the CaO as promise material for advanced pyrotechnic oxygen gasgenerators.

This work was carried out by financial backing of International Science Foundation (Grant N9K 000) and Department of Science and Scientific Politics of RF. We are indebted to Dr. I.B.Kudinov (Kurnakov's Inst. of Inorg. Chem., Moscow) and Dr. G.I.Nikishin (Zelinskii's Inst. of Org. Chem., Moscow) for helpful discussion and support.

REFERENCES

1. W.H.Schechter, R.R.Miller, R.M.Bovard, C.B.Jackson, J.R.Pappenheimer, *Industr. and Engin. Chem.*, **1950**, 42 2348.
2. M.M.Markowitz, D.A.Boryta, *J. Phys. Chem.*, **1965**, 69, 1114.
3. A.E.Harvey, M.T.Edmison, E.D.Jones, R.A.Seybert, K.A.Catto, *J. Am. Chem. Soc.*, **1954**, 76, 3270.
4. M.M.Markowitz, *US. Pat. US 3.293.187*, from 20.12.1966.
5. T.L.Thompson, *Pat. Ger. DE 2.142.185*, from 02.02.1972.

6. H.Gao, W.Ma, Y.Zhang, F.Shi, Pat. China CN 1.035.248, from 06.09. **1989**.
7. Y.C.Zhang, J.C.Cannon, PST Int. Appl. WO 93.17.962, from 16.09. **1993**.
8. W.H.Schechter, US. Pat. US 2.469.414, from 10.05. **1949**.
9. C.E.Heintz, Pat. Ger. DE 2.709.265, from 15.09. **1977**.
10. I.Araki, M.Hattori, K.Kitikoga, Jap. Pat. JP 78.44.902, from 02.12. **1978**.
11. K.I.Zvinenko, V.N.Sorotskii, S.P.Gradusov, S.S.Georgievskii L.D.Puchkov, S.P.Gamayunov, L.M.Eksel, Avt. Svid. USSR, SU 1.691.293, from 15.11. **1991**.
12. S.S.Georgievskii, S.P.Gradusov, L.M.Eksel, K.I.Zvinenko, N.V.Izotova, L.D.Puchkov, S.M.Sinelnikov, Avt. Svid. USSR. SU 1.682.301 from 01.10. **1991**.
13. J.Robinet, Pat. Ger. DE 3.502.157, from 01.08. **1985**.
14. J.S.Greer, Pat. Ger. DE 4.030.083, from 11.04. **1991**.
15. Y.C.Zhang, J.C.Cannon, PCT Int. Appl. WO 92.18.423, from 29.10. **1992**.
16. Y.C.Zhang, J.C.Cannon, US Pat. US 5.198.147, from 30.03. **1993**.
17. Y.C.Zhang, J.C.Cannon, PCT Int. Appl. WO 93.17.961, from 16.09. **1993**.
18. K.W'rster, Pat. Ger. DE 579.424, from 08.06. **1933**.
19. I.G. Farbenindustrie Akt.-Ges. in Frankfurt a.M. Pat. Ger. DE 636.639, from 24.09. **1936**.
20. Y.C.Zhang, G.Kshirsagar, J.C.Cannon, Ind. and Eng. Chem. Res., **1993**, 32, 966.
21. Z.K.Nikitina, V.Ya.Rosolovskii, Zh. Inorg. Chem., **1993**, 38, 1465.
22. W.K.Rudloff, E.S.Freeman, J. Phys. Chem, **1970**, 74, 3317.
23. M.Shimokawabe, R.Furuichi, T.Ishii, Thermochim. Acta., **1977**, 20, 347.
24. T.Nagaishi, J.Yoshimura, M.Matsumoto, S.Yoshinaga, Kyushu Sangyo Daigaku Kogakubu Kenkyu Hokoku, **1981**, 18, 19.
25. L.W.Collins, Inorg. Chim. Acta., **1980**, 39, 53.
26. A.A.El-Awad, A.A.Said, K.M.Abd-El-Salaam, Thermochim. Acta, **1988**, 126, 17.
27. J.S.Lee, C.W.Huang, J. Thermal Anal., **1993**, 40, 357.

28. S.Yamamoto, T.Asaba, Kogyo Kayaku, **1952**, 13, 235.
29. T.Wydeven, J.Catal., **1970**, 19, 162.
30. Z.G.Feng, Y.X.Pan, Y.S.Wu, J.H.Zhao, Huaxue Tongbao, **1988**, (N.9), 43.
31. S.Morishima, H.Iwakura, N.Kakuta, Nippon Kagaku Kaishi, **1991**, 1172.
32. H.Iwakura, N.Kakuta, A.Ueno, K.Kishi, J.Kato Ind. ang Eng. Chem. Res., **1991**, 30, 778.
33. Y.C.Zhang, G.Kshirsagar, J.E.Ellison, J.C.Cannon, Ind. and Eng. Chem. Res., **1993**, 30, 2863.
34. Y.C.Zhang, G.Khirsagar, J.E.Ellison, J.C.Cannon, Thermochim. Acta, **1993**, 228, 147.
35. J.C.Cannon, Y.C.Zhang, J. Thermal. Anal., **1994**, 41, 981.
36. J.F.O'Brien, Proc. of the Iowa Acad. Sci., **1959**, 66, 194.
37. T.Ishii, R.Furuichi, S.Shimada, Asahi Garasu Kogyo Gijutsu Shoreikai Kenkyu Hokoku, **1972**, 20, 53.
38. T.Ishii, R.Furuichi, C.Okawa, Hokkaido Daigaku Kogakubu Kenkyu Hokoku, **1974**, 71, 163.
39. Metal Ions in Biological Systems, V.20, Concepts on Metal Ion Toxicity. Ed. H.Siegel, N.Y. and Basel.: Marcel Dekker Inc. 1986.
40. R.M.Gabr, A.M.El-Awad, M.M.Girgis, J. Thermal Anal., **1991**, 37, 249.
41. F.Freund, H.Wengeler, R.Martens, J. Chim. Phys., **1980**, 77, 837.
42. M.M.Freund, F.Freund, F.Batllo, Phys. Rev. Lett., **1989**, 63, 2096.
43. F.Freund F. G.C.Maiti, F.Battlo, M.Baerns, J. Chim. Phys. (Phys-Chim. Biol), **1990**, 87, 1467.
44. A.K.Galway, G.M.Laverty, Thermochim. Acta, **1993**, 228, 359.
45. V.A.Griva, V.I.Rozenband, Zh. Phys. Chem., **1980**, 54, 2679.
46. F.Freund, H.Gentsch, Ber. Deutsche Keram. Ges., **1967**, 44, 51.
47. R.Martens, H.Gentsch, F.Freund, J. Catal., **1976**, 44, 366.
48. Yu.L.Seleznev, G.D.Chukin, L.A.Arbutova, T.V.Ignateva, Dokl. Ac. Sci. USSR, **1989**, 307, 1169.
49. J.B.Wallace, K.H.Oehr, US Pat. US 5.071.815, from 10.12.1991.

50. T.Grzybek, G.C.Maiti, D.Scholz, M.Baerns, Appl. Catal., **1993**, A107,, 115.
51. V.V.Klyucharev, A.P.Razumova, S.V.Karachinskii, I.V.Solopov Inorg. Mater., **1995**, 31, 111.
52. Ya. Sestak, Theory of Thermal Analysis. M.: Mir. 1987. (In Rus.) P.259.
53. Z.K.Nikitina, V.P.Babaeva, N.V.Krivtsov, V.D.Sasnovskaya, Zh. Inorg. Chem., **1989**, 34, 984.
54. Z.I.Grigorovich, G.N.Lyubimova, A.P.Razumova, V.Ya. Rosolovskii, Avt. Svid. USSR, SU 856.972, from 23.08. **1981**.
55. V.Ya.Bruner, Yu.P.Kalina, Izv. Ac. Sci. Latv. SSR, **1986**, 226.
56. D.G.Lemesheva, V.Ya.Rosolovskii, Avt. Svid. USSR, SU 1.281.507, from 07.01. **1987**.
57. C.R.Milne, G.D.Silcox, D.W.Pershing, D.A.Kirchgessner, Ind. and Eng. Chem. Res., **1990**, 29, 139.
58. Powder Diffraction File, JCPDS, Swarthmore, 1977.
59. D.A.Anderson, E.S.Freeman, Nature, **1962**, 195, 1297.
60. E.L.Charsley, J. Thermal Anal., **1993**, 40, 1399.
61. S.Yamamoto, Y.Shinnaka, J. Phys. Soc. Japan, **1983**, 52, 3080.
62. N.E.Shmidt, L.N.Golushina, G.A.Sharpataya, V.P.Babaeva, Zh. Phys. Chem. **1984**, 58, 2928.
63. S.K.Syal, S.R.Yoganarasimhan, J. Solid St. Chem., **1974**, 10, 332.
64. J.M.Molepo, R'ntgenographische und Thermochemische Untersuchungen 'ber die Phasenumwandlungen der Perchlorate Einwertiger Metalle, Dissertation. Hannover, 1975.
65. Thermal Constants of Substances, Ed. V.P.Glushko, V.10, M.: VINITI, 1981. (In Rus.)
66. V.V.Klyucharev, A.P.Razumova, in Actual Problems of the Fundamental Sci., V.5. Chemistry. M.: MGTU. P.11. (in Rus.)
67. V.V.Klyucharev, A.P.Razumova, in Workshop of the 10th Congress on Thermal Analysis. Hatfield. ICTA. 1992. P.107.
68. I.I.Volnov, Peroxide Substances of Alkali-earth metals, M.: Nauka. 1983.

Table 1.

Sample: 1 M of Salt - 1 M of Dopants	Temperature °C	
	Start of the exothermic decomposition	Peak of the exothermic decomposition
KClO ₄	609	646
KClO ₄ - Ca(OH) ₂	525	544
KClO ₄ - CaO ₂	509	514
KClO ₄ - CaO	478	498
KClO ₄ - NiO	484	506
NaClO ₄	529	582
NaClO ₄ - Ca(OH) ₂	519	552
NaClO ₄ - CaO ₂	447	502
NaClO ₄ - CaO	430	460
NaClO ₄ - NiO	410	430

In all experiments the phase transition of the KClO₄ was at 300°C, NaClO₄ at 302°C.

ESTIMATION OF THERMODYNAMIC STABILITY CONDITIONS AND
PERSPECTIVES FOR SYNTHESIS OF COVALENT CARBON NITRIDE

Victor Odintsov, Vitaly Pepekina
Institute of Chemical Physics, Russian Academy of Sciences,
4 Kosygin Street, Moscow, 117977, Russia

ABSTRACT

The present work is devoted to determination of conditions of thermodynamic stability of carbon nitride having structure of $\beta\text{-C}_3\text{N}_4$. The thermodynamic functions of crystalline covalent carbon nitride required for thermodynamic reckoning of parameters of formation of carbon nitride were determined on the base of the Debye's theory with the characteristic temperature varied in the range from 1000 to 2500 K. The formation enthalpy of carbon nitride was estimated on the base of the energy of atomization and formation enthalpy of a mixture of atomized carbon and nitrogen. The resulted quantity of the standard formation enthalpy of covalent carbon nitride at 298.15 K made up 4.47 kcal/mol. Thermodynamic computations were accomplished with the use of the Automated System of Thermodynamic Reckonings and Algorithms ASTRAL. Behavior of the gaseous phase of a chemical system was described by the BKW-RR equation of state. Carbon nitride was considered to be incompressible. The region of thermodynamic stability of covalent carbon nitride is computed. It is shown that in contrast to the carbon condensation into graphite the pressure of condensation of $\beta\text{-C}_3\text{N}_4$ when adding other chemical elements to a thermodynamic system can not only increase but decrease as well. Consideration of detonation and explosion processes in high explosives shows a way for practical synthesis of covalent carbon nitride.

Nitrides constitute an important class of ceramic materials. Among them are well known nitrides of boron, aluminum, silicon. In this connection it seems rather strange that up to now carbon nitride has not obtained yet; though there is no any a priori restriction for its existence and the number of chemical compounds consisting of only carbon and nitrogen is quite great. The interest to carbon nitride has significantly risen since the time when on the base of a simple scale model with exponential dependence of the bulk modulus of a crystalline substance on the covalent bond length with correction on its "ionization" Cohen [1] proposed that the solid formed from carbon and nitrogen atoms with covalent inter-atom bonds

can have the value of bulk modulus higher than that of diamond. Since the hardness of a material is directly connected with its bulk modulus then it followed from the Cohen's estimation that there was a possibility of existence of the substance harder than diamond.

Later Liu and Cohen [2] published the results of ab initio calculations of structural and electronic properties of the hypothetical compound $\beta\text{-C}_3\text{N}_4$. A first principles pseudopotential total energy calculation on the system was performed. The resulting value of bulk modulus (427 GPa) obtained by fitting the total energy as a function of volume to Murnaghan's equation of state [3] occurred to be by 10% less than it was predicted by the scale model and less than the bulk modulus value of diamond (443 GPa). Nevertheless, the possibility of existence of the new substance with the compressibility value close to that of diamond aroused great interest to it and attempts to synthesize this substance [4-9].

In this connection it is interesting to find out the possibility of existence of such substance and conditions of its thermodynamic stability. Liu and Cohen [2] noticed that the chosen structure of the C-N system ($\beta\text{-C}_3\text{N}_4$) was only a prototype and there was no reason a priori to believe that this structure was the most stable one. However, the moderately large cohesive energy suggested that there was a good chance that this structure could exist at least in a metastable state.

The present work is devoted to a determination of the conditions of thermodynamic stability of carbon nitride in the structure of $\beta\text{-C}_3\text{N}_4$. In this structure each carbon atom is connected by the identical bonds with four nitrogen atoms placed practically in the vertexes of a tetrahedron, and each nitrogen atom is connected with three carbon atoms by the same bonds coordinated in an almost trigonal-planar arrangement. Such atomic coordination suggests sp^3 hybrids on the carbon atoms and sp^2 hybrids on the nitrogen atoms.

Just as the phase diagram of carbon was computed for determination of conditions of diamond thermodynamic stability [10] one can compute conditions of formation of $\beta\text{-C}_3\text{N}_4$ for what it is necessary to know the thermodynamic functions of this substance.

Thermodynamic functions of crystalline substance are quite well described by the Debye's approximation [11] that is proved by a good correlation

between the graphite—diamond equilibrium line computed with the use of the theory of Debye for determination of the diamond thermodynamic functions [10] and the phase diagram of carbon [12] based on the experimental data.

To use the Debye's theory for a calculation of the thermodynamic functions of covalent carbon nitride one should know its characteristic Debye temperature. Proceed from the value of Debye temperature of diamond (1840 K) one can assume that the Debye temperature of carbon nitride should have the same order. Therefore the basic value of characteristic temperature for the crystalline structure $\beta\text{-C}_3\text{N}_4$ is accepted in this work equal to 1500 K.

The formation enthalpy of carbon nitride is estimated on the base of the energy of atomization and formation enthalpy of a mixture of atomized carbon and nitrogen. The atomization energy is calculated as the energy required for breaking all chemical bonds in 1 mole of carbon nitride with formation of 3 moles of atomized carbon and 4 moles of atomized nitrogen. Since the calculated length of a bond in $\beta\text{-C}_3\text{N}_4$ (0.147 nm [21]) and the C-N bond length in a methylamine molecule (0.1474 nm [13]) practically coincide then the breakage energy of a C-N bond in carbon nitride is accepted to be equal to 80 kcal/mol what corresponds to the energy of bond breakage of the carbon and nitrogen atoms in methylamine (80.7 kcal/mol [14]). The resulting quantity of the standard enthalpy of formation of covalent carbon nitride at 298.15 K makes up 4.47 kcal/mol.

Thermodynamic computations were conducted with the use of the Automated System of Thermodynamic Reckonings and Algorithms ASTRAL based on the methods described in [15]. Behavior of the gaseous phase of thermochemical system was described by the equation of state of Becker-Kistiakowsky-Wilson widely used in thermodynamic computations of detonation and explosion processes in high explosives and improved in [16] (BKW-RR). Carbon nitride was assumed incompressible.

The computed dependence of pressure of $\beta\text{-C}_3\text{N}_4$ formation on the temperature of system consisting of only carbon and nitrogen is presented in Fig. 1 in comparison with the phase diagram of carbon [10,12]. Unlike to diamond having the other solid phase — graphite, carbon nitride apparently does not have another solid phase of the same composition. That is why the line of formation of carbon nitride in Fig. 1 corresponds not to the

66 - 4

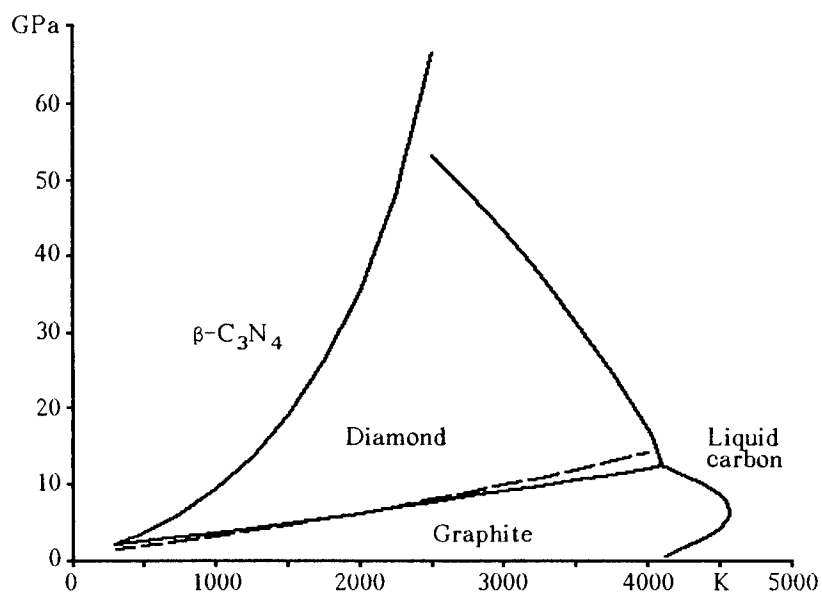


Fig. 1. The condensation line of $\beta\text{-C}_3\text{N}_4$ on the phase diagram of carbon by Bundy [12]. Dashed line — the diamond-graphite equilibrium computations [10].

phase transition but to formation of the new substance. Moreover, in contrast to the equilibrium of condensed phases the pressure and temperature of which are fixed independently of the system composition, the pressure of solid carbon nitride formation can vary at a fixed temperature value in dependence on the system composition similar to that what is observed in the case of carbon condensation into graphite under low pressures [10].

It should be noticed that in the case of presence of the solid phase of C_3N_4 with another crystal structure and less density the pressure of thermodynamic stability of β -structure at a given temperature would be not less but rather higher than in the case under consideration. For example, the carbon condensation pressure into diamond phase computed in the absence of possibility of graphite formation is several orders less than the real graphite-diamond equilibrium pressure and a bit higher than the pressure of carbon condensation into graphite.

The influence of composition of a chemical system on the boundary of a region of thermodynamic stability of carbon nitride is illustrated by dependences given in Fig. 2. Unlike carbon condensation into graphite [10] the pressure of β - C_3N_4 condensation can not only increase as in the case of addition of chemically reacting water to the C-N system (line 1) but decrease as well by diluting the C-N system with inert helium (line 2, the helium covolume in computations was arbitrarily assumed to be 100).

The use of 1500 K as the characteristic Debye temperature while calculating the thermodynamic functions of covalent carbon nitride is rather arbitrary. Therefore a question arises about influence of the Debye temperature quantity on a location of the region of thermodynamic stability of covalent carbon nitride. The answer on the question is given by the graph of β - C_3N_4 condensation pressure dependences on temperature computed with the different values of Debye temperature in an interval from 1000 to 2500 K and given in Fig. 3. From the graph it follows that the boundary of thermodynamic stability region moves insignificantly and the choice of the value of 1500 K can be considered as quite good estimation of Debye temperature for calculation of the thermodynamic functions of covalent carbon nitride.

The two ways of synthesis of superhard materials the region of thermodynamic stability of which falls on the superhigh pressures are known: 1) synthesis in the thermodynamic stability region — so called High Pres-

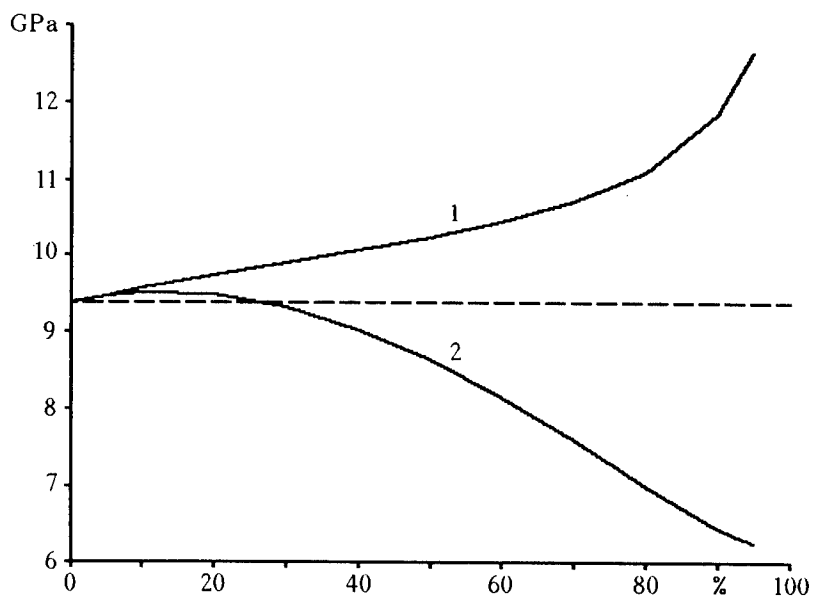


Fig. 2. Dependence of condensation pressure of $\beta\text{-C}_3\text{N}_4$ on molar percentage of addition to a C-N system at $T = 1000$ K and $\phi_D = 1500$ K. Lines correspond to the addition of: 1 — water with possibility of chemical reacting; 2 — inert helium. The dashed line — without any addition.

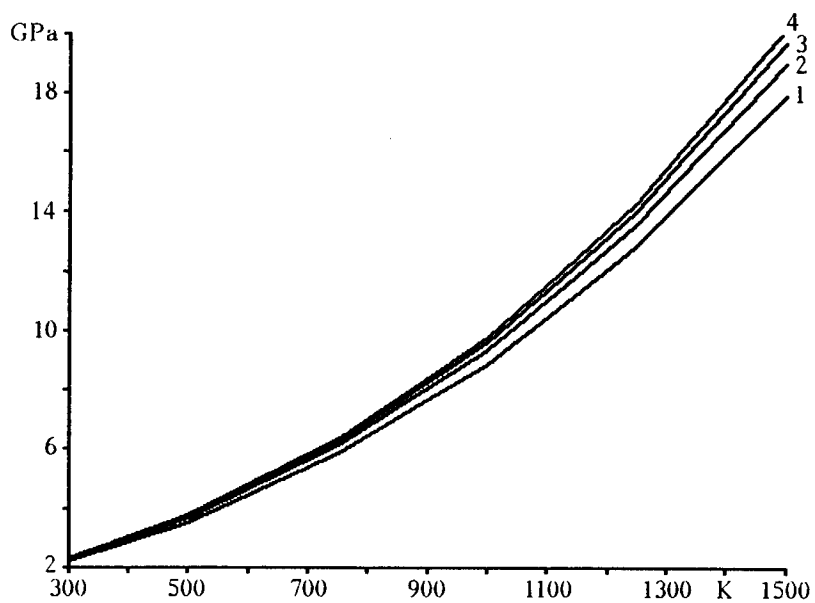


Fig. 3. Dependence of condensation pressure of $\beta\text{-C}_3\text{N}_4$ on temperature of a C-N system for different values of Debye temperature: 1 - 1000 K, 2 - 1500 K, 3 - 2000 K, and 4 - 2500 K.

sure-High Temperature (HPHT) synthesis, and 2) synthesis of thin films on a surface under low and superlow pressures outside the thermodynamic stability region — so called Chemical Vapor Deposition (CVD) synthesis.

By now discovery of traces of a film of covalent carbon nitride is supposed only in experiments on CVD synthesis [8,9]. There is no one communication in a literature about obtaining carbon nitride by the HPHT method. And this result comes to a good agreement with the computed in the present work region of thermodynamic stability of covalent carbon nitride.

To substantiate the previous statement let us consider one of the main processes of the HPHT method of synthesis of superhard materials — a detonation of high explosives. The detonation parameters of triaminotrinitrobenzene (TATB) $C_6H_6N_6O_6$, cyanurtriazide (CTA) C_3N_{12} , and triazido-tricyanobenzene (TATCB) C_9N_{12} are presented by points in Fig. 4 in comparison with the regions of thermodynamic stability of bulky and dispersed diamond [16,17] and covalent carbon nitride. It follows from comparison of the detonation parameters and thermodynamic stability regions that in detonation products there can be formed diamond (what has being already used for a long time while synthesizing ultra-dispersed diamond) but not carbon nitride. Indeed, even in the low-temperature detonation products of TATB the quite high (for detonation products of high explosives) pressure is not high enough for carbon nitride condensation. Parameters of the products while unloading from the Chapman-Jouguet point modelled in computations of isentropic expansion are depicted in Fig. 4 by solid lines originating from the points corresponding to the Chapman-Jouguet states. These lines are placed far from the line of carbon nitride condensation and go almost parallel to it. This means that the conditions in detonation products are far from that required for carbon nitride synthesis, and the process of detonation of high explosives itself cannot be considered as the promising one for synthesis of covalent carbon nitride.

One more process related to the HPHT method which is promising for synthesis of diamond consists in the adiabatic explosion of a high explosive under constant volume with following isochoric cooling the explosion products [17]. Let us see whether this process can be used for the carbon nitride synthesis.

In Fig. 5 the points represent the computed parameters of adiabatic explosion of the three explosives mentioned above and the lines originating

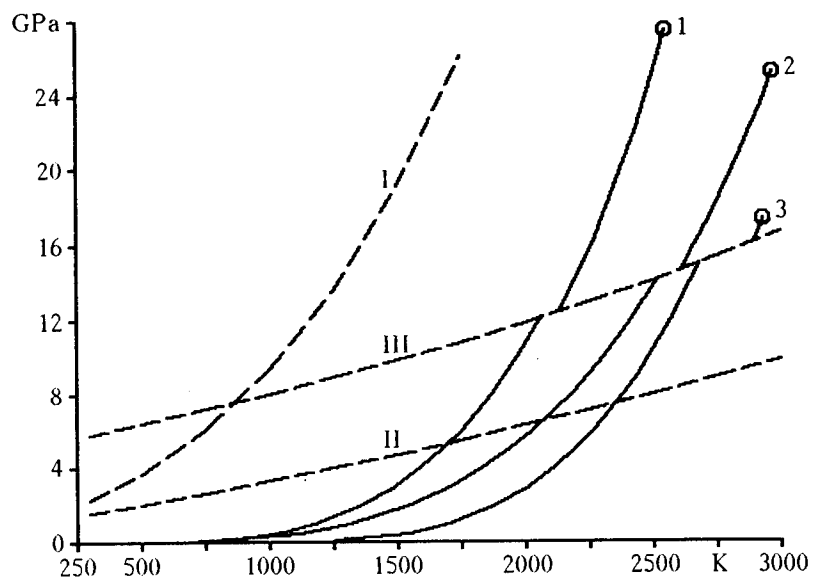


Fig. 4. Computed parameters of detonation and following isentropic expansion of detonation products of TATB (1), CTA (2), and TATCB (3) in comparison with the condensation line of $\beta\text{-C}_3\text{N}_4$ (I) and equilibrium lines of bulky (II) and dispersed (III) solid phases of carbon.

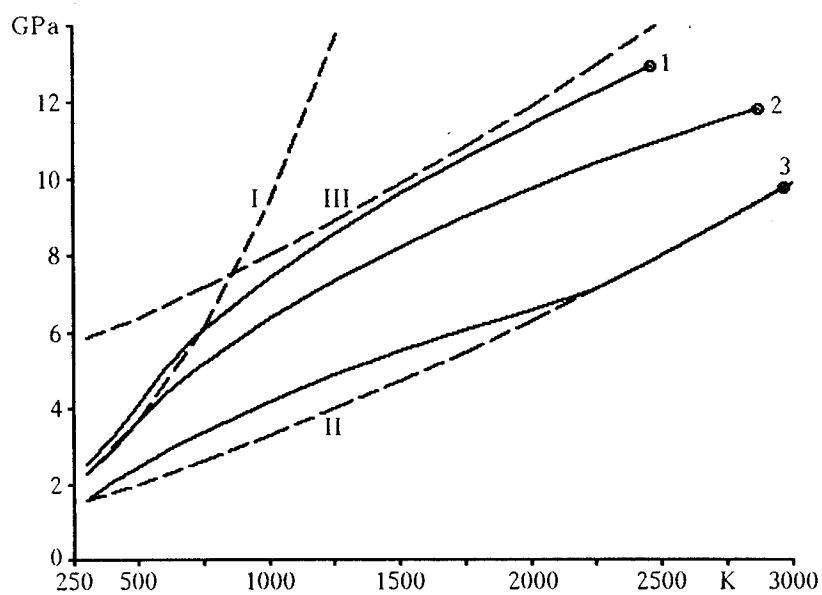


Fig. 5. Computed parameters of adiabatic explosion and following isochoric cooling of explosion products of TATB (1), CTA (2), and TATCB (3) in comparison with the condensation line of $\beta\text{-C}_3\text{N}_4$ (I) and equilibrium lines of bulky (II) and dispersed (III) solid phases of carbon.

from these points represent the parameters of isochoric cooling of explosion products in comparison with the lines of phase equilibrium of bulky and dispersed solid carbon [16,17] and the line of $\beta\text{-C}_3\text{N}_4$ appearance. It follows from Fig. 5 that while isochoric cooling the point corresponding to the states of explosion products move first into the region of thermodynamic stability of diamond and then, while further temperature decreasing, into the region of carbon nitride stability.

Thus, from the theoretical point of view the process of adiabatic explosion of high explosive with following isochoric cooling of explosion products can be used for synthesis of covalent carbon nitride. However, for its practical application one can put forward at least two obstacles. Firstly, it is impossible to keep the volume of explosion products unchanged under such high pressures and temperatures which are reached at an explosion of high explosive. Secondly, explosion products come into the region of thermodynamic stability of carbon nitride at a rather low temperature. But for condensation of a significant amount of carbon nitride in a system consisting of carbon and nitrogen the required amount of carbon can be obtained only from diamond already formed, i.e. formation of $\beta\text{-C}_3\text{N}_4$ is performed by means of evaporation of carbon from diamond and condensation of carbon vapor with nitrogen.

As a result of the undertaken consideration of the detonation and explosion processes in high explosives one can conclude that these processes hardly can be directly used for synthesis of carbon nitride. This conclusion is indirectly confirmed by the fact that by now carbon nitride has not been yet discovered neither in the detonation nor in explosion products.

Knowledge of the region of thermodynamic stability of carbon nitride allows to purposefully research new possibilities and processes for synthesizing this substance within the bounds of the HPHT way.

There
15.03.95

References

1. Cohen M.L. — Phys. Rev., 1985, V. B32, p. 7988.
2. Liu A.Y., Cohen M.L. Prediction of New Low Compressibility Solids. — Science, 1989, V. 245, p. 841.
3. Murnaghan F.D. — Proc. Nat. Acad. Sci. U.S.A., 1944, V. 30, p. 244.
4. Sekine T., Kanda H., Bando Y et al. A Graphitic Carbon Nitride. — J. Materials Sci. Lett., 1990, V. 9, p. 1376.
5. Maya L., Cole D.R., Hagaman E.W. Carbon—Nitrogen Pyrolyzates: Attempted Preparation of Carbon Nitride. — J. Am. Ceram. Soc., 1991, V. 74, No. 7, p. 1686.
6. Schnick W. Carbon(IV) Nitride C_3N_4 — A New Material Harder Than Diamond? — Angew. Chem. Int. Ed. Engl., 1993, V. 32, No. 11, p. 1580.
7. Niu C., Lu Y.Z., Lieber C.M. — Science, 1993, V. 261, p. 334.
8. Yu K.M., Cohen M.L., Haller F.E., et al. Observation of crystalline C_3N_4 . — Phys. Rev., 1994, V. B49, No. 7, p. 5034.
9. Song H.W., Cui F.Z., He X.M., et al. Carbon Nitride Films Synthesized by NH_3 -ion-beam-assisted Deposition. — J. Phys.: Condens. Matter, 1994, V. 6, p. 6125.
10. Gubin S.A., Odintsov V.V., Pepekin V.I. Diagram of Phase States of Carbon and Its Consideration in Computations of Detonation Parameters. — Khimicheskaya Fizika (Chem. Phys.), 1986, V. 5, No. 1, p. 111. (Russ.).
11. Tsan Sue-Sen. Physical Mechanics. — Moscow: "Mir", 1965. (Russ.).
12. Bundy F.P. — J. Geophys. Res., 1980, V. 85, No. B12, p. 6930.
13. Wells A.F. Structural Inorganic Chemistry. — Oxford: Clarendon Press, 1986.

14. Brief Handbook of Physical and Chemical Quantities. Ed. by Ravdel A.A. and Ponomarev A.M. — Leningrad: "Khimiya", 1983, p. 218. (Russ.).
15. Gubin S.A., Odintsov V.V., Pepekin V.I. Thermodynamic Computations of Complex Chemical Systems. — Moscow, Mosc. Phys. Eng. Inst., 1987. (Russ.).
16. Gubin S.A., Odintsov V.V., Pepekin V.I. Thermodynamic Computation of Ideal and Non-ideal Detonation. — Fizika Goreniya i Vzryva (Phys. of Combust. and Explos.), 1987, No. 4, p.75. (Russ.).
17. Gubin S.A., Odintsov V.V., Pepekin V.I. Thermodynamic Calculations of Detonation Parameters. — Proc. 16-th Int. Pyrotechnics Seminar, Sweden, 1991, p. 325.

DEFLAGRATION AND DETONATION PREDICTIONS USING A NEW EQUATION OF STATE

by

L. Durães, J. Campos and J. C. Gois

Lab. of Energetics and Detonics
Mech. Eng. Dep. - Fac. of Sciences and Technology
University of Coimbra - 3000 Coimbra - PORTUGAL

Abstract

Design and production of energetic materials requires prediction of dynamic properties and pollutants from its combustion products. Dynamic properties are generally correlated to the theoretical adiabatic isobar and isochor combustion conditions - deflagration regime. Detonation regime is identified to Chapman Jouguet condition. The following text presents the general structure of THOR code, to calculate equilibrium thermodynamic properties and final compositions of gas and solid species, as a function of the initial composition of energetic system. Used new equation of state, named H_L , is a Boltzmann equation of state type, but now based on physical intermolecular potential of gas components instead of correlations from final experimental results. The presented equation and formulations show an excellent correlation with experimental results of type cases: isobar and isochor adiabatic combustions and Chapman Jouguet detonation. The most delicate predictions are related to the detonation conditions. The validation of preceding formulations and proposed equation of state has been done calculating, initially, the properties of reactive gaseous mixtures, in order to neglect the influence of solid products. Secondly, it was correlated to experimental results of a fundamental study case: mixtures of nitromethane - polymethylmetacrylate, changing its initial density by adding glass-microballoons. Finally, it is presented the most sensible case - detonation of condensed energetic materials: TMN, NM, HMX, RDX, PETN, TATB, TNT, AN, NG and NC(12,6%N). Obtained results and correlations prove the validity of used code and proposed equation of state.

1. INTRODUCTION

Design and production of energetic materials, propellants and explosives, requires the prediction of the thermodynamic properties of its combustion products. Curing agents, plasticizers, crosslinkers, stabilizers and antioxidants are also important to optimise mechanical and energetic properties of this kind of molecules and mixtures (vd. Timnat, 1987). Theoretical prediction codes of combustion products properties are based in thermodynamic equilibrium of products, for the minimum value the Gibbs free energy. They need a thermal equation of state. The most simple equation of state is the Perfect Gases EoS. More complex equations of state have been developed, like the Boltzmann EoS, based on a virial type equation, necessary when the initial energetic material is in condensed phase and when combustion conditions are under high pressure and temperature.

The following text presents the general structure of THOR code, to calculate equilibrium compositions of gas and solid species, as a function of initial composition of an energetic system. The description of a new equation of state, named H_9 , it is based on the same assumptions of a Boltzmann equation of state, i.e. on physical intermolecular potential of gas components, instead of correlations to final experimental results. In order to discuss the validity of selected equation of state and calculations, it is also presented the correlations between theoretical and the experimental results, existing in the open bibliography, for some gaseous mixtures and condensed explosives. Theoretical evaluations concern adiabatic conditions, identified to isobar and isochor combustions and Chapman-Jouguet detonations. The most delicate predictions are related to the detonation conditions.

The theoretical prediction of combustion products, using THOR code, is based on theoretical work of Heuzé et al., 1985, 1989, and later modified (vd. IEPG Reports, 1989, and Campos, 1991) in order to calculate the composition and thermodynamic properties of explosive compositions, for isobar and isochor adiabatic conditions and a Chapman-Jouguet detonation. Several equations of state are used, namely BKW, Boltzmann, H_9 , H_{12} and JCZ3 (vd. Heuzé, 1989). Results have been compared within themselves and with results of other codes referred in open literature (Quatuor Code from Heuzé et al., 1985, using BKW EoS of the TIGER Code (vd. Chaiken, 1975) and using the KHT EoS of the Tanaka Code, (Tanaka, 1983). The BKW, H_9 and H_{12} EoS are generally selected for calculations. The first equation EoS is the most common in bibliography and the others are the natural development of a Boltzmann EoS type, with similar results to the KHT and JCZ3 EoS (vd. Tanaka, 1983, Chaiken, 1975, and Heuzé, 1989).

2. CHEMICAL EQUILIBRIUM CONDITIONS

A classical combustion system is generally a CHNO system. It is possible to consider up to m atomic species ($m < 20$) and form n chemical components with these atomic species ($n < 40$). Among these n chemical components, m are considered "basic" chemical components and $n - m$ "non basic". The selection "ab initio" of the "basic" chemical components depends on the equivalence ratio r of the mixture, related to the stoichiometry ($r = 1$). This value must be the one which significant concentrations in final products composition are expected.

For a CHNO system it has been selected (vd. , Manson, 1976, Heuzé, 1989)

- CO_2 , H_2O , O_2 and N_2 for poor mixtures ($r < 1$),
- CO_2 , H_2 , H_2O and N_2 for rich mixtures ($r > 1$) of low initial density, and, C(s) , CO_2 , H_2O and N_2 for rich mixtures of high initial density (initial condensed or solid components).

When Cl atomic species is added must be assume HCl as a "basic" chemical component.

The mass balance yields a linear system involving m equations. In order to solve the problem it is necessary to add more $(n-m)$ equations. These $n-m$ equilibrium equations are determined by the method of Lagrange multipliers or the equilibrium constants (vd. Manson, 1976, Brinkley, 1947, White et al, 1958). Consequently the system of equations is formed by m linear atomic mass balance equations and $(n-m)$ non linear equilibrium equations.

In order to determine the chemical concentration of n components, for imposed P and T conditions, two methods can be used:

- the chemical affinity method, proposed by Heuzé et al., 1985, 1989;

- solving first the system composed by the m "basic" components, and secondly adding one by one more components, optimising the relative concentration inside the group reported to the same atomic species, for the minimum value of global Gibbs free energy $G = \sum x_i \mu_i$, being the Gibbs free energy of each component $\mu_i = G_{0i}(T) + R T \ln P + R T \ln (x_i)$.

The values of $G_{0i}(T)$ are the Gibbs free energy as a function of temperature. This second method is slower than the first, but avoid numeric problems (vd. Campos, 1991).

The selection of components are dependent of atomic initial composition. For a classical CHNO system it is assumed an equilibrium composition of CO_2 , CO , H_2O , N_2 , O_2 , H_2 , OH , NO , H , N , O , HCN , NH_3 , NO_2 , N_2O , CH_4 gases and two kinds of solid carbon (graphite and diamond). When the initial mixture include Cl species, HCl and Cl_2 are expected in final products. Reported data are from JANAF Thermochemical Tables, 1971, and polynomial expressions of Gordon and McBride, 1971. The glass shell of glass microballoons, used to sensitise some propellants and explosives, was considered SiO_2 in two phases, solid and gas. It is assumed as inert in reaction.

The solution of composition problems involves simultaneously:

- the thermodynamic equilibrium, obtained with the mass and species balance, and the equilibrium condition $G=G_{\min}(P,T,x_i)$, previously described, applying to the condensed phase the model proposed by Tanaka, 1983,

- the thermal equation of state (EoS),

- the energetic equation of state, related to the internal energy $E = \sum x_i e_i(T) + \Delta e$, $e_i(T)$ being calculated from JANAF Thermochemical Tables, 1971, and polynomial expressions of Gordon and McBride, 1971,

- the combustion regime, being $P_b=P_0$, constant, for the isobar adiabatic combustion (equal initial and final total enthalpy $H_b=H_0$), the isochor adiabatic combustion being $V_b=V_0$, constant, (equal initial and final internal energy E) and the Chapman-Jouguet condition

67 - 4

(mass, momentum and energy balances and $dp/dV]_S = [(P-P_0) / (V-V_0)]$) for the detonation regime, based on the assumption that the detonation velocity D is obtained adding sound velocity a_0 with particular velocity u_p ($D=a_0+u_p$).

3. H_L EQUATION OF STATE

The proposed equation of state is based on the same assumptions of H9 and H12 EoS, proposed by Heuzé, 1985, taking the general expression

$$\frac{P V}{n R T} = \sigma (V, T, X_i)$$

where V represents the volume, T the temperature and X_i the mass fraction. The second term, σ , represents a fifth order polynome, derived from a Boltzmann EoS, traducing very well the behaviour of gaseous mixtures at high temperatures and pressures:

$$\sigma (V, T, X_i) = 1 + x + 0,625 x^2 + 0,287 x^3 - 0,093 x^4 + 0,014 x^5$$

with

$$x (V, T, X_i) = \frac{\Omega}{V T^{3/\alpha}}$$

and

$$\Omega = \sum_{i=1}^s X_i \omega_i$$

The α represents the exponent of the intermolecular potential. Heuzé, 1985, has proposed for α the values 9 and 12, based on theoretical and experimental correlations. This approach lead to H9 and H12 EoS. The values of ω_i are also dependants of each gas component and Heuzé, 1986, to obtain its value, tooks the same procedure. Their values are independent of the chosen α constant.

The HL EoS takes to α the value of 13.5 proposed by Chirat et al, 1981, Brown, 1989, Bugaut et al, 1989, and Zerilli et al, 1989. Consequently the ω_i can be calculated assuming

$$x = \frac{\sum_{i=1}^s X_i \omega_i}{V T^{3/\alpha}}$$

and, by a similar procedure of a Boltzmann type EoS,

$$x = \frac{B}{V} = \frac{\sum_{i=1}^s X_i B_i}{V} ,$$

it can be possible

$$\frac{\sum_{i=1}^s X_i \omega_i}{V T^{3/\alpha}} = \frac{\sum_{i=1}^s X_i B_i}{V} ,$$

which allows

$$\frac{\omega_i}{T^{3/\alpha}} = B_i \quad (i = 1, \dots, s) ,$$

being B_i the covolume of component i .

Now

$$\omega_i = B_i T^{3/\alpha} .$$

Using a simplified rigid sphere model (vd. Montanelli, 1978)

$$B_i = \frac{2}{3} \pi r_{0i}^3 N_{AV} ,$$

where r_{0i} is the molecular radius and N_{AV} the Avogadro number ($N_{AV} = 6,02 \times 10^{23}$ molec/mol), it can be obtained

$$\omega_i = \frac{2}{3} \pi r_{0i}^3 T^{3/\alpha} N_{AV}$$

with

$$T = \theta \frac{\varepsilon}{k}$$

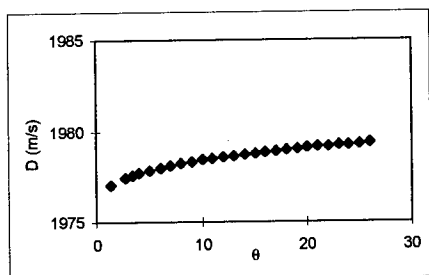


Fig. 1 - Detonation velocity of H_2 /Air mixture. as a function of adimensional temperature θ .

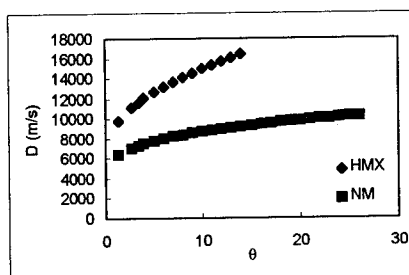


Fig. 2 - Detonation velocity of HMX and NM explosives, as a function of adimensional temperature θ .

In these equations, θ is an adimensional temperature, k the Boltzmann constant ($k = 1,380 \times 10^{-23}$ J/K), being the values of r_{0i} and ε/k presented by Heuzé et al, 1985. Several θ values

have been tried. They have great influence on predicted dynamic properties of products of condensed reactive mixtures. An example of its influence, on detonation velocity of an gaseous and condensed reactive mixture, respectively H_2 / Air and HMX, NM, is presented in Fig. 1 and 2. The value $\theta = 1.4$ has been considered the best constant value. Calculated values of ω_i , for $\theta = 1.4$, are presented in Table I.

Table I - Calculated values of ω_i (cc K^{1/3} / mole) for H_L EoS.

	ω_i		ω_i		ω_i
CO ₂	326.8	N ₂	261.5	NO	239.1
CO	261.5	H ₂	112.9	CH ₄	328.6
H ₂ O	152.7	O ₂	208.7	NH ₃	181.7

4. THEORETICAL PREDICTIONS, RESULTS AND DISCUSSION

The validation of preceding formulations and presented equation of state was done initially calculating the properties of reactive gaseous mixtures in order to neglect the influence of solid products, for the most delicate situation - detonation conditions. In Table II it is shown the selected reactive mixtures. Figure 3 presents calculated detonation velocity, pressure and temperature, as a function of chosen EoS and experimental results. The obtained pollutants concentration is presented in Figure 4.

Table II - Reactive mixtures used in calculations.

Gaseous Mixtures	H ₂ + O ₂	H ₂ + Air	CH ₄ + O ₂	CH ₄ + Air	C ₂ H ₂ + O ₂	C ₂ H ₂ + Air	C ₂ H ₄ + O ₂	C ₂ H ₄ + Air	C ₃ H ₈ + O ₂	C ₃ H ₈ + Air
Explosives	TNM	NM	HDX	RDX	PETN	TATB	TNT	AN	NG	NC*

(*) 12,6 % N.

The fundamental study case is based in nitromethane (NM), a pure chemical, liquid, very known, homogeneous explosive, changing its initial density by adding small percent of glass microballoons (GMB), used generally to sensitize emulsion explosives (vd. Gois et al, 1993). GMB are type C15/250 (supplied by 3M Corporation) with 1 μ m wall thickness and an effective density about $150 \pm 3 \text{ kg.m}^{-3}$. They were sieved in different granulometric classes. Three of them (Table III) were selected to study the effect of GMB on detonation velocity. Detonation velocity, referred to infinite diameter, (obtained by extrapolation), decreases linearly with increasing GMB concentration.

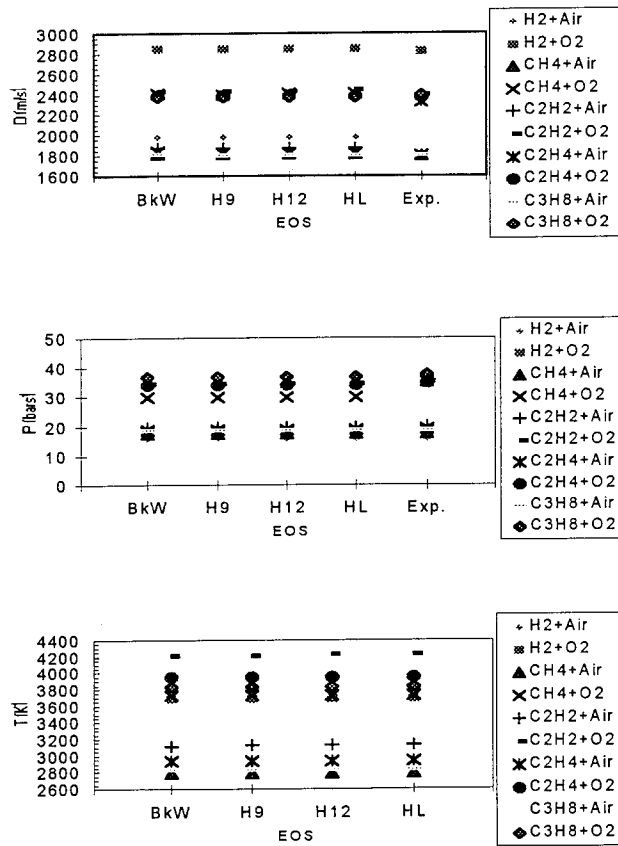


Fig. 3 - Detonation velocity, pressure and temperature of gaseous mixtures.

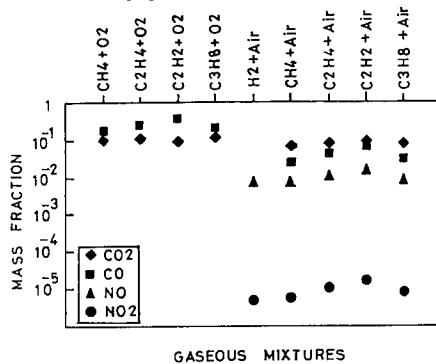


Fig. 4 - Pollutants concentration from gaseous mixtures.

Table III - Density of NM/PMMA-GMB mixtures, as a function of mass fraction (X) and the mean particle size of GMB (d_{p50}).

d_{p50} (μm)	45	75	100
$d_{p10}-d_{p90}$ (μm)	37-50	25-110	34-154
0	1.13	1.13	1.13
0.5	-	1.09	-
1	1.09	-	-
1.44	-	-	0.95
X (%)	1.04	0.97	-
2	1.00	-	-
3	0.96	-	-
4.36	-	0.79	0.68
5	0.90	-	-
6.5	-	-	-

For low GMB concentration its values (vd. Fig. 5) show an excellent correlation with theoretical predictions using H_L EoS. For high GMB concentration the influence of GMB is more important.

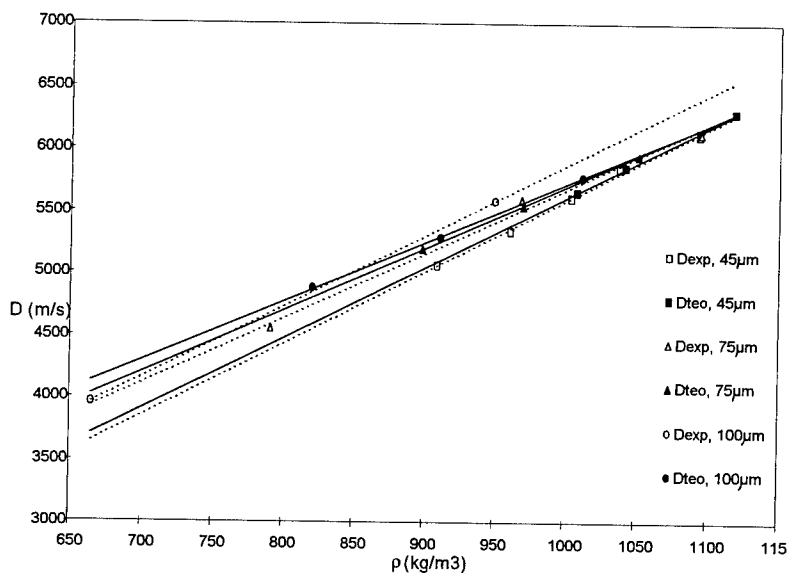


Fig. 5 - Experimental and calculated detonation velocity of NM - PMMA mixtures with GMB of indicated mean diameter.

The most sensible cases are detonation of condensed explosives: TMN, NM, HMX, RDX, PETN, TATB, TNT, AN, NG and NC(12,6%N) (vd. Table II). Figs. 6, 7 and 8 show the detonation velocity, pressure and pollutants concentration of these energetic materials.

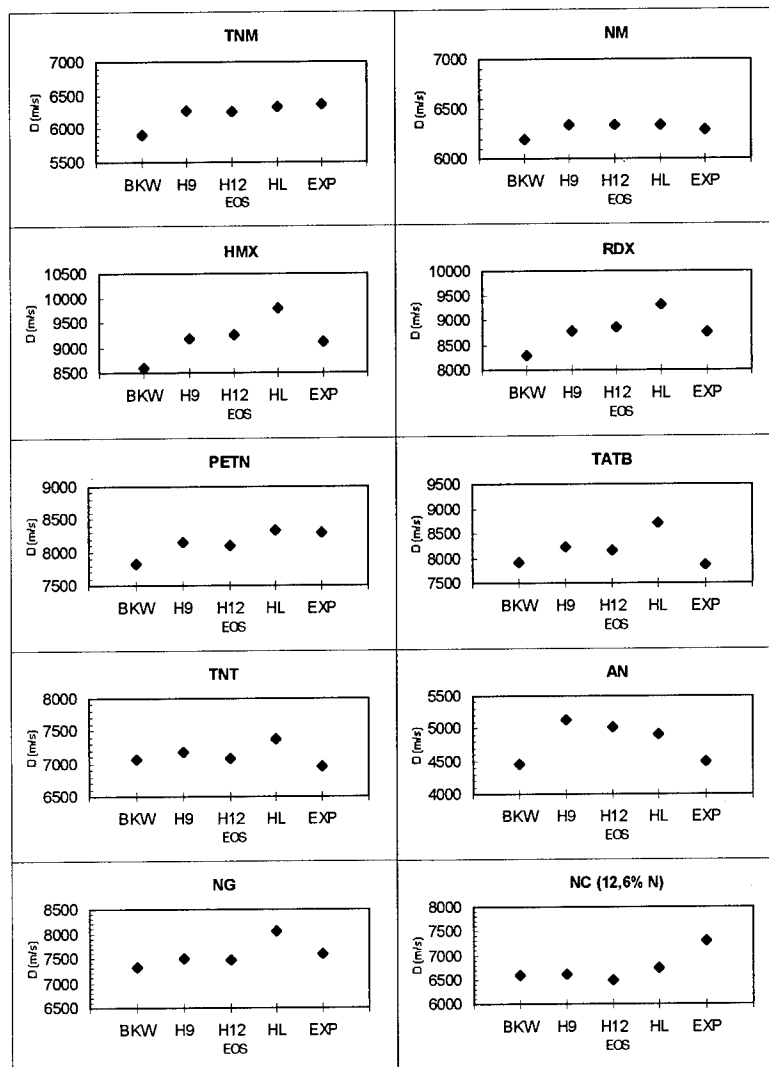


Fig. 6 - Detonation velocity of explosives.

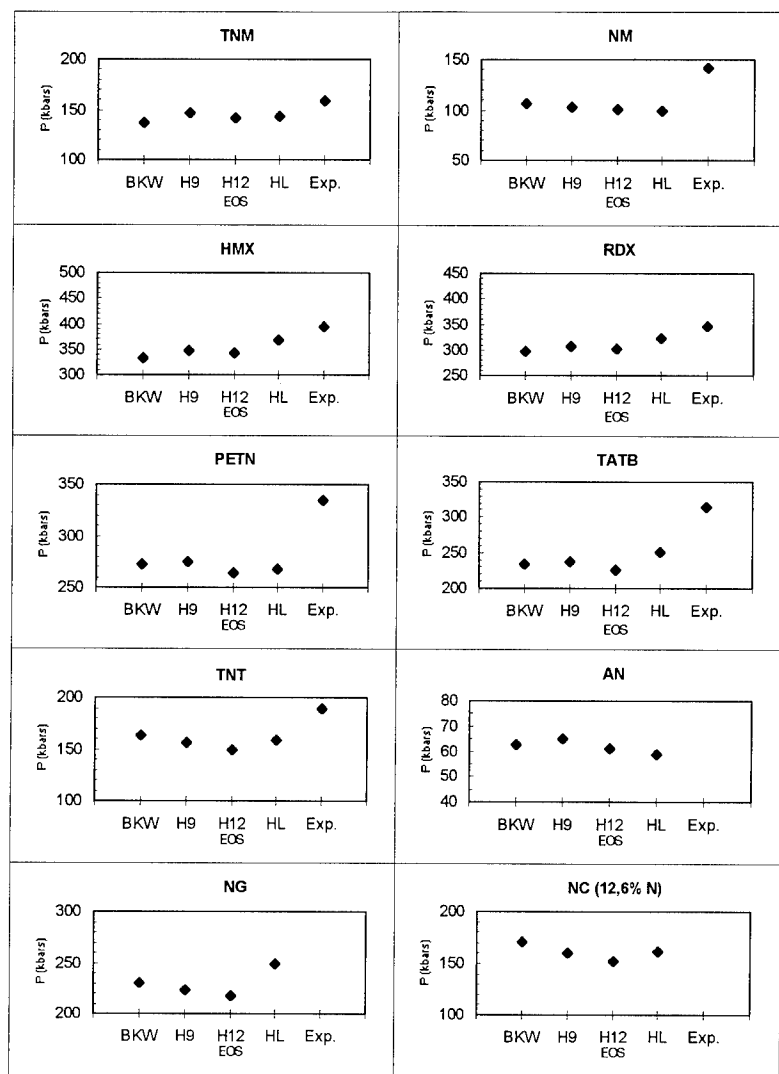


Fig. 7 - Detonation pressure of explosives.

The preceding equations and formulations show an excellent correlation with experimental results of general cases: isobar and isochor adiabatic combustions and Chapman-Jouguet detonation. The most delicate predictions, related to the detonation conditions, are presented.

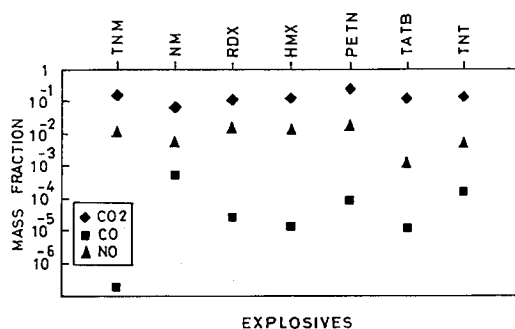


Fig. 8 - Pollutants concentration from explosives.

Analysis of the calculated combustion and detonation products allows to conclude:

- there is no influence of EoS selected to predict combustion products of gas reactants, the influence is insignificant in detonation regime,
- there is a great influence of EoS selected to predict combustion products of condensed reactants, specially in detonation regime.

In general, it is observed a very good correlation between detonation theoretical values using H_L EoS and other EoS. The correlation of theoretical predictions with experimental values, referred to infinite charge diameter, show a very good correlation for the condensed reactive mixtures of equivalence ratio near the stoichiometry. Predicted values, using H_L EoS, are very sensible to the existence of excess of carbon for the richest mixtures.

5. CONCLUSIONS

The present proposed H_L EoS is based on the same assumptions of H9 and H12 EoS but it is based on physical intermolecular potential of gas components instead of correlations to final experimental results.

The preceding equations and formulations show an excellent correlation with experimental results of general cases: isobar and isochor adiabatic combustions and Chapman-Jouguet detonation. The most delicate predictions, related to the detonation conditions, are presented. There is no influence of EoS selected to predict combustion products of gas reactants, and its influence is insignificant in detonation regime. Combustion products of condensed reactants, specially in detonation regime are dependent of chosen EoS.

The correlation of theoretical predictions with experimental values, referred to infinite charge diameter, show a very good correlation for the condensed reactive mixtures of equivalence ratio

ratio near the stoichiometry. Predicted values, using H_L EoS, are very sensible to the existence of excess of carbon for the richest mixtures.

Obtained results and correlations prove the validity of used code and proposed equation of state.

REFERENCES

- BRINKLEY, J.S.R. - *Calculation of the equilibrium composition of systems of many constituents*. «J. Chem. Phys.», 15, 1947, p.107.
- BROWN, W. B. - *Sensitivities of Adiabatic and Gruneisen Gammas to Errors in Molecular Properties of Detonation Products*. «Proceedings of the 9th Symposium (International) on Detonation», Vol. I, 1989, p.513-524.
- BUGAUT, F. et al - *Theoretical Prediction of High Explosives Efficiency: Application to NTO*. «Proceedings of the 7th Symposium (International) on Detonation», Vol. I, 1989, p.489-497.
- CAMPOS, J. - *Thermodynamic calculation of solid and gas combustion pollutants using different equations of state*. «Proceedings of First International Conference on Combustion Technologies for a Clean Environment», Vilamoura, Algarve, Portugal, 1991.
- CAMPOS, J., PORTUGAL, A. AND GOIS, J. C. - *Toxic fumes from industrial explosives*. «Proceedings of First International Conference on Combustion Technologies for a Clean Environment», Vilamoura, Algarve, 1991.
- CHAIKEN, R. F., COOK, E. B., AND RUHE, T. C. - *Toxic fumes from explosives: ammonium nitrate - fuel oil mixtures*. «Report of Investigation n° 7867 », Pittsburgh Mining and Safety Research Center, Pittsburgh, Pa., U. S. A, 1975.
- CHIRAT, R. ; PITTION-ROSSILON, G. - *Detonation Properties of Condensed Explosives Calculated with an Equation of State Based on Intermolecular Potentials*. «Proceedings of the 7th Symposium (International) on Detonation», 1981, p.703-715.
- GOIS, J.C.; CAMPOS, J. AND MENDES, R. - *Shock initiation of nitromethane - PMMA mixtures with glass microballoons*. «Proceedings of the 10th Symposium (International) on Detonation», 1993.
- GORDON, S., MC BRIDE, B.J. - *Computer Program for calculation of complex chemical equilibrium compositions, rocket performance incident and reflected shocks and chapman-jouguet detonations*. «Report NASA SP 273», NASA Lewis Research Center, 1971.
- HEUZÉ, O., BAUER, P, PRESLES, H. N. AND BROCHET, C. - *The equations of state of detonation products and their incorporation into the quatuor code*. «Proceedings of the Eighth Symposium (International) on Detonation», Albuquerque Conventional Center, New Mexico, 1985, p. 762 - 769.
- HEUZÉ, O. - *Cálculo numérico das propriedades das misturas gasosas em equilíbrio termodinâmico*. Universidade de Coimbra, Portugal, 1989.
- HEUZÉ, O. - *Equations of State of Detonation Products: Influence of the Repulsive Intermolecular Potencial*. «Physical Review», 34 (1), 1986, p.428-432.

- HEUZÉ, O., PRESLES, H. N., BAUER, P. - *Computation of Chemical Equilibria*. «J. Chem. Phys.», 83 (9), 1985, p.4734-4735.
- IEPG - PORTUGUESE RESEARCH GROUP - CAMPOS, J., LUZ, P. AND MARQUES, C. - *BKW - KHT - H9 equation of state calculations*. «Report of Progress of Technological Area 25, Cooperative Technical Programme I», Portugal, 1989, 1990.
- JANAF - *Thermochemical Tables* - 2nd Edition. National Bureau of Standards, Washington DC. 1971.
- KUBOTA, N. - *Survey of Rocket Propellants and Their Combustion Characteristics*. «Combustion Characteristics of Rocket Propellants», 1984, p.1-52.
- MANSON, N. - *Cours de Hautes Temperatures*. École Nationale Supérieure de Mécanique et d'Aérotechnique, Poitiers, France, 1976.
- MONTANELLI, T. - *Calcul de la Composition de Mélanges Gaseux dans le Cas de Mélanges de Gaz Réels à l'Aide des Seconds Coefficients du Viriel*. Laboratoire d'Énergétique et de Détonique - Université de Poitiers, 1978.
- TANAKA, K. - *Detonation properties of condensed explosives computed using the Kihara-Hikita-Tanaka equation of state*. «Report from National Chemical Laboratory for Industry», Ibaraki, Japan, 1983.
- TIMNAT, I. M. - *Advanced chemical rocket propulsion*. Academic Press, London, 1987.
- WHITE, W.B., JOHNSON, S.M., DANTZIG, G.B. - *Chemical Equilibrium in Complex Mixtures*. «J. Chem. Phys.», 28, 1958, p. 751.
- ZERILLI, F. J. ; JONES, H. D. - *Calculations of Detonation Pressures for Homologous Series of Polynitroaliphatic Explosives Using a Fluid Perturbation Equation of State and a New Chemical Equilibrium Computer Program*. «Proceedings of the 7th Symposium (International) on Detonation», Vol. I, 1989, p.461-468.

Multidimensional DDT Modeling of Energetic Materials

M. R. Baer, E. S. Hertel and R. L. Bell

Sandia National Laboratories, Albuquerque, New Mexico 87185 USA*

ABSTRACT

To model the shock-induced behavior of porous or damaged energetic materials, a non-equilibrium mixture theory has been developed and incorporated into the shock physics code, CTH. The foundation for this multiphase model is based on a continuum mixture formulation given by Baer and Nunziato. In this nonequilibrium approach, multiple thermodynamic and mechanics fields are resolved including the effects of relative material motion, rate-dependent compaction, drag and heat transfer interphase effects and multiple-step combustion.

This multiphase mixture model provides a thermodynamical and mathematically consistent description of the self-accelerated combustion processes associated with deflagration-to-detonation and delayed detonation behavior which are key modeling issues in safety assessment of energetic systems. An operator-splitting method is used in the implementation of this model, whereby phase diffusion effects are incorporated using a high resolution transport method. Internal state variables, forming the basis for phase interaction quantities, are resolved during the Lagrangian step requiring the use of a stiff matrix-free solver. Remapping of these mixture phase variables is conducted to preserve overall mixture-averaged mass, momentum and energy.

Benchmark calculations are presented which simulate low-velocity piston impact on a propellant porous bed and experimentally-measured wave features are well replicated with this model. This mixture model introduces micromechanical models for the initiation and growth of reactive multicomponent flow that are key features to describe shock initiation and self-accelerated deflagration-to-detonation combustion behavior. To complement one-dimensional simulation, two-dimensional numerical calculations are presented which indicate wave curvature effects due to the loss of wall confinement.

INTRODUCTION

Hazards analysis studies for weapon systems safety and surety assessment includes consideration of a variety of accidental scenarios whereby impact conditions can lead to direct shock initiation or other modes of combustion such as deflagration-to-detonation transition (DDT) and delayed detonation (XDT). These modes of combustion can self-accelerate into detonation due to the behavior of the energetic material microstructure. In particular, the coupled thermal/chemical/mechanical response of internal boundaries is the key issue for assessing the violence of reaction resulting from combustion of the energetic material.

A continuum multiphase model has been developed which describes well the self-accelerated combustion of granular materials as demonstrated in references 1 and 2. A variety of energetic

*This work performed at Sandia National Laboratories supported by the U.S. Department of Energy under contract DE-AC04-94AL85000

materials, including explosives and propellants, has been experimentally and theoretically studied to provide a foundation for simulation in multidimensional analyses. This multiphase model has been recently incorporated into the Sandia National Laboratories shock physics code - CTH³. The interaction of rapid combustion with deformable confinement is a critical aspect of sustained accelerated combustion; thus, simulation of real systems requires the capability of resolving multidimensional, multi-material large deformation, strong shock wave physics.

In the sections to follow, the mixture formulation is outlined and the numerical implementation of this model into the CTH shock physics code is described. One and two-dimensional calculations are presented which provide a benchmark for the nonequilibrium mixture theory.

THEORETICAL FOUNDATIONS

The equations of motion for a multiphase mixture are outlined in this section and recast to a finite volume formulation for shock physics analyses. The full derivation of this description is not repeated here (see Reference 1); hence, only the final forms of the conservation laws are described. Mixture theory is based on the concept that separate phases simultaneously occupy regions of space. Thus, a multiphase material possesses independent thermodynamic and kinematic fields. Multiple balance laws are used to describe a locally averaged thermal, mechanical and chemical response of a collection of condensed phases or gas-filled pores. In contrast to single phase continuum mechanics, a mixture average for a multiphase flow includes the effects of internal boundaries (or phase interfaces) across which the interchange of mass, momentum and energy takes place. These important micro-scale models are the new features of the multiphase description in the shock physics code, CTH.

Modern developments of continuum mixture theory provide the framework for a thermodynamically-consistent description of nonequilibrium processes of fully-compressible reactive mixtures. A unique feature of this approach is the treatment of volume fraction as an independent kinematic variable allowing compressibility of all phases without any compromise on compaction behavior. Specifically, the theory of reactive mixtures firmly establishes balance equations using the Second Law of Thermodynamics in the determination of admissible constitutive relationships for a system of multiphase equations that are well-posed⁴.

As a brief introduction to mixture theory, consider a region in space that is occupied by two phases (denoted by subscript a) - condensed (subscript s) and gas (subscript g). At some appropriate scale, each phase is viewed as occupying every spatial location in the field. Physically, this is not the case since each phase occupies a volume distinct from the other. Thus, to represent the discrete nature of the mixture, each phase is assigned independent thermodynamic and kinematic states. At each point a phase material density, $\gamma_a(x,t)$, is defined which represents the mass per unit volume occupied by each phase and the space displaced by that phase is the volume fraction, $\phi_a(x,t)$. (Volume fraction is a relative fraction of space occupied by material regardless of material type - the fraction of space treated as void is excluded.) Of the fraction of space occupied by the mixture, saturation implies that $\sum \phi_a = 1$ and the density of the local mixture is the sum of partial densities, $\rho = \sum \rho_a$ where $\rho_a = \gamma_a \phi_a$.

In generalized mixture theory, each phase is allowed to have independent velocities, $\dot{\mathbf{v}}_a = \dot{\mathbf{v}}_a(x, t)$, and the conservation equations for each phase are expressed as:

$$\text{Mass:} \quad \dot{\rho}_a = -\rho_a \nabla \cdot \dot{\mathbf{v}}_a + c_a^\dagger \quad (1)$$

$$\text{Momentum:} \quad \rho_a \dot{\dot{\mathbf{v}}}_a = \nabla \cdot \underline{\sigma}_a + \rho_a \dot{\mathbf{b}}_a + \dot{\mathbf{m}}_a^\dagger - \dot{\mathbf{v}}_a c_a^\dagger \quad (2)$$

$$\text{Energy:} \quad \rho_a \dot{e}_a = \underline{\sigma}_a : \dot{\nabla} \dot{\mathbf{v}}_a + \rho_a r_a + e_a^\dagger - (\dot{\mathbf{m}}_a^\dagger - \dot{\mathbf{v}}_a c_a^\dagger) \cdot \dot{\mathbf{v}}_a - c_a^\dagger \left(e_a + \frac{\dot{\mathbf{v}}_a \cdot \dot{\mathbf{v}}_a}{2} \right) \quad (3)$$

By definition, the Lagrangian material derivative is given as: $\dot{f}_a = \partial f / \partial t + \dot{\mathbf{v}}_a \cdot \nabla f$. In these conservation equations, c_a^\dagger is the mass exchange between phases due to chemical reaction, $\dot{\mathbf{b}}_a$ is the external body force, $\dot{\mathbf{m}}_a$ is the momentum exchange resulting from the forces acting on phase boundaries, e_a is the internal energy of each phase, r_a is the external energy source, and e_a^\dagger includes the energy exchange due to heat transfer and the irreversible work done at phase boundaries. The symmetric stress tensor, $\underline{\sigma}_a$, is expressed in terms of the phase pressure, p_a , and the shear stress $\underline{\tau}_a$; thus $\underline{\sigma}_a = -\phi_a p_a \mathbf{I} + \underline{\tau}_a$ where $tr(\underline{\tau}_a) = 0$.

Consistent with the derivations used in mixture theory, summation of each balance equation over all phases yields the response of the total mixture corresponding to the well known equations of motion for a single phase material. The following constraints are imposed on the phase interactions: $\sum c_a^\dagger = 0$, $\sum \dot{\mathbf{m}}_a^\dagger = 0$, and $\sum e_a^\dagger = 0$. The total mixture equations (the identical balance laws solved in CTH) are given (in Eulerian form) as follows:

$$\text{Total Mass:} \quad \dot{\rho} = -\rho \nabla \cdot \mathbf{v} \quad (4)$$

$$\text{Total Momentum:} \quad \rho \dot{\mathbf{v}} = \nabla \cdot \underline{\boldsymbol{\sigma}} + \rho \mathbf{b} \quad (5)$$

$$\text{Total Energy:} \quad \rho \dot{e} = \underline{\boldsymbol{\sigma}} : \nabla \mathbf{v} + \rho r \quad (6)$$

where the overdot denotes the mixture material derivative. By definition, the mixture velocity is the barycentric (mass-averaged) velocity defined as: $\dot{\mathbf{v}} = \sum \rho_a \dot{\mathbf{v}}_a / \rho$ and the phase diffusion velocity (discussed later in this section) is given as $\dot{\mathbf{u}}_a = \dot{\mathbf{v}}_a - \dot{\mathbf{v}}$.

In considering two phases, the restrictions from the Second Law of Thermodynamics suggest admissible forms of phase interaction. For the sake of brevity, the algebraic manipulation will not be repeated here (see Reference 1) and the final forms of these interactions are given as follows:

$$\text{Mass Exchange} \quad c_s^\dagger = c_g^\dagger \quad (7)$$

$$\text{Momentum Exchange} \quad \dot{\mathbf{m}}_s^\dagger = -\dot{\mathbf{m}}_g^\dagger = \delta (\dot{\mathbf{v}}_g - \dot{\mathbf{v}}_s) + c_s^\dagger \dot{\mathbf{v}}_i + p_i \nabla \phi_s \quad (8)$$

$$\text{Energy Exchange} \quad e_s^\dagger = -e_g^\dagger = \dot{\mathbf{m}}_s^\dagger \dot{\mathbf{v}}_s + h (T_g - T_s) + c_s^\dagger \left(e_i - \frac{v_s^2}{2} \right) + W_i^\dagger \quad (9)$$

where the interfacial velocity is defined as, $\dot{\mathbf{v}}_i = (\dot{\mathbf{v}}_s + \dot{\mathbf{v}}_g)/2$, the interfacial surface stress is $p_i = p_g$, the interfacial total energy is $e_i = e_s$ and the dissipative compaction work is defined as: $W_i^\dagger = -(p_s - \beta_s) \cdot \left(\dot{\phi}_s - c_s^\dagger / \gamma_s \right)$. The momentum and energy exchange coefficients representing micro-scale boundary layer effects, δ and h , are modeled as functions of local flow conditions and specific surface area. Finally, after including appropriate equations of state for each phase, closure is obtained by imposing a rate description for volume fraction consistent with the Second Law of Thermodynamics. The evolutionary equation for solid volume fraction is

$$\dot{\phi}_s - c_s^\dagger / \gamma_s = \frac{\phi_s \phi_g}{\mu_c} (p_s - p_g - \beta_s) \quad (10)$$

where the intragranular stress, β_s is defined and the rate of volume fraction change is controlled by the compaction viscosity, μ_c . It is noted that this nonequilibrium multiphase description is somewhat different than that previously implemented in CTH as the multiple pressure and

temperature model. This description implies a slightly different set of mixture rules because the volume fraction is treated as an independent kinematic variable. With this new formulation there is no requirement to renormalize energies, and the local pressure remains a volume fraction-weighted average of individual phase pressures. The rate of change of volume fraction is related directly to the local state of pressure nonequilibrium and includes the effects of combustion.

Having established the general equations of motion for a two-phase description, the model equations are recast into a form consistent with the shock physics modeling in CTH. To recast the equations of motion into integral form, a Lagrangian material derivative is defined as:

$d/dt = \partial/\partial t + \dot{\mathbf{v}} \cdot \nabla$ and $\frac{d}{dt} \int_{\beta} f dV = \int_{\beta} \frac{\partial f}{\partial t} dV + \oint_{\partial\beta} f \dot{\mathbf{v}} \cdot d\mathbf{A}$. Following algebraic manipulation, equation (1), for the gas phase mass conservation, is rewritten as:

$$\frac{d}{dt} \int_{\beta} \rho_g dV = - \int_{\beta} c_s^{\dagger} dV - \oint_{\partial\beta} \rho_g \dot{\mathbf{u}}_g \cdot d\mathbf{A} \quad (11)$$

Simply stated, this equation expresses that the time rate of change of gas mass equals the rate of mass generation as the solid phase decomposes to a gas minus the diffusion of gas mass in or out of the mixture-averaged volume.

In a similar transformation, the gas momentum conservation equation is recast into the following integral form:

$$\frac{d}{dt} \int_{\beta} \rho_g \dot{\mathbf{v}}_g dV = - \oint_{\partial\beta} \dot{\mathbf{n}} \cdot (\phi_g p_g \mathbf{I}) dA + \int_{\beta} \rho_g \dot{\mathbf{b}}_g dV - \int_{\beta} \dot{\mathbf{m}}_s dV + \oint_{\partial\beta} \rho_g \dot{\mathbf{v}}_g \dot{\mathbf{u}}_g \cdot d\mathbf{A} \quad (12)$$

This equation shows that the rate of change of gas momentum is balanced by the pressure forces, body forces, interphase momentum exchange (such as drag) with the last term corresponding to the diffusion of momentum in or out of the mixture-averaged volume.

For gas energy conservation, it is convenient to resolve the total gas energy, $E_g = e_g + (\dot{\mathbf{v}}_g \cdot \dot{\mathbf{v}}_g)/2$, and the integral balance equation for gas phase energy is given as:

$$\frac{d}{dt} \int_{\beta} \rho_g E_g dV = - \oint_{\partial\beta} \dot{\mathbf{n}} \cdot (\dot{\mathbf{v}}_g \phi_g p_g) dA - \oint_{\partial\beta} \dot{\mathbf{n}} \cdot (\dot{\mathbf{u}}_g \rho_g E_g) dA + \int_{\beta} (S_g - e_s^{\dagger}) dV \quad (13)$$

In the above balance laws for gas phase momentum and energy, the stress matrix has been simplified to the form: $\underline{\sigma}_g = -\phi_g p_g \mathbf{I}$, and the energy source includes the body forces:

$S_g = \dot{v}_g \cdot \rho_g \dot{\vec{b}}_g + \rho_g r_g$. This integral equation states that the rate of change of gas energy (including gas phase kinetic energy) is balanced by the work done by the gas pressure forces, the diffusion of gas energy in or out of the mixture-averaged volume and the volumetric energy gain (or loss) due to sources and the interphase exchange of energy occurring at phase boundaries.

To transform Equation 10 into appropriate integral form, it is convenient to resolve the solid phase material density field using the solid phase mass conservation equation. After some algebraic manipulation, this field equation is given as:

$$\frac{d}{dt} \int_{\beta} \gamma_s dV = - \int_{\beta} \gamma_s \frac{(1 - \phi_s)}{\mu_c} (p_s - p_g - \beta_s) dV - \oint_{\partial\beta} \gamma_s \dot{u}_s \cdot dA \quad (14)$$

In general, additional rate equations of the form: $\partial f_a / \partial t + \dot{v}_a \cdot \nabla f_a = f_a^\dagger$ transform to an integral equation using the phase mass conservation equation (1) yielding:

$$\frac{d}{dt} \int_{\beta} \rho_a f_a dV = \int_{\beta} (\rho_a f_a^\dagger + f_a c_a^\dagger) dV - \oint_{\partial\beta} \rho_a f_a \dot{u}_a \cdot dA \quad (15)$$

All of the details to the combustion description, momentum and energy phase interaction and additional heat transfer relationships are given in References 1 and 2. For a two-phase mixture, the velocity components for only one phase and the mixture average need to be resolved. Thus, if the gas phase and mixture averaged velocities are known, then the solid phase velocity is given as $\dot{v}_s = (\rho \dot{v} - \rho_g \dot{v}_g) / (\rho - \rho_g)$ and the solid phase diffusion velocity is determined by $\dot{u}_s = \rho_g (\dot{v} - \dot{v}_g) / (\rho - \rho_g)$.

NUMERICAL IMPLEMENTATION

The shock physics code, CTH, is a multi-material, multi-dimensional Eulerian finite volume code which serves as the platform for implementing the reactive multiphase mixture model. Details of the base code and its material models are not given here and the interested reader is referred to References 5 and 6 for such information.

The current version of CTH uses an Eulerian mesh which is fixed in space. Mixture-averaged conservation equations, in finite volume form, are solved in a Lagrangian step, and distorted cells are remapped back to a fixed mesh. In addition to overall conservation equations, internal state variables are solved using various material models⁷.

In this mixture theory, it is important to note that the overall mixture quantities are never modified; thus, conservation of mass, momentum and energy for the total system are preserved. Mixture rules dictate how these quantities are proportioned for the various phases. Additionally, the local flow velocity is recognized as being a mass-averaged quantity.

The phase conservation equations, given by Equations 11-15, have a common mathematical structure. All of these equations have source and phase diffusion terms. The phase diffusion terms represent advection in or out of the cells following phase diffusion velocity fields. Incorporating these effects is performed using operator splitting whereby all phase quantities are diffused in or out of cells, then the phase quantities are allowed to interact during the Lagrangian step. The methodology of this approach is based on earlier work described in Reference 8.

During the transport step, a Flux-Corrected Transport (FCT)⁹ method is used to incorporate phase diffusion effects and internal boundary conditions are implemented with a variant of virtual cell embedding (VCE)¹⁰. This positivity-preserving high order algorithm does not introduce artificial smearing at material interfaces. It is noted that for shocked flows, phase diffusion quantities are weak and significant only in boundary layer regions.

Typical of multiphase simulation, the interactions of phases occur with greatly disparate time-scales, and thus sources are mathematically stiff. Since explicit time differencing (even with subcycling) is inaccurate, an algorithm based on asymptotic semi-analytical solutions is used for the phase interactions¹¹. As expected, the internal state variables related to the local volume fractions must be accurately resolved to preserve consistency of the numerical solutions. Following the Lagrangian step, the volume fractions for the single mixed phase material are mapped into a single field which are then passed into the remap step. These quantities are subsequently reassembled for equation of state evaluation for the next time step. Sound speed constraints are brought into place for evaluation of Courant conditions.

In the next section, a benchmark numerical solution is discussed in which shock-induced reaction occurs in a porous propellant bed. Although phase diffusion effects are minor in this application, strong phase interactions occur. As such, this example provides a good test problem for the proposed numerical strategy.

LOW VELOCITY IMPACT SIMULATIONS

One-dimensional studies - A one-dimensional benchmark simulation of a piston-driven, low velocity impact on a porous bed of energetic material has been conducted which replicates conditions in an experiment studied by Sandusky, et al¹². A pictorial of this experiment is shown in Figure 1. A gas-driven piston impacts on a bed of NC/NG-based propellant confined in a cylindrical tube geometry.

In these tests, a compaction wave is produced after initial impact and high strain rate at the compaction front triggers low-level reactivity. This unstable process leads to rapid combustion and the formation of a fast deflagration wave and shock formation. The interactions of compaction and multi-stage combustion are clearly complex wave processes.

In the experimental studies by Sandusky and colleagues, numerous diagnostics were used to resolve various wave features¹³. Most importantly, the compaction wave front was probed using microwave interferometry and pressure gauges were used to determine various wave fields. Figure 2 displays the trajectory of the compaction wave, following a 190 m/s piston impact, measured using microwave interferometry. It is to be noted that an abrupt change in wave speed was observed well removed from the piston/propellant interface. Figure 3 displays several pressure gauge records at given location along the tube confinement wall. A weak compaction front is observed followed by the onset of rapid pressurization.

One-dimensional simulations of this experiment using the multiphase mixture model in CTH are displayed in the subsequent figures which replicate all of the features observed in the experimental test. Figure 4 displays an overlay of the volume fraction of the solid phase reactant. Numerical simulation shows a dispersive compaction wave originating from the piston/bed interface that moves at a velocity consistent with the experimental observation.

As a result of high strain rate at the dispersive compaction front, low level of reactivity occurs whereby pyrolysis (or partially decomposed) combustion products are formed in the induction zone. After approximately 100 μ s delay, energy release in the gas phase takes place as the pyrolysis products are converted to final stage combustion gases. A secondary compaction wave is formed and is supported by this reaction. When heat transfer conditions are sufficient to trigger grain burning, very rapid pressurization occurs. Eventually, the combustion wave coalesces with the primary compaction wave and an apparent abrupt change in wave speed occurs. Details of the pressurization field are provided in Figure 5.

As a demonstration of the importance of treating pressure nonequilibrium, Figure 6 displays only the gas phase component of the principle stress. In the early stages of reaction, greatly disparate pressure fields evolve. Much of the initial stress of the primary compaction wave is supported by the motion of the solid reactant material; later, it is the gas phase pressure which leads to a secondary combustion-driven reactive compaction wave.

In Figures 7 and 8, the temperature fields are shown for the gas and solid phases, respectively. As expected, greatly different temperatures arise because much of the energy release takes place in the gas phase. The effects of multi-stage combustion are clearly evident. In figure 8, it is seen that the solid phase undergoes weak compressional heating following initial impact and later gas phase pressurization enhances heat transfer from the combustion gases to the solid phase. Additional compressional heating takes place as the supported secondary compaction wave strengthens to a shock wave.

Two-dimensional simulations - In similar experimental studies conducted at LANL by McAfee, et al.¹⁴, thin wall tubes were used in DDT tests with HMX and the release of confinement near the burning region suggested the formation of multiple "shocks" prior to the onset of rapid burning. These observations are based on sequential X-ray radiographs. Only gross features of the wave fields were measured in these experiments, hence interpreted wave behavior is speculative.

A two-dimensional simulation of a weakly confined column of propellant is presented as a preliminary numerical simulation of piston impact on an energetic granular material held in weak confinement. A thin-walled steel tube, confining a NC/NG propellant, is modeled with impact conditions similar to the one-dimensional simulations discussed earlier. Figure 9 displays split image cross-sectional views of the confined granular energetic material at 50 μ s time intervals following the low velocity impact. In these CTH output plots, gas pressure contours are rendered on the left half of the plots and a dot density representation of the solid phase volume fraction is shown on the right half image plane.

At these early times following impact, it is seen that a curved compaction wave evolves as the lateral release from the wall takes place. The compaction wave is weakly supported and the weakened pressure field lessens the extent of reaction. At a later time, reaction is seen to first arise near the center of the column and a radial wave appears which leads to the secondary compaction wave. As this wave interacts with the confinement, a secondary release takes place and sustained

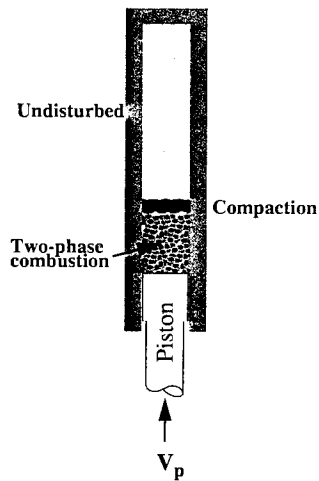


Figure 1. Piston driven compaction experiment in granular propellant porous bed.

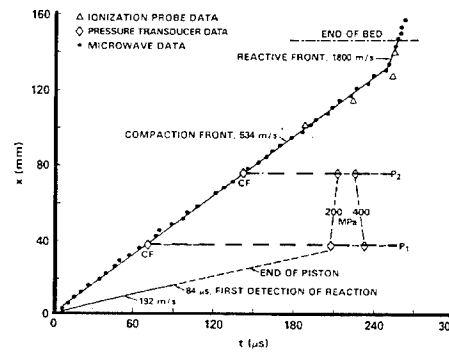


Figure 2. Experimental trajectories of wave fronts following a 190 m/s impact on a granular ball propellant bed.

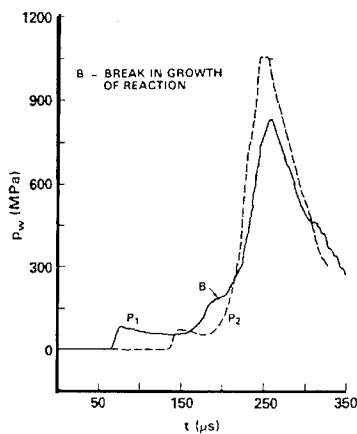


Figure 3. Pressure gauge measurements at two locations along the confined porous propellant

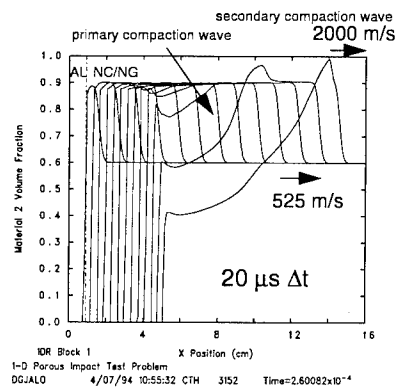


Figure 4. Overlay of volume fraction wave fields for a 190 m/s impact.

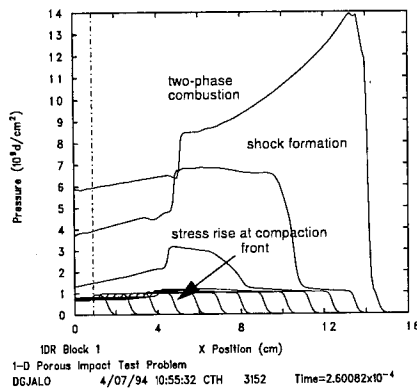


Figure 5. Overlay of pressure wave fields during impact and subsequent reaction in the porous propellant.

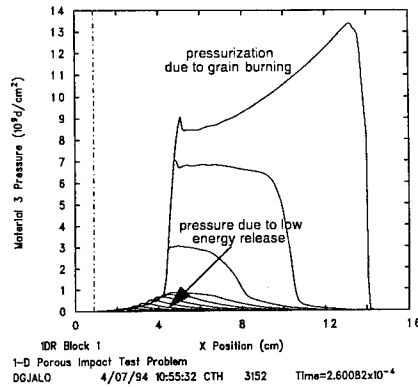


Figure 6. Gas phase pressures at 20 μ s intervals during compaction and reaction.

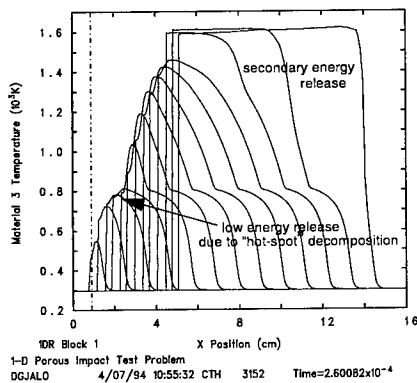


Figure 7. Overlay of gas phase temperatures in one-dimensional CTH simulation of low velocity impact.

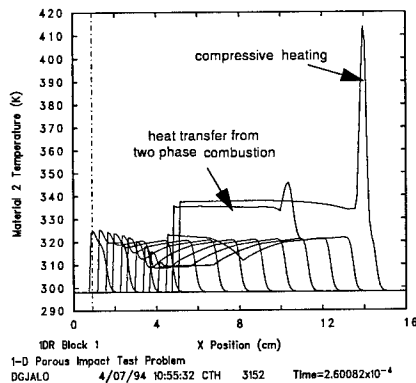


Figure 8. Overlay of solid reactant phase temperatures in one-dimensional CTH simulation of low velocity impact.

reaction greatly depends on the pressurization from low level combustion competing with the dissipation by rarefaction of confinement release. As expected, the interaction with the combustion reactions and compaction fields in multidimensional simulation is strongly influenced by the effects of confinement. Simulation of the LANL experiments may lead to a better understanding of this multidimensional behavior.

Future work is planned to simulate these low velocity experiments for a granular bed of HMX explosive. Additionally, statistical crack fracture models are being incorporated into CTH and the reactive multiphase mixture model will be coupled to address simulation of delayed detonation. Mixture theory is also being formulated to treat more than two phases and this is being incorporated as an extension for multiphase predictive capabilities.

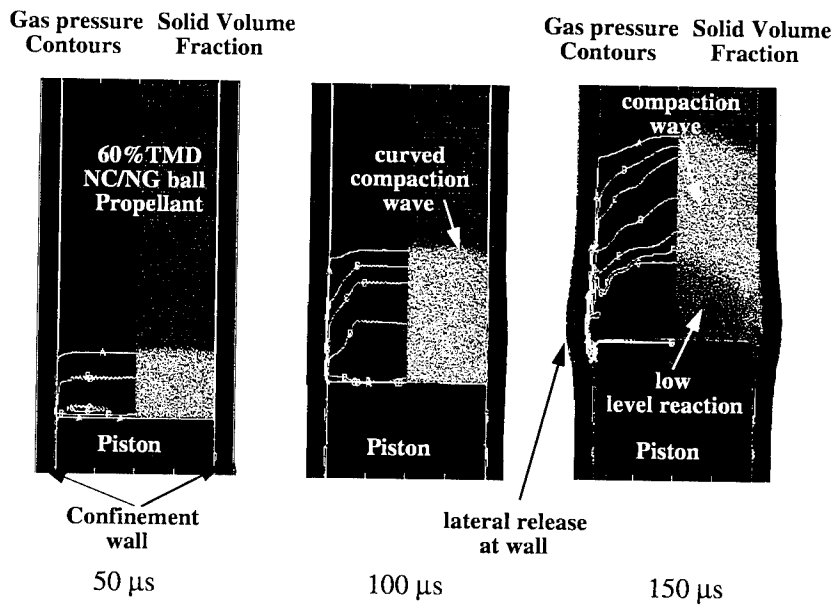


Figure 9. Two-dimensional CTH simulations of low velocity impact (200 m/s) on a weakly confined porous column of ball propellant.

SUMMARY

A nonequilibrium multiphase mixture model is described in this paper which has been implemented into shock physics analysis. The effects of strong phase interaction including combustion, momentum and energy exchange are treated by allowing mixed phases to have relative velocities and independent thermal and stress fields. An operator splitting method is described for the numerical implementation of this model.

Preliminary benchmarks of this mixture approach have addressed low-velocity impact experiments in one and two-dimensional simulations. All of the observed reactive wave behavior are replicated in the modeling. Multidimensional simulation can serve as an important numerical diagnostic for probing the nature of the complex wave fields in reactive granular materials. Future work is aimed toward using this tool with experimental studies of energetic material response to enhance predictive capabilities for weapon safety and surety assessment.

REFERENCES

1. Baer, M. R. and Nunziato, J. W., "A Two-Phase Mixture Theory for Deflagration-to-Detonation Transition (DDT) in Reactive Granular Materials," **International Journal of Multiphase Flow**, Vol. 12, 1986, pp 861-889.
2. Baer, M. R. and Nunziato, J. W., "Compressive Combustion of Granular Materials Induced by Low-Velocity Impact," **Ninth Symposium (International) on Detonation**, OCNR 113291-7, 1989, pp 293-305.
3. McGlaun, J. M., Thompson, S.L., Kmetyk, L. N. and Elrick, M.G., "A Brief Description of the Three-Dimensional Shock Wave Physics Code CTH," Sandia National Laboratories, SAND89-0607, 1990.
4. Embid, P. and M. R. Baer, "Mathematical Analysis of a Two-Phase Continuum Mixture Theory", **Continuum Mechanics and Thermodynamics**, Vol 4, 1992, pp 279-312.
5. McGlaun, J. M., "CTH Reference Manual: Lagrangian Step for Hydrodynamic Materials" Sandia National Laboratories, SAND90-2645, 1990.
6. McGlaun, J. M., "CTH Reference Manual: Cell Thermodynamics," Sandia National Laboratories, SAND91-0002, 1991.
7. Kerley, G. I., "CTH Equation of State Package: Porosity and Reactive Burn Models," Sandia National Laboratories, SAN92-0553, 1992.

8. Gross, R. J., and M. R. Baer, "A Study of Numerical Solution Methods for Two-Phase Flow," Sandia National Laboratories, SAND84-1633, 1986.
9. Boris, J. P., A. M. Landsberg, E. S. Oran, and J.H. Gardner, "LCPFCT- A Flux-Corrected Transport Algorithm for Solving Generalized Continuity Equations," Naval Research Laboratory, NRL/MR/6410-93-7192, 1993.
10. Landsberg, A. M., J. P Boris, T. R. Young and R. J. Scott, "Computing Complex Shocked Flows Through the Euler Equations," **Proceeding of the 19th International Symposium on Shock Waves**, University of Provence, Marseille, France, 1993.
11. Oran, E. S. and J. P. Boris, **Numerical Simulation of Reactive Flow**, Elsevier, pp 134-180, 1987.
12. Sandusky, H. W. and R. R. Bernecker, "Compressive Reaction in Porous Beds of Energetic Materials," **Eighth Symposium (International) on Detonation**, NSWC MP 86-194, 1985, pp. 881-891.
13. Glancy, B. C., H.W. Sandusky, P. J. Miller and A.D. Krall, "Dynamic Compaction and Compressive Reaction Studies for Single and Double-base Ball Propellants," **Ninth Symposium (International) on Detonation**, OCNR 113291-7, 1989, pp 341-353
14. McAfee, J. M., B. W. Assay, A. W. Campbell and J. B. Ramsay, "Deflagration to Detonation in Granular HMX," **Ninth Symposium (International) on Detonation**, OCNR 113291-7, 1989, pp 256-279.

BURNING RATE MODIFIERS FOR AN/HTPB-IPDI COMPOSITE SOLID PROPELLANTS FOR GAS GENERATORS

P. Carvalheira and J. Campos

Departamento de Engenharia Mecânica, Faculdade de Ciências e Tecnologia da Universidade de Coimbra, Largo de D. Dinis, P-3000 Coimbra, Portugal

G.M.H.J.L. Gadiot

TNO Prins Maurits Laboratorium, Lange Kleiweg 137, Postbus 45, 2280 AA Rijswijk, The Netherlands

ABSTRACT

Ammonium nitrate (AN) is the base component for a family of gas generator and rocket composite propellants. The chlorine free and low pollutants combustion products are their main advantages. It is known that its limitations are due not only to the phase transitions IV to III of AN crystal lattices, occurring near 305 K (32 °C) with large volume changes, but are also due to its low burning rate and high hygroscopicity. The phase transition problem is detrimental to the mechanical properties of propellants when they are subjected to thermal cycling around 305 K. The phase transition problem is generally solved through the incorporation of metal oxides of transition metals such as Ni, Cu and Zn, into the AN crystal lattice. Curing agents, plasticizers, cross linkers, stabilizers and antioxidants are also important in propellant formulations to achieve acceptable energetic and mechanical properties, processability and ageing behaviour. Hydroxyl terminated polybutadiene (HTPB) prepolymer and isophorone diisocyanate (IPDI) as curing agent are generally used as the base binder system. The objective of the present work is to select and evaluate the influence of burning rate modifiers on a standard, simple AN/HTPB-IPDI propellant formulation. Calorimetric bomb measurements show the correlation between theoretical and experimental enthalpy of reaction values, evaluating the non ideal behaviour of tested propellants. The detrimental effects of the high hygroscopicity of AN particles on propellant production was avoided by imposing low humidity ambient conditions for manufacture and storage. Phase stabilised ammonium nitrate (PSAN) was used that includes NiO (1 wt.%) as phase stabilising agent. PSAN/HTPB-IPDI compositions are tested with Iron (III) oxide and Chromium (III) oxide as burning rate modifiers. PSAN solid loading has been chosen in such a way that the effect of solid loading change in the propellant formulation does not mask the effect of the burning rate modifiers. Thermodynamic calculations indicate the range 72 - 75 % of AN solid loading to be adequate. The burning rate behaviour of the manufactured propellants was evaluated with a strand burner in the pressure range 2 - 10 MPa. The obtained results prove the applicability of this kind of propellants to gas generators.

Nomenclature

a	pre-exponential factor of Vieille's law
d	particle diameter, μm
m	mass, mg
n	pressure exponent of Vieille's law
n_i	moles of atomic species i , mol
p	pressure in Vieille's law, MPa
Q_{HHV}	gross heat of combustion at constant volume, MJ/kg
r	burning rate, mm/s
R	universal gas constant, kJ/(mol.K)
T	temperature, K
TMD	theoretical maximum density, kg/m ³
x_i	mass fraction of component i , adimensional

Greek Symbols

ρ_i	density of component i , kg/m ³
----------	--

1. Introduction

Research on AN/HTPB-IPDI propellants has gained interest for certain pyrogenic igniters and gas generators applications due to their advantages of chlorine free and low corrosive combustion products [1,2]. The phase transition IV to III in the AN crystal lattices occurring at 305 K (32 °C) with a large volume change, the high hygroscopicity of AN and low burning rate are among the disadvantages [1,3]. One solution for the phase transition problem is the incorporation of metal oxides of transition metals, such as Ni, Cu and Zn, into the AN crystal lattice [3]. Low flame temperature is another characteristic of these compositions. It can be an advantages or a disadvantage according to the application [1,2]. The hygroscopicity problem of AN is not solved yet but has been countered imposing the requirements of low humidity ambient conditions for AN/HTPB-IPDI propellants manufacture and storage [4]. The problem of low burning rate has not been solved, but progress has been made [2,5,6]. The development of new formulations and manufacturing processes for this kind of propellants might be interesting because they have a potential for low pollutant and low cost manufacturing [7].

The objective of this work is to evaluate, in a systematic way, the effect of identified burning rate modifiers for propellant formulations based in AN and HTPB-IPDI as main ingredients that might present high potential for practical applications in the near future. Phase stabilised ammonium nitrate (PSAN) was used that includes NiO (1 wt.%) as phase stabilising agent. Thermodynamic calculations indicate that AN/HTPB-IPDI propellant formulations with AN solid loading in the range 72 - 75 % have small gradients in adiabatic flame temperature and specific impulse. This small gradients allow a clear evaluation of the effect of burning rate modifiers on PSAN/HTPB-IPDI formulations allowing to neglect the influence of changes in AN solid loading from batch to batch and from composition to composition with increasing burning rate modifier. The influence of one type of Iron (III) oxide and one type of Chromium (III) oxide burning rate modifiers on selected PSAN/HTPB-IPDI composite solid propellant formulations have been investigated. All this selected composite propellant formulations include 25 wt.% HTPB-IPDI binder system. A preliminary investigation was conducted using TG/DTA thermal analysis at low heating rates (10 °C/min) and atmospheric pressure under N₂ atmospheres on the effect of this Iron(III) oxide burning rate modifier on the thermal decomposition of PSAN, of HTPB-IPDI and of the selected PSAN/HTPB-IPDI composite solid propellant formulations. This thermal analysis investigation indicates that Iron(III) oxide has a small effect on the kinetics of thermal decomposition of cured HTPB-IPDI binder and no effect on the thermal decomposition of PSAN [5]. This thermal analysis investigation was then also extended to the effect of this Chromium(III) oxide burning rate modifier on the thermal decomposition of PSAN, of HTPB-IPDI and of the selected PSAN/HTPB-IPDI composite solid propellant formulations and it indicates that Chromium(III) oxide has a noticeable effect on the kinetics of thermal decomposition of PSAN and no effect on the thermal decomposition of cured HTPB-IPDI binder [5]. Eight compositions have been selected. The propellant ingredients have been characterized, then the density of each propellant has been measured. The burning rate and the combustion wave structure were measured in a strand burner, in the pressure range 2-10 MPa, at 288 K. We expect that the methodology used in this work will allow us to predict with more confidence the effect of selected burning rate modifiers for PSAN/HTPB-IPDI formulations in other formulations with larger AN solid loading.

2. Thermodynamic Calculations

Thermodynamic calculations were performed to predict characteristics of selected AN/HTPB-IPDI propellant formulations with AN solid loading in the range 70-100 wt.%.: flame temperature, molecular weight of combustion products, isentropic compression coefficient (Γ), specific impulse and combustion products composition. The thermodynamic equilibrium calculations were performed using the NASA-Lewis CET89 code [8,9]. The AN considered was not phase stabilised. The HTPB-IPDI weight ratio in the binder is 92.32-7.68 wt.% and is typical of that used in practical composite solid propellant formulations. This binder system has excellent mechanical properties even in the low temperature end of the temperature range of most practical applications (- 60 °C to + 60 °C) [1,2,4]. The calculations were performed for isobaric adiabatic combustion at 7.0 MPa, considering an adiabatic expansion through a nozzle

in one-dimensional flow at chemical equilibrium and with an expansion ratio 70:1. Thermochemical data of propellant ingredients was obtained from reference [10]. The results for adiabatic flame temperature and specific impulse after expansion through the nozzle are presented in Fig. 1. Detailed results, presented in Figs. and Tables, can be found in Ref. [11]. Fig. 1 shows the small influence of AN solid loading on flame temperature and specific impulse in the range 72-75 wt.%, due to the relatively high level of equivalence ratio to stoichiometry. The range of AN solid loading has been chosen in order to show negligible burning rate combustion variations for small variations in AN solid loading (0-2 wt.%). Consequently, more important variations are only due to the influence of burning rate modifiers. This allows an indication that this AN solid loading range is good for propellant formulations allowing the study of the influence of burning rate modifiers on AN/HTPB-IPDI formulations.

Table 1. Thermochemical data and density of propellant ingredients

Reactant	Chemical Composition	ΔH_f^0 _{298.15} /(kcal.mol ⁻¹)	Density / (kg/m ³)	References
PSAN	H ₄ N ₂ O ₃	-87.27	1725	10
HTPB	C ₁₀ H _{15.616} N _{0.203} O _{0.196}	-10.90	901	10
IPDI	C ₁₂ H ₁₈ N ₂ O ₂	-111.40	1061	10, 12
Flexzone 6H	C ₁₈ H ₂₁ N ₂	-5.37	1290	13
Fe ₂ O ₃	Fe ₂ O ₃	-197.30	5100	14, 15
Cr ₂ O ₃	Cr ₂ O ₃	-272.20	5210	14, 16

2.1. Adiabatic Flame Temperature

The adiabatic flame temperature of the propellants in this AN solid loading range increases slightly from 1215 K to 1245 K in the range 72-75 wt.% AN, as shown in Fig. 1.

2.2. Specific Impulse

The specific impulse of the propellants in this AN solid loading range increases slightly from 1888 m/s to 1909 m/s in the range 72-75 wt.% AN, as shown in Fig. 1.

2.3. Theoretical Combustion Products Composition

Theoretical calculations of combustion products predict, in this range, no formation of carbon (graphite) in the combustion chamber but having formation of carbon (graphite) in the nozzle exit. The amount of graphite formed in the nozzle exit decreases from 0.10437 to 0.06077 when AN solid loading increases in the range 72-75 wt.%. CO is the most important pollutant [17] calculated in the nozzle exit in this AN solid loading range and it increases from 0.04493 to 0.050420 when AN solid loading increases in the range 72-75 wt.%.

3. Experimental

3.1. Propellants composition and preparation

Table 2. Composition of propellant formulations, in wt.%

	PC05	PC09	PC11	PC12	PC13	PC14	PC15
Fe ₂ O ₃	0	0.375	0.750	1.875	0	0	0
Cr ₂ O ₃	0	0	0	0	0.375	0.750	1.875
PSAN	75.000	74.625	74.250	73.125	74.625	74.250	73.125
HTPB	22.850	22.850	22.850	22.850	22.850	22.850	22.850
IPDI	1.900	1.900	1.900	1.900	1.900	1.900	1.900
Flexzone 6H	0.250	0.250	0.250	0.250	0.250	0.250	0.250

Propellant compositions studied are listed in Table 2.

The used PSAN contained 1.0 wt.% NiO as phase stabilising agent, 0.5 wt.% Petro as anticaking agent and was obtained from ICT, Germany. Significant values of measured particle size diameter distribution were: $d_{10} = 50 \mu\text{m}$; $d_{50} = 140 \mu\text{m}$; $d_{90} = 275 \mu\text{m}$, measured using a MALVERN Particle Sizer 2600 with a powder-in-air method at 15% RH and 20 °C ambient temperature.

HTPB Poly Bd R45HT was obtained from Atochem. According to the general information of Atochem its molecular weight is 2800 g/Eq, % trans-1,4 = 60, % cis-1,4 = 20, and % vinyl-1,2 = 20, hydroxyl value is 0.83 meq/g, hydroxyl number is 46.6 mg KOH/g [18]. Hydroxyl number was measured and found to be 46.5 mg KOH/g. IPDI was obtained from Fluka Ref. 59192. A ratio NCO:OH = 0.90 was used in all compositions including IPDI. This NCO:OH ratio allows to obtain a tensile strength of about 90 % of the maximum obtainable and an elongation at break of about 20 % for our binder system HTPB-IPDI taking into account the molecular weight, hydroxyl number and average functionality of this HTPB prepolymer and the values of this parameters in HTPB prepolymers studied in reference [19]. Flexzone 6H was the

antioxidant used for the binder. Burning rate modifiers used were Fe_2O_3 BayFerrox 180 (purity: 96-97 %), $d_p = 0.7 \mu\text{m}$, obtained from Bayer Chemie A.G. [15], and Cr_2O_3 (purity > 98%) $d_p = 1 \mu\text{m}$, was obtained from Aldrich, Cat. No. 20,216-9 [16].

Propellant samples were mixed in a horizontal Z blade mixer (Werner & Pfleiderer), under vacuum (absolute pressure less than 80 mbar) at temperatures in the range 313-323 K (40-50 °C). Casting was performed in a conditioned room at a temperature 18-23 °C and a relative humidity less than 20 %, at atmospheric pressure. All propellants were cast in high density polyethylene (HDPE) containers of 93.6 mm width and 151.5 mm length. The thickness of the propellant casted samples was 12-13 mm. After casting, they stayed in the conditioned room with a temperature 18-23 °C and relative humidity less than 20 %, at atmospheric pressure, for 36 hours to allow the expulsion of small bubbles formed during casting of the propellants. The propellants were cured at atmospheric pressure at 323 K (50 °C) for 10 days.

3.2. Density of propellants

The density and the mass fraction of each propellant ingredient are presented respectively in Table 1 and Table 2. The actual density of the casted propellants is presented in Table 3. The Theoretical Maximum Density (*TMD*) of propellants was calculated using equation (1). Calculated *TMD* and actual density over *TMD*, in percentage, (% *TMD*) is also presented in Table 3. For some compositions actual density over *TMD* is larger than 100.0 %. This result can be justified not only by the existence of an experimental error but also to the fact that the actual density of the cured HTPB-IPDI polymer is probably larger than the value obtained by simply applying equation (1) to this two propellant ingredients (due to the curing reaction of HTPB with IPDI). In the absence of data on mechanical properties of the tested propellants the proximity between the values of the measured and calculated densities allow us to have confidence in the quality of the manufactured propellants.

$$TMD = \left(\sum_{i=1}^n \frac{x_i}{\rho_i} \right)^{-1} \quad (1)$$

Table 3. Density of propellants

Property	PC05	PC09	PC11	PC12	PC13	PC14	PC15
density ^a /(kg/m ³)	1414	1413	1423	1426	1420	1429	1433
<i>TMD</i> ^b /(kg/m ³)	1412	1415	1418	1426	1415	1418	1427
% <i>TMD</i>	100.1	99.86	100.4	100.0	100.4	100.8	100.4

^a $\pm 5 \text{ kg/m}^3$

^b calculated

3.3. Heat of combustion measurements

The experimental measurements of heat of combustion of propellant compositions were made in a PARR 1271 oxygen bomb calorimeter. The samples were burned in excess oxygen at 3.06 MPa (450 psia) and at initial temperature 29.4 °C (85 °F) in a procedure close to standard ASTM D2015 [21], with the adaptations necessary to make measurements with these composite solid propellant samples. Five test were made for each propellant composition. The results of gross heat of combustion at constant volume, Q_{HHVv} , obtained in the measurements are shown in Table 4, in the form of average and standard deviation.

Table 4. Heat of combustion of propellant compositions

Propellant	PC05	PC09	PC11	PC12	PC13	PC14	PC15
Fe ₂ O ₃ /wt. %	0	0.375	0.750	1.875	0	0	0
Cr ₂ O ₃ /wt. %	0	0	0	0	0.375	0.750	1.875
Q_{HHVv} /(MJ/kg)	12.696	12.992	13.025	12.399	12.746	12.425	12.459
σQ_{HHVv} /(MJ/kg)	0.245	0.045	0.085	0.058	0.192	0.070	0.241
σQ_{HHVv} / %	1.93	0.35	0.65	0.47	1.51	0.56	1.93

3.4. Burning rate measurements

3.4.1. Samples

Propellants strands of 10 x 10 x 89 mm (width x length x height) were cut, with a sharp steel blade, from the propellant casted samples. Reliable ignition was successfully obtained by joining to the propellant strand a cubic ignition pellet (10 mm side length) of AP/Al/HTPB composition, allowing a smooth ignition of the propellant strand. Each propellant strand was put together with a cubic ignition pellet and held in close contact by an elastic rubber band. The set was then coated with a couple of epoxy resin layers, used as inhibitor during combustion of the propellant strand. Holes were then drilled at two planes in the propellant strand separated by 65.0 mm. Lead fuse wires were passed through these holes. The cubic ignition pellet was drilled at its middle plane to pass the nichrome ignition wire.

3.4.2. Experimental apparatus

A schematic of the experimental apparatus used for burning rate measurements is shown in Fig. 2. Burning rate measurements were carried out in an original vented strand burner with cylindrical chamber 80 mm in diameter, 225 mm in length and 1.1 dm³ in volume, designed and build at University of Coimbra (UC) and shown in Fig. 2.

Venting of the strand burner provides a constant pressure level during combustion. The venting gas inlet is at the bottom of the strand burner. The venting nozzle is of fixed geometry during each test and its geometry is selected using a program developed at UC [20]. A variety of venting nozzles is available that can be selected for optimum conditions in strand burner combustion experiments at various chamber pressures up to 10 MPa and larger. The geometry is selected in order to have the smallest cross section area of the venting nozzle, to reduce the venting nitrogen consumption, and still hold a pressure variation during the test less than 0.25 %. This pressure variation was verified in actual tests.

The ignition of the samples is performed by an electrically heated nichrome wire 0.75 mm in diameter. The ignition composition is a AP/Al/HTPB-IPDI-Flexzone 6H (64/16/18.26-1.54-0.20 wt.%) composition with AP average particle size diameter 254 μ m and Al particle size diameter less than 150 μ m, average particle size 94 μ m (Eckart Werke Grade EW 150/0).

To measure the burning rate two Lead fuse wires 0.25 mm in diameter were used. The burning rate measuring length is 65.0 mm. The fuse wires were connected to a Wheatstone bridge circuit, shown in Fig. 2, to give a voltage output step, as shown in Fig. 3, when each of the fuse wires was cut by melting by the propellant flame front. Defining the burning time as the time interval between the melting of the first fuse wire and the melting of the second fuse wire, the burning rate was calculated by dividing the distance between the two fuse wires by the burning time.

A SETRA 205 capacitive pressure transducer, of pressure range 0-3000 psia (0-20.68 MPa), was used to measure the pressure inside the strand burner during each test. The pressure transducer is mounted at the bottom of the strand burner and is electrically insulated from the strand burner body by a nylon 6 connection. The measuring volume and connections to the strand burner body are filled with synthetic lubricating engine automobile oil. The pressure level considered for each test was the measured average pressure level during the burning time.

A thermocouple type K (THERMOCOAX) of 1.0 mm diameter is used to measure the temperature of the venting gas previous to and during each test. The signals were acquired by a DATA TRANSLATION DT2812-A data acquisition board connected to a IBM PC compatible computer. All the experimental data analysis was performed in the same computer.

Table 5. Vieille's law burning rate parameters ($r = a p^n$)

Propellant	PC05	PC09	PC11	PC12	PC13	PC14	PC15
Fe ₂ O ₃ /wt. %	0	0.375	0.750	1.875	0	0	0
Cr ₂ O ₃ /wt. %	0	0	0	0	0.375	0.750	1.875
<i>p</i> range /MPa	1.5-9.9	1.1-9.9	2.0-10	2.0-10	1.2-10	1.3-10	1.3-10
<i>a</i>	0.476	0.546	0.564	0.569	0.558	0.596	0.612
<i>n</i>	0.577	0.463	0.453	0.433	0.475	0.458	0.488
correlation	0.985	0.994	0.988	0.995	0.995	0.997	0.997

4. Discussion of Results

These measurements of heat of combustion show the effect of these burning rate modifiers on the efficiency of combustion. These measurements are made at equivalence ratio conditions less than 1.0 (lean mixture) while the combustion of these propellant formulations in this strand burner are made at an equivalence ratio close to 2.34 (rich mixture), similar to the equivalence ratio in a rocket motor combustion chamber. Consequently, the results of these heat of combustion measurements have only an indicative value and the consideration of the results to the combustion conditions in a rocket motor combustion chamber must be made with care.

The measurements of heat of combustion of propellant formulations including Fe₂O₃ show an increase in Q_{HHV} when this burning rate modifier is added to the base composition in amounts 0.375-0.750 wt.%. The values of Q_{HHV} for compositions containing 0.375-0.750 wt.% of Fe₂O₃ overlap within experimental error. When 1.875 wt.% Fe₂O₃ is added to the base composition the value of Q_{HHV} shows a decrease. This is an indication that a saturation effect of Fe₂O₃ is attained for these formulations in the range 0.375-0.750 wt.% of Fe₂O₃.

The measurements of heat of combustion of propellant formulations including Cr₂O₃ overlap within experimental error with the values of Q_{HHV} for the base propellant formulation (PC05). The general trend of the average values of Q_{HHV} is to decrease when this burning rate modifier content is increased.

The typical values of heat of combustion obtained for the propellant formulations studied are about 13 MJ/kg. The values of heat of combustion for hydrocarbons like polybutadiene with a ratio n_H/n_C equal to 1.5 is about 42 MJ/kg. Because these formulations have 25.0 wt.% of binder if the heat of combustion was only due to the combustion of the hydrocarbon we would have for these composition Q_{HHV} approximately equal to 10.5 MJ/kg. We can conclude that the PSAN is only giving a minor contribution to the heat of combustion even if it is present in amounts close to 75 wt.%. With this picture in mind and the results obtained it can be concluded that the Fe₂O₃ burning rate modifier in amounts in the range 0.375-0.750 wt.% promotes the combustion of the HTPB binder system while the Cr₂O₃ burning rate modifier doesn't promotes the combustion of the HTPB binder system.

Preliminary thermal analysis investigations indicates that Cr_2O_3 has an effect on the last thermal decomposition peak of PSAN changing it from endothermic to exothermic when Cr_2O_3 is added to PSAN [6], while Fe_2O_3 has no noticeable effect on thermal decomposition of PSAN [6]. The mechanism of burning rate increase of these propellants when this Cr_2O_3 is added seems to be connected with the increase in heat generation, associated with thermal decomposition of PSAN, in the propellant surface during propellant burning.

The results of burning rate measurements with the compositions including Fe_2O_3 burning rate modifier show a monotone decrease in pressure exponent and a monotone increase in pre exponential factor of Vieille's law when this burning rate modifier is used in the range 0-1.875 wt.% content.

This Cr_2O_3 burning rate modifier promotes a larger increase in burning rate on these propellants than this Fe_2O_3 burning rate modifier, when the same amount is added, in all the pressure range 2-10 MPa as it can be seen in Table 5 and in Fig. 4. This increase is especially noticeable at medium pressures and is obtained with a low pressure exponent.

During burning experiments, it was observed the formation of tar in the exit of the strand burner venting nozzle when the burning pressure was less than 4.0 MPa for propellant formulations including Fe_2O_3 , and when the burning pressure was less than 5.0 MPa for propellant formulations including Cr_2O_3 . This fact leads to recommend to consider a burning pressure above 4.0 MPa for propellants including Fe_2O_3 , and a burning pressure above 5.0 MPa for propellants including Cr_2O_3 , in practical applications.

In consequence, it can be concluded that this Fe_2O_3 burning rate modifier is very interesting in the aspects of increasing reliability and safety (due to low n) and efficiency (due to high Q_{HHV}) of gas generators or rocket motors that use these formulations and then in a less important way by increasing performance through increased burning rate.

The formulations studied show that this Cr_2O_3 burning rate modifier has not attained saturation until an amount of 1.875 wt.% because the burning rate pre-exponential factor increases steadily with increasing Cr_2O_3 burning rate modifier content in the range 0-1.875 wt. %, while the pressure exponent oscillates in the range 0.458-0.488 in compositions including this burning rate modifier. A typical increase in burning rate in the range 4-6 MPa for propellant formulation including 1.875 wt.% Cr_2O_3 is 20 % when compared to the base formulation PC05.

This study suggests that Fe_2O_3 burning rate modifier in this type of propellants is more effective in reducing the formation of tar in the nozzle exit than Cr_2O_3 . Because tar is formed due to incomplete oxidation of the binder system HTPB-IPDI this result is in accordance with a preliminary thermal analysis investigation that indicates that this Fe_2O_3 has an effect on the thermal decomposition of the HTPB-IPDI binder system [6], and with measurements of heat of combustion that indicate that the Fe_2O_3 burning rate modifier is promoting the combustion of the binder revealed by the larger heat of combustion of propellant formulation including Fe_2O_3 when compared with the base formulation PC05 and with the formulations including Cr_2O_3 .

5. Conclusions

Calorimetric bomb measurements suggest that this Fe_2O_3 burning rate modifier increases the combustion efficiency when included in the formulation of this type of propellants while this Cr_2O_3 burning rate modifier decreases the combustion efficiency.

A saturation effect is observed on the base composition for this Fe_2O_3 burning rate modifier in the range 0.375-0.750 wt.%.

This study suggests that this Cr_2O_3 burning rate modifier in this type of propellants shows no saturation effect when used in amounts less than or equal to 1.875 wt.%. When this burning rate modifier is added it combines simultaneously a noticeable increase in burning rate pre exponential factor and a low pressure exponent, in the range 2-10 MPa. It has the disadvantage of being suspect carcinogenic. This burning rate modifier is interesting in the aspects of reliability, safety and performance of gas generators or rocket motors that use these formulations but is noxious to the environment and seems to decrease the efficiency of combustion of these propellants.

A formulation with 1.875 wt.% Fe_2O_3 burning rate proved to have a good burning behaviour for practical applications in all the pressure range 2-10 MPa, because it presents the lowest pressure exponent and the highest pre exponential factor for formulations including this burning rate modifier. Fe_2O_3 burning rate modifier also has the advantage of being non pollutant. This burning rate modifier is more interesting in improving the aspects of reliability, safety, environmental impact and efficiency of gas generators or rocket motors that use these formulations than on the aspect of performance.

This study suggests that Fe_2O_3 burning rate modifier in this type of propellants is more effective in reducing the formation of tar in the nozzle exit than Cr_2O_3 .

REFERENCES

1. Strecker, R. A. H., and Linde, D., "Gas Generator Propellants for Air-to-Air Missiles". AGARD CP-259, April 1979.
2. Korting, P. A. O. G., Zee, F. W. M., Meulenbrugge, J. J. (1987). "Performance of No Chlorine Containing Composite Propellants with Low Flame Temperatures". *AIAA/SAE/ASME/ASEE 23rd Joint Propulsion Conference*, June 29-July 2, San Diego, California.
3. Engel, W., Eisenreich, N., Deimling, A., Hermann, M., Lorenzo, M. J., Kolarik V., "Ammonium Nitrate, A Less Polluting Oxidizer". 24th International Annual Conference of ICT 1993, Karlsruhe, Federal Republic of Germany, (1993) pp. 3-1.
4. Miedema, J. R., Zee, F. W. M., Meulenbrugge, "Some Aspects of Aging of Ammonium-Nitrate Based Rocket Composite Propellants", *Environmental Testing in the 90's*, FhG ICT, Karlsruhe, 1989, p. 14-1.

5. Brewster, M. Q., Sheridan, T. A., Ishiara, A., "Ammonium Nitrate-Magnesium Propellant Combustion and Heat Transfer Mechanisms", *Journal of Propulsion and Power*, Vol. 8, No. 4, July-Aug. 1992.
6. Carvalheira, P., Gadiot, G.M.H.J.L. and de Klerk, W.P.C., Mechanism of Catalytic Effects on PSAN/HTPB Composite Solid Propellants Burning Rates. 25th International Annual Conference of ICT, Karlsruhe, Federal Republic of Germany, (1994) pp. 65-1.
7. Cooke, E.M.G., The Manufacture of High Performance Composite Propellants and Novel Charges by Batch and Continuous Extrusion Processes. *Propellants, Explosives and Pyrotechnics* 15, 235-242 (1990).
8. McBride, B. J., CET89 - Chemical Equilibrium with Transport Properties, 1989. LEW-15113 Program, Cosmic Software, The University of Georgia, Athens, U.S.A..
9. Gordon, S. and McBride, B. J., "Computer Program for Calculation of Complex Chemical Equilibrium, Rocket Performance, Incident and Reflected Shocks, and Chapman-Jouguet Detonations, NASA SP-273, Interim Revision, March 1976.
10. ICT Thermochemical Data Base, Karlsruhe, Germany, June 15, 1994.
11. Carvalheira, P., "Calculation of the Equilibrium Thermodynamic Properties of the Isobaric Adiabatic Combustion Products of AN/HTPB-IPDI Propellants at 7.0 MPa.", 26th International Annual Conference of ICT, Karlsruhe, Germany, 1995
12. Fluka Catalogue 1990/91.
13. McEntee, T. C., U.S. Patent 4,891,391, "Compositions Containing Antimicrobial Agents in Combination with Stabilizers", Jan. 2, 1990, Morton Thiokol, Inc., Chicago, Ill.
14. JANAF Thermochemical Tables, *J. Phys. Chem. Ref. Data*, Vol. 14, Suppl. 1, 1985
15. Bayferrox Data Sheet, Bayer Chemie, A.G., 1992.
16. Catalogue Handbook of Fine Chemicals, Aldrich Chemical Company, 1990-1991
17. Patrick, David R. (Ed.), *Toxic Air Pollution Handbook*, Van Nostrand Reinhold, New York, 1994.
18. Hydroxyl Terminated Poly Bd Resins Functional Liquid Polymers in Urethane Elastomers, Atochem, Elf Aquitaine, October 1990.
19. Manjari, R., Joseph, V. C., Pandureng, L. P., and Sriram, T., "Structure-Property Relationship of HTPB-Based Propellants. I. Effect of Hydroxyl Value of HTPB Resin.", *Journal of Applied Polymer Science*, Vol. 48, 271-278 (1993).
20. Carvalheira, P., "A Computer Program to Predict the Performance of a Vented Strand Burner", private communication, Departamento de Engenharia Mecânica, Faculdade de Ciências e Tecnologia da Universidade de Coimbra, February 1994.
21. ASTM D2015, "Standard Test Method for Gross Calorific Value of Solid Fuel by the Adiabatic Bomb Calorimeter".

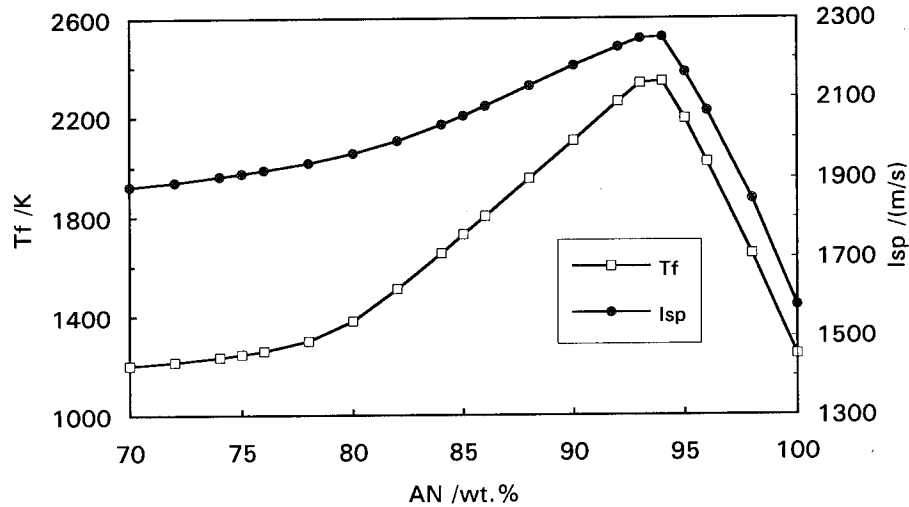


Figure 1. Evolution of the adiabatic flame temperature and specific impulse of AN/HTPB-IPDI propellant composition with AN wt. % solid loading, at 7.0 MPa and for 70:1 expansion ratio.

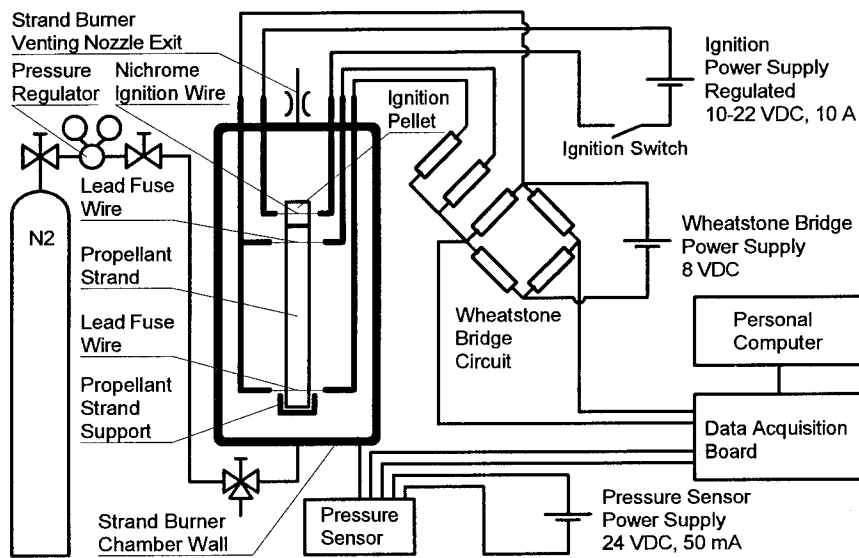


Figure 2. Schematic of the experimental apparatus used for burning rate measurements.

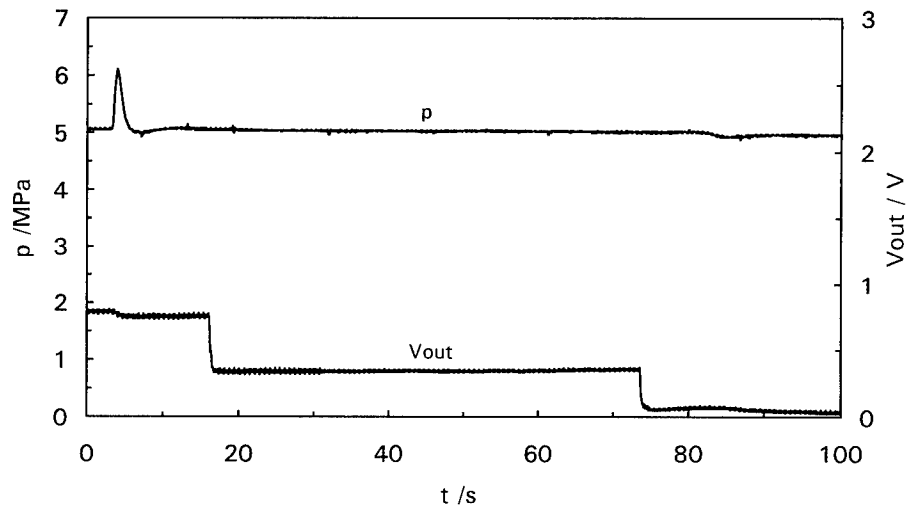


Figure 3. Evolution of pressure and voltage output of Wheatstone bridge lead fuse wire circuit during a typical measurement of propellant burning rate with the vented strand-burner.

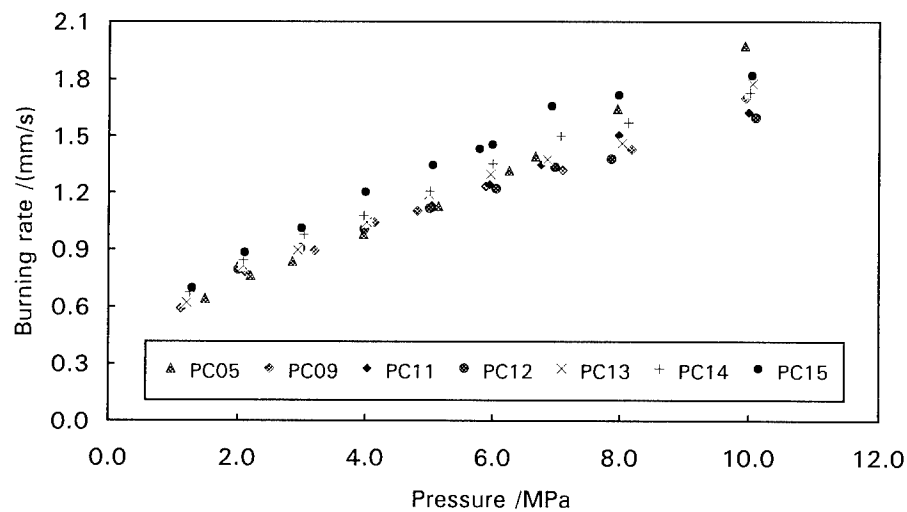


Figure 4. Burning rate behaviour of PSAN/HTPB-IPDI based propellant with and without burning rate modifiers.

COMBUSTION PHENOMENA OF BORON CONTAINING PROPELLANTS

W. Eckl, N. Eisenreich, K. Menke, Th. Rohe, V. Weiser

Fraunhofer-Institut für Chemische Technologie

Joseph-von-Fraunhoferstr. 7

76327 Pfinztal 1(Berghausen), F.R.G.

ABSTRACT

Boron containing propellants, based on AP/GAP and AP/HMX/GAP formulations, have been investigated applying fast spectroscopic, pyrometric and photographic tools. The propellants burnt at a rate of 17mm/s at 5 MPa. Adding of an iron oxide catalyst increases the rate to 20 mm/s at same pressure. The determined average pressure exponents are 0.66 without and 0.57 with iron oxide as catalyst. At pressures higher than 5 MPa, a strong decrease in the exponent is observable.

The reaction zones show high particle concentrations with temperatures from 1500 to 2000 K, varying with the adjusted nitrogen pressure. Reacting with air, the particle temperatures increase close to the evaporation temperature (2200 K) of boron dioxide. The reaction of boron with oxygen is proved by the results of spectroscopic data.

Considering an application in a Ducted Rocket, the boron is heated to the desired reaction temperature.

I. INTRODUCTION

The range of short and medium distance missiles is mainly limited by the weight of transported fuel. Therefore, air-breathing concepts of rocket propellants aim to develop new low-weight formulations.

One principle of realising such a technique is the Ducted Rocket, a propulsion unit based on two separate combustion chambers:

- the first chamber, producing hot gas and additional fuel
- the second chamber, where the additional fuel is exothermally reacting with air

In the primary gas generator, the secondary fuel is released and heated to ignition temperature for reacting with air in the secondary chamber.

Boron is one of the favourite fuels (low molar weight, high reaction enthalpy) [1-3]. In the presented work, the combustion behaviour of high boron containing propellants (FS 280, FS 314, FS 315), developed at ICT, has been investigated in a so-called optical bomb (see chapter II.) using two different atmospheres:

- Nitrogen, to simulate the first chamber
- Air, to simulate the first reactions in the secondary chamber.

Presented are results for combustion rate, flame geometry, temperature and emitted radiation to allow interpretations with reference to applications in rocket propulsion.

II. EXPERIMENTAL

The experiments were carried out in an optical bomb equipped with two opposite windows, allowing simultaneously the observation of propellant combustion up to 10 MPa by different methods (fig.1) [4]. The propellant formulations were pressed to strands of 4 x 4 x 40 mm and electrically ignited.

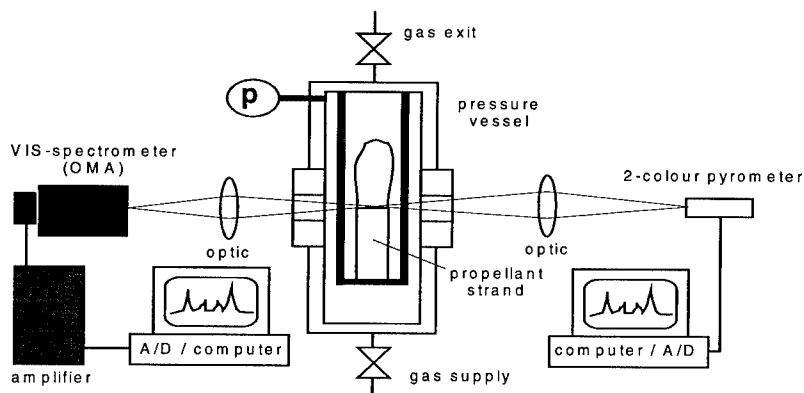


Figure 1: Experimental set-up for simultaneously spectroscopic and pyrometric investigation of propellant combustion

Visualisation of the combustion was achieved, using an automatically exposing camera (4 frames per second). The emitted radiation was detected with a Trakor Northern TN 6500 optical multichannel spectrometer (time resolution: 10 ms). Simultaneously, the combustion was

observed applying a fast two colour pyrometer developed at ICT (time resolution < 0.1 ms) [5]. The high time resolution allows detection of single boron particles.

For determining the combustion rate under nitrogen atmosphere, the strand was focused on a diode array, detecting the progressing flame front [6].

III. INVESTIGATED FORMULATIONS

The investigated propellants FS 280, FS 314 and FS 315 base on boron containing AP/GAP formulations. FS 314 and FS 315 are additionally blended with HMX (tab.1).

Sample	AP	HMX	GAP	BDNPA-F	Boron	N100	Fe ₂ O ₃
FS 280	20	--	25.6	12	40	2.4	--
FS 314	20	5	25.2	12	35	2.8	--
FS 315	20	5	24.5	11.7	35	2.8	1

Table 1: Composition of the investigated propellants (in Ma%)

The propellants were burnt in the optical bomb both in nitrogen and air atmosphere at pressures of 0.5, 2, 4 and 7 MPa. Thermodynamic calculations, applying the ICT code [7], showed the following results for adiabatic flame temperatures (in K):

Sample	2 MPa, N ₂	7 MPa, N ₂	2 MPa, Air	7 MPa, Air
FS 280	2340	2350	2840	2890
FS 314	2350	2350	2830	2880
FS 315	2350	2350	2830	2880

Table 2: Adiabatic flame temperatures in K (combustion with air: stoichiometric conditions)

Additional amount of oxygen increases the flame temperature about 500 K, proving a gain of power in the second combustion chamber without oxidator in the propellant (reduction of weight).

The calculated reaction products of FS 280 in first and after second reaction chamber are shown in table 3 assuming a pressure of 7 MPa in first reaction chamber and an adiabatic relaxation to standard conditions at frozen equilibrium for the combustion with air.

	comb. chamber, 7 MPa	nozzle exit , 0.1 MPa
Temperature in K	2350	1610
reaction products in mol%:		
CO ₂	0	5.7
H ₂ O	0	2.3
N ₂	0	77.2
CO	15.9	0.2
H ₂	18.7	0
BOH	2.9	0
HBO ₂	0.2	8.1
BO ₂	0	0.1
B ₂ O ₂	0.8	0
B ₂ O ₃	0.3	5.3
HCl	2.5	0.8
C	3.2	0
B	36.6	0
BN	18.4	0

Table 3: Equilibrium composition of important reaction products of FS 280 in first and after second combustion chamber (in mol%)

The results show, that boron is not reacting in the primary zone and, therefore, preserved for oxidation in air atmosphere (second reaction chamber). Only partially oxidised components in the gas composition like CO or H₂ are additional reactants for the air supplied second rocket chamber and increase power.

IV. RESULTS AND DISCUSSION

The investigations aimed at:

- characterisation of the process determining combustion rate and temperature,
- verifying that boron is not burnt in the first reaction step but produced with a temperature high enough to react in the second one
- investigating the reaction zone (geometry, emitted radiation, intermediate products) to clear up reaction mechanisms.

IV.1 Combustion Rate

Figure 2 shows the experimental combustion rates vs. pressure (nitrogen atmosphere). As consequence of iron oxide catalysis, FS 315 shows maximum rates and minimum mean pressure exponents (FS 315: 0.57, FS 280 and FS 314: 0.65 at 0.5 to 10 MPa). At relevant higher pressures (> 2 MPa), an even stronger effect is observable (pressure exponent: 0.4 for FS 315). Therefore, the FS 315 formulation is advantageous, both in pressure exponent and power.

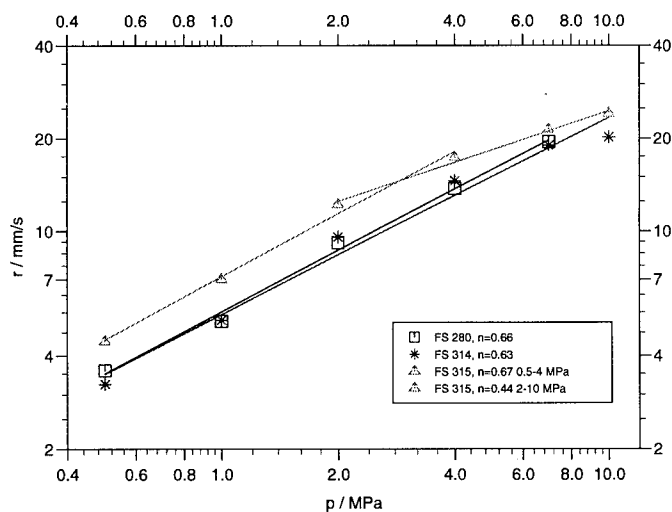


Figure 2: Combustion rate vs. reaction pressure of investigated propellants

IV.2 Flame Geometry

The shape of the reaction zone of the three investigated propellants are not significantly different (fig.3). Originated from hot particles, a lot of observed luminescent traces are observable (probably glowing boron particles). The surface of the propellant seems to be not melted. It emits with low intensity. The dark spots above FS 315 surface point at ejected small propellant fractions. No dark zone (Fizz zone) is observable.

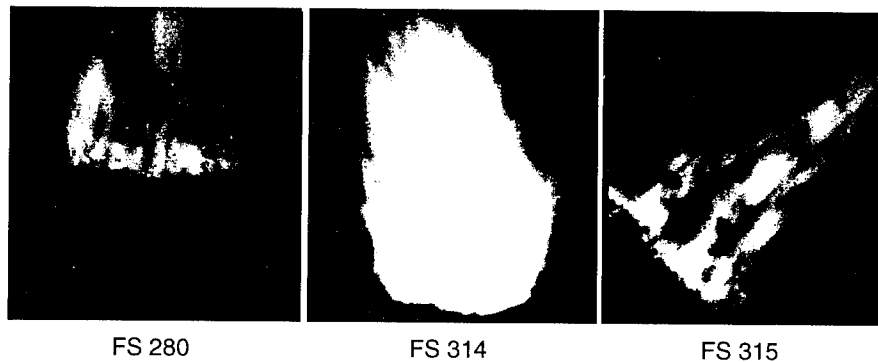


Figure 3: Combustion zones of FS 280, FS 314 and FS 315 propellants in 0.5 MPa nitrogen atmosphere



Figure 4: Combustion of FS 280 in air atmosphere (2 MPa)

The photographic investigations in air atmosphere were disturbed by strong fogging caused from water condensation at HCl molecules. Additionally, the air oxygen induces a strong non

homogeneous combustion front (fig.4). Single fractions are ejected. The observed luminescent traces are generated by hot boron particles reacting with air.

IV.3 Spectroscopy

The spectroscopic investigations aimed in the question, whether the non-burnt boron from the propellants is hot enough to react in air or not. Therefore, the combustion was investigated supplying air and nitrogen.

Figure 5 shows spectra in the intensity maximum of FS 280 with nitrogen supply at pressures of 0.5, 2, 4 and 7 MPa. Corresponding spectra with air supply to FS 315 are shown in figure 6. Pure continuous intensity contribution is observable in nitrogen atmosphere, comparable to that obtained from hot condensed matter or gas phases with high particle concentrations. The intensity is increasing with pressure caused from a higher temperature or particle density in the gas phase.

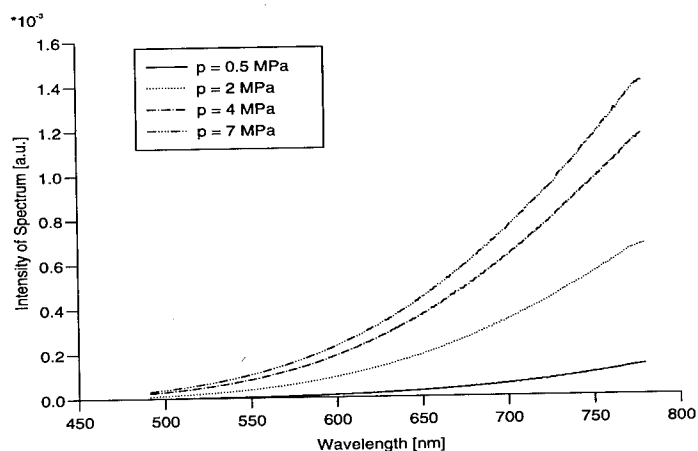


Figure 5: Spectra obtained from the gas/particle phase of FS 280 propellant at different nitrogen pressures

70 - 8

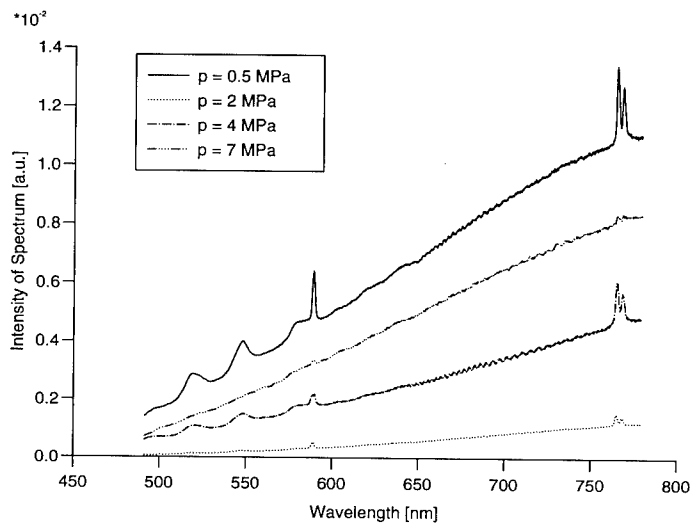


Figure 6: Spectra obtained from the gas/particle phase of FS 315 propellant at different air pressures

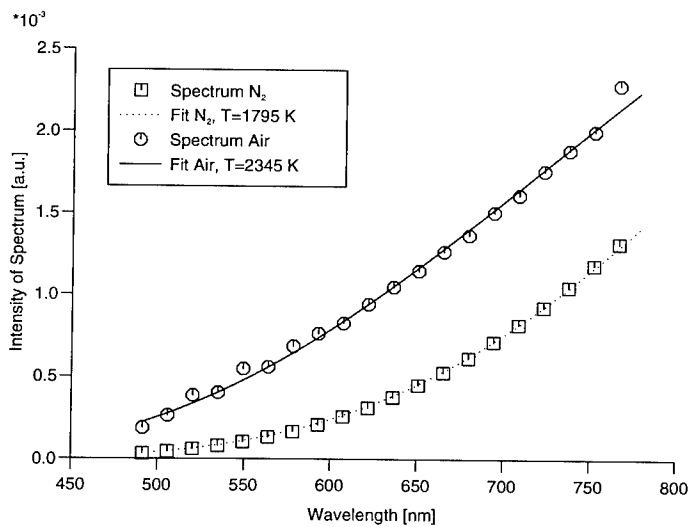


Figure 7: Least-Squares-Fit of grey radiation (Planck's radiation law) to FS 280 spectra (air and nitrogen atmosphere)

In air atmosphere (fig.6), the spectra show strong atomic lines (sodium 589 nm, potassium 766.5 and 769.9 nm) and band profiles caused by the BO_2 molecule (between 500 and 600 nm). The boron particles are reacting with air proving the assumed heating of boron by the propellant in the first reaction chamber.

The temperatures can be obtained by fitting Planck's radiation law with constant emission coefficient < 1 to the experimental data (fig.7). The obtained temperatures at various pressures are summarised in figure 8. Compared to nitrogen atmosphere, the temperatures of all propellants are 700 to 1200 K higher supplying air. This proves the additional amount of energy by boron oxidation.

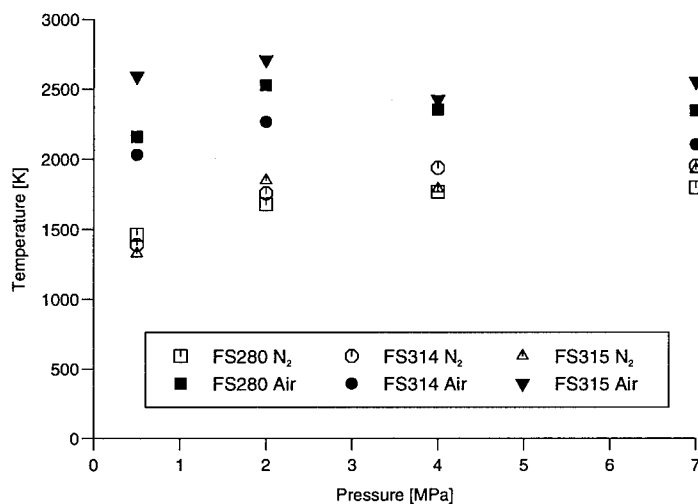


Figure 8: Temperatures at FS-propellants combustion at different pressures of air and nitrogen obtained from a grey radiation fit

IV.4 Pyrometry

The applied two colour pyrometer allows measuring temperature and integrated radiation of the reaction front with a time resolution $\Delta t < 0.1$ ms [4]. Single particles are detectable. Figures 9 and 10 show examples of temperature profiles under nitrogen (left) and air (right) atmosphere at 0.5 and 7 MPa.

At 0.5 MPa nitrogen pressure, the intensity strongly increases in the first zone, where the hot reaction zone (burning surface) is located. Strong peaks are observable in all experiments, caused by boron particles. The peak frequency is constant. During the first 5 to 10 seconds, temperatures of 1400 to 1600 K were measured, moderately decreasing up-stream. The spectroscopic investigations showed no boron oxidation in nitrogen atmosphere, therefore indicate that the boron can be considered to be inert in the first combustion chamber. 10 mm above the surface the particles are slowly cooling down.

At 7 MPa nitrogen atmosphere (fig. 10), the complete reaction zone and the area of constant temperature are extremely shortened. Higher particle temperatures of 1800 to 2000 K are obtained. The ignition temperature of boron is reached.

The combustion in air atmosphere shows a symmetrical reaction zone. The obtained temperatures are 1900 to 2000 K and are distinctively higher than in nitrogen atmosphere combustion. The temperatures increase (2000 to 2100 K) at 7 MPa pressure.

Figure 11 shows in detail temperature and intensity measurements in the upper and lower reaction zone. The upper is determined by the area of constant temperature. In the lower zone of reaction, particle peaks and temperature maxima of 1500 K coincide. In the upper zone, the minima of temperature (about 1450 K) are coincident with the intensity maxima of emitting particles. This is attributed to a slightly cooling of the boron particles.

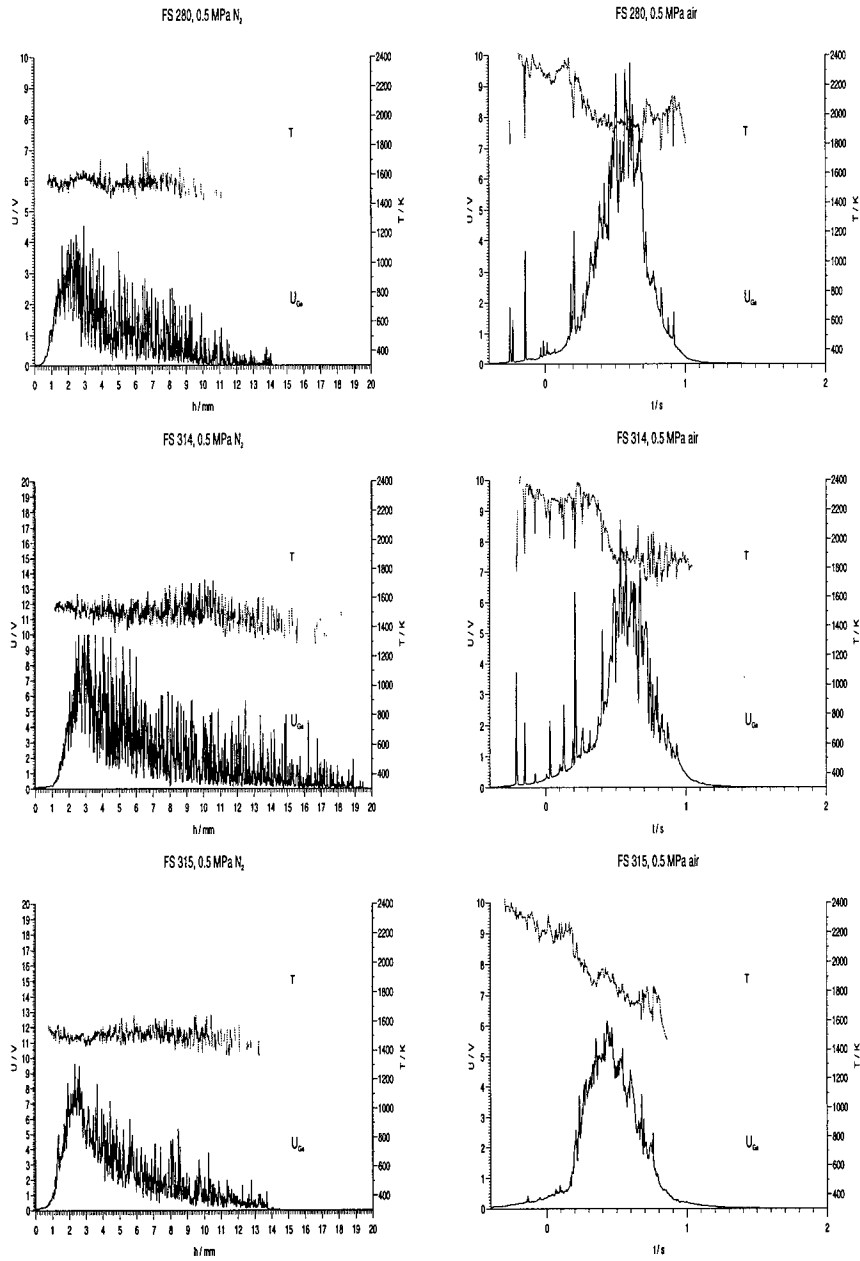


Figure 9: Progressing of temperature and intensity at 0.5 MPa in nitrogen (left) and air (right) atmosphere

70 - 12

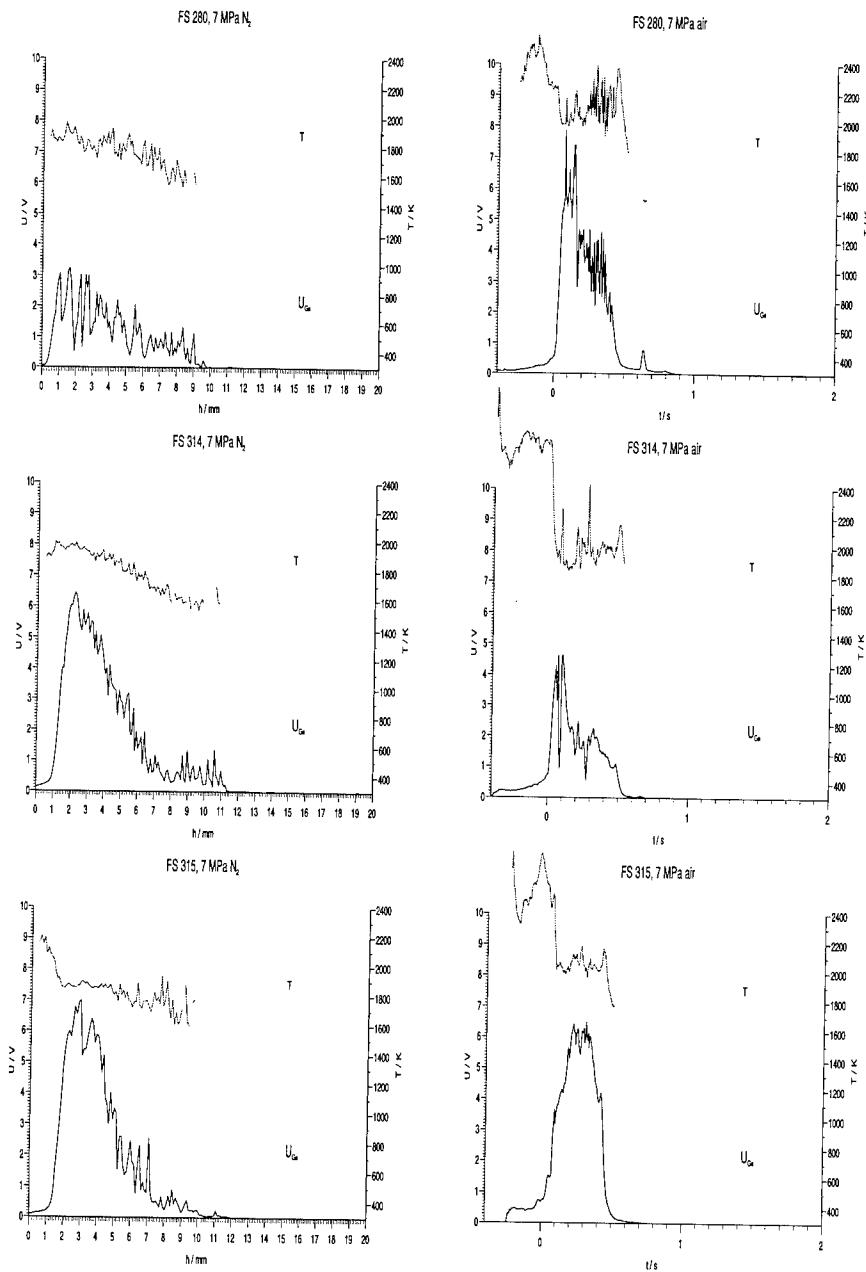


Figure 10: Progressing of temperature and intensity at 7 MPa in nitrogen (left) and air (right) atmosphere

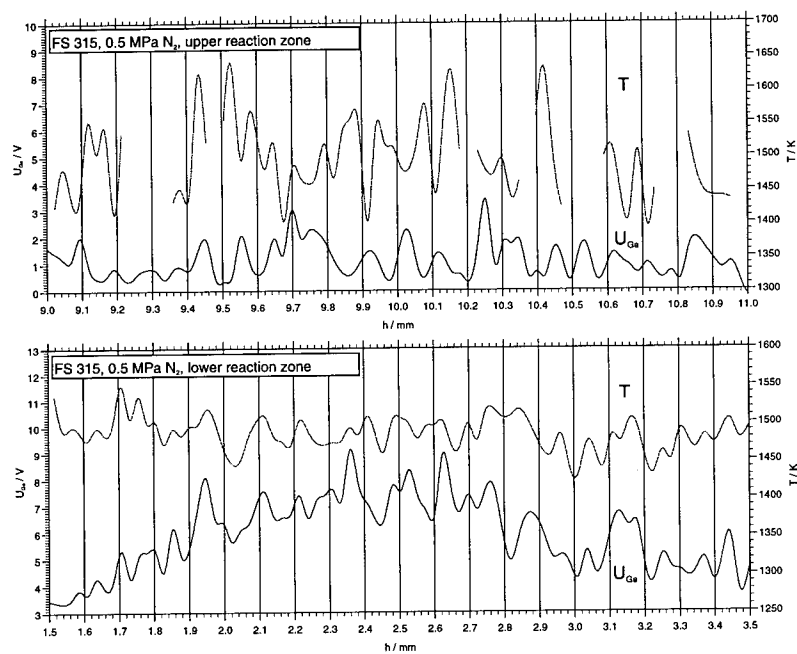


Figure 11: Intensity and temperature progress (FS 315 propellant, 0.5 MPa nitrogen) in the reaction scope 2.5 mm and 10 mm above propellant strand surface.

REFERENCES

- [1] Kuo, K. K.; Pein, R.(Ed.); Boron-based solid propellants and solid fuels; CRC Press, 1993
- [2] Liehmann, W.; Combustion of Boron-Based Slurries in a Ramburner; Propellants, Explosives, Pyrotechnics 17, 14-16 (1992)
- [3] King, M. K.; A review of studies of boron ignition and combustion phenomena at Atlantic Research Corporation over the past decade; Boron-based solid propellants and solid fuels; K. K. Kuo; R. Pein (Ed.); CRC Press, 1993
- [4] Weiser, V.; Eckl, W.; Eisenreich, N.; Pfeil, A.; Untersuchungen zum Abbrandverhalten von PSAN/GAP-Mischungen mit verschiedenen Phasenstabilisatoren; 25th International Annual Conference of ICT, 1994, pp. 25-(1-15)
- [5] W. Eckl, N. Eisenreich, W. Liehmann, H. Schneider, V. Weiser; Emission Spectroscopy and Pyrometry of Propellant Flames and Rocket Plumes; Non-Intrusive Combustion Diagnostics; (Kuo K. K., Parr T. P. ed.), Begell House, Inc. New York
- [6] W. Eckl, Th. Rohe, V. Weiser; Characterizing the combustion process of new gasgenerator propellant; 2. International Symposium on Sophisticated Car Occupant Safety Systems (AIRBAG 2000); 1994, November 29/30, Karlsruhe, Germany; pp. 35-(1-9)
- [7] Volk, F.; Bathelt, H.; Rechenprogramm zur Ermittlung thermochemischer und innenballistischer Größen, sowie von Gasdetonationsparametern, ICT-Report 3/82, 1982
- [8] CRC-Handbook of Chemistry and Physics (72nd edition), Lide, D.R. (ed.); CRC Press, 1991

DEVELOPMENT PLAN OF A NEW DETONATION THEORY

Franklin Walker
Interplay, 18 Shadow Oak Road
Danville, California, USA

ABSTRACT

The development of a very different concept and theory of the detonation of chemical explosives is presented. It is shown that a new theory of kinetics is also derived, based on a method and equation we developed for the calculation of Hugoniot (shock velocity as a function of shock pressure) values for condensed elements. Our physical-chemical model of a shock wave is based on the concept that the velocity of a shock front moving through a condensed material is a result of the momentum transfer of the shock energy by the motion of the atoms of the material at the average relative velocity of the vibrational motion, ARVV, of the atom pairs. This concept leads to the definition of physical kinetics as a nonequilibrium, nonthermal process in which chemical reaction rates are determined and regulated by the ARVVs of the bonded atoms in the condensed systems under the influence of high-velocity shocks.

The results of these studies provide the foundations for the new physical kinetics and for the different theory of detonation. Through additional development, we can now calculate accurately detonation velocities. From the concept underlying physical kinetics and with the method given herein for the calculation of detonation velocities, we present the detonation theory in which the ARVVs determine the rate of advance of the kinetic energy of the detonation wave that leads to the very high impact velocities of the atoms and molecules in the front. This impact, with its resultant compression and shear, causes massive bond scission in extremely short times in and very near the shock front, and the free atoms and radicals and other highly-activated species formed then react in very short times (tens of femtoseconds to picoseconds) to provide the chemical energy which maintains the enormous level

of kinetic energy at the detonation front. Data from more recent papers in support of this work are presented.

INTRODUCTION

When we began our early experiments on the initiation of chemical explosives more than 25 years ago, we did not anticipate the development of a new kinetics and a new theory of detonation. In fact, before we completed the early work, we had expected the results of the experiments to support the classical theories of the time. However, when we learned that our critical energy concept for initiation was probably more nearly correct than the pressure concept, and after the subsequent observation that the time to initiation of nitromethane, NM, at low shock pressures was several orders of magnitude less than the classically-proposed values, we felt that more experimentation and analysis were important. This fact became the motivation for our continued experimentation, calculation and analysis. At this early time, we did not have an explicit plan for the development of a new theory. In fact, we did not anticipate that very different or novel theories of initiation, detonation or, particularly, of shock kinetics would be required. We were told repeatedly, and sometimes heatedly, that we had made errors in our experiments or in our calculations, and we worked diligently to either find such errors or to complete new experiments and calculations which might support our early work.

As seems quite evident now, and as has been summarized in two presentations^(1,2) and in a paper⁽³⁾ published in 1994, the classical theories had serious defects, particularly as related to the time and space dimensions and the microscopic processes involved.

DEVELOPMENT OF A RESEARCH PLAN

Background

We soon became convinced from the results of a series of experiments with NM plus DETA (diethylene triamine) and from our early molecular dynamics, MD, calculations⁽¹⁻³⁾ that our first research was not in error and, very likely, that it pointed the

direction in which our future studies should proceed. From the first analysis of the shock initiation studies, in which we developed the equation which describes the critical energy fluence basis for shock initiation, it was evident that two simple equations from physics were probably basic to understanding the chemistry of the initiation and detonation of chemical explosives.

$$E_k = \frac{1}{2}mv^2 \quad (\text{kinetic energy}) \quad \text{and} \quad (1)$$

$$P - P_o = \rho U_s U_p \quad \text{or} \quad U_s = \frac{P}{\rho U_p}, \quad \text{since } P_o \ll P, \quad (2)$$

(the Hugoniot or shock velocity equations).

For, as we showed in the first paper,

$$E_c = \frac{tP^2}{\rho U_s} \quad (\text{critical energy fluence for initiation}), \quad (3)$$

depends on and is derived from Eqs. 1 and 2.

Therefore, we set out on our research to explore the ways in which kinetic energy and shock velocity, U_s , were integral to and involved in shock and detonation chemistry: in the shock structure, shock rise times, shock sensitivity, shock energy and how it is transferred and maintained, shock and detonation kinetics, shock and detonation temperatures, and detonation velocity, D .

The Development Plan

As a result of the realization that there was a critical energy fluence for the shock initiation of heterogeneous explosives, we decided to check the determinant for shock initiation in homogeneous explosives. The observations on the low-pressure initiation of NM convinced us that there were other defects in the classical theory, and we started on a search for a new theory. The plan was not developed all at once, but we devised it step-by-step as new data were obtained.

We had become well aware at this time that we would have to demonstrate and substantiate that there were many defects in the classical theory and that reviews of the new concepts and hypotheses would be highly critical. Therefore, we completed a broad

range of experiments and calculations, and we searched for corroboration in the studies of other scientists.

Two important observations made early in our studies which helped in the planning are: (1) That $8 \text{ km/s} = 8 \text{ mm/microsecond} = 8 \text{ angstroms}/10^{-13} \text{ s}$. (This shows that the shock front crosses a covalent bond in about 10^{-14} s , since the bonds are in a somewhat random orientation to the shock axis.) (2) The kinetic energy of the momentum transfer in strong shocks and detonation is stronger than the covalent bond strengths.

The development plan outlined below is summarized in Table 1.

Kinetic Energy Effects

1. Determine the structure of the initiation (where does initiation begin) in both heterogeneous and homogeneous (liquid) explosives.
2. Determine the possible acceleration of a shock front in NM at shocks less than detonation levels.
3. Study the effects of amine additives (DETA) to NM: measure the time to initiation and detonation velocity as a function of DETA concentration.
4. Calculate with MD the possibility of the momentum transfer of the kinetic energy of a shock or detonation wave and the possibility of massive bond scission at or near detonation shock energy.
5. Review the detonation calorimetry experiment of Ornellas and McGuire⁽¹⁻³⁾ with bis-trinitroethyl adipate (BTNEA). Nearly complete scission or rearrangement of the covalent bonds was reported.
6. Determine shock rise times and shock front widths. Calculate the extent and the rise time of the vibrational bond energy from the action of the kinetic energy of the shock wave.
7. Determine the strength of the shock kinetic forces in relation to the covalent bond strengths of the explosives molecules.

8. Check for correlations in reaction dynamics experiments and in detonation studies for corroboration of the new models.

9. Show that the chemical reactions in and very near the detonation front are not in thermal equilibrium and that they are not classically-thermal processes.

Shock Velocity Effects

1. Determine if U_s versus pressure, P , can be calculated accurately with MD.

2. Determine if Hugoniot of the elements can be calculated accurately, algebraically, from basic atomic properties.

3. Determine if Hugoniot for organic compounds can be calculated from the elemental Hugoniot.

4. Determine if relative vibrational velocities, RVVs, can be calculated from infrared spectroscopic and x-ray crystallographic data and also from quantum mechanics, QM, by use of the Hulbert-Hirschfelder, HH, equations.

5. Determine if a "shock barrier" to detonation velocities can be demonstrated and if it is related to the bond vibrational velocities.

6. Develop a concept of average relative vibrational velocities, ARVVs, and then develop a new "physical kinetics" based on the ARVVs.

7. Determine if the transfer of shock wave and detonation kinetic energy is shown to be a momentum transfer process by the use of new MD calculations incorporating many-body potentials and enhanced pictorial presentations.

8. Derive a simple equation for calculating D_s from the empirical equations of Kamlet and Jacobs.⁽¹⁻³⁾

9. Derive a refined equation for calculation of D_s based on the Kamlet-Jacobs work and an analysis of detonation data.

10. Derive a final detonation velocity equation from the concept of physical kinetics and the method given earlier for the calculation of the Hugoniot of organic compounds.

11. Determination of the microscopic structure of shock and detonation fronts: rise times, front widths, kinetic energy levels, energy transfer factors, bond scission and rearrangement processes, chemical reaction rates and types, maintenance of the detonation kinetic energy levels, nonequilibrium and nonthermal processes, chain reactions and free-radical mechanisms, and the ARVV and physical kinetics control of Ds.

Rationale for the Theory Development

As the work progressed, a rationale for the theory development emerged. It seemed that each new experiment or calculation or analysis (along with new data and information from the work of others in the field) appeared to be stepping stones toward new concepts and hypotheses, and they appeared to be related to either the kinetic energy aspects or the shock velocity concepts of the early work. Concise summaries of the progression of the rationale follow.

Kinetic Energy and Nonthermal Bond Scission Factors

1. Times to initiation of NM at 6.0 to 6.5 GPa are four orders of magnitude less than predicted classical values.
2. Initiation in NM occurs at and very near the shock front--not at the face first put under compression.
3. Shocks in NM at less than initiating levels cause acceleration of the shock front above hydrodynamic (unreactive) levels. The increase in shock velocity appears to be a result of chemical energy released at or near the shock front, and it is proportional to the shock pressure of a sustained (long duration) shock. Computer modelling of the experiment indicated that there was about 1 to 4% of chemical reaction of the NM at the front.
4. Detonation of NM with added DETA shows an increase in D from 6.32 to 6.7 km/s at a DETA concentration of 0.05%.
5. Calculation with the equation of Skidmore and Hart⁽¹⁾ shows that a new Chapman-Jouguet pressure, P_{CJ} , of about 19 GPa

would be required for 6.7 km/s D in NM. This large increase is a strong indication of other, fast free-radical, chain reactions providing a very high energy release rate in a nonthermal, non-equilibrium process. (Later calculation of the expected D of NM at 19 GPa by use of our final equation for the calculation of Ds from the empirical formulae of explosives gave a value of near 6.7 km/s.)

6. A detonation calorimetry study by Ornellas and McGuire⁽¹⁻³⁾ of BTNEA shows nearly complete scission (or rearrangement) of the chemical bonds of the BTNEA with random recombinations.

7. Measured shock front rise times by Harris and Presles⁽¹⁻³⁾ show shock front widths of about 15 water molecules--60 to 90 angstroms.

8. Our MD calculations of shock front widths show values of about 40 to 100 angstroms. Brenner and Robertson,⁽¹⁻³⁾ using many-body potentials, find similar rise times, shock front widths, and massive bond scissions and rearrangements.

9. Henry Eyring said very early that shock and detonation waves were momentum transfer processes and that the kinetics in detonation was not Arrhenius thermal kinetics. He named it starvation kinetics.

10. The MD calculations show that the kinetic energy of momentum transfer at near detonation shock pressures provides about 4 ev of vibrational energy in the lattice atoms in about 80 fs. This is more energy than the covalent bond strengths in RDX. MD calculations also show that the extent of bond fracture is a function of shock energy, and that near D values the scission is massive.

11. Calculations of the kinetic energy of the atoms in a moderate shock front, 4 to 5 GPa, show that it is nearly equal to the bond strengths in the covalent bonds in RDX. The kinetic energy in the detonation front of N and O atoms at 8 km/s is 4.72 and 5.34 ev, respectively.

12. Correlation of data from reaction dynamics, RD, experiments--atomic velocities, bond strengths, times to reaction, kinetic energies of atoms, etc., with data and calculations from detonation studies provides additional support for the importance of the kinetic energy factors.

13. Since the shock energy is so high in detonation, the chemical reactions that occur are not only those with the lowest activation energies, but almost any reaction pathway is available. Thus, it is highly probable that the free-radical and short chain reactions of the C,H,O,N atoms can occur in 10^{-14} to 10^{-12} s.

Shock and Vibrational Velocities Determine Kinetics

1. We derived simple but accurate equations for the calculation of the Hugoniot of elements from the atomic properties found in a periodic chart of the elements:^(4,5)

$$U_s = f(r_a, w_a, \rho) \quad (4)$$

(r_a is atomic radius, w_a is atomic weight, ρ is density)

$$U_s = \left(\frac{r_a}{w_a}\right)^{\frac{1}{4}} \cdot \rho^{-0.1} \cdot f(P) \quad (5)$$

2. Calculations of Hugoniot values by MD match the data for organic (covalent) materials.

3. Calculations of Hugoniot values for organic compounds from our calculated Hugoniots of the elements match the MD calculations and the data.

$$U_s = \sum (U_{se} f_e) \quad (6)$$

(From the empirical formulae, U_{se} is shock velocity of of the element, and f_e is the weight fraction of the element.)

4. Calculations from xray crystallography (the thermal uncertainty of atomic positions) and infrared data (vibrational frequencies) give values of the vibrational velocities of covalent atom couples.⁽⁵⁾

$$V = \nu_{cu} \quad (7)$$

(V is vibrational velocity, ν is the infrared frequency in

cm^{-1} , c is the velocity of light, and u is the relative distance traveled between the atoms in one vibration.)

5. After we observed the importance of shock velocity values in initiation and in the shock acceleration in NM, one of the first indications of the possibility that there was a physical control or "barrier" for shock velocities appeared in a plot made that showed that the detonation velocities of the known chemical explosives all fall within the range of the CH, NH, OH atomic vibrational velocities.

6. Calculations of the vibrational velocities from the H-H equations correlate well with the MD and the x-ray-infrared calculations and with the "shock barrier" graph. We obtained also U_s as a function of temperature.

7. Formulation of the hypotheses of the average relative vibrational velocities, ARVVs, of atom pairs and groups and the rates of momentum transfer of the kinetic energy of shock and detonation waves was now feasible.

8. Using the empirical equations, $P = K_6 \rho^2 \phi$ and $\phi = NM^{\frac{1}{2}} Q^{\frac{1}{2}}$, from the work of Kamlet and Jacobs, ⁽¹⁻³⁾ we derived a simple equation,

$$D = 2.45 + \frac{P^{\frac{1}{2}}}{3} \quad (8)$$

which yields a good fit to the detonation data. One curious factor is that the aliphatic explosives are mostly on one side of the average curve through the data, and the aromatics are on the other side. One interpretation of this fact is that the energy required to break up the conjugated rings in the aromatics is equal to that required to add about 0.25 km/s to the Ds.

9. From information in Paragraph eight, we derived another equation,

$$D = \left(\frac{P^{\frac{1}{2}}}{3} + 2.0 + 0.25a \right) + 0.05 \left(H_p + \frac{N_p}{20} \right) \quad (9)$$

This equation gives excellent fit to the detonation data, with a correlation coefficient of 0.991 for 14 common explosives. ⁽¹⁻³⁾ Equations 8 and 9 indicate that thermodynamic content of the

explosives molecules is a second order function, since the thermodynamic variable ϕ in the equations of Kamlet and Jacobs is taken as the constant 6 in both equations.

10. Finally, a simpler equation,

$$D = T_c \sum (U_{se} f_e), \quad (10)$$

was developed from information given above in this section. This equation gives excellent results compared to the data for all of the explosives for which we had data for comparison. The correlation coefficient is 0.976.

11. The efficacy of this equation, Eq. 10, even using P_{CJ} s calculated with the empirical equation of Kamlet and Jacobs, gives strong support for the concept of massive bond scission in detonation, since the D s are calculated simply from the empirical formulae of the explosives--the shock velocities of the elements at the P_{CJ} and the weight fraction of each element.

NEW SUPPORTING DATA FROM WORK OF OTHERS

Fortunately, there are many excellent scientists working in this area of research, and many of them have completed experiments and/or calculations related to our development plan. Short summaries from some of this work follow:

1. Simpson, Helm and Kury reported⁽⁶⁾ their studies of shocked HMX/water mixtures as compared to shocked solvent-pressed HMX. Below 6.0 GPa they observed no reaction in the HMX/water mixtures, but in the solvent pressed HMX experiments about 3 to 7% of the HMX appears to have reacted at or near the shock front to accelerate the shock. They report, "The observed higher shock velocity in the solvent-pressed data we attribute to a reaction-supported shock front."

2. Calculations of "atomic mechanics" by John Gilman⁽⁷⁾ have shown mechanical scission of covalent bonds by the impact and compression forces in a shock front.

3. Experimental studies of shocked crystal lattices by

C.S. Coffey⁽⁸⁾ have shown massive mechanical bond fracture through shear from the shock forces.

4. The results of reaction dynamics studies⁽²⁾ of a system in which a van der Waals molecule, $\text{IH}\cdots\text{OCO}$, undergoes UV photolysis which accelerates the H atom to about 20 km/s toward the OCO molecule, thus forming the transient state, TS, show the appearance of an OH signal in about 5 to 15 ps after the deconvolution of the TS. In another experiment involving the decomposition of ICN, it was reported⁽²⁾ that the TS has a lifetime of about 200 fs and a translational velocity of about 2 km/s. This shows that the TS exists for about 4 vibrations of the IC-N bond, and that the ICN molecule rotates only about 7° during this period. The energy reported to be available for this reaction is about 0.87 eV or near 7000 cm^{-1} . It is instructive to note the similarities in the physical and chemical factors in detonation and RD. The translational velocities of the atoms and radicals are in the km/s range, with the H atoms moving from perhaps 10 to 20 km/s, and the $\text{I}\cdots\text{CN}$ transient moving at 2 km/s, almost exactly covering the range seen for the vibrational velocities of the H-H couples and the C-C couples, as calculated by the H-H functions and in the MD calculations. There appear to be many fundamental correlations in these two chemical physical regimes.

5. Sharma et al. reported⁽⁹⁾ studies of initiation sites found in TATB (triaminotrinitro benzene) shocked to near initiation levels. They showed by x-ray photoelectron spectroscopy (XPS) that deposits of acetone-soluble reaction products were furoxan and furazan derivatives of TATB. Their analyses suggested that the furoxan product could react with an adjacent TATB molecule in an exothermic chain reaction to give a water molecule and a new furoxan. Thus, the shock-formed furoxan could immediately provide energy near the shock front. Sharma suggested that this reaction could be involved in the initiation of TNT as well. (It is interesting to consider, as related to the study of the HMX/water mixtures of Simpson et al., that the water formed in the TATB reaction could be a factor in the insensitivity of TATB.)

6. Tanaka et al. provide a strong defense of the new detonation theory. They report⁽¹⁰⁾ that an explosive designated as E25 (75% PETN/25% paraffin) at a density of 1.265 g/cc has a measured D of 7.230 km/s, whereas pure PETN (pentaerythritol tetranitrate) at the same density has a measured D of 6.60 km/s. Our calculation using shock velocities and the empirical formula, Eq. 10, gives a value of 7.267 km/s, within 0.51% of the measured value. The classical theory calculation missed the measured value by 14.24%--too low. The authors of the paper stated that, "All equations-of-state available to us cannot reproduce these results." We also calculated D values for an RDX/paraffin (95/5%) explosive, which reportedly had an anomalous measured value of D that was higher than for pure RDX. We calculated the D to be very close to the measured value.

7. In 1992, Brenner and Robertson et al. published⁽¹¹⁾ results of their MD studies in which they use many-body interatomic potentials to provide more realism in their calculations. Their excellent graphics show in unmistakable detail the narrow shock and detonation fronts, massive mechanical bond scission and rearrangement, free atoms and molecular fragments, and free-radical chemistry in and very near the front. These processes are non-equilibrium and nonthermal.

8. In a private communication from a paper soon to be presented,⁽¹²⁾ James Austing et al. report a calculation by our method using Eq. 10 of the D of a quite unusual explosive, TNT/ N_2O_4 (51/49%). They obtained a calculated value of 6.637 km/s, 1.6% lower than the measured value of 6.746 km/s.

9. In one of the first tests of the predictive utility of Eq. 10, I was asked by Dr. O.R. Bergmann, Manager Research Programs for Specialty Explosives, of DuPont Company, to predict the D of an explosive he needed for a special application. The composition of this explosive was PETN/NC/ATBC (63/8/29%), about 30% of inert material, with a density of 1.48 g/cc. Since I had to estimate the P_{CJ} , I may have estimated it a little too high, but I reported

to Dr. Bergmann that I expected the D to fall in the range of 7.12 to 7.34 km/s. When he later measured the D, he found a range of 6.8 to 7.1 km/s.⁽¹³⁾ He told me by phone that the prediction was very good. The average values differed by only 4%, but between the ranges the difference was only about 0.3%.

10. In support of our data that show the substantial increase in D of NM with the addition of 0.05% of DETA, recent work of Presles and Desbordes⁽¹⁴⁾ shows that the addition of 0.08% DETA to NM-acetone mixtures yields a decrease of 80% in the mean cell size in the detonation front. Addition of 0.1% DETA increased the acceptable dilution for detonation by 35.7%, and 0.03% DETA in NM reduced the critical diameter by 43%. It has been demonstrated in many experiments⁽¹⁻³⁾ that very low levels of amine additives (less than 0.1%) have large effects on detonation factors.

Each of these ten modern studies, from different scientists in different laboratories, on very different explosives, and with different experimental systems and calculational algorithms, gave results almost precisely as we had proposed from our theory--and in contradiction to expected classical results.

Related Comments

The concepts of mechanical bond scission and/or rearrangement under compression and immediate pressure reduction on the explosives molecules are both illustrated in the MD studies. Since the original bonds are gone, it is a somewhat semantic argument as to what bond scission describes.

The MD calculations also show the effects on shock sensitivity observed on a macro-scale in explosives of defects such as cracks, voids, inclusions, and lattice irregularities or damage, all of which increase sensitivity to shock initiation. More severe and higher numbers of immediate (about 10^{-13} to 10^{-10} s) bond fractures are seen in the initiation calculations at sights of the imperfections.

We stated in our early papers that bond breaking is an endothermic process. That is the reason we added chemical energy after the bond scission, at the reaction coordinates, to represent the chemical energy immediately available from the very rapid free-radical reactions. We have shown this chemical energy release rate in TATB, with a 40-angstrom detonation front width, to be almost 24 ev/ps.

CONCLUSIONS

We conclude that there is a new type of kinetics, physical kinetics, in initiation, detonation and other shock-induced reaction, and that there is a new detonation theory.

The Simplicity of Detonation

1. Thermodynamics and molecular structure determine whether or not a material will detonate, due mainly to rapid and voluminous gas formation from principally free-radical chemistry. The equation of Kamlet and Jacobs for calculating detonation pressure indicates the importance of gas formation. However, the thermodynamic factors are second-order effects in determining detonation velocities.

2. The kinetic energy of the shock or detonation waves is carried at the ARVVs by momentum transfer through the vibratory motion of the atoms, and this energy flux in the detonation front is higher than the covalent bond strengths. This leads to massive bond scission or rearrangement. This process we have designated as physical kinetics.

3. Since the explosives molecules are broken up nearly completely, there is immediate (10^{-14} to 10^{-12} s) reaction to release the major part of the chemical energy at or very near the front, and this chemical energy maintains the enormous kinetic energy of the front.

4. The ultimate determinant of the detonation velocity is the limiting ARVVs of the atomic couples, radicals or fragments from

the explosives molecules in the shock front. The D_s can then be calculated from simply the Hugoniot of the elements included in the empirical formulae of the explosives and the weight fractions of the elements.

At the end of our analyses of the many pertinent experiments and calculations we are back to the two principal physics equations with which we started: $E = \frac{1}{2}mv^2$ and $U_s = \frac{P}{\rho U_p}$, kinetic energy and shock velocity.

TABLE 1

DEVELOPMENT PLANKINETIC ENERGY

$$E_k = \frac{1}{2}mv^2$$



Determine E_c for other
Heterogeneous Explosives
Check E_c for Homogeneous
Explosives (NM)

Determine Structure of
Initiation in NM, LX-10

Check for Acceleration of Shock
Front Due to Chemical Reaction

Determine if Time to Initiation
and Detonation in NM are Functions
of DETA Concentration

Make MD Calculations of Bond

Fracture at High Shock Pressures

Make Study of Detonation Calorimetry
of BTNEA and Evidence of Massive Bond
Fracture and Rearrangement

Determine Shock Rise Times
and Shock Front Widths

SHOCK VELOCITY

$$U_s = \frac{P}{\rho U_p}$$



Calculate $U_s = f(P)$ by MD

Calculate Hugoniot of Elements
from Atomic Properties

Calculate Hugoniot of Organic
Compounds from Hugoniot of
Elements

Calculate Relative Vibrational
Velocities (RVVs) from

Infrared Spectroscopy and

X-ray Crystallography

Calculate RVVs from Hulbert-
Hirschfelder Equations

Check for Shock Barrier in Ds
and if it is Related to RVVs

Develop Concept of ARVs
and from this, Develop Concept
of Physical Kinetics

Determine E_k of Shock and Detonation Waves and Compare with Covalent Bond Strengths

Check for Correlations Between Detonation and Reaction Dynamics Factors

Determine Where Major Chemical Reaction Occurs in Shock and Detonation Waves and Time to Reaction. Is it Nonequilibrium?

Determine if Transfer of Shock Energy is by Momentum Process-- Using MD Calculations

Derive Equation for the Calculation of Ds from Kamlet-Jacobs Work

Derive Refined Equation for Calculation of Ds from K-J and Data Analysis

Derive Final D Equation from Physical Kinetics and Concept of Calculation of Hugoniot of Organic Compounds

72 - 17

RESULTS

NEW THEORIES OF PHYSICAL KINETICS AND DETONATION

(Determination of Shock and Detonation Wave Structures on a Micro-Scale: Rise Times, Widths, Energy Levels, Energy Transfer Methods, Massive Bond Scission and Rearrangement, Chemical Reaction Methods and Rates, Free-Radical and Chain Reactions, Maintenance of Shock and Detonation Wave Energy, Nonequilibrium and Nonthermal Processes in 10^{-14} to 10^{-12} s, ARVVs, and Understanding the Control of Detonation Velocities)

REFERENCES

1. F.E. Walker, Proceedings of the Twentieth International Pyrotechnics Seminar, 25-29 July 1994, Colorado Springs, CO, IIT Research Institute, Chicago, IL, pp. 941-966.
2. F.E. Walker, Proceedings of the Nineteenth International Pyrotechnics Seminar, 20-25 February 1994, Christchurch, NZ, The Fireworks Company, pp. 297-318.
3. F.E. Walker, Propellants, Explosives, Pyrotechnics 19, 315-326 (1994).
4. F.E. Walker, F.G. Walker and J.B. Walker, J. Appl. Phys. 60, 3876 (1986).
5. F.E. Walker, J. Appl. Phys. 63(11), 5548 (1988).
6. R.L. Simpson, F.H. Helm and J.W. Kury, Propellants, Explosives, Pyrotechnics 18, 150-154 (1993).
7. J.J. Gilman, Shock Compression of Condensed Matter 1989, S.C. Schmidt, J.N. Johnson and L.W. Davison (editors) Elsevier Science Publishers B.V., p. 267 (1990).
8. C.S. Coffey, Proceedings of 2nd International Workshop, Microscopic and Macroscopic Approaches to Detonation, 2-7 October 1994, St. Malo, France.
9. J. Sharma, J.W. Forbes, C.S. Coffey and T.P. Liddiard, J. Phys. Chem. 91, 5139 (1987).
10. K. Tanaka, S. Oinuma et al., Shock Compression of Condensed Matter 1989, S.C. Schmidt, J.N. Johnson and L.W. Davison (editors) Elsevier Science Publishers B.V., (1990).
11. D.W. Brenner, D.H. Robertson, et al., Microscopic Simulation of Complex Hydrodynamic Phenomena, Edited by M. Maraschal and B.L. Holian, Plenum Press, New York, NY, pp.111-123 (1992).
12. J.L. Austing, A.J. Tulis, et al., Private communication, March (1995). (Paper accepted for publication.)
13. O.R. Bergmann, Manager Research Program, Specialty Explosives, E.I. DuPont de Nemours and Company, letter of 28 October 1988.
14. H.N. Presles and D. Desbordes, Revue Scientifique et Technique de la Defense--40 Trimestre 1991, pp. 11-15.

Paper for the 26th International Annual Conference of ICT
JULY 4 - JULY 7, 1995

Experimental Phenomenon of Detonation Propagating
Along a Curved Small Charge

Feng Changgen, Wang Shushan, Jiao Qingjie, Chen Lang
Mechanics & Engineering Department
Beijing Institute of Technology
P.O. Box 327, Beijing 100081, China

& Huan Shi
Department of Applied Physics,
Changsha Institute of Technology
Changsha 410073, China

Abstract

This paper is concerned with the experimental investigation of *detonation propagation*. Attention was focused on the *velocity deficits* of detonation in a curved charge in respect to a linear one. The charge size was about $a=0.8\text{mm}-2.5\text{mm}$, where a is the size of the cross-section of the path of detonation. The relationships and their experimental formulations between the detonation velocity deficits and the charge size a or the charge curvature R were obtained respectively. The experiment showed that for some fixed sizes the detonation is prohibited in a curved charge whose curvature R is more than certain critical values. However for the same size a the detonation propagates steadily along linear charge.

Ein für Sprengkammern geeigneter ökologischer Sprengstoff für Explosivschweißen

Dipl. Ing. Aleš Vojtěch, CSc.

Lehrstuhl für Theorie und Technologie der Explosivstoffe
Universität Pardubice, Tchechische Republik

Abstract

A new agent for explosive welding was found which features are: no solid residues after detonation, the detonation products contain largely vapoured water and carbon dioxide (the explosive is environmental friendly) and using of the explosive brings, thanks its composition, minimum hygienical risks. The mentioned features make the explosive suitable for using in blasting chambers.

Zusammenfassung

Ein neuer Sprengstoff für Explosivschweißen wurde entwickelt, der dadurch gekennzeichnet ist, daß er keine festen Reste nach der Detonation hinterläßt. Die Detonationsprodukte enthalten vorwiegend Wasserdampf und Kohlendioxid, sodaß die Umwelt nicht belastigt wird. Bei der Arbeit mit dem Sprengstoff entsteht durch seine Zusammensetzung minimales Gesundheitsrisiko. Diese Eigenschaften bestimmen den Sprengstoff besonders für Arbeit in Sprengkammern.

1. Einleitung

Bearbeitung von Materialien durch Energie der Explosion ist ein Verfahren, das immer öfter in der Praxis ausgenutzt wird. Im Falle des Sprengschweißens oder Sprenghärtens muß es sich zwar nicht um große Ladungen handeln, aber diese in der offenen Luft detonierenden Ladungen belästigen die Umwelt durch Lärm und es ist immer komplizierter in den Bedingungen der bevölkerten Europa einen Platz für solches Verfahren zu finden.

So ist es günstig, die Detonation in eine Sprengkammer zu schließen. Im Falle des Sprengplakierens braucht man einen Sprengstoff, dessen Detonationsgeschwindigkeit kleiner ist, als die Schallgeschwindigkeiten in den beiden zu schweißenden Materialien. Um dies zu erzielen, werden Mischungen gemacht, in denen die brisanten Sprengstoffe mit inerten Substanzen gelöst werden. Reste dieser Inerten verbleiben jedoch auf dem Arbeitsplatz. Falls solche Mischungen in Sprengkammern benutzt werden, folgt nach einigen Schüssen Verstopfung von Lüftungsöffnungen.

2. Die Forderungen

Unser Arbeitsplatz ist mit einer Sprengkammer KVE-2 (Abb. 1.) ausgerüstet. Die Kammer ist für eine maximale Ladung von 2 kg von TNT bestimmt. Beim Schweißen mit dem bei uns dafür üblichen Sprengstoff SEMTEX S 25, der eine Mischung von Pentaerythrit und Natriumbicarbonat als Inert darstellt, setzten sich die Reste des Natriumbicarbonates überall in der Kammer, sodaß wurde bald die Ausspülung von Detonationsschwaden fast unmöglich.

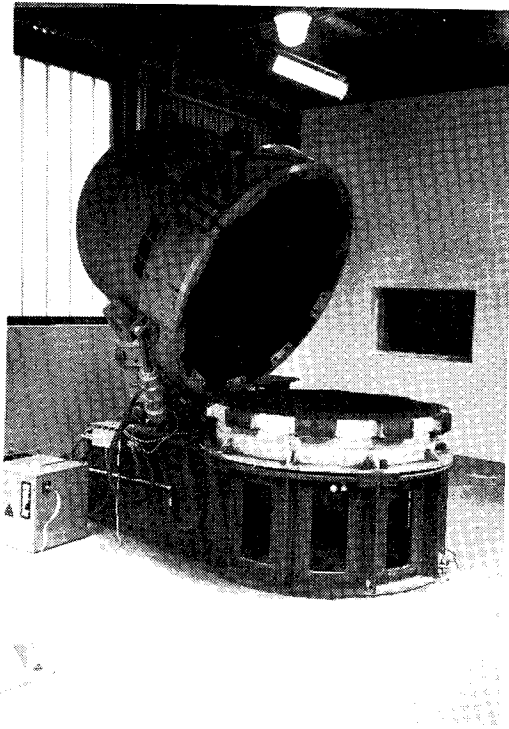


Abb. 1. Die Sprengkammer KVE-2

- Aus diesem Grund haben wir einen Sprengstoff gesucht, der :
- 1) bereits in einer Schicht von 10 mm detonieren kann, damit auch dünne Schichten plakiert werden könnten
 - 2) seine Detonationsgeschwindigkeit auch in großen Schichten unter der Grenze von 3000 m/s liegt,

- 3) nach der Detonation sollten keine festen Reste bleiben,
- 4) die Detonationsprodukten sollten vorwiegend Wasserdampf und Kohlendioxid behalten,
- 5) die Oberfläche des plakierten Matriales sollte nicht beschädigt werden.
- 6) einfache Arbeit mit dem Sprengstoff, minimales Gesundheitsrisiko

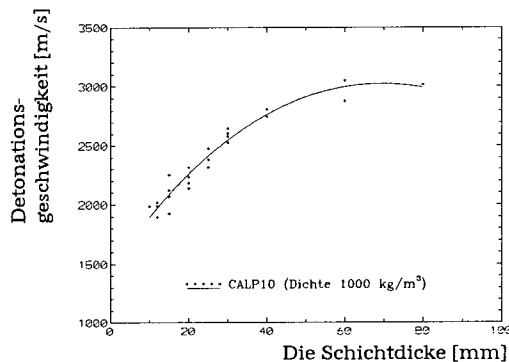


Abb. 2. : Abhängigkeit der Detonationsgeschwindigkeit von der Schichte des Sprengstoffes CALP 10

Einen solchen Sprengstoff haben wir auf der Basis von Pentrit und Amoniumnitrat gefunden und geprüft. Er ist bereits in der Schicht von 10 mm detonationsfähig, die Sauerstoffbilanz ist Null, keine festen Reste, die feinkörnige Struktur sichert, daß die Oberfläche des zu schweißenden Materiales nicht beschädigt wird. Alle sechs Punkte werden also durch diesen Sprengstoff erfüllt, das heißt, es handelt sich um einen ökologischen Sprengstoff, der besonders für Arbeit in Sprengkammern geeignet ist. Er wird als CALP 10 bezeichnet durch die Explosia Pardubice A.G. hergestellt.

3. Die Teste

Die Detonationsgeschwindigkeiten wurden an Proben gemessen, deren Grundriß 250 mal 100 mm war. Die konstante Schichtdicke wurde durch einen Holzrahmen gesichert, dessen Höhe der Schichtdicke gleich war. Der Rahmen wurde zum Blechboden befestigt, sodaß ein Kästchen entstanden ist. Die notwendige Mänge des Sprengstoffes wurde je der Schichtdicke im Voraus abgewogen und in das Kästchen plaziert, sodaß die Sprengstoffschüttdichte bei allen Proben 1 g/cm³ war.

Die Detonationsgeschwindigkeit wurde mittels zwei Paare elektrischer Kontakte auf der Basis 100 mm gemessen. Die Meßbasis wurde 150 mm von der Zündungstelle entfernt, damit sich die Detonationsgeschwindigkeit stabilisieren konnte. Die quasi-lineare Detonationsfront wurde durch eine bandförmige Übertragungsladung vom hochbrisanten SEMTEX 1A Sprengstoff gesichert.

Die Abhängigkeit der Detonationsgeschwindigkeit von der Schichtdicke zeigt die Abbildung 2.

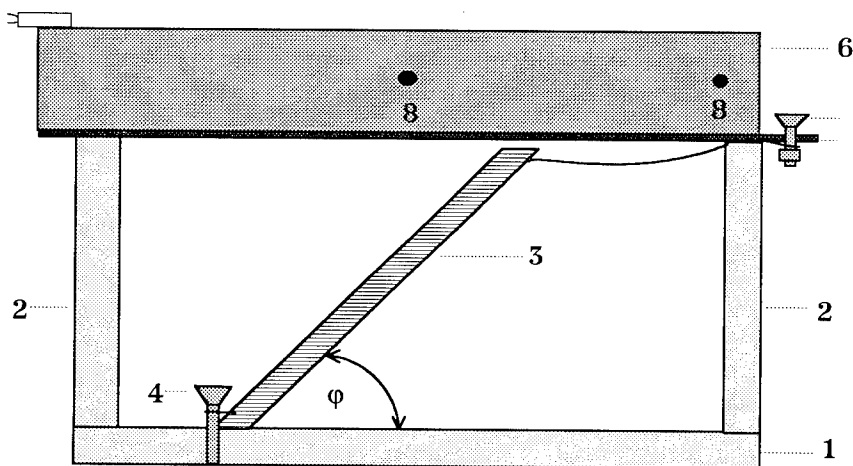


Abbildung 3 : Die fürs Detonationsgeschwindigkeit- und Flugplatteneigungswinkelmessen benutzte Zusammensetzung

Gleichzeitig mit der Detonationsgeschwindigkeit wurde auch der Flugplatteneigungswinkel gemessen, der eine wichtige Information für den Prozeß des Explosivschweißens darstellt. Zusammensetzung des Experimentes, die aus /1/ entnommen wurde, zeigt die Abbildung 3.

Die Basis der Zusammensetzung bildete eine Plexiglasplatte 200 mal 50 mm groß (1), an deren Enden sich 50 mm breite Stützen (2) befanden. Die Höhe dieser Stützen war von dem Linealwinkel (der ϕ - Winkel) abhängig. Im Falle des öftestens benutzten ϕ - Winkels 45° war es 102 mm. Auf den Stützen lagen die Blechplatte (7) und der Holzrahmen mit Sprengstoff (6). Die beiden Seiten des Holzrahmens wurden mit Öffnungen (8) für elektrische Kontakte versorgt, mit denen die Detonationsgeschwindigkeit gemessen wurde. Material der Blechplatten war Stahl, Kupfer oder Messing. Den wichtigsten Teil der Zusammensetzung bildete das Lineal (3), mit regelmäßig aufgewundenem Widerstandsdraht. Nach der Explosion wurde der Widerstandsdraht stufenweise, nach einzelnen Winden, durch die fliegende Blechplatte kurzgeschlossen, was eine Änderung in Stromspannung verursachte, die durch ein Oszillograph registriert wurde. Die Schrauben (4)

und (5) verbanden die Zusammensetzung mit der Batteriestromversorgung und Meßgerät. In der Abbildung 4 sind sie durch Punkte A und B dargestellt.

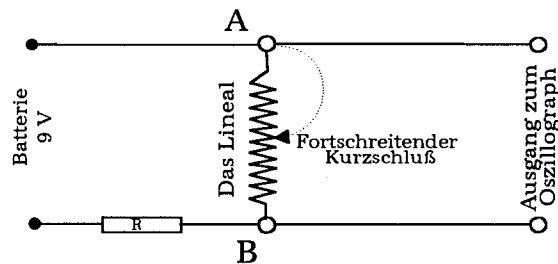


Abbildung 4 : Elektrisches Schema des Flugplatteneigungswinkelmessens

In der Abbildung 4 kann man sehen, daß der auf dem Lineal aufgewundene Widerstandsdraht mit dem Widerstand R einen Spannungsteiler bilden, sodaß der Fortschreitende Kurzschluß auf dem Lineal als eine Spannungsänderung abgelesen werden kann. Eine typische oszillographische Aufnahme zeigt die Abbildung 5.

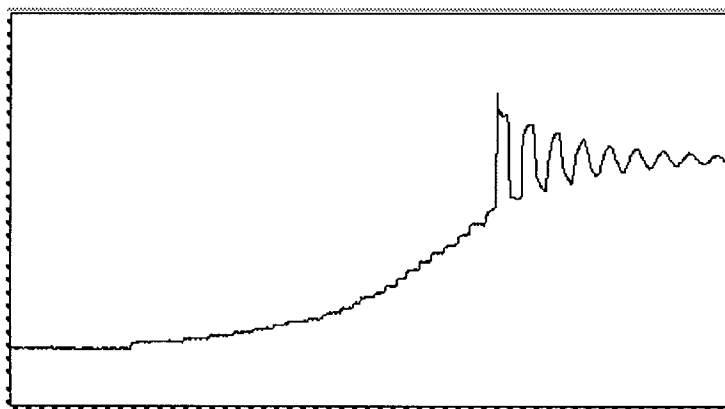


Abbildung 5 : Eine oszillographische Aufnahme des fortschreitenden Kurzschlusses auf dem Lineal

74 - 6

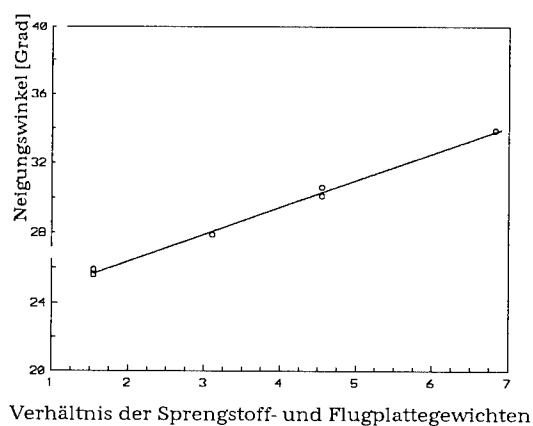


Abbildung 6 : Abhängigkeit des Flugplatteneigungswinkels von dem Verhältnis der Sprengstoff- und Flugplattengewichten

Die Zeitdifferenzen können dann bei der bekannten Geometrie und Detonationsgeschwindigkeit als Unterlage für die Blechplatteneigungswinkelberechnung dienen, und zwar nach der Formel

$$\vartheta = \arctan \frac{\Delta l \cdot \sin \varphi}{D \cdot \Delta \tau + \Delta l \cdot \cos \varphi}$$

In der Formel heißt Δl den Abstand der einzelnen Widerstandsdrahtwinden auf dem Lineal, D die Detonationsgeschwindigkeit, φ der Winkel des Lineales und $\Delta \tau$ die vom Oszillograph abgelesene Zeitdifferenz.

Die Abhängigkeit des Neigungswinkels von dem Verhältnis der Sprengstoff- und Blechplattengewichten zeigt die Abbildung 6.

4. Literatur

/1/ - Kuzmin, Maly, Paj - O metanii ploskich plastin slojami kondensirovannykh vv, Fizika vzryva 1975

TREIBSTOFF FÜR HÜLSENLOSE MUNITION AUF DER BASIS DES
PRESSBAREN NITROZELLULOSEGRANULATS

Tomáš Dosoudil

U n i v e r s i t ä t
FChT - KTTV, Čs.legií 565, 532 10 PARDUBICE
Tschechische Republik

Abstract

The modified nitrocellulose granulat has been prepared in laboratory scale. The granulat is pressable into a suitable shape for the caseless propellant elements. The pressing proceeds in dry state by increased temperature. The pressed compact elements have been tested from the pyrostatic and funktional point of view. It has been verified, that this nitrocellulose composition, on principle way, is able to perform the funktion as propellant mass in caseless and semicaseless systems.

Zusammenfassung

Im Labormasstab wurde ein modifizierter Nitrozellulosegranulat zubereitet, der im trockenen Zustand und bei erhöhter Temperatur pressbar ist, in die Form, die für hülsenlose Treibelemente erforderlich ist. Die ausgepresste Elemente wurden den pyrostatistischen Testen und Funktionsprüfungen bei verschiedenen Applikationen unterzogen.

Es wurde beglaubigt, dass die auf diesem System basierte Nitrozellulosekomposition prinzipiell die Funktion der Treibmasse erfüllen kann.

1.0 Ziel der Arbeit

Im Labormasstab wurde eine Möglichkeit beglaubigt, den auf der Nitrozellulose basierten pressbaren Granulat zu zubereiten, der für das Pressen der hülsenlosen Treibelementen verwendbar wäre.

Die Treibmasse verschiedener Energiestufen wurde pyrostatistisch testiert, sowie die ausgepresste Elemente wurden den Funktionsprüfungen in den hülsenlosen oder halbverbrennbaren Treibsystemen unterzogen.

In dieser Anfangsetappe war der Prüfungenbereich ziemlich beschränkt, mit Rücksicht auf die erste jetzige Aufgabe, die Einführungskentnisse der verfolgten Problematik festzulegen. Weiter ist es mit gründlichen Untersuchung der einzelnen Fragen zu rechnen.

2.0 Prinzip und Ergebnisse der Zubereitung und Verarbeitung des Granulats

2.1 Granulatzubereitung

Die Experimente wurden in einem Glassreaktor mit Umfang 4 L durchgeführt. Der Reaktor wurde mit einer Rühranlage mit einstellbarer Drehzahl, sowie mit einem Destillationskühler versehen.

Das Verfahren ist durch gründliche Änderungen von der Kugelpulvertechnologie abgeleitet, und besteht im Mischen des heterogenen dreiphasigen Systems, wo die Phasen wie folgt dargesetellt sind:

- a/ Wasserlösung des Tensides,
- b/ Nitrozellulose,
- c/ Lösung des synthetischen thermoplastischen Kopolymers im flüchtigen Lösungsmittelsystem.

Die Phasen b/ und c/ mischen sich zusammen und infolge des

Rührens und der Tensidwirkung zerfällt sich diese Mischung in diskrete "Lacktropfen" in der Wassenumwelt. Aus den Tropfen, durch Abdestillieren des Lösungsmittelsystems aus dem Reaktor, entsteht ein annähernd kugelförmiges Korn mit Durchmesser cca 1 - 3 mm. Das Produkt ist dann abfiltriert, durchgewaschen und ausgetrocknet.

2.2 Treibelemente

Der Granulat wurde in 4 Typen der Pressformen gefüllt und bei Temperatur 110°C mit Druck 50 MPa gepresst, um kompakte Test - bzw. Treibelemente zu gewinnen.

Infolge der Preparationsbedingungen ist in der Granulatstruktur, sowie in der Struktur der ausgepressten Elemente, die ursprüngliche Fadenform der Nitrozellulose in grosser Stufe erhalten.

Energie (als Explosionswärme gemessen) und mechanische Eigenschaften der Elemente sind durch Variieren des Stickstoffgehalts in Nitrozellulose und des Gehalts an Kopolymer in der Treibmasse einzustellen.

Gefertigte Elemente:

a/ Testelemente für pyrostatische Prüfungen in manometrischer Bombe.

b/ Treibelemente, die in der Messinghülse 9 mm Luger eingelegt wurden, um einen Wirkungsvergleich mit dem hier üblich verwendeten Pulver zu gewinnen.

c/ Treibelemente, die einen Bestandteil der Entwicklungsvariante der halbverbrennbaren Jagdladung .223 Rem darstellten.

d/ Treibelemente als hülsenlose Ladung für Entwicklungsvariante des Schlagbolzengerätes für Bauindustrie.

Alle Sorten der Elemente wurden in die Zylinderform gestaltet, mit einem zentralen Zylinderkanal (siehe Tab.1).

Tabelle 1:

Elementsorte	a/	b/	c/	d/
D (mm)	9,0	8,5	9,8	**
d (mm)	3,0	4,0	5,7	**
H (mm)	12,0	6,5	**	**
G (g)	0,90	0,40	1,5	0,25
ρ (kg.m ⁻³)	1350	1394	**	**
Q (kJ.m ⁻³)	*2481-4224	**	*2620-3111	4224

Notizen:

- D - Elementsdurchschnitt, d - Innenkanaldurchschnitt,
- H - Elementhöhe, G - Gewicht, ρ - Dichte, Q - Explosionswärme.
- * - Explosionswärmebereich nach der Zusammensetzung.
- ** - Einige Angaben werden nicht angeführt.

3.0 Pyrostatische Prüfungen

3.1 Anordnung der Experimente

Die Treibmasse wurde in der manometrischen ("ballistischen") Bombe geprüft, und zwar als Granulat (vor dem Pressen), sowie als Elemente der Kategorie a/ (nach dem Pressen).

Charakteristik der Testelemente:

Kopolymergehalt: im Bereich 2 - 14 %
 Stickstoffgehalt in Nitrozellulose: 13,22 %
 Gewicht: 0,90 g

Gemessene und ausgerechnete Größen:

t - Zeit, P - Druck, P_{\max} - Gemessener Maximaldruck,
 I_p - Impuls, d.h. Zeitintegral des Druckes.

Graphisch dargestellte Grössen:

(Siehe Abb.1 - 4)

$$P = f(t), \quad dP/dt = f(P), \quad \Gamma = f(P/P_{\max}) .$$

Für Γ - Funktion (Emission Funktion, "Vivacity") gilt ursprünglich:

$$\Gamma = d\psi / dI_p = d\psi / (Pdt), \quad \text{wobei } \psi \text{ ist relativ abgebrannte Pulvermenge.}$$

3.2 Diagramms

Der Verlauf der obig genannten Grössen wurde beim Gehalt an Kopolymer im Bereich 2 - 14 % ermittelt. Als Illustration sind weiter nur die Diagramms für 10 % angeführt (Abb. 1 - 3), und dann ein Vergleich für die funktion $\Gamma = f(P/P_{\max})$ im ganzen Bereich (Abb.4).

4.0 Funktionsprüfungen4.1 Treibelemente in der Messinghülse 9 mm Luger (Para)

Die beste Ergebnisse wurden mit den Elementen der Kategorie b/ unter den folgenden Bedingungen erreicht.

Charakteristik der Treibelemente:

Kopolymergehalt:	10 %
Stickstoffgehalt in Nitrocellulose:	13,22 %
Gewicht:	0,40 g

Anzündhütchen:	Boxer
----------------	-------

Anzündverstärkung:

Anzündsatz:	nicht angeführt
Menge:	0,07 g

Gemessene Grössen:

Geschossgeschwindigkeit $v_{12,5}$, Maximaldruck P_{\max}

Ausgerechnete Grössen:

Mittelwerte $v_{M12,5}$ $P_{M\max}$
 Mittelwerte im prozentuellen Vergleich mit den entsprechenden
 Werten nach den normalen ballistischen Forderungen
 $v_{PM12,5}$ $P_{PM\max}$

Schussanzahl: 10

Ergebnisse: $v_{PM12,5} = 107,0 \%$ $P_{PM\max} = 91,4 \%$

4.2 Halbverbrennbare Jagdladung .223 Remington

Von grösserer Menge der Experimente mit den Elementen der Kategorie c/ ist weiter nur eine Rahmenübersicht angeführt (siehe Tab.2).

Charakteristik der Treibelemente:

Kopolymergehalt: 10 - 14 %
 Stickstoffgehalt in Nitrozellulose: 11,55 - 13,22 %
 Gewicht: 1,5 g

Anzündhütchen: Boxer

Anzündverstärkung:

Anzündsatz: nicht angeführt
 Menge: 0 - 0,08 g

Gemessene Grössen:

Geschossgeschwindigkeit: v_2
 Druck: Nicht gemessen, nur nach der eventuellen Deformation des

Anzündhütchens oder der Hülse beurteilt.

Ergebnisse - Rahmenübersicht

Tabelle 2:

v_2 (m.s ⁻¹)	Druck	Nicht verbrannte Reste
778 - 979	erhöht	0
662 - 811	normal	0
610 - 650	nieder	sichtbar

4.3 Treibelemente für Schlagbolzengerät

(Elemente der Kategorie d/)

Charakteristik der Treibelemente:

Kopolymergehalt: 2 - 14 %
 Stickstoffgehalt in Nitrozellulose: 13,22 %
 Gewicht: 0,25 g

Initiierung:

Anzündsatz ohne Metallanzündhüttchen.

Gemessene Größen:

Druck: Maximaldruck in der Brennkammer P_{\max}
 Daneben wurde die Funktion des Gerätes überprüft, als Durchschlag der 5 mm dicke Stahlplatte.

Ausgerechnete Größen:

Mittelwert P_{\max}
 Massgebende Abweichung s
 Variationskoeffizient $k_v = (s / P_{\max}) \cdot 100 (\%)$

Ergebnisse:

Die besten Ergebnisse sind in Tab.3 angeführt.

Tabelle 3:

Q	GSK	n	P _{Mmax}	s	k _v	Funktion
(kJ.kg ⁻¹)	(%)	(1)	(MPa)	(MPa)	(%)	
4224	2	10	215,5	18,0	8,4	perfekt

Notizen:

Q - Explosionswärme, n - Schussanzahl,

GSK - Gehalt an synthetischen Kopolymer.

5.0 Schlussfolgerung

Aus den bisher erfahrenen Kenntnissen ergibt es sich, dass die geprüfte Nitrozellulosekomposition im Stande ist, die Funktion der Treibmasse prinzipiell zu erfüllen.

Die Applikation dieser Masse kennzeichnet sich durch das Pressen des modifizierten Nitrozellulosegranulats in der für ein Treibelement erforderlichen Form, im trockenen Zustand und bei erhöhter Temperatur.

Für die weitere Entwicklung dieser Lösung rechnet es sich mit der Fortsetzung der Arbeit, sowie mit den Prüfungen von Grösserer Anzahl und breiterem Bereich.

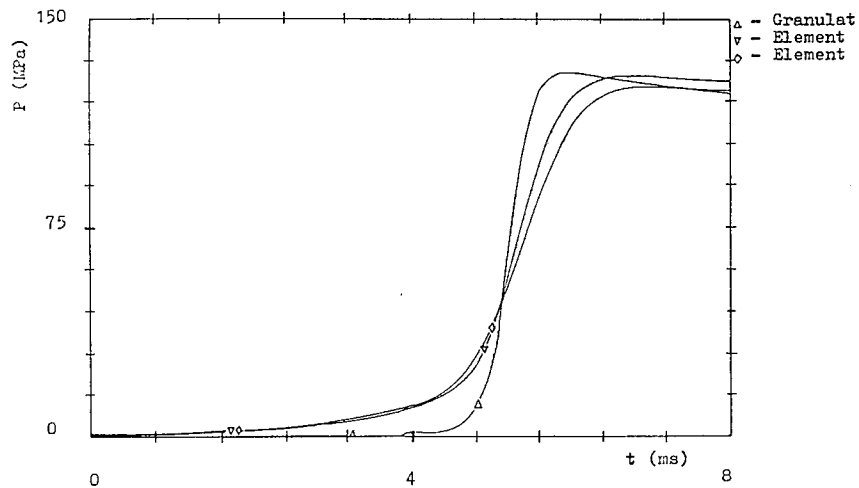


Abb.1: $P = f(t)$, Kopolymergehalt 10 %.

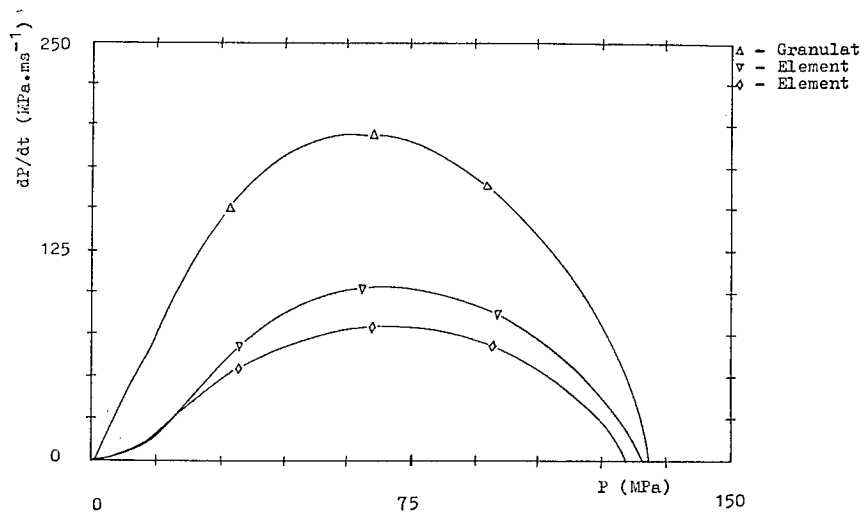


Abb.2: $dP/dt = f(P)$, Kopolymergehalt 10 %.

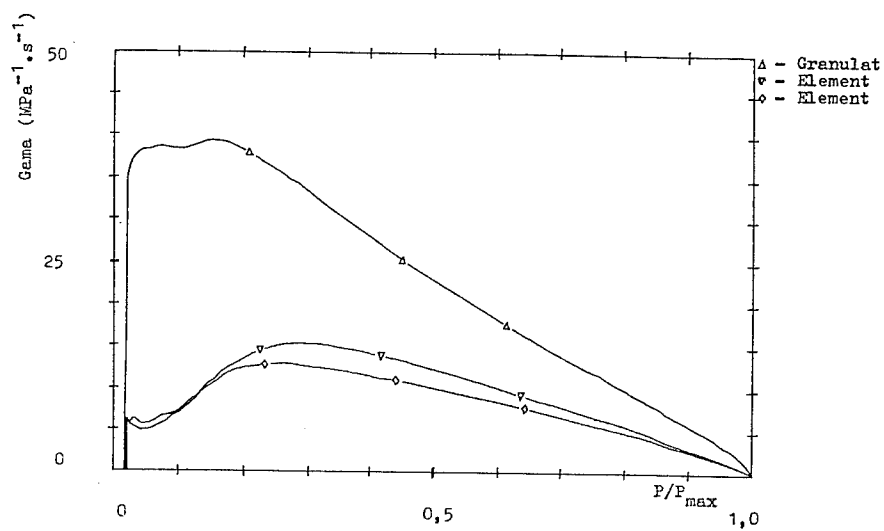


Abb.3: $\text{Gama} = f(P/P_{\text{max}})$, Kopolymergehalt 10 %.

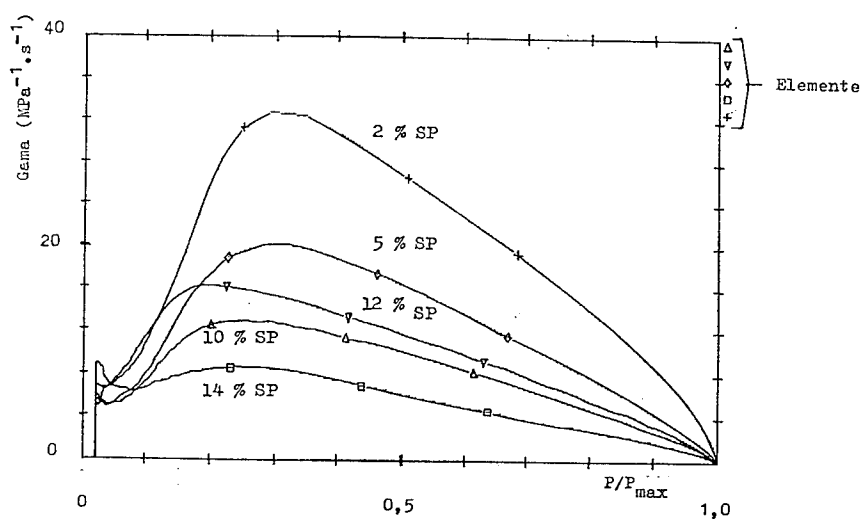


Abb.4: $\text{Gama} = f(P/P_{\text{max}})$, Kopolymergehalt ("SP") 2 - 14 %.

Solid Propellant Motor Impact Test

Masatoshi CHIBA*, Ryuichi ASANO*, Hiroyuki NAKAMURA*, Yukio HYODO*

Takehiro MATSUNAGA**, Katsumi TANAKA**

Keiji ARAI***, Takashi NAKAYAMA***, Shigeru SUZUKI***, Katsuaki KOSAKA***

* : National Space Development Agency of Japan

2-4-1 Hamamatsu-cho, Minato-ku, Tokyo, 105-60 JAPAN

** : National Institute of Materials and Chemical Research, MITI

1-1 Higashi, Tsukuba-shi, Ibaraki-ken, 305 JAPAN

*** : Nissan Motor Co., Ltd. Aerospace Div.

21-1 Matobashinmachi, Kawagoe-shi, Saitama-ken, 350-11 JAPAN

Abstract

Solid propellant motor impact tests have been conducted to establish a safety criteria for launch sites in Japan. These tests assumed that launch vehicles with solid motor falling back to the ground would be the accident mode having the highest hazard potential.

In this test, six solid motors loaded with propellant of 10 to 3600kg in weight were impacted against a massive concrete target at the velocities of 50 to 200m/s.

Two important facts were revealed by the test results. First, the TNT equivalent yield of the blast wave caused by the impact of a solid motor depends largely on the impact speed. Second, the maximum scattering distance of propellant fragments depends on the size of solid motor rather than the impact speed. In addition, the fragment scattering distance depends on the fragment size. These relations were analytically investigated and a simple prediction model was derived.

The impact numerical simulation analysis were conducted for estimating the failure mode of impacted motors. The results of computer simulations showed generally agreement with the test results, thereby confirming the validity of the simulation model.

1. Introduction

In order to establish a safety criteria for launch sites of large rocket motors, it is important to obtain information relating to the hazard potential of the solid motor. One of the accident mode having highest hazard potential is a fall-back condition from an altitude with impact on a ground surface.

In relation to the impact of solid motor, the impact test of TITAN-III booster stage solid motor conducted by NOTS⁽¹⁾ is famous. This test was carried out under a limited condition at the impact velocity of 200m/s. We have conducted the impact test using various size solid motors to obtain the fundamental data concerning the scale effects of solid motor. The blast waves and the scattering distribution of propellant fragments were mainly measured in these tests. In addition, the impact numerical simulation analysis were also carried out to estimate the failure mode of impacted motors. This report describes these results.

2. Test Procedures

The impact tests were conducted since 1991 to 1993. Solid propellant motors used in these tests and test conditions is shown in Table 1. Six solid motors were tested. The motors of test No.1~5 were loaded with HTPB based propellant, and the test No.6 motor were loaded with CTPB based propellant. The formulation of these propellants were shown also in Table 1. The test motor vehicle configuration of test No.5 is shown in Fig.1 as a typical example.

Test motor vehicles were accelerated by their own thrust on a rail track fastened to the railroad ties on the ground, and were impacted with a certain velocity against a concrete target. The outline of test procedure is shown in Fig.2. The target was constructed of reinforced concrete walls and massive earth fill. The reinforced concrete target blocks were exchanged in every test for supplying a flat surface at impact. The impact velocity of test motor vehicles was measured by optical sensor installed on the rail end at the target side. As the reference, TNT of 1~1.5kg were also exploded in near of the target front to evaluate TNT equivalent yields at impact and to examine the effects of the target configuration on the traveling of the blast waves. In a series of these tests, the pressure sensors for measuring the blast wave overpressure were located in two directions, 45deg., and 90deg. from the rail track. The tests were optically monitored and recorded by the high speed camera and VTR.

3. Results and Discussion

3.1 Impact Velocity

The measured impact velocities of the motor vehicles were shown in Table 2. The errors to the expected impact velocities were not exceeding 10% for all

test motor vehicles.

3.2 Measurements of Blast Wave

Fig.3 shows the overpressure -time histories measured at location of 20m from the target for the No.5 impact test. And Fig.4 show the ones at same location for 1kg TNT explosion test.

In these figures, the values of peak-overpressure in 45deg. direction were generally higher than that in 90deg. direction. Such directivity in propagation of blast wave were observed in all pressure records in a series of these tests. The numerical analysis relating to the propagation of blast wave for TNT explosion were carried out to examine the effects of the target wall⁽²⁾. As a results, it was shown that the higher blast pressure along 45deg. direction was caused by the shock refraction on the target wall. We concluded that the directivity of blast wave observed in these solid motor impacts were caused by the effect of reflection from the target wall.

The structures of blast wave observed in the motor impact was complicated in compared with that for TNT explosion. The blast wave structures with a precursor peak and periodical peaks are recognized in Fig.3. These wave properties were similar to the results of all motor impact tests. The growth mechanism of these wave structures is not yet clarified.

Fig.5 shows the measured peak-overpressure in 45deg. direction as a function of distance. A straight line in these figures is a best fitted regression line made by the least squares method. TNT equivalent yields of impacted motors estimated from the above-mentioned regression lines in Fig.5 were summarized in Table 2 with that in 90deg. direction. In Table 2, a TNT equivalent ratio is defined as the ratio of TNT equivalent weight to the residual propellant weight at impact.

TNT equivalent ratios are recognized to depend on the impact velocities rather than the motor vehicle sizes(or propellant gross weight) and to become high as the impact velocity increased from this summary. These results suggest that TNT equivalent yields depends on the extent of damage of the propellant grain at impact.

The value of TNT equivalent ratio in the test No.6 motor is relatively higher than that data in the test No.3 motor of almost the same test condition. This result is estimated due to the difference of used propellant type. The propellant used in the test No.6 motor is brittle.

3.3 Scattering of Fragment

The scattering distribution of fragments observed in the test No.5 motor impact test is shown in Fig.6. In Fig.6, the scattering of fragments shows an apparent tendency of concentration in the direction parallel to the impact surface of the target, suggesting the directivity of the kinetic energy release at the impact on hard target. This tendency was similar in all motor impacts. The most scattered materials was a propellant debris, and many of these debris attained far away showed that they burned on the ground where it fell.

The maximum scattering distance of propellant fragments observed in a series of these motor impact tests are summarized in Table 3. From Table 3, the maximum scattering distance of fragments are shown to strongly depend on the motor size and to extend range as the motor size increased. The effects of impact velocity on the maximum scattering distance is apparently poor.

Fig.7 shows the observed maximum scattering distance of fragments as a function of the propellant mass of impacted motors. Ref.1's data plotted in this figure. The maximum scattering distance of propellant fragments observed in Ref.1 is reported 3000 ft(914m). The solid line in the figure is a best fitted line obtained mathematically using present data. The line covers well Ref.1's data. Fig.8 shows a relation between the scattering distance and mass of propellant fragments obtained in the No.5 motor vehicle impacts. The mass of burned propellant in this figure was estimated from the area of the residue of burned propellant on the ground where it fell. The relation between propellant mass and the area of the residue was obtained preliminarily in present tests.

Large fragments show to reach far in Fig.8. The initial motion of fragment is considered to depend on a blast pressure of combustion gas ejected by the destruction of motor case at impact.

To estimate the maximum scattering distance of propellant fragment, the results in Fig.8 was examined analytically by the following method.

The motion of fragment is expressed as

$$M \frac{d^2x}{dt^2} = - Fd \cos \theta \quad M \frac{d^2y}{dt^2} = - M \cdot g - Fd \sin \theta \quad (1)$$

$$Fd = \frac{1}{2} \cdot \rho \cdot \frac{M}{D} \cdot \left\{ \left(\frac{dx}{dt} \right)^2 + \left(\frac{dy}{dt} \right)^2 \right\} \quad D = \frac{M}{Cd \cdot S}$$

where, Fd : drag force, M : mass of fragment, ρ : density of air

θ : angle of velocity vector, g : acceleration of gravity

Cd : drag coefficient, D : ballistic coefficient

S : effective cross sectional area of fragment

Equation(1) are solved under the following initial conditions.

$$x(0) = y(0) = 0, \quad \frac{dx}{dt} = V_0 \cos \theta_0, \quad \frac{dy}{dt} = V_0 \sin \theta_0$$

where, V_0 : initial velocity of fragment, θ_0 : initial angle
The solution of Eq.(1) show as a solid line in Fig.8, where the curve was obtained using the following values.

- (a). The bursting pressure was set to be 14 MPa which is the static bursting pressure of motor case.
- (b). The initial velocity of fragments was estimated from Ref.3 using the above-mentioned bursting pressure.
- (c). The values of ballistic coefficient were determined by the results of Fig.9 obtained from the recovered fragments.
- (d). Cd of 1 and θ_0 of 30° used, respectively.

Fig.8 shows that the caluculated results agree nearly well with the experimental results. The present method is considered to be useful to estimate the maximum scattering distance of fragments.

4. Impact numerical simulation analysis

The impact simulation analysis was conducted to estimate the failure mode of impacted motors. The analytical code used is 2D-axisymmetric code; AUTODYN-2D. The analytical model of the test No.5 motor vehicle(impact velocity of 100 m/s) is shown in Fig.10 as a typical example. The impact condition was assumed to be a rigid impact. Also, the initial pressure of 5.4MPa is loaded into the inner bore of propellant grain as a initial loading condition. The material properties are summarizes in Table 4. Fig.11 shows a deformation and destruction-time histories of motor vehicle at early time during impact with that of the experimental results. Both the analytical and experimental results, the propagation of deformation and destruction caused by the buckling show clearly in near the impact front of motor vehicle. From these results, the numerical simulation is considered to simulate the experimental results well quantitatively. Fig.12 summarizes the anlytical results for the test No.1~5 motor vehicle. This figure shows a weight fraction of failed propellant to the initial propellant weight at the end of motion as a function of initial impact velocities. In this results, the weight fraction of failed propellant increase in proportion to the initial impact velocities, and not depends on the motor vehicle size, apparently. Under the impact condition of 200m/s, the propellant grain estimated to destructe perfectly.

5. Conclusion

Solid propellant impact tests were conducted to establish a safety criteria for launch sites. Six solid motors loaded with propellant of 10 to 3600kg in weight were impacted against a massive concrete target at the velocities of 50 to 200m/s. Here are the summary of this study.

- (1). TNT equivalent yield of the blast wave caused by the impact of a solid motor was appeared to depend on the impact velocity rather than the motor vehicle size and to become high with the impact velocity increased. TNT equivalent yields of HTPB based solid propellant motor were estimated about 0.1% at the impact condition of 50m/s, about 2% at 100m/s and about 18% at that of 200m/s, respectively.
- (2). The maximum scattering distance of propellant fragment was appeared to largely depend on the size of solid motor and to extend range with the motor vehicle size increased. A simple prediction model was derived to estimate the maximum scattering distance of propellant fragment. This model is considered to covered the test results well.
- (3). The results of impact numerical simulation analysis conducted for estimating the failure mode of impacted motor showed generally agreement with the test results, thereby confirming the validity of the simulation model.

The method for predicting the hazard potential of large solid motors will be established on the base of these test results in the near future.

References

- (1) Vorwerk R.F '624A Solid Propellant Motor Impact Test' Technical Progress Report 381, NOTS TP 3674, U.S Naval Ordnance Test Station
- (2) Nakayama, et.al 'Blast Waves Generated by The Impact of A Solid Rocket Motor' National Symposium on Shock Waves, Jan.1992, Tokyo
- (3) Baker W.E et.al 'Workbook for Predicting Effects of Accidental Explosions in Propellant Ground Handling and Transport Systems'

Table 1. Test Conditions

Test No	Rocket Motor Size (mm)	Motor Gross Weight (kg)	Propellant Weight (kg)	Initial Chamber Pressure (MPa)	Expected Impact Velocity (m/s)
1	OD ϕ 100 L 1520	31	10.4	4.9	100
2	OD ϕ 100 L 1520	30	9.0	4.9	200
3	OD ϕ 245 L 2720	178	109	4.9	50
4	OD ϕ 245 L 2720	174	105	4.9	100
5	OD ϕ 465 L 5720	1554	996	5.39	100
6	OD ϕ 787 L 6570	4540	3603	3.43	50

OD : Outer Diameter Propellant : No1~5 HTPB/AP/Al=14/68/18wt%
 L : Overall Length No6 CTPB/AP/Al=12/68/20

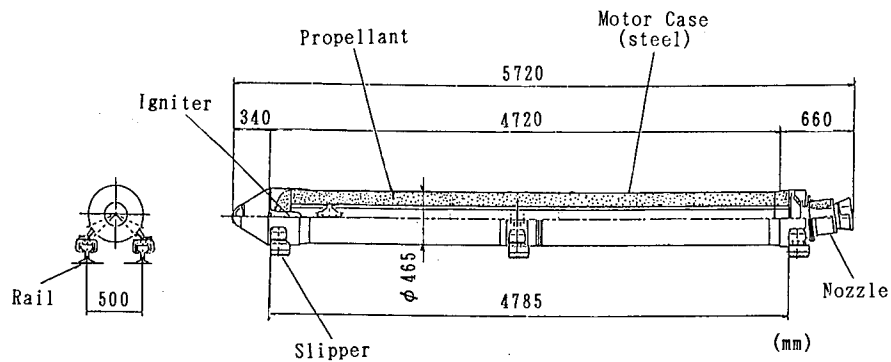


Figure 1. Test Vehicle Configuration (Test No5)

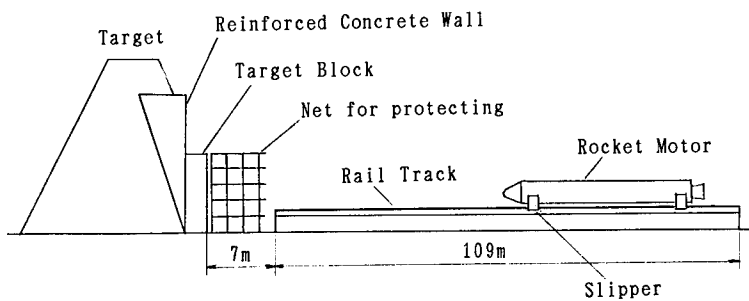


Figure 2. Experimental Set Up of Impact Test

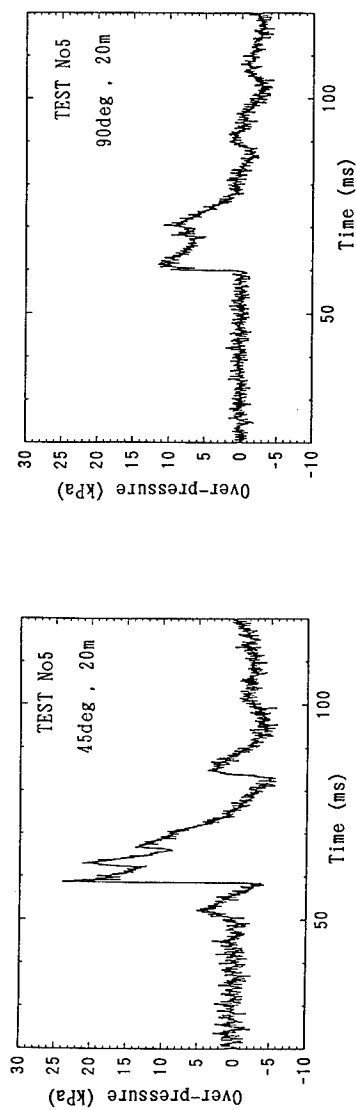


Figure 3. Measured overpressure-time histories for No. 5 Test Vehicle

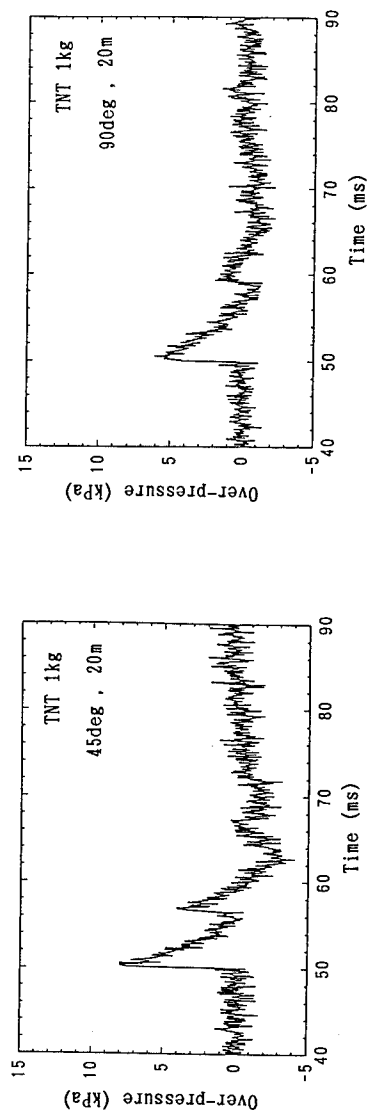


Figure 4. Measured overpressure-time histories for 1kg of TNT explosive

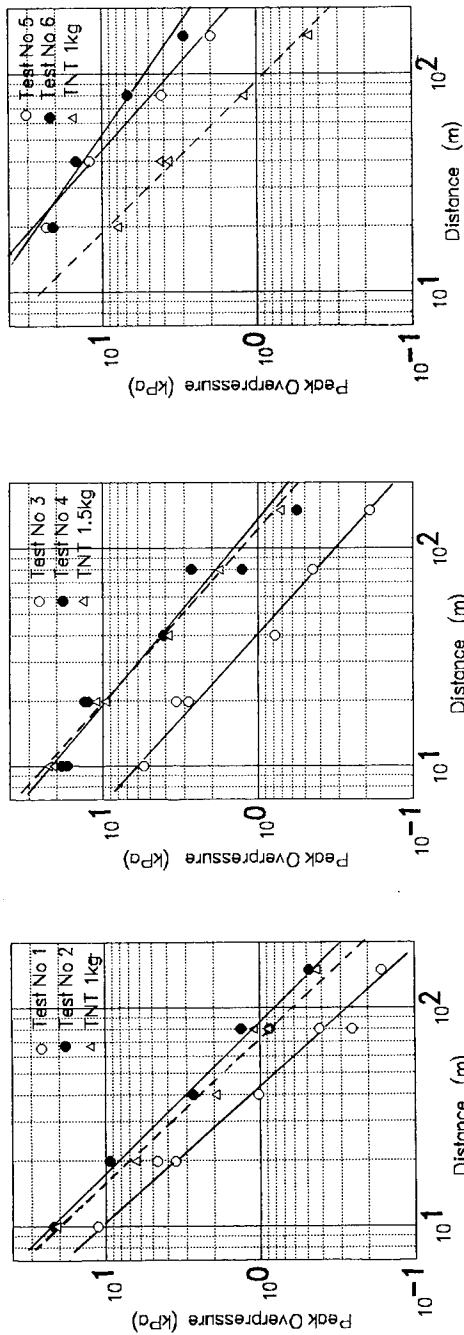


Figure 5. Relationship between peak-overpressure and distance in 45° to impact direction

Table 2. Estimated TNT equivalent yields at impact

Test No	Measured Impact Velocity (m/s)	TNT Equivalent Yields		
		TNT Eq. Weight (kg)	TNT Eq. Ratio (%)	45°
1	92	0.25	0.25	2.4
2	194	1.61	17.9	17.9
3	54	0.13	0.12	0.07
4	98	2.36	1.11	1.1
5	100	20.0	9.12	2.0
6	52	55.6	8.31	1.5
				0.23

76 - 10

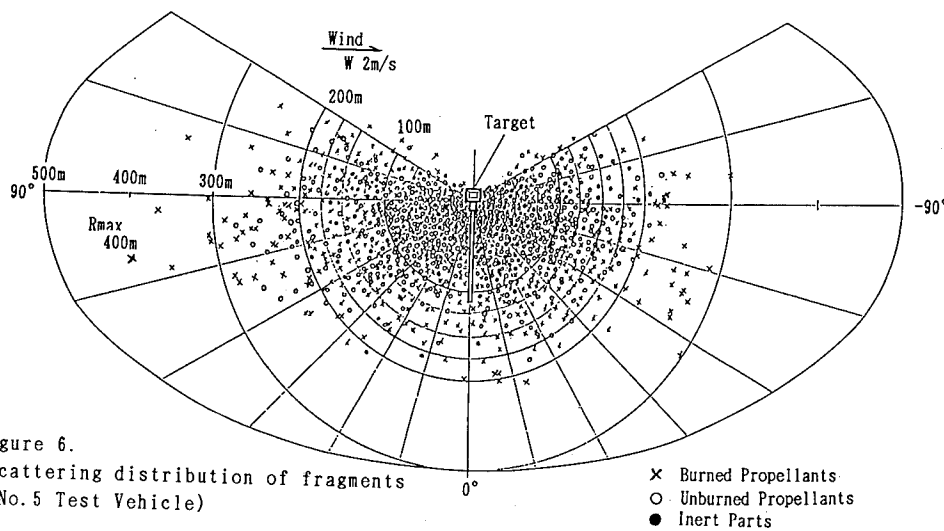


Figure 6.
Scattering distribution of fragments
(No. 5 Test Vehicle)

Table 3. Observed maximum distance of scattered fragments

Test No	Impact Velocity (m/s)	Propellant mass (kg)	Observed Maximum Scattering Distance (m)
1	92	10.4	92
2	194	9.0	110
3	54	109	205
4	98	105	235
5	100	996	400
6	52	3603	397

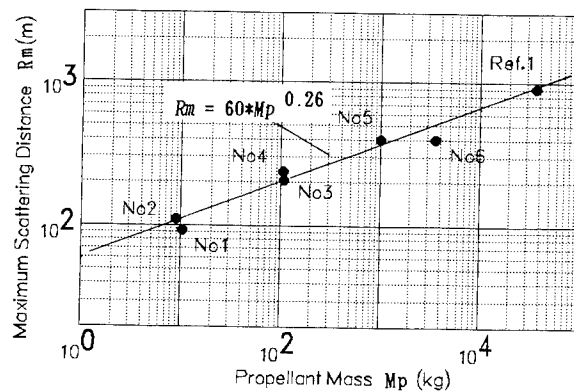


Figure 7. Relationship between
Maximum scattering range and Propellant mass

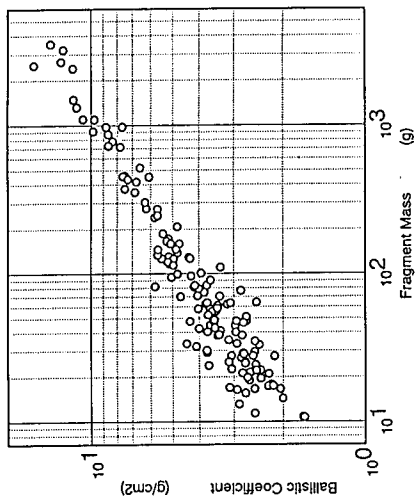


Figure 9. Relationship between ballistic coefficient and propellant fragment mass

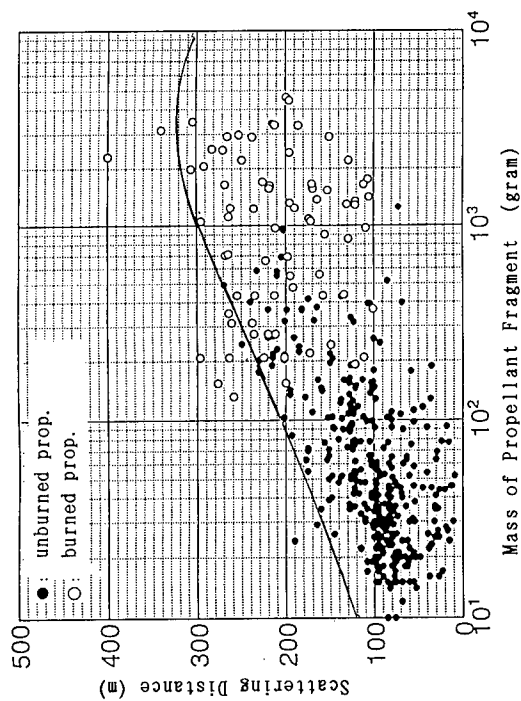


Figure 8. Relationship between scattering distance and mass of propellant fragment (Tset No. 5 motor impacts)

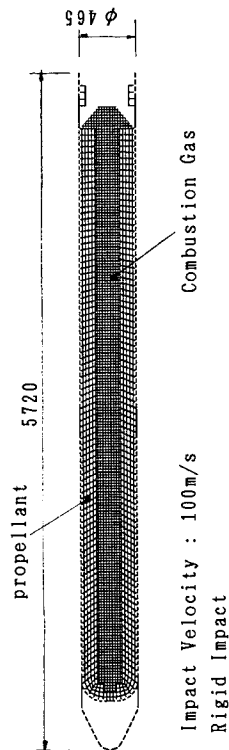
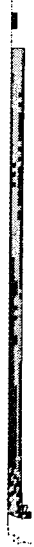


Figure 10. Impact simulation analytical model (Test No. 5 motor vehicle)

Initial Length : 5720 mm
Residual Length : 5503 mm

Time after Impact : 2 ms



ELASTIC
PLASTIC
FAILED

5102 mm

6 ms



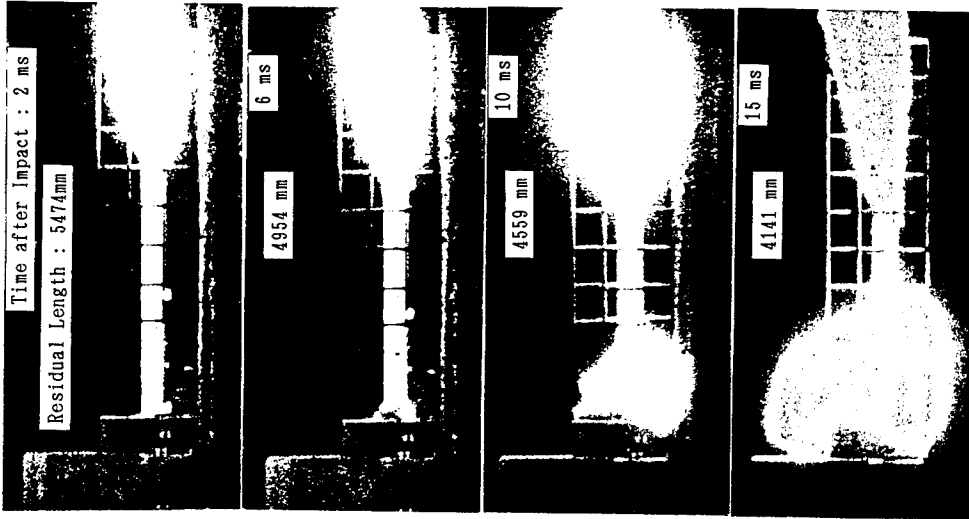
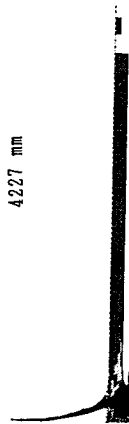
4713 mm

10 ms



4227 mm

15 ms



Time after Impact : 2 ms

Residual Length : 5474mm

4954 mm

6 ms

4559 mm

10 ms

4141 mm

15 ms

Figure 11.

Comparison of
test results
with calculated
results
(Test No. 5
motor vehicle)

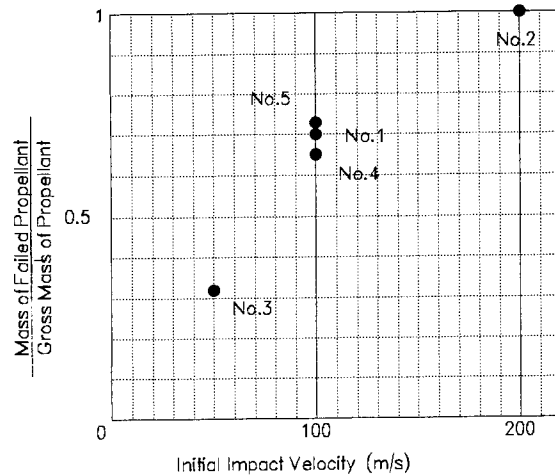


Figure 12.
Relationship between an amount of
failed propellant and impact velocity

Table 4. Material Properties

Item	Propellant	Motor Case
Material	HTPB Composite	SCM435 STEEL
Density gram/cc	1.77	7.9
Bulk Modulus Mbar	0.042	1.66
Young's Modulus Mbar	2.61E-4 *	2.001
Yield Stress Mbar	2.4E-5 *	8.18E-3
Yield Strain %	9 *	0.2
Ultimate Stress Mbar	8.5E-5 *	11.4E-3
Ultimate Strain %	64 *	16
Yield Model	Von Mises	Von Mises
Spall Pressure Mbar	-5.0E-3	-
Hugoniot EOS km/s	Us=2.232+1.98Up	-

* : Typical values at R.T(Strain rate=115/s)

Generalization of the Results of the Solid Energetic Materials Sensitivity to Impact and Friction Estimation

B.N.Kondrikov

*Mendeleev University of Chemical Technology
9 Miusskaya Sq., Moscow 125047, Russia
FAX #: (095)200-4204*

A generalization of 12 different methods of sensitivity of the solid energetic materials EM to impact and friction evaluation used in the different countries is proposed. As a ground for the generalization the critical stress data P_1 received using the strain gage and K-44-II impact machine are utilized. The values of the critical pressures P_2 obtained in experiments at static compression of the layer of explosive in the plexiglas tubes of different wall thickness and the critical pressure P_4 , produced as a result of the minimal energy of initiation W_* estimation are proportional to the P_1 value, and in fact all three of the pressures (P_1 , P_2 , P_4) are almost equal to each other. The W_* value correspondingly is proportional to P_1 square.

The results of pressure P_3 measurements necessary to obtain the explosion frequencies of 100, 50, and 0% estimated by means of the Soviet friction impact machine K-44-III (the values of $P_3(100)$, $P_3(50)$, and $P_3(0)$, corr.) are related to P_1 by the more complicated manner. At $P_1 < 7$ kbar they are proportional to P_1 . At $P_1 > 7$ kbar the main relation is $P_3 \sim P_1^2$. The quantitative explanation of this behavior is proposed.

The value of the minimal height H_0 of the 10 kg weight falling down to produce explosion in the tool #2 of the K-44-II impact machine, and the Rotter machine FF (Figure of Intensity) results are proportional to $P_1^{0.8}$ at $p_1 < 6.5$ kbar and to $P_1^{1.7}$ at $P_1 > 6.5$ kbar.

The Soviet rotating friction device I-6-2 gives the critical pressure P_6 . It is proportional to $P_1^{1.8}$. The Rotary Friction Test results FF (Figure of Friction), and the critical height, "up-and-down" value of sensitivity estimated by means of #12 Bruston tool application both correlate with P_1 as proportional to P_1^n where n is 1.4 and 1.8, corr. Only the LL data, the limiting load of BAM friction apparatus have the n -exponent essentially higher than it usually is, i.e. about 2.5. All the results obtained are logically explained.

PYROTECHNIC GENERATOR OF FLYER DISK

by

J. Ribeiro, J. Campos and R. Mendes

*Lab. of Energetics and Detonics
Mech. Eng. Dep. - Fac. of Sciences and Technology
University of Coimbra - 3000 Coimbra - PORTUGAL*

Abstract

A miniaturised pyrotechnic bomb, closed by a metallic foil, is presented. Inside, a propellant sample, as fuse head, is ignited by a small resistive wire. The expansion of the burned gases produces the rupture of the metallic foil, generating a flyer disk movement. Its acceleration is similar but slower than the observed inside the barrel of a slapper initiation device. Two used electrical pulse generators are presented. They are based on conventional electric discharge circuit, with a typical discharge energy less than 1 J, using two different kind of switches. The discharge characteristics are optimised as a function of pressure combustion inside bomb.

The experimental pressure, inside bomb, is measured and correlated with a simple combustion model. The discussion of the results seems to indicate the existence of energetic material dispersion, from the initial fuse head, before the end of combustion. Rupture of foil, generating flyer disk, is a function not only of the load pressure inside the bomb but also of the pressure rise. Flyer disk velocity seems to be able to initiate sensible secondary explosives.

1. INTRODUCTION

An electrical detonator is an electroexplosive device (EED) in which a suitable electrical waveform is supplied to a fine resistance element bridge, in such a manner to initiate the pyrotechnic charge in contact with the bridge. The role of the detonator, thus, is to convert an electrical pulse into a sustained detonation, which is then transferred to the next element in an explosive train (Austing *et al*, 1989). Generally, two methods can be considered to the explosive initiation (Dinegar, 1984) - hot wire and transmission method, pervious described as EED, and slapper foil impact initiation, (Gois *et al*, 1993), where the secondary explosive is initiated under impact of a flyer plate.

Research and development activities, over the last three decades, have been directed to improve both the electrical and pyrotechnic safeties of all EED. The improvement in the pyrotechnic safety is achieved with the stop of the use of primary explosives, which are very dangerous due to their high sensitivity to shock and temperature conditions, and to their potential pollution.

A miniaturised pyrotechnic bomb, closed by a metallic foil, is presented. Inside, a propellant sample is ignited by a small resistive wire, connected to an electrical pulse generator. The expansion of the burned gases produces the rupture of the metallic foil, generating a flyer disk

movement. Its acceleration is similar but slower than the observed inside the barrel of a slapper initiation device.

The following text presents:

- the pyrotechnic closed bomb generator of a flyer disk,
- two electrical pulse generators, based on a conventional electric discharge circuit, with a typical discharge energy less than 1 J, using two kinds of switches,
- the experimental measurements of the current and voltage drop, through the resistance of the bridge wire and fuse head,
- the experimental measurements of the pressure inside the bomb and its correlation with a simple combustion model.

2. EXPERIMENTAL SET-UP

2.1. *Flyer plate generator.*

The flying plate generator, shown in Fig. 1, is based in pyrotechnic bomb closed by a metallic foil. It includes a 5mm internal diameter and 10 mm length cylindrical combustion chamber, executed in brass and a clump screw, which locks inside a 40mg based nitro-cellulose fuse head. The chamber is closed by a 0.1mm thick copper foil, from which is generated the flyer disk. It has an accelerated movement along a 3mm diameter barrel dish. A piezoelectric pressure transducer (PCB 112A05 with 2 μ s rise time) allows the measurement of the pressure inside the chamber.

When an electrical pulse is supplied to the resistance, inside the fuse head, the heat release by Joule effect will ignite the propellant. The pressure from the combustion gases is high enough to push out a section of copper foil to form the flyer disk. The flying disk is then accelerated along a gap distance, provided by the barrel, until it reaches the target. The barrel not only must insure a suitable gap allowing the flying disk acceleration, but also act like a gun barrel providing a good obturation and an easy pushing out of the flyer plate (Rychardson et al, 1988).

2.2. *Low discharge energy electrical pulse generator*

An industrial type electrical pulse generator was used in preliminary experiments. It has an electrolic capacitor of 36 mF, usually loaded at 46 V, switched by a mechanical relay. Its unknown and not reliable internal resistance suggests the use of following system.

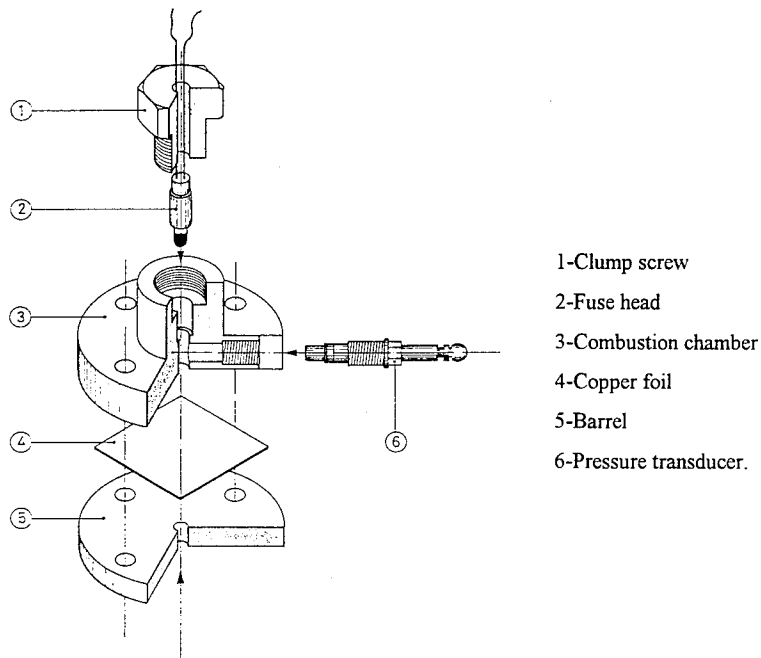


Fig. 1 - Flyer plate generator.

It is based (vd. Fig. 2) on a 2.14 mF low inductance capacitor as a source of energy, which can be charged by a medium tension generator until values of 400Volts, storing a maximum energy of 0.1712 J. The flow of current to the bridge wire is switched by an antiparallel thyristor (SCR), (RS - 353-455) allowing current peaks until 875A and with a critical rate of rise of voltage of 500V/ms.

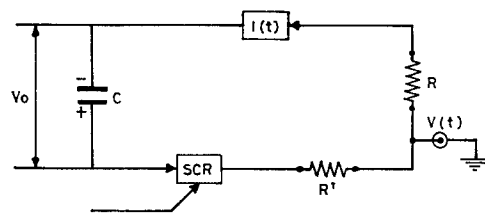


Fig. 2 - Low discharge energy electrical pulse generator circuit.

78 - 4

Figure 3 shows a discharge type curve of the capacitor, over a 1.59Ω short circuiting resistance and the potential difference throughout the resistance. It is possible to observe that the two curves are very similar, which means that the internal resistance of the electrical pulse generator is very small.

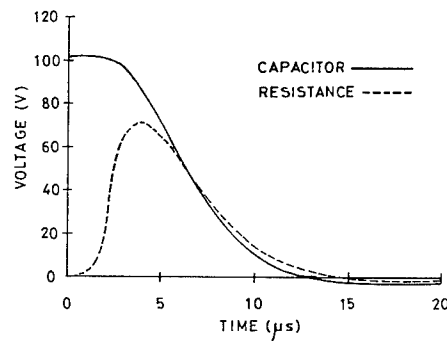


Fig. 3 - Capacitor and resistance voltage.

3. EXPERIMENTAL RESULTS AND DISCUSSION

3.1 Electric discharge characteristics

The type current and voltage difference curves through the fuse head resistance for two values of the initial capacitor voltage are shown in Fig. 4.

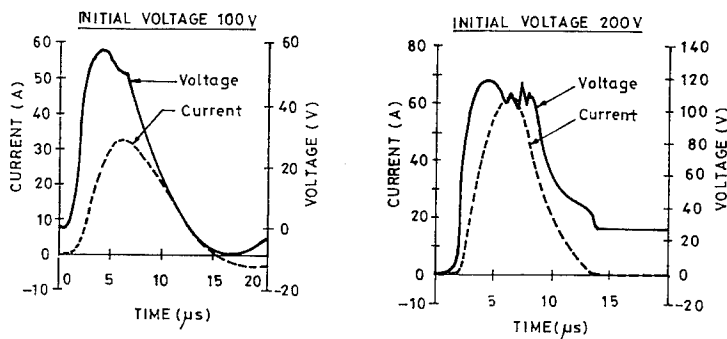


Fig. 4 - Current and voltage curves through the fuse head resistance for two initial capacitor voltages.

The analysis of the two graphics (vd. Fig. 4) suggests that all the stored energy in the case of the initial capacitor voltage of 100V, has been discharged. On the other case, for 200V initial voltage, not all the stored energy could be discharged.

The energy delivered to the fuse head resistance can be evaluated either, using the measured values of the current and voltage difference, by:

$$\int_0^t I \cdot V \cdot dt \quad (1)$$

where V is the voltage difference through the fuse head [V], I the current through [A] and t the time [s].

Assuming a constant resistance of fuse head

$$E_d = \frac{1}{2} C V^2 \left[1 - e^{\left(-2t / R_0 C \right)} \right] \quad (2)$$

where E_d is the delivered energy [J], C the capacitance [F], V_0 the initial voltage [V], t the bridge wire burst time [s] and R_0 the initial fuse head resistance [Ω].

The results obtained by numerical integration of equation 1 and analytical resolution of equation 2 are presented in Fig. 5.

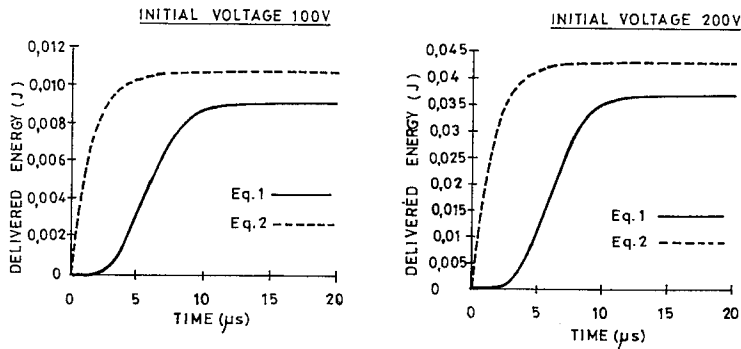


Fig. 5 - Delivered energy to the fuse head evaluated by equations 1 and 2.

The difference of obtained results, shown in Fig. 5, allow to conclude that for a two time increase in the initial capacitor voltage it is observed four times increase in the delivered energy.

3.2. Combustion and pressure rise

An example of obtained experimental pressure-time results are shown in Fig. 6. Two situations are presented:

Situation referred as A was obtained with the previous described low discharge energy electrical pulse generator, for a initial capacitor voltage of 100V,

Situation referred as B was obtained using the previous described, industrial type electrical pulse generator, with an 36 mF electrolytic capacitor, loaded at 46V, and with an mechanical relay as switch.

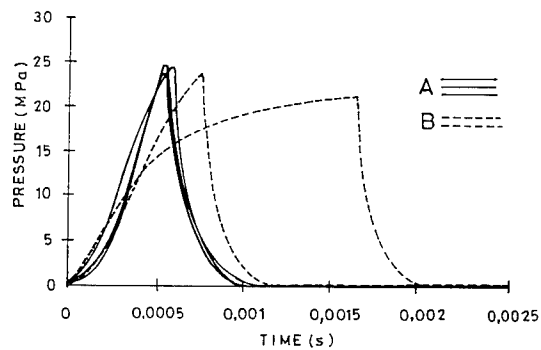


Fig. 6 - Pressure time variation for two experimental situations.

The differences observed between these two types of pressure-time profiles are suggested to be justified by electrical pulse energy. Pressure-time profiles of the situation A do not present significative differences. On the other way, pressure-time profiles of the situation B, present significant differences. This fact can be explained by the reliable behaviour of the mechanical switch.

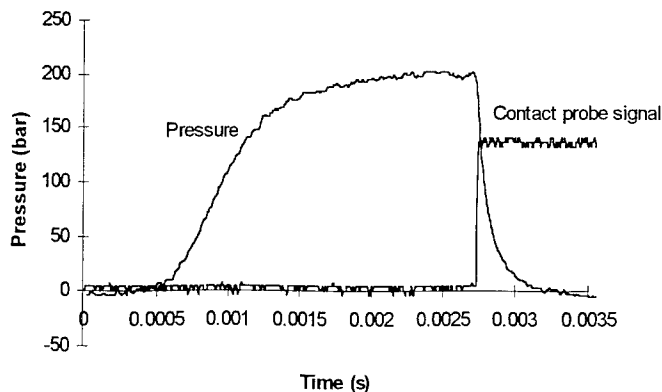


Fig. 7 - Pressure-time variation for a loading density of 0.152g/cm^3

3.3. Preliminary evaluation of flyer disc acceleration

The preliminary pressure-time experimental results can be seen on Fig. 7 and 8. It is possible to observe the pressure chamber relief when the copper plate is pushed out from the foil. The variation of the pressure rise rate and the maximum pressure value is a function of loading density, defined as the relation between the mass of propellant and the chamber volume.

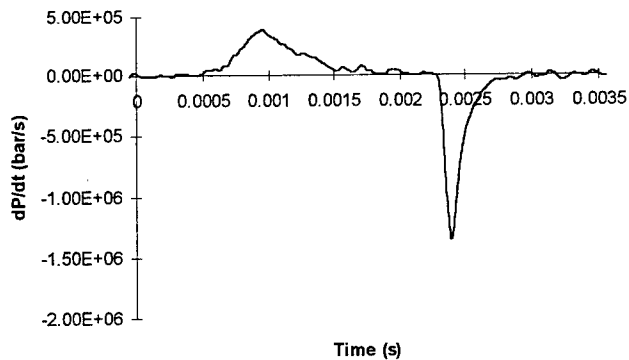


Fig. 8 - Pressure rate variation for a loading density of 0.152g/cm^3

Evaluation for the flyer plate velocity after a 7mm of travelling distance, predicts a velocity of 620m/s which seems to be in accordance with the measured travelling time.

3.4. Pressure time variation discussion

The experimental pressure-time profiles were correlated with those calculated by a simple combustion model, where the fuse head propellant is assumed to be spherical. It is based on the following equations:

- mass balance

$$\frac{\partial P}{\partial t} = \frac{P}{T} \frac{\partial T}{\partial t} + \frac{P}{V_g} \cdot 4\pi \cdot r^2 \cdot \frac{\partial r}{\partial t} - \frac{\rho_p \cdot R \cdot T}{M} \cdot \frac{4\pi \cdot r^2}{V_g} \cdot \frac{\partial r}{\partial t} \quad (3)$$

- energy balance, assuming all the energy, generated by propellant combustion, is absorbed by the combustion gases

$$\frac{\partial T}{\partial t} = \frac{\Delta H_R \cdot 4\pi \cdot r^2 \cdot \frac{\partial r}{\partial t}}{c_{p_g} \cdot \frac{P \cdot M}{R \cdot T} \cdot \left(V_c - \frac{4}{3} \pi \cdot r^3 \right)} \quad (4)$$

- Vieille law

$$\frac{\partial r}{\partial t} = a \cdot P^n \quad (5)$$

where P is the pressure inside the combustion chamber [Pa], t time [s], T combustion gas temperature [K], V_g total gas volume inside the combustion chamber [m³], r propellant radius [m], ρ_p propellant specific mass [m³/kg], R universal gas constant [J.mol⁻¹.K⁻¹], M molar mass of combustion gases [kg/mol], ΔH_R reaction enthalpy [J/kg], c_{pg} specific heat at constant pressure of the combustion gases [J.kg⁻¹.K⁻¹], a Vieille's law pre-exponential factor, and n Vieille's law exponential factor.

An example of correlation of the experimental and calculated pressure-time profiles is shown in Fig. 9. This result seems to indicate the existence of energetic material dispersion, from the initial fuse head, before the end of combustion.

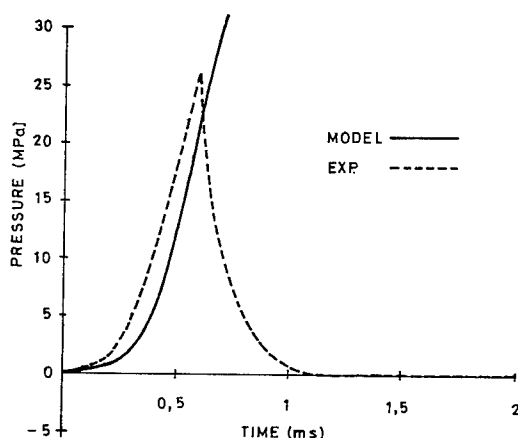


Fig. 9 - Example of correlation of experimental and calculated pressure time profiles.

4. CONCLUSIONS

A miniaturized pyrotechnic bomb, closed by a metallic foil, having inside a propellant sample as a fuse head, ignited by a small resistive wire, is presented. The expansion of burned gases produces the rupture of the metallic foil generating a flyer disk movement. The discharge characteristics are optimized as a function of combustion inside the bomb.

The flyer disk velocity, correlated with experimental measurements of pressure inside the bomb, seems to be able to initiate sensible secondary explosives. The discussion of the results,

based in a simple combustion model, seems to indicate the dispersion of the energetic material from the initial fuse head, before the end of combustion. Rupture of foil, generating flyer disk, is a function not only of the load pressure inside the bomb, but also a function of the pressure rise.

References

- AIAA, 1984. *Fundamentals of solid propellant combustion*. Prog. in Astronautics and Aeronautics Series. Edited by Kuo, K.K. and Summerfield, M., vol. 90, USA.
- AUSTING, J.L., TULIS, A.J., HARDINE, D.J., JOYCE, R.P. and URBANSKI, E, 1989. Capacitor-discharge initiation of a detonator containing a vacuum-deposited thin-film chromium bridge. *Propellants, Explosives and Pyrotechnics*, vol. 13, pp.129-134.
- DINEGAR, R.H., 1984. High-temperature-stable detonators. Proc. of *12th Symposium on Explosives and Pyrotechnics*, San Diego, USA.
- GOIS, J., CAMPOS, J. AND MENDES, R. , 1993. - Shock Initiation of Nitromethane-PMMA Mixtures with Glass Microballoons. Proc. of *10th International Detonation Symposium*, Boston, USA.
- GRIEF, D. and COLEY, G., 1984. Performance Criteria for Small Slapper Detonators. Proc. of *12th Symposium of Explosives and Pyrotechnics*, San Diego, USA.
- KUBOTA, N., 1984. Survey of rocket propellant and their combustion characteristics. Prog in Astronautics and Aeronautics, AIAA, vol. 90, pp.1-52.
- RYCHARDSON, D., NORTHEAST, E., and RYAN, P., 1988. *An Exploding Foil Flying Plate Generator*. Internal Report of the Materials Research Laboratory of the Defense Science and Technology Organisation. Melbourne, Australia.
- UEE-EXPLOSIVOS, 1989. *Detonadores Eléctricos y Equipos Accesorios*. Edited by UEE, Spain.

SPECTRAL EMISSION FROM POOL FIRES OF VARIOUS FUELS - CONSIDERING TRANSIENT STRUCTURES

V. Weiser, M. Weindel, A. Hoffmann, W. Eckl, N. Eisenreich

Fraunhofer Institut für Chemische Technologie,
Joseph-von-Fraunhofer-Str. 7, D-76327 Pfinztal,
Germany

Abstract

With special regard to short-time structure nitromethane, methanol, 2-propanol and isooctane have been investigated, applying NIR/IR spectrometer systems based on rotating filter wheels and with a scan rate of 50 scans/s. The resulting spectra have been analysed for emitting species, their concentration and temperature of gas and particle phase. Temperatures and optical depth have been determined, comparing calculated spectra to experimental data (wavelength region 1 - 10 μm). Assuming a simple flame ball model, the observed profiles can be explained.

Introduction

Pool fires play an important role as model fires for industrial flame hazards of chemicals and compounds like petrol products, solvents, metals (sodium) , plastics and toxic monomers (isocyanates). Their main destructive potential comes out of radiated heat and toxic smoke gases (Bagster 1989). This is also of interest within smaller accidental fires like burning containers of chemicals emitting toxic gases endangering enclosed employees. Pool fires are atmospheric turbulent diffusion flames with fluctuation of flame front caused by strong heat and mass transfer. Reaction is starting, if local ignitions conditions are reached. Therefore even small fires are very complex reaction systems with inhomogenous flame fronts and transient structures of 1 to 10 Hz (Brötz 1983).

Effective fire fighting requires knowledge of reaction mechanism and toxic products. Previously applied radiation and concentration diagnostics are limited to low scan rates and

cannot resolve the instationary flame structures, essential for detailed understanding of physical and chemical reaction aspects. But just these short time structures would be a decisive factor in an efficient flame modelling (DiBlasi 1990). Applying fast emission spectrometers (20 to 100 Hz) allows identification of the main reaction zones by simultaneous determination of pyrometric and chemical properties. Additionally, time-resolved concentration and temperature profiles of reactants like H_2O , CO , CO_2 , C_xH_y and NO can be determined simultaneously and non-intrusive.

Previous investigations on pool fires showed, that local and temporal fluctuations of flame shape display no random character, but recurrent self similar structures. Periodically a flame ball is formed at the flame base and ascends driven by buoyancy (Brötz 1978, Zukoski 1984, Weiser 1991). It is assumed that this structure is formed by inflaming the diffusive mixed air and fuel vapour when reaching the lower ignition limit. Expanding flame gases prevent further supply of oxygen. After the flame ball rises upstream surrounding air entrains to the continuously evaporating fuel. This phenomena of ascending flame structures can also be observed in parts of big hazardous fires.

Experimental

A steel pool (diameter 113 mm, height 40 mm) was filled with fuel to 1 mm below surface. The fuel level was considered to be constant during the measurements started 30 seconds past ignition with 50 spectra/s scan rate. The temperature of the fuel ranged between 20 and 25°C and was not affected perceptibly because of the short combustion period. Used fuels were methanol, 2-propanol, nitromethane and isooctane.

The spectrometers consist of two fast rotating interference filter wheels with wavelength regions from 1200 - 2500 nm (InSb-detector) and 2450 - 14000 nm (InSb/HgCdTe-sandwich-detector), developed at ICT. They allow a time resolution down to 10 ms per scan. The calibration was carried out from reference spectra of a black body radiator. The optics was focused on the flame axis in heights of 20, 100, 180 and 300 mm.

Results

Mean spectral radiation of different flame regions

The spectral intensity of emitting flame gases is depending on temperature, concentration of IR-active gas compounds and emitting pathlength. A reduced data analysis, using mean spectra, allows identifying chemical species in different flame regions. Fig. 1(a)-(d) shows emission spectra of investigated pool fires 20 and 180 mm above surface, resulting in 30 consecutive scans and assembling both NIR and IR filter wheel spectra.

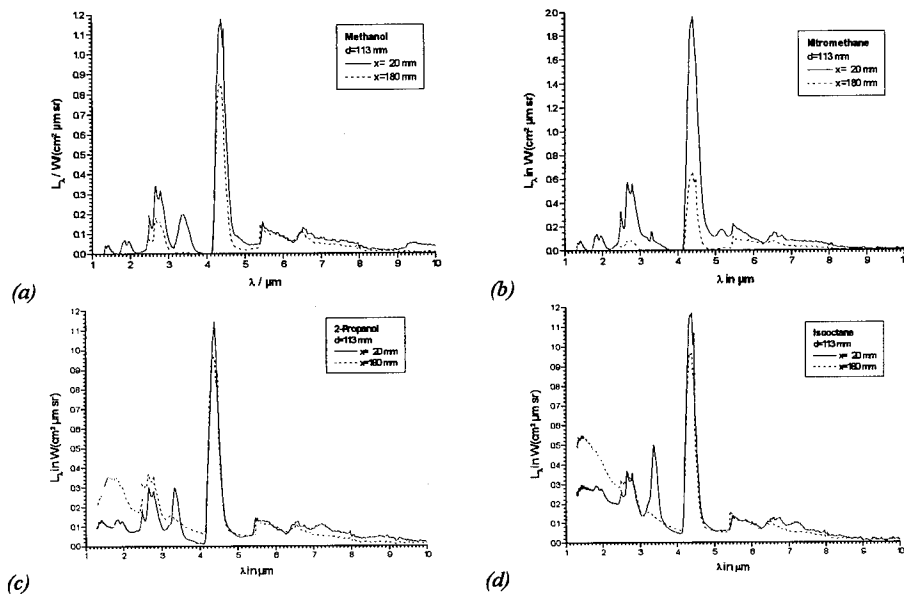


Fig. 1: Time mean spectra of investigated pool fires 20 mm and 180 mm above surface. (a) methanol, (b) nitromethane, (c) 2-propanol, (d) isooctane

In the lower flame region (20 mm spectra) high concentrations of hydrocarbons and partially oxidized species were detected. In upper regions (180 mm spectra, dashed lines) only water and carbondioxide can be determined (compare with results of gasanalytics, Tab. 1 (Hoffmann 1994))

In all spectra the strong bands of CO₂ at 2.7 and 4.3 μm , the optical thin water bands at 1.3, 1.8 and 2.7 μm and the optical thick water band from 5.5 to 8 μm can be observed. Additionally, 20 mm above surface C-H vibrational-stretching bands at 3.3 μm can be found. At 7 μm the water bands are overlapped by emissions of hydrocarbons, indicating large amounts of unburned hydrocarbons in the lower flame region. Furthermore the spectrum of methanol at 20 mm above surface shows weak CO emissions at 4.8 μm and at the same height nitromethane has a weak NO band at 5.2 μm . These NO bands, appearing only in spectra of nitromethane, indicate that the combustion product NO is splitted from nitromethane, but not created by the thermal mechanism proposed by Zeldovich, 1946. This behaviour of nitrocompounds during atmospheric combustion has been described by Gröbel, 1994. The spectra of 2-propanol and isooctane show continuous radiation up to 4 μm , emitted by soot particles. The high soot emission in the upper flame region suggest that soot is formed by cracking of fuel molecules at advanced combustion state.

	height	CH ₄	CO	CO ₂	O ₂	NO _x
methanol	20 mm	5	9	6.5	1	0.1
nitromethane		15	15	6	5	0.9
2-propanol		12	6.5	7.5	0.5	0.5
isooctane		14	5	7	0.5	0.7
methanol	180 mm	0	1	4	15	0
nitromethane		0.5	0.5	4	18	0.4
2-propanol		0.5	0.5	4	15	0.3
isooctane		2	1	4	15	0.1

Tab. 1: Concentrations of most important dry flame gas components of investigated fuels (mol%)

Time-resolved spectra

Qualitative considerations

The time-resolved spectra exhibit periodical structures, repeating at frequency from 6 to 7 Hz (see Weiser 1991). Fig. 2 and 3 show waterfall plots of methanol and 2-propanol flames at two heights (20 and 180 mm above surface). In the lower flame region the intensities of H₂O-, CH- and CO₂-bands follow a sinus curve. Strong fluctuations of the flame in the upper region lead to complete decrease of measured intensity. C-H bands and maximum soot emission

appear simultaneously. This indicates alternating structures dominated, on the one hand, by soot and unburned hydrocarbons and, on the other hand, by completely oxidized combustion products.

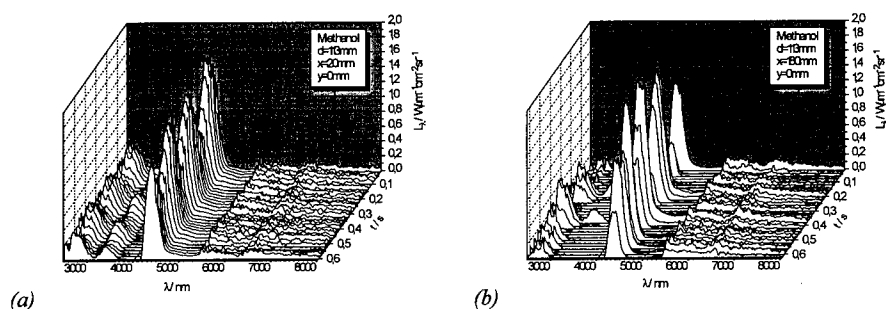


Fig. 2: Waterfall plot of time-resolved flame spectra of methanol. (a) $x = 20$ mm, (b) $x = 180$ mm.

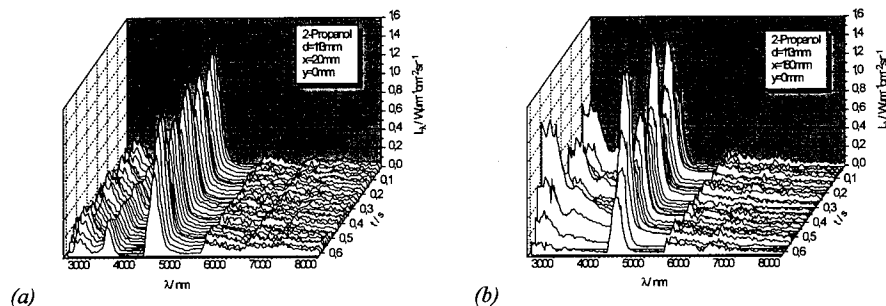


Fig. 3: Waterfall plot of time-resolved flame spectra of 2-propanol. (a) $x = 20$ mm, (b) $x = 180$ mm.

If soot and unburned hydrocarbons are assigned to the proposed flame ball structure, the intensity alternation in the time-resolved spectra can be explained as ascending flame balls. Time-resolved spectra of nitromethane and isooctane show similar profiles.

For a detailed analysis, band regions assigned to the products were integrated and normalised. Fig. 4 and 5 show the profiles of CO_2 (4.1 to 4.7 μm), H_2O (5.5 to 6.3 μm), CH (3.2 to 3.6 μm) and soot continuum (3.7 to 4.1 μm). Soot continuum has been subtracted to correct the CH -profile. Water and carbondioxide profiles show the same behaviour. An obvious phase shift can be observed 20 mm above surface caused by pure or pyrolyzed fuel. In the upper flame region this shift disappears. Therefore in the lower flame combustion end products and high fuel concentrations are alternating. In upper flame regions only the passing flame ball

structure, filled with a high amount of unburned hydrocarbons is detected. The results indicate soot formation caused by thermal degradation of hydrocarbons at the exterior zone of the flame ball.

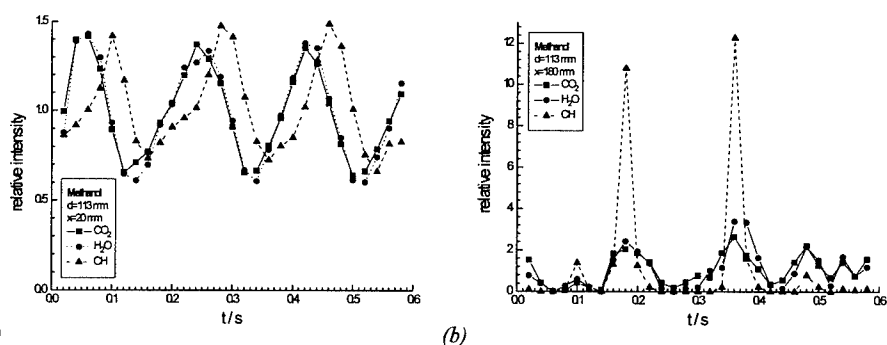


Fig. 4: Normalised time profile of various product specific band regions in the case of methanol. (a) $x = 20$ mm, (b) $x = 180$ mm.

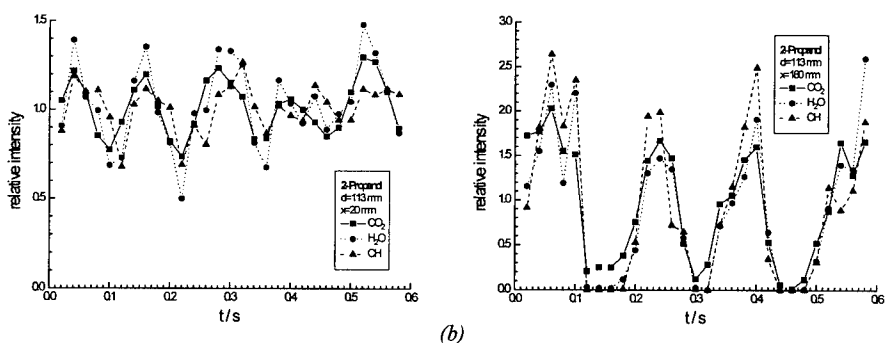


Fig. 5: Normalised time profile of various product specific band regions in the case of 2-propanol. (a) $x = 20$ mm, (b) $x = 180$ mm.

Quantitative considerations

A quantitative data analysis has been applied by using band modelling. The used computer program BAM can calculate NIR/IR-spectra (1 - 10 μm) of inhomogeneous gas mixtures of H_2O (with bands around 1.3, 1.8, 2.7 and 6.2 μm), CO_2 (with bands around 2.7 and 4.3 μm), CO , NO and HCl and can take in consideration emission of soot particles. It is based on the

single line group model (see Ludwig et al. 1973) and makes also use of tabulated data of H_2O and CO_2 in this reference. Because there are so many unknown parameters influencing the emission spectrum of an inhomogeneous gas mixture, only a simplified model can be employed. Therefore we have assumed that there is just one emitting layer of undefined thickness, constant temperature, constant concentration of the various gases and soot particles in thermal equilibrium. These assumptions lead to a reasonable number of parameters, which can be determined by fitting calculated spectra to experimental data.

Because we have used two spectrometers, which were not synchronised, only the spectrum of the NIR- or IR-spectrometer can be fitted at once. A further complication is induced by high absorption of the CO_2 band at $4.3\text{ }\mu\text{m}$ and the H_2O band at $6.3\text{ }\mu\text{m}$. For these bands the assumption of a homogenous layer is a very poor one, because also not-emitting regions have significant effect on measured intensity. As a result, we have analysed only the NIR-spectrum from $1.7 - 2.2\text{ }\mu\text{m}$ dominated by the $1.8\text{ }\mu\text{m}$ band of water, since the $1.3\text{ }\mu\text{m}$ band of water is very weak and has a bad signal/noise ratio. With this restriction, temperature and „concentration length“ (concentration * length) of water and soot particles have been determined by fitting. Representative fitted spectra are given in Fig. 6(a)-(d) and Fig. 7(a)-(d) shows time profiles of fitted parameters. For methanol and nitromethane temperature is almost constant, but is fluctuating for 2-propanol and isooctane. These fluctuations are probably a consequence of the high heat radiation of the soot particles.

The concentration of water shows the expected periodic behaviour. Another interesting result is the high correlation of water and soot concentration fluctuations in the case of 2-propanol and isooctane.

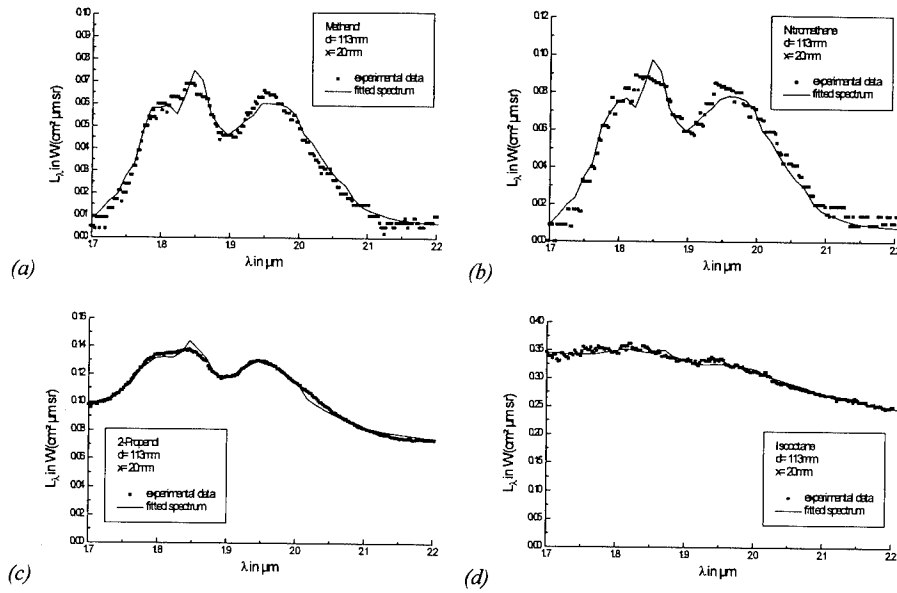


Fig. 6: Typical sampled spectra in the region of the 1.8 μm water band of (a) methanol, (b) nitromethane, (c) 2-propanol and (d) isooctane 20 mm above the surface. The solid curves are fitted theoretical spectra calculated with BAM.

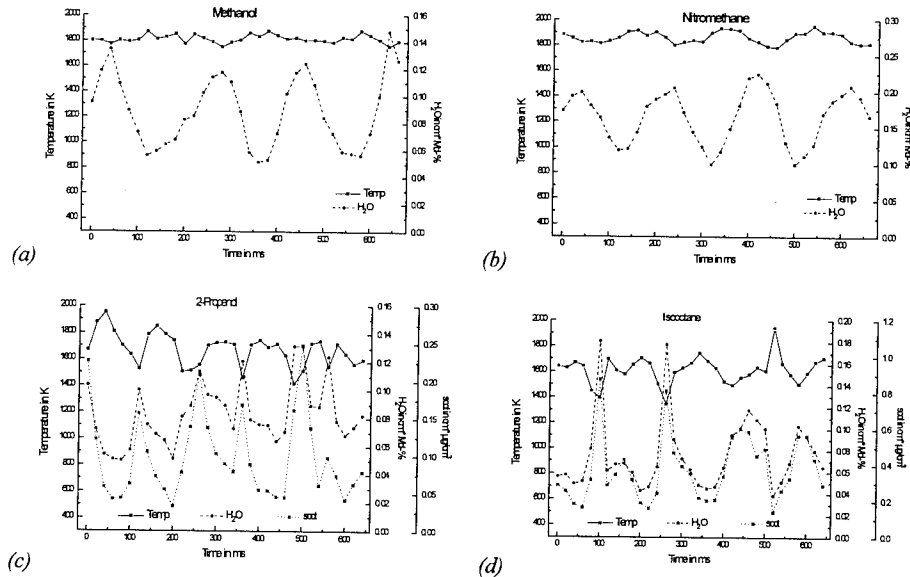


Fig. 7: Temperature and concentration*pathlength of H_2O and soot as result of fitting calculated spectra to experimental data: (a) methanol, (b) nitromethane, (c) 2-propanol and (d) isooctane 20 mm above the surface.

References

- Bagster, D. F.; Pitblado, R. M.;** Thermal hazards in the process industry; Chem. Eng. Prog., 85(7), 69-75 (1989)
- Brötz, W.; Schönbucher, A.;** Wärme- und Stofftransport in Tankflammen; Chem.-Ing.-Tech. 50 (1978) Nr. 8, S. 573-585
- Brötz, W.; Schönbucher, A.; R. Lucas.; Schieß, N.;**Kohärente Kurzzeit-Strukturen und momentane Brechzahl-, Dichte- und Temperaturprofile in einer n-Hexan-Tankflamme; Ber. Bunsen-Ges. Phys. Chem., 87, 951-958 (1983)
- Di Blasi, C.; Crescitelli, S.; Russo, G.;** Model of pulsating flame spread across liquid fuels; 23rd Symp. (Int.) on Comb., The Combustion Inst., 1990/pp. 1669-1675
- V. Gröbel, H.H. Krause, V. Weiser;** Investigation of exhaust gas products in the thermal disposal of waste munition using nitrocellulose and TNT as examples; from: Conversion of Polymer Wastes & Energetics; ed. Krause, H.H.; Penninger J.M.L.; ChemTec Publishing; Toronto, Canada, 1994
- Hoffmann, A.;** Vergleich von Flammenspektren mit zeitgemittelten, IR-absorptiv bestimmten Gaskonzentrationen in Modelltankflammen, diploma thesis at Universität Karlsruhe TH, 1994
- Ludwig, C.B.;** Malkmus, W.; Reardon, J.E.; Thomson, J.A.L.; Handbook of Infrared Radiation from Combustion Gases, NASA SP-30980 (1973)
- Weiser, V.;** Eisenreich, N.; Krause, H.; Experimentelle Untersuchungen von Flammgeometrie, Temperaturverteilung und Konzentrationsfeldern in Modell-Tankflammen verdampfender, flüssiger Brennstoffe; Int. Annu. Conf. ICT, 22nd(Combust. React. Kinet.), 101/1-101/14 (1991)
- Zeldovich, Y. B.;** Acta Physicochem. USSR 1946, 21, 577
- Zukoski, E. E.;** Cetegen, B. M.; Kubota, T.; Visible structure of buoyant diffusion flames, 20th Symp. (Int.) on Comb., The Combustion Inst., 1994/pp. 361-366

**THERMAL ANALYSIS STUDIES ON THE ZIRCONIUM-POTASSIUM PERCHLORATE-
NITROCELLULOSE PYROTECHNIC SYSTEM**

B.Berger¹, E.L.Charsley², J.J.Rooney² and S.B.Warrington²

1. Gruppe für Rüstungsdienste, Feuerwerkerstrasse 39, CH-Thun 2, Switzerland.
2. Thermal Analysis Consultancy Service, Leeds Metropolitan University, Calverley Street, Leeds, LS1 3HE, U.K.

ABSTRACT

The influence of nitrocellulose on the reaction between zirconium and potassium perchlorate has been investigated quantitatively by differential scanning calorimetry, chemical analysis using ion specific electrodes and simultaneous thermogravimetry-differential thermal analysis-mass spectrometry using a unit calibrated for carbon dioxide measurement. The increase in the extent of reaction produced by the addition of nitrocellulose to the binary composition containing 10% zirconium, has been shown to be significantly larger than that predicted from measurements on potassium perchlorate-nitrocellulose mixtures.

DSC measurements on the exothermicity of reaction of zirconium-potassium perchlorate-1% nitrocellulose compositions, containing from 10-90% zirconium, have shown good agreement with results obtained using adiabatic combustion calorimetry. The solid state reaction between zirconium and potassium perchlorate, measured by DSC under non-ignition conditions, therefore represents the major component of the pyrotechnic combustion reaction.

INTRODUCTION

Previous studies on the zirconium-potassium perchlorate-nitrocellulose (NC) pyrotechnic system, using simultaneous thermogravimetry-differential thermal analysis-mass spectrometry (TG-DTA-MS) showed that zirconium and potassium perchlorate gave an exothermic solid state reaction, in the region of 400°C, which overlapped with the decomposition of unreacted potassium perchlorate (1). Quantitative measurements were made on this solid state reaction by differential scanning calorimetry (DSC) and by chemical analysis using ion-specific electrodes (ISE) to measure the potassium perchlorate and chloride contents of the reaction products (2).

The experiments were carried out on the 40% Zr-59% KClO₄-1% NC composition and enabled the amount of potassium perchlorate reacted to be established quantitatively as a function of temperature. By comparison of the DSC peak area measurements on the potassium perchlorate transition before and after reaction with the results from the perchlorate electrode, the DSC technique was found to provide an excellent ancillary method for the determination of the extent of the perchlorate reaction. A comparison of the amount of potassium chloride formed in the reaction with the amount of perchlorate reacted showed that the solid state reaction could be represented by the equation :- $2\text{Zr} + \text{KClO}_4 \rightarrow 2\text{ZrO}_2 + \text{KCl}$.

The simultaneous TG-DTA-MS experiments, carried out on compositions containing 10% zirconium, showed that the addition of low levels of nitrocellulose appeared to increase the exothermicity of this solid state reaction (1). It was also observed that potassium perchlorate reacted exothermically with the carbonaceous residue, formed by the decomposition of nitrocellulose at about 200°C. This reaction took place in the region of the zirconium -potassium perchlorate reaction and resulted in the production of carbon dioxide.

In the present work, the DSC and ISE techniques have been applied to quantify the influence of nitrocellulose on the reaction. This has been carried out by comparing the increase in the extent of reaction on addition of nitrocellulose to the binary composition containing 10% zirconium, with the magnitude of the reaction between potassium perchlorate and nitrocellulose. The results have been supplemented by quantitative MS measurements on the amounts of CO₂ evolved.

In addition, DSC has been used to investigate the influence of zirconium content on the exothermicity of reaction under non-ignition conditions for ternary $\text{Zr-KClO}_4\text{-NC}$ compositions containing from 10-90% zirconium and 1% nitrocellulose.

EXPERIMENTAL

The zirconium (Degussa grade CX) had a mean particle size of $1.7\mu\text{m}$, and a purity of 96.5% (as total Zr + Hf). The potassium perchlorate had a particle size of $<60\mu\text{m}$, and a purity of $>99\%$. The nitrocellulose was type 220.E, with a nitrogen content of 12.1%. The compositions were prepared in a Turbula mixer before granulation with the nitrocellulose to give a grain size of about 0.5mm.

DSC experiments were carried out, using a Du Pont 9900 unit, in purified argon with zirconium powder as an internal oxygen getter. Samples were heated at 5°C min^{-1} in alumina crucibles fitted with platinum lids. Calibration for temperature and enthalpy was carried out using the fusion of high purity samples of indium, tin, lead, zinc and aluminium. Analysis of reaction products, prepared by heating a composition to different temperatures in the DSC apparatus, for perchlorate and chloride content was performed using ion-specific electrodes (ISE) (Orion Models 33-81 & 94-17B). Full details of the experimental procedures have been given previously (2).

Simultaneous TG-DTA-MS measurements were carried out using a Stanton Redcroft STA 1500 linked via a jet separator interface to a VG Micromass quadrupole mass spectrometer (3). The experiments were performed using 10mg samples, heated at 5°C min^{-1} in alumina crucibles with alumina lids. Since the aim of the present experiments was to obtain a quantitative measurement of the amount of CO_2 formed, modifications were made to the experimental procedure given previously. The present experiments were carried out in an atmosphere of helium containing 232ppm argon. By continuous monitoring of the argon signal, it was possible to correct for any changes in the mass spectrometer sensitivity during the experiments. A stable gas flow was achieved by using a digital flowmeter and controller (Brooks Models 5850TR & 5878).

The mass spectrometer was calibrated for CO_2 by measuring the amount of CO_2 evolved from cadmium carbonate which decomposes in the temperature range $250\text{-}350^\circ\text{C}$. Different weights of a 2% cadmium carbonate-98% alumina mixture

were chosen to cover the range 10-450 μ g CO₂ and a linear correlation was observed between the MS peak area and the amount of CO₂ evolved. The accuracy of the method was estimated to be $\pm 6\%$.

RESULTS AND DISCUSSION

Studies on the Reaction between Potassium Perchlorate and Nitrocellulose

A series of DSC experiments was carried out to investigate the reaction between potassium perchlorate and nitrocellulose using mixtures containing 1%, 3.2% and 9.1% by weight of nitrocellulose. Measurements were made initially on 5mg samples and in view of the small peaks obtained with the lower nitrocellulose mixtures a second set of experiments was carried out using 15mg samples to obtain better defined curves.

Typical curves obtained using 15mg samples are shown in Fig.1. All three mixtures showed a broad exothermic reaction starting at about 325°C with a peak temperature in the region of 400°C. The temperature at which the reaction was completed could be seen to increase with increasing nitrocellulose content. Measurement of the peak areas gave a linear increase with increasing nitrocellulose content and this is illustrated in Fig.2, which also shows the good agreement between the results obtained at the two weight levels.

Chemical analysis of the residues from 15mg samples of the 9.1% nitrocellulose mixture heated to completion of the reaction in the region of 470°C showed reasonable agreement between the amount of perchlorate reacted and the amount of chloride formed, indicating direct conversion of the perchlorate to the chloride. The measurements showed that about 5.1% of the potassium perchlorate had reacted. Assuming that the reaction takes place according to the equation :- $\text{KClO}_4 + 2\text{C} \rightarrow \text{KCl} + 2\text{CO}_2$, then 0.9% of carbon would be required for the amount of perchlorate reacted. This represents 10% by weight of the nitrocellulose present in the 9.1% nitrocellulose mixture, which is similar to the amount of carbonaceous residue formed by heating nitrocellulose to 500°C (1).

The results of the mass spectrometry measurements on the three

perchlorate-nitrocellulose mixtures are shown in Fig.3, together with a curve for a mixture containing 1 % nitrocellulose with 99% powdered fused alumina. It can be seen from the latter curve that the CO_2 loss from the nitrocellulose decomposition, at about 200°C , extended into the region where the carbonaceous nitrocellulose residue was oxidised by the perchlorate, resulting in two overlapping peaks. The onset of the perchlorate-nitrocellulose residue reaction could be seen to start in the region of 350°C , with a peak maximum at about 400°C .

The total amount of CO_2 evolved is plotted as a function of nitrocellulose content in Fig.4 and can be seen to increase in a linear manner. The values obtained for the second peak, after correction for the contribution from the nitrocellulose decomposition, are also plotted in Fig.4 and, in agreement with the DSC experiments, these also showed a linear increase with nitrocellulose content. From the slope of the line, a value of 3.7mg of CO_2 per g of mixture for 1% nitrocellulose was given. This represents the reaction of 0.9% carbon for the mixture containing 9.1 % nitrocellulose, which is in good agreement with the values estimated from the chemical analysis measurements and thus confirms the proposed reaction mechanism.

Influence of Nitrocellulose on the Zirconium-Potassium Perchlorate Reaction

DSC studies were carried out to establish quantitatively the influence of nitrocellulose on the reaction between zirconium and potassium perchlorate. The compositions chosen for the study were:- 10% Zr-90% KClO_4 , 10% Zr-89% KClO_4 -1% nitrocellulose and 10% Zr-85% KClO_4 -5% nitrocellulose.

Typical DSC curves for the three compositions, using 5mg samples, are shown in Fig.5, together with a curve for the 96.8% KClO_4 -3.2% nitrocellulose mixture. There was some variation in the peak shapes from different experiments on the same zirconium compositions. Some experiments on the binary composition showed evidence of a shoulder on the leading edge of the curve, while for the composition with 1 % nitrocellulose, a shoulder was sometimes seen on the trailing edge of the peak. The mixtures containing 5% nitrocellulose showed good reproducibility.

It can be seen that the presence of nitrocellulose has influenced the

temperature at which the reaction commenced. In the case of the binary zirconium composition, the reaction appeared to start in the region of the perchlorate phase transition, whereas the addition of 1 % nitrocellulose had introduced a small plateau between the phase transition and the onset of reaction. The 5% nitrocellulose composition was closer in behaviour to the binary composition.

The curves clearly show that the introduction of nitrocellulose into the binary zirconium composition has resulted in a substantial increase in the reaction exothermicity. This increase was observed mainly in the initial part of the reaction which is in the region where the exothermic reaction in the perchlorate-nitrocellulose mixtures took place, as can be seen from curve D.

The peak areas for the binary zirconium compositions, which have been measured between the completion of the perchlorate phase transition above 300°C and the onset of KClO_4 -KCl eutectic fusion at about 500°C, are listed in Table 1.

Table 1

DSC Peak Area Measurements for 10% Zirconium Compositions

MEASUREMENT	% NITROCELLULOSE		
	0	1	5
DSC Peak Area /J g ⁻¹	730 ± 19	854 ± 12	987 ± 18

Considering the uncertainty in the establishment of the baseline introduced by the aforementioned transitions, the area measurements showed reasonable reproducibility. However, the measured increase of 17% in the peak area for the addition of 1 % nitrocellulose to the binary mixture was considerably higher than expected from the measurements on the perchlorate-nitrocellulose mixtures. From the plot of DSC peak area v nitrocellulose content for these mixtures, a heat output of 38J g⁻¹ per percent nitrocellulose was obtained. Thus the increase in peak area would only have been expected to be of the order of 5% in the ternary composition.

The influence of nitrocellulose at the 5% level can be seen to be less marked than at the 1% level giving an overall increase of 35% in the peak area. This however is still significantly higher than the predicted increase of about 25% from the perchlorate-nitrocellulose measurements.

The possibility that part of the increase in exothermicity could be due to the reaction of the gaseous decomposition products of the nitrocellulose with the zirconium was investigated by DSC. 15mg samples of a 90.9% zirconium-9.1% nitrocellulose mixture were heated under the standard conditions and revealed a shallow exothermic reaction, with a peak temperature of 270°C, which overlapped with the main exothermic decomposition peak of the nitrocellulose at 205°C. This higher temperature reaction was absent in experiments carried out under the same conditions on a mixture prepared using 9.1% nitrocellulose with powdered fused alumina in place of the zirconium. However the contribution of this reaction to the main exothermic reaction in the ternary systems starting above 350°C would not be significant.

A set of experiments was carried out to determine the influence of nitrocellulose on the solid-solid reaction between zirconium and potassium perchlorate by chemical analysis. 15mg samples were heated to 440°C to avoid complications due to the decomposition of the perchlorate, which was found to be accelerated in the presence of the reaction products ZrO_2 and KCl (1). Duplicate ISE measurements for perchlorate and chloride content and a single DSC measurement for perchlorate content were carried out on each composition. The results are given in Table 2 and show reasonable agreement between the techniques, although the chloride figures for the composition containing 5% nitrocellulose are lower than the perchlorate figures.

Chemical analysis measurements on the 90.9% KClO_4 -9.1% nitrocellulose mixture showed that about 5% of the potassium perchlorate had reacted with nitrocellulose. This would result in the reaction of about 0.6% perchlorate when nitrocellulose is incorporated at the 1% level in a 10% zirconium ternary composition. The results shown in Table 2 show an increase in the extent of reaction over 3 times greater than expected. This is in agreement with the DSC measurements and suggests that the presence of nitrocellulose enhances the reaction between zirconium and potassium perchlorate. The analysis results also

Table 2

Chemical Analysis Results for 10% Zirconium Compositions heated to 440°C

MEASUREMENT	% NITROCELLULOSE		
	0	1	5
KClO ₄ Reduction /% (ISE)	4.6 ± 0.2	7.3 ± 0.8	11.4 ± 0.8
KClO ₄ Reduction /% (DSC)	5.8	7.8	11.3
KCl Formed /%	5.2 ± 0.1	7.2 ± 0.2	9.8 ± 0.1

confirm that the influence of nitrocellulose has a lesser effect at the 5% level where an increase of about 1.2 times the predicted value was given.

The mass spectrometry traces for CO₂ showed reasonable reproducibility in peak shapes, although there was some variation in the magnitude of the peaks. Representative curves for the binary and ternary zirconium compositions are shown in Fig.6, together with that for the 99% KClO₄-1% nitrocellulose mixture. Although the evolution of CO₂ in the second reaction stage started at a lower temperature in the presence of zirconium, the effect was less marked than observed previously at higher heating rates (1). The overall level of CO₂ evolution was similar for both the ternary composition containing 1% nitrocellulose and the 99% KClO₄-1% nitrocellulose mixture which gave values of 8.0 ± 1.5 and 7.8 ± 0.3 mg CO₂ per g of mixture, respectively.

In the case of the ternary mixture containing 5% nitrocellulose there appeared to be a small reduction in the amount of CO₂ evolved. Thus a value of 31.8 ± 3.3 mg CO₂ per g of mixture was obtained, compared with a value of 39.8 ± 3.2 calculated from the experiments on the perchlorate-nitrocellulose mixture, although further experiments would be required to confirm this.

Influence of Zirconium Content on the Exothermicity of Reaction

The variation in the exothermicity of reaction of the zirconium-potassium perchlorate-nitrocellulose system with zirconium content was investigated by

measurement of the DSC peak areas for compositions containing 10-90% zirconium. Duplicate experiments were carried out by heating 5mg samples under the standard conditions to 520°C.

The curves for the 20%, 50% and 70% zirconium compositions are shown in Fig.7. It can be seen that as the zirconium content was increased the shoulder visible on the leading edge of the DSC peak became increasingly prominent. A similar shoulder was observed on the DTA peak obtained in the aerial oxidation of zirconium (1). The exothermic peak at about 500°C, in the region of the KClO_4 -KCl eutectic fusion, became less marked as the zirconium content was increased, and above the 50% zirconium level merged into the trailing edge of the main peak.

The results of the area measurements are plotted in Fig.8 together with those obtained by adiabatic combustion calorimetry (4). The good agreement between the measurements suggests that the reaction being studied by DSC under non-ignition conditions represents the major component of the combustion reaction.

Both techniques show an exothermicity maximum in the region of 60% zirconium which is in good agreement with the stoichiometric value of 56.8% zirconium calculated from the equation:- $2 \text{Zr} + \text{KClO}_4 \rightarrow 2 \text{ZrO}_2 + \text{KCl}$ and therefore lend support to the previously postulated reaction mechanism.

CONCLUSIONS

It has been shown that the carbonaceous residue produced by the decomposition of nitrocellulose, at about 200°C, reacts with potassium perchlorate in the region of 400°C and that there is a linear relationship between the exothermicity of reaction and the nitrocellulose content over the range studied (1-9.1%). The extent of the perchlorate reaction as measured by chemical analysis and the amount of carbon dioxide produced, as determined by mass spectrometry, are consistent with the reaction:- $\text{KClO}_4 + 2 \text{C} \rightarrow \text{KCl} + 2 \text{CO}_2$, where the amount of carbon oxidised represents about 10% of the nitrocellulose present.

DSC studies have confirmed that when nitrocellulose is incorporated at the 1% level into binary compositions containing 10% zirconium, an increase in exothermicity is produced that is approximately three times greater than that expected from measurements on the potassium perchlorate-nitrocellulose mixtures. The exothermicity contribution from the reaction of the gaseous decomposition products of nitrocellulose with zirconium was found to be negligible.

Studies by chemical analysis, on samples heated to 440°C, similarly showed an increase some three times greater than expected for the amount of potassium perchlorate reacted, thereby indicating that the presence of nitrocellulose had resulted in an increase in the extent of the reaction between zirconium and potassium perchlorate.

The variation in the exothermicity of reaction with zirconium content has been measured by DSC for compositions containing 10-90% zirconium. The agreement between the DSC and adiabatic combustion calorimetry studies suggested that the reaction in the region 325°C to 520°C, observed by DSC under non-ignition conditions, represented the major component of the pyrotechnic combustion reaction. The zirconium content corresponding to the maximum exothermicity given by the DSC was in good agreement with the value of 56.8% Zr calculated from the previously postulated reaction equation:- $2 \text{Zr} + \text{KClO}_4 \rightarrow 2 \text{ZrO}_2 + \text{KCl}$.

ACKNOWLEDGEMENT

We would like to thank Mr A.J.Brammer of the Thermal Analysis Consultancy Service, Leeds Metropolitan University for his skilled technical assistance.

REFERENCES

1. B.Berger, E.L.Charsley, S.B.Warrington, Propellants, Explos., Pyrotech., in press.
2. B.Berger, E.L.Charsley, J.J.Rooney, S.B.Warrington, Thermochim. Acta, in press.
3. E.L. Charsley, S.B. Warrington, T.T. Griffiths and J. Queay, Proc. 14th International Pyrotechnic Seminar, RARDE, 1989, 763.
4. B. Berger and B.Haas, Proc. 3e Congres International de Pyrotechnie Spatiale et 12th International Pyrotechnic Seminar, Association Francaise de Pyrotechnie, 1987, 265.

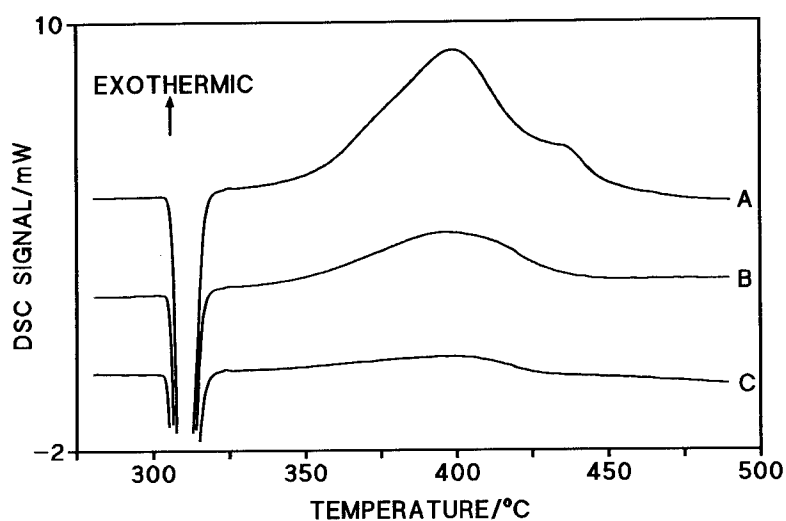


FIG 1 DSC CURVES FOR KClO_4 -NITROCELLULOSE MIXTURES CONTAINING (A) 9.1% NC, (B) 3.2% NC (C) 1% NC (Sample weight, 15mg; heating rate, 5°C min^{-1} ; atmosphere, argon)

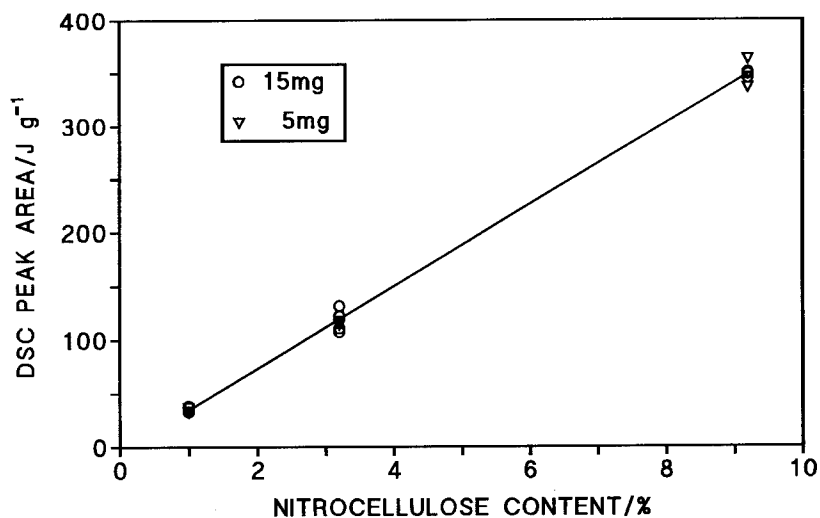


FIG 2 PLOT OF DSC PEAK AREA v NITROCELLULOSE CONTENT FOR A SERIES OF KClO_4 -NC MIXTURES

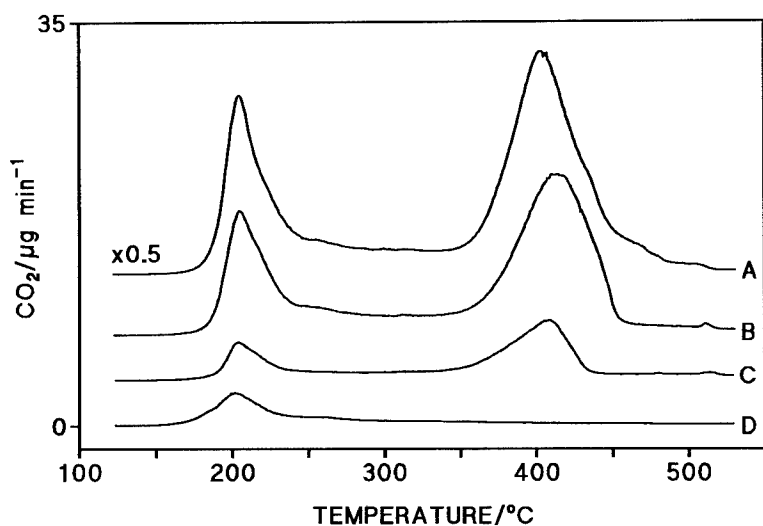


FIG 3 CO_2 CURVES FOR KClO_4 -NITROCELLULOSE MIXTURES WITH (A) 9.1% NC, (B) 3.2% NC, (C) 1% NC AND (D) A 1% NC -99% Al_2O_3 MIXTURE (sample weight, 10mg; heating rate, 5°C min^{-1} ; atmosphere, helium)

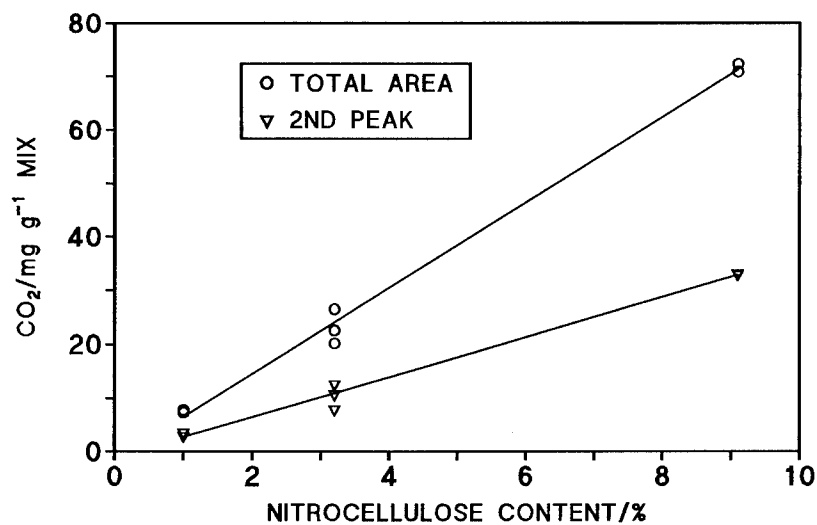


FIG 4 PLOT OF CO_2 EVOLVED v NITROCELLULOSE CONTENT FOR A SERIES OF KClO_4 -NC MIXTURES

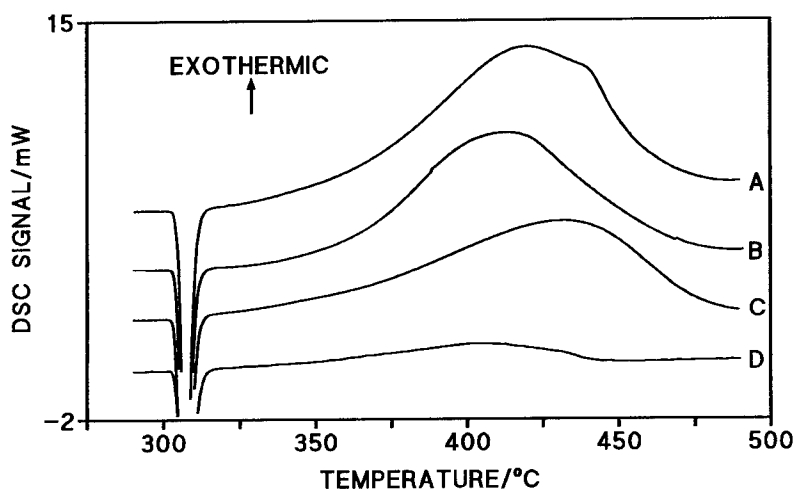


FIG 5 DSC CURVES FOR (A) 10% Zr-85% KClO_4 -5% NC
(B) 10% Zr-89% KClO_4 -1% NC, (C) 10% Zr-90% KClO_4 ,
(D) 96.8% KClO_4 -3.2% NC (Sample weight, 5mg;
heating rate 5°C min^{-1} ; atmosphere, argon)

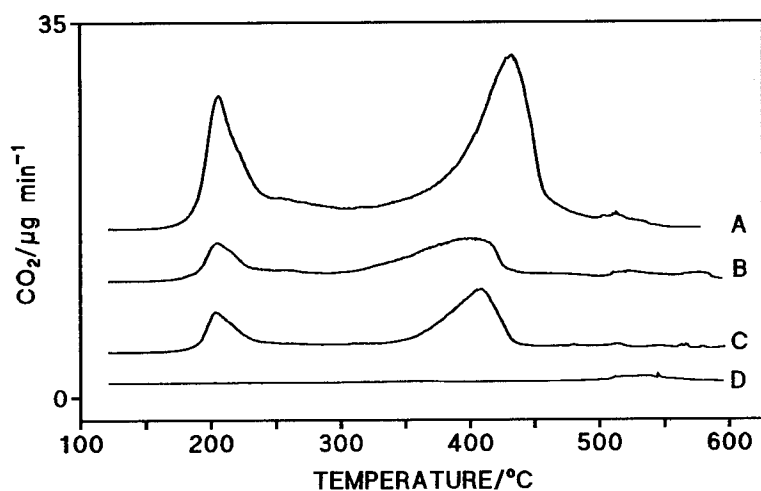


FIG 6 CO_2 CURVES FOR (A) 10% Zr-85% KClO_4 -5% NC
(B) 10% Zr-89% KClO_4 -1% NC, (C) 99% KClO_4 -1% NC
(D) 10% Zr-90% KClO_4 (Sample weight, 10mg; heating
rate, 5°C min^{-1} ; atmosphere, helium)

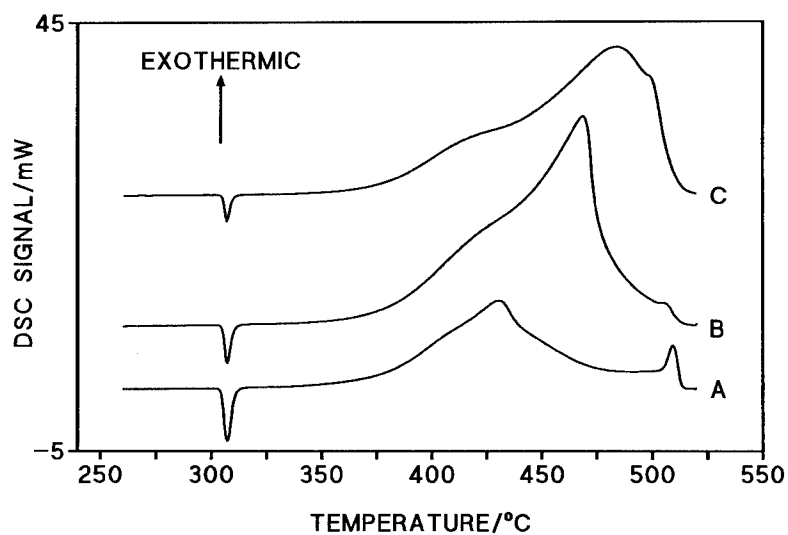


FIG 7 DSC CURVES FOR (A) 20% Zr-79% KClO_4 -1% NC, (B) 50% Zr-49% KClO_4 -1% NC, (C) 70% Zr-29% KClO_4 -1% NC MIXTURES (Sample weight, 5mg; heating rate, 5°C min^{-1} ; atmosphere, argon)

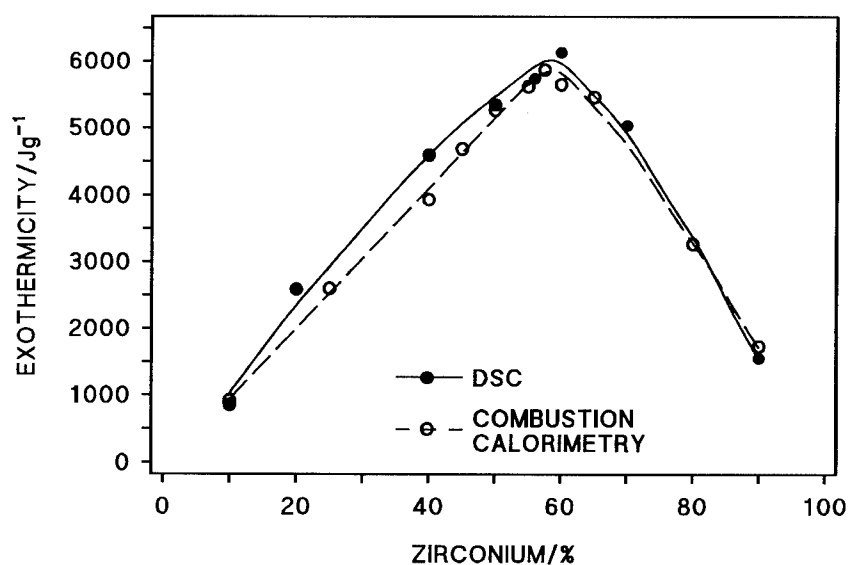


FIG 8 EXOTHERMICITY MEASUREMENTS FOR THE ZIRCONIUM-POTASSIUM PERCHLORATE-NITROCELLULOSE SYSTEM

A PYROTECHNIC MULTI LAUNCH ROCKET SYSTEM SIMULATOR

Michael Cartwright and members of 32 A.T.O.C.

Chemical Systems Group,
School of Mechanical Materials and Civil Engineering
Cranfield University, Royal Military College of Science,
Shrivenham, Swindon, U.K. SN6 8LA

Abstract

The paper describes the design, prototype production and trial of a cheap Multi Launch Rocket System simulator pyrotechnic device suitable for use in a training role. The system was required to cover a 30 m radius area with a sub-munition density of 1 per 20 m². From safety considerations the constraints applied were :-

- No high explosive materials

- Electrical initiation for remote firing

- Air burst

- Sub-munitions and main munition should represent no

- Hazard to unprotected troops in the open

- Sub munitions to function on the ground and not in the air

The final design consisted of a tube launched munition with 150 sub munitions, dispersed at the apogee of the flight by a burster charge, which also ignited delays on the sub munitions, such that they would reach the ground seconds before functioning. The components used were manufactured from readily available materials, which required the minimum of modification. The standard cardboard firework launch tube was easily deployed in the training area, prior to an exercise, either by burying to > half its length, or free standing, surrounded by sandbags and was capable of repeat use. 10 successful launches have been achieved from the same tube. Simple electric match initiation of the launch propellant started the necessary complete delay sequence. Further work on the use of biodegradable components, which represent a minimal environmental impact, and reduction of the fragments from the main munition body are in progress.

Introduction

During the academic phase of the training programme for Ammunition Technical Officers, the students undertake a munition design project. The purpose of the project is to provide the students with practical applications for the classroom theory before they handle live munitions. By involving the students in projects, safety procedures are developed before mistakes can prove costly.

The second purpose of this project was to demonstrate a safe and cheap training device to simulate the effects of an incoming MLRS weapon for use during training exercises. The munition specification was :-

- a) Tube Launched
- b) Air Bursting
- c) Cover a 30 metre radius with a density of one sub-munition per 20 m²
- d) Sub-munitions should function on the ground
- e) Should represent no hazard to unprotected troops in the open
- f) Contains No High Explosive Compounds
- g) Primary initiation must be electrical

On the basis of the original specification 150 sub-munition would need to be dispersed from the main munition over the target area. The project divided into three areas

Sub Munitions - Dimensions and contents

Main Munition - Arrangement of sub-munitions
 Delay Element
 Bursting charge

Propulsion System - How to lift the payload to the desired height.

Each of these topics was further subdivided for experimental purposes but with the understanding that they were often inter-dependant. The mass of the sub-munitions would dictate the lifting capacity required. Also the safety distances for the device should it malfunction in the most harmful manner

would influence the height for the air burst and hence the propulsion system and delay mechanism. All of the components would be simple to manufacture in view of the limited experience of the operators.

Sub-Munition

The standard issue MK 8 Thunderflash contains 12 g of a Potassium perchlorate/Magnesium/Carbon 57/37/6 flashpowder. After preliminary trials this composition was discarded on the grounds of limited noise production, poor storage properties and sheer size of the completed munition with over 1.8 Kg of flashpowder without any packaging and operating components. After further trials of a range of materials and mixtures on a 70/30 mixture of potassium chlorate and aluminium was selected as the active filling. 1g samples of this mixture, when suitably enclosed, provided the same noise effect as the standard thunderflash for an order of magnitude less material. Submunitions would have to be ignited by the bursting charge but should only function after they had reached the ground. In order to guarantee this aspect a delay element, with a burn time of 2 seconds longer than the time taken for the submunition to fall to the ground from the burst position, would be required. The delay would have to be ignited by the burster charge. This would involve additional material in the sub-munition and determine the dimensions of the sub-munitions.

In order to provide the correct confinement for the flash powder to function correctly the delay element must seal one end of the sub-munition. After limited trials a simple polymer bonded pyrotechnic composition based on potassium perchlorate oxidiser and hydrocarbon fuel was chosen. Inclusion of strontium oxalate helped to control the burn rate and also produced a red light output from the burning delay making the falling submunitions clearly visible at nighttime, thus reducing a potential hazard. After mixing the composition to a paste, it was hand pressed, against a mandrill, into one end of a 2 mm wall thickness, 12 mm i.d., 25 mm long, wrapped cardboard tube,

to a depth of 12 mm which was sufficient to give an 10 seconds delay when ignited. Note in figure 1a the indent at the flash powder end of the delay element which ensures adequate confinement of the flash powder during initiation. The polymer resin was partially cured and then an additional cap of first fire mixture added figure 1 a. Again a polymer fuel with potassium perchlorate oxidiser was used but with the strontium oxalate replaced by potassium benzoate and 5% aluminium added. Full curing of the polymer occurred during warming overnight in an oven at 60 °C. It was important that the delay element bonded to the cardboard wall so that the flame could not penetrate prematurely into the flash powder. When dry 1 g of the flash powder, prepared from carefully dried and sieved ingredients, was added to the cavity and the open tube end sealed with a plastic cup, see figure 1(b) Devices made with wet ingredients gave reduced performance. These sub-munitions were manufactured in groups of twenty and stored in the magazine, until sufficient number had been made, when they were loaded into the main munition, at the remote handling facility.

Main Munition

The main munition was a 160 mm length of 140 mm o.d., 5mm wall thickness, plastic piping, fitted with two machined plastic end plates as shown in the figure 2. The design carried in the central hole the delay device, which would be ignited by the propelling charge and then itself ignite the bursting charge. The design allowed the lid to be shed and the sub-munitions dispersed without shattering the body. The base was held in position using an epoxy resin glue as was the central delay, a standard black powder 4 second delay element used in firework displays. The bursting charge of 20 g blackpowder was spread over the base of the assembled container and covered with a cardboard disc.

The submunitions were arranged in layers in three concentric circles on Cambric cloth circles and taped, with their igniter end in contact with the Cambric see figure 3. The four layers were then placed in the munition body in the

configuration shown in figures 4 and 5. The central hole in each layer was filled with a Cambric tube containing black powder, which sat in contact with the main delay element. After loading all the submunitions the empty space within the body was filled with black powder and the lid was press fitted into place. A gas tight seal was formed by wrapping a light adhesive tape round the joint. The complete munition had an all-up weight of 2 Kg which was considerably less than a similar munition using black powder and thunder flash fillings throughout (Minimum 5.3 Kg). Trials with thinner walled main bodies were unsuccessful due to failures in the launch tube causing ignited submunitions to be ejected from the launch tube.

Launch System

The main munition would be launched from a vertically mounted, firework industry standard, 6" diameter 3' long cardboard tube either ground buried to a depth of two feet, see figure 6 or free standing surrounded by sandbags along its length. This ensured that, in the event of a complete deflagration on initial launch, the device would be completely safe. Propelling charge was black powder contained in a plastic cup press fitted to the base of the main munition with either, an Igniting Safety Fuse Electric or, an electric match embedded in the powder, see figure 7. ISFE ignition gave most reliable initiation. Trials were conducted, using inert fillings, for a range of lifting charges in the 20 to 50 g range, since the windage, occurring around of the munition, was greater than the modelling programme could accommodate. Flight times were measured, see figure 8, and the heights reached calculated using Newton's laws of motion. Half the flight time gave time to maximum height and for 40 g lifting charge this was 4 secs giving a muzzle velocity of $\sim 47 \text{ m s}^{-1}$. Using a 2.5 second delay the munition would reach a height of 86 m before initiating the bursting sequence. This was a minimum safety height for a complete deflagration on initiation. Assuming submunitions continue to fly in a vertical direction then a minimum of

81 - 6

an 8 second delay would be required to ensure the submunitions reached the ground before functioning and hence the 10 second delay chosen for the submunitions.

Field Trials

Each sub component in the system was chosen after extensive trials as a separate unit. The final complete assembly was then trialled and any modifications required made before a final trial scheme was undertaken. In these latter trials safety, as well as performance, were assessed. Two trials involved deliberately omitting the lifting charge thereby initiating complete munitions in the launch tube. Although the cardboard tube was severely damaged no fragments escaped from the sandbagged enclosure or were ejected other than vertically into the air from the partially buried tube giving a minimum user safety distance of 50 metres.

Ten working trials of the complete munition were undertaken with the following results:-

None initiated in the launch tube.

Two tumbled in flight scattering unlit submunitions

Two resulted in total initiation by the bursting charge at heights of ~ 90 m due to the lid failing to eject.

Two dispersed the submunitions over a 10 m radius due to the lid being ejected too easily

Final four were successful with < 5% of submunition failures

Area covered 25 x 40 m approximately

Noise Measurements

Part of the project was to produce a munition with the same noise foot-print as a standard thunderflash. Noise levels are very difficult to measurement since the output is of a very short duration. However an environmental noise meter was erected 50 m from functioning sub munitions and the peak output was found to be 130 dB which is comparable with that from the standard Mk 8 thunderflash. This can only

be a guide to environmental health effects. Further work would be required if a completed munition were to be made.

Further Work

Although the system has been tested for short term stability and compatibility. If a completed munition is to be made then long term stability and compatibility studies will be required. Also the complete munition may require some form of water proofing to give it an adequate shelf life. Since it is only designed as a training round then long term stability is not required. Further work would develop a system, which would not require the careful site preparation used here even though firing preparation time was only 30 minutes for the assembled device. A vehicle mounted system would increase it's flexibility

CONCLUSIONS

Final Project Design

Sub-Munition

Will contain 1 g of a 70/30 KClO_4/Al (Pyro Grade) Flash powder in a cardboard tube 28 mm by 12 mm i.d. sealed with a plastic cap initiated by a 10 seconds pyrotechnic delay element

Main Munition

Will be a 6" calibre with 4 layers of 40 submunitions

Will use a 3.5 or 4 s pressed gunpowder primary delay element

Ejection will be by a base plate energised with ~ 30 g gunpowder

Launch System

Use commercially available cardboard or Plastic launch tube

40 g gunpowder propelling charge held in a plastic cone at
the base of the munition
ISFE (or Electric Match) initiation

BIBLIOGRAPHY

- J. A. Conklin, "The Chemistry of Pyrotechnics - Basic Principles and Theory ", Marcel Dekker Inc N.Y., 1994
- R.M. Estcourt, "A report on the Thunderflash Trial", Report ITDU, Warminster
- J. Kemp, "The Effects of Environment on Pyrotechnic Stores", ATO report RMCS 1975
- Rev. R. Lancaster, " Fireworks - Principles and Practice ", Chemical Publishing Company Inc. N.Y. 1993
- M.A. Wilson, "Development of Pyrotechnic Photoflash Composition MRL(X)210", DSTO Report MRL 1989
- R.F. Powell, "Noise in the Military Environment", Brassey's Defence Publishers, 1988

Acknowledgements

The Syndicate Members who performed the work were :-

Capt. A.R. Hornsby R.L.C.

Capt. J.P. Plante R.L.C.

Capt J.C. Yarymowich

Lt. D.J. Beckett R.L.C.

Lt C.J. Henson R.L.C.

Lt A.J. Taylor R.L.C.

2nd Lt. E.J. Sinclair R.L.C.

WO1 G. Richardson Military Advisor & range supervisor

The assistance of the following is gratefully acknowledged

Dr. C Hodges	Chemical Systems Group
Rev. R. Lancaster	Kimbolton Fireworks
M. Armstrong	Theatrical Pyrotechnics
B. Cook	Standard Fireworks
I. Hornsby	March May Manufacturing
N. Birch	Vale of the White Horse District Council

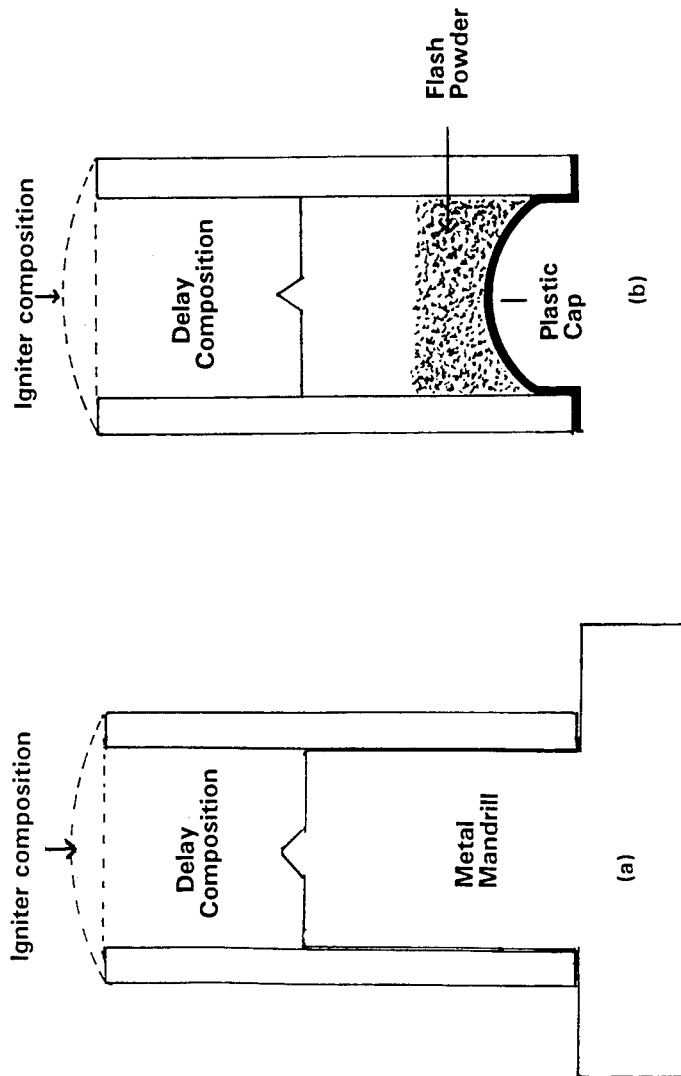
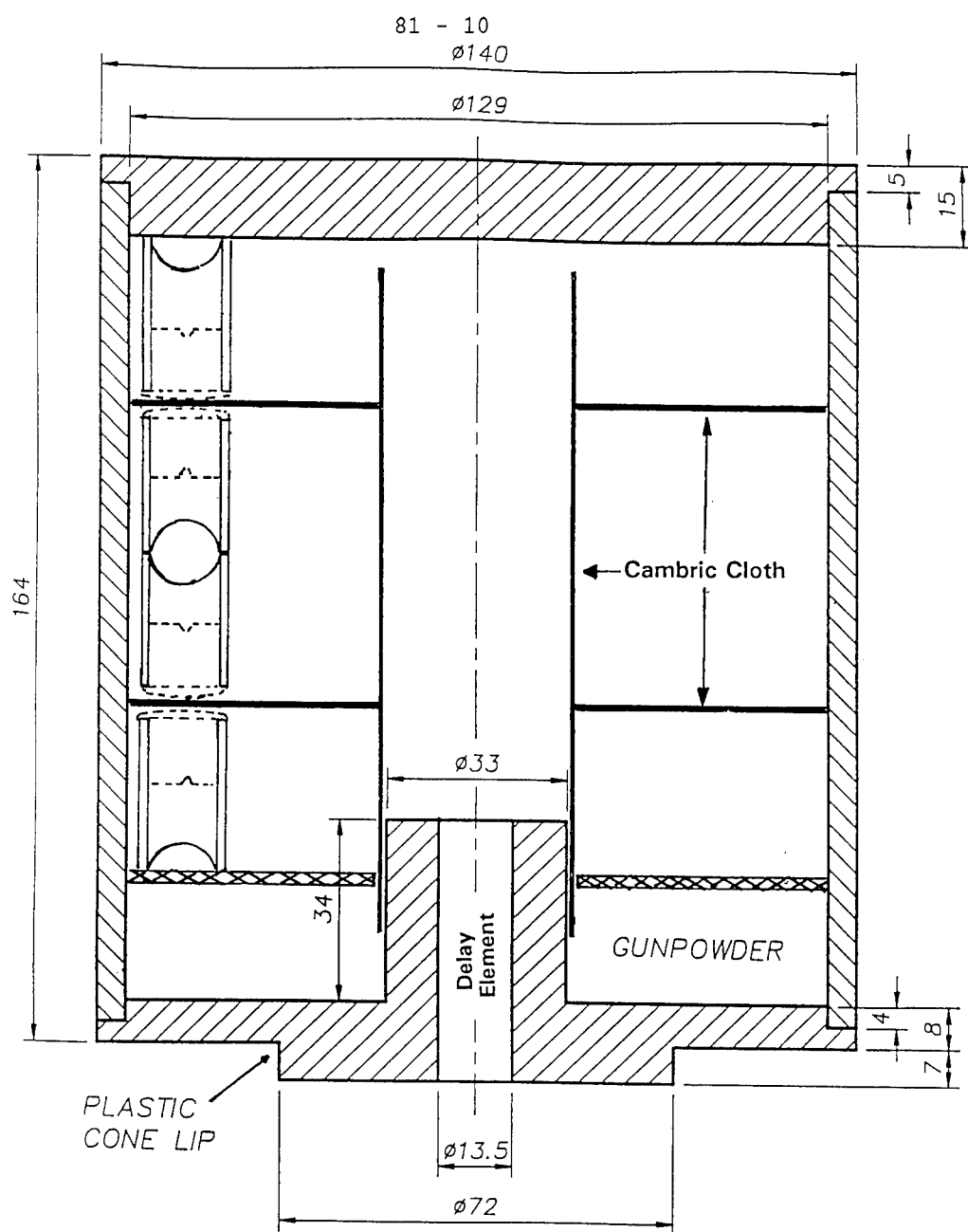


Figure 1 (a) Filling of cardboard tube submunition with delay composition, using the mandrill and (b) completed submunition containing flash powder sealed with the plastic cap



Dimensions are in millimetres

Figure 2 Cross-section of main munition body showing lip for plastic cone containing lifting charges and central delay holder. Also shown is the arrangement of the sub-munitions on the cambric cloth

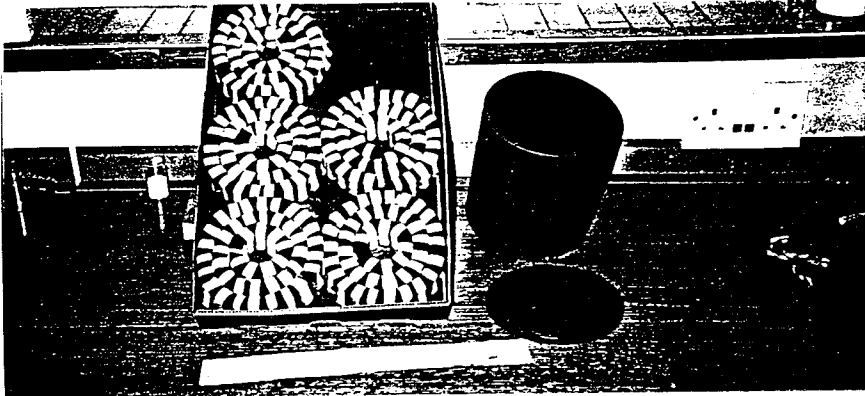


Figure 3 Munition body and lid with tray of sub-munitions assembled onto cambric strips ready for packing Note the central hole

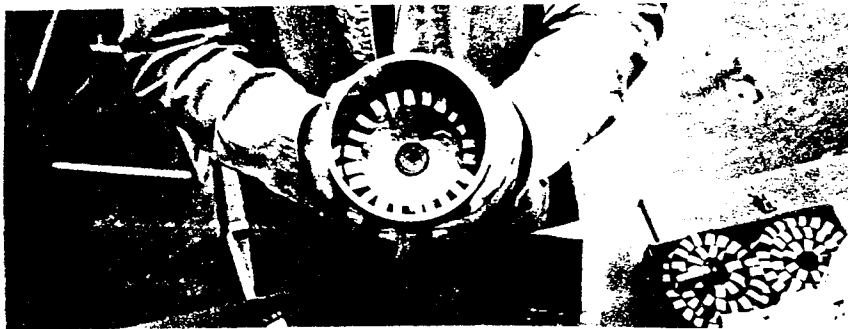


Figure 4 Main munition shown with the outer ring of the bottom layer in place. The wick from the primary delay and the cardboard ejection plate are visible beneath the sub-munitions

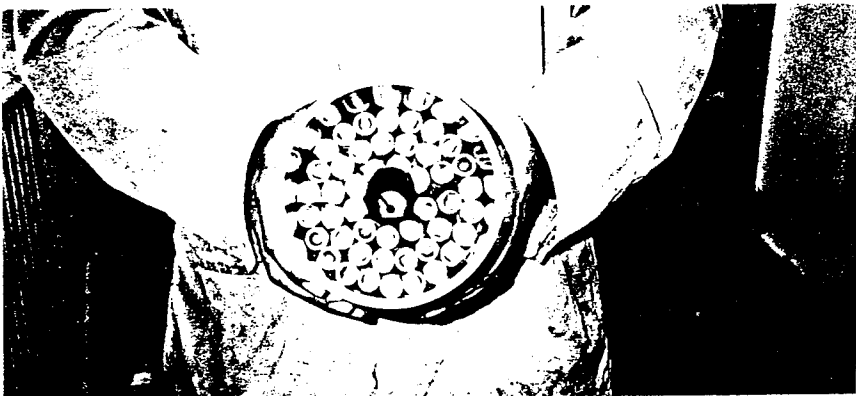


Figure 5 Main munition shown with second layer in place.

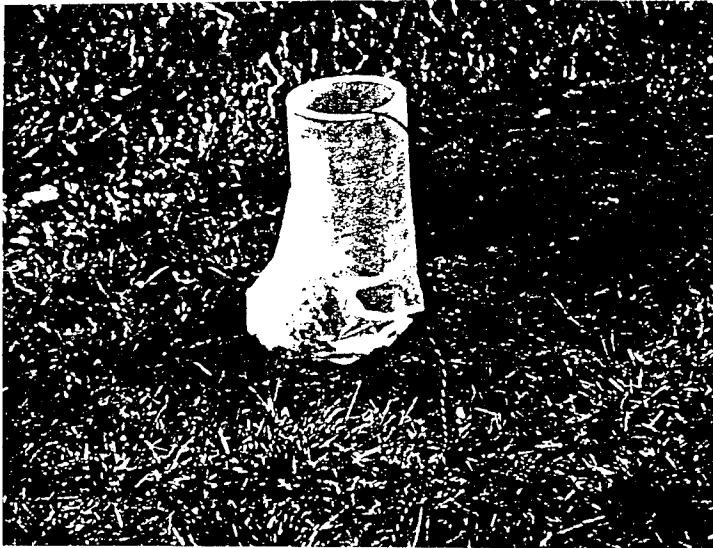


Figure 6 Launch tube buried to half its length ready for firing



Figure 7 Plastic cone holding propelling charge and ISFE fitted to the bottom of a test munition

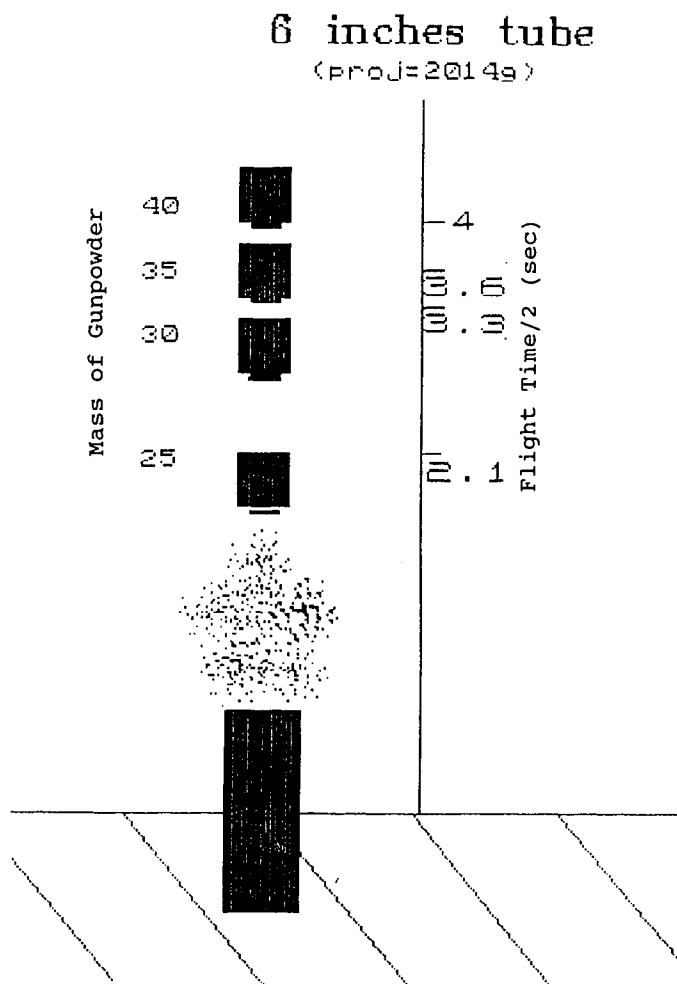


Figure 8 Schematic of Time to Apogee (Half flight time) against mass of blackpowder propelling charge.

**OPTICAL CHARACTERISATION OF A HIGH PRESSURE REACTION CHAMBER
FOR DEGRADATION PROCESSES OF ENERGETIC MATERIALS IN
SUPERCRITICAL WATER**

B. Michelfelder, W. Eckl, M. Herrmann, N. Eisenreich, Th. Hirth, H. Krause
Fraunhofer Institut für Chemische Technologie,
Joseph-von-Fraunhofer-Str. 7, D-76327 Pfinztal,
Germany

Abstract

A high pressure facility including an optical reaction chamber has been designed allowing observation of degradation processes of propellants and explosives in supercritical water combustion.

The first investigations aimed in an optical characterisation of the cell. The results showed the strong influence of water at the adjusted conditions of different temperatures and pressures. The obtained results may help to improve the application of emission spectroscopic based diagnostics by including the determined wavelength dependence of the transmission coefficient into the equation of radiative transfer. The experimental work will be continued, investigating the combustion processes of military relevant substances in supercritical water conditions.

Introduction

Former investigations showed that supercritical water oxidation is an innovative process with high destruction efficiency for degradation of military waste [1 - 4]. The physical properties of supercritical water have been published in various papers [5, 6].

To achieve high conversion ratio, the reactions must be accelerated to avoid problems of the normally used long tube reactor. A practical concept is an high pressure combustion chamber because due to the higher reaction temperature the reaction zone is much smaller so that for example the corrosion problems will be limited in an defined area.

To improve the combustion kinetic data like radical concentration and temperature must been known. The quantitative observation of degradation processes in supercritical water, applying spectroscopic diagnostics, needs a complete optical characterisation of the reaction cell. Therefore, in a first step a facility including an optical combustion chamber has been designed allowing detailed investigation of the reaction mechanism.

Experimental

To produce a diffusion flame a cylindrical high pressure cell made of a high temperature nickel based alloy is used with a 80 mm o. d. and 30 mm i. d. with an inner volume of 30 cm³. In the longitudinal axis sapphire windows with a diameter of 8 mm which are sealed on gold foils are mounted to observe the visible flame and to analyze the reaction zone by different spectroscopic methods. In the middle of the cylinder axis the cell is equipped with four drillings to adapt high pressure pipes in an angle of 90°. Three of them are used to feed the different fluids in the fourth a thermocouple is mounted to measure the temperature of the contents in the cell. The cell can be heated electrically.

The fuel and the oxidizer are each fed in pressure intensifiers (406, 412) with a pressure of 100 bar. The low pressure side of the pressure intensifiers is filled with hydraulics oil. It is pressurized by nitrogen. The nitrogen is pressurized by a compressor (400) up to 140 bar and fed into a pressure vessel (401). So the mass-flow of the fuel and the oxidizer can be regulated by the valves in the hydraulics oil. The intensifier ratio of 1:8 of the pressure intensifiers allows to compress the gases up to 1100 bar.

Via sensitive high pressure valves (407, 414) the fuel and the oxidizer are fed from the pressure intensifiers into the high pressure cell. The oxidizer is fed through the drilling below the cell through a nozzle with a diameter of 0.5 mm, the fuel is feed through a pipe at the side of the cell.

The water is fed in the cell from the top either through a manual pump (102) or via a hydraulic powered pressure intensifier (301).

The combustion products can be taken up in pressure intensifiers (302, 305) through the water in and outlet drilling on top of the cell. The hydraulic oil of the pressure intensifiers can be drained off through a valve (316), so the pistons in the intensifiers move slowly back and take up a part of the cell contents. So the combustion products are continuously feed out of the cell and can be analyzed separately.

Technical Data of the Facility:

- pressure up to 1000 bar
- temperature 500°C
- three separate mass-flows:
 - water
 - fuel
 - oxidiser
- volume of the intensifiers: 500 ml
- max. duration of experiments: 20 - 30 min.
- central control unit behind a safety wall

Technical Data of the Spectrometer:

- Optical Multichannel Analyser Spectrometer
- used range 250 - 550 nm
- minimum exposure time of diode array about 10 ms
- grating with 2400 grooves per mm
- intensified diode array 1024 elements
- wavelength resolution 1 nm

Fig. 1: Experimental setup of the high pressure facility

Results and Conclusions

Figure 2 shows the transmission of sapphire windows at different states of wear applied in the reaction chamber. The transmission in the UV and VIS of new sapphire is comparable to quartz (70 - 90% transmission). The graphics proves, that even after a short use in the supercritical water, the transmission in the ultraviolet spectral range is strongly decreased to 20 to 30%. Further application reduces the transparency to 5% in the whole investigated spectral range. Polishing with diamond paste increases the transmission coefficient to 0.2 in the UV and 0.5 in the VIS.

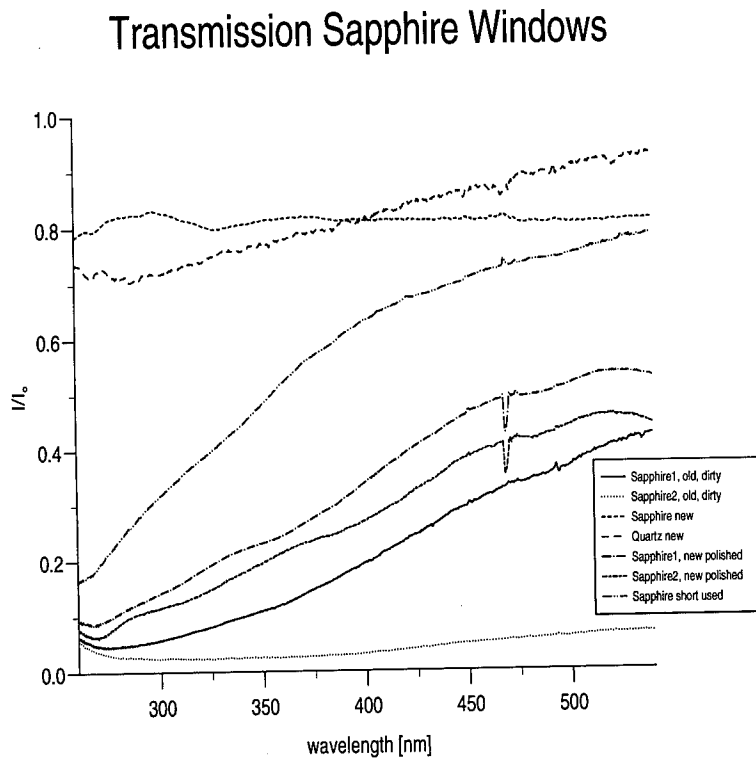


Fig. 2: Transmission of sapphire windows (spectral range 250 to 550 nm)

To investigate the optical influence of cold water (300 K), the transmission I at different pressures normalised to the intensity recorded from the cell without water I_0 , has been determined. The wavelength dependent intensity distribution is given in Figure 3. A strong absorption has been detected at 300 nm. In the visible spectral range, the intensity ratio I/I_0 rises from 0.8 to 1.1, depending on pressure. From Fresnel-Equations the reflection at the sapphire surfaces can be calculated. With cold water, the transmission increases about 10% (density 1000 kg/m³). Assuming constant density (cold water) the pressure dependence on optical geometry can be worked out. The sapphire windows (with plane surfaces at 0 MPa) are getting a spherical surface at high pressure, which is shifting the focus of the optics 'lens effect', so that scattered light of the inner cell is observed in dependence of pressure and wavelength. Maximum transmission is observed between 20 to 30 MPa. This dependence is shown in detail for 500 nm in the same plot.

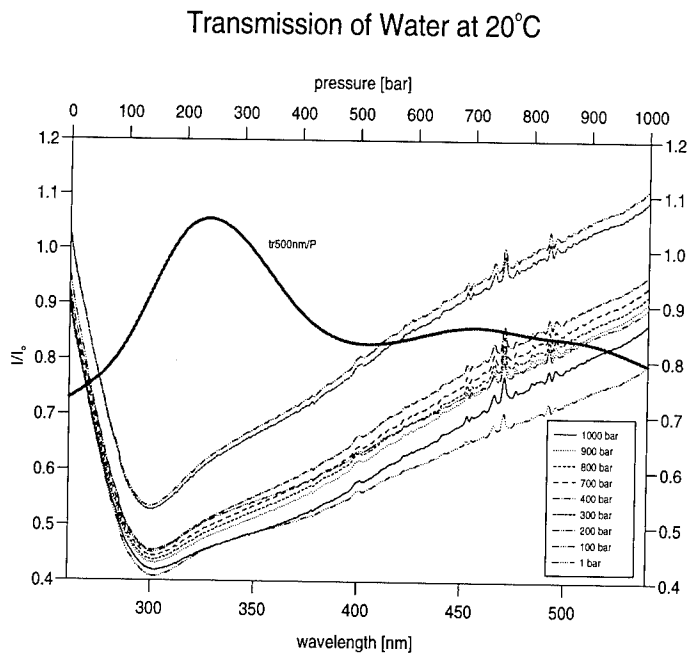


Fig. 3: Transmission of water at 300 K

In supercritical state, the transmission behaviour changes (see Fig. 4). The minimum is shifted to shorter wavelength about 280 nm. The intensity ratio I/I_0 in the UV increases to 0.9. Observed transparency in the VIS is at any wavelength more than 100%. Minimum transmission has been detected at 30 MPa. A significant change happens between 50 and 60 MPa. An additional pressurising to 100 MPa leads to continuous increase of transmission. Additional in the hot state the pressure dependence of the density is playing a role, so that at diminished density the absorption is getting smaller while the 'lens effect' at high temperatures is increasing.

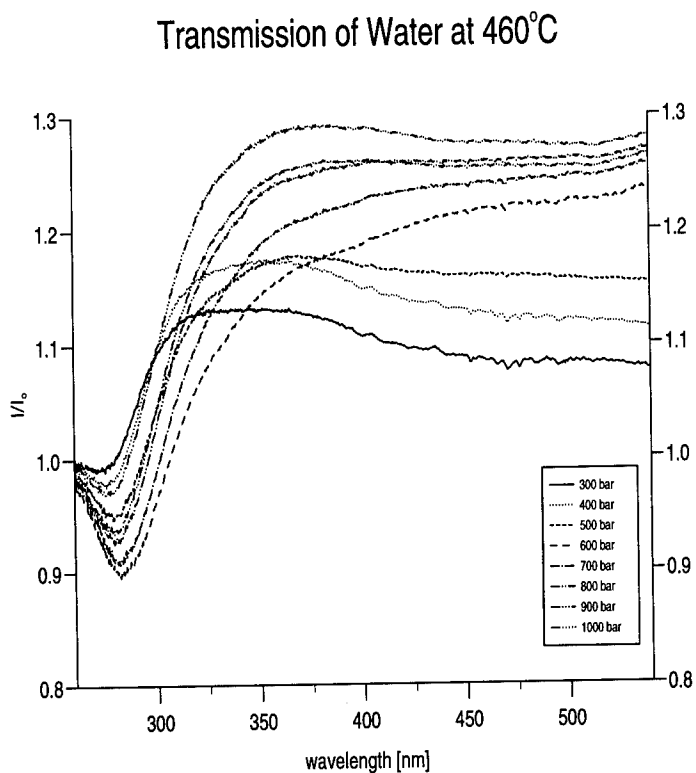


Fig. 4: Transmission of water at 733 K

This fundamental investigations show as an example the exigency of a detailed determination of optical characterisation working at supercritical conditions. Applying emission spectroscopic diagnostics without this detailed knowledge may lead to wrong results. Former spectroscopic investigations of supercritical water combustion determined the temperature from the intensity distribution of the A-X 0-0 band of OH [7, 8] at 309 nm. Considering the here obtained results may lead to an improvement of this diagnostic method by including the wavelength dependent transmission into the equation of radiative transfer.

The experimental work will be continued, investigating the combustion processes in supercritical water of military relevant substances. Degrading abandoned polluted areas and toxical waste especially heavy metals in pyrotechnic formulations will be of future interest.

References

- [1] **S. Buelow, R. Dyer, C. Rofer, J. Atenico**, Destruction of Propellant Components in Supercritical Water, Los Alamos National Laboratory, LA-UR-90-1338
- [2] **S.J. Buelow, R.B. Dyer, C. K. Rofer, J.H. Atenico, J.D. Wander**, Advanced Techniques for Soil Remadiation: Destruction of propellant Components in Supercritical Water, Los Alamos Form No. 836 R4 St.No 2629 5/81
- [3] **Th. Hirth, H. Krause, N. Eisenreich**, Zersetzung von Treib- und Explosivstoffendurch Prozesse in überkritischem Wasser - I. Aufbau der Versuchsanlage, ICT-Bericht 17/91
- [4] **Th. Hirth, N. Eisenreich, H. Krause, G. Bunte**, Entsorgung von Treib- und Explosivstoffen durch Prozesse in überkritischem Wasser, 23. Internationale Jahrestagung ICT. Pfinztal
- [5] **M. Modell**, Supercritical Fluid Technology in Hazardous Waste Treatment, Modell Development Corporation, Cambridge, MA 02138, USA

[6] **W. Schilling, E.U. Franck**, Combustion and Diffusion Flames at High Pressures to 2000 bar, Ber. Bunsenges. Chem 92 (1988), 631

[7] **E. U. Franck, Th. Hirth, G. Pohsner, J. Steinle**, Combustion and Flames to 1000 bar, Poster presented at the 23th Symposium on Combustion, The Combustion Institute, Orleans, France July 22-27, 1990

[8] **W. Eckl, N. Eisenreich**, Temperatures of Flames Obtained from Band Profiles of Diatomic Molecules, Bull. Soc. Belg. Vol 101, N010, 1992

ANALYSIS OF THE LONG TERM STABILITY DATA

Jan Petržílek

Research Institute for Industrial Chemistry, Synthesia a.s.
532 17 Pardubice - Semtín, Czech Republic

ABSTRACT

12,469 samples of 62 propellant types produced in Synthesia a.s. and stored under normal conditions were periodically tested for chemical stability and obtained data set analyzed. Results of heat test at 100 °C, Bergmann - Junk test and vacuum stability test are discussed with respect to chemical composition of samples and duration of their storing. The conclusion is, that supposed drop of values of heat test at 100 °C during storage of propellant was relatively small for double base propellants. A significant increase in results of this test was observed during first period of storing for some nitroglycerine and single base propellants. In case of selected single base propellants we can observe that the dependencies of 100 °C and Bergmann - Junk test results on duration of storing are strongly nonlinear and non monotonous and that the difference between the computed curves for individual tests is significant.

INTRODUCTION

Heat test at 100 °C, Bergmann - Junk test at 132 °C and manometric vacuum stability test in vacuum (STABIL)^(1,2) have been mostly used to check propellant chemical stabilities in Czech Republic and former Czechoslovakia. Several tenths of thousand measurements have been performed during last forty years and the results indicate some interesting features of these tests.

THEORETICAL PART

Heat test at 100 °C⁽³⁾ : 10 g sample is heated at 100 °C in glass test tube until the appearance of yellow, red or brown fumes are observed. The test tube is closed one hour after beginning of heating, stopper is removed from the tube for 10 minutes once in 24 hours.

Stability test according to Bergmann - Junk⁽³⁾ : 5 g dried sample of single base propellant is heated 5 hours at 132 °C, released gases are dissolved in water and titrated. The value obtained by recalculating of total volume of released acid gases to nitrogen oxide is a measure of chemical stability.

Vacuum stability test (STABIL)⁽¹⁻²⁾ : Evacuated test tube containing 2 g of sample is heated 5 hours at 115 °C. The value obtained by recalculating of total volume of gases released during 20 hours to nitrogen oxide is a measure of chemical stability.

DATA ANALYSIS

12,469 samples of 62 propellant types produced in Synthesia a.s. within 1947 and 1988 were stored under normal conditions in magazines and periodically tested for chemical stability. Analyzed data set contains 20,517 results of heat test at 100 °C and additional results of other tests (i.g. Bergmann - Junk test or vacuum stability test) if performed. The propellant types discussed can be divided into these groups: single base (marked Nc, Nc F, NC Cl), and double base groups - nitroglycerine (compositions Ng 7.85, Ng 8.85, Ng 9.0, Ng 12.0, Ng KV, Ng R1, NBL - 60, vz. 43 and TPH - G) or diglycoldinitrate (compositions Dg 7.5, Dg 8.0, Dg 8.15, Dg 8.5, Dg 9.0, Dg RM, Dg RMCl). Figure 1 shows content of stabilizer (ethylcentralite) and heat of explosion of the double base propellants discussed. All of single base propellants are stabilized by diphenylamine and those marked Nc F are surface treated by ethylcentralite.

The results of heat test at 100 °C for the above mentioned propellant compositions are shown in figure 2 by boxplots, figures 3 and 4 demonstrate, how the results change with years of storage under normal conditions (local regression⁽⁴⁾ and 99 % confidence intervals were used for computation and graphing; 4010 resp. 4257 measurements were used).

Boxplots in figure 5 are based on 4411 measurements of Bergmann - Junk test of 17 selected single base propellant types. The first seven types (of very similar chemical composition and without surface treatment) were chosen to illustrate dependence of measured results of stability test on duration of storing in magazine. These relations are graphed in figures 6 and 7. The computed shapes of curves were not dependent on the date of production of the propellant and on type of propellant (it was proved by graphing of parts of this data set).

Results of vacuum stability test of TPH - G propellant are shown in figure 8.

CONCLUSIONS

When comparing the results of heat test at 100 °C of double base propellants, the mean values computed for each type of propellant are in good accordance with its chemical composition (the test gives higher values for higher stabilizer content and lower values for higher heat of explosion of the sample). Supposed drop of values of heat test at 100 °C during propellant storage for individual types of propellants is relatively small, even in case of low stabilized propellants (NBL, Dg RM). On the contrary, a significant increase of results of heat test at 100 °C during first five years of storing was observed at some highly stabilized nitroglycerine propellants (TPH - G, Vz. 43 and Ng 7.85). The hypothesis of increasing chemical stability of last mentioned highly stabilized propellant types is also supported by vacuum stability test dependence shown in figure 8.

Higher levels of heat test at 100 °C results were measured for single base propellants containing diphenylamine and ethylcentralite than for those without centralite, but the same trend was observed in case of Bergman - Junk test. Dependencies of results of heat test

83 - 4

at 100 °C and Bergman - Junk test on duration of storing, measured for the same sample are shown in figures 6 and 7. It is obvious that the computed curves are non linear, non monotonous and that their shapes differ significantly for individual tests.

Interpretation of the above mentioned results is complicated but on the basis of these results it is possible to eliminate the hypothesis of significant decrease of propellant chemical stability during first 15 years of storing.

Double based propellants

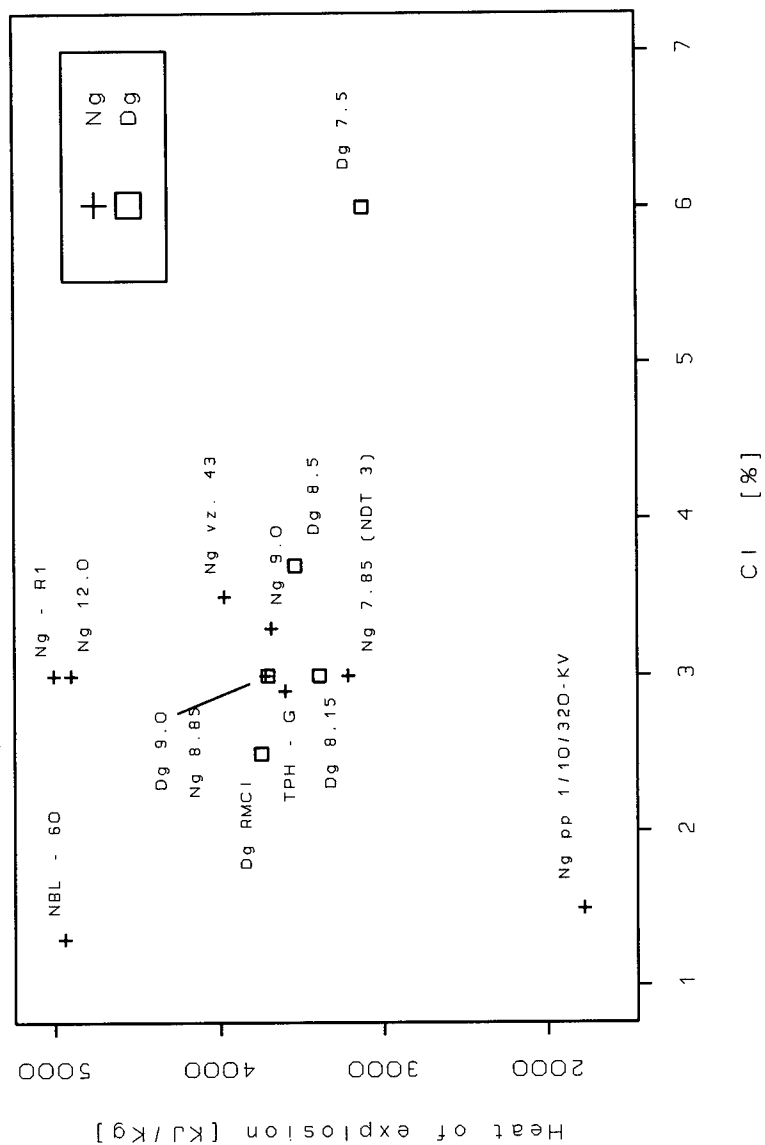


Figure 1

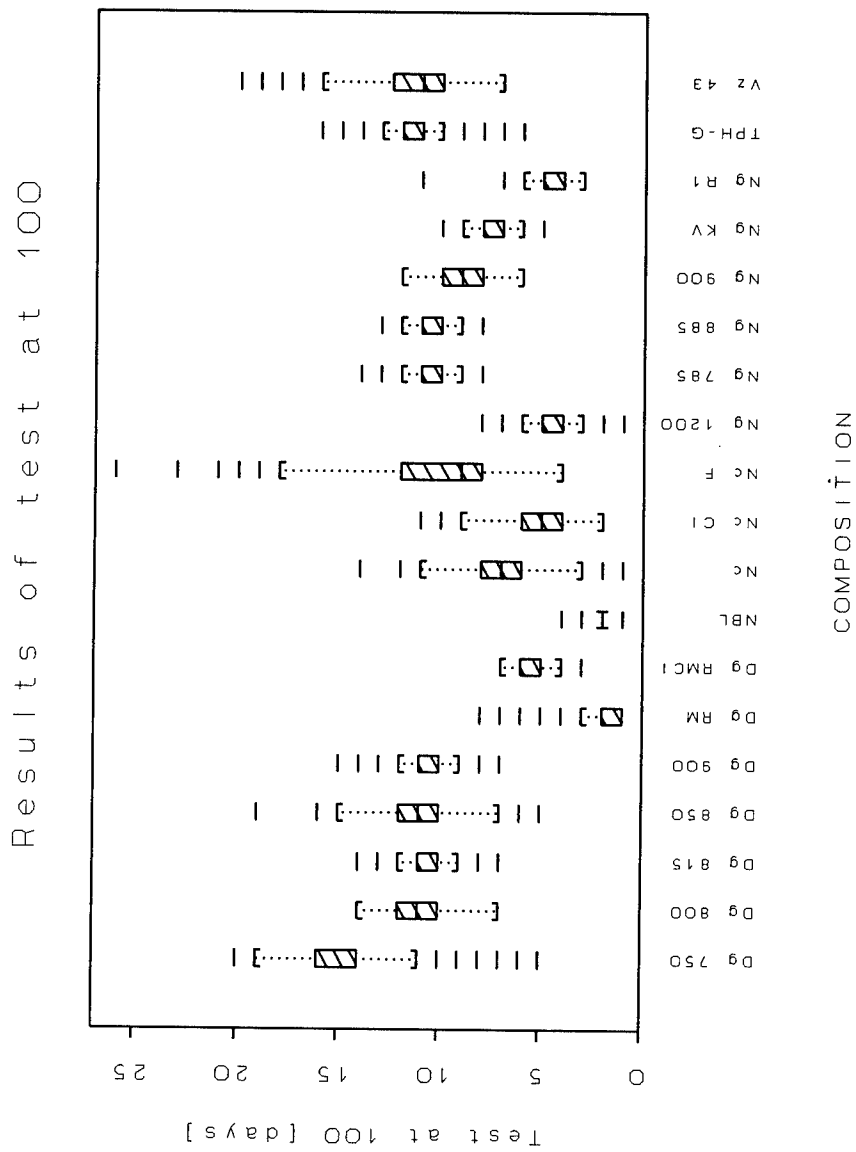


Figure 2

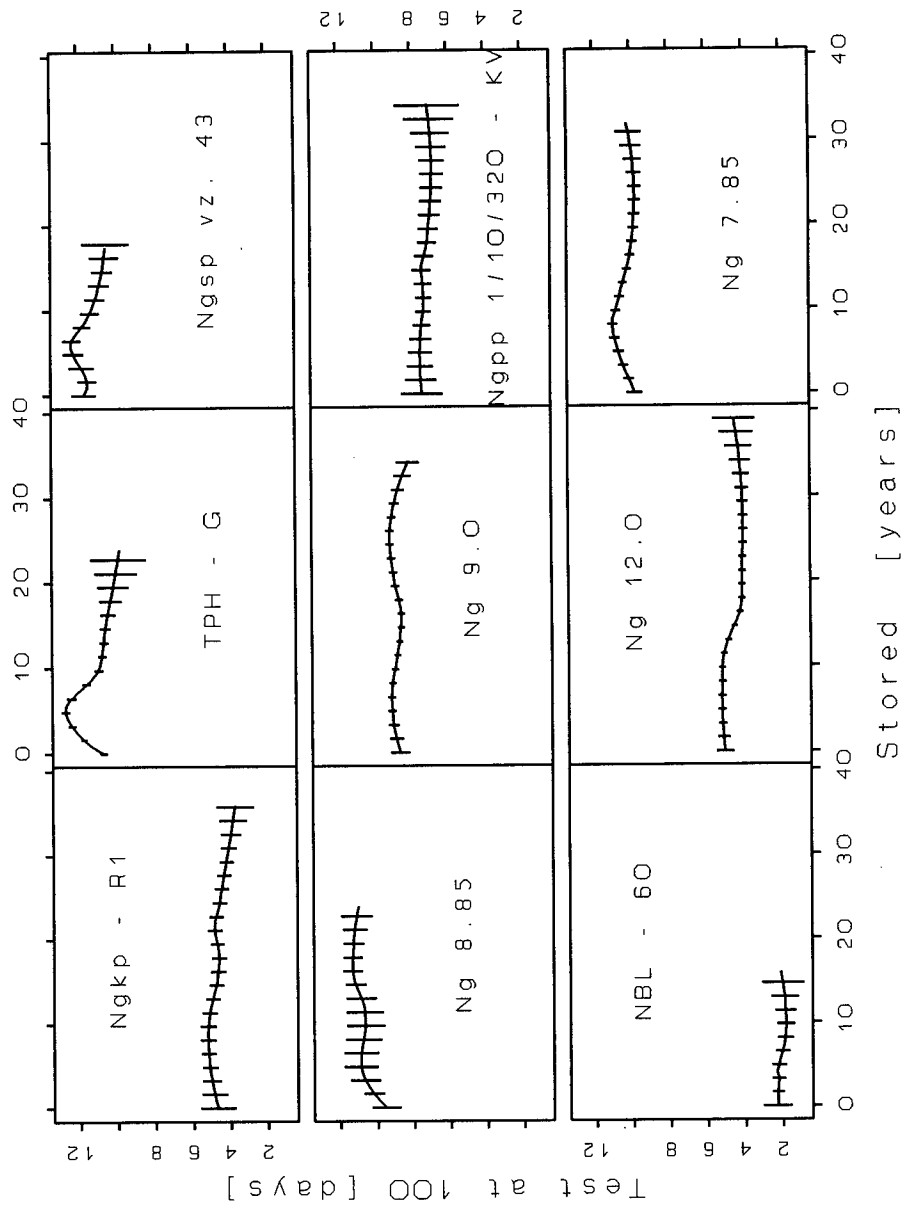


Figure 3 Nitroglycerine propellants

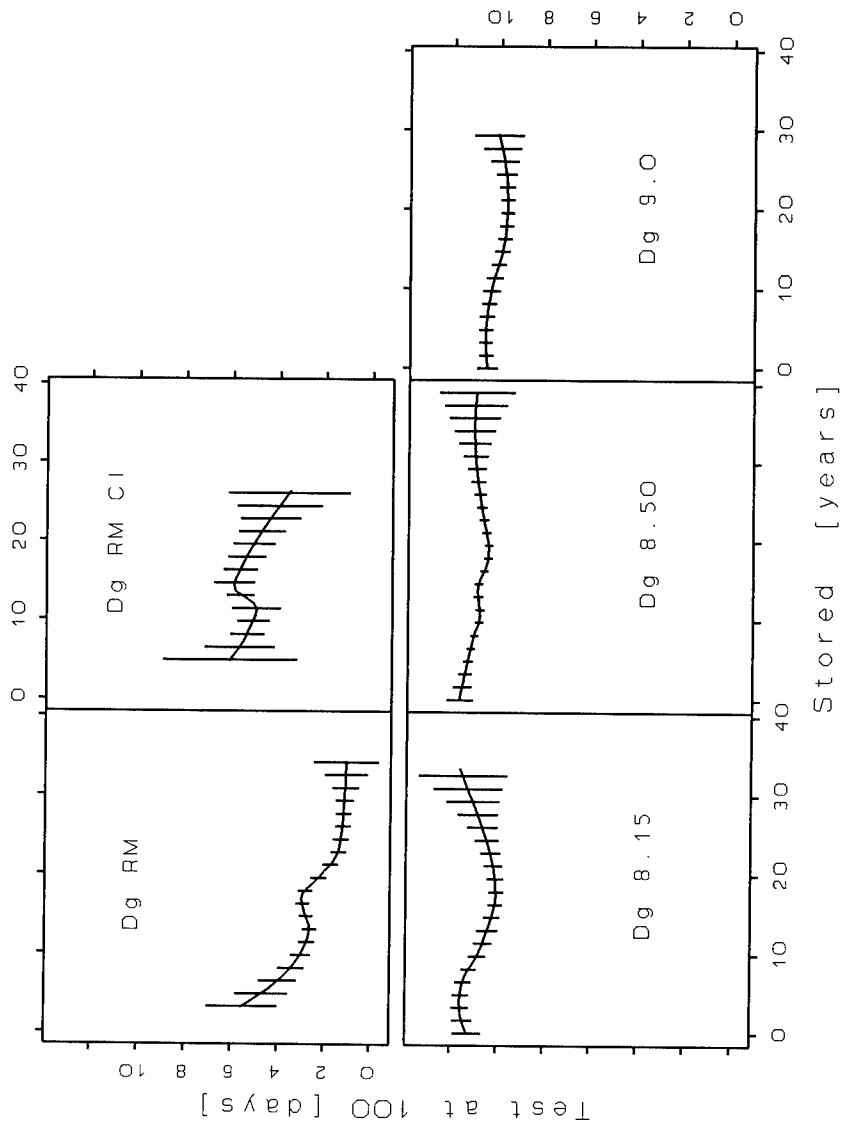


Figure 4 Diglycoldinitrate propellants

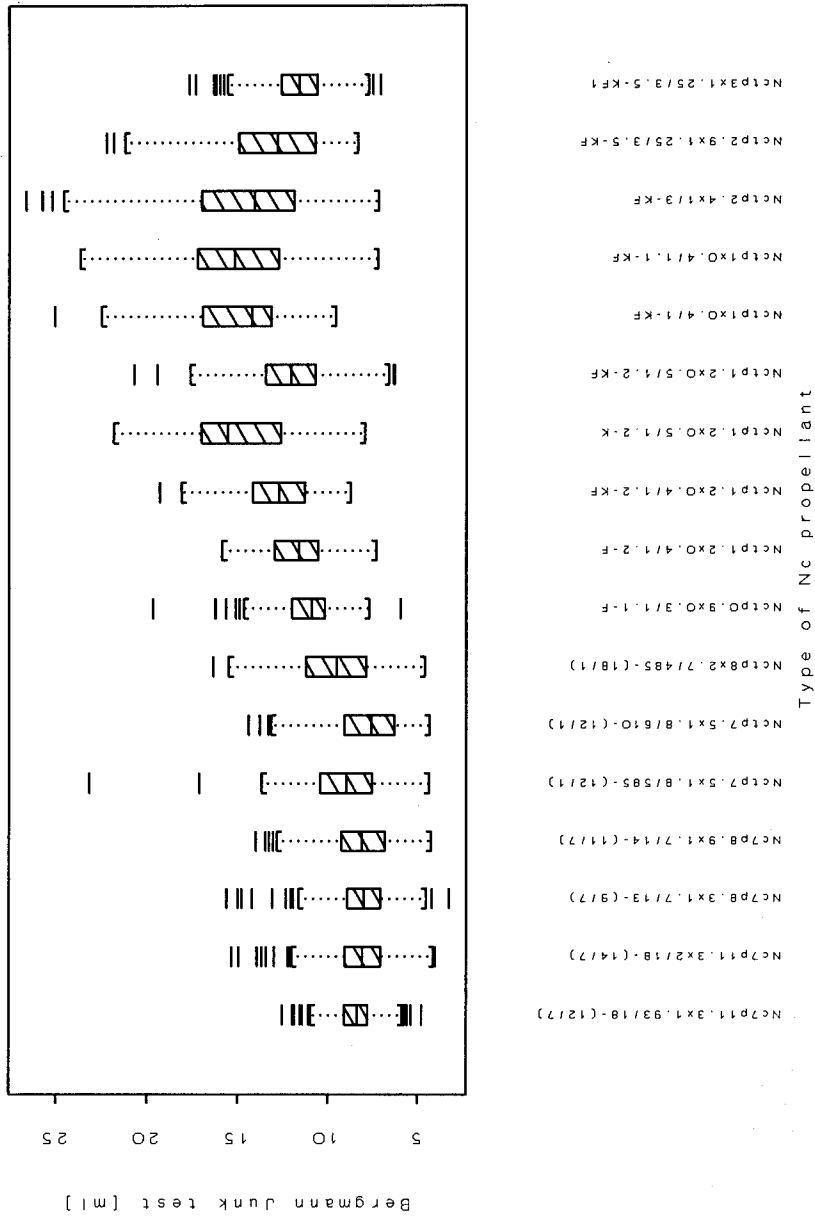


Figure 5 Nitrocellulose propellants

83 - 10

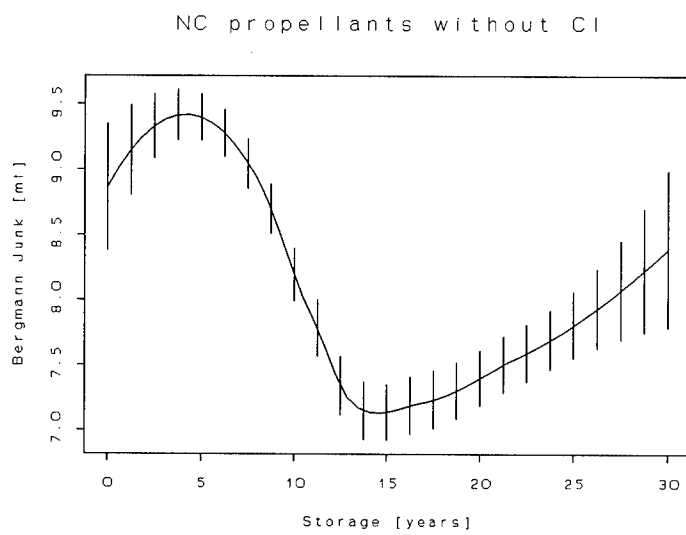


Figure 6

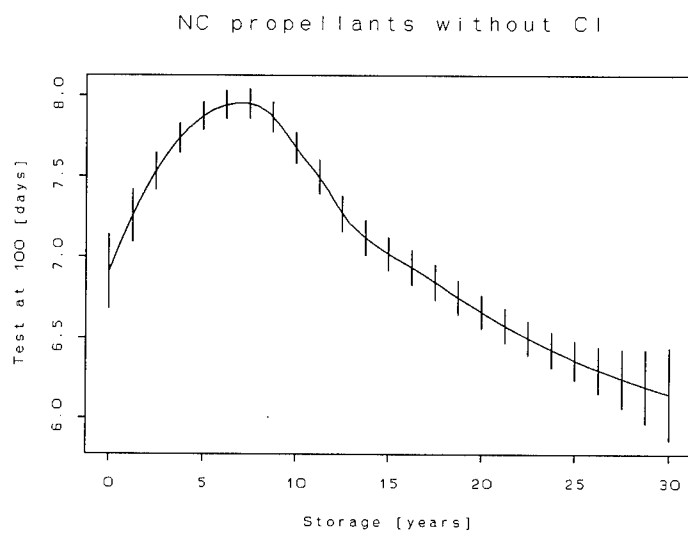


Figure 7

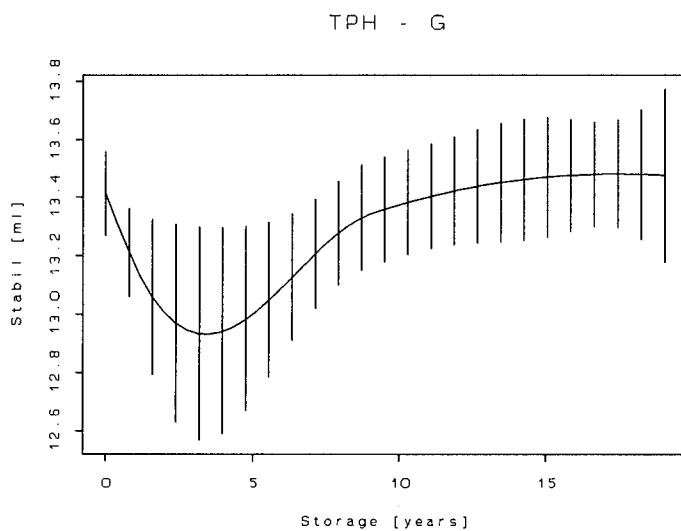


Figure 8

REFERENCES

1. Kučera V., Havráňková E.: Propellants, Explosives, Pyrotechnics 13 (1988), 186-188.
2. Havráňková E., Pilná B.: Propellants, Explosives, Pyrotechnics 14 (1989), 118-121.
3. Československá státní norma, ČSN 668102, bezdýmné prachy, metody zkoušení, 28.3.1978.
4. Chambers J.M., Hastie T.J.: Statistical models in S, Chapman & Hall, 1990.

Heat flow calorimetric investigations of primers

Stephan Wilker, Gabriele Pantel, Manfred Kaiser, Uldis Ticmanis

Bundesinstitut für Chemisch-Technische Untersuchungen beim BWB (BICT)
Großes Cent, D-53913 Swisttal

Abstract

Some components of the sintox primer composition, which was introduced into German ammunition in the early 1980's, were investigated by isothermal heat flow calorimetry. From the obtained data kinetic parameters such as activation energy and frequency factor were calculated by linear regression analysis. The heat flow calorimetric results were compared with those coming from "classical" thermoanalytical methods such as DTA, TG and DSC, where tetracene with $E_A = 205$ kJ/mol showed a very good agreement, while diazole reveals a much smaller activation energy (127 kJ/mol) at the investigated temperature range (80 to 50°C). There is no evidence for a change in the reaction mechanism or the activation energy of the decomposition reaction in the interesting temperature range as it is usually found in propellants.

We also looked at the specific heat production rate of primer compositions (sintox and sinoxide). From all results we calculated the shelf life time of the explosives, where a loss of 60% of the tetracene resp. diazole content in two complete primers is assumed.

Zusammenfassung

Einige Verbindungen, die in Sintox-Anzündhütchen (welche in den frühen achtziger Jahren in die deutsche Munition eingeführt wurden) enthalten sind, wurden mit Hilfe der isothermen Wärme-flußkalorimetrie untersucht. Aus den erhaltenen Daten wurden kinetische Parameter wie Aktivierungsenergie und vorexponentieller Faktor mittels linearer Regression ermittelt. Die wärme-flußkalorimetrischen Daten wurden mit jenen, die in den sog. "klassischen" thermoanalytischen Methoden wie DSC (DDK), DTA oder TG gewonnen wurden, verglichen. Dabei konnte für Tetrazen mit $E_A = 205$ kJ/mol eine sehr gute Übereinstimmung beobachtet werden, während Diazol im untersuchten Temperaturbereich (80 bis 50°C) eine deutlich niedrigere Aktivierungsenergie (127 kJ/mol) aufweist. Es ergaben sich keine Hinweise für einen Wechsel im Reaktionsmechanismus oder der Aktivierungsenergie im genannten Temperaturbereich, wie sie gewöhnlicherweise bei der Untersuchung von Treibladungspulvern gefunden werden.

Wir haben ebenfalls die spezifische Wärmeproduktionsrate von kompletten Anzündhütchen (Sintox und Sinoxid) gemessen und von allen untersuchten Explosivstoffen Gebrauchslebenszeiten (wobei ein Tetrazen- bzw. Diazolverlust von 60% zugrundegelegt wurde) berechnet.

1. The sintox composition

During the 1970's people became conscious about the health risks of the reaction products of primer mixtures while using ammunition with sinoxide primers. Especially the lead content of the sinoxide composition was criticized, the threshold limit value for lead was exceeded on an average 6.6 fold in the area of the supervising personnel, when they were exposed to the emissions for 8 hours a day. Even high levels of lead concentrations could be found in the blood of firers and supervisory personnel [1].

So a new, lead-, barium- and antimony-free primer composition was developed by the Dynamit Nobel AG in the years between 1977 and 1980 [2]. As well as the sinoxide composition it consists of a sensitizer, a primary explosive material and a pyrotechnic system (table 1) [3].

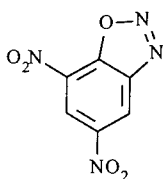
Table 1

Chemical structure of sinoxide and sintox compositions

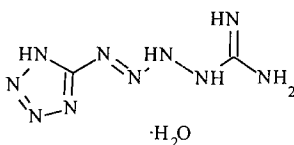
composition	sinoxide	sintox
sensitizer	tetracene	tetracene
primary explosive material	lead triciniate (lead styphnate)	diazole
pyrotechnic system	Ba(NO ₃) ₂ /Sb ₂ S ₃ /CaSi	ZnO ₂ /Ti/CaSi/Al
energetic filling material		propellant (double-base)

In addition the double-base propellant .30 carbine is used as an energetic filler in sintox primers.

After successful investigations about the stability and reliability of the sintox primer composition it was introduced into the German army's ammunition in the early 1980's [2,3]. But still some questions about the chemical stability remain unanswered [7b], combined with several problems connected with the shelf life prediction of the new primer composition.



Diazole (2,4-dinitro-6-diazophenole)



Tetracene

2. Heat flow measurements

A relatively new method for checking the stability of explosives is the isothermal heat flow calorimetry. It gives us additional information about the kinetics of the decomposition reaction to the well-established thermoanalytical methods like DTA, DSC and TG [4]. By combining these results with those of the heat flow calorimetry a reliable description of the kinetics of the decomposition reactions can be made. The method of isothermal heat flow calorimetry was developed in the 1960's and 70's [5]. In the past decade a new generation of capable heat flow calorimeters were produced.

The heat flow measurements were conducted in a TAM microcalorimeter. The data were collected with a 486-SX25 IBM-compatible computer.

The basic principle is that the heat produced by any process within the sample is completely exchanged with a surrounding heat sink which is maintained at a constant temperature. If a chemical reaction occurs in the sample a small temperature difference arises which causes a (small) heat flow. With highly sensitive thermopiles around the reaction vessel these small temperature differences, which are directly proportional to the heat flow, can be detected. The functional design of a heat flow calorimeter is outlined in figure 1 [6].

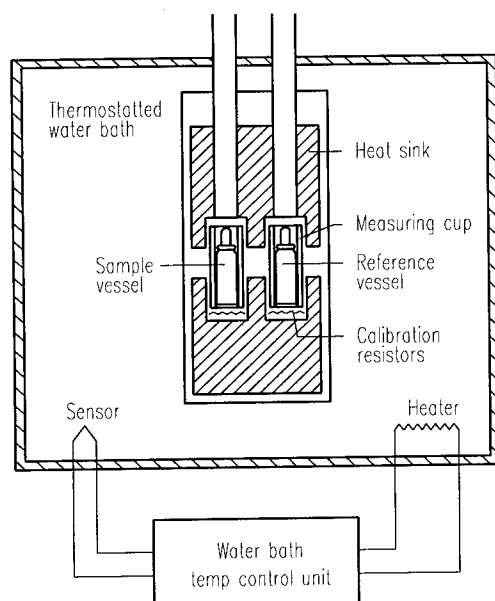


Figure 1: Functional design of a heat flow calorimeter

Before a measurement can be carried out an accurate calibration of the sample and the reference vessel has to be made.

From the resulting specific heat production rates which are recorded at different constant bath temperatures the kinetic parameters of the decomposition reaction can be calculated according to (1), where a reaction with zero order and a temperature independent frequency factor are assumed.

$$q = C' \cdot e^{-\frac{E_A}{RT}} \quad (1)$$

with q = specific heat production rate [$\mu\text{W/g}$]
 C' = preexponential (frequency) factor [W/kg]
 E_A = activation energy [kJ/mol]
 R = universal gas constant [$\text{J/K}\cdot\text{mol}$]
 T = ambient (bath) temperature [K]

An Arrhenius plot ($\lg q$ vs. $10^3/T$) gives us both values of C' and E_A , from which life time predictions can be made (see below).

3. Results

We measured the specific heat production rate of single components of the sintox composition as well as of complete sintox and sinoxide primers.

3.1 Diazole and tetracene

About 1.8 g of each compound were introduced into the sample vessel. The reference vessel remained empty. The preceding calibration occurred with two empty vessels. Typical heat flow curves of these compounds are sketched in figures 2 and 3.

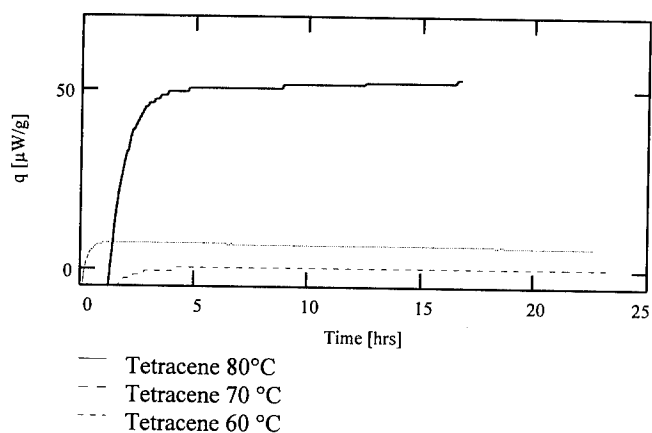


Figure 2: Heat flow measurements of tetracene at different temperatures

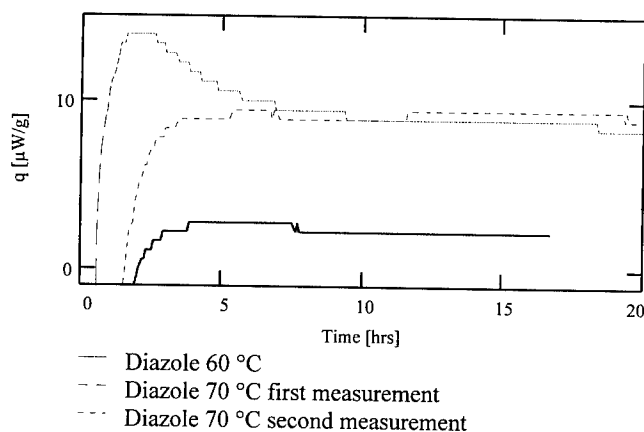


Figure 3: Heat flow measurements of diazole at different temperatures

As can be seen, there are huge differences between the behaviour of diazole and tetracene. Whereas the shape of the diazole curve (at least at the investigated range of decomposition) is more similar to a typical propellant decomposition process with a constant value of q at the end of the measurement, tetracene reveals a constant increase of heat generation with time. This fact requires a different method of evaluation (see chapter 3.2).

It can also be seen, that the second measurement of the same sample of diazole at 70°C shows different behaviour in the beginning (no preliminary "dirt" effects) but nearly the same constant q in the end.

In the case of diazole it is possible to use the constant heat production rate for the calculation of the kinetic parameters like it is usually realized with propellant measurements. The shape of the tetracene heat production rate makes it nearly impossible to find a period with constant q , especially at elevated temperatures ($> 70^\circ\text{C}$, see table 2 and figure 2). The method of evaluation using an autocatalytic model is outlined in chapter 3.2.

The specific heat production rates of these two compounds are presented in table 2.

Table 2
specific heat production rates of diazole and tetracene [$\mu\text{W/g}$]

bath temperature [$^\circ\text{C}$]	diazole ^{a)}	tetracene ^{b)}	tetracene ^{c)}	tetracene ^{d)}
80	48,9	36,8	56,7	39,2/41,0
75	31,4	18,4	-	16,2/16,3
70	15,2	5,20	6,72	6,4/ 6,2
65	6,36	1,90	-	2,05/ 1,98
60	4,08	0,79	0,45	0,33/ 0,30
50	1,69	e)	e)	e)

a) constant heat production rate

b) average of two values after 20 h

c) value after 60 h

d) value after 15/20 h with a defined small hole in the cap of the sample vessel¹

e) no evaluation of data possible because the specific heat production rate is too small

- not determined

The Arrhenius plot of the diazole experiments is presented in figure 4.

¹ The defined small hole in the caps of the sample vessel causes a certain evaporation of volatiles off the sample and simulates more precisely the conditions in primers. As can be seen the decrease of the specific heat production rates (compared with the experiments with a tightly closed vessel) is much bigger at elevated temperatures, whereas at 65°C the values are in good agreement with the "closed vessel" experiments (entry 2)

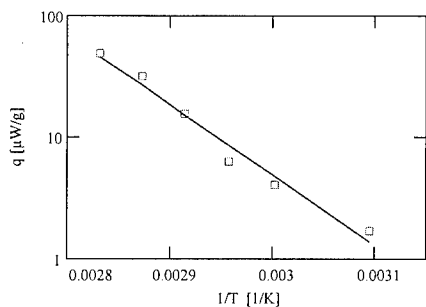


Figure 4. Arrhenius plot of diazole

3.2 Evaluation of kinetic data of tetracene

Although during the measurements only a relatively small reaction degree is obtained, a systematic increase - at least at higher temperatures - of the heat production rate during an isothermal period can be observed. This is due to an autocatalytic acceleration of the reaction and is compatible with TG and DSC measurements of tetracene. So an evaluation after a reaction model of zero order is no longer sufficient but has to be replaced by a more relevant equation like the model of first order with autocatalysis. It also must be mentioned that the autocatalysis constant B, which stands for the degree of acceleration might only be determined somewhat inexactly because of the small turnover rate. The reaction model of first order with autocatalysis is described by the following equation (2):

$$q = (1 - \alpha) * [1 + (B - 1) * \alpha] * c' * e^{\frac{-E_A}{R * T}} \quad (2)$$

with $c' = 1000 \cdot \Delta H \cdot A$ [W/kg]
 ΔH = reaction enthalpy (here 600 J/g)
 A = (usual) frequency factor (s^{-1})
 α = reaction degree
 B = autocatalysis constant²
 $f(\alpha) = (1 - \alpha) \cdot [1 + (B - 1) \cdot \alpha]$

The reaction degree α can be calculated from $\Delta h / \Delta H$ (Δh stands for the sum of the partial reaction enthalpies of every entry until the point of evaluation). The kinetic parameters were estimated from the logarithmic form of (2). If one plots $\ln(q/f(\alpha))$ vs. $1/T$ a straight line should result if the kinetic model is correct.

In table 3 the calculated values of c' , the activation energy and constant B are collected.

² If B takes the value 1, we have a simple first order kinetic model without autocatalysis

Table 3

Calculated kinetic data for tetracene

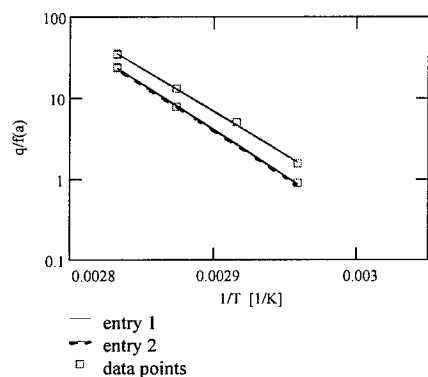
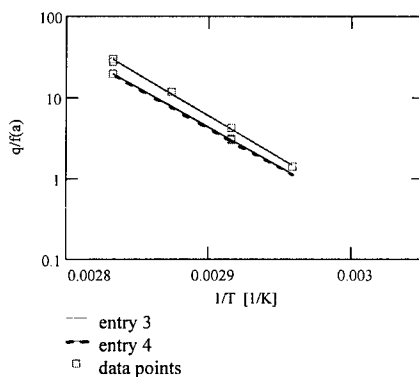
entry a)	c' [W/kg]	E _A [kJ/mol]	B	s
1	4,4 · 10 ³⁰	218	38	0,055
2	6,7 · 10 ²⁸	205	46	0,051
3	1,2 · 10 ²⁸	200	56	0,086
4	2,9 · 10 ²⁶	191	64	0,017

1 and 2: small hole in the cap (cf. table 2)

3 and 4: closed sample vessel

s: standard deviation between measured and calculated heat production rate q

The plots of these results are collected in figures 5 and 6.

Figure 5. modified Arrhenius plot of tetracene
- entries 1 and 2Figure 6. modified Arrhenius plot of
tetracene - entries 3 and 4

3.3 Sinoxide and sintox primers

The sample vessel was filled with 26 or 28 primers respectively, the reference vessel contained about the same number of empty delaborated metal cups. The preceding calibration was carried out with empty metal cups in both vessels. Typical heat flow curves of these primers are sketched in figures 7 and 8.

84 - 8

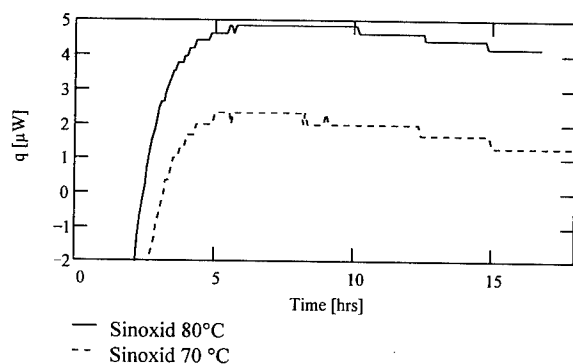


Figure 7: Heat flow measurements of sinoxide primers at different temperatures

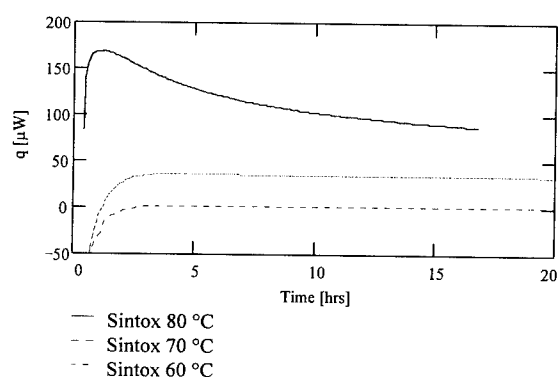


Figure 8: Heat flow measurements of sintox primers at different temperatures

For the evaluation of data we used the constant q values at the end of each measurement. Because of the inhomogenities of the samples material we obtained remarkable differences in double determinations (see table 4). Only the marked* entries are used for further calculations and are presented in figures 8 and 9. The results of the investigations are collected in table 4.

Table 4
specific heat production rates of complete sintox and sinoxide primers [$\mu\text{W/g}$ tetracene]

bath temperature [$^{\circ}\text{C}$]	sinoxide (DM 1032B1)	sintox (DM 1448)
80	73,7/143	1624*/618
75	12,8/153*	944*/304
70	a) /50,5*	622*/ 93
65	5,86/11,7*	146*/133
55	a) / a)	31,0*/ 21,3
45	a) / a)	11,0*/ -

a) no evaluation of data possible because the specific heat production rate is too small
- not determined

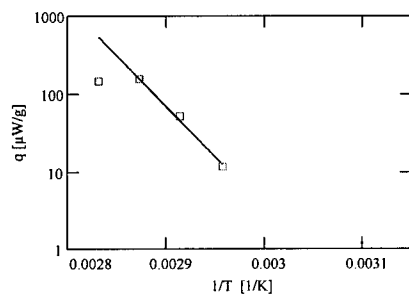


Figure 9: Arrhenius plot of sinoxide primers

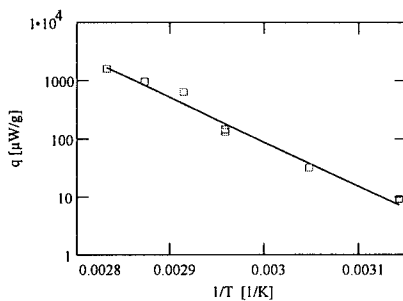


Figure 10: Arrhenius plot of sintox primers

3.4 Kinetic data of the decomposition reactions

From the obtained heat flow results the activation energies and the frequency factors are calculated. Both values were fitted by a linear regression analysis. They are collected in table 5. In table 6 a comparison between heat flow calorimetric and thermoanalytical (DSC, TG, DTA) [7, 8] results is presented.

Table 5

Kinetic data of primer compounds and primer compositions

compound		diazole	tetracene	sinoxide ^{a)}	sintox ^{a)}
activation energy	[kJ/mol]	127	205 ^{b)}	252	146
frequency factor	[W/kg]	$3,1 \cdot 10^{17}$	$6,7 \cdot 10^{28}$ ^{b)}	$9,7 \cdot 10^{36}$	$6,1 \cdot 10^{21}$
storage temperature ^{c)}	[°C]	59	56	57	35
shelf life time at 30°C	[yrs]	280 ^{d)}	> 1000 ^{e)}	> 1000 ^{e)}	86 ^{e)}

a) referring to the tetracene content

b) entry 2 of table 3

c) the storage temperature for a lifetime of 10 years

d) the period of time, in which 60% of the diazole content is lost

e) the period of time, in which a total loss of 60% of the tetracene content [7b] occurs.

The calculation is according to (3) [9]

$$t = 0.60 \cdot \frac{\Delta H \cdot 10^6}{86400 \cdot 365 \cdot q_{303}} \quad (3)$$

with ΔH = heat of reaction [J/g]

q_{303} = specific heat production rate at 303 K, calculated from kinetic parameters according to (1) [μ W/g]

Table 6

Comparison between heat flow calorimetric and thermoanalytical results [7, 8]

compound		diazole	tetracene	sinoxide	sintox
activation energy ^{a)}	[kJ/mol]	127	205	252	146
frequency factor C' ^{a)}	[W/kg]	$3,1 \cdot 10^{17}$	$6,7 \cdot 10^{28}$	$9,7 \cdot 10^{36}$	$6,1 \cdot 10^{21}$
activation energy ^{b)}	[kJ/mol]	178	200 ^{d)}	259 ^{c)}	176
frequency factor C' ^{b)}	[W/kg]	$1,1 \cdot 10^{24}$	-	$2,7 \cdot 10^{37}$	-
method		TG, DSC, NMR	DSC	isothermal TG	dynamic TG
temperature range	[°C]	80-150	110-150	85-95	110-140
storage temperature ^{e)}	[°C]	66	57	64	51

a) from heat flow calorimetric investigations

b) from thermoanalytical methods as described in line 6

c) for an Avrami-Erofeev reaction model $[f(\alpha) = (1-\alpha) \cdot (-\ln(1-\alpha))^p]$ d) evaluation according to Kissinger [10] from different heating rates from 0.1 to 1 K·min⁻¹ and different peak temperatures

e) the storage temperature for a lifetime of 10 years

4 Discussion

Both diazole and tetracene show a linear Arrhenius plot and easy-to-calculate kinetic data. Between 80 and 50°C seem to be no changes in reaction mechanism or activation energy at lower temperatures, as they can be regularly found e.g. in propellants³.

While the activation energy of the decomposition reaction of diazole only a value of about 130 kJ/mol was found, it is much higher in the case of tetracene. The tetracene results ($E_A = 205$ kJ/mol) are in good agreement with the data gained by other thermoanalytical methods. The kinetic model of a zero-order rate constant seems to be correct for the investigated early state of decomposition of diazole. The reaction of tetracene is better described by a first-order autocatalytic model. After 66 hrs the total reaction degree α of tetracene is at 1,29 % (80°C) or at 0,55 % (65°C), respectively⁴.

Comparing sinoxide and sintox primers it is obvious that the specific heat production rate of the sintox composition is much higher. The reason for this is the higher tetracene content and is somewhat lower stability in this mixture. The heat produced by the decomposition reactions are added, which makes it difficult to do a correct calculation of the total activation energy and of the total frequency factor. But it could be shown that the heat production between 80 and 60°C is mainly due to the decomposition of tetracene in the interesting temperature region between 100 and 20°C. So the calculation of the shelf life time of the sintox primers is mainly the result of the decomposition reaction of tetracene.

³ The latest results of our investigations show a remarkably "high" amount of heat generation of tetracene at 50°C (0.3-0.4 μW/g). It was not possible to find out, whether this is an artefact due to impurities/inhomogenities or whether there is a change in activation energy at these low temperatures. Until the conference begins we will have found it out and present it on the poster.

⁴ Comparison of the total energy emitted with the reaction enthalpy (600 J/g)

The only heat generating compound of the sinoxide composition is tetracene, the "inorganic" materials and lead styphnate are quite stable even at temperatures above 100°C. With the relatively small tetracene content in these primers the specific heat production rate is smaller compared with that of pure tetracene. The different chemical surrounding of tetracene in these primers (compared with the pure microcrystalline material we used for our first investigations) causes a different behaviour, e.g. no autocatalytical increase of the heat production is observed at 80°C.

It is obvious, that a good agreement of the storage temperatures for a lifetime of ten years in all cases except sintox primers between heat flow calorimetry and other thermoanalytical methods is found (tables 5 and 6). The observed differences with sintox might be due to the decomposition of the nitrocellulose containing sealing lac.

5 Conclusions

It could be demonstrated that it is possible to determine the specific heat production rate of primer compounds and compositions by isothermal heat flow calorimetry. From these data the kinetic parameters of the decomposition reactions could be calculated according to Arrhenius. In the case of pure tetracene a first-order reaction model with autocatalysis was used.

They are in the case of tetracene and sinoxide in good agreement with the values obtained by other thermoanalytical methods, whereas the decomposition reaction of diazole has a remarkably lower activation energy compared with the TG/DSC/NMR results obtained at 80-150°C. Nevertheless the storage temperature for a lifetime of ten years does not differ markedly caused by "kinetic compensation".

Because of the complexity of the decomposition reactions in the sintox composition (three different "unstable" compounds [double-base propellant, diazole and tetracene] are present) it is not easy to calculate reliable kinetic parameters. But it can be predicted that at room temperature no measurable heat production might be observed.

References

- [1] *Deutsches Waffen-Journal* 3/1983, p.45 ff.
- [2] R. Hagel, K. Redecker, "Sintox - A New, Non-Toxic Primer Composition by Dynamit Nobel AG", *Propellants, Explosives, Pyrotechnics* **11**, 184-187 (1986); *Deutsches Patent* DE 3321943 A1, 20.12.1984.
- [3] J. Knappworst, "Schadstoffarme Munition mit Sintox-Anzündung", *Deutsches Waffen-Journal* 10/1994, 1508-1515.
- [4] G. Krien, "Thermoanalytical Determination of Tetracene in Primer Mixtures", *Propellants and Explosives* **4**, 53-55 (1979) and references cited therein; G. Krien, "Über Anwendungsmöglichkeiten der DTA und der TG", *Explosivstoffe* **13**, 205-223 (1965).
- [5] J. Hansson, "Testing propellants by microcalorimetry" *LKB Application Note* 337 (1983); I. Wadsö, "Microcalorimetry", *Symp.Chem.Probl.Conn.Stabil.Explos.* **5**, 93-105 (1979); M. Frey, "Stabilitätsuntersuchungen an Treibladungspulvern und Sprengstoffen mittels Wärme flußkalorimetrie", *Symp.Chem.Probl.Conn.Stabil.Explos.* **5**, 345-359 (1979); E. Lion, M. Rat "Application de la microcalorimétrie isotherme à l'étude de la stabilité des poudres pour armes - corrélation avec d'autres techniques de caractérisation", *SNPE NT N° 93/83/CRB/NP* (1983).
- [6] ThermoMetric - "TAM - Thermal Activity Monitor for highly sensitive isothermal analyses".
- [7] a. W. Scheunemann, U. Ticmanis, "Anzündhütchen DM 1448 - Untersuchung von Qualifikationsmustern", *BICT Bericht* 330/13683/94;
b. U. Ticmanis, W. Scheunemann, "Unsicherheiten in der Beurteilung der Langzeitstabilität von Zündmitteln aus Ergebnissen standardisierter Prüfmethode", *BICT Bericht* 330/11993/92;
c. M. Kaiser, U. Ticmanis, "Thermal Stability of Diazodinitrophenole", *Thermochimica Acta* (1995), in press.
- [8] M. Kaiser, W. Scheunemann, U. Ticmanis, "Advanced Methods for the Determination of Primary Explosives", *ICT Jahrestagung* **26**, 1995.
- [9] J. Zierath, G. Pantel, "Arbeitsvorschrift für die Bestimmung der chemischen Stabilität mittels Wärme flußkalorimetrie", *BICT Bericht* 110/10383/91; *TL 1376-0600, Teil 30a* (Methode 2.51.1) (1993).
- [10] H.E. Kissinger, *Analyt. Chem.* **29**, 1702-1706 (1957)

THERMOANALYTISCHE CHARAKTERISIERUNG VON PYROPHOREN METALLOORGANISCHEN VERBINDUNGEN

Thomas S. Fischer, Achim Pfeil, Norbert Eisenreich

Fraunhofer-Institut für Chemische Technologie, Joseph-von-Fraunhoferstr. 7,
76327 Pfinztal, D

Anthony C. Jones, A.B. Leese, Simon Rushworth, Graham Williams

Epichem Limited, Power Road Bromborough, Wirral, Merseyside L62 3QF,
UK

Kurzfassung

Erste Ergebnisse thermoanalytischer Untersuchungen (DSC, EGA) an Trimethylaluminium (TMAI), Triethylgallium (TEGa) und Trimethylindium (TMIn) werden beschrieben.

Abstract

Preliminary results on the thermal decomposition of trimethylaluminium, triethylgallium and trimethylindium by DSC and EGA are presented.

Einleitung

Metallorganische Verbindungen wie die Trialkyle von Aluminium, Gallium und Indium sind Ausgangskomponenten bei der Herstellung von Halbleitern durch Verfahren wie MOCVD (metalorganic chemical vapour deposition) oder MOMBE (metalorganic molecular beam epitaxy) [1-3]. Dabei entsteht das hochreine Metall durch Pyrolyse.

Die Verbindungen sind thermisch instabil, stark pyrophor und können sich explosionsartig zersetzen [4, 5]. Die Kenntnis der thermischen Zersetzung und ihrer sicheren Handhabung angesichts der steigenden Produktion und des damit verbundenen scaling-up werden unverzichtbar.

Ergebnisse

Typische DSC finger prints sind in den Bildern 1 und 2 dargestellt. Drei Reaktionsintervalle dominieren: Endothermer Peak unterhalb 100 °C, breiter exothermer Peak bei 200-400 °C und endothermer Peak zwischen 400-600 °C. Die Lage des letzteren Peaks erwies sich als abhängig von der Einwaage.

Die Trimethyle sind bei Normaltemperatur fest, die höheren Trialkyle wie TEGa auf Grund der voluminösen Liganden flüssig. Der endotherme Peak im ersten Intervall ist die Phasenumwandlung fest-flüssig, mit Onset-Temperaturen bei 13 °C und 87 °C für TMAI bzw. TMIn. Die sich unmittelbar anschließende Umwandlung in die Gasphase ist im Diagramm wenig ausgeprägt, ebenso die Dissoziation des Dimers TMAI in das Monomer. Die Dimerisationswärme ist gering (- 10.2 kcal/Mol per AlCH₃Al-Brücke, [6]) und TMAI dissoziiert bei 130 °C [7].

Der Peak im Intervall 200 bis 400 °C (die Onset-Temperaturen sind 254, 280 und 230°C für respektive TMAI, TEGa, TMIn) markiert exotherme Zersetzung, die dabei freiwerdende Energie ist beträchlich: 1 kJ/g für TMAI, ca. 0.75 kJ/g für TEGa und 1,5 kJ/g für TMIn. Diese Zersetzung wurde für TMGa im Hochvakuum näher untersucht [7,8]. Charakterisch ist hier der C-Ga Bindungsbruch oberhalb 380 °C unter Bildung von Methylradikalen und Dimethylgallium. Durch intramolekularen H-Transfer entsteht Methan. Die

Zersetzung von TMAI und TMIn erfolgt analog, bei TEGa bildet sich durch β -Elimination Äthan.

Im EGA-Experiment (evolved gas analysis, [9]) wurde die Methanbildung bis 270 °C verfolgt. Dazu wurde TMAI bei vergleichbarer Rate wie im DSC-Experiment linear aufgeheizt und die entstehenden Gase in Absorption on-line FTIR-spektroskopisch registriert. Bild 3 zeigt ein solches Thermogramm. Die Methanbildung ist linear und über das gesamte Intervall beobachtbar. TMAI selbst ist bei 270 °C vollständig abgebaut. Die Profile sind in Bild 4 dargestellt. Das von TMAI folgt (reziprok) zunächst dem von Methan, doch nur bis 130 °C. Hier knickt es ab, das Szenario wird komplex.

Die Komplexität äußert sich durch Auftreten von Transienten (854 cm^{-1}), Bandenaufspaltung ($2942, 700, 651\text{ cm}^{-1}$) oder unveränderter Bandenintensität (Intensität der Bande bei 775 cm^{-1} bleibt unverändert bis 150 °C).

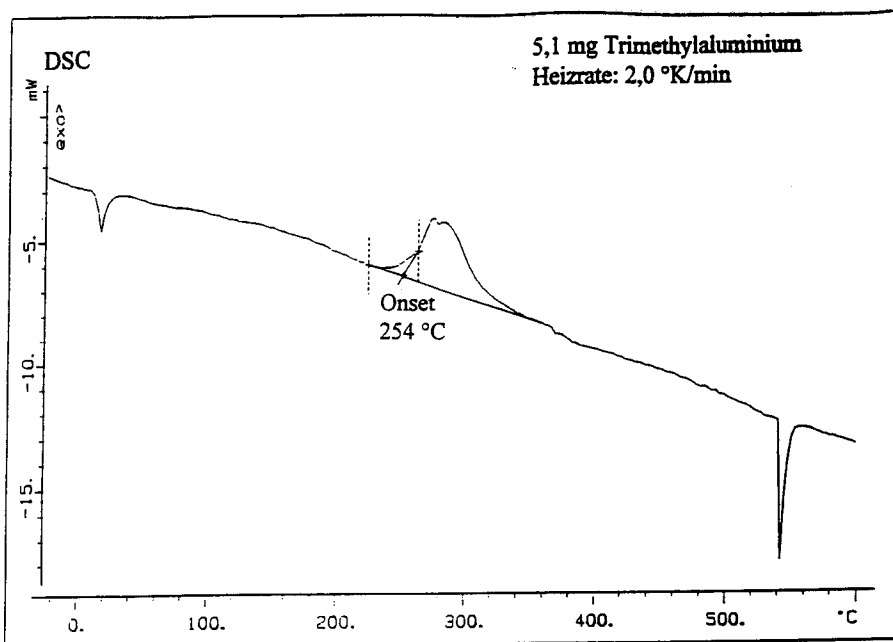
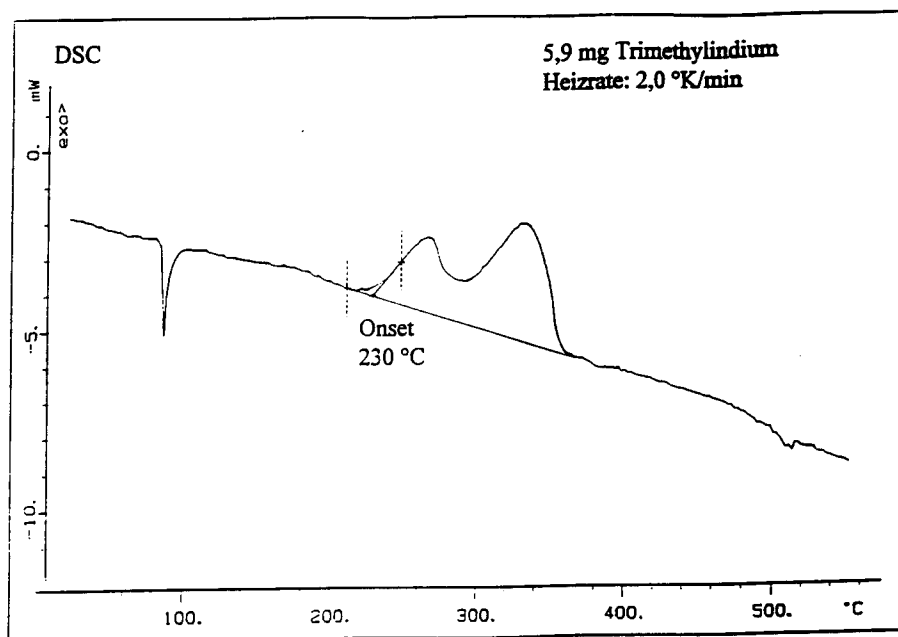
Das IR-Spektrum bei 50 °C stimmt mit den Literaturwerten des dimeren TMAI überein [10, 11]. Die CH₃-Schwingungen dominieren das Spektrum. Dies sind Streckschwingungen ($3000\text{--}2800\text{ cm}^{-1}$), Deformationen ($1260\text{--}1200\text{ cm}^{-1}$) und Rockingdeformationen ($780\text{--}600\text{ cm}^{-1}$). Die Al-C-Gerüstschwingungen liegen unterhalb 600 cm^{-1} im FIR, außerhalb des Detektionslimits unserer Apparatur. Im Unterschied zu den CH₃-Banden sind diese stark symmetrieabhängig und damit sensibel für Veränderungen im Ligandenbereich.

Danksagung

Wir danken der Europäischen Union für ihre finanzielle Unterstützung.

Literatur

- [1] A.C. Jones et al., Routes to Ultra-Pure Alkyls of Indium and Gallium and their Adducts with Ethers, Phosphines and Amines, *Journal of Crystal Growth* 68 (1984) 1.
- [2] D.F. Foster et al., Purification of group III metal alkyls using nitrogen donor ligands, *Chemtronics* 3 (1988) 38.
- [3] A.C. Jones, Metalorganic Precursors for Vapour Phase Epitaxy, *Journal of Crystal Growth* 129 (1993) 728.
- [4] I. Sax, *Dangerous Properties of Industrial Materials* (6th ed.), Van Nostrand Reinhold, New York (1984).
- [5] R. M. Content, Control Methods for Metals and Metalloids in III-V Materials Vapor-Phase Epitaxy, in 'Hazard Assessment and Control Technology in Semiconductor Manufacturing', *Industrial Hygiene Science Series*, Chelsea, Michigan (1989).
- [6] D.B. Chambers, G.E. Coates, F. Glockling, M. Weston, *J. Chem. Soc. (A)* (1969) 1712.
- [7] T.R. Gow, R. Lin, A.L. Backman, R. I. Masel, *Vacuum* 41 (1990) 951.
- [8] D.W. Squire, C.S. Dulcey, M.C. Lin, *Chem. Phys. Lett.* 131 (1968) 112.
- [9] H. Krause, N. Eisenreich, A. Pfeil, *Thermochimica Acta* 149 (1989) 349.
- [10] T. Ogawa, *Spectrochim. Acta*, 24A (1968) 15.
- [11] J.R. Hall, L.A. Woodward, E.A.V. Ebsworth, *Spectrochim. Acta*, 20 (1964) 1249.

**Bild 1: DSC-Diagramm von TMAI****Bild 2: DSC-Diagramm von TMIn**

The graph plots Optical Density (OD) against temperature in Celsius for two compounds: TMAL (1207) and Methan (3016). The x-axis ranges from 60 to 175°C. The left y-axis (0 to 0.45) corresponds to TMAL (1207), and the right y-axis (0 to 0.16) corresponds to Methan (3016). TMAL (1207) shows a decreasing trend, while Methan (3016) shows an increasing trend.

Temperature (°C)	TMAL (1207) OD	Methan (3016) OD
60	0.45	0.00
100	0.30	0.05
120	0.15	0.09
130	0.12	0.10
140	0.10	0.11
150	0.08	0.12
160	0.06	0.13
170	0.05	0.14

Bild 4: Profile der Methanbildung (Bande bei 3016 cm⁻¹) und TMAI-Zersetzung (Bande bei 1207 cm⁻¹)

P86

Thermisches Zersetzungsverhalten von AN/GAP-Mischungen

J. Böhnlein-Mauß, Th. Härdle, Th. Keicher, S. Löbbecke, A. Pfeil, V. Weiser

ICT, Pfinztal, D

Kurzfassung

Die Arbeit charakterisiert den katalysierenden Einfluß des Vanadium/Molybdän-Mischoxides auf die Pyrolyse und das Abbrandverhalten von AN/GAP-Festtreibstoffproben.

The poster characterizes the catalytic influence of the Vanadium/Molybdenum-mixed oxides on the pyrolysis and the burning behavior of AN/GAP-solid propellant samples.

1. Einleitung

Ammoniumnitrat (AN) bietet sich als Oxidator für raucharm abbrennende, wenig empfindliche Treibstoffe an. Der Einsatz ist begrenzt durch

- Phasenübergänge des AN und damit verbundene Volumenänderungen
- geringen Energiegehalt
- schlechte Anzündbarkeit.

Durch Einsetzen von phasenstabilen AN-Typen [1-3], energetischen Bindern wie Glycidylazidpolymer (GAP) und energetischen Weichmachern [4-7] sowie speziellen Abbrandmoderatoren [8,9] erscheinen diese Schwierigkeiten prinzipiell überwindbar. Doch sind die bisher praktisch erzielten Ergebnisse hinsichtlich der erreichten Abbrandgeschwindigkeit und des Druckexponenten begrenzt [9].

Die Arbeiten zeigen auf, daß sich Abbrandgeschwindigkeit und Druckexponent in AN-FTS durch Metalloxide beeinflussen lassen. Von besonderem Interesse sind dabei die Mischoxide des Vanadium und Molybdän (MoVO), da sie die Abbrandeigenschaften verbessern, ohne die Stabilität zu verschlechtern [8].

Die vorliegende Arbeit greift diesen Moderatortypus heraus. Sie charakterisiert dessen Einfluß auf die Pyrolyse und das Abbrandverhalten von AN/GAP-Festtreibstoffproben.

2. Experimente

Eingesetzt wurden Mischungen aus AN und GAP im Gewichtsverhältnis 2:1, wobei GAP mit N100 ($R=0.75$) gehärtet vorlag. Die Mischungen wurden einmal zusatzfrei (AG-00) und zum anderen mit einem katalysierenden Zusatz, hier V-Mo-Oxid (AG-01) und V-Mo-Oxid/Ruß (AG-02), mit einem Gewichtsanteil von jeweils 3% untersucht. Mischoxide dieses Typs wirken bei Verbrennungsreaktionen selektiv oxidativ auf Kohlenwasserstoffe und selektiv reduktiv auf Stickoxide.

Diese Mischungen wurden pyrolytisch in einem thermoanalytischen Reaktor (Evaporated Gas Analysis EGA) [10] und der Abbrand in einer optischen Bombe untersucht [11,12].

3. Ergebnisse und Diskussion

Bild 1 zeigt ein typisches Produktspektrum, wie es von den Mischungen durch den EGA-Reaktor, gekoppelt an ein IR-Spektrometer, erhalten wurde. Die Hauptprodukte sind CO_2 , N_2 , HCN und NH_3 . In Bild 2 sind die zugehörigen Reaktionsprofile für die Spezies CO_2 dargestellt. Die Funktion der Zusätze äußert sich hier durch eine Verschiebung des Reaktionsintervalls nach niederen Temperaturen hin ($\Delta T=40$ K). Weiterhin wurde die Bildung von CO und der Stickoxide NO_2 , NO und N_2O signifikant eingeschränkt. Ein Einfluß der Ruß-Komponente war nicht ausgeprägt. Die Wirkung der katalysierenden Zusätze bei der Verbrennung wurde durch visuelle Veränderungen der Reaktionszonen und deren Temperaturen, sowie durch die Druckabhängigkeit der Abbrandrate und der unterschiedlichen Schlackenzusammensetzung charakterisiert.

Bild 3 zeigt die erzielten Abbrandraten und deren Druckabhängigkeit. Die Kurven folgen dem Vielle'schen Gesetz. Die Zusätze erhöhen deutlich die Abbrandrate und senken signifikant den Druckexponenten (von 0.72 auf 0.55). Dabei ist die Lebhafte bis zu dem Faktor 3 angehoben.

Weiterhin äußert sich die erhöhte Reaktivität der Mischungen mit katalysierendem Zusatz in der veränderten visuellen Erscheinung der Reaktionszonen und deren Temperaturen. Neben einer stabilen Verbrennungsfront auf der Oberfläche mit schnellen, stark exothermen Entgasungsreaktionen bildete sich darüber ein kegelförmiges Gerüst aus Abbrandresten/Schlacken mit langsamer exothermer Umsetzung. Während auf der Oberfläche der additivfreien Probe getrennt reagierende AN-Zentren auftraten, erschien die Abbrandoberfläche der zusatzhaltigen Proben als eine stark leuchtende Einheit mit deutlich erhöhten Temperaturen. Bild 4 vergleicht die berechnete adiabatische Verbrennungstemperatur mit den experimentell gefundenen Werten.

Weiterhin sind die C,H-Anteile der Schlacken dieser Proben gegenüber der additivfreien minimal und bestehen im Wesentlichen aus Metalloxid.

4. Fazit

Reaktionsmechanistisch erhöht Mo-V-Oxid die Geschwindigkeit der primären Reaktionen zwischen AN und GAP. Sie führen insgesamt bei der Feststoffpyrolyse und auf der Abbrandoberfläche zu thermisch niedrigen Reaktionsintervallen, gebündelten Reaktionszentren und erhöhtem Umsatz.

5. Literatur

- [1] B.A. Zentner, M.L. Chan und D.A. Ciaramitaro, Ageing Stability of AN Propellants, Naval Air Warfare Center Division, China Lake/CA, Informal Paper 1992.
- [2] W. Engel, N. Eisenreich, A. Deimling, M. Hermann, M.J. Lorenzo, V. Kolarik, AN, A Less Polluting Oxidizer, 24th Int. Annual ICT Conference, Karlsruhe 1993.
- [3] K.D. Thiel, Verbesserung des Herstellungsverfahrens für phasenstabilisiertes AN, ICT-Bericht 18, 1992.
- [4] A. M. Helmy, AIAA, SAE, ASME, ASEE Joint Propulsion Conference, 23d, San Diego/CA June 29-July 2, 1987, AIAA Paper 87-1725, pp. 11.
- [5] T. Keicher, Darstellung und Eigenschaften von Azidpolyestern mit endständigen Hydroxylgruppen, Wissenschaftliche Schriftenreihe ICT, Band 5, 1993.
- [6] K. B. Brehler, K. Menke, Signaturarme Raketenfesttreibstoffe, ICT-Bericht 5, 1993.
- [7] M.E. Colclough, H. Desai, R.W. Millar, N.C. Paul, M.J. Stewart, P. Golding, Polymers for Advanced Technologies 5 (1994) 554.
- [8] J. Böhnlein-Mauß, K.P. Brehler, K. Menke, Wenig empfindliche Festtreibstoffe, ICT-Bericht 5, 1994.
- [9] P.F.V. Carvalho, G.M.H.J.L. Gadiot, W.P.C. de Klerk, Mechanism of Catalytic Effects On PSAN/HTPB Composite Propellants Burning Rates, 25th Int. Annual ICT Conference, Karlsruhe 1994.
- [10] H. Krause, N. Eisenreich, A. Pfeil, Thermochemica Acta, 149 (1989), 349-356,
- [11] V. Weiser, W. Eckl, N. Eisenreich, A. Pfeil; Untersuchungen zum Abbrandverhalten von PSAN/GAP-Mischungen mit verschiedenen Phasenstabilisatoren; ICT-Bericht 13/93
- [12] W. Eckl, N. Eisenreich; Photographie und Spektroskopie des Abbrandes von Composite-Festtreibstoffen in einer optischen Bombe, ICT-Bericht 10/92

**EXPERIMENTAL STUDY OF DDT IN AN
HETEROGENEOUS EXPLOSIVE COMPOSITION**

D. LEMOINE, L. GAUTIER, H. CHERIN, R. BELMAS

COMMISSARIAT A L'ENERGIE ATOMIQUE

Centre d'Etudes du Ripault

B. P. n ° 16

37260 MONTS (FRANCE)

ABSTRACT

Thermal test results allow us to identify the key-phenomenons governing combustion-to-deflagration-to-detonation transition in an HMX pressed composition. A simple, but efficient, model is developed on the basis of these results.

INTRODUCTION

Most of the published studies devoted to DDT deal with powdered low density explosives. Comprehensive analyses and efficient models have been developed in this area. Published results on DDT in explosive compositions are far more scarce.

The study presented here deals with DDT phenomenon in a pressed HMX composition.

Violent reactions have been observed when this composition is heated to a sufficiently high temperature, under strong confinement.

The aim of our work was to identify the physical mechanisms governing the transition from regular laminar burning to deflagration and, in some cases to detonation.

1. THERMAL TESTS

1.1. Closed bomb combustion (see figure 1)

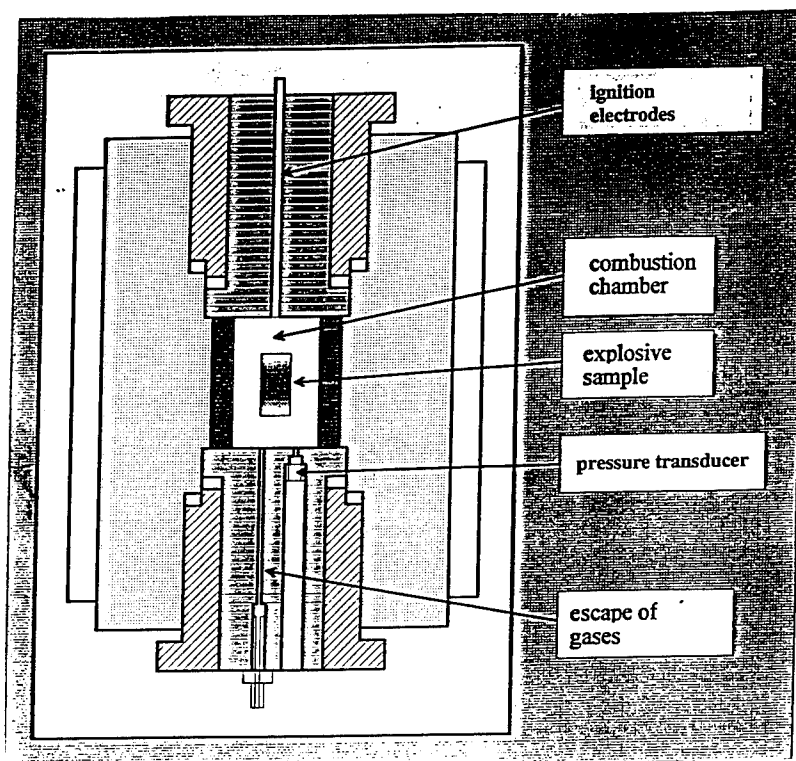


Figure 1

Several tests were performed on HMX (X1) and TATB-HMX (TX1) compositions with different loading densities Δ (Δ is the ratio of the sample volume and of the combustion chamber volume).

The pressure profiles $P(t)$ were recorded as a function of time and the pressurization curves $\frac{dP}{dt} = f(P)$ were plotted (see figure 2).

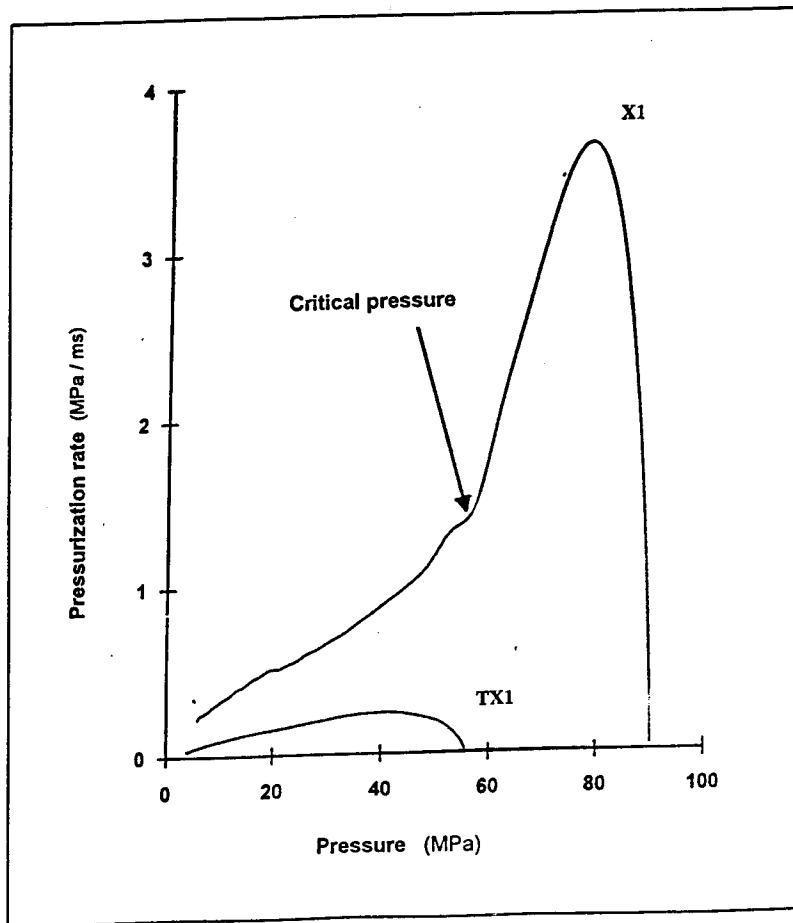


Figure 2

We can notice that the TX1 curve is perfectly regular, indicating that the combustion is normal and laminar, and that the explosive sample decreases in size when burning but remains cylindrical. This point was verified by interrupting the test at different times and observing the partially burnt samples.

At the opposite, the X1 curve shows a critical pressure P_c by 50 MPa. Below this value, the composition burns normally. Above this pressure, an abnormal combustion develops, leading to high pressurization rate. This rate increases very fast with the loading density (see figure 3) and it is obvious that, for high values of Δ , the abnormal combustion will result in a compressive wave in the explosive.

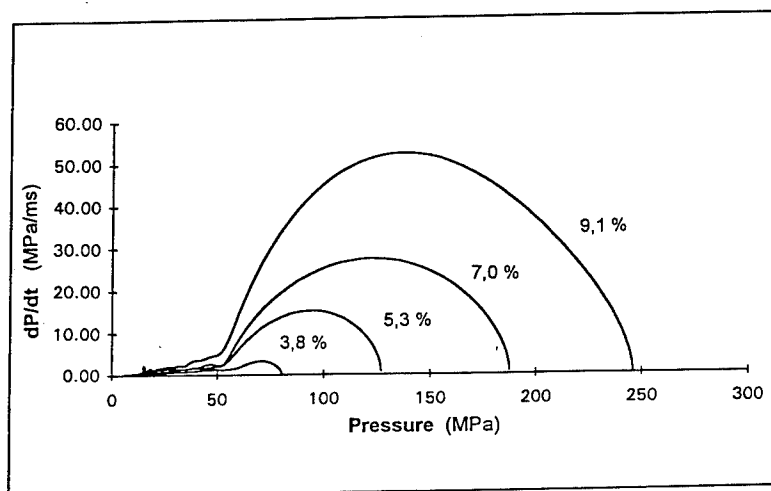


Figure 3

1.2. Confined thermal induction test (see figure 4)

A strongly confined cylindrical explosive sample is heated by a heating plate, the temperature of which rises linearly with time at 3°C/s . Thermocouples are implemented in the explosive and the decomposition gases pressure is measured inside the vessel.

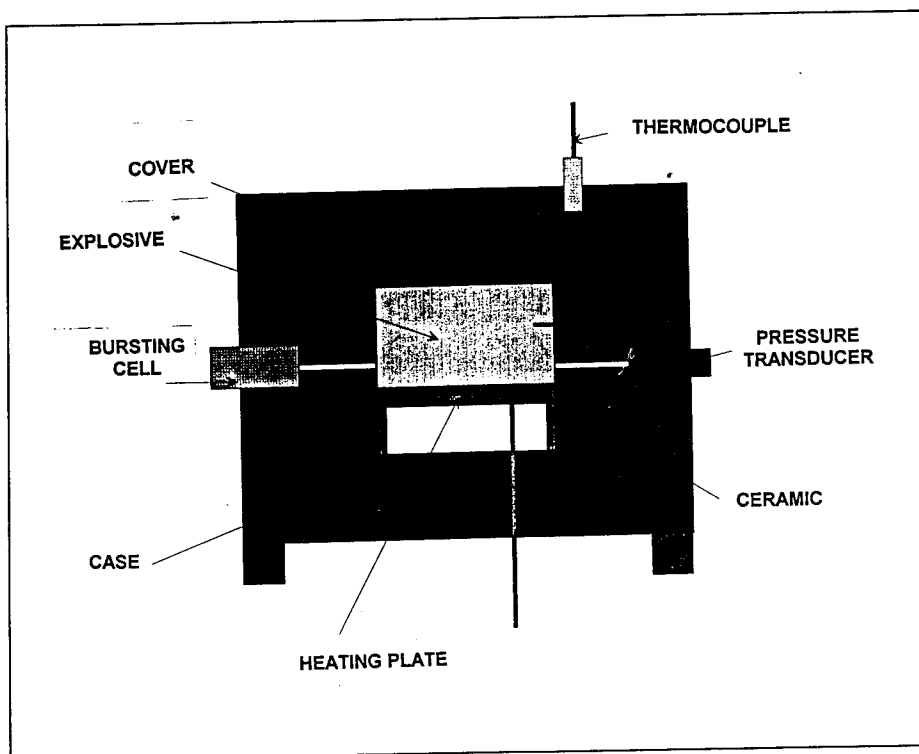


Figure 4

Detonations issued from DDT are observed when X1 ignites.

On the contrary, only pneumatic explosions and case ruptures are obtained with TX1.

The $P(t)$ measurement (figure 5) shows, for X1, a very important phenomenon. After X1 ignition, the pressure rises slowly as the gases diffuse in the gaps and dead volumes. Then, the pressure rate grows with the pressure and, consequently, the burning velocity increases.

At this point, a very sharp pressure rise is observed when the explosive pressure reaches 50 MPa. This value is to be compared to the critical pressure value observed in closed bomb experiments.

87 - 6

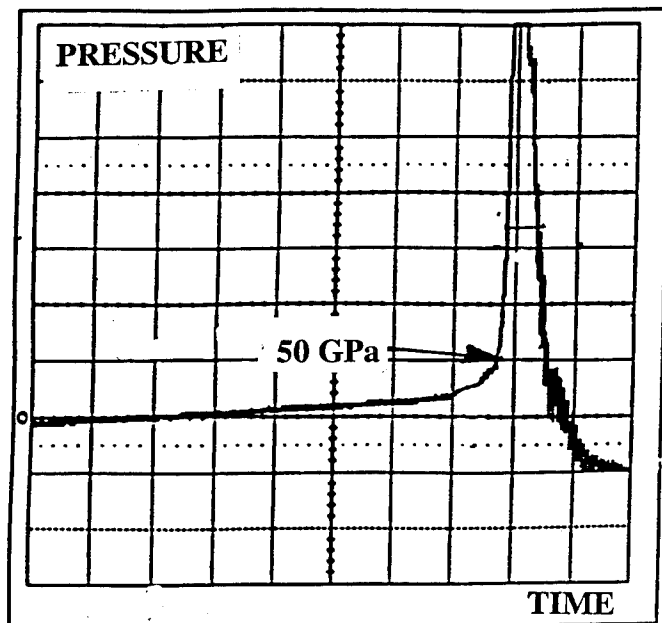


Figure 5

2. DDT MECHANISM

The physical DDT mechanism deduced from the previous results is as follows.

- 1) The explosive experiments laminar combustion with relatively slow pressure and burning velocity increases.
- 2) The pressure reaches the critical value and the combustion becomes abnormal.
- 3) A sharp pressure rise is generated in the explosive, resulting in a compressive wave formation and, in some cases, in a shock wave, depending on experimental set-up geometry and case strength.

- 4) The compressive and shock waves produce micro structural hot spots leading to a partial or total SDT process, depending on sample and case geometries.

3. MODELLING

The key phenomenon previously identified is the sudden sharp pressure rise taking place for pressures above the critical value.

As a result, an efficient modelling must accurately describe the laminar and abnormal combustion and the decomposition gases thermodynamic behaviour.

3.1. Combustion modelling

Below the critical pressure, the burning velocities measured with the strand burner and the closed bomb (assuming, in this case, a regular regression of the sample) are equal (see figure 6).

Above this pressure, the burning area increases, due to sample fragmentation or similar phenomenon.

Thus, the apparent burning velocity determined with the closed bomb results is far higher the actual velocity as can be deduced from strand burner measurements (figure 6).

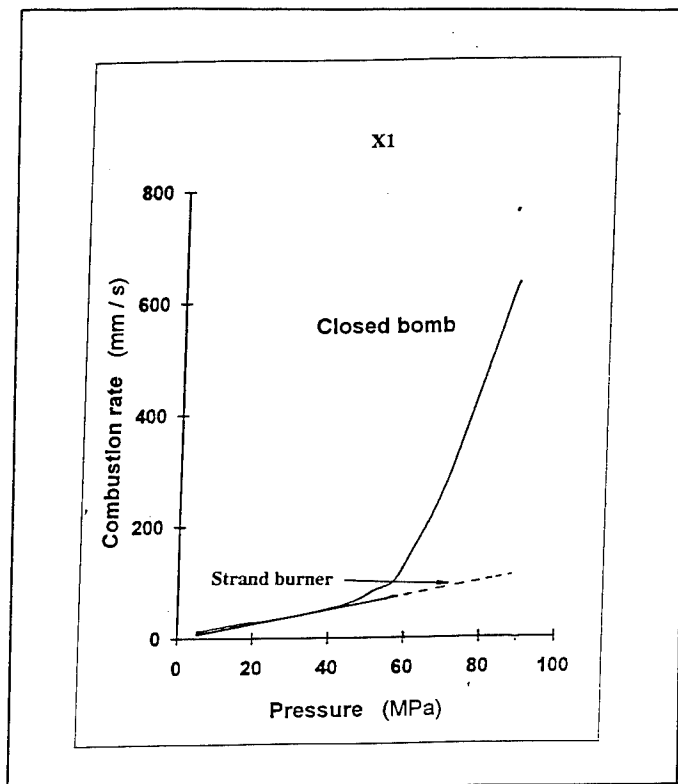


Figure 6

This is due to the fact that the conservation of the cylindrical geometry is no more valid above P_C .

However, from a pure modelling point of view, the results (energy release, pressure rise) are the same if we consider a decreasing cylindrical sample with an apparent burning velocity.

This convenient modelling strategy has been chosen for our simulations.

The burning velocity is then calculated using two power laws : $V_C = a_i P^{b_i}$ where a_i and b_i are different below and above P_C .

3.2. Gases EOS

We use the second order virial EOS :

$$PV = nRT \left(1 + \frac{B(T)}{V} + \frac{C(T)}{V^2} \right)$$

Where : V is the gases volume,

R is the perfect gases constant,

T is the temperature,

n is the number of gases moles,

B and C are coefficients depending only on temperature and gases compositions.

3.3. Energy equation

It is given by :

$$\Delta U = \Delta W + \Delta Q, \text{ with } \Delta W = - \int_1^2 P dV \text{ and } \Delta Q = \Delta H^r (m_1 - m_2)$$

where : U is the internal system energy,

ΔW is the mechanical work,

ΔQ is the heat released by the combustion,

ΔH^r is the heat of reaction,

m is the released mass of gases.

3.4. Additional assumptions

The case is supposed to be adiabatic and keeping constant internal volume.

3.5. Comparisons with experiments

Several comparisons are presented on figures 7 and 8, where are plotted respectively :

87 - 10

- $P_m/\Delta = f(P_m)$, where P_m is the maximum pressure obtained in a closed bomb test for a given Δ ,
- $\frac{dP}{dt} = f(P)$ for several loading densities.

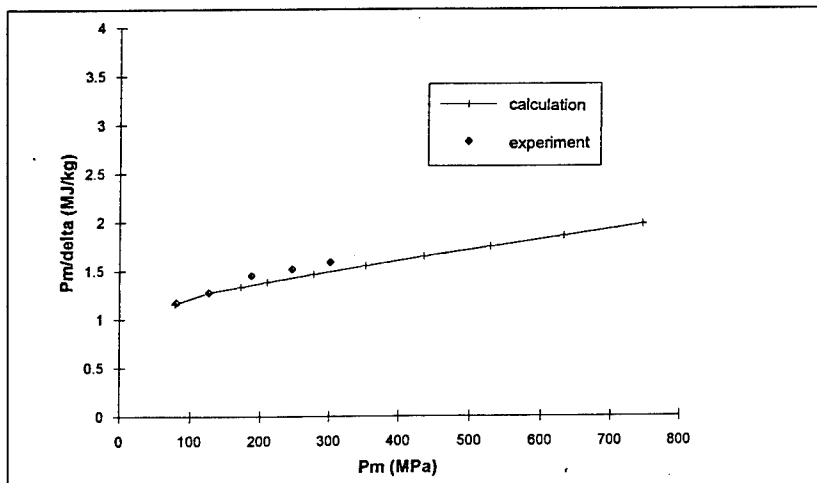


Figure 7

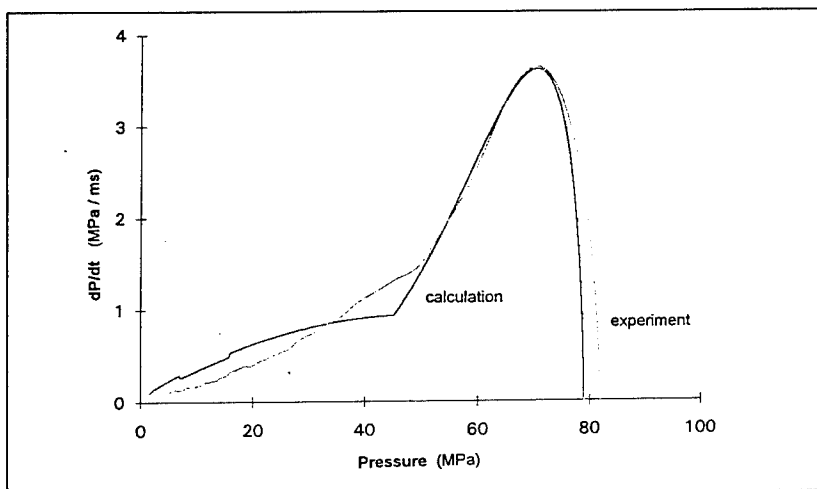


Figure 8

We obtain a very good agreement which validates the model.

CONCLUSION

We have identified that abnormal combustion and resulting sharp pressure rise are the key phenomenons governing DDT in X1 composition.

A modelling of these phenomenons has been developed and agrees well with experiments.

The next step will be the junction of the combustion model and of an hydrodynamic code, in order to analyse the compressive and shock wave formations and the resulting SDT.

Investigation of Thermal Decomposition and
Impact Sensitivity of Pyrotechnic Mixtures

W. Li F. S. Niu S. H. Jin Y. X. Hu Q. C. Song

Beijing Institute of Technology
College of Chemical Engineering and Materials Science
P. O. BOX 327, Beijing, 100081, P. R. C.

ABSTRACT

A study has been made of the thermal decomposition and impact sensitivity of mixture of KNO_3 with potassium o-hydrogen phthalate, sodium salicylate and benzoate respectively. Kinetic data of thermal decomposition of these mixtures demonstrate that under high temperature (for example 1000K) the rate constants k are quite different and the value of k for sodium salts are obviously higher than that of potassium salt. But the impact sensitivity of mixtures mentioned above is similar. From the view of point of hot spots theory, data of thermal decomposition are not consistent with impact sensitivity. It is desired to study these problems in more details.

INTRODUCTION

Whistling agent (WA) is one of the important ingredient in pyrotechnic compositions. The impact sensitivity of its mixture with oxidant KNO_3 is of great interest for designing pyrotechnic compositions, but studies on it have been limited^[1]. In the present paper, a study has been made of thermal decomposition and impact sensitivity of mixtures of WA (including potassium hydrogen phthalate PHP, sodium benzoate SB,

sodium salicylate SS) and KNO_3 . The dynamic stress under impact of these mixtures has been determined for understanding the role of mechanical behavior for these mixtures under impact.

EXPERIMENTAL

The drop-weight sensitivity of all samples were determined using a KAST impact apparatus fitted with a 5kg hammer. The test samples each weighed $50 \pm 2\text{mg}$, and the results were obtained by performing a minimum of 25 trails in accordance with the Bruceton procedure. The thermal decomposition properties were assessed using PCR-1 DTA.

RESULTS AND DISCUSSION

The determination of formal chemical kinetic parameters of thermal decomposition of mixtures of WA and KNO_3 have been made using differential thermal analysis technique (DTA). The DTA data have been calculated with the help of equation of Kissinger H. [2] and Ozawa T. [3]. Table 1 illustrates the data of apparent energy activation values (E) and preexponential factor (A).

Table 1 Formal kinetic data of thermal decomposition of mixtures KNO_3 -WA

Samples	E/kJ \cdot mol ⁻¹	lgA	k _{725°C}
PHP	229.69 \pm 0.84	14.2	1.60 \times 10 ²
SS	150.74 \pm 1.27	12.2	2.16 \times 10 ⁴
SB	483.71 \pm 6.25	28.33	1.15 \times 10 ¹¹
PHP- KNO_3	130.44 \pm 2.68	8.66	6.94 \times 10 ¹
SS- KNO_3	161.67 \pm 0.34	15.10	4.56 \times 10 ⁹
SB- KNO_3	270.03 \pm 0.60	18.36	1.79 \times 10 ⁴

The data in Table 1 show that there is difference between kinetic properties of these mixtures. The biggest value of E is 488.7 kJ/mol for SB, and the smallest one is 150.7 kJ/mol for SS. All the values of E for mixtures are lower than that of WA alone. For example, E of SB-KNO₃ is 0.56 times of SB, E of PHP-KNO₃ is 0.58 times of PHP. The value of E for SS-KNO₃ is somewhat larger than that of SS alone. The difference between the reaction rate constants k under 726°C is great for these three mixtures and the values of mixtures ranked in increasing order are as follows: $k_{SS-KNO_3} > k_{SB-KNO_3} > k_{PHP-KNO_3}$.

The results of critical height H_{50} of these mixtures are listed in Table 2.

Table 2 Critical height of WA-KNO₃ mixtures (5kg hammer)

Samples	H_{50}/cm		\bar{H}_{50}/cm
	NO.	1. 2.	
PHP-KNO ₃	76.4	72.1	74.3 ± 2.2
SS-KNO ₃	64.3	74.6	69.5 ± 5.2
SB-KNO ₃	65.9	73.6	69.8 ± 3.9

It has been demonstrated that the impact sensitivity of mixtures is quite similar and almost as the same as tetryl, but obviously lower than that of KClO₃ mixtures^[4-6]. Comparing the data illustrated in Table 1 and Table 2, it can be found that the H_{50} values of PHP-KNO₃ with the smallest $k_{726^\circ\text{C}}$ is 5 centimeters higher than the others. However, for the other mixtures there is some contradiction between thermal decomposition parameter $k_{726^\circ\text{C}}$ and H_{50} . The $k_{726^\circ\text{C}}$ value of SS-KNO₃ is bigger than that of SB-KNO₃, but their impact sensitivity are in the same level. Therefore, it is necessary to investigate the dynamic stress of mixtures under impact for understanding this result.

Table 3 illustrates the results of determining dynamic stress using stress-determining system^[7].

Table 3 Dynamic stress of WA-KNO₃ mixtures

Samples	σ /kN			$\bar{\sigma}$ /kN
	NO. 1.	2.	3.	
PHP-KNO ₃	26.4	23.6	22.4	24.1±1.5
SS-KNO ₃	26.0	25.6	23.6	25.1±1.0
SB-KNO ₃	20.4	20.4	23.6	21.5±1.4

The data listed in Table 3 show that under the same impact condition the maximum stress produced in these three mixtures are almost similar. It means that the possibility of the generation of hot spots in these mixtures are quite similar. And, the difference between their impact sensitivity is not large. But it is different to find out any simple correlation between $k_{726}^{\circ}\text{C}$ and H_{50} . This suggests that the influence of thermal decomposition of mixtures on their impact sensitivity is complicated, especially, for SS-KNO₃ and SB-KNO₃.

CONCLUSION

The PHP-KNO₃, SS-KNO₃ and SB-KNO₃ have similar impact sensitivity and dynamic mechanical properties. But the thermal decomposition properties of these three mixtures are different. Data obtained from the experiments show that it is difficult to find out a simple correlation between the $k_{726}^{\circ}\text{C}$ and H_{50} for WA-KNO₃ mixtures, but the $k_{726}^{\circ}\text{C}$ has somewhat effect on its impact sensitivity. The impact sensitivity of pyrotechnic samples is determined by their chemical kinetic behaviors and dynamic behaviors under impact.

REFERENCES

1. Hu Yuxiao Personal communication, 1992.
2. Kissinger H.E. Anal. Chem. 1957, 29, 1702-1707.
3. Ozawa T. Bull. Chem. Soc. Japan. 1965, 38, 1881-1886.
4. Song Quancai, Hu Yuxiao. "An investigation of impact sensitivity of some pyrotechnic compositions" Proc. of explo., propellants soc. China, 1990 (in Chinese).
5. Huscain G., Rees G.J. Propellants, Explosives, Protechnics, 1990, 15: 43-47
6. Oztap Selcuk. Pyrotechnica, 1990, 13: 19-21. CA. Vol115 11864d
7. Song Quancai, Wei Huazhen. Explosion and Shock Waves, 1990, 10 244-248. (in Chinese).

The Dounreay-Silver-II-Process and Its Industrial Application for the Disposal of Pyrotechnic Materials

Jörg Hedtmann

SubSea Offshore Ltd.

- Environmental Technologies Division -

Greenwell Base, Greenwell Road

Aberdeen AB1 4AX

Scotland

ABSTRACT

Pyrotechnic materials can, when disposed of in the conventional ways of incineration and open pit burning, release environmentally hazardous and toxic products. This is mainly due to their organic contents, namely the organo-halides.

In addition, due to contamination and degradation of the materials, they become increasingly unstable with age, making the handling of old pyrotechnics dangerous for personnel and equipment. In this aspect, pyrotechnics by far outweigh other explosives. In some old contaminated sites pyrotechnics can be found mixed with munitions of any kind, adding a further hazard to their disposal.

The Dounreay-Silver-II-Process has been successfully applied to destroy a wide range of organics, including high explosives, chemical warfare agents and industrial toxic compounds, either individually or in a mixed feed, making it very versatile. Silver-II additionally has proven itself for the destruction of the compound containing hardware, as demonstrated with the destruction of a simulated rocket body filled with VX and DNT. It thus can significantly reduce the need for the handling of unstable products and the hazards emanating from delaboration procedures.

These facts make the Dounreay-Silver-II-Process a very promising candidate for the disposal of pyrotechnics, too, especially in a mobile plant configuration. The solution can thus be brought to the problem.

The presentation will explain the principle chemistry behind Silver-II, highlight some of the experiments, which were conducted with military products and finally demonstrate the concept of a mobile plant as envisaged for the safe and uncomplicated disposal of organic compounds, including pyrotechnics.

1. Introduction

Pyrotechnics which can no longer be used because they are stored longer than their safe storage life permits, or which have been stored in improper conditions, or which are recovered during the course of a remediation project, have to be disposed of. The choice of disposal method is usually restricted by safety and environmental impact considerations as laid out in the respective regulations for health and safety and environmental compliance. The priority, however, is the removal of a risk posed by those materials, as deteriorating pyrotechnics can become highly unstable. Here they often exceed the danger potential of explosives. A suitable disposal method has therefore to be chosen that ensures that pyrotechnics can be destroyed safely and without unlawful pollution of the environment.

Amongst other methods those which have been popular in the past are controlled open-air combustion and incineration or recycling of the pyrotechnic compounds. Both methods have their problems:

1.1 Open-Air Combustion:

Pyrotechnics by their very nature emit light, sound, and smoke. As these emissions themselves are not environmentally friendly, their by-products often pose a substantial hazard. However, there is a tendency now to develop environmentally benign pyrotechnic charges. The open-air combustion of the materials or the controlled explosion (at least for the foreseeable future) can therefore be ruled out as an environmentally acceptable option.

1.2 Incineration or Recycling of the Pyrotechnic Compounds:

In order to recycle pyrotechnic materials they have to be extracted from their container in a delaboration stage. As mentioned above, very often these old pyrotechnics become unstable and thus unpredictable. They can be set off by physical handling or machining, causing damage and injuring personnel. Thus, even lengthy transports to specialised facilities become problematic, especially on the over crowded road systems of central Europe.

When considering incineration one has to bear in mind that a number of substances used in pyrotechnic charges demand special waste incinerators to prevent the forming of toxic by-products, such as dioxins and di-benzo-furanes in the case of some organic mixtures. But even in circumstances, where the incineration technology is appropriate, the "psychology of incineration", e.g. its influence on public perception could make the operation difficult, lengthy and thus costly.

A possible solution should exclude any of these disadvantages and should preferably also minimise transport and handling of these hazardous products. One solution for pyrotechnics containing organics is the Dounreay-Silver-II-Process.

2. The Dounreay-Silver-II Process

2.1 The Process Development

The Dounreay-Silver-II-Process was developed by the U.K. Atomic Energy Authority (AEA) and was originally targeted at destroying radio-active contaminated organic wastes from the re-processing of spent nuclear fuel (Tributyl-Phosphate / Odourless Kerosene). In the development stage it was soon realised that this process could be applied to a wide range of organic compounds and a large number of organics have since been successfully destroyed in a pilot plant at the AEA-facilities in Dounreay, Scotland.

As the very nature of the process allows the safe handling and destruction of military compounds, external tests were conducted, destroying a number of explosives and propellants, and recently, chemical warfare agents. These experiments shall be described to explain the attractive features of the Silver-II process.

2.2 Process Description

The process utilises Silver in its 2+ oxidation state, which is one of the strongest oxidising agents. The whole process takes place in a strong nitric acid environment. Ag^{2+} -ions are generated within an electro-chemical cell similar to those used in the chlorine manufacturing industry. The cell is divided by a fluoropolymer cation exchange membrane (typically Du Pont Nafion 324) to prevent mixing of the anolyte and catholyte. This membrane has shown excellent chemical resistance in this highly oxidising and strong acid process environment, however, its ion exchange properties are not utilised in this process.

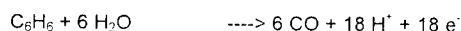
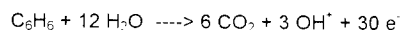
The anode is coated with platinum whereas the cathode is composed of stainless steel.

The cell assembly is a standard electrolyser, internally manifolded, resulting in a minimum number of external process connections. This eases maintenance and results in higher reliability. The cell design has proved reasonably tolerant of solids contained in the waste streams and particulate sizes of up to 1 mm have not shown to cause any problems of membrane fouling or blockage. This is also an important aspect when treating waste materials.

In nitric acid solution Ag(II) exists as AgNO_3^+ , a dark brown complex. Its reaction with organics takes place by a number of mechanisms, one of which is the formation of highly reactive OH and NO_3 radicals with the water. Ag(II) also reacts directly with many organic molecules, often forming radicals as intermediates.

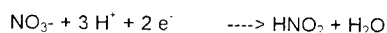
When the organic feedstock is added to the anolyte solution the dark brown Ag(II) colour disappears quickly, indicating a relatively low concentration of AgNO_3^+ in the solution. As a result of the ongoing oxidation of the organics, carbon monoxide and carbon dioxide are formed, along with a number of inorganic products from any hetero-atoms which might have been present. The oxygen in the carbon oxides arise from the water molecules in the anolyte.

The overall process can be described as follows, using the benzene oxidation as an example:



High efficiencies (80% to 90%) were achieved by Ag(II) oxidation of some saturated hydrocarbons at an anode current density of 10 kA/m^2 . Usually, however, the current density is restricted to 5 kA/m^2 or less to avoid exceeding the limiting data of the membrane.

The catholyte solution is of similar composition as the anolyte, however, due to migration of Ag^+ and H^+ ions through the membrane, the Silver concentration in the catholyte is somewhat higher as in the anolyte. The main reaction at the cathode is the reduction of nitric acid to nitrous acid:



The nitrous acid decomposes further to form nitrous oxides (NO_x), which, together with the HNO_2 can be regenerated to form nitric acid.

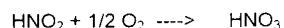
2.3 An Integrated System

Figure 1 shows the simplified block diagram of the process. The process can run continuously or in a batch configuration without altering a great number of details. The

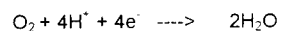
organic feedstock, i.e. the waste to be destroyed is added to the anolyte circuit in a suitable format, e.g. shredded to a particle size less than 1mm (however, this is not necessary at the expense of time). Water is added to compensate for the loss of water in the reaction i.e. through the formation of CO and CO₂ and the migration of H⁺ ions through the membrane. The CO and CO₂ is fed through a scrubbing system in order to prevent acid fumes, residual organic species etc. to vent into the atmosphere.

On the cathode side of the process the catholyte solution is fed through a reflux column to recycle the nitrous acid into NO_x and nitric acid. In addition, air is used to oxidise the NO_x to NO₂.

This reaction can be described as :



The thus regenerated nitric acid is fed back into the catholyte circuit or held in a storage tank. At the same time water is formed at the cathode by the reaction.



The hydronium ions consumed in this reaction are those generated in the oxidation of the organic in the anolyte and the subsequent migration of those ions through the membrane. The surplus water thus generated must be distilled off from the catholyte and can either be discharged or recycled as make-up water for the organic feed stock in the anolyte circuit. The added advantage of this reaction is, off course, that no hydrogen is allowed to form, which could pose a hazard to the operation of a Silver-II plant. The concentration of organic feed in the water can be varied over a wide range, allowing for great flexibility in the water flow and the associated plant lay-out.

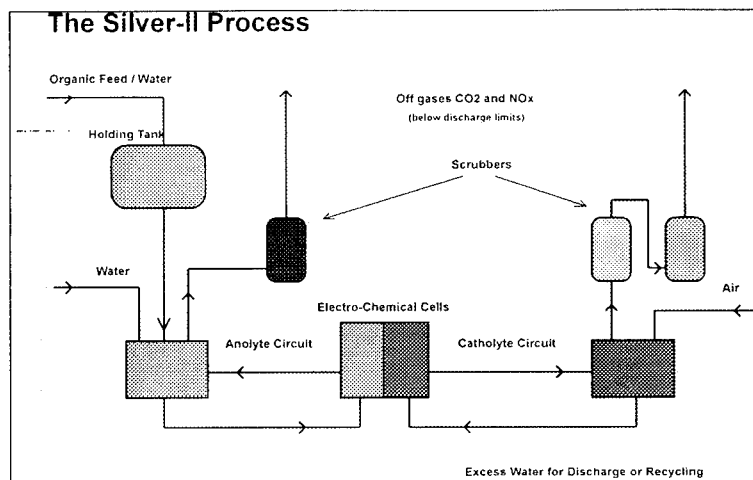


Figure 1: Simplified Process Flow Diagram

2.4 Application of the Process

There is an ever extending range of organic materials being tested in the process, including aliphatic and aromatic hydrocarbons, phenols, organo-phosphorus compounds, organo-sulphurous compounds, chlorinated aliphatic and aromatic compounds, including PCB's (see table 1). A list of some of the destroyed substances is attached. As this list can obviously never be complete, it does, however, give a good indication of the practical application of the process. Substances known to be ineffectively destroyed, are certain plastics and silicon-lubricants.

The efficiency of the process is usually very high, can be determined from measuring the CO + CO² production and comparing it with the values obtained from theoretical calculations based on the cell current. If the efficiency approaches 100%, a small amount of NO_x is often produced from the anolyte, suggesting the involvement of nitric acid in the oxidation of the organics. The loss of nitric acid is, however, very small as the reduction products from the nitric acid are very quickly re-oxidised in the very oxidising anolyte.

Aliphatic

- Kerosene (C12 to C16 hydrocarbons)
- Tributyl Phosphate (TBP)
- Dodecane
- Octanic Acid
- Tri-Ethanol-Amine
- Butanol
- mixed Aliphatic Amines
- 2-Chloroethyl-Ethyl-Sulphide
- 2-Methoxy-Ethanol
- Di-Methyl-Formamide
- Methanol
- Chloroform
- Isopropanol
- Methylene Chloride
- Tetra-Hydrofuran
- Dioxan

Aromatic

- Phenol
- Toluene
- Xylene
- Tri-Tolyl Phosphate
- Di-Nitro-Phenol
- Chlorobenzene
- Tri-Chlorobenzene
- Nitrosobenzene
- Chloro-Fluoro-Benzoic Acid (CFC)
- p-Toluene-Sulphonic Acid
- mixed PCB isomers

Explosives, Propellants and Chemical Warfare Agents

- Nitroglycerin
- DEMEX
- Nitrocellulose
- Nitroguanidine
- RDX
- Agent GB (Sarin)
- Agent VX
- Agent GA (Tabun)
- Agents HD, HT, THD (Sulphur Mustard)
- SDG3 (Decontamination agent)
- Decon 90 (Decontamination agent)
- DNT
- TNT
- m-Nitro-p-Toluidine

Table 1: Substrates Successfully Destroyed using the Silver-II-Process

2.5 Inorganic Hetero-Atoms

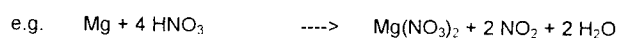
Pyrotechnics are a combination of:

- organic compounds containing atoms of inorganic elements (e.g. phosphorous, sulphur)
- reactive metals, e.g. magnesium
- metal oxides, e.g. titanium oxide
- metal nitrates
- metal chlorates
- other compounds.

Sulphur and phosphorous do not interfere with the process, if their concentration in the anolyte is kept limited. The inorganic component is oxidised to the mineral acid cation, e.g. nitrogen to nitrate ions, phosphorous to phosphate ions, chlorine to chloride ions etc.

In the case of metals, or their oxides, salts or complexes etc. these usually become dissolved in the hot nitric acid and the strong oxidising conditions. These metals are then transformed to their highest oxidation state. The presence of these species has not been found to interfere with the process, on the contrary: in cases, where the metal in its highest oxidation state is an oxidant itself (e. Mn, Cr, etc) it becomes beneficial for the process.

However, the concentrations in the anolyte must not be allowed to become excessive. Hydrogen would not be formed in this reaction.



Titanium oxide will not react with the nitric acid. Also, being in its highest valency state, it will not be oxidised by the Silver-II process. It is expected that titanium oxide will remain unreacted after exposure to the Silver-II process.

Metal nitrates and metal chlorates will dissolve in the anolyte solution. The chlorate ions may be oxidised to their highest oxidation state (perchlorate ions) and would not be reduced to chloride gas.

3.0 Practical Tests

3.1 Explosives and Propellant

A number of experiments were carried out by AED to assess the suitability of the Dounreay-Silver-II-process for the destruction of explosives and propellants. They are summarised below:

The experience with the destruction of a great variety of compounds gave no indication, why explosives should not be successfully destroyed in this process. Explosives and propellants by their very nature are reactive and as an added benefit, their production is usually facilitated using highly concentrated nitric acid, which is also one of the process consumables.

As indicated above, the process can cope with large amounts of water in the feed-stream, thus making it well suited to process materials which have been extracted from shells utilising steaming or water-jetting technologies

This feature would also allow the treatment of the highly bio-toxic pink and red water emanating from the manufacture of explosives. The discharge from the Silver-II-plant, however, could directly be discharged without detrimental effects on the environment.

3.1.1 The Experiments

Table 2 summarises the experimental conditions during the destruction of three explosives and one triple base propellant. The cell used was a flanged 'H'-cell configuration with the anolyte and catholyte compartments separated by a Nafion 324-ion exchange membrane.

After pre-heating the anolyte to ca 80-85°C a current was passed through the apparatus to generate Ag^{2+} . 5g of the substance under test was then added to the dark brown solution. This dark colour faded during the process and it was this change in colour that was taken as a qualitative measure for the completion of the reaction. The analysis of the anolyte solution used for the four runs showed a TOC (total organic carbon) - content of 200 ppm.

The compounds to be tested were:

- a) RDX
- b) TNT
- c) DEMEX 100 (plastic explosive)
- d) Triple Base propellant (50% nitro-guanidine
25% nitro-cellulose and
25% nitro-glycerine)

Anolyte:	8M HNO_3 / 0.5 M AgNO_3
Temperature:	80-90 degrees C
Anode:	Platinum Foil, 10 cm^2
Catholyte:	12 M HNO_3
Temperature:	60 degrees C
Cathode:	Stainless Steel, 10 cm^2
Sample Size:	5 g, all added at start of run
Gas Analysis:	Varian 3400 gas chromatograph Poraplot Q column, 30 m x 0.32 m ID Finnegan ITD 800, direct coupled Bio Rad S600 FTIR spectrophotometer 10 cm gas cell, NaCl plates
TOC Analysis:	Ionics 555 TC analyser

Table 2: Experimental Details, Explosives Destruction

3.1.2 Summary of Results:

As limited, small scale batch trials, these experiments were designed as "proof-of-principle". They have, however, conclusively shown that Ag(II) - electrochemical oxidation can effectively destroy a variety of explosives and a triple base propellant. There have not been any extra-ordinary observations during the experiments, the substances used behaved similar to other, moderately reactive compounds.

During the destruction of nitramine explosives considerable amounts of N_2O were produced. No volatile organic compounds were detected in the off gases.

There have been no observations of any violent or adverse reactions at any stage and no other nitrogen oxides but N_2O were produced.

3.2 Chemical warfare Agents

Further "proof-of principle" experiments were performed at CBDE, Porton Down, under the auspices of AEA. These test involved the destruction of a number of chemical warfare agents, namely :

- a) agent GA (Tabun)
- b) agent GB (Sarin)
- c) agent VX
- d) pure S-mustard
- e) weapons grade S-mustard
- f) thickened S-mustard (Zäh-LoSt)

In a further experiment a model M55-rocket (aluminium-shell) was destroyed, containing VX and DNT.

The experiments were conducted in a test-rig constructed by AEA Technology at Dounreay. It was based on a standard ICI FM 01 electro-chemical cell. For the commissioning phase simulants with a similar structure to the compounds under study were used (TBP, DNT).

CBDE personnel provided the agents and the subsequent analysis.

3.2.1 Destruction of Pure Agents

The agent was oxidised to carbon dioxide, carbon monoxide, mineral acids and protons. The silver I in the anolyte solution was recycled through the electrochemical cell to continuously regenerate silver II ions.

The anolyte offgas composition was measured throughout the experiment and used, along with the offgas flowrate and cell current, to calculate the electrochemical efficiency of the Silver II process of the destruction of each agent. The electrochemical efficiency is a measure of the amount of current required to destroy the agent and does not reflect the final level of organic destruction which can be achieved.

The anolyte offgas also contained varying levels of nitrous oxide and volatile organic alkyl nitrates.

The protons formed in the anolyte by the destruction of the chemical agents were transferred to the catholyte as part of the electrochemical process. The protons were consumed in the nitric acid reduction and formed water, they did not combine to form hydrogen.

The gaseous reaction products from the oxidation of the agents destrained in the anolyte vessel and passed through a -10 C condenser to remove any volatilised agent, water vapour, acid vapour etc. The dried gas then passed through a flowmeter before being passed through a sodium hydroxide scrubber and discharged. The purpose of the sodium hydroxide scrubber was to remove any agents which may have passed through the condenser.

The anolyte nitric acid and sodium hydroxide solutions were sampled at regular intervals throughout the experiment. The catholyte nitric acid and sodium results show that the organo-phosphorus agents could not be detected by the analytical instrumentation by the end of the first hour of the experiment. Traces of the S-mustard agents were still present at the end of the second hour but were undetectable by the end of the experiment.

3.2.2 Experiments simulating destruction of M55 rockets

The M55 rocket was simulated by sealing a mixture of VX and DNT in a small aluminium capsule. The simulated aluminium capsule was placed into the anolyte solution and dissolved so that the VX and DNT were exposed to contact with the anolyte solution.

The agent and DNT were totally destroyed by the action of the Silver II process. These experiments were carried out with the anolyte temperature controlled at 50°C and 90°C.

3.2.3 Experimentation Results

The peak carbon-basis electrochemical efficiencies for the destruction of the various agents are shown below:

a) Tributyl phosphate at 90°C	71%
b) Tributyl phosphate at 50°C	72%
c) Agent GA (Tabun) at 50°C	41%
d) Agent GB (Sarin) at 50°C	62%
e) Agent VX at 50°C	47%
f) Agent HD (distilled S-mustard) at 50°C	87%
g) Agent HT (weapons grade G-mustard) at 50°C	77%
h) Agent THD (thickened S-mustard) 50°C	40%
i) TBP simulant M55 rocket at 50°C	32%
j) VX simulant M55 rocket at 50°C	40%
k) VX simulant M55 rocket at 90°C	48%

The chemical agents were completely destroyed by the Silver II process to below the limit of detection of the analytical instruments used.

The experiments show that the carbon content of the chemical agents is more effectively destroyed when the Silver II process is operated at 90°C rather than 50°C.

4. Industrial Plant Configuration

The Dounreay Silver-II Process as described above is not the ideal process for the mass throughput destruction of materials, as e.g. incinerators. The relatively low cost and availability of incineration capacity makes stationary Silver-II plants relatively cost ineffective, and it would probably take a long time, before emission regulations and general safety considerations alone would give Silver-II an advantage. However, from the start of the Silver-II development until now, the relative cost difference between incineration and Silver-II has decreased substantially.

On the other hand the Silver-II process, being low temperature, low pressure, lends itself quite ideally to a modular, mobile or transportable design for the destruction of materials, which are very hazardous, difficult to move or unacceptable for incineration (Figure 2).

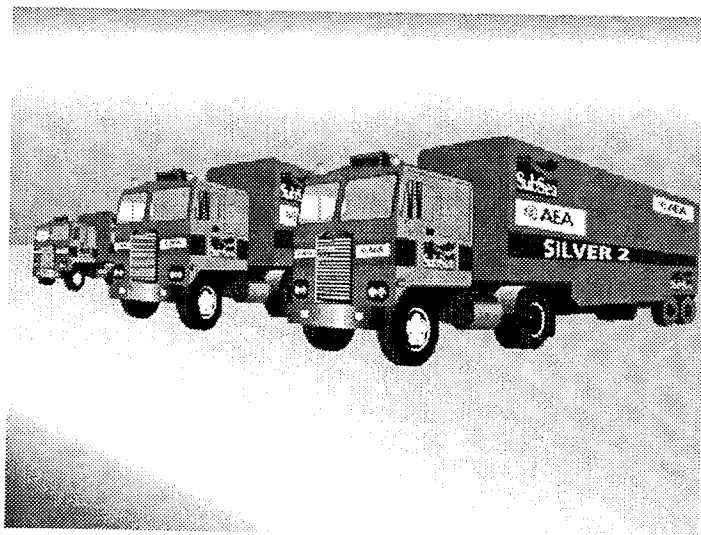


Figure 2: Taking the Process to the Problem

An operational plant would consist of a number of standard ISO-containers fitted with electro-chemical circuits, scrubbers, control and instrumentation and power supply. Where necessary, this set-up could be complemented by the addition of a power generator. A number of concepts exist for plant sizes between 4kW and 360kW, based on standard size units. These can easily be upgraded by the addition of more modules, until the required through-put is achieved.

As the process is non-discriminative, a plant lay-out for the worst case scenario (super-toxic, highly explosive) would cover all eventualities without major plant modification. It seems therefore ideal for situations, where a mixed feed of unknown composition is to be expected (e.g. demil remediation projects). However, in well defined application scenarios a plant could be adapted to suit.

The process can be relatively easy interfaced to complementary technologies, e.g. a delaboration unit. From the delaboration stand, which can be remote-controlled or manual, the product can be directly fed into the process. This is made easy by the relatively widespread use of water or steam for the extraction of product from the containing shell. Water is needed for the process thus there is no need for a water separation stage before feeding the product into the destruction unit, at the same time reducing the complexity of the plant and the water treatment stages.

5. Summary and Conclusions

The Dounreay Silver-II process seems a feasible technology for the destruction of military and civilian pyrotechnics, i.e. those containing organic compounds. It is not a viable alternative to purely non-organic destruction, although a certain percentage of inorganic compounds does not harm the operation of the process.

Where the bulk destruction of low-hazardous compounds is required, or where materials are non-problematic for conventional technologies, the Silver-II process cannot commercially compete, especially against incineration. However, products from incineration could be further treated by Silver-II. It is therefore seen as a complementary rather than an alternative technology.

The process can be applied to a very wide range of liquid and solid organic materials. These materials can also be treated in a "mixed feed", making it very versatile.

Organic compounds are converted to give carbon dioxide, water and small quantities of inorganic salts and nitrous oxides, depending on the feedstock. All of these effluents / off-gases can be treated by readily available technology or discharged.

The process does not give rise to toxic species, such as dioxins or dibenzofurans which have been detected in the discharges of incinerators. The organic inventory within the process is kept to a low and thus safe level.

The process operates at low temperatures and ambient pressure, reducing the risk of inadvertent leakage into the environment. It can be rendered inert in seconds, by simply switching off the electrical supply.

The modular concept makes the process ideal for containerisation, allowing to take the solution to the problem. In many cases this is the safer alternative to moving hazardous compounds to centralised disposal facilities. It is anticipated that a mobil pilot plant will be in operation by the end of the year, destroying recovered non-stockpile chemical rounds in a remediation project for the MoD.

6. Literature

1. Rapsch/Tiedemann (Hrsg.): Schutzmaßnahmen bei der Gefährdungsabschätzung von Rüstungsaltslasten, Berlin 1994
2. Thome-Kozmiensky (Hrsg.): Management zur Sanierung von Rüstungsaltslasten, Berlin 1992
3. D.F. Steele: The Safe and Environmentally Benign Destruction of Explosives Using Electro-Chemical Oxidation, Paper presented to the International Seminar on Demilitarisation Technology for Explosives and Explosive Ordnance, RMCS-Cranfield, November 1991
4. D.F. Steele: Electro-Chemical Destruction of Toxic Organic Industrial Waste, in Platinum Metals Rev., 1990, 34, (1), 10-14
5. AEA Technology-Datasheet: AEA's Silver-II Process
6. AEA / SSOL Internal Test-Reports and Protocols
7. D.F. Steele, J.P. Wilks, W. Batey: The Electro-Chemical Destruction of Waste Reprocessing Solvent and Ion Exchange Resins, Paper presented to 1992 Incineration Conference: Thermal Treatment of Radioactive Hazardous, Chemical, Mixed and Medical Wastes, Albuquerque, May 1992
8. J. Hedtmann, Dr. R. Häber: Unexploded Ordnance Devices: Detection, Recovery and Disposal, Paper presented to NATO-Advanced Research Workshop on Sea-Dumped Chemical Ammunition, Moscow 1995

Größenanalyse von Feststoffpartikeln mit Hilfe der Laserbeugungsspektrometrie am Beispiel von Gasgeneratorkomponenten

Particle Size Determination of Gasgenerator Components by Laser Light Scattering

U. Teipel , U. Förter-Barth

Fraunhofer Institut für Chemische Technologie (ICT)
Postfach 1240, 76318 Pfinztal

Zusammenfassung

Zur Charakterisierung disperser Partikelkollektive ist die Kenntnis der Partikelgröße und der Partikelgrößenverteilung von entscheidender Bedeutung. Bei der Vielzahl an Meßverfahren, die zur Partikelgrößenanalyse zur Verfügung stehen, findet die Laserbeugungsspektrometrie aufgrund der kurzen Analysezeiten und der guten Reproduzierbarkeit der Meßergebnisse immer größere Anwendung.

Die Laserbeugungsspektrometrie ist ein optisches Meßverfahren, welches die Information einer Streulichtverteilung, die durch Wechselwirkung mit den Partikeln gestörte Ausbreitung von Lichtwellen bedingt ist, zur Ermittlung der Partikelgrößenverteilung auswertet.

In diesem Beitrag werden Ergebnisse der Charakterisierung von Komponenten von Gasgenerator - Reaktionsmischungen mittels Laserbeugungsspektrometrie vorgestellt.

1 Einleitung

Für die Komponenten einer Reaktionsmischung von Airbag - Gasgeneratoren, wie z.B. Brennstoff-, Oxidator-, Katalysatorpartikel, ist die Partikelgröße und die Partikelgrößenverteilung neben der Partikelgestalt und den Oberflächeneigenschaften eine wichtige Produkteigenschaft. Insbesondere im Hinblick auf Stoffumwandlungs- und Reaktionsvorgänge ist die Partikelgröße und die von ihr abhängige spezifische Oberfläche der Partikel von entscheidender Bedeutung.

2 Meßverfahren der Partikelgrößenanalyse

Zur Bestimmung von *Partikelgrößen* und deren *Verteilungen* stehen die verschiedensten *Meßverfahren* zur Verfügung. Sie unterscheiden sich insbesondere durch ihr physikalisches Prinzip und durch ihren möglichen Meßbereich. Zu den bekanntesten klassischen Verfahren zählen die *Trennverfahren* (Siebung, Sichtverfahren), die *Sedimentationsanalyse* und die *Zählverfahren*.

Eine weitere Gruppe Meßverfahren zur Partikelgrößenanalyse sind die *optischen Meßmethoden* und die *Ultraschallspektrometrie*.

Die *optischen Meßverfahren* werden i.a. in Verfahren, welche die Streuung von Licht an Partikeln nutzen, und abbildende Verfahren unterteilt. Für die abbildenden Verfahren seien an dieser Stelle beispielhaft die Kurzzeitfotografie und die Impulsholografie genannt. Bei den Streulichtmethoden, zu denen auch das im folgenden näher erläuterte Verfahren der Laserbeugung gehört, steckt die Information in der durch Wechselwirkung mit den Partikeln gestörten Ausbreitung der Lichtwellen. Die gemessenen Lichtsignale können sofort in elektrische Signale umgewandelt werden, was eine sehr schnelle Ermittlung der gesuchten Verteilung ermöglicht. Ein weiterer Vorteil der optischen Meßmethoden besteht in der Möglichkeit der In-line-Messung, d.h. bei einer entsprechenden optischen Zugänglichkeit des Mehrphasensystems (z.B. nicht zu hohe Partikelkonzentration) ist die Messung der Partikelgröße ohne Störung der Strömung möglich. Im folgenden wird das Verfahren der Laserbeugungsspektrometrie näher erläutert.

2.1 Laserbeugungsspektrometrie

Die Laserbeugungsspektrometrie ist ein Meßverfahren der Partikelgrößenanalyse, das die Streuung von Licht an Partikeln ausnutzt, um die Partikelgrößenverteilung zu bestimmen. Die von einem Partikel bei Einwirkung eines Lichtstrahls ausgehende Streulichtstrahlung läßt sich anhand des sogenannten "Mie-Parameters" α unterschiedlichen Bereichen zuordnen.

$$\alpha = \frac{\pi \cdot x}{\lambda} \quad (1)$$

Je nach Lichtwellenlänge λ und Partikeldurchmesser x unterscheidet man folgende Bereiche des Streuverhaltens :

- $\alpha \ll 1$ Bereich der Rayleigh-Streuung
- $0,1 < \alpha < 10$ Bereich der Mie-Streuung
- $\alpha \gg 1$ Gültigkeitsbereich der geometrischen Optik
(Fraunhofer-Bereich)

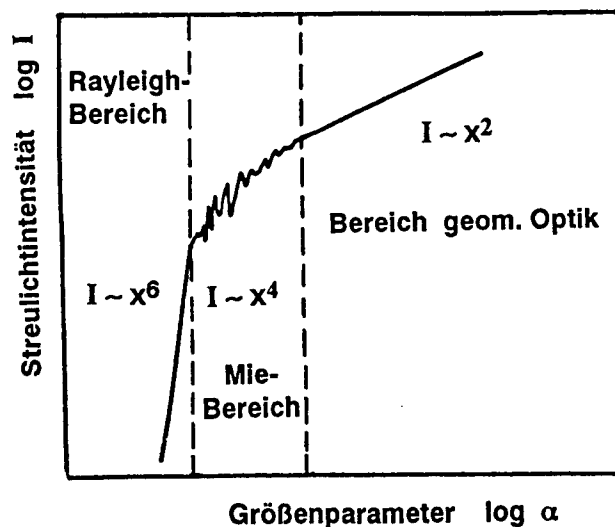


Abb. 1: Funktion der Streulichtintensität vom Partikelgrößenparameter α

Die *Rayleigh-Streuung* ist durch eine vollständige Symmetrie in Richtung des ein- und ausfallenden Lichtes gekennzeichnet, d.h. das Licht streut nach vorne und hinten gleich stark. Im Rayleigh-Bereich ist somit keine Streulicht-Partikelgrößenanalyse durchführbar.

Im *Mie-Bereich* ist eine Partikelgrößenanalyse mittels Streulicht ab einer Partikelgröße von etwa $0,1 \mu\text{m}$ realisierbar. Mit zunehmendem Mie-Parameter α gewinnt der in Vorwärts-Richtung gestreute Anteil des Lichtes an Intensität; der nach hinten gestreute Anteil wird schwächer. In Abb.2 ist das Streulichtverhalten an Wassertropfen ($n = 1,33$) unterschiedlicher Größe ($\alpha = 1$, $\alpha = 6$, $\alpha = 30$) in Abhängigkeit vom Streuwinkel φ als Polardiagramm dargestellt. Man erkennt, wie sich mit wachsendem Tropfendurchmesser ein Maximum der Streuintensität um den Streuwinkel $\varphi = 0$ ausbildet.

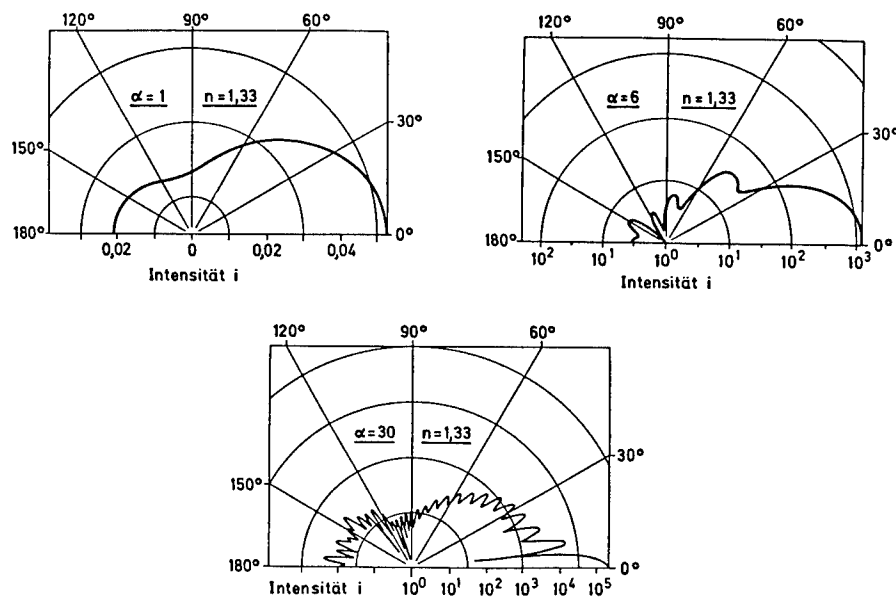


Abb. 2 : Lichtstreuung an kleinen Partikeln (Polardiagramme der *Mie-Streuung*) / 2 /

Im Gültigkeitsbereich der *geometrischen Optik* ($\alpha \gg 1$) sind Streulicht-Partikelgrößenanalysen unproblematisch. Der engste Vorwärtsbereich der Streuung (Streuwinkel $\varphi \rightarrow 0$) wird im wesentlichen durch die Beugung bestimmt. Die Streulichtanteile der Brechung und Reflexion sind hier vernachlässigbar. In diesem Bereich ergibt sich weitgehende Übereinstimmung mit den Beugungserscheinungen, die an einer Kreisscheibe beobachtet wurden und als *Fraunhofer-Beugung* bekannt sind / 3 /.

Zwischen der Partikelgröße und der Streuwinkelverteilung besteht ein direkter Zusammenhang (siehe Abb. 2). Eine exakte Berechnung dieses Zusammenhangs ist mit Hilfe der *Theorie nach "Mie"* möglich / 4, 5 /. Hierzu ist allerdings die Kenntnis des komplexen Brechungsindex m des zu untersuchenden Materials erforderlich :

$$m = n - i \cdot \kappa \quad (2)$$

mit: n = Brechungsindex

$$\kappa = \text{Absorptionsindex} : \quad \kappa = \frac{k \cdot \lambda}{4 \cdot \pi \cdot n} ; \quad k = \text{Absorptionskoeffizient}$$

Durch den komplexen Brechungsindex wird die optische Stoffeigenschaft eines homogenen Fluids beschrieben. Da die Angaben (n, k) oft nicht vorhanden sind, arbeitet man in vielen Fällen mit einer Näherungslösung, der sogenannten *Fraunhofer-Näherung* / 6 /.
Fraunhofer-Näherung / 6 /.

Diese Fraunhofer-Näherungslösung, bei der angenommen wird, daß die betrachteten Partikel kugelförmig und absorbierend seien, ist nur für die Streuung im engen Vorwärtsbereich, wo die auftretende Streulichtintensität im wesentlichen aus der Beugung der einfallenden Lichtquelle an der Partikeloberfläche stammt, erfüllt. Dies trifft insbesondere für Partikel mit einem Durchmesser $x > 3\text{-}5 \mu\text{m}$ zu.

Die vom Partikeldurchmesser x und vom radialen Abstand zur optischen Achse r abhängige Streulichtintensitätsverteilung $I(r, x)$ wird für ein Partikel durch Gleichung (3) beschrieben :

$$I(r, x) = I_0 \left(\frac{\pi x^2}{4f} \right)^2 \cdot \left(\frac{2J_1 \left(\frac{\pi x r}{\lambda f} \right)}{\left(\frac{\pi x r}{\lambda f} \right)} \right)^2 \quad (3)$$

Dabei steht f für die Brennweite und J_1 für die Besselfunktion 1-Art, 1-ter Ordnung.

Bei Untersuchungen an einem Partikelkollektiv erfolgt eine additive Überlagerung der von den einzelnen Partikeln erzeugten Streulichtintensitäten. Aus den gemessenen Streulichtintensitätsverteilungen kann die Partikelgrößenverteilung der Probe berechnet werden [7].

Meßgerät

Laserbeugungsspektrometer werden für Messungen von Partikelgrößen im Bereich von $0,1\ \mu\text{m}$ bis $2000\ \mu\text{m}$ angeboten, wobei verschiedene Meßbereiche unter Verwendung eines Detektors durch Variation der Brennweite eingestellt werden können. Die in diesem Beitrag vorgestellten Ergebnisse wurden mit dem Laserbeugungsspektrometer "Mastersizer X" der Fa. Malvern Instruments ermittelt. In Abb.3 ist der prinzipielle Aufbau eines Laser-Streulichtspektrometers dargestellt.

Das Meßgerät besteht aus einer Sendeeinheit, von der aus der He-Ne-Laserstrahl mit einer Wellenlänge $\lambda = 632,8\ \text{nm}$ ausgesendet wird, und einer Empfängereinheit, die die Abbildungsoptik und die Detektorelektronik enthält. Die Sender- und Empfängereinheit können auf einer optischen Bank montiert oder z.B. für Untersuchungen von Mehrphasenströmungen in eine Anlage eingebaut werden.

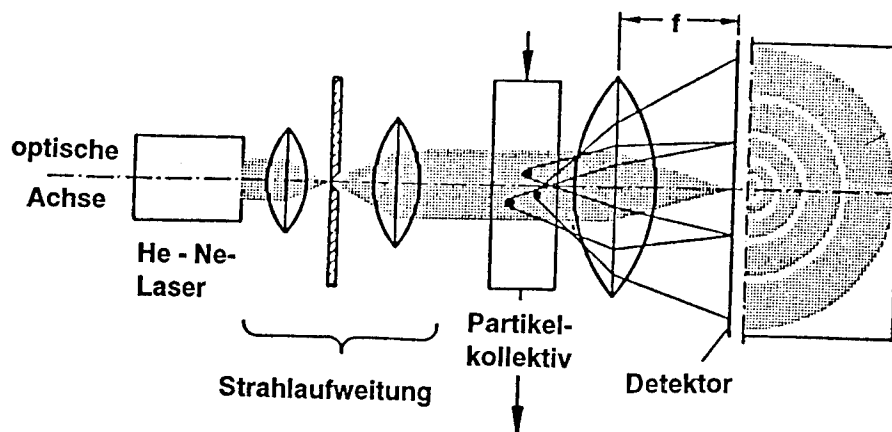


Abb. 3 : Prinzipieller Aufbau eines Laserbeugungsspektrometers

Die zu untersuchenden Partikel werden in einer kontinuierlichen Phase, die gegenüber den Partikeln keine Lösungseigenschaften aufweisen darf, suspendiert. Diese Suspension durchströmt eine Durchflußküvette, die von dem aufgeweiteten, parallelen Lichtstrahl durchleuchtet wird.

Das von den Partikeln gebeugte Licht bildet auf dem halbkreisförmigen Detektor ein radialsymmetrisches Beugungsbild. Bei kugelförmigen Partikeln besteht das Beugungsbild aus konzentrischen dunklen und hellen Ringen (Beugungsringe). Aus der gemessenen, radialen Intensitätsverteilung dieser Beugungsringe kann auf die Partikelgrößenverteilung des Kollektives geschlossen werden.

Besonders gut geeignet ist dieses Verfahren für Partikelgrößen $x \geq 3\text{-}5 \mu\text{m}$. Für kleinere Partikel, insbesondere, wenn die Partikelgröße im Bereich der Lichtwellenlänge ($\lambda = 632,8 \text{ nm}$) liegt, gibt die *Fraunhofer-Näherung* die realen Verhältnisse nur ungenügend wieder. In diesem Größenbereich liegt ein entscheidender Einfluß des komplexen Brechungsindex der Partikel auf die Meßergebnisse vor. Bei Kenntnis des Brechungsindex und des Absorptionskoeffizienten sollte die Berechnung der Größenverteilung mit Hilfe der *Mie-Theorie* durchgeführt werden. Die *Mie-Theorie* findet ebenfalls Anwendung, wenn bei transparenten Partikeln der Brechungsindex-Unterschied zwischen den Partikeln und der kontinuierlichen Phase gering ist, bzw. wenn der Quotient $n^* = n_p/n_k \rightarrow 1$.

Ein entscheidender Vorteil der Laserbeugungsspektrometrie liegt in der geringen Meßzeit, insbesondere im Vergleich zu einigen nicht-optischen Meßverfahren.

3 Versuchsergebnisse

Im folgenden werden Untersuchungen zur Bestimmung der Partikelgröße und der Partikelgrößenverteilung von **Airbag-Gasgenerator-Komponenten** am Beispiel von Katalysatoren mit Hilfe der Laserbeugungsspektrometrie vorgestellt.

Die Partikel werden in einer gegenüber den Partikeln unlöslichen, kontinuierlichen Phase dispergiert und durch die Messküvette gefördert. Für die untersuchten wasserunlöslichen metallischen Katalysatoren diente Wasser (Brechungsindex $n_k = 1,330$) als kontinuierliche Phase. Die Berechnung der Größenverteilung eines Partikelkollektivs wurde mit der *Fraunhofer-Näherungslösung* und mit Hilfe der *Theorie von Mie* durchgeführt.

Abb. 4 zeigt die nach der *Fraunhofer-Näherung* ausgewerteten Volumensummen- $Q_3(x)$ und Volumendichteverteilung $q_3(x)$ einer Gasgenerator-Katalysatorfraktion mit einem Medianwert $x_{50,3} = 53,5 \mu\text{m}$. Die Lageparameter dieser Verteilungsbreite betragen $x_{10,3} = 17,2 \mu\text{m}$ und $x_{90,3} = 114,5 \mu\text{m}$.

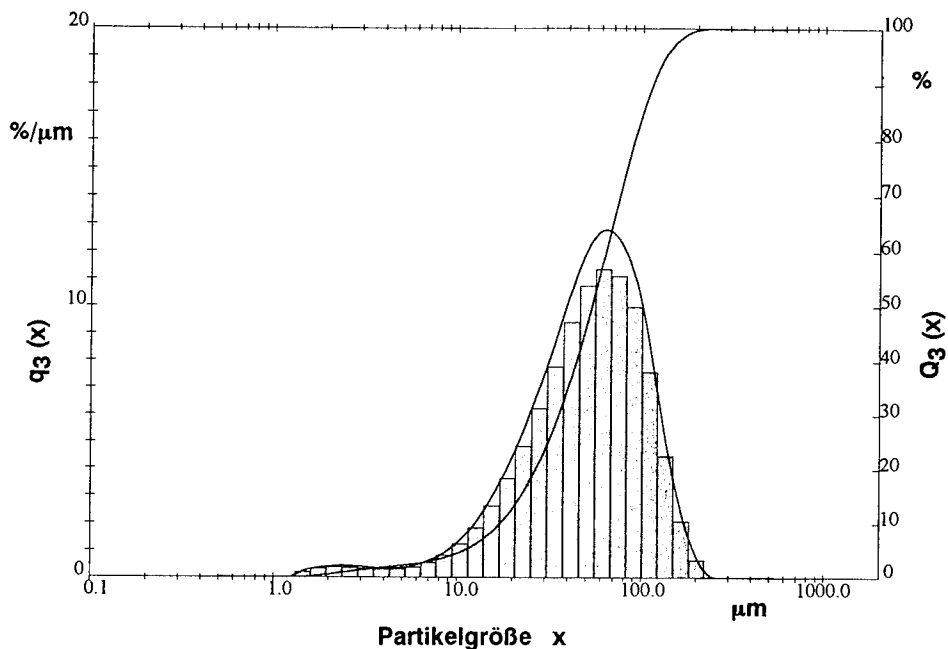


Abb. 4 : Volumensummen- $Q_3(x)$ und Volumendichteverteilung $q_3(x)$:
Metallischer Katalysator (Kat.4) , Auswertung : Fraunhofer

In diesem Größenbereich und bei Partikeln mit metallischer Oberfläche ergeben die Auswertung nach der *Fraunhofer-Näherung* und die Auswertung nach der *Mie-Theorie* mit dem entsprechenden Brechungsindex ($n=1,7$ und $n=1,9$) und Absorptionskoeffizienten $k=0,1$ identische Werte der Verteilung (siehe Abb. 5).

Der Medianwert dieser Katalysatorpartikelfraktion beträgt bei der Auswertung nach der *Mie - Theorie* $x_{50,3} = 54,4 \mu\text{m}$ und die Lageparameter der Verteilungsbreite betragen $x_{10,3} = 17,8 \mu\text{m}$ und $x_{90,3} = 115,7 \mu\text{m}$.

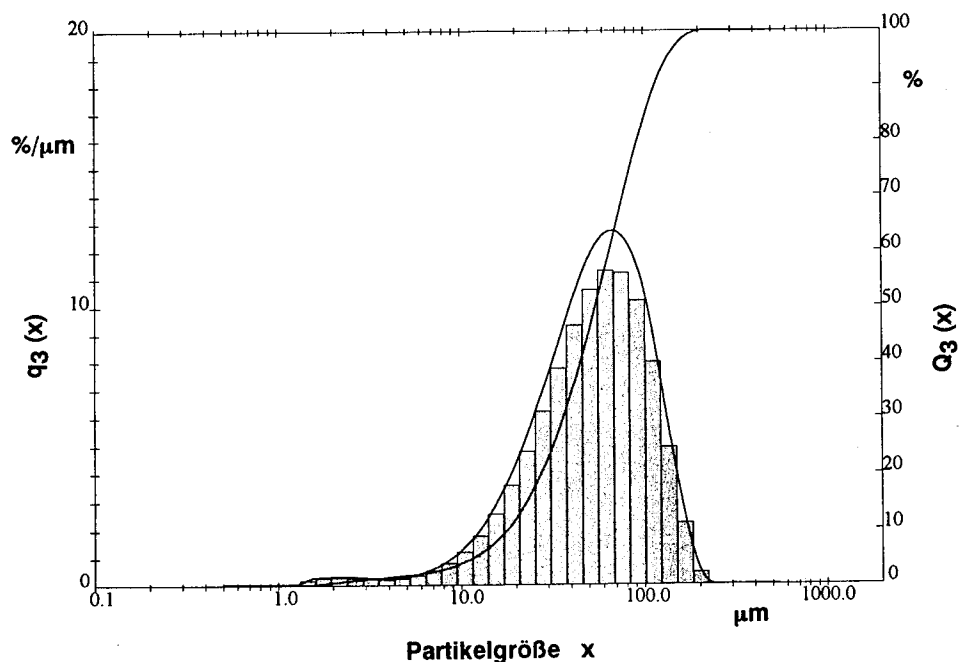


Abb. 5 : Volumensummen- $Q_3(x)$ und Volumendichteverteilung $q_3(x)$:
 Metallischer Katalysator (Kat.4) , Auswertung : Mie $n = 1,7$; $k = 0,1$

Für eine weitere Fraktion metallischer Katalysatorpartikel ergab die Auswertung nach der *Fraunhofer-Näherungslösung* ein Medianwert von $x_{50,3} = 11,8 \mu\text{m}$. Die Auswertung der Partikelgrößenverteilung nach der Theorie von *Mie* ergab ein Medianwert $x_{50,3} = 12,3 \mu\text{m}$. Auch für die Breite der Partikelgrößenverteilung ergaben sich für diese Fraktion nahezu identische Werte.

Diese Ergebnisse machen deutlich, daß in diesem Größenbereich und bei Partikeln mit metallischer Oberfläche die Berechnung der Partikelgrößenverteilung nach der *Fraunhofer Näherung* und der *Mie-Theorie* keinen Unterschied der Partikelgröße liefert .

Bei der Bestimmung der Größenverteilung von kleineren ($\alpha < 10$), transparenten Partikeln mit Hilfe der Laserbeugungsspektrometrie ist die Anwendung der Mie Theorie erforderlich, da bei der Auswertung nach der Fraunhofer-Näherungslösung ein nicht vorhandener Feinanteil ermittelt wird. Nähere Information siehe / 12 /.

Zusammenfassend kann festgestellt werden, daß die Bestimmung der Partikelgröße und der Partikelgrößenverteilung mit Hilfe der Laserbeugungsspektrometrie für Feststoffpartikel, Suspensionen, Emulsionen und Aerosolen erfolgen kann. Bei einer notwendigen Dispergierung der Partikel kann die kontinuierliche Phase bezüglich der Löslichkeit und des Brechungsindexverhältnisses auf die zu untersuchenden Partikel abgestimmt werden.

4 Literatur

- /1/ *Leschonski, K.:* Messung von Partikel- und Porengrößenverteilungen
in: Ullmanns Encyklopädie der technischen Chemie. Bd 5, S. 725-753

- /2/ Hochschulkurs "Staubabscheiden". Institut für Mechanische Verfahrenstechnik und Mechanik (Prof. F. Löffler), Universität Karlsruhe 1992

- /3/ *Fraunhofer, J.:* Bestimmung des Brechungs- und Farbzerstreuungsvermögens verschiedener Glasarten.
Gilberts Annalen der Physik, 56 (1817) S. 193 ff.

- /4/ *Mie, G.:* Beiträge zur Optik trüber Medien.
Annalen der Physik, 25 (1908), S. 377-445

- /5/ *Kerker, M. :* The Scattering of Light.
Academic Press, New York and London (1969)

- /6/ *Airy, G.B. :* On the diffraction of an object glass with circular aperture.
Trans. Camb. Phil. Soc. 5 (1835), S. 283 - 290

- /7/ *Heuer, M.; Leschonski, K.:* Results obtained with a new Instrument for the Measurement of Particle Size Distributions from Diffraction Patterns. Part. Charact., 2 (1985), S. 7-13

- /8/ *Bürkholz, A.; Polke, R.:* Laser Diffraction Spectrometers / Experience in Particle Size Analysis. Part. Charact. 1 (1984), S. 153-160

- /9/ *Vielhaber, U.; Wachering, H.:* Partikelgrößenbestimmungen im Bereich 0,1 - 2000 µm. Malvern-Laserstreulichtanalyse, Verfahrenstechnik 11/1990

- /10/ *Sommer, H. T.:* Performance of optical Particle Counters: Comparison of Theory and Instrument.
Proc. of the 37th Annual Technical Meeting of the Institute of Environmental Sciences. San Diego, 06.-10.05.91

- /11/ *Bauckhage, K.:* Nutzung unterschiedlicher Streulichtanteile zur Partikelgrößenbestimmung in dispersen Systemen.
Chem.-Ing. Techn. 65 (1993) 10, S. 1200-1205
- /12/ *Teipel, U.; Siegl, T.; Akse, N. :* Größenanalyse transparenter Partikel mit Hilfe der Laserbeugungsspektrometrie.
Proc. der 23. Jahrestagung der Gesellschaft für Umweltsimulation ,
Pfinztal, 9-11. März 1994

STUDIES ON INFRARED SCREENING SMOKES

Amarjit Singh, SB Avachat, LK Bankar, Haridwar Singh
HIGH ENERGY MATERIAL RESEARCH LABORATORY, PUNE - 411021.

A B S T R A C T

This paper describes the experimental set up for evaluation of pyrotechnic smoke compositions for anti-thermal role using IR spectroradiometer and presents results for a few pyrotechnic smoke compositions based on hexachloroethane and hexachlorobenzene. The morphology and elemental compositions of aerosols generated from some pyrotechnic smoke compositions were studied using scanning electron microscope coupled to energy dispersive X-ray spectrometer. Results obtained reveal that smoke compositions producing large amount of carbon particles from various hydrocarbons were more effective in attenuating radiation as compared to compositions which produce various inorganic particles. The result of percentage attenuation have been discussed in the light of the information available and data generated during present study. An attempt has also been made to explain the relative mode of action by IR screening smokes.

1. INTRODUCTION :

In the modern battlefield, a large numbers of sophisticated opto-electronic systems like lasers, image-intensifiers, active sights, passive night vision devices called thermal imagers, etc. are in use⁽¹⁾, which provide the weapon system unparalleled accuracy, first strike capability and killing power. Several infra-red (IR) countermeasures are underdevelopment to these modern systems. Some of these are :

- (i) Paint films of low emissivity to minimise the temperature contrast between surface of vehicle and surroundings⁽²⁾.
- (ii) Use of special material nets, mats, umbrellas to reduce the thermal signature of targets⁽³⁾.
- (iii) Infra-red jammers, which confuse IR seekers of incoming missiles⁽⁴⁾.
- (iv) Infra-red decoy flares and chaff, which protect targets by distraction and seduction⁽⁵⁾.
- (v) Heat suppression techniques for engines and use of exhaust pipes for diluting the exhaust gases by air⁽⁶⁾.
- (vi) Utilisation of 'stealth' techniques, whereby it is possible to reduce the signature of the target by suitable design and by chemical and electronic applications⁽⁷⁾. and
- (vii) Use of smoke screens.

Smoke screens can be produced using mortars, guns, hand grenades, grenade launchers mounted on tanks and armoured personnel carriers (APCs)⁽⁸⁾ and can reduce the effectiveness of conventional weapons by three to four times and blinding smoke by as much as fifteen times⁽⁹⁾. In addition to a large number of uses of smokes in civil and defence fields, smokes can degrade

the effectiveness of guidance and control systems of modern weapons and are believed to be more effective than even high explosives in limiting their effectiveness⁽¹⁰⁻¹⁵⁾.

Since IR countermeasures using smoke screen is cheap, free from electronic jamming, practical and easily deployable, a number of studies have been carried out⁽¹⁶⁻²⁸⁾ in the past. These studies broadly cover theoretical predictions, facilities for evaluation of IR screening smokes and the determination of optical properties of pyrotechnic smokes using either IR spectrophotometer/FTIR. However, compositional details are not available for pyrotechnic smoke formulations. Moreover, only hexachloroethane (HCE) based smoke composition has been tried and no formulations using hexachlorobenzene (HCB) based smoke compositions are mentioned. However, a recent review article on IR smokes, covers their formulation, processing and evaluation⁽²⁹⁾.

In the present study, a number of compositions based on hexachloroethane and hexachlorobenzene along with various oxidisers, metallic fuels and other additives were formulated, processed and evaluated. IR smoke studies include evaluation for anti-thermal role using IR spectroradiometer and morphology and elemental composition of aerosols produced. The attenuation results obtained for the various pyrotechnic smoke compositions have been discussed and mechanism of action of IR screening smoke explained.

2. EXPERIMENTAL :

Nine pyrotechnic smoke compositions were formulated and were pelleted (dia 40mm, dead load 12 tons), using hydraulic press. The processing technique followed is as described in The Text Book of Filling⁽³⁰⁾. The broad compositional details are given in Table - 1 and Table - 2. Even though the range is given, only one composition was studied. The pelleted smoke compositions were ignited inside an aluminium cubical chamber of volume 1.82m^3 (with windows on opposite walls that could be opened or closed) placed in between the source of IR radiation and IR spectroradiometer (Model SR-5000, M/s.RMP, France) as shown in Fig.1. The smoke produced was stirred for 5-10 secs. for uniform mixing of particulate materials. Using 150 W IR lamp as source and pyroelectric lithium tantalate detector, measurements were carried out in radiometric mode (IR output Vs time) in wavelength bands 2-2.4 μm , 3-5 μm and 8-13 μm . The distance between the IR radiometer and source was 12 meters. The % attenuation was computed using the formula

$$\% \text{ Attenuation} = \frac{I_0 - I_s}{I_0} \times 100$$

WHERE, I_0 represents radiant intensity of source without smoke screen.

I_s represent radiant intensity of source with smoke screen

Measurements were also repeated using indium antimonide/mercuric cadmium telluride (InSb/MCT) sandwich detector (cooled by liquid nitrogen) in radiometric mode as well as spectral mode

(wavelength Vs. IR output) and attenuation obtained at 3.7 μm and 10.6 μm discrete wavelengths. In these experiments, the IR lamp source was replaced by a 3 kW hot plate connected to a rheostat.

The morphology of the aerosol was determined separately using scanning electron microscope (JEOL, Model JSM-840, Japan). The aerosol particles were generated by combustion of 2g pelleted smoke composition (20mm dia and dead load 10 tons) in an enclosure of dimensions 1.4 x 0.8 x 1.1 metres. The aerosol particles were allowed to settle on SEM specimen studs having double sided adhesive tape by using a buchner funnel and vacuum pump. Thereafter, the specimen studs were coated with a thin layer of carbon using the coating unit. The SEM observations were conducted using an accelerated voltage of 20 kV (kilovolts). Only few representative micrographs are presented in this paper. The qualitative elemental compositions of aerosol particulates (observed under SEM) were simultaneously determined for elements sodium and subsequent elements of higher atomic number using energy dispersive X-ray spectrometer (Kevex International Corporation, USA). The results are given in Table 3. The electron micrographs of particulates generated from few pyrotechnic smoke compositions are shown in photographs 1 to 4. The spectrograms obtained from the particulates from various pyrotechnic smoke compositions are shown in Fig.2 to Fig.8.

3. RESULTS & DISCUSSIONS :

It can be seen from results (Table 1) that smoke compositions HCE, anthracene, $KClO_4$ (Compn. No.1), HCE anthracene Mg. powder (Compn. No.2), HCB, ZnO, Mg/Al alloy (Compn. No.3), HCB, anthracene, Mg. powder (Compn. No.4) produced average attenuation of 92 to 99% in 2-2.4 μm , 77 to 97% in 3-5 μm and 33 to 41% in 8-13 μm wave bands respectively, whereas compositions containing HCE, Al, $CaSi_2$, Silicon (Compn.No.5), HCE,Al, TiO_2 (Compn.No.6), HCE, Al, ZnO (Compn.No.7) gave average attenuation of 16 to 53% in 2-2.4 μm , 11 to 49% in 3-5 μm and 13-22% in 8-13 μm range respectively. Compositions HCE, ZnO, $CaSi_2$, KNO_3 (Compn.No.8), HCE, ZnO, $CaSi_2$, KNO_3 , Rosin (Compn. No.9) have given average attenuation 40 to 65% in 2-2.4 μm , 32 to 38% in 3-5 μm and 5 to 8% in 8-14 μm range respectively. These results indicate that the compositions based on HCE,anthracene, $KClO_4$ (Compn.No.1), HCE, anthracene, Mg powder (Compn.No.2), HCB, ZnO, Mg/Al alloy (Compn.No.3), HCB, anthracene, Mg powder (Compn.No.4) are more effective than compositions containing HCE, Al, $CaSi_2$, Silicon (Compn. No.5), HCE, Al, TiO_2 (Compn.No.6), HCE, Al, ZnO (Compn. No.7), HCE, ZnO, $CaSi_2$, KNO_3 (Compn.No.8), HCE,ZnO, $CaSi_2$, KNO_3 , Rosin (Compn.No.9) in attenuating radiation. This is also borne out by the results given in Table 2, where attenuation produced at specific wavelengths 3.7 μm and 10.6 μm are higher for compositions HCE, anthracene, $KClO_4$ (Compn.No.1) HCE,anthracene Mg. powder (Compn. No.2), HCB, ZnO, Mg/Al alloy (Compn. No.3), HCB, anthracene, Mg. powder (Compn. No.4) as compared to HCE, Al, $CaSi_2$, Silicon (Compn.No.5), HCE, Al, TiO_2 (Compn.No.6), HCE, Al,

ZnO (Compn.No.7) HCE,ZnO, CaSi₂, KNO₃ (Compn.No.8), HCE, ZnO, CaSi₂, KNO₃, Rosin (Compn. No.9). Highest attenuation produced by composition HCE, anthracene, KClO₄ (Compn.No.1). HCE, anthracene, Mg (Compn.No.2), HCB, ZnO, Mg/Al alloy (Compn.No.3), HCB, anthracene. Mg powder (Compn.No.4) may be due to high concentration of carbon particles produced during thermal decomposition of the hydro carbon to produce carbon particles. This is corroborated by oxygen balance of the compositions studied (Table 1). Compositions having higher (negative) oxygen balance show higher attenuation due to comparatively more carbon/carbonaceous matter formation. A large number of primary carbon particles build aggregates in the form of chains or clusters due to the adsorption on to the surface of the growing particles. Due to this adsorption, the new layers are always oriented parallel to the existing surface. Also several particles join by collision while they grow and aggregates are formed by further carbon deposition on these initially loose aggregates. It is a known fact that carbon black rearranges to graphitic order beginning at the particle surface, at temp. above 1200°C and assume polyhedral shape at 3000°C⁽³¹⁾. It is also reported that giant cage like molecules containing 60 or more carbon atoms in the form of balls can be formed during the carbon vaporising process. These are called buckyballs and possess optical limiting qualities due to the large size of molecule⁽³²⁾. The major contributing factor towards effectiveness of carbon producing pyrotechnic smoke composition in attenuating IR radiation is aggregates of carbon in form of chains and clusters of 400 um length as well as round cage like molecules of

about 100 um diameter. These carbon aggregates are suspended in the aerosol due to other inorganic particulates (like $MgCl_2$, $ZnCl_2$ etc.) and the thermal lift due to the pyrotechnic reaction would assist in suspending the large sized carbon aggregates.

TABLE 1 : ATTENUATION PRODUCED BY SMOKE AT DIFFERENT WAVELENGTH BANDS UNDER LOW HUMIDITY (<50% RH) USING PYROELECTRIC DETECTOR.

Sr. No.	Ingredients of smoke compn.	Nominal %	Ave. % attenuation at wavelength bands (Max. variation $\pm 4\%$)			Oxygen Balance
			2-2.4 μm	3-5 μm	8-13 μm	
1.	Hexachloroethane Anthracene Pot. perchlorate	15-40 15-40 30-50	94	83	33	-72.6
2.	Hexachloroethane Magnesium powder Anthracene	40-80 15-25 05-30	92	77	36	-82.5
3.	Hexachlorobenzene Zinc oxide Mg/Al alloy (50:50)	40-80 05-20 10-20	99	97	41	-49.2
4.	Hexachlorobenzene Anthracene Magnesium powder	40-80 05-30 15-25	95	78	41	-109.6
5.	Hexachloroethane Aluminium Calcium silicide Silicon	40-85 01-10 05-15 05-15	48	49	22	-25.7
6.	Hexachloroethane Aluminium Titanium dioxide	40-85 05-15 15-35	16	11	13	-10.6
7.	Hexachloroethane Aluminium Zinc oxide	20-70 05-15 30-70	53	25	14	-10.2
8.	Hexachloroethane Zinc oxide Calcium silicide Potassium nitrate	20-60 20-60 10-25 01-05	40	32	05	-9.5
9.	Hexachloroethane Zinc oxide Calcium silicide Potassium nitrate Rosin ($\text{C}_{20}\text{H}_{30}\text{O}_2$)	20-60 20-60 10-25 01-05 01-10	65	38	08	-14.0

**TABLE 2 : ATTENUATION PRODUCED BY SMOKE AT SPECIFIC WAVELENGTHS
UNDER LOW HUMIDITY (<50% RH) USING CMT/InSb SANDWICH
DETECTOR.**

Sr. No.	Ingredients of smoke compn.	Nominal %	Ave.% attenuation at wavelength (Max. variation $\pm 4\%$)			
			SPECTRAL MODE		RADIOMETRIC MODE	
			3.7um	10.6um	3.7um	10.6um
1.	Hexachloroethane Anthracene Pot.perchlorate	15-40 15-40 30-50	68	30	71	44
2.	Hexachloroethane Magnesium powder Anthracene	40-80 15-25 05-30	71	26	75	37
3.	Hexachlorobenzene Anthracene Magnesium powder	40-80 05-30 15-25	87	34	82	39
4.	Hexachloroethane Aluminium Calcium silicide Silicon	40-85 01-10 05-15 05-15	31	22	32	24
5.	Hexachloroethane Aluminium Titanium dioxide	40-85 05-15 15-35	11	11	12	16
6.	Hexachloroethane Aluminium Zinc oxide	20-70 05-15 30-70	24	13	30	15
7.	Hexachloroethane Zinc oxide Calcium silicide Potassium nitrate	20-60 20-60 10-25 01-05	26	10	26	09
8.	Hexachloroethane Zinc oxide Calcium silicide Potassium nitrate Rosin (C ₂₀ H ₃₀ O ₂)	20-60 20-60 10-25 01-05 01-10	18	02	27	08

**TABLE 3 : MORPHOLOGY AND ELEMENTAL COMPOSITION OF AEROSOLS PRODUCED
FROM PYROTECHNIC SMOKE COMPOSITIONS**

Sr. No.	Ingredients of smoke compn.	Nominal %	Morphology	Size	Elemental Composition of particle
1.	Hexachloroethane Anthracene Pot.perchlorate	15-40 15-40 30-50	Carbon chains, fibrous porous multi layer alongwith inorganic particles & spherical hollow carbonaceous particles	More than 200 um long carbon chains CaCl_2 particles are spherical & size 10um, KCl is irregular shape of 5 um, AlCl_3 particle is round of size 6um, SiCl_4 is irregular shaped of size 10um.	K, Cl, Ca, Al, Si.
2.	Hexachloroethane Magnesium powder Anthracene	40-80 15-25 05-30	- " -	More than 400um long carbon chains, thickness 1.3um. Spherical hollow carbonaceous particles of diameter approx. 100 um. KCl particle of size 3.5 um & less, round MgCl_2 particles of size 2-3 um and less.	K, Cl, Mg, Si.
3.	Hexachlorobenzene Zinc oxide Mg/Al alloy(50:50)	40-80 05-20 10-20	Long carbon chains fibrous porous multi-layer alongwith inorganic particulates and spherical hollow carbonaceous particles	More than 300um long carbon chain. Small MgCl_2 & ZnCl_2 particles	Mg, Cl, Zn, Si.
4.	Hexachloroethane Aluminium Calcium silicide Silicon	40-85 01-10 05-15 05-15	Oval shaped particles joined together to give a chain and also irregular shaped particles	Oval shaped particle have size 5-20 um and chain length 100um	Si, Al, Cl - large amounts K, Ca - Small amounts
5.	Hexachloroethane Aluminium Titanium dioxide	40-85 05-15 15-35	Spherical masses & irregular shaped particulate	The spherical masses have size approx. 30um and consist of agglomerates of chlorides (& oxides) of K, Si, Al, Ti & Fe. The irregular shaped particles have size 5-25um and consist of chlorides (& oxide) of Al, Si, K, Ca & Fe	<u>Spherical masses</u> K, Cl - Large amount. Al, Si, Ti - Small amount. <u>Irregular shaped particles</u> a) Al, Si - large amounts Ca, K, Ca, Fe - Small amt. b) Al, Cl - Large amount K - Small amount
6.	Hexachloroethane Aluminium Zinc oxide	20-70 05-15 30-70	Chain of particles & agglomerates of particles	The individual particles in the chain have size less than 1 um The chain has length 150um. The agglomerates of particles have size 100 um.	Cl, Zn - Large amounts Si - Small amounts
7.	Hexachloroethane Zinc oxide Calcium silicide Potassium nitrate	20-60 20-60 10-25 01-05	Individual irregular shaped, agglomerates of particles & chain of particles	Individual particles have size less than 10um. Agglomerates are 75um size & chain is 60 um long.	<u>Individual particles</u> : Ca - Large amounts Si - Small amounts <u>Agglomerates & Chain</u> Zn, Cl - Large amounts Ca, Si - Small amounts

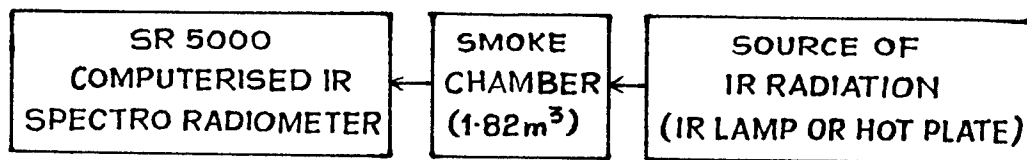


FIG.1: EXPERIMENTAL SET UP FOR RADIOMETRIC STUDY.

⁹²⁻¹³ ENERGY DISPERSIVE X-RAY SPECTROGRAMS OF SMOKE PARTICULATES

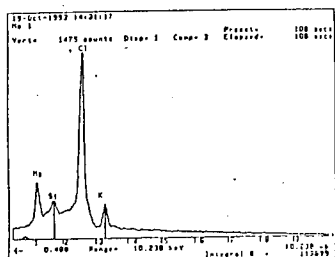
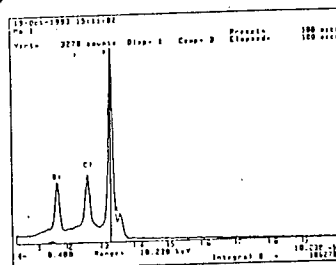
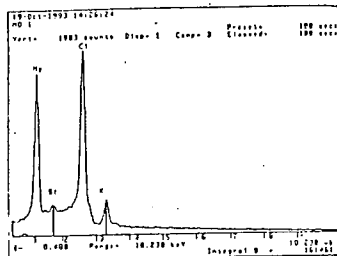
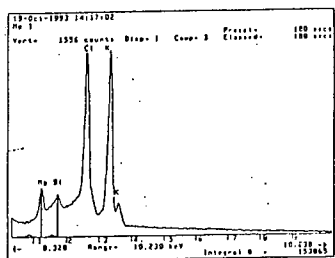


FIG.2 : SMOKE COMPOSITION HCE + ANTHRACENE + MAGNESIUM

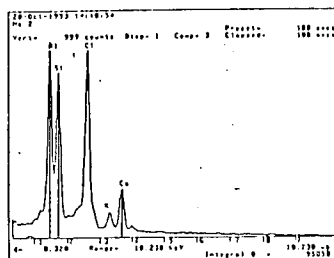
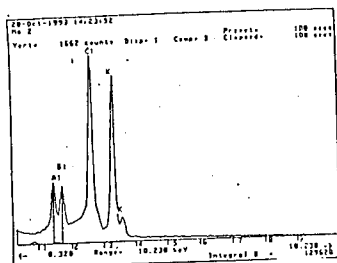


FIG.3 : SMOKE COMPOSITION HCE + KClO₄ + ANTHRACENE

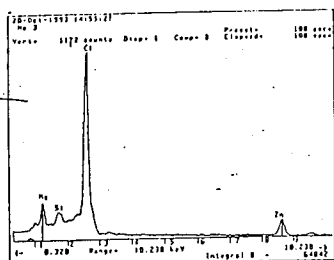


FIG.4 : SMOKE COMPOSITION HCB + ZnO + MAGNESIUM

02 - 14

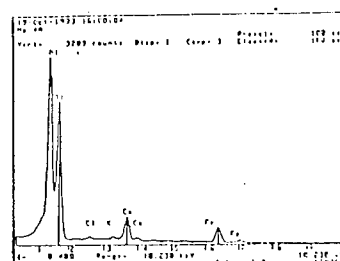
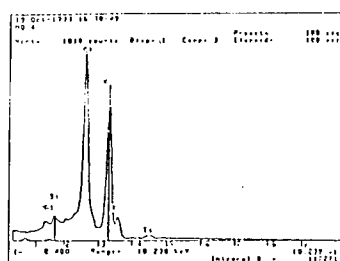
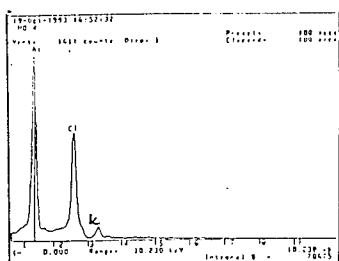


FIG.5 : SMOKE COMPOSITION HCE + TiO₂ + ALUMINIUM

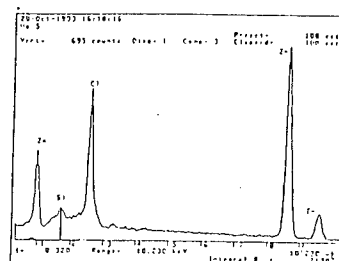


FIG.6 : SMOKE COMPOSITION HCE + ZnO + ALUMINIUM

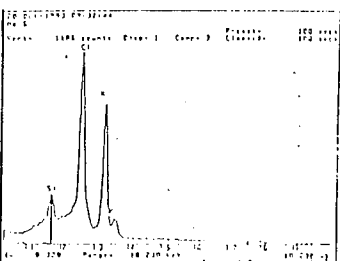
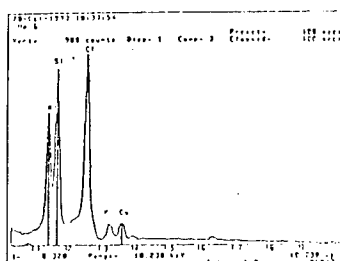
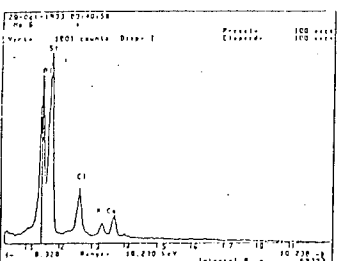


FIG.7 : SMOKE COMPOSITION HCE + ALUMINIUM + CaSi₂ + SILICON

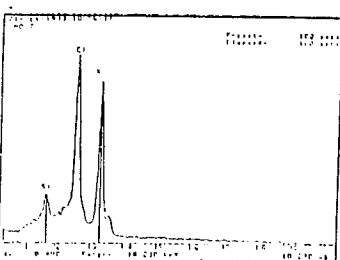
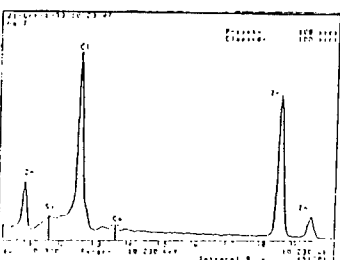
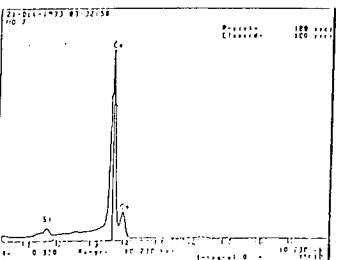
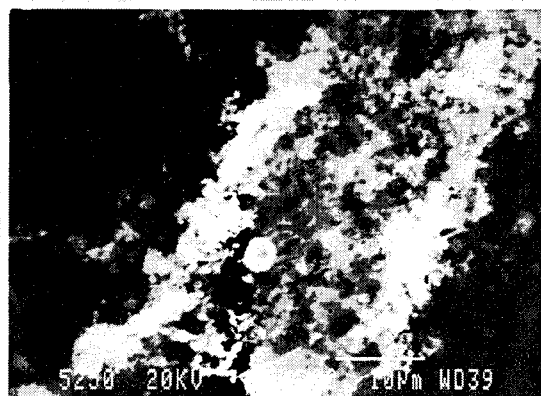
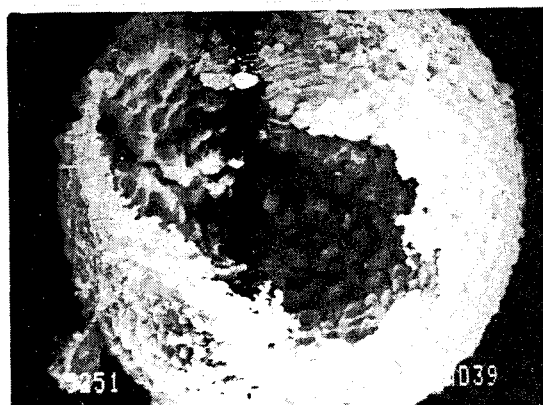


FIG.8 : SMOKE COMPOSITION HCE + CaSi₂ + KNO₃ + ZnO

^{92 - 15}
ELECTRON MICROGRAPHS OF
SMOKE PARTICULATES

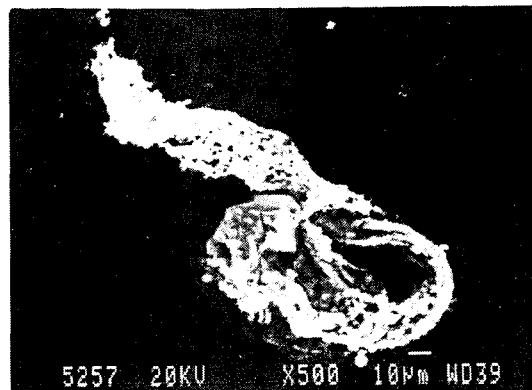


PHOTOGRAPH 1: SMOKE COMPN HCE + ANTHRACENE + Mg.

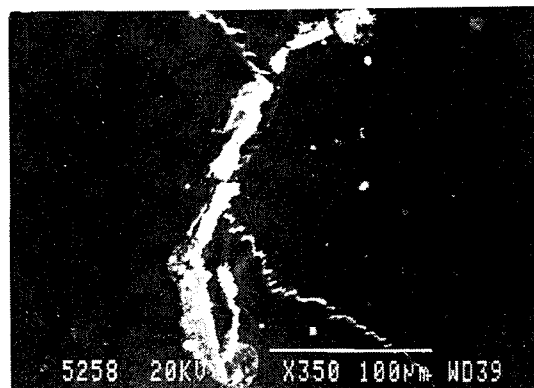


PHOTOGRAPH 2: SMOKE COMPN HCE + ANTHRACENE + Mg.

92 - 16



PHOTOGRAPH 3: SMOKE COMPN HCE + KClO_4 + ANTHRACENE



PHOTOGRAPH 4: SMOKE COMPN HCB + ZnO + Mg .

REFERENCES

1. A.L. Rodgers, I.B.R. Fowler, T.K. Garland - Collins, J.A. Gould, D.A. James and W. Roper, "Surveillance and Target Acquisition Systems", Brassey's Battlefield Weapons Systems and Technology, Vol. VII, Brassey's Defence Publishers, Oxford, 1983, PP 91-120.
2. R.M. Ogorkiewicz, "Countermeasures for Tanks Beating Smart Munition", IDR 1, 55 (1989).
3. Barracuda, "Can we Rely on Advanced Reconnaissance Methods in a World of Camouflage", Mil Tech., 11, No. 6/87, 133, (June 1987).
4. D.G. Kiely, "Naval Electronic Warfare", Brassey's Battlefield Weapons Systems & Tech., Vol. V, Brassey's Defence Publishers, Oxford, 1988, PP 52 & 62.
5. Infrared Military Systems, Part I (US Army Material Command, Engineering Design Hand Book, AMC Pamphlet 706-127), Alexandria VA, USA.
6. M. Hammick, "Invisible art of camouflage", IDR 8/1992, 749-754 (1992).
7. M. Leibstone, "Stealth : The US advance technology bombers", Mil Tech., Vol. X, Issue No. 9/86, 219-224 (1986).
8. P.R. Courtney-Green, "Ammunition for the land battle", Brassey's New Battlefield Weapon Systems & Technology Series, Vol. 4, Brassey's (UK) Ltd., 1991, PP 71 & 193-202.
9. C.N. Donnelly, "Soviet Tactics for Overcoming NATO Anti-tank Defences", IDR, 12, 1105-1106 (1979).
10. Amarjit Singh & S.G. Avachat, "Behind the Smoke Screen" Science Reporter, Vol. 31, No. 12, 13-16, (Dec'1994).
11. G.C. Holst, "Tactical Smoke Increases Survivability", Armour, 94, 20 (May-June 1984) .
12. Design of Ammunition for Pyrotechnic Effects (US Army Material Command, Engineering Design Handbook, Military Pyrotechnic Series, Part 4, (AMC Pamphlet 706-188) Alexandria VA, USA) (1974), 3-33.
13. J.C. Cackett, "Monograph on Pyrotechnic Compositions" (Royal Armament Research & Development Establishment, Fort Halstead, Sevenoaks, Kent, England), 1965, PP 99.
14. S. Walter, "Military Fuzes and Pyrotechnics", Armada, Internat, 10, 22 (Feb 1986).

15. F. Hopfgarten, "IR - Screening Smoke", Pyrotechnic, Basic Principles, Technology, Applications. Proceedings of 16th Int. ICT-Jahrestagung, 1985 combined with 10th Int. Pyrotechnic Seminar, Karlsruhe, FRG, July 1985, p 79-2.
16. P. Twardawa, G. Roy & B. Evans, "Canadian Evaluation of Infrared Smoke and Screening Systems", Proceedings of 16th Int. ICT Jahrestagung, Karlsruhe, FRG, July 1985, p 28-1.
17. F. Hopfgarten, P. Collvin, "Studies of IR & Visible Screening Smoke", Proceedings of 16th International ICT-Jahrestagung, Karlsruhe, FRG, July 1985, p 29-1.
18. J.T. Hanley & E.J. Mack, "A Chamber Investigation of the IR & Visible Obscuration" Properties of Pyrotechnically generated smokes", CALSPAN Report No. 7278-1 (1985). (Prepared for Naval Research Laboratory, Washington D.C., U.S.A.).
19. J. T. Hanley, B.J. Wattle & E.J. Mack, "Extinction Characteristics of Pyrotechnically generated Alkali Halide Smoke", CALSPAN Report No. 6855-M-1 (1981) (Prepared for Dept. of the Navy, Washington D.C., U.S.A.)
20. W. Scheunemann, "IR Optical Properties of a Pyrotechnic Screening Smoke", Propellants and Explosives 4, 95-97 (1979).
21. Li Fang and Lao Yunliang, "An Estimation of the Maximum Extinction Coefficient for the Spherical Particle Dispersion", 15th Int Pyro Seminar, Boulder, Colorado, July 1990, p 637, IIT Research Institute, Chicago, Illinois, USA.
22. Matti Harkoma, Harri Lippo & Matti Hemmila, "The IR spectra measurements of aerosols using a Laboratory scale dispersive IR Spectrometer", 16th Int. Pyro Seminar, Jonkoping, Sweden, June 1991, p 71, The Royal Swedish Academy of Sciences.
23. Jin Sik, Hwang, Suk Jong, Oh Chang Sik Kim, "Prediction of extinction coefficients and screening characteristics by the small particles in the IR wavebands," 16th Int. Pyro Seminar, Jonkoping, Sweden, June 1991, p 440, The Royal Swedish Academy of Sciences.
24. Luo Yunhua, Chen Zuoru, Tan Tiande, "A new method of determining Infrared spectral characteristics of screening smoke", 17th Int. Pyro Seminar, Vol. I, Beijing, China, October 1991, p 124, Beijing Institute of Technology.
25. Zhou Jin, Miao Yunkun, "IR Optical properties at 10.6 micron of a pyrotechnic screening smoke", 17th Int. Pyro Seminar, Vol. I, Beijing, China, October 1991, p 183-188, Beijing Institute of Technology.

26. Xiao Jianjun, Yao Yuliang, "A new thermodynamic model for phosphorus derived smoke droplets", 17th Int. Pyro Seminar, Vol. I, Beijing, China, October 1991, p 151-156, Beijing Institute of Technology.
27. Xiao Jianjun, Yao Yuliang, "Optical properties of phosphorus derived smokes", 17th Int. Pyro. Seminar, Vol. I, Beijing, China, 1991, p 157-162, Beijing Institute of Technology.
28. Amarjit Singh, S.G. Avachat, S.A. Joshi & Haridwar Singh, "Evaluation of pyrotechnic smoke for anti infrared and anti laser roles", Propellants, Explosives, Pyrotechnics. "In Press".
29. Amarjit Singh, S.G. Avachat and Haridwar Singh, "Infrared Screening Smokes - A review", Journal of Scientific & Industrial Research, Vol. 53, 667-673, (1994).
30. "The Text Book of Filling", 1958 Chapter 6, PP 1-16 (Ministry of Supply, UK).
31. Wolfgang Gerhartz, "Ullmann's Encyclopedia of Industrial Chemistry", VCH Verlagsgesellschaft, Weinheim, Federal Republic of Germany, Vol. A5, 1986, PP 140-143.
32. B. Anderberg, "Protection & Countermeasures against Laser Weapons", Military Technology, Vol XVII, Issue 5, 20-30 (May 1993).

**A PROPOSED SCHEME FOR THE EVALUATION OF MATERIALS
WITH PYROTECHNICS IN ROCKET MOTOR IGNITERS**

Barry Merchant and Mike Keeton

British Aerospace Defence Limited
Royal Ordnance
Rocket Motors Division
Summerfield, Kidderminster
Worcs, DY11 7RZ
(United Kingdom)

ABSTRACT

A proposed scheme for the assessment of materials with pyrotechnic compositions currently processed at Royal Ordnance Rocket Motors Division is described. Central to the scheme is that testing must not only address the long term reliability and functioning of an igniter but also the on-site process safety requirements.

INTRODUCTION

All materials contained in an explosive device such as a rocket motor igniter have to be physically and chemically compatible with each other and the explosive constituents. The prime requirement of any testing is to ensure safety and reliability during both manufacture and the service life of the store. The on-site requirement includes evaluation of materials such as process aids, adhesives, potting agents, seals etc which may present a safety hazard during assembly, whilst service aspects are concerned with the long term functioning of the device.

Generally there is less data available with regard to the interaction of materials with pyrotechnic composition than, for example, that available for the rocket propellant. This possibly emanates from difficulty in applying a testing scheme involving pyrotechnics as opposed to double based propellants. Propellants can be assessed by stabilizer depletion or gas evolution, using methods which are amenable to quantitative analysis. In the case of pyrotechnics however, reactive gas volumes are usually low and no stabilizer is present.

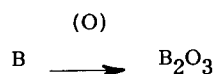
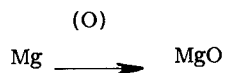
A typical pyrotechnic igniter device is shown in Fig 1. In this design powder and pellets comprising of magnesium and potassium nitrate are used and typifies modern igniter construction. All materials with the exception of the metal components, which by experience are known not to present a hazard would have to undergo assessment. This could be simply read-across from similar devices or, when this is not possible, by the scheme described.

The two pyrotechnic formulations most commonly used in solid rocket motor igniter systems are

1.	%
Boron	30
Potassium Nitrate	70
Volatiles	0.25 max.
Material retained on a 600 um sieve Nil	
2.	%
Magnesium	42.0
Potassium Nitrate	50.0
Protective Resin	8.0
Volatiles	0.20 max.
Material retained on a 600 um sieve Nil	

By nature the compositions are highly reactive. A characteristic of pyrotechnic is the adverse effect moisture even in small amounts has on performance. With magnesium mixtures a protective resin is incorporated to coat the magnesium particles to minimize the effect of moisture ingress. Moisture can lead to corrosion of the device and gas evolution, giving rise to rupture of sealing foils in extreme cases. Therefore when considering the use of a material in the proximity of powder or pellets a critical examination of the material, and any associated moisture must be undertaken. For example any system based on a condensation reaction must be treated with caution.

Tests which measure any oxidation of the fuel for example,



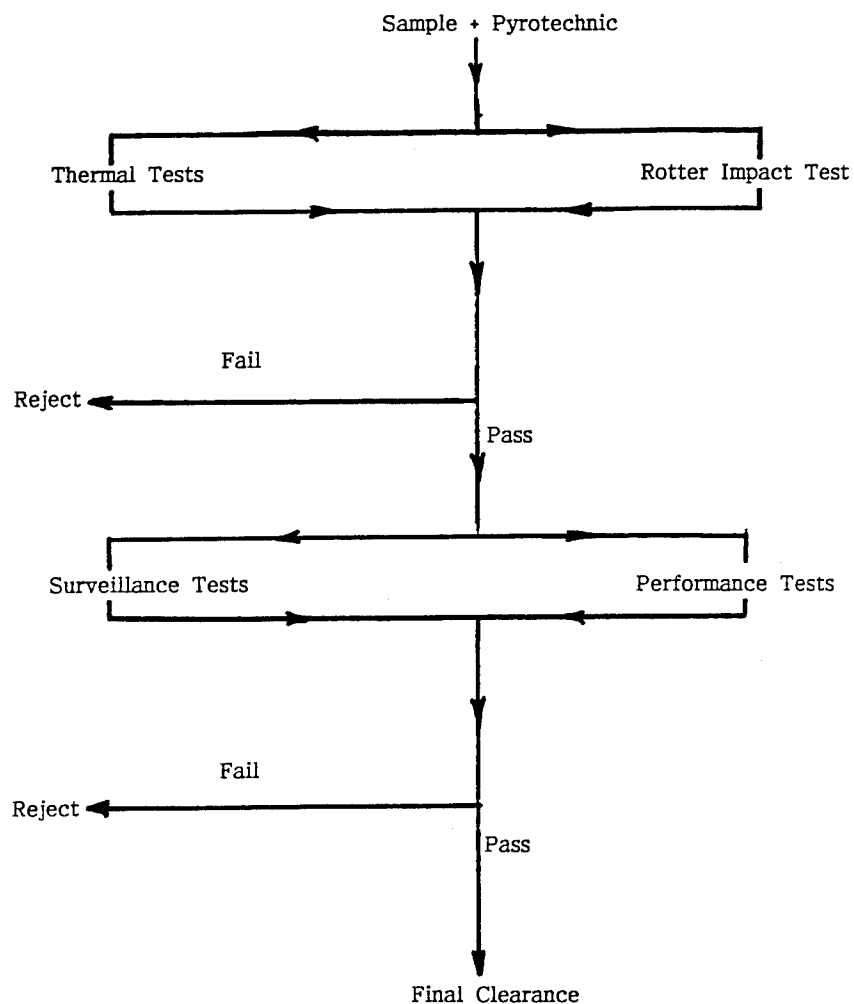
would appear to offer a solution to measuring the ability of a composition to function satisfactorily. However it has been demonstrated that even with significantly reduced levels of fuel (upto 50%) in a fresh mixture, can continue to give acceptable proof tests. Despite this the measurement of Mg/MgO ratio is not completely dismissed since degradation rate can be monitored and may be significant in obtaining an overall picture. The proposed scheme recognises that life prediction tests are not possible with pyrotechnics in the same way as those applied to propellant. The scheme is designed however to verify safety and confirm continued performance to the design standard.

Where a material would be rejected by the test scheme the Technical Authority may call for a further critical assessment using tests better suited to individual service requirements. This is relevant where the initiator has no alternative material to use. If there is any doubt about the interpretation of results the Laboratory Manager or Technical Authority must be consulted.

93 - 4

PROPOSED SCHEME

The test scheme is shown diagrammatically thus,



ACCELERATED AGEING

The scheme recognises that elevated temperature tests provide a means of compressing time scales. The aged tests are compared to appropriate control samples stored at ambient temperature and in a dry atmosphere.

SAMPLE PREPARATION

The test material is finely divided such that an intimate mix of pyrotechnic is obtained. This is particularly significant for both impact and thermal tests since both tests require milligram quantities.

SAFETY TESTS

1. Rotter Impact Test

This test is to measure any increase of sensitivity due to impact when a material is present in intimate contact. The test consists of a 5 kg falling drop weight striking an anvil containing the test sample. The basic composition is compared to the composition containing the material under test. Any increase in sensitivity is identified by a reduction in the drop height. Drop heights are set using the 'Bruceton Staircase' method and determine the height at which there is a 50% probability of an event.

Typically	B.KNO ₃	39 cms (Median Height)
	Mg. KNO ₃	88 cms (Median Height)

2. Thermal Characteristics

Procedures applied to measure heat flow such as Differential Scanning Calorimetry (DSC) or Thermal Gravimetry (TG) can be used to investigate safety and deterioration of a composition. DSC can provide an indication of any exothermic/endothermic reaction between the pyrotechnic and substrate, of importance when considering process safety, and may provide evidence of degradation particularly with boron based composition. It is known that boron degradation products give rise to an exothermic transition in the range 110-140°C. TG tests can identify breakdown of a material with the possible evolution of moisture. Materials which yield or generate moisture can be assessed by storing small amounts of pyrotechnic in close proximity with large amounts of material at ambient and elevated temperatures. The pyrotechnic is then examined to identify any deterioration as a result of any vapours emanating from the test material.

STABILITY

To improve the chemical stability of pyrotechnic compositions a number of precautions can be taken.

- i) Coat magnesium particles with waterproof coating
- ii) Prevent moisture from entering the composition by using only non hygroscopic ingredients. Carrying out all filling operations in a dry atmosphere and sealing in the composition hermetically.
- iii) Fill with compositions containing the least, practical amount of moisture and then extract the remainder by drying techniques or by an accelerated corrosion.

It is possible to incorporate some of these recommendations for the filling of rocket motor igniters.

1. Use compositions in which the magnesium is blown and coated with a protective resin.
2. Dry the powders to below 0.2% moisture/volatile content.
3. Fill in buildings with a dry atmosphere e.g. less than 65% relative humidity.

The effectiveness of these precautions are assessed on,

1. Foil Distention Trials

Foil distention is a known problem associated with moisture in igniter pyrotechnic powders and arises despite the fact that the total volatile matter of the powder is closely monitored during production. Clearly this is dependant on a gas tight seal being obtained in the igniter during manufacture. By monitoring distention, it is possible to determine whether or not gas generation will pose a problem.

The foil covering the pyrotechnic, Figure 1 and photograph 1 can be measured for distention just after manufacture using a gauge similar to that shown in photograph 2. Trials for monitoring distention are:-

- a) Measurement of igniters returned from service
- b) Investigation of the effect of storage environment on foil distention
- c) Determination of foil burst pressure

In the first case igniters form part of a long term service life surveillance programme and they are measured at regular intervals. Alternatively igniters can be made specifically for the trials and placed on accelerated ageing storage at +40°C in an attempt to force the failure of the igniter foils. Results of this type of trial (Reference 1) are shown in Figure 2 and normally exhibit a rapid rise in extension followed by a plateau. This is usually attributed to the rapid rate of corrosion to begin with which slows down as the layer of oxidation products on the magnesium surface increases in thickness.

To determine the pressure at which the foil bursts and hence the safety factor, empty cans are prepared to the normal production standards i.e. with a normal crimp load and protective finish. The cans are then assembled to a suitable jig fitted with a linear transducer to measure the distention of the foil. Before nitrogen is fed into the can through the fuze housing at a rate of 2 bar per minute. The mean values from 10 trials plotted on a graph of pressure, against distention in relation to pressure are shown in Figure 3. The foils eventually failed at a distention of nearly 0.9 inches (22.9 mm).

This simple method of monitoring, indicated that the precautions taken to improve stability work well. The pressures being produced were far lower than those needed to damage the device, in the example shown.

2. Performance Test

The ballistic performance of igniters (and hence the pyrotechnic) can be assessed by assembling them into vented vessels (Figure 4) and measuring the pressure generated against time after the device is initiated. A typical pressure time record for Mg/KNO₃ and B/KNO₃ pyrotechnics is shown in Figure 5. It is possible to measure accurately certain specific parameters for example,

93 - 8

- i) The maximum pressure, P.MAX (bar gauge)
- ii) The ignition delay, $t_d(s)$
- iii) The rise time, $t_i(s)$
- iv) The action time, $t_a(s)$
- v) The pressure integral, P.Int (bar g s)

By doing this for a number of igniters during development, statistically derived limits for the parameters can be obtained.

The state of the pyrotechnic within the igniter can be assessed by removing it and the Total Volatile Content of this powder and the chemical composition can be determined, to investigate decay rates.

To determine the effect of pyrotechnic stability on performance, the igniter is subjected to a sequence of trials similar to that shown in Table 1.

TABLE 1

Pyrotechnic Stability Tests

SerialNumber	1	2	3	4	5	6	7	8	9	10
Accelerated Ageing	X	X	X	X	X	X	X	X	X	X
DropTest	X	X	X	X	X	X	X	-	-	-
Vibration Trial	X	X	X	X	X	X	X	-	-	-
(°C)	-10	+43	+43	-10	+43	-10	-10			
Temp/Humidity Cycling	-	-	-	X	X	X	X	X	X	X
Disassembly	X	-	-	-	-	-	-	-	-	X
ProofFiring	-	X	X	X	X	X	X	X	X	-
(°C)				+20	+20					

The results from these sequential trials, can vary from igniter type to igniter type. The different pyrotechnic filling, B/KNO₃ or Mg/KNO₃, as well as the hardware may effect the results.

Typical test results for Mg/KNO₃ based igniters are shown in Table 2 (Reference 2) and Table 3 (Reference 1).

TABLE 2

Total Volatile Matter Content

Igniter Serial No.	Powder TVM Spec Limit	Actual Powder TVM Level
1	0.20%	0.13%
10	0.20%	0.25%

93 - 10

TABLE 3

Pyrotechnic Free Magnesium/Total Magnesium Ratio

Sample	% Volatile Matter	Free % Magnesium	% Total Magnesium	Ratio Free/Total
Stored	0.17	40.3	43.0	0.94
Stored	0.14	36.0	38.8	0.93
Control	0.11	38.6	40.8	0.94

The powders removed can be seen to be "free running" and whilst the TVM levels indicate some slight moisture uptake, possibly through a failure of the hermetic seal. Degradation does not appear to be significant.

A statistically significant number of aged igniter firings were compared with the ballistic specifications for fresh material and demonstrated to fall within these limits.

TABLE 4

Ballistic Firing Data from Aged Igniters

Description	Aged Igniters (Mean)	Control Limits	
		Min	Max
DelayTime	0.016		0.030
RiseTime	0.004		0.016
ActionTime	0.205	0.158	0.256
PressureMax	11.48	8.0	14.0
PressureIntegral	1.19	1.035	

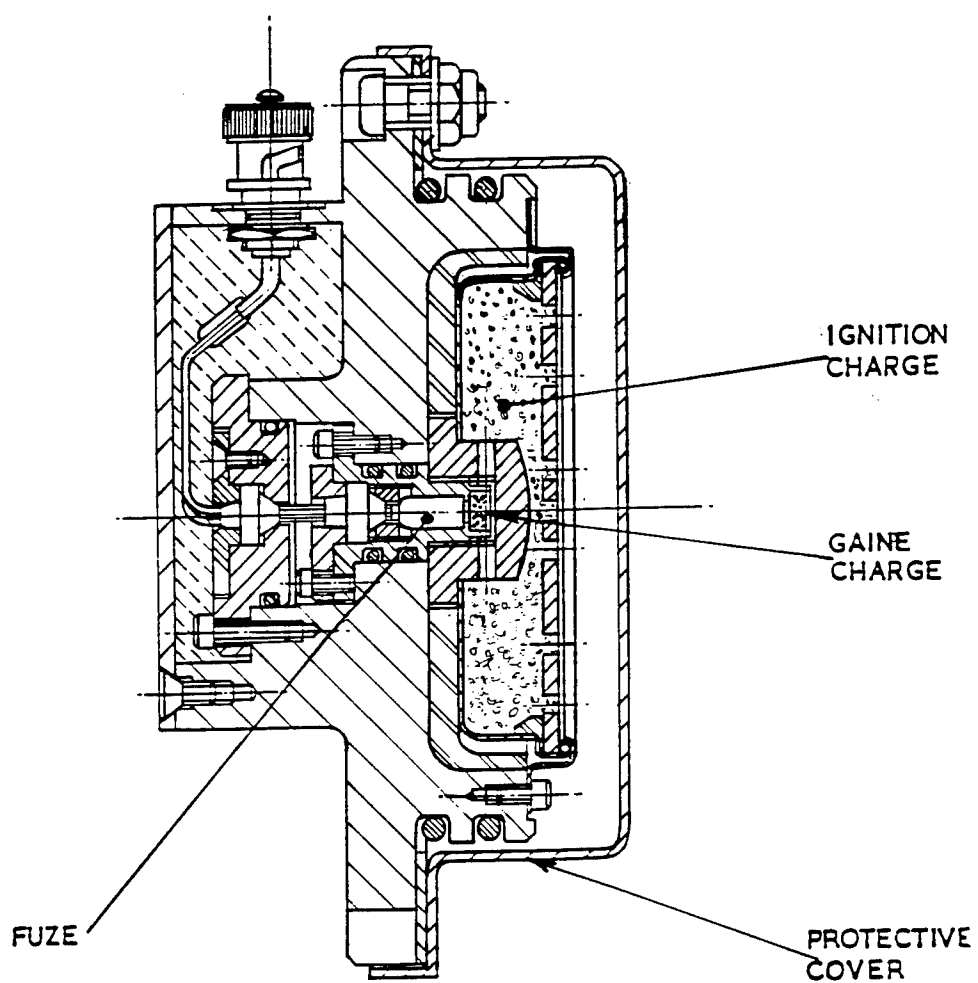
By testing devices in this way it is possible to determine the stability the pyrotechnic and hence the useful life of the device. It has been found in practice that by following the criteria stipulated for igniter filling, the satisfactory functioning of well sealed pyrotechnic devices can exceed 10 years.

REFERENCES

1. A.H. Trapp et al Royal Ordnance, Rocket Motors Division -
unpublished data
2. A.C. Mason et al Royal Ordnance, Rocket Motors Division -
unpublished data.

93 - 12

Figure 1
Boost Motor Igniter



93 - 13

Figure 2
Storage Time Against Distention

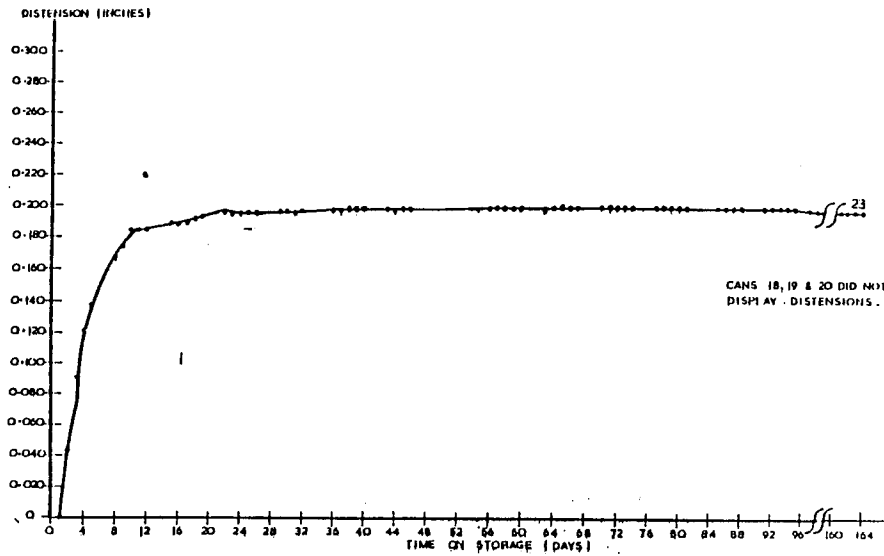


Figure 3
Internal Pressure Against Distention for Physical
Tests on Empty Cans

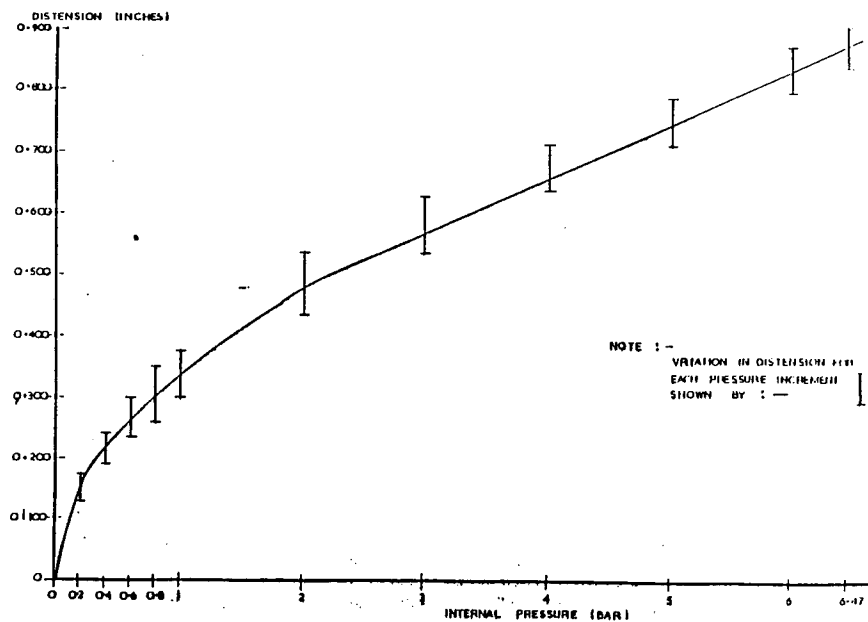


Figure 4
Vented Vessel

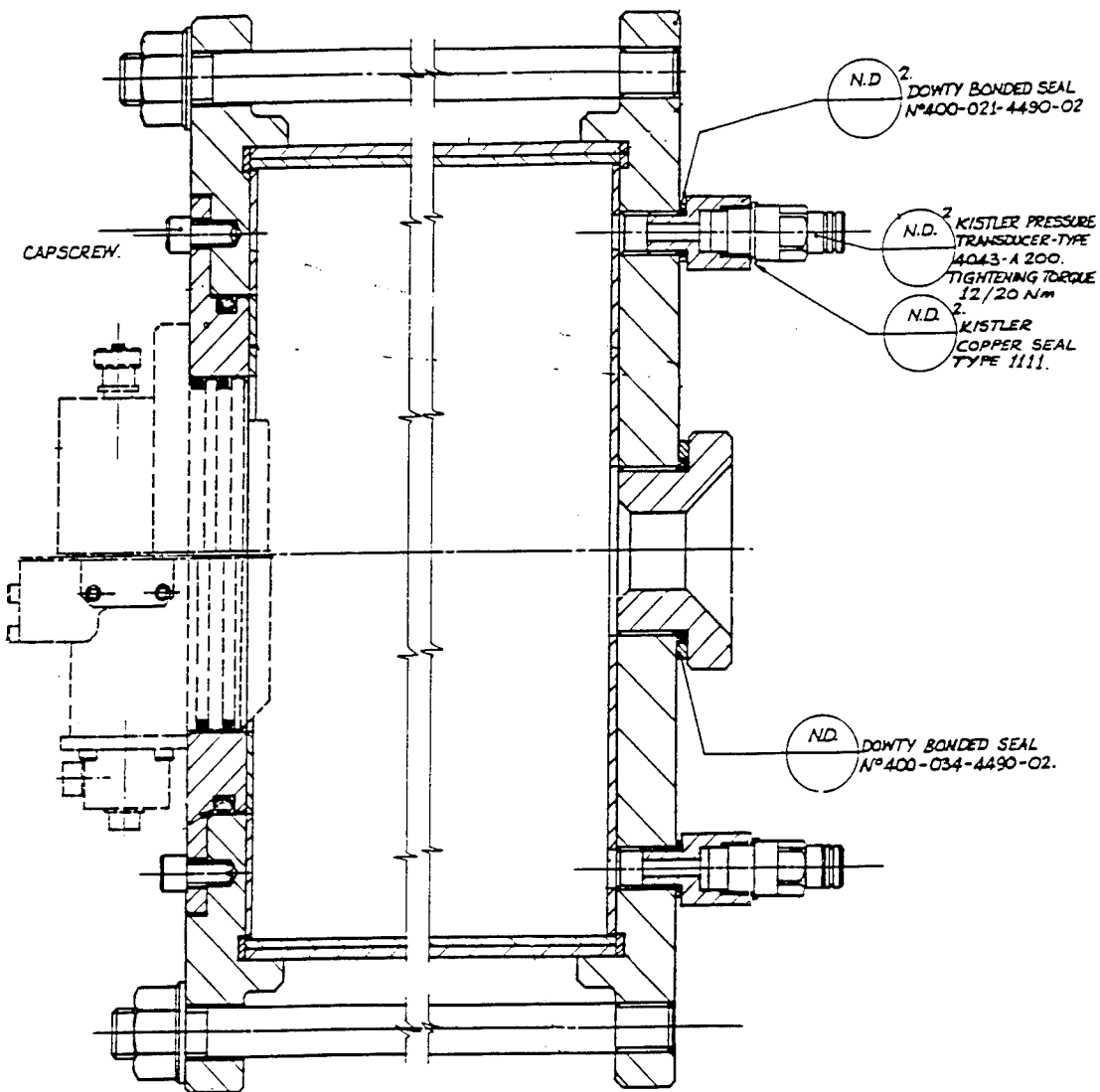
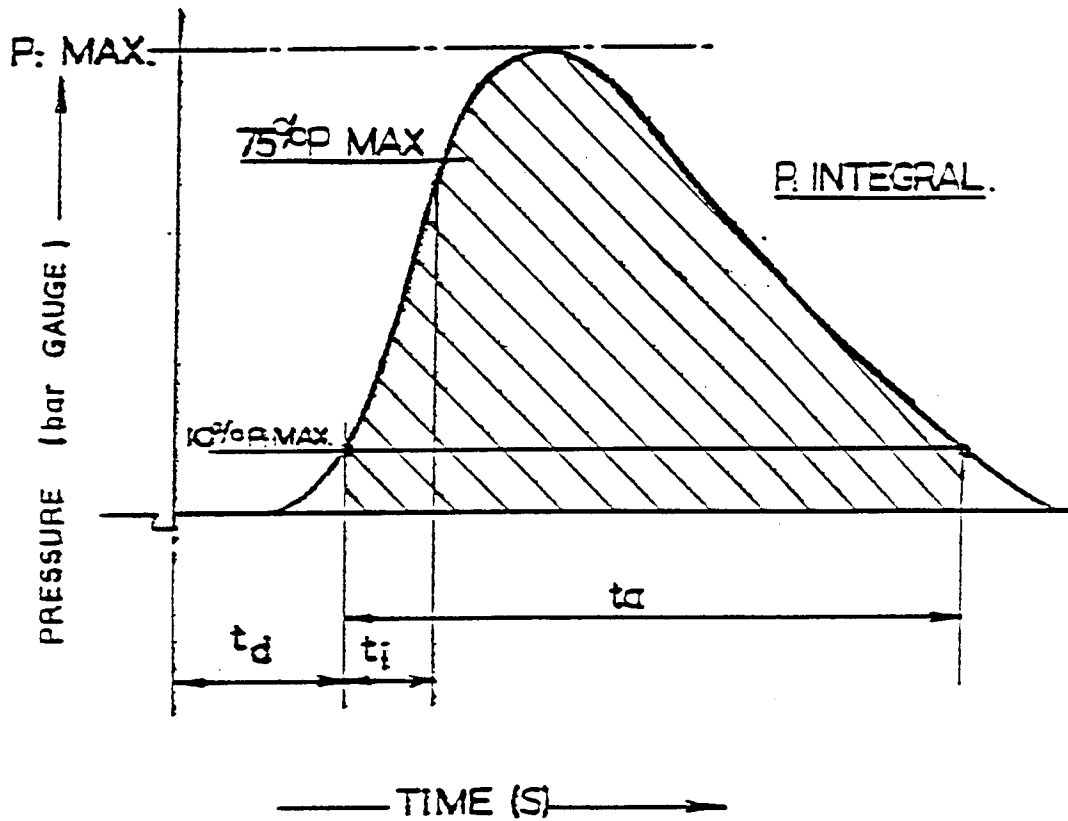


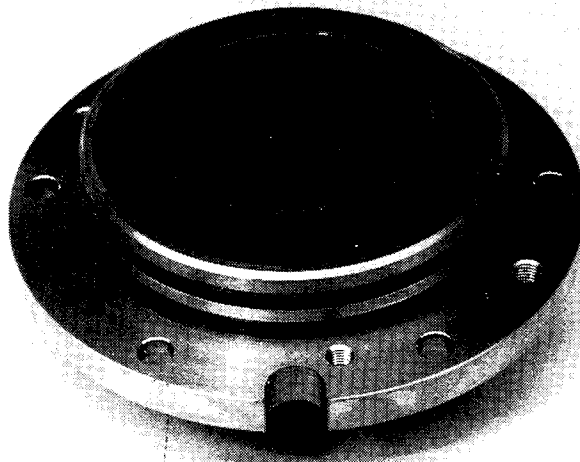
Figure 5
Pressure - Time Record



DEFINITIONS

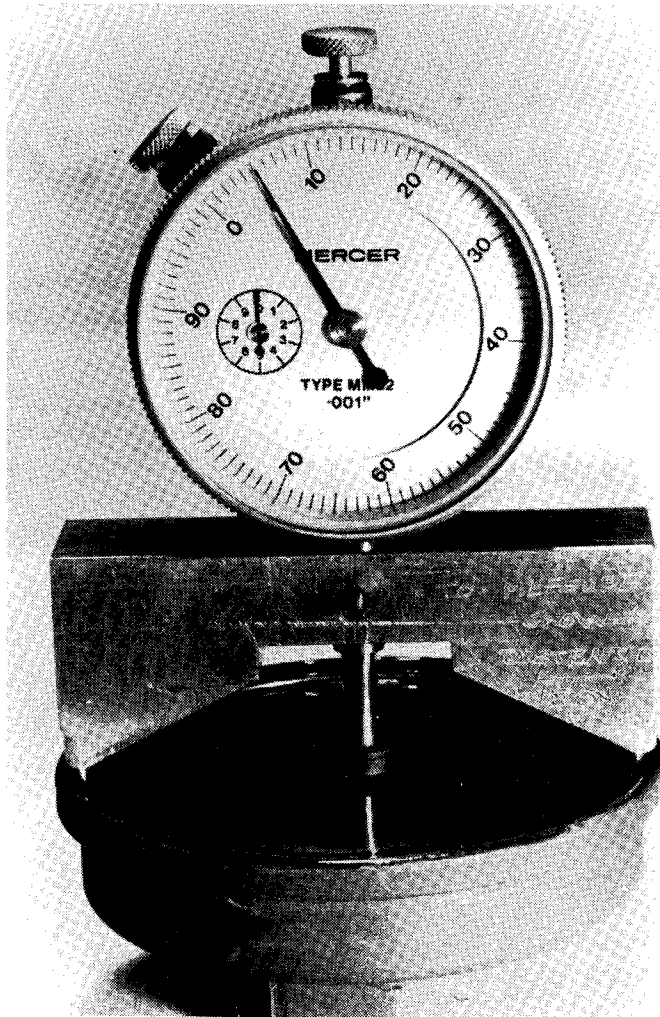
03 - 16

Photograph 1



93 - 17

Photograph 2



Spektroskopische Untersuchungen zum Abbrandverhalten von HTPB- und GAP-Platten mit Borzusatz in einer ebenen Stufenbrennkammer

Hensel, C. und Clezki, H.

DLR, Hauptabteilung Raumfahrtantriebe, Lampoldshausen

Abstract

Zur Untersuchung des Verbrennungsverhaltens von borhaltigen Festbrennstoffen für den Einsatz in Stauantrieben wurden HTPB- und GAP-Platten mit und ohne Borzusatz eingesetzt. Hierbei sollte geklärt werden, wie sich die spontanen Lichtemissionen bestimmter Spezies, wie z.B. OH, CH und BO_2 erkennen sind. Beim Abbrand von HTPB allein zeigt sich im gesamten sichtbaren Spektralbereich eine starke kontinuierliche Lichtemission, die durch die thermische Strahlung von Rußpartikeln hervorgerufen wird, sodaß im untersuchten Spektralbereich lediglich bei OH im ultravioletten einzelne Peaks in befriedigender Intensität erkennbar sind. Bei GAP hingegen, das eine geringe Rußneigung aufweist, lassen sich die Bandensysteme von OH, CH und CN bei nur geringem Untergrund relativ gut darstellen. Beim Einsatz von Bor macht sich sowohl bei GAP als auch bei HTPB eine starke kontinuierliche Strahlung bemerkbar, die der thermischen Emission der heißen Borpartikel, bei HTPB aber auch den Rußpartikeln, zuzuordnen ist, sodaß lediglich OH befriedigend darstellbar ist. Im grünen Spektralbereich lassen sich zwei nicht besonders stark ausgeprägte Maxima erkennen, die der BO_2 -Emission zugeordnet werden können.

In order to get a better understanding in the combustion behaviour of boron containing solid fuels for ramjet applications, the spontaneous light emission in a dump combustor has been investigated with a spectrometer. Pure HTPB shows a strong continuous emission which can be related to the thermal radiation of soot. Only the emissions OH with the band head at 306 nm can be seen above the continuous emission. GAP has a low sooting behaviour and shows structure of the spectra of OH, CN, CH and C₂ relatively good. If boron is added both to HTPB and GAP, the burning boron particles produce a strong continuous emission, so that only OH can be detected with a sufficient intensity. In the green region two not very distinct maxima have been detected both for HTPB and GAP, which can be related to BO_2 emission.

Einleitung

Der Einsatz von pulverförmigem Bor in Feststoffstauantrieben ist wegen seines hohen volumetrischen Heizwertes von großem Interesse. Hierbei steht einer schnellen und vollständigen Verbrennung der Borpartikel entgegen, daß diese sich beim Entzündungsvorgang mit einer flüssigen Oxidschicht überziehen und der weitere Oxidationsprozeß somit behindert wird [1]. Erst bei höheren Temperaturen dampft diese Schicht ab und erlaubt die weitere Umsetzung der Borpartikel.

Zur grundlegenden Untersuchung der Verbrennungsvorgänge in Feststoffstau-brennkammern wird eine ebene Stufenbrennkammer eingesetzt, bei der über seitliche Fenster eine Beobachtungsmöglichkeit gegeben ist. In einer solchen Kammer kann überprüft werden, ob über die auftretende Lichtemission Rückschlüsse auf das Verbrennungsverhalten ziehbar sind.

Reine Kohlenwasserstoffflammen zeigen bekanntlich Bandensysteme bestimmter beim Verbrennungsvorgang auftretender Spezies wie z.B. OH, CH oder C_2 in unterschiedlicher Ausprägung. Allerdings können solche Spektren, insbesondere bei Diffusionsflammen, durch eine kontinuierliche Strahlung, die durch heiße Rußpartikel hervorgerufen wird, überlagert sein. Inwieweit nun die dem Festbrennstoff zugesetzten Borpartikel ebenfalls durch thermische Strahlung die Ausprägung der Bandenstrahlung von OH, CH und BO_2 überlagern, soll in dieser Arbeit gezeigt werden. So wurden in früheren Untersuchungen von Liehmann [2] und von Morrison [3] Emissionsspektren im sichtbaren und infraroten Spektralbereich bei Metall/Kohlenwasserstoff-Slurrybrennern aufgenommen. Wie sich aber Emissionsspektren bei einem Feststoffabbrand ausbilden, soll in dieser Arbeit gezeigt werden.

Experimenteller Aufbau

Die für die Untersuchungen eingesetzte ebene Stufenbrennkammer (engl. dump combustor) ist in Abb. 1 dargestellt. Ein H_2/O_2 -Brenner heizt den der Brennkammer zuzuführenden Luftstrom auf bis zu $500^\circ C$ auf. Die Breite der Kammer beträgt 150 mm, die Höhe 45 mm und die Stufenhöhe 20 mm. Die Brennstoffplatten von 198 mm Länge und 100 mm Breite werden oberflächenbündig in den Boden eingesetzt. Seitliche versetzbare Quarzfenster von 45 mm Höhe und 25 mm Breite erlauben den Einblick in die Kammer für Kameras und den Spektrometer. Für die hier vorgestellte Untersuchung waren die Fenster so montiert, daß das Fensterende mit dem Ende der Brennstoffplatte abschloß. Zur Reduzierung der Fensterbelegung durch Ruß und Borpartikel wurde eine Fensterspülung eingesetzt, bei der ein Stickstoffstrom über der gesamten Kammerhöhe parallel zur Scheibe geführt wird. Unterhalb der Stufe ist ein weiterer Brenner montiert, dessen Flamme durch einen Schlitz kurzfristig auf die Plattenoberfläche gelenkt wird um diese zu entzünden.

Für die spektroskopischen Untersuchungen wurde ein 0,22 m Gitterspektrometer (Typ 1681) von Tracor Northern mit einem 512-kanaligen Diodendetektorkopf eingesetzt. Die Aufbereitung und Aufzeichnung der ermittelten Daten erfolgt mittels der TN 6500 Analyseeinheit desselben Herstellers. Die optische Ausrichtung des Spektrographen war so gewählt, daß ein Objekt, welches in 13 mm Höhe über dem Kammerboden und in der Mitte zwischen den beiden seitlichen Fenstern positioniert ist, auf den Eingangsschlitz abgebildet wird (siehe Abb. 2). Die im folgenden dargestellten Spektren sind aus mehreren aufeinanderfolgenden Spektren der gesamten Aufnahmezeit gemittelt. Weitere Daten zur Verfahrensweise und zur Einstellung des Gerätes sind in [4] enthalten.

Als Videokamera wurde überwiegend eine Dicam-2 mit UV-durchlässigem Objektiv eingesetzt. Schmalbandige Interferenzfilter von Schott wurden vor das Objektiv gesetzt um die Lichtemission im Bereich der jeweiligen zu untersuchenden Bandenemission zu selektieren.

Die für diese hier vorgestellten Versuche eingesetzten Festbrennstoffe sind in Tab. I aufgeführt. Die Herstellung der GAP-Platten erfolgte durch das Fraunhofer-Institut für Chemische Technologie in Pfinztal. Die Borpartikel von H.C. Starck waren amorph und hatten einen mittleren Durchmesser von etwa 1 µm.

1. 91,6% HTPB ; 8,4% Isophorondiisocyanat
2. 64,1% HTPB ; 5,9% " ; 30% Bor
3. 88,6% GAP ; 11,4% N100
4. 79,8% GAP ; 10,2% N100 ; 10% Bor

Tab. I Zusammensetzung der verwendeten Festbrennstoffe (Gew.-%)

Versuchsergebnisse und Diskussion

Die spontane Emission des Bandensystems von OH um die Bandenköpfe bei 306,4 und 306,8 nm konnte eindeutig identifiziert werden. Hierbei tritt, wie in Abb. 3 ersichtlich ist, ein deutlicher Untergrund bei HTPB auf. GAP hingegen, Abb. 4, zeigt ein deutlich besser ausgeprägtes Spektrum, dessen Linienintensitäten mit zunehmender Temperatur T_L des der Brennkammer zugeführten Luftstromes deutlich zunehmen. Desweiteren sind in diesem Spektrum einige Linien vorhanden, die dem Element Zinn zuzuordnen sind, das dem in geringer Menge als Katalysator für die Aushärtung zugegebenen Dibutylzinndilaurat entstammt.

Bei GAP mit Borzusatz (Abb. 5) nimmt der Untergrund im Verhältnis zu den Bandenemissionen des OH deutlich zu. Bei $T_L = 500^\circ\text{C}$ erkennt man einen deutlichen Anstieg zu niedrigeren Wellenlängen hin, was möglicherweise auf eine höhere Verbrennungstemperatur hindeutet, da ein weiteres Bandensystem von OH um 294 nm erkennbar wird. Dies ist in geringer Ausprägung auch bei reinem GAP bei $T_L = 500^\circ\text{C}$ vorhanden. Das sich ergebende Spektrum bei 400°C in

Abb. 5 besitzt aufgrund einer übermäßig starken Fensterbelegung während des Versuchs niedrige Intensitäten und ist somit nicht repräsentativ.

In Abb. 6 ist das Emissionsspektrum von GAP im Bereich von etwa 400 bis 435 nm dargestellt. Das Bandensystem von CH mit dem Bandenkopf bei 431,1 nm, das von CN mit dem Kopf bei 415,2 nm, sowie Ausläufer des C_2 -Bandensystems sind sehr deutlich zu erkennen. Bei GAP mit Borzusatz tritt der Einfluß der kontinuierlichen Strahlung in Abb. 7 deutlich hervor, sodaß CH und CN nur schlecht darstellbar sind. Diese kontinuierliche Strahlung dürfte hier hauptsächlich der thermischen Emission der heißen Borpartikel zuzuschreiben sein, da GAP eine geringe Rußneigung aufweist und der Untergrund in Abb. 6 im Vergleich zu dem in Abb. 7 relativ niedrig ist. Bei HTPB hingegen sind, sowohl mit als auch ohne Borzusatz, wegen der ausgeprägten Kontinuumsstrahlung aufgrund der starken Rußneigung des Brennstoffes die CH-Banden über dem Untergrund kaum erkennbar.

In Abb. 8 sind die Spektren der spontanen Emissionen im grünen Spektralbereich von mit Bor versetztem GAP dargestellt. Hier ist eine starke kontinuierliche Strahlung bemerkbar über die die Emissionen von BO_2 nur relativ gering herausragen. Bei reinem GAP, hier nicht präsentiert, sind im gesamten grünen Spektralbereich relativ geringe Signalintensitäten ohne ausgeprägte Emissionsbanden registriert worden. Dies deutet ebenfalls darauf hin, daß der Untergrund bei Borzusatz, wie bereits oben vermutet, durch die thermische Emission der heißen Borpartikel hervorgerufen wird. Die Abnahme der Signalintensitäten mit zunehmendem T_L ist möglicherweise, aufgrund von CCD-Kamera-Aufnahmen mit vorgesetztem Filter für den BO_2 -Emissionsbereich ($ZW=547,7$ nm, $HW=2,7$ nm), mit der Vergrößerung des Abstandes der Emissionszone von der Brennstoffoberfläche mit zunehmendem T_L nach oben hin erklärt werden, da der Spektrograph auf den unteren Kammerbereich eingestellt war. Dies muß allerdings durch weitere Untersuchungen erhärtet werden.

In Abbildung 9 ist eine Folge von fünf aufeinanderfolgenden CCD-Kameraaufnahmen mit vorgesetztem OH-Filter ($ZW=310,1$ nm; $HW=6,9$ nm) zu sehen. Hierbei war die Belichtungszeit 350 μs und die Bildfolgefrequenz 15 Hz. Die Anströmung auf den Bildern erfolgt von links. Eine starke vertikale Bewegung der Hauptintensitätszone ist aus der Abfolge der Bilder ersichtlich. Hierbei dringt diese bis zur Brennkammerdecke vor, während unmittelbar über der Brennstoffplatte sich Gebiete mit geringer Emission ergeben.

Literatur

- [1] Meinköhn, D.,
The Ignition of Boron Particles,

- Combustion and Flame, 59, pp. 225 (1985)
- [2] Liehmann, W.,
Combustion of Boron-Based Slurries in a Ramburner,
22nd Int. Annual Conf. of ICT, Karlsruhe, July 2-5 1991
 - [3] Morrison, M. E., Scheller, K.,
Spectral Characteristics of Hydrocarbon-Air Flames Containing Aluminium,
Magnesium and Boron,
Combustion and Flame, 13, pp. 93 (1969)
 - [4] Hensel, C.,
Diplomarbeit RWTH Aachen, Interner Bericht DLR, IB 645-95/5, 1995
 - [5] Mavrodineanu, R., Boiteux, H.,
Flame Spectroscopy,
John Wiley & Sons, New York, 1965

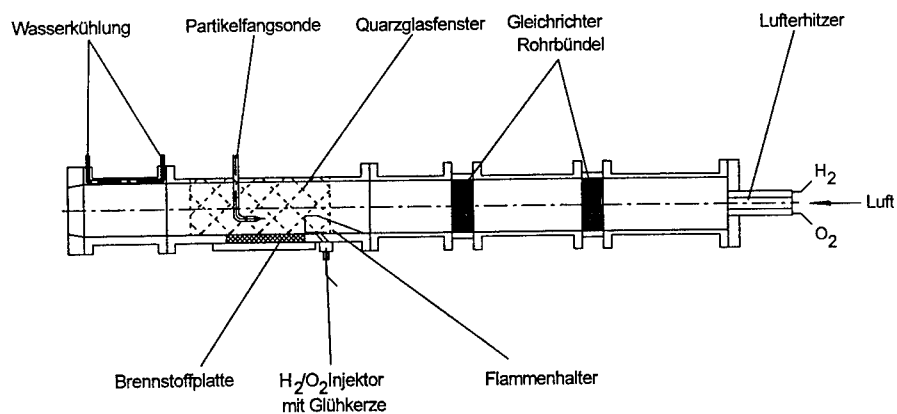


Abb. 1 Skizze des Prüfstandes mit ebener Stufenbrennkammer und Lufterhitzer

94 - 6

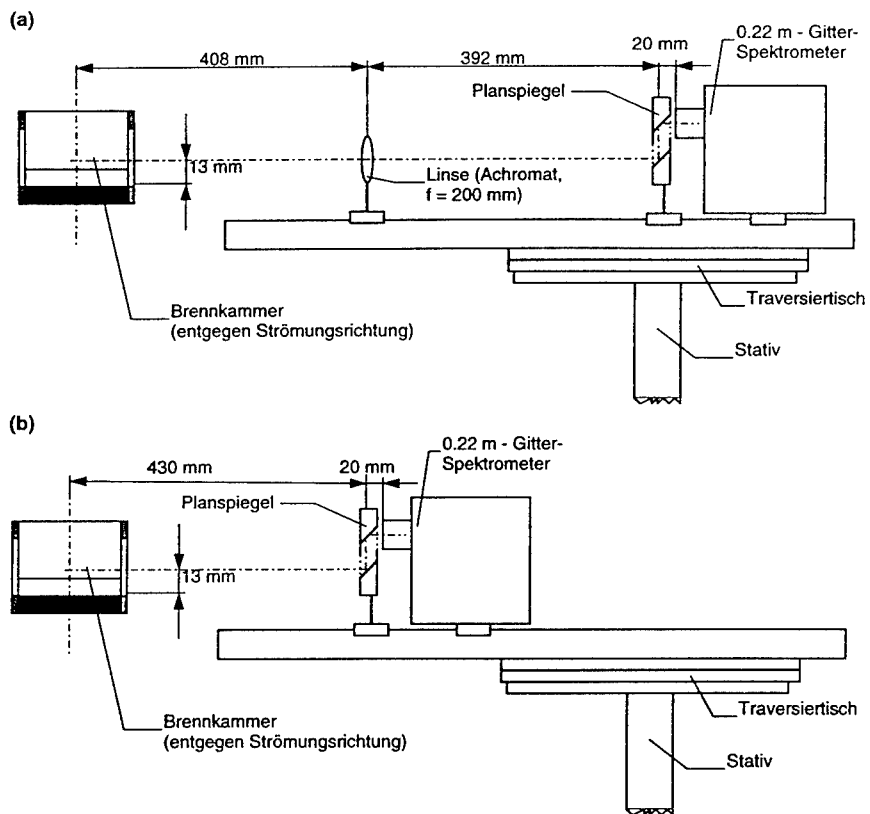


Abb. 2 Versuchsaufbau für emissionsspektroskopische Messungen
a.) im sichtbaren Spektralbereich
b.) im UV-Bereich

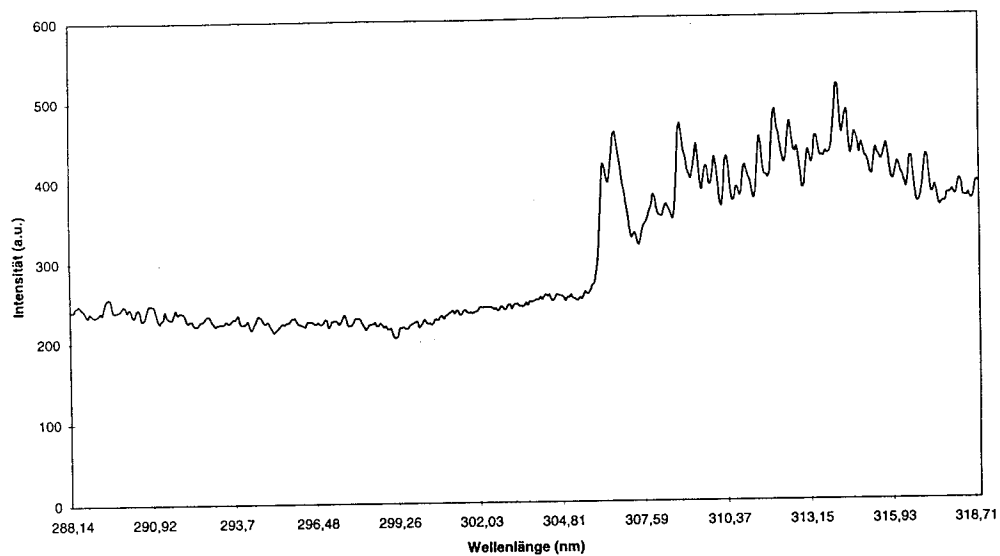


Abb. 3 OH-Spektrum von HTPB ohne Borzusatz; $T_L = 500^\circ\text{C}$

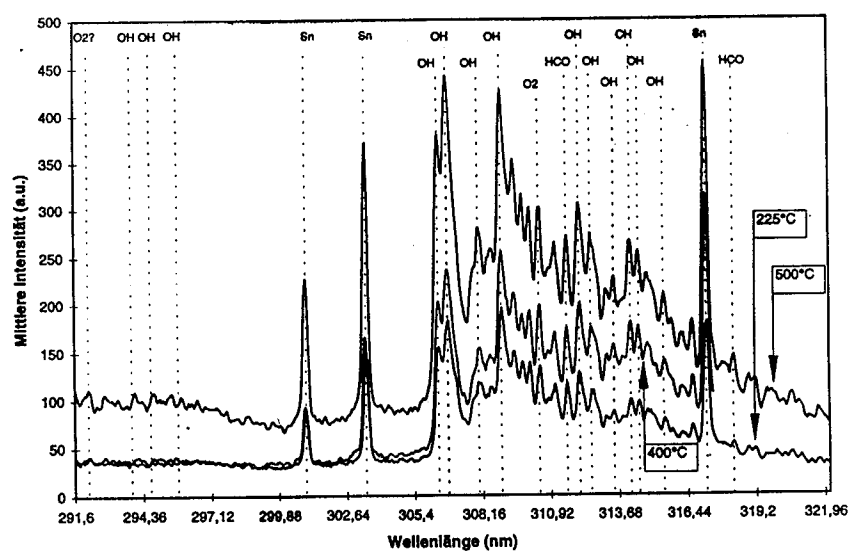


Abb. 4 OH-Spektrum von GAP ohne Borzusatz

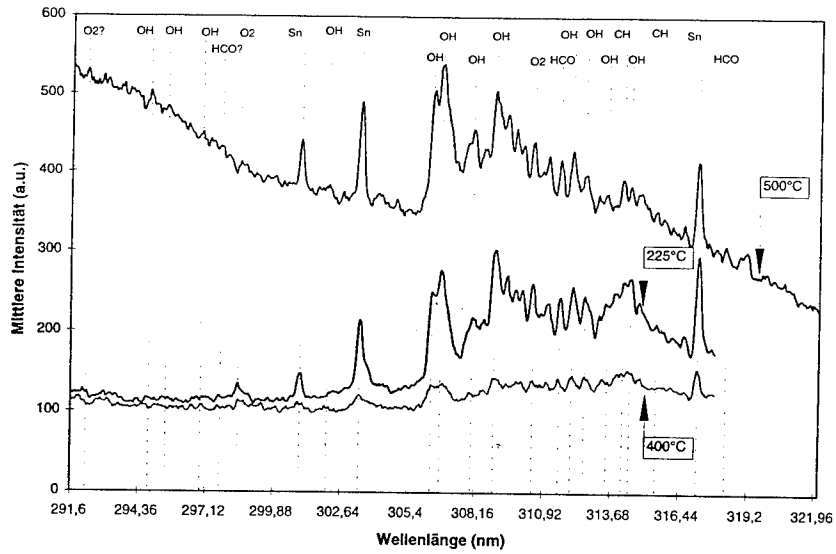


Abb. 5 OH-Spektrum von GAP mit 10% Borzusatz

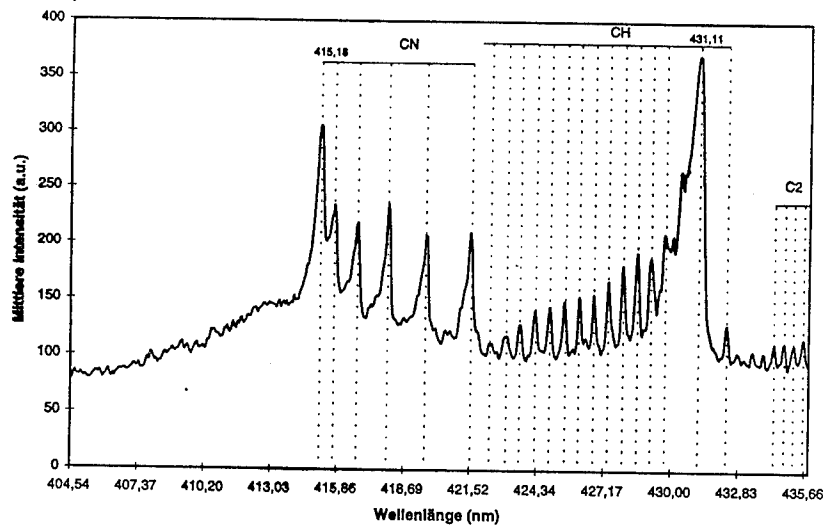


Abb. 6 CH-Spektrum von GAP ohne Borzusatz; $T_L = 500^\circ\text{C}$

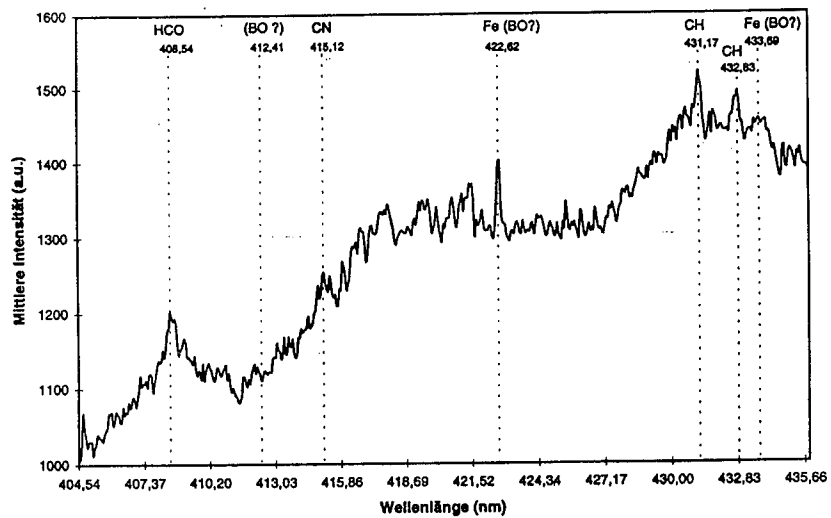


Abb. 7 CH-Spektrum von GAP mit 10% Borzusatz; $T_L = 500^\circ\text{C}$

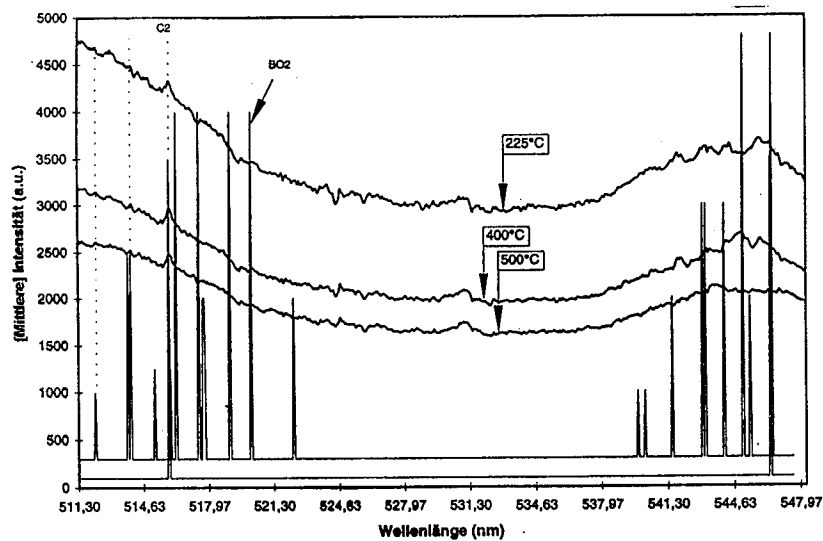


Abb. 8 BO_2 -Spektrum von GAP mit 10% Borzusatz;
(Peaks der beiden unteren Linien kennzeichnen Positionen von Linien
und Intensitäten theoretischer Spektren von BO_2 und C_2 nach
z.B. [5])

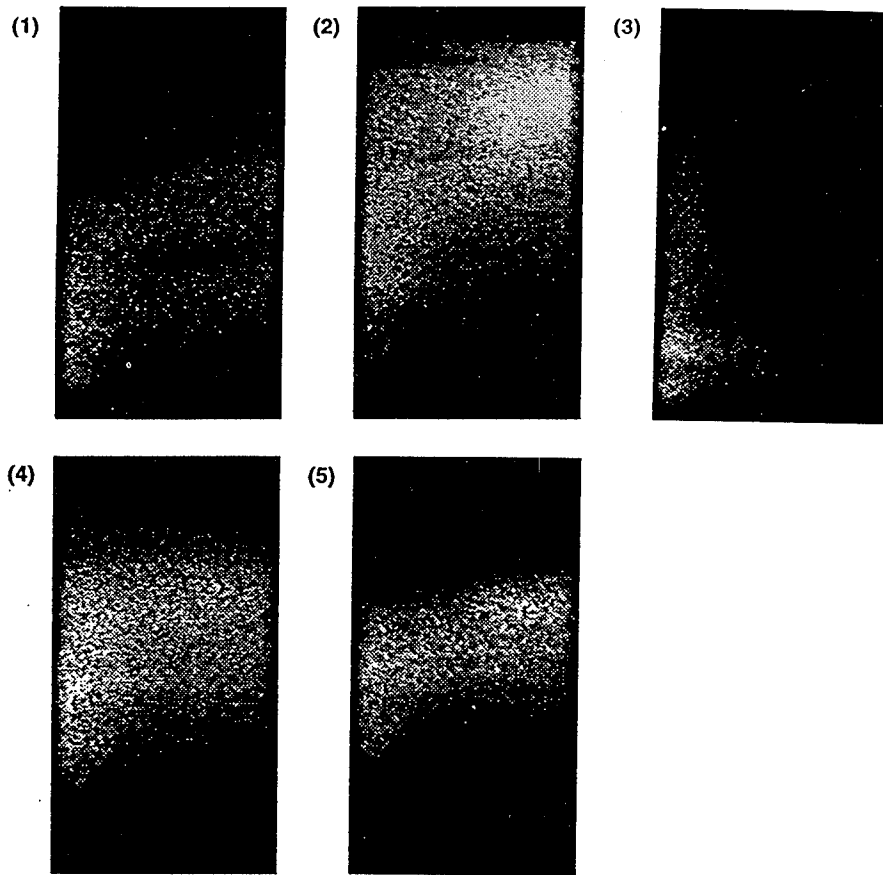


Abb. 9 Sequenz von CCD-Kameraaufnahmen im OH-Spektralbereich;
GAP ohne Borzusatz

Entwicklung einer kombinierten Gas- und Partikelprobennahmesonde
für den Einsatz in einer Feststoffstaubrennkammer

Ciezeki, H. und Schwein, B.

DLR, Hauptabteilung Raumfahrtantriebe, Lampoldshausen

Zur Untersuchung des Abbrandverhaltens von HTPB-Festbrennstoffplatten mit Borzusatz in einer ebenen Stufenbrennkammer wurde eine wassergekühlte Absaugsonde entwickelt mit der gleichzeitig gasförmige stabile Reaktionszwischenprodukte in einem Probenbehälter, sowie die Feststoffphase auf einem Filter aufgefangen werden können. Aus der anschließenden Analyse wurden Konzentrationsverteilungen für gasförmige Stoffe mittels eines Gaschromatographen, sowie B_2O_3 mittels eines naßchemischen Verfahrens ermittelt. Die Probennahmepositionen waren zwischen 8 mm bzw. 4 mm und 24 mm bzw. 28 mm über der Brennstoffplatte in drei verschiedenen Meßebenen 60 mm, 97 mm und 171 mm hinter der Flammenhalterstufe senkrecht zur Brennstoffoberfläche.

Hierbei zeigte sich, daß CO , CO_2 und H_2 mit zunehmendem Abstand von der Brennstoffoberfläche in allen drei Meßebenen abnehmen und der Sauerstoffanteil zunimmt. Methan wurde in der hintersten Meßebene bei 4 mm Höhe mit 0,2 % gemessen. Weitere Kohlenwasserstoffe konnten im Rahmen der Meßgenauigkeit und der verwendeten Säule nicht ermittelt werden. Bei etwa 28 mm Höhe sind keine gasförmigen Verbrennungsprodukte mehr vorhanden und die Zusammensetzung der Gasprobe entspricht der Luft, wie sie vom Lufterhitzer des Prüfstandes der Brennkammer zugeführt wird.

Die Konzentration von B_2O_3 in der auf dem Filter aufgefangenen Feststoffphase nimmt tendenziell mit zunehmendem Abstand von der Brennstoffoberfläche bis 24 mm zu. Über den weiteren Verlauf kann keine Aussage infolge fehlender Messungen gemacht werden. Durch die relativ geringen Probenmengen und die somit ungenauere Analyse können die Schwankungen im Kurvenverlauf hervorgerufen werden.

Bei ausgesuchten Probennahmepositionen wurden mittels eines Rasterelektronenmikroskops Aufnahmen der aufgefangenen Feststoffphase erzeugt. Hierbei sind sowohl plattenartige, bzw. kristalline Strukturen als auch amorphe zu erkennen. Bei 4 mm Höhe und 171 mm hinter der Stufe zeigen eine Vielzahl der Platten Löcher und tropfenartige Gebilde auf ihrer Oberfläche.

P96

UV-VIS-SPEKTROSKOPISCHE ERFASSUNG VON IN UNTER- UND ÜBERKRITISCHEM KOHLENDIOXID GELÖSTEN NITROAROMATEN

S. Löbbecke, G. Bunte, T. Härdle, H. Krause

Fraunhofer-Institut für Chemische Technologie ICT, Joseph-von-Fraunhofer-Straße 7,
D-76327 Pfinztal/Berghausen

KURZFASSUNG

Eine Meßapparatur wird vorgestellt, mit der in unter- und überkritischem CO_2 gelöste Nitroaromaten bis in den Spurenbereich UV-VIS-spektroskopisch erfaßt werden. Das besondere spektroskopische Verhalten dieser Lösungen bei Drücken bis 400 bar und Temperaturen bis 150 °C wird beschrieben.

A measuring device is presented, which is capable to detect trace amounts of nitroaromatic compounds dissolved in sub- and supercritical CO_2 by UV-VIS-spectroscopy. The specific spectroscopic behavior of these solutions at pressures up to 400 bar and temperatures up to 150 °C is described.

1 EINLEITUNG UND PROBLEMSTELLUNG

Energetische Substanzen wie z.B. TNT und andere Nitroaromaten weisen sehr gute Lösungseigenschaften in unter- und überkritischem Kohlendioxid auf.

Extraktionsverfahren unter Einsatz von überkritischem CO_2 (SC- CO_2) als Extraktionsmittel (angels.: supercritical fluid extraction SFE) ermöglichen somit den Austrag von TNT und seinen Abbauprodukten aus unterschiedlichen Matrices, wie z.B. kontaminierten Böden [1].

Aufgrund der Tatsache, daß die analytischen Informationen über die mittels SFE extrahierten Substanzen zur Zeit ausschließlich durch Analysenmethoden erhalten werden, die dem Extraktionsvorgang nachgeschaltet werden, ist die Entwicklung einer on-line-Analysentechnik für SFE-Verfahren von großem Interesse.

Mit der Verfügbarkeit einer solchen - z.B. spektroskopischen - on-line-Analytik für SF-Extraktionen würde bereits parallel zum Extraktionsverlauf die Möglichkeit zur Identifizierung und Quantifizierung der extrahierten Analyten bestehen. Eine unmittelbare Überwachung des Extraktionsvorganges sowie dessen schnelle Bewertung und Optimierung wären somit möglich.

2 EXPERIMENTELLES

Vor diesem Hintergrund wurde eine Meßapparatur zur Simulation einer UV-VIS-spektroskopischen on-line-Analytik für SFE-Verfahren entwickelt, mit der Untersuchungen an gasförmigem sowie insbesondere flüssigem und überkritischem Kohlendioxid vorgenommen werden können. Abbildung 1 zeigt den optischen Aufbau. Die Konstruktion und der Aufbau der Meßapparatur ist hinsichtlich der besonderen Anforderungen hoher Temperatur- und Druckbeständigkeit ($T \leq 150\text{ }^{\circ}\text{C}$, $p \leq 400\text{ bar}$) ausgelegt.

Als Kernstück der Meßapparatur wurde eine optische Hochdruckzelle (Abb. 2) entwickelt, die so konzipiert ist, daß sie neben der hohen Druck- und Temperaturbeständigkeit eine einfache und kostengünstige Konstruktion aufweist, die einen vielseitigen Einsatz der Meßzelle (u.a. Vermessung verschiedener Schichtdicken, Option für Fluoreszenzmessungen) erlaubt.

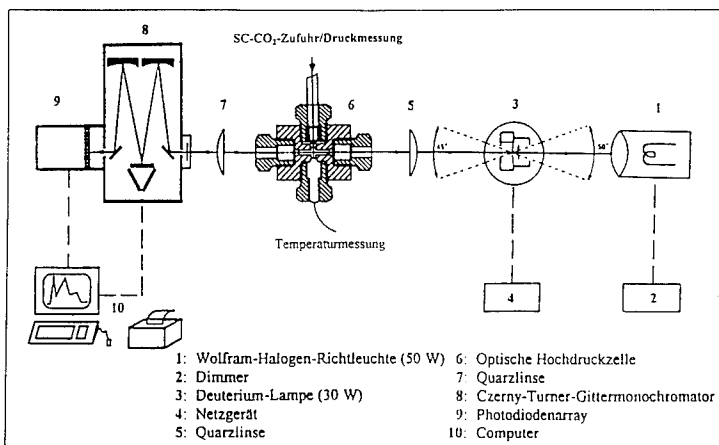


Abb.1: Schematische Darstellung der Meßanordnung zur UV-VIS-Spektroskopie

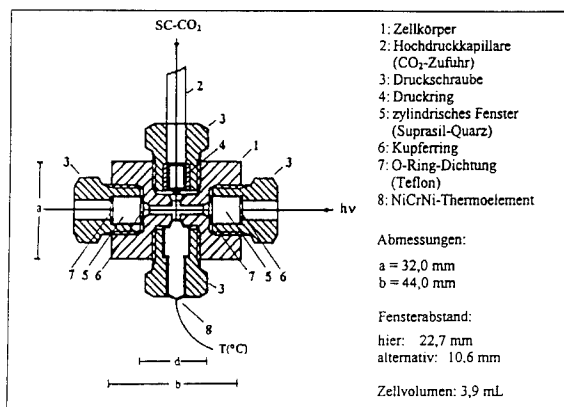


Abb.2: Schematischer Querschnitt durch die optische Hochdruckzelle

3 ERGEBNISSE

Die UV-VIS-spektroskopischen Eigenschaften von Kohlendioxid wurden über einen weiten Druck- und Temperaturbereich ($p = 1 - 400$ bar, $T = 20 - 150$ °C) erfaßt. Dabei läßt sich zeigen, daß die Transmissionseigenschaften des CO_2 im kurzwelligen UV-VIS-Spektralbereich dichteabhängig sind (Abb. 3). Eine Erhöhung der CO_2 -Dichte führt infolge zunehmender Brechungseffekte (Abb. 4) zu einer verringerten Transparenz des CO_2 im Wellenlängenbereich 190 bis maximal 400 nm. Desweiteren ist zu beobachten, daß kurzzeitige Dichte- und somit Brechungsindex-Inhomogenitäten des CO_2 , die infolge von Druck- oder Temperaturänderungen auftreten können, kurzzeitige Intensitätsschwankungen der das CO_2 transmittierenden Strahlung zur Folge haben. Diese lassen sich durch geeignete apparative Maßnahmen, die Wärmekonvektion und Druckgradienten verhindern, unterdrücken.

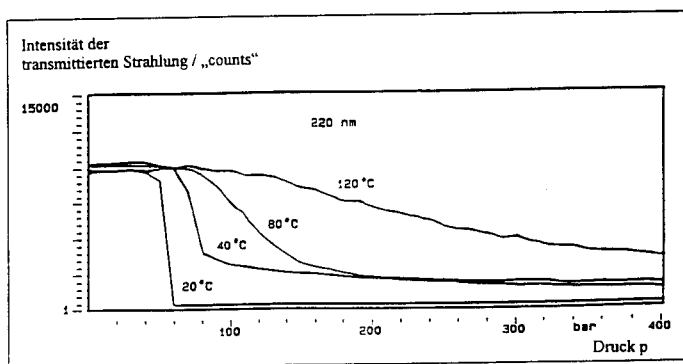


Abb. 3: Die CO_2 -Transparenz in Abhängigkeit von Druck und Temperatur am Beispiel der Wellenlänge $\lambda = 220$ nm

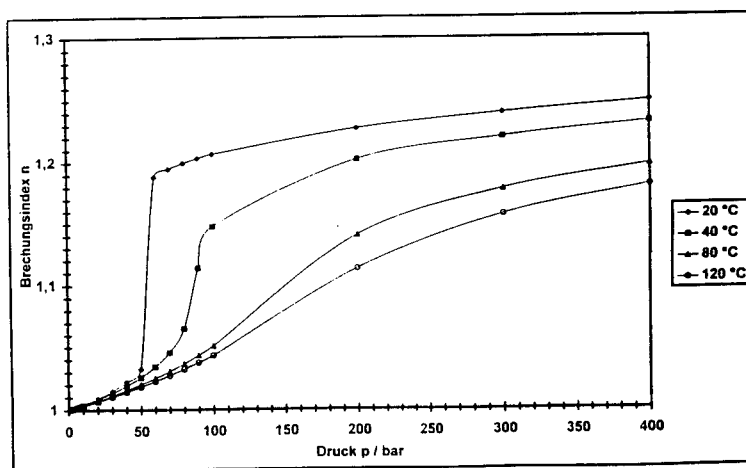


Abb. 4: Verlauf des CO_2 -Brechungsindex für vier isotherme Druckerhöhungen (berechnet auf der Grundlage der spezifischen Lorentz-Lorenz-Refraktionsgleichung für $\lambda = 546$ nm) [2]

Mittels UV-VIS-spektroskopischer Untersuchungen an in unter- und überkritischem CO_2 gelösten Nitroaromaten (2,4,6-Trinitrotoluol und dessen Abbauprodukt 4-Amino-3-nitrotoluol) wurde die spektroskopische on-line-Erfassung von Analyten simuliert, die mit komprimiertem Kohlendioxid aus einer Sprengstoff-kontaminierten Bodenprobe extrahiert werden.

Die Identifizierung der in SC-CO_2 gelösten Analyten erfolgt anhand ihrer charakteristischen Absorptionsbanden. Eine Quantifizierung der Nitroaromaten ist bis in den ppm-Bereich möglich.

Es läßt sich zeigen, daß die charakteristischen Absorptionsbanden der in SC-CO_2 gelösten Analyten gegenüber Lösungen in klassisch organischen Lösungsmitteln mitunter drastischen, hypsochromen Verschiebungen (um bis zu 50 nm) unterliegen. Zusätzlich ist eine schwächer ausgeprägte, bathochrome Absorptionsbanden-Verschiebung bei zunehmender CO_2 -Dichte bzw. -Polarität zu beobachten.

Abbildung 5 zeigt diese Effekte am Beispiel der Transmissionsspektren von in SC-CO_2 gelöstem 4-Amino-3-nitrotoluol.

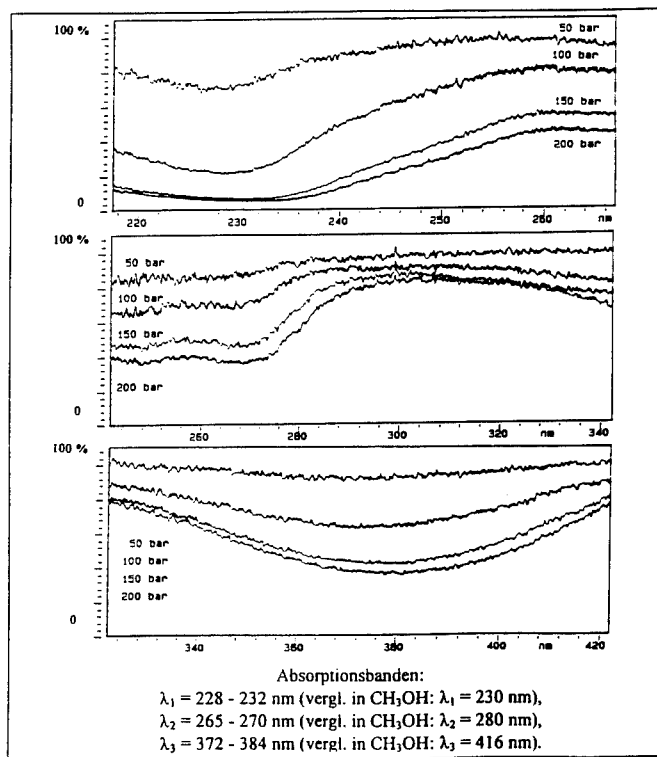


Abb. 5: Transmissionsspektren von in unter- und überkritischem CO_2 gelöstem 4-Amino-3-nitrotoluol ($T = 80^\circ\text{C}$):
vollständiges Lösen des Analyten mit zunehmender CO_2 -Dichte unter bathochromer Absorptionsbanden-Verschiebung

4 LITERATUR

- [1] G. Bunte, Th. Hirth, H. Krause, A. Kroll,
„Extraktion von Explosivstoffen aus Böden mit überkritischem Kohlendioxid“,
25. ICT-Jahrestagung, Karlsruhe (1994)

- [2] E. P. Kholodov, N. I. Timashenko, A. L. Yaminov,
„Determining the density and polarisability of CO₂ on the basis of experimental
data on the refractive index“,
Therm. Eng. (Engl. Transl.) 19, 126 (1972)

Übersicht über die Themen der ICT-Jahrestagungen seit 1982

- | | |
|------|--|
| 1982 | <p>„Verwendung von Kunststoffen für Treib- und Explosivstoffe“
 „Use of Plastic Materials for Propellants and Explosives“
 „Utilisation des matières plastiques dans les propergols et explosifs“</p> |
| 1983 | <p>„Gütesicherung und Überwachung von Treib- und Sprengmitteln“
 „Production Control and Surveillance of Propellants and High Explosives“
 „Assurance de la qualité et surveillance de propergols et explosifs“</p> |
| 1984 | <p>„Technologie von Treib- und Sprengmitteln“
 „Technology of Propellants and High Explosives“
 „Technologie des poudres et explosifs“</p> |
| 1985 | <p>„Pyrotechnik: Grundlagen, Technologie, Anwendung“
 „Pyrotechnics: Basic Principles, Technology, Application“
 „Pyrotechnique: Bases fondamentales, technologie, applications“</p> |
| 1986 | <p>„Analyse von Treib- und Explosivstoffen - Chemische und physikalische Methoden“
 „Analysis of Propellants and Explosives - Chemical and Physical Methods“
 „Analyse des poudres et d'explosifs - Méthodes chimiques et physiques“</p> |
| 1987 | <p>„Technologie von energiereichen Stoffen - Herstellung und Verarbeitung, Beurteilung der Produkteigenschaften“
 „Technology of Energetic Materials - Manufacturing and Processing, Valuation of Product Properties“
 „La technologie de substances de haute énergie - Préparation et traitement, Evaluation des caractéristiques du produit“</p> |
| 1988 | <p>„Verbrennungs- und Detonationsvorgänge“
 „Combustion and Detonation Phenomena“
 „Phénomènes de combustion et de détonation“</p> |
| 1989 | <p>„Umweltprüfung in den 90ern“
 „Environmental Testing in the 90's“
 „Les essais d' environnement dans les années 90“</p> |
| 1990 | <p>„Technologie von Kunststoffcompounds und energiereichen Materialien“
 „Technology of Polymer Compounds and Energetic Materials“
 „Technologie des compounds et matières à haute energie“</p> |
| 1991 | <p>„Verbrennung und Reaktionskinetik“
 „Combustion and Reaction Kinetics“
 „Cinétique de combustion et de réaction“</p> |
| 1992 | <p>„Entsorgung von Energiestoffen und Polymeren“
 „Waste Management of Energetic Materials and Polymers“
 „Gestion des déchets de matières énergétiques et de polymères“</p> |
| 1993 | <p>„Unempfindliche und umweltfreundliche Treib- und Explosivstoffe“
 „Energetic Materials - Insensitivity and Environmental Awareness“
 „Le propergols et explosifs peu sensibles et non polluants“</p> |
| 1994 | <p>„Chemische Energieträger - Methoden der Analytik und Charakterisierung, Testverfahren“
 „Energetic Materials - Analysis, Characterization and Test Techniques“</p> |